THE LITHOGEOCHEMICAL AND MINERALOGICAL SETTING OF TURBIDITE HOSTED ARSENIC-GOLD DEPOSITS IN THE LOWER PALAEOZOIC OF SCOTLAND.

by

Paul R. Duller, B.Sc.

Volume Two

Thesis submitted to the
University of Strathclyde for the Degree
of Doctor of Philosophy

Department of Applied Geology,
University of Strathclyde,
GLASGOW,
Scotland,
G1 1XJ.

December 1989.

FOLDOUTS

Fold-Out 1

Glendinning Regional Geochemical Traverse

This diagram displays the results of multi-element geochemistry upon a series of interbedded greywackes and mudstones of Late Llandovery and Wenlock age, defined as the Hawick Group.

Both greywacke (n=305) and mudstone (n=197) samples were collected from the same locality (whenever possible) on a series of cross-strike traverses in the Glendinning Study area (see text). Samples were grouped on the basis of stratigraphy, lithology and numerical order to aid the assessment and interpretation of the complex inter-relationships that exist within this dataset.

This diagram presents the results of 22,080 analytical and calculated values.

Glendinning Regional Geochemistry

1196

Fold-Out 2

The Southern Uplands Composite Geochemical Traverse

This fold-out diagram displays the results of multi-element geochemistry upon a number of petrographically defined greywacke formations in the Southern Uplands. Samples from each formation have been grouped in ascending numerical order and combined with other formations to create a composite geochemical profile (n=861).

The Marchburn, Blackcraig, Scar and Pyroxenous Formations are defined by Floyd (1983) on petrographic evidence to have been derived from one or more volcanic terrains as opposed to the Afton, Shinnel and Intermediate Formations which were derived from a cratonic terrain. The Hawick Formation, is defined in this study as a cratonic derived greywacke containing in addition, a significant proportion of carbonate.

Please note the inverted stratigraphy displayed on this diagram in order to mirror the actual north-south juxtaposition of each formation across the Southern Uplands. It should also be noted that this diagram graphically displays the results of 24,969 analytical and 12,915 calculated values (total 37,884).

The Southern Uplands: Composite Geochemical Traverse.

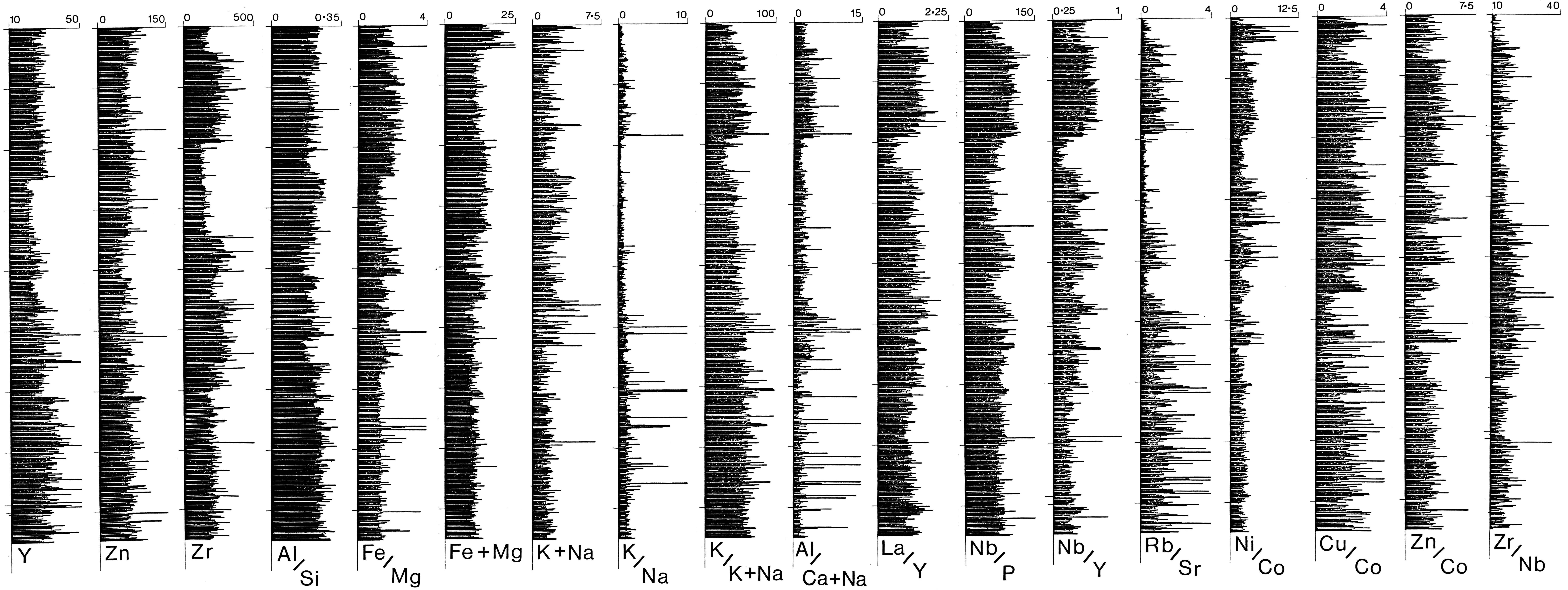

10 50 Y
0 150 Zn
0 500 Zr
0 0·35 Al/Si
0 4 Fe/Mg
0 25 Fe+Mg
0 7·5 K+Na
0 10 K/Na
0 100 K/K+Na
0 15 Al/Ca+Na
0 2·25 La/Y
0 150 Nb/P
0·25 1 Nb/Y
0 4 Rb/Sr
0 12·5 Ni/Co
0 4 Cu/Co
0 7·5 Zn/Co
10 40 Zr/Nb

1197

Fold-Out 3

The Glendinning As-Sb-Au Deposit, Southern Scotland : Borehole Lithogeochemistry

This diagram displays the results of multi-element geochemistry upon a series of interbedded greywackes, siltstones and mudstones of Wenlock age (n=170) sampled from four boreholes drilled in proximity to the Louisa Antimony Mine, Glendinning. The location and characteristics of each borehole is defined below:

Borehole No.	1	2	3	4
Samples	n=33	n=44	n=82	n=11
Grid Ref.	[3139,9652]	[3147,9693]	[3143,9669]	[3135,9671]
Elevation	290.0m	380.1m	317.1m	316.6m
Inclination	50	50	60	50
Azimuth	098	103	104	287
Depth	85.27m	118.82m	197.82m	84.87m

When viewed in conjunction with fold-out 1 (detailing background variation in the host rocks to this deposit) the effects of hydrothermal alteration and mineralization may be easily recognised (see text for detailed explanation).

Please note that the length of each borehole section displayed on the fold-out is directly related to the number of samples and their relative position in each hole rather than depth, and as such this diagram can only be used for comparative purposes. This diagram presents the results of 7,480 determined and calculated values.

The Glendinning As-Sb-Au Deposit, Southern Scotland: Borehole Geochemistry.

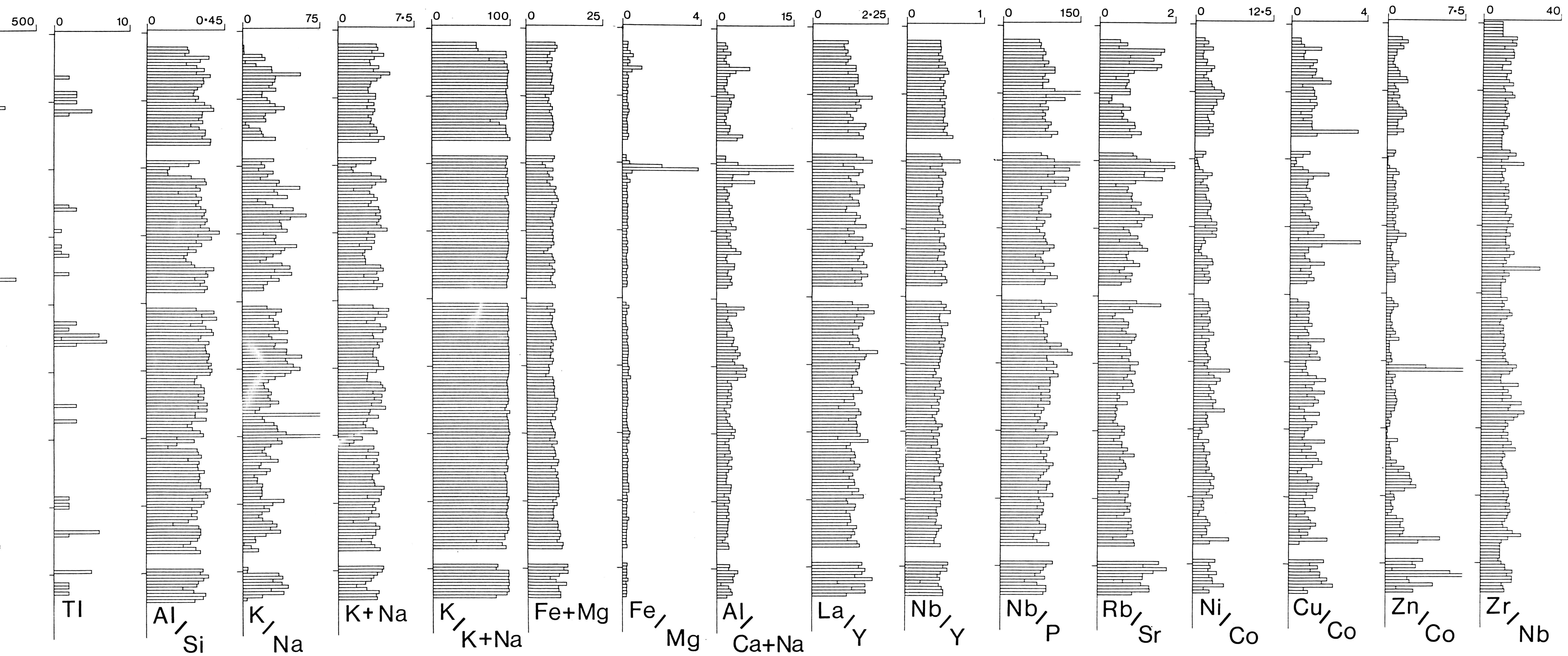

500
0 10
Tl
0 0·45
Al/Si
0 75
K/Na
0 7·5
K+Na
0 100
K/K+Na
0 25
Fe+Mg
0 4
Fe/Mg
0 15
Al/Ca+Na
0 2·25
La/Y
0 1
Nb/Y
0 150
Nb/P
0 2
Rb/Sr
0 12·5
Ni/Co
0 4
Cu/Co
0 7·5
Zn/Co
0 40
Zr/Nb

Fold-Out 4

The Longford Down Geochemical Traverse

This fold-out diagram displays the results of multi-element geochemistry upon a number of petrographically defined greywacke formations in the Longford Down. Samples were assigned to their respective Formations on the basis of petrographic examination (Morris, 1983) grouped in ascending numerical order and combined with other formations to create a composite geochemical profile (n=225). Here again the strat igraphy defined by Morris (op.cit.) has been inverted in order to present a true North-South traverse across the Longford Down. This diagram displays the results of 10,800 analytical and calculated values.

The Longford Down: Geochemical Traverse.

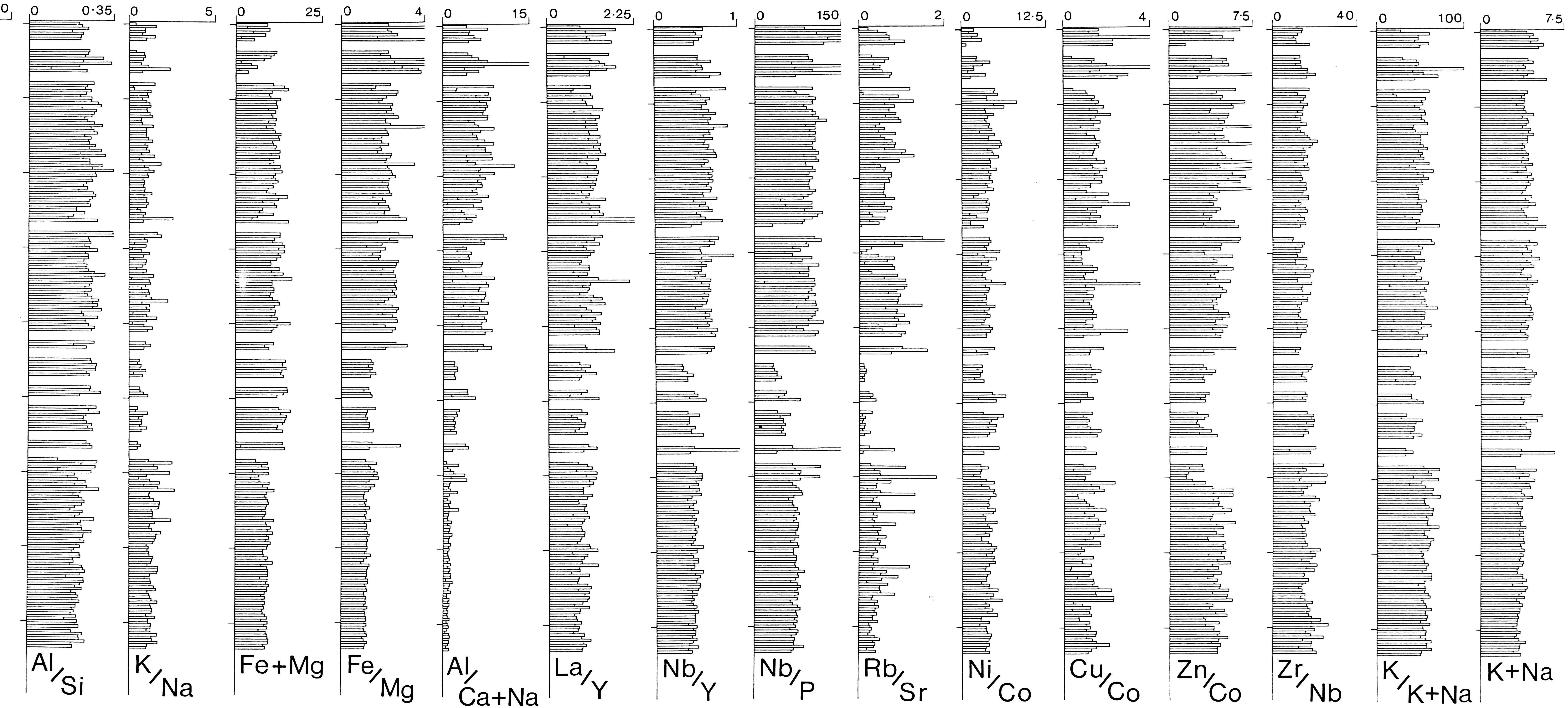

0
0 0·35
Al/Si
0 5
K/Na
0 25
Fe+Mg
0 4
Fe/Mg
0 15
Al/Ca+Na
0 2·25
La/Y
0 1
Nb/Y
0 150
Nb/P
0 2
Rb/Sr
0 12·5
Ni/Co
0 4
Cu/Co
0 7·5
Zn/Co
0 40
Zr/Nb
0 100
K/K+Na
0 7·5
K+Na

Fold-Out 5

The Rhinns of Galloway Geochemical Traverse

This fold-out diagram displays the results of multi-element geochemistry upon Greywackes sampled at approx 150-200m intervals, during a Coastal traverse of Southwest Scotland. This diagram may be divided into three sections: the first, traverse A-B was undertaken on the eastern margin of Loch Ryan, as opposed to the second, on the western margin. The remaining samples (forming the major part of this study) were collected on a 42km traverse of the western margin of the Rhinns of Galloway; from Corsewall Point in the North, south to the Mull of Galloway.

Traverse A-B: Currarie Point [20550,57790]
south to Laight [20598,57030].

Traverse C-D: Milleur Point [20200,57370]
south to Clachan Heughs [20350,57040].

Please note that the Corsewall, Kirkcolm and Portpatrick Formations (Kelling, 1969) are synonymous with the Marchburn, Afton, Scar (Portpatrick basic) and Shinnel (Portpatrick acid) Formations of Floyd (1983). In addition the position of the (Silurian) Pyroxenous, Intermediate and Hawick Formations are identified by this study (see text). This fold-out diagram displays the results of 12,386 (n=279) determined and calculated values.

The Rhinns of Galloway : Geochemical Traverse.

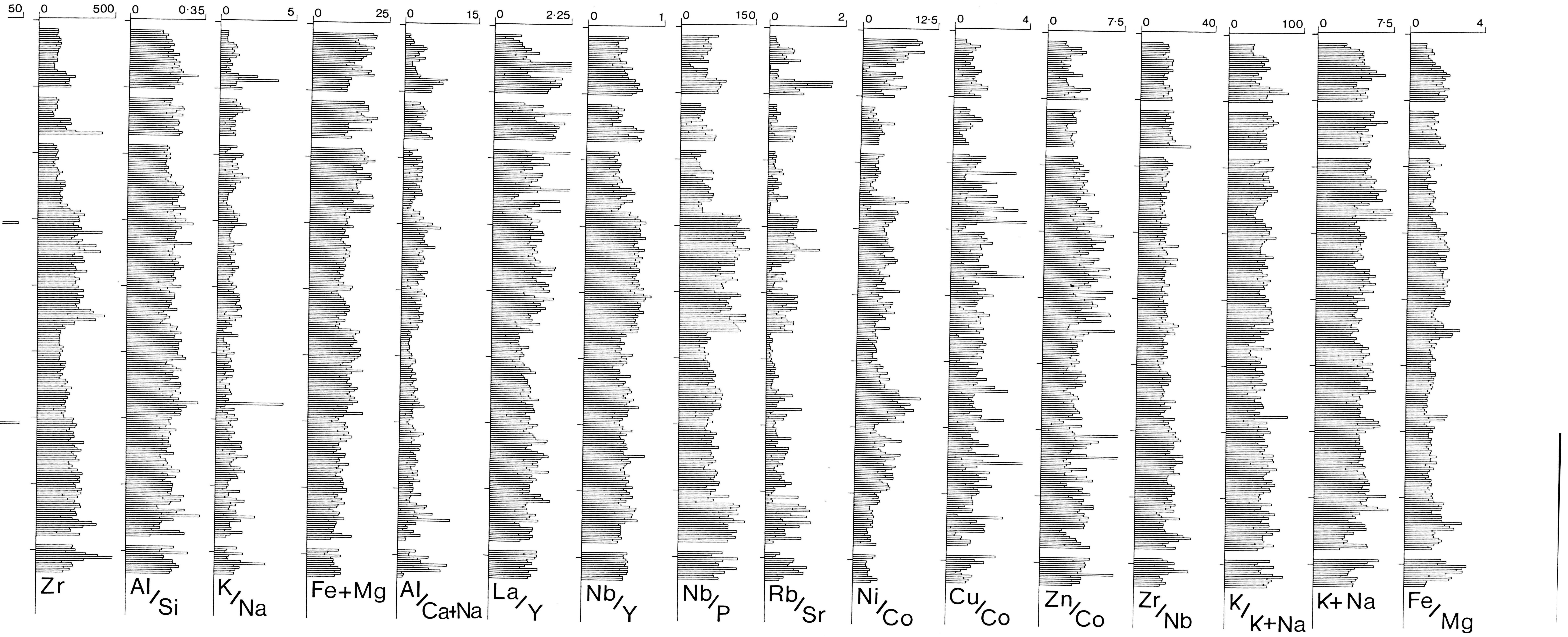

50
0 500
Zr
0 0·35
Al/Si
0 5
K/Na
0 25
Fe+Mg
0 15
Al/Ca+Na
0 2·25
La/Y
0 1
Nb/Y
0 150
Nb/P
0 2
Rb/Sr
0 12·5
Ni/Co
0 4
Cu/Co
0 7·5
Zn/Co
0 40
Zr/Nb
0 100
K/K+Na
0 7·5
K+Na
0 4
Fe/Mg

Fold-Out 6

Interformational Studies

This fold-out diagram displays the results of two multi-element geochemical studies evaluating the effects of inter-formational variation within a greywacke sequence.

The first study, The Tweed Bridge Section (30977, 62434) defines the nature of major, minor and trace element variation present within a single, massive turbidite bed, 4m in thickness, sampled at 30cm intervals (n=12).

The second study, The Talla Linn Section (31415,62009) defines the nature of major, minor and trace element variation present within a succession of closely spaced, interbedded greywacke units (>20cm in width) sampled over a traverse 30m in length (n=20).

This diagram summarises the results of 1408 analytical and calculated values.

Interformation Studies

FIGURES

LIST OF FIGURES

FIGURES

1 - British Isles Location Map (conical projection). Note the position of the Southern Uplands in the central portion of the diagram with respect to the Midland Valley of Scotland, Longford-Down Inlier and Lake District.

2 - Thesis methodology and philosophy. This diagram presents a graphical summary of the methodology and philosophy undertaken during this PhD project, extending from the initial concepts and hypothesis, through a process of sampling, analysis and interpretation in an iterative fashion in order to generate the models and conclusions presented within this thesis.

3 - Relationship between the Ordinance survey national numerical grid and the grid reference lettering system. This diagram presents an outline map of Northern England and Scotland in relation to the UK national grid system. Any area located within this map may be defined to the nearest 10m in terms of a unique 10 figure grid reference (ie 55555 33333) This map will assist the reader to locate the approximate position of any geochemical sample site within the UK field areas. Unfortunately an extension of this grid system into Eire during the Longford Down sampling program was not possible. Please note that the Irish National Grid System was used to provide unique sample site positions within the Longford Down.

4a- Major structural lineaments in the UK (after Haszledine 1986). This map depicts a number of major N-S lineaments identified during research upon structural controls of Carboniferous sedimentation. The first appearance of a number of of these structures correspond with the first occurrence of lamprophyre dykes during Late Silurian (Pridoli) times. In addition the hypothesis postulated within this thesis is that there is a significant correlation between lineaments, intrusions and gold mineralisation in Southern Scotland.

4b- Location of the Glendinning As-Sb-Au deposit with respect to the Southern Uplands Shatter Belt. A major lineament identified not only by Hazledine (1986) but earlier by Peach and Horne (1899) is depicted upon current 1:50,000 BGS maps of this area as a linear "shatter belt". This belt comprises of sparsely exposed, highly brecciated greywacke and mudstones forming a zone up to 1.5km in width. If this belt is extrapolated at a scale of 1:50,000 south of its last known outcrop, it is observed to pass within 1km of the Glendinning deposit.

5 - The occurrence of gold mineralisation in the UK (from Collins 1977). Note that the only gold occurrence in the Southern Uplands is reported as medieval alluvial workings in the Leadhills area.

6 - Southern Uplands of Scotland Location Map. (Based upon the U.K. National Survey 1:250,000 map). This map details the extent of the Southern Uplands field area and defines the unique numerical grid system used for identifying the location of individual samples within this region.

7a- Location of the Glendinning Deposit in Southern Scotland. Schematic representation of the location of the Glendinning Deposit in relation to both the Southern Uplands and Scotland.

7b- Location of Arsenopyrite hosted gold mineralisation in the Southern Uplands of Scotland. This diagram displays the relative positions of the five main arsenopyrite-gold deposits studied within the Southern Uplands (Chapter 5).

8 - Occurrences of Gold mineralisation in Ireland (after Jones, 1986). This map clearly illustrates the widespread nature of gold mineralisation in Ireland. Note the concentration of gold mineralisation associated with Lower Palaeozoic and Caledonian lithologies in contrast to the Upper Palaeozoic.

9 - Location of the Clontibret deposit in Southern Ireland. A schematic representation of the position of the Clontibret As-Sb-Au deposit in relation to Eire and the Northern Ireland border.

10- Detailed mine plans and sections of the Clontibret deposit after Wilbur (1978) and Morris (1986). Note the limited extent of underground mining activity,

FIGURE 1


SHETLAND
OUTER ISLES THRUST
MOINE THRUST ZONE
FORELAND
NORTHERN HIGHLANDS
GREAT GLEN FAULT
CENTRAL HIGHLANDS
HIGHLAND BOUNDARY FAULT
MIDLAND VALLEY GRABEN
SOUTHERN UPLANDS FAULT
SOUTHERN UPLANDS
IAPETUS SUTURE
DONEGAL
TYRONE
NORTH MAYO
OX MOUNTAINS
CLEW BAY
SOUTH MAYO
CONNEMARA
LONGFORD-DOWN INLIER
LAKE DISTRICT
ISLE OF MAN
ANGLESEY
NORTH WALES
WELSH BORDERS
CENTRAL WALES
LEINSTER
SOUTHERN IRELAND
SOUTH WALES
POST-CARBONIFEROUS COVER
SOUTH-WEST ENGLAND
MILES
KILOMETRES

FIGURE 2

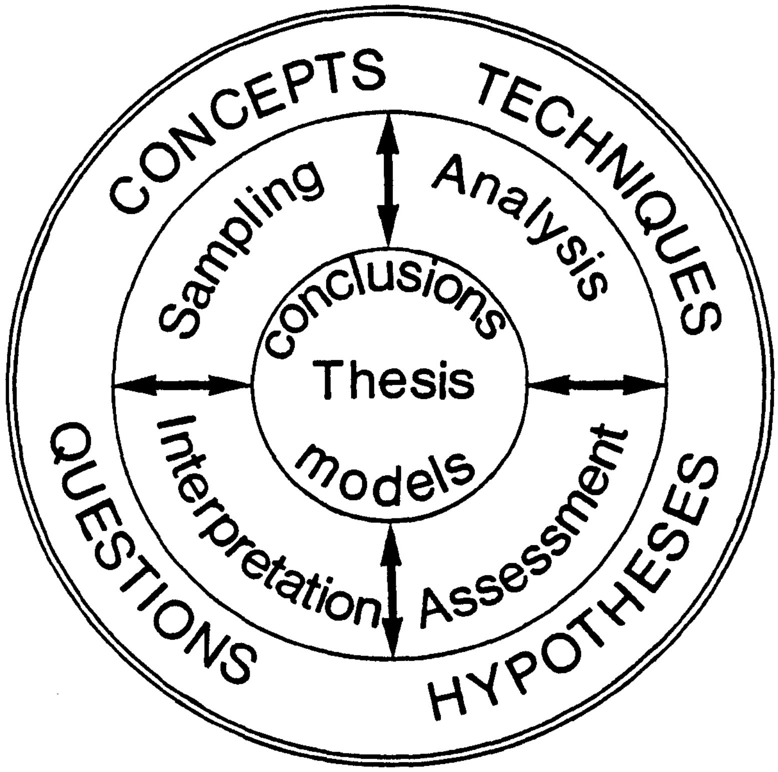
CONCEPTS
TECHNIQUES
QUESTIONS
HYPOTHESES
Sampling
Analysis
Interpretation
Assessment
conclusions
Thesis
models

FIGURE 3

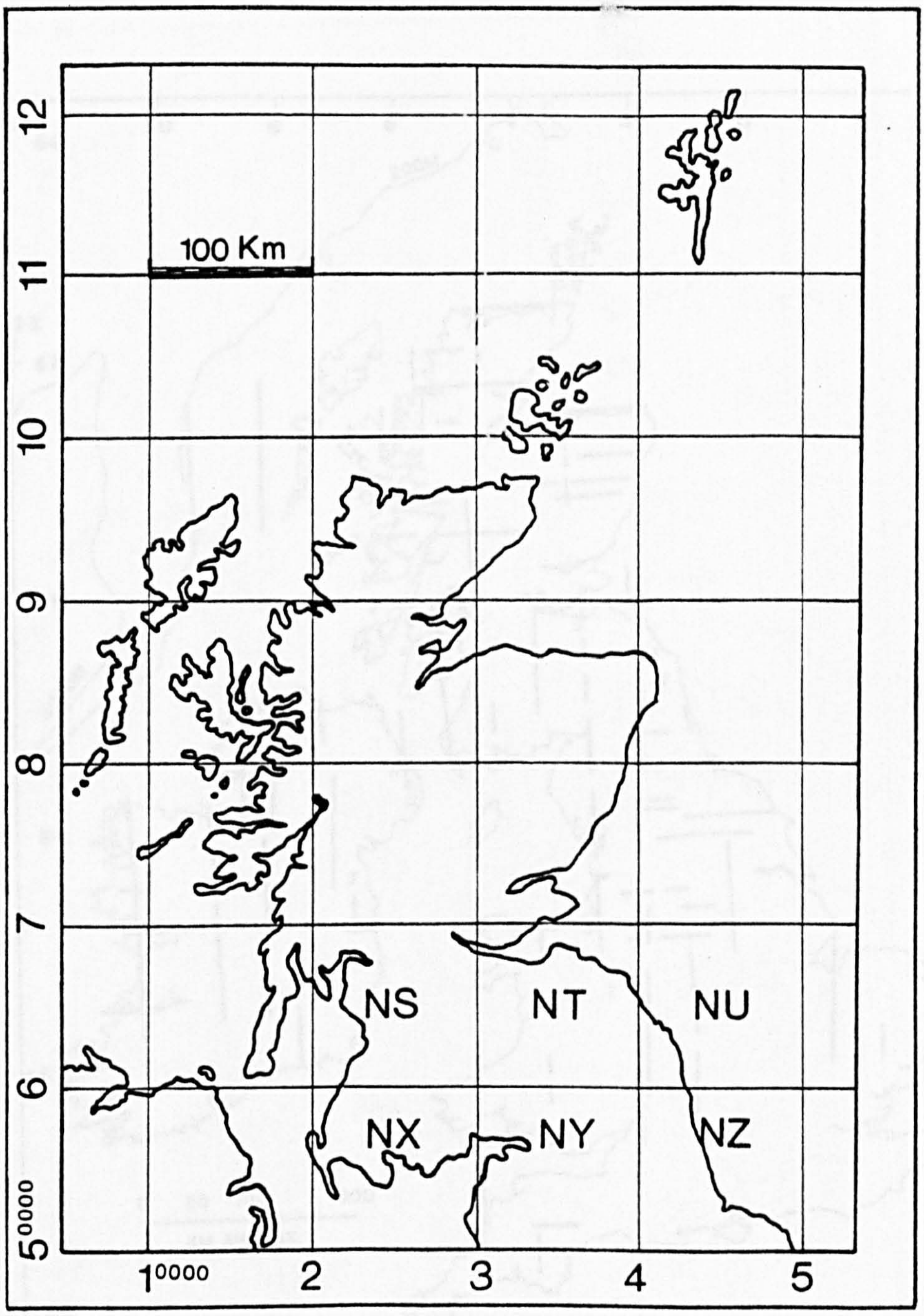

FIGURE 4a

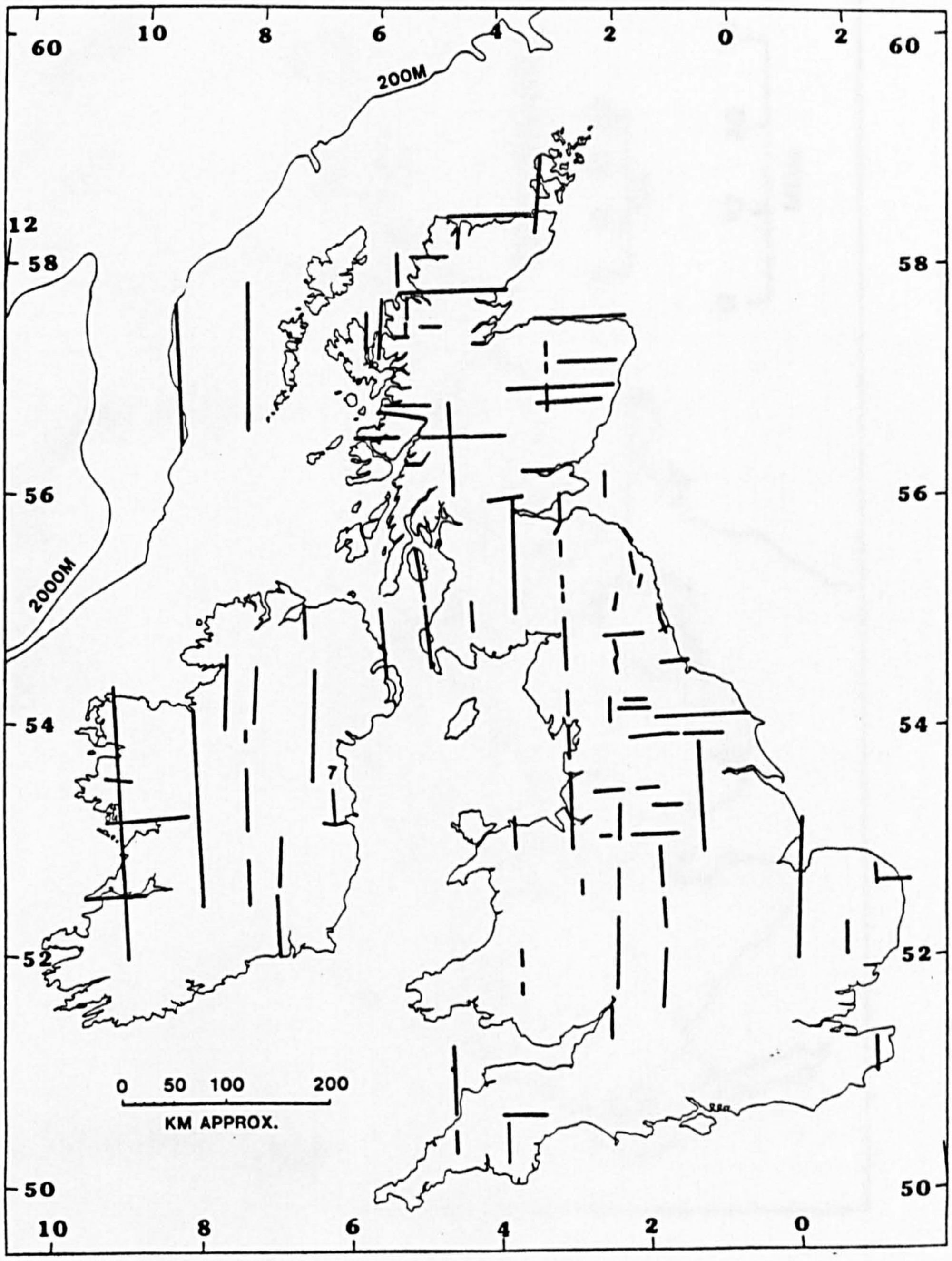

60
10
8
6
4
2
0
2
60
200M
12
58
58
56
56
2000M
54
54
7
52
52
0 50 100 200
KM APPROX.
50
50
10
8
6
4
2
0

FIGURE 4b

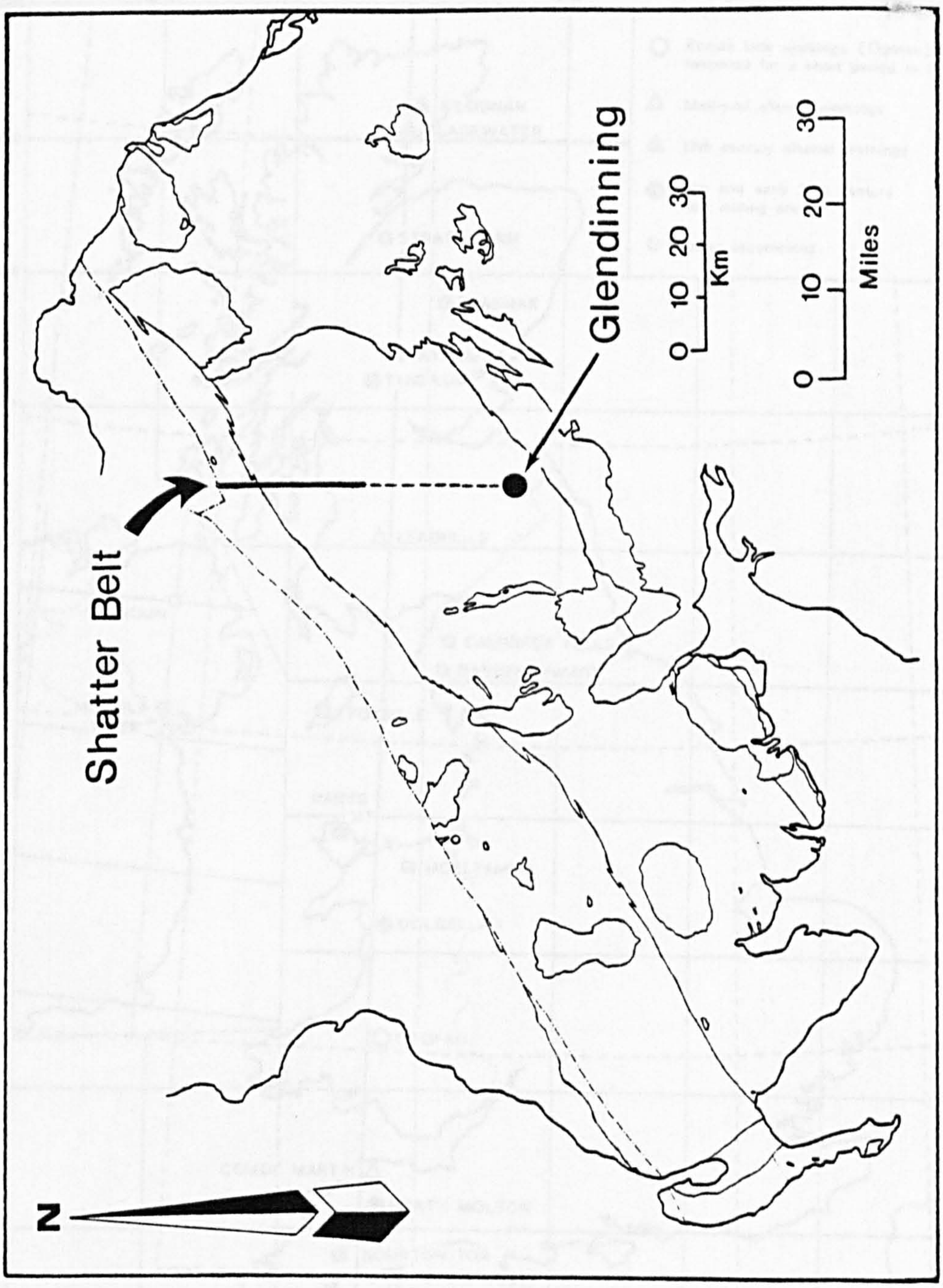

FIGURE 5

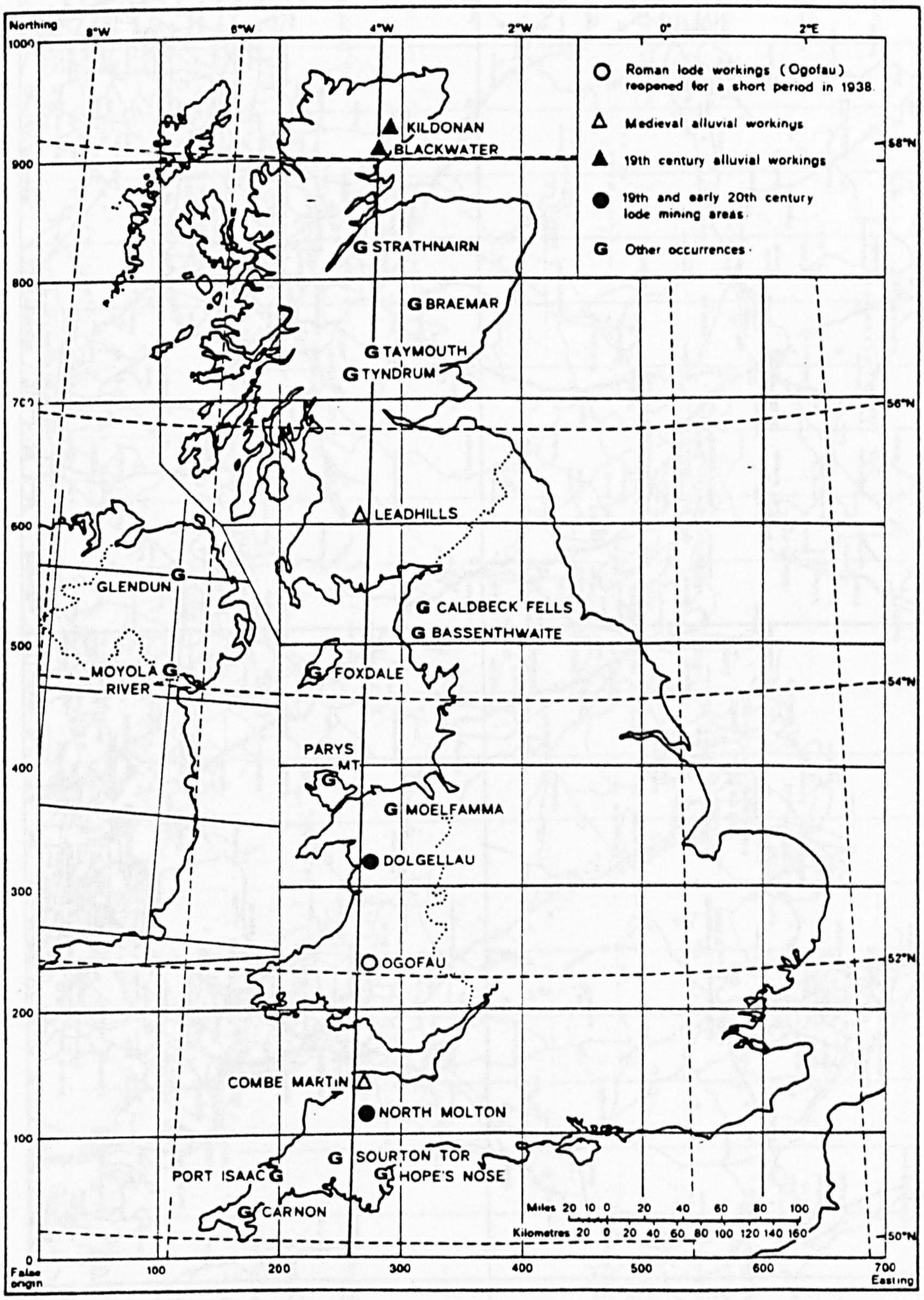
Northing
8°W
6°W
4°W
2°W
0°
2°E
1000
900
800
700
600
500
400
300
200
100
0
False origin
100
200
300
400
500
600
700
Easting
58°N
56°N
54°N
52°N
50°N
Roman lode workings (Ogofau) reopened for a short period in 1938.
Medieval alluvial workings
19th century alluvial workings
19th and early 20th century lode mining areas.
Other occurrences.
KILDONAN
BLACKWATER
STRATHNAIRN
BRAEMAR
TAYMOUTH
TYNDRUM
LEADHILLS
GLENDUN
CALDBECK FELLS
BASSENTHWAITE
MOYOLA RIVER
FOXDALE
PARYS MT
MOELFAMMA
DOLGELLAU
OGOFAU
COMBE MARTIN
NORTH MOLTON
SOURTON TOR
HOPE'S NOSE
PORT ISAAC
CARNON
Miles 20 10 0 20 40 60 80 100
Kilometres 20 0 20 40 60 80 100 120 140 160

FIGURE 6

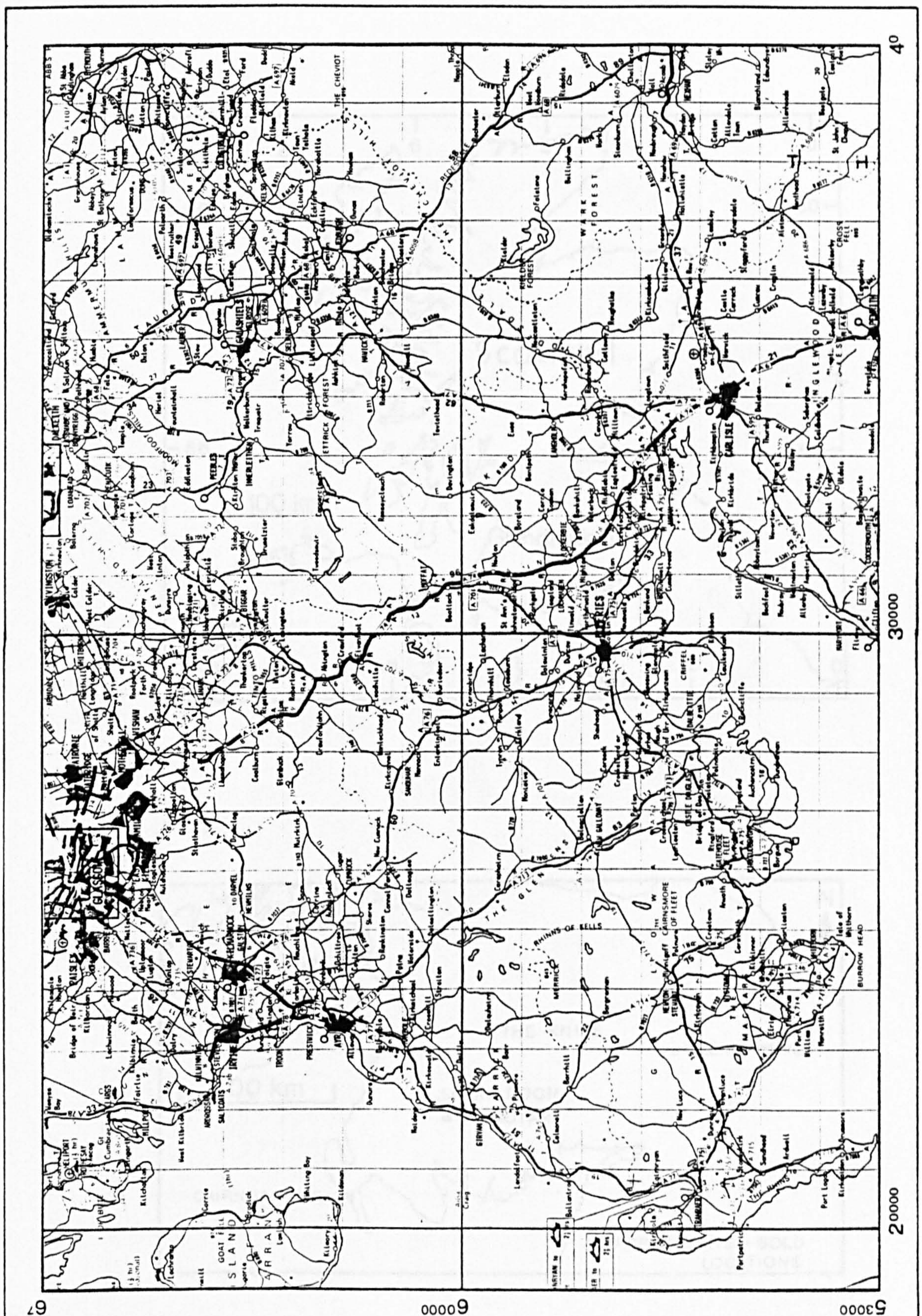

FIGURE 7

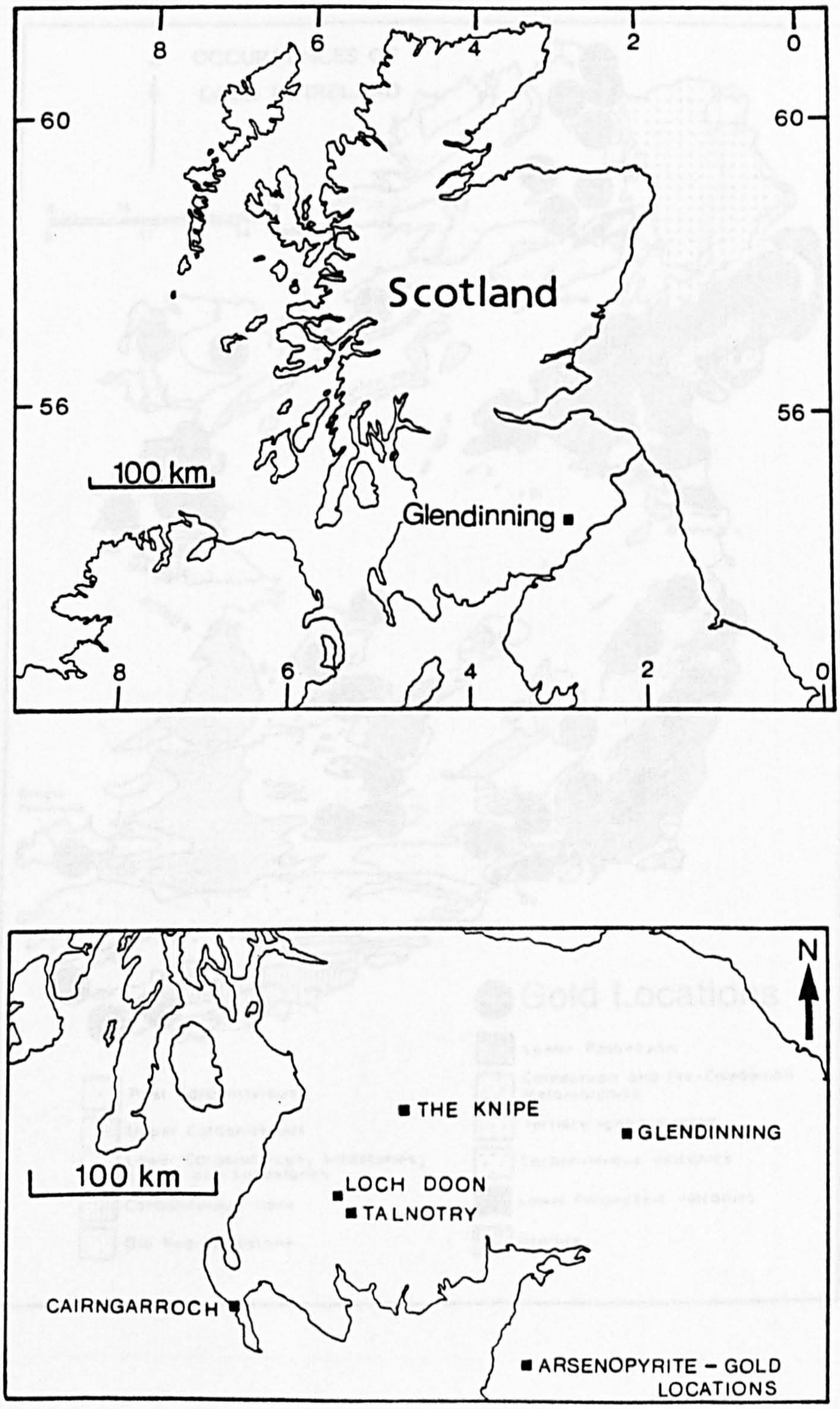
8
6
4
2
0
60
60
Scotland
56
56
100 km
Glendinning
8
6
4
2
0
N
THE KNIPE
GLENDINNING
100 km
LOCH DOON
TALNOTRY
CAIRNGARROCH
ARSENOPYRITE - GOLD LOCATIONS

FIGURE 8

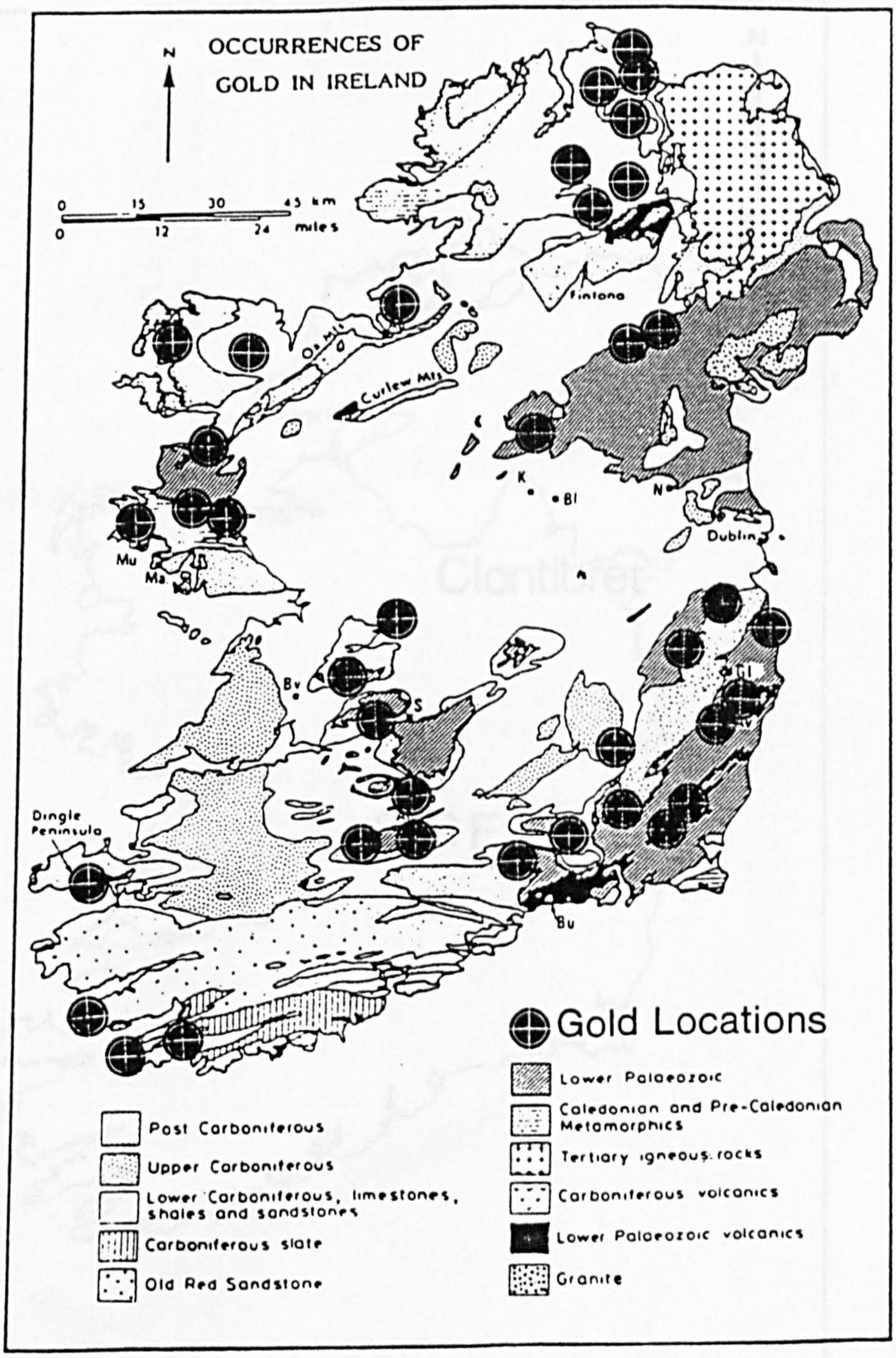
OCCURRENCES OF
GOLD IN IRELAND
N
0 15 30 45 km
0 12 24 miles
Fintona
Ox Mts
Curlew Mts
K
Bl
N
Dublin
Mu
Ma
Bv
S
Av
Dingle
Peninsula
Bu
Gold Locations
Lower Palaeozoic
Caledonian and Pre-Caledonian
Metamorphics
Tertiary igneous rocks
Carboniferous volcanics
Lower Palaeozoic volcanics
Granite
Post Carboniferous
Upper Carboniferous
Lower Carboniferous, limestones,
shales and sandstones
Carboniferous slate
Old Red Sandstone

FIGURE 9

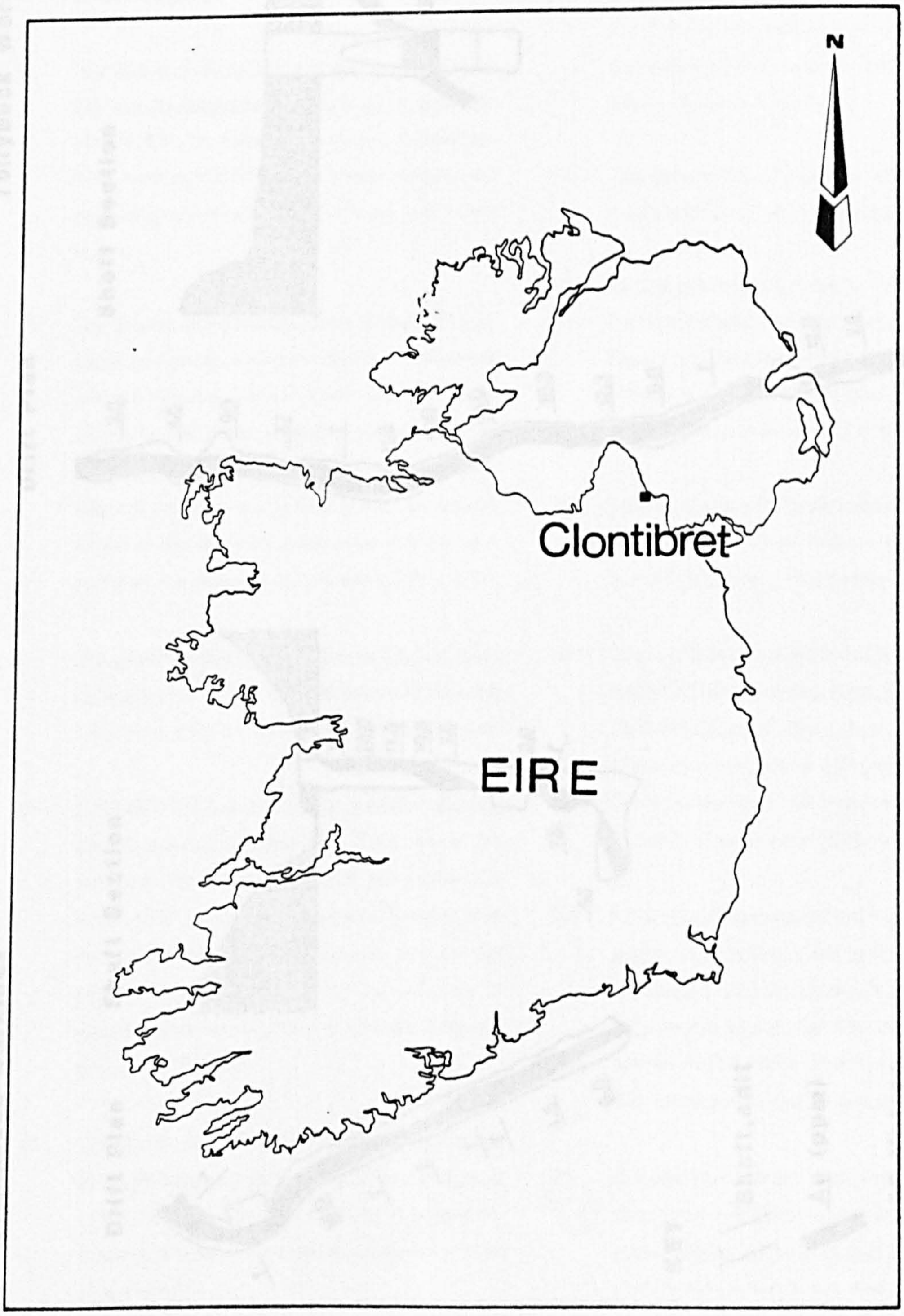

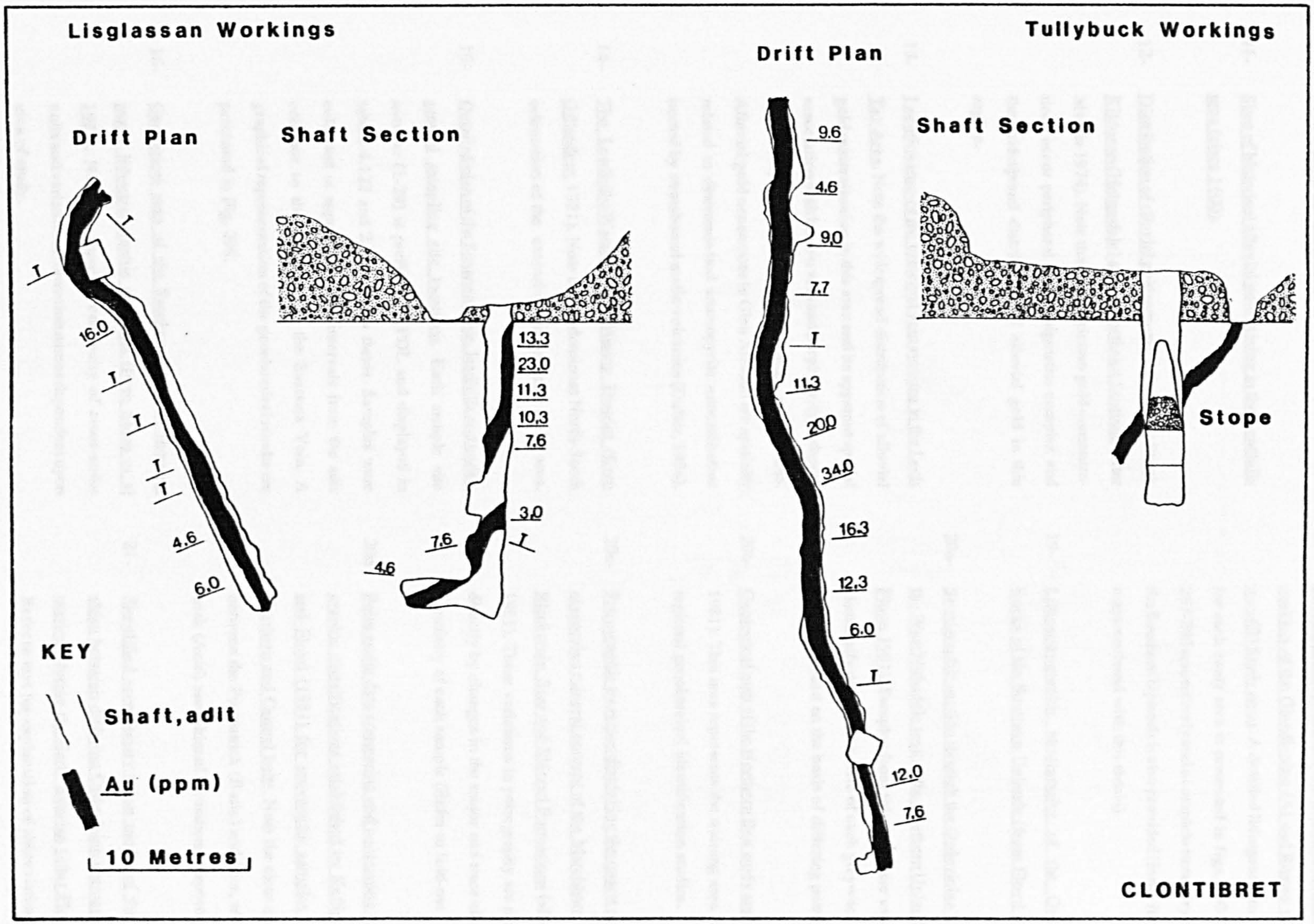

Lisglassan Workings
Drift Plan
Shaft Section
Tullybuck Workings
Drift Plan
Shaft Section
Stope
16.0
T
4.6
6.0
13.3
23.0
11.3
10.3
7.6
3.0
7.6
4.6
9.6
4.6
9.0
7.7
11.3
20.0
34.0
16.3
12.3
6.0
12.0
7.6
KEY
Shaft,adit
Au (ppm)
10 Metres
CLONTIBRET

FIGURE 10

considerable drift thickness (>8m) and the extremely high (34ppm) Au assay values located during the 1950's sampling programs.

11- Sites of historical alluvial gold mining in the Leadhills area (circa 1600).

12- Distribution of alluvial gold mineralisation in the Strath Kildonan (Helmsdale) area of northeast Scotland (after Michie 1974). Note that the maximum gold concentrations occur peripheral to the migmatite complex and the widespread distribution of alluvial gold in this region.

13- Location map of the principal vein systems in the Loch Tay Area. Note the widespread distribution of alluvial gold mineralisation in this area and its apparent spatial association with known vein and porphyry-type deposits, namely Corrie Buie, Tomnadashan, and Comrie. Alluvial gold occurences in Glen Almond are spatially related to disemminated arsenopyrite mineralisation hosted by stratabound mafic volcanics (Duller, 1986).

14- The Leadhills-Wanlockhead Mining District (from Gillanders, 1981). Note the predominant North-South orientation of the extensive suite of veins in this area.

15- Detailed plan of the Susanna Mine, leadhills and underground sampling site locations. Each sample site number (1-29) is prefixed by PDL and displayed in tables 4.122 and 2.119 of this thesis. Samples were collected at approximate 5m intervals from the adit entrance to the contact with the Susanna Vein. A graphical representation of the geochemical results are presented in Fig. 298.

16- Geological map of the Southern Uplands showing major lithostratigraphic divisions (from Stone et al 1987). Note the apparent continuity of cross-strike units and variation in formation names dependent upon area of study.

17- Structural map of the Southern Uplands identifying major faults and boundaries between belts (After Leggett 1979). A detailed summary of the lithostratigraphic units (I to X) is presented in the previous diagram (fig.16).

18- Location map of the Southern Uplands defining the position of the Glendinning (A) and Rhinns of Galloway (B) Study areas. A detailed lithogeochemical atlas for each study area is presented in figs. 160-224 and 267-295 respectively and a complete summary atlas for the Southern Uplands is also provided (in the form of 22 maps enclosed with this thesis).

19- Lithopetrographic stratigraphy of the Ordovician Rocks of the Southern Uplands (from Floyd 1981).

20a- Stratigraphic section through the Ordovician Rocks of the West Nithsdale area of the Southern Uplands (from Floyd 1981). Samples from this area were used to chemically define the nature of each greywacke formation recognised on the basis of differing petrography.

20b- Geological map of the Northern Belt study area (Floyd, 1981). This area represents the training area for regional geochemical identification studies.

20c- Petrographic traverses displaying the quartz and ferromagnesian mineral content of the Marchburn, Afton, Blackcraig, Scar and Shinnel Formations (after Floyd 1981). These variations in petrography are mirrored directly by changes in the major and trace element chemistry of each sample (Refer to fold-out 2).

20d Point count data comparing and contrasting the petrographic classifications established by Kelling (1969) and Floyd (1981) for greywacke samples from the Northern and Central belts. Note the clear correlation between the Portpatrick (Basic) and Scar, and Portpatrick (Acid) and Shinnel formations respectively.

21- Simplified accretionary prism model of the relationships between differing Ordovician petrographic formations during the Early Silurian (after Floyd,1983). Refer to text for explanation of abbreviations.

22- Geological map of the Fleet granite and surrounding area (from Leake et al 1978). Note the complex zoning pattern within the granite mass and the location of small peripheral intrusions.

FIGURE 11

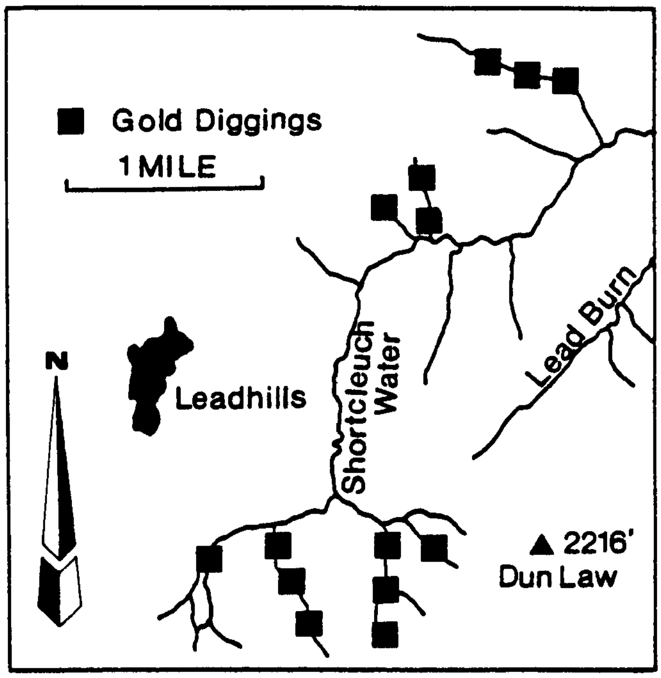
Gold Diggings
1 MILE
N
Leadhills
Shortcleuch Water
Lead Burn
▲ 2216'
Dun Law

FIGURE 12

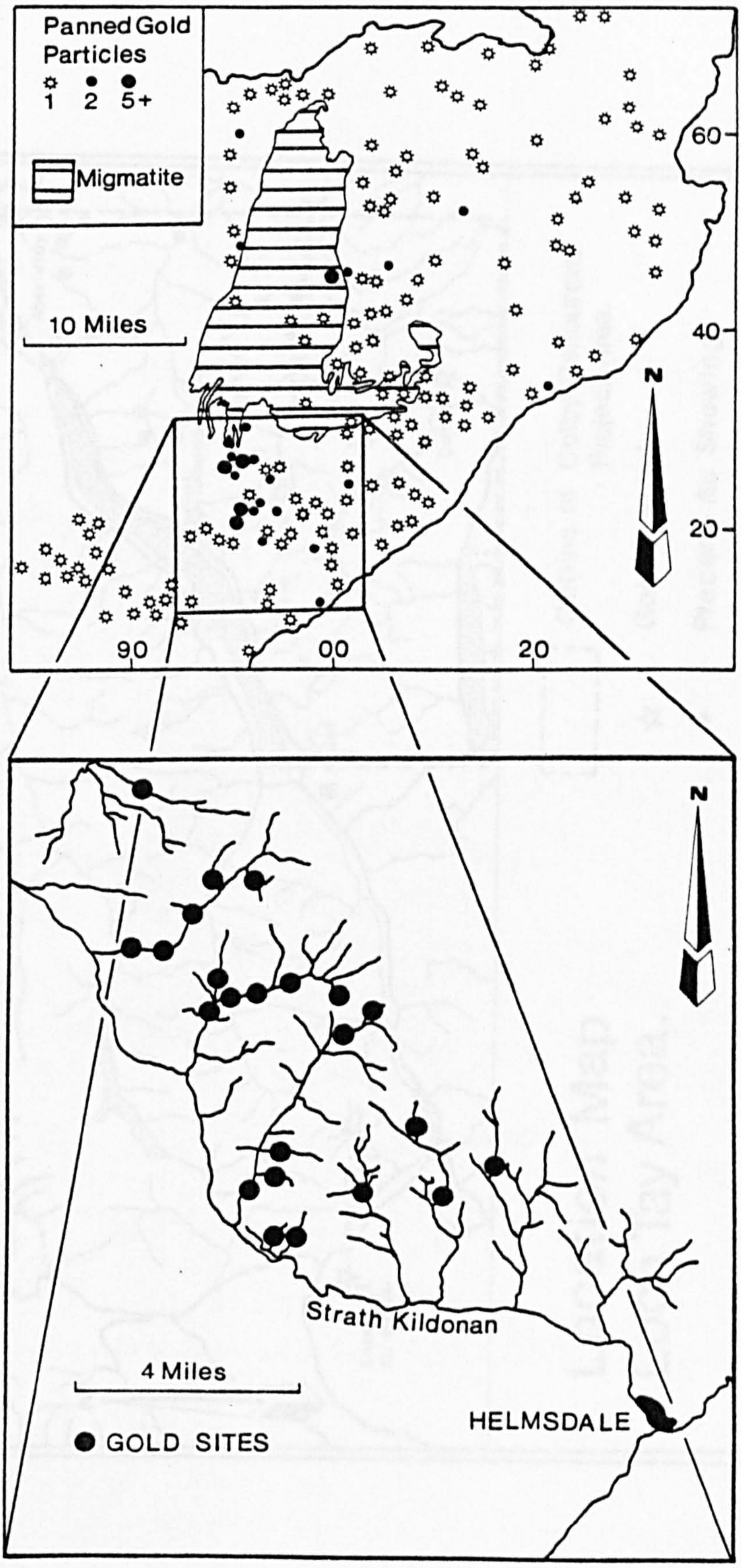
Panned Gold Particles
1 2 5+
Migmatite
10 Miles
60
40
20
N
90
00
20
N
Strath Kildonan
4 Miles
GOLD SITES
HELMSDALE

FIGURE 13

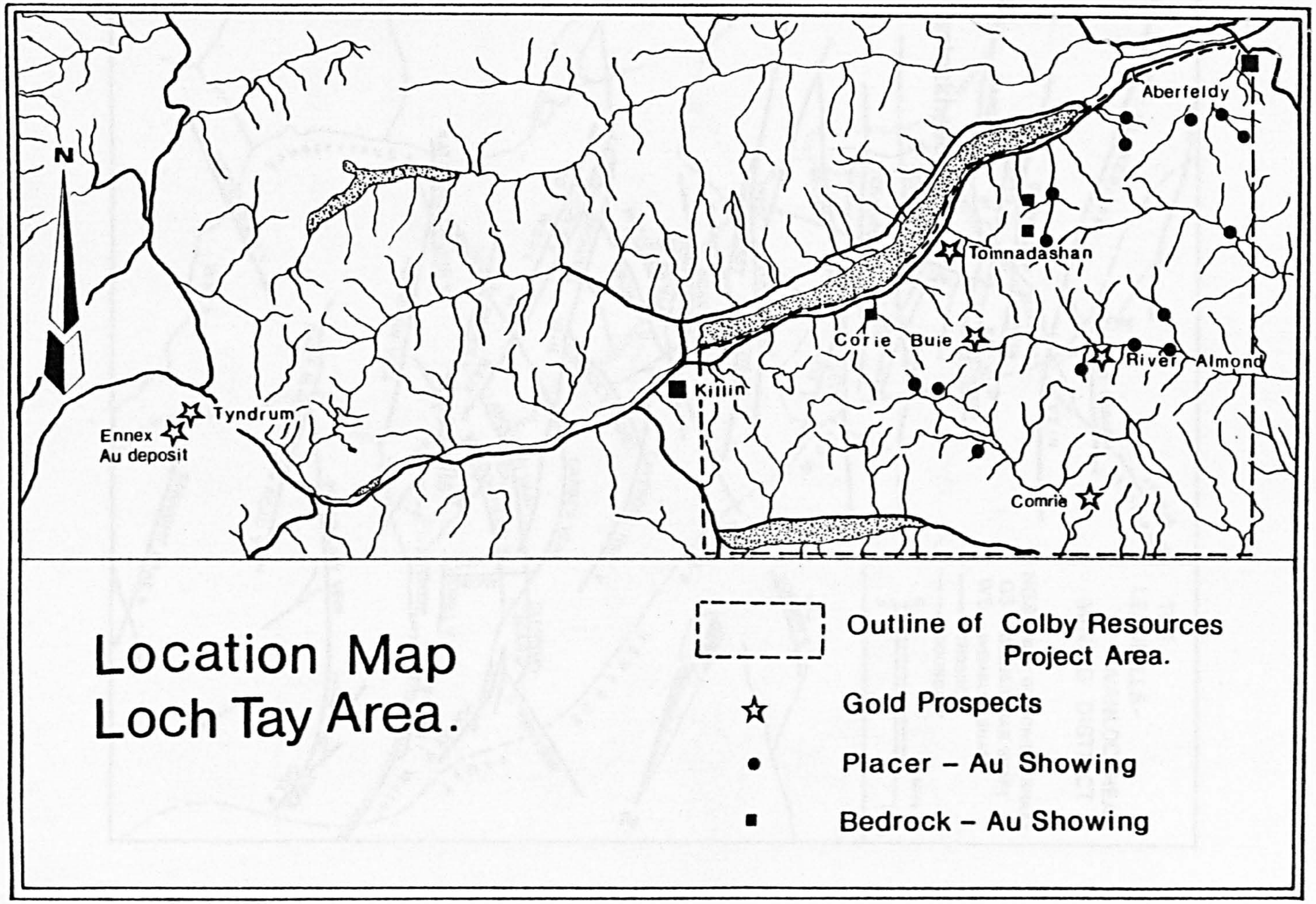
N
Aberfeldy
Tomnadashan
Corrie Buie
River Almond
Killin
Tyndrum
Ennex
Au deposit
Comrie
Location Map
Loch Tay Area.
Outline of Colby Resources Project Area.
Gold Prospects
Placer – Au Showing
Bedrock – Au Showing

FIGURE 14

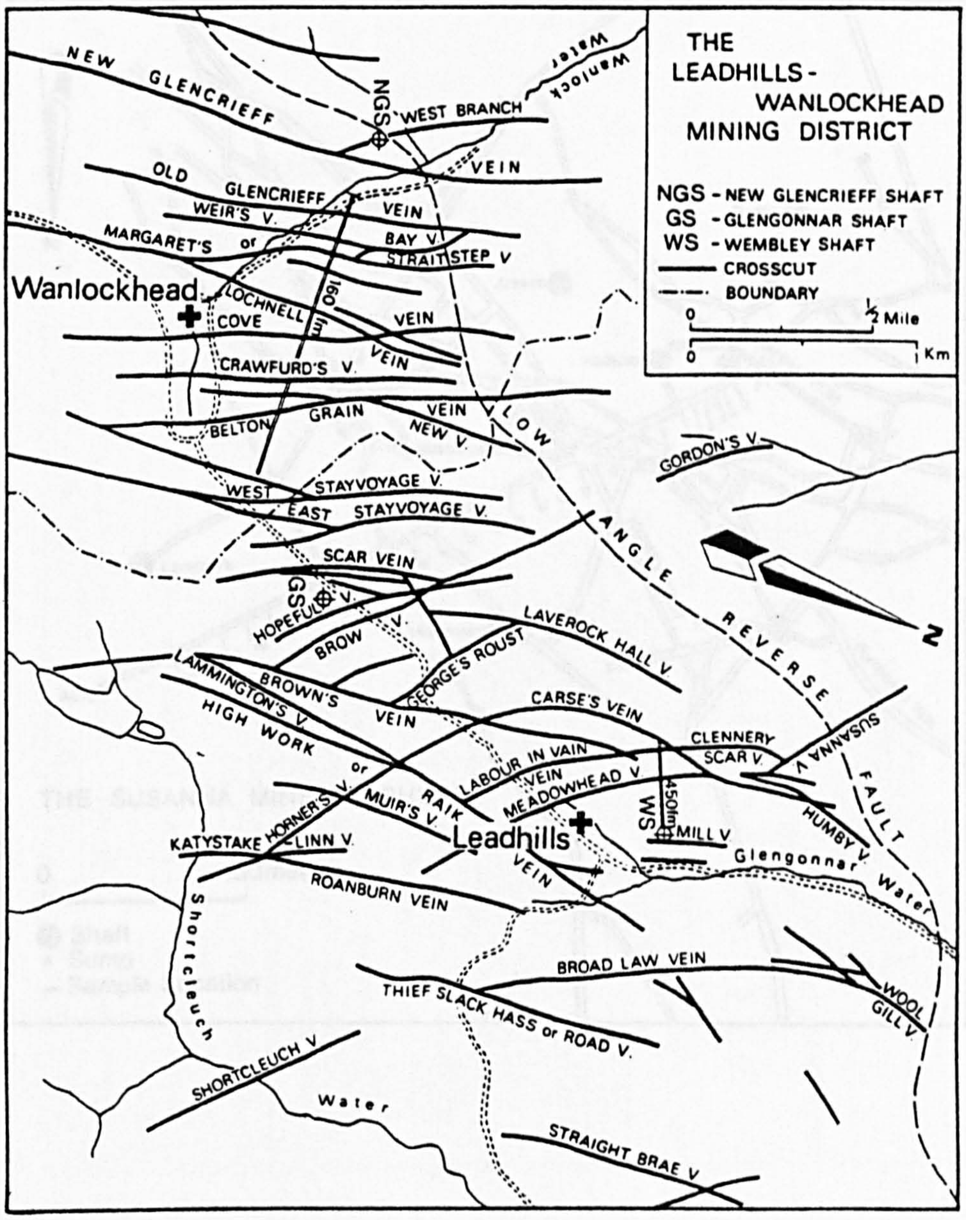
THE LEADHILLS - WANLOCKHEAD MINING DISTRICT
NGS - NEW GLENCRIEFF SHAFT
GS - GLENGONNAR SHAFT
WS - WEMBLEY SHAFT
CROSSCUT
BOUNDARY
0
½ Mile
0
1 Km
N
Wanlock Water
NEW GLENCRIEFF
NGS
WEST BRANCH
VEIN
OLD GLENCRIEFF VEIN
WEIR'S V.
MARGARET'S or BAY V.
STRAIT STEP V
Wanlockhead
LOCHNELL VEIN
COVE VEIN
160 fm
CRAWFURD'S V.
BELTON GRAIN VEIN
NEW V.
LOW ANGLE REVERSE FAULT
GORDON'S V.
WEST STAYVOYAGE V.
EAST STAYVOYAGE V.
SCAR VEIN
GS
HOPEFUL V.
BROW V.
LAVEROCK HALL V
GEORGE'S ROUST
BROWN'S VEIN
LAMMINGTON'S V
HIGH WORK or RAIK
CARSE'S VEIN
CLENNERY SCAR V.
SUSANNA V
LABOUR IN VAIN VEIN
MEADOWHEAD V
WS
450fm
MILL V
HUMBY V
HORNER'S V.
MUIR'S V.
Leadhills
KATYSTAKE
LINN V.
VEIN
Glengonnar Water
ROANBURN VEIN
Shortcleuch
BROAD LAW VEIN
WOOL GILL V.
THIEF SLACK HASS or ROAD V.
SHORTCLEUCH V
Water
STRAIGHT BRAE V

FIGURE 15

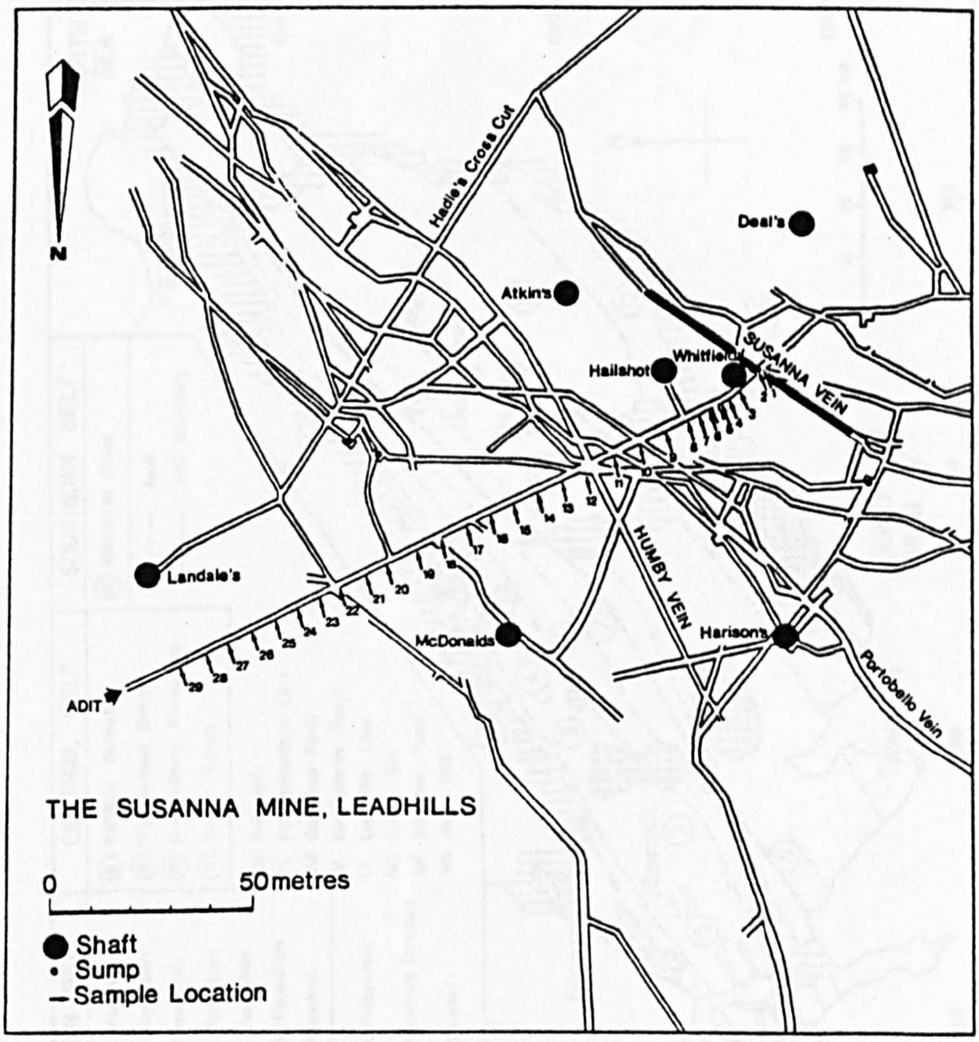

THE SUSANNA MINE, LEADHILLS

FIGURE 16

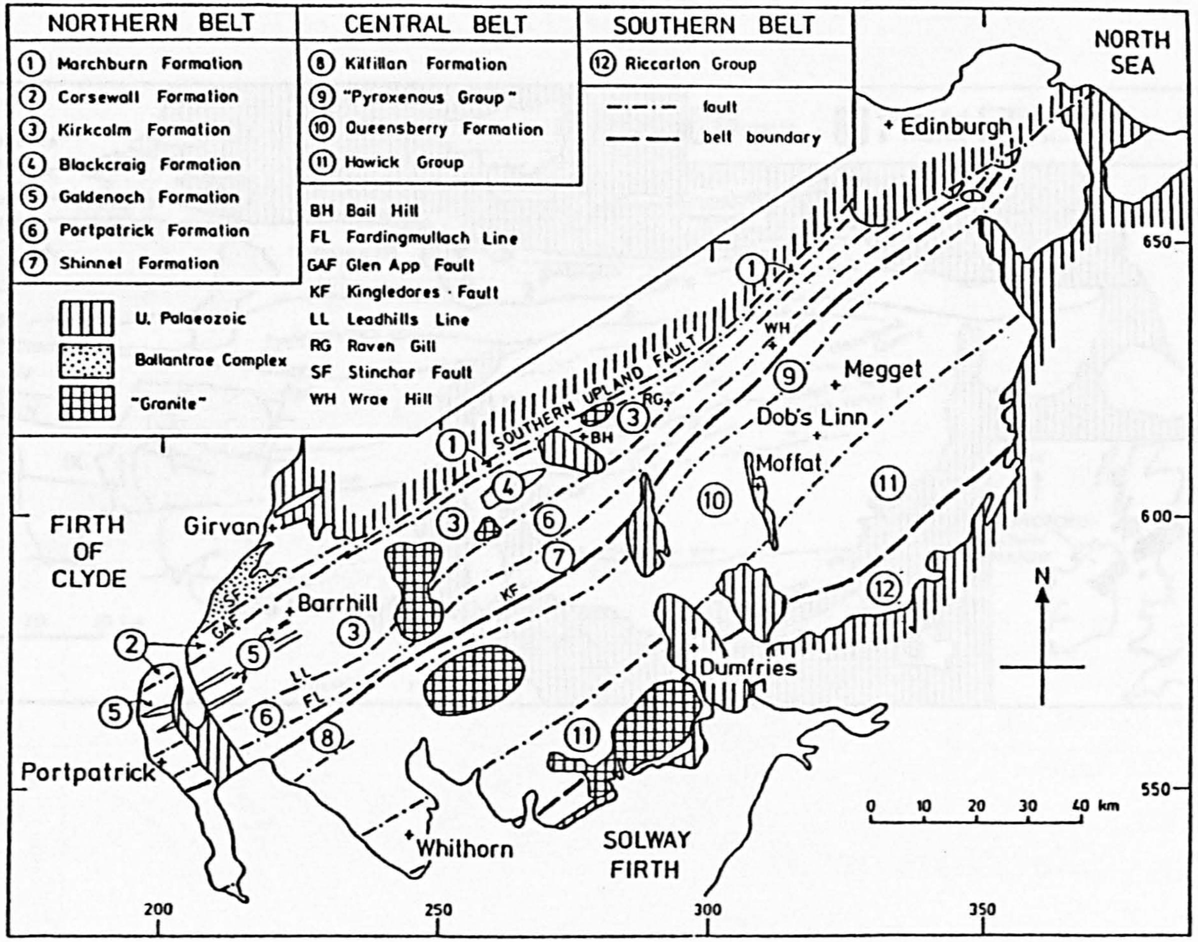
NORTHERN BELT
1 Marchburn Formation
2 Corsewall Formation
3 Kirkcolm Formation
4 Blackcraig Formation
5 Galdenoch Formation
6 Portpatrick Formation
7 Shinnel Formation
CENTRAL BELT
8 Kilfillan Formation
9 "Pyroxenous Group"
10 Queensberry Formation
11 Hawick Group
SOUTHERN BELT
12 Riccarton Group
fault
belt boundary
U. Palaeozoic
Ballantrae Complex
"Granite"
BH Bail Hill
FL Fardingmullach Line
GAF Glen App Fault
KF Kingledores Fault
LL Leadhills Line
RG Raven Gill
SF Stinchar Fault
WH Wrae Hill
NORTH SEA
Edinburgh
SOUTHERN UPLAND FAULT
Megget
Dob's Linn
Moffat
FIRTH OF CLYDE
Girvan
Barrhill
Dumfries
Portpatrick
Whithorn
SOLWAY FIRTH
N
0 10 20 30 40 km
650
600
550
200
250
300
350

FIGURE 17

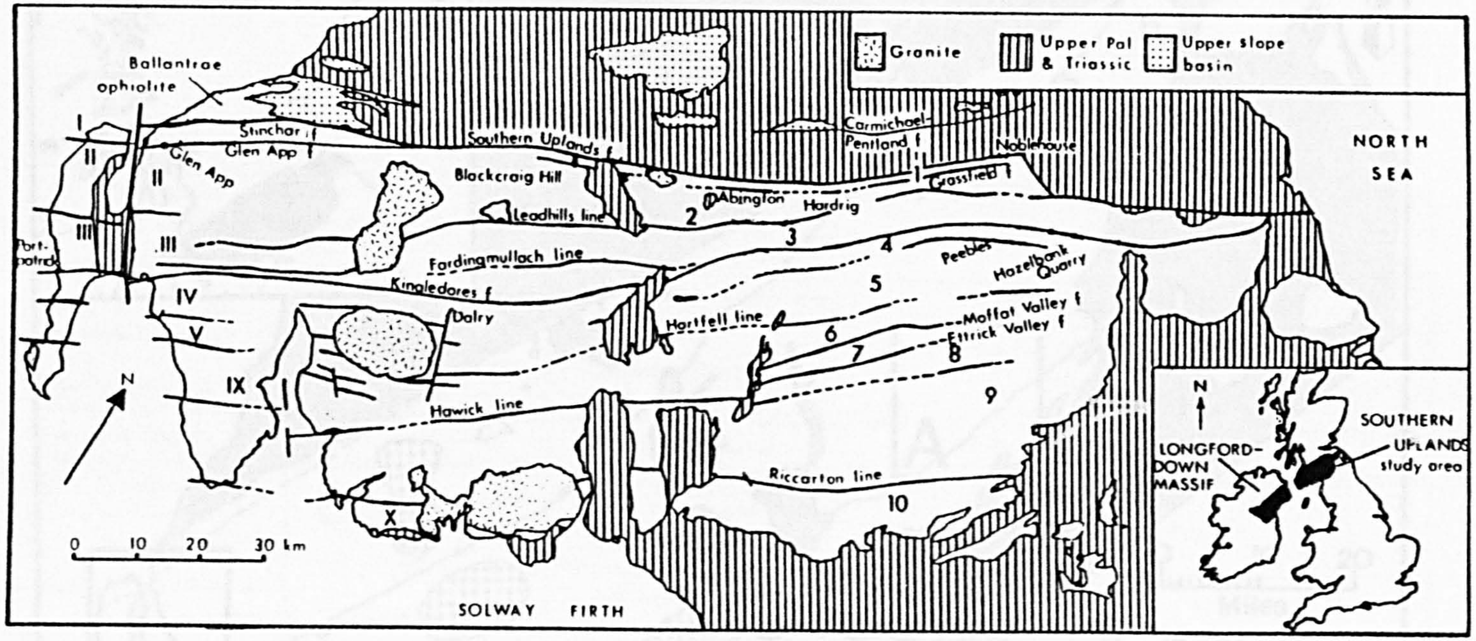

Granite
Upper Pal & Triassic
Upper slope basin
Ballantrae ophiolite
Stinchar f
Glen App f
Glen App
Southern Uplands f
Carmichael-Pentland f
Noblehouse
Grassfield f
NORTH SEA
Blackcraig Hill
Abington
Hardrig
Leadhills line
Fardingmullach line
Kingledores f
Peebles
Hazelbank Quarry
Dalry
Hartfell line
Moffat Valley f
Ettrick Valley f
Hawick line
Riccarton line
Port-patrick
N
0 10 20 30 km
SOLWAY FIRTH
SOUTHERN UPLANDS study area
LONGFORD-DOWN MASSIF
I
II
III
IV
V
IX
X
1
2
3
4
5
6
7
8
9
10

FIGURE 18

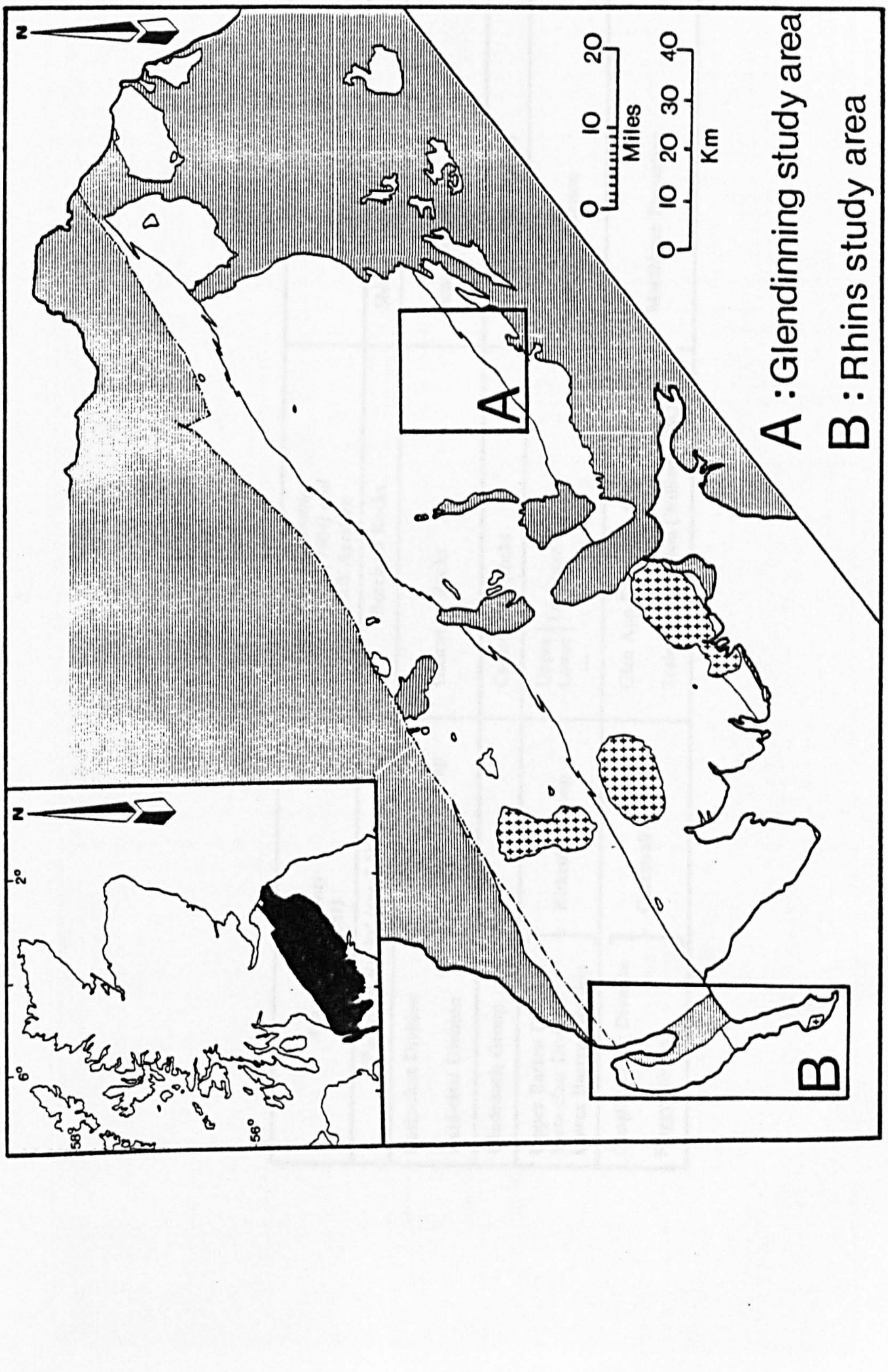
N
A
B
0 10 20
Miles
0 10 20 30 40
Km
A : Glendinning study area
B : Rhins study area
6°
2°
58°
56°

FIGURE 19

Rhinns of Galloway (Kelling 1961)	*NW Wigtonshire (Welsh 1964) and SW Ayrshire*	*W Nithsdale* (FLOYD 1981)
'Portayew Rocks' (see 1.5)	Boreland Rocks	Shinnel Formation
Basic-clast Division Acid-clast Division } Portpatrick Group	Glenwhan Rocks	Scar Formation
Gladenoch Group	Cairnerzean Rocks	Blackcraig Formation
Upper Barren Division Meta-clast Division Lower Barren Division } Kirkcolm Group	Upper Lower } Lochryan Rocks —	Afton Formation
Conglomeratic Division Flaggy Division } Coreswall Group	Glen App Formation (Walton 1961) Traboyack Division (Williams 1962)	Marchburn Formation

FIGURE 20a/b/c

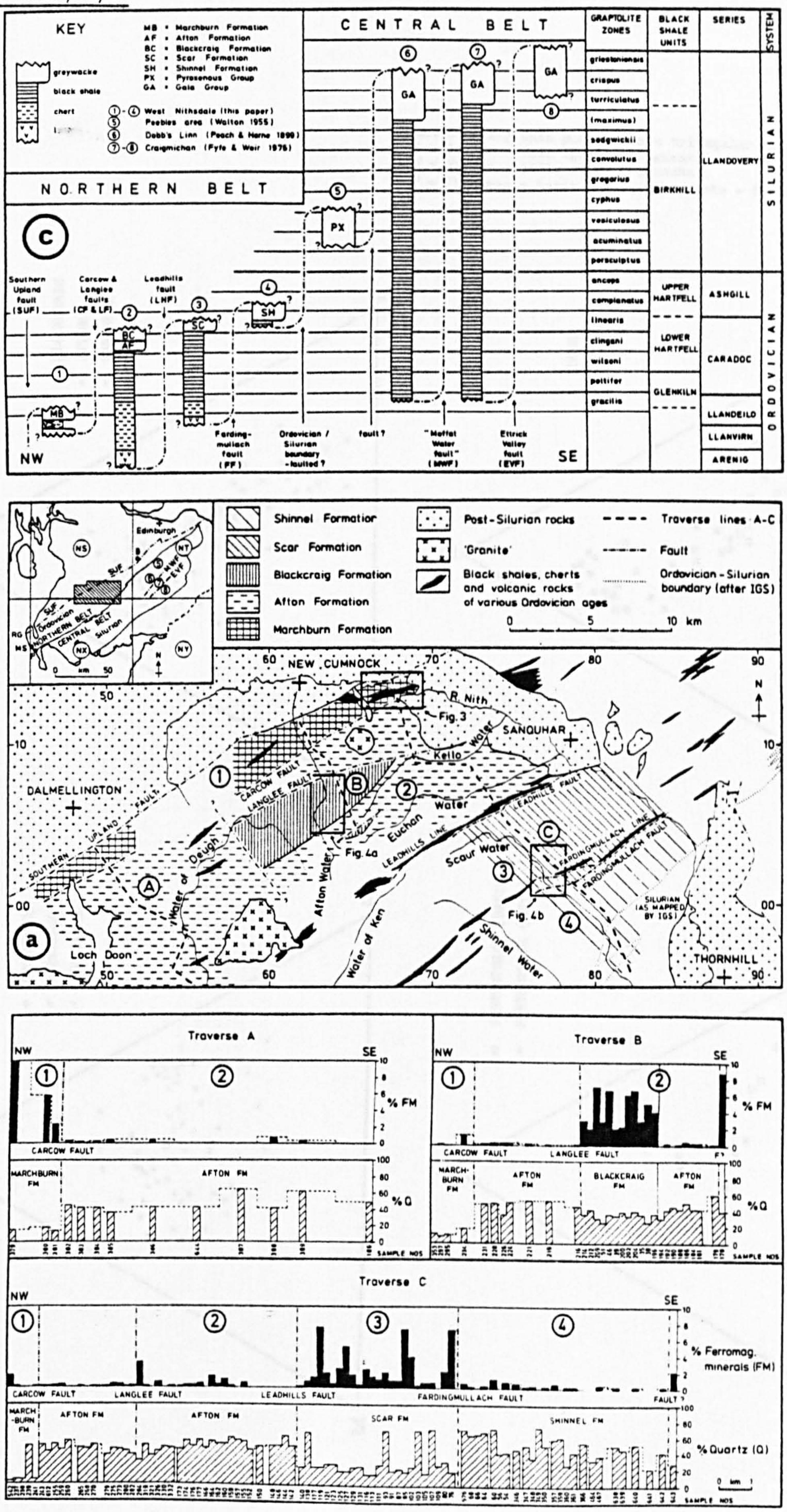

FIGURE 20d

Point counting data plotted on a triangular diagram.
Q = Quartz + acid igneous fragments + metamorphic fragments
M = Matrix + sedimentary fragments
F = Feldspar + basic igneous fragments + ferromags.

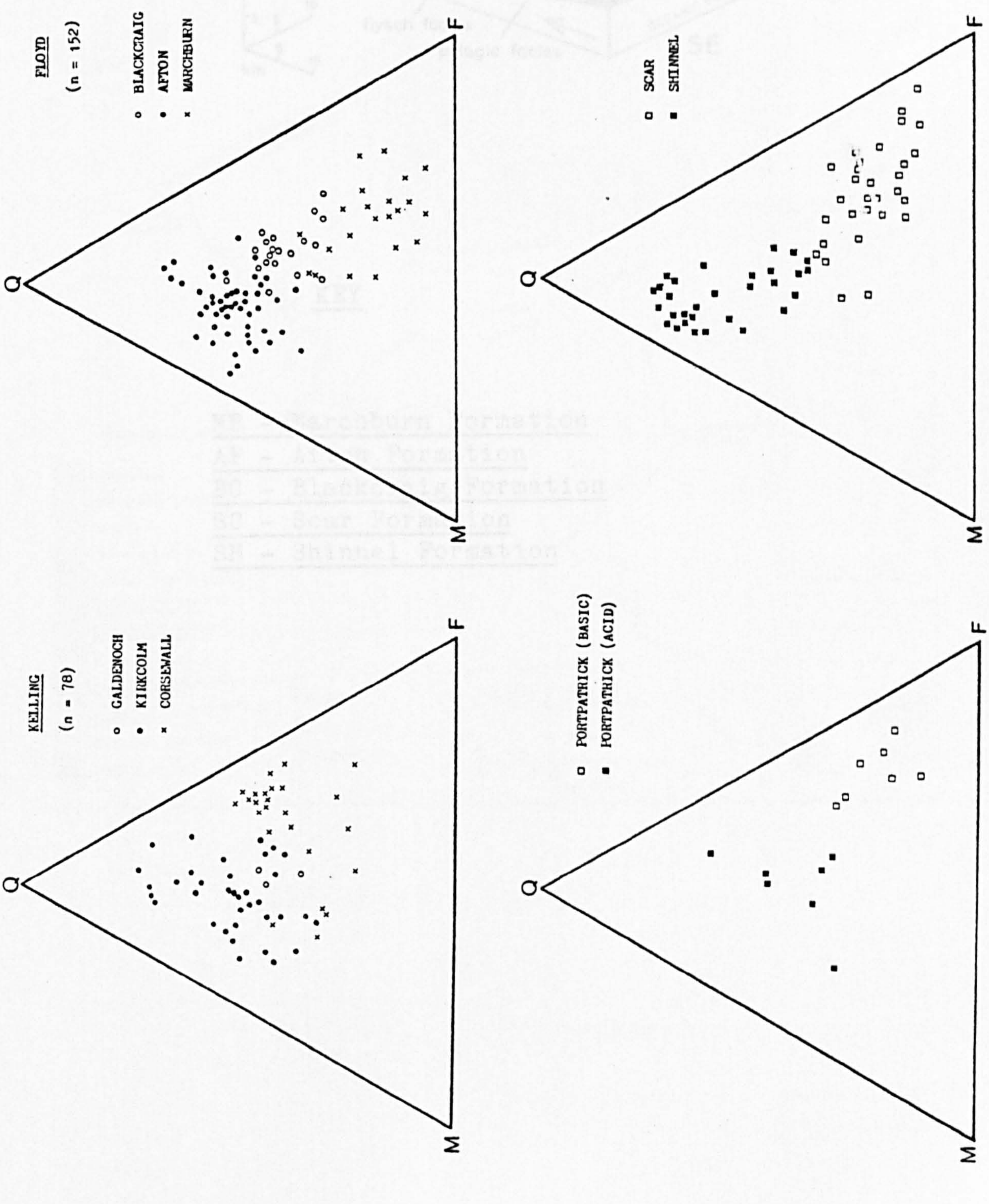

FIGURE 21

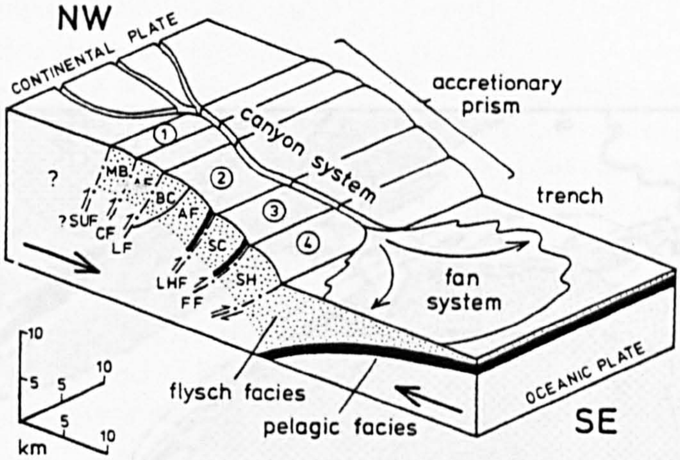

KEY

MB - Marchburn Formation
AF - Afton Formation
BC - Blackcraig Formation
SC - Scar Formation
SH - Shinnel Formation

FIGURE 22

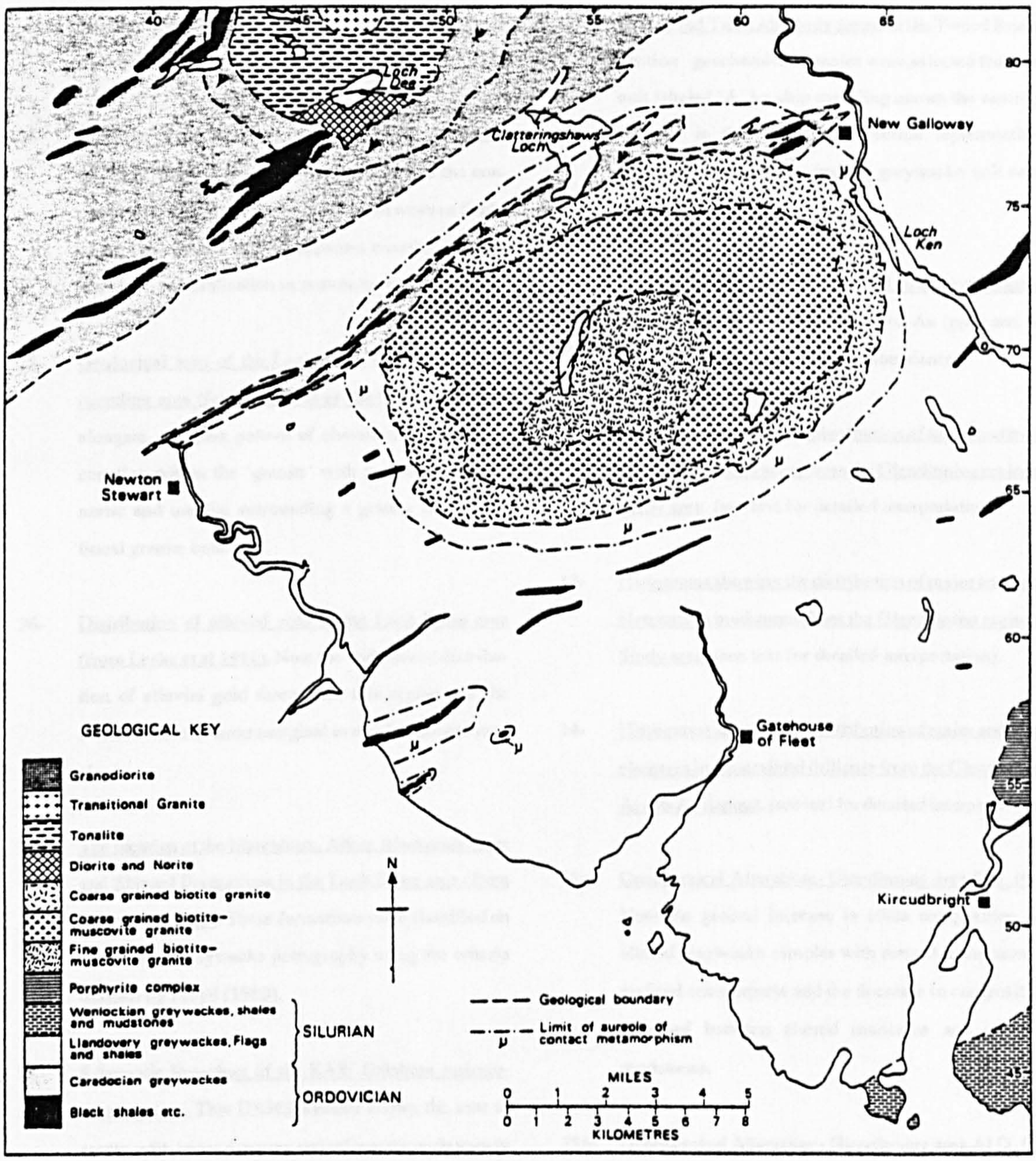
Loch Dee
Clatteringshaws Loch
New Galloway
Loch Ken
Newton Stewart
Gatehouse of Fleet
Kircudbright
GEOLOGICAL KEY
Granodiorite
Transitional Granite
Tonalite
Diorite and Norite
Coarse grained biotite granite
Coarse grained biotite-muscovite granite
Fine grained biotite-muscovite granite
Porphyrite complex
Wenlockian greywackes, shales and mudstones
Llandovery greywackes, Flags and shales
Caradocian greywackes
Black shales etc.
SILURIAN
ORDOVICIAN
N
Geological boundary
Limit of aureole of contact metamorphism
MILES
KILOMETRES

23- Drainage geochemistry map of the Fleet granite and surrounding area (from Leake et al 1978). Note the apparent strike-parallel nature of the turbidite unit contacts and the apparent cross strike variation in geochemistry.

24- Location of old metalliferous mines in the vicinity of the Fleet Granite, Southwest Scotland. Note the concentration of Pb/Zn deposits in the south western flanks of the fleet granite and the apparent zonation towards As/Cu/Ni mineralisation in proximity to the granite.

25- Geological map of the Loch Doon Granite and surrounding area (from Leake et al 1981). Note the N-S elongate, complex pattern of chemical/ petrographic zonation within the 'granite' with peripheral diorite, norite and tonalite surrounding a granite and transitional granite core.

26- Distribution of alluvial gold in the Loch Doon area (from Leake et al 1981). Note the widespread distribution of alluvial gold throughout this region and the concentration in areas marginal to small igneous intrusions.

27- The location of the Marchburn, Afton, Blackcraig, Scar and Shinnel Formations in the Loch Doon area (from Leake et al 1981). These formations were classified on the basis of greywacke petrography using the criteria defined by Floyd (1980).

28- Schematic flowchart of the RAW Database management system. This DBMS System allows the user to create, edit, append, merge and reformat a wide variety of numerical data stored in self-formating relational data files. Two forms of editing are provided, namely sample and variable editing. Sample editing allows individual sample records to be modified or removed whereas variable oriented editing allows variables to be generated or transformed for each and every sample record in the data file. A variety of tabulation options enables the user to specify the format of the report output, immediately prior to report creation.

29- Sandstone classification diagram (Modified after Dott 1964, McBride 1963). See diagram for explanatory notes.

30- Measured stratigraphic sections from the Tweed Bridge and Talla Linn study areas. In the Tweed Bridge Section geochemical samples were selected from the unit labeled 'A' by chip sampling across the outcrop, whereas in the Talla Linn Section representative samples from each interbedded greywacke unit were sampled.

31- Scottish Lamprophyre arsenic and gold geochemistry. Note the strong correlation between Au (ppb) and As (ppm) with increasing element abundance.

32- Histograms showing the distribution of major and trace elements in greywackes from the Glendinning regional Study area. (see text for detailed interpretation).

33- Histograms showing the distribution of major and trace elements in mudstones from the Glendinning regional Study area. (see text for detailed interpretation).

34- Histograms showing the distribution of major and trace elements in mineralised drillcore from the Glendinning As-Sb-Au deposit. (see text for detailed interpretation).

35a- Geochemical Alteration:- Glendinning area SiO_2 (%) Note the general increase in silica composition for altered greywacke samples with respect to the unmineralised counterparts and the decrease in composition reflected between altered mudstone and regional mudstones.

35b- Geochemical Alteration:- Glendinning area Al_2O_3 (%) Note the general increase in Al composition reflected in altered samples.

35c- Geochemical Alteration:- Glendinning area TiO_2 (%) Note the enhanced TiO_2 levels present in mudstone samples in comparison with the interbedded greywacke counterparts.

36a- Geochemical Alteration:- Glendinning area Fe_2O_3 (%) Note the depletion of iron in both altered greywacke and mudstone samples respectively.

FIGURE 23

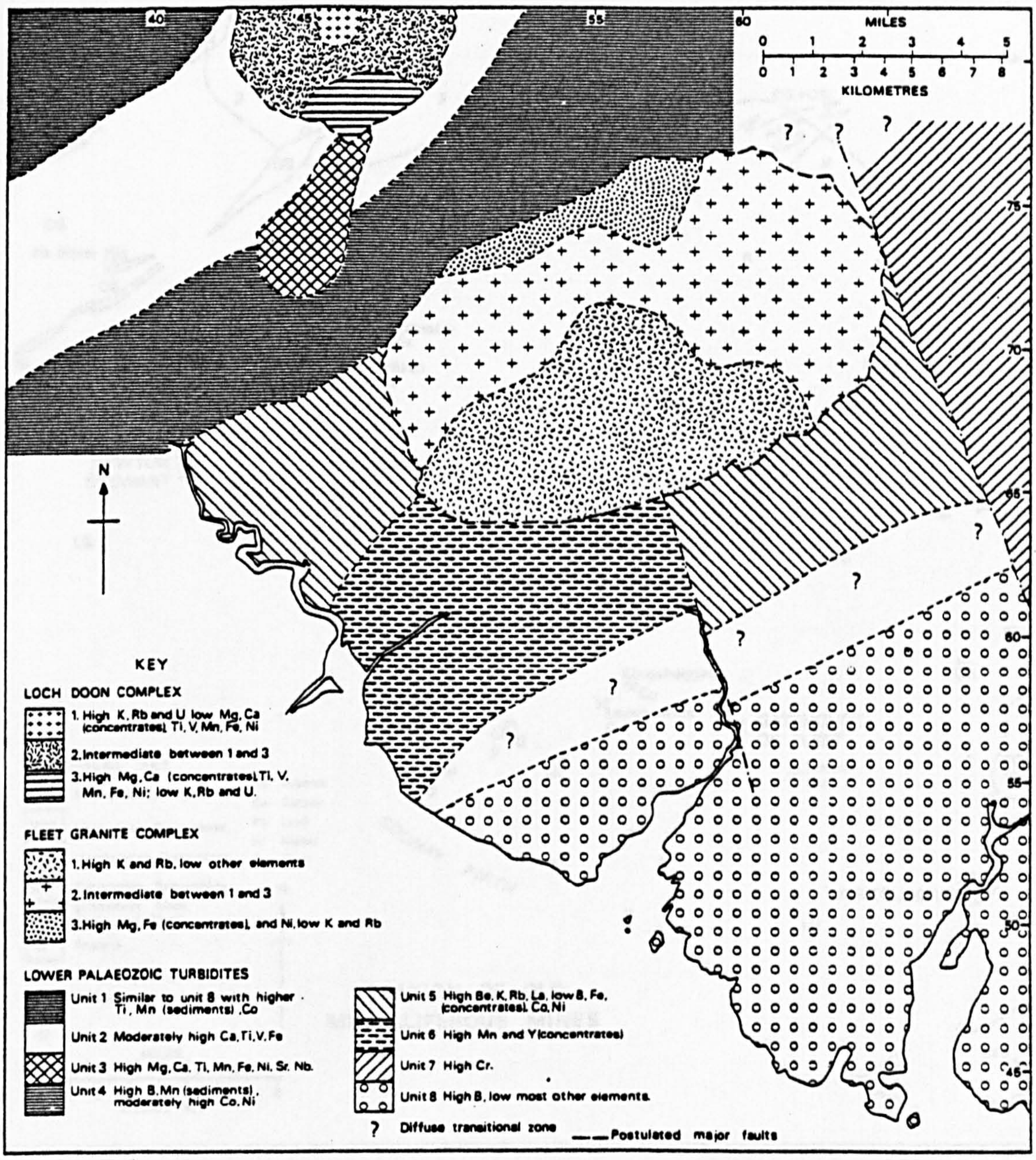
40
45
50
55
60
MILES
0 1 2 3 4 5
0 1 2 3 4 5 6 7 8
KILOMETRES
75
70
65
60
55
50
45
N
KEY
LOCH DOON COMPLEX
1. High K, Rb and U low Mg, Ca (concentrates), Ti, V, Mn, Fe, Ni
2. Intermediate between 1 and 3
3. High Mg, Ca (concentrates), Ti, V, Mn, Fe, Ni; low K, Rb and U.
FLEET GRANITE COMPLEX
1. High K and Rb, low other elements
2. Intermediate between 1 and 3
3. High Mg, Fe (concentrates), and Ni, low K and Rb
LOWER PALAEOZOIC TURBIDITES
Unit 1 Similar to unit 8 with higher Ti, Mn (sediments), Co
Unit 2 Moderately high Ca, Ti, V, Fe
Unit 3 High Mg, Ca, Ti, Mn, Fe, Ni, Sr, Nb.
Unit 4 High B, Mn (sediments), moderately high Co, Ni
Unit 5 High Be, K, Rb, La, low B, Fe, (concentrates), Co, Ni
Unit 6 High Mn and Y (concentrates)
Unit 7 High Cr.
Unit 8 High B, low most other elements.
? Diffuse transitional zone
Postulated major faults

FIGURE 24

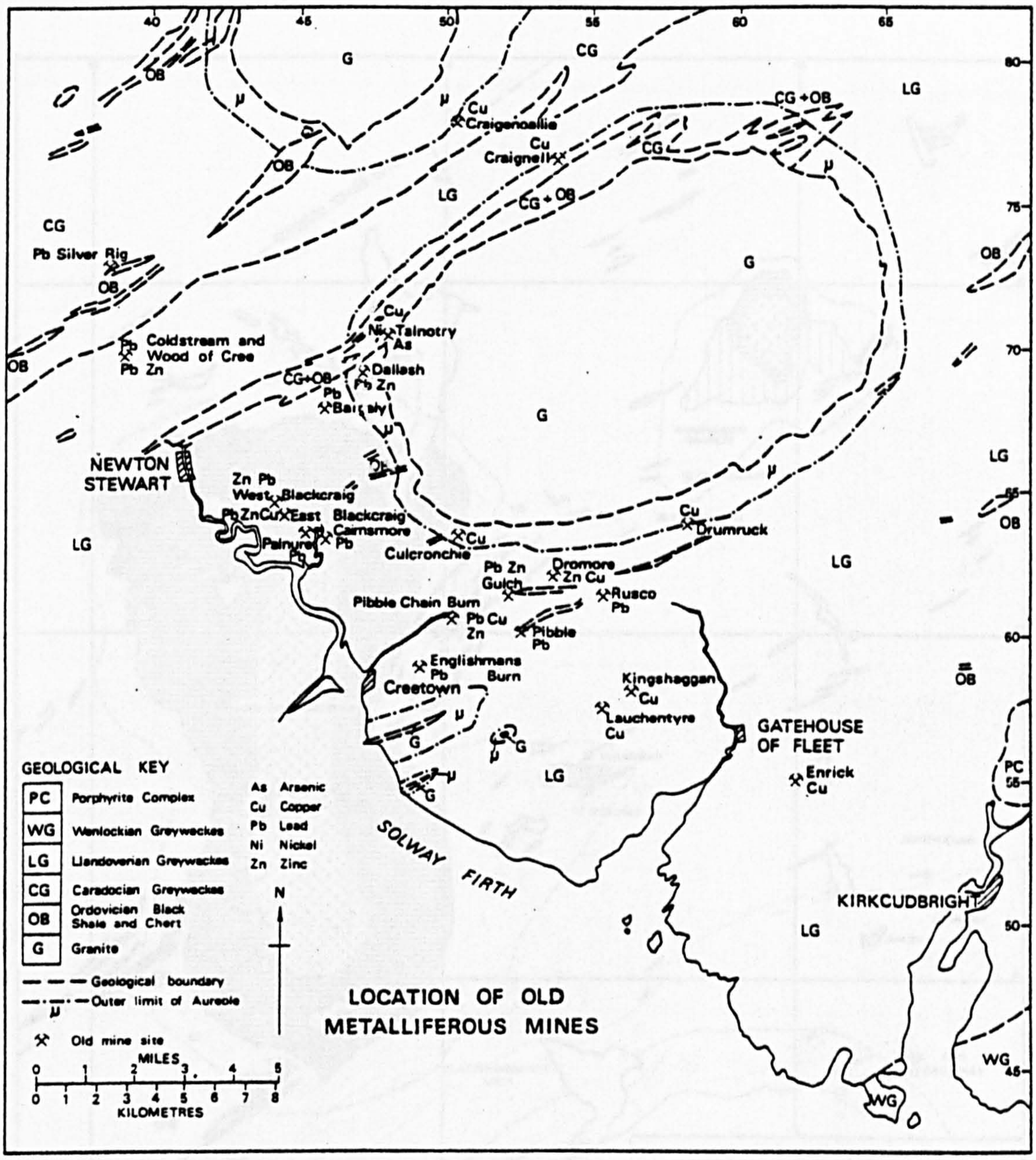
G
CG
LG
OB
CG+OB
µ
Cu Craigenoallie
Cu Craignell
Pb Silver Rig
Pb Coldstream and Wood of Cree Pb Zn
Cu Ni Talnotry As
Dallash Pb Zn
Pb Bargaly
NEWTON STEWART
Zn Pb West Blackcraig
Pb Zn Cu East Blackcraig
Cairnsmore Pb
Palnure Pb
Cu Culcronchie
Cu Drumruck
Pb Zn Gulch
Dromore Zn Cu
Rusco Pb
Pibble Chain Burn Pb Cu Zn
Pibble Pb
Englishmans Pb Burn
Creetown
Kingshaggan Cu
Lauchentyre Cu
GATEHOUSE OF FLEET
Enrick Cu
SOLWAY FIRTH
KIRKCUDBRIGHT
PC
WG
GEOLOGICAL KEY
PC Porphyrite Complex
WG Wenlockian Greywackes
LG Llandoverian Greywackes
CG Caradocian Greywackes
OB Ordovician Black Shale and Chert
G Granite
As Arsenic
Cu Copper
Pb Lead
Ni Nickel
Zn Zinc
N
Geological boundary
µ Outer limit of Aureole
Old mine site
MILES
0 1 2 3 4 5
0 1 2 3 4 5 6 7 8
KILOMETRES
LOCATION OF OLD METALLIFEROUS MINES
40 45 50 55 60 65
80 75 70 65 60 55 50 45

FIGURE 25

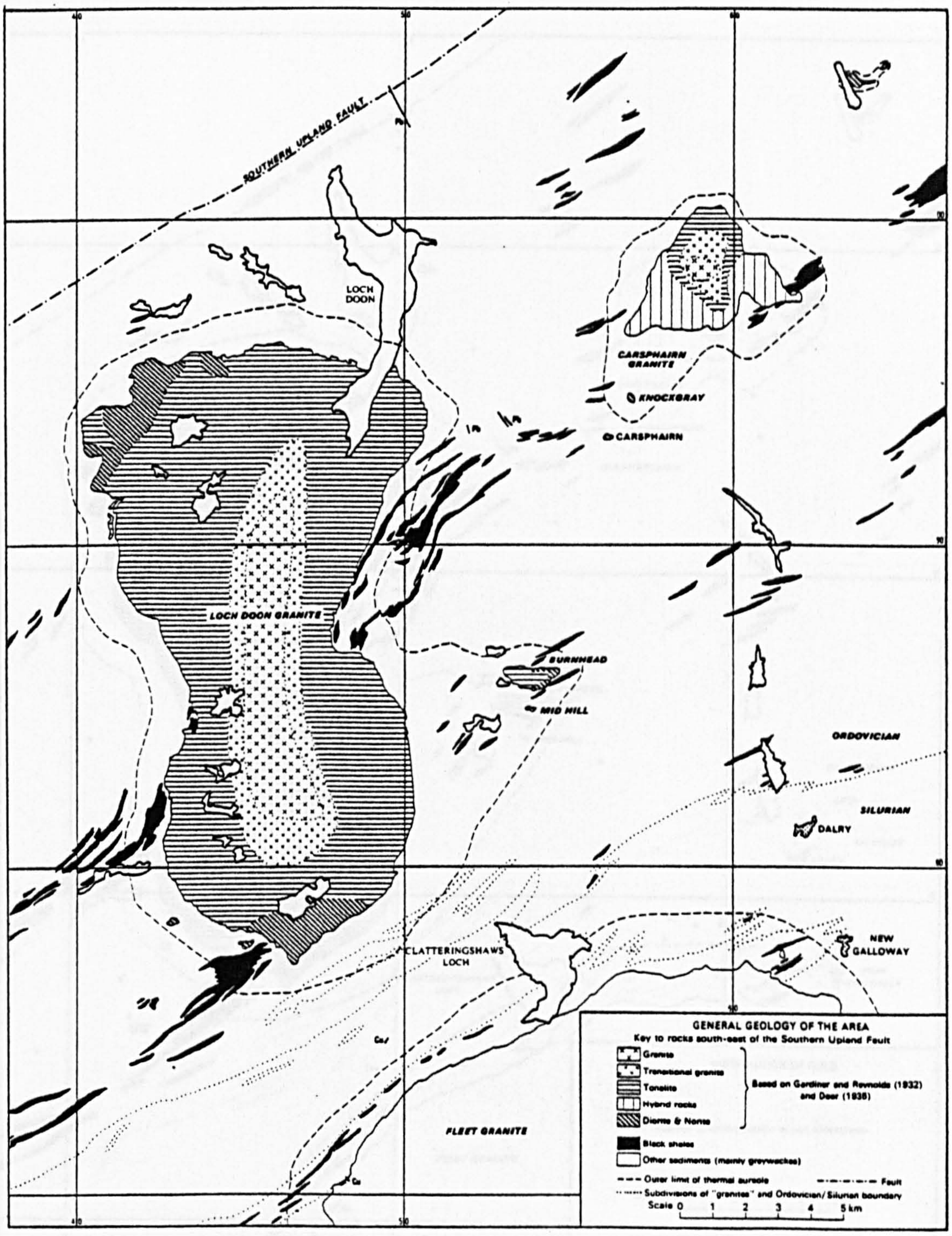
SOUTHERN UPLAND FAULT
LOCH DOON
CARSPHAIRN GRANITE
KNOCKGRAY
CARSPHAIRN
LOCH DOON GRANITE
BURNHEAD
MID HILL
ORDOVICIAN
SILURIAN
DALRY
NEW GALLOWAY
CLATTERINGSHAWS LOCH
FLEET GRANITE
GENERAL GEOLOGY OF THE AREA
Key to rocks south-east of the Southern Upland Fault
Granite
Transitional granite
Tonalite
Hybrid rocks
Diorite & Norite
Based on Gardiner and Reynolds (1932) and Deer (1938)
Black shales
Other sediments (mainly greywackes)
Outer limit of thermal aureole
Fault
Subdivisions of "granites" and Ordovician/Silurian boundary
Scale 0 1 2 3 4 5 km

FIGURE 26

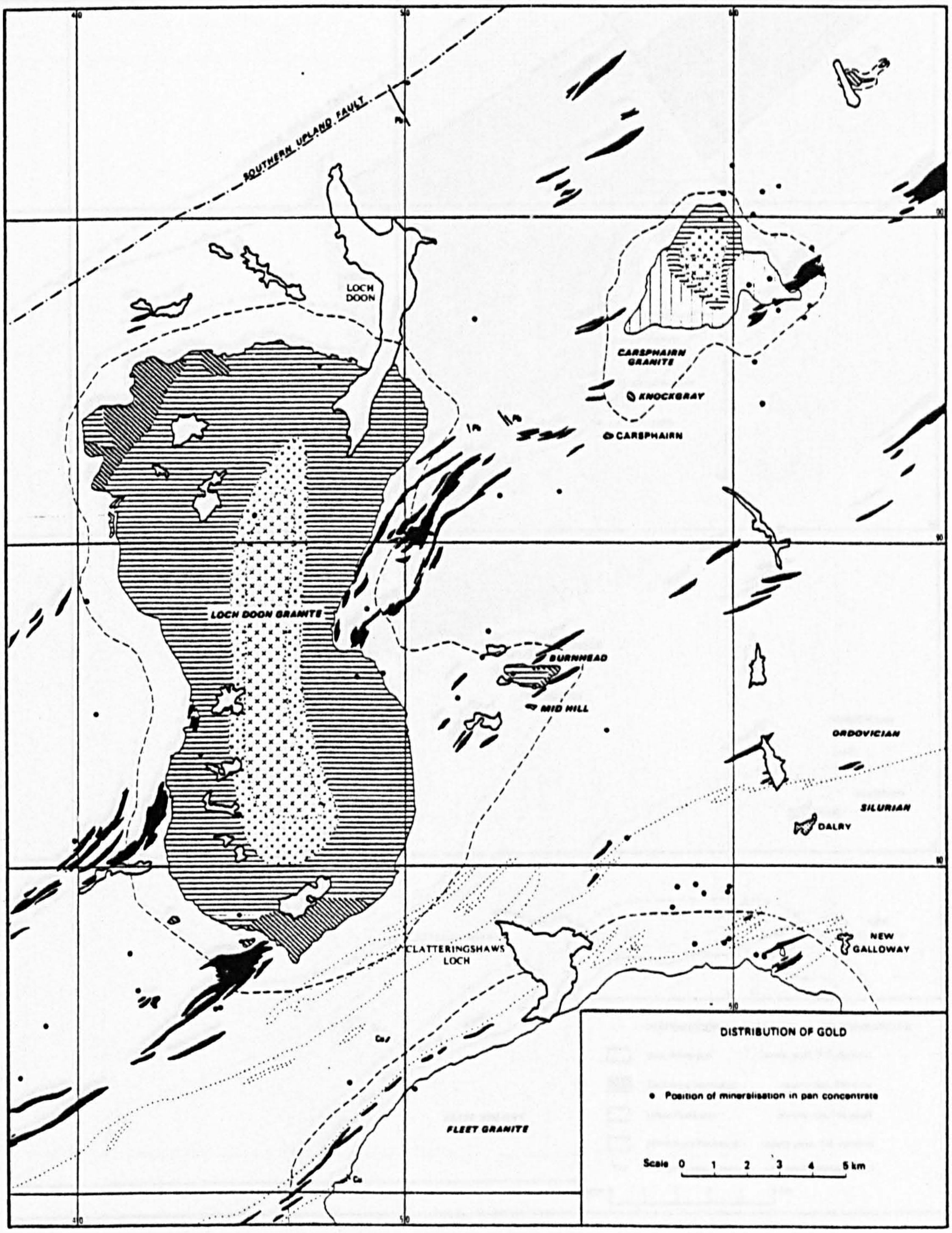
SOUTHERN UPLAND FAULT
LOCH DOON
CARSPHAIRN GRANITE
KNOCKGRAY
CARSPHAIRN
LOCH DOON GRANITE
BURNHEAD
MID HILL
ORDOVICIAN
SILURIAN
DALRY
NEW GALLOWAY
CLATTERINGSHAWS LOCH
FLEET GRANITE
DISTRIBUTION OF GOLD
Position of mineralisation in pan concentrate
Scale 0 1 2 3 4 5 km

FIGURE 27

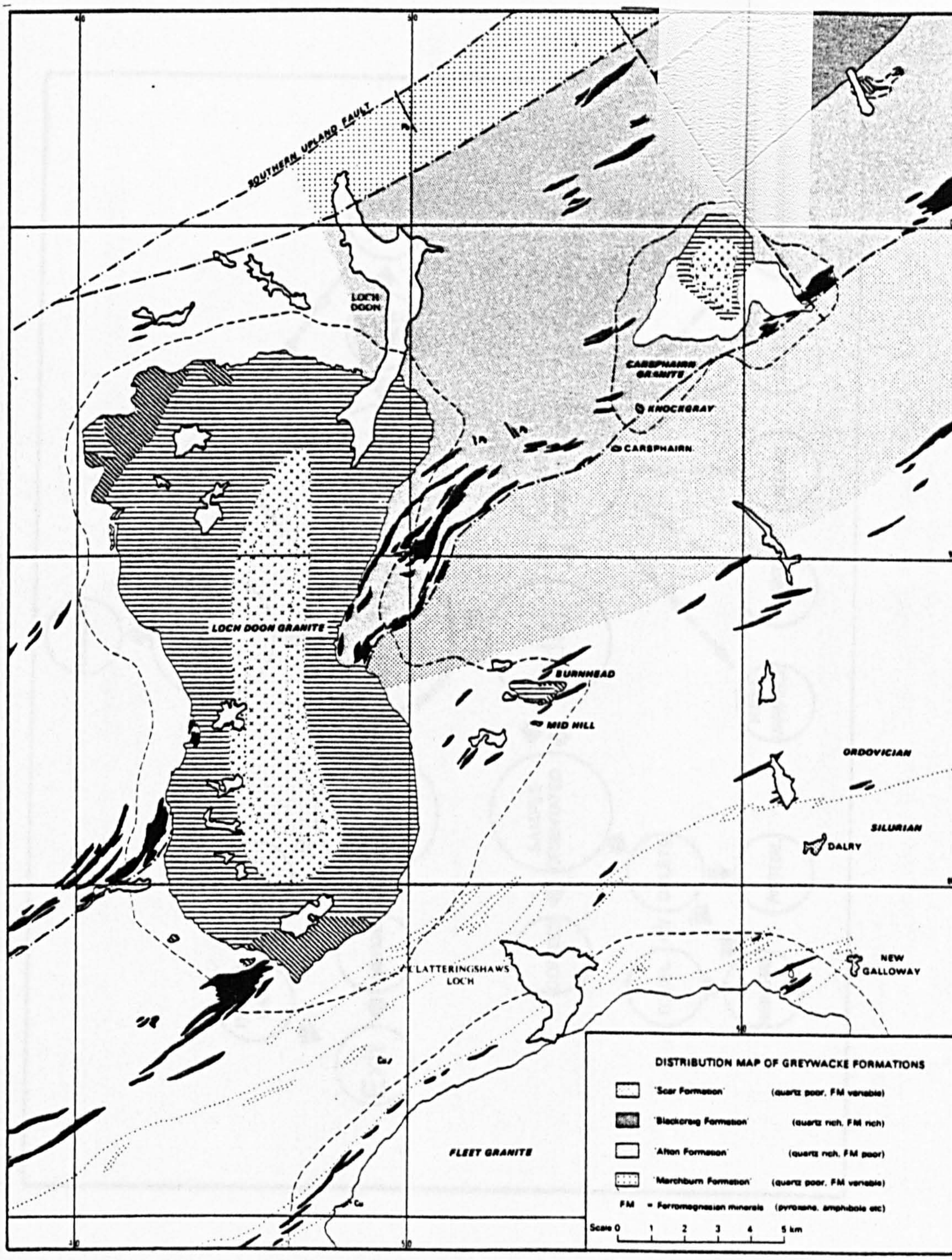
SOUTHERN UPLAND FAULT
LOCH DOON
CARSPHAIRN GRANITE
KNOCKGRAY
CARSPHAIRN
LOCH DOON GRANITE
BURNHEAD
MID HILL
ORDOVICIAN
SILURIAN
DALRY
CLATTERINGSHAWS LOCH
NEW GALLOWAY
FLEET GRANITE
DISTRIBUTION MAP OF GREYWACKE FORMATIONS
'Scar Formation' (quartz poor, FM variable)
'Blackcraig Formation' (quartz rich, FM rich)
'Afton Formation' (quartz rich, FM poor)
'Marchburn Formation' (quartz poor, FM variable)
FM = Ferromagnesian minerals (pyroxene, amphibole etc)
Scale 0 1 2 3 4 5 km

FIGURE 28

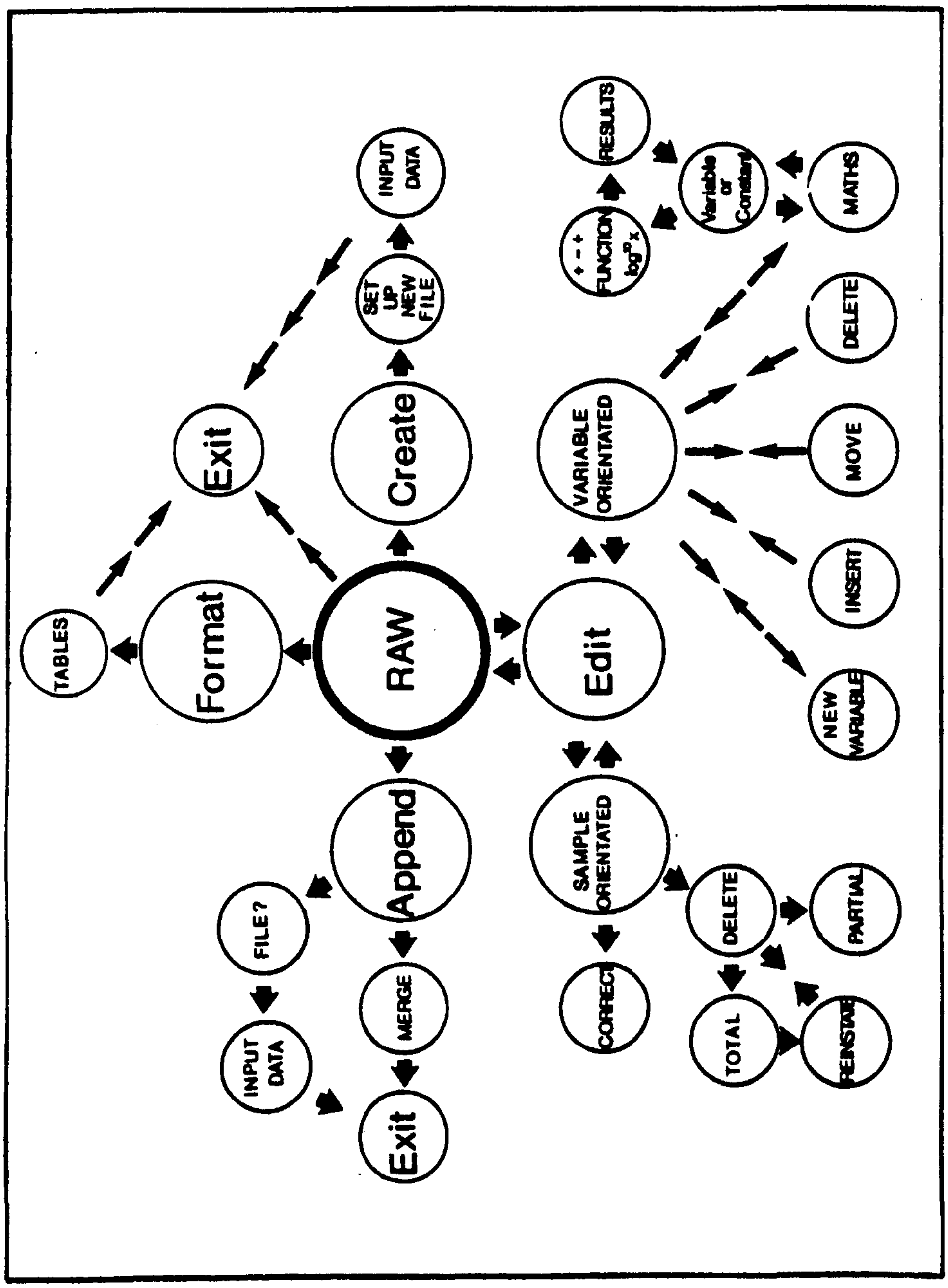
RAW
Create
SET UP NEW FILE
INPUT DATA
Exit
Format
TABLES
Append
FILE ?
INPUT DATA
MERGE
Exit
Edit
VARIABLE ORIENTATED
NEW VARIABLE
INSERT
MOVE
DELETE
MATHS
Variable or Constant
RESULTS
+ - ÷ FUNCTION $\log^{n} x$
SAMPLE ORIENTATED
CORRECT
DELETE
PARTIAL
TOTAL
REINSTATE

FIGURE 29

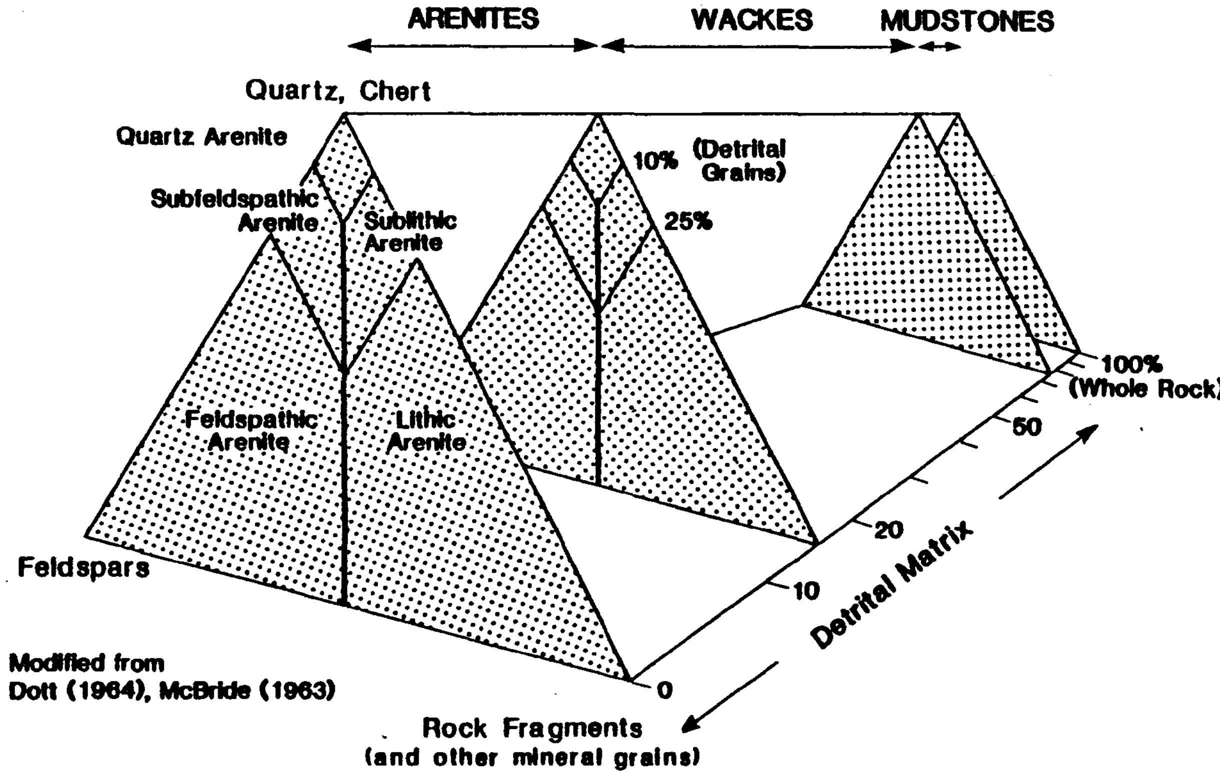

SANDSTONE CLASSIFICATION

Explanatory Notes.

This classification considers detrital components only. Lithological terms (as defined above) are prefixed for authigenic phases (including clays and carbonates) where they constitute 10% or more of the whole rock e.g. Calcareous QUARTZ ARENITE.

FIGURE 30

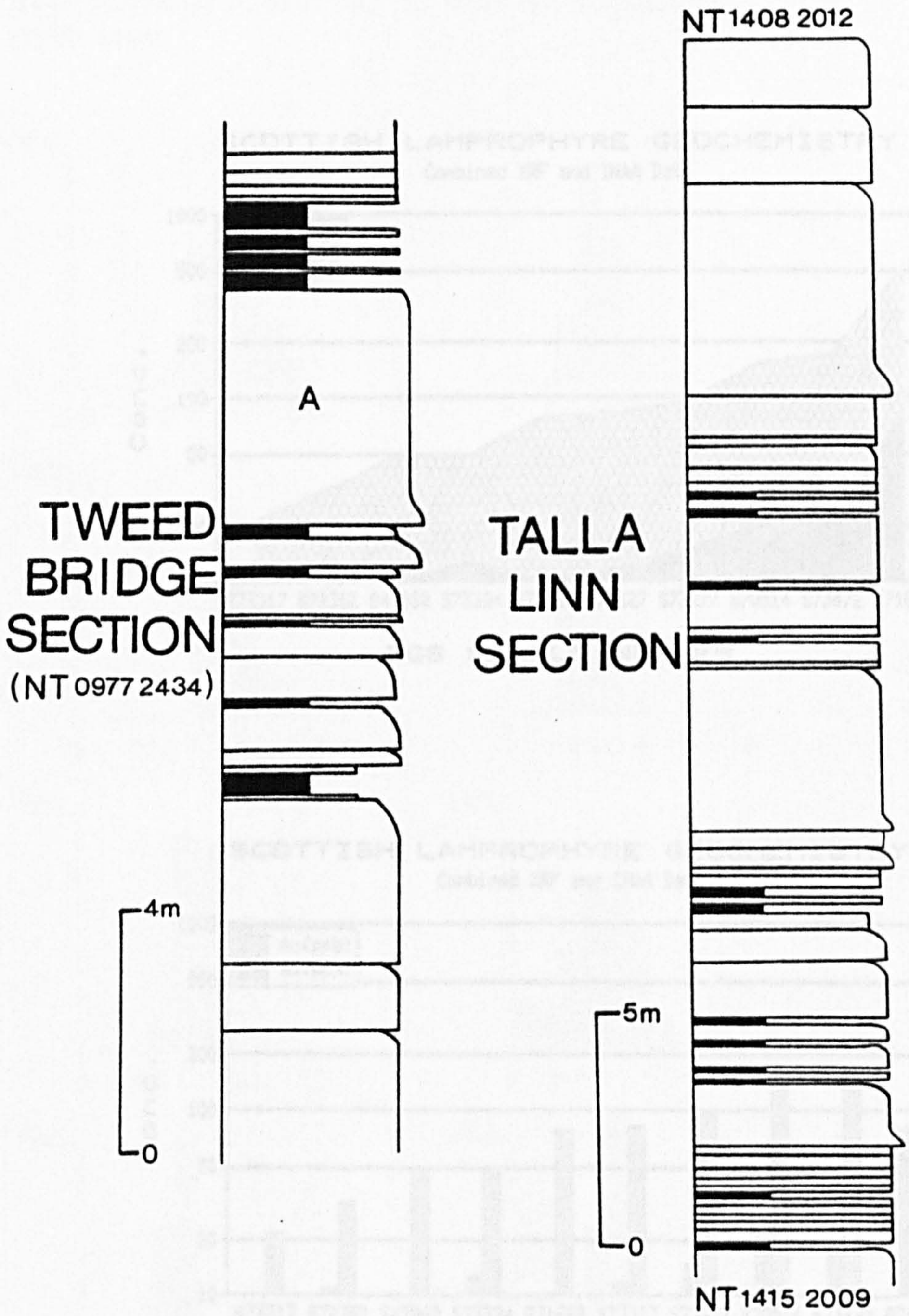
NT 1408 2012
A
TWEED
BRIDGE
SECTION
(NT 0977 2434)
TALLA
LINN
SECTION
4m
0
5m
0
NT 1415 2009

FIGURE 31

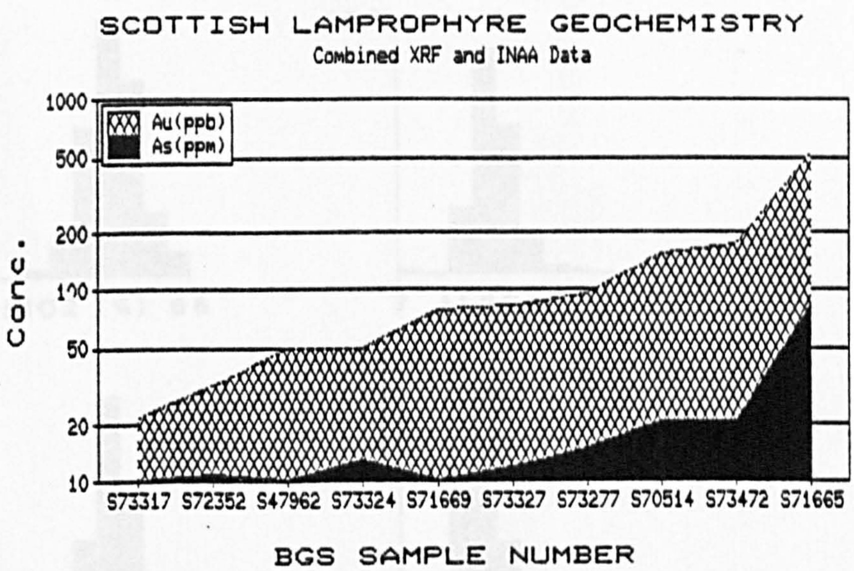
SCOTTISH LAMPROPHYRE GEOCHEMISTRY
Combined XRF and INAA Data
Au(ppb)
As(ppm)
1000
500
200
100
50
20
10
Conc.
S73317 S72352 S47962 S73324 S71669 S73327 S73277 S70514 S73472 S71665
BGS SAMPLE NUMBER

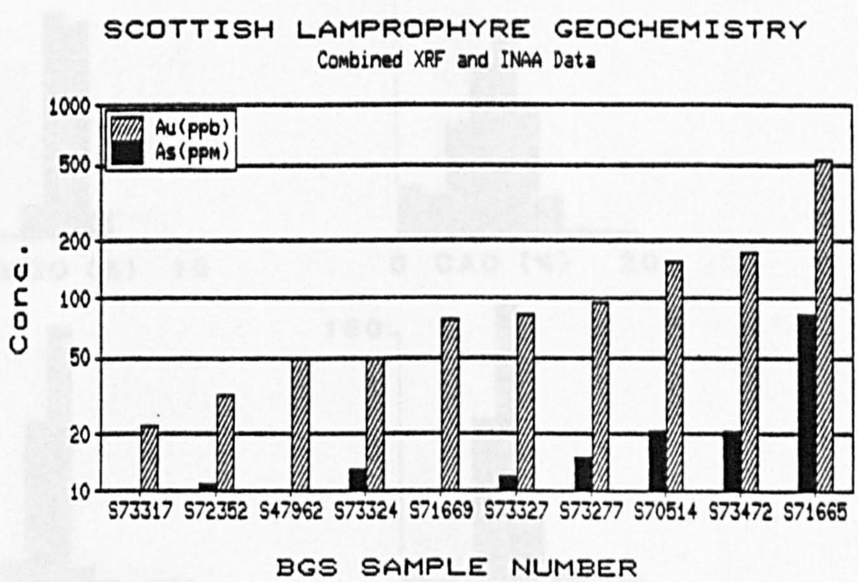
SCOTTISH LAMPROPHYRE GEOCHEMISTRY
Combined XRF and INAA Data
Au(ppb)
As(ppm)
1000
500
200
100
50
20
10
Conc.
S73317 S72352 S47962 S73324 S71669 S73327 S73277 S70514 S73472 S71665
BGS SAMPLE NUMBER

FIGURE 32

Histograms showing the distribution of major and trace elements in greywackes from the Glendinning study area.

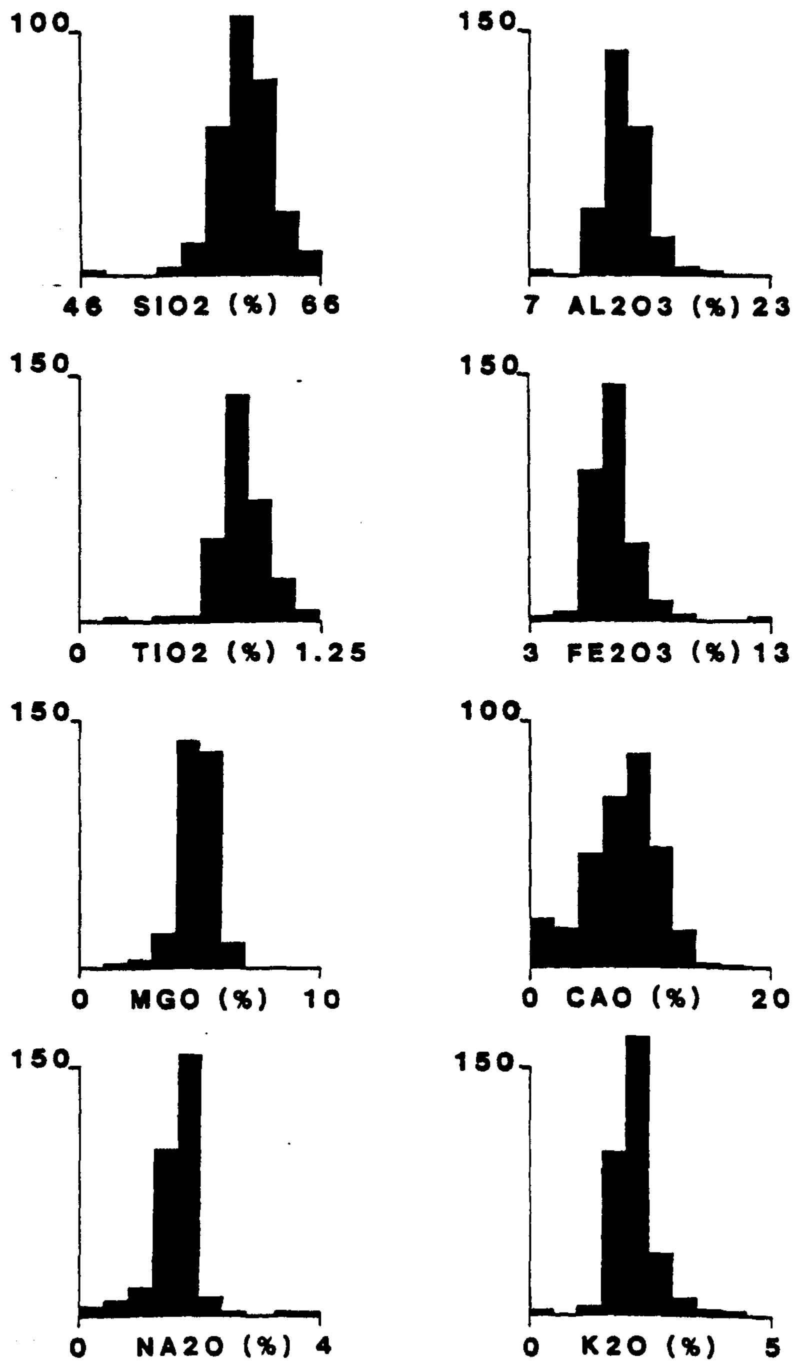

FIGURE 32 cont:

Histograms showing the distribution of major and trace elements in greywackes from the Glendinning study area.

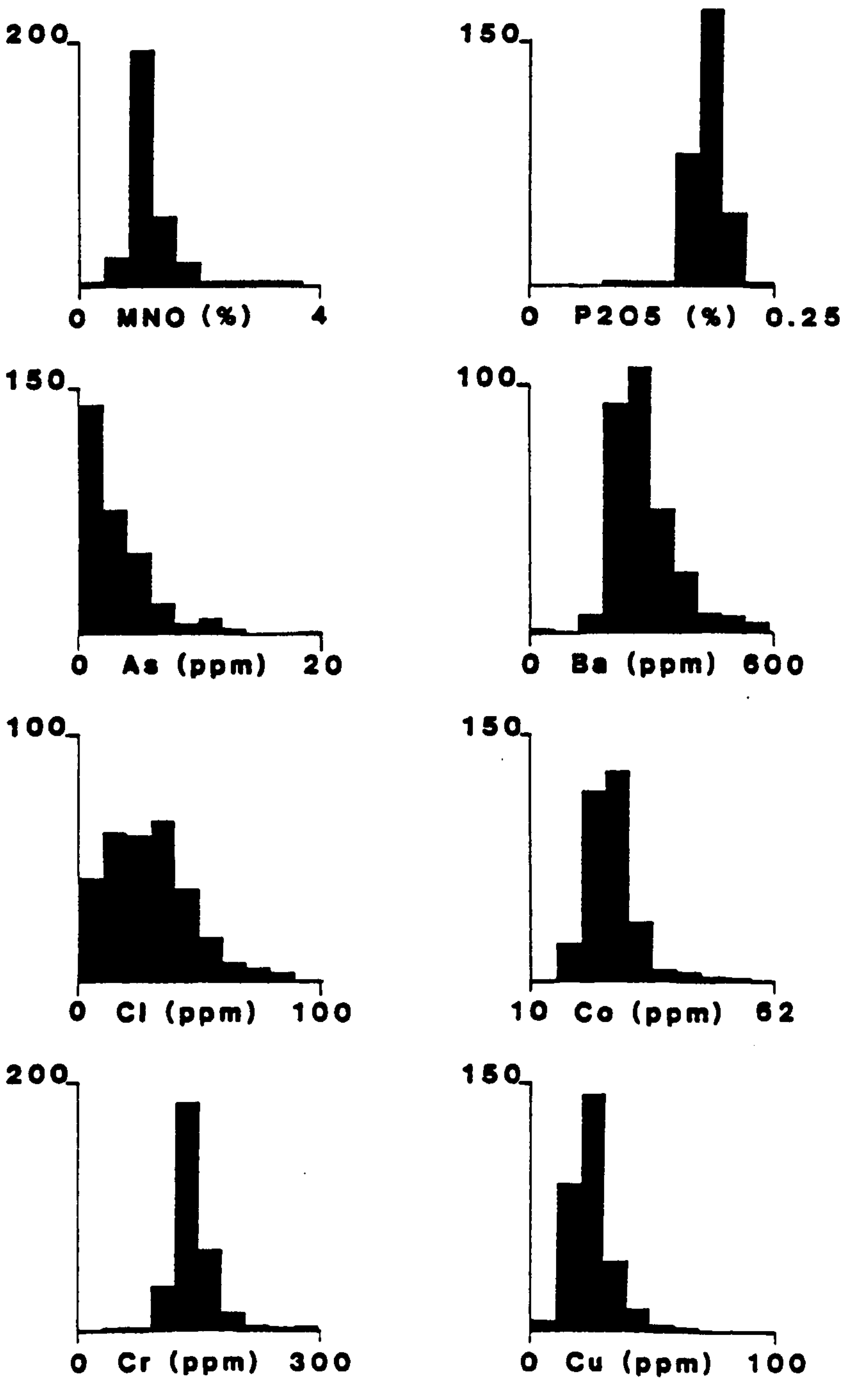

FIGURE 32 cont:

Histograms showing the distribution of major and trace elements in greywackes from the Glendinning study area.

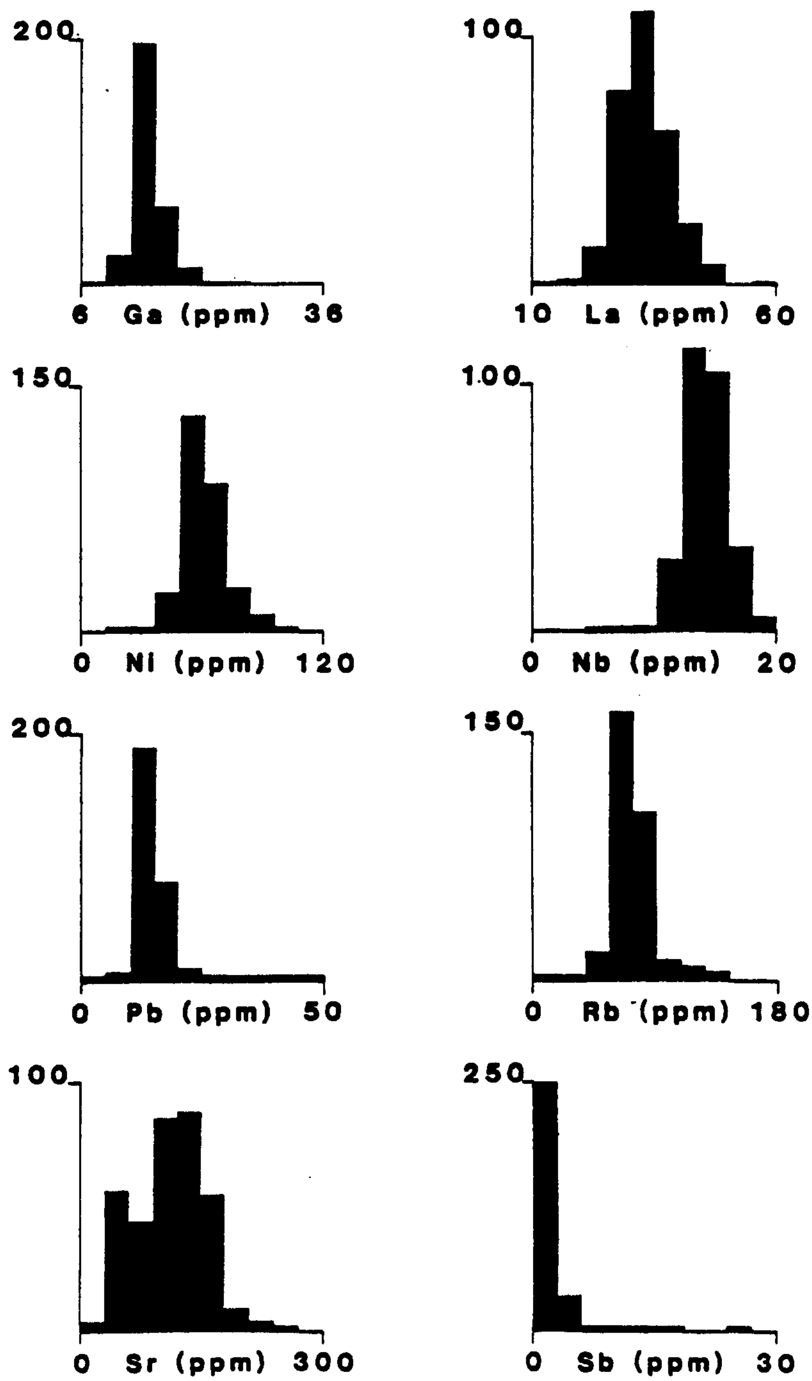

FIGURE 32 cont:

Histograms showing the distribution of major and trace elements in greywackes from the Glendinning study area.

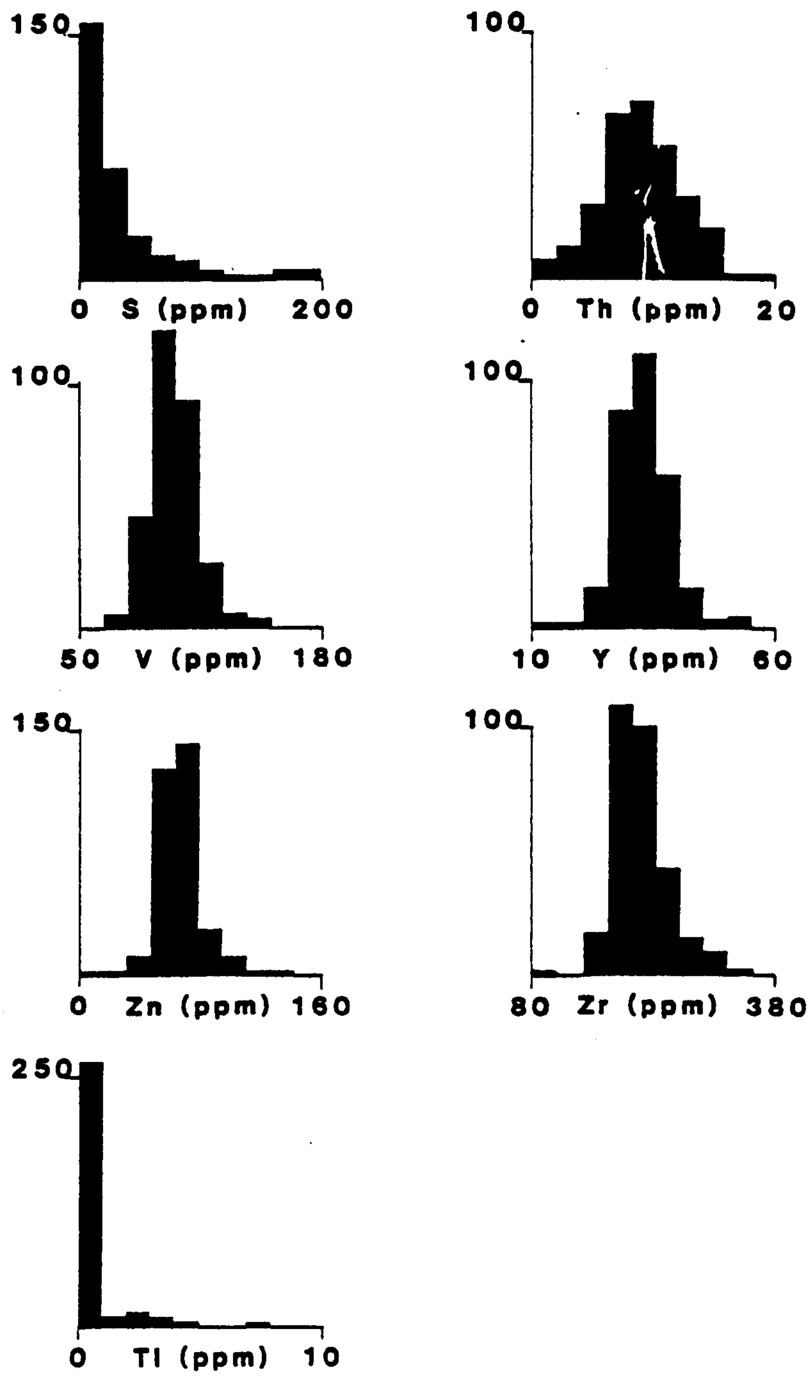

FIGURE 33

Histograms showing the distribution of major and trace elements in mudstones from the Glendinning study area.

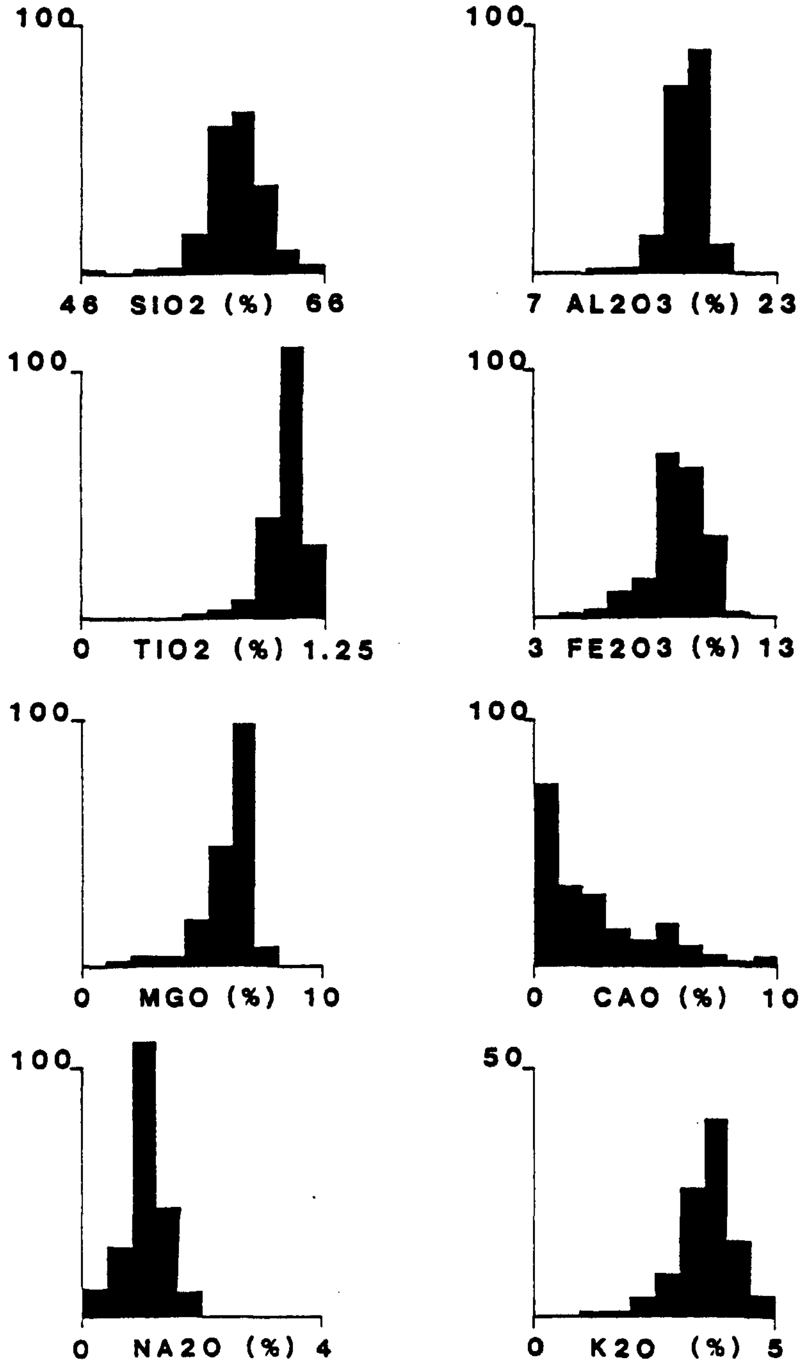

FIGURE 33 cont:

Histograms showing the distribution of major and trace elements in mudstones from the Glendinning study area.

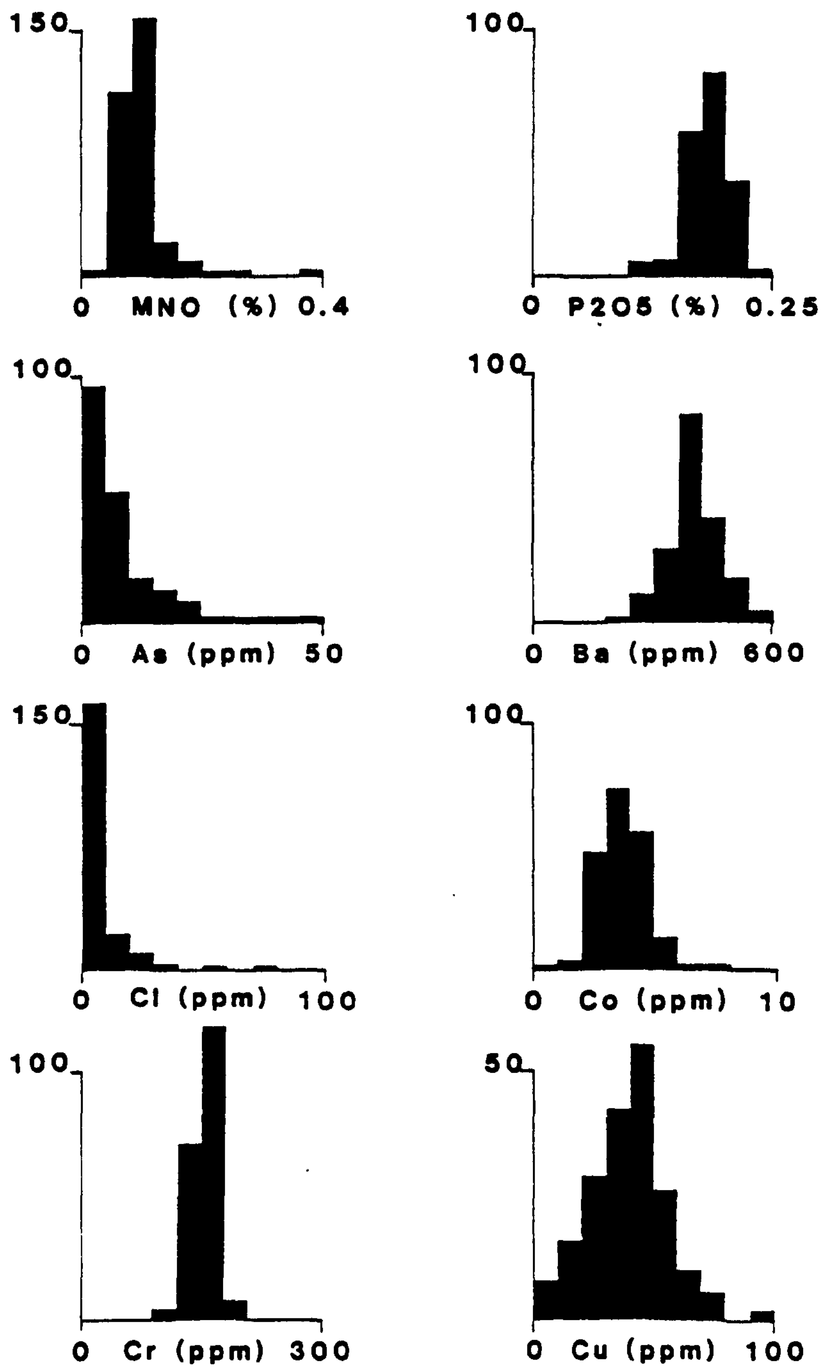

FIGURE 33 cont:

Histograms showing the distribution of major and trace elements in mudstones from the Glendinning study area.

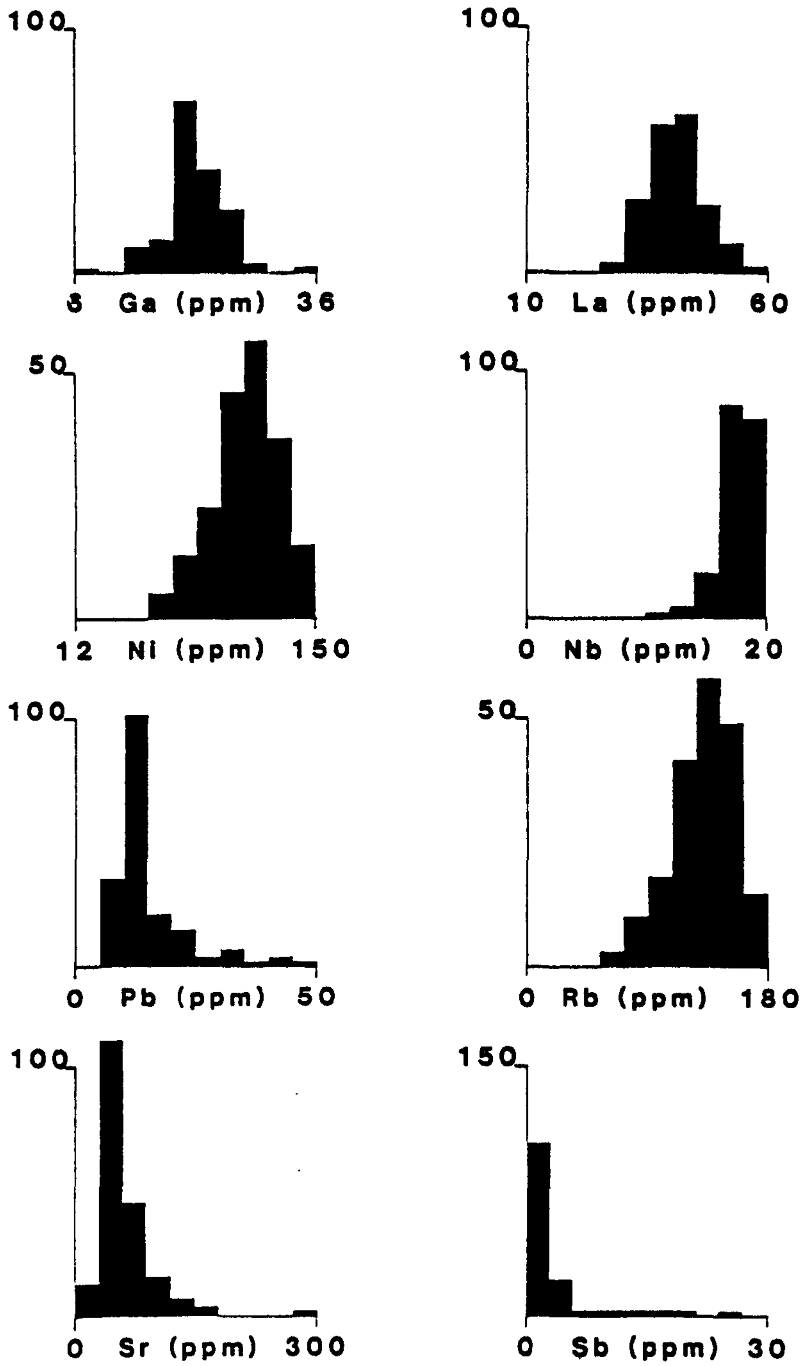

FIGURE 33 cont:

Histograms showing the distribution of major and trace elements in mudstones from the Glendinning study area.

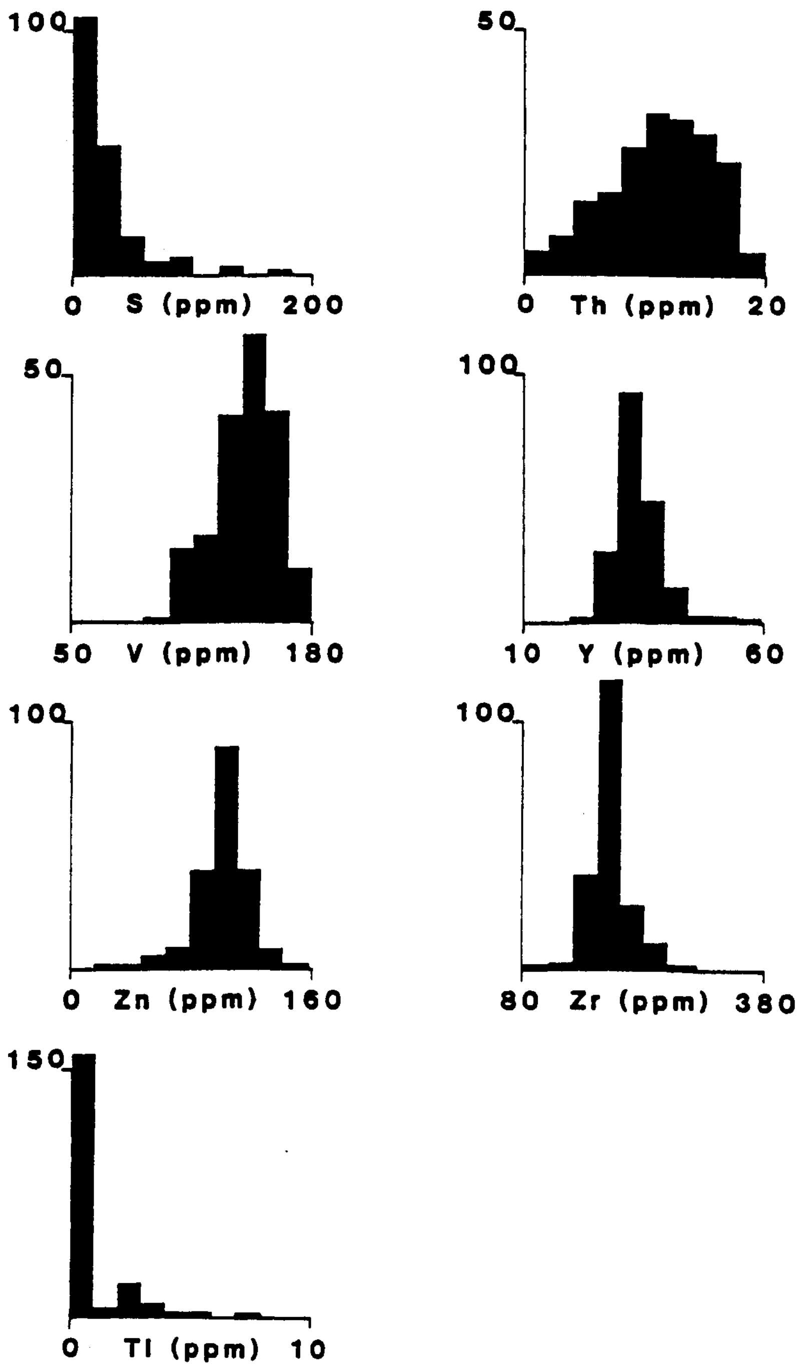

FIGURE 34

Histograms showing the distribution of major and trace elements in mineralised drill core from the Glendinning Au-As-Sb deposit.

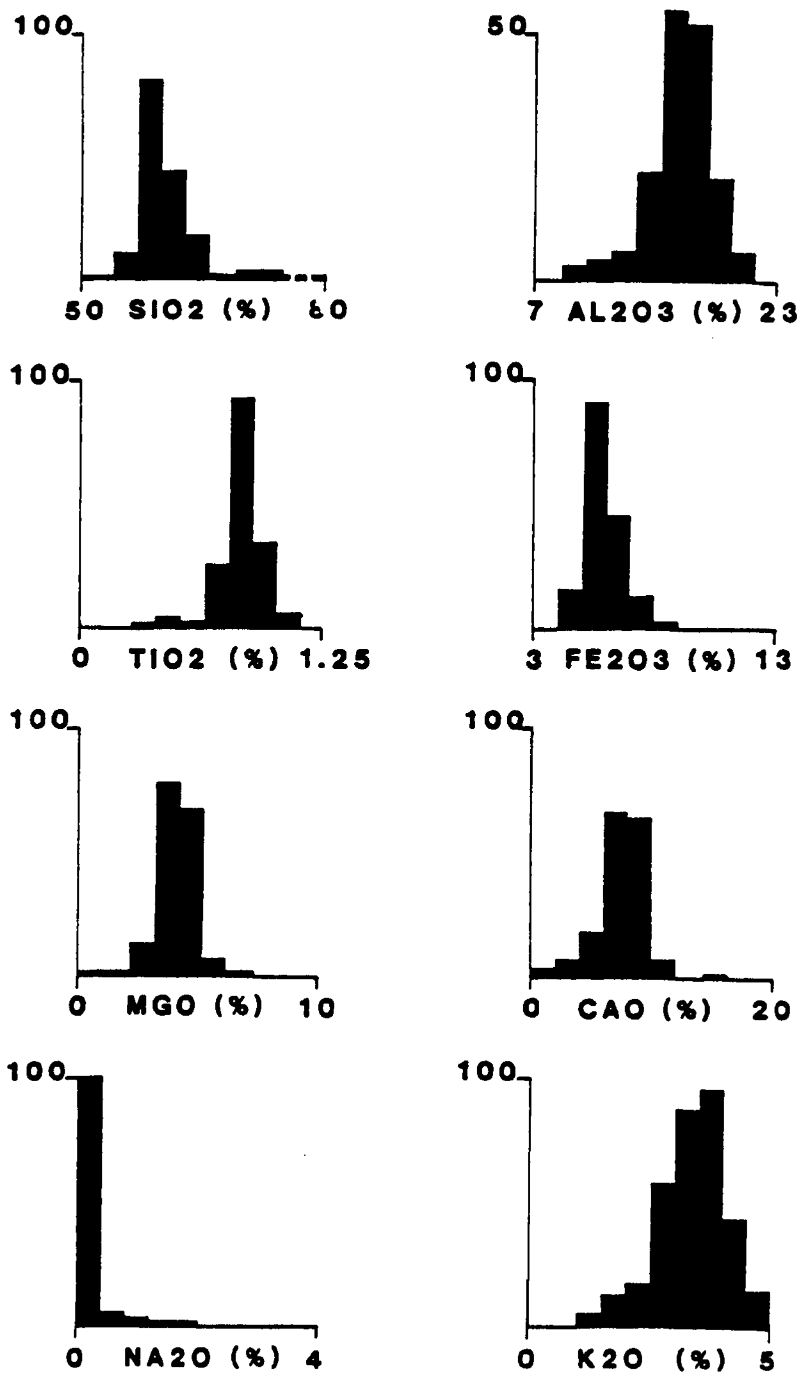

FIGURE 34 cont:

Histograms showing the distribution of major and trace elements in mineralised drill core from the Glendinning Au-As-Sb deposit.

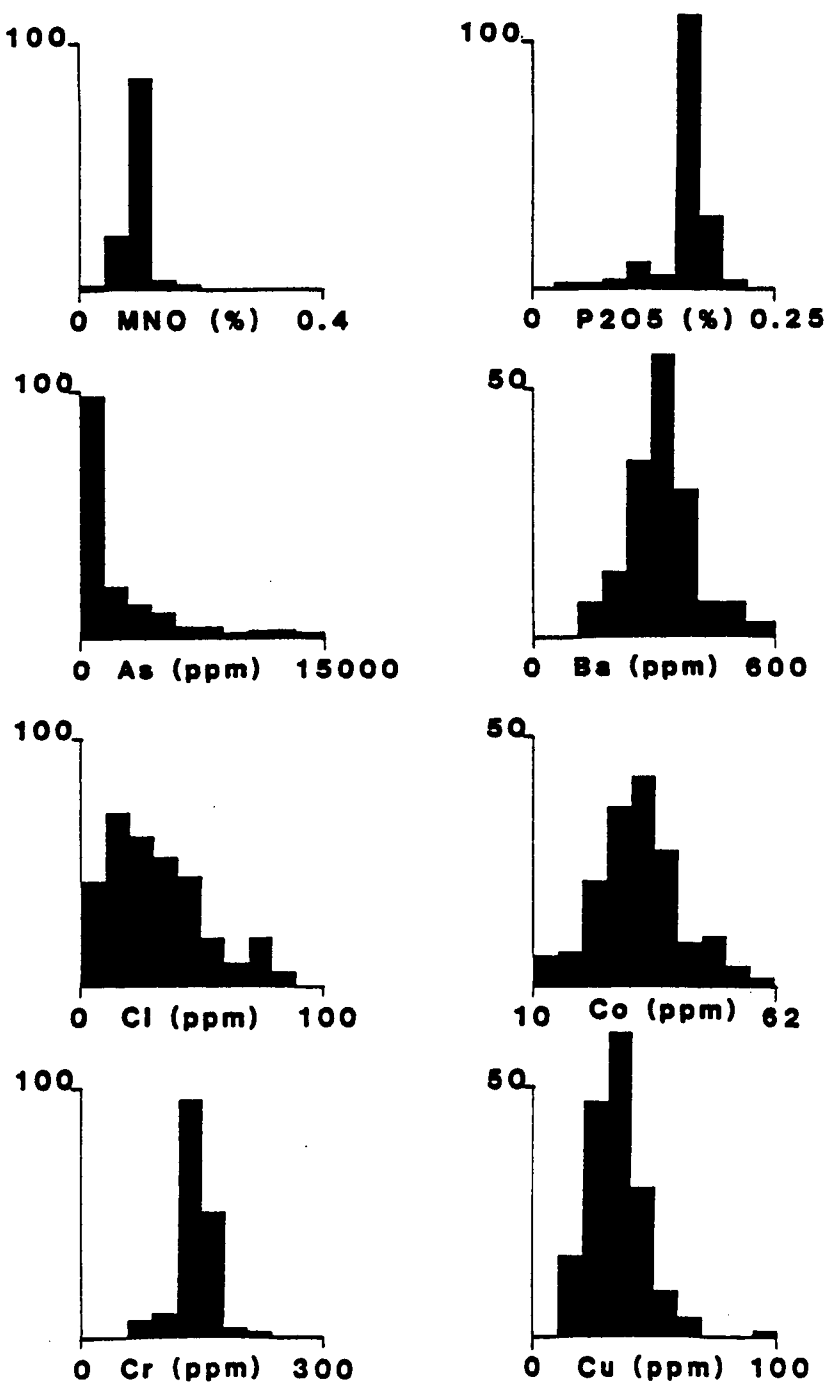

FIGURE 34 cont:

Histograms showing the distribution of major and trace elements in mineralised drill core from the Glendinning Au-As-Sb deposit.

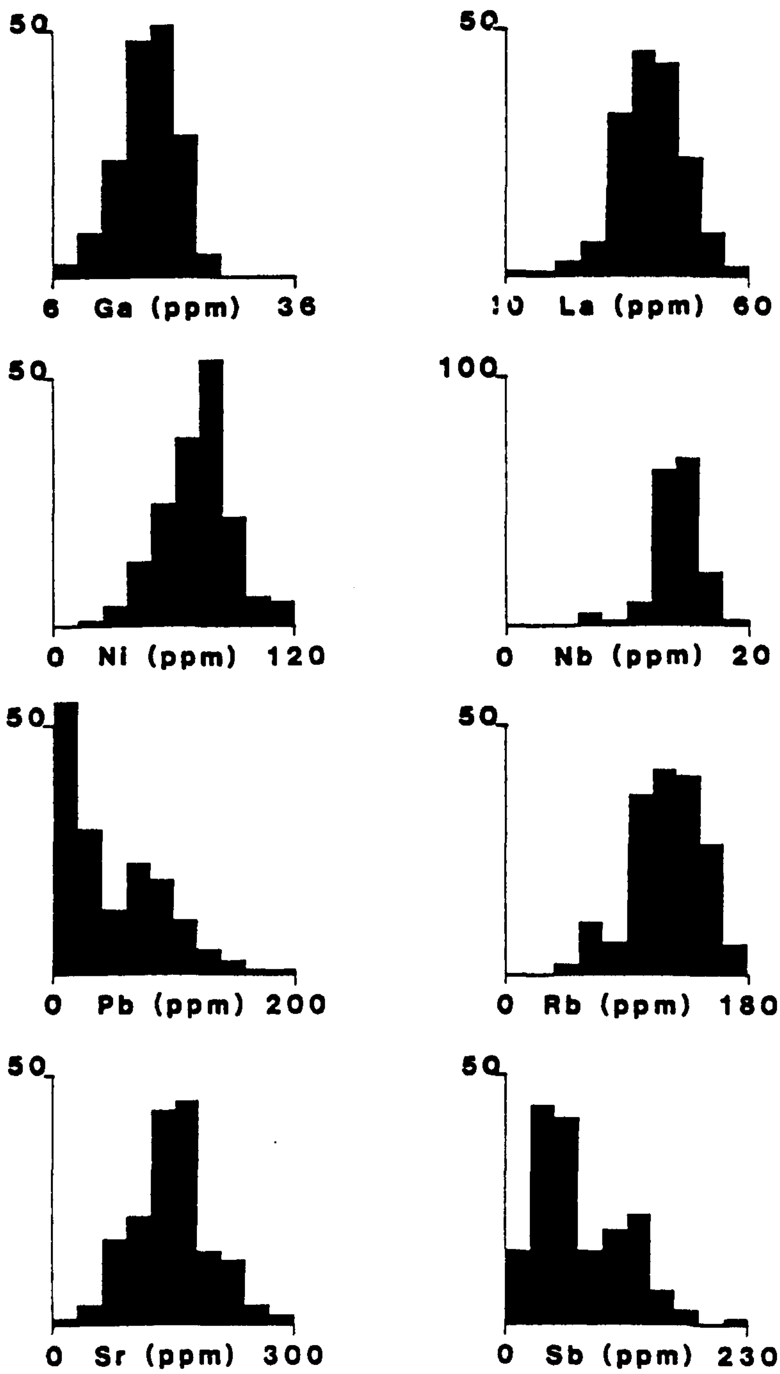

FIGURE 34 cont:

Histograms showing the distribution of major and trace elements in mineralised drill core from the Glendinning Au-As-Sb deposit.

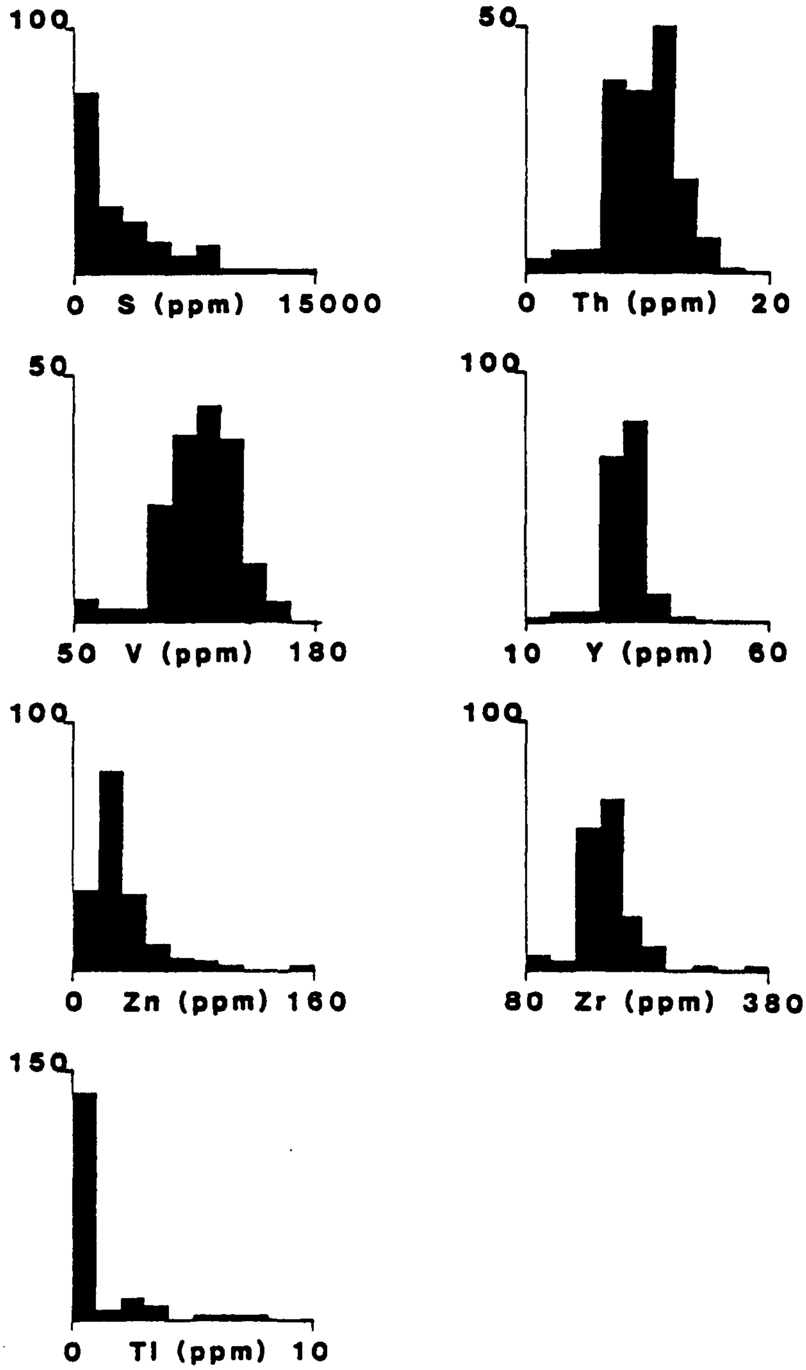

FIGURE 35 a/b/c

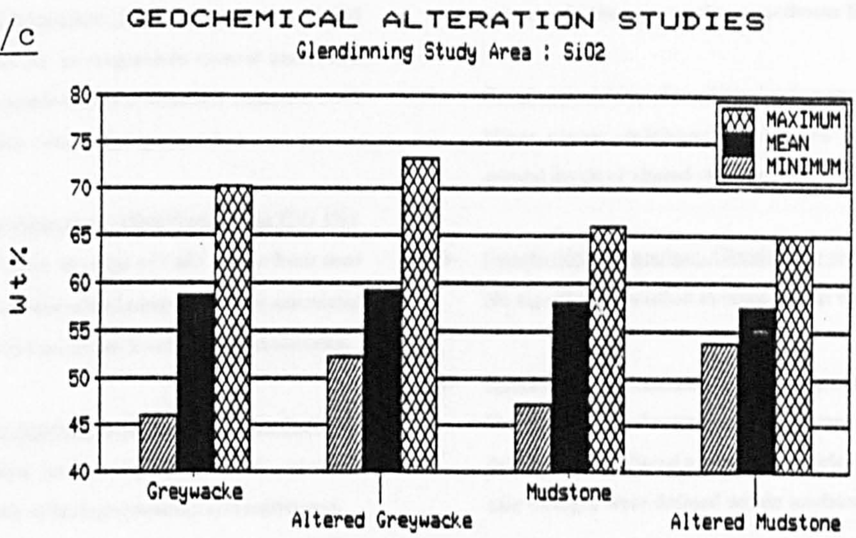

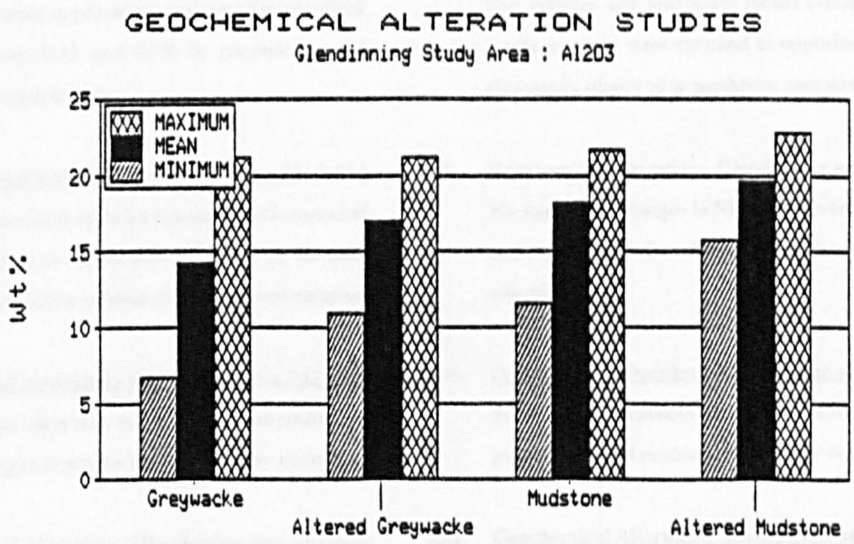

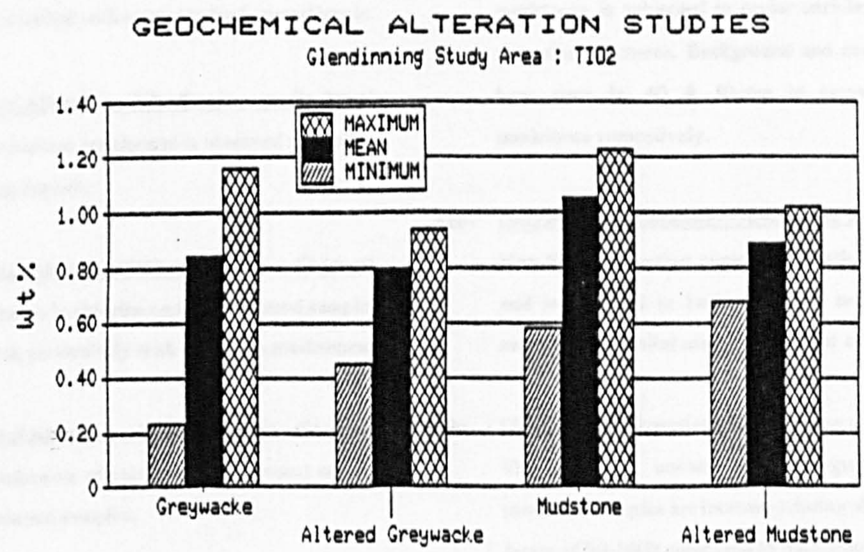

36b- Geochemical Alteration:- Glendinning area MgO (%)
Note the decrease in magnesium content associated with altered samples and the enhanced minimum level associated with mineralised greywackes.

36c- Geochemical Alteration:- Glendinning area CaO (%)
Note the decrease in range of CaO values from non-mineralised to mineralised samples, and the associated increase in CaO minimum levels in altered samples.

37a- Geochemical Alteration:- Glendinning area Na_2O (%)
Note the major sodium depletion effects associated with alteration of both greywackes and mudstones.

37b- Geochemical Alteration:- Glendinning area K_2O (%)
Note the increase in potassium content of mineralised samples (mean 0.75 and 0.5% in greywackes and mudstones respectively).

37c- Geochemical Alteration:- Glendinning area MnO (%)
Note the minor increase in background MnO content of altered samples as opposed to the relatively constant average composition of altered and unaltered samples.

38a- Geochemical Alteration:- Glendinning area P_2O_5 (%)
This diagram illustrates that the P_2O_5 composition of both lithologies is relatively unaffected by alteration.

38b- Geochemical Alteration:- Glendinning area As (ppm)
As expected arsenic levels are enriched in this deposit by a factor of >1000 with respect to background levels.

38c- Geochemical Alteration:- Glendinning area Ba (ppm)
Only minor barium enrichment is observed within the Glendinning deposit.

39a- Geochemical Alteration:- Glendinning area Cl (ppm)
Minor increases in chlorine content of altered samples are observed, particularly with respect to mudstones.

39b- Geochemical Alteration:- Glendinning area Co (ppm)
Minor enrichments of cobalt (2-5ppm mean) are observed in altered samples.

39c- Geochemical Alteration:- Glendinning area Cr (ppm)
No significant variation are observed in the chromium content of either greywacke or mudstone lithologies.

40a- Geochemical Alteration:- Glendinning area Cu (ppm)
Minor copper enrichment is observed in the background levels of altered samples.

40b- Geochemical Alteration:- Glendinning area Ga (ppm)
No significant variation in composition was detected.

40c- Geochemical Alteration:- Glendinning area La (ppm)
Enrichment of La background and average levels were defined only in altered greywacke samples. No significant changes were defined within mudstone samples.

41a- Geochemical Alteration:- Glendinning area Ni (ppm)
The average and maximum nickel content of greywacke samples were enriched in opposition to depletion trends observed in mudstone samples.

41b- Geochemical Alteration:- Glendinning area Nb (ppm)
No significant changes in Nb content were defined. As such, it may be inferred that Nb was immobile during alteration.

41c- Geochemical Alteration:- Glendinning area Pb (ppm)
Substantial increases in the lead content of both altered greywackes and mudstones is clearly defined.

42a- Geochemical Alteration:- Glendinning area Rb (ppm)
The rubidium content of both greywackes and mudstones is subjected to major enrichment during alteration processes. Background and average levels have risen by 40 & 30ppm in greywackes and mudstones respectively.

42b- Geochemical Alteration:- Glendinning area Sr (ppm)
Note that the strontium content mirrors that of rubidium and is enriched in both mudstone and greywacke samples in a similar manner and order of magnitude.

42c- Geochemical Alteration:- Glendinning area Sb (ppm)
The antimony content of both greywacke and mudstone samples are increased during alteration by a factor of 50-1000 compared to background values.

FIGURE 36 a/b/c

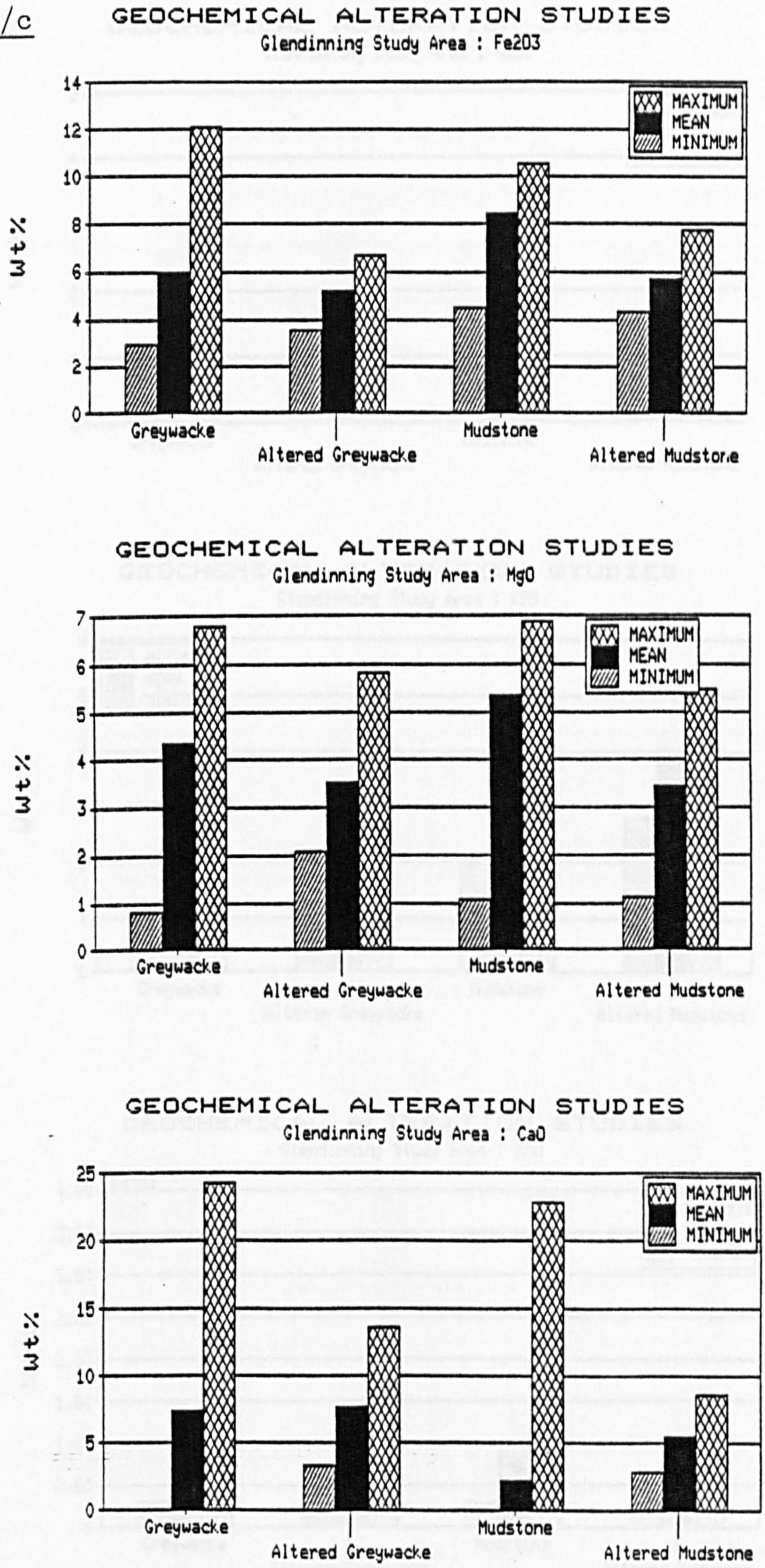

FIGURE 37 a/b/c

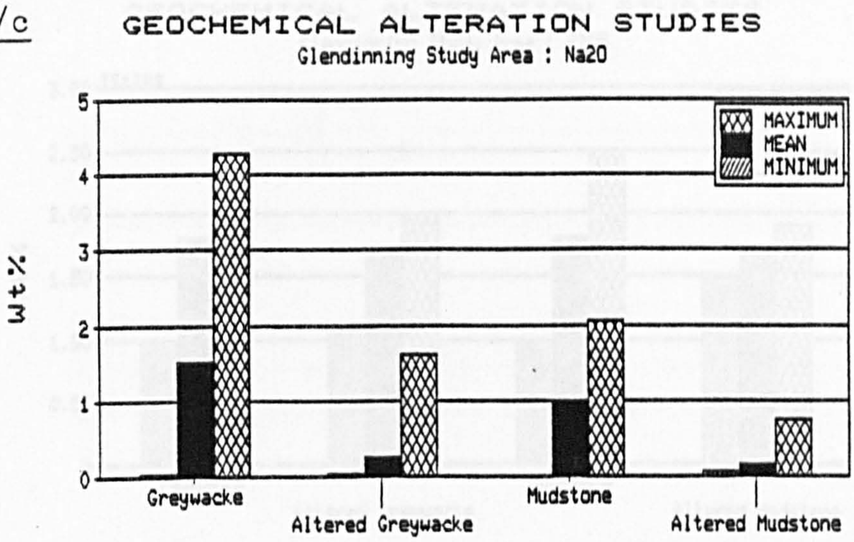

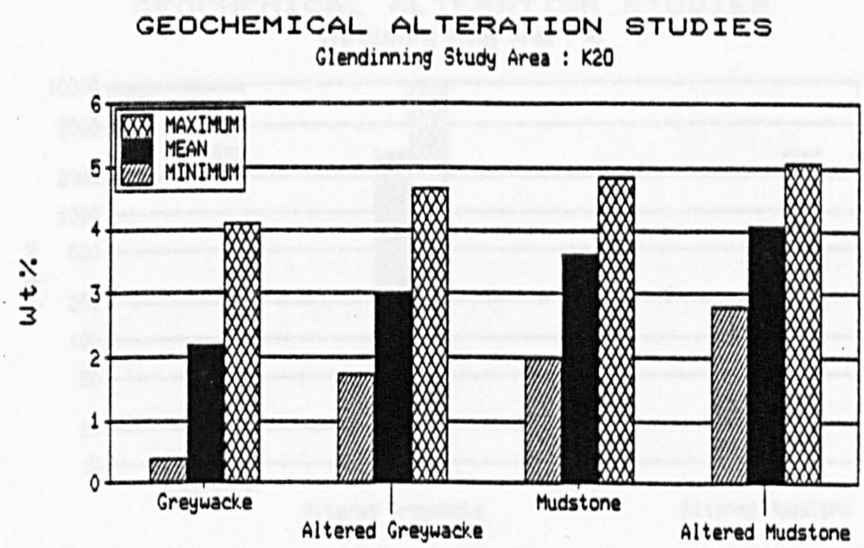

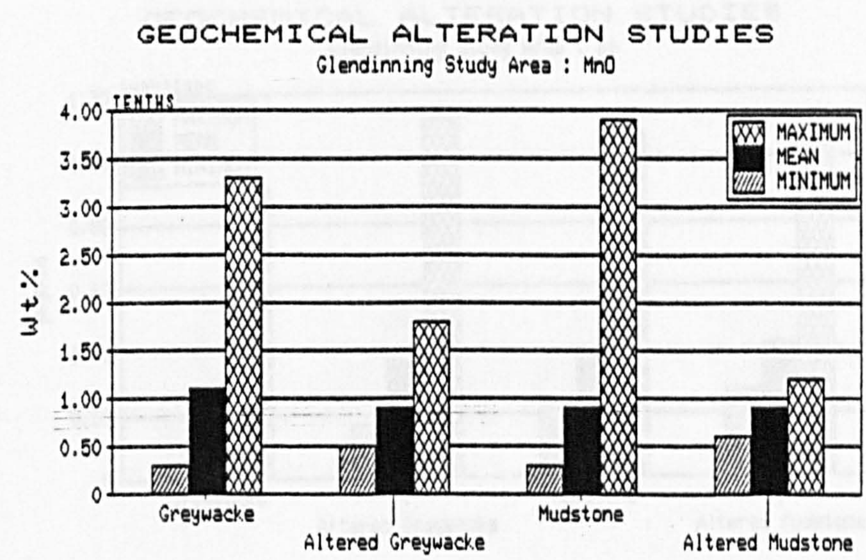

FIGURE 38 a/b/c

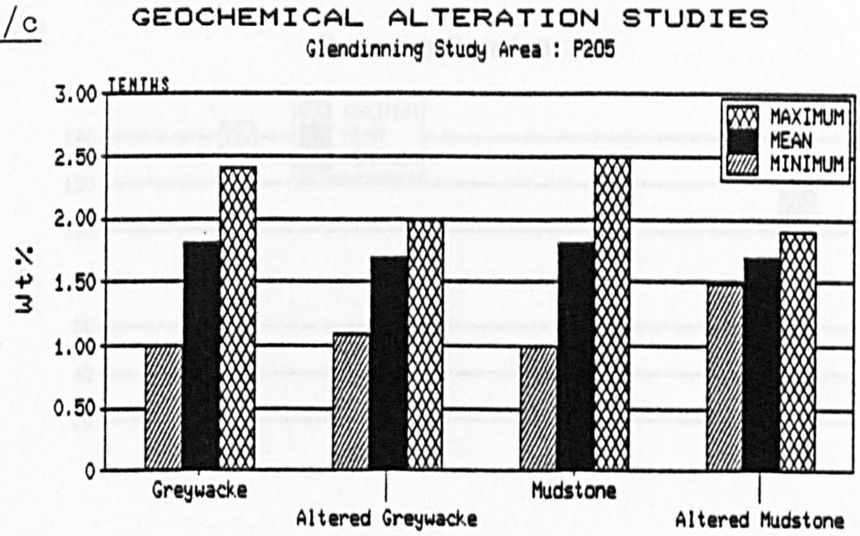

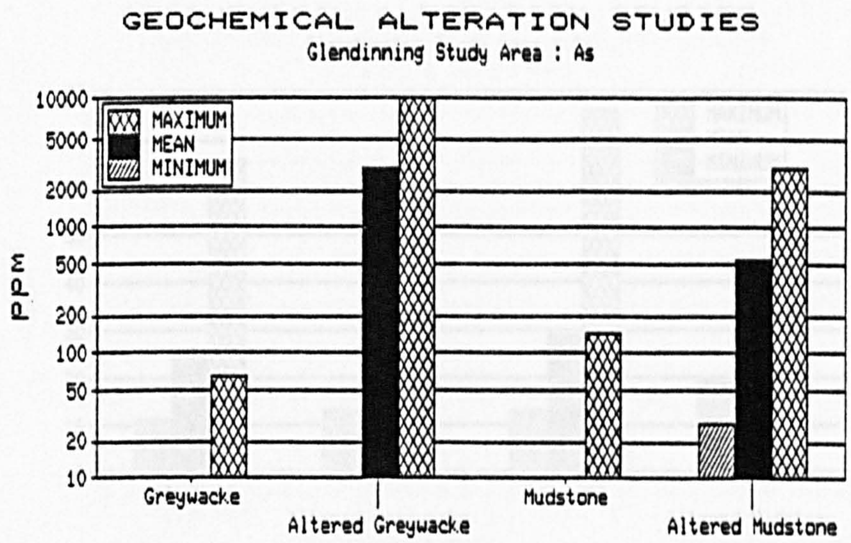

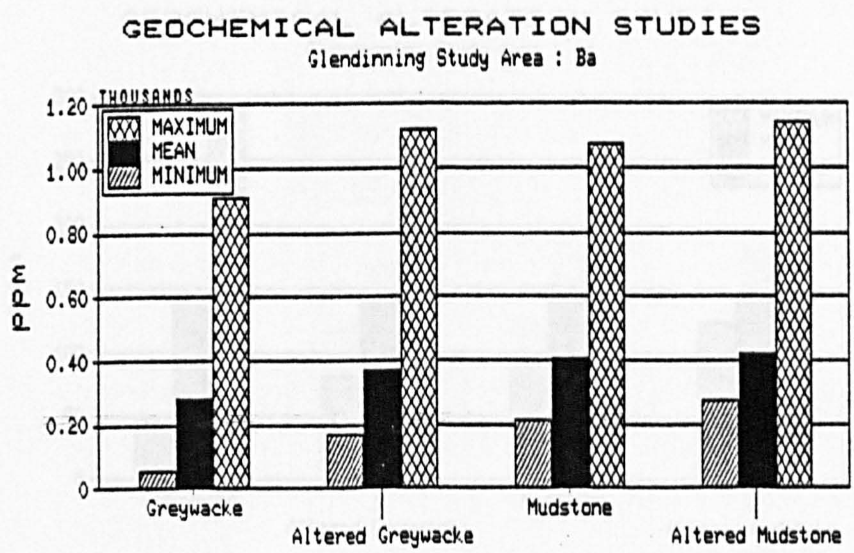

FIGURE 39 a/b/c

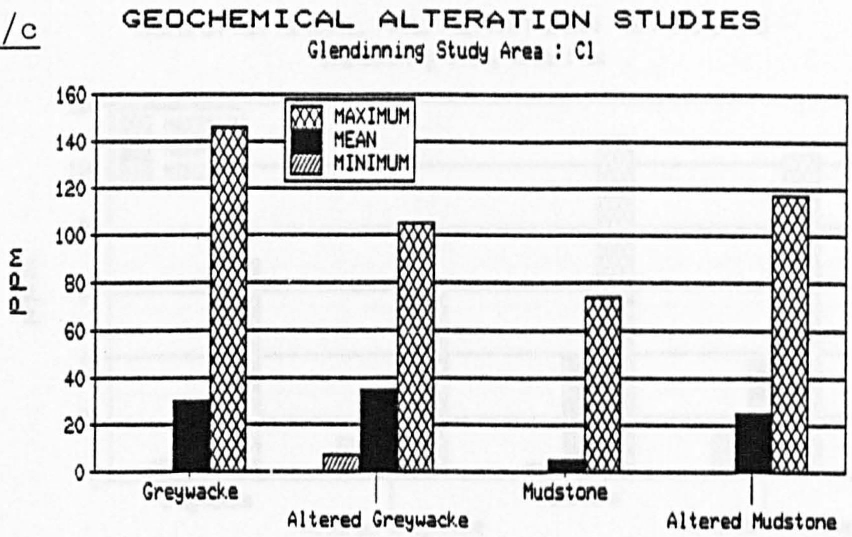

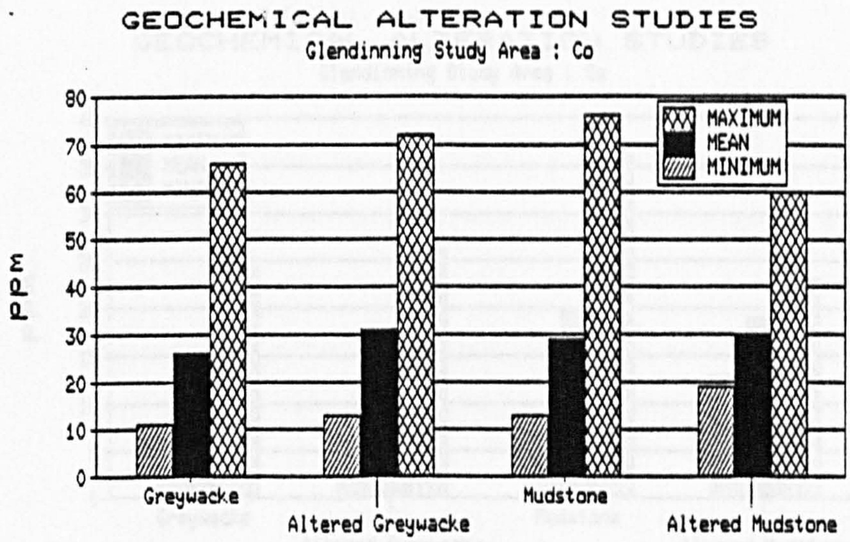

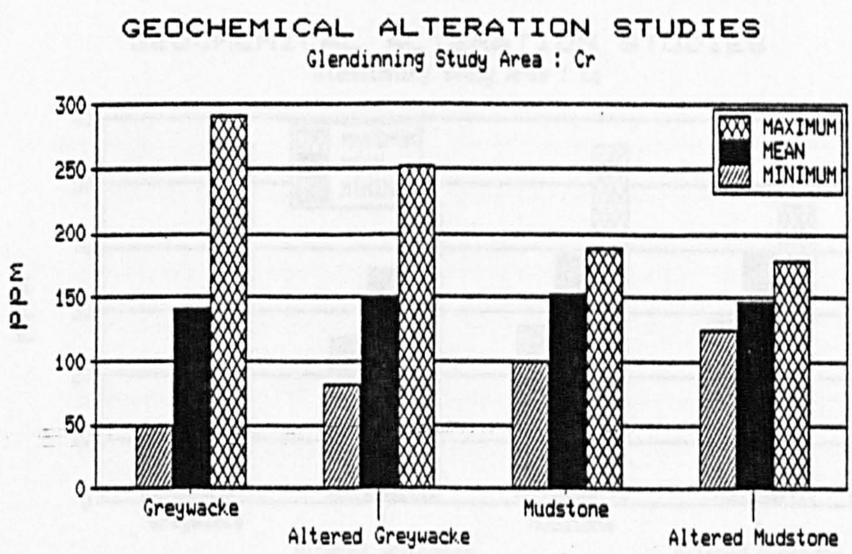

FIGURE 40 a/b/c

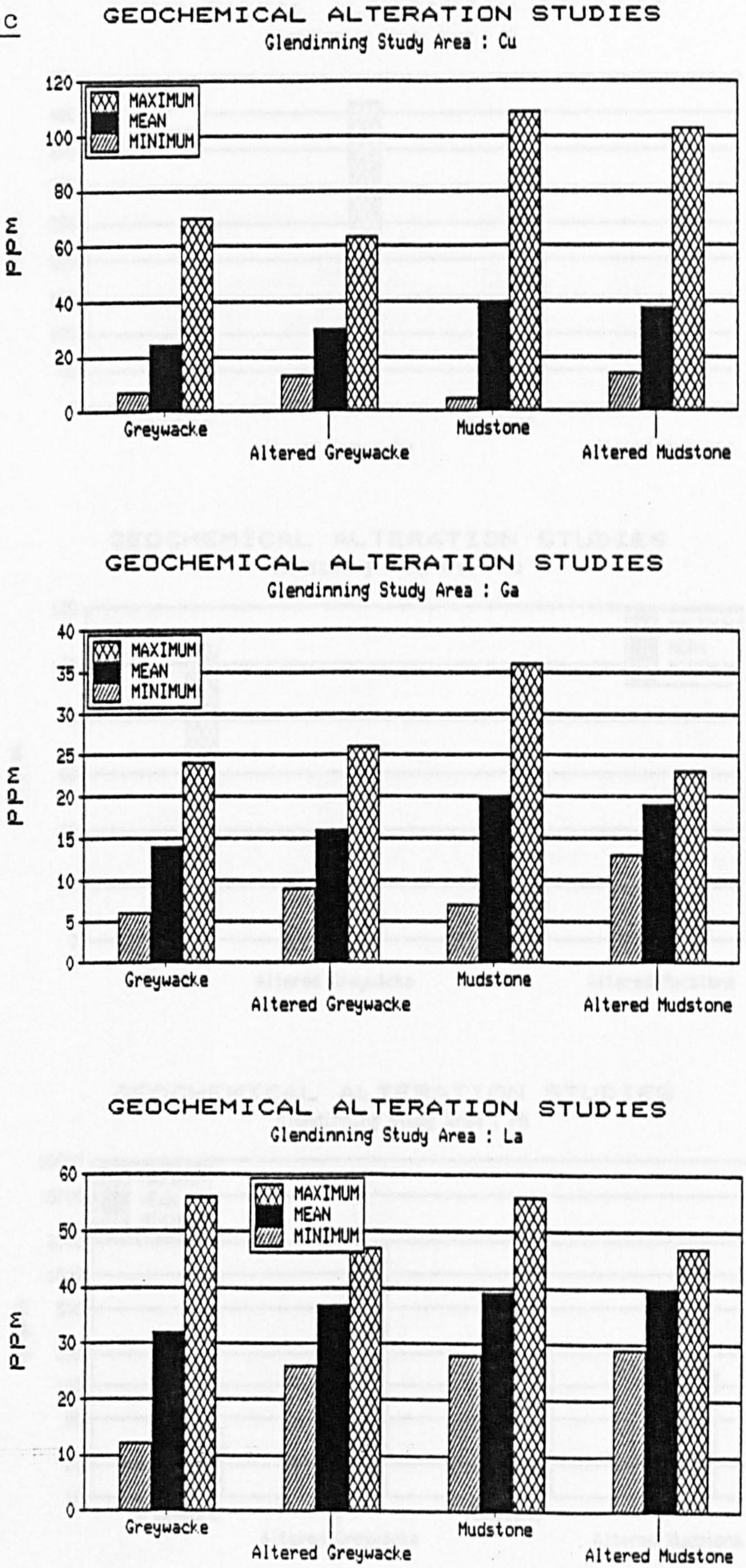

FIGURE 41 a/b/c

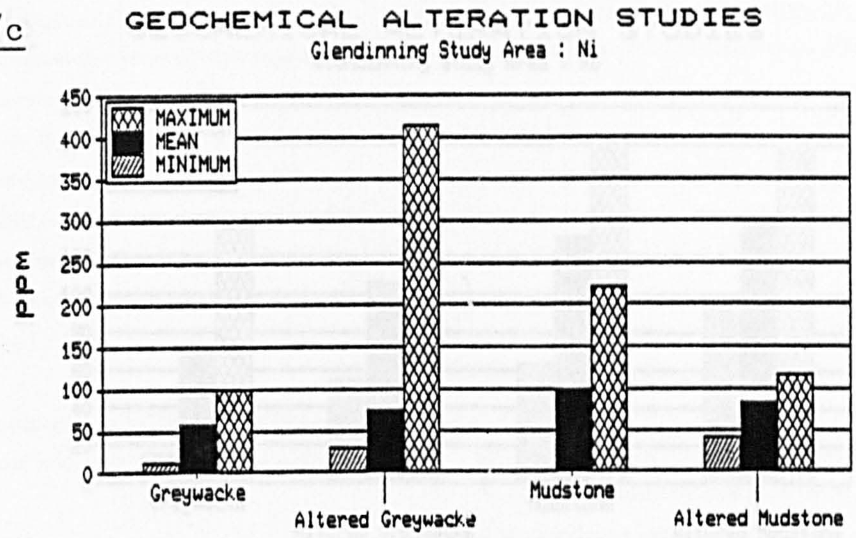

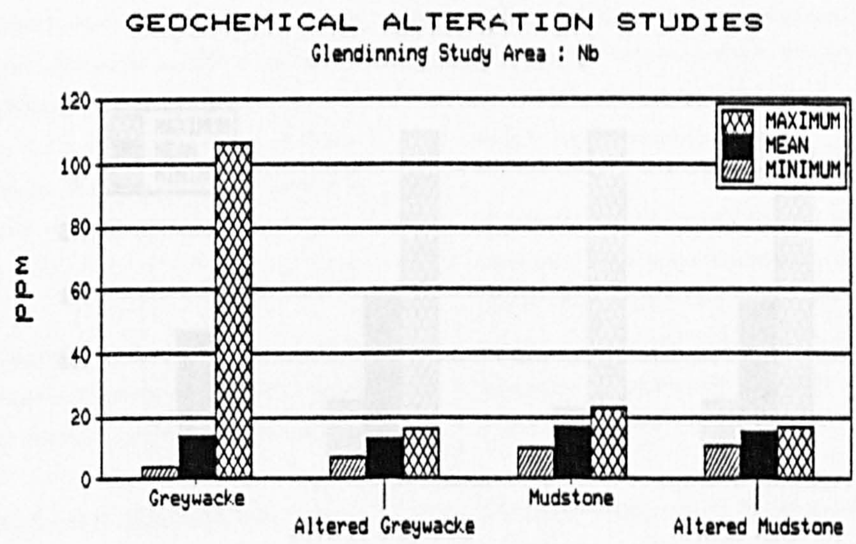

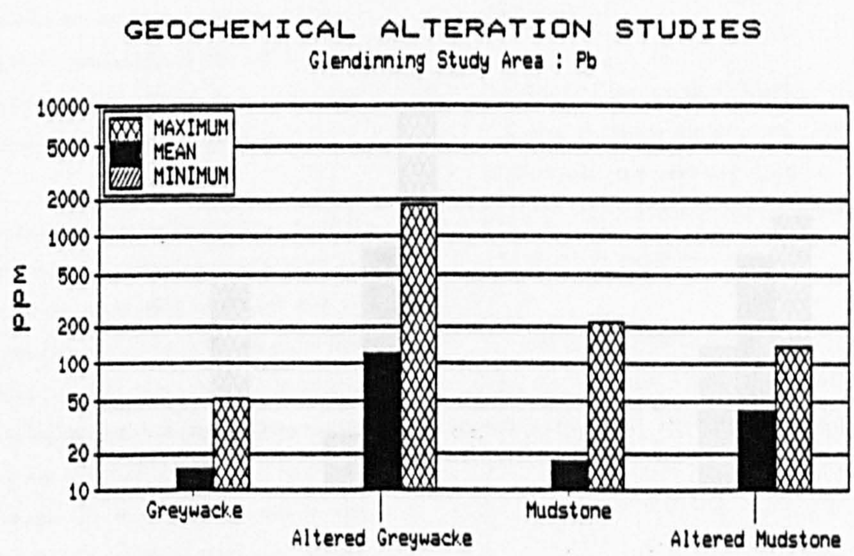

FIGURE 42 a/b/c

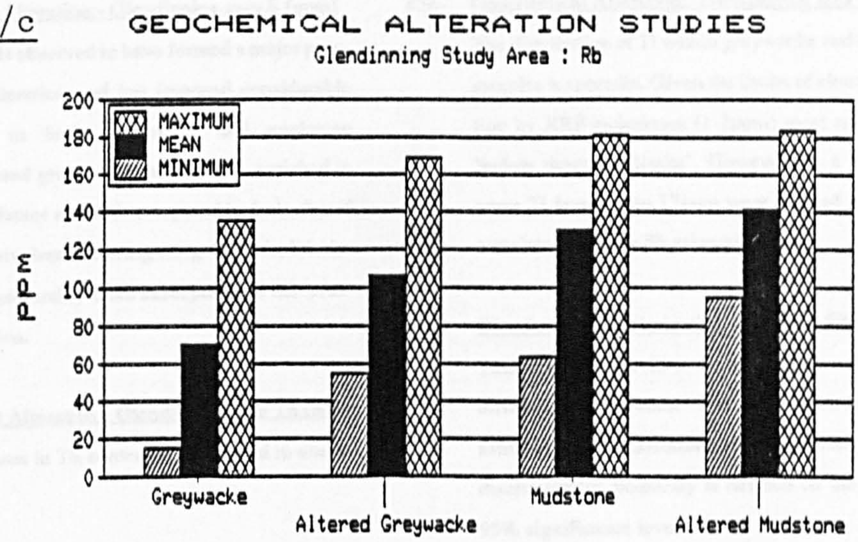

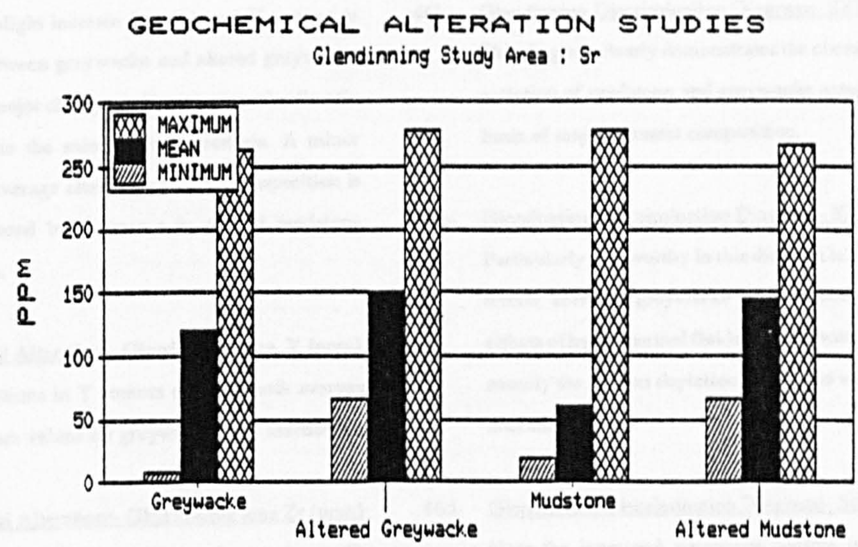

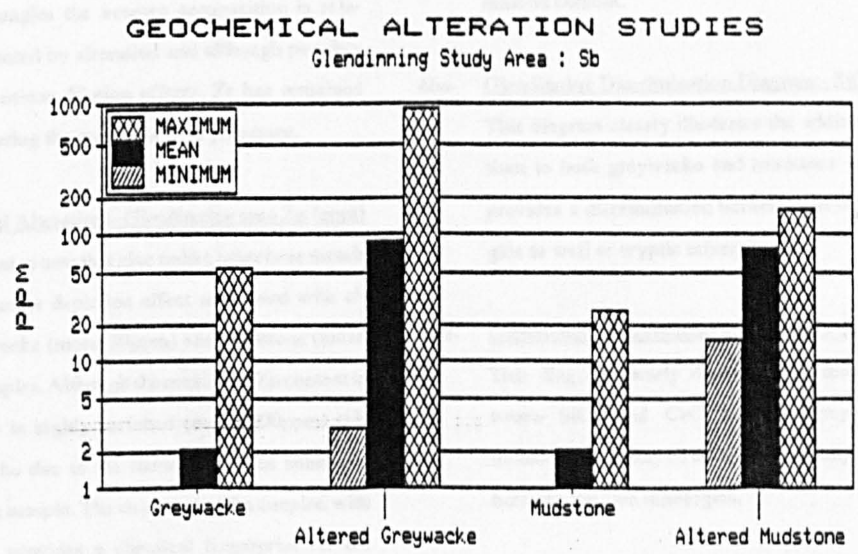

43a- Geochemical Alteration:- Glendinning area S (ppm)
Sulphidation is observed to have formed a major process during alteration and has imposed considerable enrichments in both greywacke and mudstone samples. Altered greywacke samples are enriched in sulphur by a factor of 100% compared to their altered mudstone equivalents inferring that greywacke lithologies were considerably more succeptable to this process of alteration.

43b- Geochemical Alteration:- Glendinning area Th (ppm)
Minor increases in Th content are observed in altered samples.

43c- Geochemical Alteration:- Glendinning area V (ppm)
Although a slight increase in minimum V content is observed between greywacke and altered greywacke samples no major changes in V content can be directly attributable to the mineralising processes. A minor increase in average altered greywacke composition is counterbalanced by decreases in altered mudstone composition.

44a- Geochemical Alteration:- Glendinning area Y (ppm)
Minor depletions in Y content occur in both average and maximum values for greywackes and mudstones.

44b- Geochemical Alteration:- Glendinning area Zr (ppm)
Although characteristic decreases in maximum Zr contents are observed in both altered greywacke and mudstone samples the average composition is relatively unaffected by alteration and although possibly affected by minor dilution effects, Zr has remained immobile during the mineralisation processes.

45a- Geochemical Alteration:- Glendinning area Zn (ppm)
It is important to note that zinc unlike other base metals displays a major depletion effect associated with altered greywacke (mean 30ppm) and mudstone (mean 60ppm) samples. Although the maximum Zn content in greywackes is highly enriched (max 2000ppm) this value may be due to the incorporation of sphalerite (ZnS) in the sample. The depletion of Zn coupled with that of Na provides a chemical fingerprint for the location and identification of Glendinning type deposits in this terrain.

45b- Geochemical Alteration:- Glendinning area Tl (ppm)
The distribution of Tl within greywacke and mudstone samples is sporadic. Given the limits of element detection by XRF techniques (1-2ppm) most analyses fell 'below detection limits'. However, in a number of cases Tl levels upto 17ppm were located and clearly correlated with As-Sb mineralisation.

46a- Glendinning Discrimination Diagram:- SiO_2 vs Al_2O_3
This diagram provides a chemical classification to differentiate between mudstone and greywacke samples from the Glendinning regional study area. The discrimination boundary is defined on the basis of a 95% significance level.

46b- Glendinning Discrimination Diagram:- SiO_2 vs Fe_2O_3
This diagram clearly demonstrates the chemical differentiation of mudstone and greywacke samples on the basis of major element composition.

46c- Glendinning Discrimination Diagram:- SiO_2 vs Na_2O
Particularly noteworthy in this diagram is the differentiation between greywacke and mudstone, and the effects of hydrothermal fluids on upon both lithologies, namely the sodium depletion associated with wallrock alteration.

46d- Glendinning Discrimination Diagram:- SiO_2 vs K_2O
Note the increased potassium content of mudstone samples interpreted as reflecting an increased clay mineral content.

46e- Glendinning Discrimination Diagram:- SiO_2 vs Sr
This diagram clearly illustrates the addition of strontium to both greywacke and mudstone samples and provides a discrimination between individual lithologies as well as cryptic mineralisation.

46f- Glendinning Discrimination Diagram:- SiO_2 vs CaO
This diagram clearly illustrates the relationship between SiO_2 and CaO in both greywackes and mudstones and may be used to chemically differentiate between the two lithologies.

47a- Glendinning Discrimination Diagram:- SiO_2 vs V
Note the increased vanadium content in mudstones

FIGURE 43 a/b/c

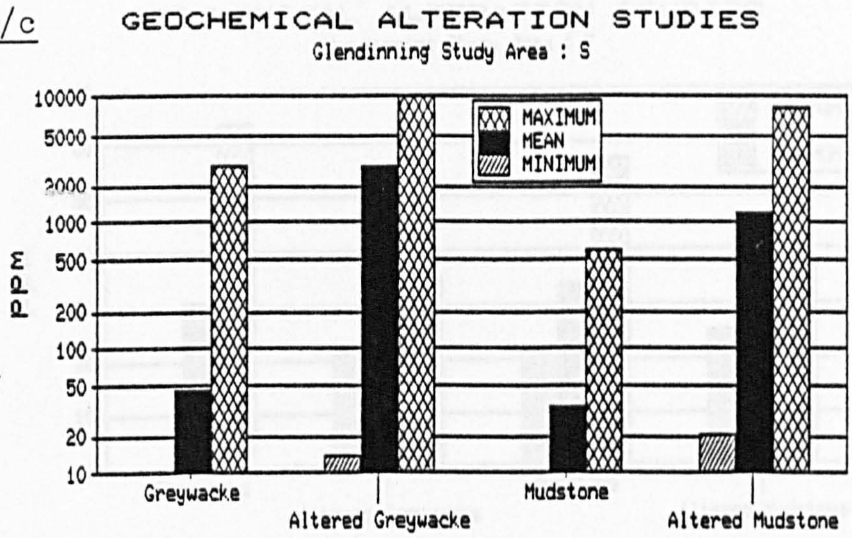

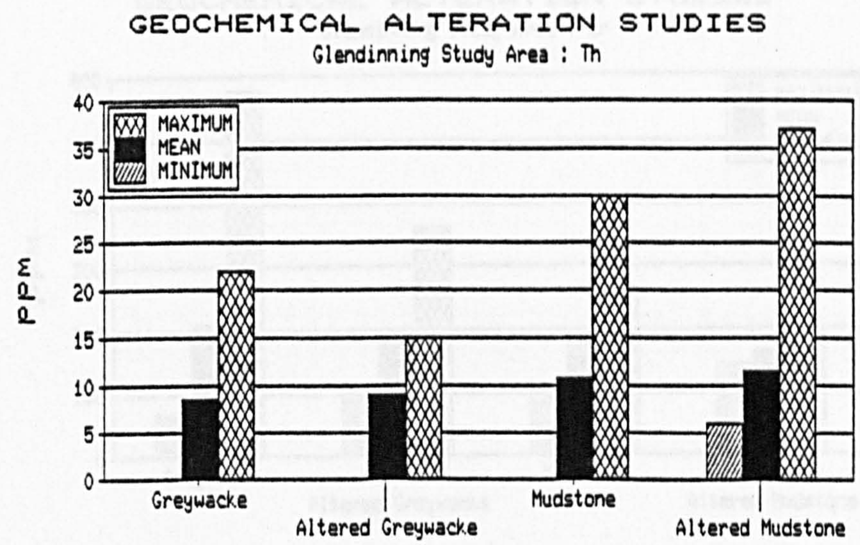

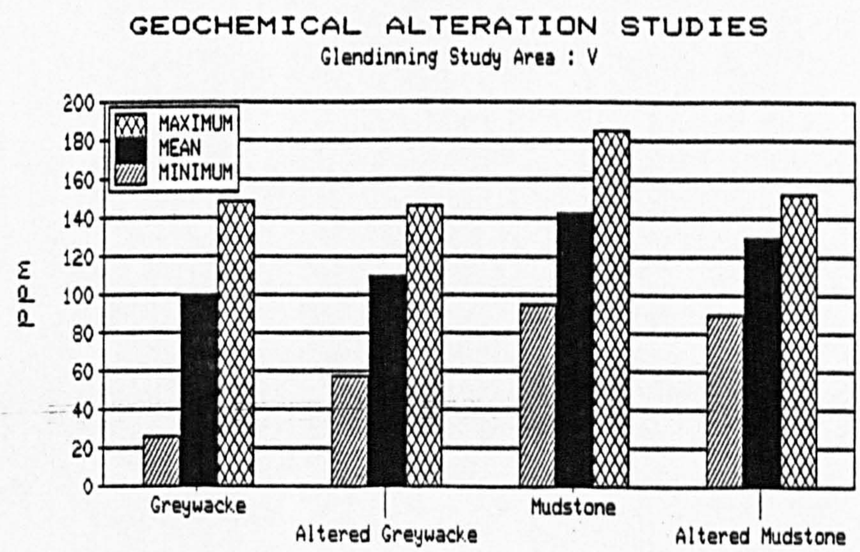

FIGURE 44 a/b

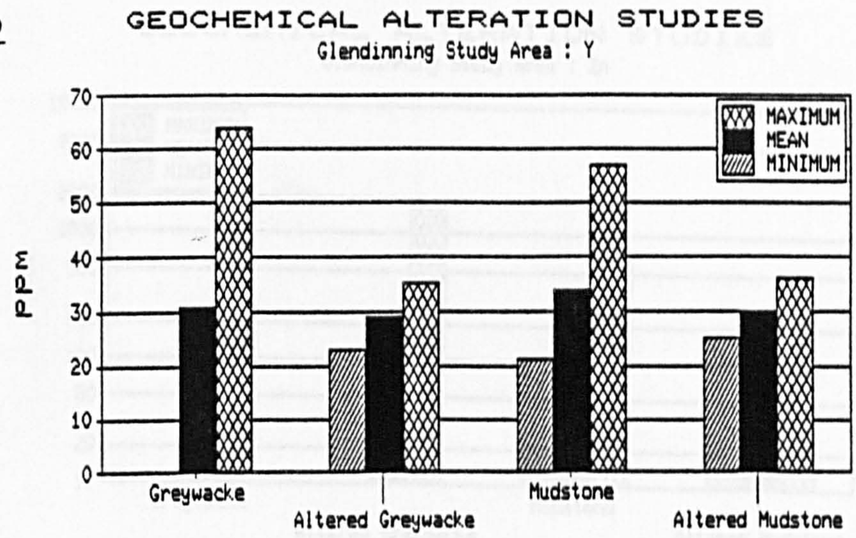
GEOCHEMICAL ALTERATION STUDIES
Glendinning Study Area : Y
PPM
70
60
50
40
30
20
10
0
MAXIMUM
MEAN
MINIMUM
Greywacke
Altered Greywacke
Mudstone
Altered Mudstone

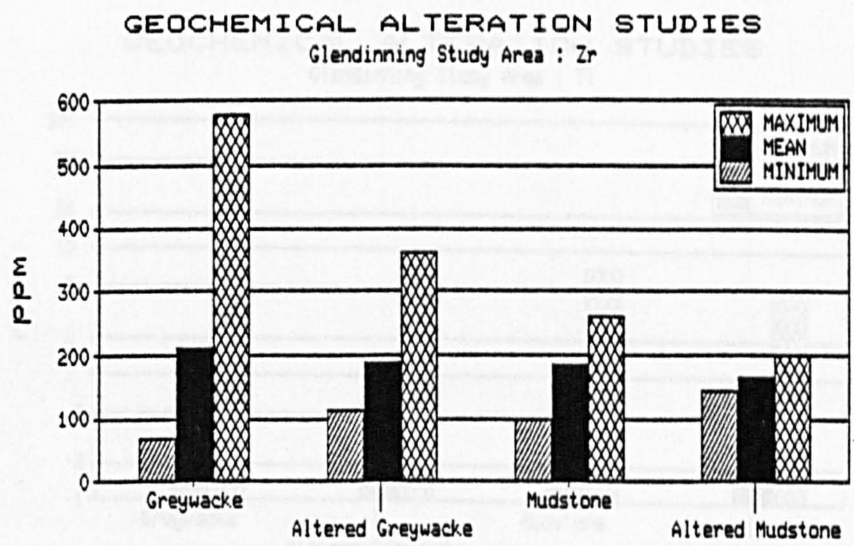
GEOCHEMICAL ALTERATION STUDIES
Glendinning Study Area : Zr
PPM
600
500
400
300
200
100
0
MAXIMUM
MEAN
MINIMUM
Greywacke
Altered Greywacke
Mudstone
Altered Mudstone

FIGURE 45 a/b

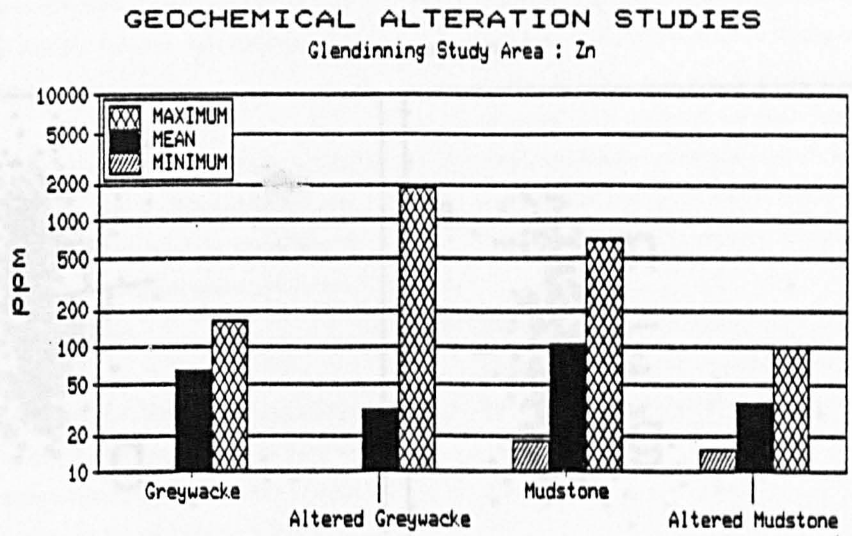
GEOCHEMICAL ALTERATION STUDIES
Glendinning Study Area : Zn
10000
5000
2000
1000
500
200
100
50
20
10
ppm
MAXIMUM
MEAN
MINIMUM
Greywacke
Altered Greywacke
Mudstone
Altered Mudstone

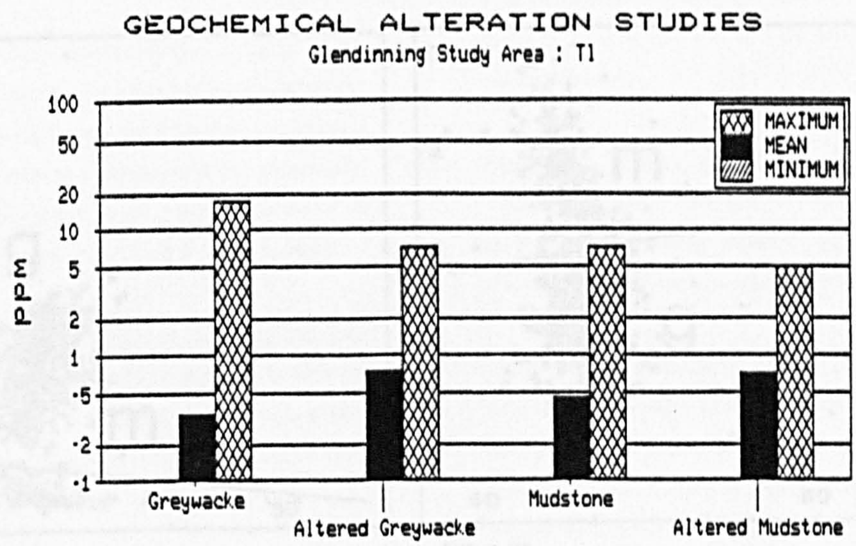
GEOCHEMICAL ALTERATION STUDIES
Glendinning Study Area : Tl
100
50
20
10
5
2
1
·5
·2
·1
ppm
MAXIMUM
MEAN
MINIMUM
Greywacke
Altered Greywacke
Mudstone
Altered Mudstone

FIGURE 46 a-f

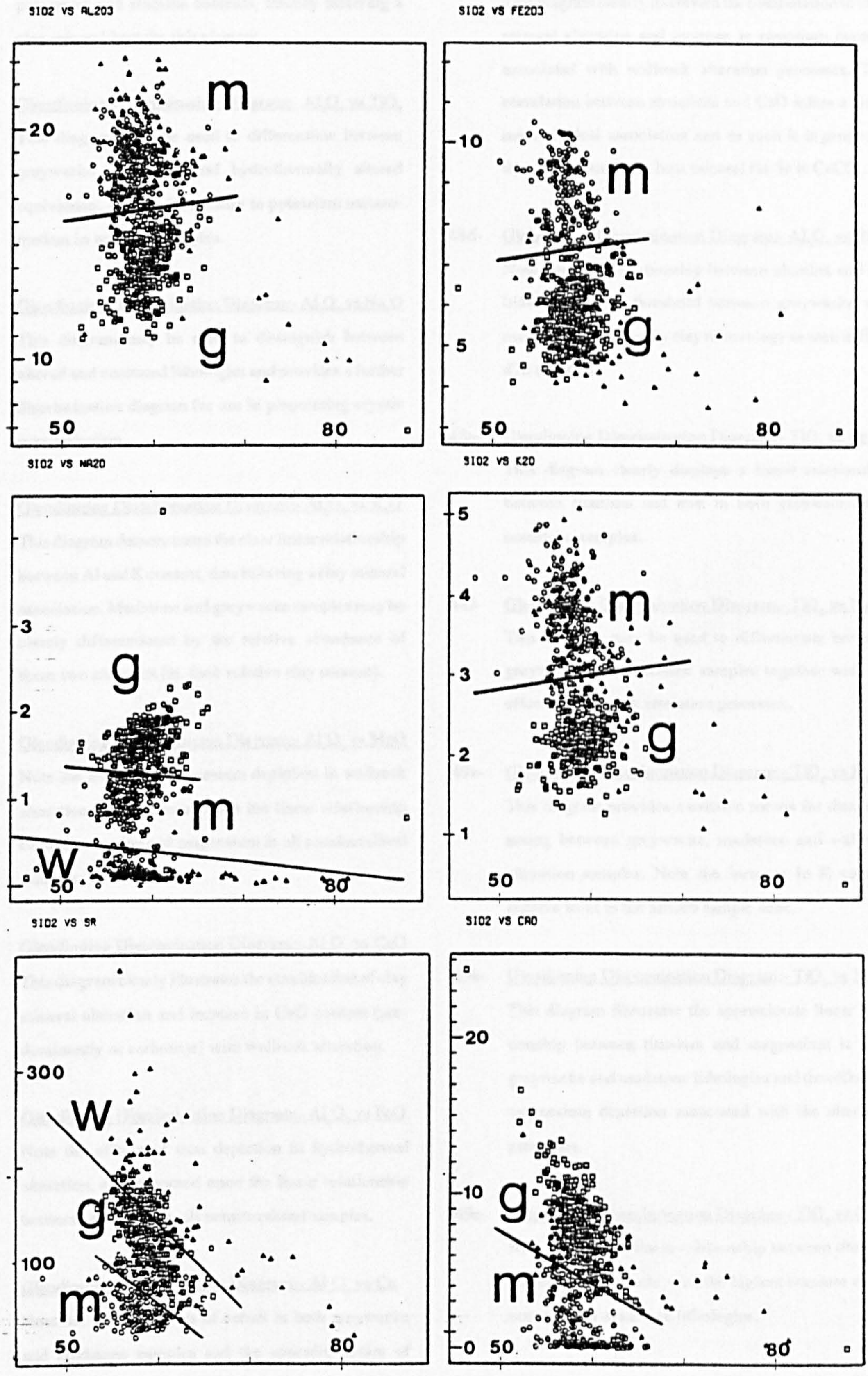

G - Greywacke, M - Mudstone, W - Wallrock Alteration

which correlates well with similar increases in both potassium and alumina contents, thereby inferring a clay mineral host for this element.

47b- Glendinning Discrimination Diagram:- Al_2O_3 vs TiO_2
This diagram may be used to differentiate between greywacke, mudstone and hydrothermally altered equivalents, due predominantly to potassium metasomatism in wallrock samples.

47c- Glendinning Discrimination Diagram:- Al_2O_3 vs Na_2O
This diagram may be used to distinguish between altered and unaltered lithologies and provides a further discrimination diagram for use in pinpointing cryptic mineralisation.

47d- Glendinning Discrimination Diagram:- Al_2O_3 vs K_2O
This diagram demonstrates the clear linear relationship between Al and K content, thus inferring a clay mineral association. Mudstone and greywacke samples may be clearly differentiated by the relative abundance of these two elements (ie. their relative clay content).

47e- Glendinning Discrimination Diagram:- Al_2O_3 vs MgO
Note the effects of magnesium depletion in wallrock alteration, superimposed upon the linear relationship between alumina and magnesium in all unmineralised samples.

47f- Glendinning Discrimination Diagram:- Al_2O_3 vs CaO
This diagram clearly illustrates the combination of clay mineral alteration and increase in CaO content (predominantly as carbonate) with wallrock alteration.

48a- Glendinning Discrimination Diagram:- Al_2O_3 vs FeO
Note the effects of iron depletion in hydrothermal alteration, superimposed upon the linear relationship between Al and Fe in all unmineralised samples.

48b- Glendinning Discrimination Diagram:- Al_2O_3 vs Co
Note the uniform levels of cobalt in both greywacke and mudstone samples and the sporadic nature of cobalt enrichment associated with mineralised samples.

48c- Glendinning Discrimination Diagram:- Al_2O_3 vs Sr
This diagram clearly illustrates the combination of clay mineral alteration and increase in strontium content associated with wallrock alteration processes. The correlation between strontium and CaO infers a close mineralogical association and as such it is proposed that the predominant host mineral for Sr is $CaCO_3$.

48d- Glendinning Discrimination Diagram:- Al_2O_3 vs Rb
Note the linear relationship between alumina and rubidium with the threshold between greywacke and mudstone controlled by clay mineralogy as seen in figs. 47d and 48a.

48e- Glendinning Discrimination Diagram:- TiO_2 vs Fe_2O_3
This diagram clearly displays a linear relationship between titanium and iron in both greywacke and mudstone samples.

48f- Glendinning Discrimination Diagram:- TiO_2 vs Na_2O
This diagram may be used to differentiate between greywacke and mudstone samples together with the effects of wallrock alteration processes.

49a- Glendinning Discrimination Diagram:- TiO_2 vs K_2O
This diagram provides a suitable means for discriminating between greywacke, mudstone and wallrock alteration samples. Note the increase in K content relative to Ti in the altered sample suite.

49b- Glendinning Discrimination Diagram:- TiO_2 vs MgO
This diagram illustrates the approximate linear relationship between titanium and magnesium in both greywacke and mudstone lithologies and the effects of magnesium depletion associated with the alteration processes.

49c- Glendinning Discrimination Diagram:- TiO_2 vs CaO
Note the inverse linear relationship between titanium and calcium contents, with the highest titanium values occurring in mudstone lithologies.

49d- Glendinning Discrimination Diagram:- TiO_2 vs Rb
This diagram clearly illustrates the addition of rubidium during hydrothermal alteration of both lithologies.

FIGURE 47 a-f

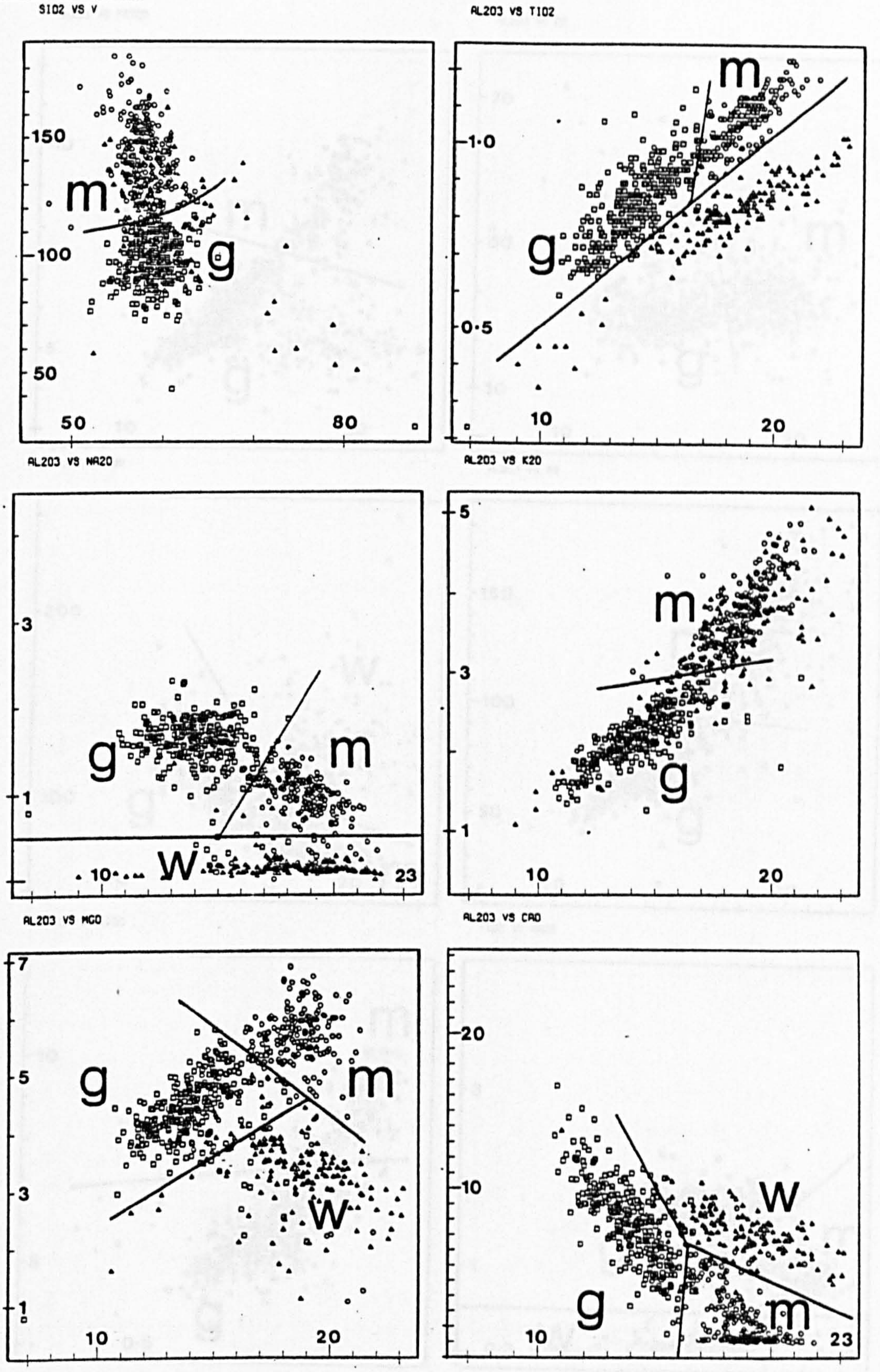

G - Greywacke, M - Mudstone, W - Wallrock Alteration

FIGURE 48 a-f

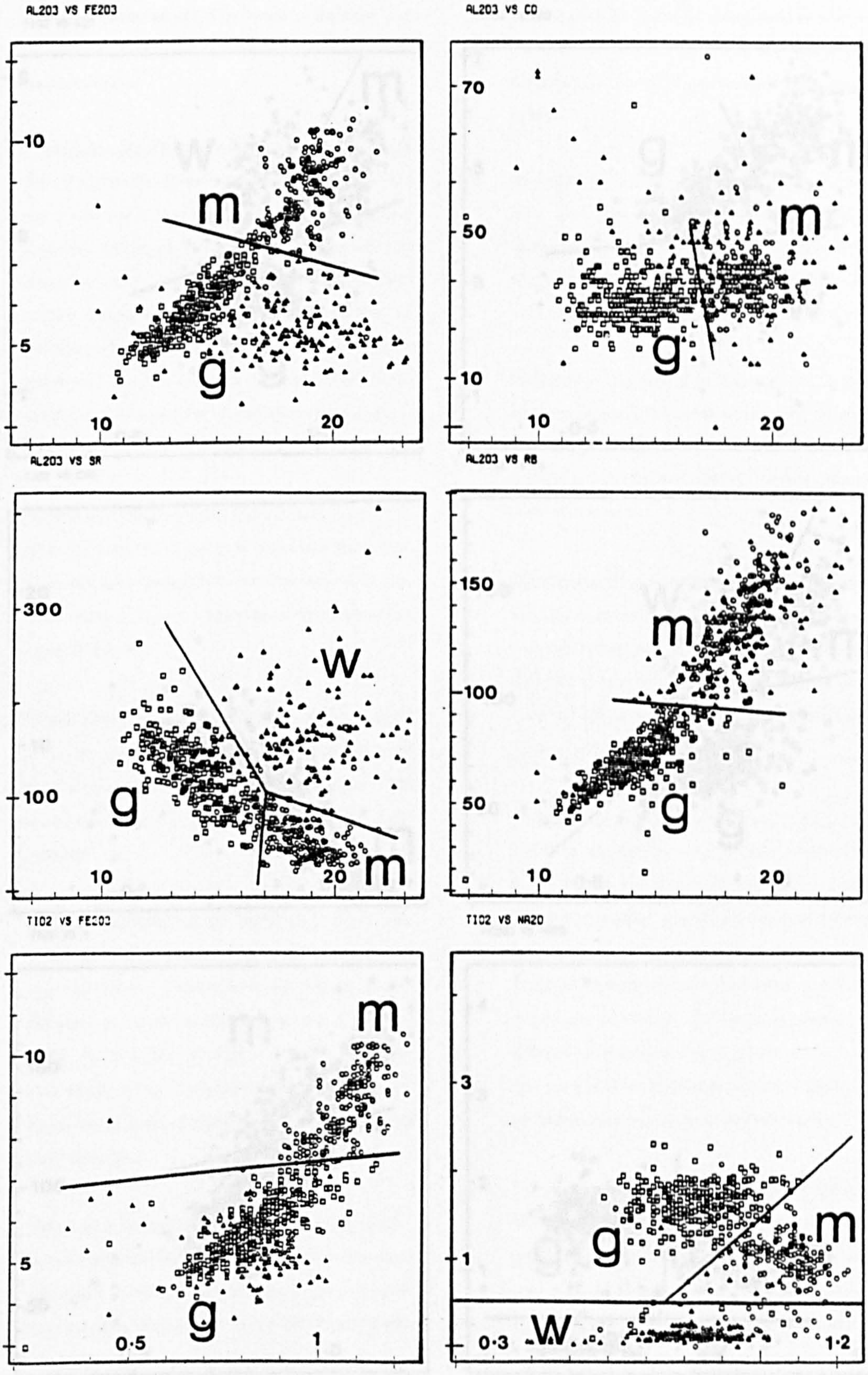

G - Greywacke, M - Mudstone, W - Wallrock Alteration

FIGURE 49 a-f

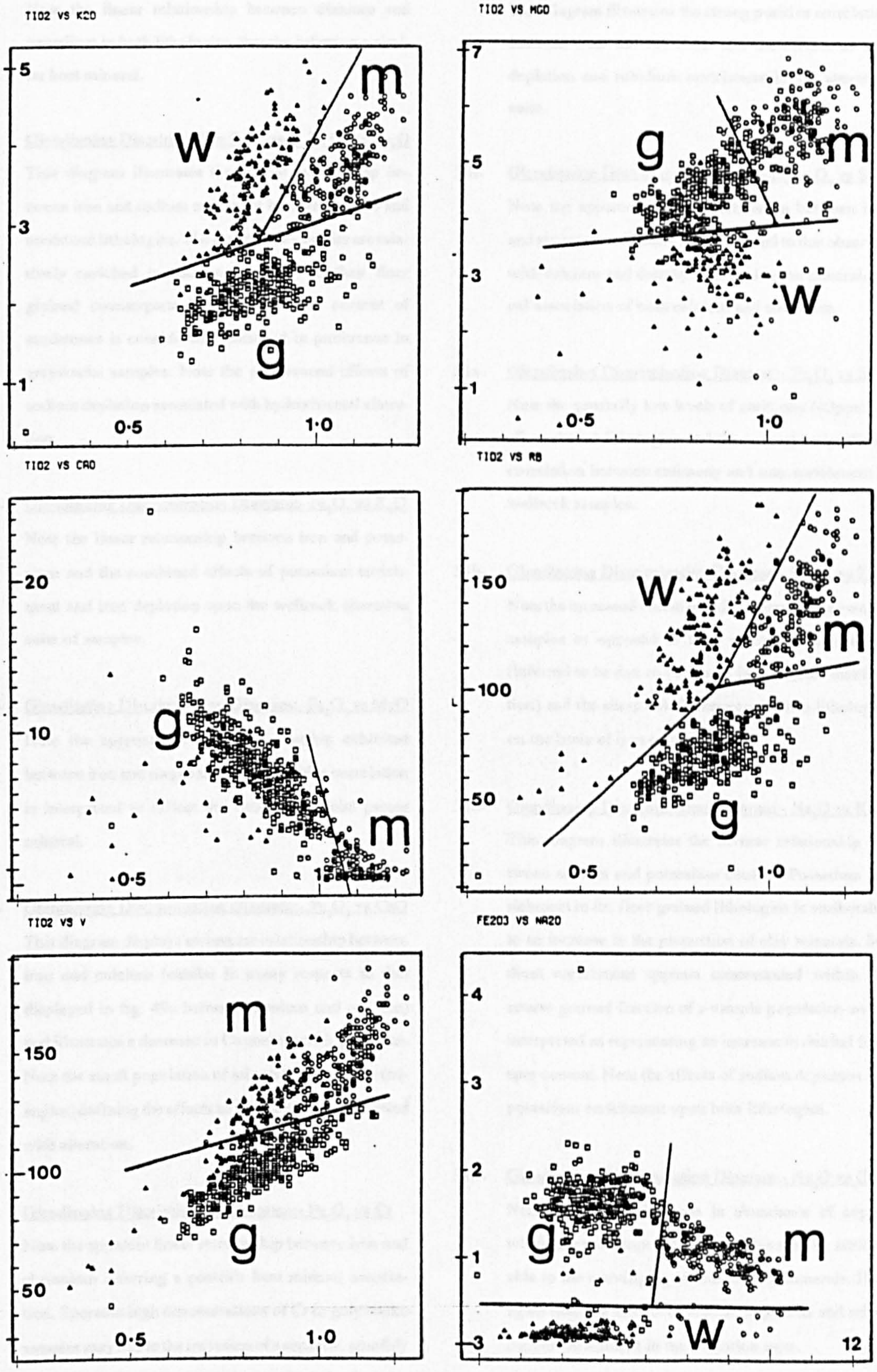

G - Greywacke, M - Mudstone, W - Wallrock Alteration

49e- Glendinning Discrimination Diagram:- TiO_2 vs V
Note the linear relationship between titanium and vanadium in both lithologies, thereby inferring a similar host mineral.

49f- Glendinning Discrimination Diagram:- Fe_2O_3 vs Na_2O
This diagram illustrates the spatial relationship between iron and sodium content of both greywacke and mudstone lithologies. The greywacke samples are relatively enriched in sodium compared to their finer grained counterparts however the iron content of mudstones is considerably enriched in preference to greywacke samples. Note the pronounced effects of sodium depletion associated with hydrothermal alteration.

50a- Glendinning Discrimination Diagram:- Fe_2O_3 vs K_2O
Note the linear relationship between iron and potassium and the combined effects of potassium enrichment and iron depletion upon the wallrock alteration suite of samples.

50b- Glendinning Discrimination Diagram:- Fe_2O_3 vs MgO
Note the approximate linear relationship exhibited between iron and magnesium. This positive correlation is interpreted to reflect the nature of a joint parent mineral.

50c- Glendinning Discrimination Diagram:- Fe_2O_3 vs CaO
This diagram displays an inverse relationship between iron and calcium (similar in many respects to that displayed in fig. 49c between titanium and calcium) and illustrates a decrease in Ca content with grain size. Note the small population of mineralised samples (triangles) defining the effects of iron depletion associated with alteration.

50d- Glendinning Discrimination Diagram:- Fe_2O_3 vs Cr
Note the apparent linear relationship between iron and chromium inferring a possible host mineral association. Sporadic high concentrations of Cr in greywacke samples may due to the inclusion of a separate, possibly monomineralic source, such as detrital chromite grains.

50e- Glendinning Discrimination Diagram:- Fe_2O_3 vs Rb
This diagram illustrates the strong positive correlation between iron and rubidium and the effects of iron depletion and rubidium enrichment in the alteration suite.

50f- Glendinning Discrimination Diagram:- Fe_2O_3 vs Sr
Note the apparent inverse relationship between iron and strontium reflecting a similar trend to that observed with calcium and thereby reaffirming the mineralogical association of both calcium and strontium.

51a- Glendinning Discrimination Diagram:- Fe_2O_3 vs Sb
Note the generally low levels of antimony (<3ppm) in all unaltered lithologies and the lack of a significant correlation between antimony and iron enrichment in wallrock samples.

51b- Glendinning Discrimination Diagram:- Fe_2O_3 vs Zr
Note the increased variation in Zr content in greywacke samples as opposed to their mudstone equivalents (inferred to be due to variances in grain size distribution) and the sharp cutoff between the two lithologies on the basis of iron content.

51c- Glendinning Discrimination Diagram:- Na_2O vs K_2O
This diagram illustrates the inverse relationship between sodium and potassium content. Potassium enrichment in the finer grained lithologies is attributable to an increase in the proportion of clay minerals. Sodium enrichment appears concentrated within the course grained fraction of a sample population and is interpreted as representing an increase in detrital feldspar content. Note the effects of sodium depletion and potassium enrichment upon both lithologies.

51d- Glendinning Discrimination Diagram:- Na_2O vs Cu
Note the general increase in abundance of copper within the mudstone lithologies. This may be attributable to the scavenging effects of clay minerals. Here again note the effects of sodium depletion and minor copper enrichment in the alteration suite.

51e- Glendinning Discrimination Diagram:- Na_2O vs Co
Note the narrow range of cobalt composition present in both lithologies and the effects of minor cobalt enrich-

FIGURE 50 a-f

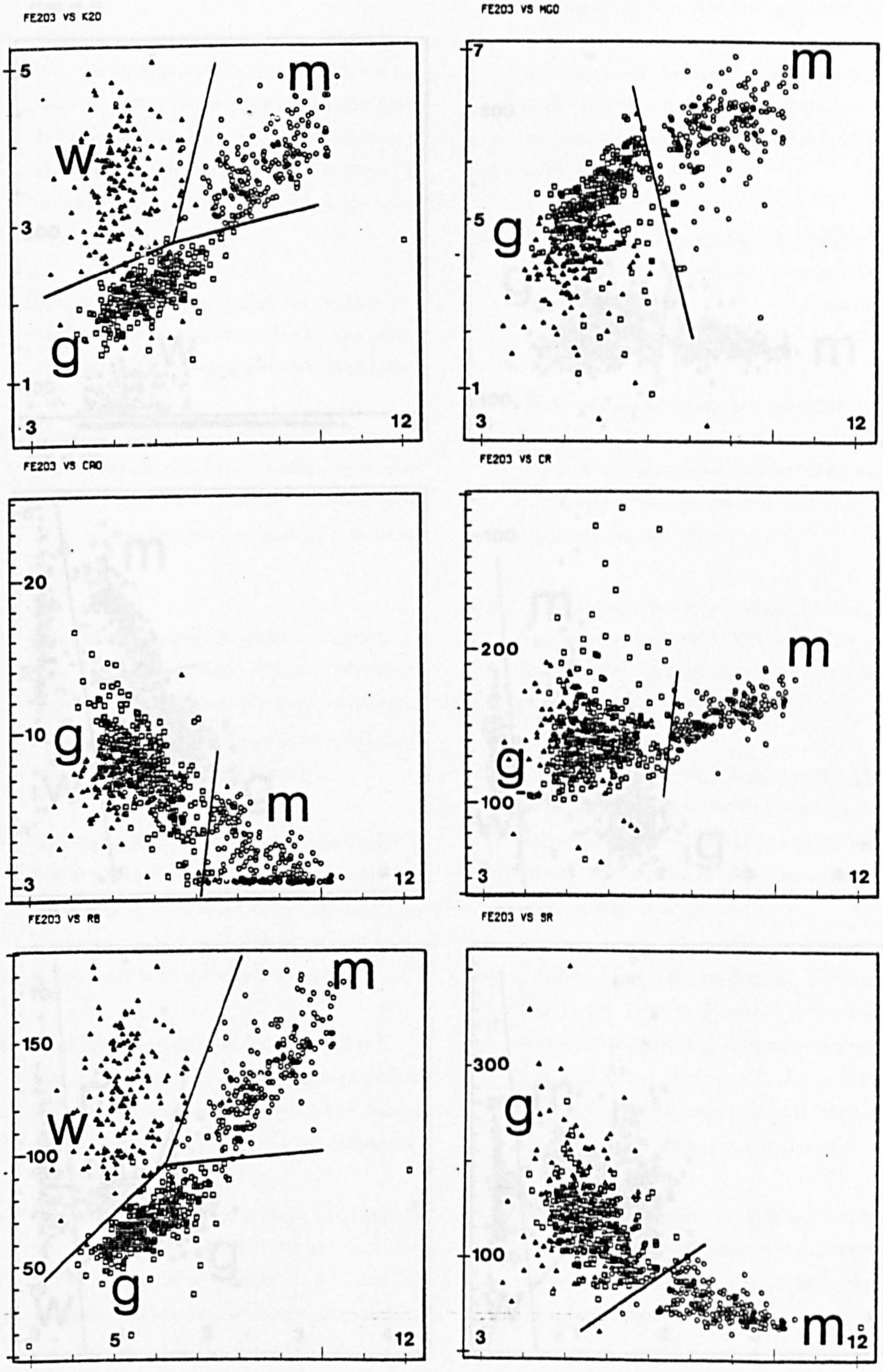

G - Greywacke, M - Mudstone, W - Wallrock Alteration

FIGURE 51 a-f

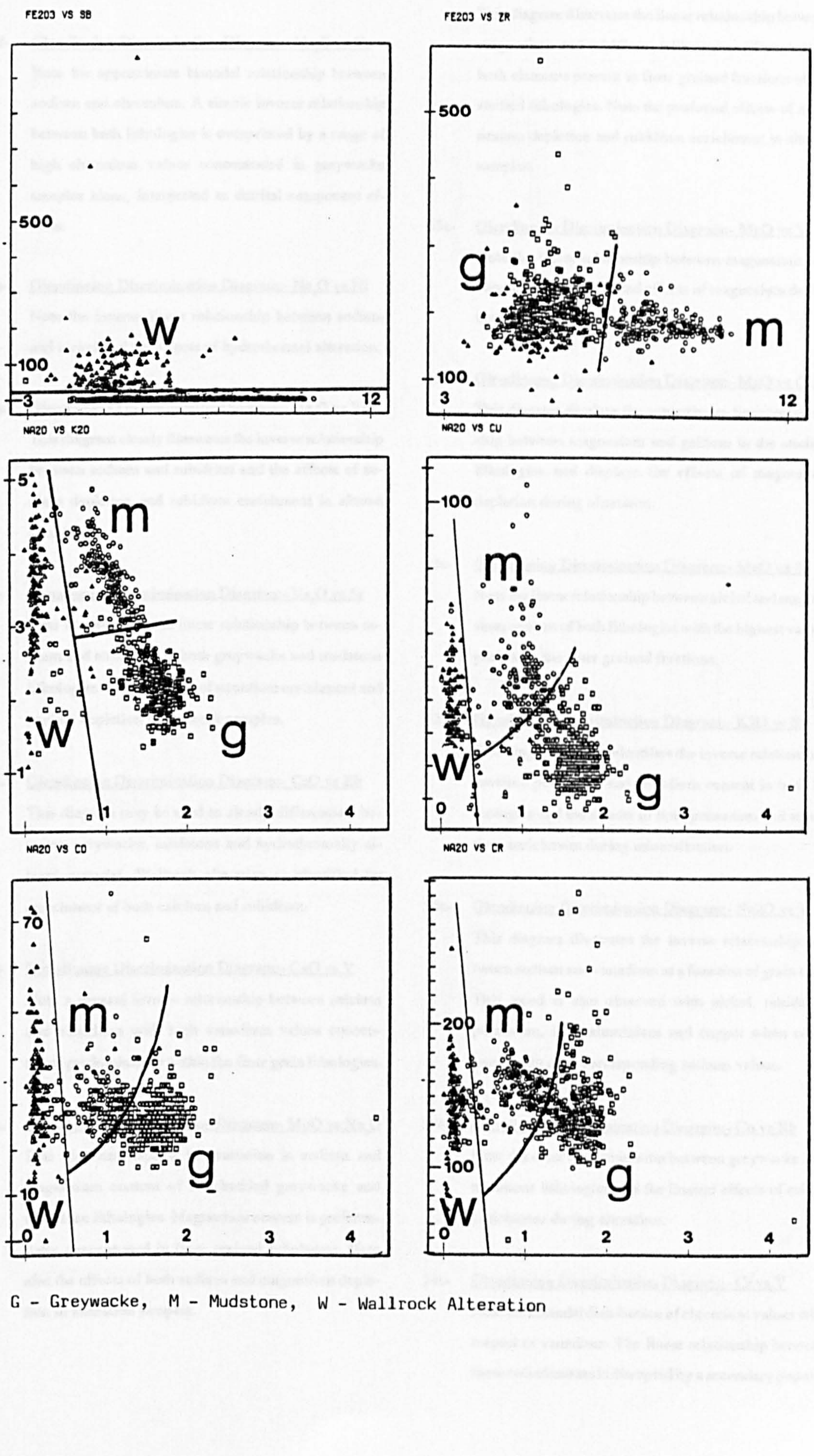

G - Greywacke, M - Mudstone, W - Wallrock Alteration

ment during hydrothermal alteration.

51f- Glendinning Discrimination Diagram:- Na_2O vs Cr
Note the approximate bimodal relationship between sodium and chromium. A simple inverse relationship between both lithologies is overprinted by a range of high chromium values concentrated in greywacke samples alone, interpreted as detrital component effects.

52a- Glendinning Discrimination Diagram:- Na_2O vs Ni
Note the inverse linear relationship between sodium and nickel and the effects of hydrothermal alteration.

52b- Glendinning Discrimination Diagram:- Na_2O vs Rb
This diagram clearly illustrates the inverse relationship between sodium and rubidium and the effects of sodium depletion and rubidium enrichment in altered samples.

52c- Glendinning Discrimination Diagram:- Na_2O vs Sr
Note the approximate linear relationship between sodium and strontium in both greywacke and mudstone lithologies and the effects of strontium enrichment and sodium depletion in wallrock samples.

52e- Glendinning Discrimination Diagram:- CaO vs Rb
This diagram may be used to clearly differentiate between greywacke, mudstone and hydrothermally altered material. Wallrock alteration is identified by enrichment of both calcium and rubidium.

52f- Glendinning Discrimination Diagram:- CaO vs V
Note a general inverse relationship between calcium and vanadium with high vanadium values concentrated predominantly within the finer grain lithologies.

53a- Glendinning Discrimination Diagram:- MgO vs Na_2O
This diagram displays the variation in sodium and magnesium content of interbedded greywacke and mudstone lithologies. Magnesium content is preferentially concentrated in finer grained lithologies. Note also the effects of both sodium and magnesium depletion in alteration samples.

53b- Glendinning Discrimination Diagram:- MgO vs Rb
This diagram illustrates the linear relationship between magnesium and rubidium, with increased content of both elements present in finer grained fractions of the studied lithologies. Note the profound effects of magnesium depletion and rubidium enrichment in altered samples.

53c- Glendinning Discrimination Diagram:- MgO vs V
Note the linear relationship between magnesium and vanadium and the limited effects of magnesium depletion on the sample population.

53d- Glendinning Discrimination Diagram:- MgO vs Ga
This diagram displays the approximate linear relationship between magnesium and gallium in the studied lithologies and displays the effects of magnesium depletion during alteration.

53e- Glendinning Discrimination Diagram:- MgO vs Ni
Note the linear relationship between nickel and magnesium content of both lithologies with the highest values present in the finer grained fractions.

53f- Glendinning Discrimination Diagram:- K2O vs Sr
This diagram clearly identifies the inverse relationship between potassium and strontium content in both lithologies and the effects of both potassium and strontium enrichment during mineralisation.

54a- Glendinning Discrimination Diagram:- Na2O vs V
This diagram illustrates the inverse relationship between sodium and vanadium as a function of grain size. This trend is also observed with nickel, rubidium, potassium, iron, aluminium and copper when compared with their corresponding sodium values.

54b- Glendinning Discrimination Diagram:- Co vs Rb
Note the clear discrimination between greywacke and mudstone lithologies and the limited effects of cobalt enrichment during alteration.

54c- Glendinning Discrimination Diagram:- Cr vs V
Note the bimodal distribution of chromium values with respect to vanadium. The linear relationship between these two elements is disrupted by a secondary popula-

FIGURE 52 a-f

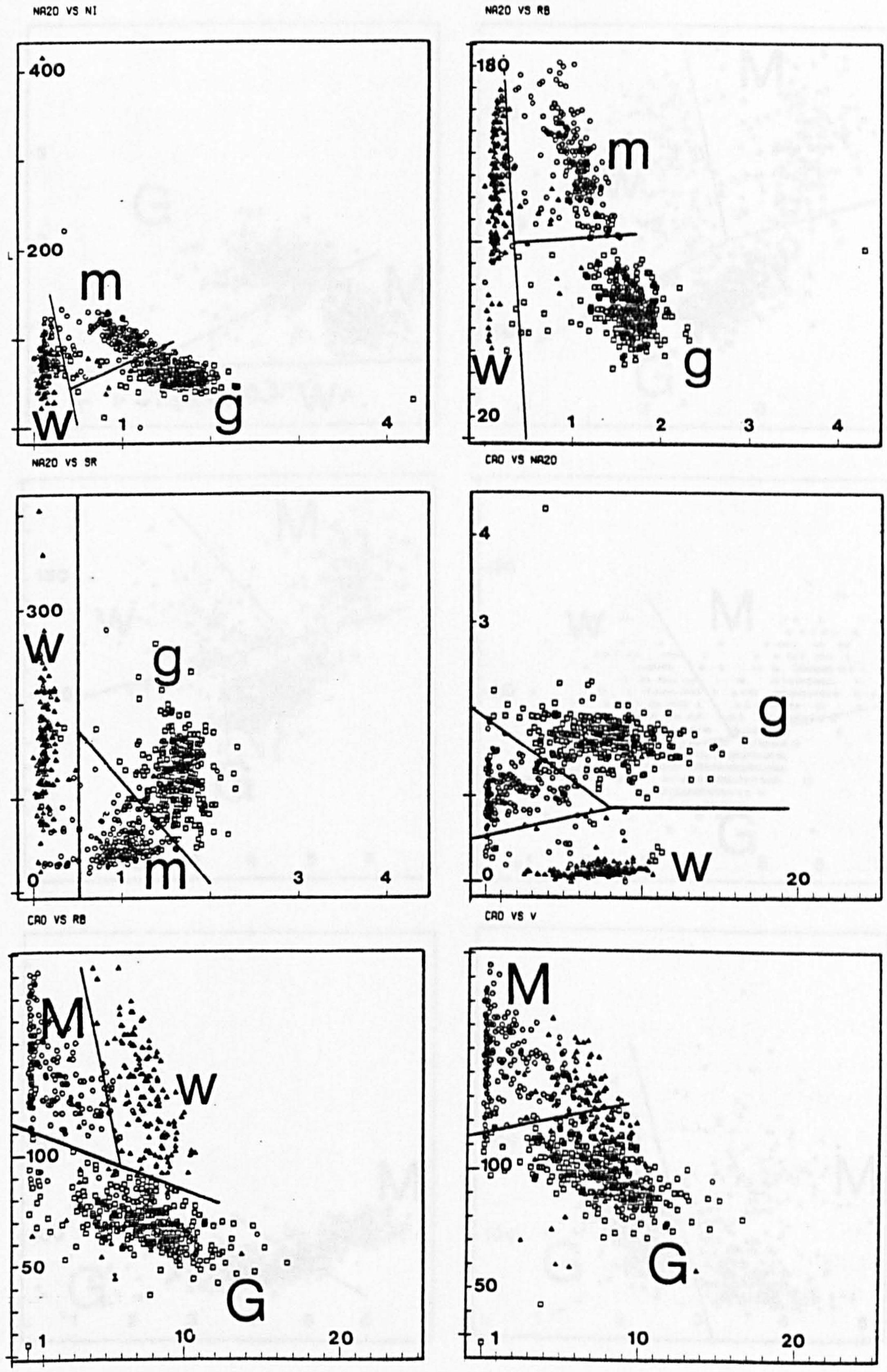

G - Greywacke, M - Mudstone, W - Wallrock Alteration

FIGURE 53 a-f

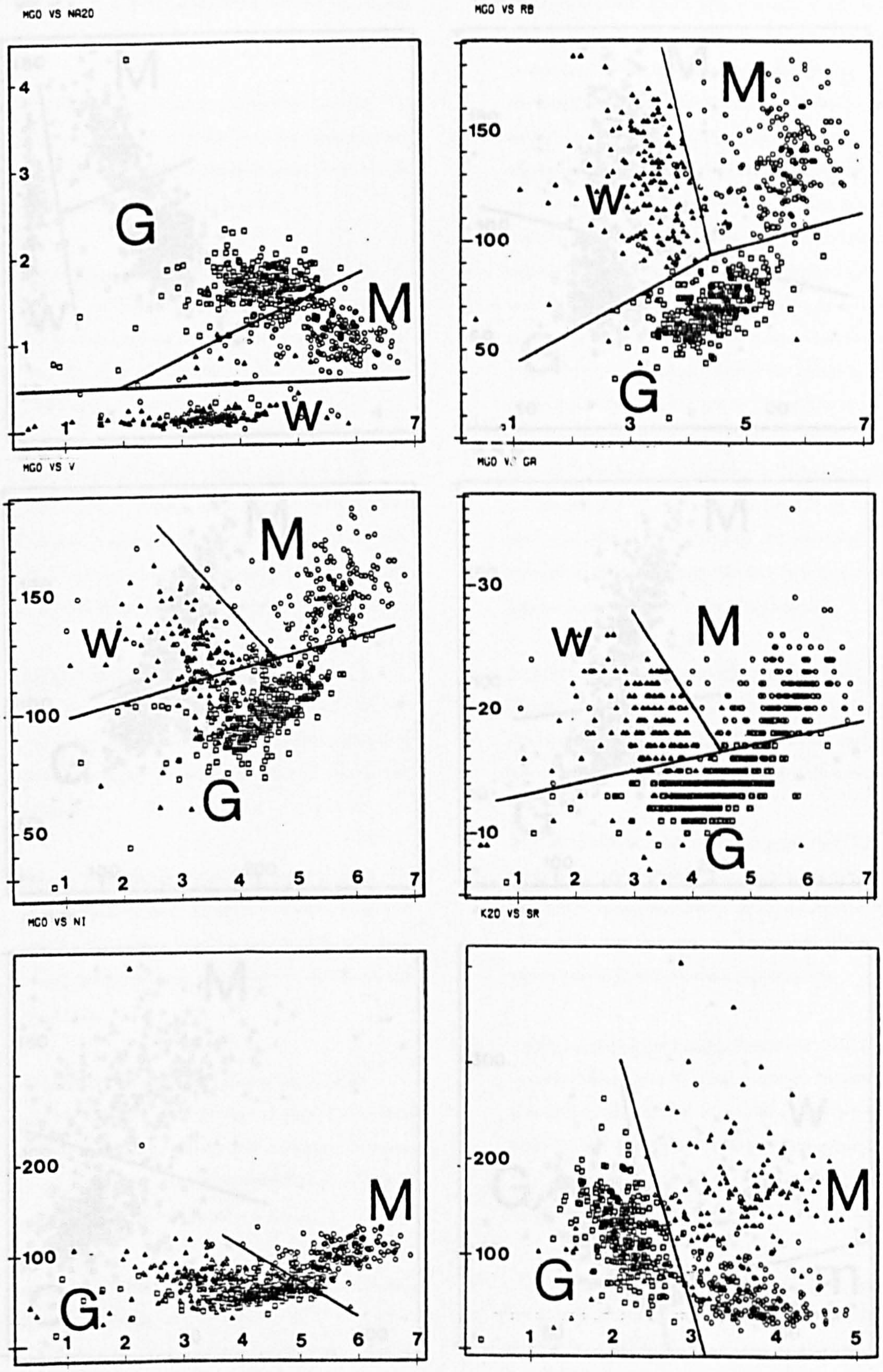

G - Greywacke, M - Mudstone, W - Wallrock Alteration

FIGURE 54 a-f

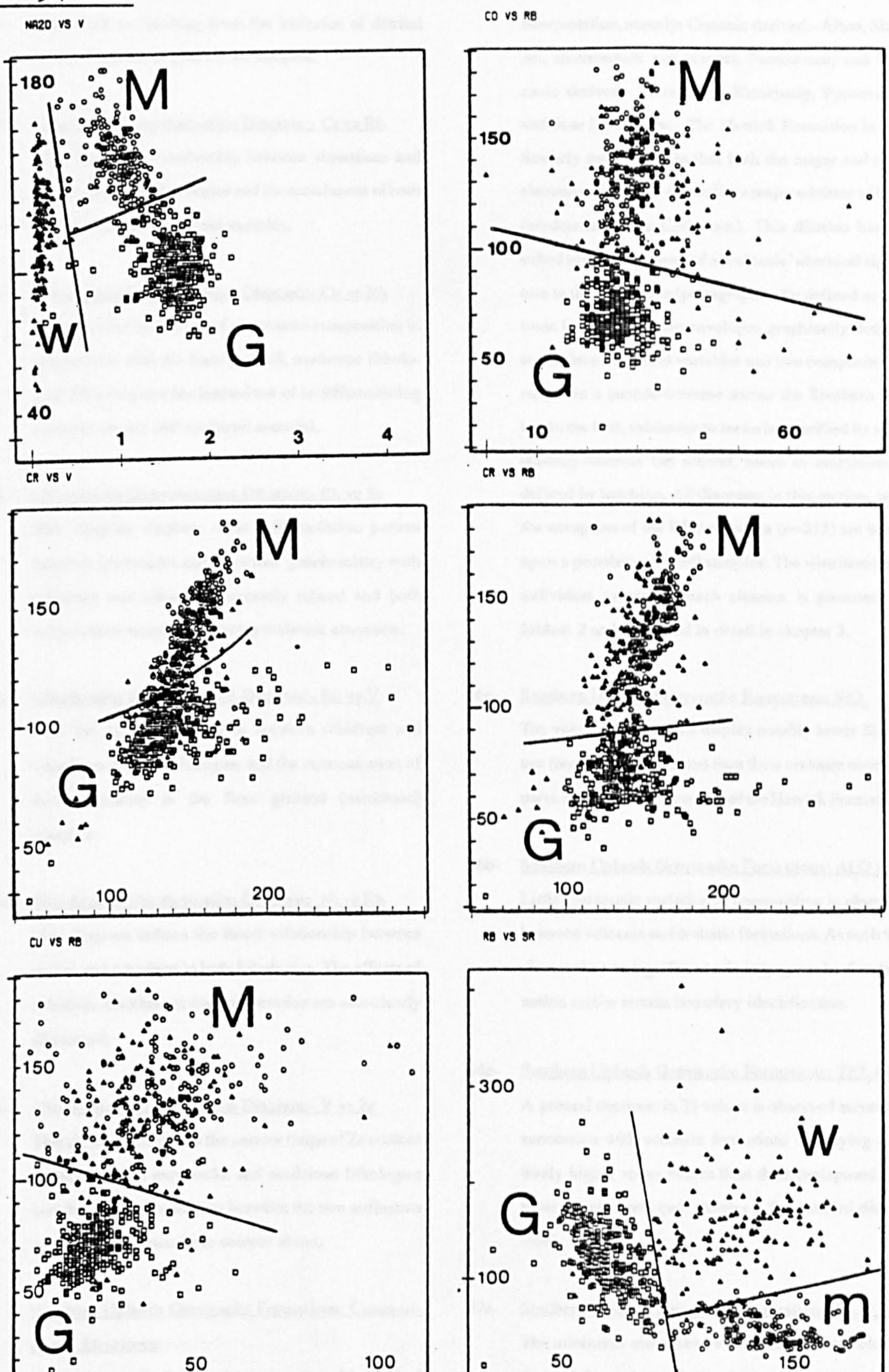

G - Greywacke, M - Mudstone, W - Wallrock Alteration

tion of high Cr values which has previously been interpreted as resulting from the inclusion of detrital chromite grains in greywacke samples.

54d- Glendinning Discrimination Diagram:- Cr vs Rb
Note the linear relationship between chromium and rubidium in both lithologies and the enrichment of both elements in the finer grain samples.

54e- Glendinning Discrimination Diagram:- Cu vs Rb
Note the confined range of greywacke composition in comparison with the finer grained, mudstone lithologies. This diagram has limited use of in differentiating between altered and unaltered material.

54f- Glendinning Discrimination Diagram:- Rb vs Sr
This diagram displays clear differentiation pattern between greywacke and mudstone geochemistry with rubidium and strontium inversely related and both subjected to enrichment during wallrock alteration.

55a- Glendinning Discrimination Diagram:- Rb vs V
Note the positive correlation between rubidium and vanadium in both lithologies and the concentration of these elements in the finer grained (mudstone) samples.

55b- Glendinning Discrimination Diagram:- Ni vs Rb
This diagram defines the linear relationship between nickel and rubidium in both lithologies. The effects of rubidium enrichment during alteration are also clearly illustrated.

55c- Glendinning Discrimination Diagram:- V vs Zr
This diagram illustrates the narrow range of Zr content defined in both greywacke and mudstone lithologies and defines the boundaries between the two sediments on the basis of vanadium content alone.

56- Southern Uplands Greywacke Formations: Compositional Envelopes
The following 13 figures display a series of individual element compositional envelopes and present a graphical summary of the variations displayed by differing petrographic formations across the Southern Uplands. The eight greywacke formations described here may be sub-divided into two main categories in order to aid interpretation, namely: Cratonic derived:- Afton, Shinnel, Intermediate and Hawick Formations; and Volcanic derived:- Marchburn, Blackcraig, Pyroxenous and Scar Formations. The Hawick Formation is particularly noteworthy in that both the major and trace element contents are diluted by a major addition of CaO (predominantly as Carbonate). This dilution has resulted in the assignment of a 'volcanic' chemical signature to this formation (petrographically defined as cratonic in origin). These envelopes graphically demonstrate three statistical variables and two compositional ranges in a pseudo-traverse across the Southern Uplands; the first, minimum to mean is identified by solid shading whereas the second, mean to maximum is defined by hatching. All diagrams in this section, with the exception of the REE elements (n=213) are based upon a population of 699 samples. The distribution of individual values for each element is presented in foldout 2 and discussed in detail in chapter 5.

56a- Southern Uplands Greywacke Formations: SiO_2
The volcanic formations display notably lower Si values (mean and maximum) than their cratonic counterparts. Note the low Si content of the Hawick Formation.

56b- Southern Uplands Greywacke Formations: Al_2O_3(%)
Little systematic variation in composition is observed between volcanic and cratonic formations. As such this element has no significant role in greywacke discrimination and/or terrain boundary identification.

56c- Southern Uplands Greywacke Formations: TiO_2 (%)
A general decrease in Ti values is observed across the succession with volcanic formations displaying relatively higher mean values than their juxtaposed cratonic counterparts (see chapter 5 for detailed discussion).

57a- Southern Uplands Greywacke Formations: Fe_2O_3 (%)
The minimum and mean Fe compositions of volcanic derived formations display higher values than their cratonic counterparts and mirror the Ti compositions with a trend towards decreasing values across the sucession.

FIGURE 55 a-f

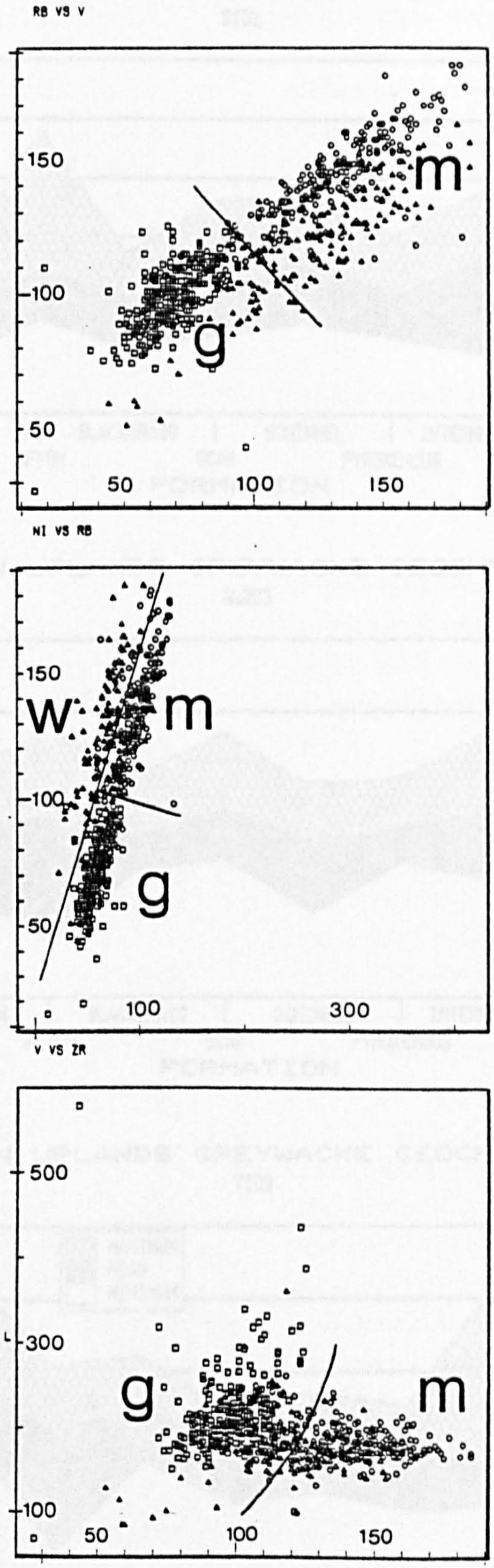

G - Greywacke, M - Mudstone, W - Wallrock Alteration

FIGURE 56

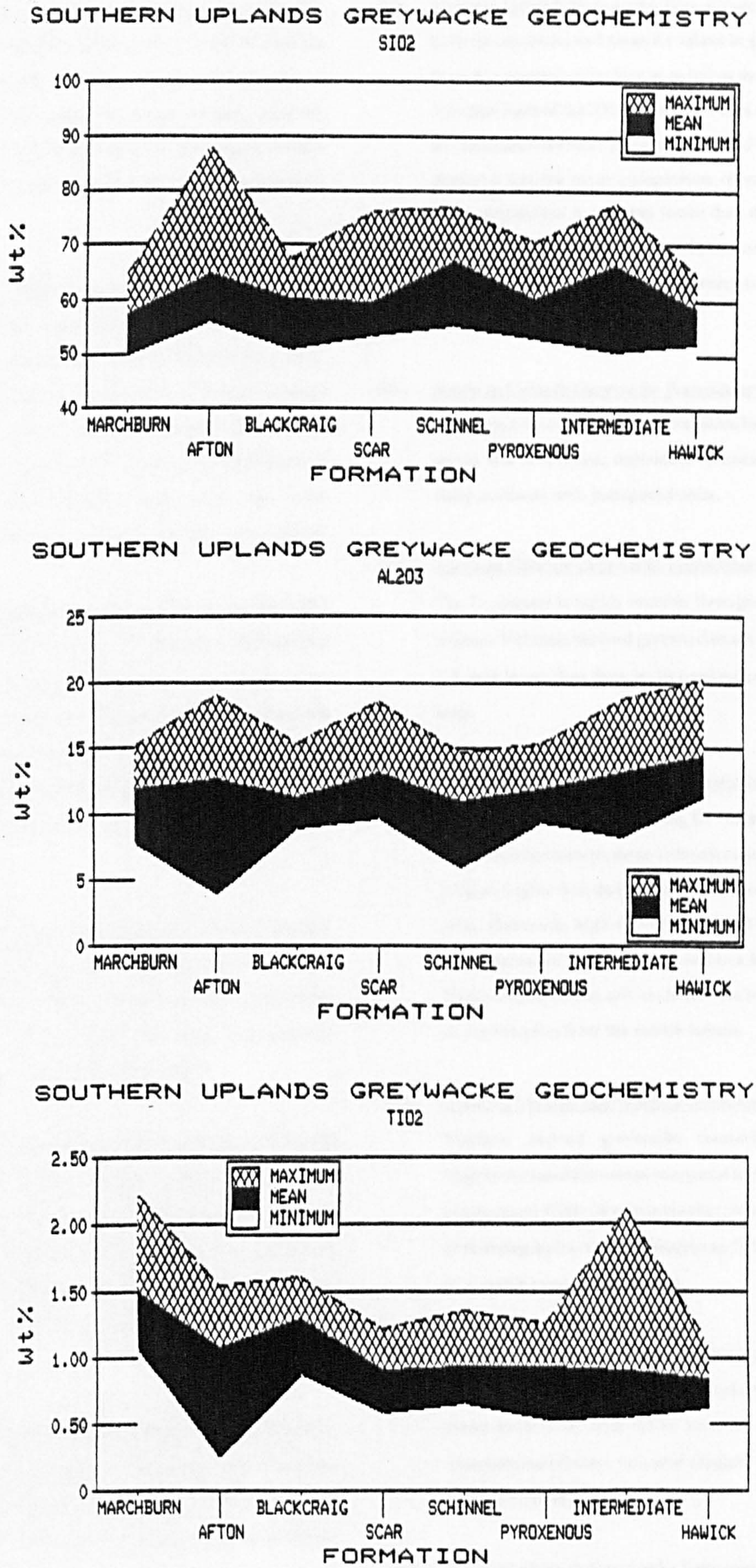
SOUTHERN UPLANDS GREYWACKE GEOCHEMISTRY
SIO2
Wt%
100
90
80
70
60
50
40
MAXIMUM
MEAN
MINIMUM
MARCHBURN
AFTON
BLACKCRAIG
SCAR
SCHINNEL
PYROXENOUS
INTERMEDIATE
HAWICK
FORMATION
SOUTHERN UPLANDS GREYWACKE GEOCHEMISTRY
AL2O3
Wt%
25
20
15
10
5
0
MAXIMUM
MEAN
MINIMUM
MARCHBURN
AFTON
BLACKCRAIG
SCAR
SCHINNEL
PYROXENOUS
INTERMEDIATE
HAWICK
FORMATION
SOUTHERN UPLANDS GREYWACKE GEOCHEMISTRY
TIO2
Wt%
2.50
2.00
1.50
1.00
0.50
0
MAXIMUM
MEAN
MINIMUM
MARCHBURN
AFTON
BLACKCRAIG
SCAR
SCHINNEL
PYROXENOUS
INTERMEDIATE
HAWICK
FORMATION

57b- <u>Southern Uplands Greywacke Formations: MgO (%)</u>
MgO values closely follow that of Ti and Fe with the highest contents occurring in the volcanic derived Marchburn Formation. The mean volcanic composition is 1.5-3.0% higher than its juxtaposed cratonic counterpart and as such provides a useful discrimination index.

57c- <u>Southern Uplands Greywacke Formations: CaO (%)</u>
The Ca content varies systematically across the sucession. With the exception of the Hawick Formation, cratonic derived greywackes have 2-3% lower average content than their volcanic counterparts. The Hawick Formation is however, characterised by the highest Ca content of any formation in this study, due to the significant input of carbonate from the source terrain.

58a- <u>Southern Uplands Greywacke Formations: Na_2O (%)</u>
The Na content reflects the variation in petrography across the succession with mean compositions of volcanic derived greywackes up to 0.8% higher than their cratonic counterparts. The effects of Na depletion associated with hydrothermal activity are markedly developed in the Afton, Intermediate and Hawick (cratonic) formations.

58b- <u>Southern Uplands Greywacke Formations: K_2O (%)</u>
Systematic differences in mean composition between cratonic and volcanic derived greywacke formations are illustrated (volcanic 0.5% lower than cratonic) particularly during Ordovician times.

58c- <u>Southern Uplands Greywacke Formations: MnO (%)</u>
Although the MnO content is generally low (<0.25%) systematic variations between cratonic and volcanic derived greywacke formations exist with the former relatively depleted with respect to its volcanic counterpart (mean volcanic composition is 0.05% higher than cratonic).

59a- <u>Southern Uplands Greywacke Formations: P_2O (%)</u>
This diagram illustrates a subtle trend towards decreasing P content across the succession with notably higher values occurring in the volcanic Marchburn Formation.

59b- <u>Southern Uplands Greywacke Formations: As (ppm)</u>
Both the minimum and mean As values in greywackes from this succession lie close to, or below the analytical detection limit of the XRF (2-3ppm). From a review of the univariate statistics pertaining to this diagram it is observed that the mean composition of volcanic derived greywackes is 1-2 ppm lower than the cratonic samples. This diagram illustrates the numerous occurrence of elevated arsenic levels (several tens of ppm) across this succession.

59c- <u>Southern Uplands Greywacke Formations: Ba (ppm)</u>
Although there is no systematic variation in Ba content across this succession, individual formations exhibit sharp contrasts with juxtaposed units.

60a- <u>Southern Uplands Greywacke Formations: Co (ppm)</u>
The Co content is highly variable throughout the succession. Volcanic derived greywackes are on average 5-8 ppm lower than their juxtaposed cratonic equivalents.

60b- <u>Southern Uplands Greywacke Formations: Cr (ppm)</u>
A systematic trend of decreasing Cr values across the succession occurs with mean volcanic composition 30-150ppm higher than their juxtaposed cratonic counterparts. Extremely high Cr values up to 1100ppm are characteristic of the Marchburn and to a lesser extent, Blackcraig formation and are indicative of an ultrabasic contribution from the source terrain.

60c- <u>Southern Uplands Greywacke Formations: Cu (ppm)</u>
Volcanic derived greywacke formations display slightly elevated Cu values compared to their cratonic counterparts. High Cu values maybe related to a variety of differing styles of mineralisation and identify targets of possible exploration interest.

61a- <u>Southern Uplands Greywacke Formations: Ga (ppm)</u>
Highly consistent Ga values are displayed across the entire succession, with subtle variation (3-4ppm) in composition between volcanic (higher) and cratonic (lower) derived formations.

61b- <u>Southern Uplands Greywacke Formations: La (ppm)</u>
Systematic variations in La content occur across the

FIGURE 57 a-c

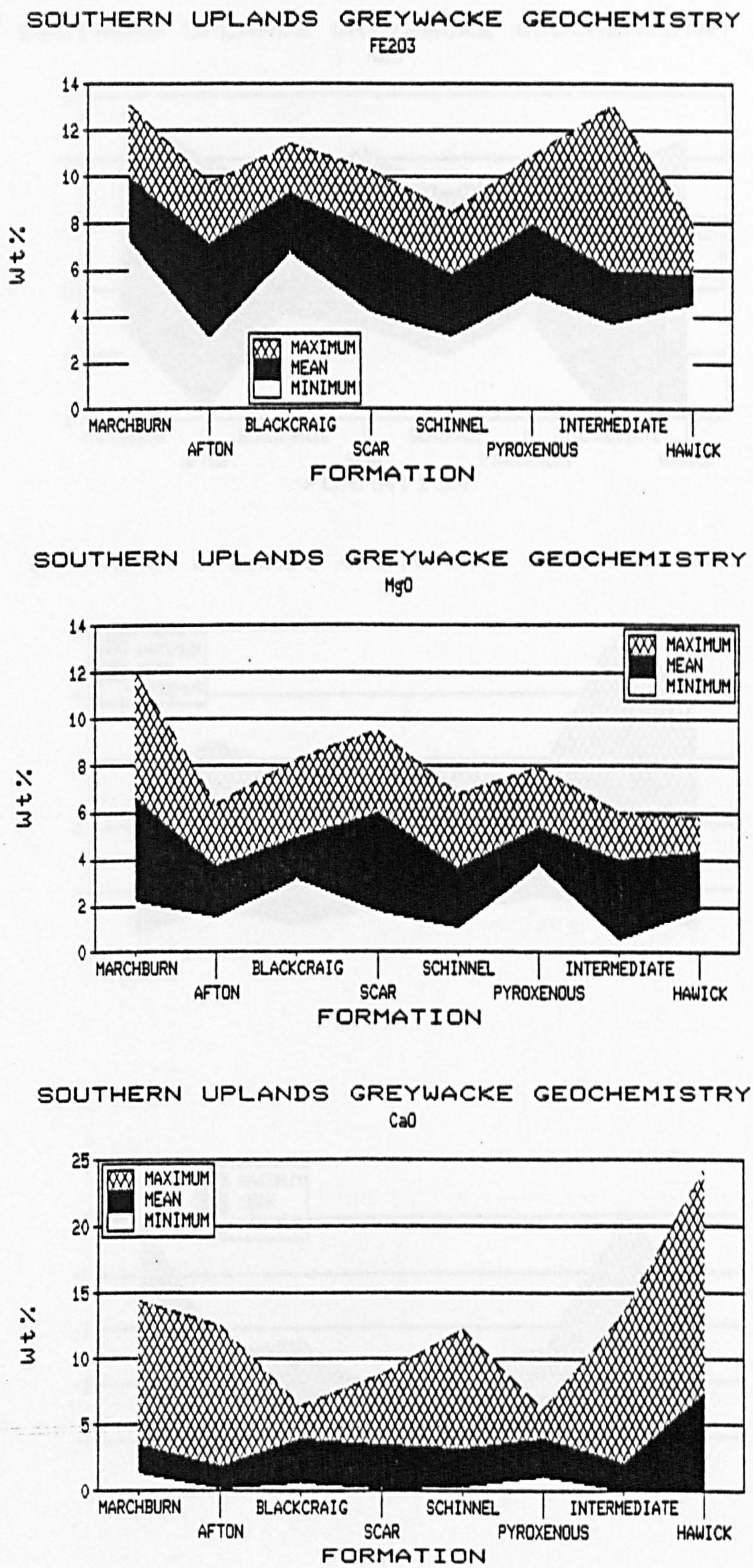
SOUTHERN UPLANDS GREYWACKE GEOCHEMISTRY
FE203
Wt%
MAXIMUM
MEAN
MINIMUM
MARCHBURN
AFTON
BLACKCRAIG
SCAR
SCHINNEL
PYROXENOUS
INTERMEDIATE
HAWICK
FORMATION
SOUTHERN UPLANDS GREYWACKE GEOCHEMISTRY
MgO
Wt%
MAXIMUM
MEAN
MINIMUM
FORMATION
SOUTHERN UPLANDS GREYWACKE GEOCHEMISTRY
CaO
Wt%
MAXIMUM
MEAN
MINIMUM
FORMATION

FIGURE 58 a-c

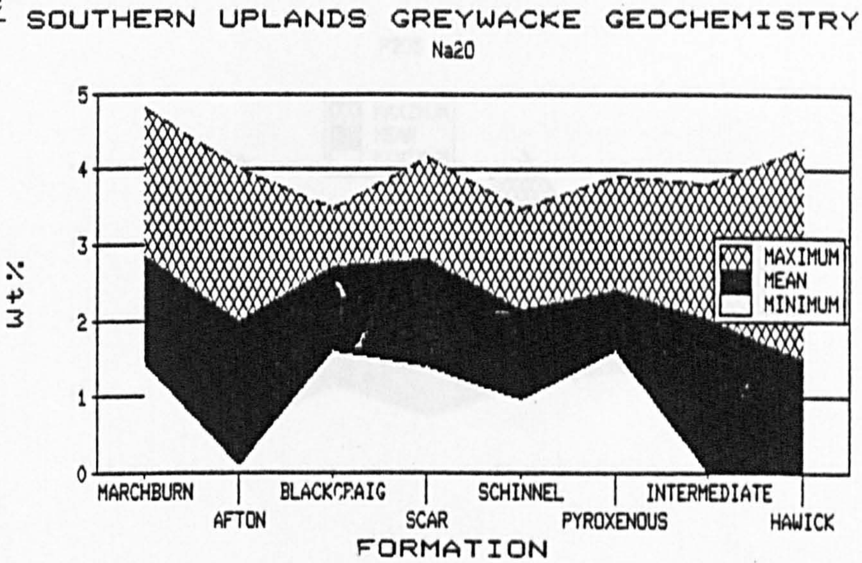
SOUTHERN UPLANDS GREYWACKE GEOCHEMISTRY
Na2O
Wt%
MAXIMUM
MEAN
MINIMUM
MARCHBURN
AFTON
BLACKCRAIG
SCAR
SCHINNEL
PYROXENOUS
INTERMEDIATE
HAWICK
FORMATION

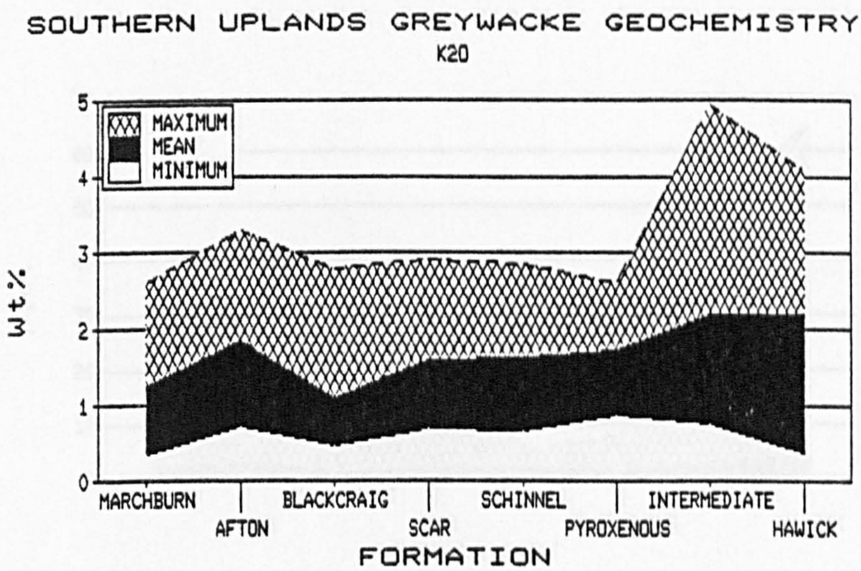
SOUTHERN UPLANDS GREYWACKE GEOCHEMISTRY
K2O
Wt%
MAXIMUM
MEAN
MINIMUM
MARCHBURN
AFTON
BLACKCRAIG
SCAR
SCHINNEL
PYROXENOUS
INTERMEDIATE
HAWICK
FORMATION

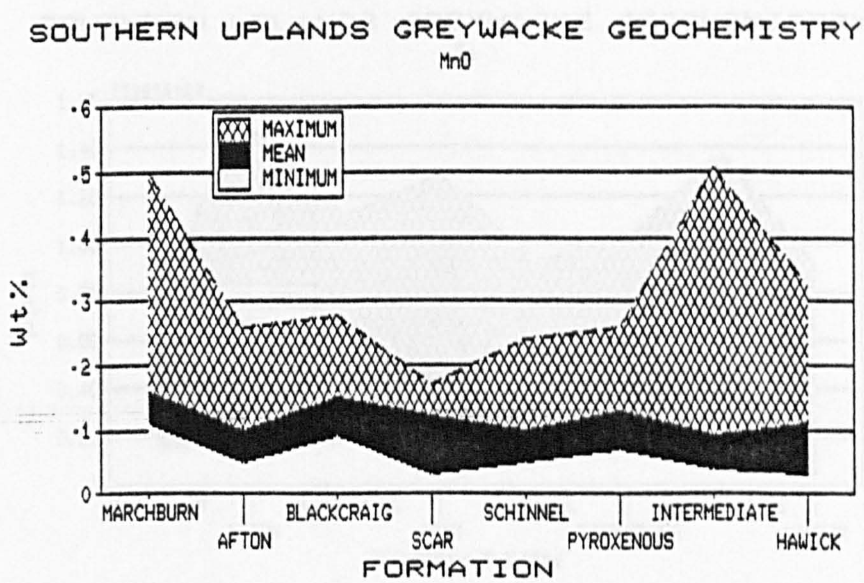
SOUTHERN UPLANDS GREYWACKE GEOCHEMISTRY
MnO
Wt%
MAXIMUM
MEAN
MINIMUM
MARCHBURN
AFTON
BLACKCRAIG
SCAR
SCHINNEL
PYROXENOUS
INTERMEDIATE
HAWICK
FORMATION

FIGURE 59 a-c

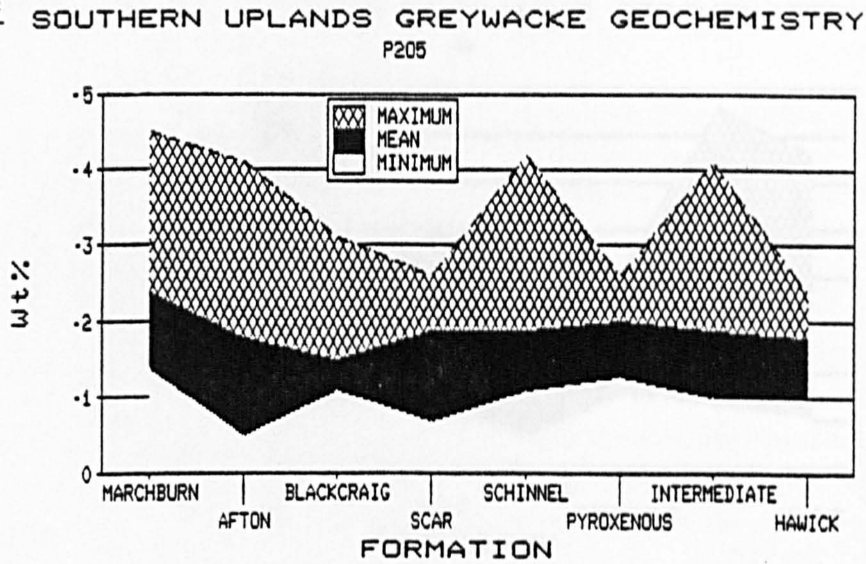
SOUTHERN UPLANDS GREYWACKE GEOCHEMISTRY
P205
wt%
MAXIMUM
MEAN
MINIMUM
·5
·4
·3
·2
·1
0
MARCHBURN
AFTON
BLACKCRAIG
SCAR
SCHINNEL
PYROXENOUS
INTERMEDIATE
HAWICK
FORMATION

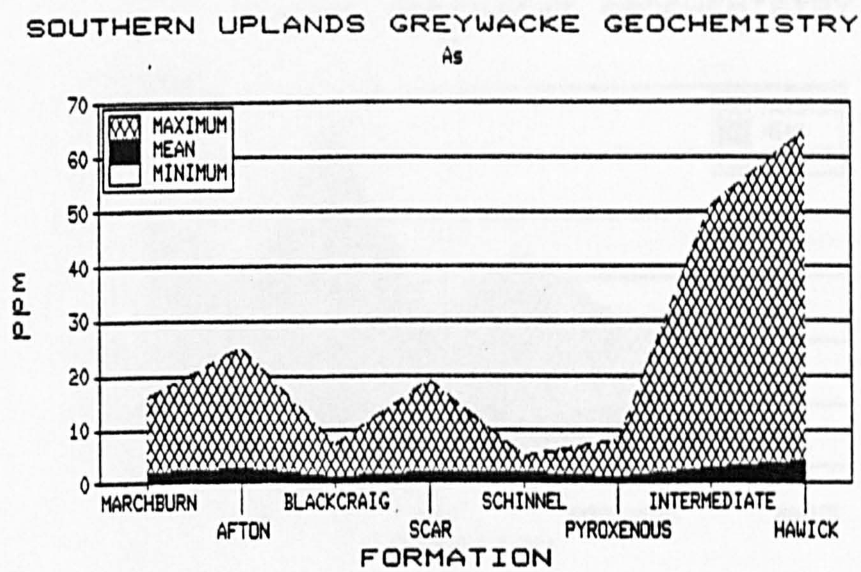
SOUTHERN UPLANDS GREYWACKE GEOCHEMISTRY
As
ppm
MAXIMUM
MEAN
MINIMUM
70
60
50
40
30
20
10
0
MARCHBURN
AFTON
BLACKCRAIG
SCAR
SCHINNEL
PYROXENOUS
INTERMEDIATE
HAWICK
FORMATION

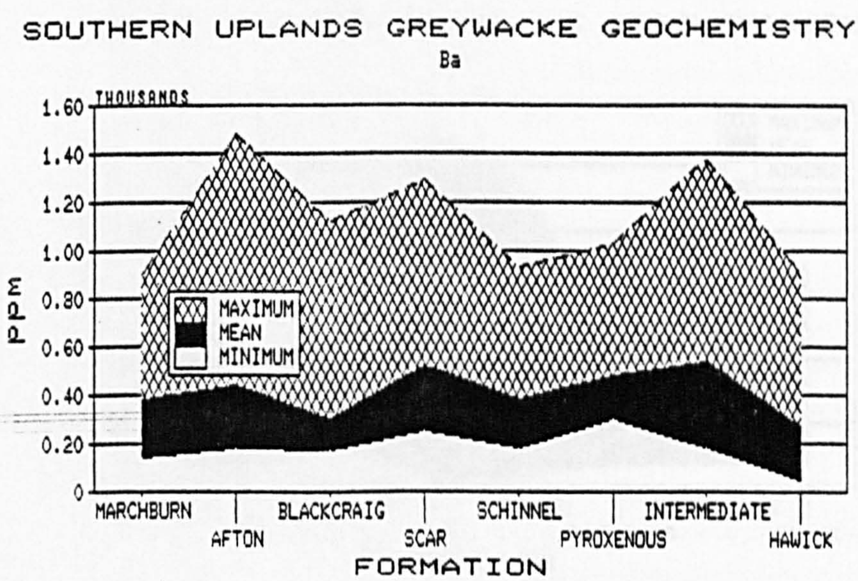
SOUTHERN UPLANDS GREYWACKE GEOCHEMISTRY
Ba
THOUSANDS
ppm
MAXIMUM
MEAN
MINIMUM
1.60
1.40
1.20
1.00
0.80
0.60
0.40
0.20
0
MARCHBURN
AFTON
BLACKCRAIG
SCAR
SCHINNEL
PYROXENOUS
INTERMEDIATE
HAWICK
FORMATION

FIGURE 60 a-c

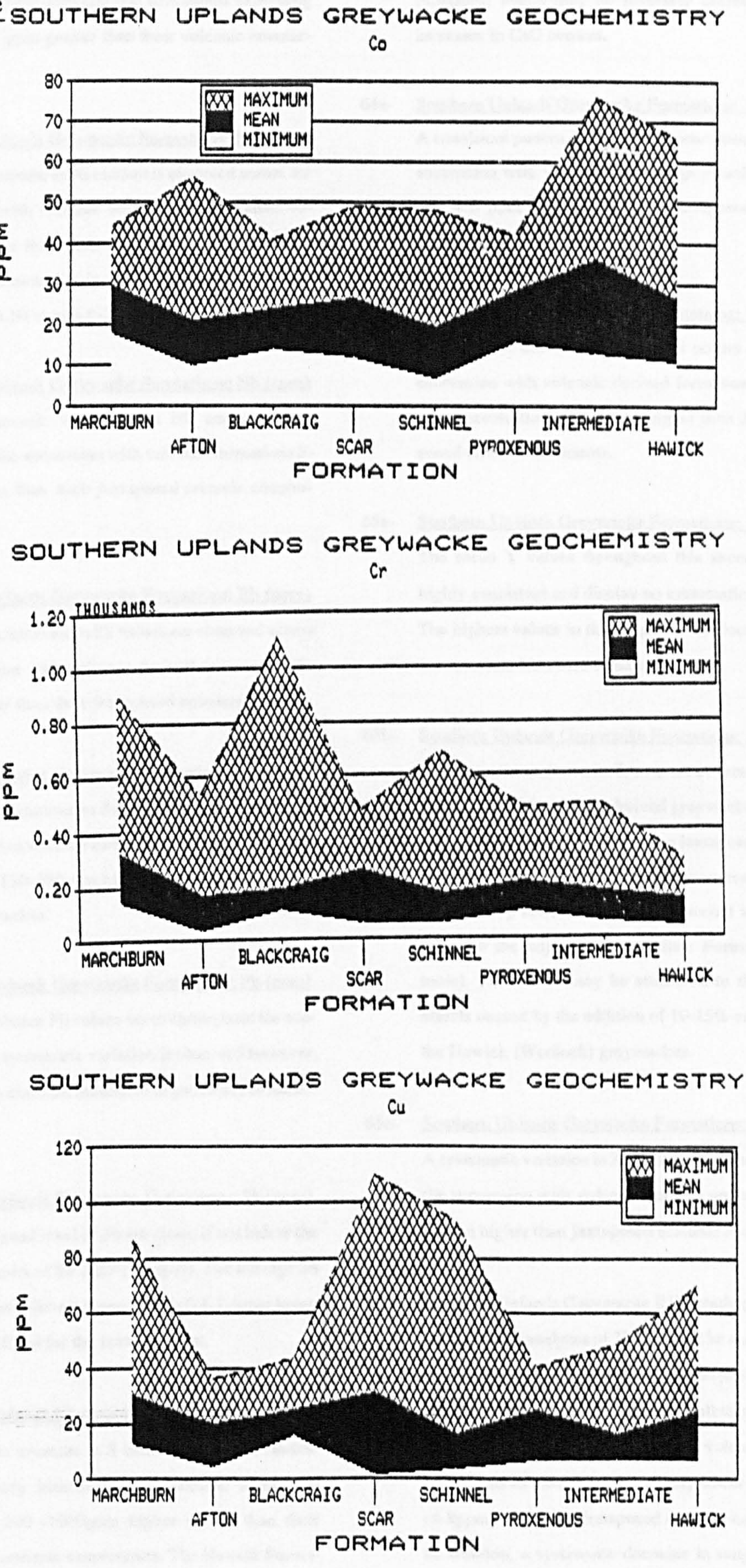
SOUTHERN UPLANDS GREYWACKE GEOCHEMISTRY
Co
PPM
0
10
20
30
40
50
60
70
80
MAXIMUM
MEAN
MINIMUM
MARCHBURN
AFTON
BLACKCRAIG
SCAR
SCHINNEL
PYROXENOUS
INTERMEDIATE
HAWICK
FORMATION
SOUTHERN UPLANDS GREYWACKE GEOCHEMISTRY
Cr
THOUSANDS
PPM
0
0.20
0.40
0.60
0.80
1.00
1.20
MAXIMUM
MEAN
MINIMUM
MARCHBURN
AFTON
BLACKCRAIG
SCAR
SCHINNEL
PYROXENOUS
INTERMEDIATE
HAWICK
FORMATION
SOUTHERN UPLANDS GREYWACKE GEOCHEMISTRY
Cu
PPM
0
20
40
60
80
100
120
MAXIMUM
MEAN
MINIMUM
MARCHBURN
AFTON
BLACKCRAIG
SCAR
SCHINNEL
PYROXENOUS
INTERMEDIATE
HAWICK
FORMATION

entire succession with cratonic formations exhibiting levels 10-15 ppm greater than their volcanic counterparts.

61c- Southern Uplands Greywacke Formations: Ni (ppm)
A general decrease in Ni content is observed across the succession, with volcanic units defined by values 40-60ppm higher than their cratonic counterparts. The Marchburn Formation is again characterised by extremely high Ni values (>250ppm).

62a- Southern Uplands Greywacke Formations: Nb (ppm)
Subtle systematic variations in Nb content occur throughout the succession with volcanic formations 5-15ppm lower than their juxtaposed cratonic counterparts.

62b- Southern Uplands Greywacke Formations: Rb (ppm)
A systematic increase in Rb values are observed across the succession with volcanic derived formations 20-30ppm lower than their juxtaposed counterparts.

62c- Southern Uplands Greywacke Formations: Sr (ppm)
Systematic variations in Sr content occur throughout this succession with the mean composition of volcanic formations 130-200ppm higher than the cratonic derived greywackes.

63a- Southern Uplands Greywacke Formations: Pb (ppm)
Highly consistent Pb values occur throughout the succession. No systematic variation is observed however, anomalous values are indicative of proximity to mineralisation.

63b- Southern Uplands Greywacke Formations: Sb (ppm)
The background level of Sb are close, if not below the detection limits of the XRF (1-3ppm). The average Sb content of the volcanic formations is 0.4-1.6ppm lower than that defined for the cratonic units.

63c- Southern Uplands Greywacke Formations: S (ppm)
A systematic decrease in S content across the succession is clearly identified, with volcanic formations containing 200 -1000ppm higher values than their juxtaposed cratonic counterparts. The Hawick Formation is characterised by extremely low values (<50ppm) which may be inversely correlated with increases in CaO content.

64a- Southern Uplands Greywacke Formations: Th (ppm)
A consistent pattern of Th values occur throughout the succession with volcanic derived greywackes generally 4-6 ppm lower than their juxtaposed cratonic counterparts.

64b- Southern Uplands Greywacke Formations: V (ppm)
A systematic decrease in V content occurs across the succession with volcanic derived formations exhibiting concentration 50-100ppm higher than their juxtaposed cratonic sediments.

65a- Southern Uplands Greywacke Formations: Y (ppm)
The mean Y values throughout this succession are highly consistent and display no systematic variation. The highest values in this sequence are located in the Intermediate Hawick Formation.

65b- Southern Uplands Greywacke Formations: Zr (ppm)
A systematic variation in Zr content occurs across the succession with volcanic derived greywackes displaying values 100-150ppm lower than juxtaposed cratonic greywacke. The Hawick Formation however, displays significantly lower values than expected when compared to the adjacent Intermediate Formation (cratonic). This factor may be attributed to the dilution effects caused by the addition of 10-15% carbonate to the Hawick (Wenlock) greywackes.

65c- Southern Uplands Greywacke Formations: Zn (ppm)
A systematic variation in Zn content is observed across the succession with volcanic derived greywackes 10-30ppm higher than juxtaposed cratonic sediments.

66a- Southern Uplands Greywacke REE study : La (ppm)
REE element analyses of 213 greywacke samples were undertaken by ICP following the techniques outlined in chapter 2. Although La displays relatively consistent values, this diagram shows the mean volcanic derived formations to have a comparatively lower La content (6-8ppm) than their juxtaposed cratonic counterparts. In addition, a systematic decrease in range, coupled with an increase in minimum values is observed across

FIGURE 61 a-c

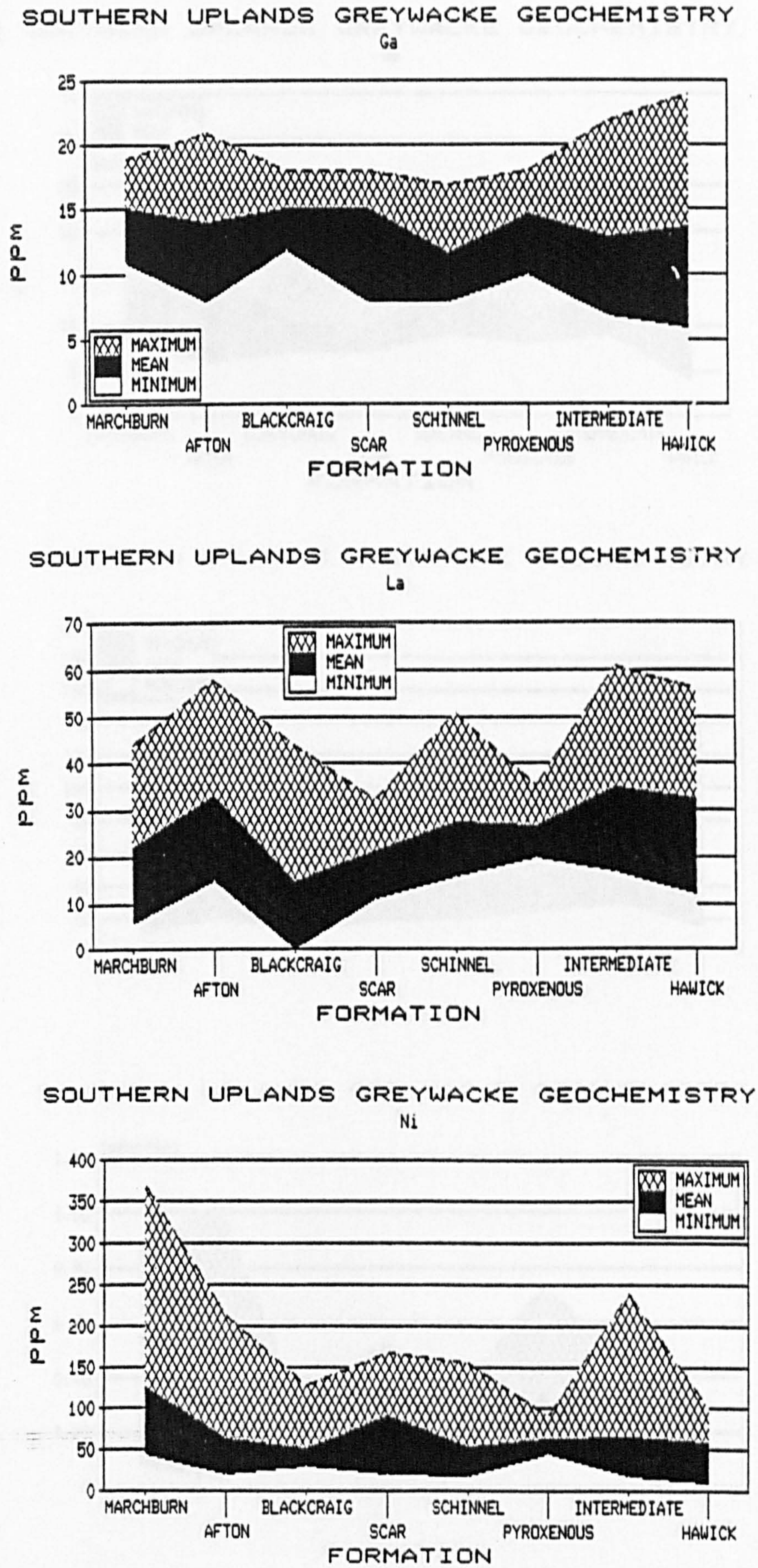
SOUTHERN UPLANDS GREYWACKE GEOCHEMISTRY
Ga
PPM
0
5
10
15
20
25
MAXIMUM
MEAN
MINIMUM
MARCHBURN
AFTON
BLACKCRAIG
SCAR
SCHINNEL
PYROXENOUS
INTERMEDIATE
HAWICK
FORMATION
SOUTHERN UPLANDS GREYWACKE GEOCHEMISTRY
La
PPM
0
10
20
30
40
50
60
70
MAXIMUM
MEAN
MINIMUM
MARCHBURN
AFTON
BLACKCRAIG
SCAR
SCHINNEL
PYROXENOUS
INTERMEDIATE
HAWICK
FORMATION
SOUTHERN UPLANDS GREYWACKE GEOCHEMISTRY
Ni
PPM
0
50
100
150
200
250
300
350
400
MAXIMUM
MEAN
MINIMUM
MARCHBURN
AFTON
BLACKCRAIG
SCAR
SCHINNEL
PYROXENOUS
INTERMEDIATE
HAWICK
FORMATION

FIGURE 62 a-c SOUTHERN UPLANDS GREYWACKE GEOCHEMISTRY

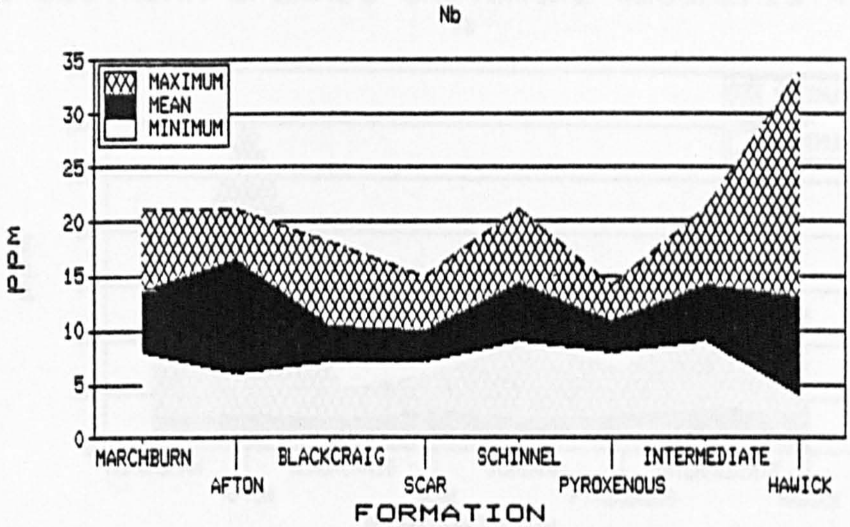

SOUTHERN UPLANDS GREYWACKE GEOCHEMISTRY

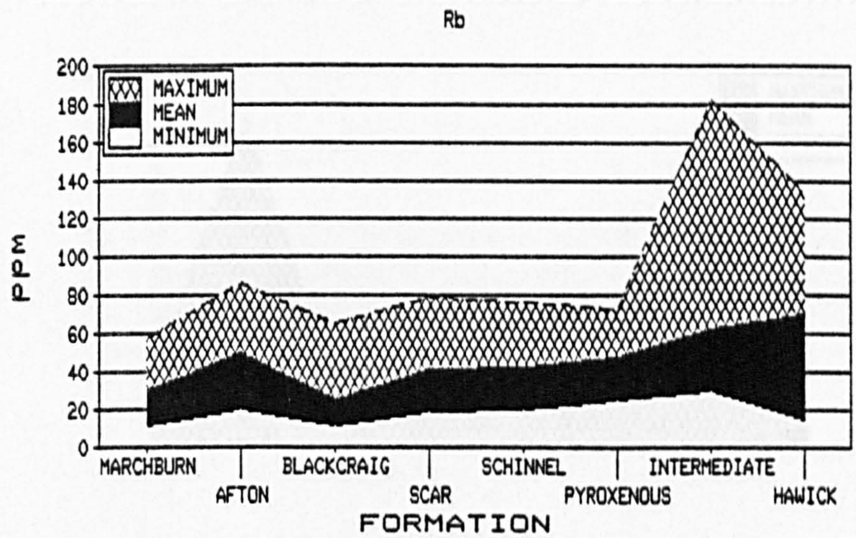

SOUTHERN UPLANDS GREYWACKE GEOCHEMISTRY

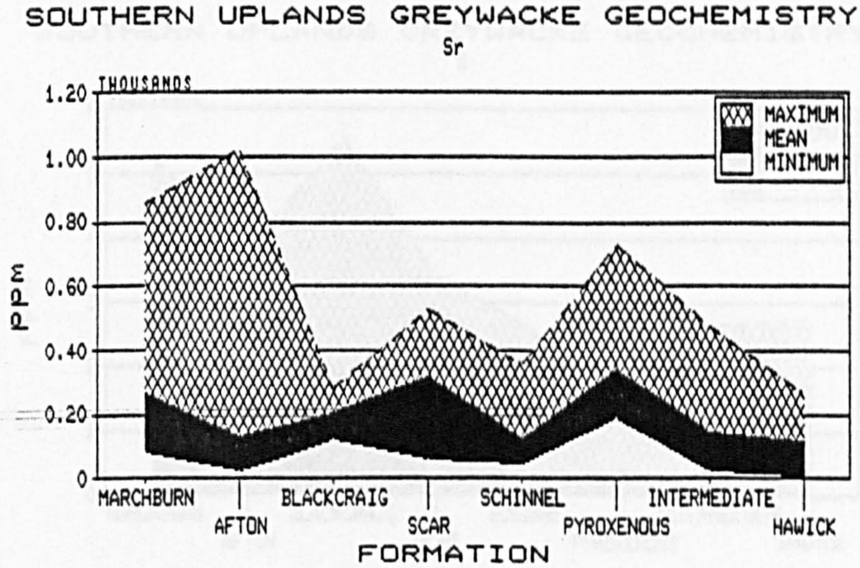

FIGURE 63 a-c

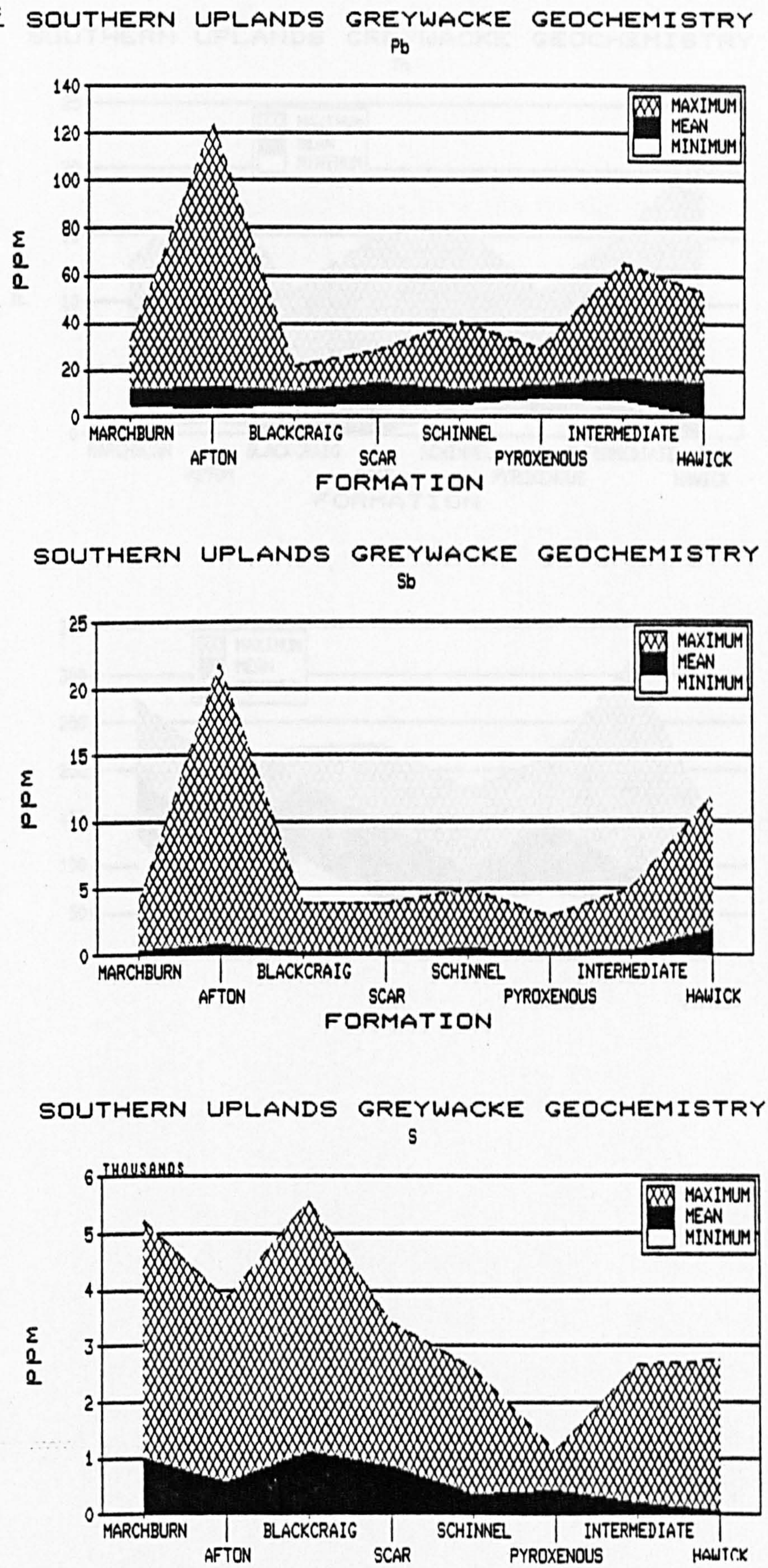
SOUTHERN UPLANDS GREYWACKE GEOCHEMISTRY
Pb
MAXIMUM
MEAN
MINIMUM
PPM
0
20
40
60
80
100
120
140
MARCHBURN
AFTON
BLACKCRAIG
SCAR
SCHINNEL
PYROXENOUS
INTERMEDIATE
HAWICK
FORMATION
SOUTHERN UPLANDS GREYWACKE GEOCHEMISTRY
Sb
MAXIMUM
MEAN
MINIMUM
PPM
0
5
10
15
20
25
MARCHBURN
AFTON
BLACKCRAIG
SCAR
SCHINNEL
PYROXENOUS
INTERMEDIATE
HAWICK
FORMATION
SOUTHERN UPLANDS GREYWACKE GEOCHEMISTRY
S
THOUSANDS
MAXIMUM
MEAN
MINIMUM
PPM
0
1
2
3
4
5
6
MARCHBURN
AFTON
BLACKCRAIG
SCAR
SCHINNEL
PYROXENOUS
INTERMEDIATE
HAWICK

FIGURE 64 a-c

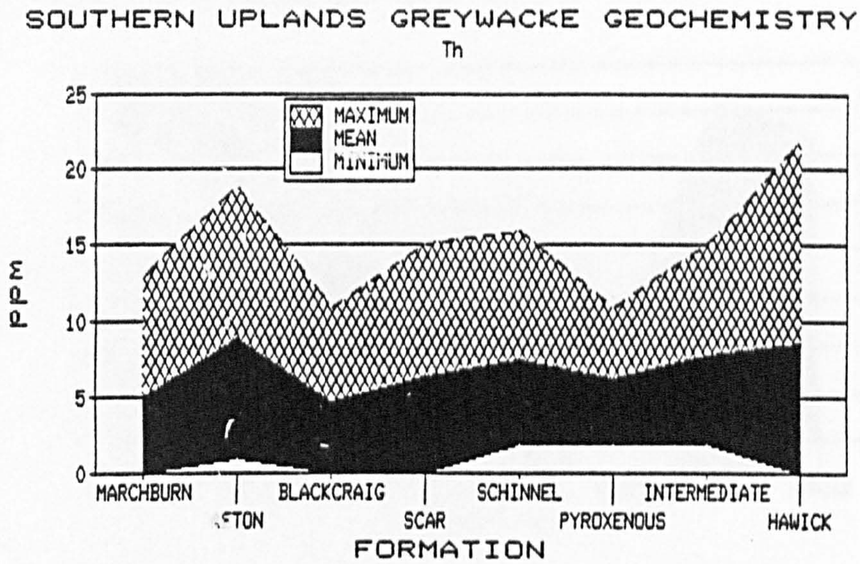
SOUTHERN UPLANDS GREYWACKE GEOCHEMISTRY
Th
MAXIMUM
MEAN
MINIMUM
PPM
25
20
15
10
5
0
MARCHBURN
AFTON
BLACKCRAIG
SCAR
SCHINNEL
PYROXENOUS
INTERMEDIATE
HAWICK
FORMATION

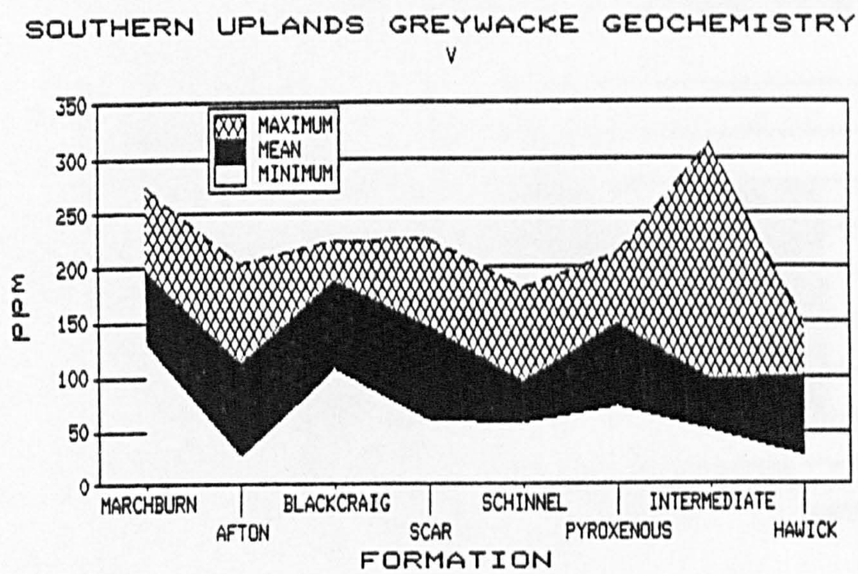
SOUTHERN UPLANDS GREYWACKE GEOCHEMISTRY
V
MAXIMUM
MEAN
MINIMUM
PPM
350
300
250
200
150
100
50
0
MARCHBURN
AFTON
BLACKCRAIG
SCAR
SCHINNEL
PYROXENOUS
INTERMEDIATE
HAWICK
FORMATION

FIGURE 65 a-c

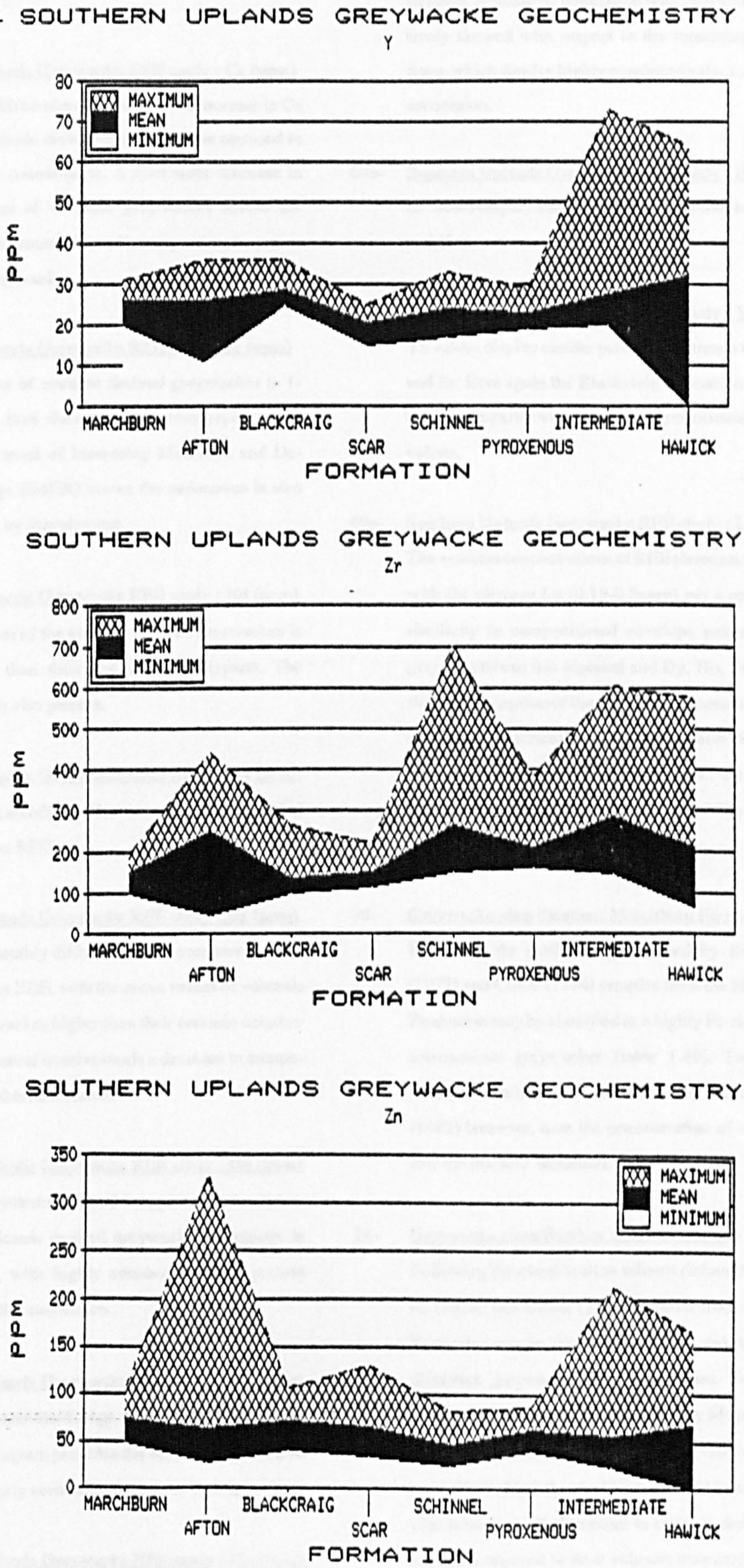
SOUTHERN UPLANDS GREYWACKE GEOCHEMISTRY
Y
MAXIMUM
MEAN
MINIMUM
PPM
0
10
20
30
40
50
60
70
80
MARCHBURN
AFTON
BLACKCRAIG
SCAR
SCHINNEL
PYROXENOUS
INTERMEDIATE
HAWICK
FORMATION
SOUTHERN UPLANDS GREYWACKE GEOCHEMISTRY
Zr
MAXIMUM
MEAN
MINIMUM
PPM
0
100
200
300
400
500
600
700
800
MARCHBURN
AFTON
BLACKCRAIG
SCAR
SCHINNEL
PYROXENOUS
INTERMEDIATE
HAWICK
FORMATION
SOUTHERN UPLANDS GREYWACKE GEOCHEMISTRY
Zn
MAXIMUM
MEAN
MINIMUM
PPM
0
50
100
150
200
250
300
350
MARCHBURN
AFTON
BLACKCRAIG
SCAR
SCHINNEL
PYROXENOUS
INTERMEDIATE
HAWICK
FORMATION

the succession.

66b- Southern Uplands Greywacke REE study : Ce (ppm)
This diagram illustrates the comparative increase in Ce content of cratonic derived greywackes as opposed to their volcanic counterparts. A systematic increase in the Ce content of volcanic greywackes across the succession is counterbalanced by respective decreases in cratonic greywackes.

66c- Southern Uplands Greywacke REE study : Pr (ppm)
The Pr content of cratonic derived greywackes is 1-2ppm higher than their volcanic counterparts. The general REE trend of Increasing Minimum and Decreasing Range (IMDR) across the succession is also demonstrated by this element.

67a- Southern Uplands Greywacke REE study : Nd (ppm)
The Nd content of the cratonic derived greywackes is again higher than their volcanic counterparts. The IMDR trend is also present.

67b- Southern Uplands Greywacke REE study : Sm (ppm)
Sm displays markedly similar element variations to that of the previous REE.

67c- Southern Uplands Greywacke REE study : Eu (ppm)
Eu displays notably different profile compared to that of the previous REE, with the mean values of volcanic derived greywackes higher than their cratonic counterparts and a general trend towards a decrease in composition across this succession.

68a- Southern Uplands Greywacke REE study : Gd (ppm)
Little if any systematic trend is apparent between cratonic and volcanic derived greywacke formations in this diagram, with highly consistent values present across the entire succession.

68b- Southern Uplands Greywacke REE study : Dy (ppm)
The tightly constrained range of the Blackcraig Formation on this diagram provides the only misnomer on an otherwise highly consistent pattern of values.

68c- Southern Uplands Greywacke REE study : Ho (ppm)
The Blackcraig Formation again shows a tightly constrained, leptokurtic population with distribution positively skewed with respect to the remaining Formations, which display highly consistent values across the succession.

69a- Southern Uplands Greywacke REE study : Er (ppm)
Er values display similar patterns and trends to both Dy and Ho.

69b- Southern Uplands Greywacke REE study : Yb (ppm)
Yb values display similar patterns and trends to Dy, Ho and Er. Here again the Blackcraig Formation provides the only disparity within a relatively consistent series of values.

69c- Southern Uplands Greywacke REE study : Lu (ppm)
The weakest concentrations of REE elements are found with the element Lu (0.19-0.5ppm) yet a remarkable similarity in compositional envelope pattern is displayed between this element and Dy, Ho, Er and Yb. With the exception of the Blackcraig Formation values are highly consistent, with a trend towards decreasing range across the succession. In general, the volcanic formations exhibit the greatest variability in both magnitude and range.

70- Greywacke classification: Marchburn Formation
Following the methodology defined by Blatt et al. (1972) and Crook (1974) samples from the Marchburn Formation may be classified as a highly Fe-rich, quartz intermediate greywackes (table 1.49). Total alkali contents lie within the field defined by Maynard et al. (1982) however, note the concentration of values below the Na/K=1 threshold.

71- Greywacke classification: Afton Formation
Following the classification scheme defined by Blatt et al. (1972) and Crook (1974) samples from the Afton Formation may be classified as Fe-rich, quartz intermediate/rich greywackes/lithic sandstones. Total alkali contents lie within the field defined by Maynard et al. (1982) however, the concentration of values centered upon the Na/K=1 threshold is indicative of a considerable increase in K_2O content in cratonic derived sediments as opposed to their volcanic counterparts.

FIGURE 66 a-c

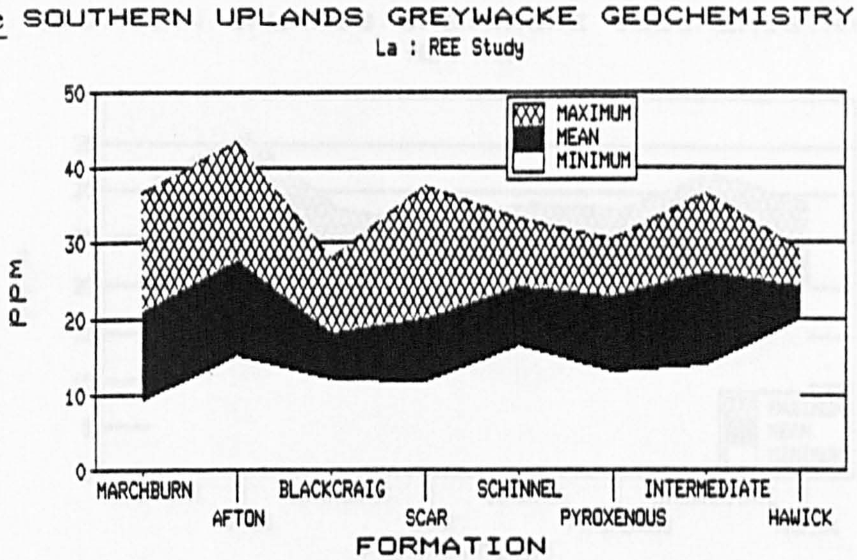
SOUTHERN UPLANDS GREYWACKE GEOCHEMISTRY
La : REE Study
MAXIMUM
MEAN
MINIMUM
50
40
30
20
10
0
PPM
MARCHBURN
AFTON
BLACKCRAIG
SCAR
SCHINNEL
PYROXENOUS
INTERMEDIATE
HAWICK
FORMATION

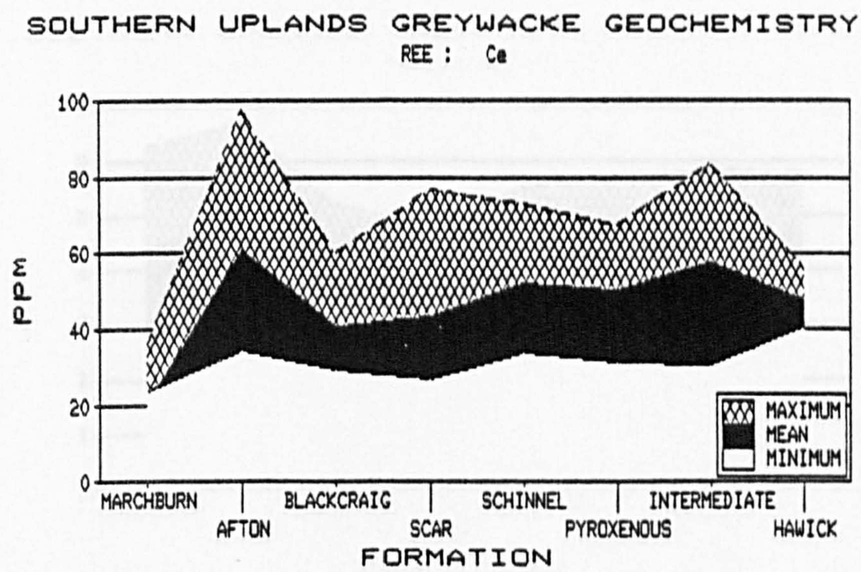
SOUTHERN UPLANDS GREYWACKE GEOCHEMISTRY
REE : Ce
100
80
60
40
20
0
PPM
MAXIMUM
MEAN
MINIMUM
MARCHBURN
AFTON
BLACKCRAIG
SCAR
SCHINNEL
PYROXENOUS
INTERMEDIATE
HAWICK
FORMATION

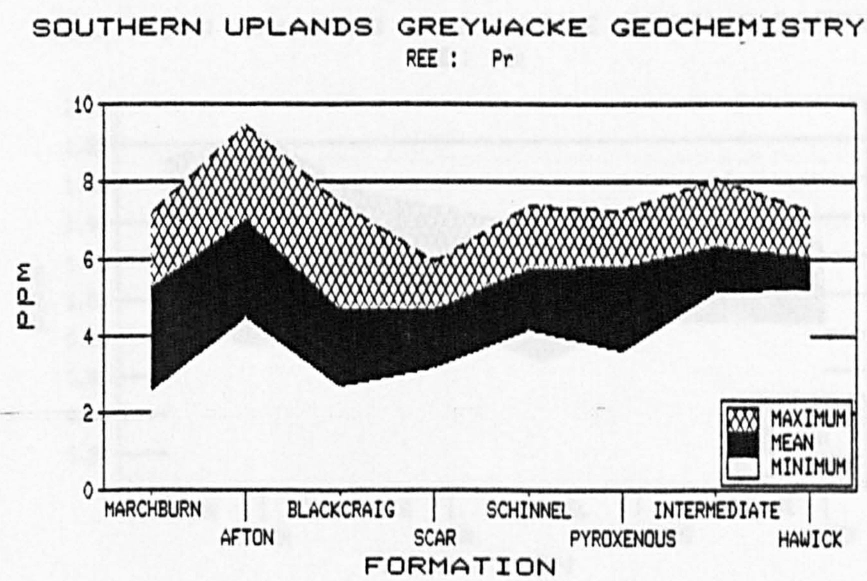
SOUTHERN UPLANDS GREYWACKE GEOCHEMISTRY
REE : Pr
10
8
6
4
2
0
PPM
MAXIMUM
MEAN
MINIMUM
MARCHBURN
AFTON
BLACKCRAIG
SCAR
SCHINNEL
PYROXENOUS
INTERMEDIATE
HAWICK
FORMATION

FIGURE 67 a-c

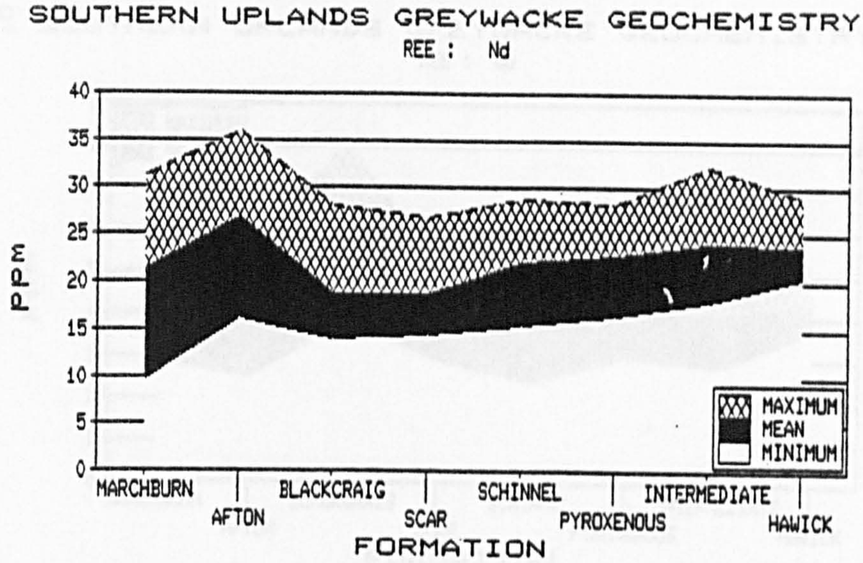
SOUTHERN UPLANDS GREYWACKE GEOCHEMISTRY
REE : Nd
PPM
0
5
10
15
20
25
30
35
40
MAXIMUM
MEAN
MINIMUM
MARCHBURN
AFTON
BLACKCRAIG
SCAR
SCHINNEL
PYROXENOUS
INTERMEDIATE
HAWICK
FORMATION

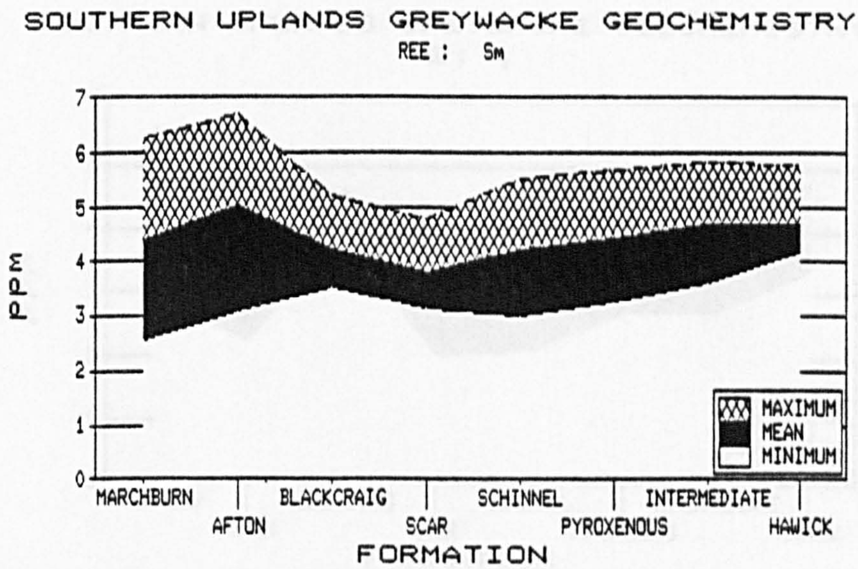
SOUTHERN UPLANDS GREYWACKE GEOCHEMISTRY
REE : Sm
PPM
0
1
2
3
4
5
6
7
MAXIMUM
MEAN
MINIMUM
MARCHBURN
AFTON
BLACKCRAIG
SCAR
SCHINNEL
PYROXENOUS
INTERMEDIATE
HAWICK
FORMATION

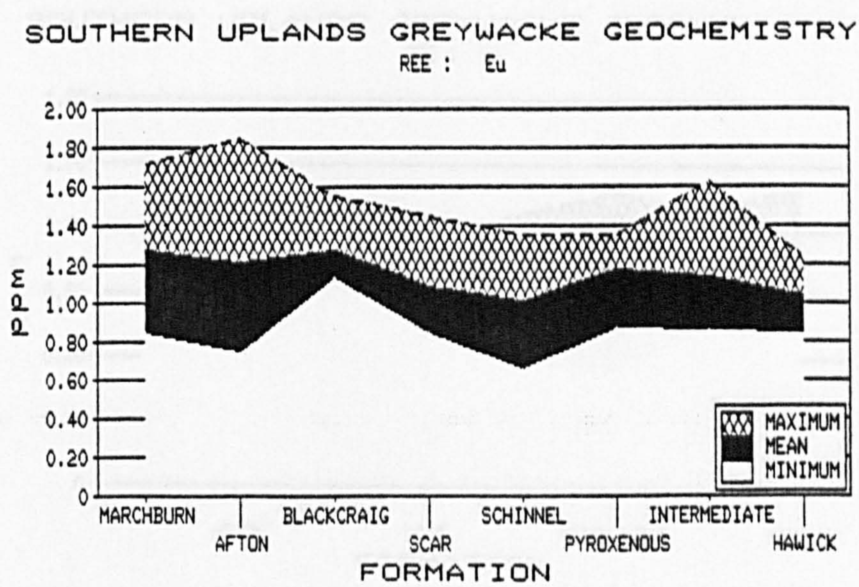
SOUTHERN UPLANDS GREYWACKE GEOCHEMISTRY
REE : Eu
PPM
0
0.20
0.40
0.60
0.80
1.00
1.20
1.40
1.60
1.80
2.00
MAXIMUM
MEAN
MINIMUM
MARCHBURN
AFTON
BLACKCRAIG
SCAR
SCHINNEL
PYROXENOUS
INTERMEDIATE
HAWICK
FORMATION

FIGURE 68 a-c

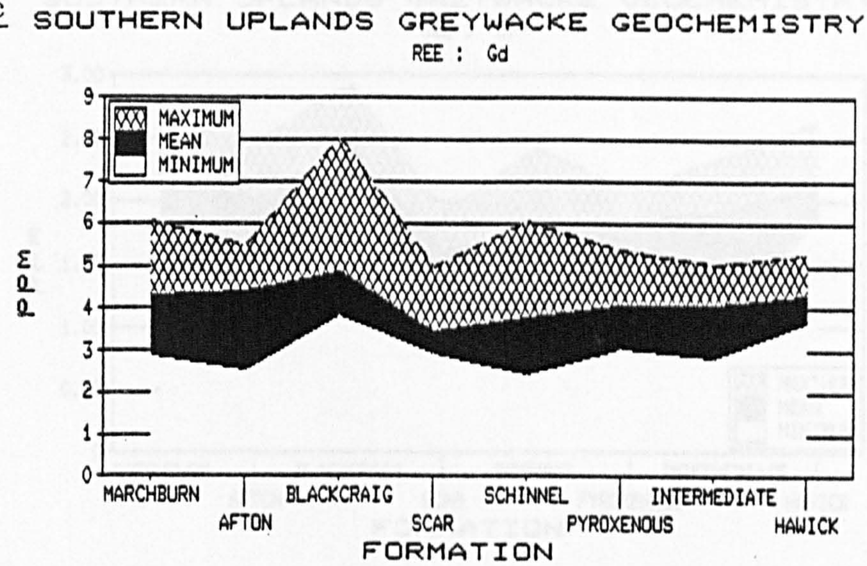
SOUTHERN UPLANDS GREYWACKE GEOCHEMISTRY
REE : Gd
MAXIMUM
MEAN
MINIMUM
PPM
0
1
2
3
4
5
6
7
8
9
MARCHBURN
AFTON
BLACKCRAIG
SCAR
SCHINNEL
PYROXENOUS
INTERMEDIATE
HAWICK
FORMATION

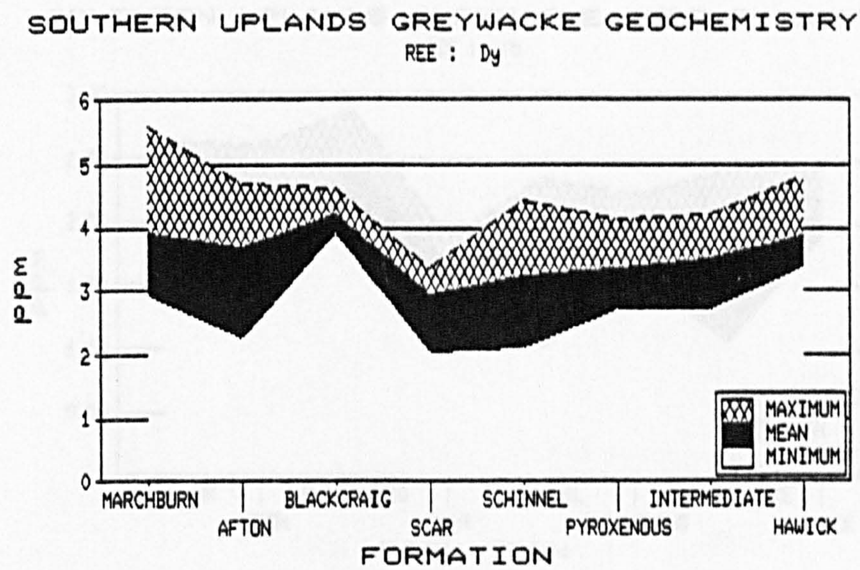
SOUTHERN UPLANDS GREYWACKE GEOCHEMISTRY
REE : Dy
PPM
0
1
2
3
4
5
6
MAXIMUM
MEAN
MINIMUM
MARCHBURN
AFTON
BLACKCRAIG
SCAR
SCHINNEL
PYROXENOUS
INTERMEDIATE
HAWICK
FORMATION

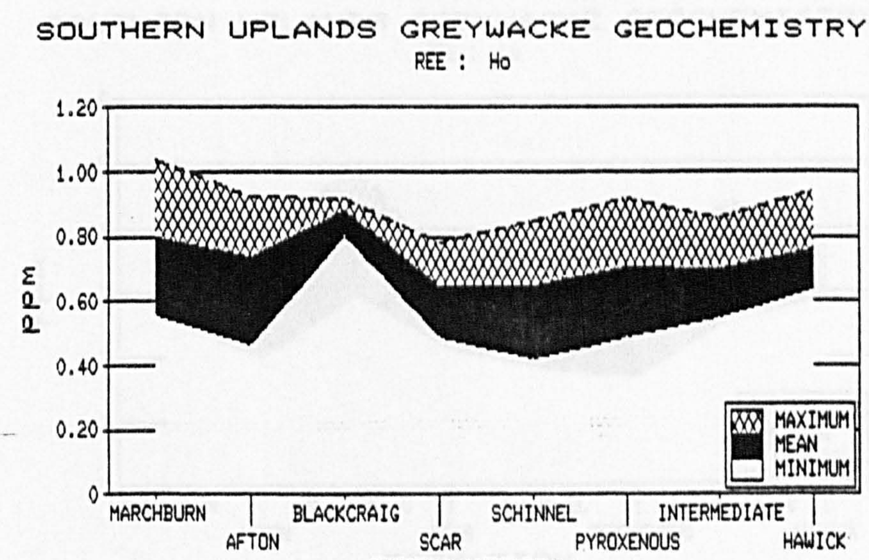
SOUTHERN UPLANDS GREYWACKE GEOCHEMISTRY
REE : Ho
PPM
0
0.20
0.40
0.60
0.80
1.00
1.20
MAXIMUM
MEAN
MINIMUM
MARCHBURN
AFTON
BLACKCRAIG
SCAR
SCHINNEL
PYROXENOUS
INTERMEDIATE
HAWICK
FORMATION

FIGURE 69 a-c

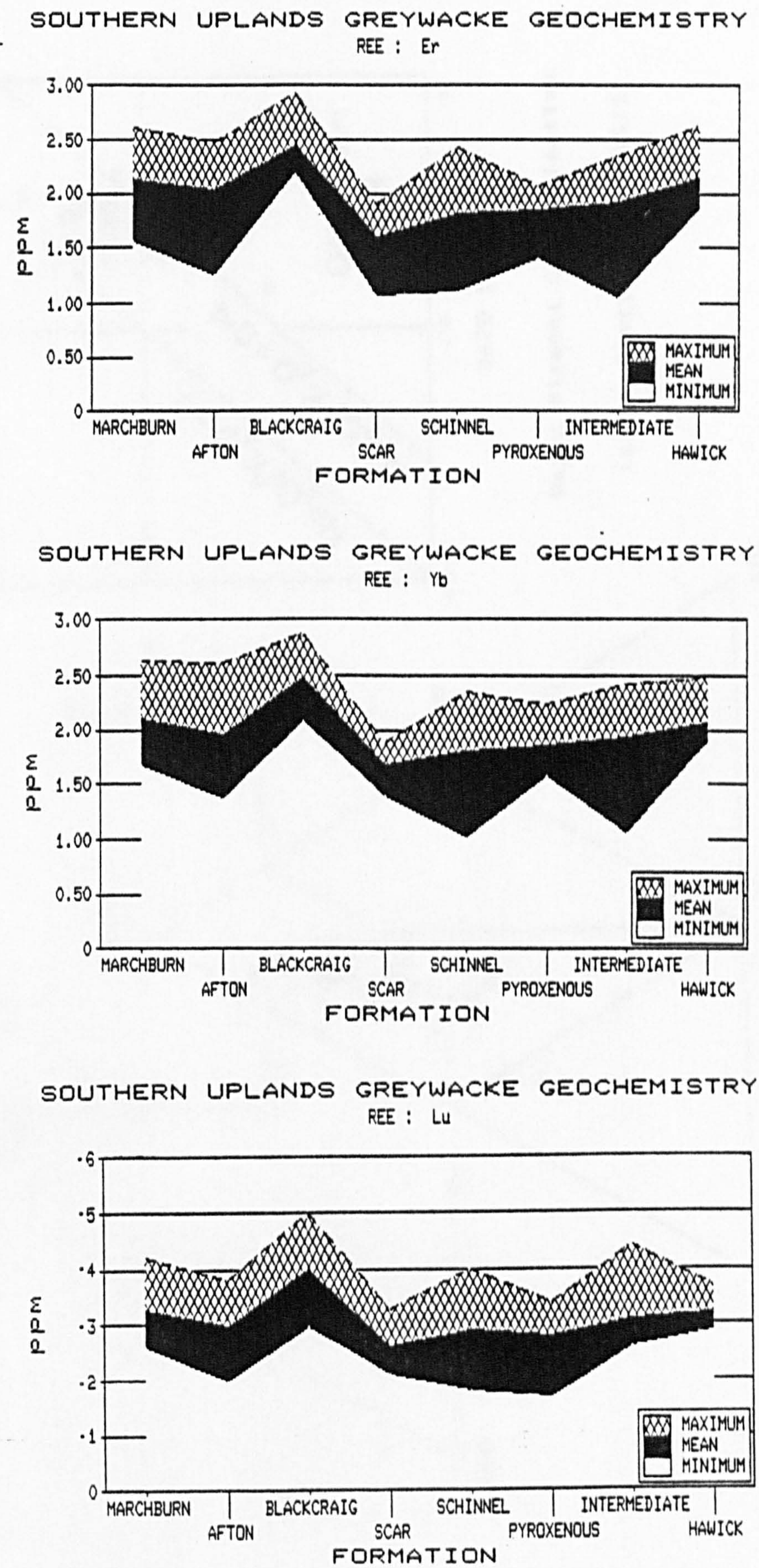
SOUTHERN UPLANDS GREYWACKE GEOCHEMISTRY
REE : Er
PPM
3.00
2.50
2.00
1.50
1.00
0.50
0
MAXIMUM
MEAN
MINIMUM
MARCHBURN
AFTON
BLACKCRAIG
SCAR
SCHINNEL
PYROXENOUS
INTERMEDIATE
HAWICK
FORMATION
SOUTHERN UPLANDS GREYWACKE GEOCHEMISTRY
REE : Yb
PPM
3.00
2.50
2.00
1.50
1.00
0.50
0
MAXIMUM
MEAN
MINIMUM
MARCHBURN
AFTON
BLACKCRAIG
SCAR
SCHINNEL
PYROXENOUS
INTERMEDIATE
HAWICK
FORMATION
SOUTHERN UPLANDS GREYWACKE GEOCHEMISTRY
REE : Lu
PPM
·6
·5
·4
·3
·2
·1
0
MAXIMUM
MEAN
MINIMUM
MARCHBURN
AFTON
BLACKCRAIG
SCAR
SCHINNEL
PYROXENOUS
INTERMEDIATE
HAWICK
FORMATION

FIGURE 70

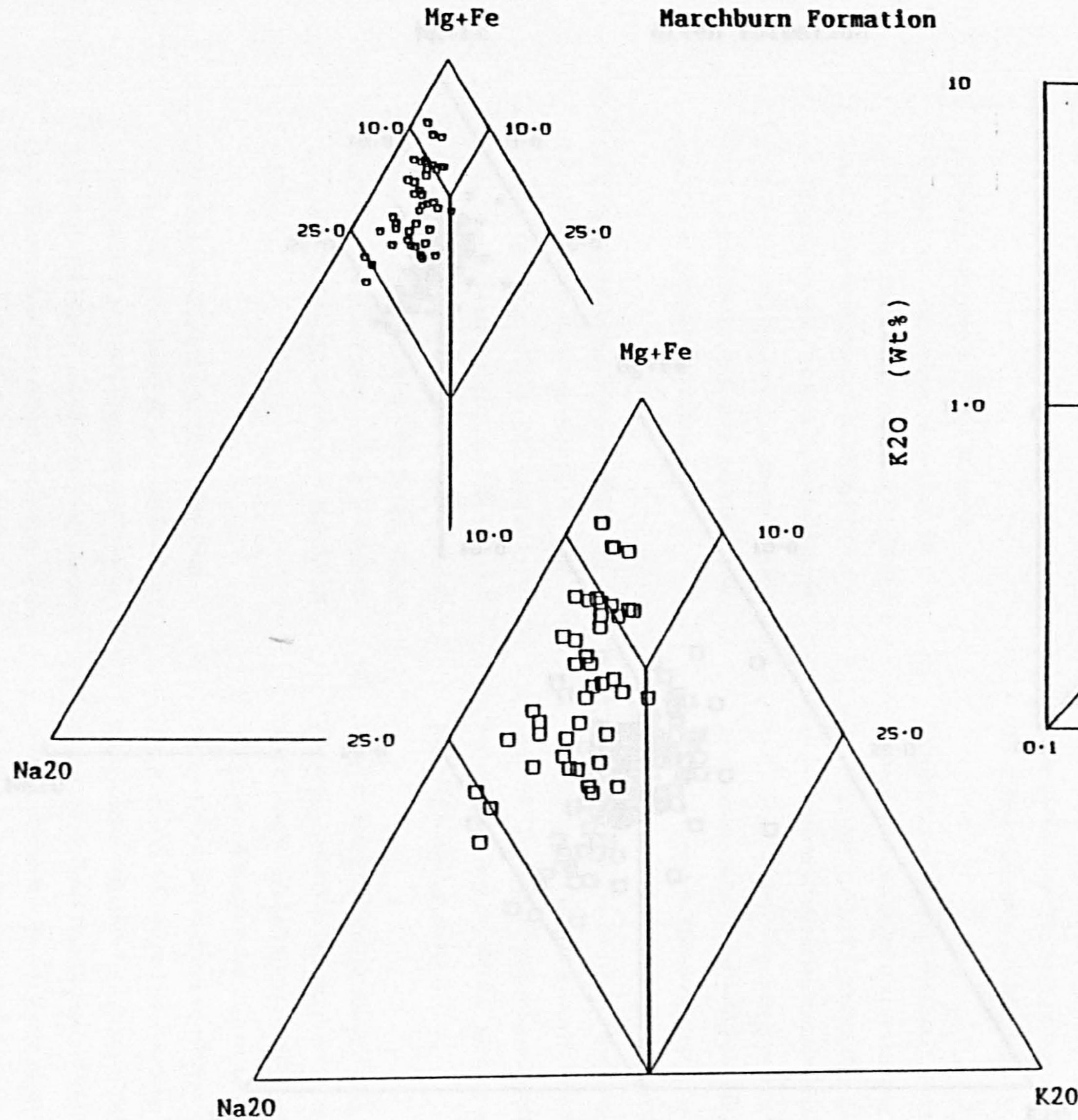

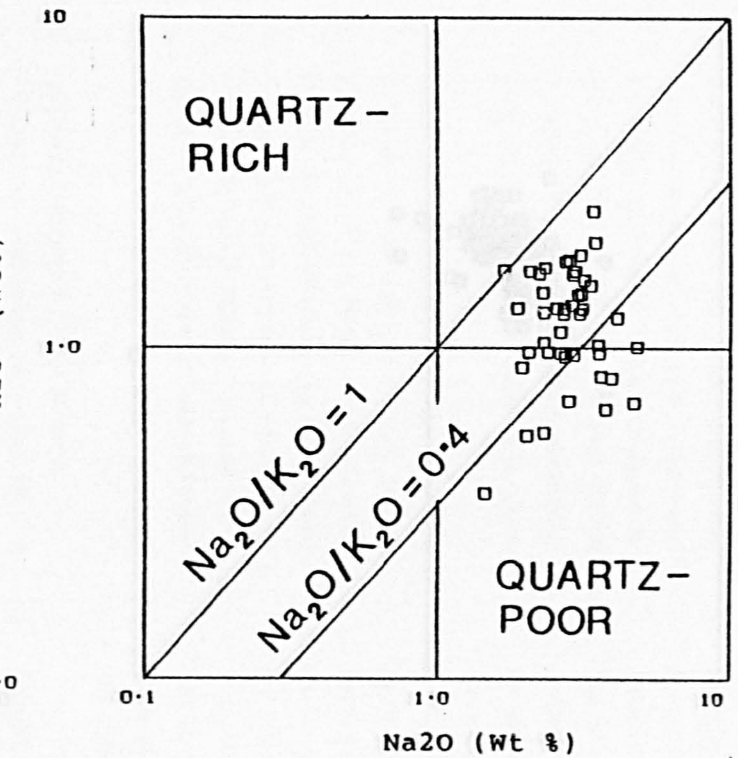

Major Element Classification

(after Blatt et. al. 1972)

FIGURE 71

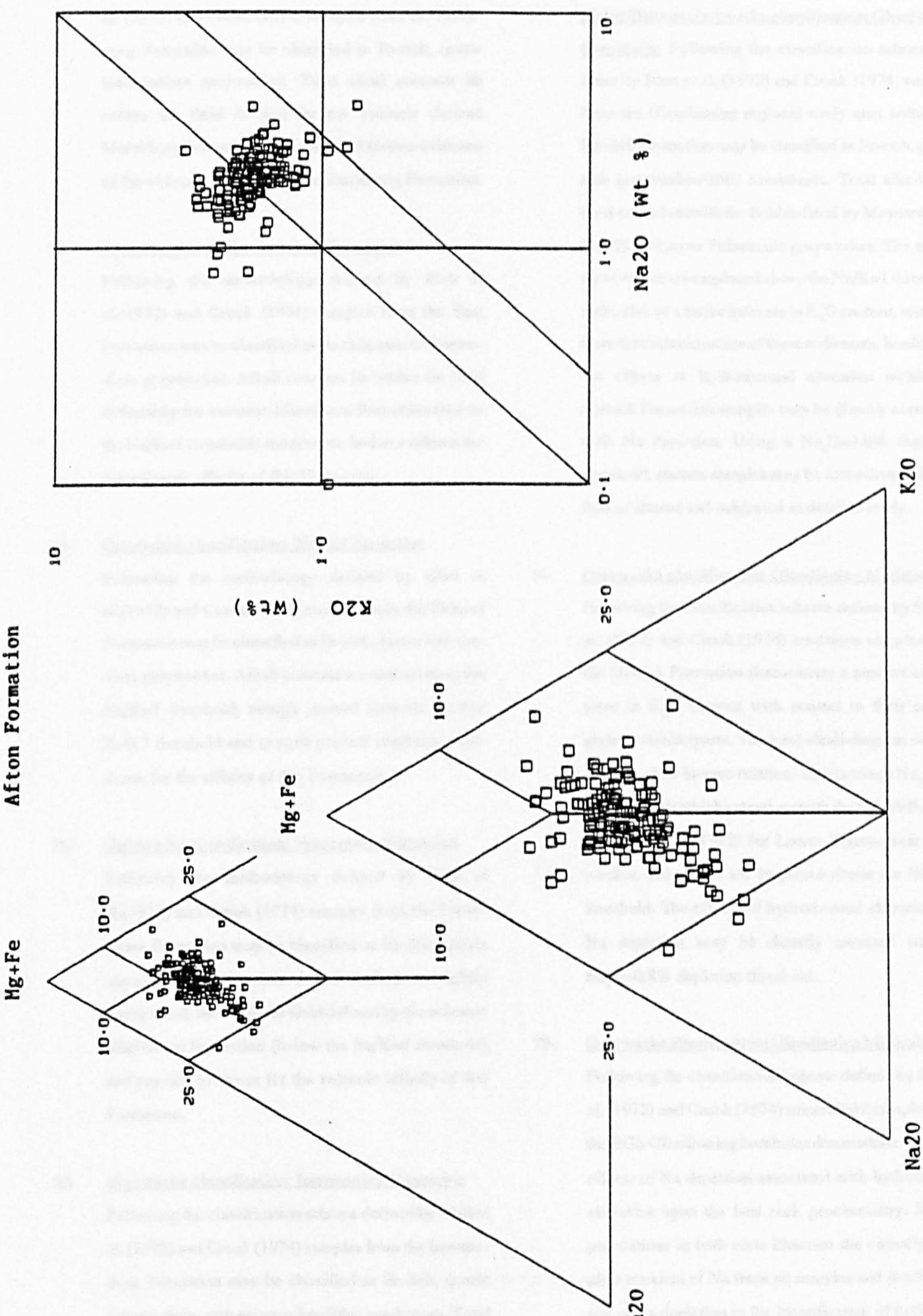

72- Greywacke classification: Blackcraig Formation
Following the classification scheme defined by Blatt et al. (1972) and Crook (1974) samples from the Blackcraig Formation may be classified as Fe-rich, quartz intermediate greywackes. Total alkali contents lie within the field defined by the volcanic derived Marchburn Formation, and provided further evidence of the volcanic affinities of the Blackcraig Formation.

73- Greywacke classification: Scar Formation
Following the methodology defined by Blatt et al.(1972) and Crook (1974) samples from the Scar Formation may be classified as Fe-rich, quartz intermediate greywackes. Alkali contents lie within the field defined by the volcanic Marchburn Formation (below the Na/K=1 threshold) and provide further evidence for the volcanic affinity of this Formation.

74- Greywacke classification: Shinnel Formation
Following the methodology defined by Blatt et al.(1972) and Crook (1974) samples from the Shinnel Formation may be classified as Fe-rich, quartz intermediate greywackes. Alkali contents are centred upon the Na/K=1 threshold, though skewed towards the Na/K=0.7 threshold and as such provide conflicting evidence for the affinity of this Formation.

75- Greywacke classification: Pyroxenous Formation
Following the methodology defined by Blatt et al.(1972) and Crook (1974) samples from the Pyroxenous Formation may be classified as Fe-rich, quartz intermediate greywackes. Alkali contents are tightly constrained, lie within the field defined by the volcanic Marchburn Formation (below the Na/K=1 threshold) and provide evidence for the volcanic affinity of this Formation.

76- Greywacke classification: Intermediate Formation
Following the classification scheme defined by Blatt et al. (1972) and Crook (1974) samples from the Intermediate Formation may be classified as Fe-rich, quartz intermediate -rich greywackes/lithic sandstones. Total alkali contents lie within the field defined by Maynard et al. (1982) however, values are centered upon the Na/K=1 threshold, indicative of an increase in K_2O content with respect to the juxtaposed Pyroxenous Formation, and the cratonic nature of these sediments.

77- Major Element Greywacke classification: Glendinning Greywacke Following the classification scheme defined by Blatt et al. (1972) and Crook (1974) samples from the Glendinning regional study area within the Hawick Formation may be classified as Fe-rich, quartz rich greywackes/lithic sandstones. Total alkali contents extend outwith the field defined by Maynard et al. (1982) for Lower Palaeozoic greywackes. The majority of values are emplaced above the Na/K=1 threshold, indicative of a major increase in K_2O content, resulting from the cratonic nature of these sediments. In addition, the effects of hydrothermal alteration within the Hawick Formation samples may be directly correlated with Na depletion. Using a Na_2O=1.0% depletion threshold, sixteen samples may be immediately identified as altered and subjected to detailed study.

78- Greywacke classification: Glendinning Mudstone
Following the classification scheme defined by Blatt et al. (1972) and Crook (1974) mudstone samples from the Hawick Formation demonstrate a positive enrichment in K_2O content with respect to their coarser grained counterparts. The total alkali diagram demonstrates a clear inverse relation- ship between Na_2O and K_2O contents which extend outwith the field defined by Maynard et al.(1982) for Lower Palaeo- zoic greywackes. All values are emplaced above the Na/K=1 threshold. The effects of hydrothermal alteration and Na depletion may be directly assessed using a Na_2O=0.8% depletion threshold.

79- Greywacke classification: Glendinning Mineralisation
Following the classification scheme defined by Blatt et al. (1972) and Crook (1974) mineralised samples from the BGS Glendinning boreholes demonstrate the major effects of Na depletion associated with hydrothermal alteration upon the host rock geochemistry. Sample populations in both plots illustrate the virtually complete removal of Na from all samples and justifies the use of Na depletion in the identification of hydrothermally altered samples in the regional sample set.

80- Th-Co-Zr/10 Greywacke Classification
The discrimination diagram defined by Bhatia (1985)

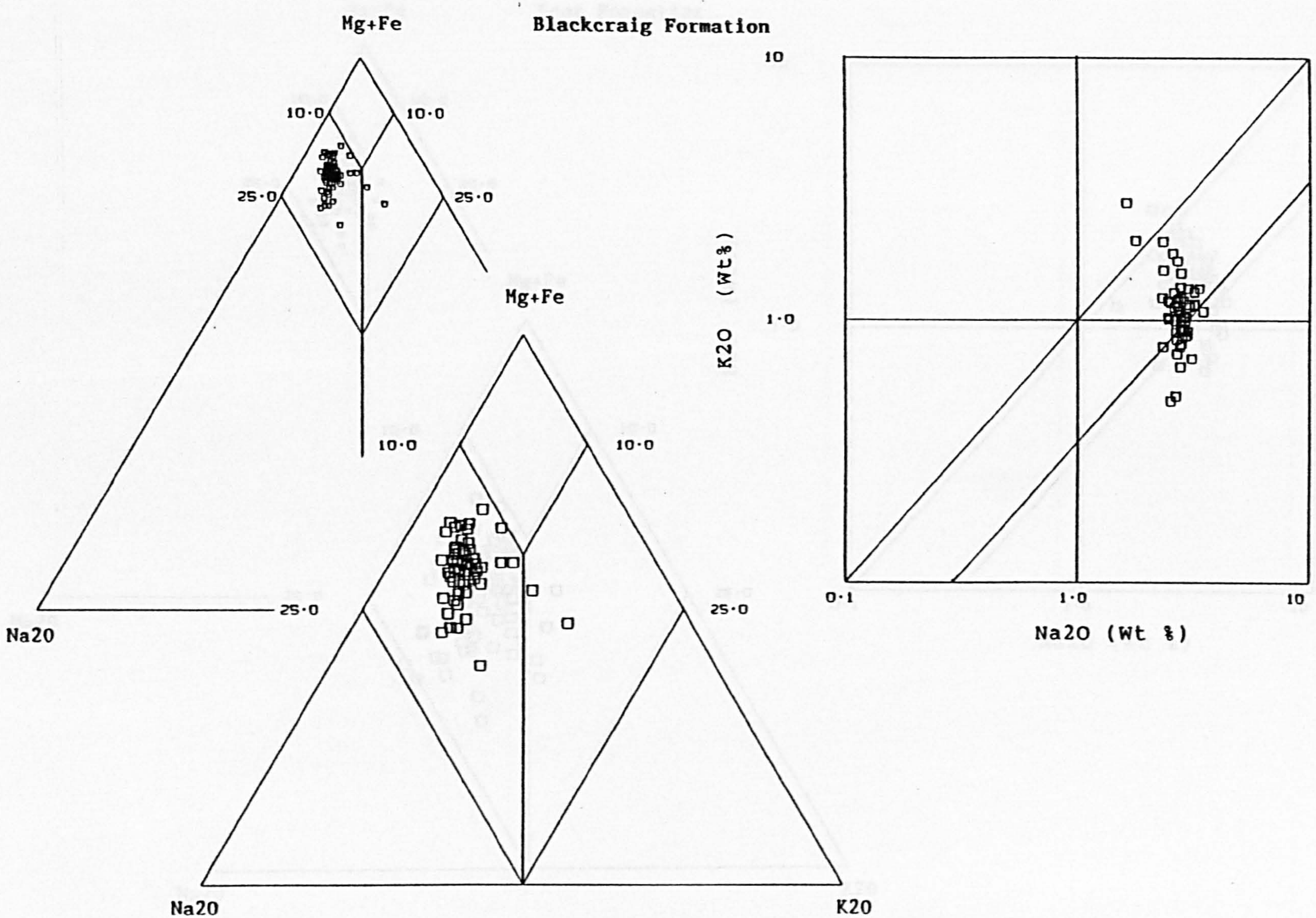

Blackcraig Formation
Mg+Fe
10·0
10·0
25·0
25·0
10·0
25·0
Na2O
Mg+Fe
10·0
10·0
25·0
25·0
Na2O
K2O
10
1·0
K2O (Wt%)
0·1
1·0
10
Na2O (Wt %)

FIGURE 72

FIGURE 73

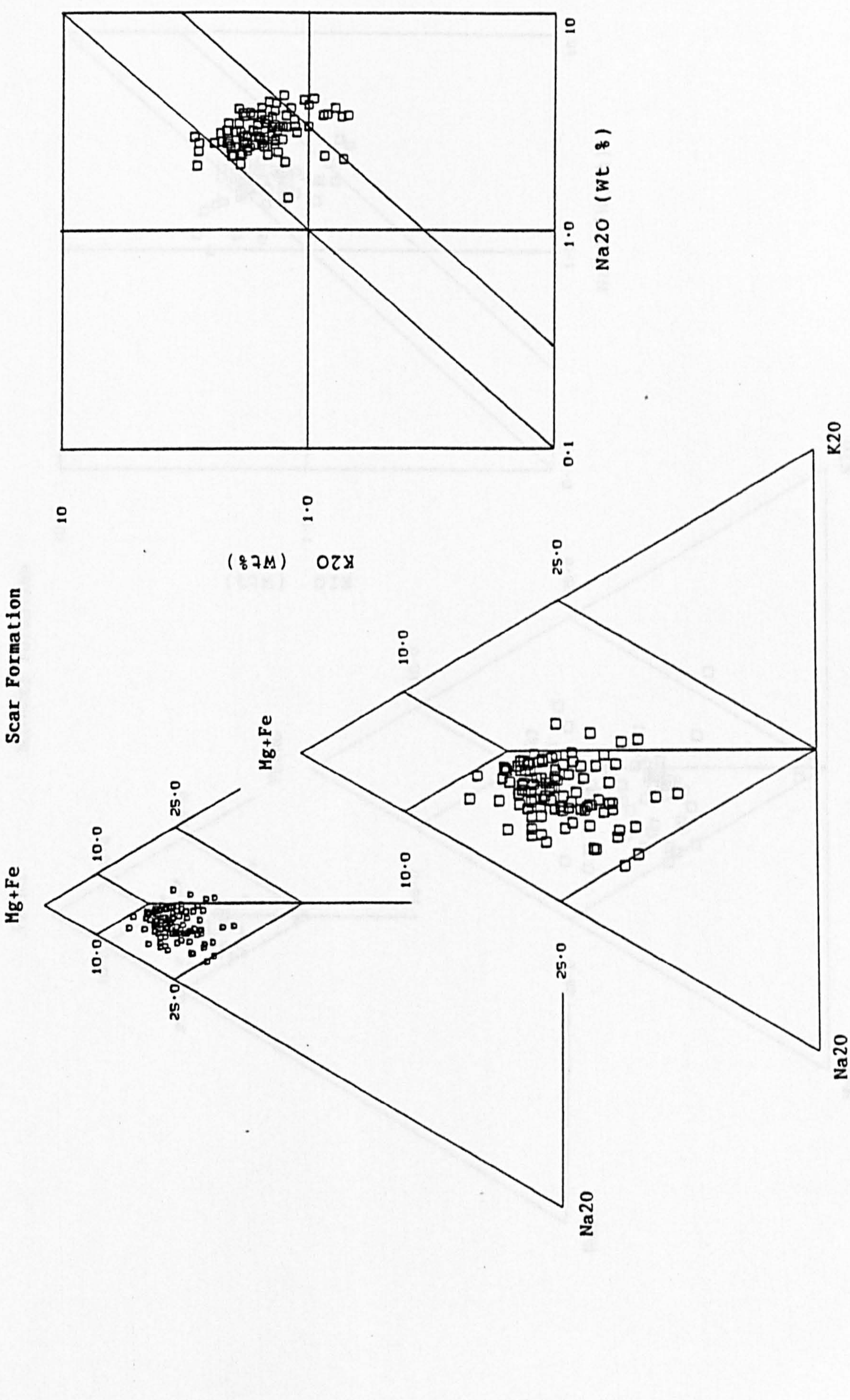

FIGURE 74

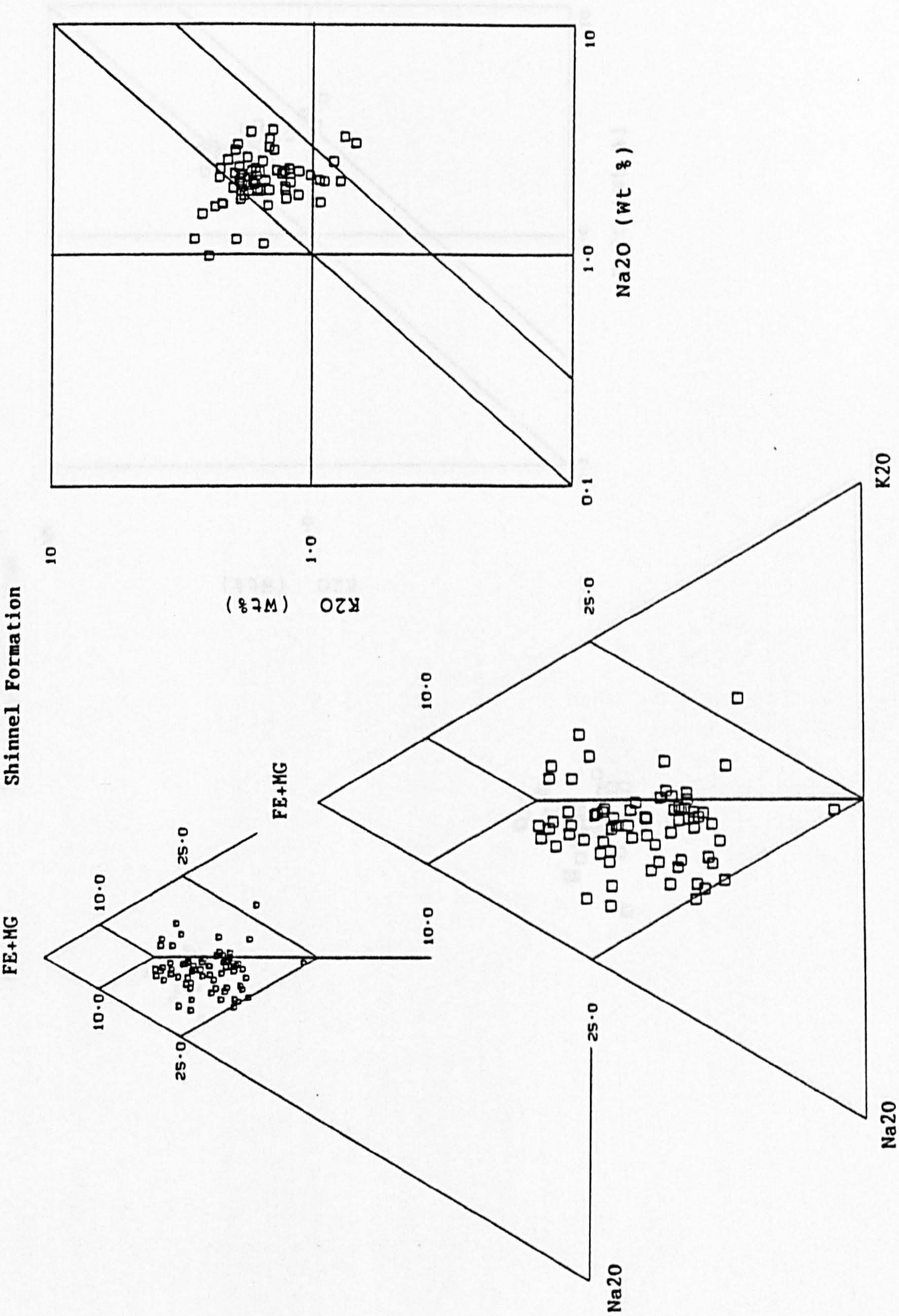
Shinnel Formation
Na2O (Wt %)
K2O (Wt%)
10
1.0
0.1
FE+MG
K2O
Na2O
10.0
25.0

FIGURE 75

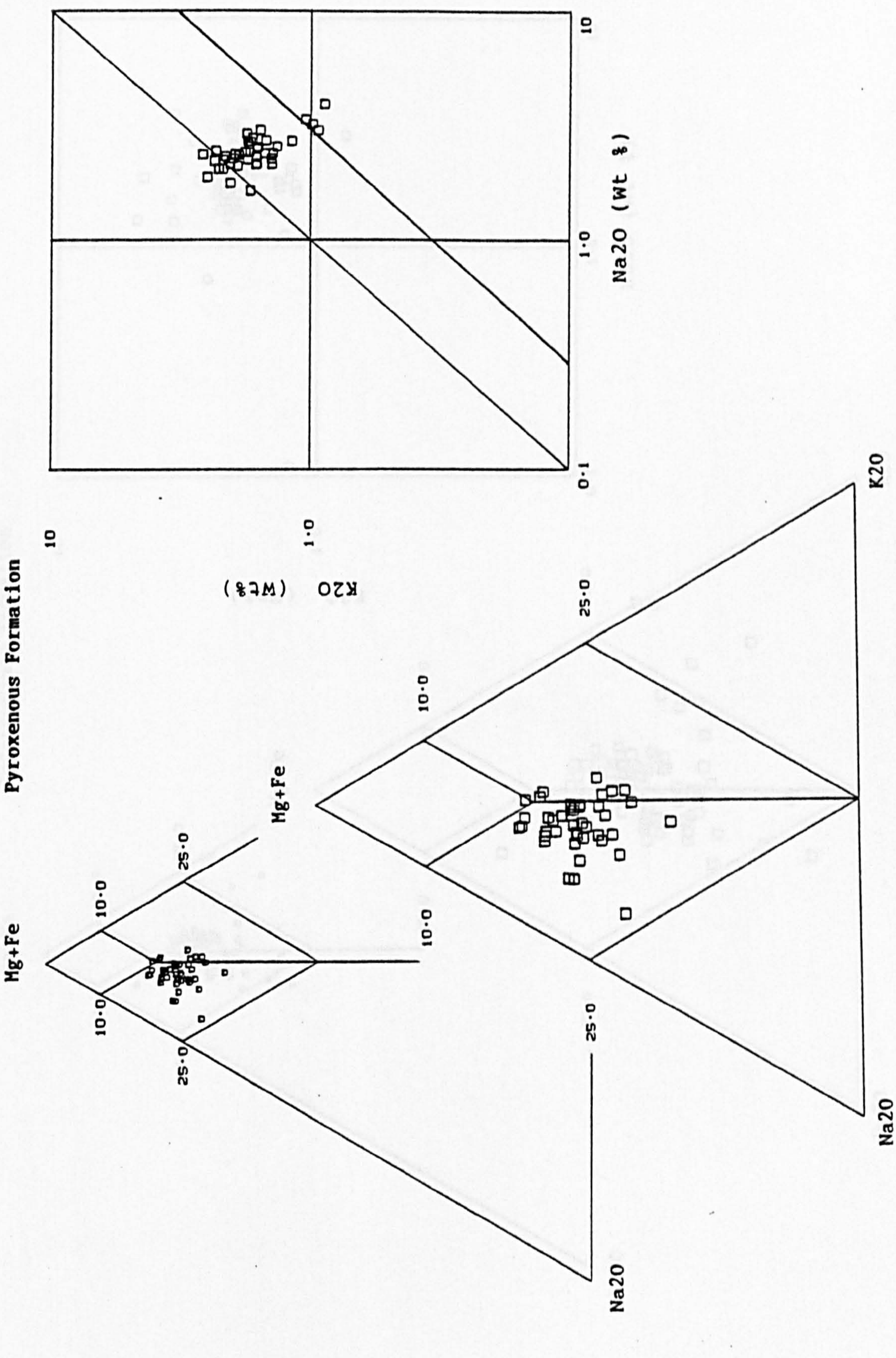

Pyroxenous Formation
K2O (Wt%)
Na2O (Wt %)
0·1
1·0
10
Mg+Fe
K2O
Na2O
10·0
25·0

FIGURE 76

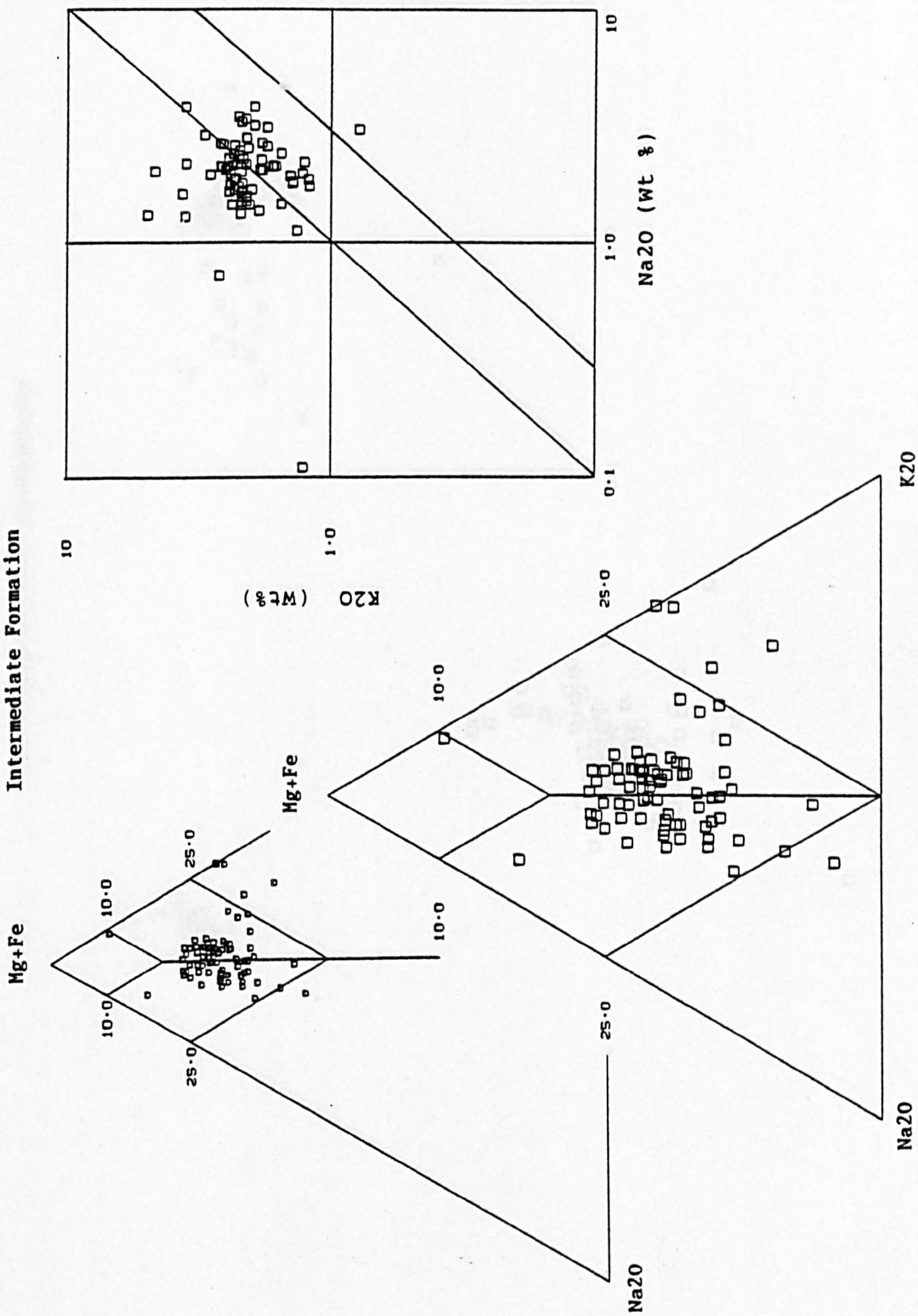
Intermediate Formation
K2O (Wt%)
Na2O (Wt %)
10
1·0
0·1
Mg+Fe
Na2O
K2O
10·0
25·0

FIGURE 77

Glendinning Greywacke Geochemistry

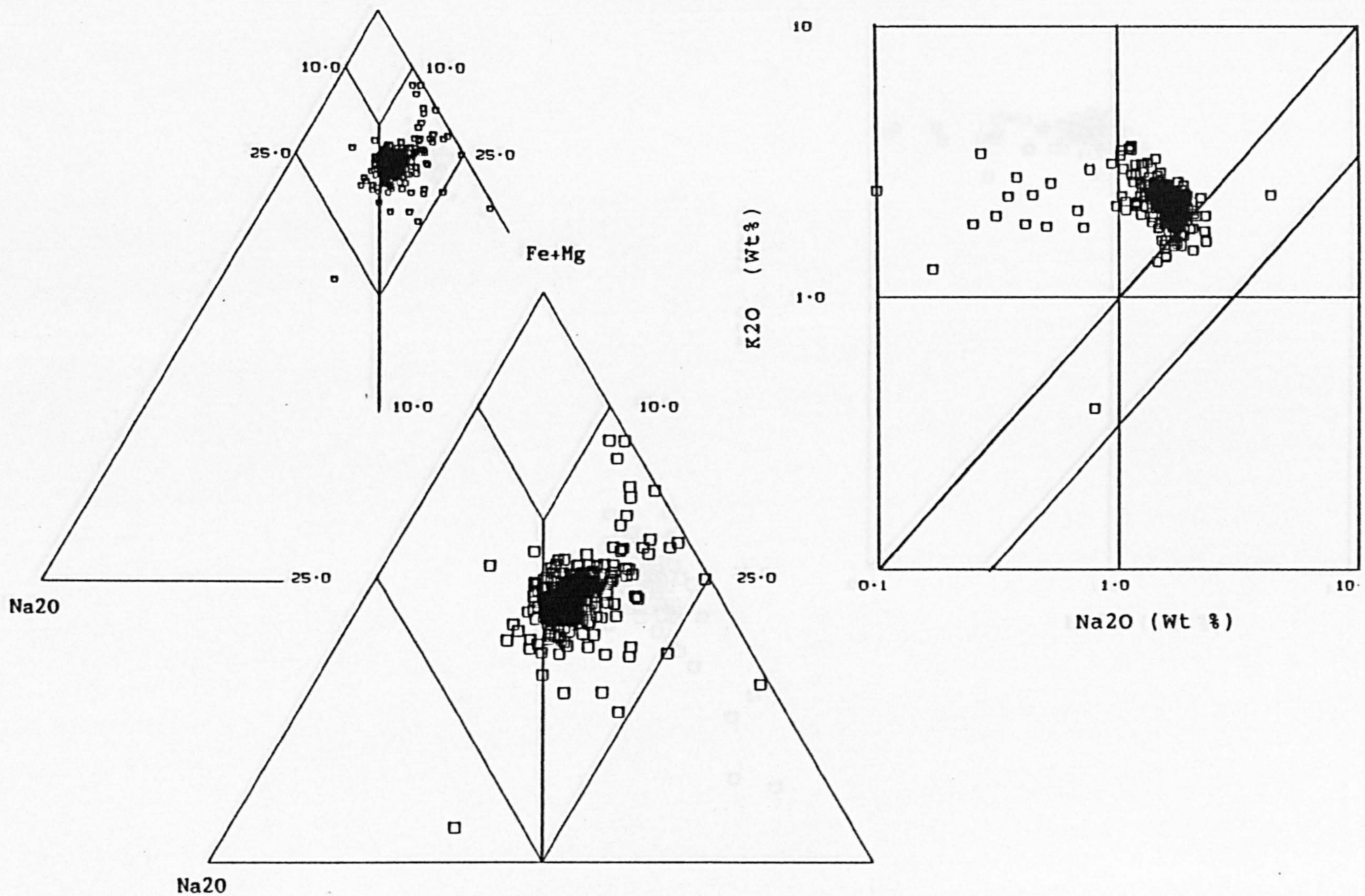

FIGURE 78

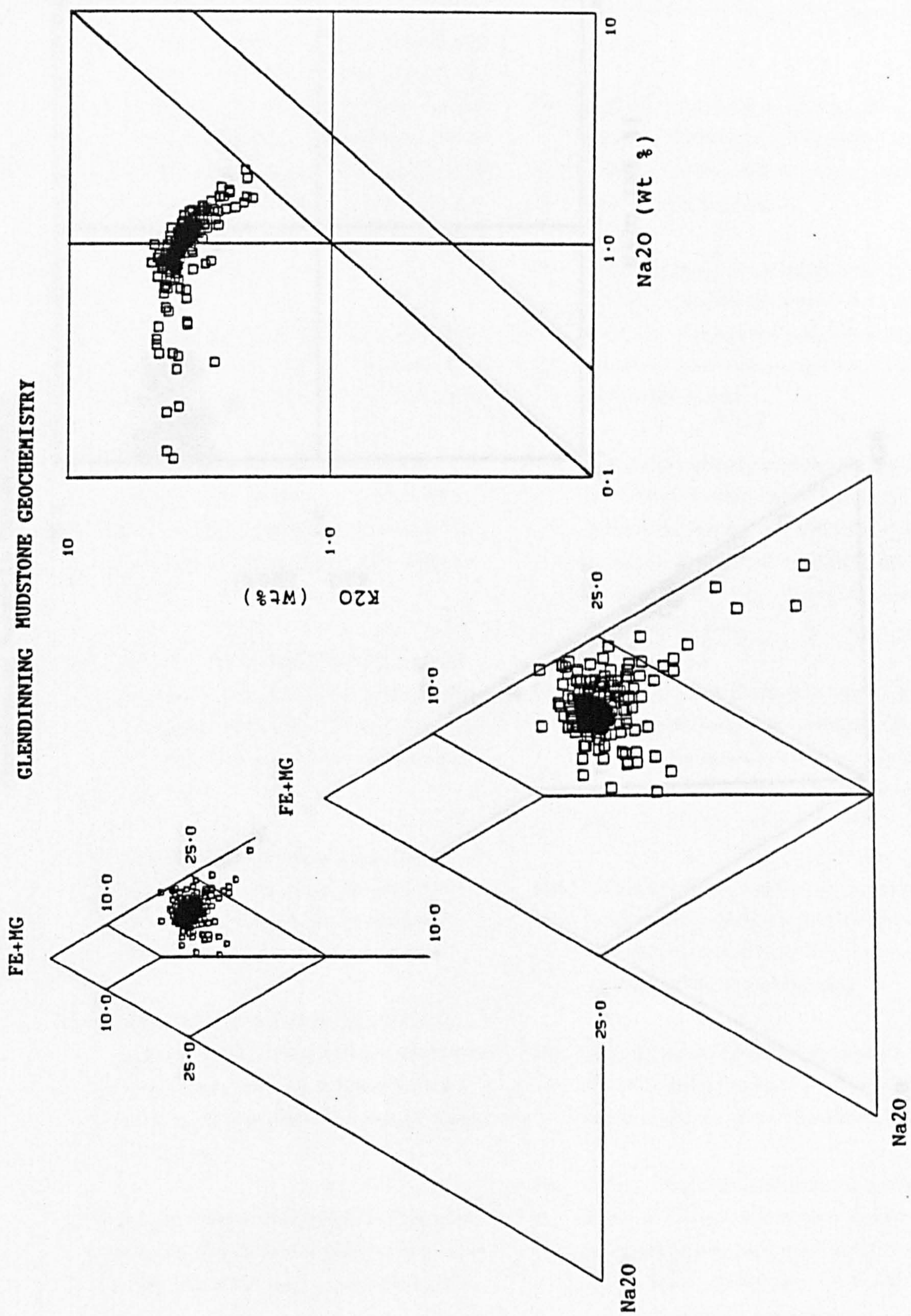
GLENDINNING MUDSTONE GEOCHEMISTRY
K2O (Wt%)
Na2O (Wt %)
0·1
1·0
10
FE+MG
Na2O
10·0
25·0

FIGURE 79

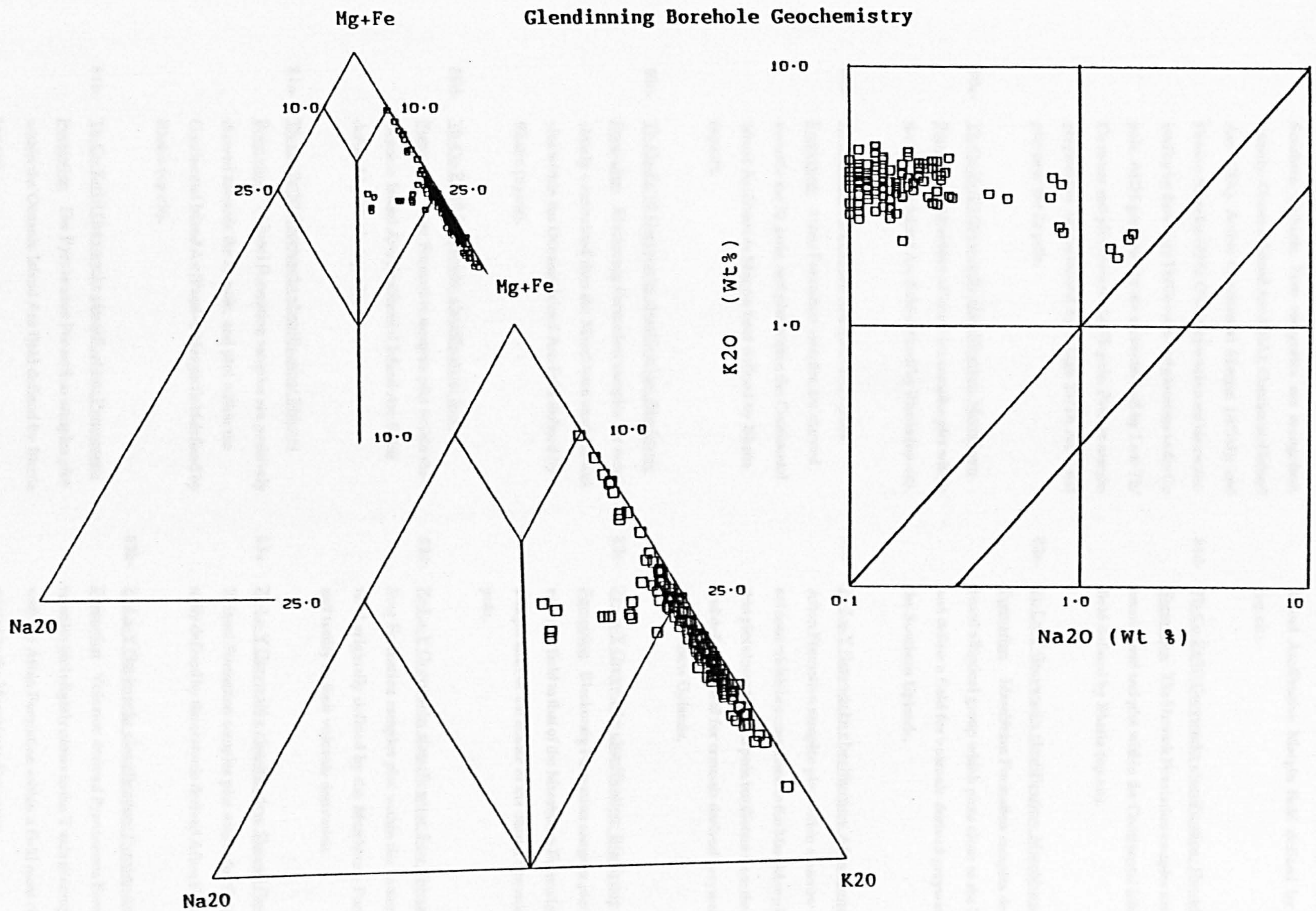
Glendinning Borehole Geochemistry
Mg+Fe
10·0
10·0
25·0
25·0
10·0
25·0
Na2O
Mg+Fe
10·0
10·0
25·0
Na2O
K2O
10·0
1·0
K2O (Wt%)
0·1
1·0
10
Na2O (Wt %)

may be used to classify the distinct provenance types and tectonic setting of differing petrofacies in the Southern Uplands. Four categories are recognised, namely: Oceanic Island Arc (OIA); Continental Island Arc (CIA); Active Continental Margin (ACM); and Passive Margins (PM). OIA greywackes are characterised by by their high Th/Co ratio and plot close to the Co pole. ACM greywackes are characterised by Low Th/Co ratios and plot close to the Th pole. Passive margin greywackes characterised by a high Zr/Th ratio and plot near the Zr pole.

80a- Th-Co-Zr/10 Greywacke classification: Marchburn Formation. Marchburn Formation samples plot within the Oceanic Island Arc field defined by Bhatia (op.cit).

80b- Th-Co-Zr/10 Greywacke classification: Afton Formation. Afton Formation samples are skewed towards the Zr pole, and plot within the Continental Island Arc/Passive Margin field defined by Bhatia (op.cit).

80c- Th-Co-Zr/10 Greywacke classification: Blackcraig Formation Blackcraig Formation samples are more closely constrained than the Marchburn samples and plot within the Oceanic Island Arc field defined by Bhatia (op.cit).

80d- Th-Co-Zr/10 Greywacke classification: Scar Formation Scar Formation samples plot within the Oceanic Island Arc/Continental Island Arc fields defined by Bhatia (op.cit).

81a- Th-Co-Zr/10 Greywacke classification: Shinnel Formation Shinnel Formation samples are positively skewed towards the Zr pole, and plot within the Continental Island Arc/Passive Margin field defined by Bhatia (op.cit).

81b- Th-Co-Zr/10 Greywacke classification: Pyroxenous Formation The Pyroxenous Formation samples plot within the Oceanic Island Arc field defined by Bhatia (op.cit).

81c- Th-Co-Zr/10 Greywacke classification: Intermediate Formation The Intermediate Formation samples plot in a similar position to the Shinnel Formation, are skewed towards the Zr pole and lie within the Continental Island Arc/Passive Margin field defined by Bhatia (op.cit).

81d- Th-Co-Zr/10 Greywacke classification: Hawick Formation The Hawick Formation samples are tightly constrained and plot within the Continental Island Arc field defined by Bhatia (op.cit).

82a- Zr-La-Y Greywacke classification: Marchburn Formation Marchburn Formation samples define a broad elliptical group which plots close to the Zr pole and define a field for volcanic derived greywackes in the Southern Uplands.

82b- Zr-La-Y Greywacke classification: Afton Formation Afton Formation samples plot within a narrow elliptical zone which in comparison to the Marchburn Formation plot closer to the Zr pole but distant from the Y pole and defines a field for cratonic derived greywackes in the Southern Uplands.

82c- Zr-La-Y Greywacke classification: Blackcraig Formation Blackcraig Formation samples plot within a similar field to that of the Marchburn Formation, with a slight shift of the center of the cluster towards the Y pole.

82d- Zr-La-Y Greywacke classification: Scar Formation Scar Formation samples plot within the center of the field originally defined by the Marchburn Formation and testify to their volcanic derivation.

83a- Zr-La-Y Greywacke classification: Shinnel Formation Shinnel Formation samples plot within the field originally defined by the cratonic derived Afton Formation.

83b- Zr-La-Y Greywacke classification: Pyroxenous Formation Volcanic derived Pyroxenous Formation samples plot slightly closer to the Y axis in comparison with the Afton Formation within a field most closely related to the Marchburn Formation.

83c- Zr-La-Y Greywacke classification: Intermediate Formation Cratonic derived Intermediate Formation

FIGURE 80

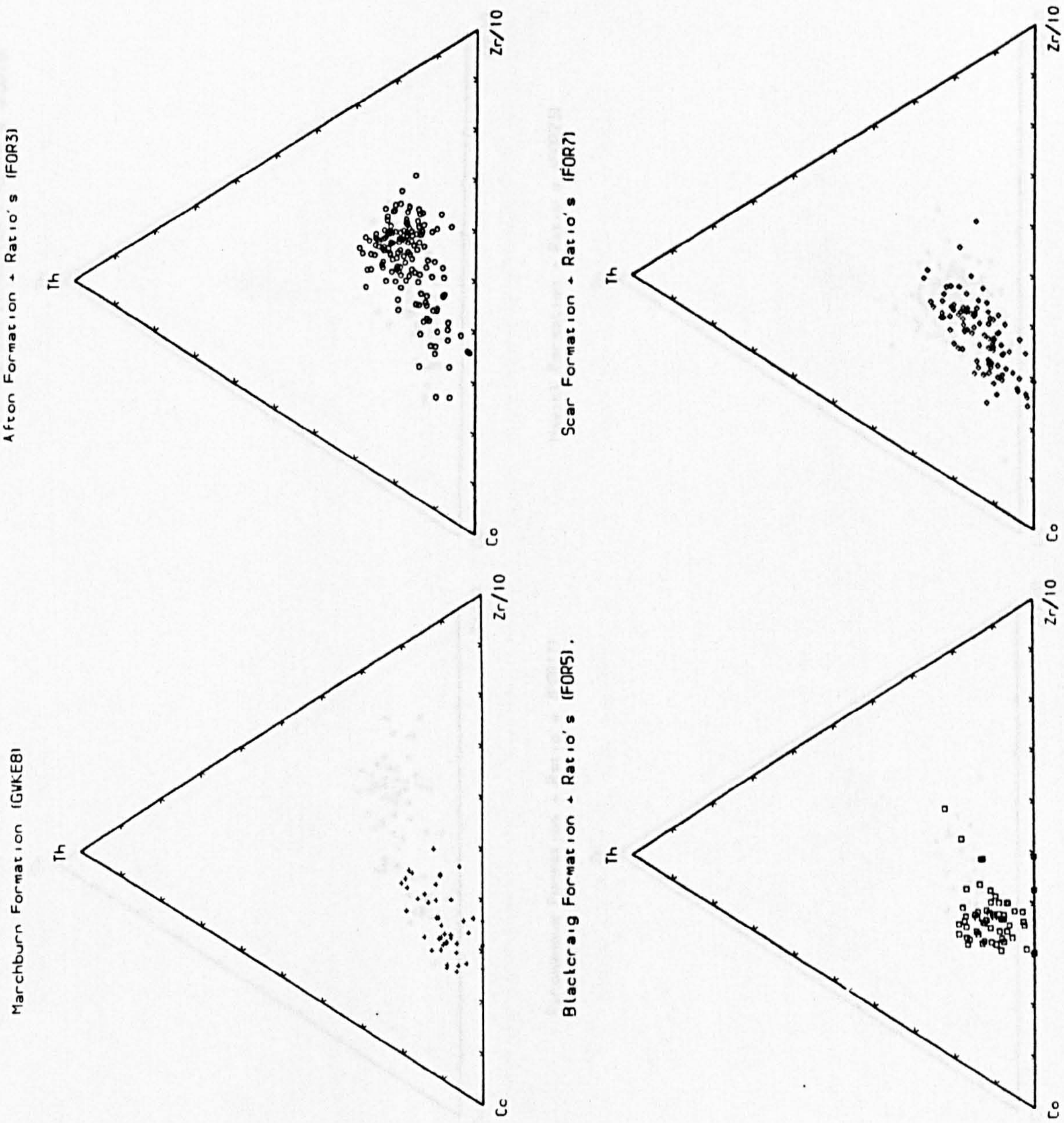
Afton Formation + Ratio's (FOR3)
Scar Formation + Ratio's (FOR7)
Marchburn Formation (GWKE8)
Blackcraig Formation + Ratio's (FOR5).
Th
Zr/10
Co

FIGURE 81

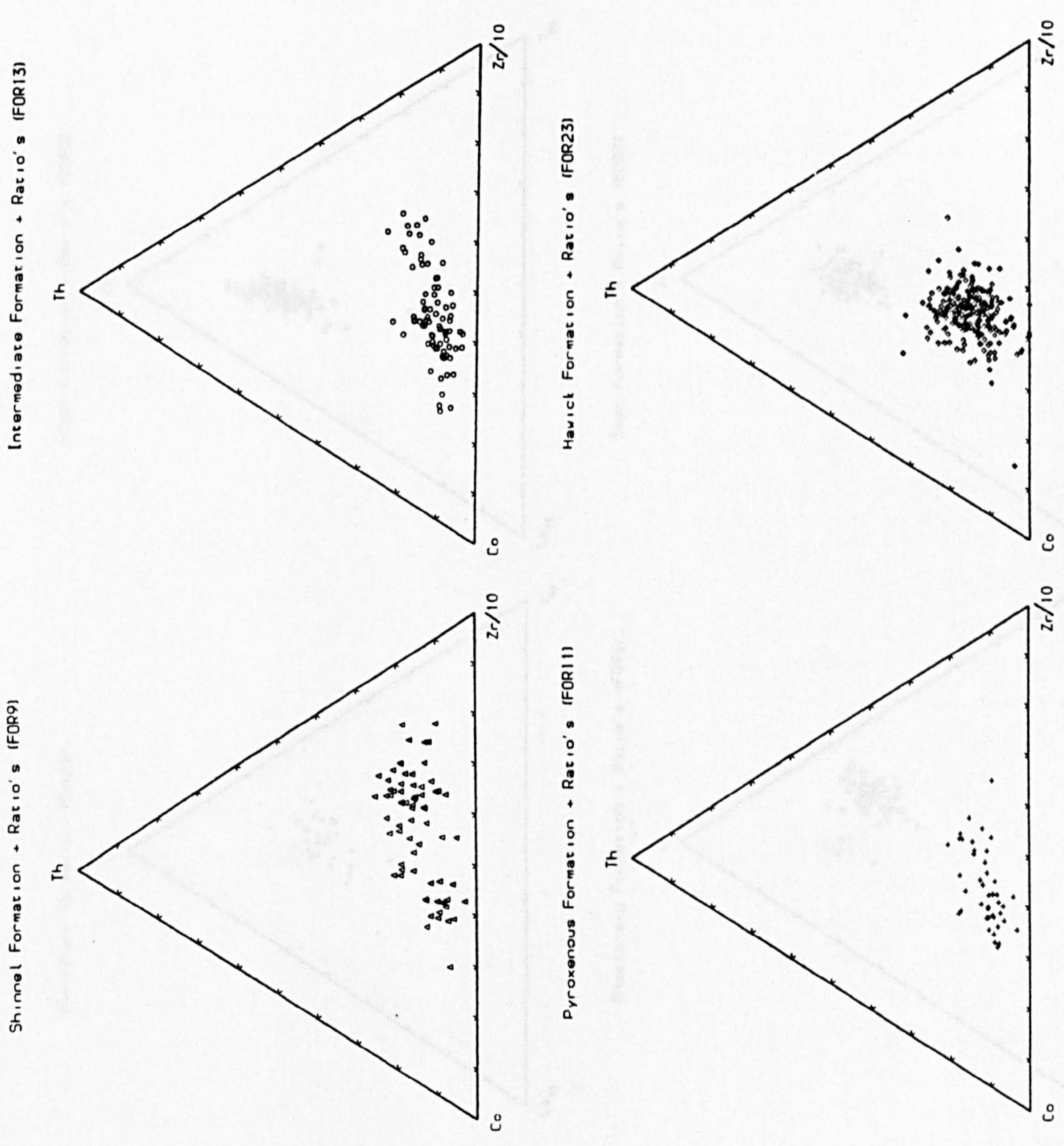
Shinnel Formation + Ratio's (FOR9)
Intermediate Formation + Ratio's (FOR13)
Pyroxenous Formation + Ratio's (FOR11)
Hawick Formation + Ratio's (FOR23)
Th
Co
Zr/10

FIGURE 82

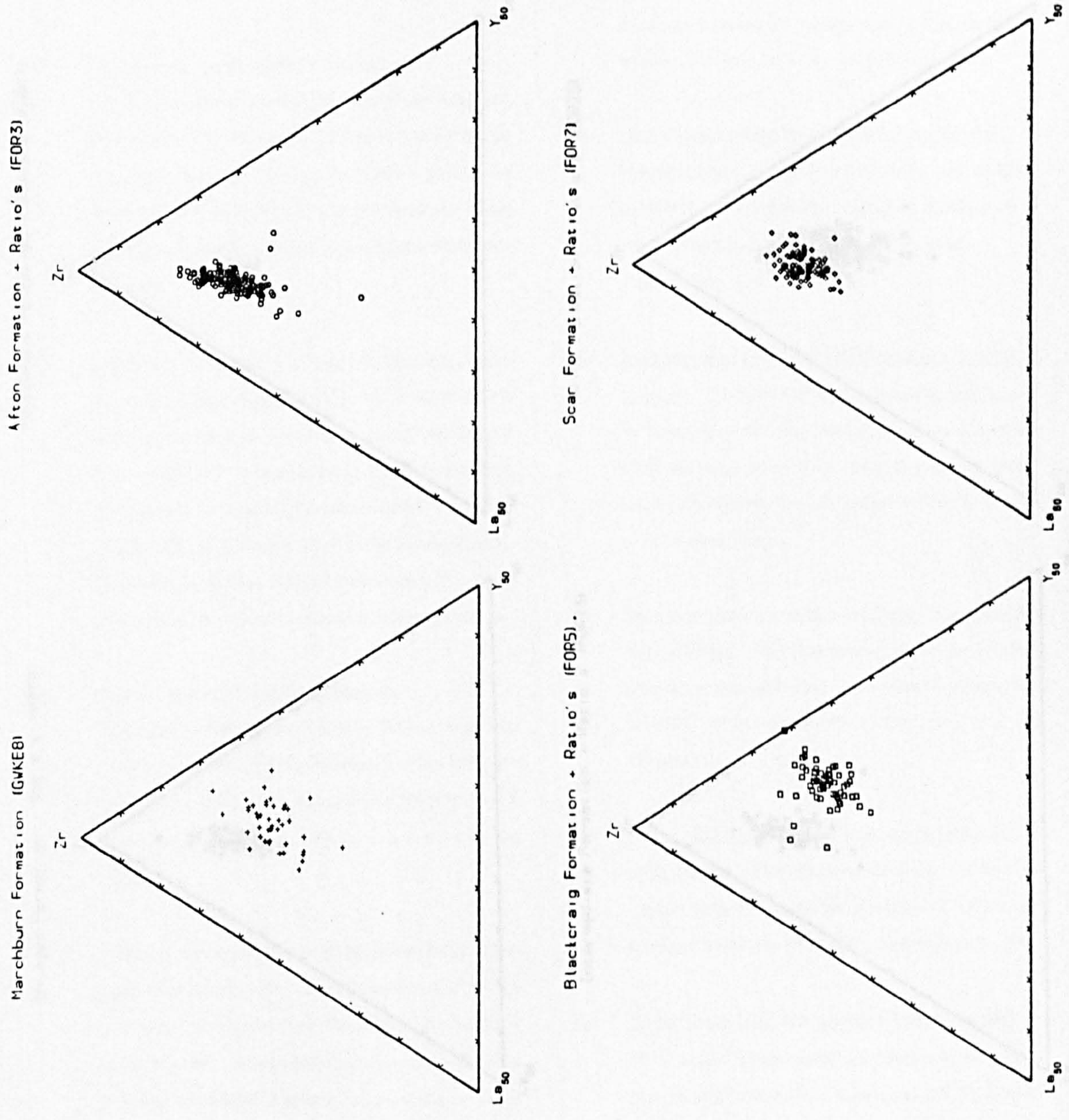
Afton Formation + Ratio's (FOR3)
Zr
Y_{50}
La_{50}
Scar Formation + Ratio's (FOR7)
Zr
Y_{50}
La_{50}
Marchburn Formation (GWKE8)
Zr
Y_{50}
La_{50}
Blackcraig Formation + Ratio's (FOR5).
Zr
Y_{50}
La_{50}

FIGURE 83

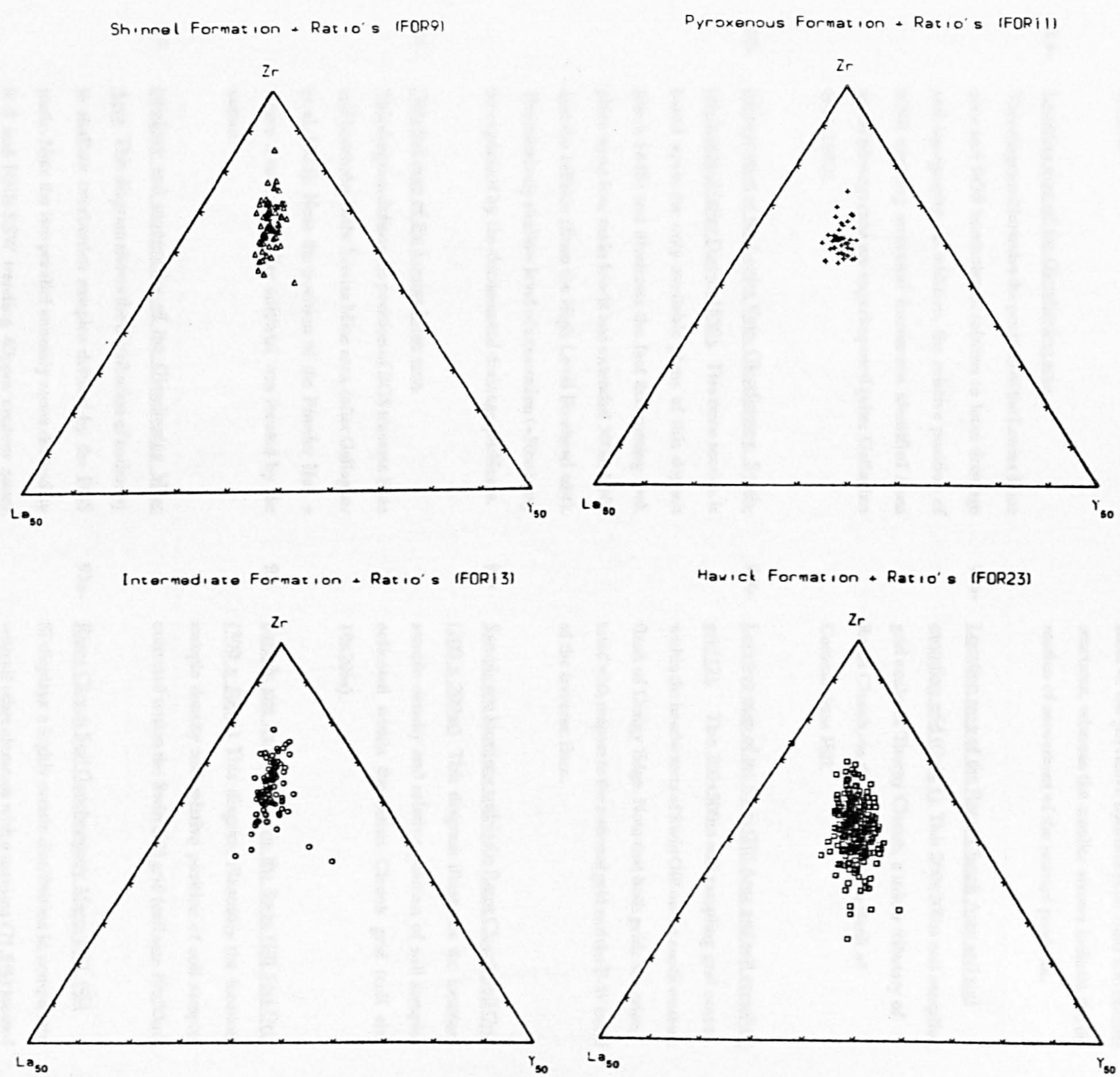
Shinnel Formation + Ratio's (FOR9)
Zr
La_{50}
Y_{50}
Pyroxenous Formation + Ratio's (FOR11)
Zr
La_{50}
Y_{50}
Intermediate Formation + Ratio's (FOR13)
Zr
La_{50}
Y_{50}
Hawick Formation + Ratio's (FOR23)
Zr
La_{50}
Y_{50}

samples plot with a narrow field initially defined by the Afton Formation.

83d- Zr-La-Y Greywacke classification: Hawick Formation Hawick Formation samples display the widest distribution and extending further away from the Zr pole than any previous group. This trend may be partially attributed to the dilution effects of added carbonate upon the system.

84- Location map of the Glendinning area. This diagram illustrates the position of the Louisa Mine area and BGS boreholes in relation to local drainage and topography. In addition, the relative position of NNE trending structural lineaments identified from aerial photographs are superimposed (after Gallagher et al.,1983).

85- Mine section of the Louisa Vein, Glendinning, Southern Scotland (after Dirom, 1850). This mine section is based upon the only available plans of this deposit (circa 1840) and illustrates the fact that mining took place upon four main levels and extended 300m NNE into the hillside (from the High Level Forehead adit). The relatively shallow level of excavation (~50m) may be explained by the documented drainage problems.

86- Detailed map of the Louisa Mine area. This diagram defines the position of BGS traverse lines and boreholes in the Louisa Mine area. (after Gallagher et al.,1983). Note the position of the Powder Hut, a where a second smaller adit/trial was located by the author.

87- Geology and topography of the Glendinning Mine Area This diagram shows the distribution of antimony in shallow overburden samples defined by the BGS study. Note the two parallel anomaly zones defined by N-S and NNE-SSW trending 40ppm contour zones (from Gallagher et al 1983).

88- Hypothetical E-W trending section through the Glendinning deposit. This diagram presents a generalised cross section through the Glendinning deposit defining the approximate dimensions of the alteration zone/pipe (stippled) and anastamosing network of mineralised veins and breccias (black).

89- Summary of geochemical net additions and depletions within the wallrocks adjacent to quartz-stibnite vein mineralisation at Glendinning. This diagram illustrates the major, minor and trace element enrichments and depletions associated with the alteration at Glendinning. The large arrows indicate the direction of movement of the pervasive hydrothermal fluid and soluble reactants, whereas the smaller arrows indicate the direction of movement of the reacted products.

90a- Location map of the Rams Cleuch Area and soil sampling grid (Grid 1). This 200x200m soil sampling grid encloses Thorny Cleuch, a minor tributary of Rams Cleuch, on the north western flank of Commonbrae Hill.

90b- Location map of the Swin Gill Area and soil sampling grid (2). This 300x500m soil sampling grid occurs within the headwaters of Swin Gill on the south western flank of Craigy Edge. Note that both grids are orientated with respect to the national grid and the E-W trend of the traverse lines.

91- Sample site locations within the Rams Cleuch Soil Grid (200 x 200m) This diagram illustrates the location, sample density and relative position of soil samples collected within the Rams Cleuch grid (cell size 10x20m).

92- Sample site locations within the Swin Gill Soil Grid (300 x 500m) This diagram illustrates the location, sample density and relative position of soil samples collected within the Swin Gill grid (cell size 10x50m).

93a- Rams Cleuch Soil Geochemistry Maps: SiO_2 (%) Si displays a highly erratic distribution in comparison with all other elements with a maxima (71.5%) located in the north-western corner of the grid area. The zones of As-Sb mineralisation defined by this study (see below) are not identified by Si values and lie within a broad tract of the grid defined by the <50 percentile threshold (clear). Details of the contour levels for both the Swin Gill and Rams Cleuch geochemical grids are presented in table 1.42.

FIGURE 84

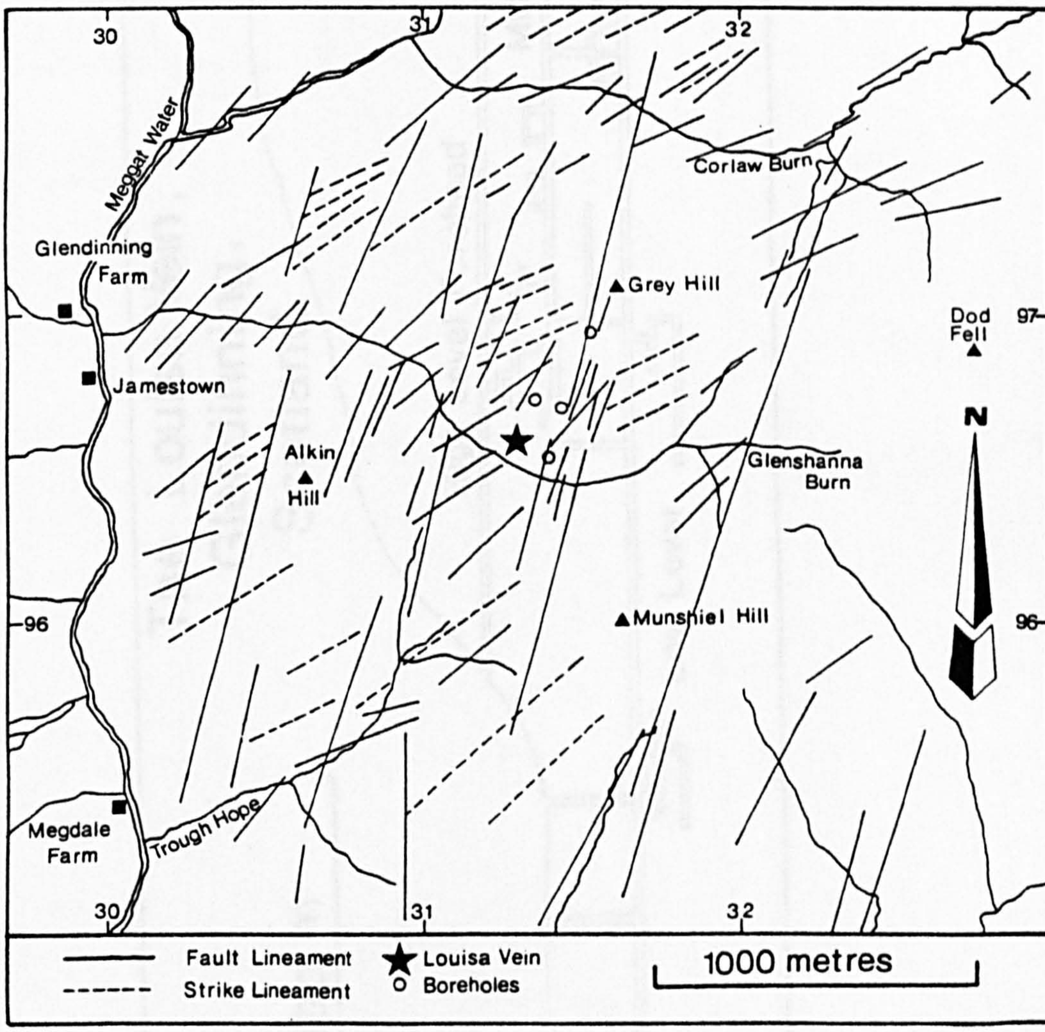
30
31
32
Meggat Water
Glendinning Farm
Jamestown
Corlaw Burn
Grey Hill
Dod Fell
97
N
Alkin Hill
Glenshanna Burn
Munshiel Hill
96
Megdale Farm
Trough Hope
Fault Lineament
Strike Lineament
Louisa Vein
Boreholes
1000 metres

FIGURE 85

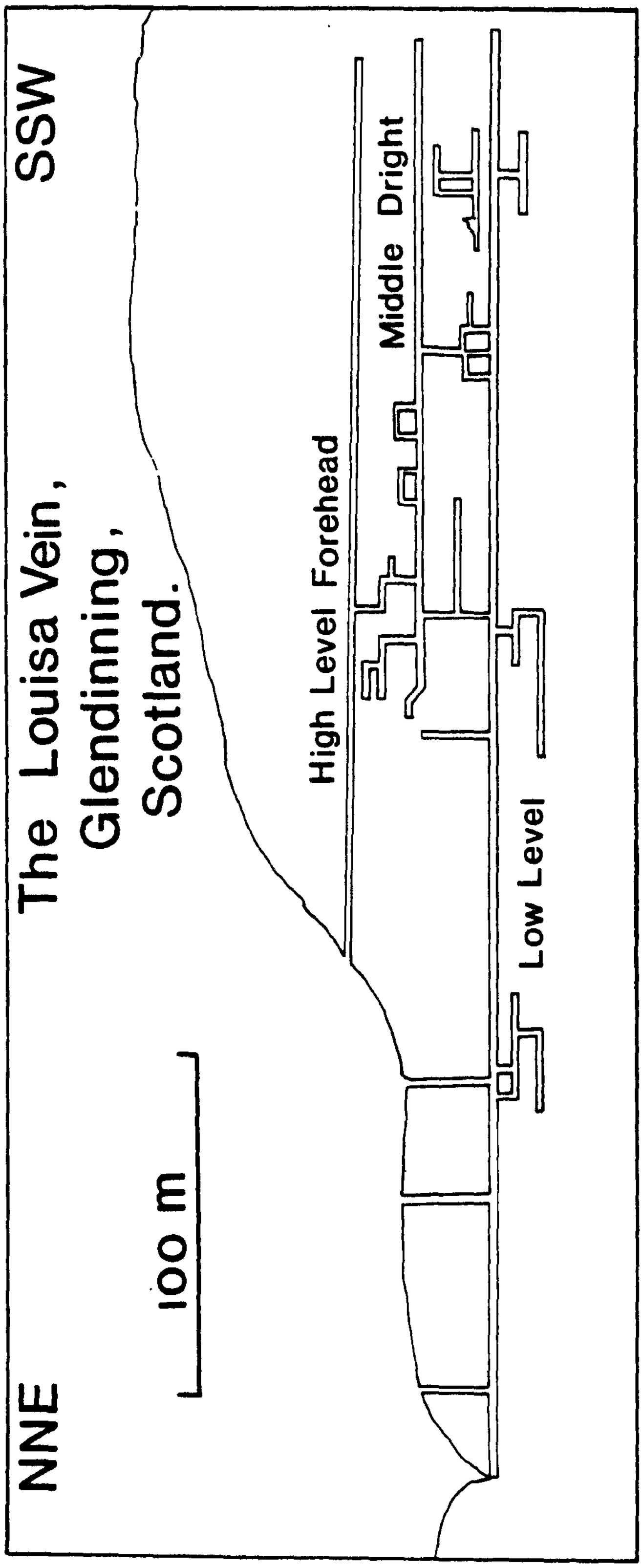
The Louisa Vein,
Glendinning,
Scotland.
SSW
NNE
100 m
High Level Forehead
Middle Dright
Low Level

FIGURE 86

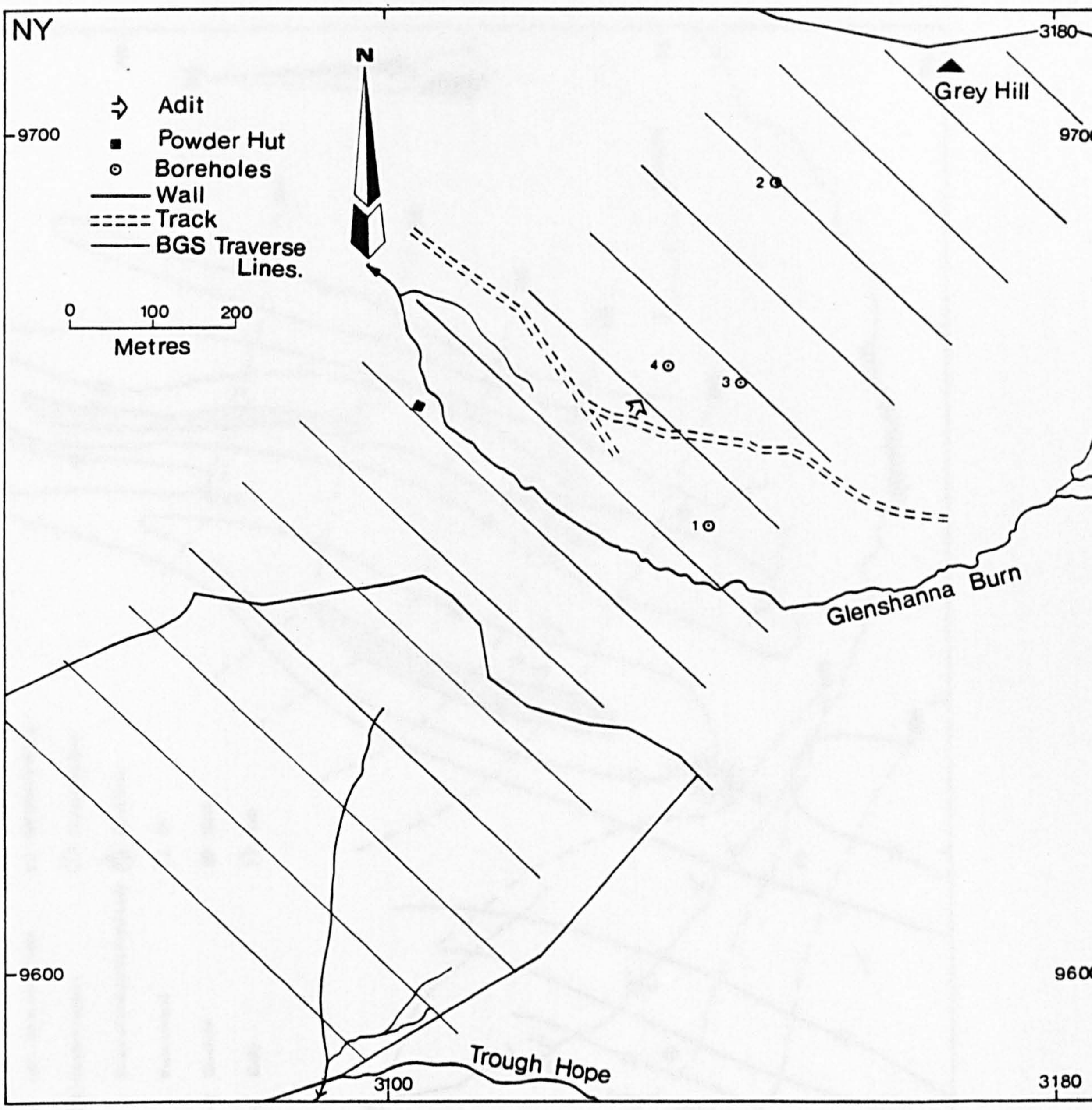
NY
N
Adit
Powder Hut
Boreholes
Wall
Track
BGS Traverse
Lines.
0
100
200
Metres
9700
9700
3180
Grey Hill
2
4
3
1
Glenshanna Burn
9600
9600
Trough Hope
3100
3180

FIGURE 87

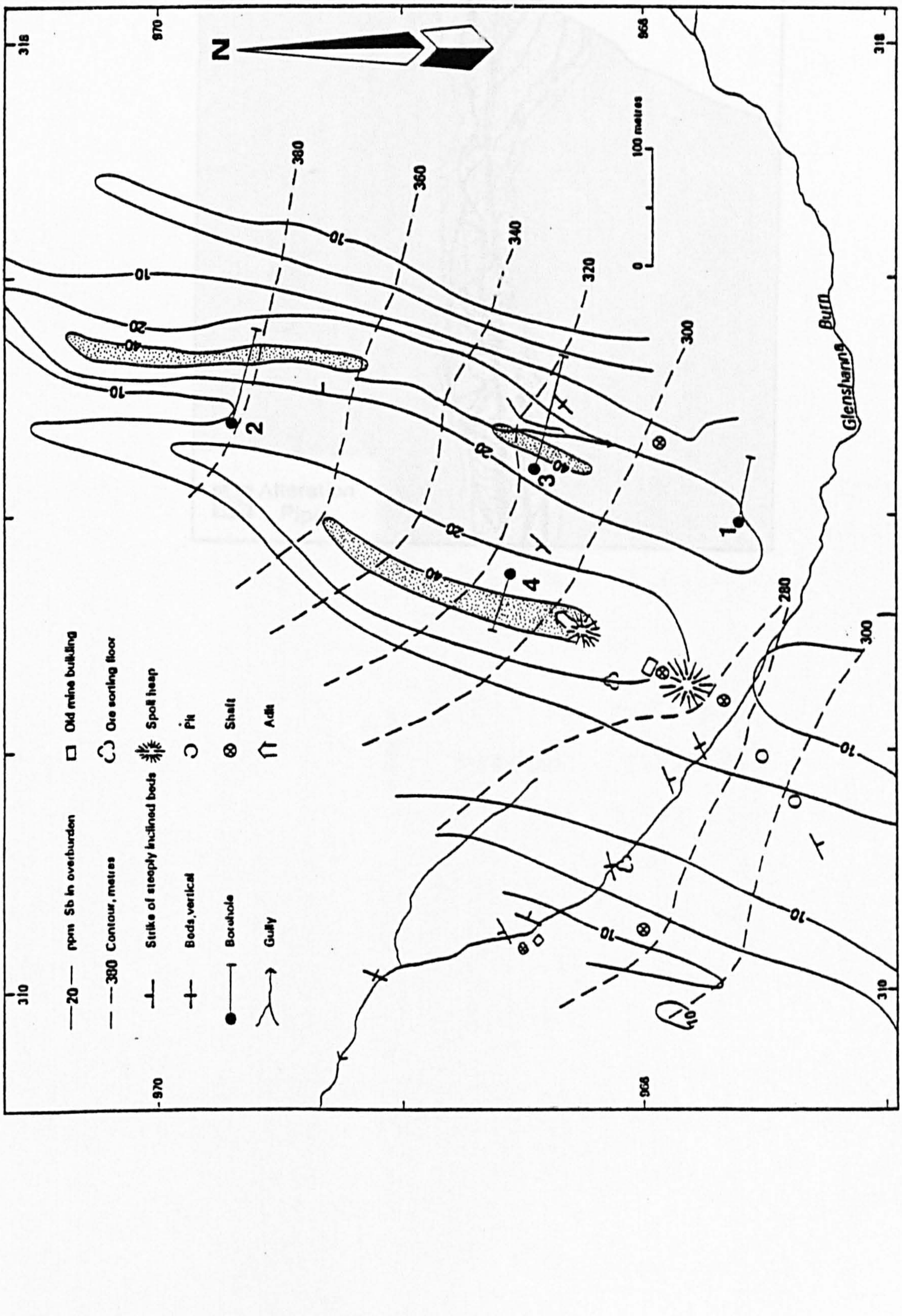

N
100 metres
0
—20— ppm Sb in overburden
– – 380 Contour, metres
Strike of steeply inclined beds
Beds, vertical
Borehole
Gully
Old mine building
Ore sorting floor
Spoil heap
Pit
Shaft
Adit
Glenshanna Burn
380
360
340
320
300
280
10
20
40
1
2
3
4
310
318
970
968

FIGURE 88

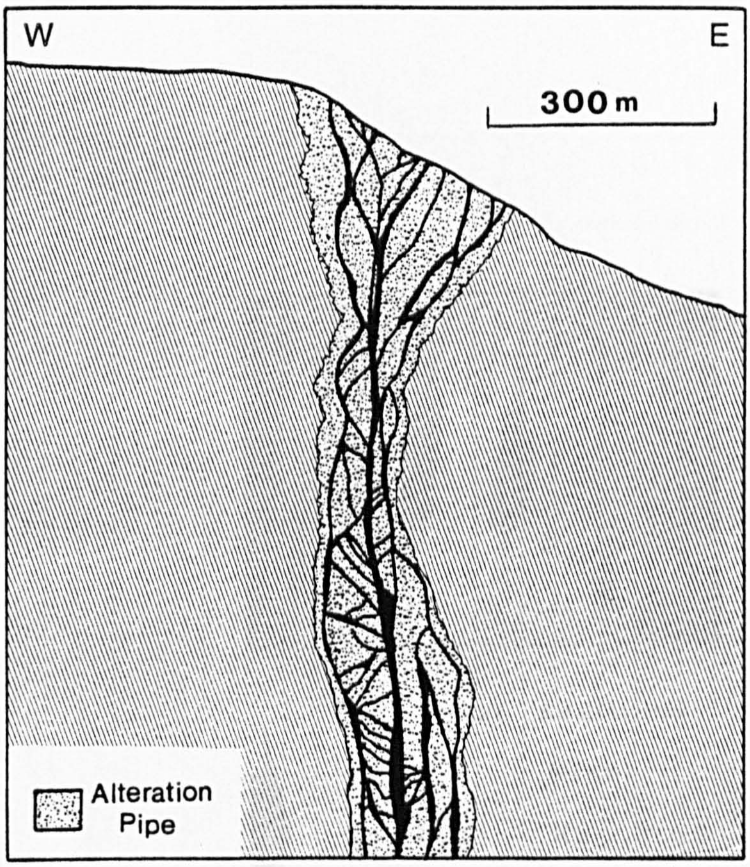

FIGURE 89

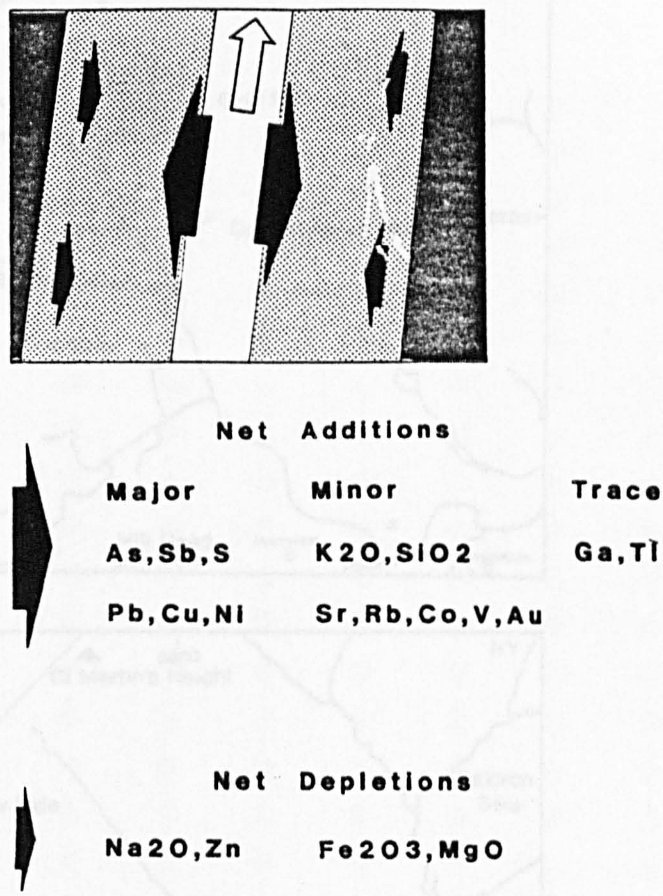
Net Additions
Major
Minor
Trace
As,Sb,S
K2O,SiO2
Ga,Ti
Pb,Cu,Ni
Sr,Rb,Co,V,Au
Net Depletions
Na2O,Zn
Fe2O3,MgO

FIGURE 90

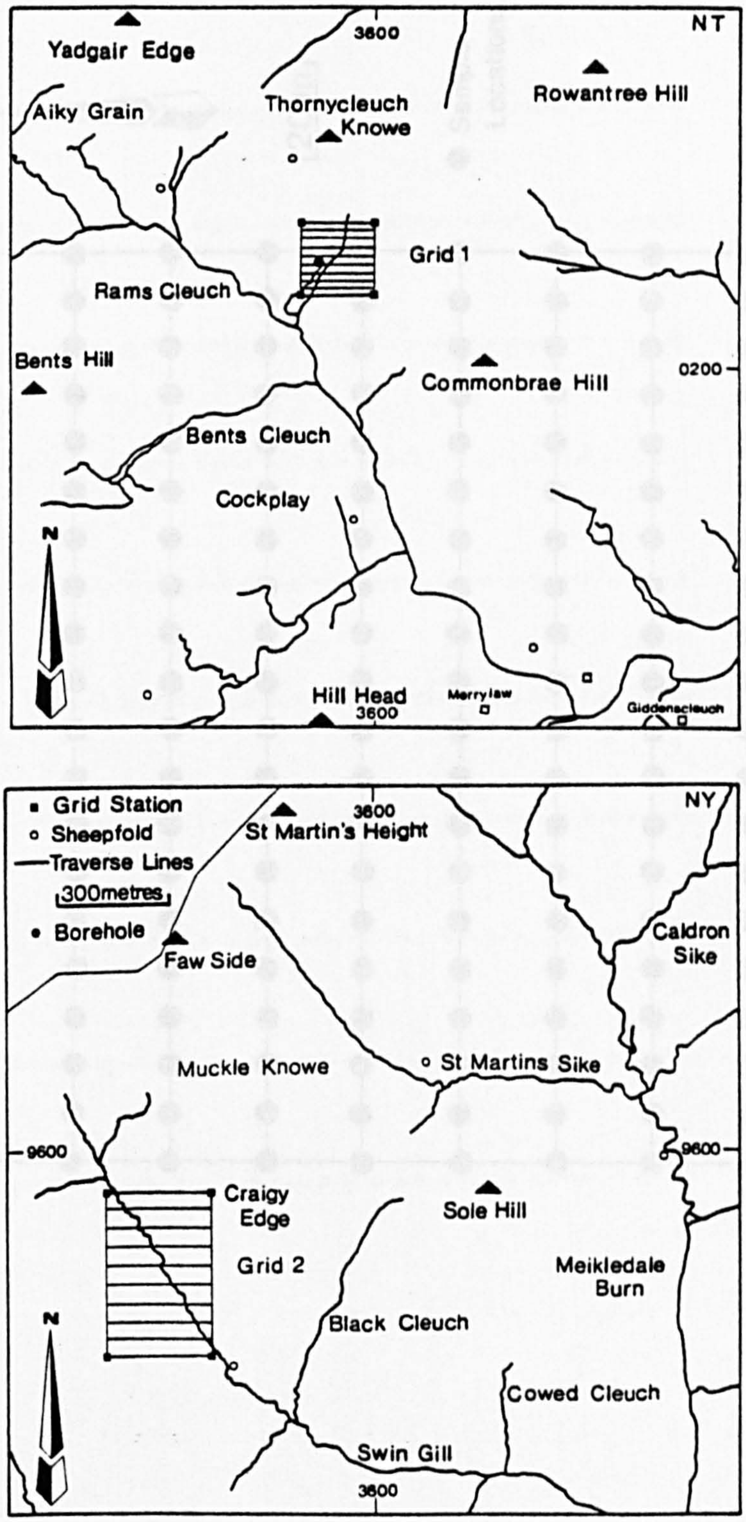
NT
Yadgair Edge
3600
Aiky Grain
Thornycleuch
Knowe
Rowantree Hill
Grid 1
Rams Cleuch
Bents Hill
Commonbrae Hill
0200
Bents Cleuch
Cockplay
N
Hill Head
3600
Merrylaw
Giddenscleuch
NY
Grid Station
Sheepfold
Traverse Lines
300metres
Borehole
3600
St Martin's Height
Faw Side
Caldron
Sike
Muckle Knowe
St Martins Sike
9600
9600
Craigy
Edge
Sole Hill
Grid 2
Meikledale
Burn
N
Black Cleuch
Cowed Cleuch
Swin Gill
3600

FIGURE 91

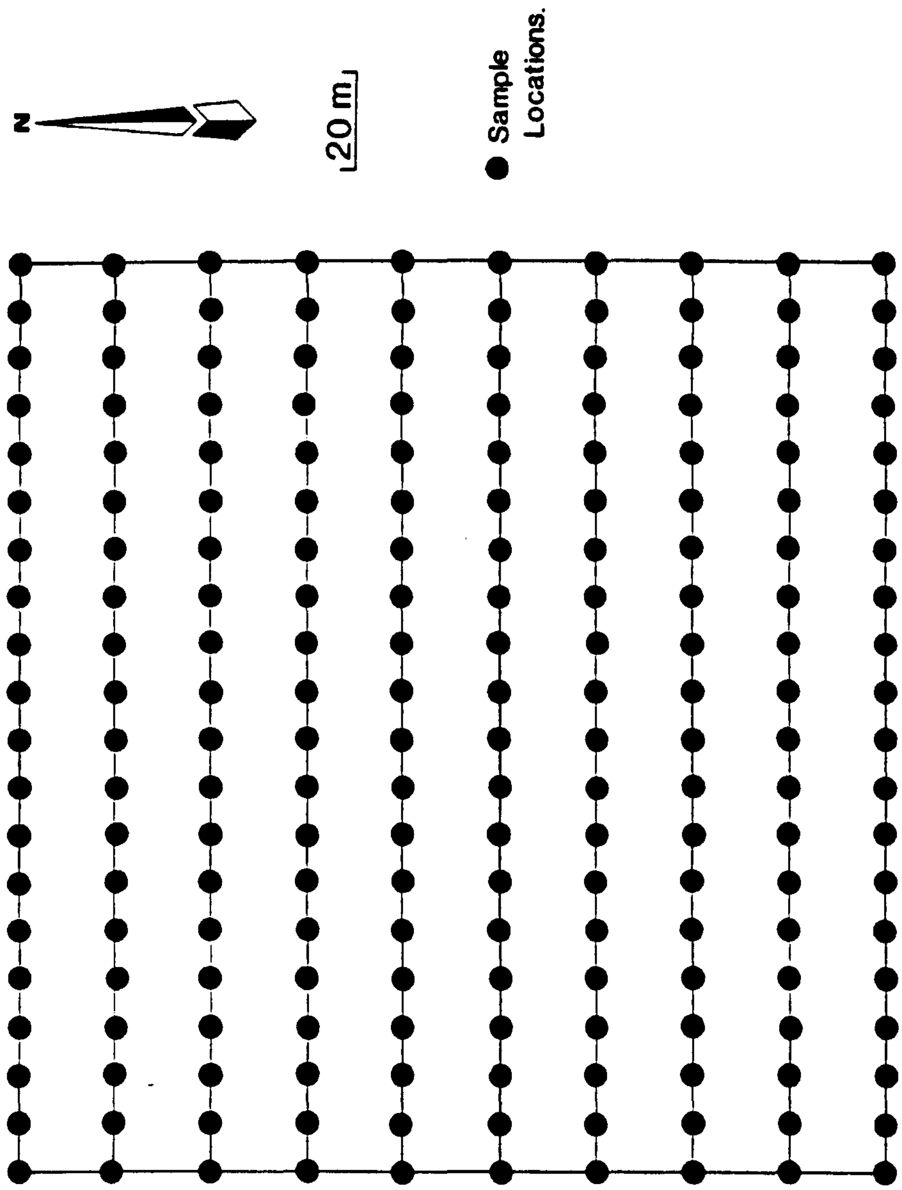

FIGURE 92

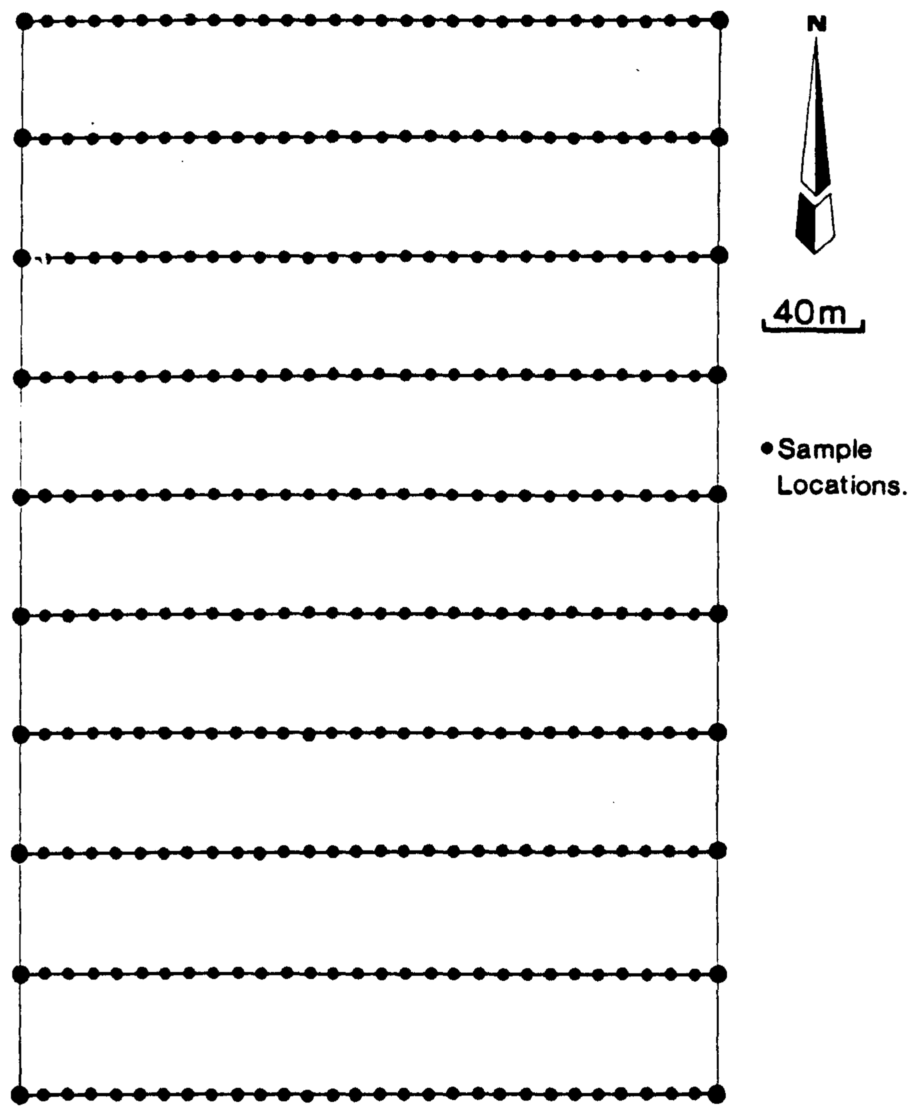

93b- Rams Cleuch Soil Geochemistry Maps: Al_2O_3 (%)
Al values display a broad correlation with As and define an envelope to the main NNE trending As-Sb structure transecting the western half of the survey grid. The second As-Sb structure is identified by Al values but, to a more limited extent.

93c- Rams Cleuch Soil Geochemistry Maps: Fe_2O_3 (%)
Fe values (max 11.69%) clearly outline the location of the two main As-Sb anomalies. In addition, a third Fe anomaly is defined lying parallel to but between the main NNE trending zones. This third zone weakly correlates with Al, Na, As, Sb, Zn and Sr.

93d- Rams Cleuch Soil Geochemistry Maps: MgO (%)
Mg values (max 4.00%) demonstrate a clear inverse relationship with both As and Sb with Mg depletion 'holes' enveloping areas of maximum concentration. High Mg levels located in the upper central portion of the grid and spatially correlates with Al, Na, Ba and S.

93e- Rams Cleuch Soil Geochemistry Maps: Na_2O (%)
Na values (max 1.02%, min 0.25%) closely follow the trends identified by Mg and define a clear inverse relationship with As, Sb and other mineralisation related elements. A sodium depletion envelope surrounds both the main and secondary As-Sb anomalies.

93f- Rams Cleuch Soil Geochemistry Maps: K_2O (%)
K values (max 4.6%) appear closely related to Al but provides little correlation with the sulphide group elements (Fe-As-Sb-Cu-Pb-Zn-Tl).

93g- Rams Cleuch Soil Geochemistry Maps: As (ppm)
This diagram provides clear evidence of a major NNE trending, As-bearing linear structure crosscutting the central portion of the grid area. This zone (max 27ppm) forms an envelope to a similar Sb enriched zone and is interpreted in terms of wallrock hosted disseminated arsenopyrite marginal to a stibnite bearing, quartz vein system. A second, relatively minor zone is defined in the eastern margin of the grid corresponding to significant Sb values.

93h- Rams Cleuch Soil Geochemistry Maps: Sb (ppm)
Sb values (max 20ppm) closely follow the trends described previously for As, although individual zones appear relative constrained in comparison to their arsenic counterparts. A third parallel anomaly zone, previously defined by Fe values is highlighted by elevated Sb levels.

94a- Rams Cleuch Soil Geochemistry Maps: Cu (ppm)
Cu values (max 56ppm) define trends which closely mimic those of As-Sb and related elements. The two main linear feature defined by As anomalies transecting the grid area is clearly identified by Cu, as is the more weakly developed third zone parallel to, but separating the other two.

94b- Rams Cleuch Soil Geochemistry Maps: Pb (ppm)
Pb values (max 101ppm) are strongly correlated with As values with their respective soil maps being virtually identical. Pb values also correlate well with Sb, Cu, Zn, Sr and Tl.

94c- Rams Cleuch Soil Geochemistry Maps: Zn (ppm)
Zn values (max 134ppm) follow the general trends identified by both As and Sb, however they are less well constrained than their respective base metal counterparts (Pb-Cu).

94d- Rams Cleuch Soil Geochemistry Maps: Ba (ppm)
The distribution of Ba values (max 551ppm) is considerably simplified in comparison with most other elements, and defines a single NNE trending linear feature which broadens in the upper part of the grid area. This feature follows the greneral trend of the main As-Sb linear, however it occurs on the eastern margin of this zone (the footwall).

94e- Rams Cleuch Soil Geochemistry Maps: S (ppm)
S values (max 3382ppm) are notable for their their lack of coherence with the main zones of As-Sb enrichment. Only the southern most section the the main As anomaly (>95%) is identified by any form of sulphur enrichment. Elsewhere, within the grid area sulphur anomalies form peripheral to zones of Sb enrichment. In general, sulphur correlates weakly with Fe only and may be attributed to the presence of syndiagenetic pyrite.

FIGURE 93

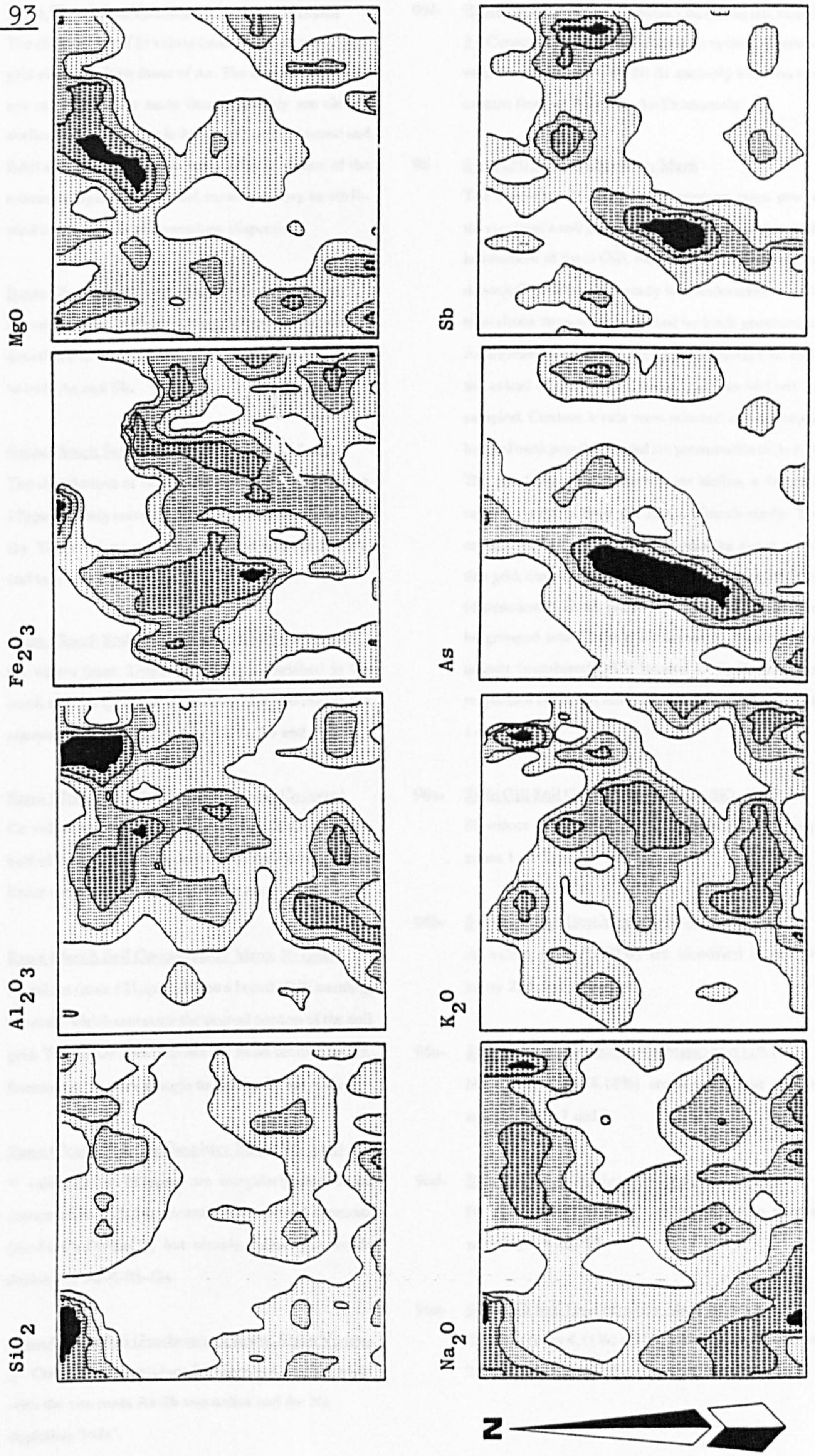

94f- Rams Cleuch Soil Geochemistry Maps: Sr (ppm)
The distribution of Sr values (max 144ppm) within this grid closely follow those of As. The central and southern sections of the main linear anomaly are clearly outlined by Sr values as is the location of the second and third anomaly zones. The more variable nature of the eastern margin of individual anomalies may be attributed to the effects of downslope dispersion.

94g- Rams Cleuch Soil Geochemistry Maps: Rb (ppm)
Rb values (max 162ppm) are considerably more erratic than those of Sr, and in general are inversely correlated to both As and Sb.

94h- Rams Cleuch Soil Geochemistry Maps: Tl (ppm)
The distribution of highly anomalous Tl values (max 17ppm) closely correlate with the main linear As anomaly. These values are also correlated with As and Pb, and to a lesser extent Cu, Zn and Sr.

95a- Rams Cleuch Soil Geochemistry Maps: Ga (ppm)
Ga values (max 27ppm) are weakly enriched in the south eastern quadrant of the soil grid and mirror the anomaly trends delineated by Al, K, Rb and V.

95b- Rams Cleuch Soil Geochemistry Maps: Co (ppm)
Co values (max 88ppm) are enriched in the southern half of the grid area, particularly in the vicinity of the linear structures defined by As-Sb anomalies.

95c- Rams Cleuch Soil Geochemistry Maps: Ni (ppm)
Ni values (max 121ppm) define a broad NNE trending anomaly which crosscuts the central portion of the soil grid. This linear zone follows the trend defined by Ba, forming an eastern margin to the As-Sb anomaly.

95d- Rams Cleuch Soil Geochemistry Maps: V (ppm)
V values (max 183ppm) are irregularly distributed compared to with the mineralisation related elements (As-Sb-Cu-Pb-Zn-Tl) but closely follow the trends defined by Al-K-Rb-Ga.

95e- Rams Cleuch Soil Geochemistry Maps: Eigen Vector-2
Contoured eigenvalues for eigen vector 2 correlate with the two main As-Sb anomalies and the Na depletion 'hole'.

95f- Rams Cleuch Soil Geochemistry Maps: Eigen Vector-3
Contoured eigenvalues for eigen vector 3 correlate with the main Ba-Zn-Pb-Ni-Sr anomaly trend on the eastern flank of the main As-Sb anomaly.

96 - Swin Gill soil Geochemistry Maps
The following 21 'grey-scale' contour maps present the results of a soil geochemical study undertaken in the headwaters of Swin Gill, 4km east of the Glendinning deposit (Fig. 90b). This study was undertaken in order to evaluate stream sediment and bedrock geochemical As-Sb anomalies. A soil grid approximately four times the extent of the Rams Cleuch grid was laid out and sampled. Contour levels were selected on a percentile basis of each population and are presented in table 1.42. The resulting geochemical maps define a far more complex pattern than the Rams Cleuch study. Two orientations of geochemical anomalies occur within this grid, namely NNE-SSW (9 structures) and NW-SE (4 structures). These geochemical anomaly zones may be grouped into 13 main structures or chemical lineaments (numbered 1-13) located in fig.99 with their respective chemical associations documented in table 1.69.

96a- Swin Gill Soil Geochemistry Maps: SiO_2 (%)
Si values (Max 69.31%) are identified in anomaly zones 1, 2, 3, 6, 8, 9 and 11.

96b- Swin Gill Soil Geochemistry Maps: Al_2O_3 (%)
Al values (max 21.02%) are identified in anomaly zones 2, 3, 5, 6, 9 and 11.

96c- Swin Gill Soil Geochemistry Maps: MgO (%)
Mg values (max 4.18%) are identified in anomaly zones 2, 3, 5, 7 and 9.

96d- Swin Gill Soil Geochemistry Maps: Fe_2O_3 (%)
Fe values (max 14.38%) are identified in anomaly zones 3, 5, 6 and 12.

96e- Swin Gill Soil Geochemistry Maps: K_2O (%)
K values (max 4.11%) are identified in anomaly zones 2, 3, 5, 6, 8, 11 and 12.

FIGURE 94

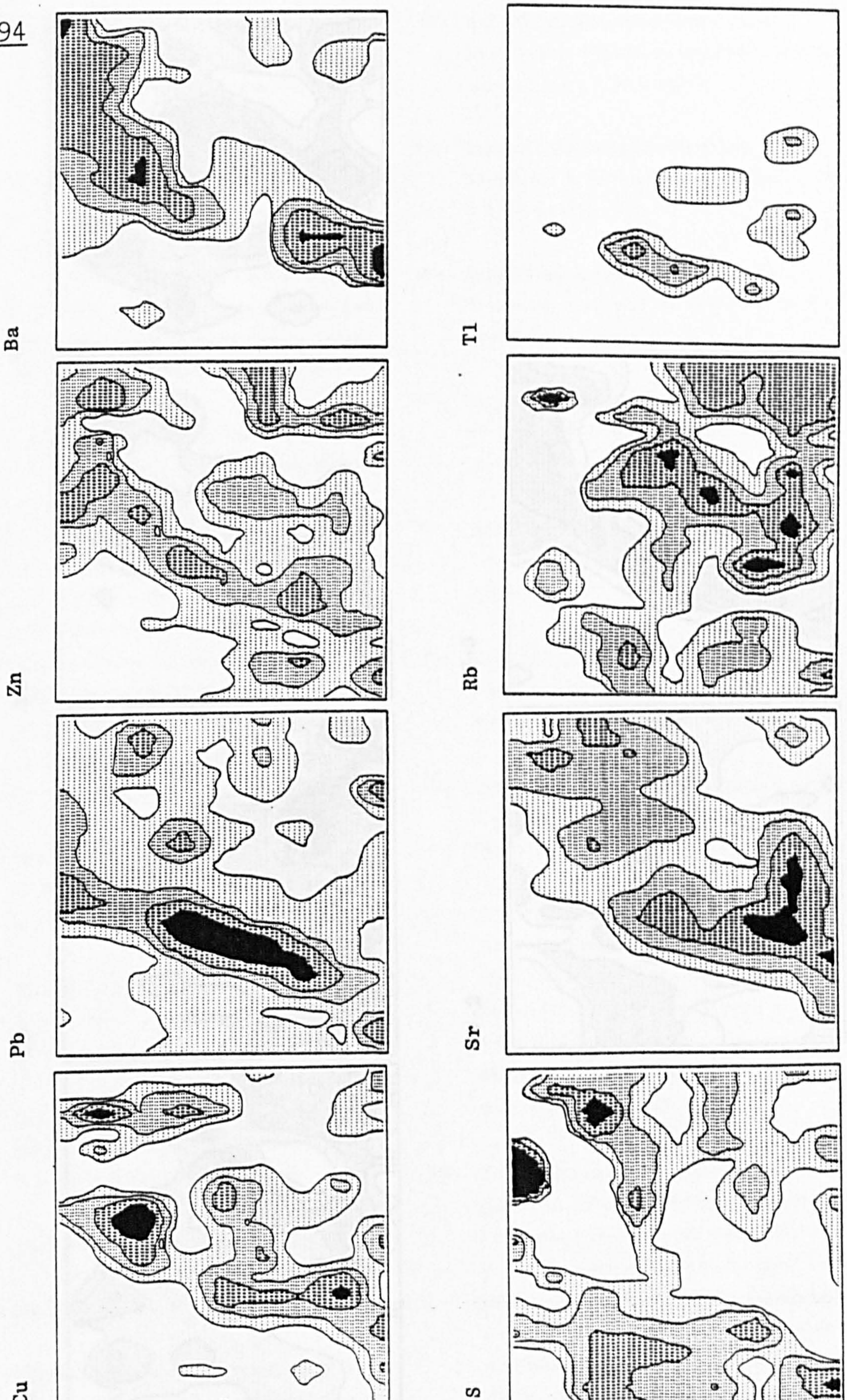

FIGURE 95

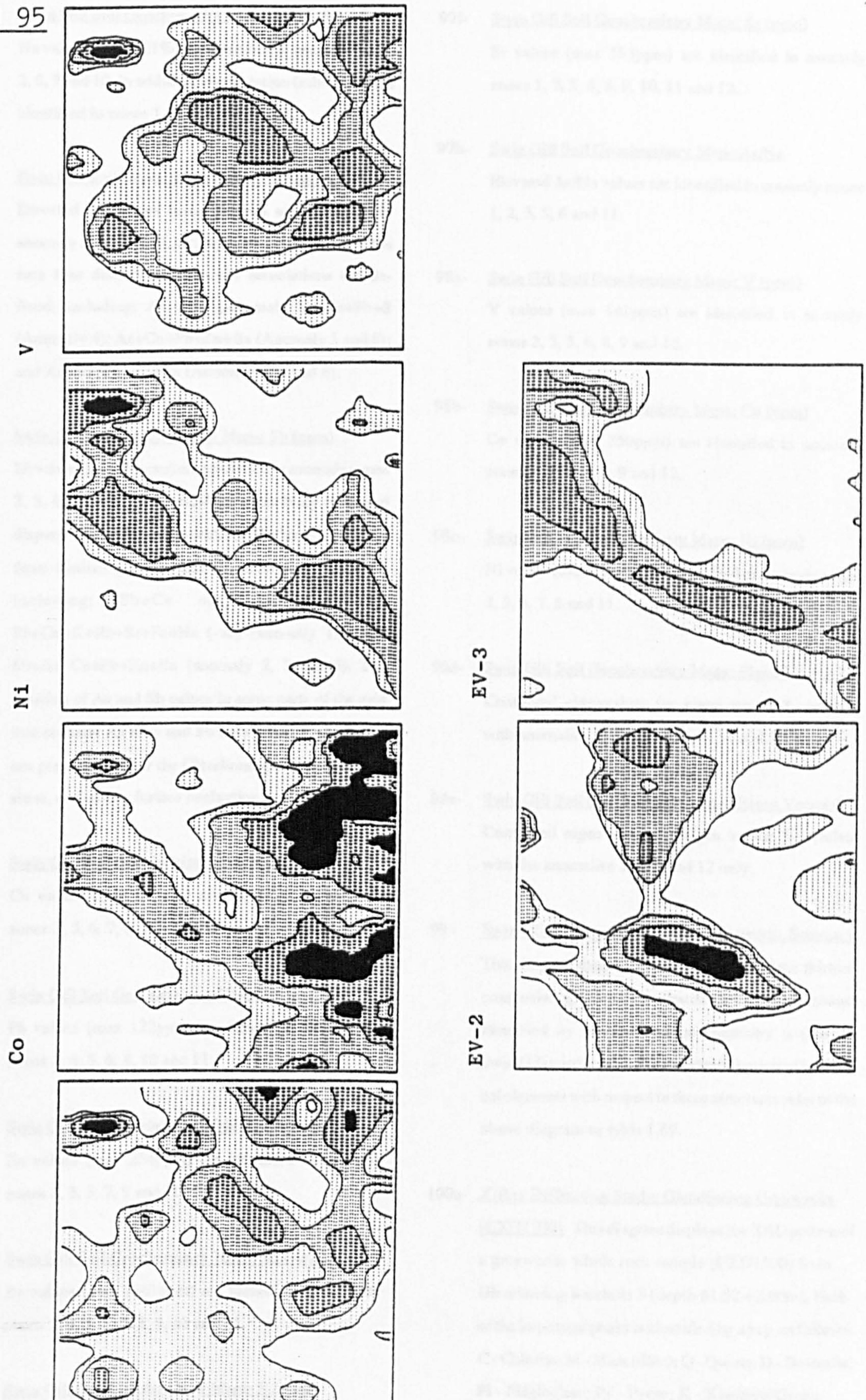

96f- Swin Gill Soil Geochemistry Maps: Na_2O (%)
Na values (max 1.21%) are identified in anomaly zones 2, 6, 9 and 10. In addition, Na depletion (min 0.26%) is identified in zones 1, 3, 4, 5, 11 and 12.

96g- Swin Gill Soil Geochemistry Maps: As (ppm)
Elevated As values (max 65ppm) are identified in anomaly zones 1, 2, 3, 4, 5, 6, 8, 10 and 11. Within this area four distinct geochemical associations are defined, including: As Only (Anomaly 1); As+Pb+S (Anomaly 4); As+Cu+Pb+Zn+Ba (Anomaly 5 and 8); and As+Sb+Pb+Zn+Ba (Anomaly 2, 3 and 6).

96h- Swin Gill Soil Geochemistry Maps: Sb (ppm)
Sb values (max 34ppm) are identified in anomaly zones 2, 3, 6, 12 and 13 but exhibits a relatively restricted dispersion in comparison with As. Within the grid area three distinct geochemical associations are defined, including: Sb+Cu only (anomaly 13); Sb+Cu+K+Rb+Sr+Fe+Na (-ve) (anomaly 12); and Sb+As+Cu+Pb+Zn+Ba (anomaly 2, 3 and 6). The division of As and Sb values in some parts of the grid into separate As only and Sb only zones is an enigma not present in either the Glendinning or Rams Cleuch areas, and merits further evaluation.

97a- Swin Gill Soil Geochemistry Maps: Cu (ppm)
Cu values (max 68ppm) are identified in anomaly zones 3, 5, 6, 7, 8, 12 and 13.

97b- Swin Gill Soil Geochemistry Maps: Pb (ppm)
Pb values (max 122ppm) are identified in anomaly zones 3, 4, 5, 6, 8, 10 and 11.

97c- Swin Gill Soil Geochemistry Maps: Zn (ppm)
Zn values (max 254ppm) are identified in anomaly zones 2, 3, 5, 7, 9 and 10.

97d- Swin Gill Soil Geochemistry Maps: Ba (ppm)
Ba values (max 1561ppm) are identified in anomaly zones 2, 3, 5, 6, 7, 8, 9, 10 and 11.

97e- Swin Gill Soil Geochemistry Maps: S (ppm)
S values (max 5312ppm) are identified in anomaly zones 2, 3, 4, 6, 7 and 10.

97f- Swin Gill Soil Geochemistry Maps: Sr (ppm)
Sr values (max 183ppm) are identified in anomaly zones 1, 3, 5, 6, 8, 9, 10, 11 and 12.

97h- Swin Gill Soil Geochemistry Maps:As/Na
Elevated As/Na values are identified in anomaly zones 1, 2, 3, 5, 6 and 11.

98a- Swin Gill Soil Geochemistry Maps: V (ppm)
V values (max 141ppm) are identified in anomaly zones 2, 3, 5, 6, 8, 9 and 12.

98b- Swin Gill Soil Geochemistry Maps: Co (ppm)
Co values (max 350pp [illegible]) are identified in anomaly zones 2, 3, 5, 7, 8, 9 and 12.

98c- Swin Gill Soil Geochemistry Maps: Ni (ppm)
Ni values (max 85ppm) are identified in anomaly zones 2, 3, 5, 7, 8 and 11.

98d- Swin Gill Soil Geochemistry Maps: Eigen Vector-2
Contoured eigenvalues for eigen vector 3 correlate with anomalies 1, 2, 3, 4, 5, 6, 8, 10 and 12.

98e- Swin Gill Soil Geochemistry Maps: Eigen Vector-3
Contoured eigenvalues for eigen vector 3 correlate with the anomalies 2, 3, 6 and 12 only.

99 - Swin Gill Composite Soil Anomaly trends: Summary
This diagram summarises the locations of the thirteen composite geochemical structures (anomaly zones) identified by shallow soil geochemistry within the Swin Gill survey grid. For the identification of individual elements with respect to these structures refer to the above diagram or table 1.69.

100a- X-Ray Diffraction Study: Glendinning Greywacke (CXD1500) This diagram displays the XRD pattern of a greywacke whole rock sample (CXD1500) from Glendinning borehole 3 (depth 61.92-62.00m). Each of the important peaks is identified by a key, as follows: C - Chlorite; M - Mica (illite); Q - Quartz; D - Dolomite; Pl - Plagioclase; Py - Pyrite; K - Kaolinite Group (dickite); and Si - Siderite. The results of a semiquanti tative whole rock and clay fraction analysis for this sample together with CXD1551, CXD1552 and CXD

FIGURE 96

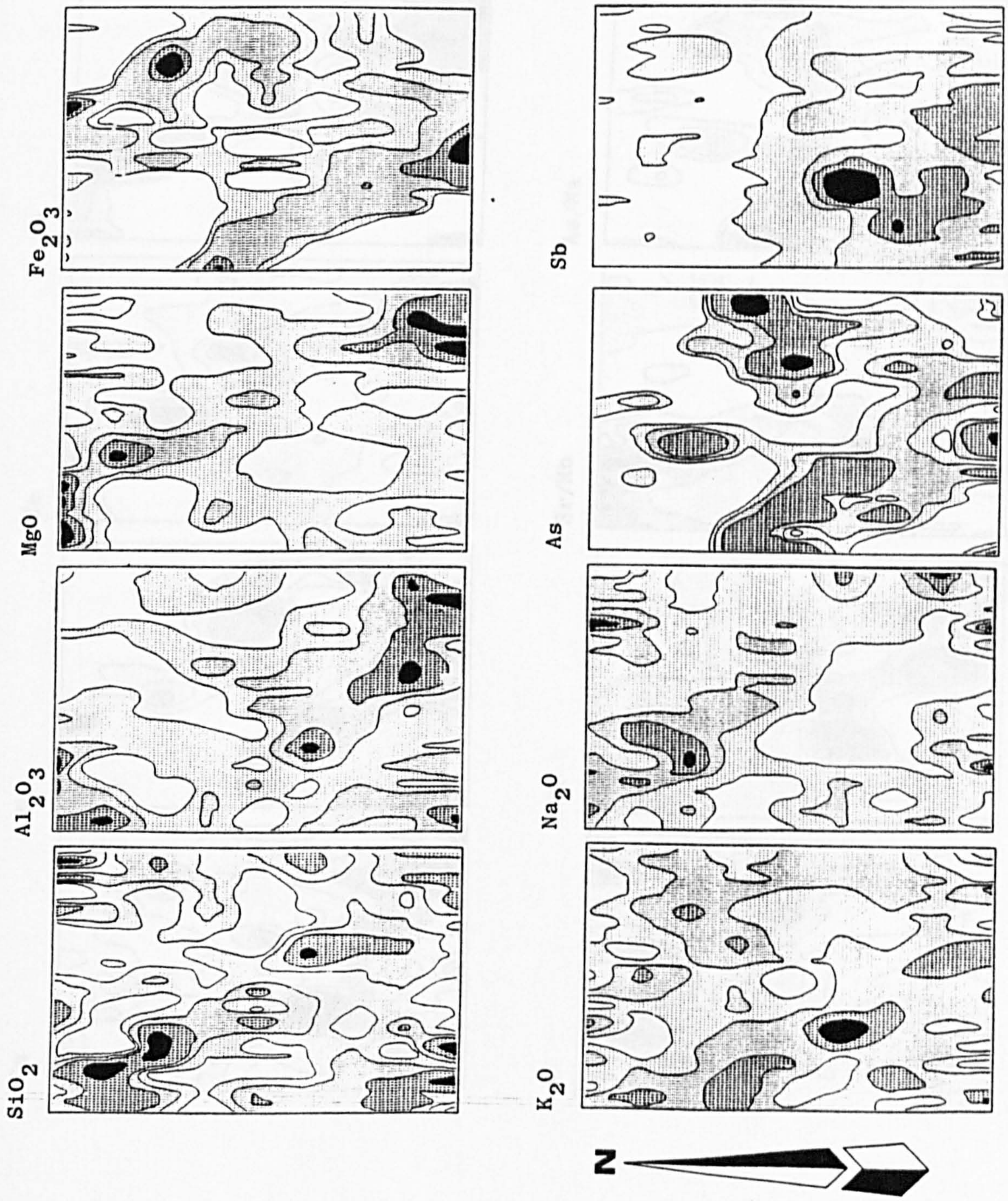

FIGURE 97

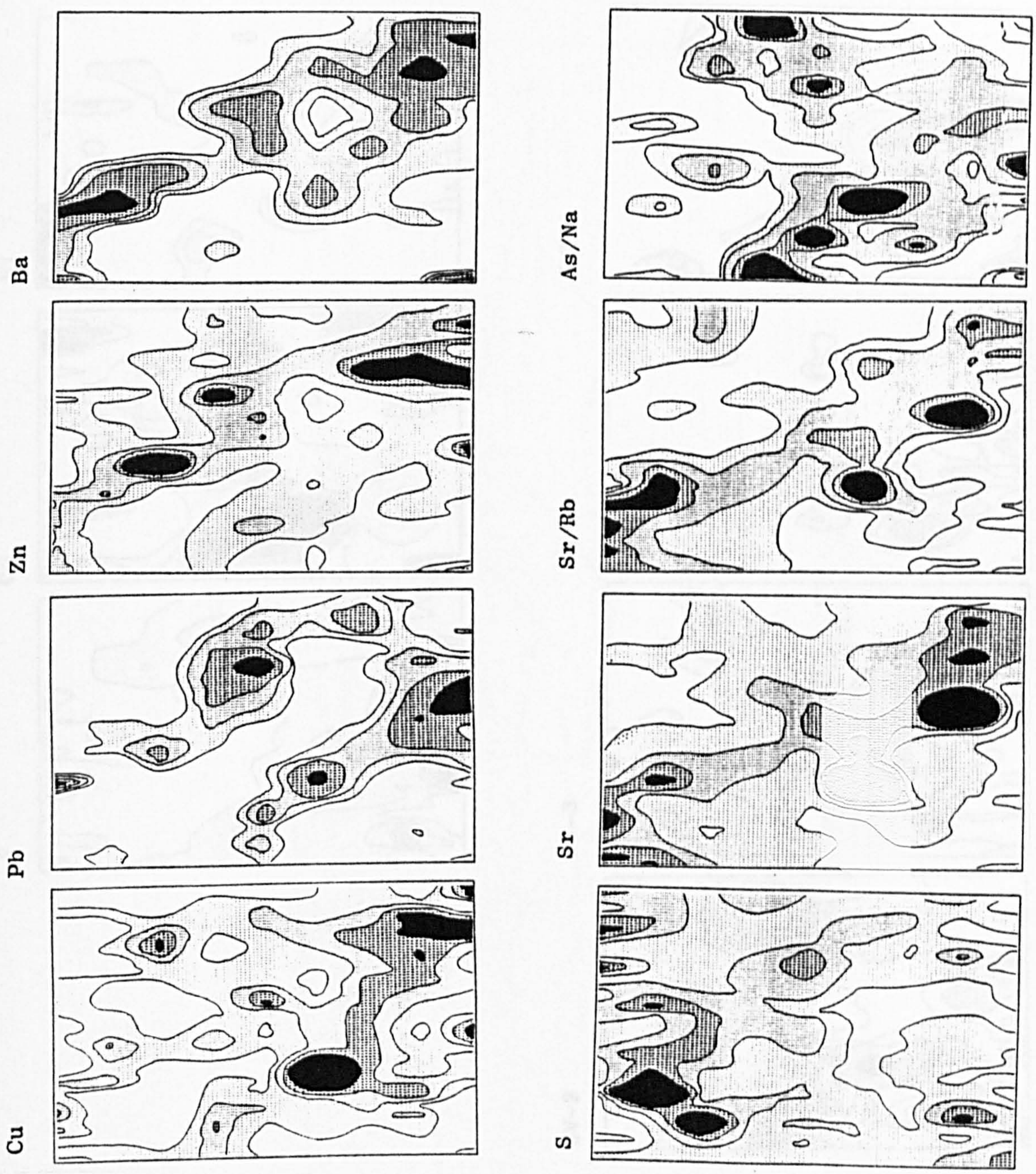

FIGURE 98

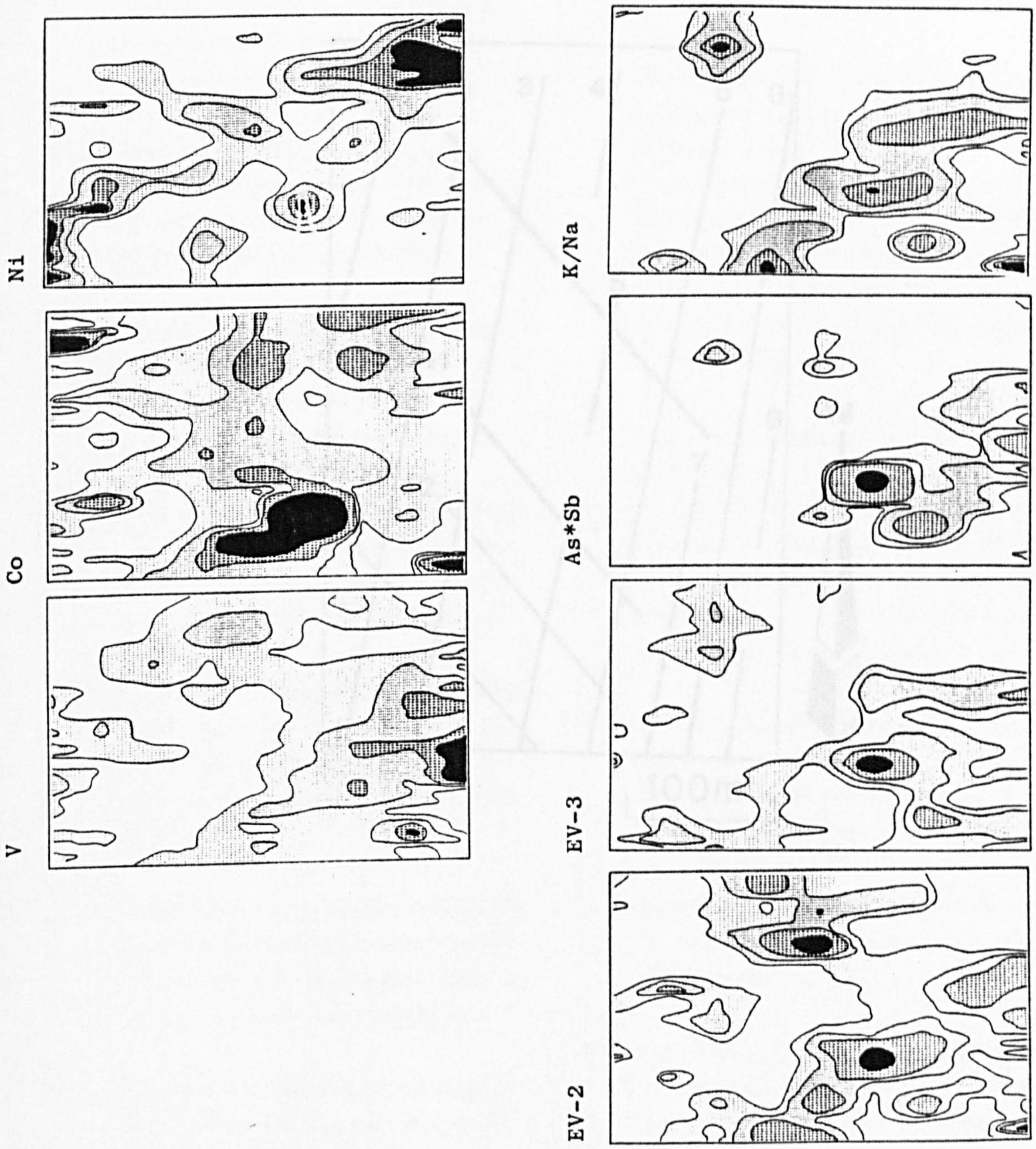

FIGURE 99

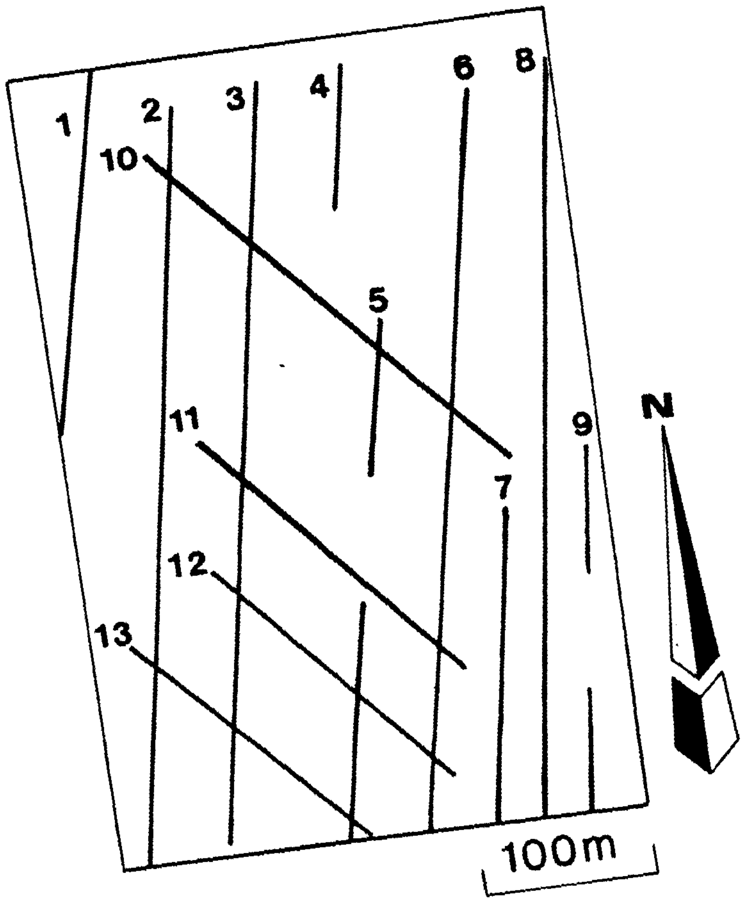

2001 are presented in table 1.01.

100b- X-Ray Diffraction Study: Glendinning Mudstone (CXD1552) This diagram displays the XRD pattern of a mudstone whole rock sample (CXD 1552) from Glendinning borehole 3 (depth 165.40-165.55m).

101a- X-Ray Diffraction Study: Glendinning Greywacke (CXD1551) This diagram displays the XRD pattern of a greywacke whole rock sample (CXD 1551) from Glendinning borehole 3 (depth 126.60-126.66m).

101b- X-Ray Diffraction Study: Glendinning Mudstone (CXD2001) This diagram displays the XRD pattern of a mudstone whole rock sample (CXD 2001) from Glendinning borehole 3 (depth 79.38-79.42).

102a- X-Ray Diffraction Study: Clay Fraction (CXD1500) This diagram displays the XRD pattern of a greywacke <2 micron clay fraction sample (CXD 1500) from Glendinning borehole 3 (depth 61.92-62.00m).

102b- X-Ray Diffraction Study: Clay Fraction (CXD1552) This diagram displays the XRD pattern of a mudstone <2 micron clay fraction sample (CXD 1552) from Glendinning borehole 3 (depth 165.40-165.55m).

103a- X-Ray Diffraction Study: Clay Fraction (CXD1551) This diagram displays the XRD pattern of a greywacke <2 micron clay fraction sample (CXD 1551) from Glendinning borehole 3 (depth 126.60-126.66m).

103a- X-Ray Diffraction Study: Clay Fraction (CXD2001) This diagram displays the XRD pattern of a mudstone <2 micron clay fraction sample (CXD 2001) from Glendinning borehole 3 (depth 79.38-79.42m).

104- X-Ray Diffraction Study : Alunite, Kaolinite and Dickite This diagram displays the standard XRD patterns of alunite (ref:4-865); kaolinite (ref:29-1488) and Dickite (ref: 10-446) used for comparative purposes to evaluate the mineralogical composition of greywackes, mudstones and mineral concentrates from the Glendinning deposit and elsewhere in the Southern Uplands.

105- X-Ray Diffraction Study : Galena, Arsenopyrite, Stibnite, Pyrite, marcasite and chalcopyrite This diagram displays the standard XRD patterns of Galena (ref:5-592); arsenopyrite (ref:14-218); stibnite (ref: 6-474); Pyrite (ref:6-710) marcasite (ref:3-799) and chalcopyrite (ref:25-288) used for comparative purposes to determine the composition of mineral concentrates from the Glendinning deposit and elsewhere in the Southern Uplands.

106- X-Ray Diffraction Study: Tetrahedrite, tennantite, jamesonite, pyrrhotite and sphalerite This diagram displays the standard XRD patterns of tetrahedrite (ref:24-1318); Jamesonite (13-461); Tennantite (11-102); Pyrrhotite (ref 20-534 and 29-724) and sphalerite (ref:5-566) used for comparative purposes to determine the composition of mineral concentrates from the Glendinning deposit and elsewhere in the Southern Uplands.

107- X-Ray Diffraction Study: Zinckenite, Semseyite and Fuloppite This diagram displays the standard XRD patterns of zinckenite (ref:7-334); semseyite (ref:22-1130) and fuloppite (ref:22-648) used for comparative purposes to determine the composition of mineral concentrates from the Glendinning deposit.

108- X-Ray Diffraction Study: Arsenic, antimony, gold & mercury This diagram displays the standard XRD patterns of gersdorffite (ref:12-705); native arsenic (ref:5-632); native antimony (ref:5-562); Gold (ref:4-784) and mercury (ref: 17-863 and 9-253) used to determine the composition of mineral concentrates from the Glendinning deposit.

109- Arsenopyrite Geothermometry: Univariant temperature-sulphur activity diagram (after Kretchmar and Scott 1976) Plot of the sulphur activity-tenperature projection of buffered assemblages involving arsenopyrite in the Fe-As-S system (after Barton,1969; Scott and Barnes, 1971). The stability fields of arsenopyrite are contoured in atomic % arsenic (after Kretchmar and Scott,1976) and form the basis of the arsenopyrite geothermometer.

FIGURE 100

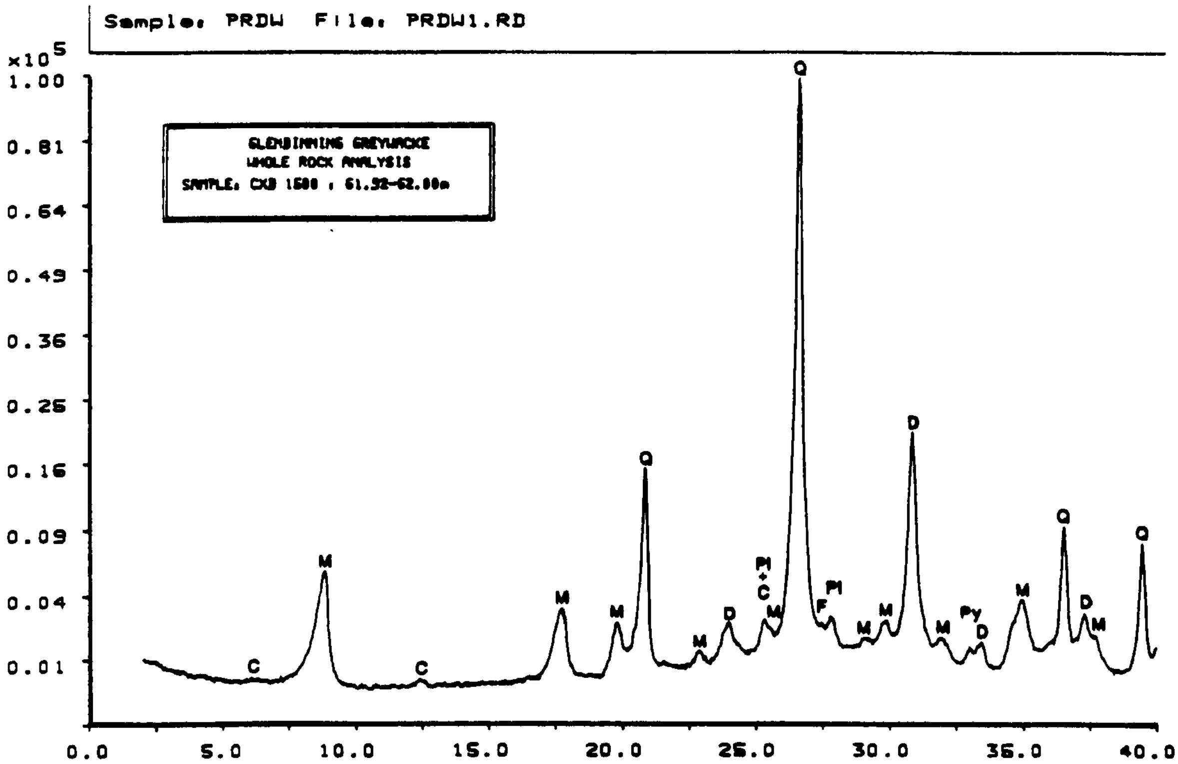
Sample: PRDW File: PRDW1.RD
x10^5
1.00
0.81
0.64
0.49
0.36
0.25
0.16
0.09
0.04
0.01
GLENDINNING GREYWACKE
WHOLE ROCK ANALYSIS
SAMPLE: CXB 1500 : 61.92-62.00m
Q
D
Q
Q
Q
M
M
M
M
Pl + C
M
D
Pl
F
M
M
M
Py
D
M
D
M
C
C
0.0
5.0
10.0
15.0
20.0
25.0
30.0
35.0
40.0

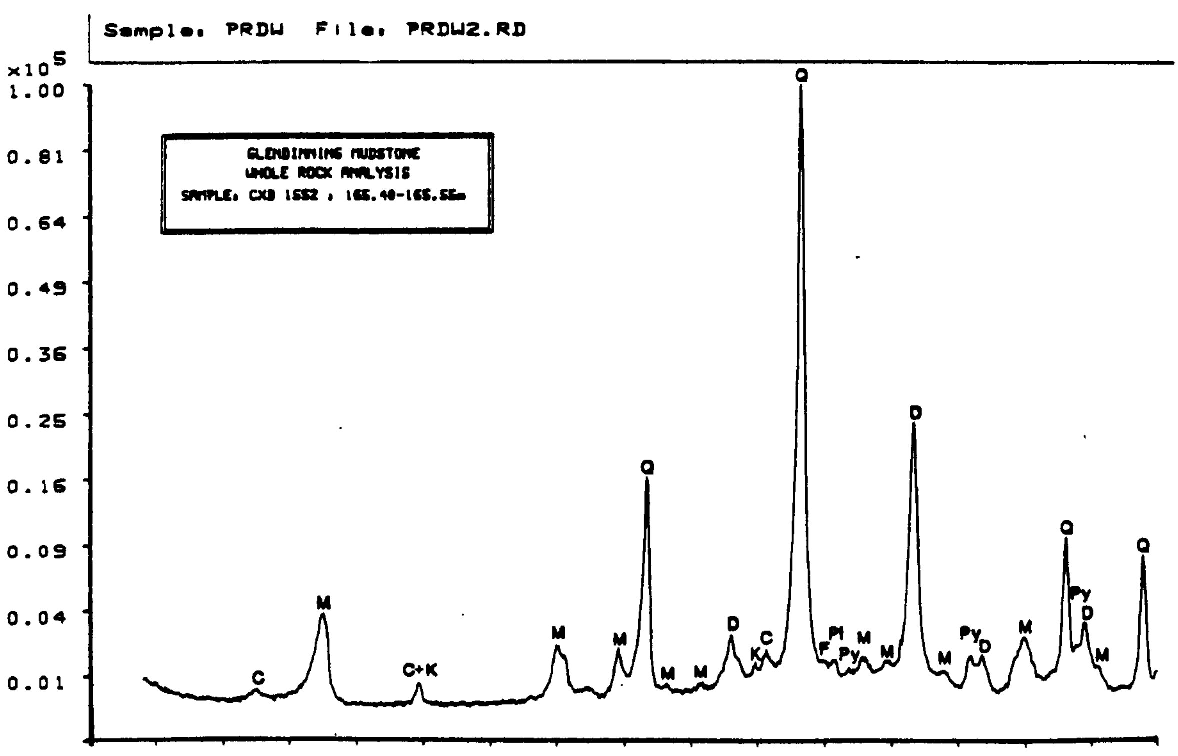
Sample: PRDW File: PRDW2.RD
x10^5
1.00
0.81
0.64
0.49
0.36
0.25
0.16
0.09
0.04
0.01
GLENDINNING MUDSTONE
WHOLE ROCK ANALYSIS
SAMPLE: CXB 1552 : 165.40-165.55m
Q
D
Q
Q
Q
M
M
M
D
K
C
Pl
F
Py
M
M
Py
D
M
M
Py
D
M
M
M
C
C+K
M
0.0
5.0
10.0
15.0
20.0
25.0
30.0
35.0
40.0

FIGURE 101

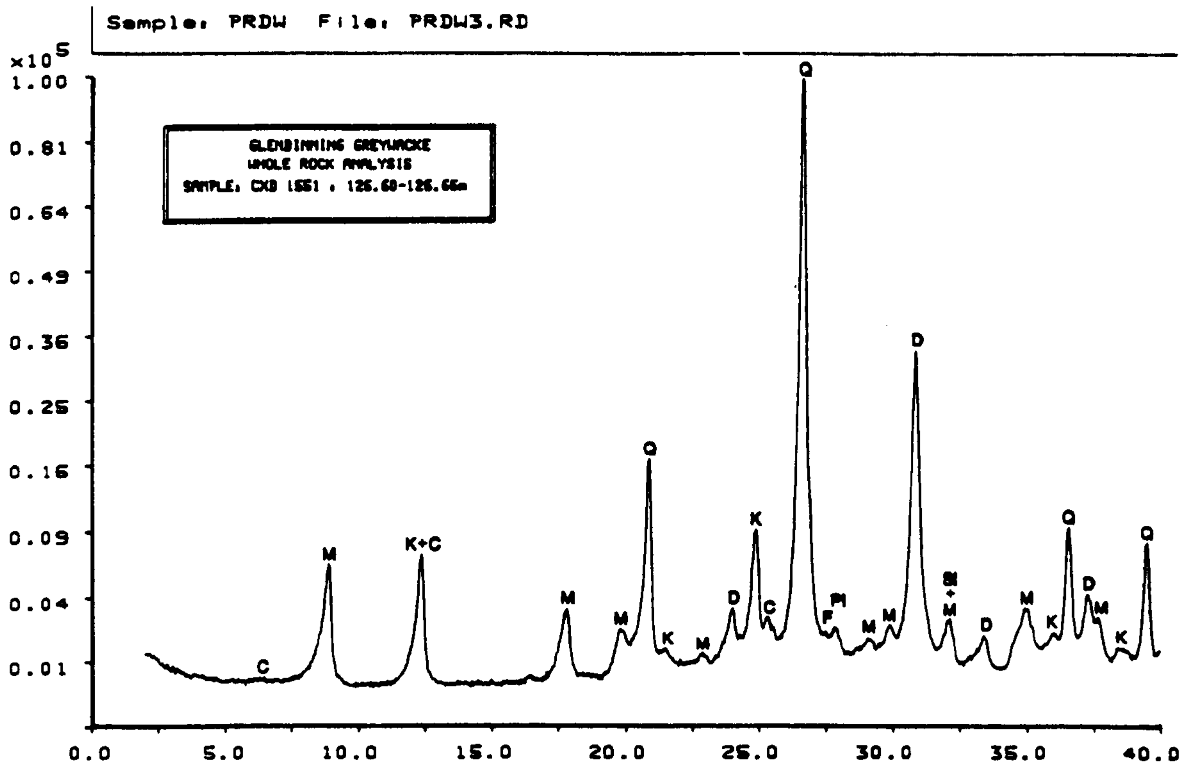
Sample: PRDW File: PRDW3.RD
$\times 10^5$
1.00
0.81
0.64
0.49
0.36
0.25
0.16
0.09
0.04
0.01
GLENDINNING GREYWACKE
WHOLE ROCK ANALYSIS
SAMPLE: CXB 1551 : 126.60-126.66m
0.0
5.0
10.0
15.0
20.0
25.0
30.0
35.0
40.0

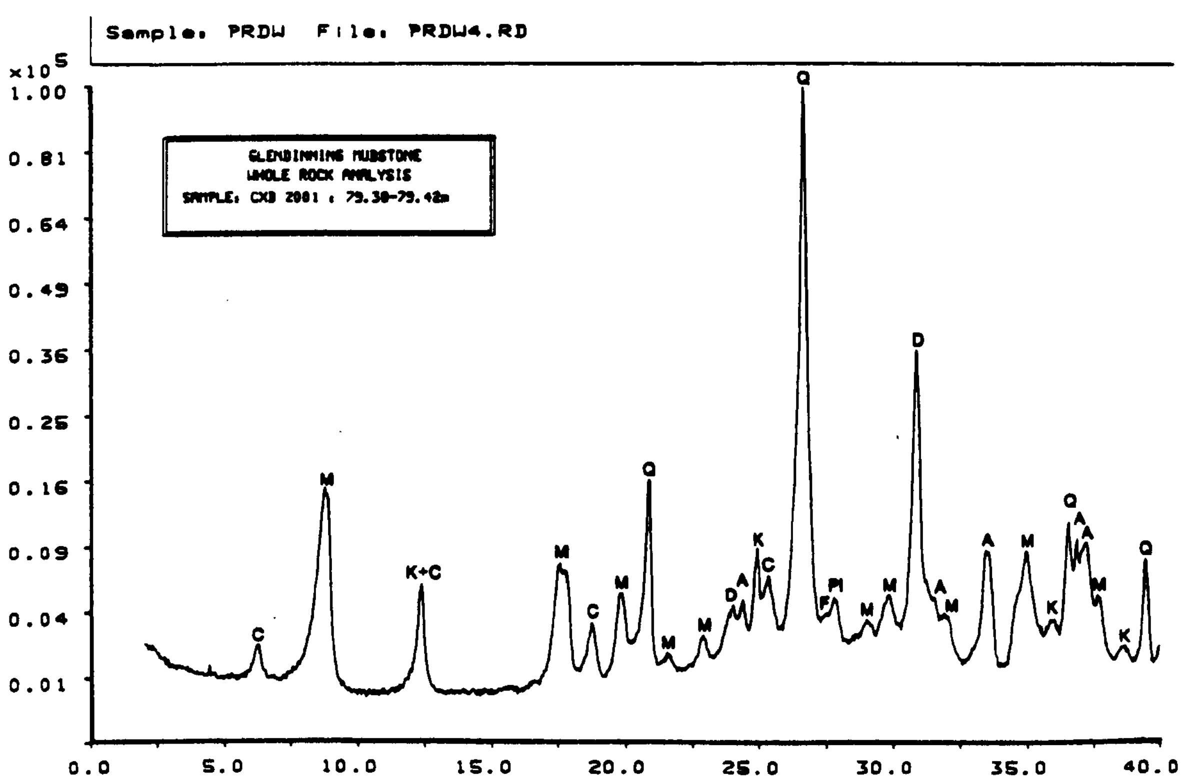
Sample: PRDW File: PRDW4.RD
$\times 10^5$
1.00
0.81
0.64
0.49
0.36
0.25
0.16
0.09
0.04
0.01
GLENDINNING MUDSTONE
WHOLE ROCK ANALYSIS
SAMPLE: CXB 2001 : 79.30-79.42m
0.0
5.0
10.0
15.0
20.0
25.0
30.0
35.0
40.0

FIGURE 102

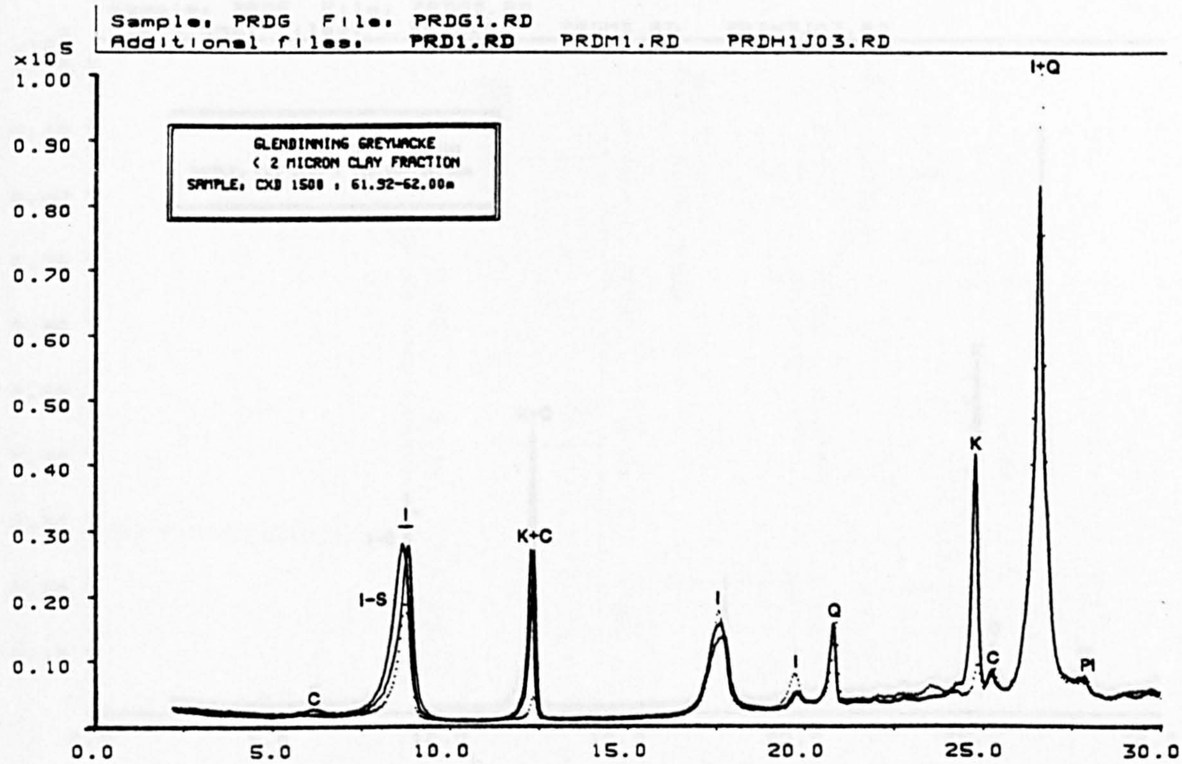
Sample: PRDG File: PRDG1.RD
Additional files: PRD1.RD PRDM1.RD PRDH1J03.RD
GLENDINNING GREYWACKE
< 2 MICRON CLAY FRACTION
SAMPLE: CXB 1508 : 61.92-62.00m
x10^5
I-S
I
K+C
I
I
Q
K
C
I+Q
Pl
C

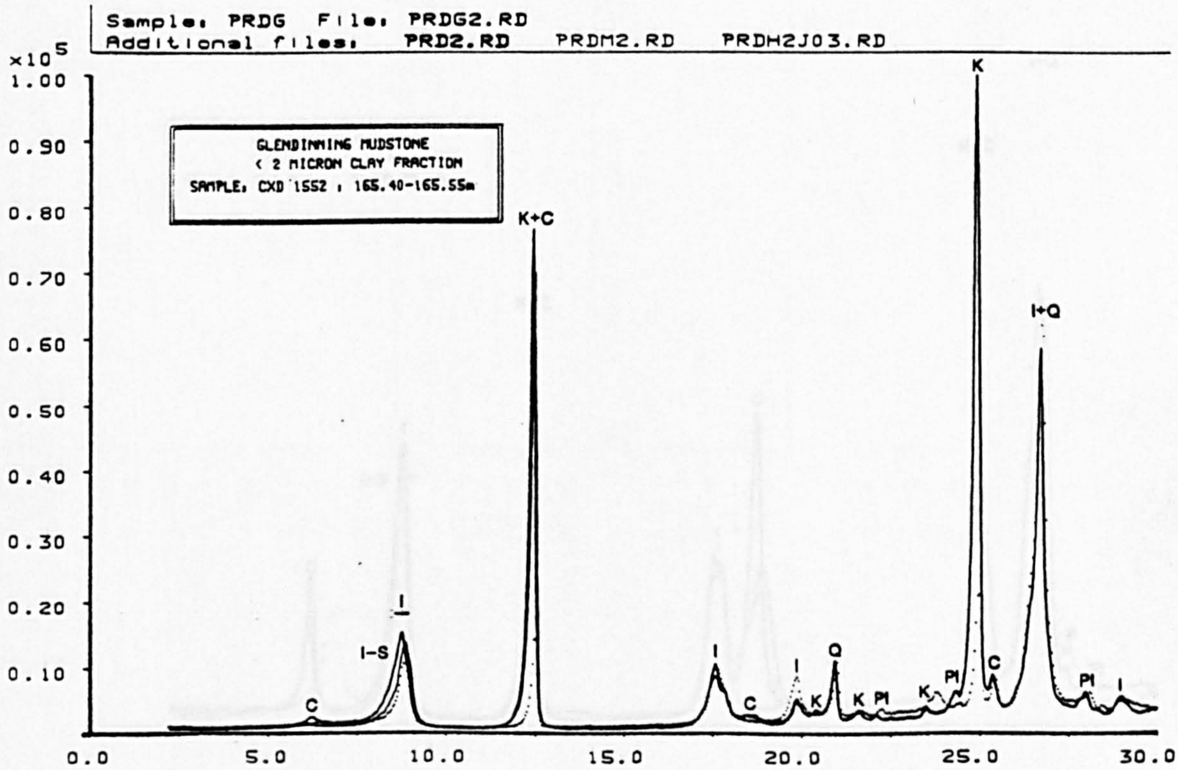
Sample: PRDG File: PRDG2.RD
Additional files: PRD2.RD PRDM2.RD PRDH2J03.RD
GLENDINNING MUDSTONE
< 2 MICRON CLAY FRACTION
SAMPLE: CXD 1552 : 165.40-165.55m
x10^5
K+C
K
I+Q
I-S
I
C
I
C
I
K
Q
K
Pl
K
Pl
C
Pl
I

FIGURE 103

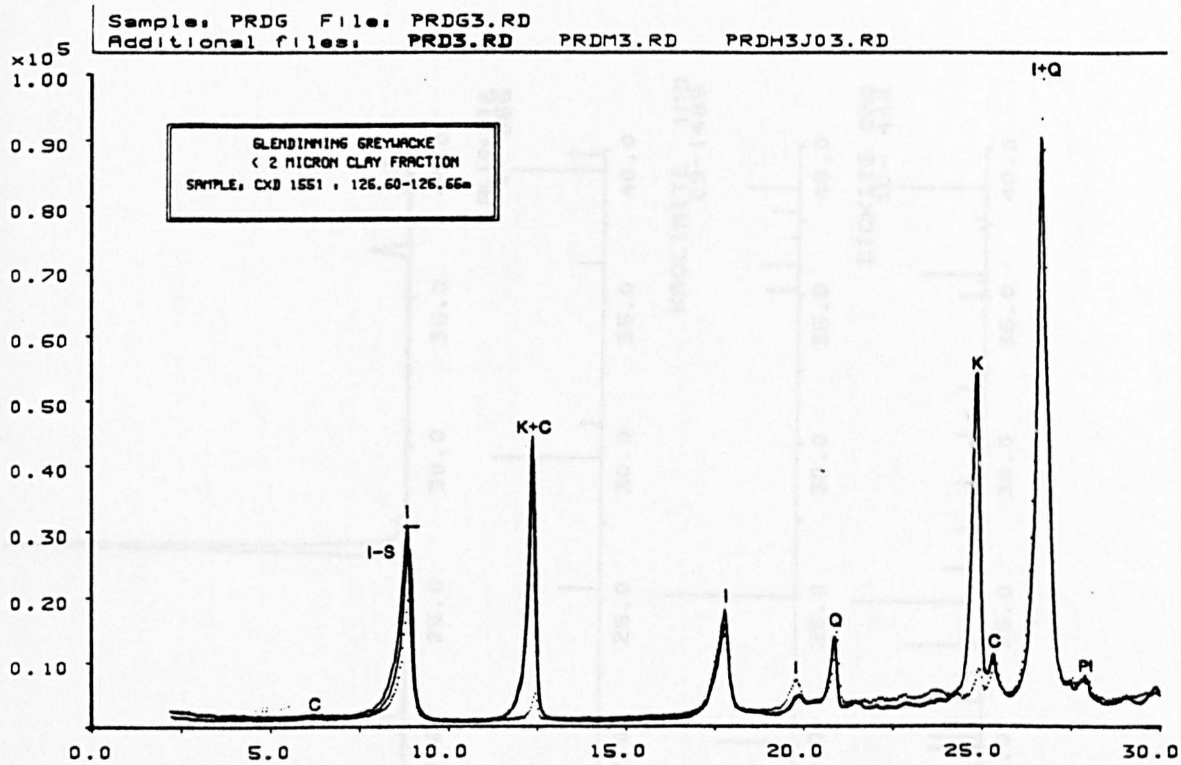
Sample: PRDG File: PRDG3.RD
Additional files: PRD3.RD PRDM3.RD PRDH3J03.RD
x10^5
GLENDINNING GREYWACKE
< 2 MICRON CLAY FRACTION
SAMPLE: CXD 1551 : 126.60-126.66m
I+Q
K+C
K
I
I-S
C
Q
Pl
0.0 5.0 10.0 15.0 20.0 25.0 30.0

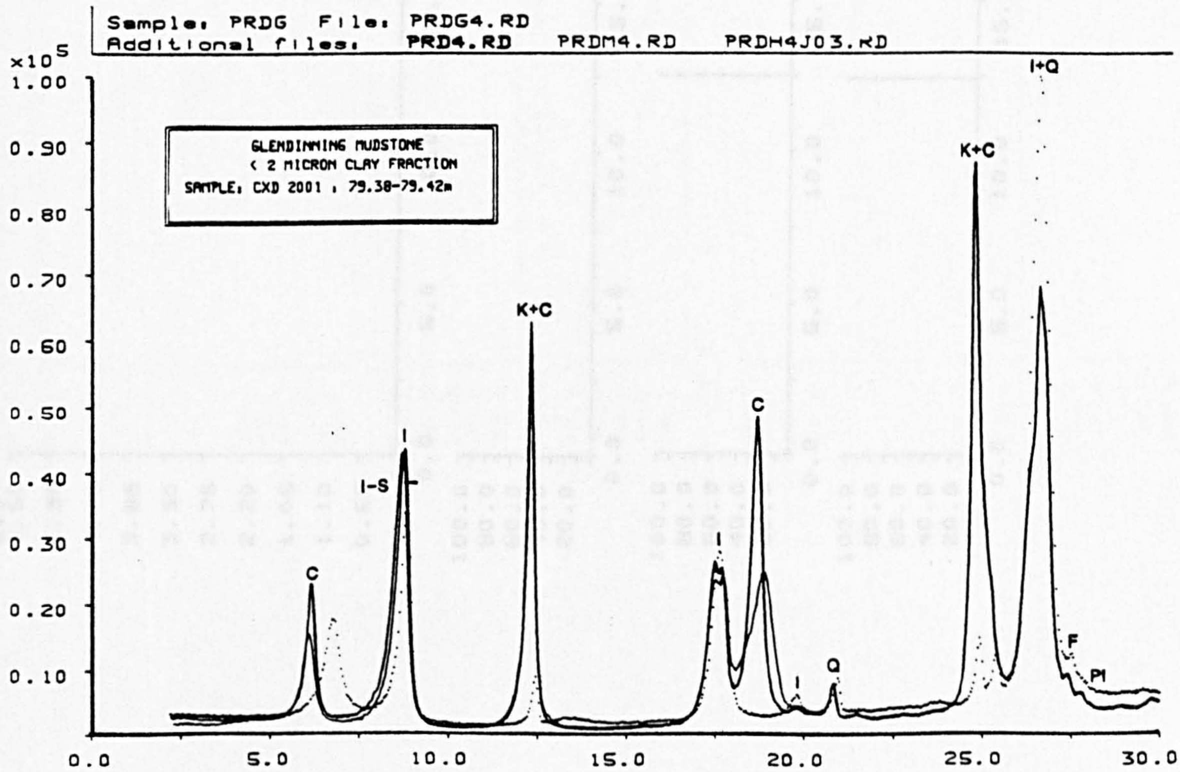
Sample: PRDG File: PRDG4.RD
Additional files: PRD4.RD PRDM4.RD PRDH4J03.RD
x10^5
GLENDINNING MUDSTONE
< 2 MICRON CLAY FRACTION
SAMPLE: CXD 2001 : 79.38-79.42m
I+Q
K+C
C
I
I-S
Q
F
Pl
0.0 5.0 10.0 15.0 20.0 25.0 30.0

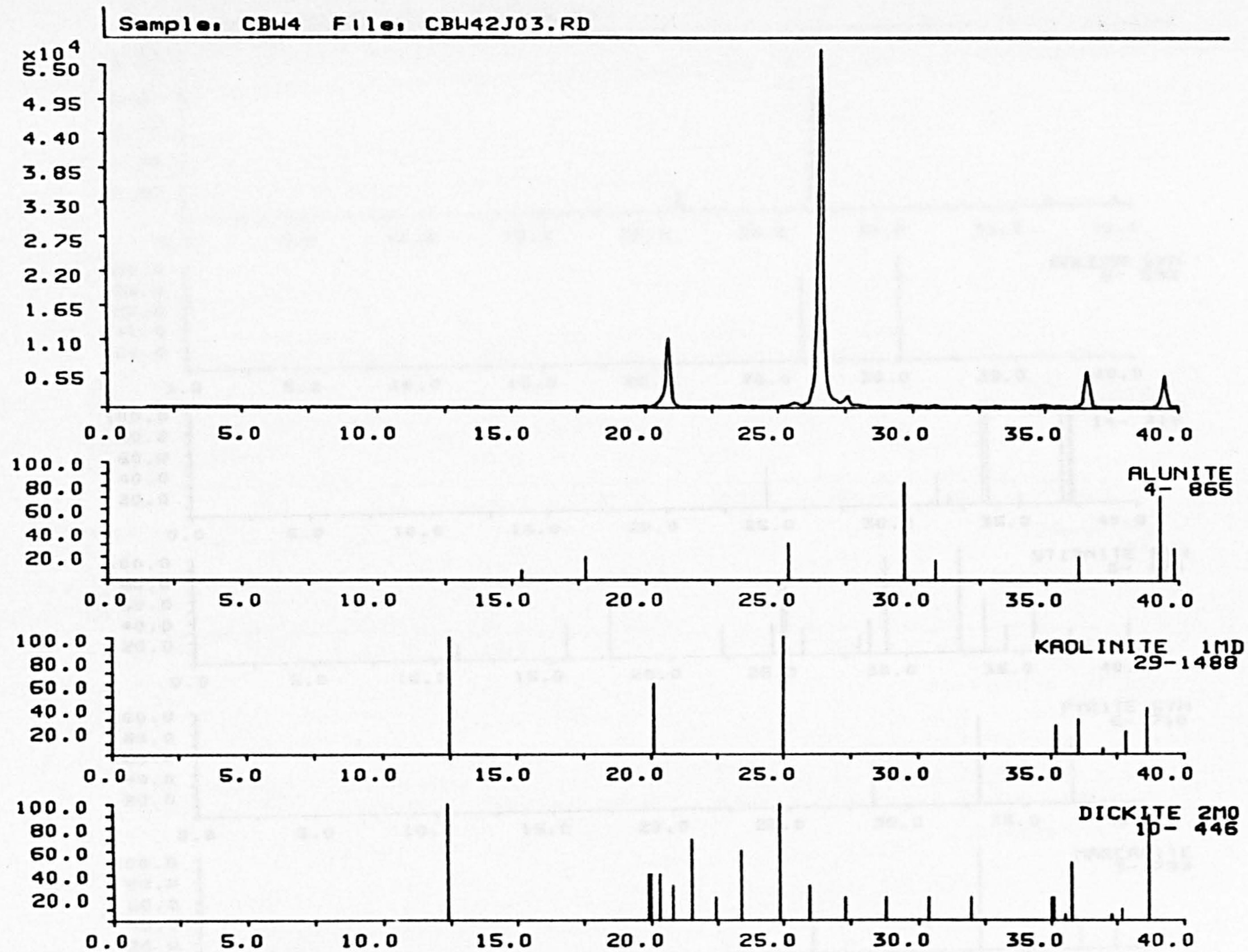

Sample: CBW4 File: CBW42J03.RD
x10^4
5.50
4.95
4.40
3.85
3.30
2.75
2.20
1.65
1.10
0.55
0.0 5.0 10.0 15.0 20.0 25.0 30.0 35.0 40.0
100.0 80.0 60.0 40.0 20.0
ALUNITE
4- 865
KAOLINITE 1MD
29-1488
DICKITE 2M0
10- 446

FIGURE 104

FIGURE 105

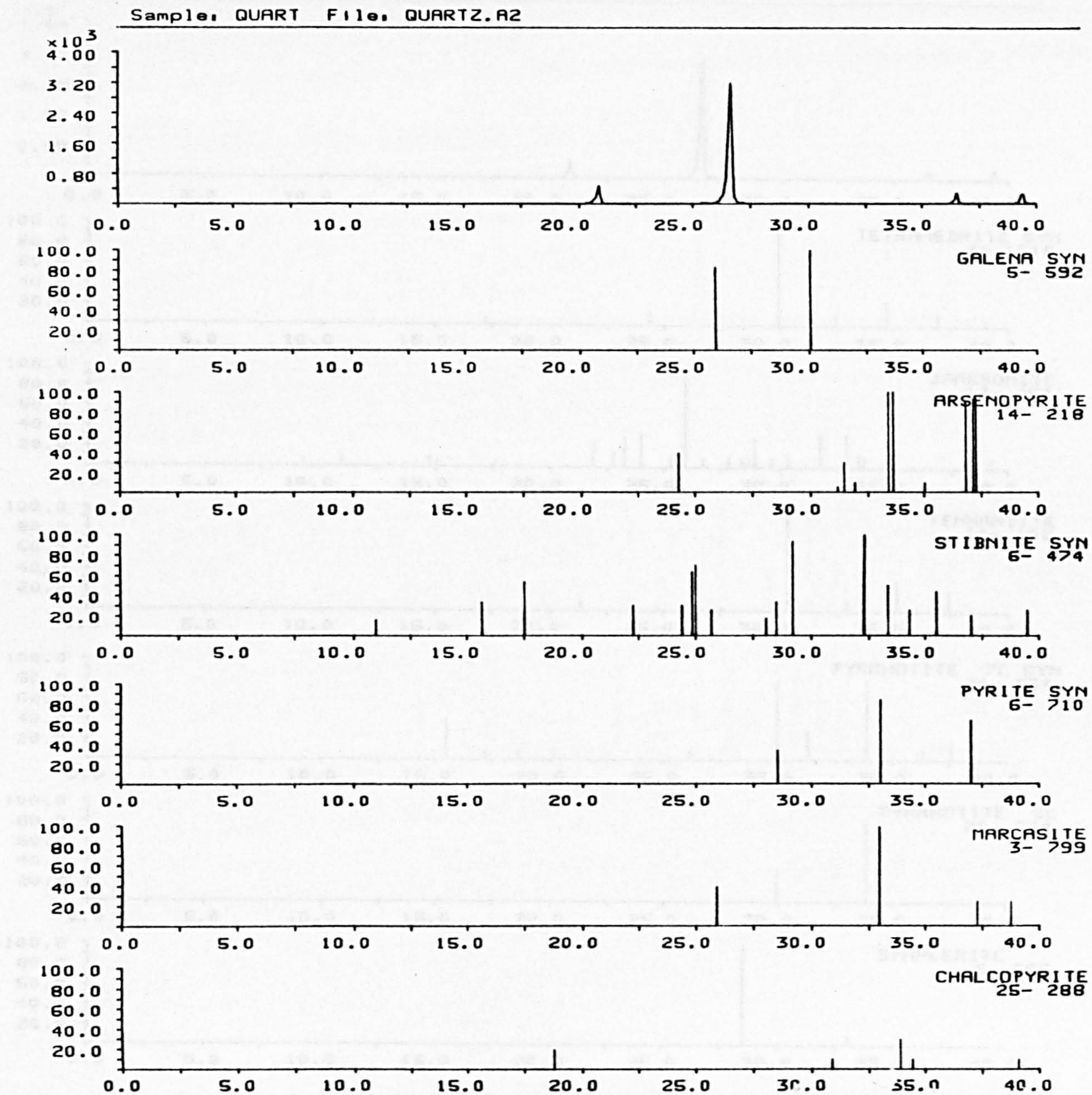

Sample: QUART File: QUARTZ.A2
x10^3
4.00
3.20
2.40
1.60
0.80
0.0 5.0 10.0 15.0 20.0 25.0 30.0 35.0 40.0
GALENA SYN
5- 592
100.0 80.0 60.0 40.0 20.0
ARSENOPYRITE
14- 218
STIBNITE SYN
6- 474
PYRITE SYN
6- 710
MARCASITE
3- 799
CHALCOPYRITE
25- 288

FIGURE 106

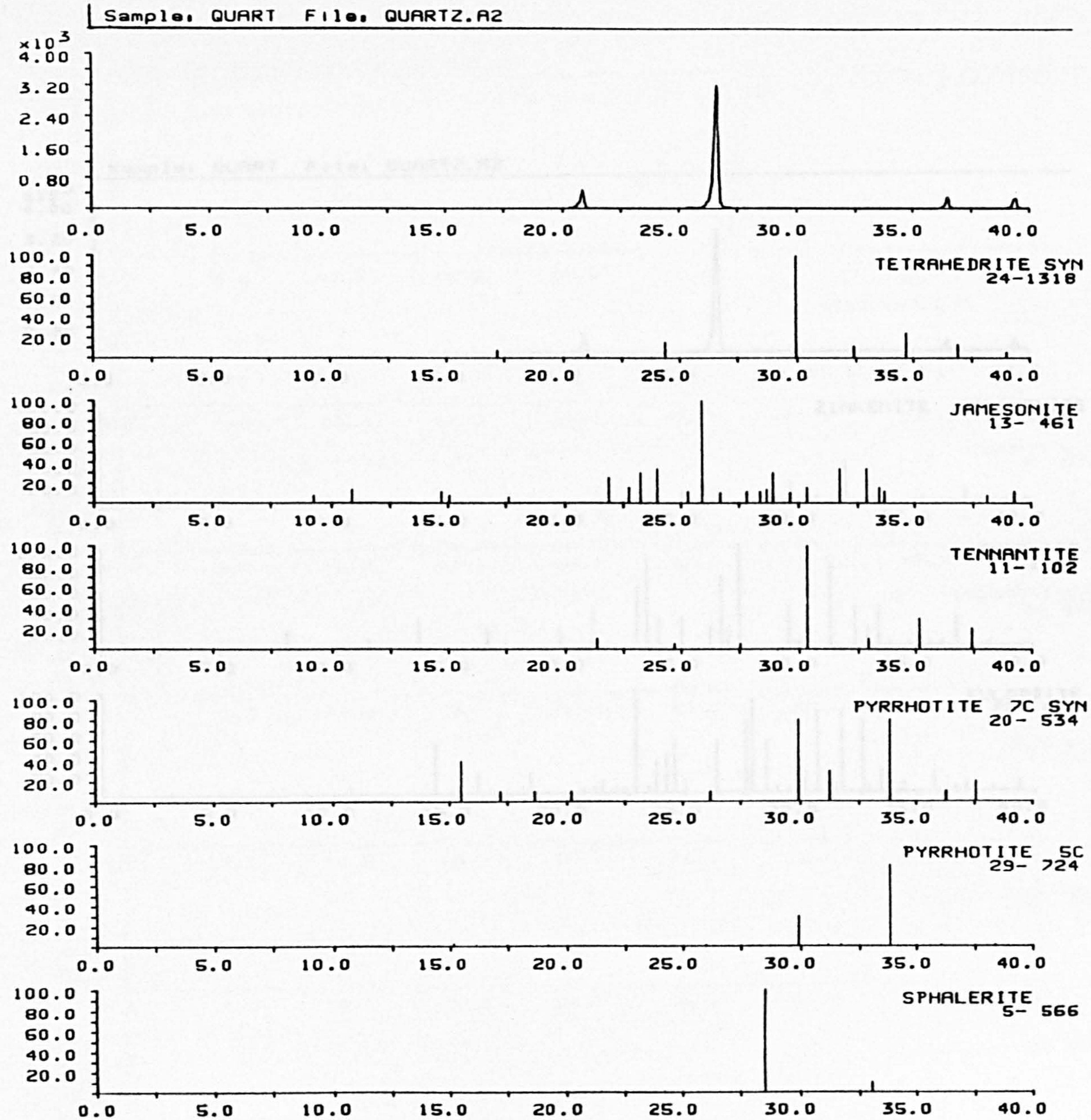
Sample: QUART File: QUARTZ.A2
x10^3
TETRAHEDRITE SYN
24-1318
JAMESONITE
13- 461
TENNANTITE
11- 102
PYRRHOTITE 7C SYN
20- 534
PYRRHOTITE 5C
29- 724
SPHALERITE
5- 566

FIGURE 107

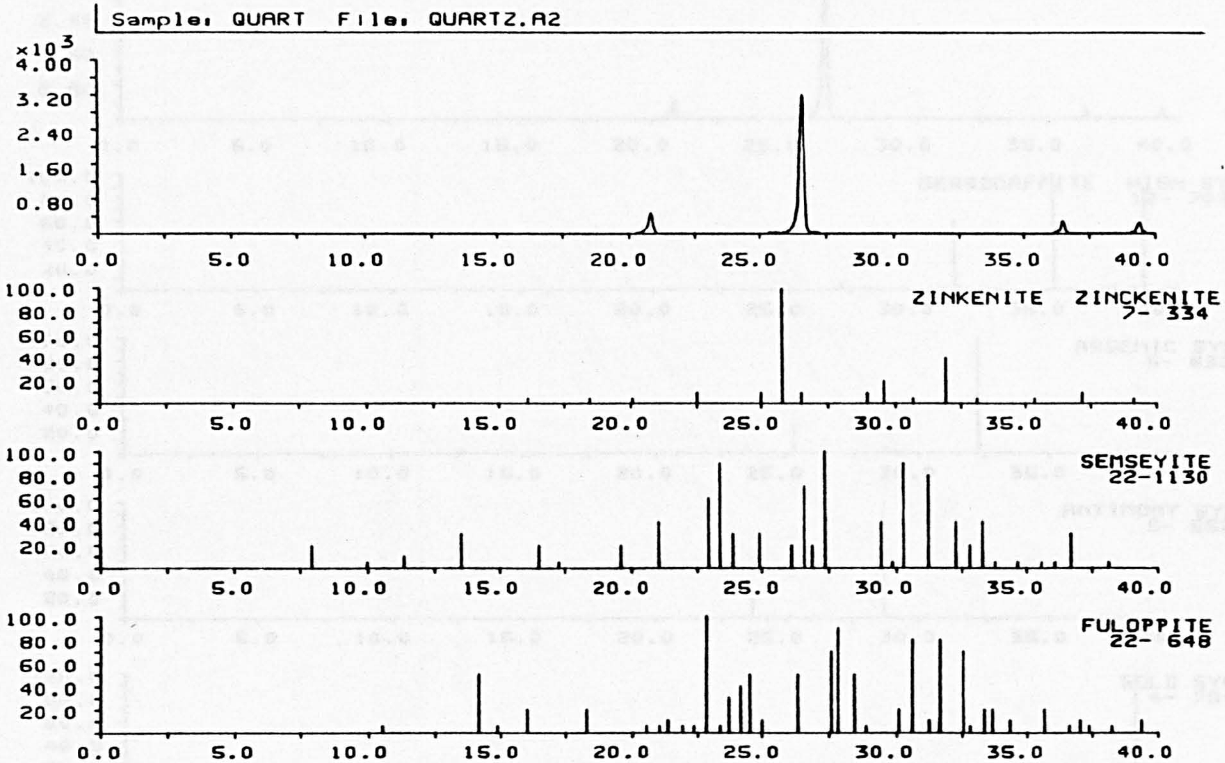
Sample: QUART File: QUARTZ.A2
x10^3
4.00
3.20
2.40
1.60
0.80
0.0 5.0 10.0 15.0 20.0 25.0 30.0 35.0 40.0
100.0
80.0
60.0
40.0
20.0
ZINKENITE ZINCKENITE
7-334
SEMSEYITE
22-1130
FULOPPITE
22-648

FIGURE 108

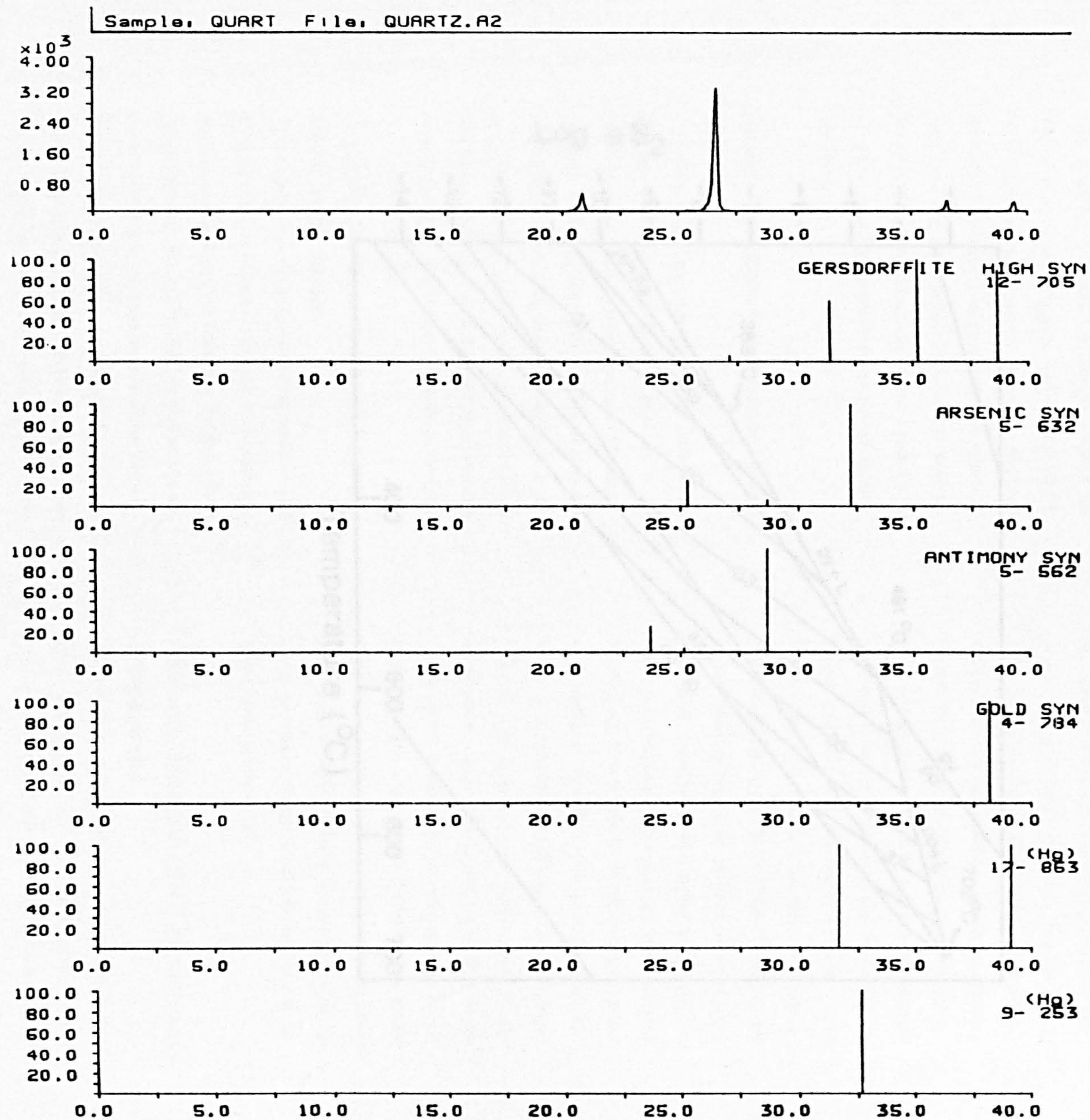

Sample: QUART File: QUARTZ.A2
x10^3
GERSDORFFITE HIGH SYN
12- 705
ARSENIC SYN
5- 632
ANTIMONY SYN
5- 562
GOLD SYN
4- 784
(Hg)
17- 863
(Hg)
9- 253

FIGURE 109

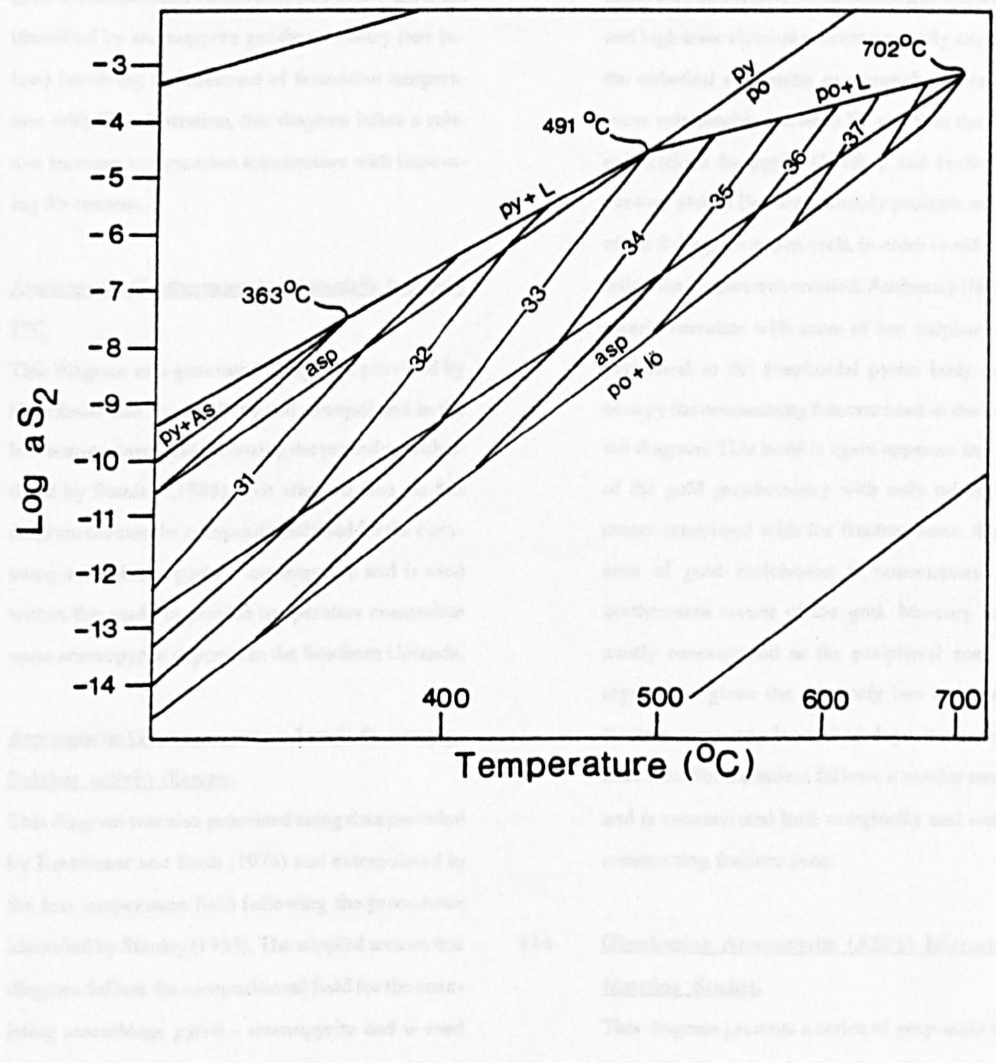
Log a S2
-3
-4
-5
-6
-7
-8
-9
-10
-11
-12
-13
-14
400
500
600
700
Temperature (°C)
702°C
491 °C
363°C
py
po
po+L
py+L
py+As
asp
asp
po+lö
31
32
33
34
35
36
37

110- Arsenopyrite Geothermometry: Univariant temperature-Sb wt% diagram (after Gamyanin 1976)

This diagram presents an additional geothermometer based upon the level of antimony substitution in arsenopyrite, as described by Gamyanin (1976). Note the general substitution line (T°C=20 x Sb wt% + 255) and error bars (±10°C). Analyses of arsenopyrites from the Southern Uplands plot within the shaded field on this diagram within a 255-280°C (±10°C) temperature range. In opposition to the trend identified by arsenopyrite geothermometry (see below) involving the decrease of formation temperature with Sb substitution, this diagram infers a relative increase in formation temperature with increasing Sb content.

111- Arsenopyrite Geothermometry: Atomic% Arsenic - T°C

This diagram was generated using data provided by Kretchmar and Scott (1976) and extrapolated in the low temperature field following the procedures identified by Stanley (1983). The stippled area on this diagram defines the compositional field for the coexisting assemblage pyrite - arsenopyrite and is used within this study to provide temperature constraints upon arsenopyrite deposits in the Southern Uplands.

112- Arsenopyrite Geothermometry: Atomic % Arsenic - Sulphur activity diagram

This diagram was also generated using data provided by Kretchmar and Scott (1976) and extrapolated in the low temperature field following the procedures identified by Stanley (1983). The stippled area on this diagram defines the compositional field for the coexisting assemblage pyrite - arsenopyrite and is used within this study to provide constraints upon sulphur activity during the formation of arsenopyrite deposits in the Southern Uplands.

113- Glendinning Stratiform Pyrite Microchemical Mapping study

This diagram presents a series of 'grey-scale' contour maps detailing the results of a micro-geochemical investigation of the trace element content of synsedimentary framboidal pyrite cluster and accompanying authigenic / epigenetic overgrowths associated with mineralisation. Microprobe analysis were undertaken using a 20 micron grid spacing (n=174) within a 250x250 micron grid. The results of this study are presented in table 4.19 together with summary statistics in table 2.19. Sulphur values illustrate a concentric structure defining the approximate extent of relic framboidal pyrite. This cluster is crosscut by a series of fractures the most notable of which virtually subdivides the grain into two halves. This fracture is infilled by authigenic pyrite exhibiting a low sulphur and high trace element content normally attributed to the euhedral epigenetic overgrowth. Given the inverse relationship between Fe and S in the formula calculations for pyrite (Fe+S=2 and Fe:S~1:1) the contour plot of Fe values simply presents an inverse of the S diagram and as such, in order to aid interpretation the Fe plot was omitted. Antimony (Sb) values clearly correlate with areas of low sulphur content, peripheral to the framboidal pyrite body and also occupy the crosscutting fracture zone in the centre of the diagram. This trend is again apparent in a review of the gold geochemistry with only minor enrichments associated with the fracture zone, the major area of gold enrichment is concentrated in the northeastern corner of the grid. Mercury is dominantly concentrated in the peripheral zone of the crystal and given the relatively low content in the fracture zone, may have been deposited marginally later than Sb. Cadmium follows a similar tend to Sb and is concentrated both marginally and within the crosscutting fracture zone.

114- Glendinning Arsenopyrite (ASP1) Microchemical Mapping Studies.

This diagram presents a series of grey-scale contour maps detailing the results of a micro-geochemical investigation of the major and trace element content of breccia hosted arsenopyrite from the Glendinning deposit. Microchemical analyses were undertaken over ½ of a rhombic shaped arsenopyrite crystal (180x60 microns in cross-section) using a 10 micron analysis grid (n=72). The results of this study are presented in table 4.01 together with summary statistics in table 2.01. Grid sizes, coordinates and mapping boundaries for all microchemical studies are presented in table 1.15 and 1.50.

FIGURE 110

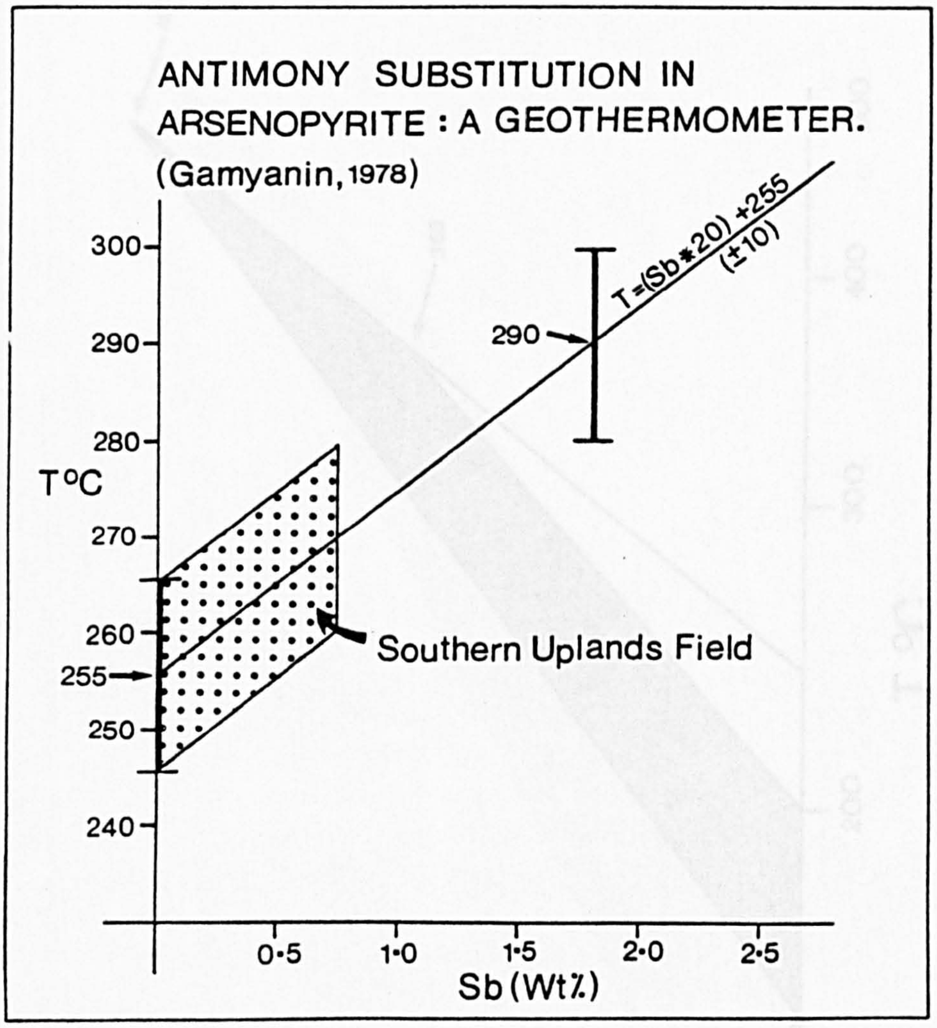
ANTIMONY SUBSTITUTION IN
ARSENOPYRITE : A GEOTHERMOMETER.
(Gamyanin, 1978)
T=(Sb*20) +255
(±10)
290
300
290
280
270
260
255
250
240
T°C
Southern Uplands Field
0·5
1·0
1·5
2·0
2·5
Sb (Wt%)

FIGURE 111

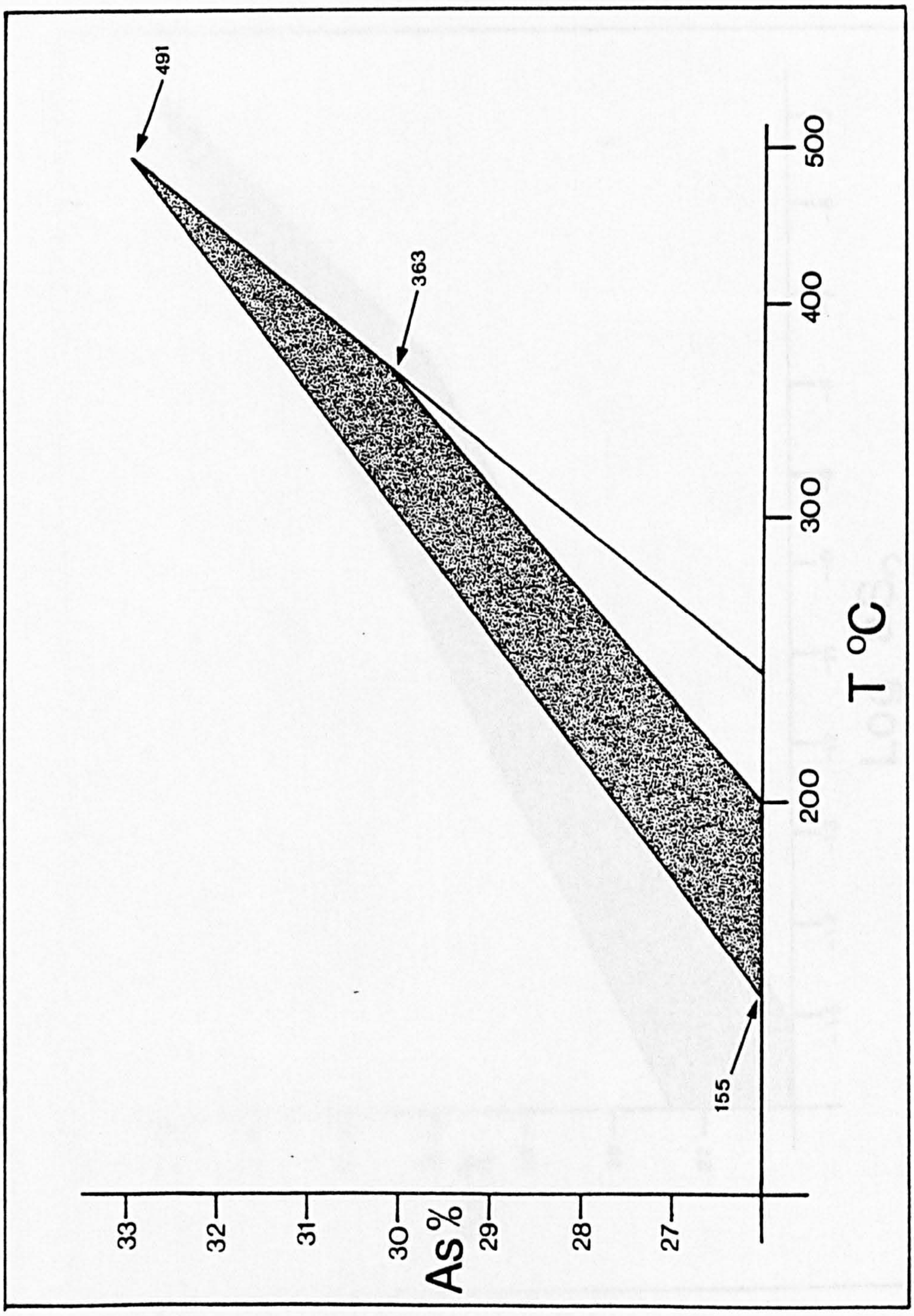

FIGURE 112

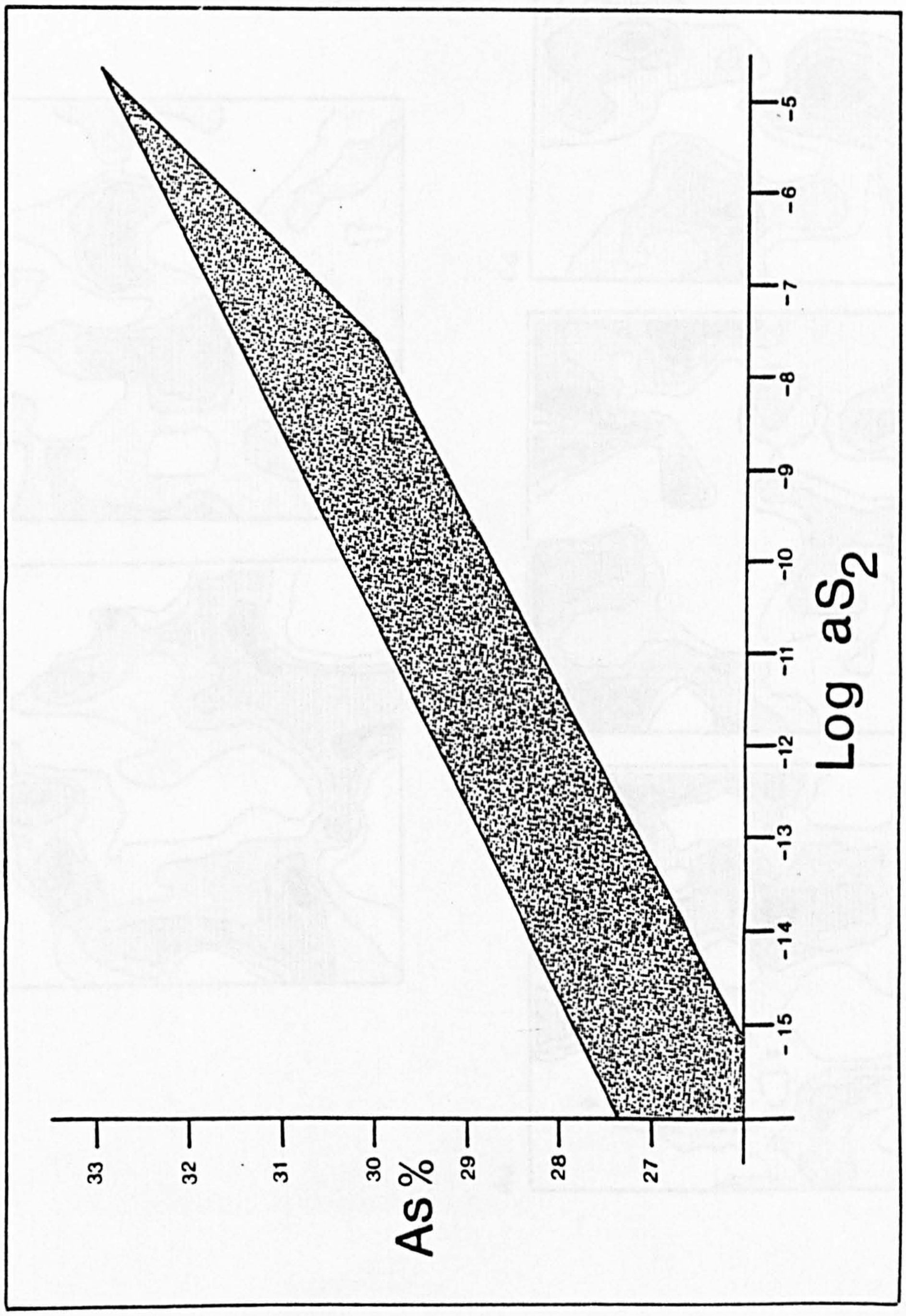

FIGURE 113

Glendinning Stratiform Pyrite: Major and Trace Element Geochemistry.

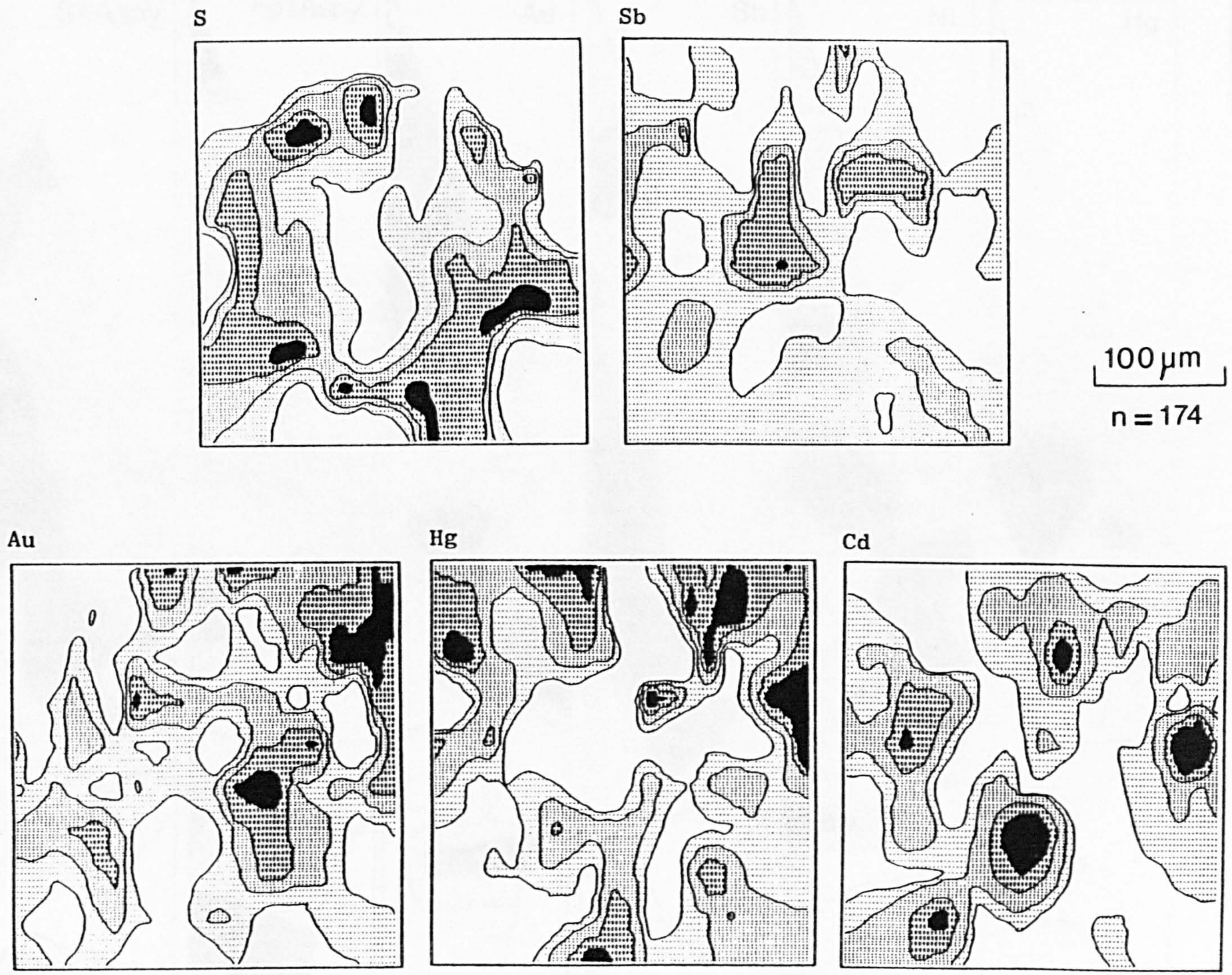

FIGURE 114

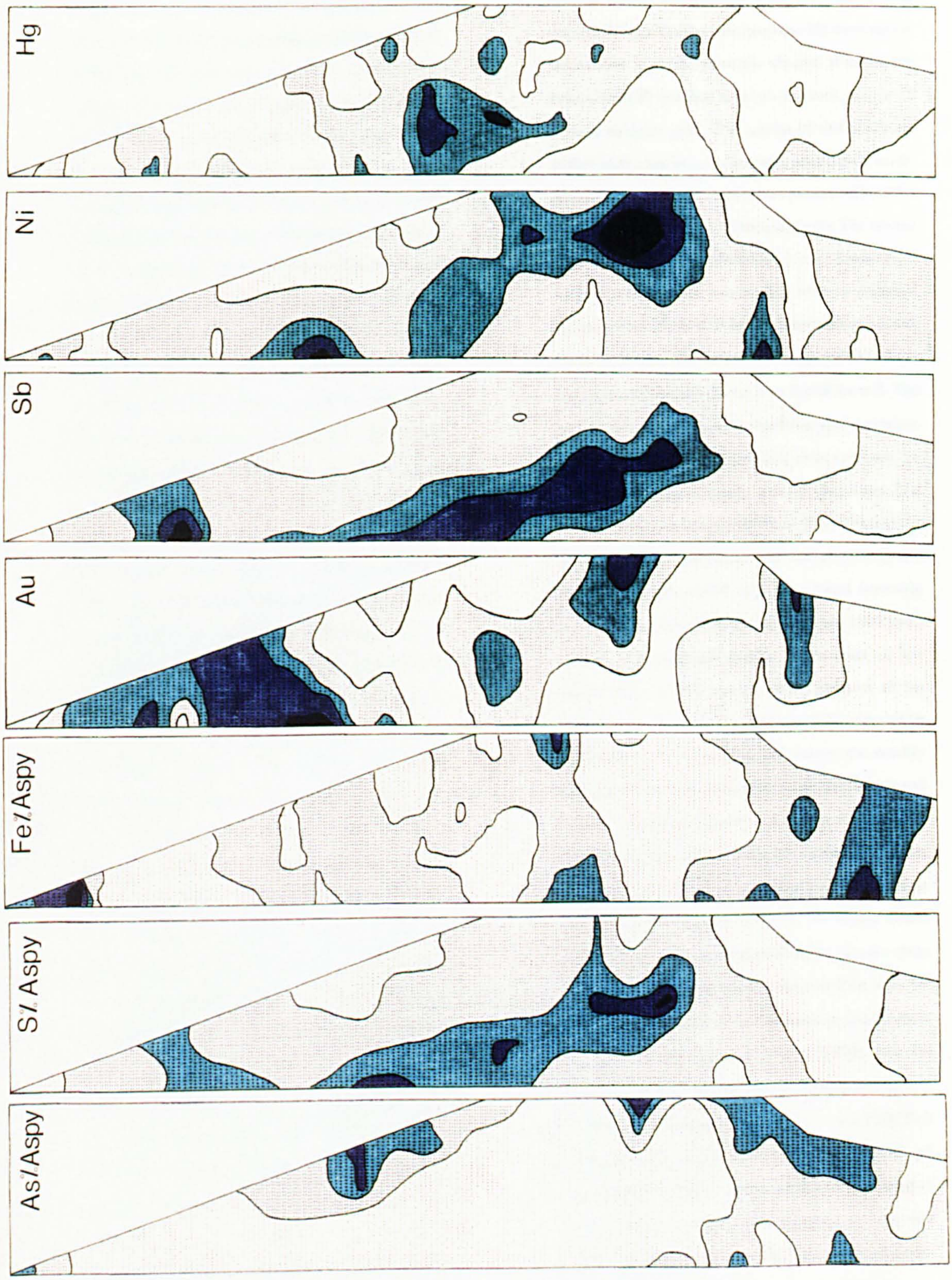

The atomic %Fe in arsenopyrite (Fe%Aspy) plot illustrates a relatively sporadic distribution (note that Fe values (range: 32.85-33.60 At.%S) exhibit minimal variation with respect to either As or S). The atomic %As in arsenopyrite (As%Aspy) plot exhibits clear evidence for an As enriched margin (max: 31.97 at.%As) and depleted core (min: 27.93 at.%As) to the crystal. The atomic %S in arsenopyrite (S% Aspy) plot displays a relatively enriched core zone (max: 38.38) and depleted margin (min: 34.74) a trend inversely related to that of arsenic. Au values (max: 1500 ppm) indicate a preferential enrichment in areas of low arsenic/high sulphur values within the crystal core and illustrate an inverse relationship with arsenic concentration. Sb values are notably enriched within the crystal core (max: 7400ppm) and exhibit a marked concentric zonation parallel to crystal margins. Sb is positively correlated with sulphur and inversely correlated with arsenic values. Ni values (max: 1700ppm) follow the trends ident- ified by both Au and Sb and are concentrated in low arsenic/ high sulphur zones within the core of the crystal. It should be noted however that the greatest concentration of both Ni and Au coincide within this zone, and are located marginal to the highest Sb concentrations. Hg values (max: 5200ppm) follow the trends identified by Ni and Au, and form a peripheral zone to areas of highest Sb content. With reference to the arsenopyrite geothermometer of Kretchmar and Scott (1976) both the temperature and sulphur activity during the period of crystal formation may be obtained (figs 109, 111 and 112). This study indicates that crystal is intensely zoned and as such the variation in As content may be used to infer the presence of a low temperature core and relatively high temperature margin. In detail, deposition took place over a wide range of temperatures (240-350°C) with a greater portion of values confined to a 290-330°C range. Sulphur activity (aS_2) is also lower in the crystal core (10^{-14} to 10^{-11}) than the margin 10^{-11} to 10^{-6}) with average values in the 10^{-11} to 10^{-7} field. The antimony substitution geothermometer defined by Gamyanin (1978) displayed in fig. 110 may be used to infer deposition temperatures in the range 255-270°C (±10°) with the Sb rich core zones deposited at slightly elevated values to their rim zones.

115- <u>Glendinning Arsenopyrite (ASP2) Microchemical Mapping Studies</u>

This diagram presents a series of grey-scale contour maps of the major and trace element content of breccia hosted arsenopyrite from the Glendinning deposit. Microchemical analyses (n=25) were undertaken over a small, rhombic shaped arsenopyrite crystal (40x20 microns in cross- section) using a 10 micron analysis grid. The results of this study together with a statistical summary, grid sizes, coordinates and mapping boundaries are presented in tables 4.02 and 2.02, 1.15 and 1.50 respectively. The atomic %Fe in arsenopyrite (Fe%Aspy) plot illustrates a relatively concentric distribution with an enriched margin (max: 33.90 at.% Fe) and depleted core (min: 32.14 at.% Fe). Note that the range of Fe%Aspy values is considerably lower than that of As or S. The atomic %As in arsenopyrite (As%Aspy) plot exhibits similar trends to Fe and provides clear evidence for As enriched margins (max: and core depletion. The atomic %S in arsenopyrite (S%Aspy) plot displays a strongly enriched core zone (max: 38.60 at.% S) and depleted margin (34.90 at.% S) a trend inversely related to that of arsenic. Au values (max: 1200 ppm) indicate a preferential enrichment in areas of low arsenic/high sulphur values within the core of the crystal and illustrate a strong positive correlation with sulphur concentration. Sb values are notably enriched (max: 4100 ppm) within the crystal core and exhibit a marked positive correlation with sulphur and inverse correlation with As values. Hg values (max: 10,500 ppm) display little systematic variation with respect to either As or S. Ni values (max: 700ppm) are relatively enriched within the core of the crystal and follow the trends identified by both Au and Sb. With reference to the arsenopyrite geothermometer of Kretchmar and Scott (1976) both the temperature and sulphur activity during crystal formation may be obtained (figs 109, 111 and 112). This study indicates that the crystal is strongly zoned and as such, the variation in As content may be used to infer the presence of a low temperature core and relatively high temperature rim zone. In detail, deposition took place over a wide temperature range with average values confined to a 280-350°C range. Sulphur activity (aS_2) is also lower in the crystal core (10-

FIGURE 115

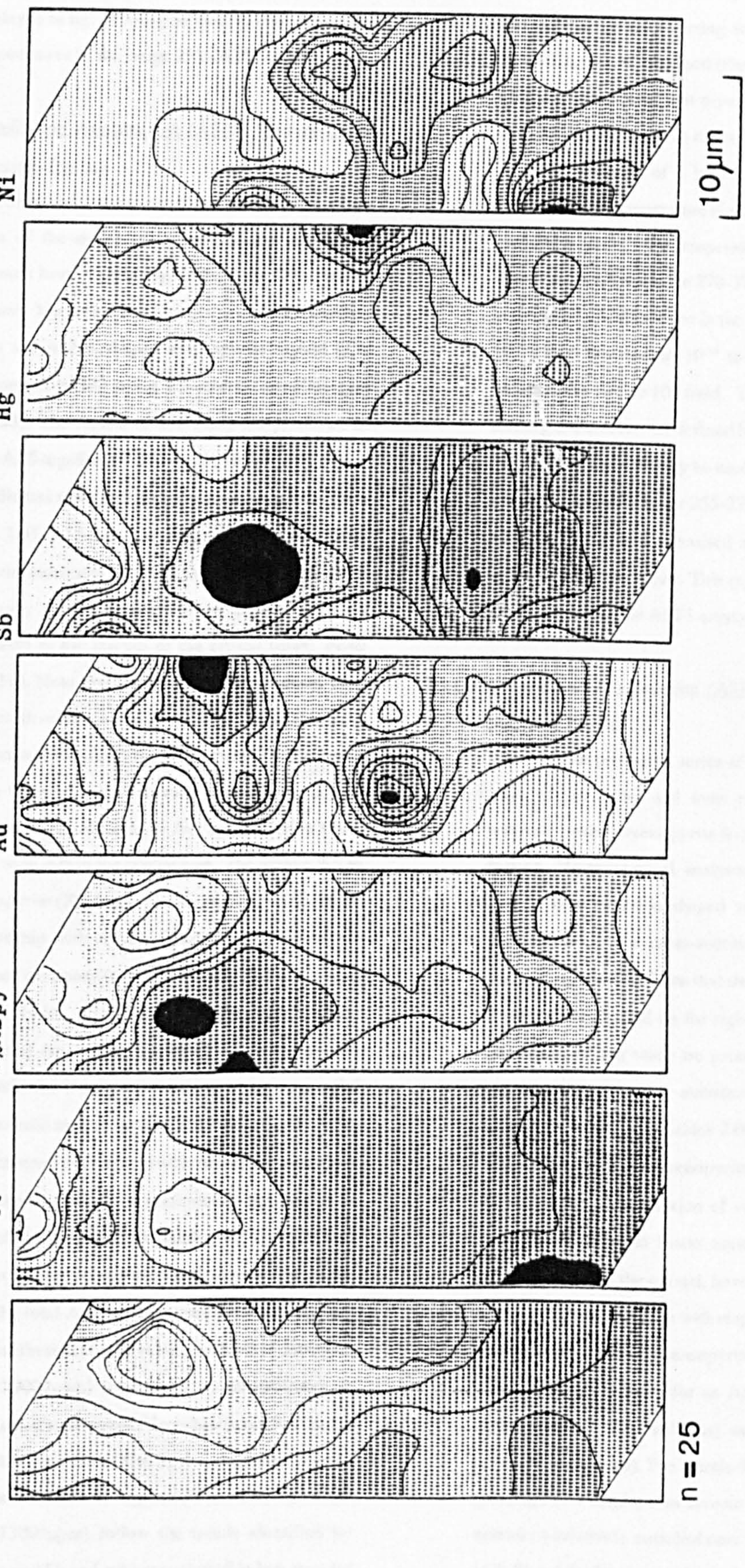

^{16} to 10^{-11}) than the margin 10^{-11} to 10^{-6}) with average values in the 10^{-11} to 10^{-7} field. The antimony substitution geothermometer defined by Gamyanin (1978) displayed in fig. 110 may be used to infer deposition temperatures in the range 255-263°C (±10°).

116- Glendinning Arsenopyrite (ASP5) Microchemical Mapping Studies

This diagram presents a series of grey-scale contour maps of the major and trace element content of wallrock hosted arsenopyrite from the Glendinning deposit. Microchemical analyses were undertaken upon a rhombic shaped arsenopyrite crystal (250 microns in width) using a 5 micron sampling grid (n=323). The results of this study are presented in table 4.05 together with summary statistics, grid size, coordinates and mapping boundaries are presented in table 2.05, 1.15 and 1.50, respectively. The atomic %Fe in arsenopyrite (Fe%Aspy) plot illustrates a relatively systematic distribution with values concentrated in the margin of the crystal (max: 29.40 at.% Fe). Note that Fe values exhibit minimal variation with respect to either As or S. The atomic %As in arsenopyrite (As% Aspy) plot exhibits clear evidence for preferential As enrichment in the crystal margins (max: 33.28 at.% As) and depletion (min: 26.25 at.% As) in the crystal core. The atomic %S in arsenopyrite (S%Aspy) plot displays an antipathetic relationship with arsenic, illustrated by a relatively enriched core zone (max: 41.23 at.% S) and depleted margin (min: 33.44 at.% S). Sb values (max: 7300ppm) are notably enriched within the crystal core and exhibit a strong concentric zonation parallel to the crystal margin. Sb is positively correlated with S and inversely correlated with As values. Au values (<3000ppm) indicate a preferential enrichment in areas of low arsenic/high sulphur values and illustrate an inverse relationship with arsenic concentration. The total Au plot illustrates the relatively random distribution of gold values in excess of 3000ppm (max: 29000ppm) interpreted as sub-microscopic inclusions of native gold. Hg values (max: 8500ppm) follow the trends identified by Au, and form a peripheral zone to areas of highest Sb content. Ni values (max: 13000ppm) follow the trends identified by both Au and Sb and are concentrated in low arsenic/high sulphur zones within the core of the crystal. With reference to the arsenopyrite geothermometer of Kretchmar and Scott (1976) both the temperature and sulphur activity during the period of crystal formation may be obtained (figs 109, 111 and 112). This study indicates that crystal is intensely zoned and that the variation in As content may be used to infer the presence of a low temperature core and relatively high temperature rim. In detail, deposition took place over a wide temperature range with average values confined to the 270-370°C range. Sulphur activity (aS_2) is also lower in the crystal core (10^{-16} to 10^{-10}) than the margin 10^{-10} to 10^{-6}) with average values in the 10^{-12} to 10^{-8} field. The antimony substitution geothermometer defined by Gamyanin (1978) displayed in fig. 110 may be used to infer deposition temperatures in the range 255-270°C (±10°) with the Sb rich core zones deposited at slightly elevated values to their rim zones. This crystal shows marked similarities with the ASP1 crystal (fig. 114).

117- Glendinning Arsenopyrite (ASP6) Microchemical Mapping Studies

This diagram presents a series of grey-scale contour maps of the major and trace element content of wallrock hosted arsenopyrite from the Glendinning deposit. Microchemical analyses were undertaken over ½ of a rhombic shaped arsenopyrite crystal (120x150 microns in cross-section) using a 5 micron analysis grid (n=97). Note that the central portion of the crystal is situated on the right of each diagram. The results of this study are presented in table 4.06 together with summary statistics, coordinates and mapping boundaries in tables 2.06, 1.15 and 1.50. The atomic %Fe in arsenopyrite (Fe%Aspy) plot illustrates the concentration of values (max: 33.58 at.% Fe) in a broad linear zone crosscutting the central portion of the crystal, however the Fe values exhibit minimal variation with respect to either As or S. The atomic %As in arsenopyrite (As%Aspy) plot exhibits clear evidence for an As enriched crystal margins (max: 32.86 at.% As) and a depleted core (min: 28.44 at.% As). The atomic %S in arsenopyrite (S%Asp) plot displays an inverse relationship with arsenic; a relatively enriched core zone (max: 39.39 at.% S) and depleted crystal margin (min: 35.50 at.%

FIGURE 116

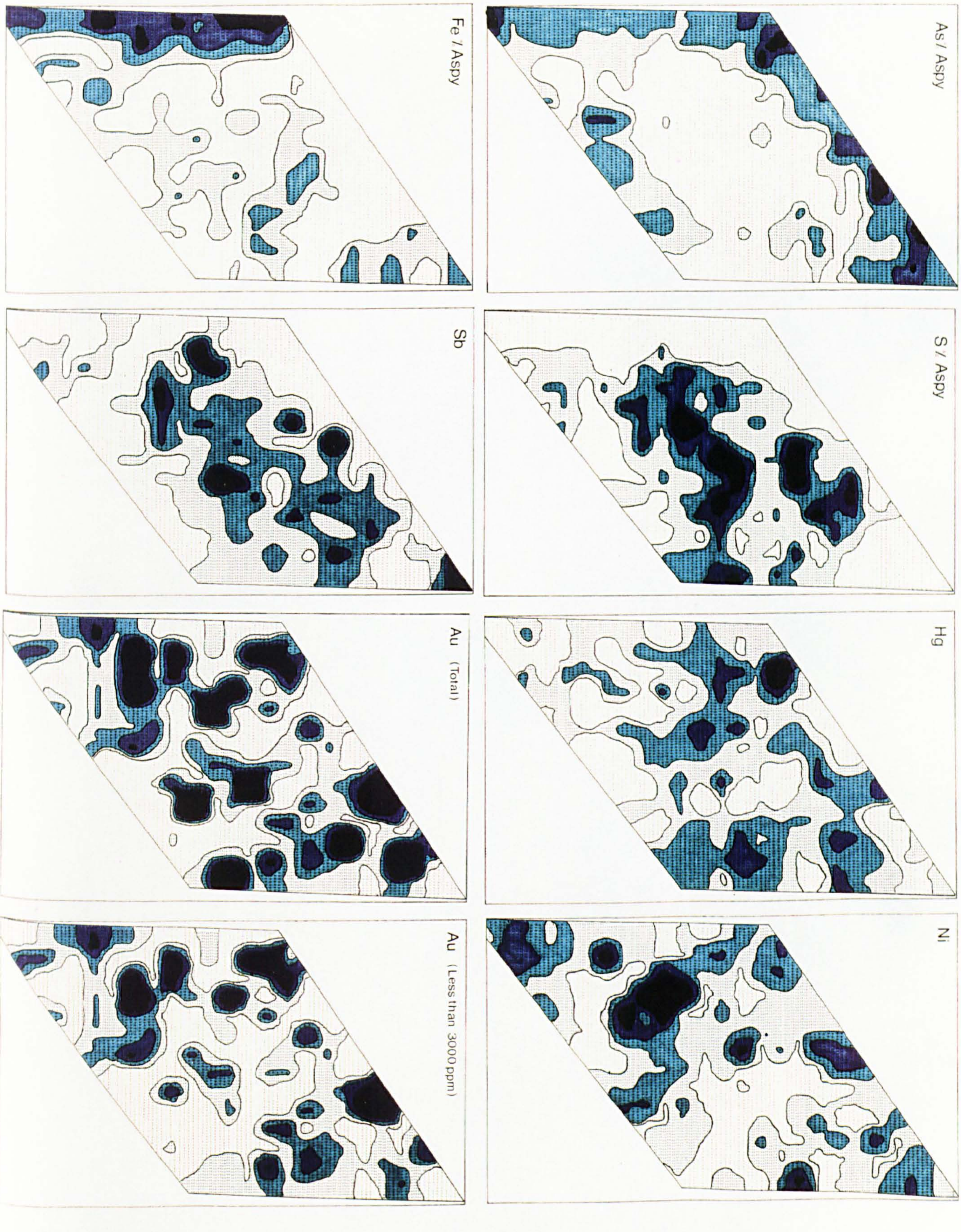

FIGURE 117

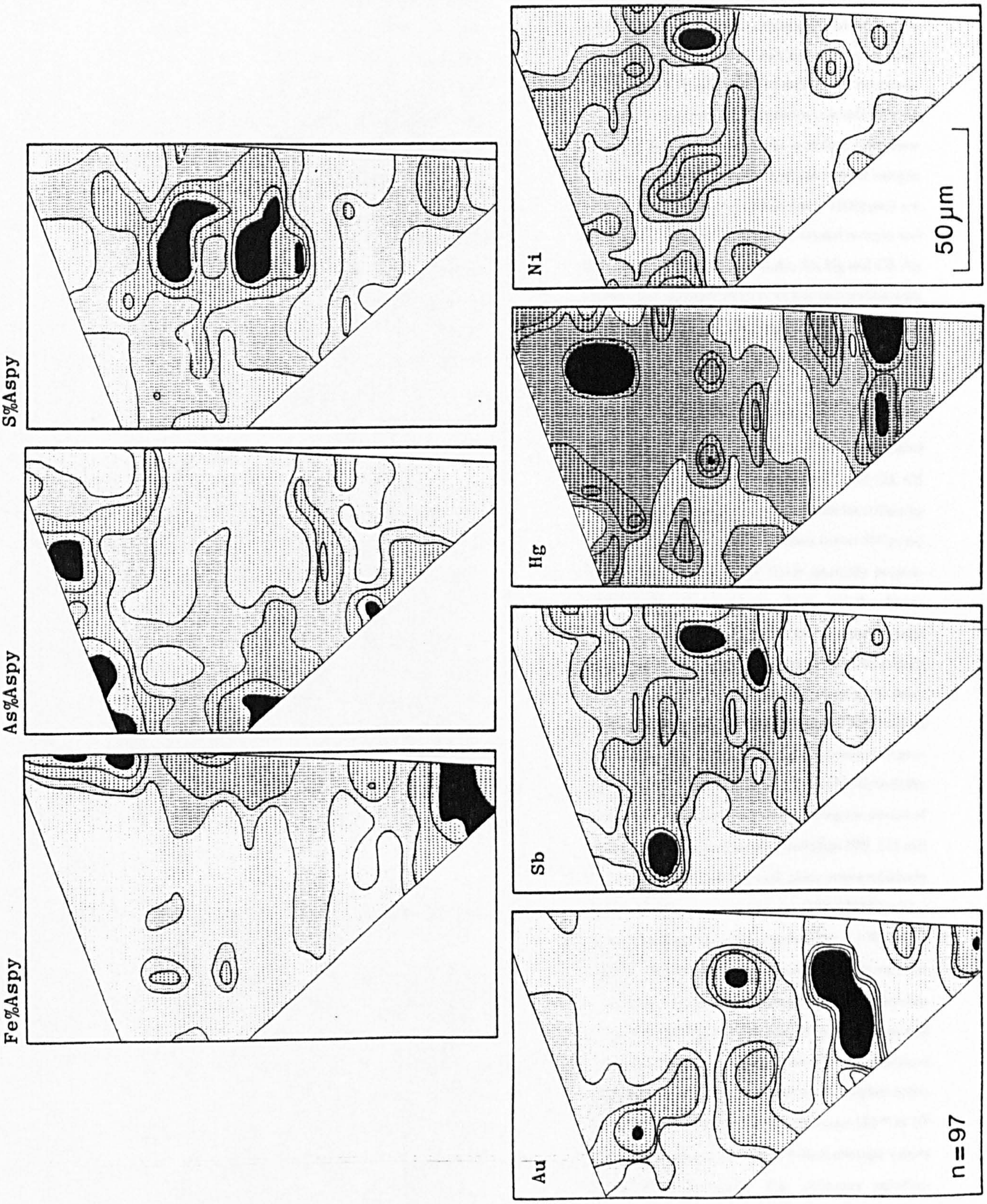

S). Au values (max: 23,700ppm) indicate a preferential enrichment in areas of low arsenic values within the crystal. Sb values (max: 7500ppm) are enriched in areas of arsenic deficiency, notably within the crystal core. Sb is positively correlated with sulphur and, to a lesser extent Au and inversely correlated with arsenic values. Hg values (max: 14,900ppm) follow the general trends identified by sulphur values and highlight peripheral zones adjacent to areas of highest Sb content. Ni values (max: 8400ppm) follow the trends identified by Sb and are concentrated in low arsenic/high sulphur zones within the core of the crystal. With reference to the arsenopyrite geothermometer of Kretchmar and Scott (1976) both the temperature and sulphur activity during the period of crystal formation may be obtained (figs 109, 111 and 112). This study indicates that crystal is intensely zoned and that the variation in As content may be used to infer the presence of a low temperature core and relatively high temperature margin. Arsenopyrite deposition took place over a wide temperature range with a greater portion of values confined to a 250-330°C range. Sulphur activity (aS_2) is also lower in the crystal core (10^{-13} to 10^{-10}) than the margin 10^{-10} to 10^{-5}) with average values concentrated in the 10^{-12} to 10^{-8} field. Here again, the antimony substitution geothermometer defined by Gamyanin (1978) displayed in fig. 110 may be used to infer deposition temperatures in the range 255-270°C (±10°) with the Sb rich core zones deposited at slightly elevated values to their rim zones.

118- The Knipe Arsenopyrite (ASP7) Microchemical Mapping Studies

This diagram presents a series of grey-scale contour maps of the major and trace element content of wallrock hosted arsenopyrite from the Knipe deposit. Analyses were undertaken over ½ of a rhombic shaped arsenopyrite crystal (70x 50microns in cross-section) using a 5 micron analysis grid (n=49). Note that the central portion of the crystal is situated at the top of each diagram. The results of this study are presented in table 4.07 together with summary statistics, coordinates and mapping boundaries in tables 2.07, 1.15 and 1.50. The atomic %Fe in arsenopyrite (Fe% Aspy) plot illustrates the enrichment of values (max: 33.78 at.% Fe) adjacent to the crystal margin however, Fe values exhibit minimal variation with respect to either As or S. The atomic %As in arsenopyrite (As% Aspy) plot exhibits enriched crystal margins (max: 29.69 at.% As) and a deficient core zone (min: 24.79 at% As). The atomic %S in arsenopyrite (S% Asp) plot displays an inverse relationship with arsenic, with a relatively enriched core zone (max: 41.55 at.% S) and a depleted crystal margin (min: 36.89 at.% s). Au values (max 1800ppm) are enriched in zones adjacent to the crystal margin and are positively correlated with As, Sb, Hg and Cd. Ag values (max 600ppm) display a close correlation with S enrichment and As deficiency. Sb values are enriched (max: 8600ppm) in zones of weak arsenic deficiency (notably within the crystal core) and positively correlated with Au, Hg, Cd. Hg values (max:6600ppm) follow the general trend identified by sulphur and correlate with Au, Sb and Cd. Cd values (max: 800ppm) follow the trends identified by Fe, S, Sb and Hg whereas Ni values (max: 500 ppm) present an small, isolated, linear anomaly perpendicular to the crystal margin. In general, the chemical zonation identified within this wallrock hosted arsenopyrite from the Knipe deposit exhibits close similarities with wallrock hosted arsenopyrite from the Glendinning deposit (see chapter 6 for detailed discussion). With reference to the arsenopyrite geothermometer of Kretchmar and Scott (1976) both the temperature and sulphur activity during the period of crystal formation may be obtained (figs 109, 111 and 112). In detail, deposition took place over a relatively restricted range of temperatures (150-310°C) with a greater portion of values confined to a 170-250°C range. Although the trends identified in above arsenic plot are not as well developed as in the Glendinning plots (see fig. 116) the zonation present may still be used to infer the presence of a low temperature core and higher temperature rim zone. Sulphur activity (aS_2) is also lower in the crystal core (10^{-16} to 10^{-12}) than the margin 10^{-12} to 10^{-7}) with average values in the 10^{-16} to 10^{-11} field. The antimony substitution geothermometer defined by Gamyanin (1978) displayed in fig. 110 may be used to infer deposition temperatures in the range 255-272°C (±10°).

FIGURE 118

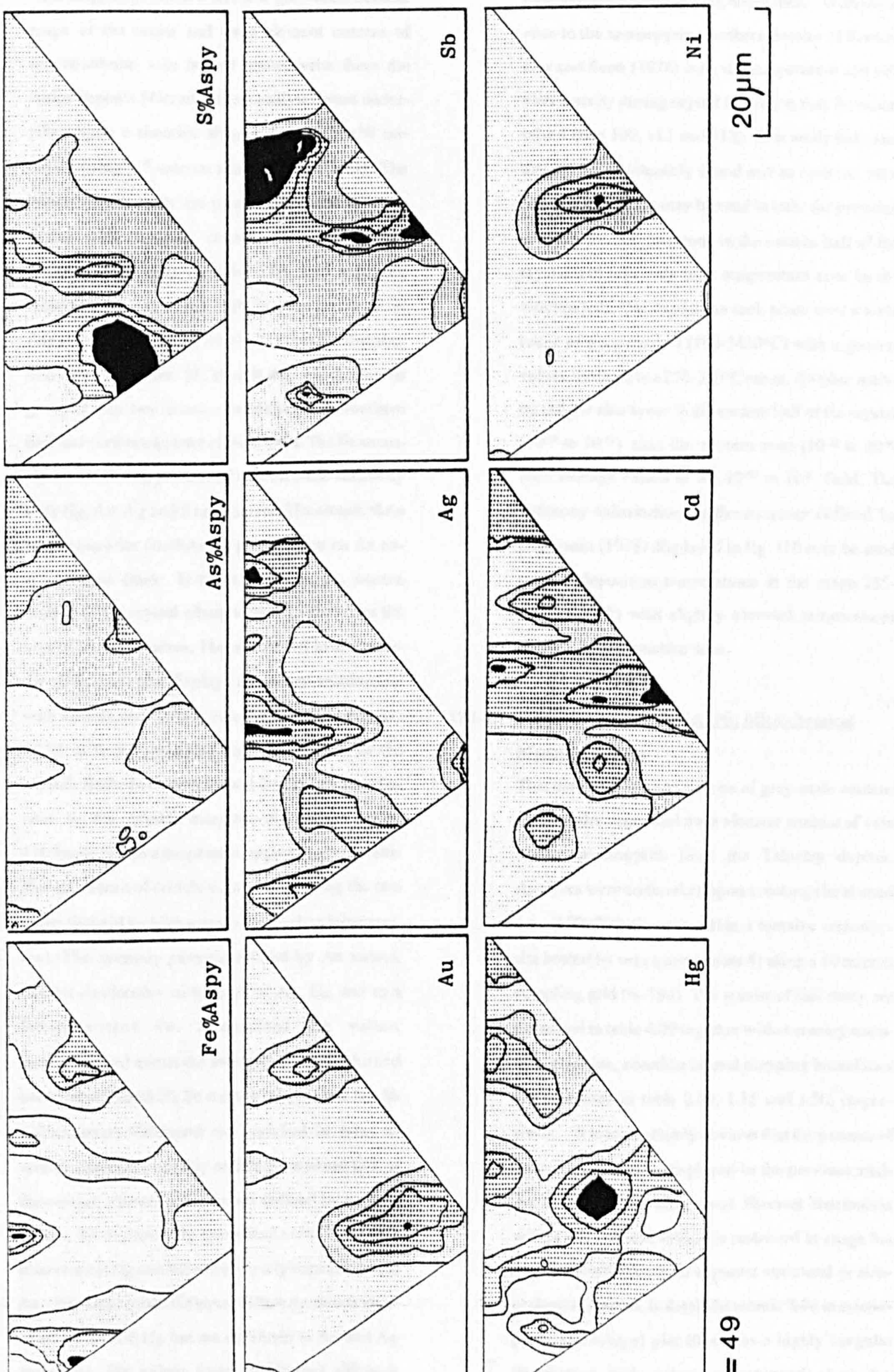

119- The Knipe Arsenopyrite (ASP8) Microchemical Mapping Studies

This diagram presents a series of grey-scale contour maps of the major and trace element content of quartz-stibnite vein hosted arsenopyrite from the Knipe deposit. Microchemical analyses were undertaken upon a rhombic shaped crystal (50x30 microns) using a 5 micron analysis grid (n=61). The results of this study are presented in table 4.08 together with summary statistics, coordinates and mapping boundaries in tables 2.08, 1.15 and 1.50, respectively. The atomic %Fe in arsenopyrite (Fe% Aspy) plot illustrates a relatively sporadic distribution of values (max: 35.26 at.% Fe) which may be grouped into two zones, crosscutting the southern half and northern quarter of the crystal. The Fe anomaly trends (>90th percentile) exhibit some similarity with Hg, Au, Ag and S enrichment. The atomic %As in arsenopyrite (As%Aspy) plot defines an As enriched zone (max: 32.99 at.% As) in the eastern section of the crystal which virtually subdivides the crystal into two halves. The atomic %S in arsenopyrite (S%Aspy) plot displays an inverse relationship with arsenic and defines an enrichment zone (max: 38.72 at.% S) occupying the western half of the crystal. Both maximum As and S zones occur adjacent to the crystal margins. Au values (max: 1100ppm) define a concentric, approximate rhombic shaped pattern of enrich- ment, crosscutting the two zones defined by high arsenic and high sulphur content. The anomaly patterns defined by Au values, exhibit similarities with those of Ag, Hg and to a lesser extent Fe. Anomalous Ag values (max:600ppm) mimic the trends identified by Au and correlate with both Ni, Fe and to a lesser extent Hg. Sb values (max: 6900ppm) are enriched in areas of arsenic depletion, notably within the western half of the crystal, mirroring the trends defined by sulphur values. Sb is positively correlated with S and to a lesser extent Hg and Ni; and inversely correlated with As. Ni values (max: 600ppm) follow the trends identified by Sb and Hg but are unrelated to Au and Ag anomalies. Hg values (max: 6100ppm) although sporadic follow the general trends identified by Sb values and form peripheral zones adjacent to areas of highest Sb content. Cu values are enriched in both the crystal core and in areas of anomalous Hg values in the crystal margin. Cu values (max: 1000ppm) appear unrelated to Au and Ag anomalies. With reference to the arsenopyrite geothermometer of Kretchmar and Scott (1976) both the temperature and sulphur activity during crystal formation may be ascertained (figs 109, 111 and 112). This study indicates that crystal is intensely zoned and as such the variation in As content may be used to infer the presence of a low temperature zone in the eastern half of the crystal and relatively high temperature zone in the western half. Ore deposition took place over a wide range of temperatures (190-?450°C) with a general values confined to a 250-350°C range. Sulphur activity (aS_2) is also lower in the eastern half of the crystal (10^{-16} to 10^{-11}) than the western zone (10^{-12} to 10^{-5}) with average values in the 10^{-12} to 10^{-8} field. The antimony substitution geothermometer defined by Gamyanin (1978) displayed in fig. 110 may be used to infer deposition temperatures in the range 255-270°C (±10°) with slightly elevated temperatures defined for the western zone.

120- Talnotry Arsenopyrite (ASP9) Microchemical Mapping Studies

This diagram presents a series of grey-scale contour maps of the major and trace element content of vein hosted arsenopyrite from the Talnotry deposit. Analyses were undertaken upon a rectangular shaped area (100x200microns) within a massive arsenopyrite hosted by vein quartz (plate 4) using a 10 micron sampling grid (n=194). The results of this study are presented in table 4.09 together with summary statistics, grid size, coordinates and mapping boundaries are presented in table 2.09, 1.15 and 1.50, respectively. It is immediately obvious that the patterns of concentric zonation displayed in the previous studies, is absent from this crystal. Element distribution within this massive crystal is restricted in range but highly variable, with no apparent structural or mineralogical control. In detail the atomic %Fe in arsenopyrite (Fe%Aspy) plot illustrates a highly irregular distribution with values concentrated along the northern and southern margin of the crystal and within the centre of the grid area (max: 34.18 at.% Fe). The atomic %As in arsenopyrite (As% Aspy)

FIGURE 119

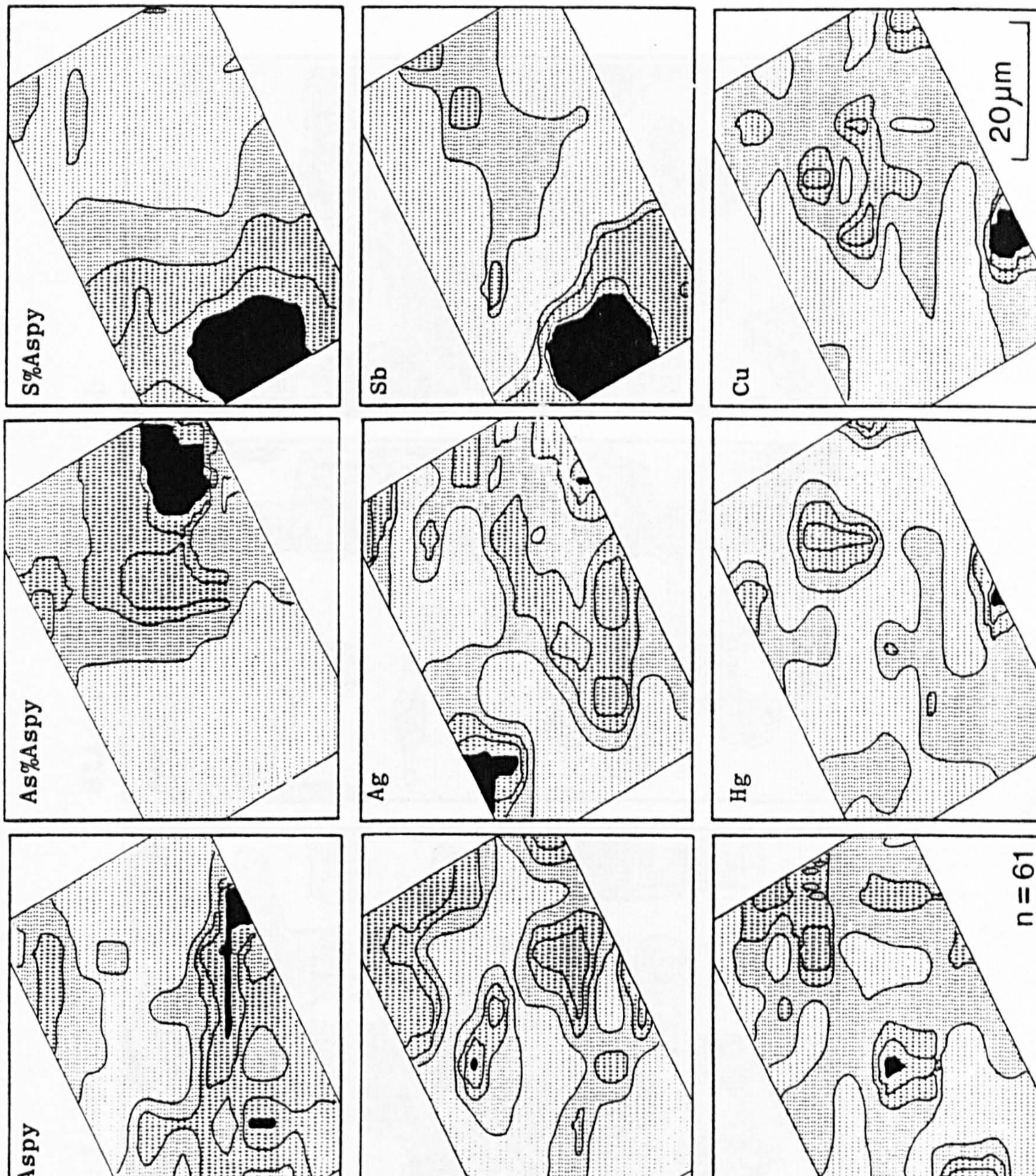

FIGURE 120

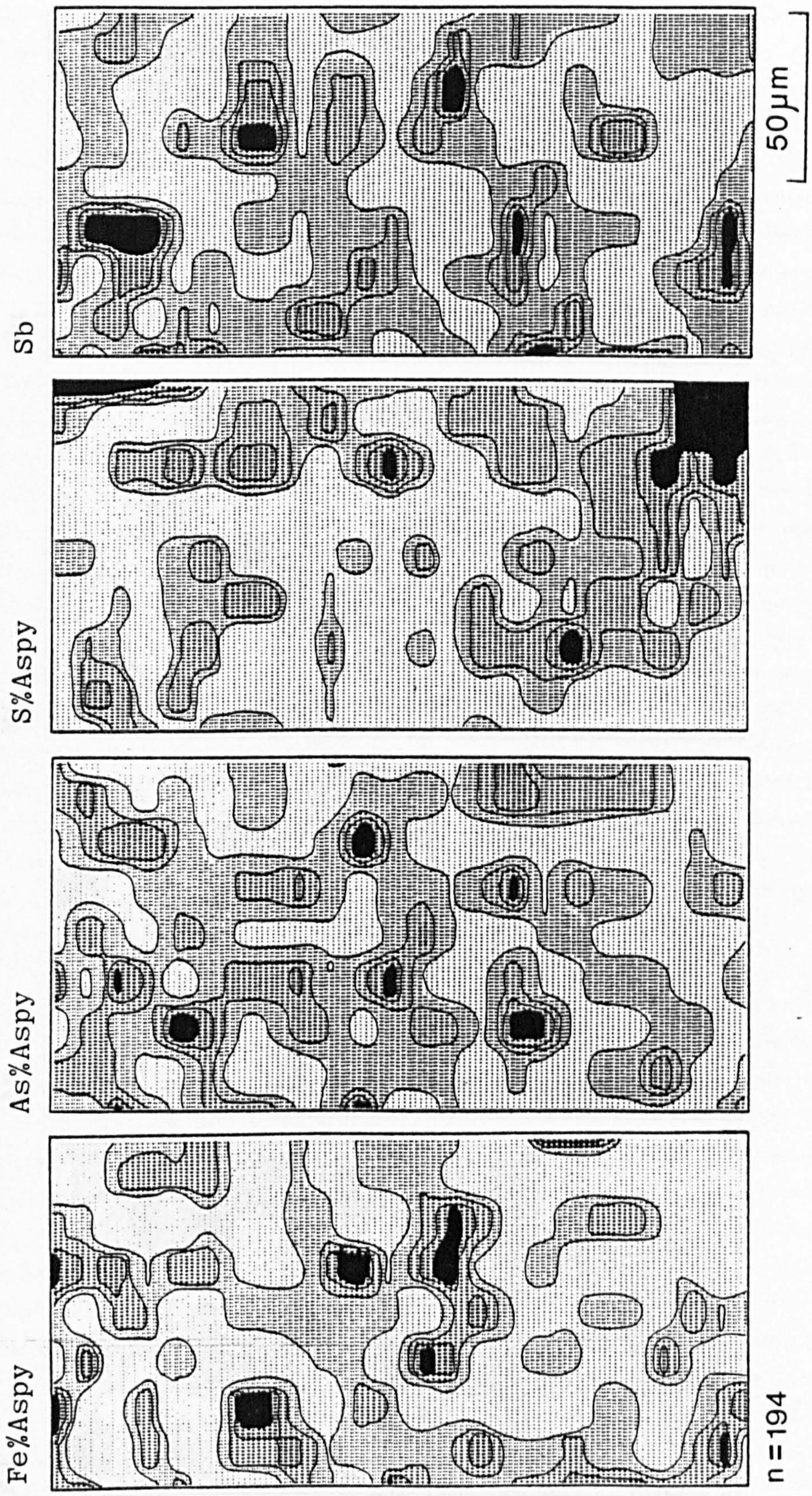

FIGURE 120 cont:

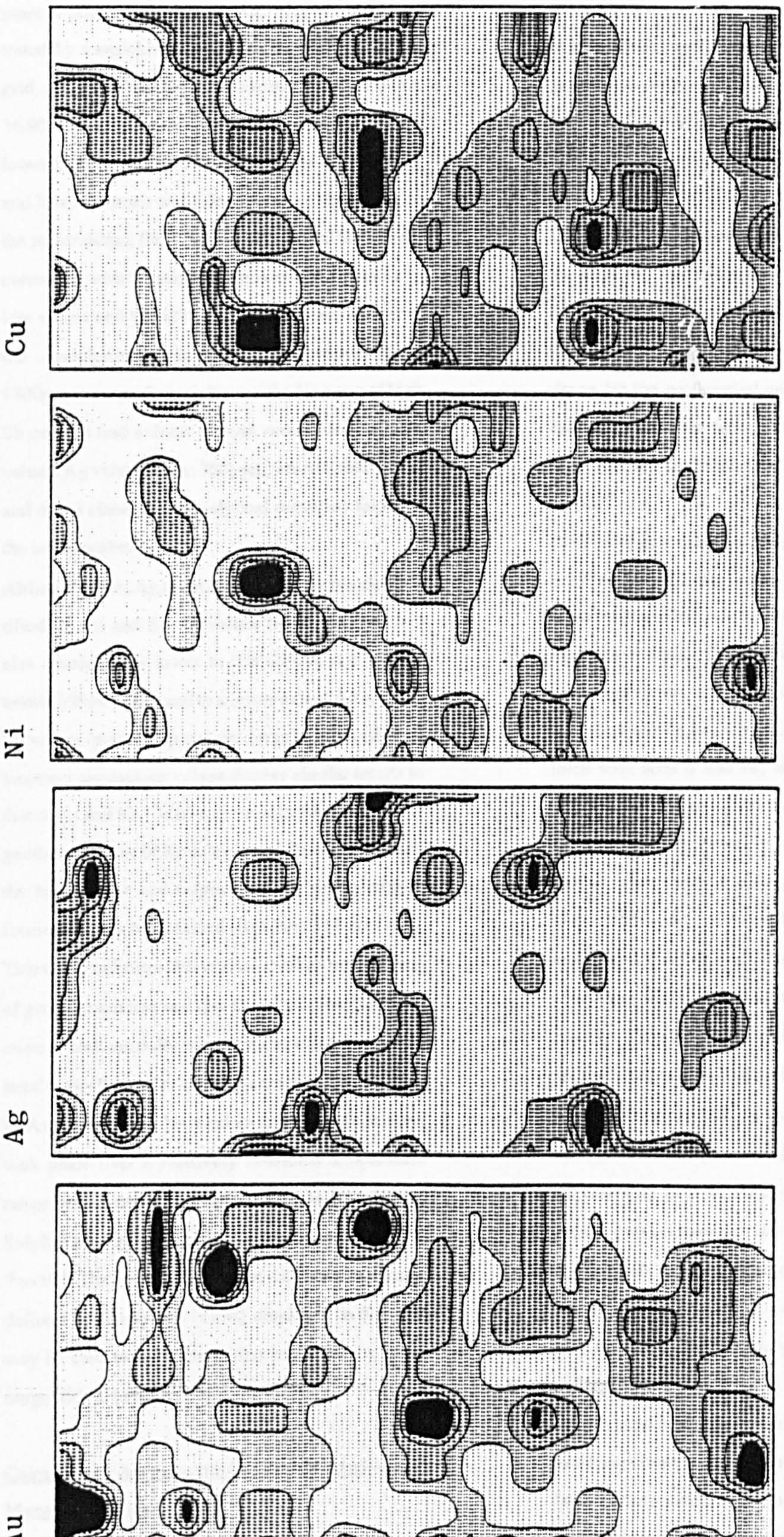

plot exhibits a complex, convoluted distribution with some evidence for As enrichment in areas of low Fe content (max: 33.31at.% As). The atomic %S in arsenopyrite (S%Aspy) plot displays a relatively more subtle inverse relationship with arsenic, illustrated by a enrichment on the eastern margin of the grid, particularly in the south eastern quadrant (max: 36.80 at.% S). Sb values (max: 900ppm) are notably lower than those observed in both the Glendinning and Knipe deposit and infer antimony deficiency in the mineralising fluid system. Sb may be tentatively correlated with S enrichment however the extremely low values and variable distribution make such spatial correlation problematic. Au values (max: 1400ppm) are preferentially enriched in areas of high Sb content and exhibit a weak association with Fe values. Ag values (max: 300ppm) are extremely low, and occur close to the analytical detection limits of the microprobe.

Although weak, Ag anomalies follow the trends identified by Au and Sb. Ni values (max: 500ppm) are also considerably lower in this deposit and exhibit trends following Fe and to a lesser extent Au and Ag. Cu values (max: 900ppm) are irregularly distributed, however anomalous values display similar trends to that of As and Sb. With reference to the arsenopyrite geothermometer of Kretchmar and Scott (1976) both the temperature and sulphur activity during crystal formation may be obtained (figs 109, 111 and 112). This study indicates that crystal exhibits no evidence of growth zonation and that the microchemical variation is both spatially complex and apparently unrelated to any form of mineralogical control. Variations in As content may be used to infer that deposition took place over a relatively restricted temperature range with average values confined to 300-350°C. Sulphur activity (aS_2) is also confined to a range 10^{-10} to 10^{-8}. The antimony substitution geothermometer defined by Gamyanin (1978) displayed in fig. 110 may be used to infer deposition temperatures in the range 255°C (±10°).

121- <u>Cairngarroch Arsenopyrite (ASP10) Microchemical Mapping Studies</u>

This diagram presents a series of grey-scale contour maps of the major and trace element content of vein hosted arsenopyrite from the Cairngarroch deposit. Microchemical analyses were undertaken on a square shaped arsenopyrite crystal (50 microns in diameter) using a 5 micron sampling grid (n=74). The results of this study are presented in table 4.10 together with summary statistics, grid size, coordinates and mapping boundaries are presented in tables 2.10, 1.15 and 1.50, respectively. The atomic %Fe in arsenopyrite (Fe%Aspy) plot illustrates a relatively systematic distribution with values concentrated in the southern half of the crystal, notably close to the crystal margins (max: 35.13 at.% Fe). The atomic %As in arsenopyrite (As% Aspy) plot exhibits evidence for the preferential enrichment in the crystal margins, notably in the western quadrant (max: 32.92 at.% As) and depletion (min: 28.47 at.% As) in the crystal core. The atomic %S in arsenopyrite (S%Aspy) plot displays an inverse relationship with both As and Fe anomalies, illustrated by a small relatively enriched core zone (max: 40.38 at.% S) and northern margin. Sb values (max: 1000ppm) are notably enriched within the crystal core and in areas of both S and Fe enrichment. Sb is positively correlated with both S and Fe; and inversely correlated with As values. Au values (max: 8700ppm) indicate a preferential enrichment in areas of low arsenic/high iron+sulphur concentrations, and are poorly related to Sb values. Ag values (max:700ppm) follow the trends identified by Au; are concentrated within the core zone, and occur marginal to areas of high Sb content. Ni values (max: 1000ppm) define isolated anomaly zones marginal to the crystal rims and follow trends identified by both Fe and Sb and are concentrated in high arsenic/ high iron zones within the rim of the crystal. With reference to the arsenopyrite geothermometer of Kretchmar and Scott (1976) both the temperature and sulphur activity during crystal formation may be ascertained (figs 109, 111 and 112). This study indicates that crystal is strongly zoned and that the variation in As content may be used to infer the presence of a small, relatively low temperature core zone and high temperature rim. In detail, deposition took place over a wide temperature range with average values confined to the 250-350°C field. Sulphur activity (aS_2) is lower in areas

FIGURE 121

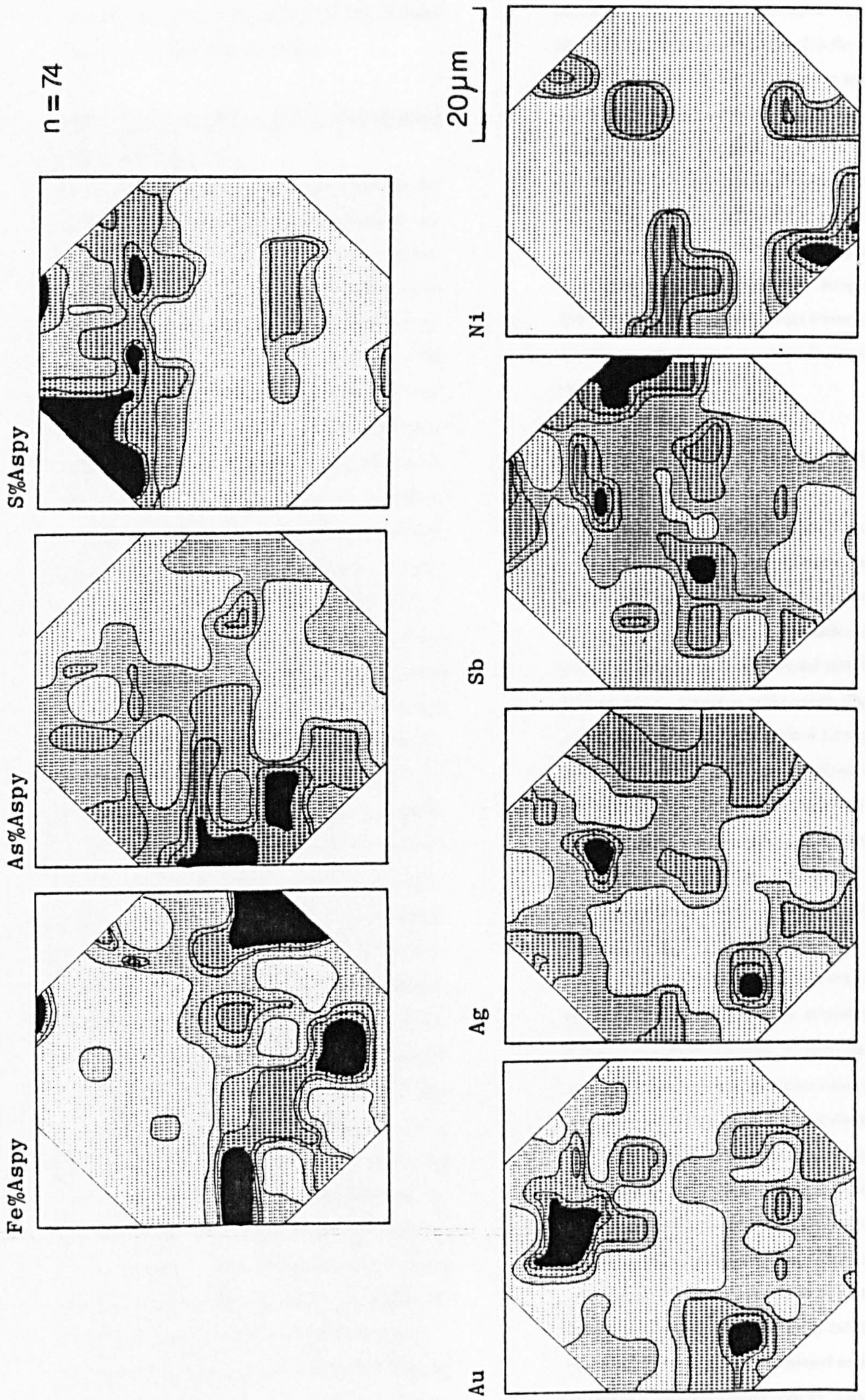

of arsenic deficiency such as the crystal core and northern margin with values 10^{-12} to 10^{-7}. The antimony substitution geothermometer defined by Gamyanin (1978) displayed in fig. 110 may be used to infer deposition temperatures of 255°C (±10°) with the Sb rich zones deposited at slightly elevated values to their depleted counterparts.

122- Cairngarroch Arsenopyrite (ASP11) Microchemical Mapping Studies

This diagram presents a series of grey-scale contour maps of the major ar d trace element content of vein hosted arsenopyrite from the Cairngarroch deposit. Microchemical ar lyses were undertaken on a rhomb shaped ars nopyrite crystal (200x200 microns in size) using a 5 micron grid (n=254). The results of this study are presented in table 4.11 together with summary statistics, grid size, coordinates and mapping boundaries are presented in tables 2.11, 1.15 and 1.50, respectively. The atomic %Fe in arsenopyrite (Fe%Aspy) plot illustrates a relatively systematic distribution with values generally concentrated in the margins of the crystal (max: 35.13 at. % Fe). The atomic %As in arsenopyrite (As% Aspy) plot exhibits evidence for preferential enrichment in the rim zones of the crystal (max: 32.43 at.% As) and depletion (min: 29.19 at.% As) in the crystal core. The atomic %S in arsenopyrite (S%Aspy) plot displays an inverse relationship with As anomalies, illustrated by a relatively enric- hed core zone (max: 37.99 at.% S) and western margin. Sb values (max: 1000 ppm) are notably enriched within the crystal core following the trends identified by S enrich- ment and As deficiently. Sb is positively correlated with both S and Fe; and inversely correlated with As. Au values (max: 8700ppm) indicate a sporadic enrichment in the core of the crystal, in areas of low arsenic and/or high iron+ sulphur concentrations. Au values also follow the trends identified by Sb and Ag anomalies. Ag values (max: 700ppm) follow the trends identified by both Sb and As, and are concentrated within the core zone. Ni values (max: 400ppm) define isolated anomaly zones concentrated within the crystal core and follow trends identified by both Sb and Ag.

The arsenopyrite geothermometer of Kretchmar and Scott (1976) enables both the temperature and sulphur activity during crystal formation to be ascertained (figs 109, 111 and 112). This study indicates that crystal is strongly zoned and that the variation in As content may be used to infer the presence of a relatively low temperature core zone and high temperature crystal rim. In detail, deposition took place over a temperature range confined to the 250-350°C field. Sulphur activity (aS_2) is lower in areas of arsenic deficiency such as the crystal core and western margin with values ranging from 10^{-12} to 10^{-9} whereas arsenic enriched margins exhibit values from 10^{-10} to 10^{-7}. The antimony substitution geothermometer defined by Gamyanin (1978) displayed in fig. 110 may be used to infer deposition temperatures of 255°C (±10°) with the Sb rich core zones deposited at slightly elevated values to their depleted marginal counterparts.

123- Cairngarroch Arsenopyrite (ASP12) Microchemical Mapping Studies.

This diagram presents a series of grey-scale contour maps of the major and trace element content of vein hosted arsenopyrite from the Cairngarroch deposit. Microchemical analyses were undertaken on a rhomb shaped arsenopyrite crystal (60x60 microns in size) using a 5 micron grid (n=64). The results of this study are presented in table 4.12 together with summary statistics, grid size, coordinates and mapping boundaries are presented in tables 2.12, 1.15 and 1.50, respectively. The atomic %Fe in arsenopyrite (Fe%Aspy) plot illustrates a relatively systematic distribution with values generally concentrated (max: 33.68 at. % Fe) in the core of the crystal (an inverse trend to that of the previous crystal from this deposit). The atomic %As in arsenopyrite (As% Aspy) plot exhibits evidence for preferential enrichment in the core and north eastern rim zone of the crystal (max: 32.92 at.% As) and depletion (min: 29.04 at.% As) in the remaining crystal margins. The atomic %S in arsenopyrite (S%Aspy) plot displays an inverse relationship with As anomalies, and exhibits enriched crystal margins (max: 40.38 at.% S). Sb values (max: 800ppm) are enriched both within the crystal core and in marginal areas exhibiting S enrichment. Sb is positively correlated with both S and Fe; and inversely correlated with As. Au values (max:

FIGURE 122

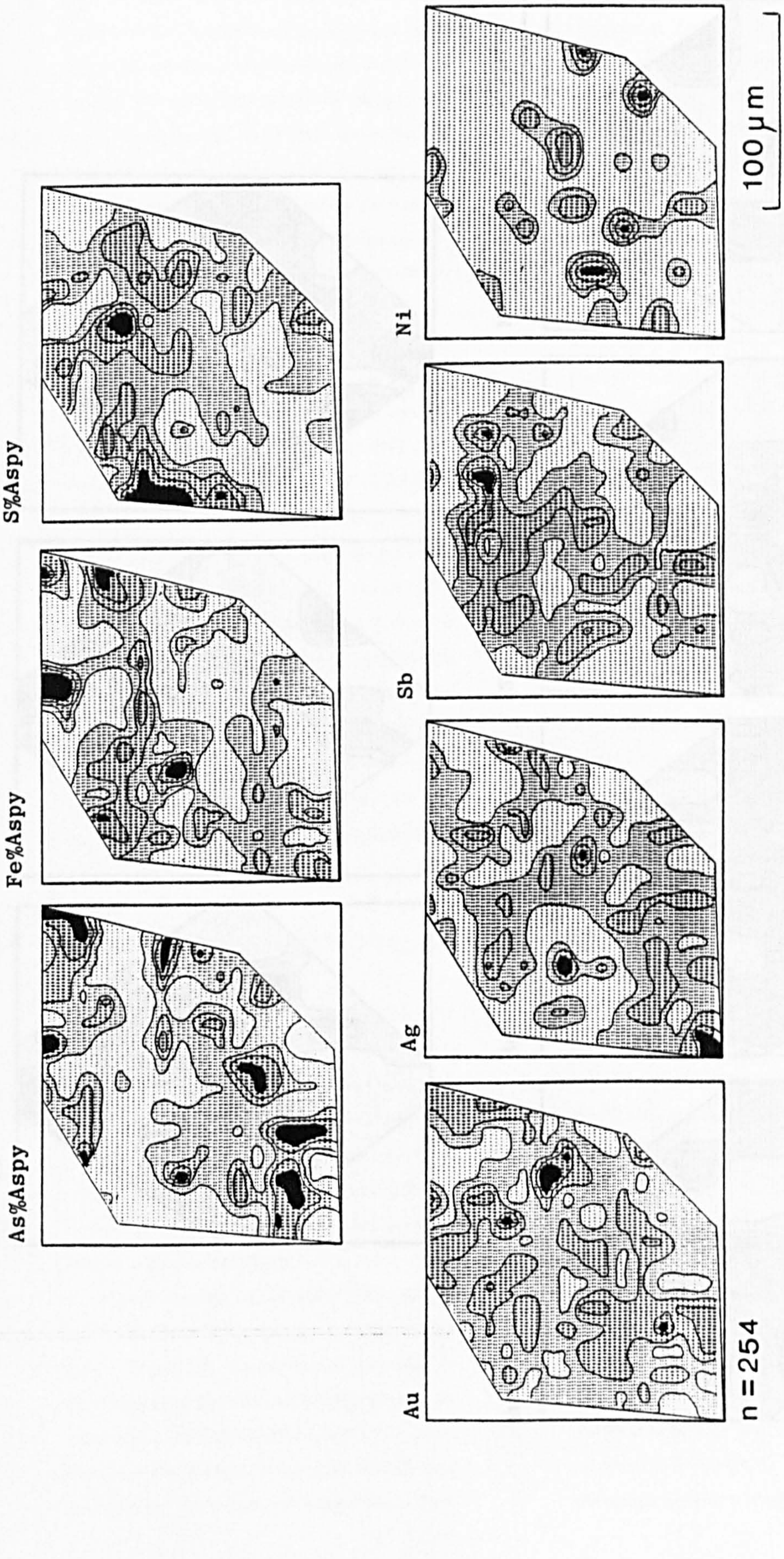

FIGURE 123

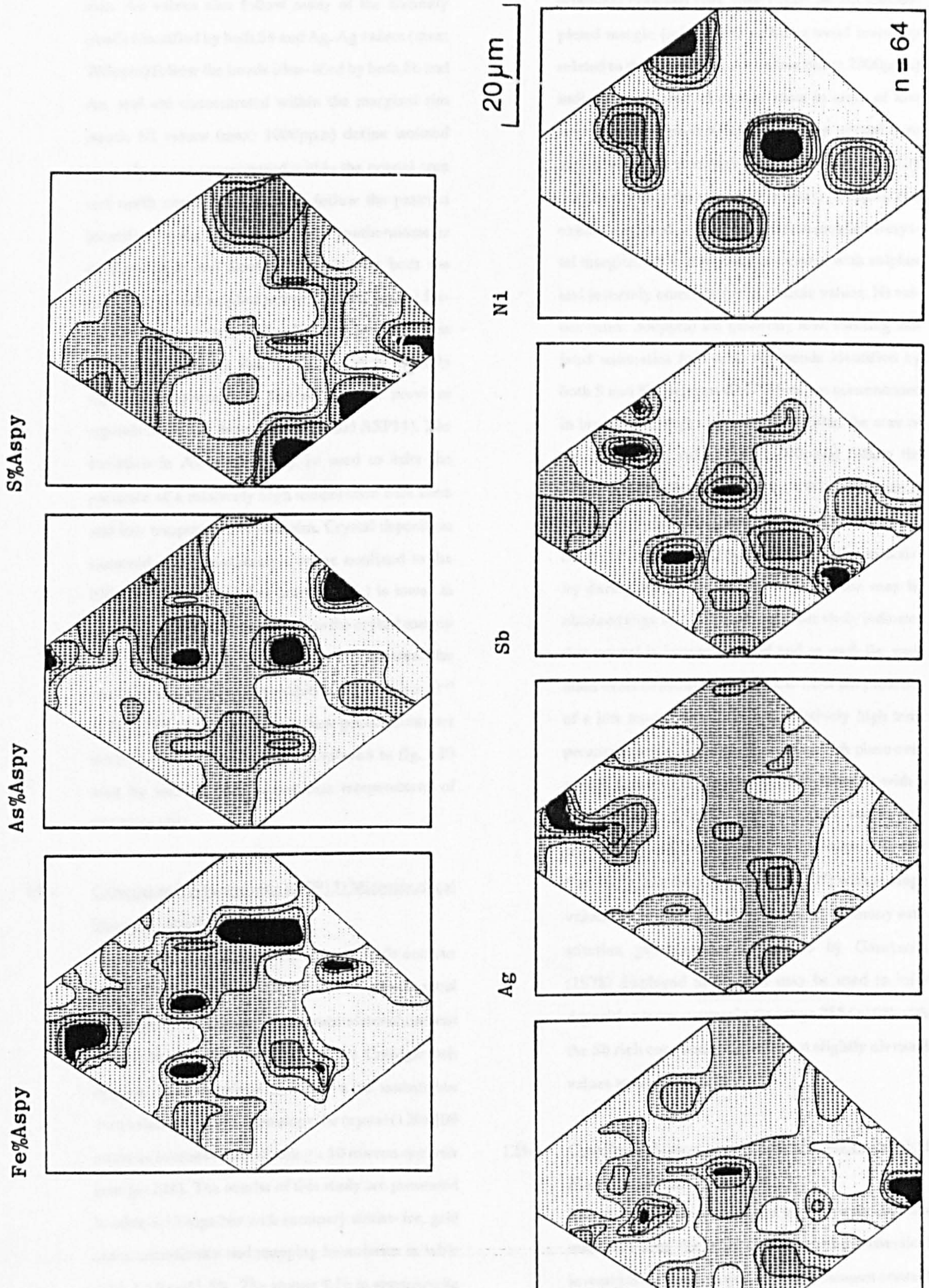

1500 ppm) are enriched in the rim zones of the crystal in areas of low arsenic and high sulphur concentration. Au values also follow many of the anomaly trends identified by both Sb and Ag. Ag values (max: 700ppm) follow the trends iden- ified by both Sb and Au, and are concentrated within the marginal rim zones. Ni values (max: 1000ppm) define isolated anomaly zones concentrated within the crystal core and north eastern margin, and follow the patterns identified by As. The arsenopyrite geothermometer of Kretchmar and Scott (1976) enables both the temperature and sulphur activity during crystal formation to be ascertained (figs 109, 111 and 112). This study indicates that this small crystal is strongly zoned, but inversely to that defined for previous crystals from this deposit (ASP10 and ASP11). The variation in As content may be used to infer the presence of a relatively high temperature core zone and low temperature crystal rim. Crystal deposition occurred over a temperature range confined to the 250-350°C field. Sulphur activity (aS_2) is lower in areas of arsenic deficiency such as the crystal margin with values ranging from 10^{-12} to 10^{-9} whereas the arsenic enriched core zone exhibits values from 10^{-10} to 10^{-7}. The antimony substitution geothermometer defined by Gamyanin (1978) displayed in fig. 110 may be used to infer deposition temperatures of 255°C (±10°).

124- Cairngarroch Arsenopyrite (ASP13) Microchemical Mapping Studies.

This diagram presents a series of grey-scale contour maps detailing the results of a micro-geochemical investigation of the major and trace element content of vein hosted arsenopyrite from the Cairngarroch deposit. Microchemical analyses were undertaken over a rhombic shaped arsenopyrite crystal (130x100 microns in cross-section) using a 10 micron analysis grid (n=144). The results of this study are presented in table 4.13 together with summary statist- ics, grid sizes, coordinates and mapping boundaries in table 2.13, 1.15 and 1.50. The atomic %Fe in arsenopyrite (Fe%Aspy) plot illustrates a relatively sporadic distribution (range: 32.20-33.80 At. %Fe). The atomic %As in arsenopyrite (As%Aspy) plot exhibits clear evidence for an As enriched margin (max: 31.40 at.%As) and depleted core (min: 29.26 at.%As). The atomic %S in arsenopyrite (S% Aspy) plot displays a relatively enriched core zone (max: 38.26) and depleted margin (min: 35.70 at.%S) a trend inversely related to that of arsenic. Au values (max: 2000ppm) indicate a preferential enrich- ment in areas of low arsenic/high sulphur values within the crystal core and southwestern margin. Sb values are notably enriched within the crystal core (max: 900ppm) and exhibit a marked concentric zonation parallel to crystal margins. Sb is positively correlated with sulphur and inversely correlated with arsenic values. Ni values (max: 300ppm) are generally low, forming isolated anomalies following the trends identified by both S and Sb. In general Ni values are concentrated in low arsenic/high sulphur zones within the core of the crystal. Ag values (max: 600ppm) follow the trends identified by S, Sb and Au. With reference to the arsenopyrite geothermometer of Kretchmar and Scott (1976) both the temperature and sulphur activity during the period of crystal formation may be obtained (figs 109, 111 and 112). This study indicates that crystal is intensely zoned and as such the variation in As content may be used to infer the presence of a low temperature core and relatively high temperature margin. In detail, deposition took place over a wide range of temperatures (240-340+°C) with a 95% of values confined to a 260-300°C range. Sulphur activity (aS_2) is also lower in the crystal core (10^{-12} to 10^{-10}) than the margin 10^{-10} to 10^{-8}) with average values in the 10^{-11} to 10^{-9} field. The antimony substitution geothermometer defined by Gamyanin (1978) displayed in fig. 110 may be used to infer deposition temperatures in the range 255 (±10°) with the Sb rich core zones deposited at slightly elevated values to their rim zones.

125- Clontibret Arsenopyrite (ASP14) Microchemical Mapping Studies.

This diagram presents a series of grey-scale contour maps detailing the results of a micro-geochemical investigation of the major and trace element content of vein hosted arsenopyrite from the Clontibret Sb-As-Au deposit, in Southern Ireland. Microchemical analyses were undertaken over a rhombic shaped arsenopyrite crystal (100x80 micron cross-section)

FIGURE 124

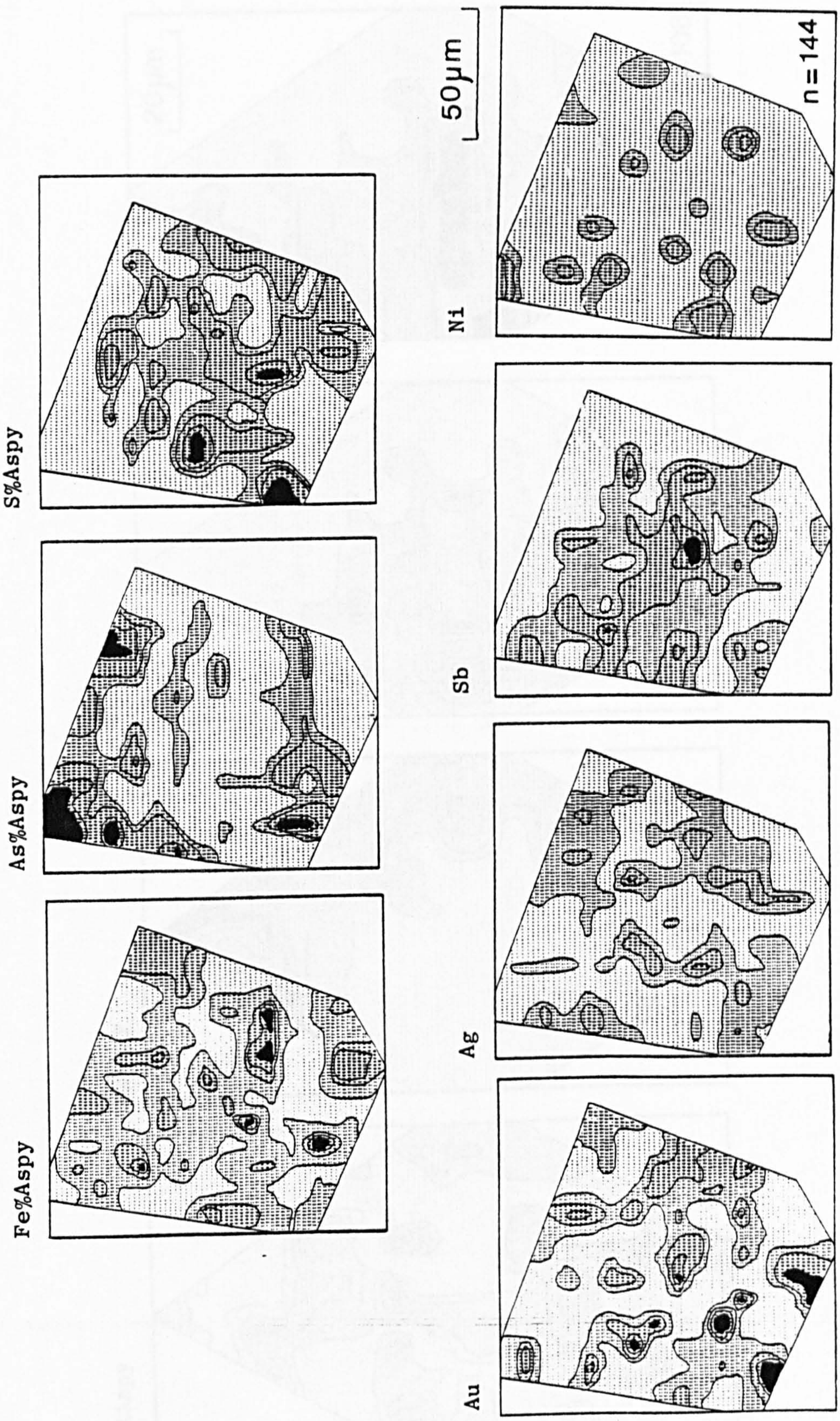

FIGURE 125

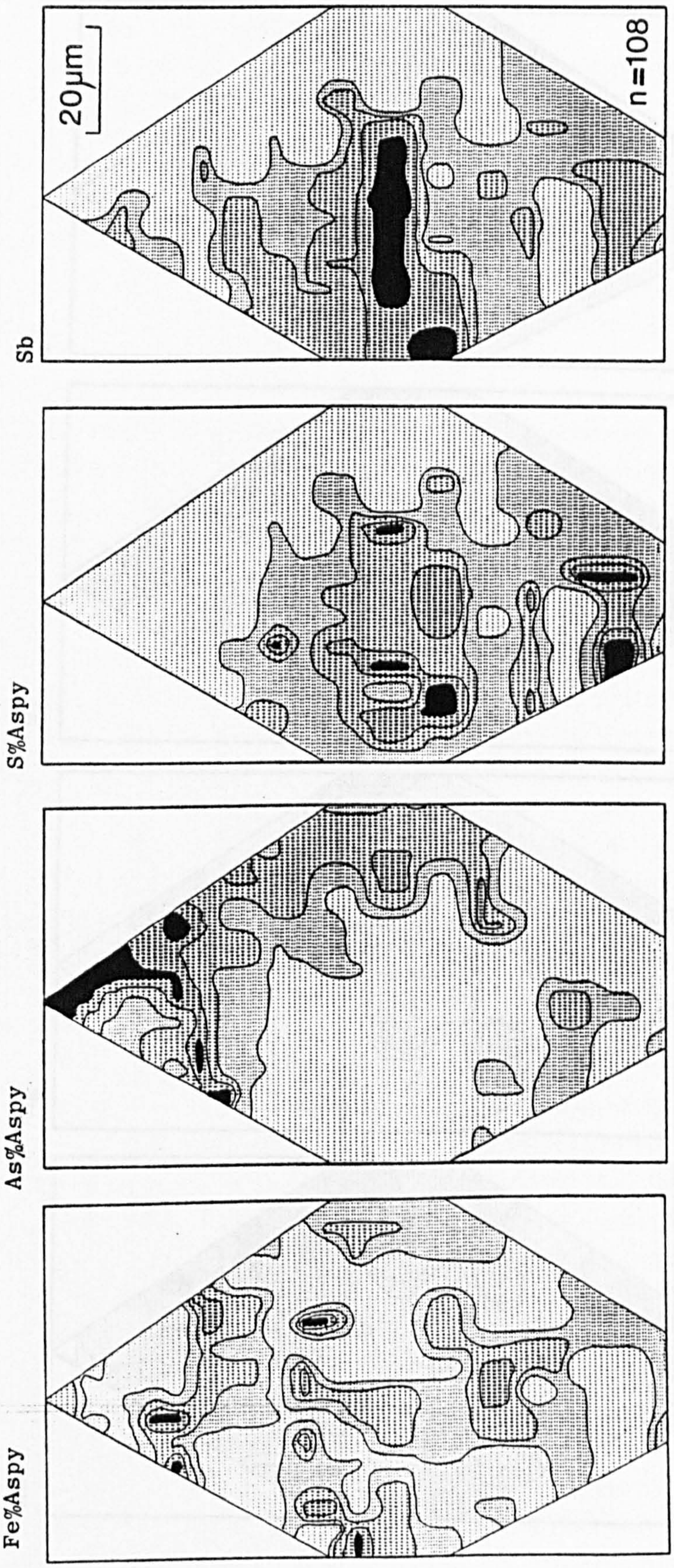

FIGURE 125 cont:

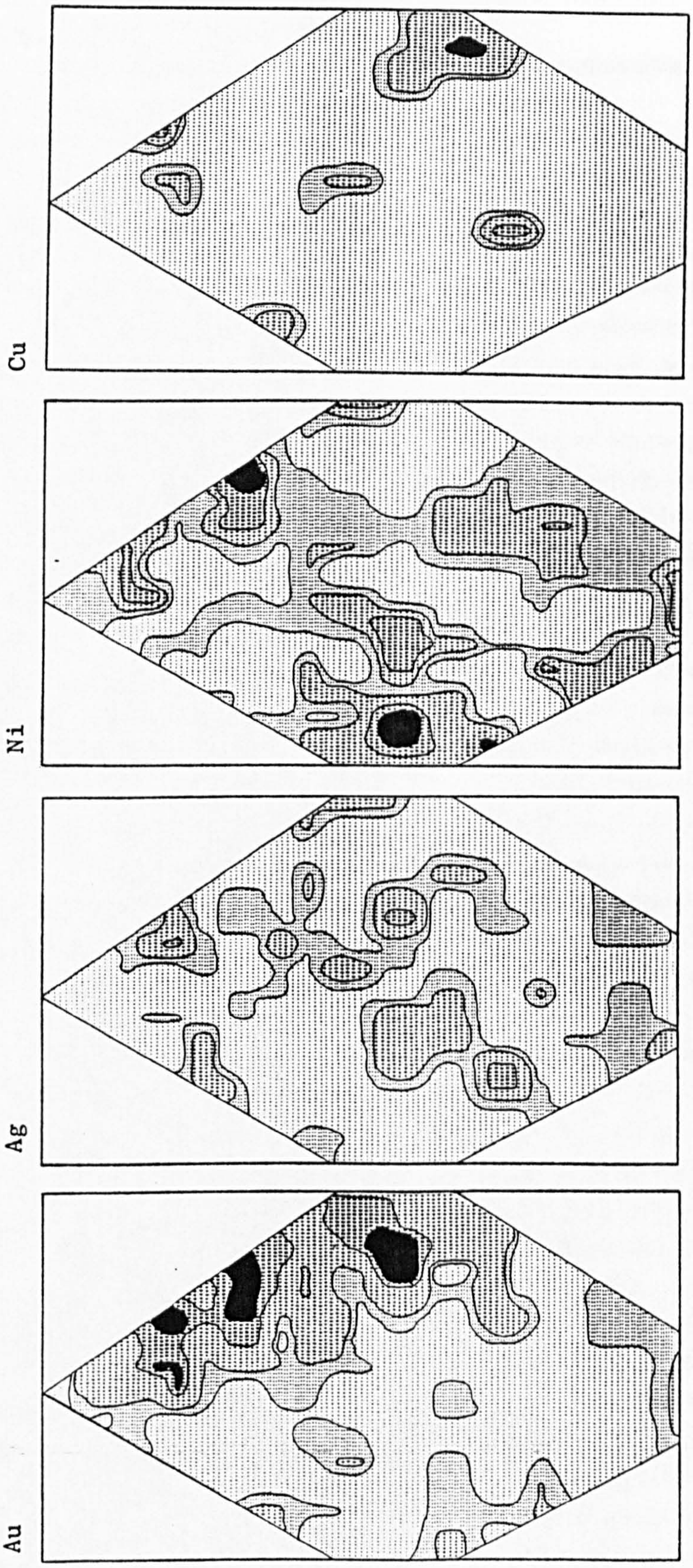

using a 5 micron analysis grid (n=108). The results of this study are presented in table 4.14 together with summary statistics, grid sizes, coordinates and mapping boundaries in tables 2.14, 1.15 and 1.50, respectively. The atomic %Fe in arsenopyrite (Fe%Aspy) plot illustrates a relatively sporadic distribution (max: 33.17 At.%Fe). The atomic %As in arsenopyrite (As%Aspy) plot exhibits clear evidence for an As enriched margin (max: 32.32 at.%As) and depleted core (min: 30.01 at.%As). The atomic %S in arsenopyrite (S% Aspy) plot displays a relatively enriched core zone (max: 36.92 at.%S) and depleted margins (min: 34.74 at.%S) a trend inversely related to that of arsenic. Sb values are notably enriched within the crystal core (max: 48000ppm) and exhibit a concentric zonation, parallel to crystal margins. Sb is positively correlated with S and inversely correlated with As values. Au values (max: 1700ppm) indicate preferential enrichment in areas of high arsenic/low sulphur values within the crystal margin. Ag values (max: 100ppm) are concentrated within the core of the crystal, however their low concentration, close to that of the analytical detection limit invalidated the observed relationship. Ni values (max: 500ppm) are generally low, and cluster in the margins of the crystal. These values closely follow the trends identified by Fe and to a lesser extent Sb. Cu, Zn and Co values all lie below the analytical detection limit and are not discussed further. With reference to the arsenopyrite geothermometer of Kretchmar and Scott (1976) both the temperature and sulphur activity during crystal formation may be ascertained (figs 109, 111 and 112). This study indicates that the crystal is intensely zoned and the variation in As content may be used to infer the presence of a low temperature core and relatively high temperature rim zone. Sb substitution is confined to areas of As deficiency whereas maximum Au values are located in areas of sulphur deficiency. Ore deposition took place over a wide range of temperatures (300-420°C) with 95% of values confined to a 320-380°C range. Sulphur activity (aS_2) is also lower in the core of the crystal (10^{-11} to 10^{-9}) than the margin 10^{-9} to 10^{-6}) with average values in the 10^{-10} to 10^{-8} field. The antimony substitution geothermometer defined by Gamyanin (1978) displayed in fig. 110 may be used to infer deposition temperatures in the range 255-351°C (±10°) with the Sb rich core zones deposited at highly elevated values to their rim zone counterparts.

126- Clontibret Arsenopyrite (ASP15) Microchemical Mapping Study.

This diagram presents a series of grey-scale contour maps detailing the results of a micro-geochemical investigation of the major and trace element content of wallrock hosted arsenopyrite from the Clontibret Sb-As-Au deposit, in Southern Ireland. Microchemical analyses were undertaken over a small, rhombic shaped arsenopyrite crystal (70x50 microns in cross-section) using a 5 micron analysis grid (n=102). The results of this study are presented in table 4.15 together with summary statistics, grid sizes, coordinates and mapping boundaries in tables 2.15, 1.15 and 1.50, respectively. The atomic %Fe in arsenopyrite (Fe% Aspy) plot illustrates a relatively sporadic distribution (max: 32.95 At.%Fe). The atomic %As in arsenopyrite (As% Aspy) plot exhibits clear evidence for an As enriched margin (max: 32.53 at.%As) and depleted core (min: 30.13 at.%As). The atomic %S in arsenopyrite (S% Aspy) plot displays a relatively enriched core zone (max: 37.36 at.% S) and depleted margins (min: 34.87 at.%S); a trend inversely related to that of arsenic. Sb values are notably enriched within the crystal core (max: 5400ppm) and exhibits a zonation pattern mirroring that of S, inversely related to As values. Au values (max: 3200ppm) are higher than their vein hosted counterparts and may be used to indicate preferential enrichment in areas of high arsenic - low sulphur values within the crystal margin. Ag values (max: 200ppm) follow the trend identified for Au and are concentrated within the margin of the crystal. The low Ag concentration however, close to the analytical detection limit of this technique casts doubt upon the validity of the observed relationship. Ni values (max: 600ppm) are generally low, clustering in the core of the crystal and forming an envelope to zones of Fe enrichment. In general Ni values are concentrated in low arsenic/high sulphur zones within the core of the crystal. Cu, Zn and Co values all lie below the analytical detection limit and are not discussed further. With reference to the arsenopyrite geothermometer

FIGURE 126

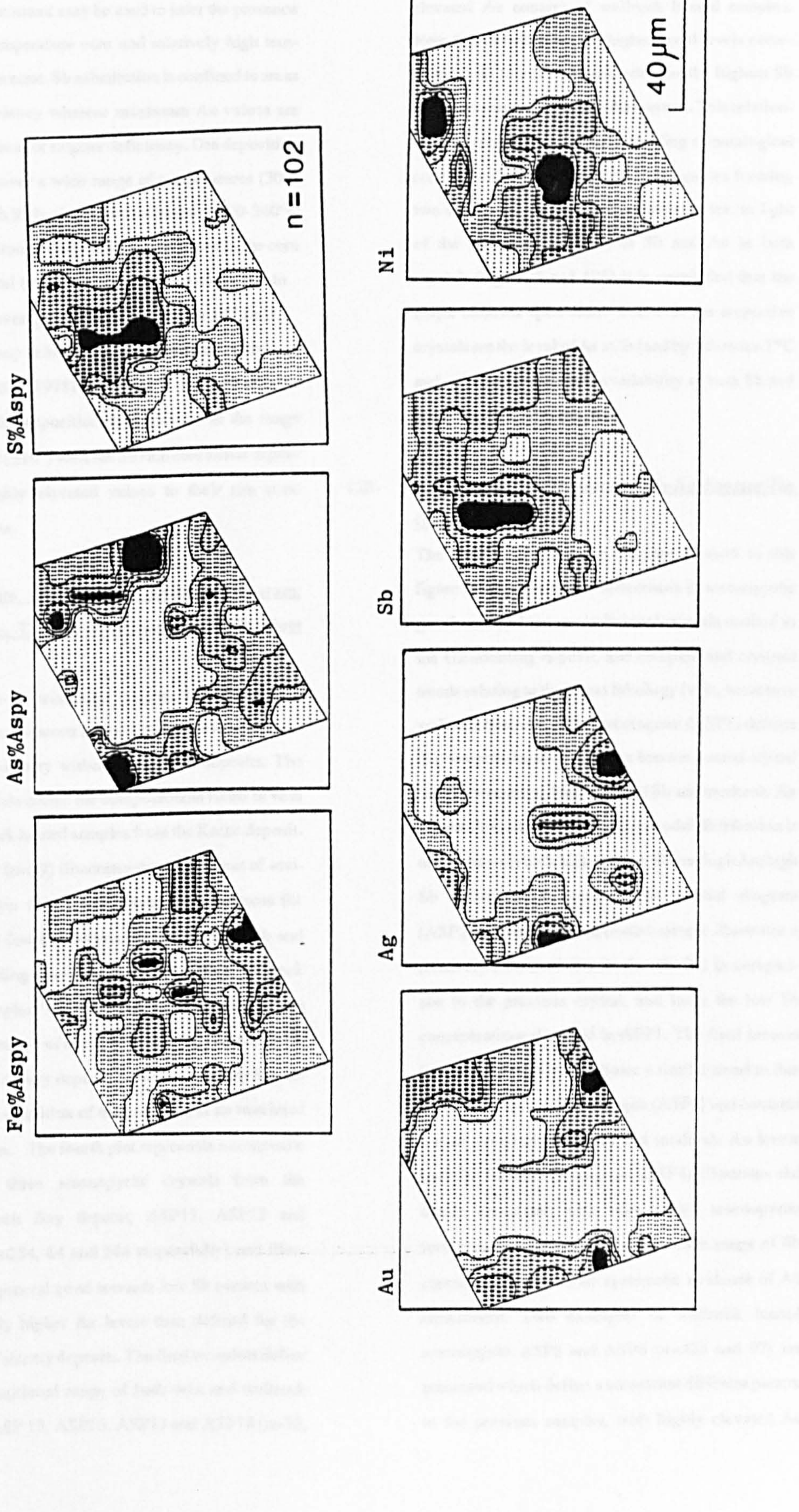

of Kretchmar and Scott (1976) both the temperature and sulphur activity during crystal formation may be ascertained (figs 109, 111 and 112). This study indicates that the crystal is intensely zoned and the variation in As content may be used to infer the presence of a low temperature core and relatively high temperature rim zone. Sb substitution is confined to areas of As deficiency whereas maximum Au values are located in areas of sulphur deficiency. Ore deposition took place over a wide range of temperatures (300-420°C) with 95% of values confined to a 320-360°C range. Sulphur activity (aS_2) is a'so lower in the core of the crystal (10^{-11} to 10^{-7}) than the margin 10^{-9} to 10^{-6}) with average values in th 10^{-10} to 10^{-8} field. The antimony substitution gec thermometer defined by Gamyanin (1978) displayed in fig. 110 may be used to infer deposition temperatures in the range 255-265°C (±10°) with the Sb rich core zones deposited at highly elevated values to their rim zone counterparts.

127- <u>Arsenopyrite geochemistry As-Sb-Au diagram: The Knipe, Talnotry, Cairngarroch and Clontibret deposits</u>.

The As-Sb-Au triangular diagram may be used to compare and contrast major differences in arsenopyrite geochemistry within the studied deposits. The first two plots define the compositional fields of vein and wallrock hosted samples from the Knipe deposit. Plot ASP7 (n=49) illustrates the enrichment of antimony within vein hosted arsenopyrite whereas the ASP8 plot (n= 61) defines the depletion of Sb and corresponding enrichment of Au within wallrock hosted samples. The third plot, ASP9 (n=74) defines the composition of massive vein hosted arsenopyrite from the Talnotry deposit; note the extremely low Sb and Au composition of the sample and its restricted distribution. The fourth plot represents a composite study of three arsenopyrite crystals from the Cairngarroch Bay deposit, ASP11, ASP12 and ASP13 (n=254, 64 and 144 respectfully) and illustrates the general trend towards low Sb content with consistently higher Au levels than defined for the Knipe or Talnotry deposits. The final two plots define the compositional range of both vein and wallrock samples ASP 15, ASP16, ASP17 and ASP18 (n=32, 102, 69 and 50 respectfully) from the Clontibret Sb-As-Au deposit, in Southern Ireland. This diagram illustrates the enriched levels of Sb and low Au values within vein hosted samples; and the reduced Sb and elevated Au content of wallrock hosted samples. Note that in both plots the highest gold levels correspond with low Sb content, whereas the highest Sb levels correspond with low Au content. This relationship is inferred to have an overriding mineralogical control, with both Sb and Au rich samples forming two end-members in a solid-solution series. In light of the spatial distribution of Sb and Au in both crystals (figs 125 and 126) it is concluded that the major controls upon subst- itution in the respective crystals are the level of As at.% (and by inference T°C and sulphur activity) and availability of both Sb and Au at the time of deposition.

128- <u>Arsenopyrite geochemistry As-Sb-Au diagram:The Glendinning Deposit</u>

The As-Sb-Au triangular diagram is used in this figure to illustrate major differences in arsenopyrite geochemistry between individual crystals studied in the Glendinning deposit, and compare and contrast trends relating to their host lithology (vein, breccia or wallrock hosted). The first diagram (ASP1) defines the compositional fields for a breccia hosted crystal (n=72) containing high levels of Sb and moderate Au values. A weak trend towards bimodal distribution is observed with both high Au/low Sb and high Au/high Sb end-members present. The second diagram (ASP2) a further breccia hosted sample illustrates a relatively restricted distribution (n=26) in comparison to the previous crystal, and lacks the low Sb concentrations depicted in ASP1. The final breccia hosted crystal (ASP3) follows a similar trend to that established by the first example (ASP1) and contains a wide range of Sb values and moderate Au levels (n=35). The fourth diagram (ASP4) illustrates the trends associated with vein hosted arsenopyrite (n=56) in this deposit, namely: a wide range of Sb content with little or no systematic evidence of Au enrichment. Two examples of wallrock hosted arsenopyrite ASP5 and ASP6 (n=323 and 97) are presented which define a somewhat different pattern to the previous samples, with highly elevated Au

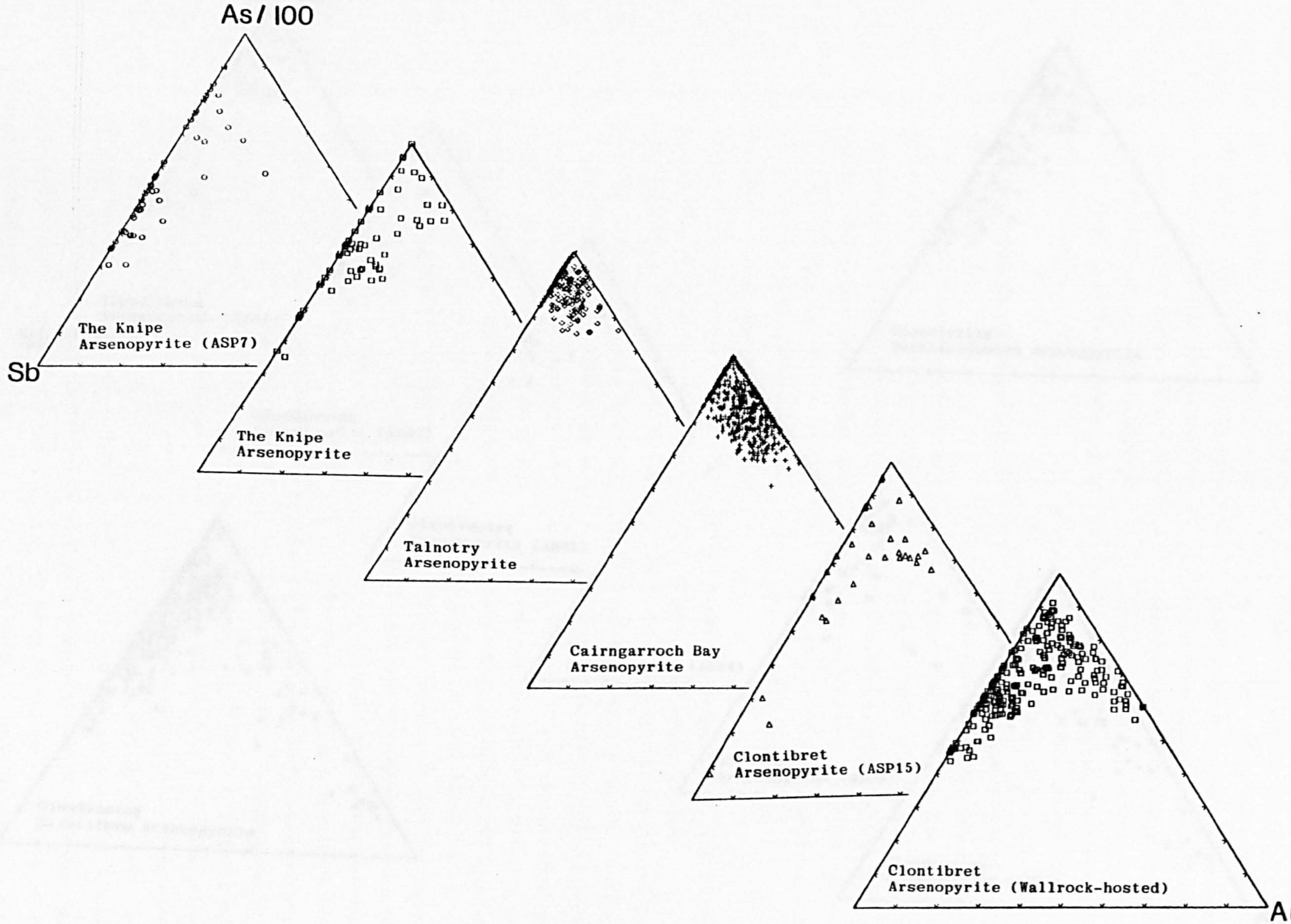
As/100
Sb
Au
The Knipe
Arsenopyrite (ASP7)
The Knipe
Arsenopyrite
Talnotry
Arsenopyrite
Cairngarroch Bay
Arsenopyrite
Clontibret
Arsenopyrite (ASP15)
Clontibret
Arsenopyrite (Wallrock-hosted)

FIGURE 127

FIGURE 128

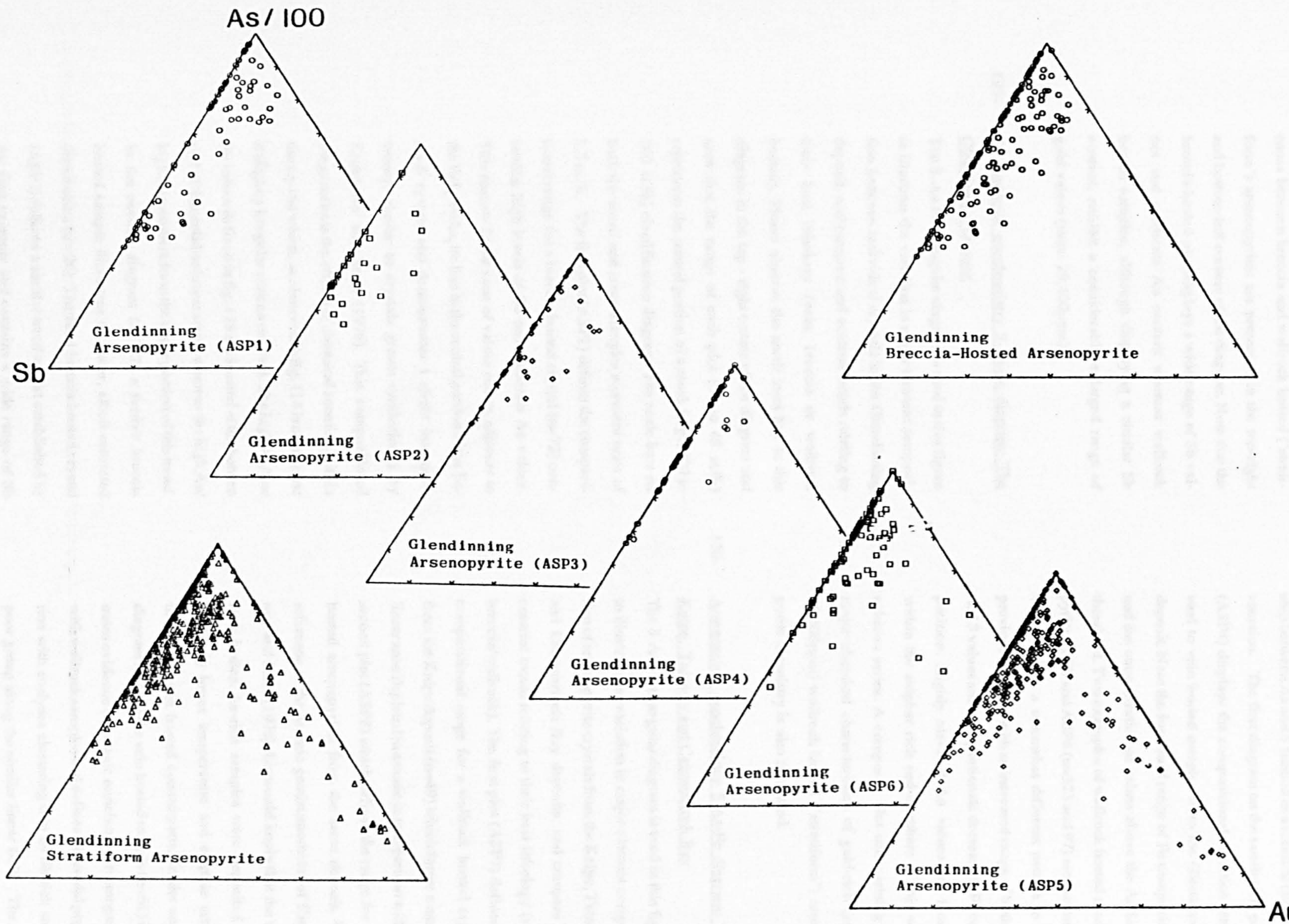
As/100
Sb
Au
Glendinning
Arsenopyrite (ASP1)
Glendinning
Arsenopyrite (ASP2)
Glendinning
Arsenopyrite (ASP3)
Glendinning
Arsenopyrite (ASP4)
Glendinning
Arsenopyrite (ASP6)
Glendinning
Arsenopyrite (ASP5)
Glendinning
Breccia-Hosted Arsenopyrite
Glendinning
Stratiform Arsenopyrite

values located in the low Sb field of each diagram. Two composite plots summarising the major differences between breccia and wallrock hosted ('stratiform') arsenopyrites are presented in the top-right and bottom-left corners of the diagram. Note that the breccia-hosted plot displays a wide range of Sb values and moderate Au content whereas wallrock hosted samples, although displaying a similar Sb content, exhibit a considerably enlarged range of gold values (max: 29,400ppm).

129- <u>Arsenopyrite geochemistry S-As-Fe diagram: The Glendinning Deposit</u>

The S-As-Fe triangular diagram is used in this figure to illustrate the variation in major element composition between individual crystals in the Glendinning deposit, and compare and contrast trends relating to their host lithology (vein, breccia or wallrock hosted). Please observe the small inset key to this diagram in the top - right corner of the diagram and note that the range of each plot (30 to 45 at.%) represents the central portion of a much larger (00 to 100 at.%) classification diagram. The scale bars on both the small and large triangles represent units of 1.5 at.%. The first plot (ASP1) defines the compositional range for a breccia hosted crystal (n=72) containing high levels of Sb and moderate Au values. This narrow linear zone of values occurs adjacent to the FeS_2-$FeAs_2$ tie line in the central portion of the Fe-As-S system and demonstrates a slight iron deficiency, similar to crystals grown synthetically by Kretchmar and Scott (1976). This compositional range reflects the effects of chemical zonation within the crystal which, as observed in fig. 114 is concentric if slightly irregular with no reversal. The high Au/low Sb values defined in fig. 128 are located at the bottom end of this solid-solution series whereas the high Au/high Sb members form the upper portion of this trend. In the second diagram (ASP2) a further breccia hosted sample illustrates a similar, albeit restricted distribution (n=26). The final breccia hosted crystal (ASP3) follows a similar trend to that established by the first example and contains a wide range of Sb values and moderate Au levels (n=35). The fourth diagram presents a composite plot of all (n= 133) breccia hosted samples and serves to illust- rate the trends associated with this group, namely: a narrow range of Fe content and linear solid-solution relationship between As and S formed as a result of chemical zonation. The first diagram on the continuing page (ASP4) displays the compositional variation attributed to vein hosted samples from the Glendinning deposit. Note the increased range of Fe composition and the concentration of values above the As%=36 threshold. Two examples of wallrock hosted arsenopyrite ASP5 and ASP6 (n=323 and 97) are presented which define a somewhat different pattern to the previous samples, with an increased range of both As and S values and a proportionate decrease in Fe composition. Highly elevated Au values are located within the sulphur rich end-members of this solid solution series. A composite plot summarising the major chemical characteristics of gold-rich (max: 29,400ppm) wallrock hosted ('stratiform') arsenopyrite chemistry is also presented.

130- <u>Arsenopyrite geochemistry S-As-Fe diagram: The Knipe, Talnotry and Cairngarroch Bay</u>

The S-As-Fe triangular diagram is used in this figure to illustrate the variation in major element composition of arsenopyrite crystals from the Knipe, Talnotry and Cairngarroch Bay deposits, and compare and contrast trends relating to their host lithology (vein/breccia/wallrock). The first plot (ASP7) defines the compositional range for a wallrock hosted crystal from the Knipe deposit (n=49) which forms a narrow linear zone depleted in arsenic in comparison with the second plot (ASP8) which defines the range for vein hosted arsenopyrites from the same deposit. With reference to the arsenic geothermometer of Kretchmar and Scott (1976) this would imply that the wallrock hosted Au-rich samples were deposited at a relatively lower temperature and sulphur activity than their vein hosted counterparts. In the second diagram (ASP8) the vein hosted sample (n=61) illustrates evidence of arsenic enrichment in comparison with wallrock samples and defines a bimodal population with analyses clustering into an Sb rich and Sb poor group along the similar linear field. The third diagram illustrates the restricted composition of massive arsenopyrite (ASP9) from the Talnotry deposit (n=74) located in a similar field to the anti-

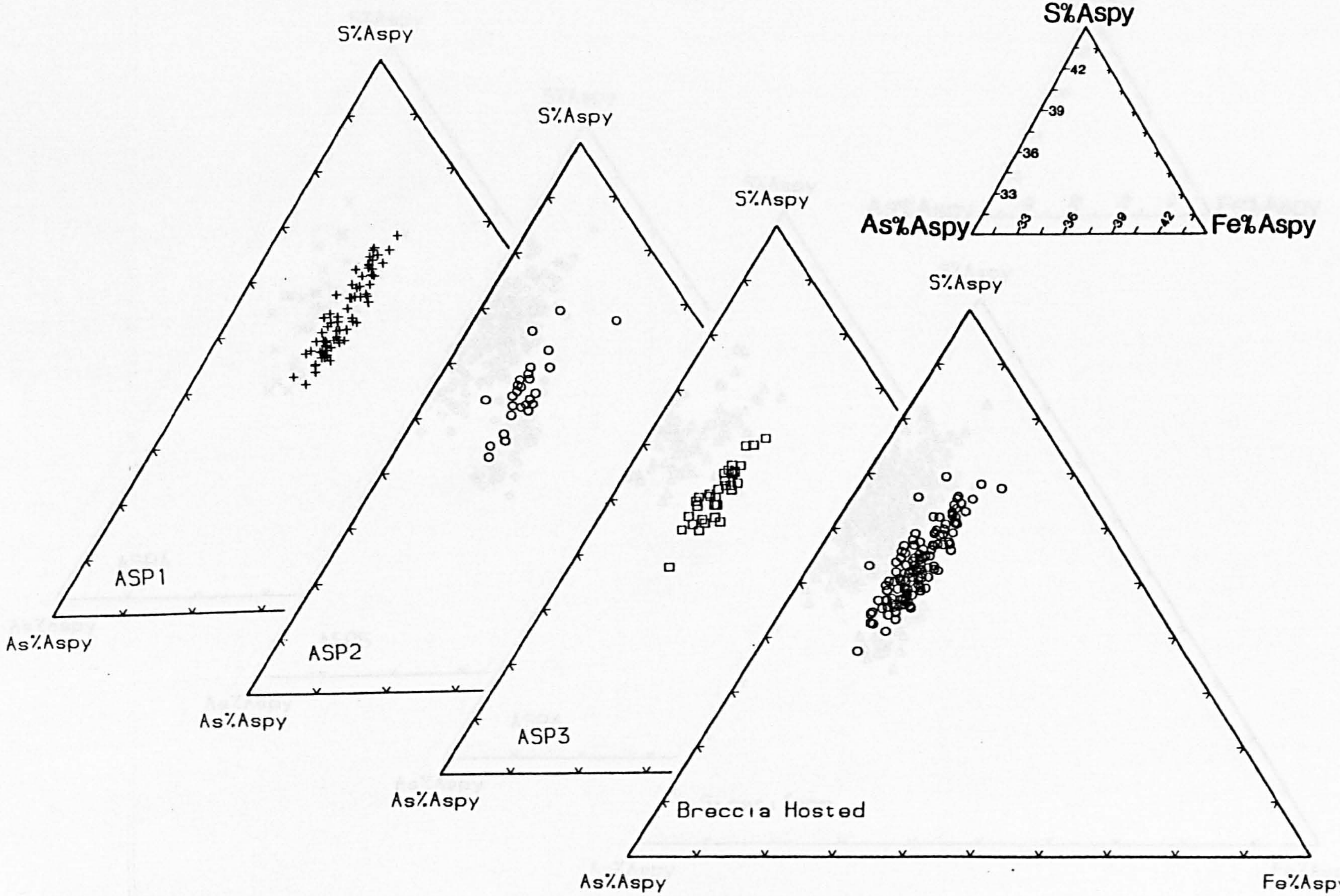
S%Aspy
As%Aspy
Fe%Aspy
42
39
36
33
ASP1
ASP2
ASP3
Breccia Hosted

FIGURE 129

FIGURE 129 cont:

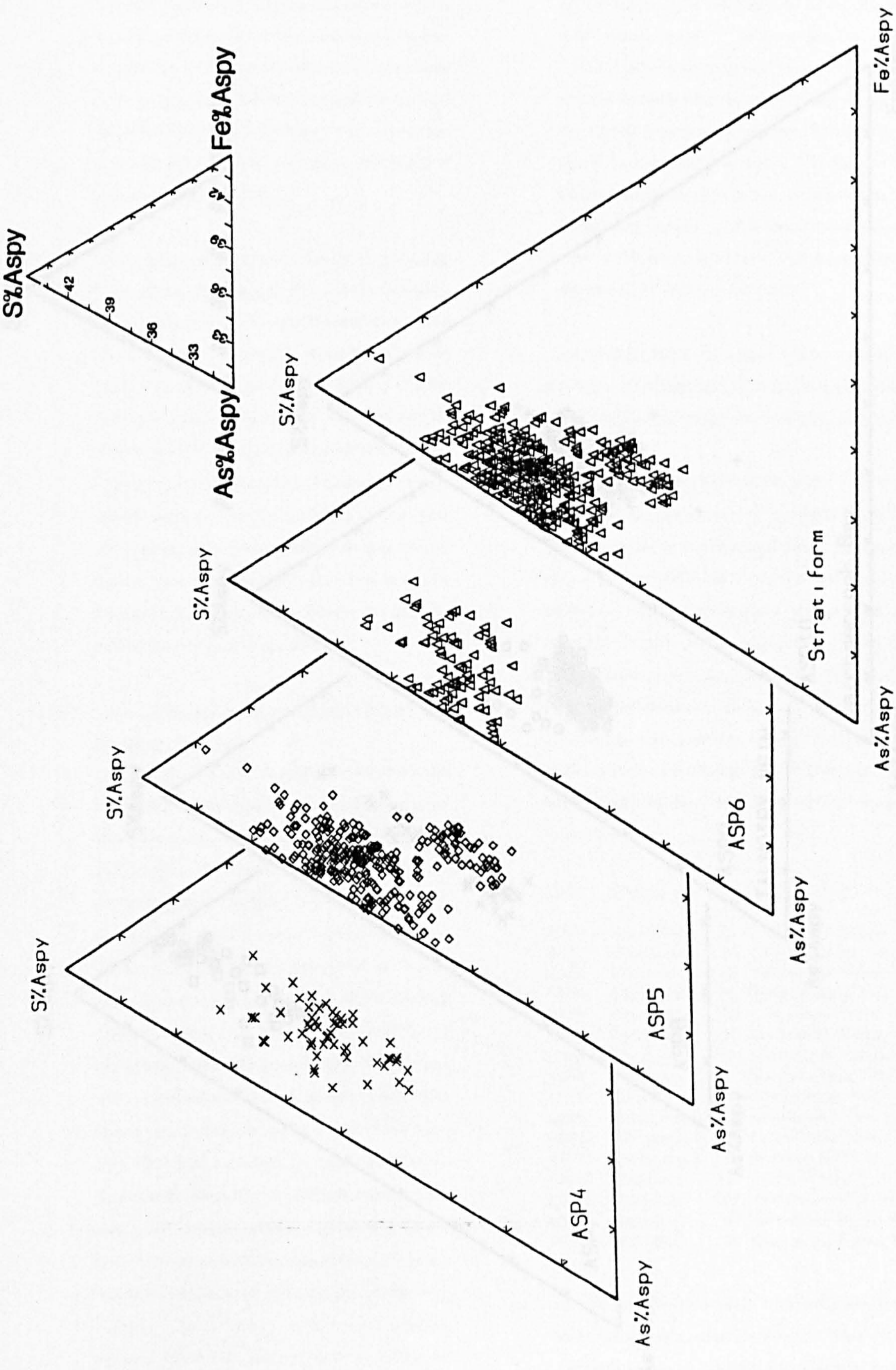

FIGURE 130

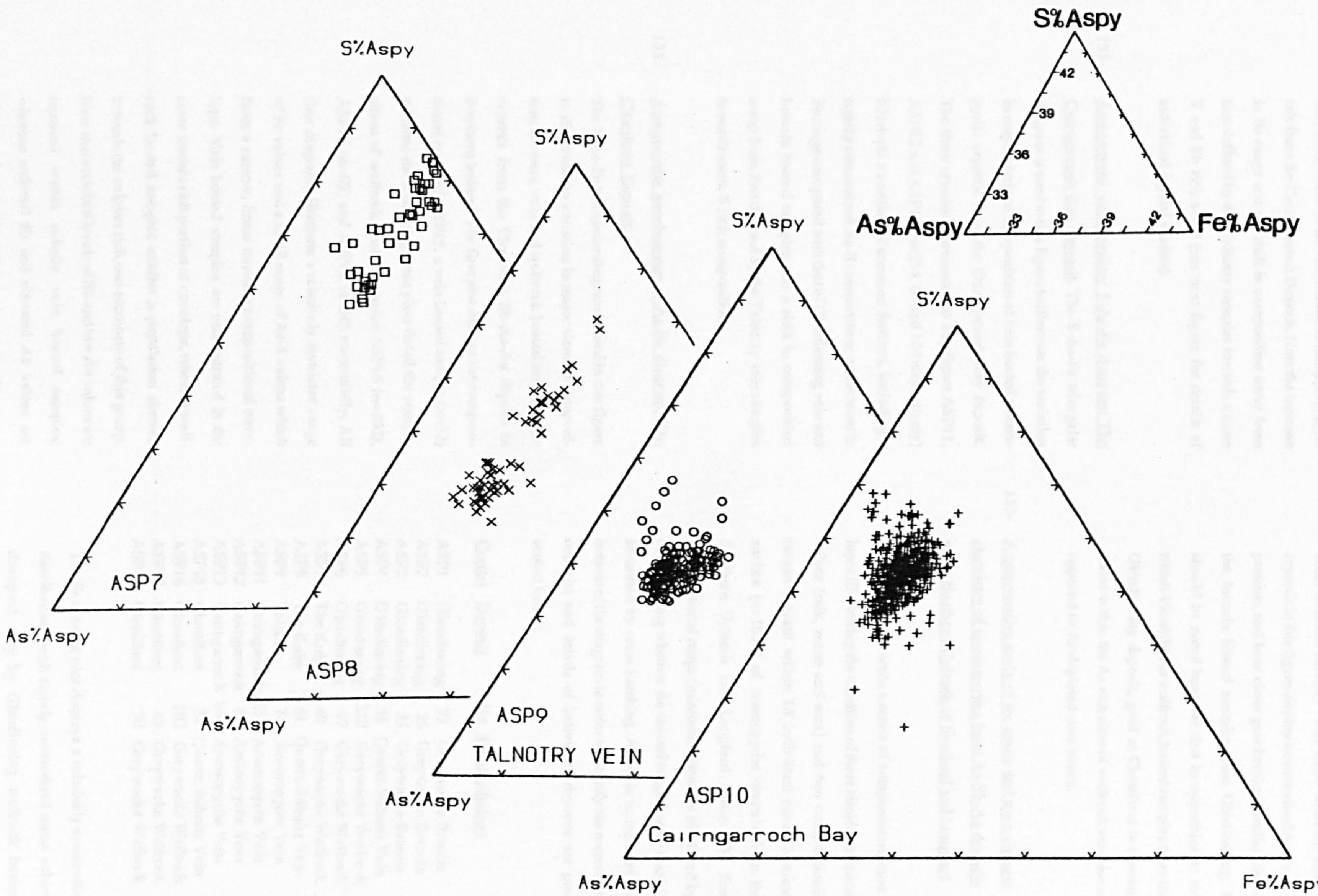
S%Aspy
As%Aspy
Fe%Aspy
42
39
36
33
ASP7
ASP8
ASP9
TALNOTRY VEIN
ASP10
Cairngarroch Bay

mony poor variety of vein and breccia hosted arsenopyrites from the Knipe and Glendinning deposits. The final diagram in this figure illustrates a composite plot (n=462) of all vein hosted arsenopyrite crystals from the Cairngarroch Deposit. Note the increase in Fe range and the shift in composition away from that defined by the Talnotry samples towards a more S and Sb rich trend (see next figure for details of individual crystal studies).

131- Arsenopyrite geochemistry S-As-Fe diagram: The Cairngarroch Bay Deposit. The S-As-Fe triangular diagram is used in this figure to illustrate the variation in major element composition of vein hosted arsenopyrite crystals from the Cairngarroch Bay deposit. The three crystals represented in this figure ASP11, ASP12 and ASP13 (n=254, 64 and 144 respectively) illustrate a number of common features, including a tightly constrained As-S composition; an increase in Fe range compared with that of Glendinning vein and breccia hosted samples and a shift in composition away from that defined by the Talnotry vein samples towards more S rich compositions.

132- Arsenopyrite geochemistry S-As-Fe diagram: The Clontibret Deposit.
The S-As-Fe triangular diagram is used in this figure to illustrate the variation in major element composition between vein and wallrock hosted arsenopyrite crystals from the Clontibret Sb-As-Au deposit in Southern Ireland. The first plot defines the compositional range of ASP15, a vein hosted sample (n=32) whereas the remaining three plots detail the composition of wallrock hosted samples ASP16 (n=102), ASP17 (n=69) and ASP18 (n=50) respectfully. All four diagrams illustrate a relatively restricted range of Fe values and a small range of As-S values which form a narrow, linear trending compositional envelope. Vein hosted samples are concentrated in the more arsenic rich portion of envelope, whereas wallrock hosted samples exhibit a population skewed towards the sulphur rich end-members of this group. Note that enriched levels of Sb and low Au values are reported within stibnite vein hosted samples; whereas reduced Sb and elevated Au values are recorded in the wallrock hosted samples. This relationship is inferred to have an overriding mineralogical control, with both Sb and Au rich samples clustering around the two end-members of the Fe-As-S solid-solution series. The three wallrock hosted crystals in this figure display a constrained As-S composition and bear close geochemical similarities to the breccia hosted samples from Glendinning. It should be noted however that in opposition to the trends identified in wallrock hosted samples from the Glendinning deposit, gold at Clontibret is concentrated within the As rich rims of wallrock samples as opposed to As depleted core zones.

133- A comparative study of the major and trace element chemistry of arsenopyrites from As-Sb-Au deposits in the Southern Uplands of Scotland and Longford Down
This diagram presents a series of compositional envelopes illustrating the variation of three simple statistical values (min, mean and max) and two compositional ranges present within 18 individual microchemical studies (n=1627) of arsenopyrite crystals from the Southern Uplands and Longford Down. The first compositional range (minimum-mean) is identified by solid shading whereas the second range (mean-max) is identified by cross hatching. A key is included at the bottom of the diagram in order to identify the respective deposits and details of individual deposits are presented below:

Crystal	Deposit	No	Host/Lithology
ASP1	Glendinning	72	Greywacke Breccia
ASP2	Glendinning	26	Greywacke Breccia
ASP3	Glendinning	35	Greywacke Breccia
ASP4	Glendinning	56	Quartz-Stibnite Vein
ASP5	Glendinning	323	Greywacke Wallrock
ASP6	Glendinning	97	Greywacke Wallrock
ASP7	The Knipe	49	Greywacke Wallrock
ASP8	The Knipe	61	Quartz-Stibnite Vein
ASP9	Talnotry	74	Arsenopyrite Vein
ASP11	Cairngarroch	254	Arsenopyrite Vein
ASP12	Cairngarroch	64	Arsenopyrite Vein
ASP13	Cairngarroch	144	Arsenopyrite Vein
ASP15	Clontibret	32	Quartz-Stibnite Vein
ASP16	Clontibret	102	Greywacke Wallrock
ASP17	Clontibret	69	Greywacke Wallrock
ASP18	Clontibret	50	Greywacke Wallrock

The Fe content plot displays a relatively systematic distribution with tightly constrained mean values disrupted only by Glendinning wallrock hosted samples ASP5 and ASP6 which exhibit strong deple-

FIGURE 131

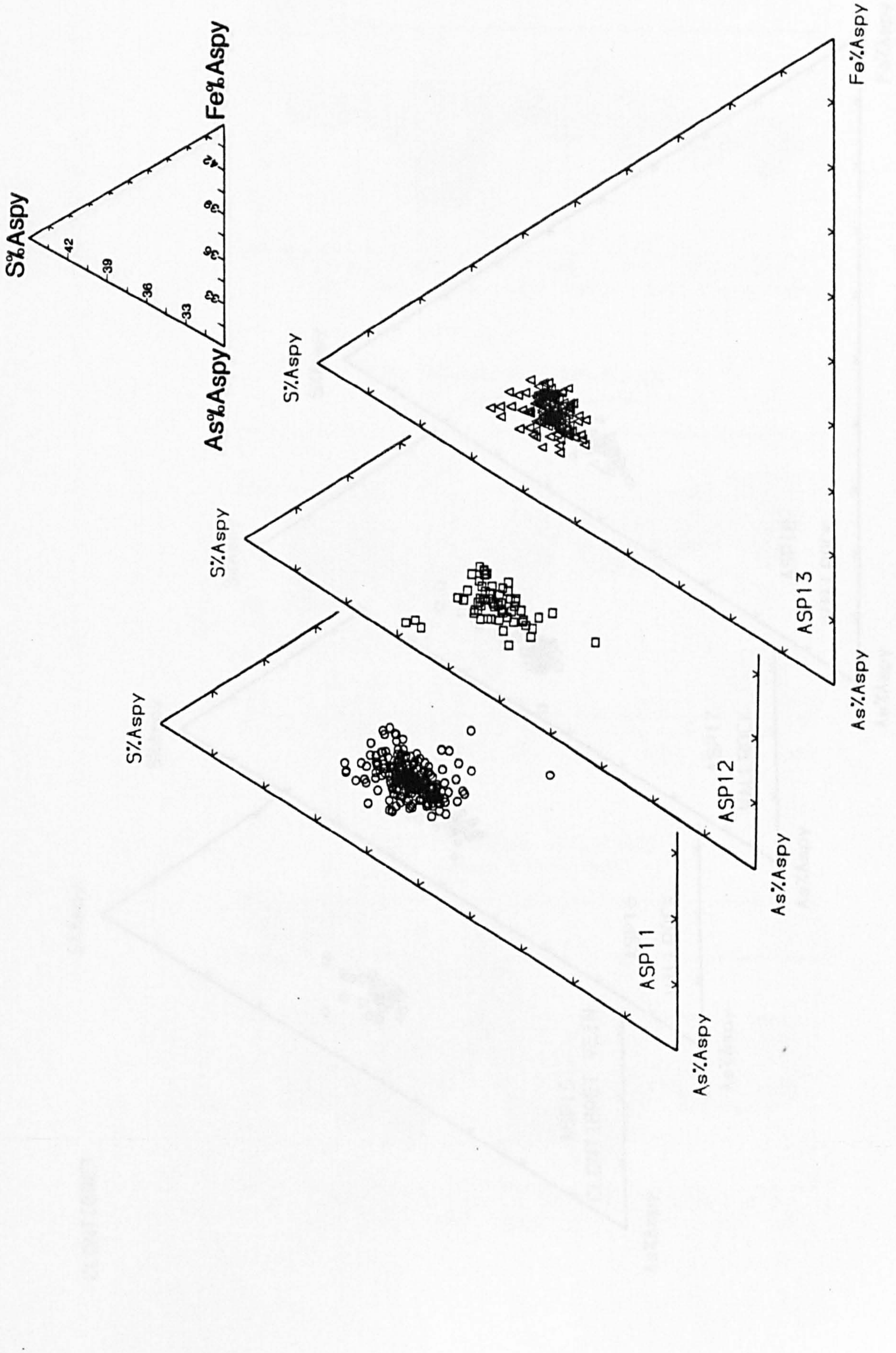

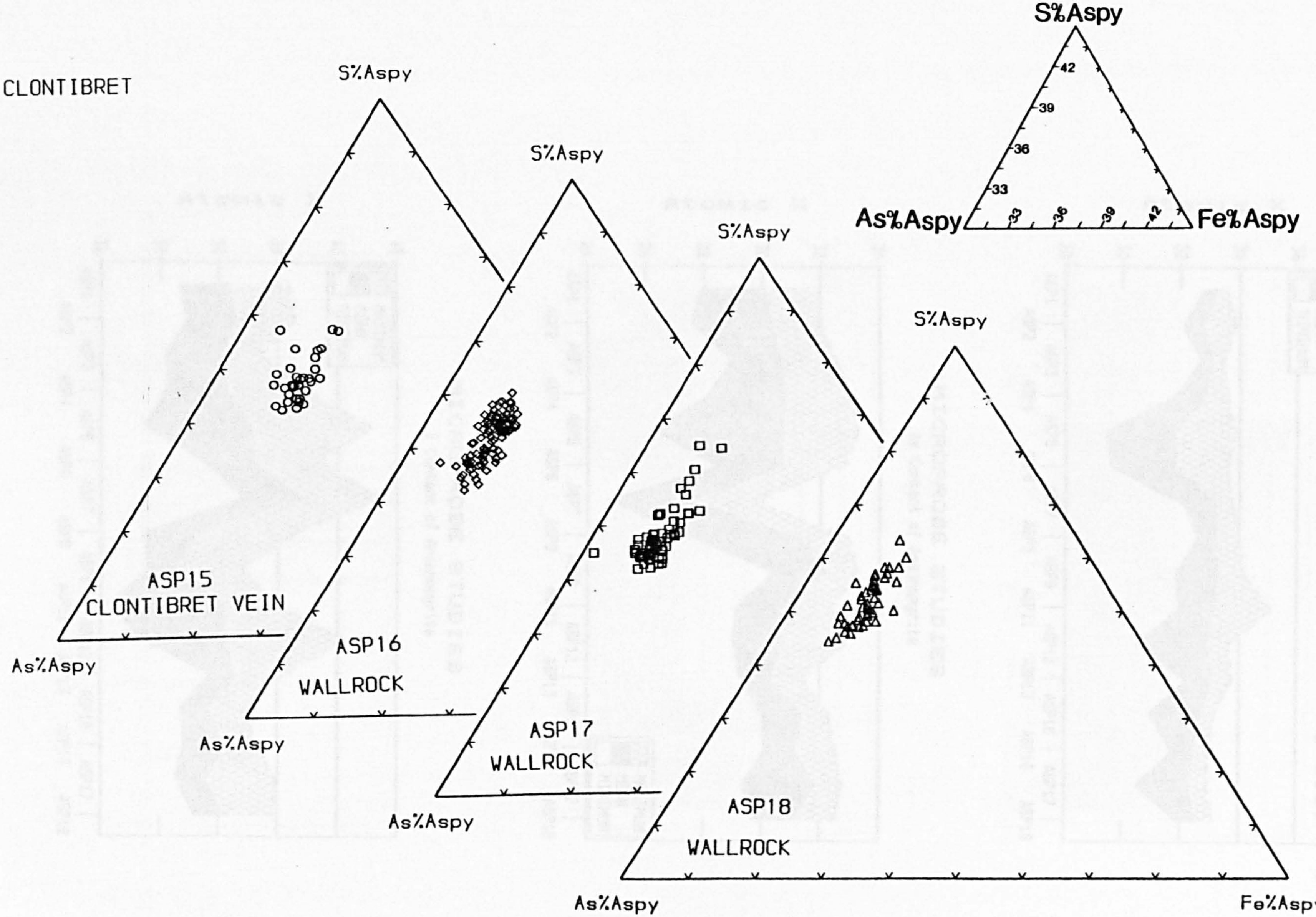
CLONTIBRET
S%Aspy
As%Aspy
ASP15
CLONTIBRET VEIN
ASP16
WALLROCK
ASP17
WALLROCK
ASP18
WALLROCK
Fe%Aspy
42
39
36
33

FIGURE 132

FIGURE 133

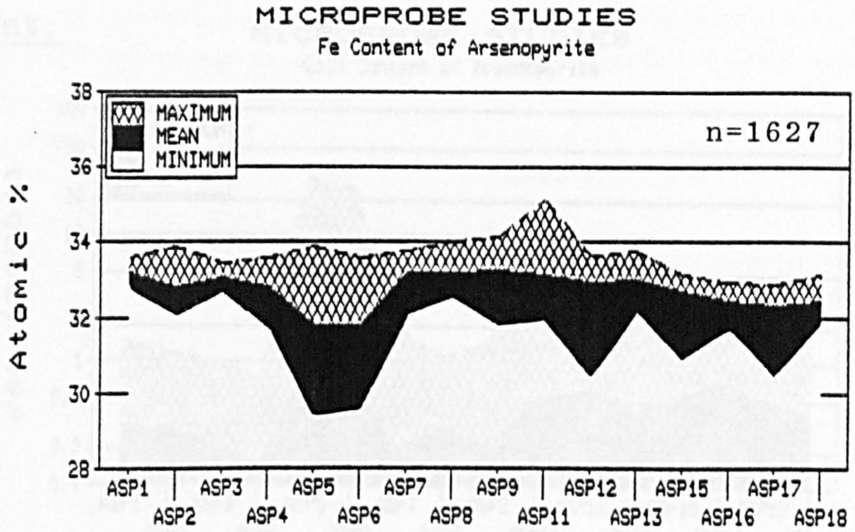
MICROPROBE STUDIES
Fe Content of Arsenopyrite
MAXIMUM
MEAN
MINIMUM
n=1627
Atomic %
38
36
34
32
30
28
ASP1
ASP2
ASP3
ASP4
ASP5
ASP6
ASP7
ASP8
ASP9
ASP11
ASP12
ASP13
ASP15
ASP16
ASP17
ASP18

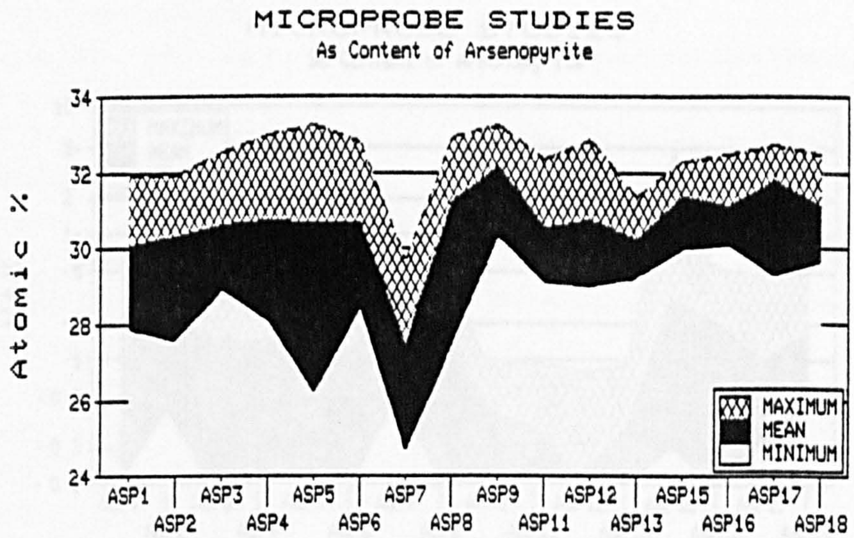
MICROPROBE STUDIES
As Content of Arsenopyrite
Atomic %
34
32
30
28
26
24
MAXIMUM
MEAN
MINIMUM
ASP1
ASP2
ASP3
ASP4
ASP5
ASP6
ASP7
ASP8
ASP9
ASP11
ASP12
ASP13
ASP15
ASP16
ASP17
ASP18

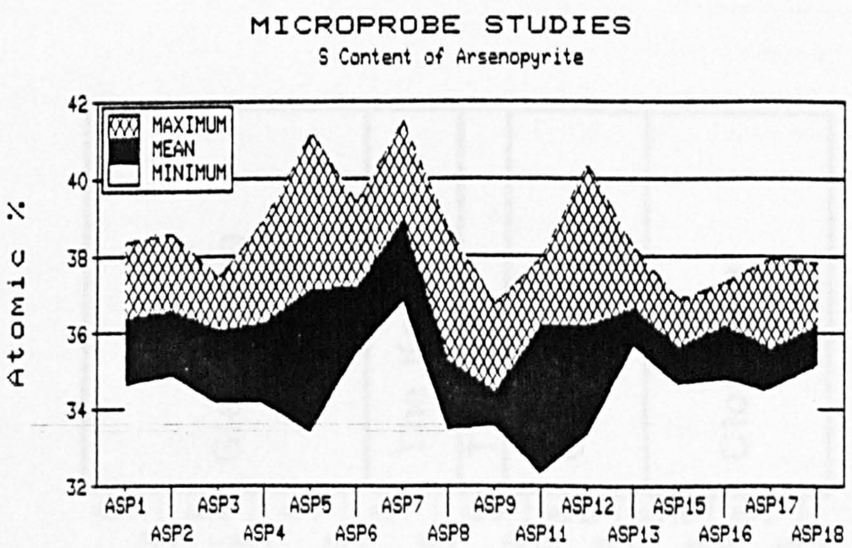
MICROPROBE STUDIES
S Content of Arsenopyrite
MAXIMUM
MEAN
MINIMUM
Atomic %
42
40
38
36
34
32
ASP1
ASP2
ASP3
ASP4
ASP5
ASP6
ASP7
ASP8
ASP9
ASP11
ASP12
ASP13
ASP15
ASP16
ASP17
ASP18

FIGURE 133 cont:

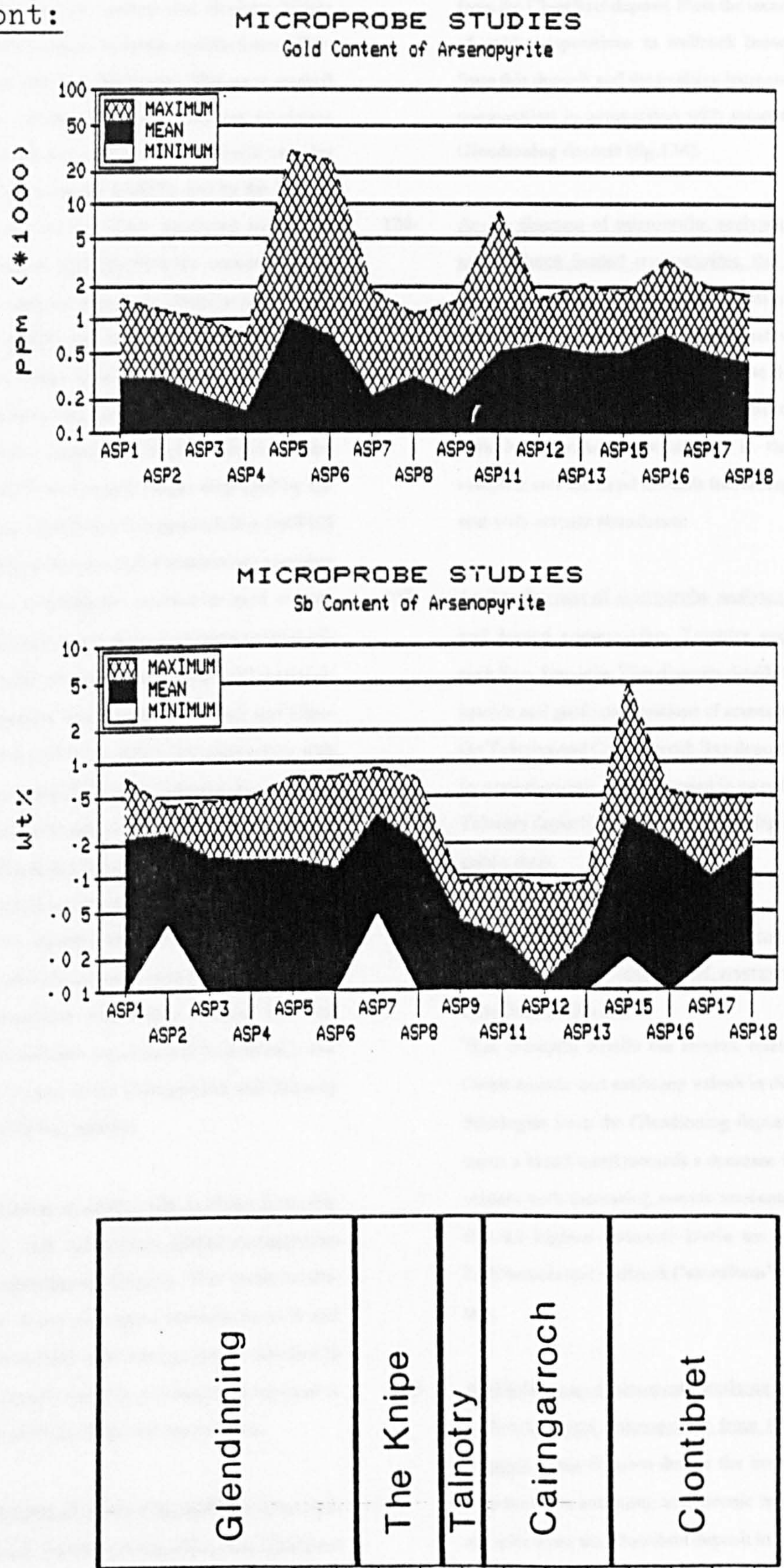

tion effects. The As content plot displays highly variable compositions between crystals from differing deposits and host lithologies. The most marked variation is displayed by extremely low minimum and mean values associated with wallrock samples from the Knipe deposit (ASP7); and by the highest minimum and mean values displayed within the Talnotry sample (ASP9). Note the consistent mean values of samples from the Glendinning deposit (ASP1 to ASP6) and the relatively increased As content of samples from the Clontibret deposit.
Sulphur contents are again highly variable with the highest mean compositions displayed by the Knipe sample (ASP7) and largest ranges displayed by the Glendinning (ASP5) and Cairngarroch Bay (ASP12) samples. The gold content plot summarises a number of features including the increase in gold content from Glendinning vein through breccia to wallrock hosted crystals; the increase in mean gold compositions of samples from the Cairngarroch and Clontibret deposit (ASP11 to ASP18) in comparison with samples from the Knipe and Talnotry deposits; and the low gold content of vein hosted arsenopyrites from the Southern Uplands. Antimony values are highly variable and displayed on a logarithmic scale (range: 0.01-10wt%, 100-100,000ppm). Note the largest mean and maximum antimony values present in quartz-stibnite vein hosted samples from the Knipe and Clontibret deposits; and the extremely low Sb values located in the Cairngarroch and Talnotry deposits (ASP9 to ASP13).

134- <u>As-Au diagram of microprobe analyses from disseminated, vein and breccia hosted arsenopyrites from the Glendinning Deposit</u> This crossplot displays little direct correlation between As at.% and gold content. Gold values are generally enriched in wallrock hosted ('stratiform') samples as opposed to their vein and breccia hosted counterparts.

135- <u>As-Au diagram of microprobe analyses from vein and wallrock hosted arsenopyrites, the Clontibret Deposit</u>.
This crossplot displays a general correlation between increased gold composition and arsenic content within both vein and wallrock hosted arsenopyrites from the Clontibret deposit. Note the increased range of gold compositions in wallrock hosted samples from this deposit and the positive increase in arsenic composition in comparison with samples from the Glendinning deposit (fig.134).

136- <u>As-Au diagram of microprobe analyses from vein and wallrock hosted arsenopyrites, the Knipe Deposit</u>. This crossplot details the variation in arsenic and gold composition in wallrock and vein hosted samples from the Knipe deposit. Note the differing arsenic composition between the two host lithologies with lower values concentrated in the wallrock samples; and the trend towards increasing gold content with arsenic abundance.

137- <u>As-Au diagram of microprobe analyses from vein and hosted arsenopyrites, Talnotry and Cairngarroch Bay Deposits</u> This diagram details the range of arsenic and gold compositions of arsenopyrites from the Talnotry and Cairngarroch Bay deposits. Note the increased arsenic values present in samples from the Talnotry deposit, which also exhibit slightly reduced gold values.

138- <u>As-Sb diagram of microprobe analyses from wallrock, vein and breccia hosted arsenopyrite in the Glendinning Deposit</u>
This crossplot details the inverse relationship between arsenic and antimony values in different host lithologies from the Glendinning deposit and illustrates a broad trend towards a decrease in antimony content with increasing arsenic concentration. Note that the highest antimony levels are developed in both breccia and wallrock ('stratiform') hosted crystals.

139- <u>As-Sb diagram of microprobe analyses from vein and wallrock hosted arsenopyrites from the Clontibret Deposit</u>. This diagram details the inverse relationship between antimony and arsenic in arsenopyrite samples from the Clontibret deposit in Southern Ireland. Note the extended range values in the wallrock hosted samples and the concentration of vein hosted samples in the low (<1000ppm) antimony/high arsenic (>31 at.%) values.

FIGURE 134

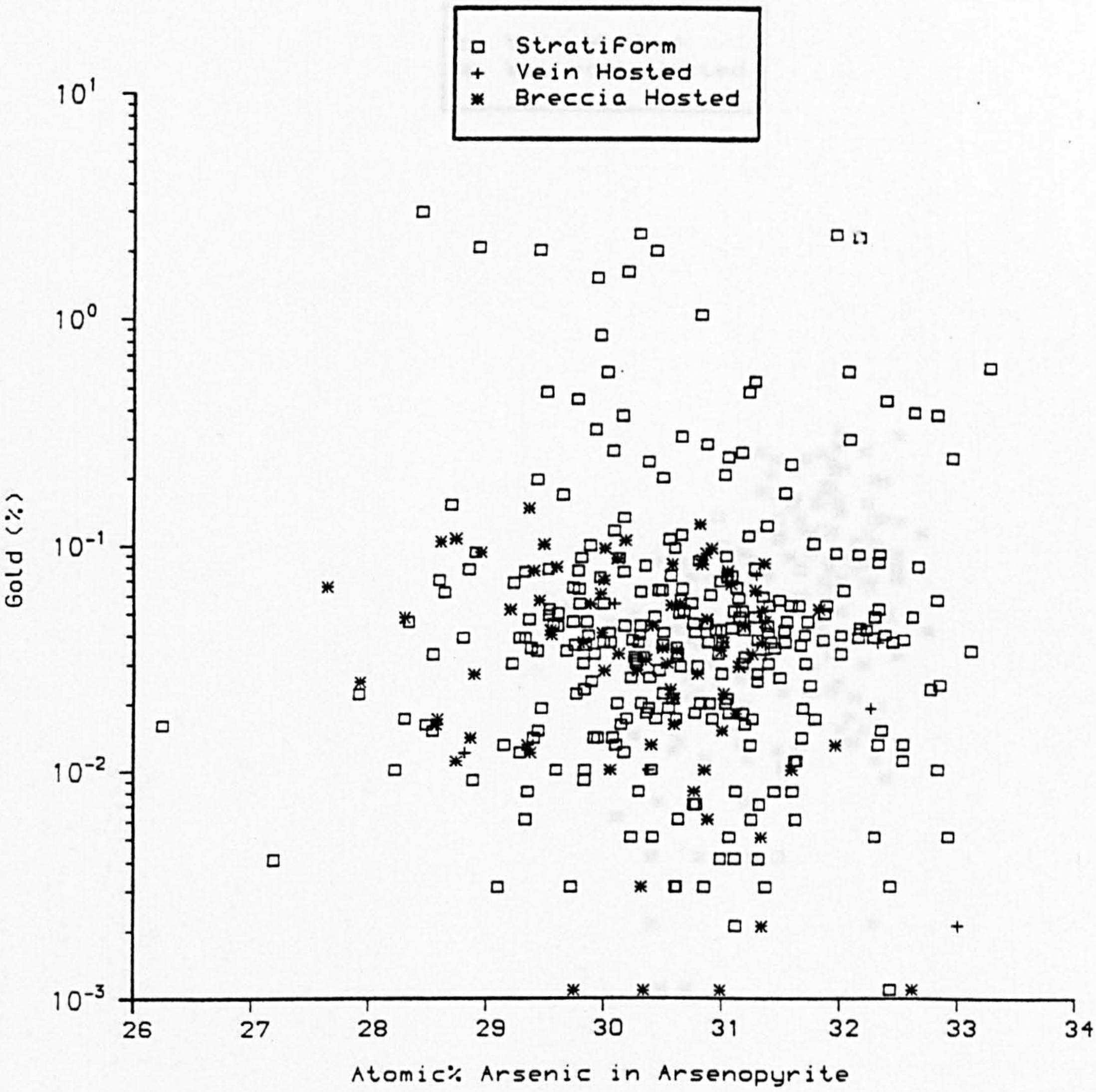

Glendinning Microprobe Studies.

FIGURE 135

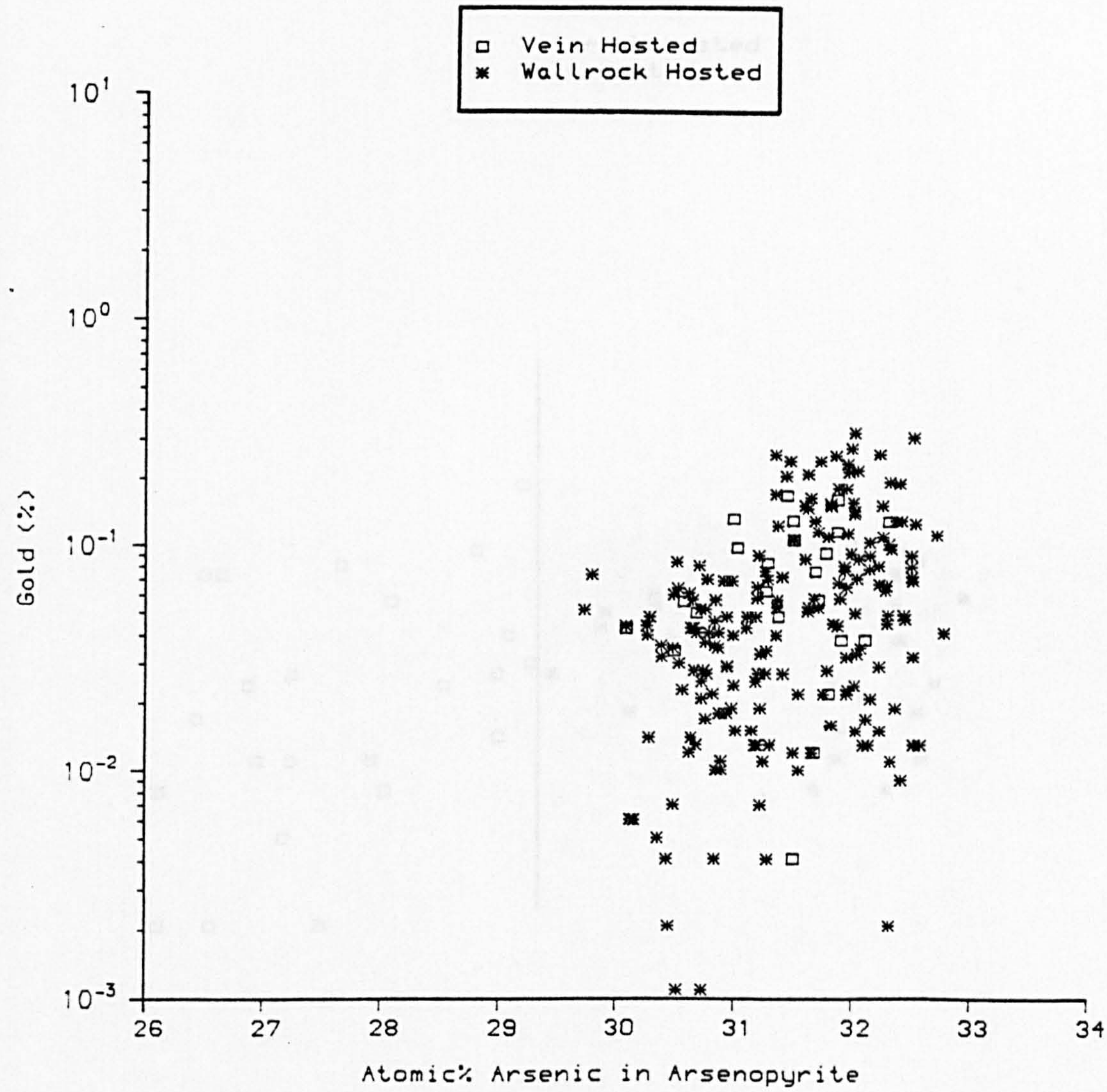

Clontibret Microprobe Studies.

FIGURE 136

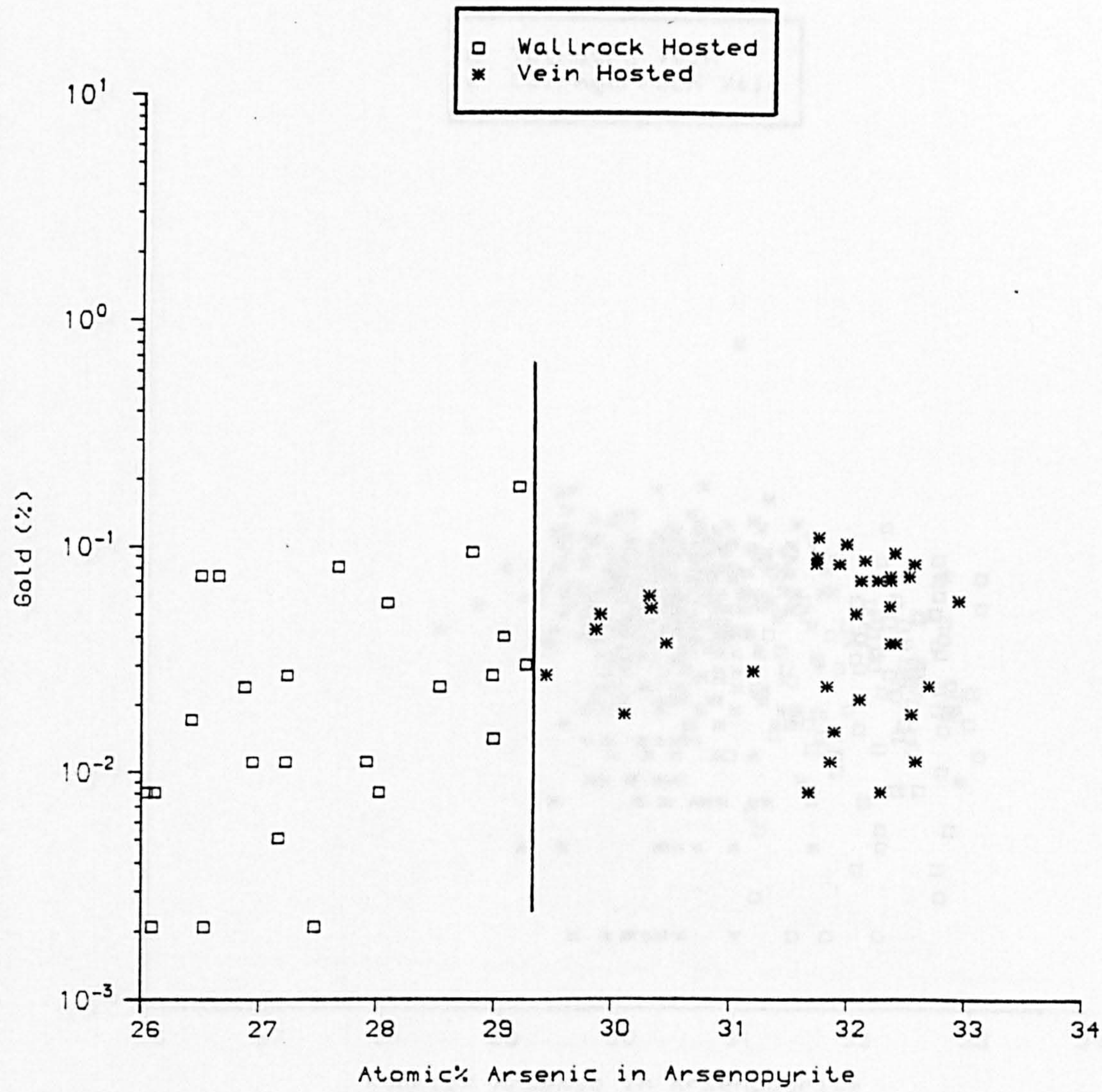

The Knipe Microprobe Studies.

FIGURE 137

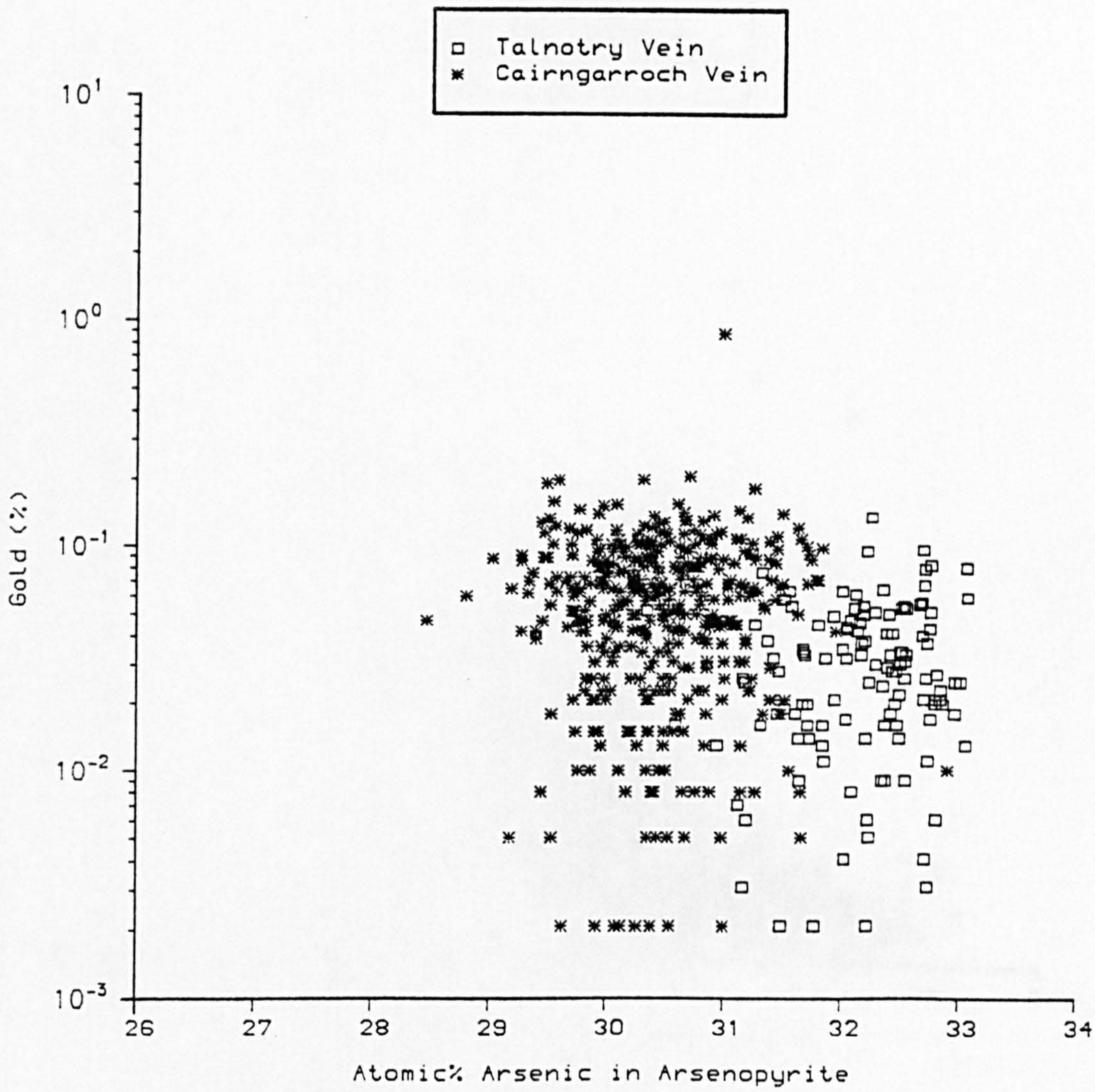

Talnotry and Cairngarroch Microprobe Studies.

FIGURE 138

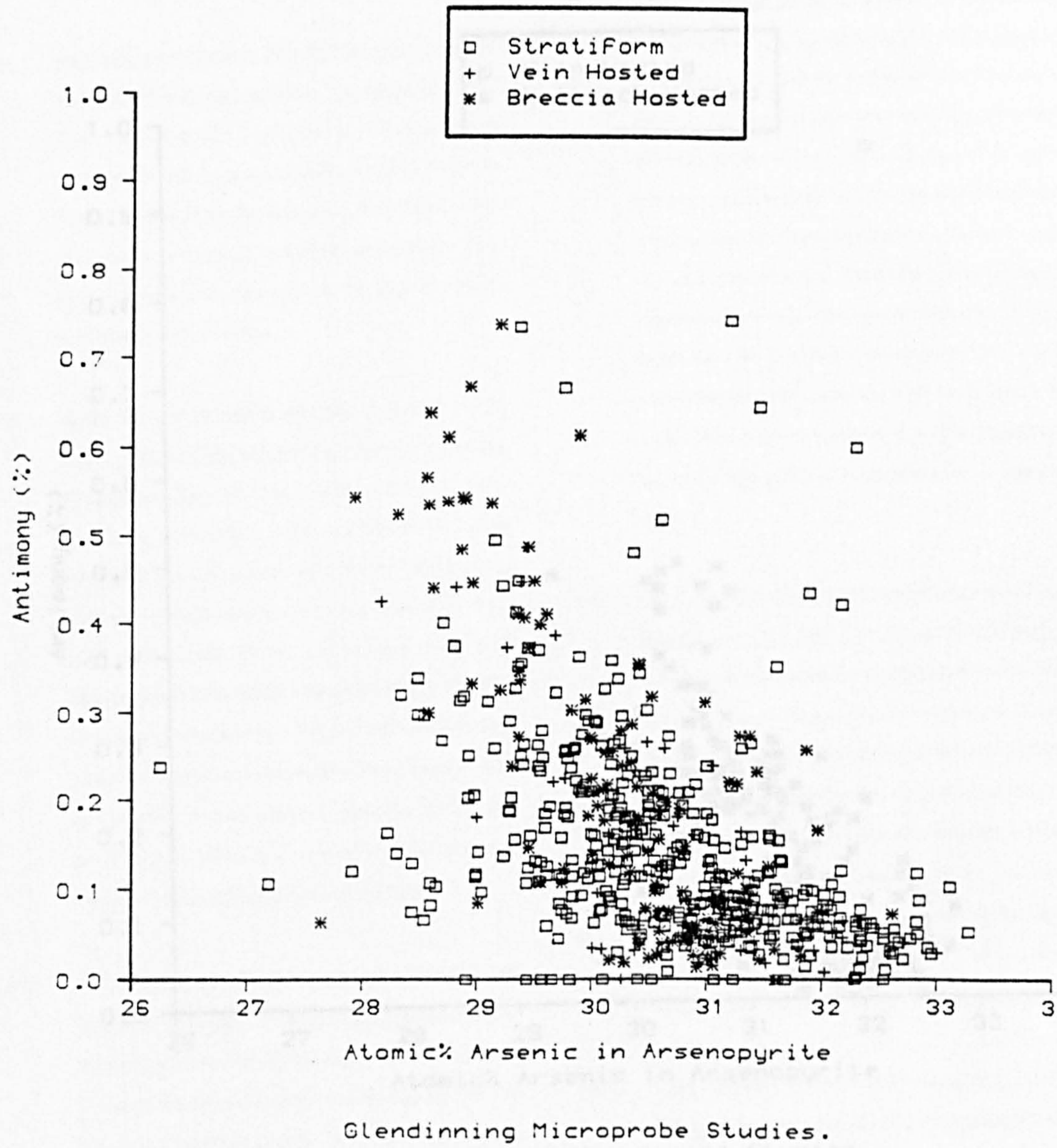
Stratiform
Vein Hosted
Breccia Hosted
Antimony (%)
1.0
0.9
0.8
0.7
0.6
0.5
0.4
0.3
0.2
0.1
0.0
26
27
28
29
30
31
32
33
34
Atomic% Arsenic in Arsenopyrite
Glendinning Microprobe Studies.

FIGURE 139

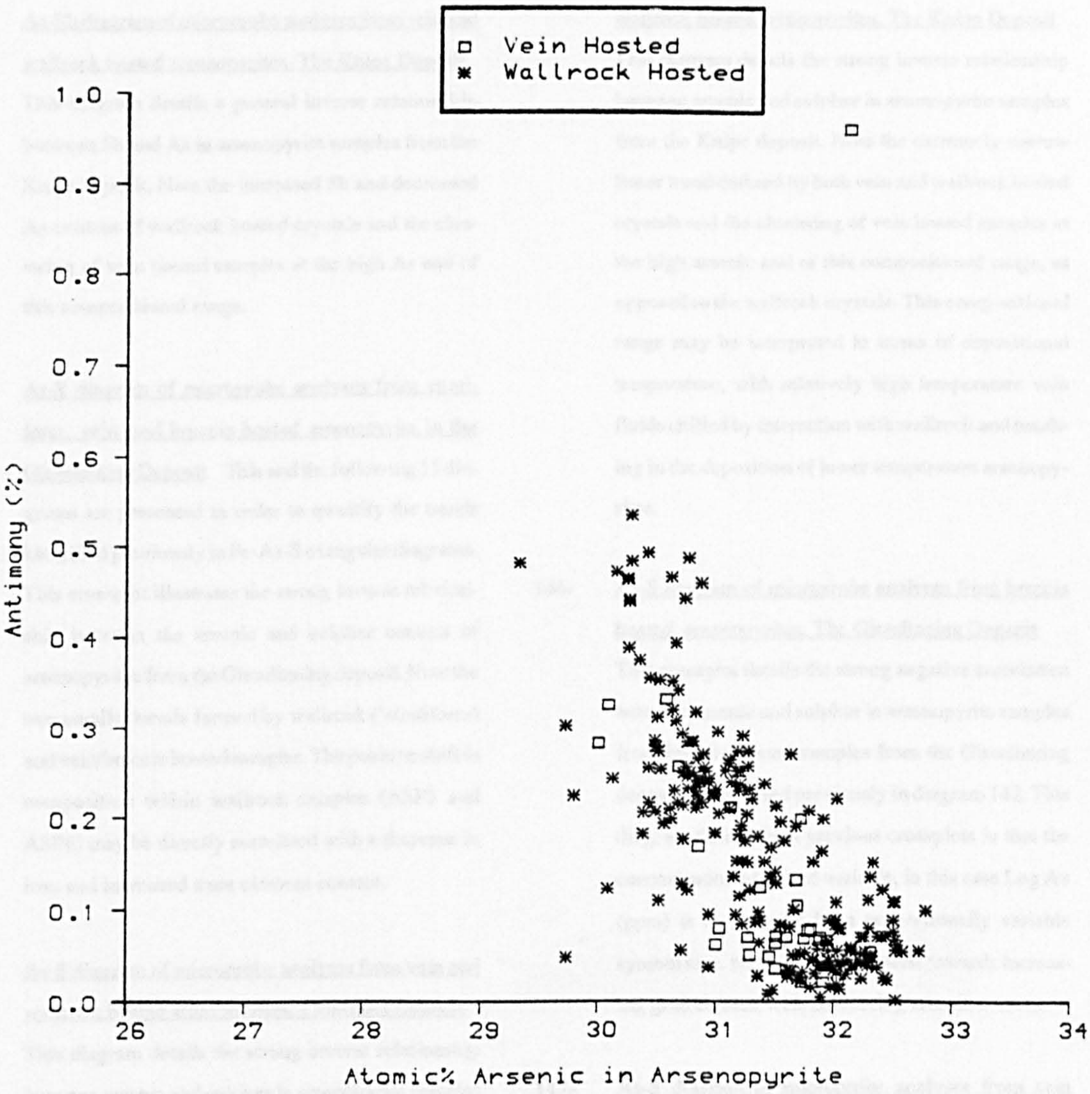

Clontibret Microprobe Studies.

140- As-Sb diagram of microprobe analyses from vein and wallrock hosted arsenopyrites, Talnotry and Cairngarroch Bay Deposits. This crossplot illustrates the extremely low concentration of antimony (<1000ppm) in arsenopyrites from the Talnotry and Cairngarroch Bay deposits. Note the increase in arsenic content within samples from the Talnotry deposit.

141- As-Sb diagram of microprobe analyses from vein and wallrock hosted arsenopyrites, The Knipe Deposit. This diagram details a general inverse relationship between Sb and As in arsenopyrite samples from the Knipe deposit. Note the increased Sb and decreased As content of wallrock hosted crystals and the clustering of vein hosted samples at the high As end of this compositional range.

142- As-S diagram of microprobe analyses from stratiform, vein and breccia hosted arsenopyrite in the Glendinning Deposit This and the following 15 diagrams are presented in order to quantify the trends identified previously in Fe-As-S triangular diagrams. This crossplot illustrates the strong inverse relationship between the arsenic and sulphur content of arsenopyrites from the Glendinning deposit. Note the two parallel trends formed by wallrock ('stratiform) and vein/breccia hosted samples. The positive shift in composition within wallrock samples (ASP5 and ASP6) may be directly correlated with a decrease in iron and increased trace element content.

143- As-S diagram of microprobe analyses from vein and wallrock hosted arsenopyrites, Clontibret Deposit This diagram details the strong inverse relationship between arsenic and sulphur in arsenopyrite samples from the Clontibret deposit. Note the narrow linear trend defined by both vein and wallrock hosted crystals and the clustering of vein hosted samples at the high end of this compositional range.

144- As-S diagram of microprobe analyses from vein and wallrock hosted arsenopyrites, the Talnotry and Cairngarroch Bay Deposits This crossplot details the strong negative correlation between arsenic and sulphur in arsenopyrite samples from both the Talnotry and Cairngarroch Bay deposits. Note the relatively narrow linear trends defined by samples from both deposits; the increased arsenic and decreased sulphur values in samples from Talnotry; and the clustering of Cairngarroch Bay samples at the low arsenic/high sulphur end of this compositional range.

145- As-S diagram of microprobe analyses from vein and wallrock hosted arsenopyrites, The Knipe Deposit This diagram details the strong inverse relationship between arsenic and sulphur in arsenopyrite samples from the Knipe deposit. Note the extremely narrow linear trend defined by both vein and wallrock hosted crystals and the clustering of vein hosted samples at the high arsenic end of this compositional range, as opposed to the wallrock crystals. This compositional range may be interpreted in terms of depositional temperature, with relatively high temperature vein fluids chilled by interaction with wallrock and resulting in the deposition of lower temperature arsenopyrites.

146- As-S diagram of microprobe analyses from breccia hosted arsenopyrites, The Glendinning Deposit This crossplot details the strong negative correlation between arsenic and sulphur in arsenopyrite samples from breccia hosted samples from the Glendinning deposit as described previously in diagram 142. This diagram differs from previous crossplots in that the concentration of a third variable, in this case Log Au (ppm) is represented by a proportionally variable symbol size. Note the general trend towards increasing gold content with decreasing arsenic content.

147- As-S diagram of microprobe analyses from vein hosted arsenopyrites, The Glendinning Deposit This diagram details a general inverse correlation between arsenic and sulphur in vein hosted arsenopyrites from the Glendinning deposit. Symbol size is directly controlled by Log Au (ppm) content. Note the lack of grouping of high gold values within the vein hosted samples.

148- As-S diagram of microprobe analyses from wallrock hosted arsenopyrites The Glendinning Deposit This crossplot details the general negative correlation

FIGURE 140

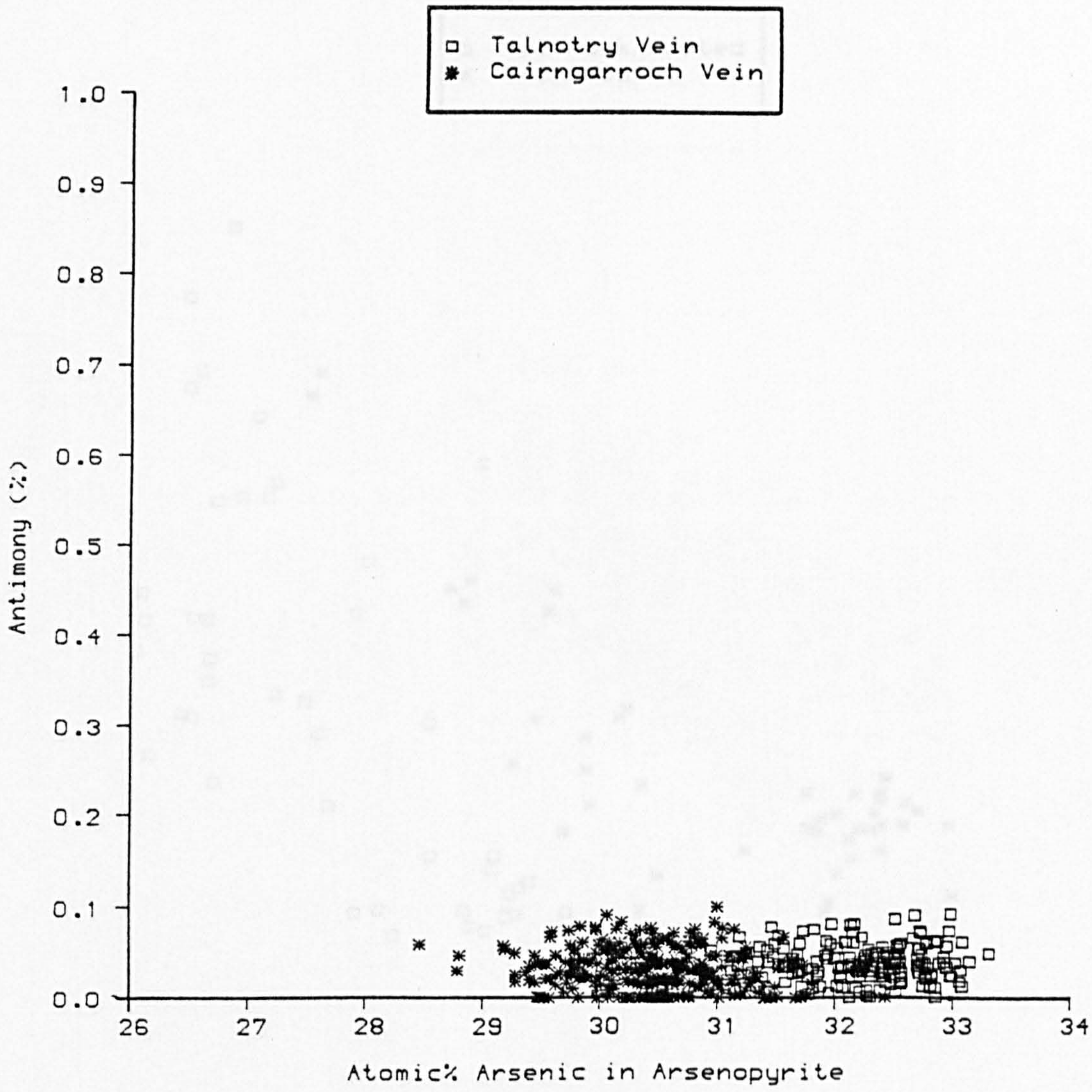

Talnotry and Cairngarroch Microprobe Studies.

FIGURE 141

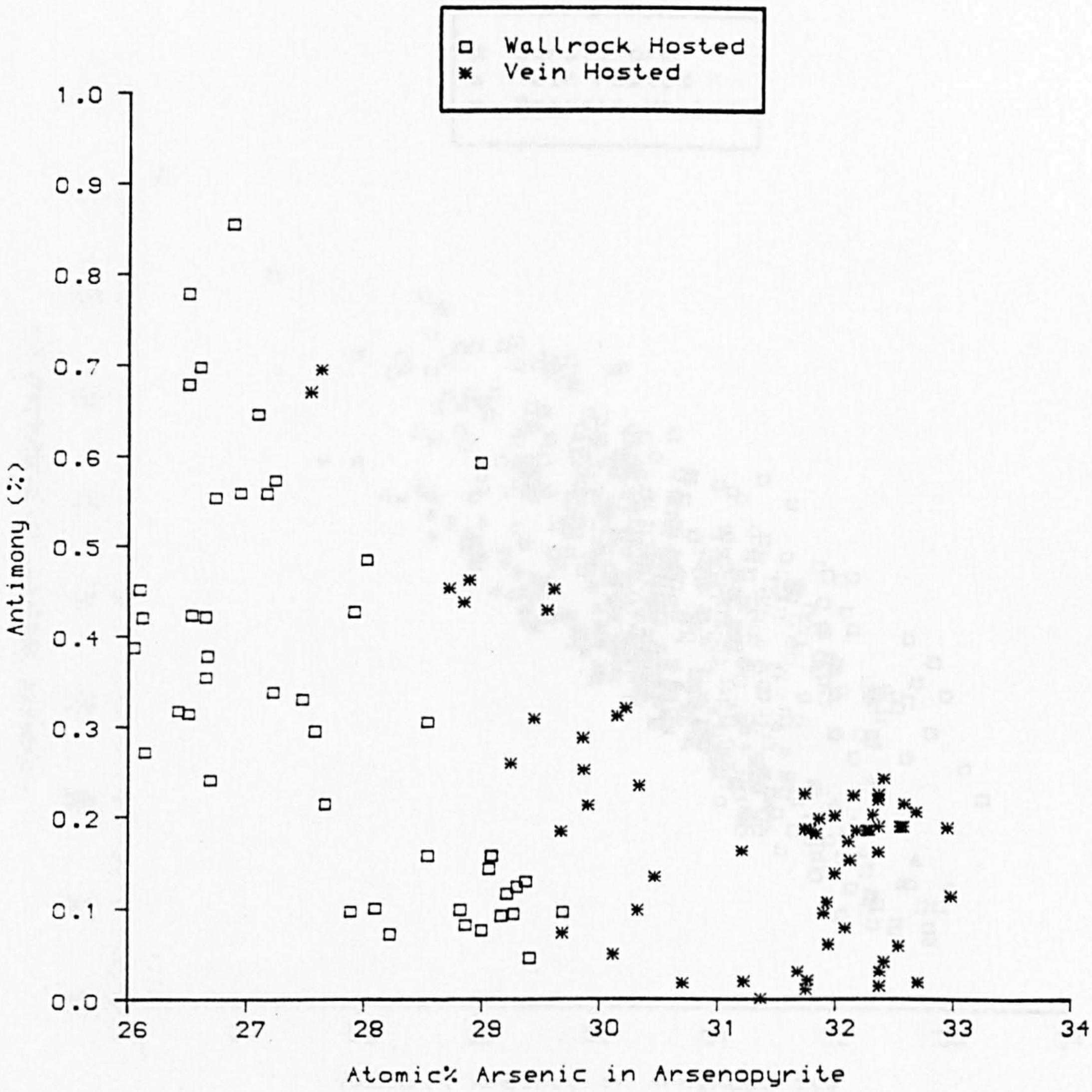

The Knipe Microprobe Studies.

FIGURE 142

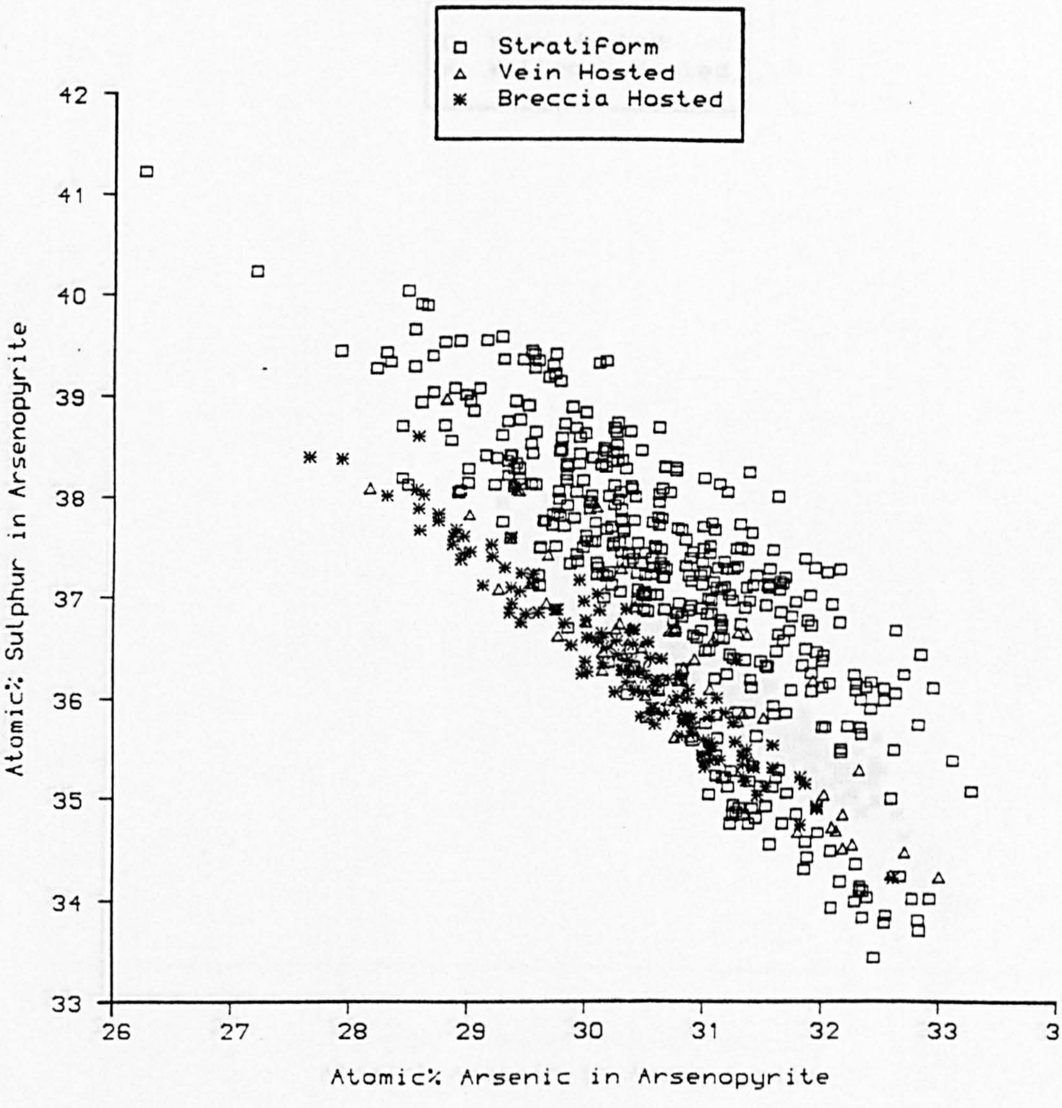

Glendinning Microprobe Studies.

FIGURE 143

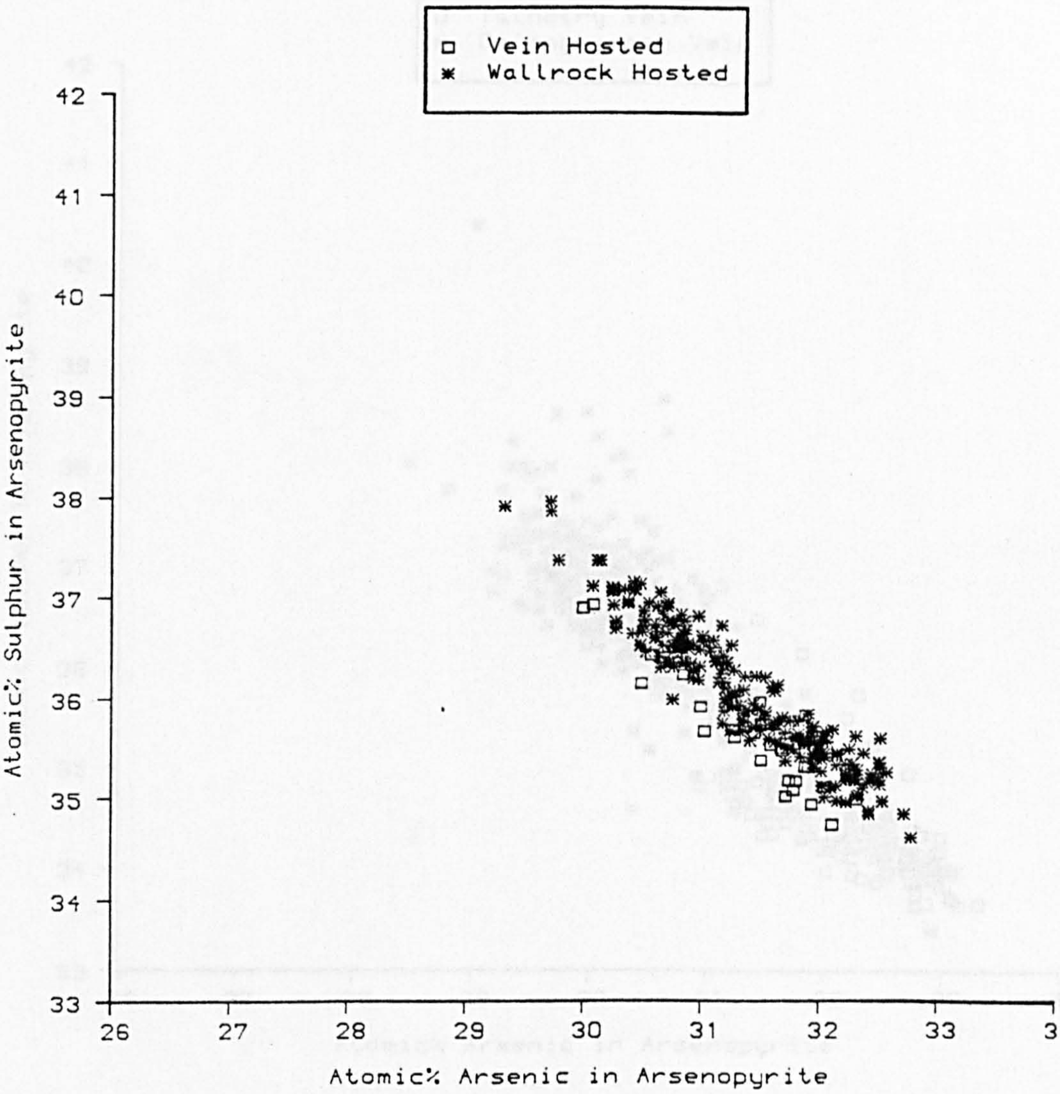

Clontibret Microprobe Studies.

FIGURE 144

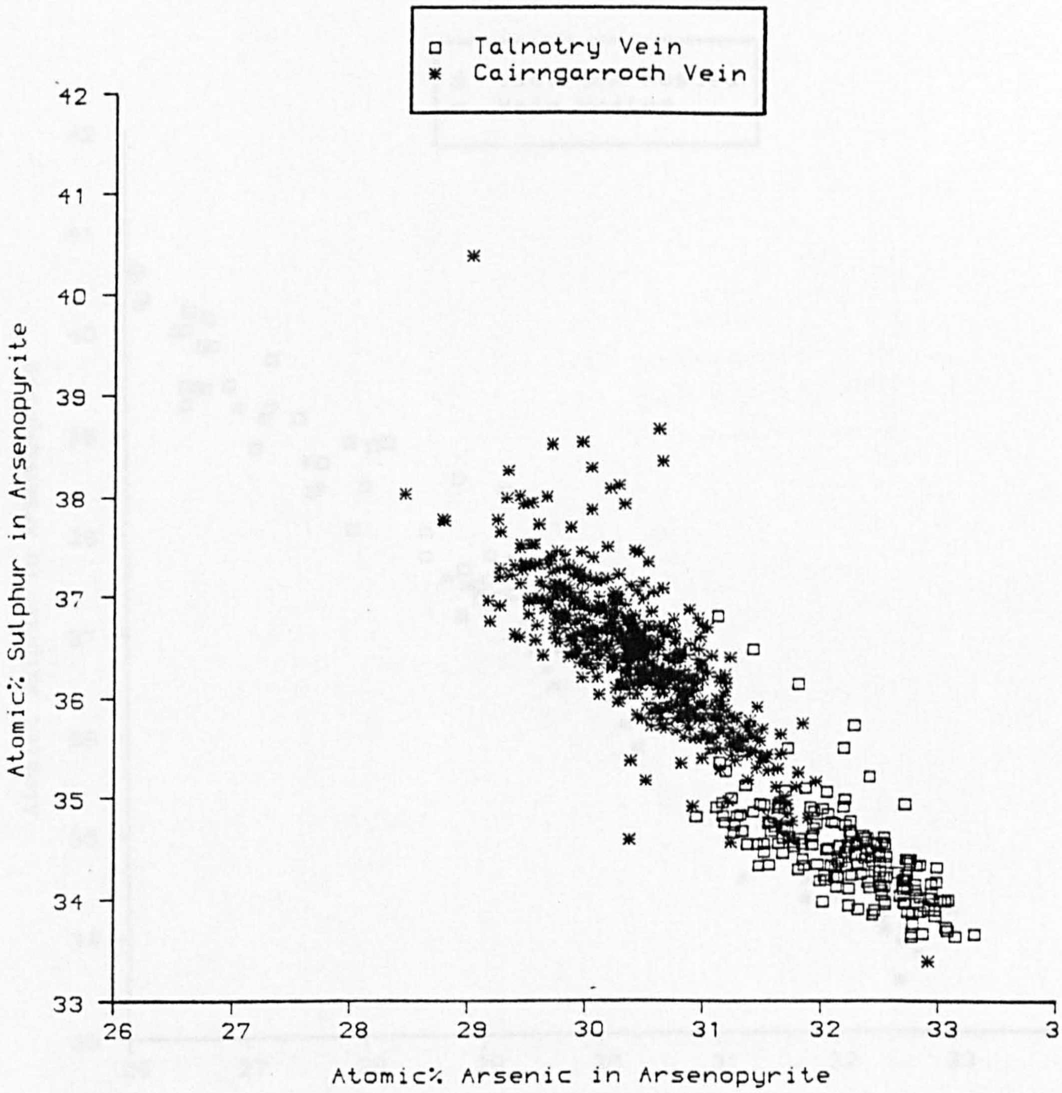

Talnotry and Cairngarroch Microprobe Studies.

FIGURE 145

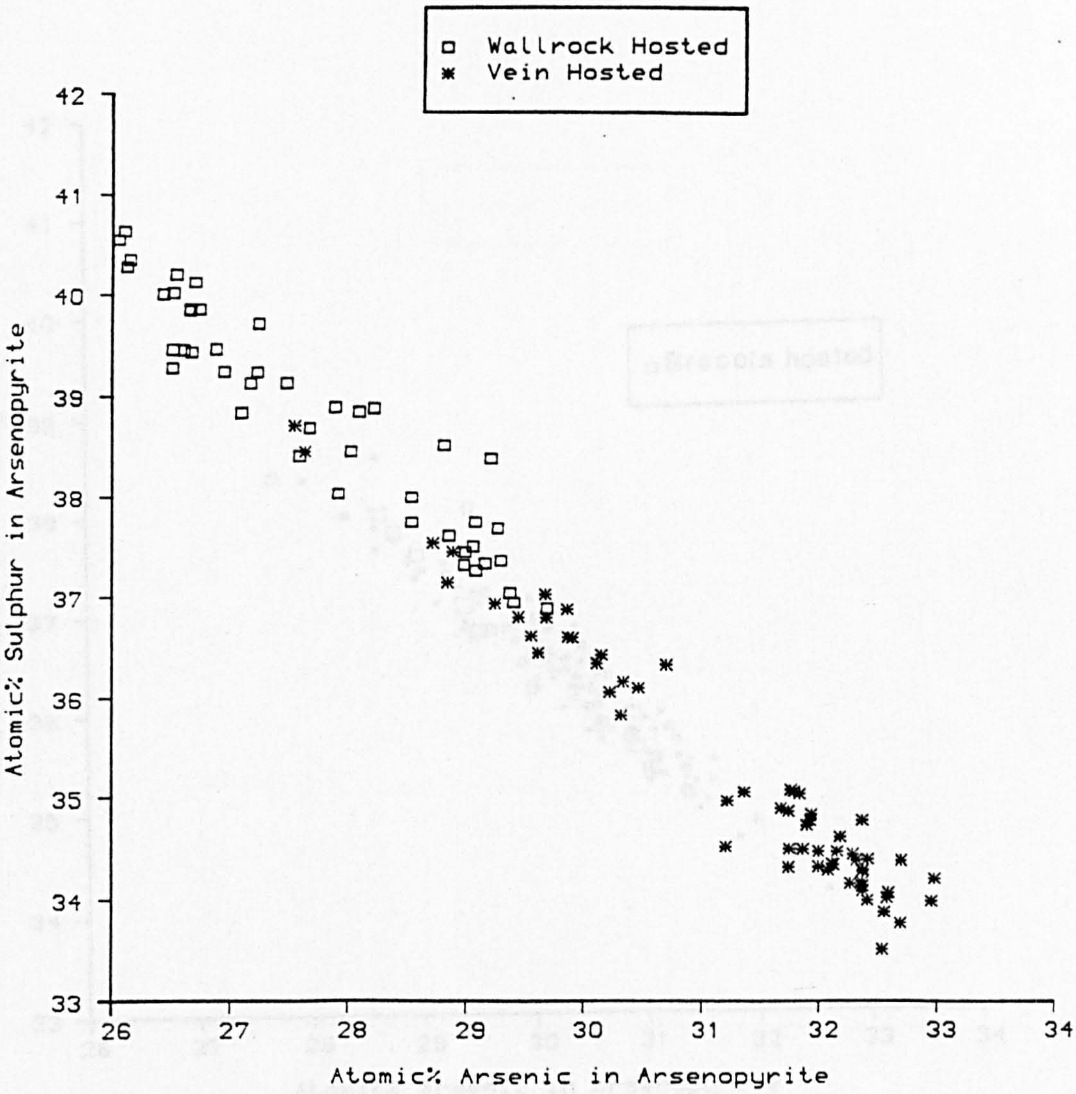

The Knipe Microprobe Studies.

FIGURE 146

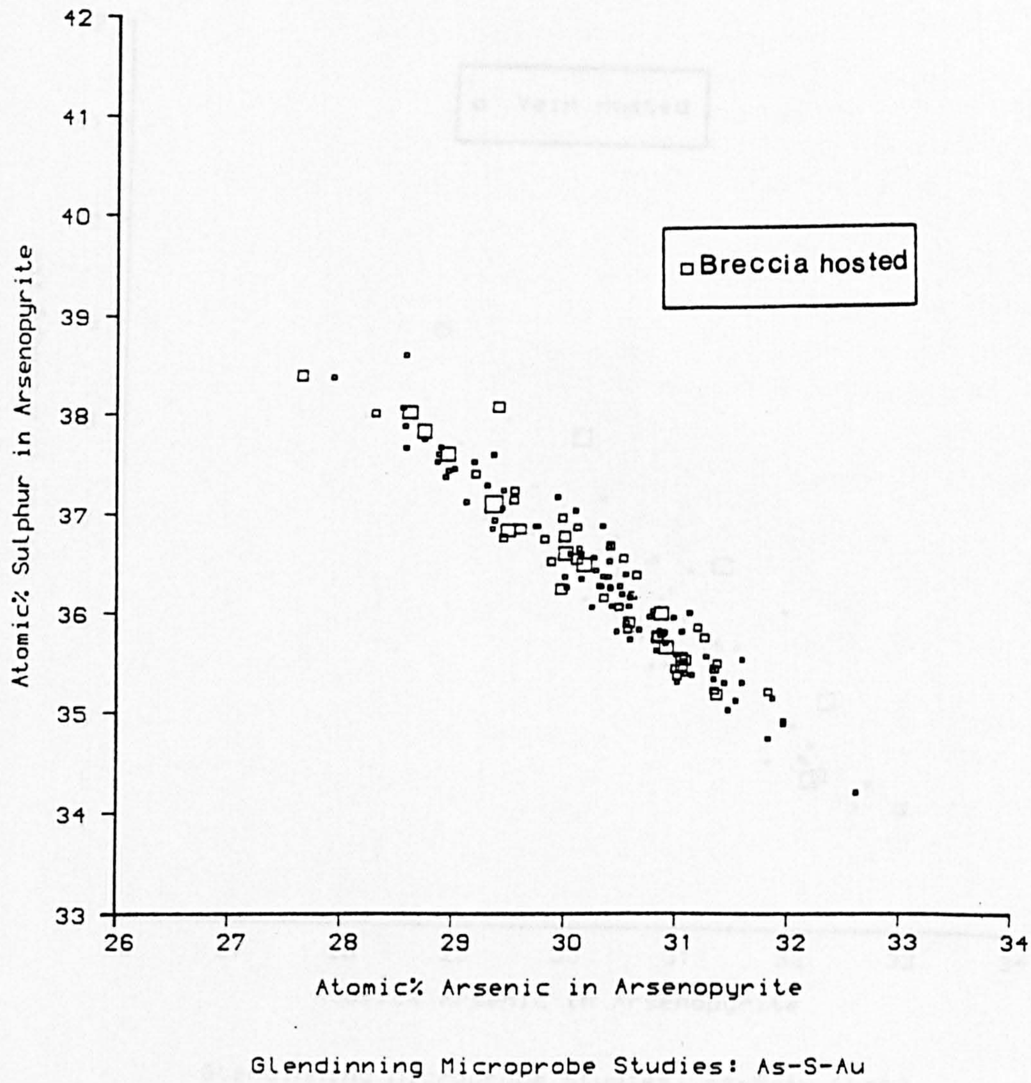

Glendinning Microprobe Studies: As-S-Au

FIGURE 147

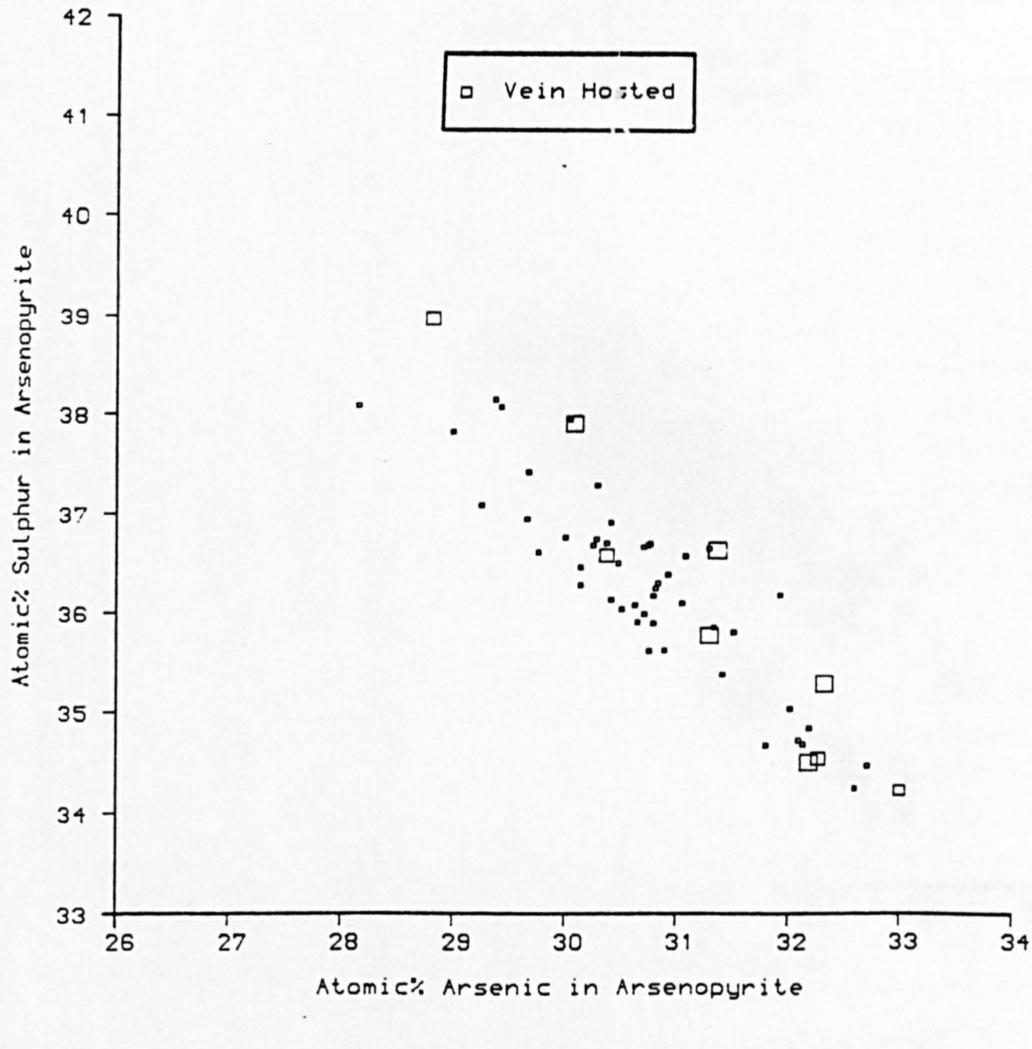

Glendinning Microprobe Studies: As-S-Au (Log)

FIGURE 148

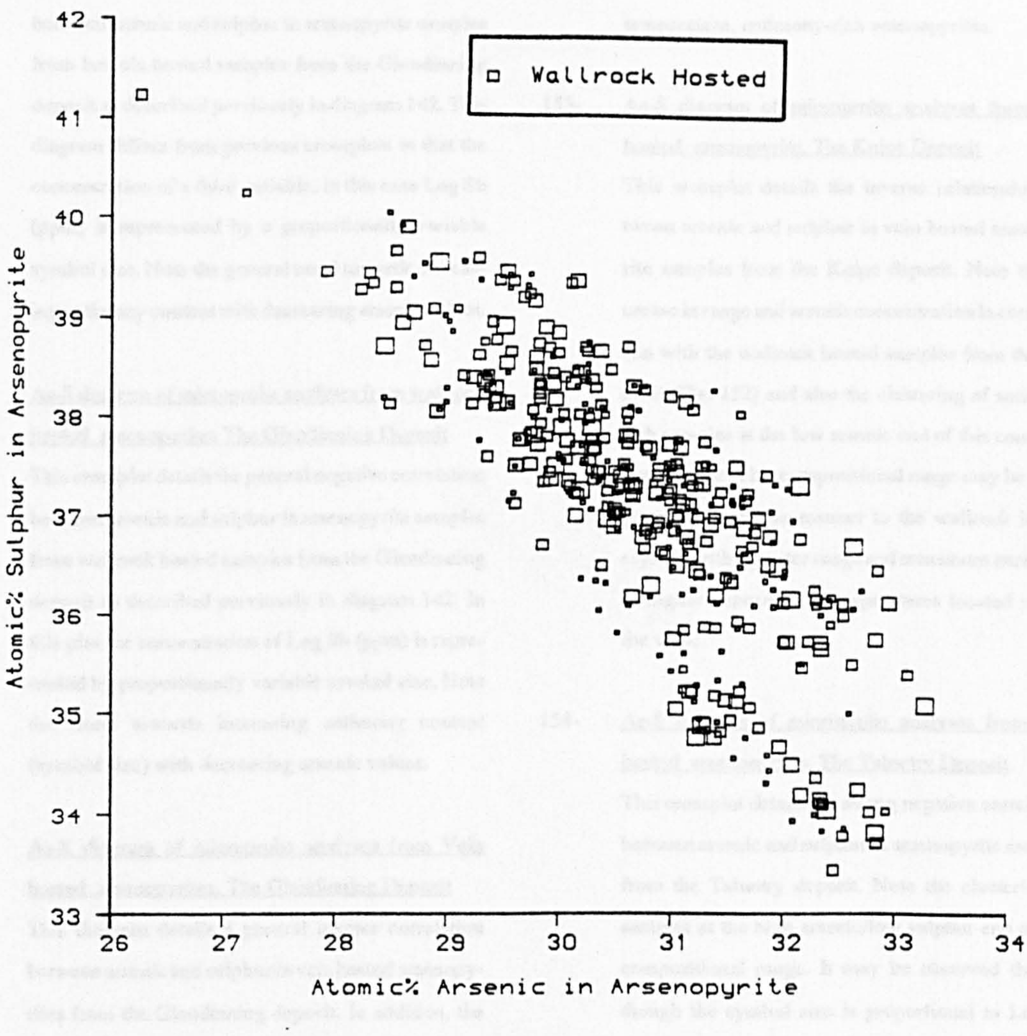
Wallrock Hosted
Atomic% Sulphur in Arsenopyrite
42
41
40
39
38
37
36
35
34
33
26
27
28
29
30
31
32
33
34
Atomic% Arsenic in Arsenopyrite
Glendinning Microprobe Studies: As-S-Au (Log)

between arsenic and sulphur in arsenopyrite samples from wallrock hosted samples from the Glendinning deposit as described previously in diagram 142. Here again, the concentration of Log Au (ppm) is represented by proportionally variable symbol size. Note the wide range of gold values displayed throughout this solid solution series.

149- <u>As-S diagram of microprobe analyses from breccia hosted arsenopyrites. The Glendinning Deposit</u>

This crossplot details the strong negative correlation between arsenic and sulphur in arsenopyrite samples from breccia hosted samples from the Glendinning deposit as described previously in diagram 142. This diagram differs from previous crossplots in that the concentration of a third variable, in this case Log Sb (ppm) is represented by a proportionally variable symbol size. Note the general trend towards increasing antimony content with decreasing arsenic values.

150- <u>As-S diagram of microprobe analyses from wallrock hosted arsenopyrites The Glendinning Deposit</u>

This crossplot details the general negative correlation between arsenic and sulphur in arsenopyrite samples from wallrock hosted samples from the Glendinning deposit as described previously in diagram 142. In this plot the concentration of Log Sb (ppm) is represented by proportionally variable symbol size. Note the trend towards increasing antimony content (symbol size) with decreasing arsenic values.

151- <u>As-S diagram of microprobe analyses from Vein hosted arsenopyrites. The Glendinning Deposit</u>

This diagram details a general inverse correlation between arsenic and sulphur in vein hosted arsenopyrites from the Glendinning deposit. In addition, the symbol size is directly controlled by the Log Sb (ppm) content. Note the grouping of high antimony values within samples containing low arsenic concentrations (ie. the low temperature end members of this group).

152- <u>As-S diagram of microprobe analyses from wallrock hosted arsenopyrite. The Knipe Deposit</u>

This diagram details the strong inverse relationship between arsenic and sulphur in wallrock hosted arsenopyrite samples from the Knipe deposit. Note the clustering of samples at the low arsenic end of this compositional range, as opposed to their vein hosted counterparts (Fig. 153). As the symbol size is directly controlled by the log Sb (ppm) content it is clear that high antimony content samples are closely grouped in the lowest arsenic fraction of this population. This compositional range may be interpreted in terms of depositional temperature, with relatively high temperature vein fluids chilled by the interaction with wallrocks and resulting in the deposition of lower temperature, antimony-rich arsenopyrites.

153- <u>As-S diagram of microprobe analyses from vein hosted arsenopyrite. The Knipe Deposit</u>

This crossplot details the inverse relationship between arsenic and sulphur in vein hosted arsenopyrite samples from the Knipe deposit. Note the increase in range and arsenic concentration in comparison with the wallrock hosted samples from this deposit (Fig. 152) and also the clustering of antimony rich samples at the low arsenic end of this compositional range. This compositional range may be interpreted in a similar manner to the wallrock hosted crystals with a greater range and maximum attributed to higher depositional temperatures located within the vein.

154- <u>As-S diagram of microprobe analyses from vein hosted arsenopyrites. The Talnotry Deposit</u>

This crossplot details the strong negative correlation between arsenic and sulphur in arsenopyrite samples from the Talnotry deposit. Note the clustering of samples at the high arsenic/low sulphur end of this compositional range. It may be observed that although the symbol size is proportional to Log Sb (ppm) content, little if any systematic variation in antimony content occurs within this group.

155- <u>As-S diagram of microprobe analyses from vein hosted arsenopyrites. Cairngarroch Deposit</u>

This crossplot details the relationship between arsenic, sulphur and antimony in arsenopyrite samples from the Cairngarroch Bay deposit. Note the clustering of samples towards the low arsenic/high sulphur end member of this compositional range. As the

FIGURE 149

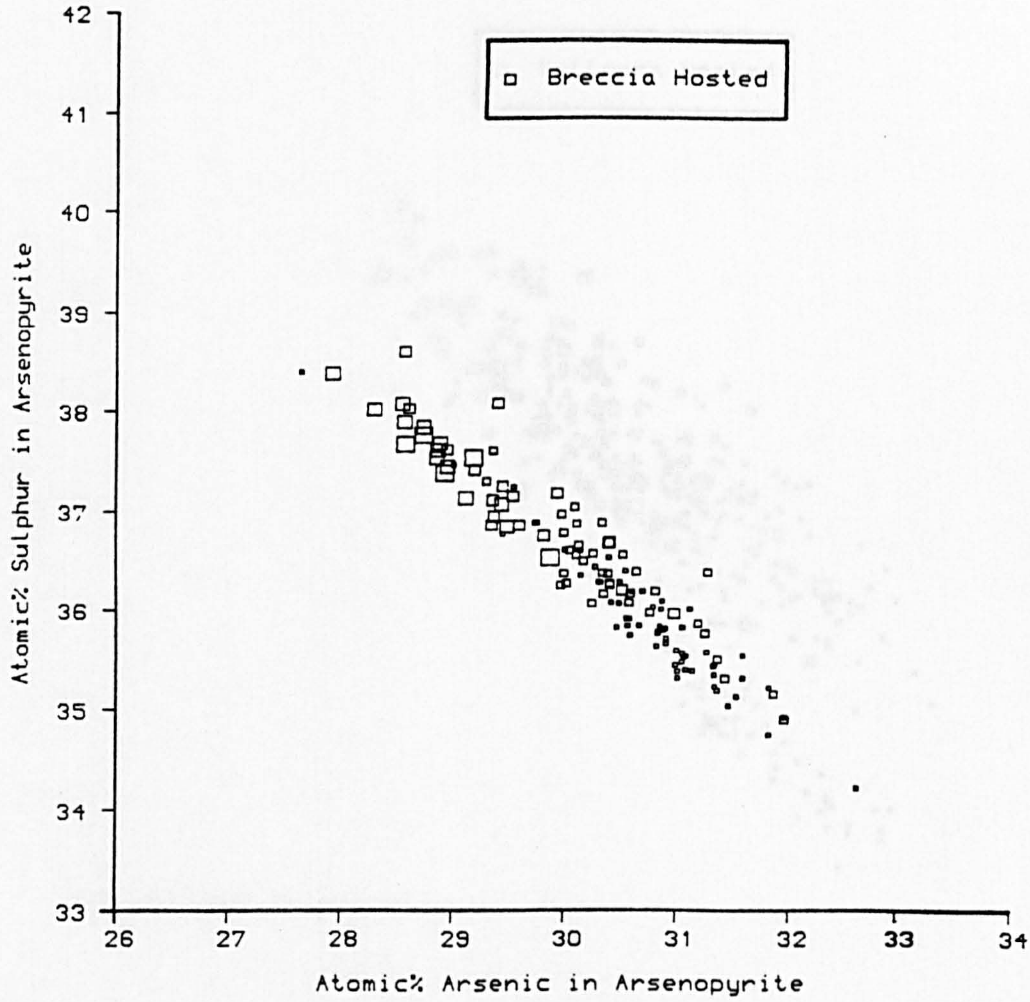

Glendinning Microprobe Study: As-S-Sb

FIGURE 150

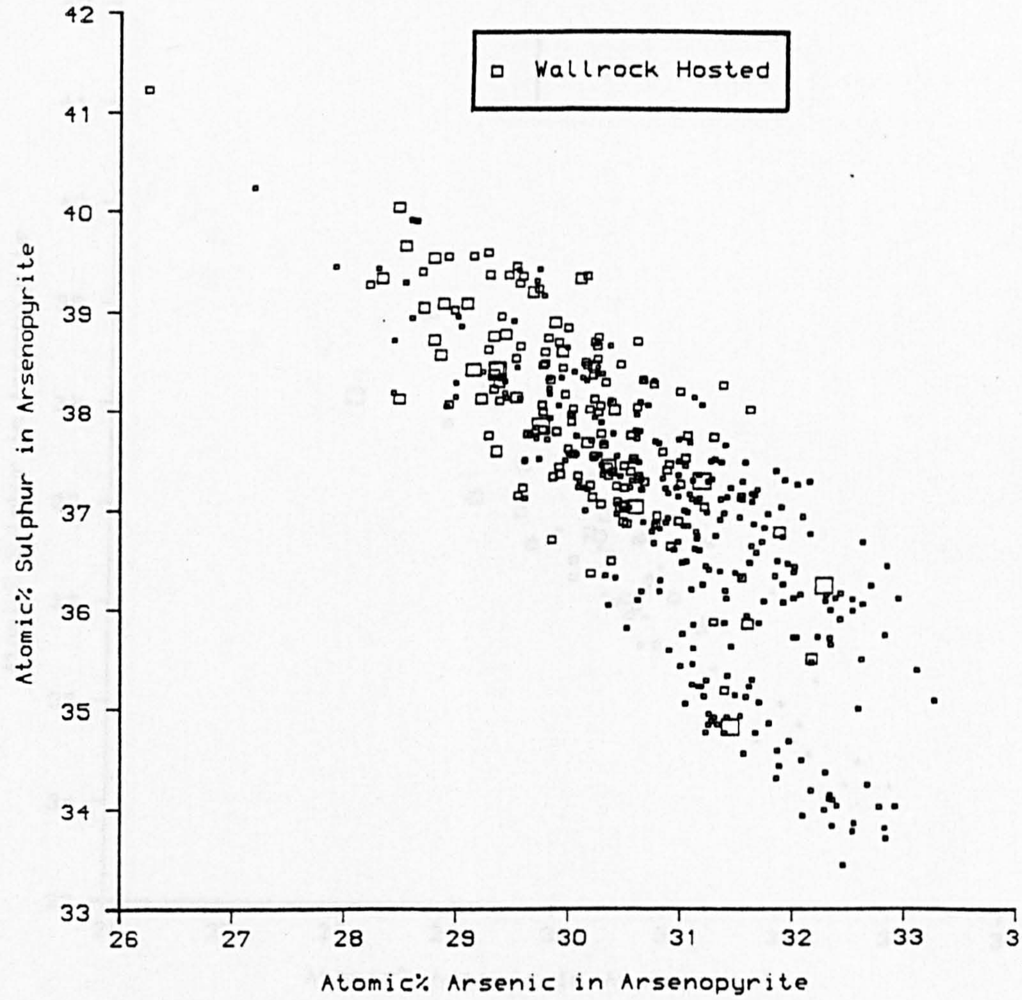

Glendinning Microprobe Study: As-S-Sb

FIGURE 151

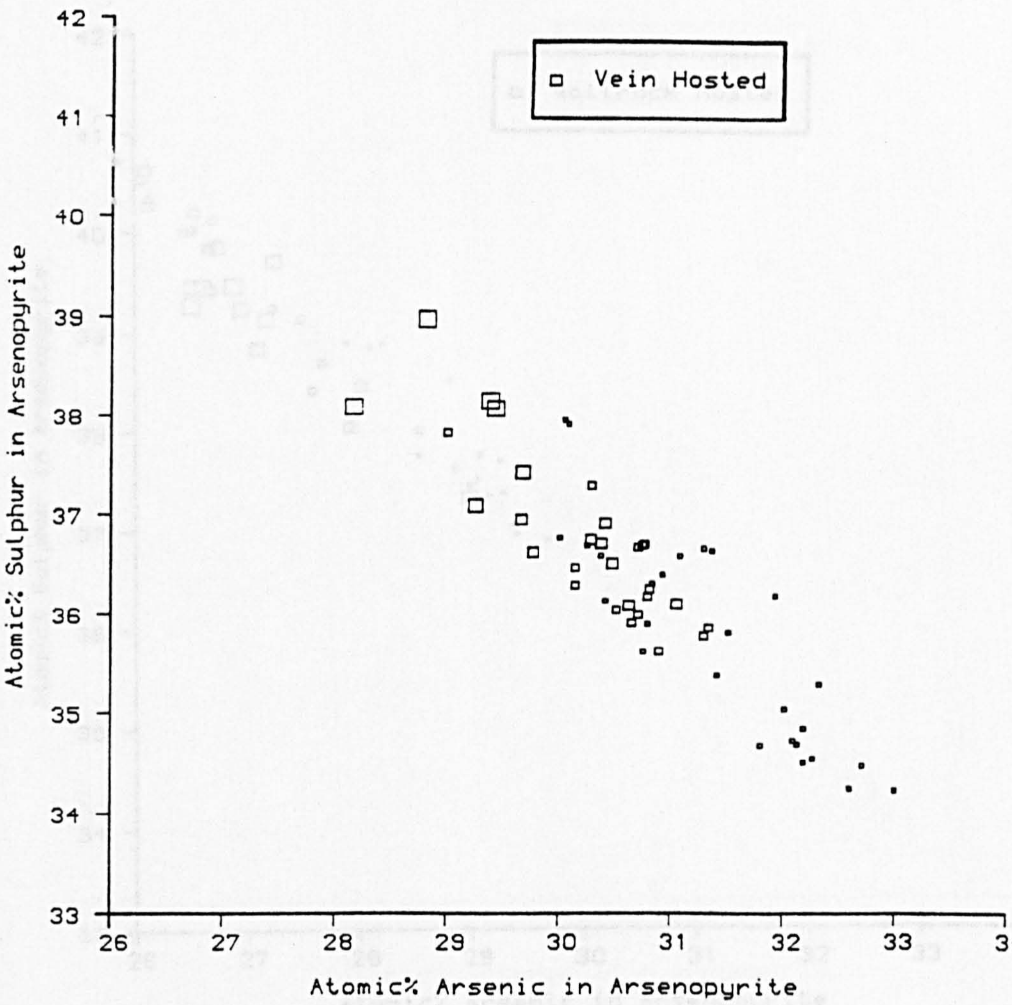

Glendinning Microprobe Study: As-S-Sb

FIGURE 152

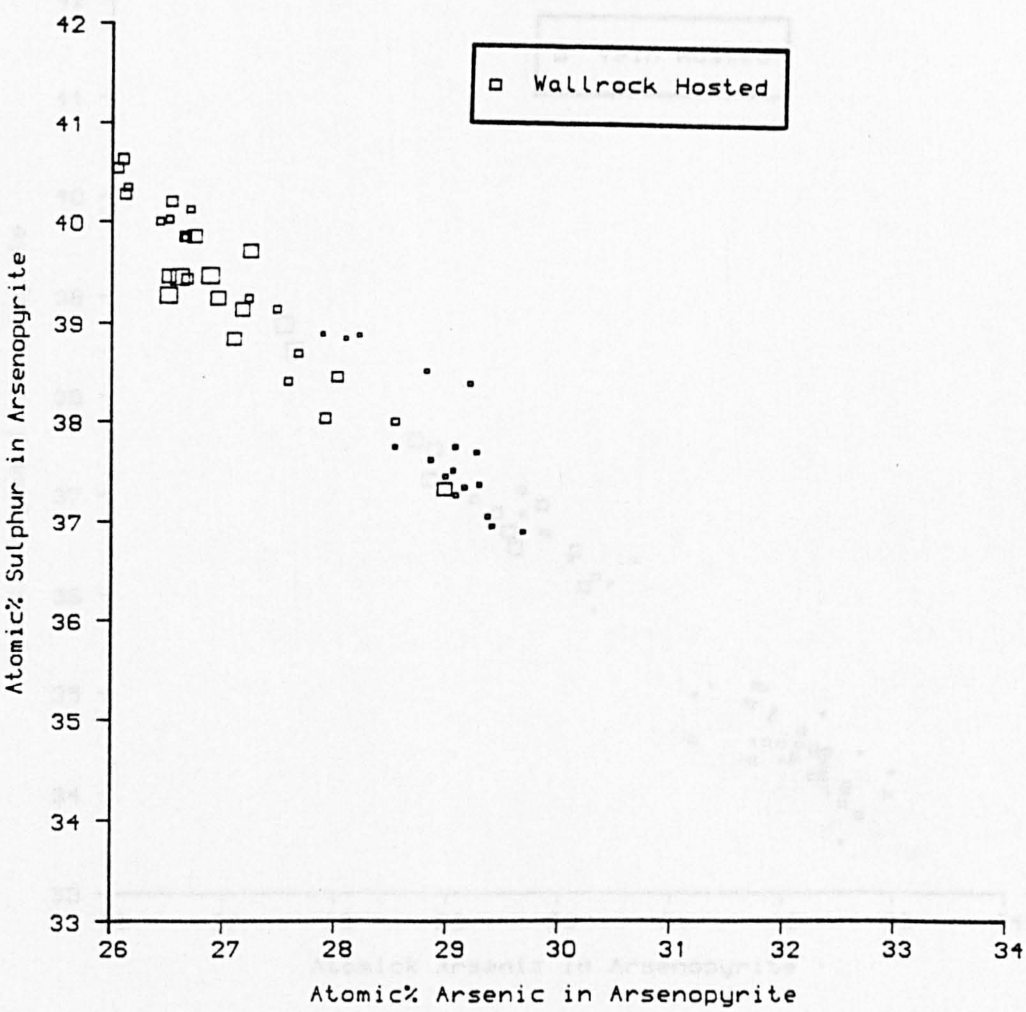

The Knipe Microprobe Study: As-S-Sb

FIGURE 153

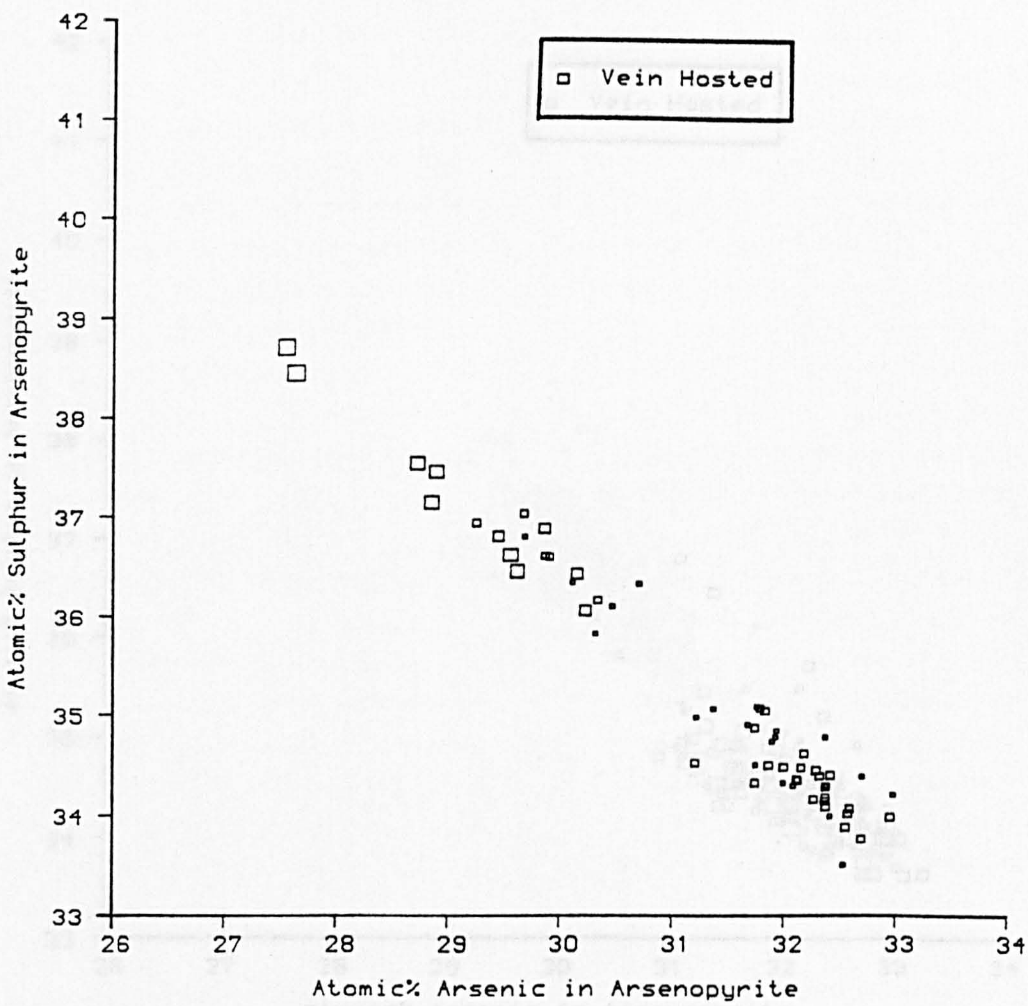

The Knipe Microprobe Study: As-S-Sb

FIGURE 154

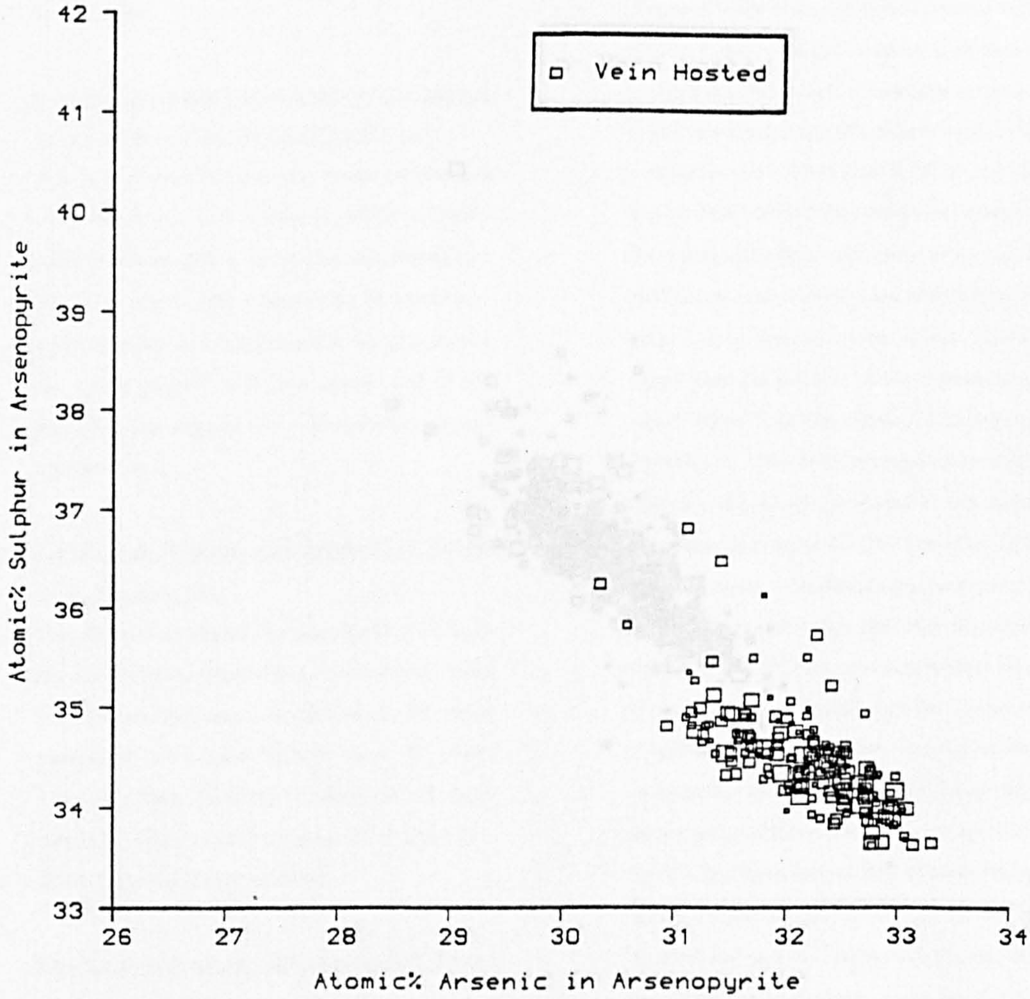

Talnotry Microprobe Study: As-S-Sb

FIGURE 155

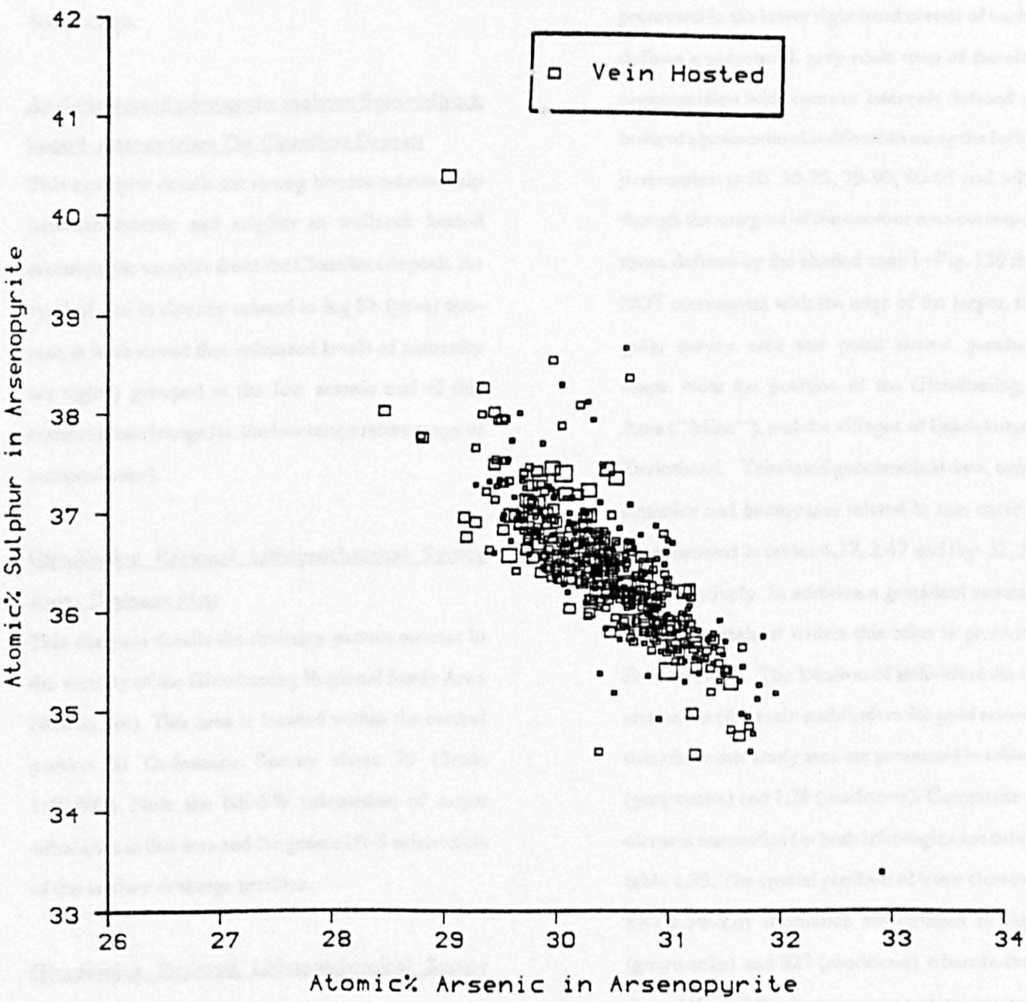

Cairngarroch Microprobe Study: As-S-Sb

symbol size is proportional to Log Sb (ppm) content, a subtle increase in antimony values is noted at the low arsenic end of this compositional range.

156- As-S diagram of microprobe analyses from vein hosted arsenopyrites, The Clontibret Deposit

This diagram details the relationship between arsenic, sulphur and antimony in vein hosted arsenopyrite samples from the Clontibret deposit. Note the extremely low levels of antimony and the lack of any systematic pattern of variation within this compositional range.

157- As-S diagram of microprobe analyses from wallrock hosted arsenopyrites The Clontibret Deposit

This crossplot details the strong inverse relationship between arsenic and sulphur in wallrock hosted arsenopyrite samples from the Clontibret deposit. As symbol size is directly related to log Sb (ppm) content, it is observed that enhanced levels of antimony are tightly grouped at the low arsenic end of this compositional range (ie. the low temperature range of compositions).

158- Glendinning Regional Lithogeochemical Survey Area: Drainage Map

This diagram details the drainage pattern present in the vicinity of the Glendinning Regional Study Area (484 sq km). This area is located within the central portion of Ordnanace Survey sheet 79 (Scale 1:50,000). Note the NE-SW orientation of major tributaries in this area and the general N-S orientation of the tertiary drainage profiles.

159- Glendinning Regional Lithogeochemical Survey Area: Contoured Region

The shaded area presented on this diagram defines the margins of the Glendinning Study Area and outlines the area subjected to grey-scale contour mapping within the Glendinning Regional Geochemical Atlas (Figs. 160-219).

160-224 Glendinning Regional Lithogeochemical Atlas

The following series of 62 maps may be grouped together in order to form the Glendinning Regional Geochemical Atlas. This atlas details the spatial and elemental variation present within the Glendinning survey area. Two maps are presented for each element for both greywacke and mudstone lithologies. On the larger of the two maps, 'point-source' geochemical data is presented with the position of individual sample sites identified by circles. The size of each circle is controlled by the elemental value, assigned to one of four ranges (Zero to Mean; Mean to Mean+1 Standard Deviation; Mean+1 Standard Deviation to Mean+2 Standard Deviations; and >2 Standard Deviations. The smaller of the two maps presented in the lower right hand corner of each page defines a contoured, grey-scale map of the element concentration with contour intervals defined on the basis of a percentile classification using the following percentiles: 0-50, 50-75, 75-90, 90-95 and >95. Although the margins of the contour area correspond to those defined by the shaded zone in Fig. 159 they do NOT correspond with the edge of the larger, rectangular survey area and point source geochemical maps. Note the position of the Glendinning Mine Area ("Mine"), and the villages of Eskdalemuir and Teviothead. Tabulated geochemical data, summary statistics and histograms related to this survey area are presented in tables 4.37, 2.47 and figs 32, 33 and 34 respectively. In addition a graphical summary of all data contained within this atlas is presented on Foldout No. 1. The location of individual As and Sb anomalies (the main pathfinders for gold mineralisation) from this study area are presented in tables 1.37 (greywacke) and 1.38 (mudstone). Composite multi-element anomalies for both lithologies are detailed in table 1.39. The spatial position of trace element (As-Sb-Cu-Pb-Zn) anomalies are defined in figs 221 (greywacke) and 223 (mudstone) whereas the position of Na and Zn depletion anomalies are presented in figs 222 (greywacke) and 224 (mudstone). Anomaly sites identified by this study and documented in table 1.39 include: the Glendinning Deposit (G); Black Syke (BS); Rams Cleuch (RC); Swin Gill (SC); Wisp Hill (WH); Philhope Loch (PL); Cat Rig (CR); Greatmoor Hill (GH); Rashigrain (R); The Shoulder (TS); Stibbiegill Head (SH); Stennies Water (SW); Linhope Burn (LB); Phaup Burn (PB); Meggat Water (MW) and Upper Stennies Water (US).

FIGURE 156

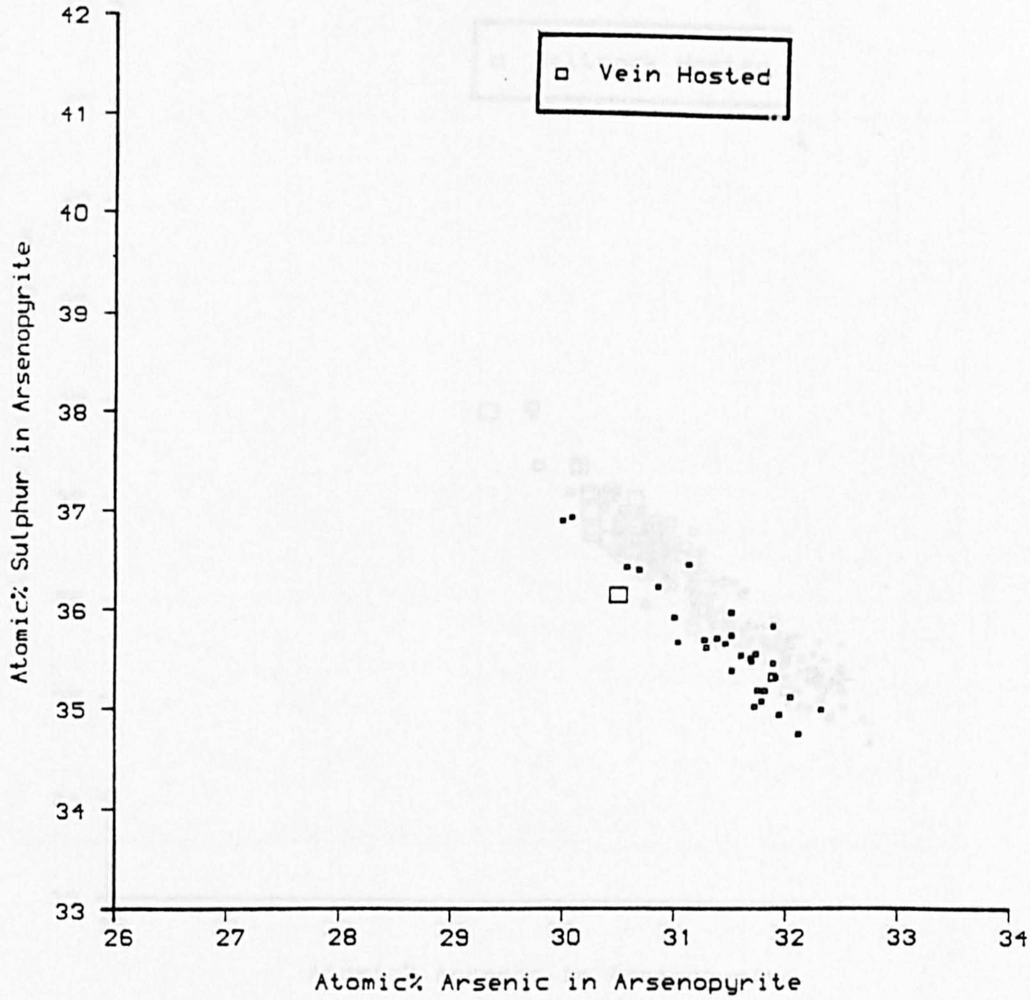

Clontibret Microprobe Study: As-S-Sb

FIGURE 157

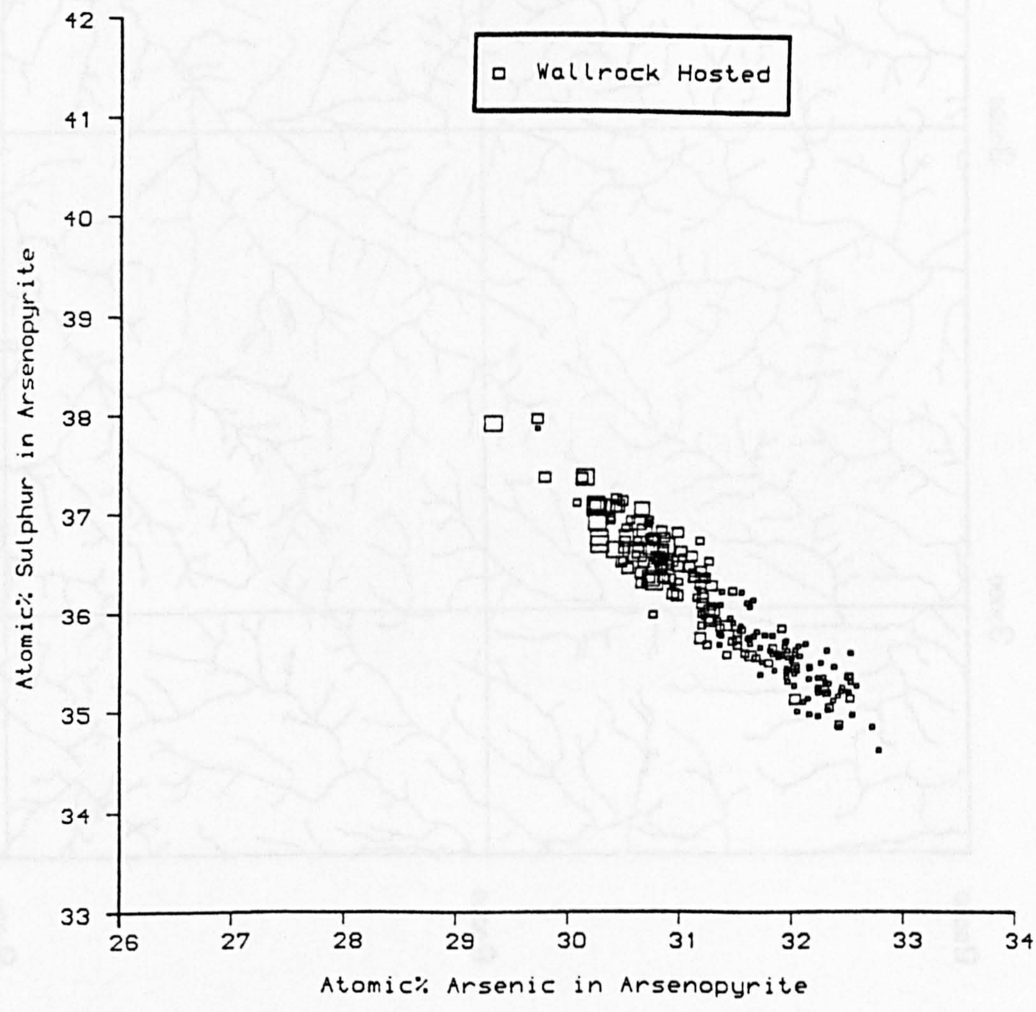

Clontibret Microprobe Study: As-S-Sb

FIGURE 158

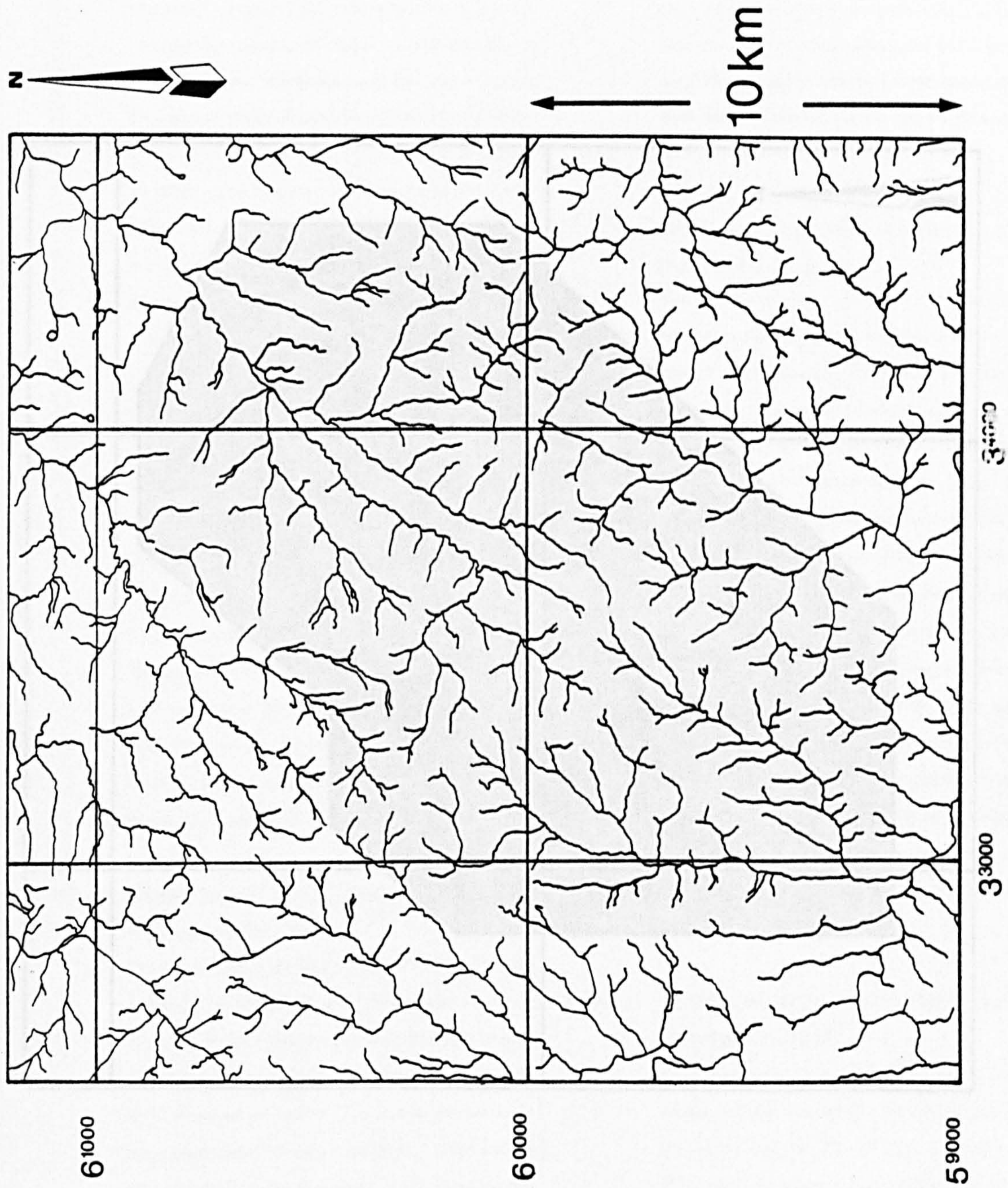

FIGURE 159

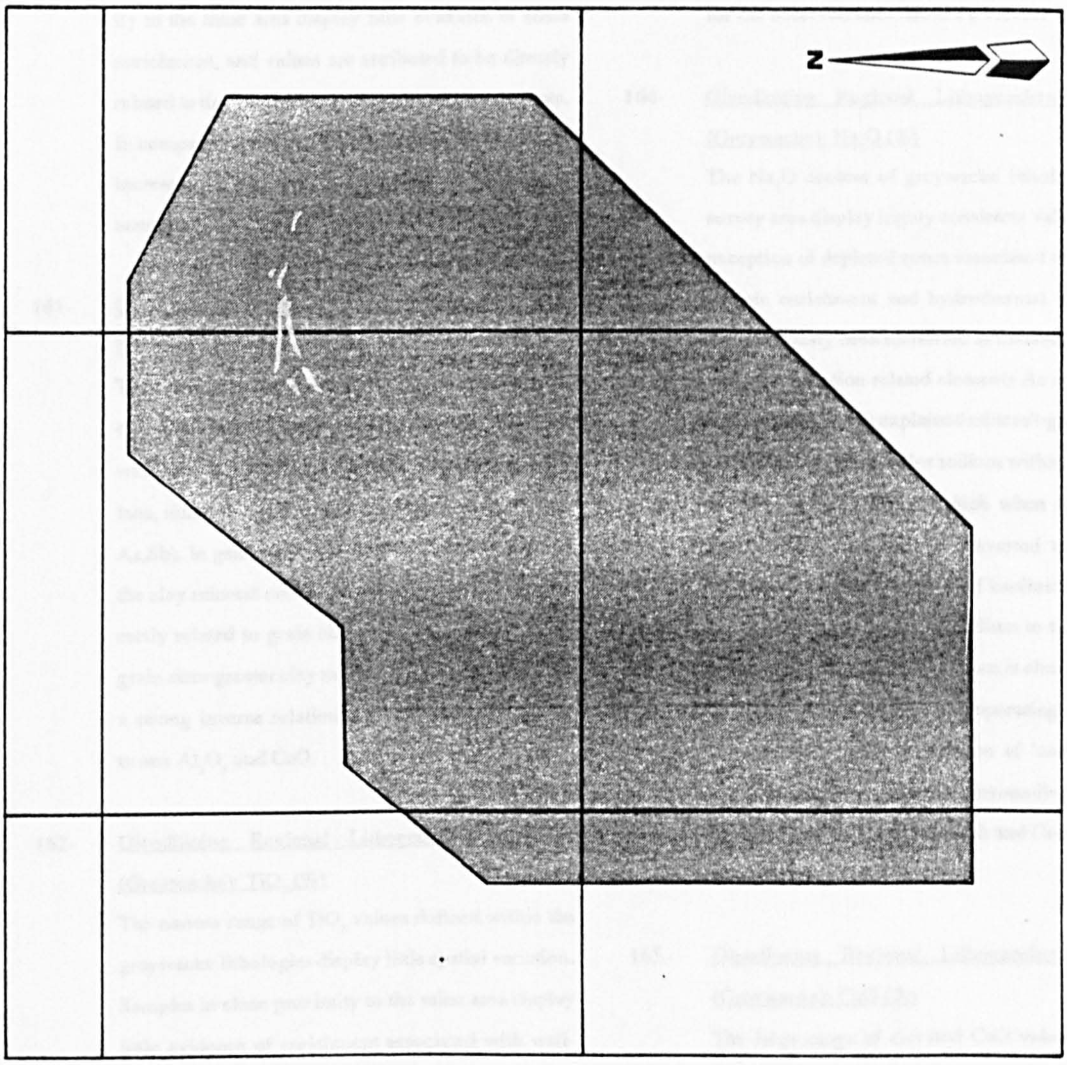

160- Glendinning Regional Lithogeochemical Atlas (Greywacke): SiO_2 (%)

The small range of SiO_2 values located in Hawick Formation greywacke lithologies display little spatial variation with relatively uniform silica values throughout this succession. Samples in close proximity to the mine area display little evidence of silica enrichment, and values are attributed to be directly related to the detrital quartz content of the sediments. In comparison with mudstone lithologies (fig.190) a increase of 4-5wt% is observed in greywacke samples.

161- Glendinning Regional Lithogeochemical Atlas (Greywacke): Al_2O_3 (%)

The alumina values defined on this point source geochemical map display little systematic variation within the study area and bear little relation to anomalous, mineralisation related trace element values (ie. As,Sb). In general, values may be directly related to the clay mineral content of the greywacke, and indirectly related to grain size of the samples (ie. finer grain size=greater clay mineral content). In addition, a strong inverse relationship may be observed between Al_2O_3 and CaO.

162- Glendinning Regional Lithogeochemical Atlas (Greywacke): TiO_2 (%)

The narrow range of TiO_2 values defined within the greywacke lithologies display little spatial variation. Samples in close proximity to the mine area display little evidence of enrichment associated with wall-rock alteration processes. The close correlation observed between TiO_2 MgO and Fe_2O_3 values may be directly related to the detrital ferromagnesian mineral content of the sediments.

163- Glendinning Regional Lithogeochemical Atlas (Greywacke): Fe_2O_3 (%)

The wide range of Fe values displayed by greywacke lithologies are generally lower than their mudstone counter parts and display little systematic variation throughout the survey area. However, anomalous values (>95%) are closely related to sites of anomalous As and Sb values including Black Syke, Rams Cleuch and Wisp Hill. This pattern is also reflected, albeit to a lesser extent within mudstone lithologies (Fig. 193). Although three main sources of iron have been identified within the greywacke (ferromagnesian minerals, Fe-rich carbonates and iron bearing sulphides) sulphidation processes associated with hydrothermal alteration are deemed to be responsible for the observed anomalous Fe values.

164- Glendinning Regional Lithogeochemical Atlas (Greywacke): Na_2O (%)

The Na_2O content of greywacke lithologies in the survey area display highly consistent values with the exception of depleted zones associated with areas of arsenic enrichment and hydrothermal activity. Na has previously been identified as inversely related to the mineralisation related elements As and Sb. This relationship may be explained mineralogically, as the dominant host mineral for sodium within these greywacke is sodic feldspar, which when subjected to hydrothermal alteration is converted to dickite (a high temperature polymorph of kaolinite) and water together with the release of sodium to the aqueous phase. As such, sodium depletion is characteristic of the mineralisation processes operating within this area. Note the relative position of 'sodium holes' displayed on the contour plot surrounding the Glendinning, Swin Gill, Rams Cleuch and Greatmoor Hill anomaly sites.

165- Glendinning Regional Lithogeochemical Atlas (Greywacke): CaO (%)

The large range of elevated CaO values identified within Hawick Formation greywackes in this study area result from an the addition of a major detrital carbonate component. This component displays a strong antipathetic relationship with SiO_2 (a 'closure' effect). The high carbonate content within the greywackes masks the subtle effects of CaO enrichment associated with hydrothermal alteration. Note that the contour plot details a slight increase in CaO levels in the south western portion of the study area.

166- Glendinning Regional Lithogeochemical Atlas (Greywacke): MgO (%)

MgO values defined on the point source geochemical map display highly uniform contents with little sys-

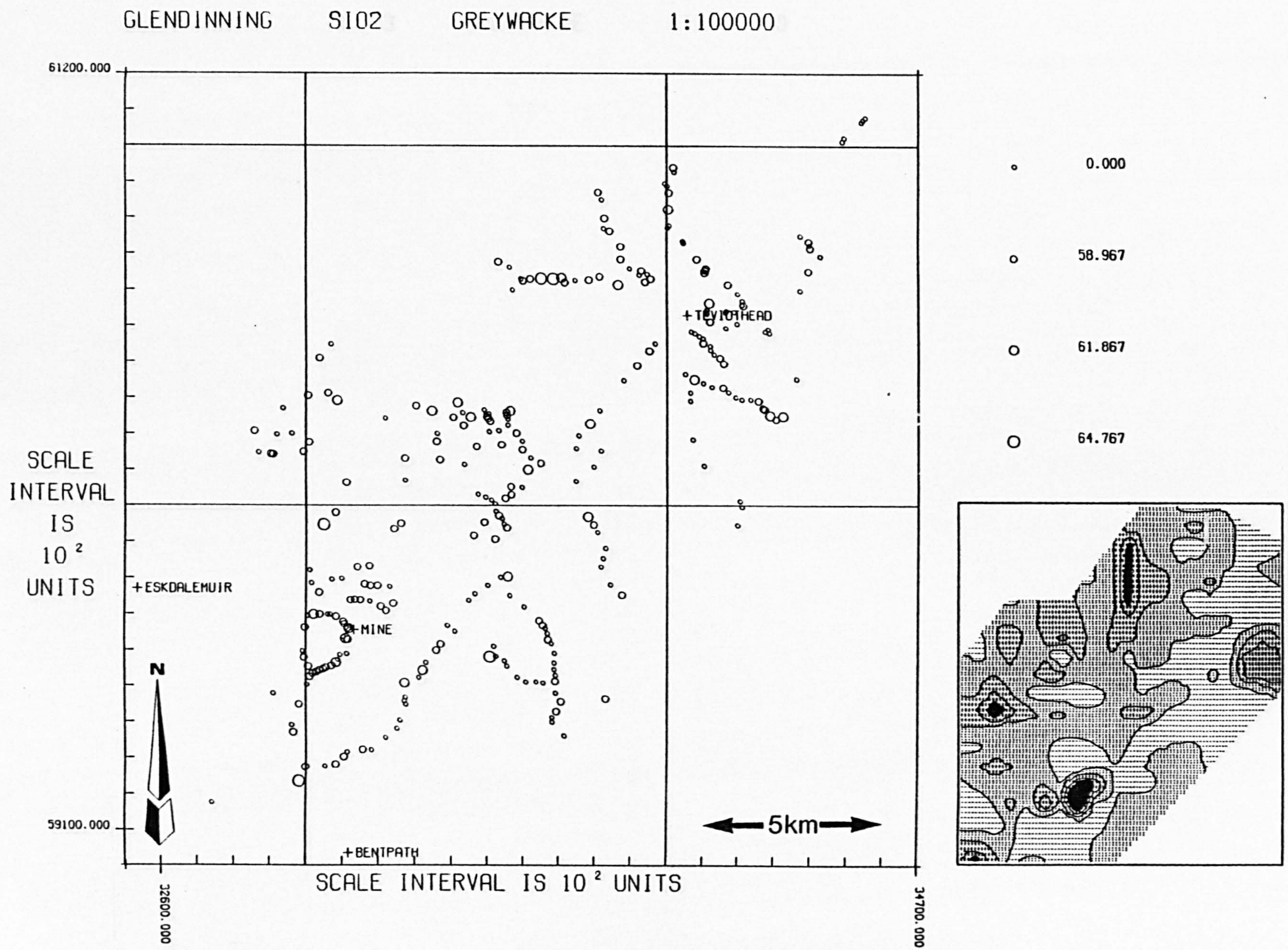
GLENDINNING SIO2 GREYWACKE 1:100000
61200.000
59100.000
SCALE INTERVAL IS 10 ² UNITS
+ESKDALEMUIR
+TEVIOTHEAD
+MINE
+BENTPATH
N
5km
SCALE INTERVAL IS 10 ² UNITS
3260.000
3470.000
0.000
58.967
61.867
64.767

FIGURE 160

FIGURE 161

GLENDINNING AL203 GREYWACKE 1:100000

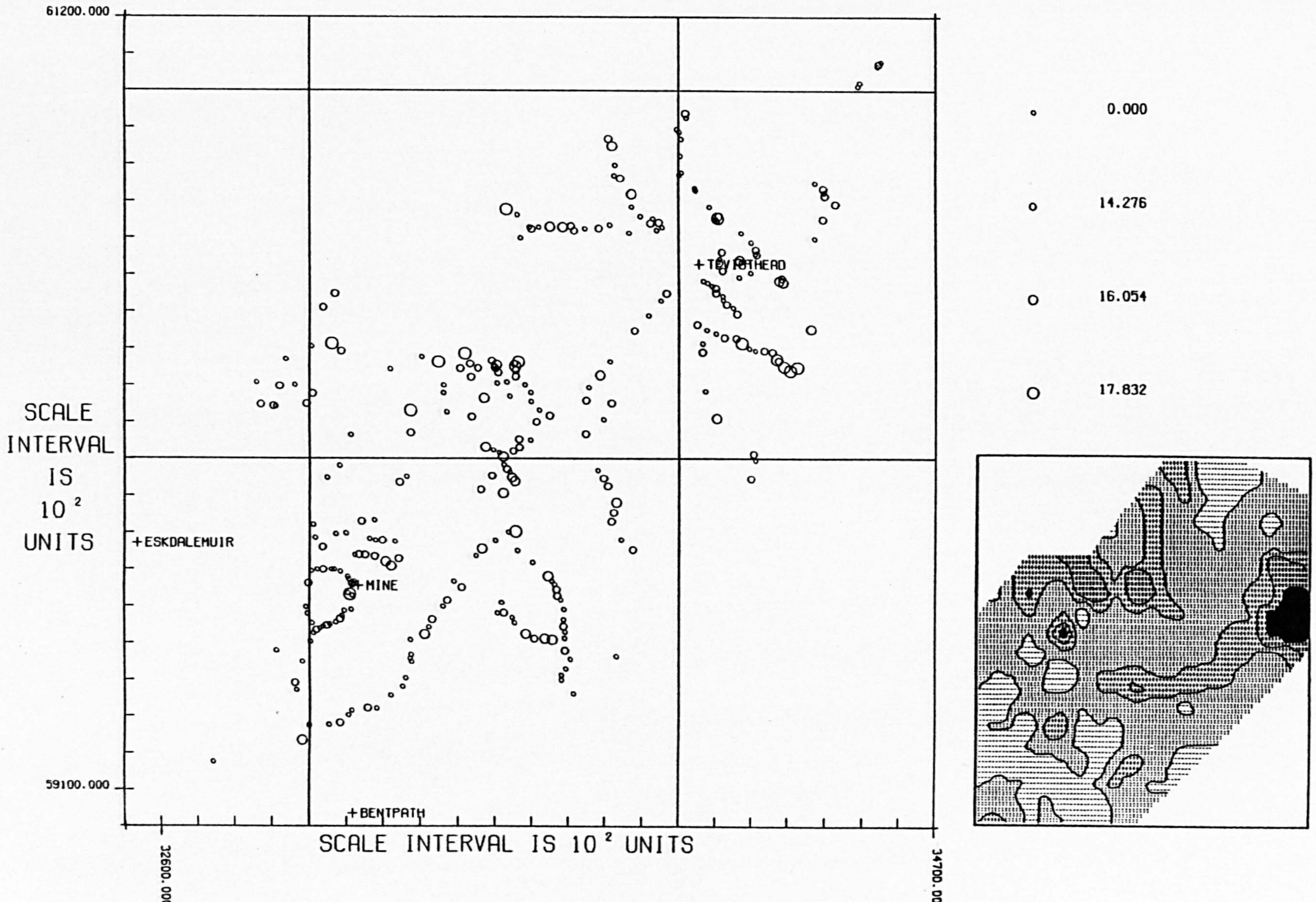

GLENDINNING TI02 GREYWACKE 1:100000

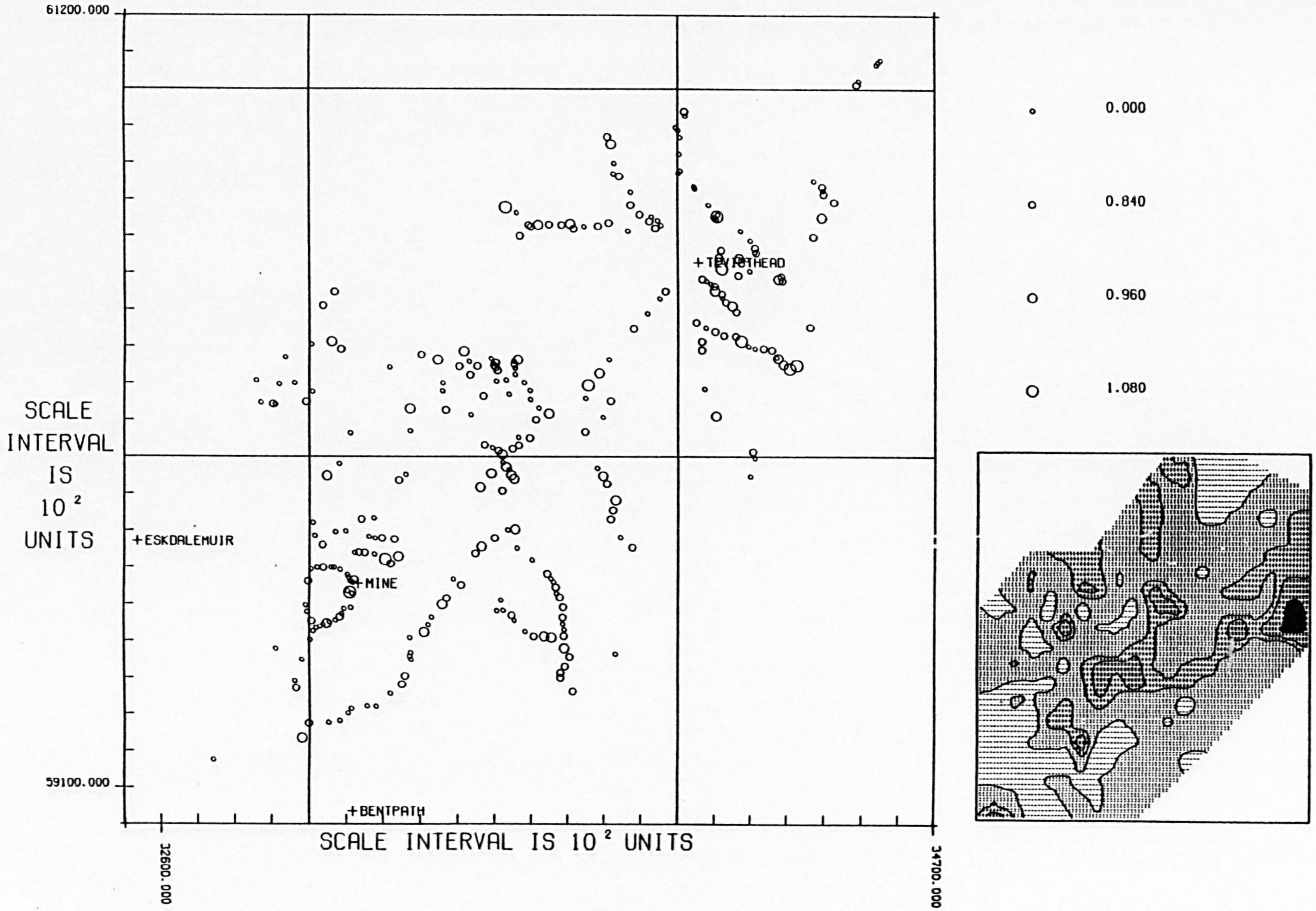

FIGURE 162

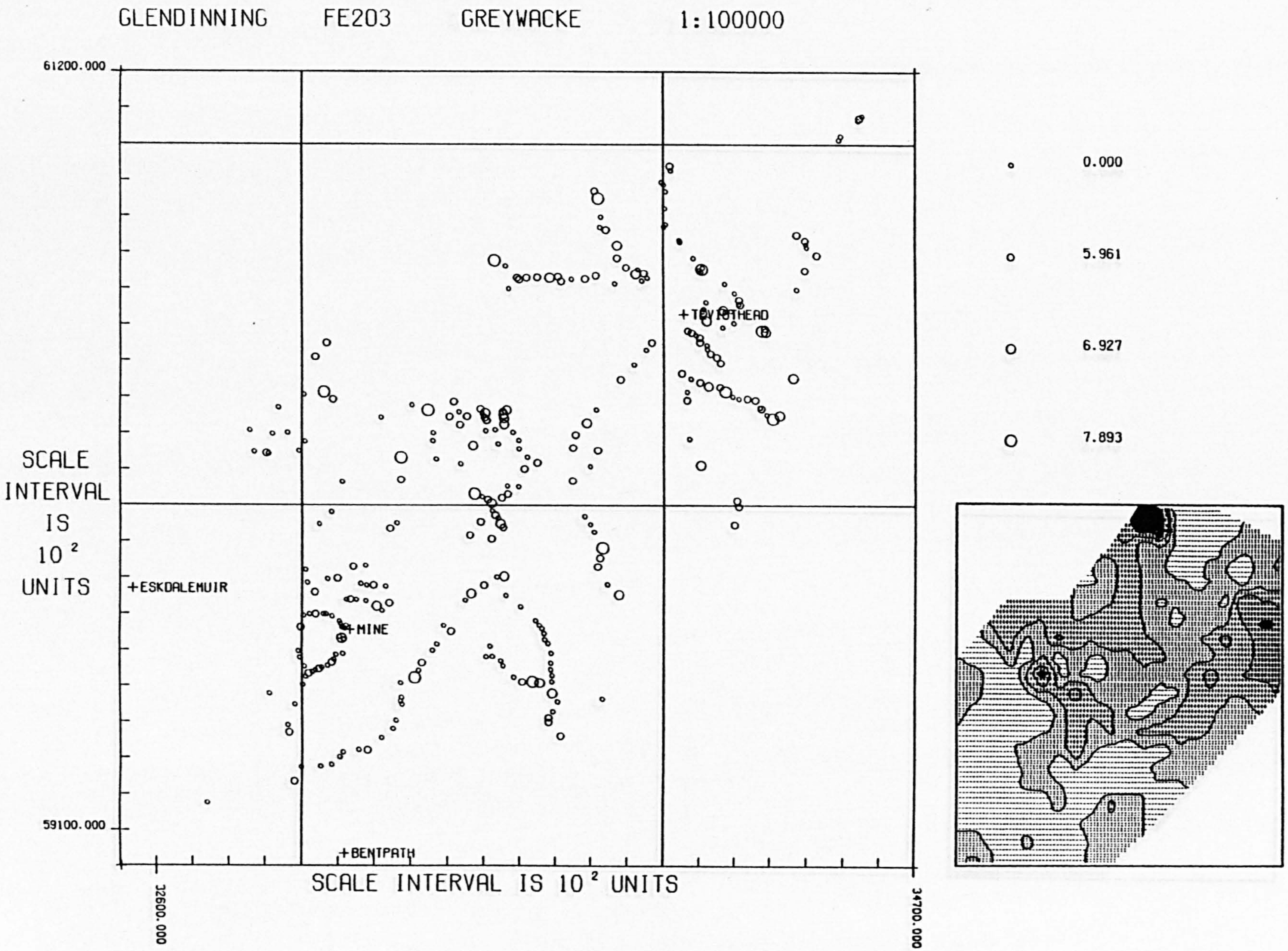
GLENDINNING FE203 GREYWACKE 1:100000
61200.000
59100.000
SCALE INTERVAL IS 10 ² UNITS
SCALE INTERVAL IS 10 ² UNITS
32600.000
34700.000
+ESKDALEMUIR
+MINE
+BENTPATH
+TEVIOTHEAD
0.000
5.961
6.927
7.893

FIGURE 163

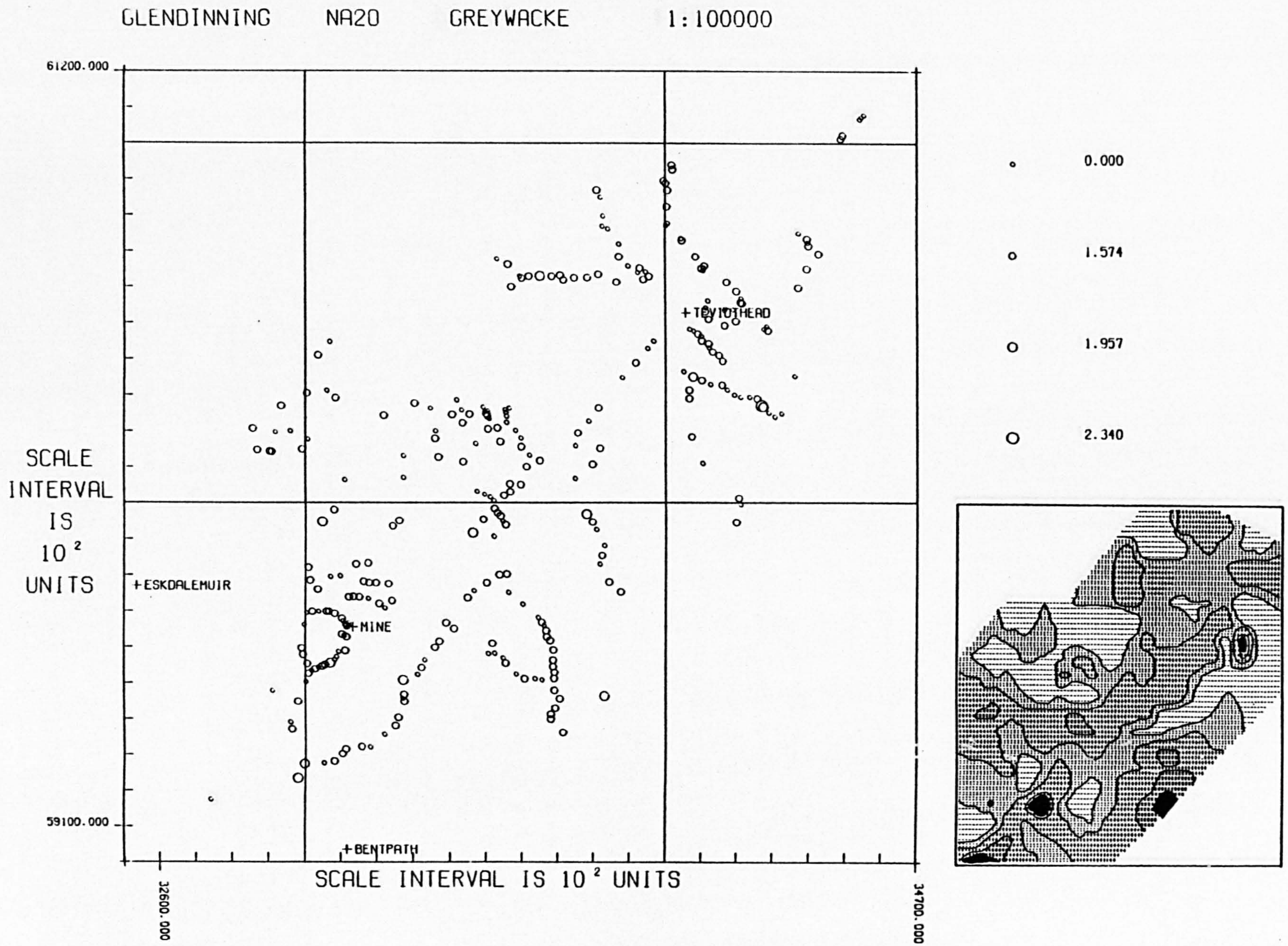
GLENDINNING NA20 GREYWACKE 1:100000
61200.000
59100.000
32600.000
34700.000
SCALE INTERVAL IS 10 ² UNITS
SCALE INTERVAL IS 10 ² UNITS
+TEVIOTHEAD
+ESKDALEMUIR
+MINE
+BENTPATH
0.000
1.574
1.957
2.340

FIGURE 164

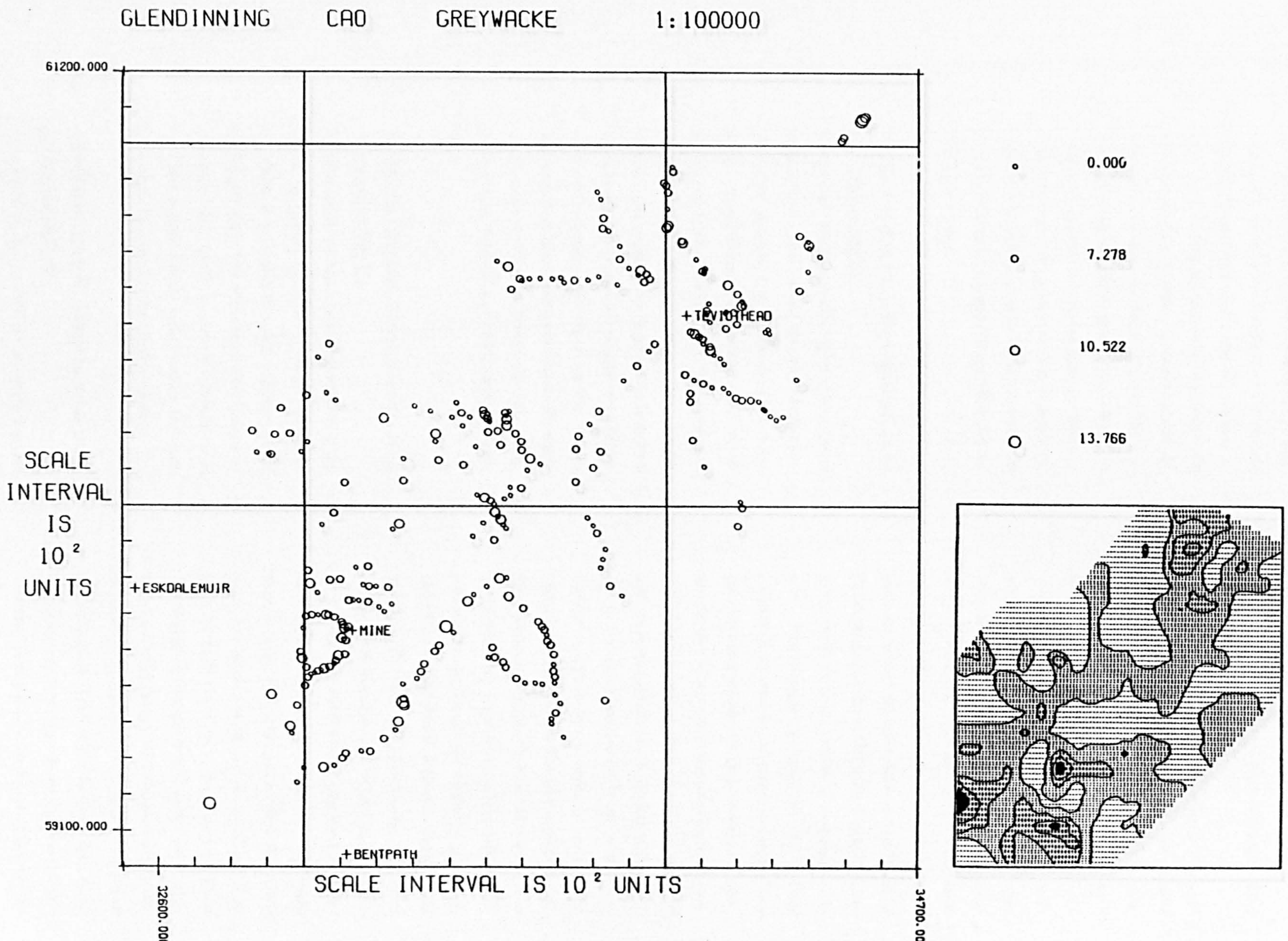
GLENDINNING CAO GREYWACKE 1:100000
61200.000
59100.000
3600.000
3700.000
SCALE INTERVAL IS 10 2 UNITS
SCALE INTERVAL IS 10 2 UNITS
+ESKDALEMUIR
+MINE
+BENTPATH
+TEVIOTHEAD
0.000
7.278
10.522
13.766

FIGURE 166

GLENDINNING MGO GREYWACKE 1:100000

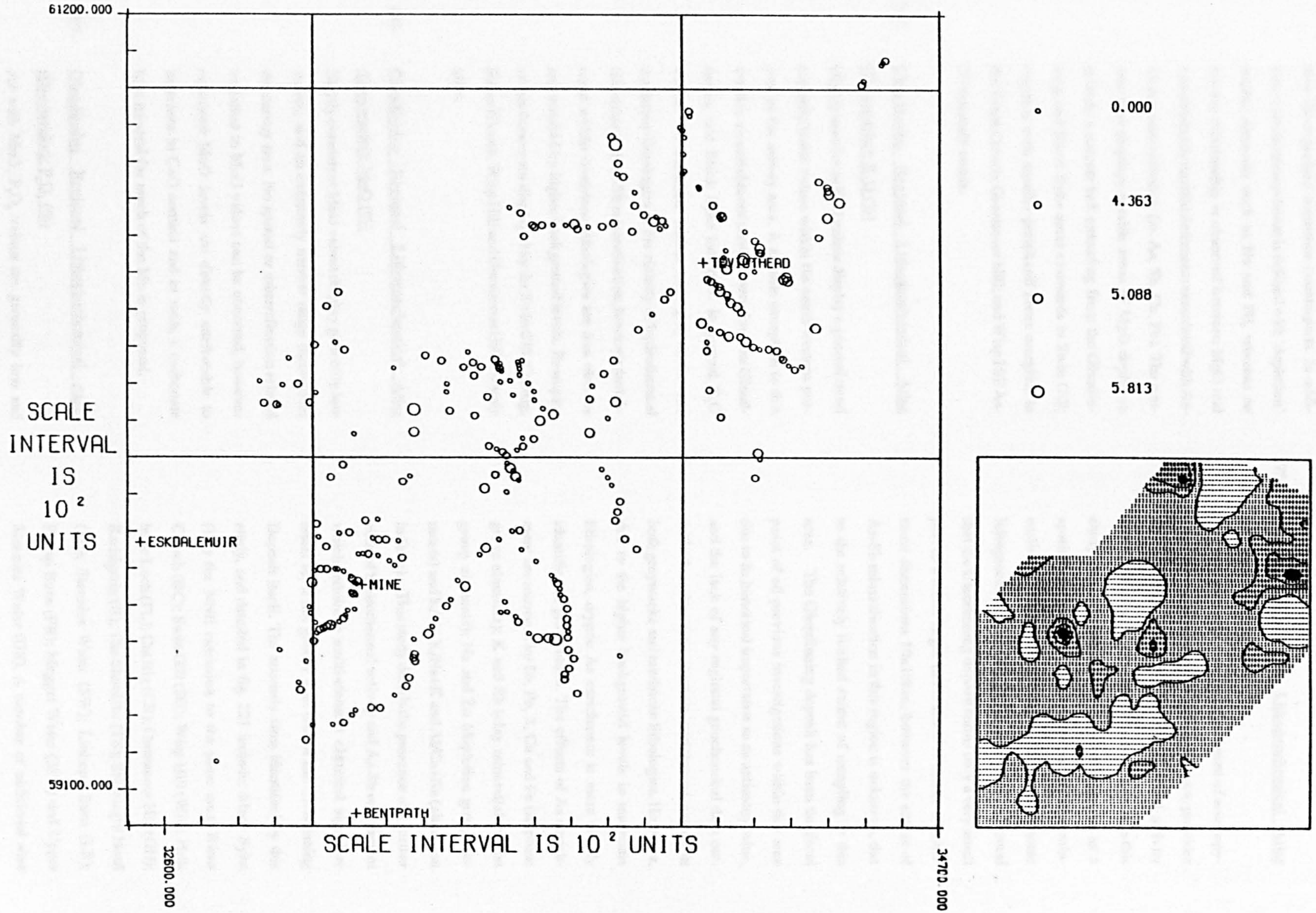

tematic variation within the study area. MgO values display a relatively restricted range compared with their finer grained mudstone counterparts. In addition, a positive correlation is defined with 'depletion' related elements such as Na and FE, whereas an inverse relationship is observed between MgO and hyrothermally enriched elements associated with As-Sb-Au mineralisation (ie. As, Sb, Cu, Pb). The contour plot displays notable areas of MgO depletion include a narrow belt extending from the Glendinning and Black Syke areas eastwards to Swin Gill; together with smaller peripheral zones marginal to the Rams Cleuch; Greatmoor Hill; and Wisp Hill As-Sb anomaly zones.

167- Glendinning Regional Lithogeochemical Atlas (Greywacke): K_2O (%)

Highly consistent K_2O values display a general trend towards lower values within the south western portion of the survey area. A notable exception to this trend is an enrichment zone surrounding the Glendinning and Black Syke localities. In general K_2O values are enriched within both greywacke and mudstone lithologies in the vicinity of hydrothermal alteration and As-Sb mineralisation, however enrichment within mudstone lithologies are less obvious and masked by higher background levels. Examples of this feature are displayed by the Swin Gill, Cat Rig, Rams Cleuch, Wisp Hill and Greatmoor Hill anomaly sites.

168- Glendinning Regional Lithogeochemical Atlas (Greywacke): MnO (%)

Highly consistent MnO values display generally low values, and an extremely narrow range throughout the survey area. No spatial or mineralisation related variation in MnO values can be observed, however enhanced MnO levels are directly attributable to increases in CaO content and as such, a carbonate host mineral for much of the Mn is proposed.

169- Glendinning Regional Lithogeochemical Atlas (Greywacke): P_2O_5 (%)

As with MnO, P_2O_5 values are generally low and display an extremely restricted (virtually constant) range of values throughout the survey area. A relatively broad, strike parallel belt of 'elevated' values, trending NE-SW is defined within the contour plot.

170- Glendinning Regional Lithogeochemical Atlas (Greywacke): As (ppm).

Arsenic, the main 'pathfinder' element of arsenopyrite hosted gold mineralisation in this area, provides an extremely useful guide to hydrothermal activity and As-Sb mineralisation in this area. Previous to this study the Glendinning deposit was regarded as a spatially isolated deposit, distant from all other mineralisation centres in the Southern Uplands. Arsenic lithogeochemical studies in this area however, reveal that the Glendinning deposit forms only a very small part of a much larger mineralisation center of minimum dimensions 10x10km, however the extent of As-Sb mineralisation in this region is unknown, due to the relatively limited extent of sampling in this area. The Glendinning deposit has been the focal point of all previous investigations within this area due to its historical importance as an antimony mine, and the lack of any regional geochemical data outwith the mine area. Arsenic enrichment occurs in both greywacke and mudstone lithologies. However, due to the higher background levels in mudstone lithologies, cryptic As enrichment is more clearly identified in greywackes. The effects of As enrichment are mirrored by Sb, Pb, S, Cu and Fe (sulphide group elements); K and Rb (clay mineral/alteration group elements); Na and Zn (depletion group elements) and K/Na, K/Na+K and Al/Ca+Na (alteration indices). This study details the presence of 8 further sites of hydrothermal activity and As-Sb enrichment which exhibit a multi-element chemical signature equal to, if not greater than that of the Glendinning Deposit itself. The anomaly sites identified by this study, and detailed in fig. 221 include: Black Syke (BS) the NNE extension to the mine area; Rams Cleuch (RC); Swin Gill (SG); Wisp Hill (WH); Philhope Loch (PL); Cat Rig (CR); Greatmoor Hill (GH); Rashigrain (R); The Shoulder (TS); Stibbiegill Head (SH); Stennies Water (SW); Linhope Burn (LB); Phaup Burn (PB); Meggat Water (MW) and Upper Stennies Water (US). A number of additional sites sites have been located which exhibit evidence of alteration and/or weak mineralisation. Grid refer-

GLENDINNING K20 GREYWACKE 1:100000

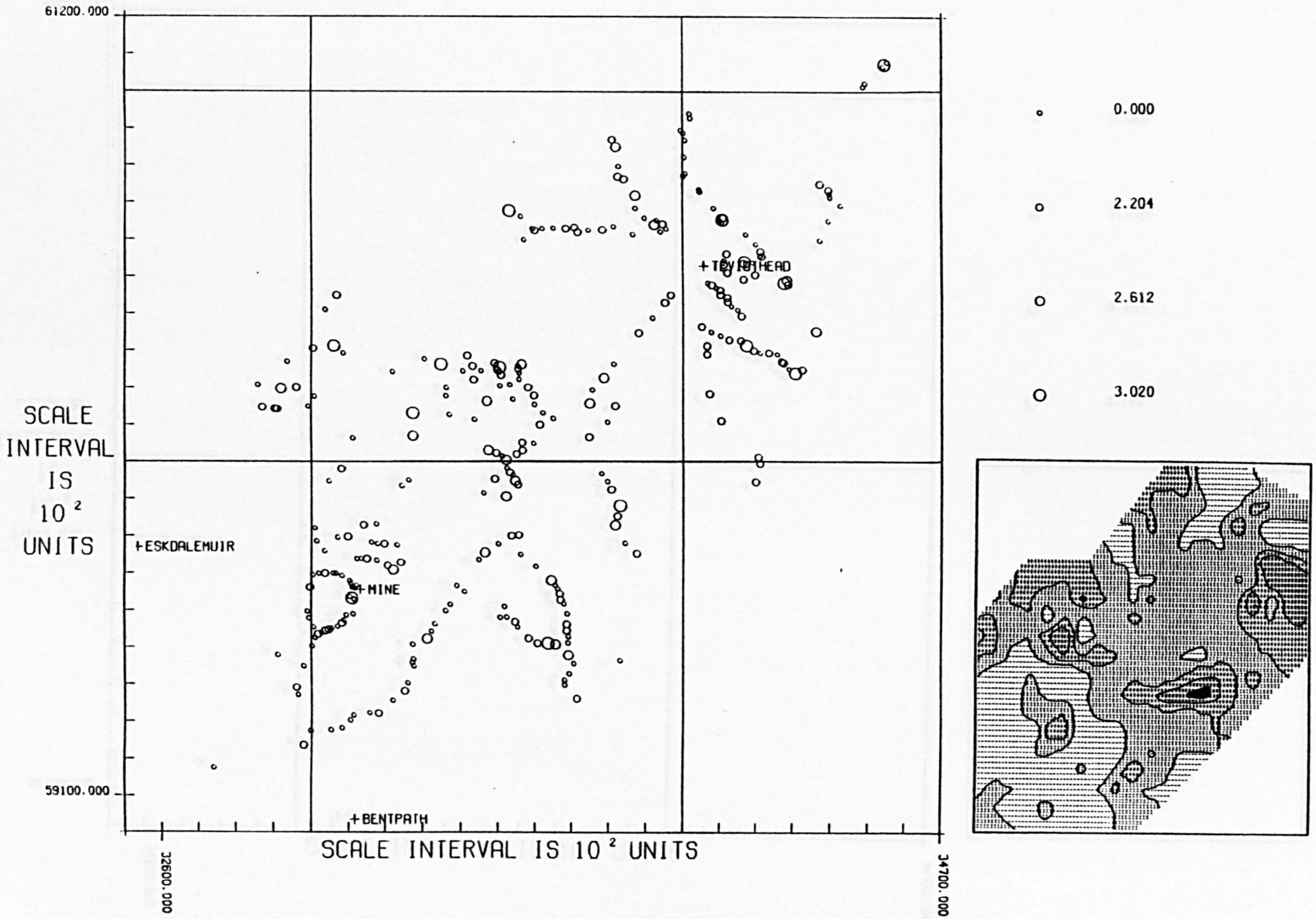

FIGURE 167

FIGURE 168

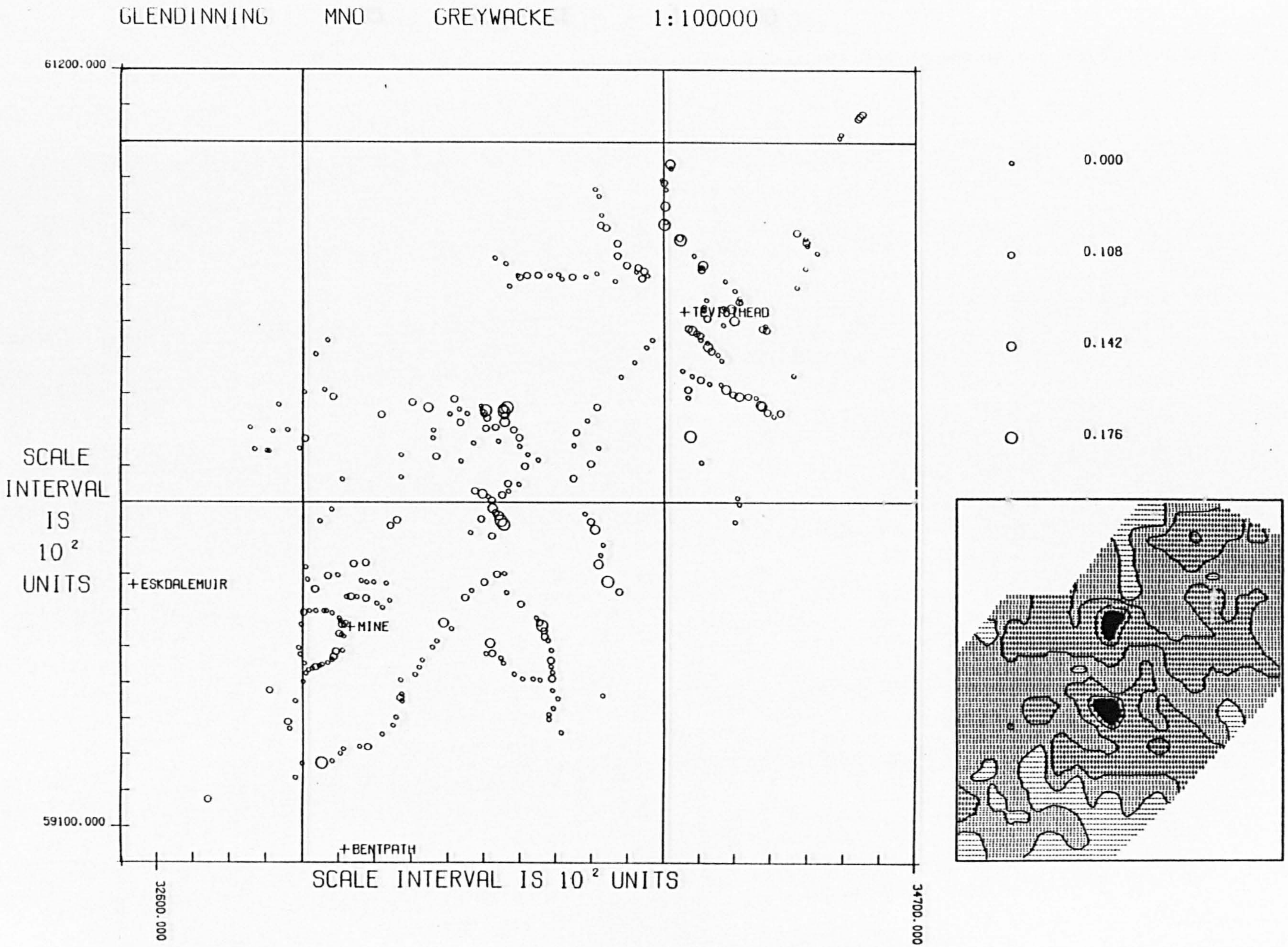
GLENDINNING MNO GREYWACKE 1:100000
61200.000
59100.000
32600.000
34700.000
SCALE INTERVAL IS 10 ² UNITS
SCALE INTERVAL IS 10 ² UNITS
+ESKDALEMUIR
+MINE
+BENTPATH
+TEVIOTHEAD
0.000
0.108
0.142
0.176

GLENDINNING P205 GREYWACKE 1:100000

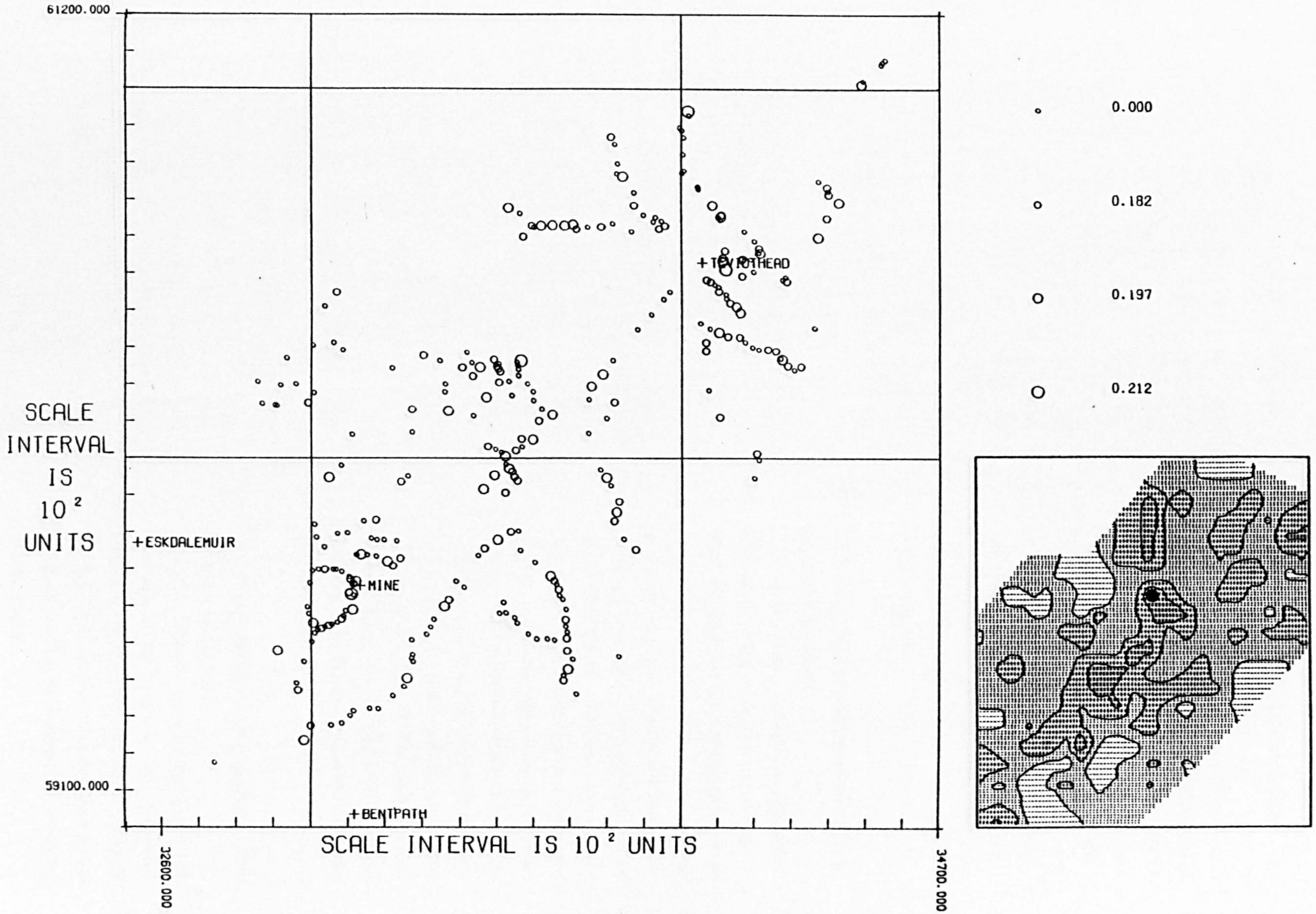

FIGURE 169

GLENDINNING ARSENIC GREYWACKE 1:100000

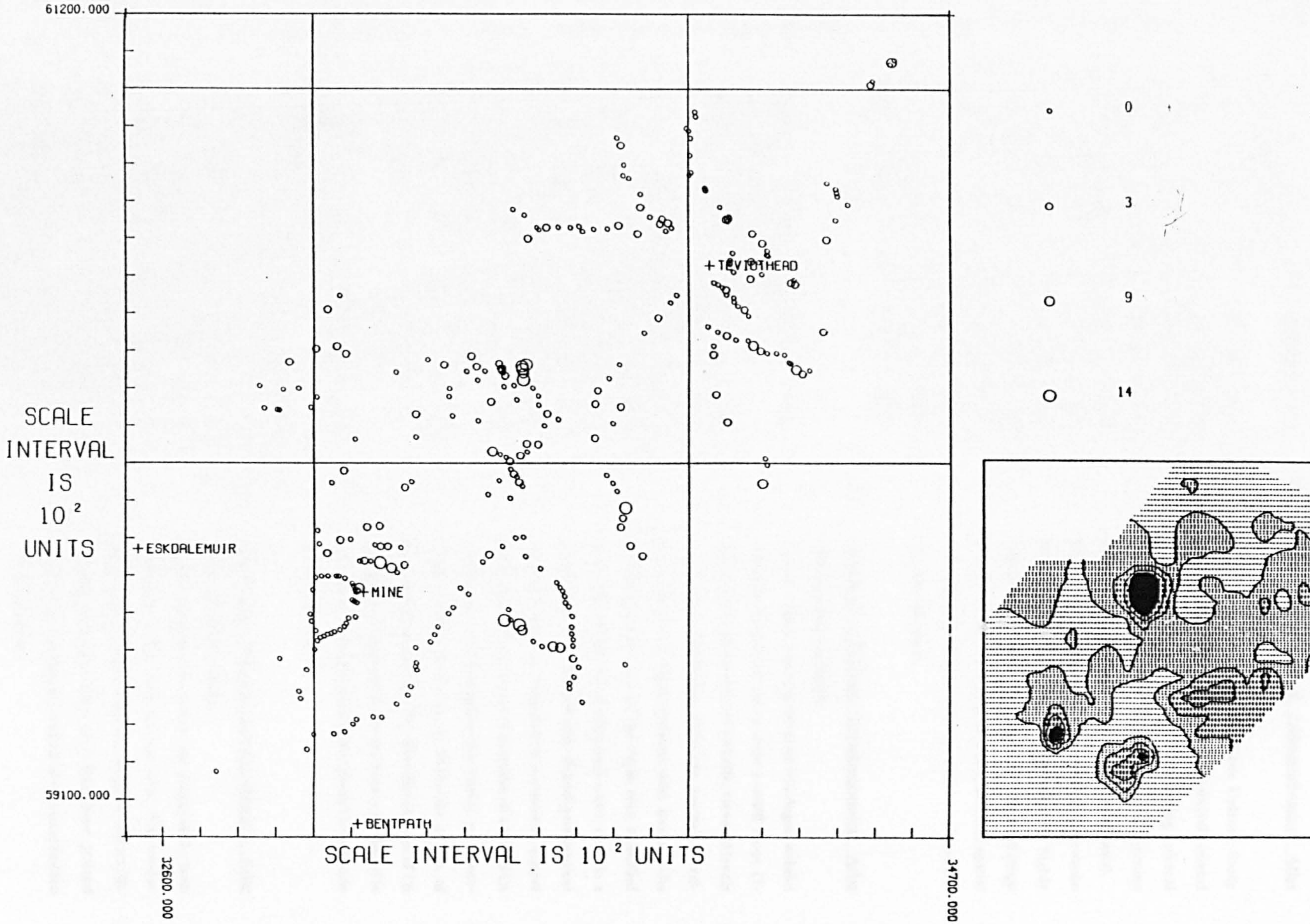

FIGURE 170

ences and element signitures relating to the above sites are detailed in tables 1.37, 1.38 and 1.39.

171- Glendinning Regional Lithogeochemical Atlas (Greywacke): Ba (ppm).

Barium displays relatively consistent values throughout the survey area with a general trend towards increasing values in the southeastern half of the study area. Greywacke samples display a relatively restricted range of values compared with their finer graine mudstone counter parts. Anomalous Ba values correlate well with zones of arsenic enrichment, particularly in greywacke lithologies. The presence of low grade Pb-Zb-Ba mineralisation in this region forms the most probable source of Ba enrichment observed in a small number of samples (max: 912ppm Ba) unrelated to As-Sb-Au mineralisation in the survey area.

172- Glendinning Regional Lithogeochemical Atlas (Greywacke): Cl (ppm).

Elevated Cl values are located in both the northern and southern sections of the survey area with a broad belt of relatively restricted values occupying the central portion of this area. Slightly elevated Cl values are associated with both the Glendinning Mine, Swin Gill and Rams Cleuch areas however the problems of Cl contamination during sample preparation invalidate the use of this data in any form of fundamental geochemical model of mineralisation.

Following this initial evaluation, Cl was removed from the analysis list and is not discussed further.

173- Glendinning Regional Lithogeochemical Atlas (Greywacke): Co (ppm).

Co values defined on the point source geochemical map display highly consistent values and a strong systematic variation within the study area. Although Co values display a restricted range (11-66ppm), anomalous values may be positively correlated with arsenic enrichment and areas of hydrothermal activity. Individual sites of Co enrichment include Glendinning, Black Syke, Swin Gill and Rams Cleuch. The trend towards high Co values throughout all samples collected within Stennies Water, to the east of the mine area is as yet unexplained, however it does result in the development of a major anomaly zone in the south western corner of the contour map.

174- Glendinning Regional Lithogeochemical Atlas (Greywacke): Cr (ppm).

As observed within the Southern Uplands Study Area, the distribution of Cr values is directly related to the proportion of detrital Cr-bearing mineral phases present within the sample (ie. ferromagnesian minerals, detrital chromite, and mafic lithoclasts).

Within the Glendinning study area both greywacke and mudstone lithologies display similar, highly consistent values; a small, relatively restricted range composition (49-290 ppm) and no systematic spatial relationship with either stratigraphic or mineralisation related trends.

175- Glendinning Regional Lithogeochemical Atlas (Greywacke): Cu (ppm).

Copper values within greywacke lithologies exhibit relatively consistent values over a small range (7-70ppm) as opposed to more variable, elevated levels in mudstone lithologies. Although, anomalous values in both rock types correlate with zones of As enrichment, only two of the eight sites identified above (Wisp Hill and Rashigrain) which contain a mineralised or hydrothermally altered geochemical signature could be identified by anomalous copper values. In addition, however a number of isolated Cu anomalies occur throughout the survey area unrelated to either As-Sb-Au or Pb-Zn-Ba phases of mineralisation (see fig. 221). This distribution of Cu anomalies throughout the survey area is attributed to the widespread occurrence of low grade Cu-dolomite veins in this region.

176- Glendinning Regional Lithogeochemical Atlas (Greywacke): Ga (ppm).

Highly consistent Ga values are displayed by both lithologies within this survey area. Greywackes exhibit an extremely narrow range of values (6-24ppm) somewhat lower than their finer grained counterparts, and display no spatial or mineralisation related variation.

FIGURE 171

GLENDINNING BARIUM GREYWACKE 1:100000

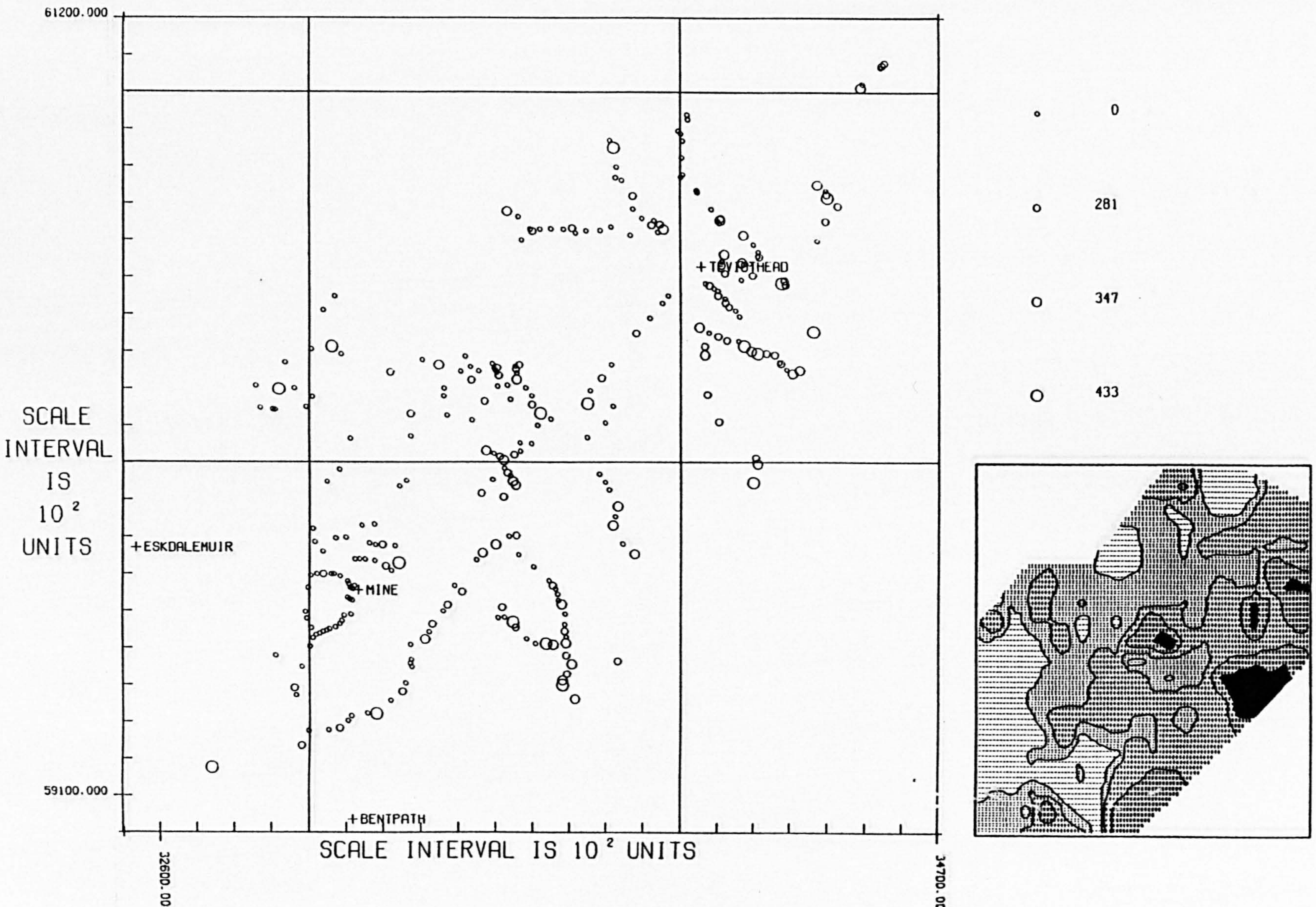

FIGURE 172

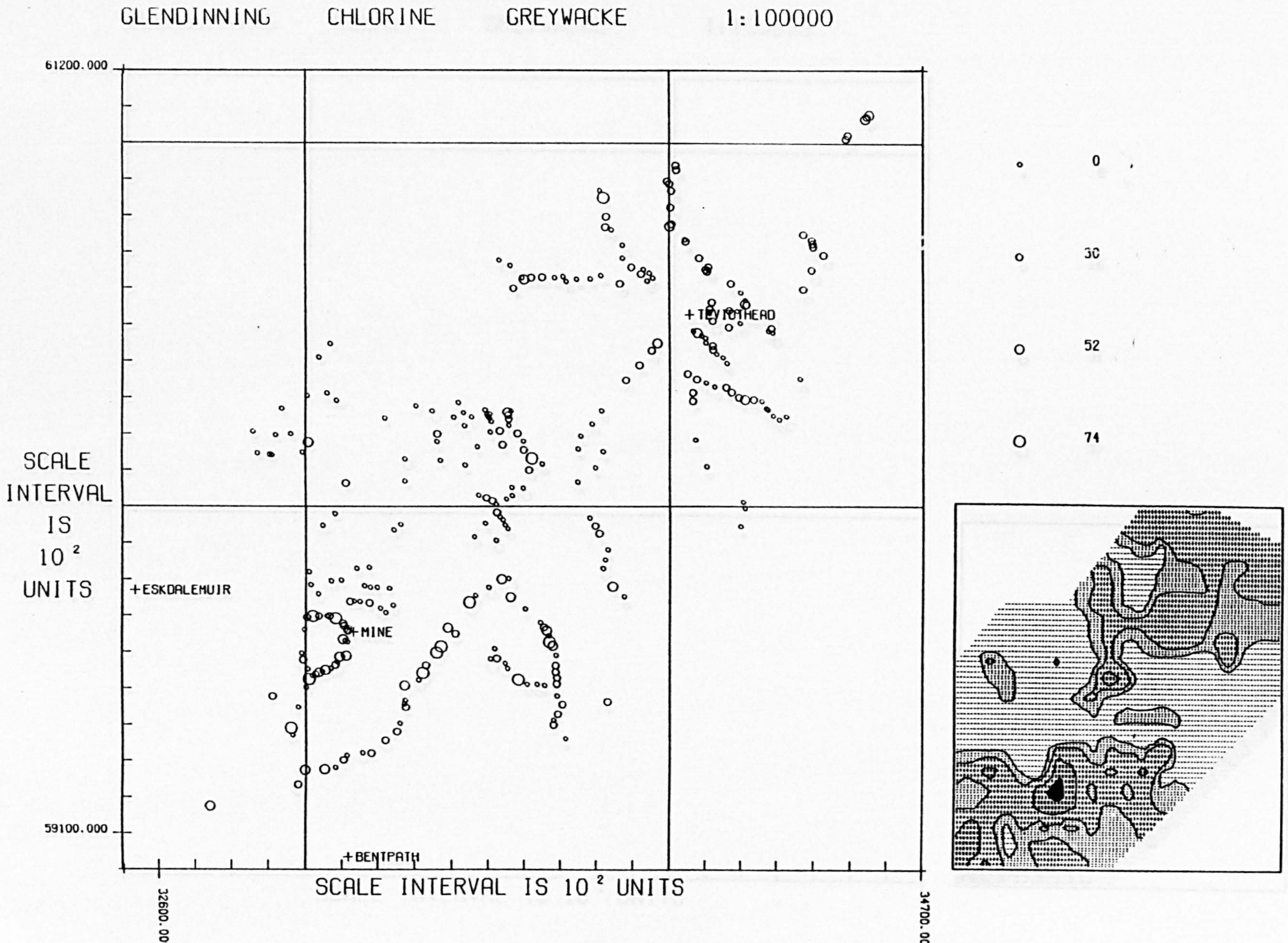
GLENDINNING CHLORINE GREYWACKE 1:100000
61200.000
59100.000
32600.000
34700.000
SCALE INTERVAL IS 10 ² UNITS
SCALE INTERVAL IS 10 ² UNITS
+ESKDALEMUIR
+MINE
+BENTPATH
+TEVIOTHEAD
0
30
52
74

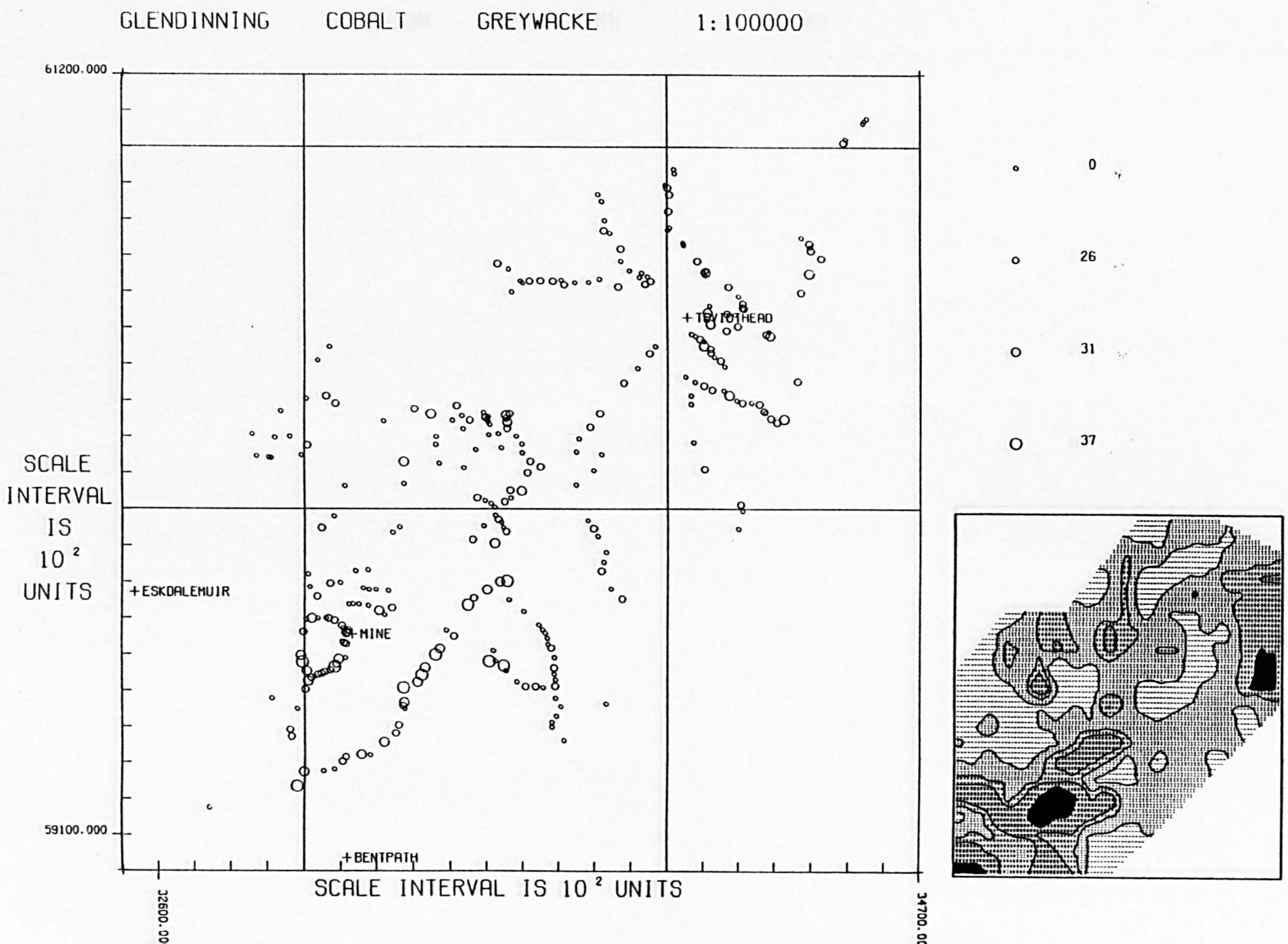
GLENDINNING COBALT GREYWACKE 1:100000
61200.000
59100.000
SCALE INTERVAL IS 10 2 UNITS
+ESKDALEMUIR
+TEVIOTHEAD
MINE
+BENTPATH
SCALE INTERVAL IS 10 2 UNITS
3600.000
3700.000
0
26
31
37

FIGURE 173

FIGURE 174

GLENDINNING CHROMIUM GREYWACKE 1:100000

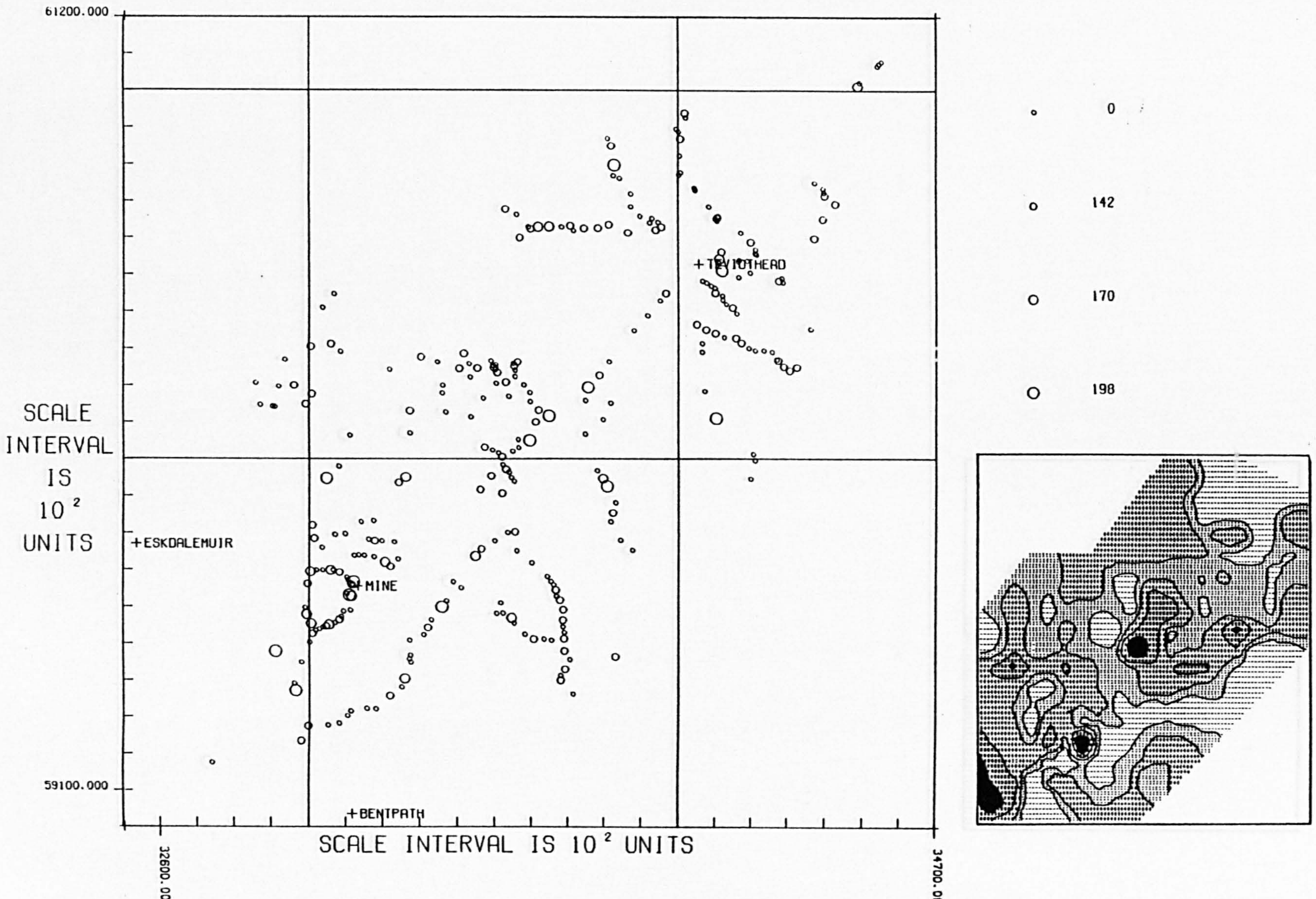

GLENDINNING COPPER GREYWACKE 1:100000

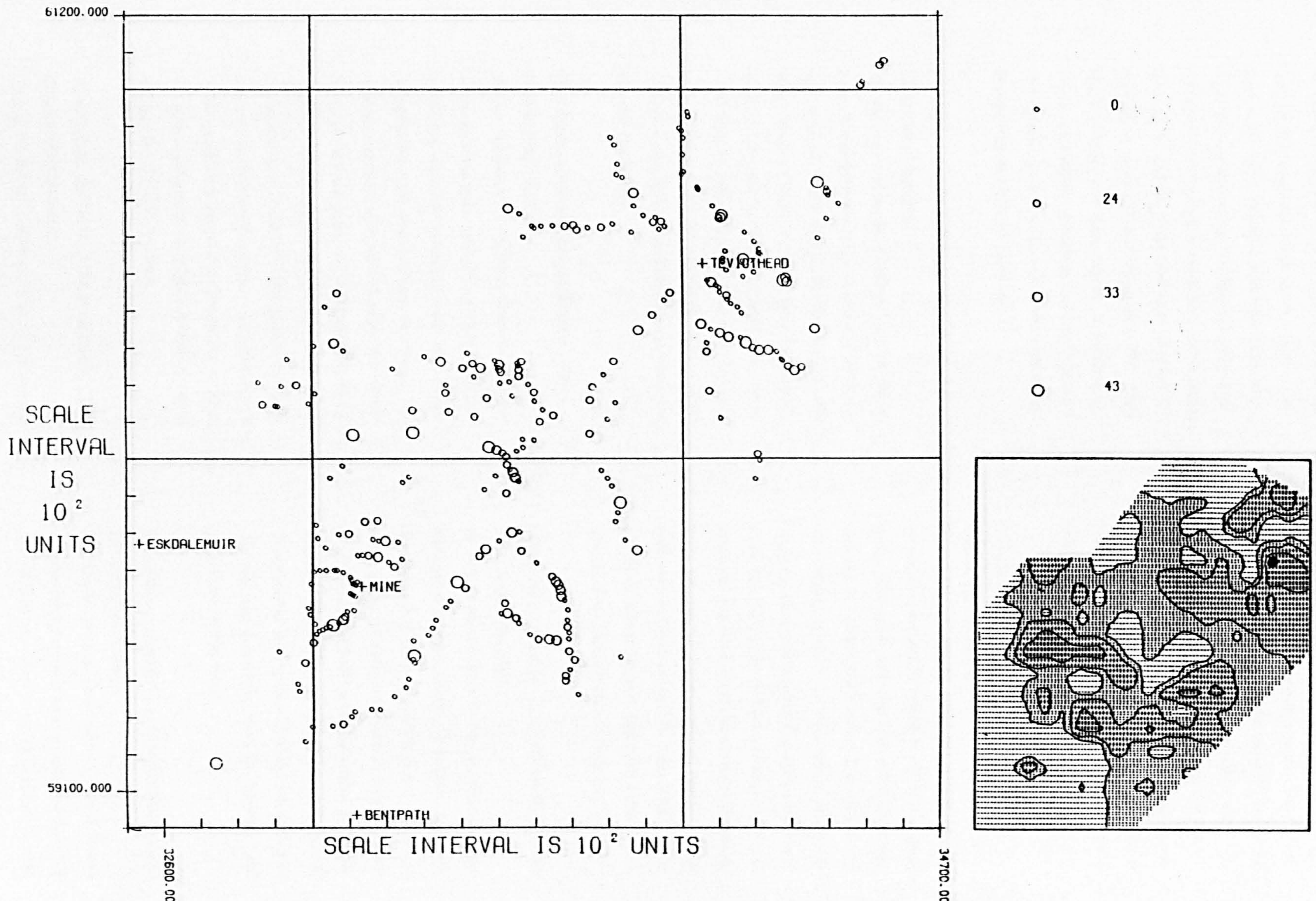

FIGURE 175

FIGURE 176

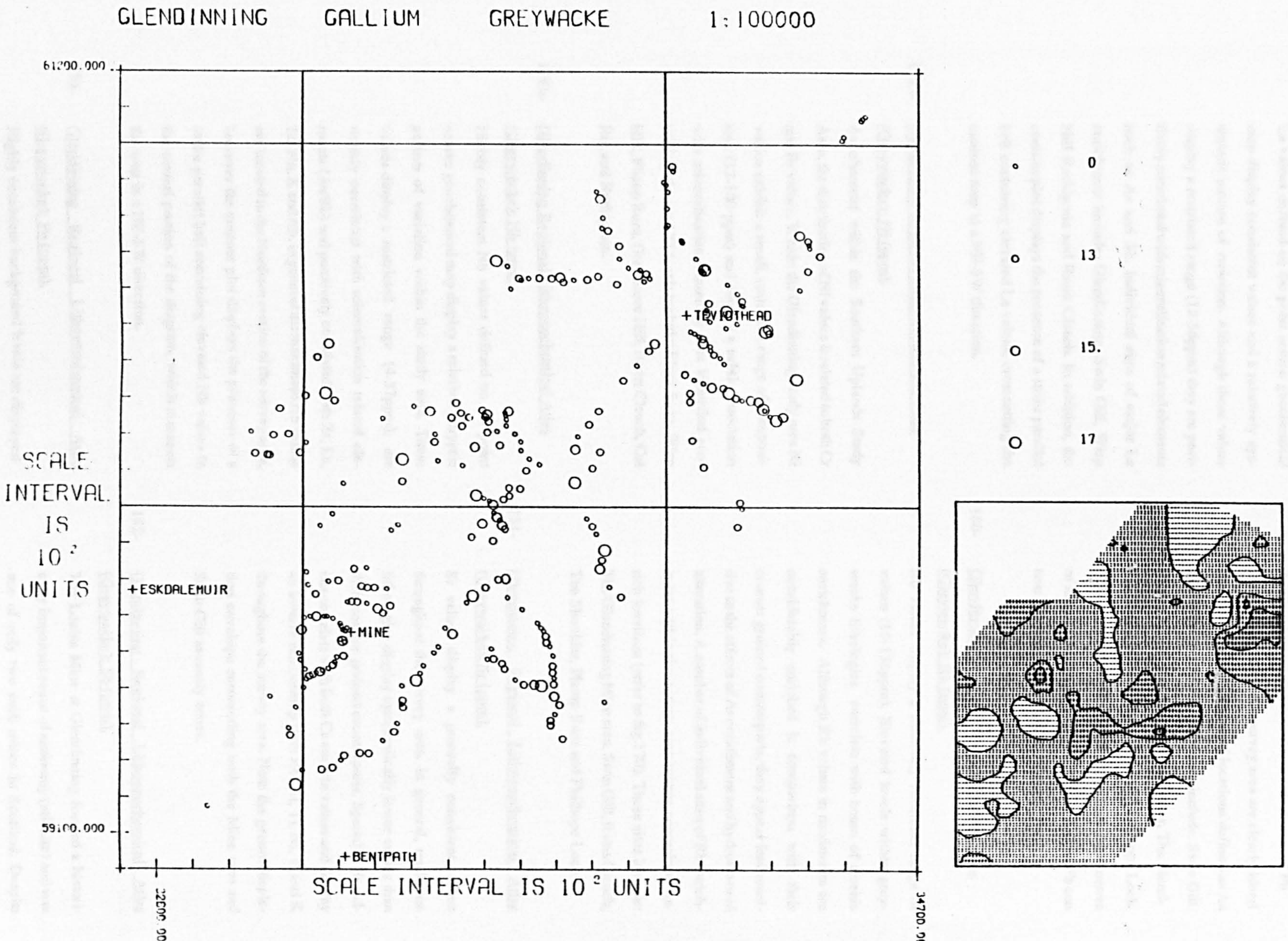
GLENDINNING GALLIUM GREYWACKE 1:100000
61200.000
59100.000
32000.000
34700.000
SCALE INTERVAL IS 10 ² UNITS
SCALE INTERVAL IS 10 ² UNITS
+TEVIOTHEAD
+ESKDALEMUIR
+MINE
+BENTPATH
0
13
15.
17

177- <u>Glendinning Regional Lithogeochemical Atlas (Greywacke): La (ppm).</u>

La values defined on the point source geochemical map display consistent values and a relatively systematic pattern of variation. Although these values display a restricted range (12-56ppm) they are positively correlated with mineralisation related elements such as As and Sb. Individual sites of major La enrichment include: Glendinning, Swin Gill, Wisp Hill Rashigrain and Rams Cleuch. In addition, the contour plot displays the presence of a strike parallel belt containing elevated La values, crosscutting the contour map in a NE-SW direction.

178a- <u>Glendinning Regional Lithogeochemical Atlas (Greywacke): Ni (ppm).</u>

As observed within the Southern Uplands Study Area, the distribution of Ni values is related to both Cr and Fe values. Within the Glendinning study area Ni values exhibit a small, restricted range of composition (12-100 ppm) and display a subtle association with mineralisation. Anomaly sites identified containing elevated Ni levels include: Black Syke, Wisp Hill, Phaup Burn, Greatmoor Hill, Rams Cleuch, Cat Rig and Rashigrain.

178b- <u>Glendinning Regional Lithogeochemical Atlas (Greywacke): Nb (ppm).</u>

Highly consistent Nb values defined on the point source geochemical map display a relatively cryptic pattern of variation within the study area. These values display a restricted range (4-37ppm); are weakly correlated with mineralisation related elements (As/Sb) and positively correlated with Zr, La, Th, Na, K and Rb. In general the maximum Nb values are located in the Northern section of the survey area, however the contour plot displays the presence of a strike parallel belt containing elevated Nb values in the central portion of the diagram, which crosscuts the map in a NE-SW direction.

179- <u>Glendinning Regional Lithogeochemical Atlas (Greywacke): Pb (ppm).</u>

Highly consistent background levels are displayed by both greywacke and mudstone lithologies. Anomalous Pb values are defined on both maps and display a close correlation with both arsenic and copper enrichment. Although these values display a restricted range (0-53ppm) individual sites of Pb enrichment within the survey area are clearly identified and mirror a number of locations defined as As anomalies in fig.170. These sites include: Swin Gill, Rams Cleuch, Cat Rig, Stennies Water, The Shoulder, Linhope Burn, Phaup Burn and Philhope Loch. Note the similarity and relative position of the centres of mineralisation highlighted on both As and Pb contour plots.

180- <u>Glendinning Regional Lithogeochemical Atlas (Greywacke): Rb (ppm).</u>

Rb values display a relatively restricted range of values (15-136ppm). Elevated levels within greywacke lithologies correlate with zones of arsenic enrichment. Although Rb values in mudstones are considerably enriched in comparison with their coarser grained counterparts, they appear less sensitive to the effects of As enrichment and hydrothermal alteration. A number of individual sites of Rb enrichment within the survey area mirror anomalous As-rich locations (refer to fig.170). These sites include: The Glendinning Mine area, Swin Gill, Rams Cleuch, The Shoulder, Phaup Burn and Philhope Loch.

181- <u>Glendinning Regional Lithogeochemical Atlas (Greywacke): Sr (ppm).</u>

Sr values display a generally consistent values throughout the survey area. In general, mudstone lithologies display systematically lower values than their coarser grained counterparts. Spatially, Sr values correlate with both Ca and Mn values and display an inverse relationship with Rb, Al, Ti, Ni, V and K throughout the survey area. Note the general depletion envelope surrounding both the Mine area and Swin Gill anomaly zones.

182- <u>Glendinning Regional Lithogeochemical Atlas (Greywacke): Sb (ppm).</u>

The Louisa Mine at Glendinning formed a historically important souce of antinomy (stibnite) and was one of only two such mines in Scotland. Despite historical exploration activity in this region the Glendinning deposit was regarded prior to this study

FIGURE 177

GLENDINNING LA GREYWACKE 1:100000

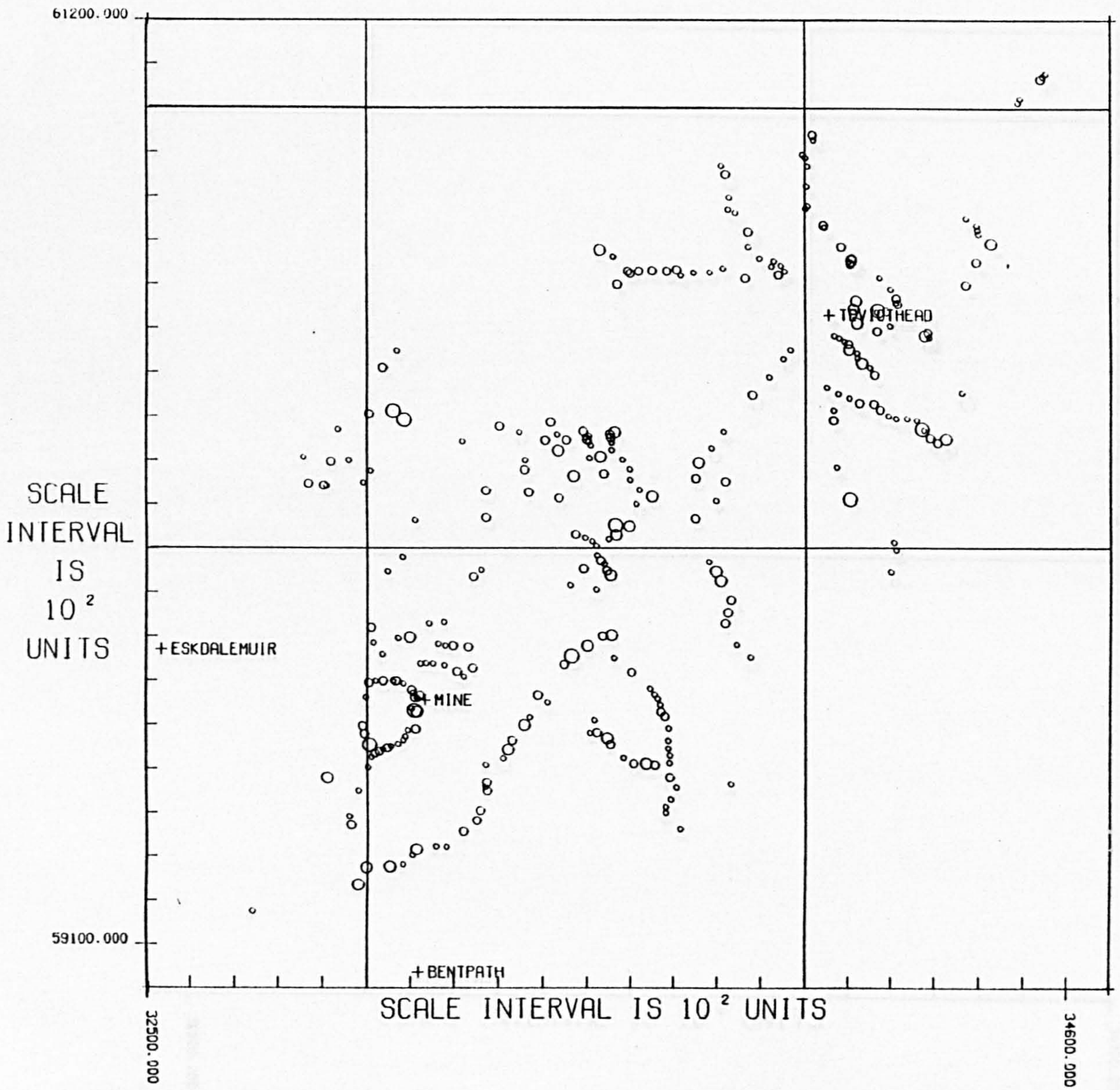

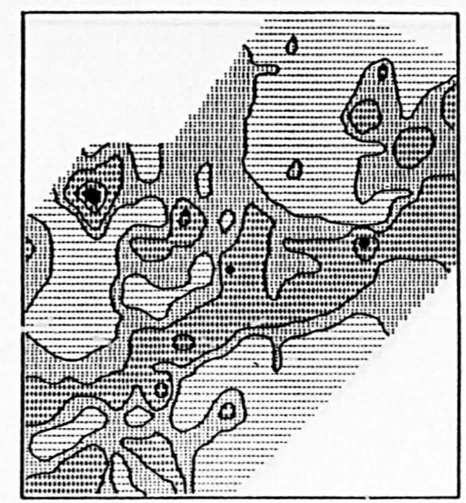

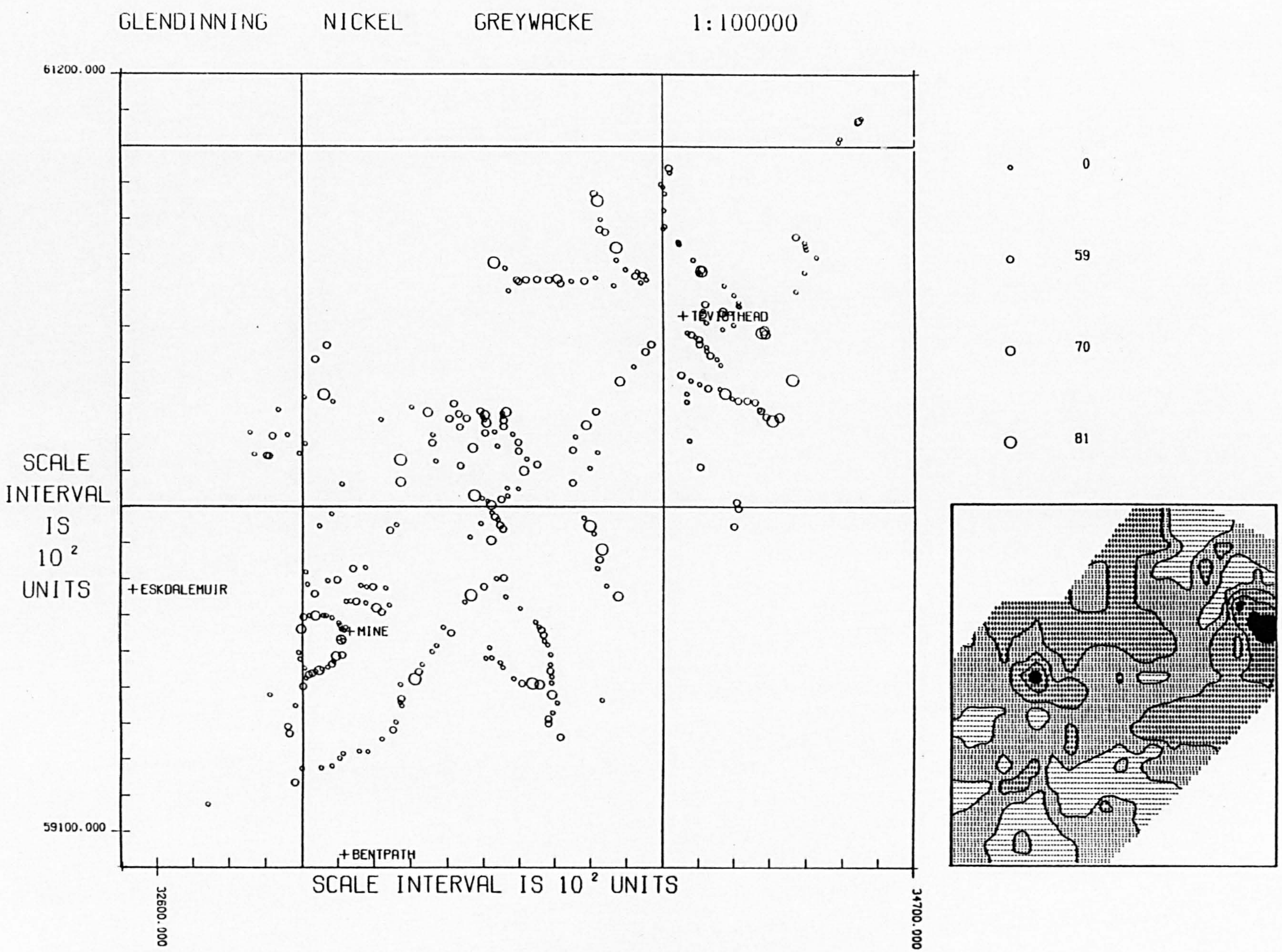
GLENDINNING NICKEL GREYWACKE 1:100000
61200.000
59100.000
SCALE INTERVAL IS 10² UNITS
+ESKDALEMUIR
+TEVIOTHEAD
+MINE
+BENTPATH
SCALE INTERVAL IS 10² UNITS
3600.000
3700.000
0
59
70
81

FIGURE 178

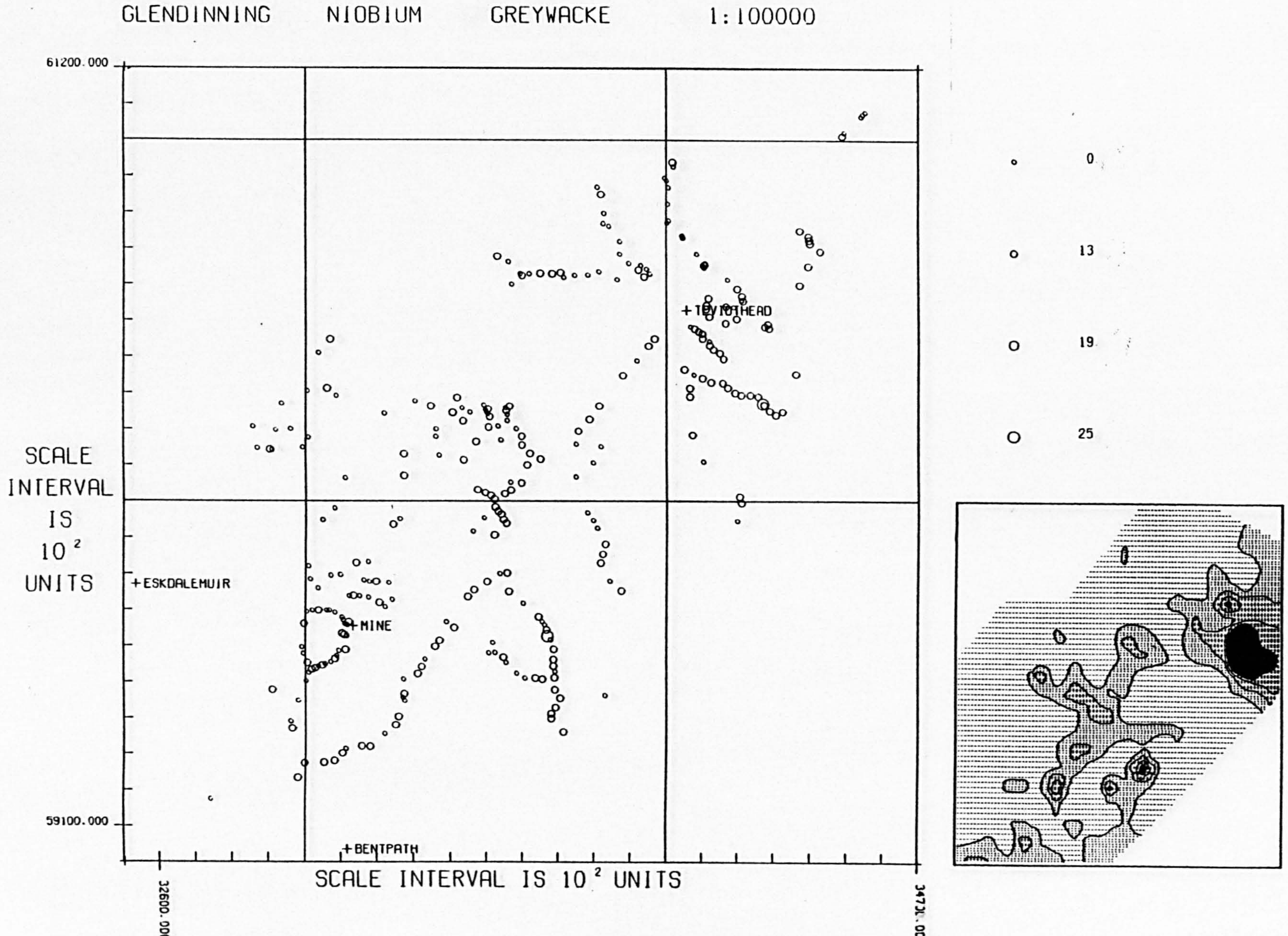
GLENDINNING NIOBIUM GREYWACKE 1:100000
61200.000
59100.000
SCALE INTERVAL IS 10 ² UNITS
+ESKDALEMUIR
+TEVIOTHEAD
+MINE
+BENTPATH
SCALE INTERVAL IS 10 ² UNITS
32600.000
34730.000
0
13
19
25

FIGURE 179

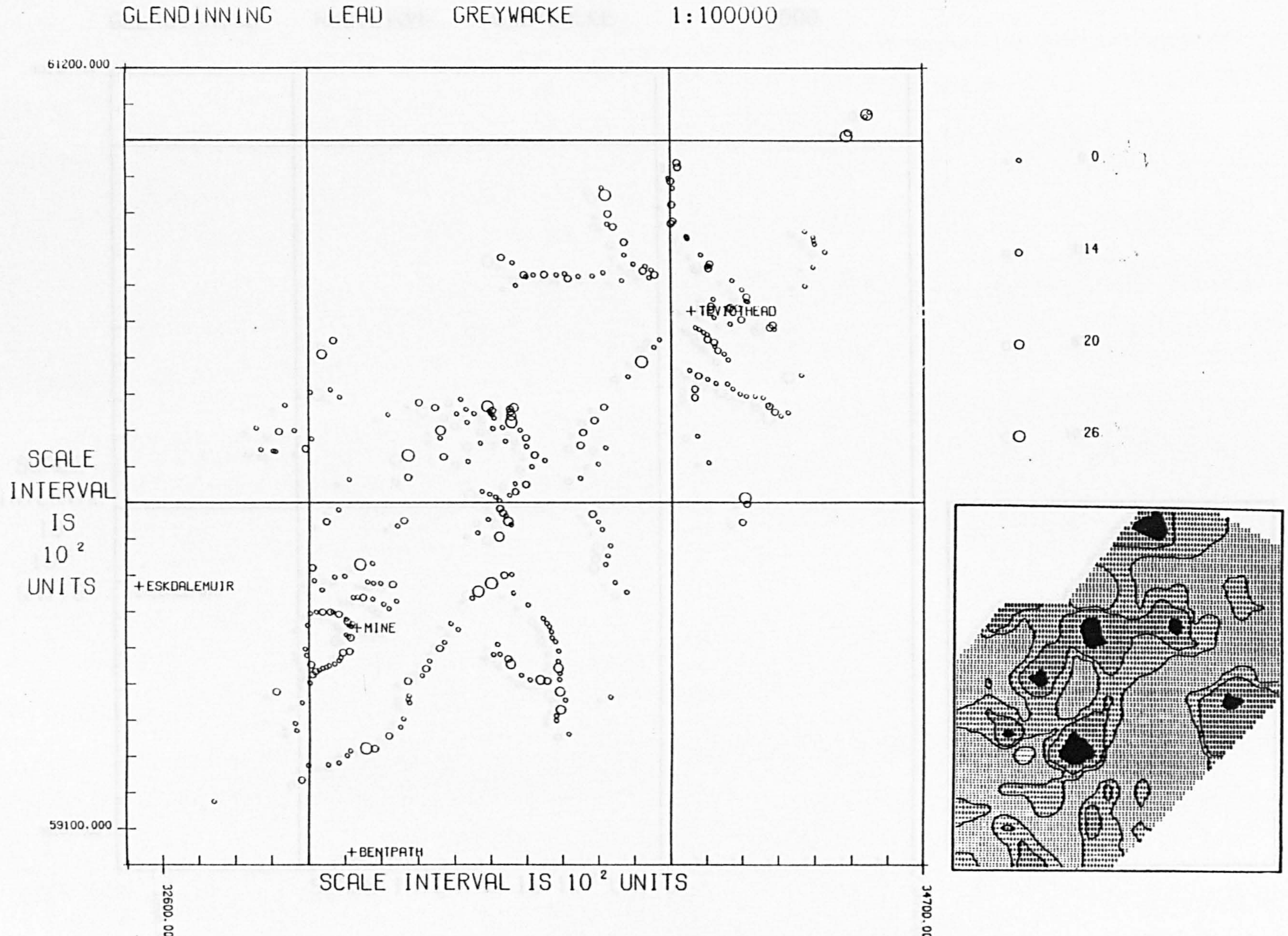
GLENDINNING LEAD GREYWACKE 1:100000
61200.000
59100.000
32600.000
34700.000
SCALE INTERVAL IS 10 ² UNITS
SCALE INTERVAL IS 10 ² UNITS
+TEVIOTHEAD
+ESKDALEMUIR
+MINE
+BENTPATH
0
14
20
26

FIGURE 179

FIGURE 180

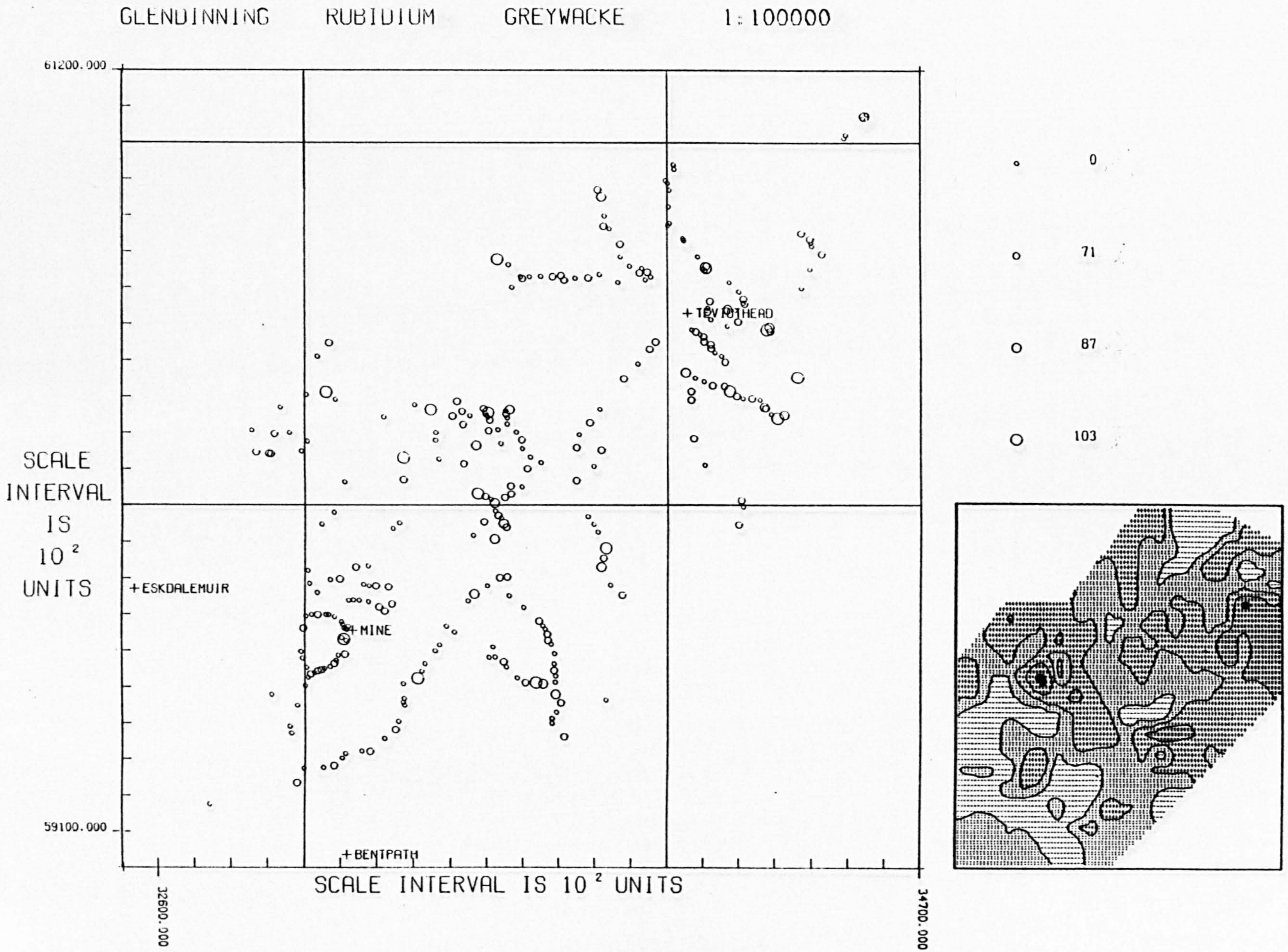

GLENDINNING RUBIDIUM GREYWACKE 1:100000
61200.000
59100.000
SCALE INTERVAL IS 10 2 UNITS
SCALE INTERVAL IS 10 2 UNITS
2600.000
34700.000
+ESKDALEMUIR
+TEVIOTHEAD
+MINE
+BENTPATH
0
71
87
103

FIGURE 181

GLENDINNING STRONTIUM GREYWACKE 1:100000

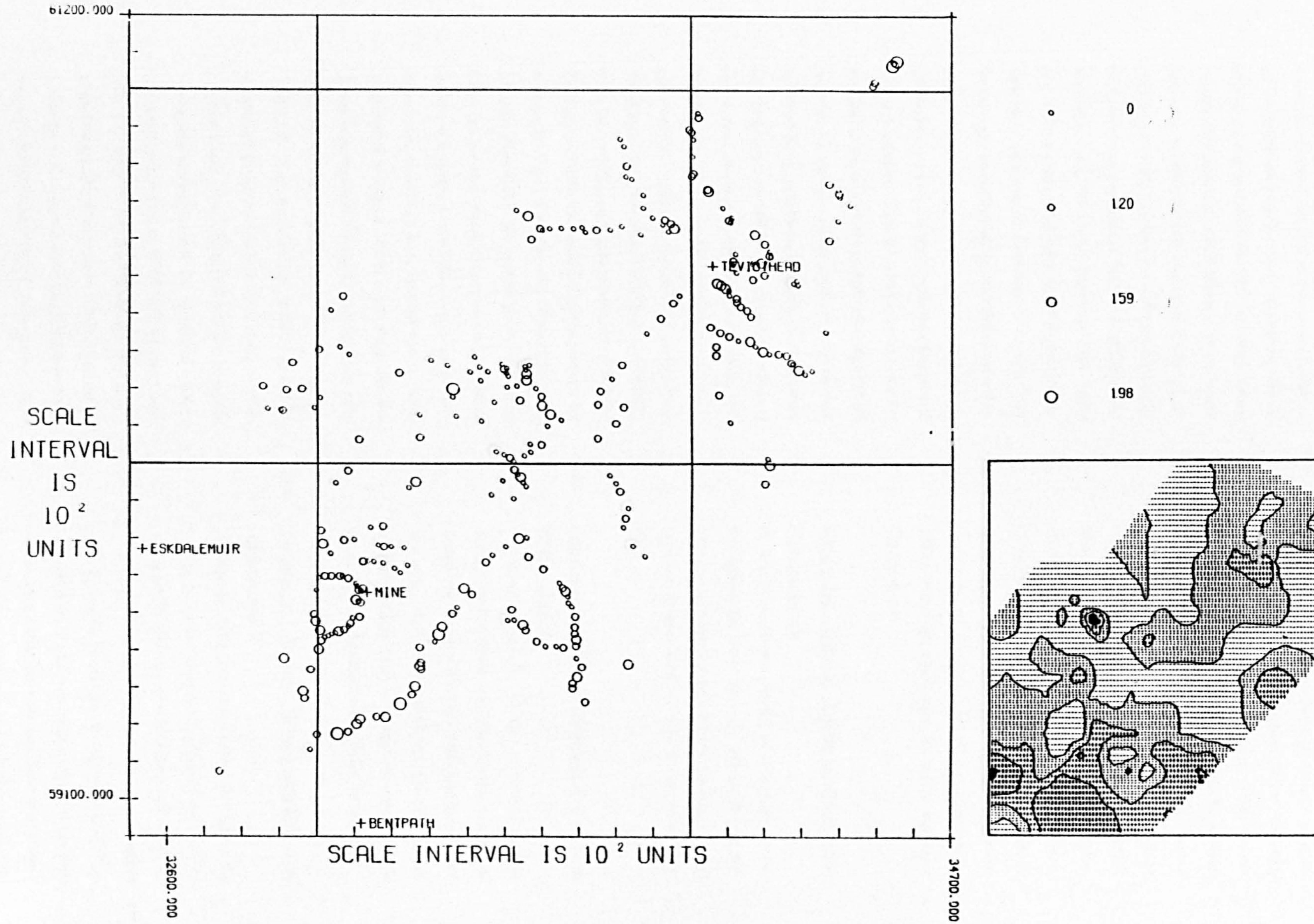

FIGURE 182

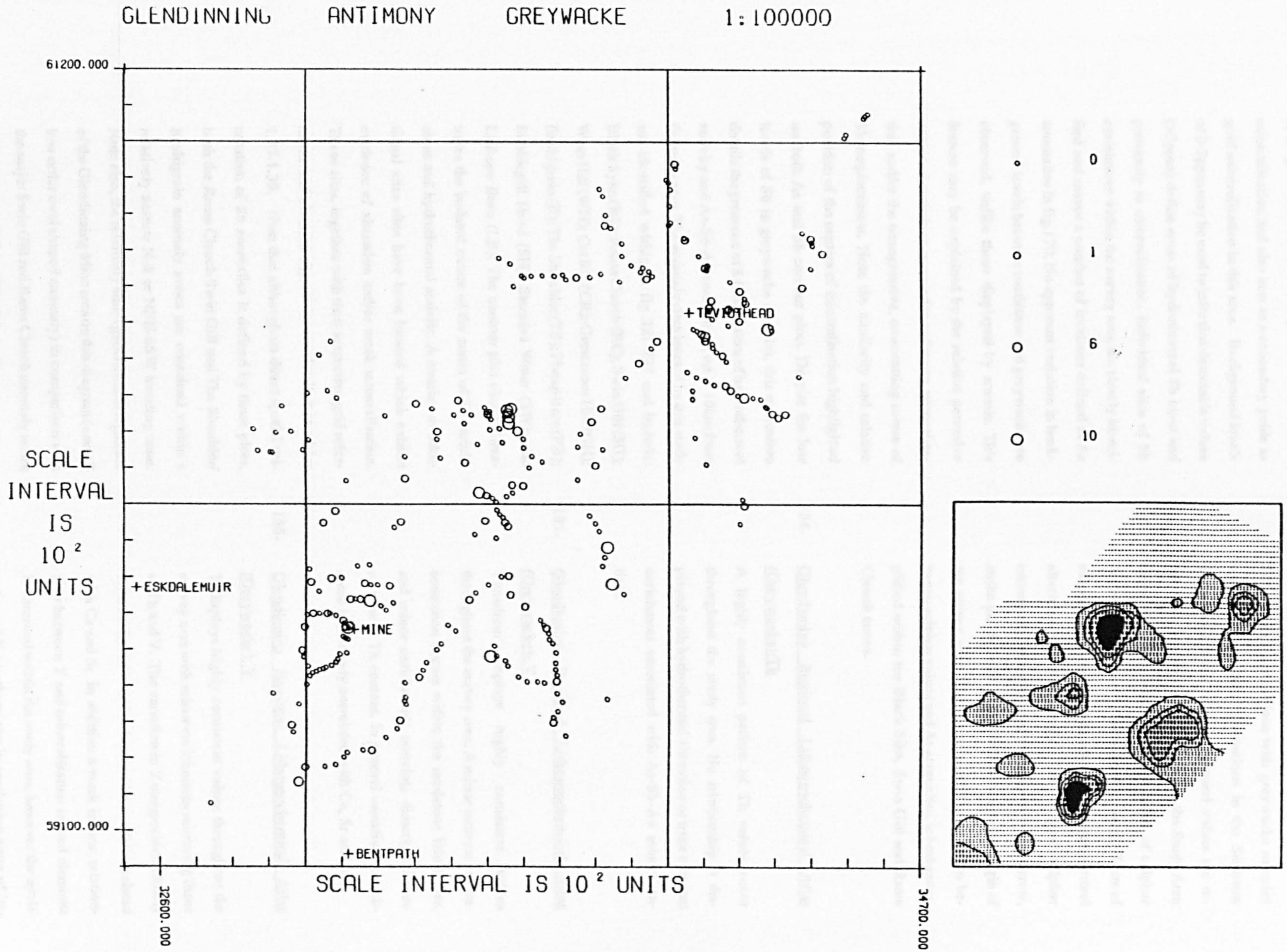
GLENDINNING ANTIMONY GREYWACKE 1:100000
61200.000
59100.000
SCALE INTERVAL IS 10 ² UNITS
+ESKDALEMUIR
+TEVIOTHEAD
+MINE
+BENTPATH
SCALE INTERVAL IS 10 ² UNITS
32600.000
34700.000
0
1
6
10

as a single isolated example of this form of turbidite hosted Sb-mineralisation. Antimony (Sb) forms the main pathfinder element for quartz hosted stibnite mineralisation and also acts as a secondary guide to gold mineralisation in this area. Background levels of 0-2ppm may be used to infer that detectable values (>5ppm) define areas of hydrothermal Sb input and proximity to mineralisation. Individual sites of Sb enrichment within the survey area are clearly identified and mirror a number of locations defined as As anomalies in fig.170. No apparent variation in background levels between mudstone and greywacke are observed, unlike those displayed by arsenic. This feature may be explained by the relative pervasive nature of arsenic as opposed to antimony mineralisation and/or the transgressive, crosscutting nature of Sb emplacement. Note the similarity and relative position of the centres of mineralisation highlighted on both As and Sb contour plots. Despite the low levels of Sb in greywacke samples, this evaluation details the presence of 8 further sites of hydrothermal activity and As-Sb-Au enrichment, up to 10km from the mine area. The anomaly sites located by this study are identified within in fig 221-223 and include: Black Syke (BS); Rams Cleuch (RC); Swin Gill (SG); Wisp Hill (WH); Cat Rig (CR); Great moor Hill (GH); Rashigrain (R); The Shoulder (TS); Phaup Burn (PB); Stibbiegill Head (SH); Stennies Water (SW); and Linhope Burn (LB). The contour plot clearly illustrates the isolated nature of the zones of Sb enrichment and hydrothermal activity. A number of additional sites sites have been located which exhibit evidence of alteration and/or weak mineralisation. These sites, together with their respective grid references and element signatures are detailed in tables 1.37-1.39. Note that although no direct spatial orientation of Sb anomalies is defined by these plots, both the Rams Cleuch Swin Gill and The Shoulder/ Rashigrain anomaly zones are contained within a relatively narrow N-S or NNE-SSW trending zone. Note also, the relatively small geochemical signiture of the Glendinning Mine area on this diagram (a small low order oval shaped anomaly) in comparison with the major Swin Gill and Rams Cleuch anomaly zones (4km ESE and 7km NE of the mine area, respectively).

183- <u>Glendinning Regional Lithogeochemical Atlas (Greywacke): S</u>

Although sulphur displays a wide range of values (0-2755 ppm) a comparison with greywacke samples collected from other formations in the Southern Uplands indicates that background values are remarkably low (mean 48ppm) within the Study Area (Hawick Formation). Anomalous levels of sulphur define areas subjected to the geochemical effects of sulphidation processes associated with hydrothermal alteration and As enrichment. The maximum sulphur concentrations are located within a relatively narrow, strike parallel belt, along the south eastern margin of the survey area. The strong spatial association between sulphur values and As anomalies, is best exemplified within the Black Sike, Swin Gill and Rams Cleuch zones.

184- <u>Glendinning Regional Lithogeochemical Atlas (Greywacke):Th</u>

A highly consistent pattern of Th values occur throughout the study area. No relationship is displayed with hydrothermal alteration or trace element enrichment associated with As-Sb-Au mineralisation.

185- <u>Glendinning Regional Lithogeochemical Atlas (Greywacke): V</u>

Vanadium displays highly consistent values throughout the survey area. A minor increase in concentration occurs within the mudstone lithologies, and minor enrichments correlate directly with increases in Th content. In general vanadium enrichment is inversely correlated with Ca, Sr and Sb.

186- <u>Glendinning Regional Lithogeochemical Atlas (Greywacke): Y</u>

Y displays highly consistent values throughout the survey area with minor enrichments mirroring those of Th and V. The variation in Y composition closely follows that of V and values are inversely correlated with Ca and Sr. In addition a weak inverse relationship between Y and mineralisation related elements is observed within the study area, however the application of Y geochemistry in predicting areas of hydrothermal alteration and possible mineralisation is

GLENDINNING SULPHUR GREYWACKE 1:100000

FIGURE 183

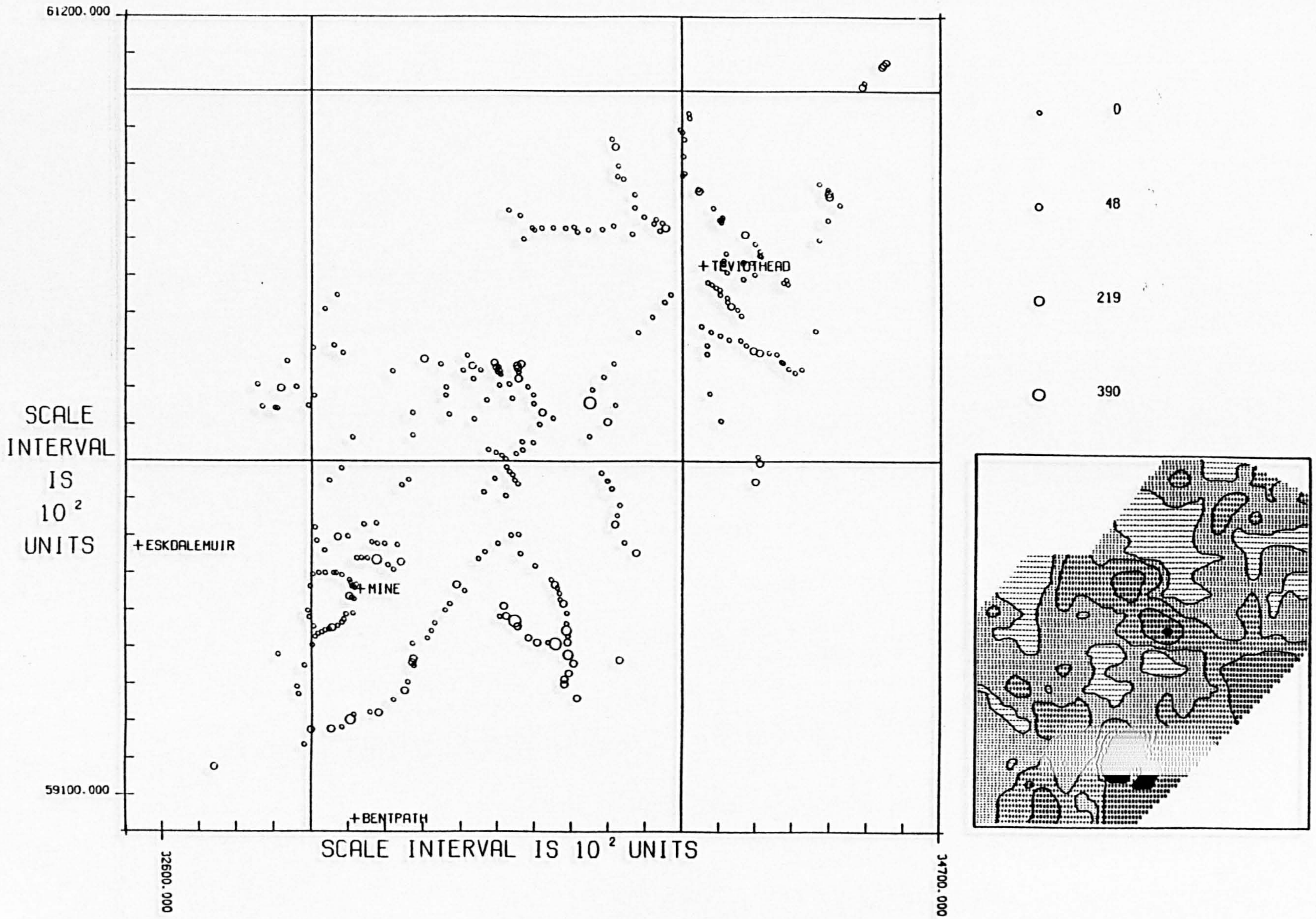

GLENDINNING THORIUM GREYWACKE 1:100000

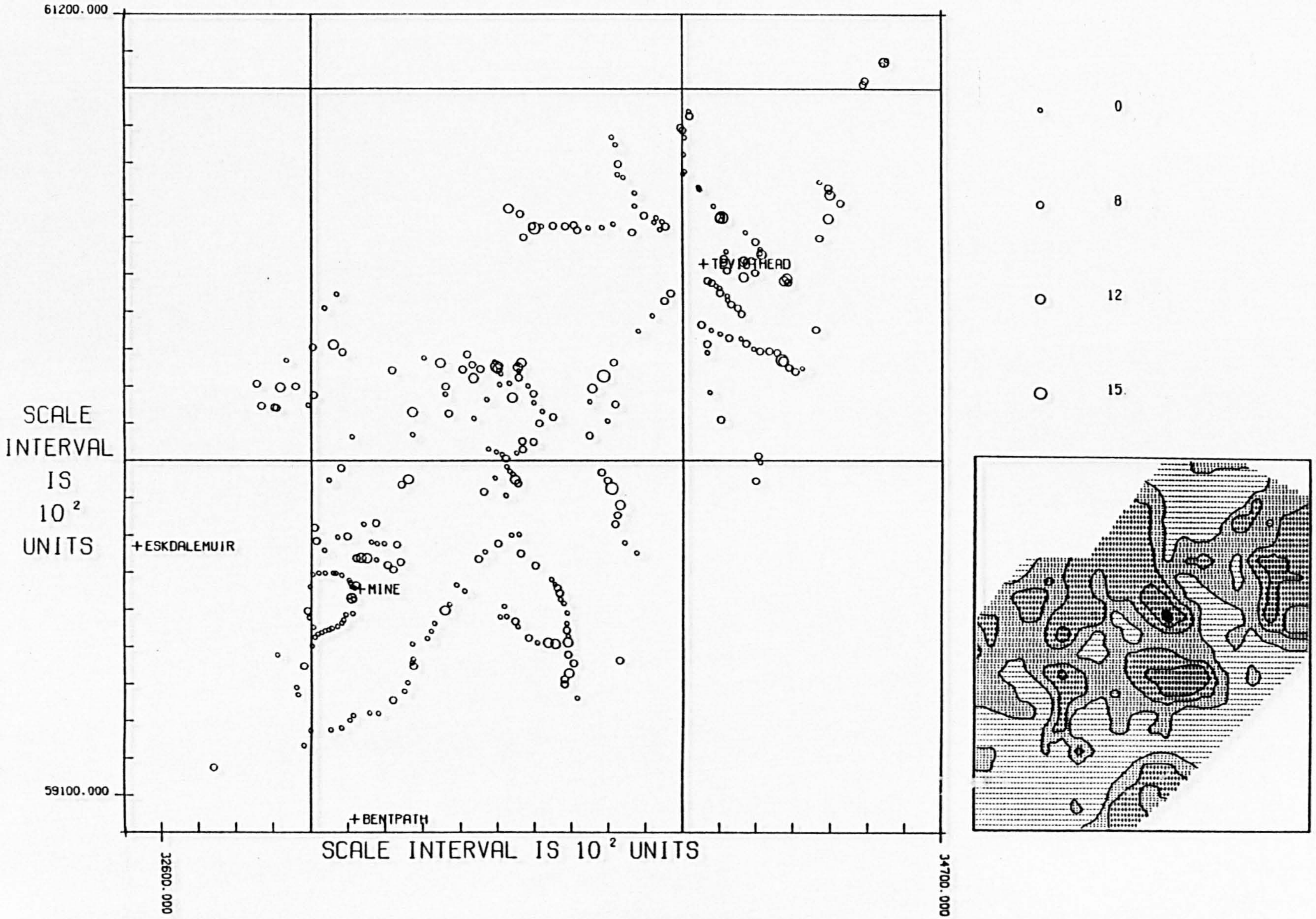

FIGURE 184

GLENDINNING VANADIUM GREYWACKE 1:100000

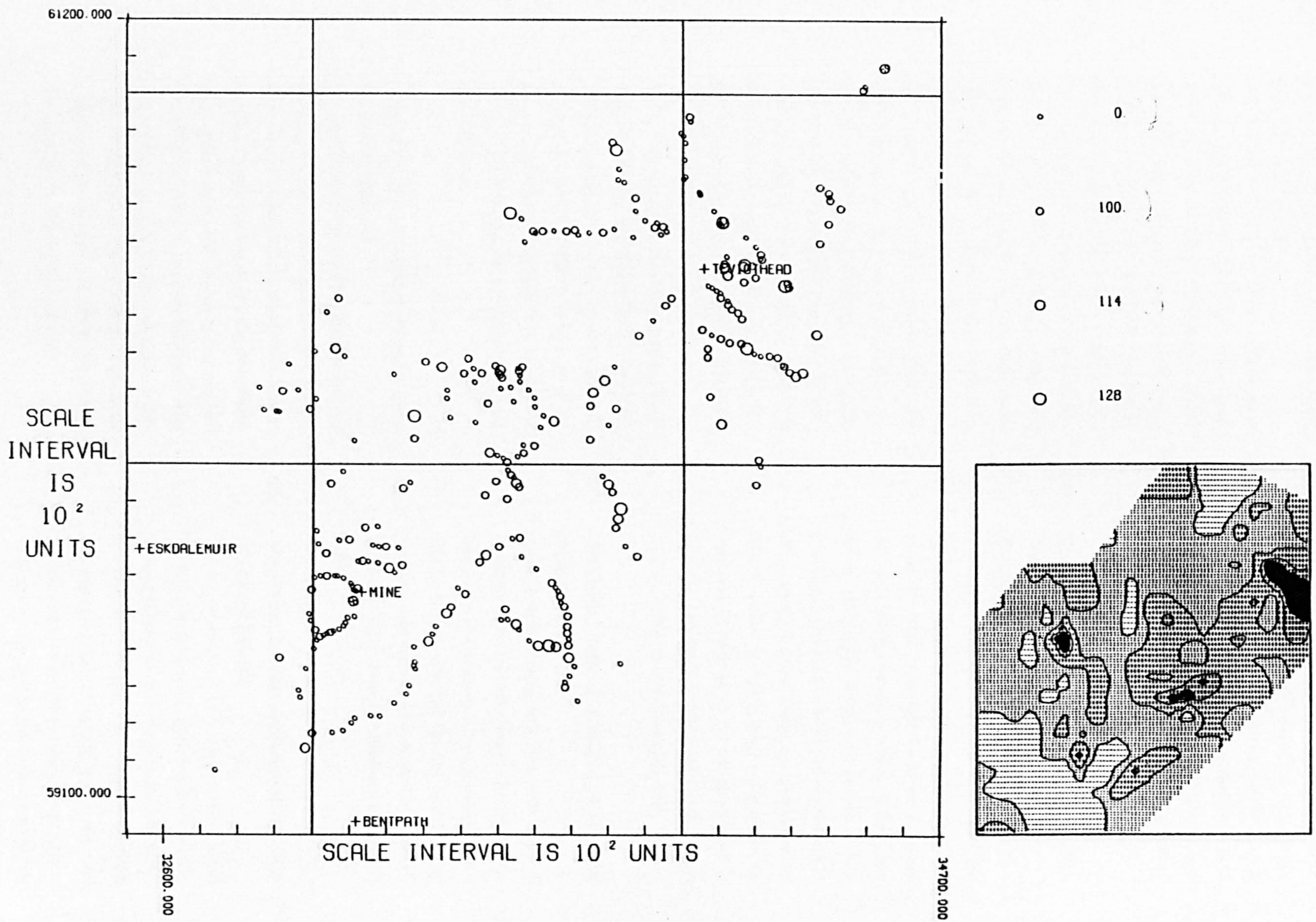

FIGURE 185

FIGURE 186

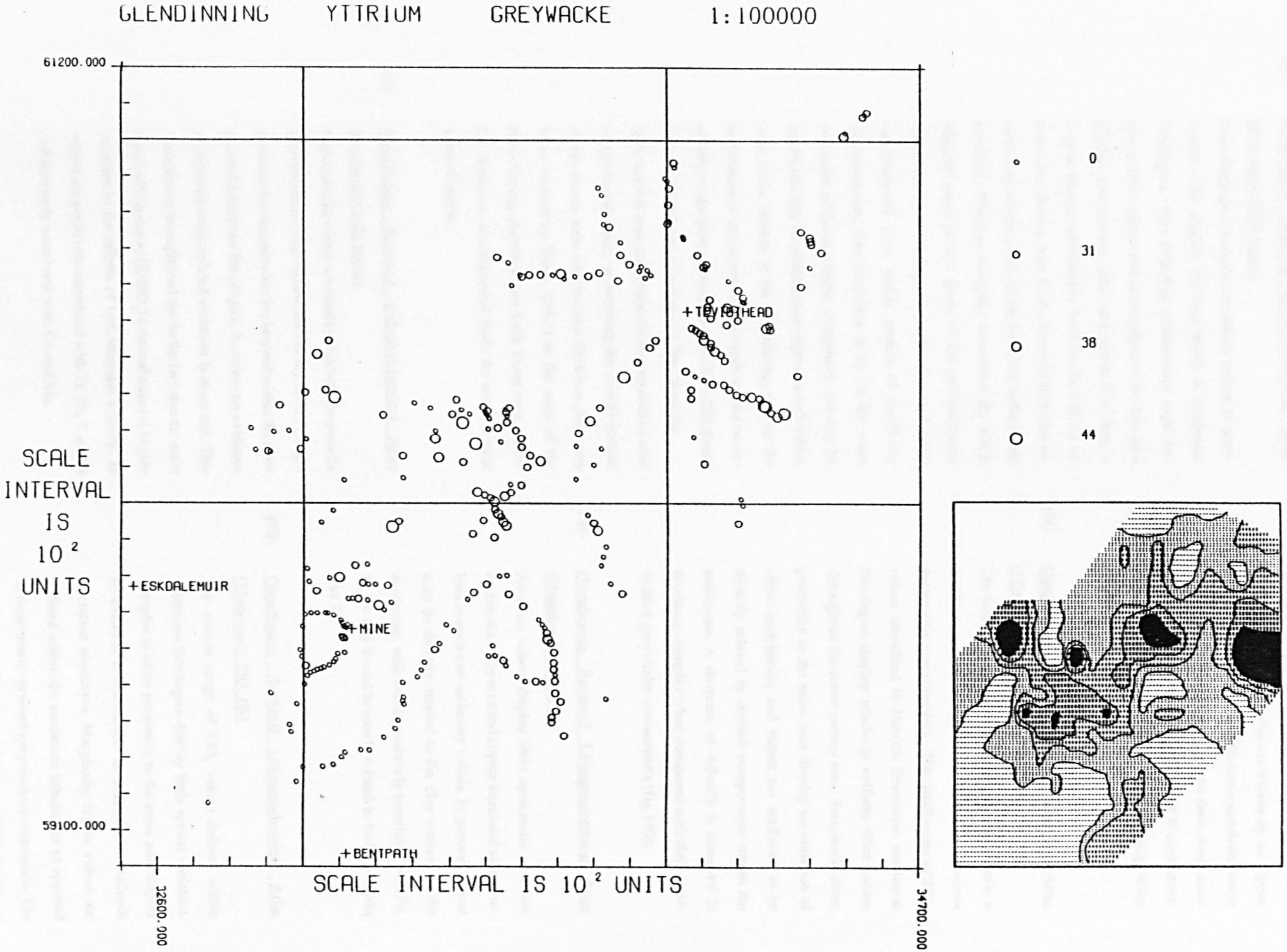

GLENDINNING YTTRIUM GREYWACKE 1:100000
61200.000
59100.000
32600.000
34700.000
SCALE INTERVAL IS 10 ² UNITS
SCALE INTERVAL IS 10 ² UNITS
+ESKDALEMUIR
+MINE
+TEVIOTHEAD
+BENTPATH
0
31
38
44

extremely limited.

187- Glendinning Regional Lithogeochemical Atlas (Greywacke): Zn (ppm).

Zinc displays relatively consistent values in greywackes with slightly elevated levels in mudstone lithologies. Two differing relationships exist between zinc values and mineralisation in this area (Duller and Harvey, 1983 and 1984): The first, a cryptic inverse relationship between Zn and As allows Glendinning type As-Au deposits to be characterised by subtle levels of Zn depletion within their wallrock; Whereas secondly, anomalous Zn levels pinpoint areas of low grade Pb-Zn mineralisation which due to overriding structural controls, is often superimposed upon earlier phases of As-Sb-Au mineralisation. Zinc depletion is by far the more pervasive of the two styles of anomaly and may be used to identfy a depletion zone approximately 400m wide in the vicinity of the Glendinning deposit. Zn enrichment is characteristic of a number of As anomaly sites in the survey area including; Swin Gill, Rams Cleuch, Rashigrain, Cat Rig and The Shoulder.

Note the N-S orientated zone of Zn anomalies located on the contour map, crosscutting the central portion of the survey area. Similar zinc depletion processes were located by Stone (1985) to the west of the Glendinning deposit in the Loch Doon area, where Zn depletion accompanied both As and Pb vein mineralisation.

188- Glendinning Regional Lithogeochemical Atlas (Greywacke): Zr (ppm).

Consistent Zr values are displayed in both greywacke and mudstones throughout the survey area. A slight decrease in concentration is observed within the finer grained mudstone lithologies, however no evidence of mineralisation related variation is observed. This feature may be explained due to the fact that the main host for Zr is zircon ($ZrSiO_4$) a detrital mineral, highly resistant to the effects of hydrothermal activity. Zr values are positively correlated with Ti, Th, Y an Nb and inversely correlated with Ca and Mn.

189- Glendinning Regional Lithogeochemical Atlas (Greywacke): Tl (ppm). Over 95% of all samples analysed within the survey area contain Tl values below detection limits (1-2ppm). Of the remaining samples, Tl levels up to 7ppm were located within the Glendinning deposit, whereas values up to 17ppm were detected outwith the Mine area and define areas of considerable exploration, given their close association with As-Sb anomalies. Sites of Tl enrichment include: Rams Cleuch, Black Syke, Cat Rig, Wisp Hill and Philhope Loch.

190- Glendinning Regional Lithogeochemical Atlas (Mudstone): SiO_2 (%)

The following series of 31 mudstone maps display a smaller number of samples (n=197) that the previous greywacke maps (n=304). The small range of SiO_2 values identified in Hawick Formation mudstone lithologies display relatively uniform silica values throughout the entire survey area. Samples in close proximity to the mine area display no evidence of silica enrichment, and values are attributed to be directly related to detrital components within the sediments. A decrease of 4-5wt% is observed in mudstone samples when compared with their interbedded greywacke counterparts (fig.160).

191- Glendinning Regional Lithogeochemical Atlas (Mudstone): Al_2O_3 (%)

Alumina values display little systematic variation within the study area and appear unrelated to anomalous arsenic and antimony values. In general, values may be directly related to the clay content of the mudstone, with values positively correlated with Fe, K, Rb and V; and inversely related to both CaO, Mn and Sr.

192- Glendinning Regional Lithogeochemical Atlas (Mudstone): TiO_2 (%)

The narrow range of TiO_2 values defined within mudstone lithologies display little spatial variation. Samples in close proximity to the mine area display no evidence of enrichment associated with wallrock alteration processes. Marginally higher values are defined within the mudstone lithologies as opposed to their coarser grained greywacke counterparts. The close correlation observed between TiO_2, MgO and Fe_2O_3 values is attributed to the detrital ferromagne-

FIGURE 187

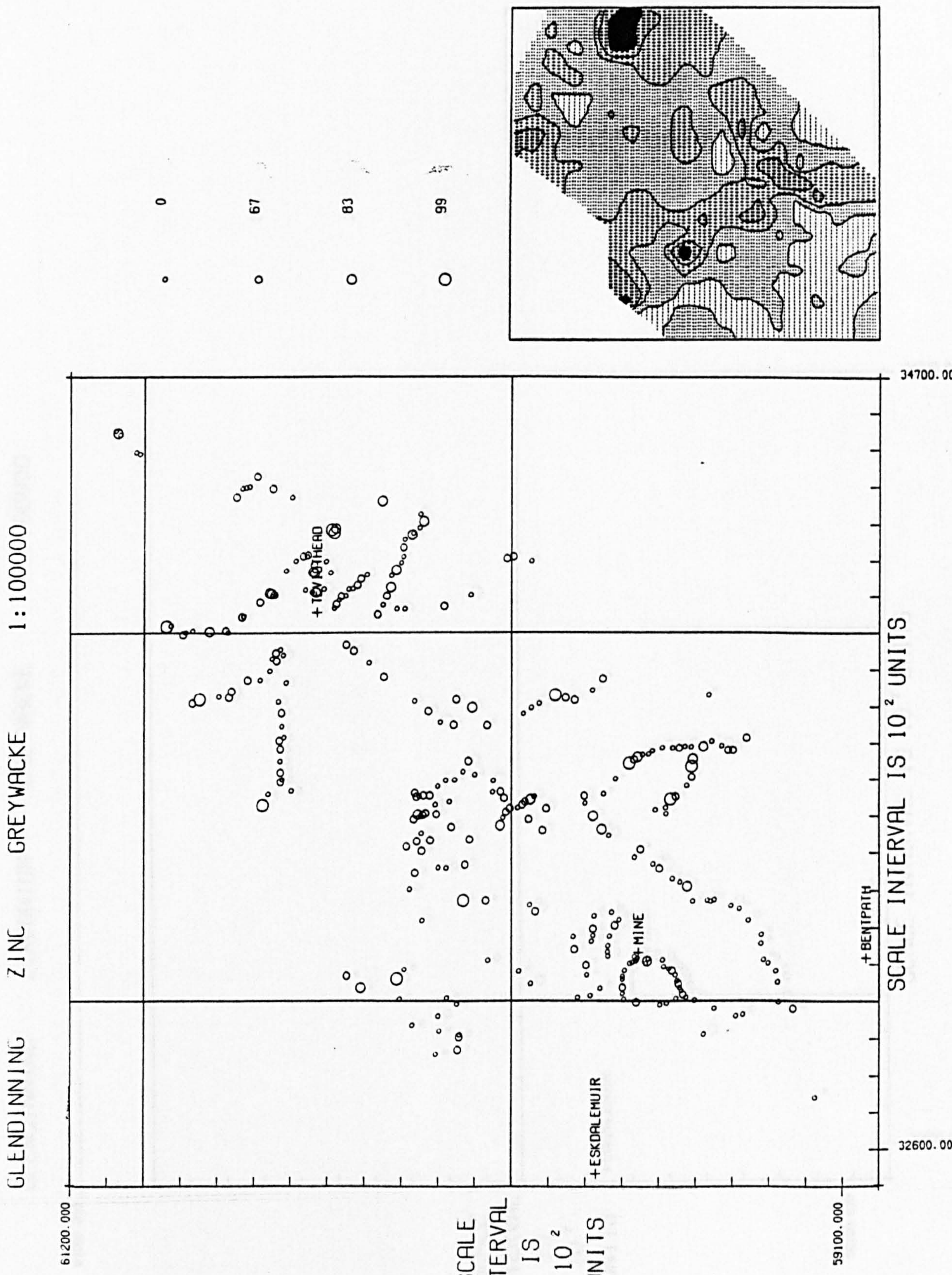
GLENDINNING ZINC GREYWACKE 1:100000
0
67
83
99
+TEVIOTHEAD
+MINE
+BENTPATH
+ESKDALEMUIR
34700.000
32600.000
61200.000
59100.000
SCALE INTERVAL IS 10² UNITS
SCALE INTERVAL IS 10² UNITS

FIGURE 188

GLENDINNING ZIRCONIUM GREYWACKE 1:100000

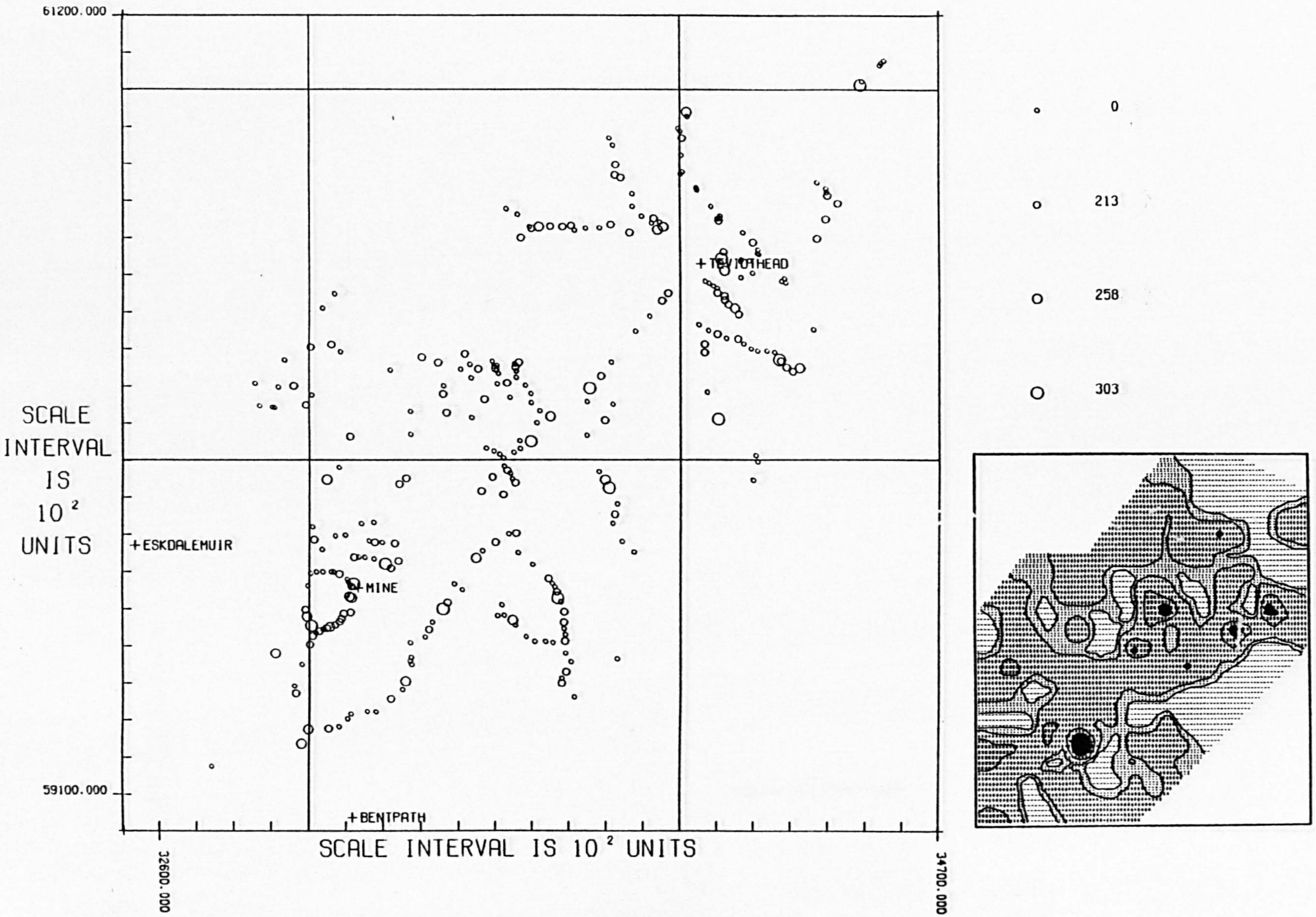

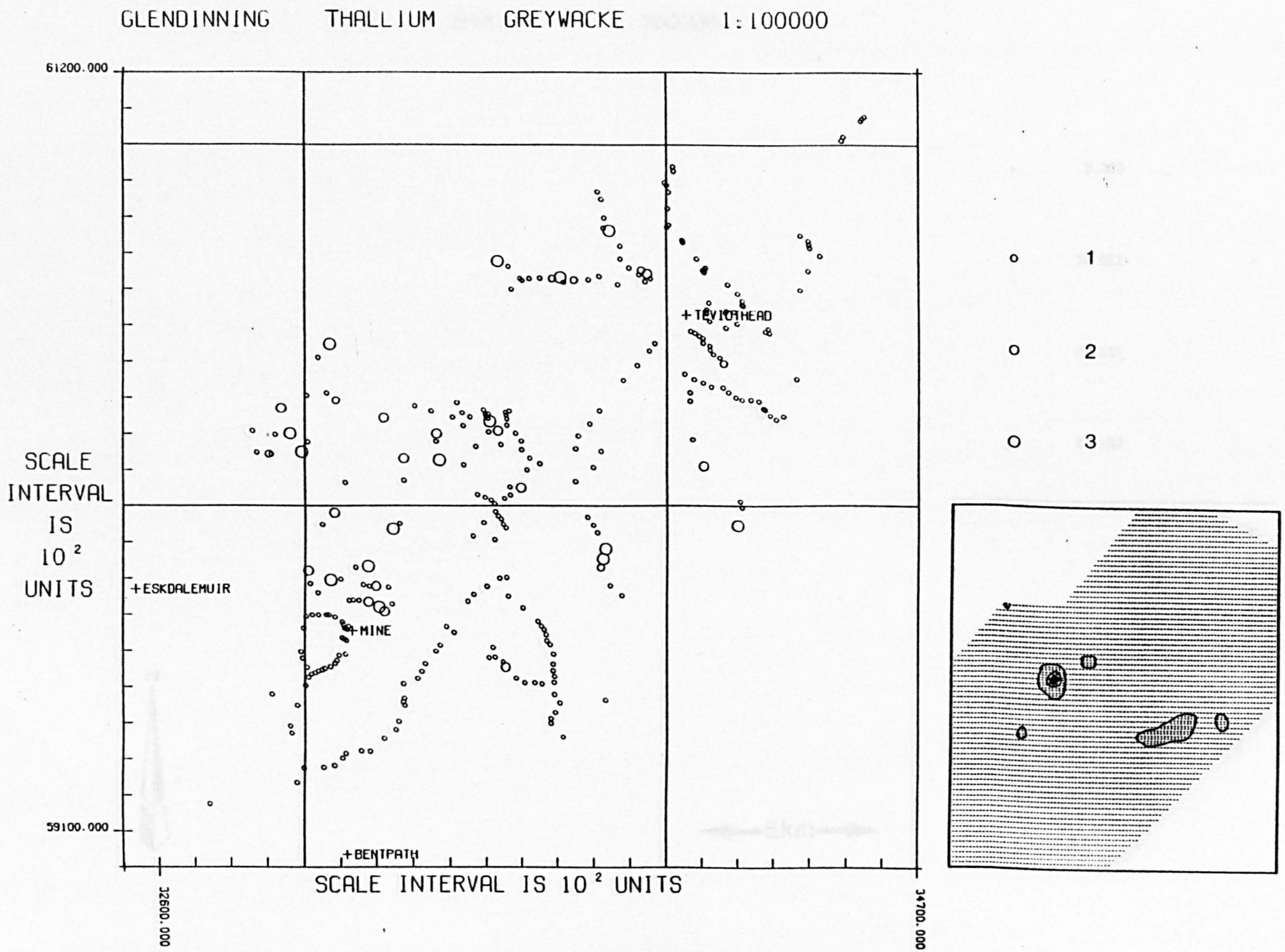

GLENDINNING THALLIUM GREYWACKE 1:100000
61200.000
59100.000
SCALE INTERVAL IS 10 ² UNITS
+ESKDALEMUIR
+TEVIOTHEAD
+MINE
+BENTPATH
SCALE INTERVAL IS 10 ² UNITS
32600.000
34700.000
1
2
3

FIGURE 189

FIGURE 190

GLENDINNING SIO2 SHALE 1:100000

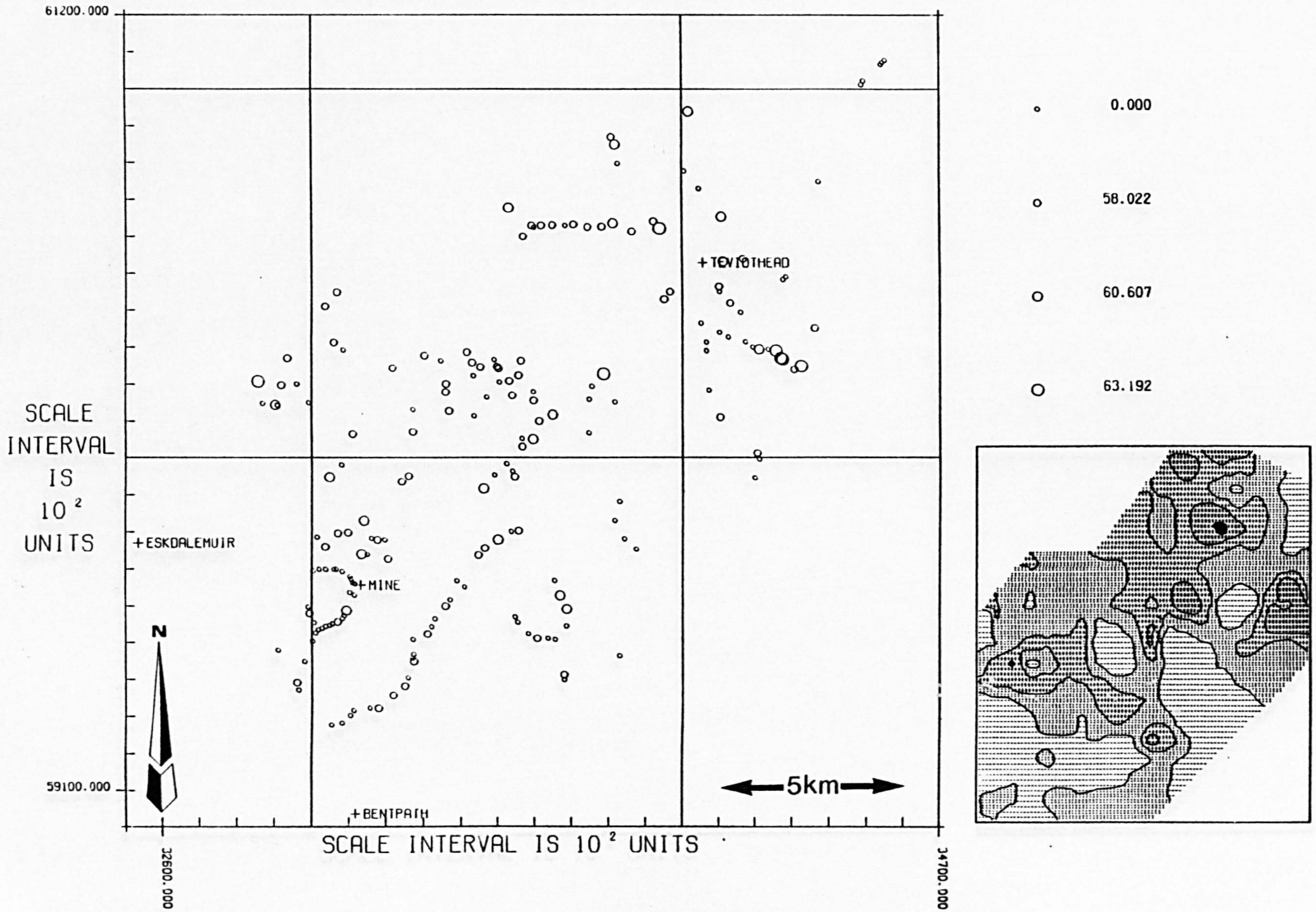

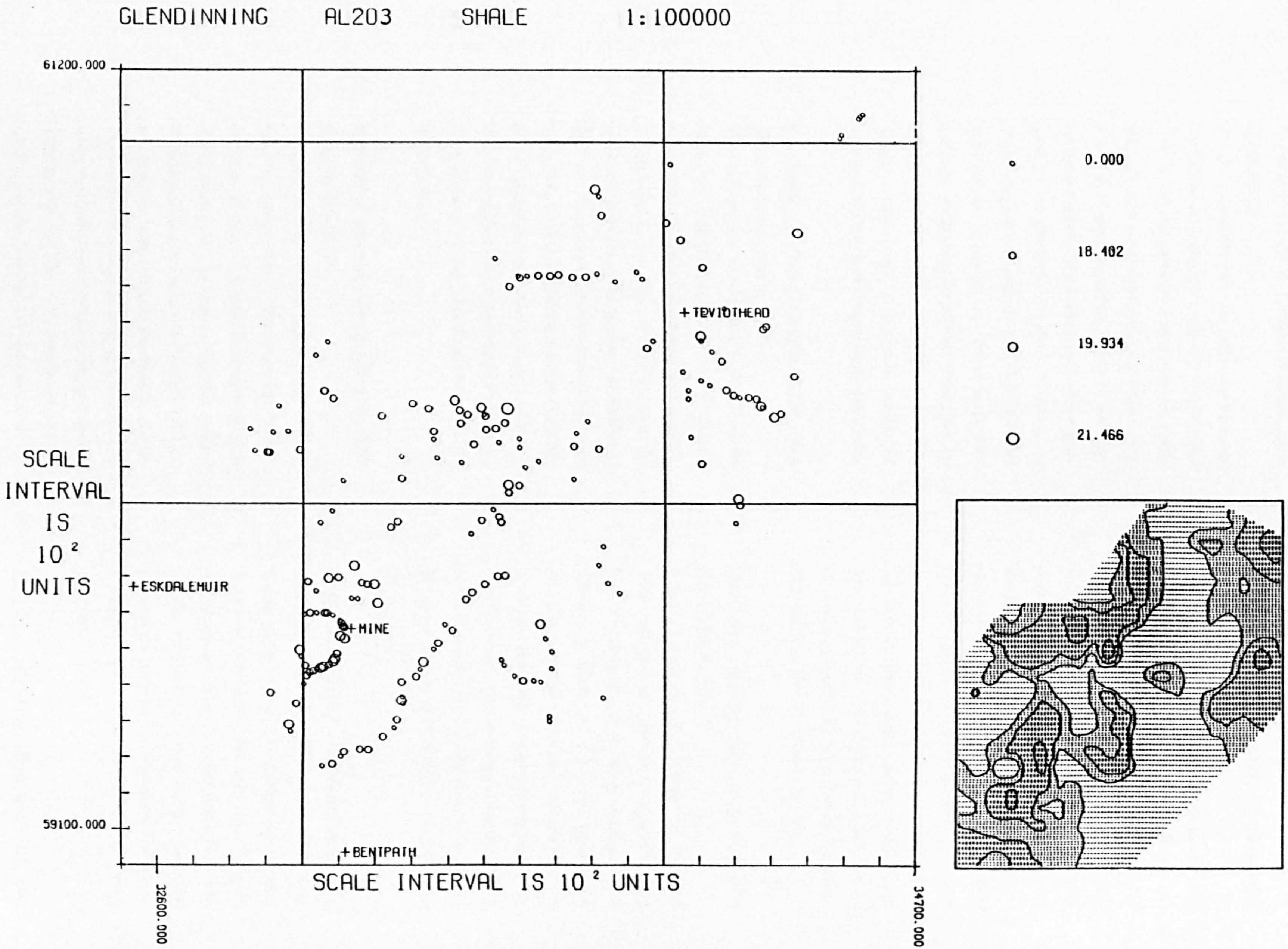
GLENDINNING AL203 SHALE 1:100000
61200.000
59100.000
SCALE INTERVAL IS 10 ² UNITS
+ESKDALEMUIR
+TEVIOTHEAD
+MINE
+BENTPATH
SCALE INTERVAL IS 10 ² UNITS
32600.000
34700.000
0.000
18.402
19.934
21.466

FIGURE 191

FIGURE 192

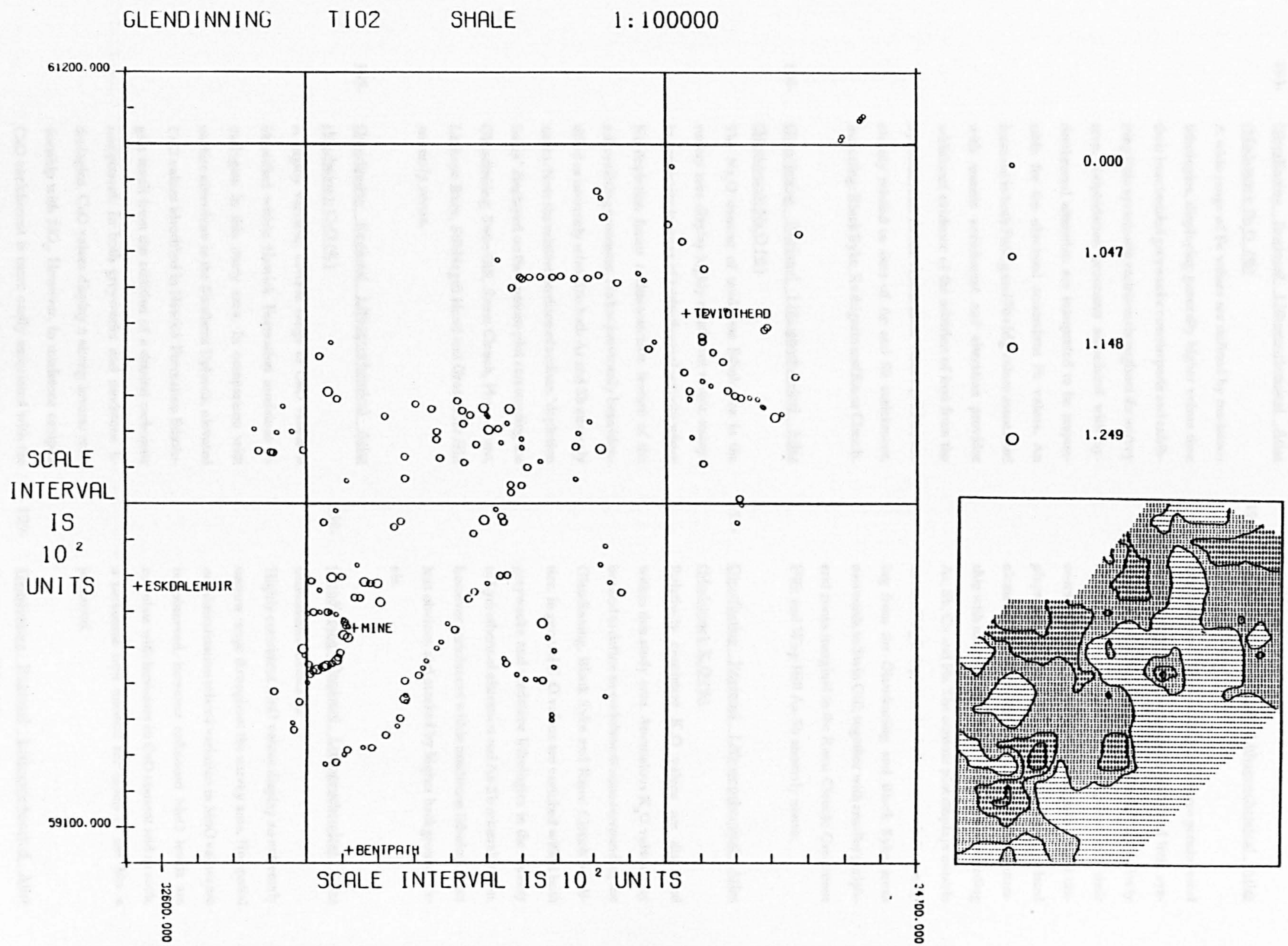
GLENDINNING TIO2 SHALE 1:100000
61200.000
59100.000
SCALE INTERVAL IS 10 2 UNITS
32600.000
34100.000
SCALE INTERVAL IS 10 2 UNITS
+TEVIOTHEAD
+ESKDALEMUIR
+MINE
+BENTPATH
0.000
1.047
1.148
1.249

sian mineral content of the sediments.

193- Glendinning Regional Lithogeochemical Atlas (Mudstone): Fe_2O_3 (%)

A wide range of Fe values are defined by mudstone lithologies, displaying generally higher values than their interbedded greywacke counterparts and exhibiting little systematic variation throughout the survey area. Sulphidation processes associated with hydrothermal alteration are interpreted to be responsible for the observed anomalous Fe values. An increase in both Fe/Mg and Fe+Mg values associated with arsenic enrichment and alteration provides additional evidence of the addition of iron from the hydrothermal fluids. Anomalous values (>95%) are closely related to sites of As and Sb enrichment, including: Black Syke, Rashigrain and Rams Cleuch.

194- Glendinning Regional Lithogeochemical Atlas (Mudstone): Na_2O (%)

The Na_2O content of mudstone lithologies in the survey area display highly consistent values, except in proximity to areas of hydrothermal activity where Na depletion forms a characteristic feature of the mineralising processes. Na has previously been identified as inversely related to both As and Sb anomaly zones. Note the relative position of sodium 'depletion holes' displayed on the contour plot surrounding the Glendinning, Swin Gill, Rams Cleuch, Phaup Burn, Linhope Burn, Stibbiegill Head and Greatmoor Hill anomaly zones.

195- Glendinning Regional Lithogeochemical Atlas (Mudstone): CaO (%)

A highly variable, diverse range of CaO values is identified within Hawick Formation mudstone lithologies in this study area. In comparison with studies elsewhere in the Southern Uplands, elevated CaO values identified in Hawick Formation lithologies result from the addition of a detrital carbonate component. In both greywacke and mudstone lithologies, CaO values display a strong inverse relationship with SiO_2. However, in mudstone samples CaO enrichment is more easily associated with the effects of hydrothermal alteration and mineralisation. Anomalous CaO values are observed in the following sites: Glendinning, Swin Gill, Phaup Burn and Rams Cleuch.

196- Glendinning Regional Lithogeochemical Atlas (Mudstone): MgO (%)

MgO values defined on the point source geochemical map display highly uniform contents and little systematic variation. MgO values display a relatively enlarged compositional range compared with their coarser grained greywacke counterparts. MgO displays a positive correlation with 'depletion' related elements such as Na and Fe, and an inverse relationship with mineralisation enriched elements including As, Sb, Cu and Pb. The contour plot displays notable areas of MgO depletion include a narrow belt extending from the Glendinning and Black Syke areas eastwards to Swin Gill; together with smaller peripheral zones marginal to the Rams Cleuch; Greatmoor Hill; and Wisp Hill As-Sb anomaly zones.

197- Glendinning Regional Lithogeochemical Atlas (Mudstone): K_2O (%)

Relatively consistent K_2O values are displayed within this study area. Anomalous K_2O values may be used to define an enrichment zone surrounding the Glendinning, Black Syke and Rams Cleuch localities. In general K_2O values are enriched within both greywacke and mudstone lithologies in the vicinity of hydrothermal alteration and As-Sb mineralisation, however enrichment within mudstone lithologies are less obvious and masked by higher background levels.

198- Glendinning Regional Lithogeochemical Atlas (Mudstone): MnO (%)

Highly consistent MnO values display an extremely narrow range throughout the survey area. No spatial or mineralisation related variation in MnO values are be observed, however enhanced MnO levels are correlate with increases in CaO content and as such, a carbonate host mineral for much of the Mn is proposed.

199- Glendinning Regional Lithogeochemical Atlas (Mudstone): P2O5 (%)

As with MnO, P_2O_5 values are generally low and

GLENDINNING FE2O3 SHALE 1:100000

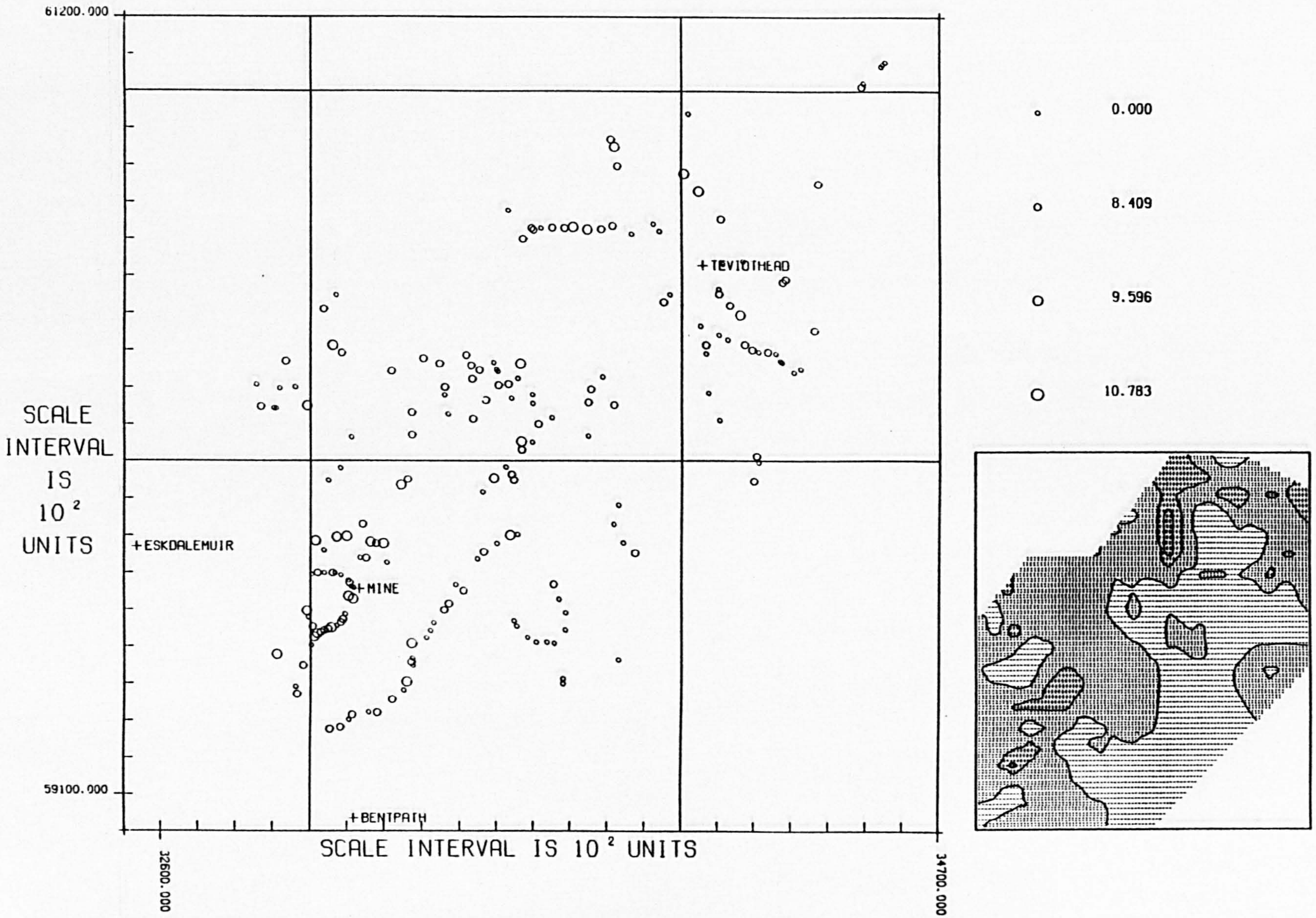

FIGURE 193

FIGURE 194

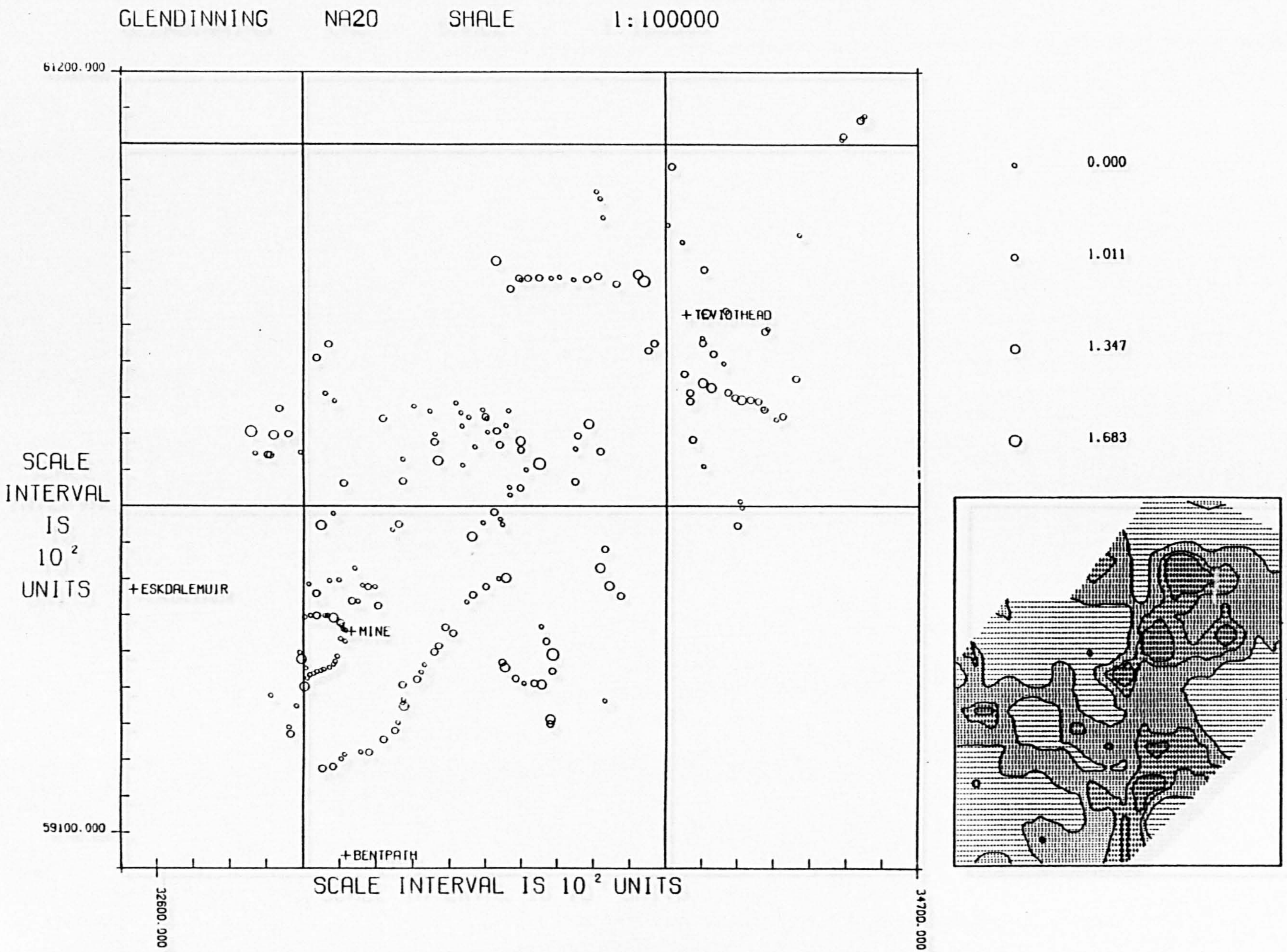
GLENDINNING NA20 SHALE 1:100000
61200.000
59100.000
SCALE INTERVAL IS 10 ² UNITS
+ESKDALEMUIR
+MINE
+TEVIOTHEAD
+BENTPATH
SCALE INTERVAL IS 10 ² UNITS
3260.000
3470.000
0.000
1.011
1.347
1.683

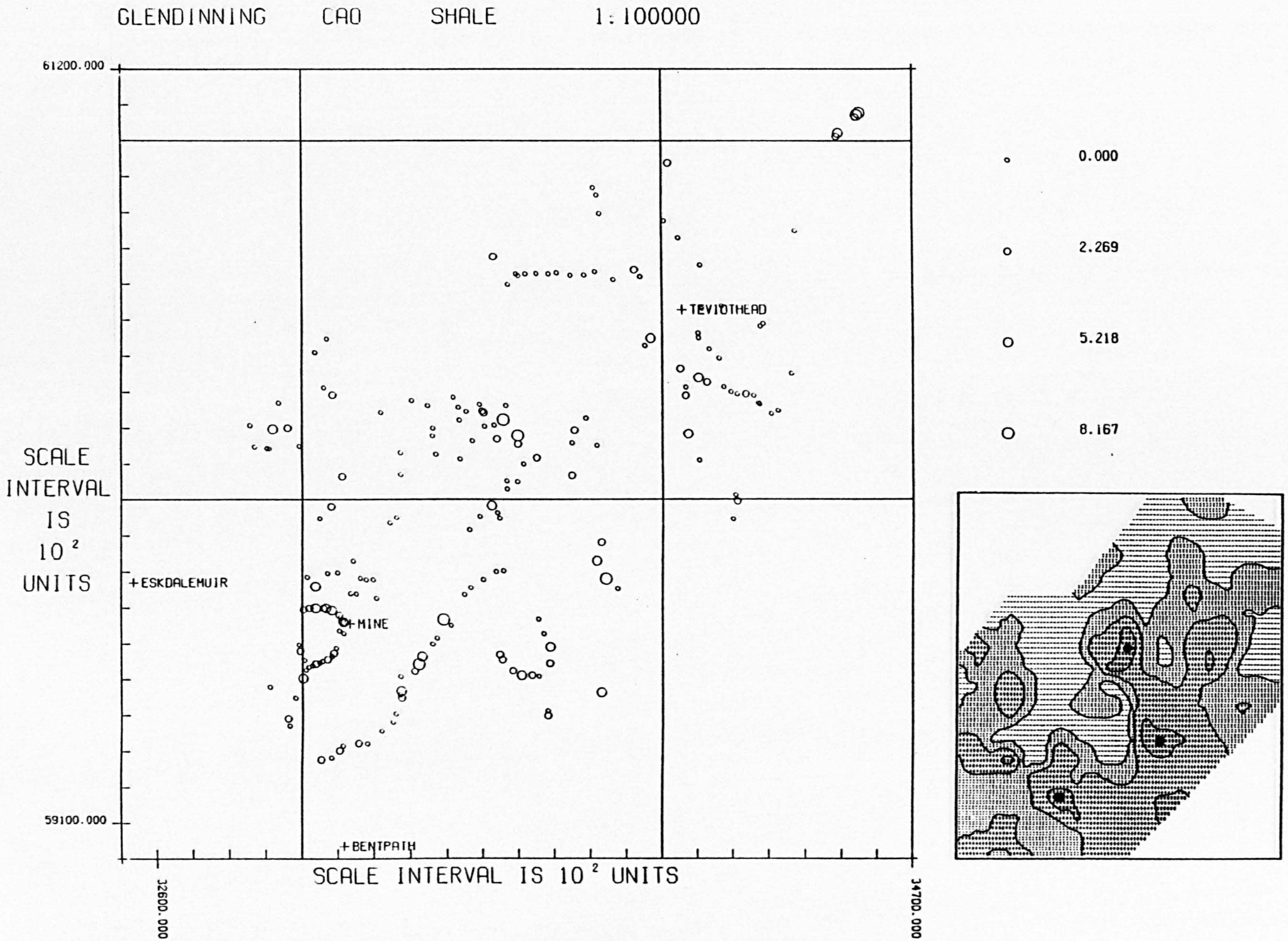
GLENDINNING CAO SHALE 1:100000
61200.000
59100.000
SCALE INTERVAL IS 10 2 UNITS
+ESKDALEMUIR
+TEVIOTHEAD
+MINE
+BENTPATH
SCALE INTERVAL IS 10 2 UNITS
32600.000
34700.000
0.000
2.269
5.218
8.167

FIGURE 195

FIGURE 196

GLENDINNING MGO SHALE 1:100000

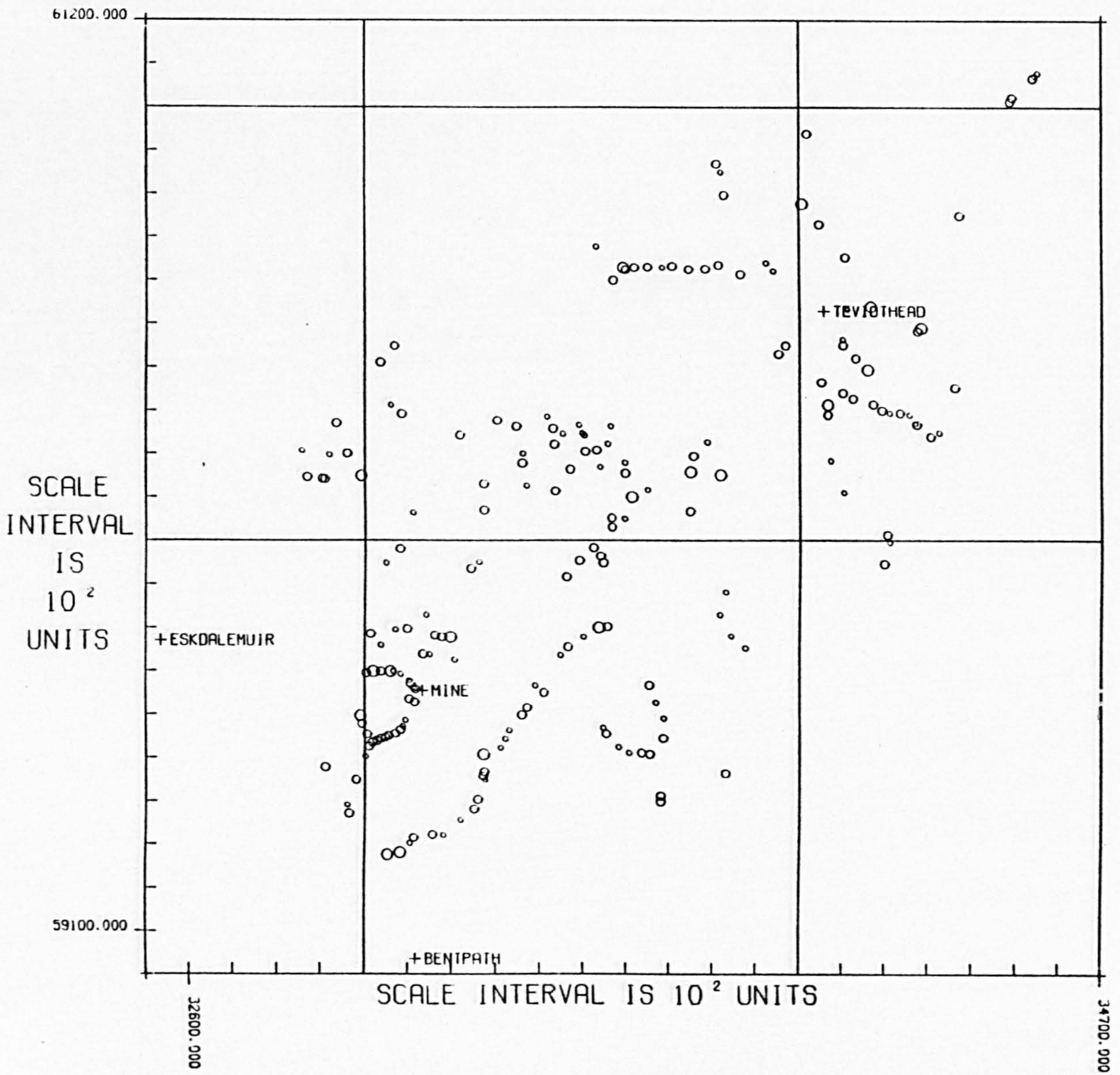

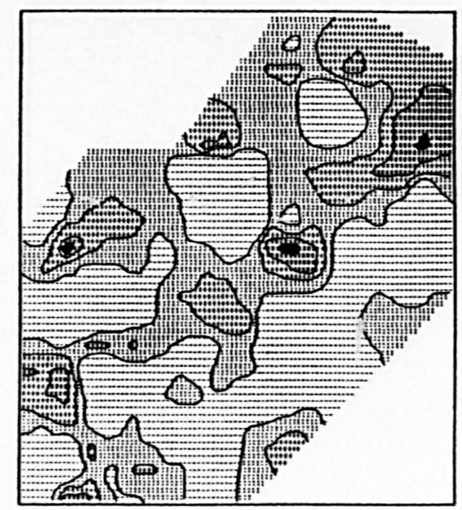

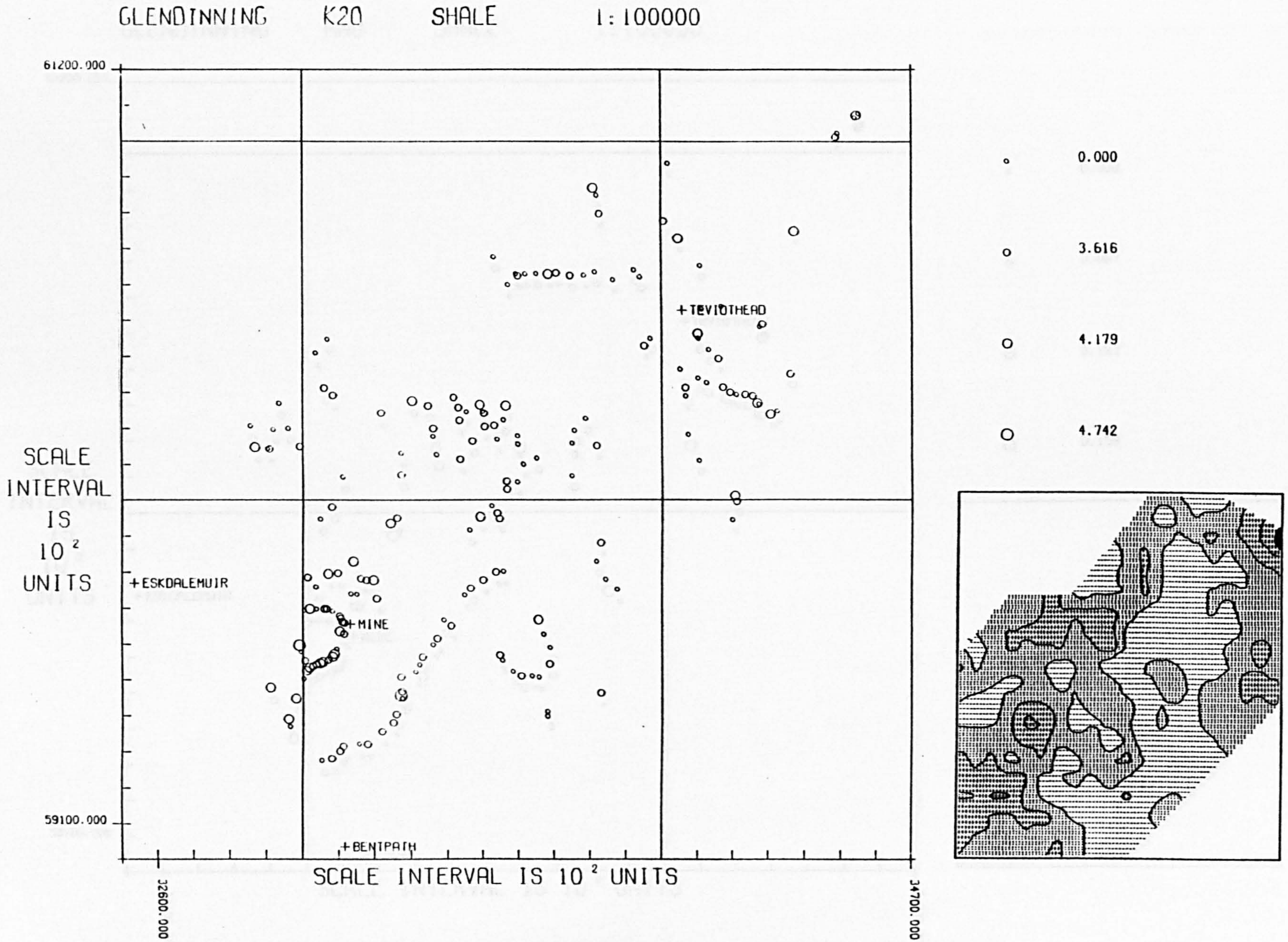
GLENDINNING K20 SHALE 1:100000
61200.000
59100.000
32600.000
34700.000
SCALE INTERVAL IS 10 ² UNITS
SCALE INTERVAL IS 10 ² UNITS
+ESKDALEMUIR
+MINE
+BENTPATH
+TEVIOTHEAD
0.000
3.616
4.179
4.742

FIGURE 197

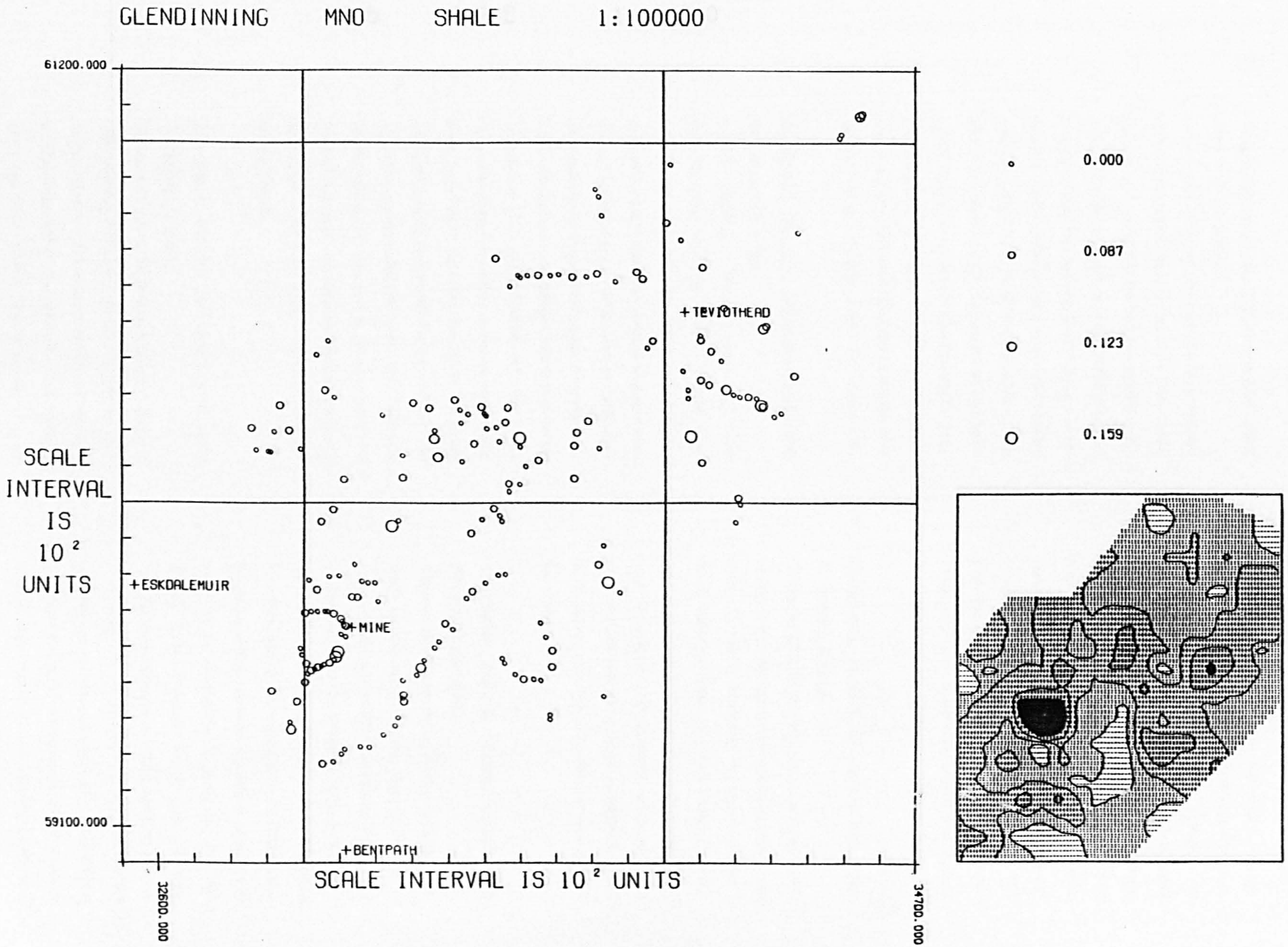
GLENDINNING MNO SHALE 1:100000
61200.000
59100.000
SCALE INTERVAL IS 10 ² UNITS
+ESKDALEMUIR
+MINE
+TEVIOTHEAD
+BENTPATH
SCALE INTERVAL IS 10 ² UNITS
32600.000
34700.000
0.000
0.087
0.123
0.159

FIGURE 198

FIGURE 199

GLENDINNING P205 SHALE 1:100000

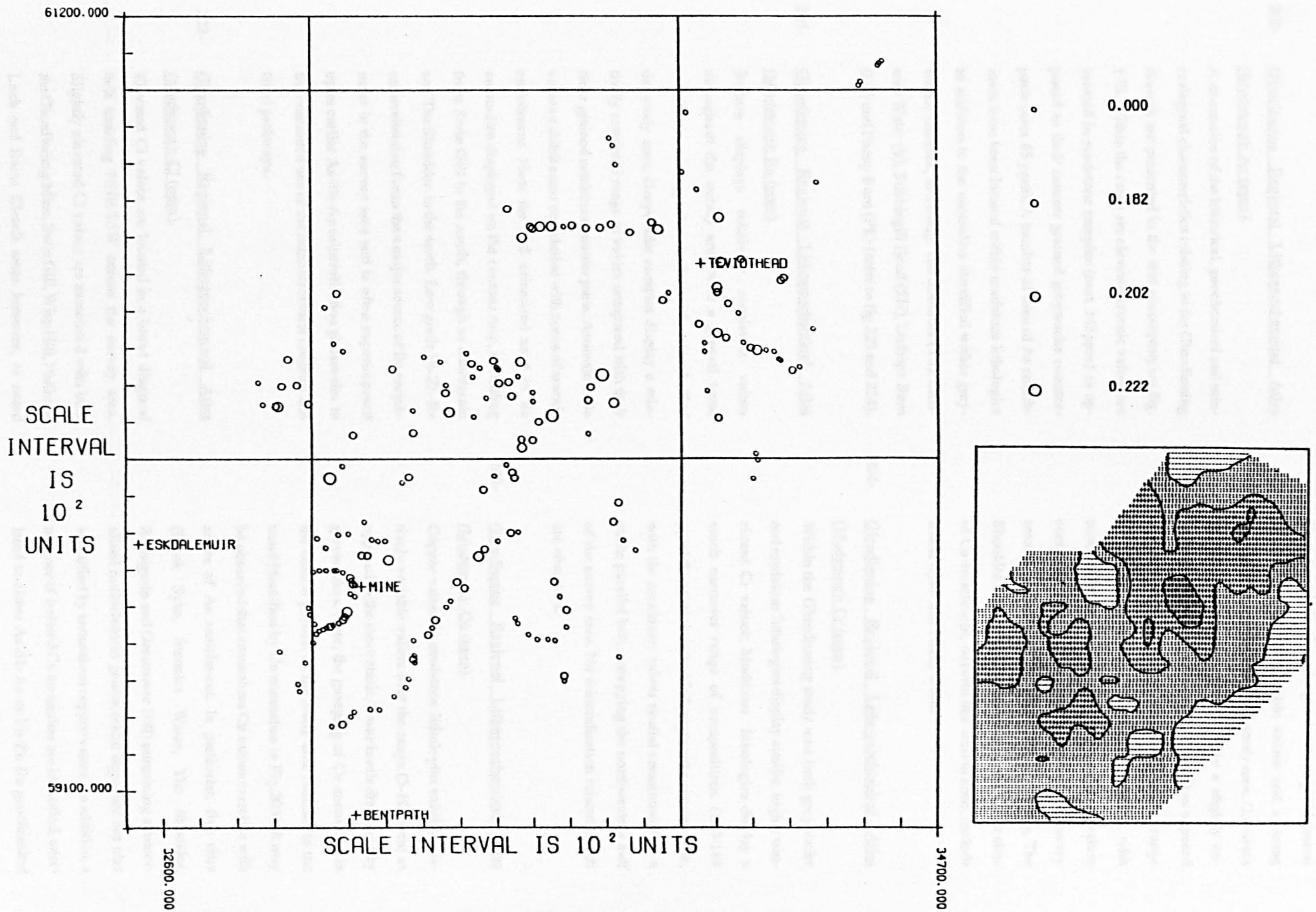

display an extremely restricted range of values throughout the survey area.

200- Glendinning Regional Lithogeochemical Atlas (Mudstone): As (ppm).
A discussion of the historical, geochemical and mineralogical characteristics relating to the Glendinning deposit are presented in the text accompanying fig. 170. Within the study are elevated arsenic values are located in mudstone samples (max 145ppm) as opposed to their coarser grained greywacke counterparts (max 65 ppm). A number of sites of As enrichment have been located within mudstone lithologies in addition to the anomalies identified within greywacke samples, including: The Shoulder (TS), Stennies Water (S), Stibbiegill Head (SH), Linhope Burn (LP) and Phaup Burn (PB) (refer to fig 223 and 224).

201- Glendinning Regional Lithogeochemical Atlas (Mudstone): Ba (ppm).
Barium displays relatively consistent values throughout the survey area with a general trend towards increasing values in the southeastern half of the study area. Greywacke samples display a relatively restricted range of values compared with their finer grained mudstone counter parts. Anomalous Ba values exhibit some correlation with zones of arsenic enrichment. Note the N-S orientated zone of Ba anomalies displayed on the contour map, extending from Swin Gill in the south, through to Rashigrain and The Shoulder, in the north. Low grade Pb-Zb-Ba mineralisation forms the a major source of Ba enrichment in the survey area and is often superimposed upon earlier As-Sb-Au mineralisation phases due to the continued use of the same structural controls and fluid pathways.

202- Glendinning Regional Lithogeochemical Atlas (Mudstone): Cl (ppm).
Elevated Cl values are located in a broad diagonal belt trending NNE-SSW across the survey area. Slightly elevated Cl values are associated with both the Glendinning Mine, Swin Gill, Wisp Hill, Philhope Loch and Rams Cleuch areas however, as noted earlier, the problems of contamination during sample preparation invalidate the use of this data in any geochemical model of mineralisation.

203- Glendinning Regional Lithogeochemical Atlas (Mudstone): Co (ppm).
Co values defined on the point source geochemical map display highly variable values and a strong systematic variation within the study area. Co values within mudstone lithologies display a slightly enlarged compositional range (13-76 ppm) as opposed to their interbedded greywacke counterparts (range 11-66ppm). Anomalous Co values correlate with zones of arsenic enrichment, with maximum values contained within the central portion of the survey area, in proximity to the Rams Cleuch, Cat Rig, The Shoulder and Rashigrain anomaly zones. Other sites of Co enrichment, outwith this central zone, include Black Syke and Phaup Burn.

204- Glendinning Regional Lithogeochemical Atlas (Mudstone): Cr (ppm).
Within the Glendinning study area both greywacke and mudstone lithologies display similar, highly consistent Cr values; Mudstone lithologies display a much narrower range of compositions (100-188 ppm) than their interbedded greywacke counterparts, with the maximum values spatial concentrated in a strike parallel belt, occupying the northwestern half of the survey area. No mineralisation related trends are observed.

205- Glendinning Regional Lithogeochemical Atlas (Mudstone): Cu (ppm).
Copper values in mudstone lithologies exhibit relatively variable values over the range (5-109ppm) as opposed to the more static, lower levels displayed by greywackes. Note, the grouping of Cu anomalies in the central portion of the study area (similar to the trend identified by Co anomalies in Fig.203). It may be observed that anomalous Cu values correlate with zones of As enrichment. In particular, five sites (Black Syke, Stennies Water, The Shoulder, Rashigrain and Greatmoor Hill) containing a mineralised multielement geochemical signature are also identified by anomalous copper values. In addition, a number of isolated Cu anomalies are identified, unrelated to either As-Sb-Au or Pb-Zn-Ba geochemical anomalies, and are attributed to the widespread occurrence of low grade Cu-dolomite vein mineralisation in this region.

GLENDINNING ARSENIC SHALE 1:100000

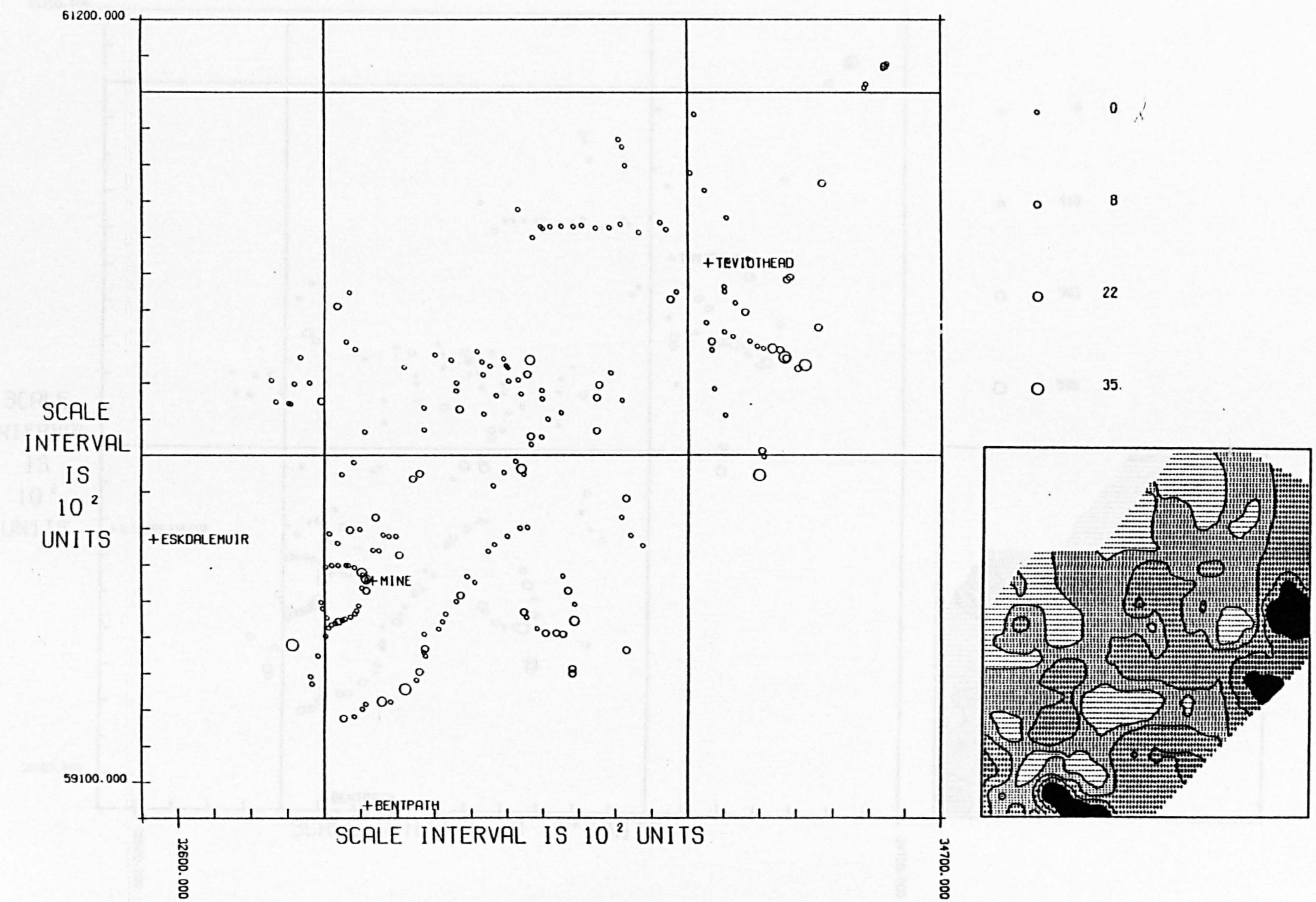

FIGURE 200

FIGURE 201

GLENDINNING BARIUM SHALE 1:100000

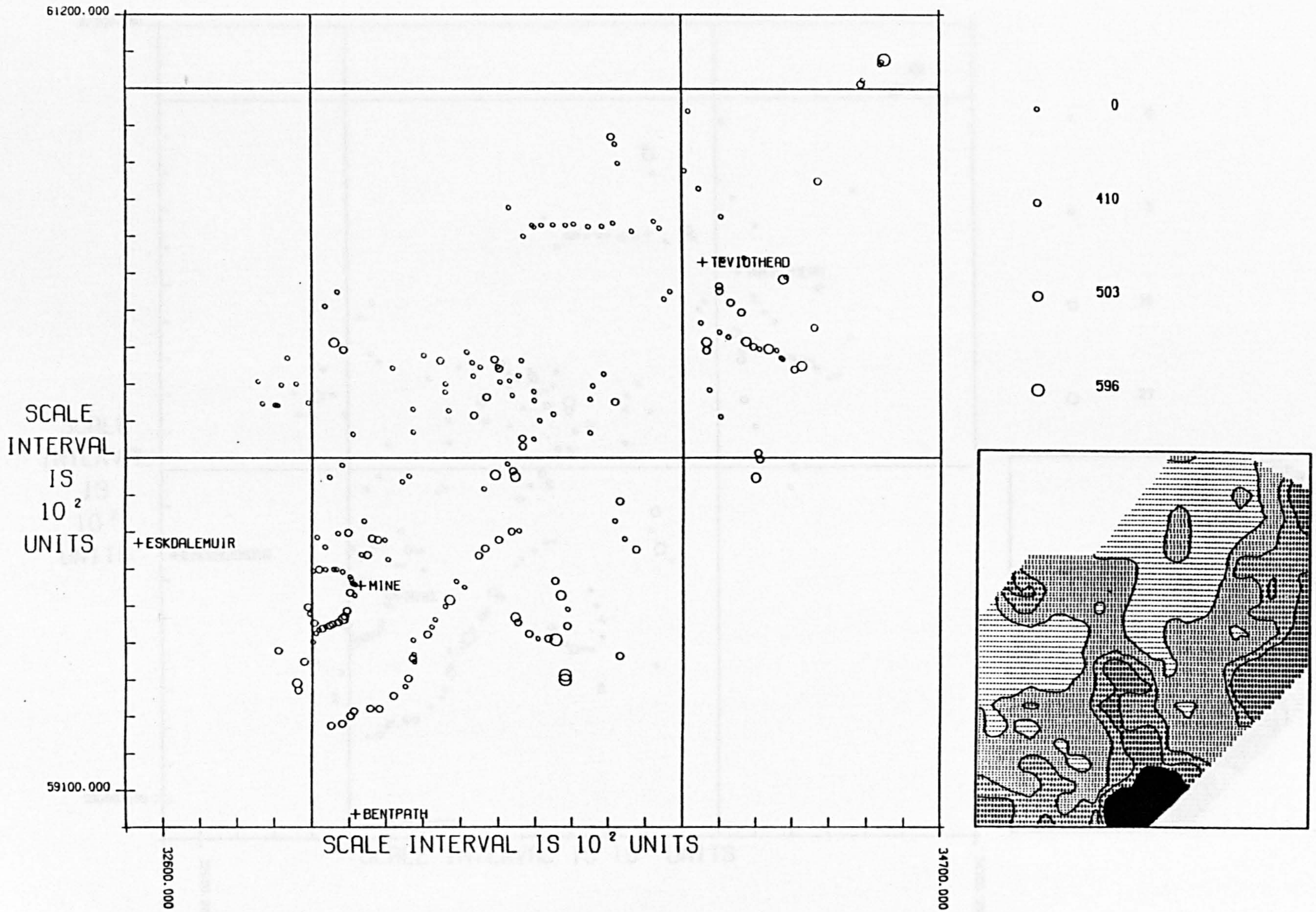

FIGURE 202

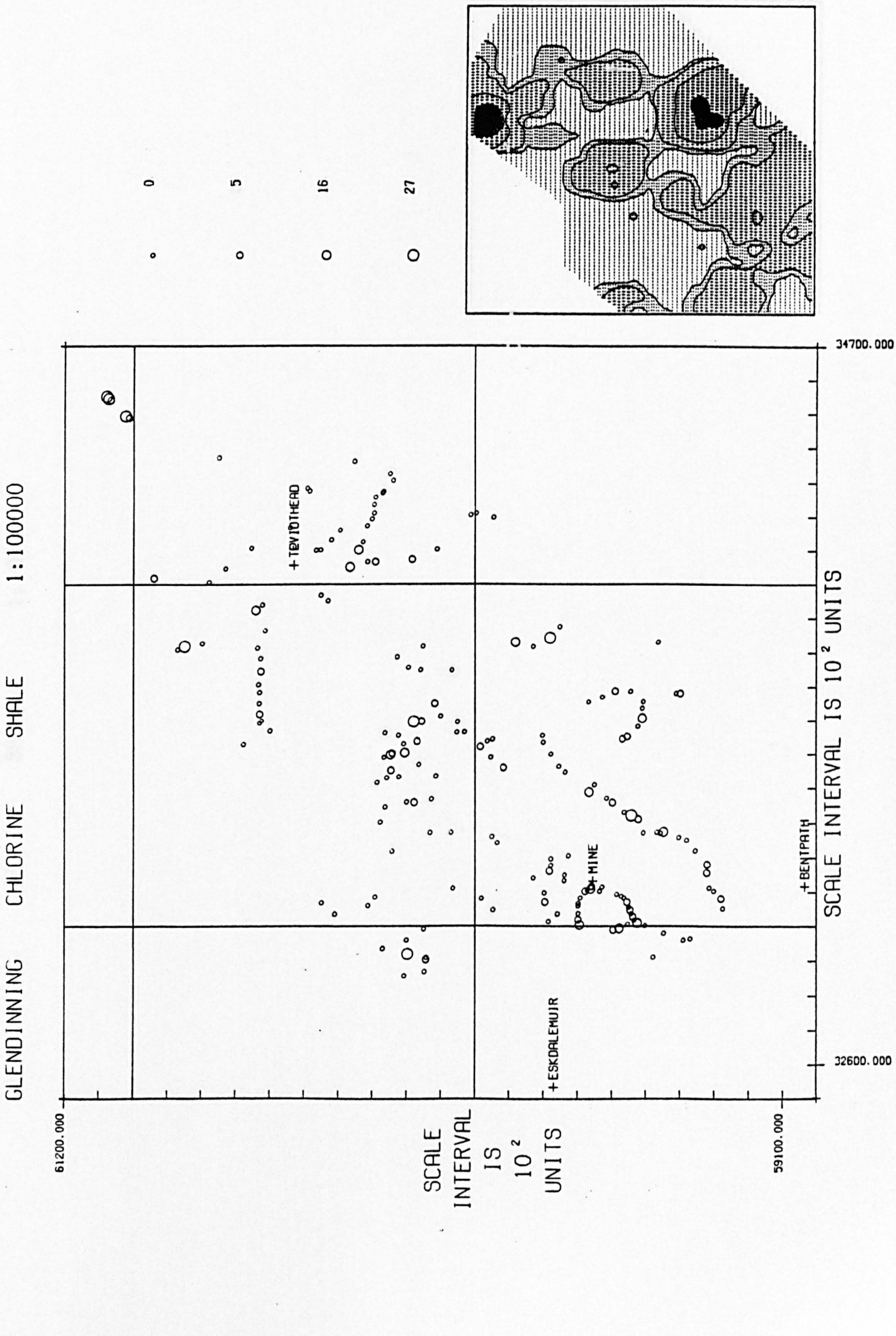
GLENDINNING CHLORINE SHALE 1:100000
0
5
16
27
+TEVIOTHEAD
+MINE
+BENTPATH
+ESKDALEMUIR
34700.000
32600.000
61200.000
59100.000
SCALE INTERVAL IS 10² UNITS
SCALE INTERVAL IS 10² UNITS

FIGURE 203

GLENDINNING COBALT SHALE 1:100000

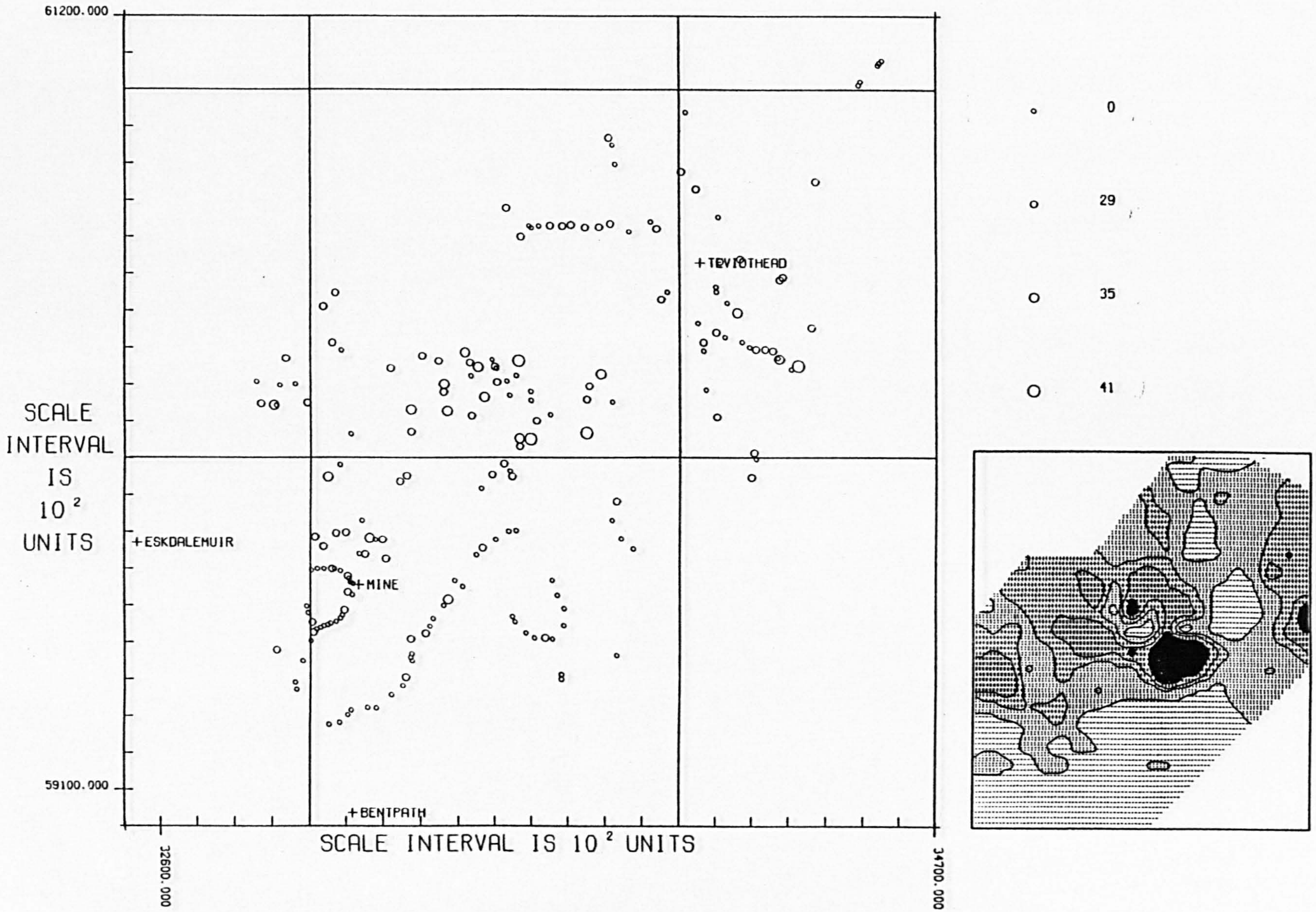

-1462-

FIGURE 204

GLENDINNING CHROMIUM SHALE 1:100000

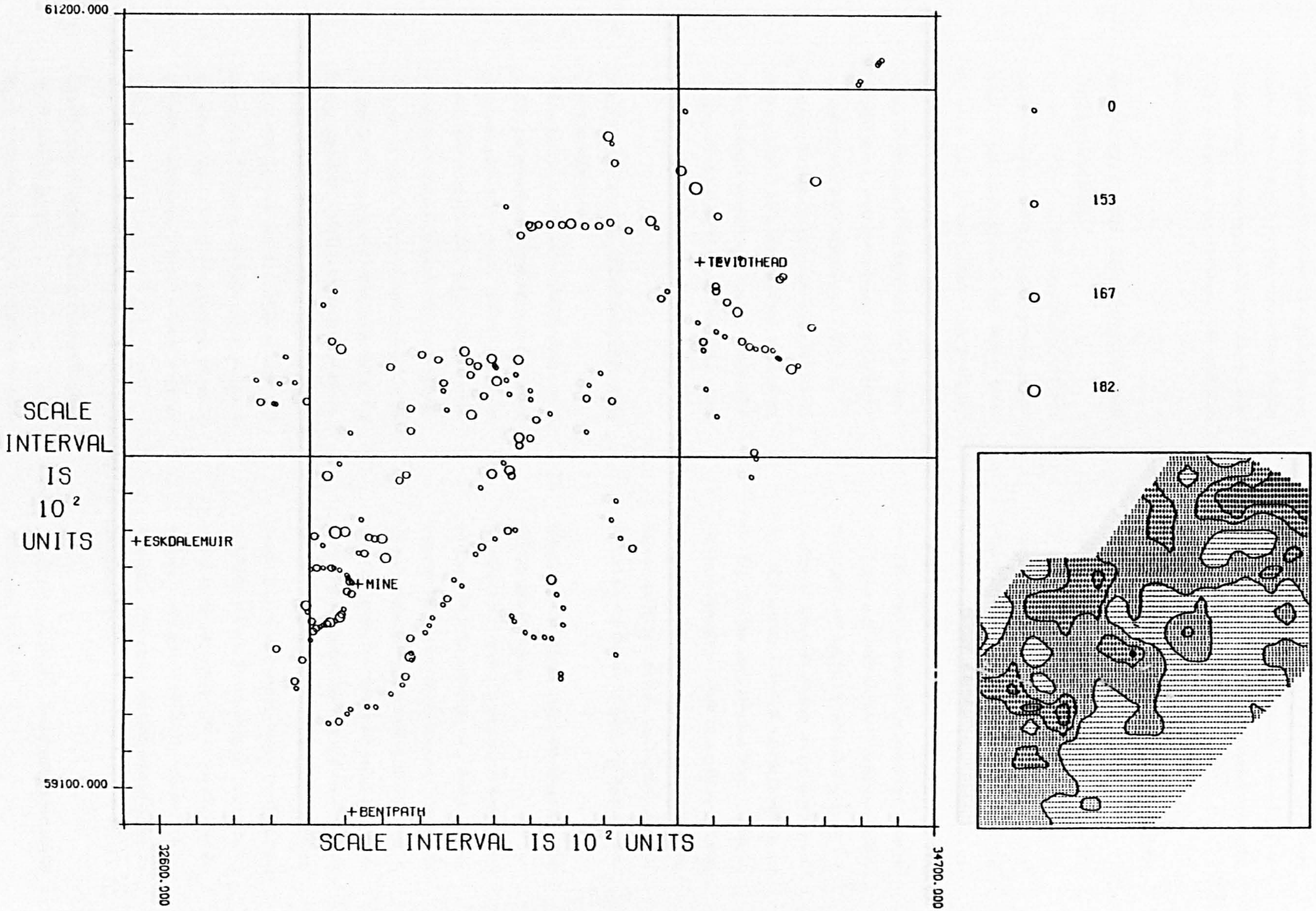

FIGURE 205

GLENDINNING COPPER SHALE 1:100000

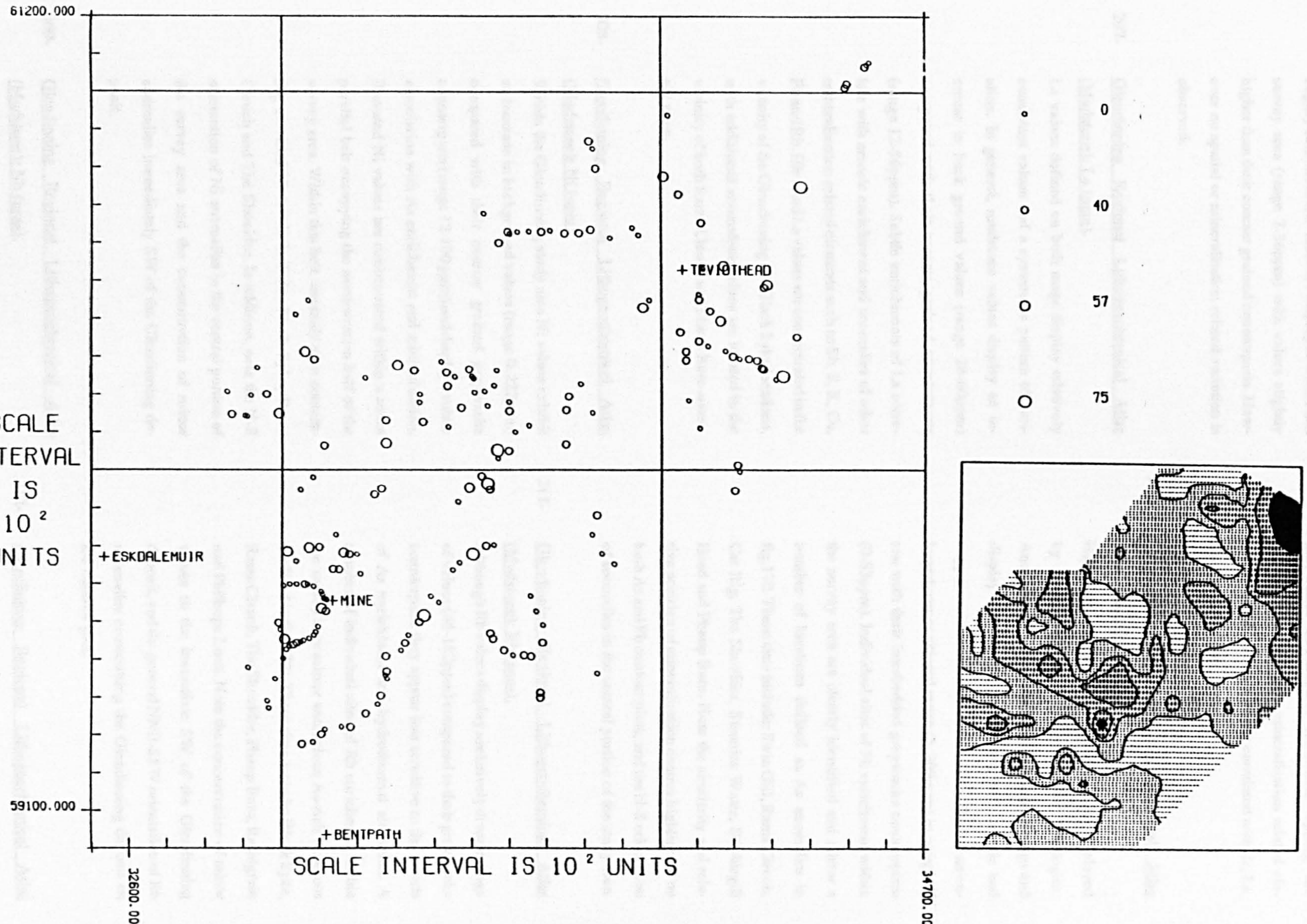

SCALE INTERVAL IS 10^2 UNITS

206- <u>Glendinning Regional Lithogeochemical Atlas (Mudstone): Ga (ppm)</u>.

Highly consistent Ga values are displayed within this survey area (range 7-36ppm) with values slightly higher than their coarser grained counterparts. However no spatial or mineralisation related variation is observed.

207- <u>Glendinning Regional Lithogeochemical Atlas (Mudstone): La (ppm)</u>.

La values defined on both maps display relatively consistent values and a systematic pattern of variation. In general, mudstone values display an increase in back ground values (range 28-60ppm) compared with their coarser grained counterparts (range 12-56ppm). Subtle enrichments of La correlate with arsenic enrichment and anomalies of other mineralisation related elements such as Sb, S, K, Cu, Pb and Rb. Elevated La values are concentrated in the vicinity of the Glendinning and Black Syke locations, with additional anomalous values are located in the vicinity of both Rams Cleuch and Phaup Burn anomaly zone.

208- <u>Glendinning Regional Lithogeochemical Atlas (Mudstone): Ni (ppm)</u>.

Within the Glendinning study area Ni values exhibit an increase in background values (range 0-222ppm) compared with their coarser grained greywacke counterparts (range 12-100 ppm) and display a subtle association with As enrichment and mineralisation. Elevated Ni values are concentrated within a strike parallel belt occupying the northwestern half of the survey area. Within this belt, anomaly sites containing elevated Ni levels include: Black Syke, Rams Cleuch and The Shoulder. In addition, note the N-S orientation of Ni anomalies in the central portion of the survey area and the concentration of minor anomalies immediately SW of the Glendinning deposit.

209- <u>Glendinning Regional Lithogeochemical Atlas (Mudstone): Nb (ppm)</u>.

Highly consistent Nb values defined on the point source geochemical map display a relatively cryptic pattern of variation within the study area. Nb values display a slight increase in background levels (minimum 10ppm) in comparison with their interbedded greywacke counterparts (minimum 4ppm); are weakly correlated with mineralisation related elements (As/Sb); and positively correlated with Zr, La, Th, Na, K and Rb.

210- <u>Glendinning Regional Lithogeochemical Atlas (Mudstone): Pb (ppm)</u>.

Highly consistent background levels are displayed by both greywacke and mudstone lithologies. Anomalous Pb values are defined on both maps and display a close correlation with both arsenic and copper enrichment. Mudstone values display an enlarged compositional range (5-209ppm) in comparison with their interbedded greywacke counterparts (0-53ppm). Individual sites of Pb enrichment within the survey area are clearly identified and mirror a number of locations defined as As anomalies in fig.170. These sites include: Swin Gill, Rams Cleuch, Cat Rig, The Shoulder, Stennies Water, Stibbiegill Head and Phaup Burn. Note the similarity and relative position of mineralisation centres highlighted on both As and Pb contour plots, and the N-S orientation of anomalies in the central portion of the study area.

211- <u>Glendinning Regional Lithogeochemical Atlas (Mudstone): Rb (ppm)</u>.

Although Rb values display a relatively diverse range of values (64-182ppm) compared to their greywacke counterparts they appear less sensitive to the effects of As enrichment and hydrothermal alteration. A number of individual sites of Rb enrichment within the survey area mirror anomalous As-rich locations (defined in fig.170). These sites include: Black Syke, Rams Cleuch, The Shoulder, Phaup Burn, Rashigrain and Philhope Loch. Note the concentration of minor values to the immediate SW of the Glendinning deposit, and the general NNE-SSW orientation of Rb anomalies crosscutting the Glendinning deposit on the contour plot.

212- <u>Glendinning Regional Lithogeochemical Atlas (Mudstone): Sr (ppm)</u>.

Sr displays generally consistent values throughout the survey area, with mudstone lithologies displaying

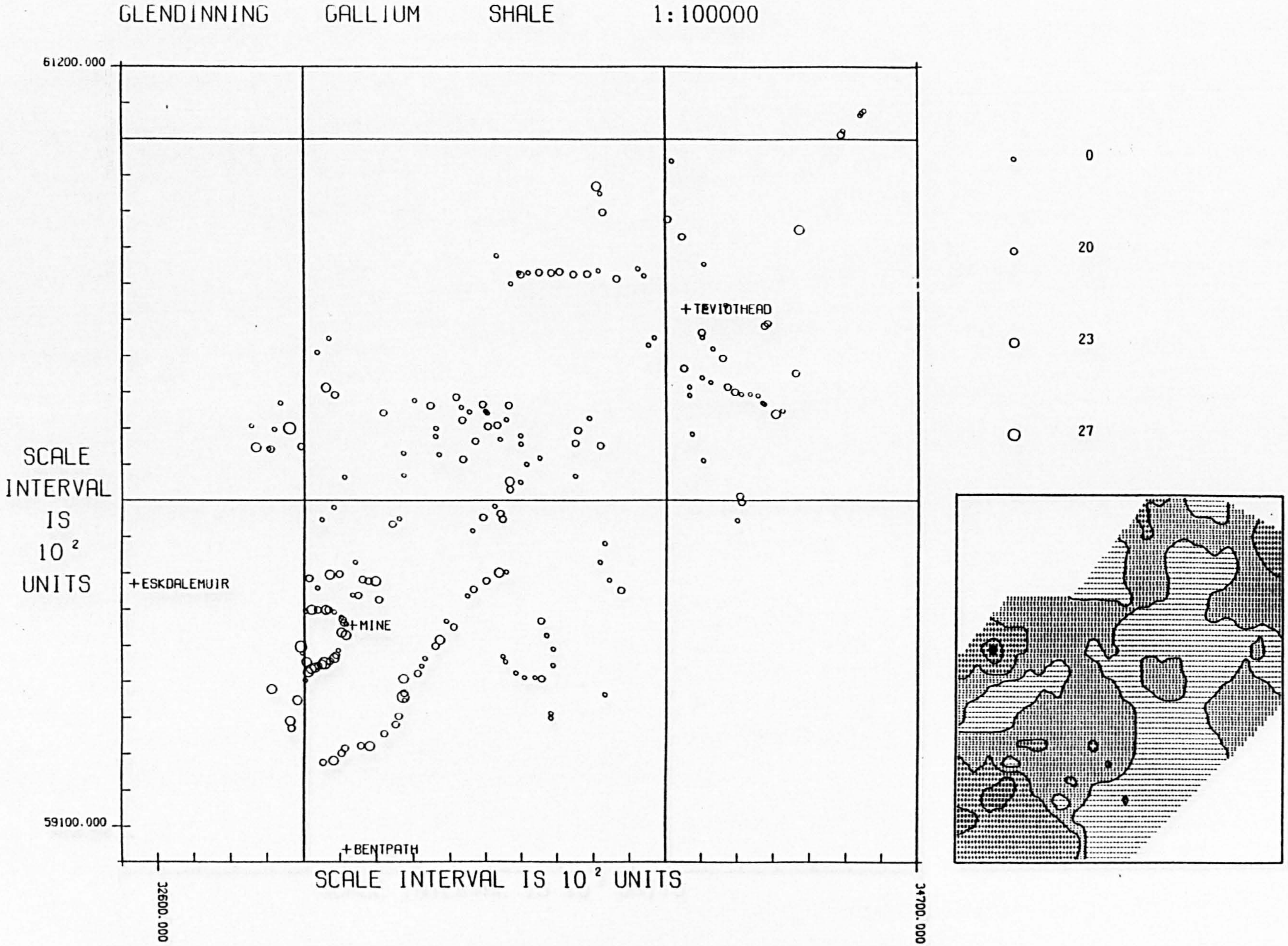
GLENDINNING GALLIUM SHALE 1:100000
61200.000
59100.000
32600.000
34700.000
SCALE INTERVAL IS 10 ² UNITS
SCALE INTERVAL IS 10 ² UNITS
+ESKDALEMUIR
+TEVIOTHEAD
+MINE
+BENTPATH
0
20
23
27

FIGURE 206

FIGURE 207

GLENDINNING LA SHALE 1:100000

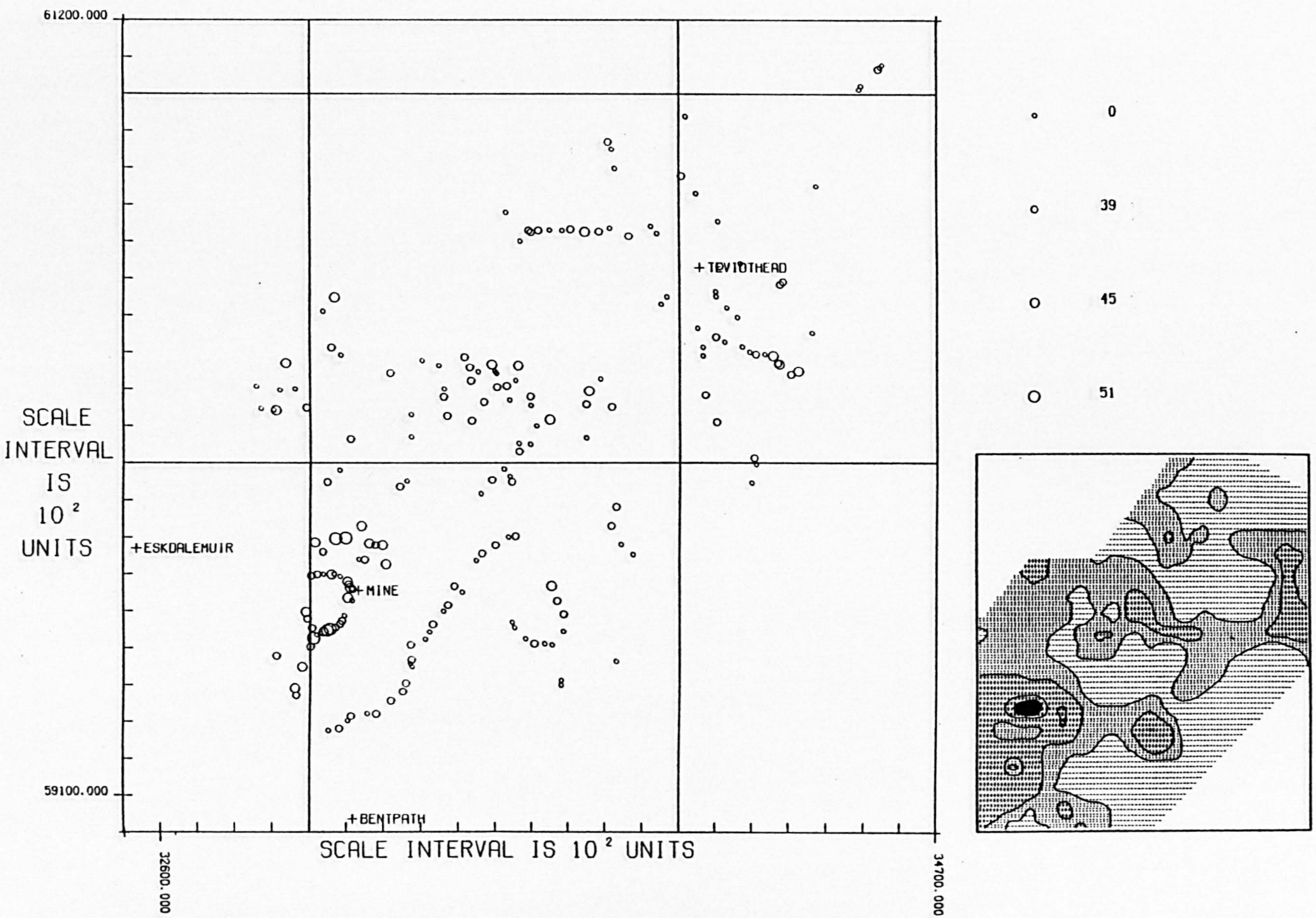

GLENDINNING NICKEL SHALE 1:100000

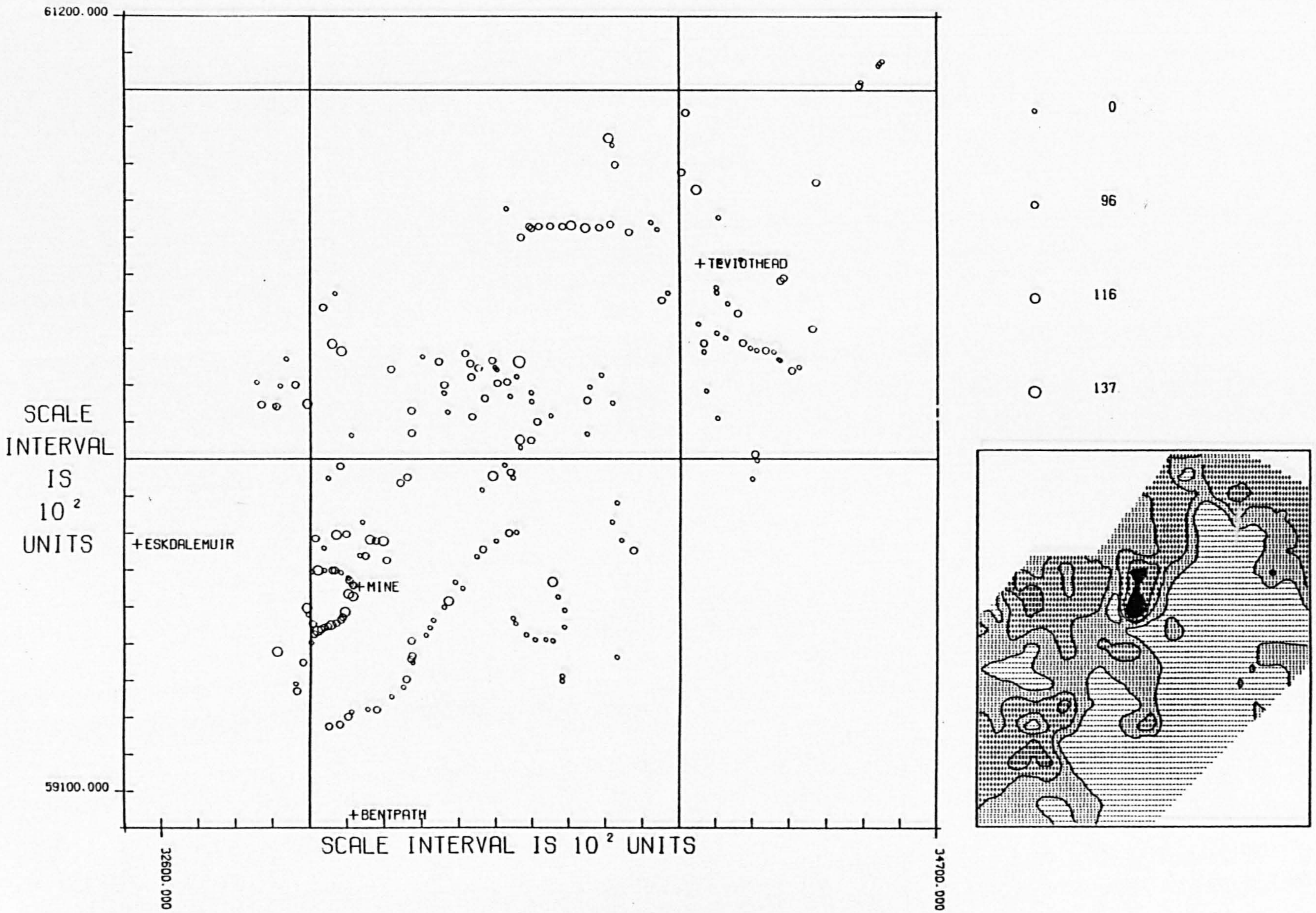

FIGURE 208

GLENDINNING NIOBIUM SHALE 1:100000

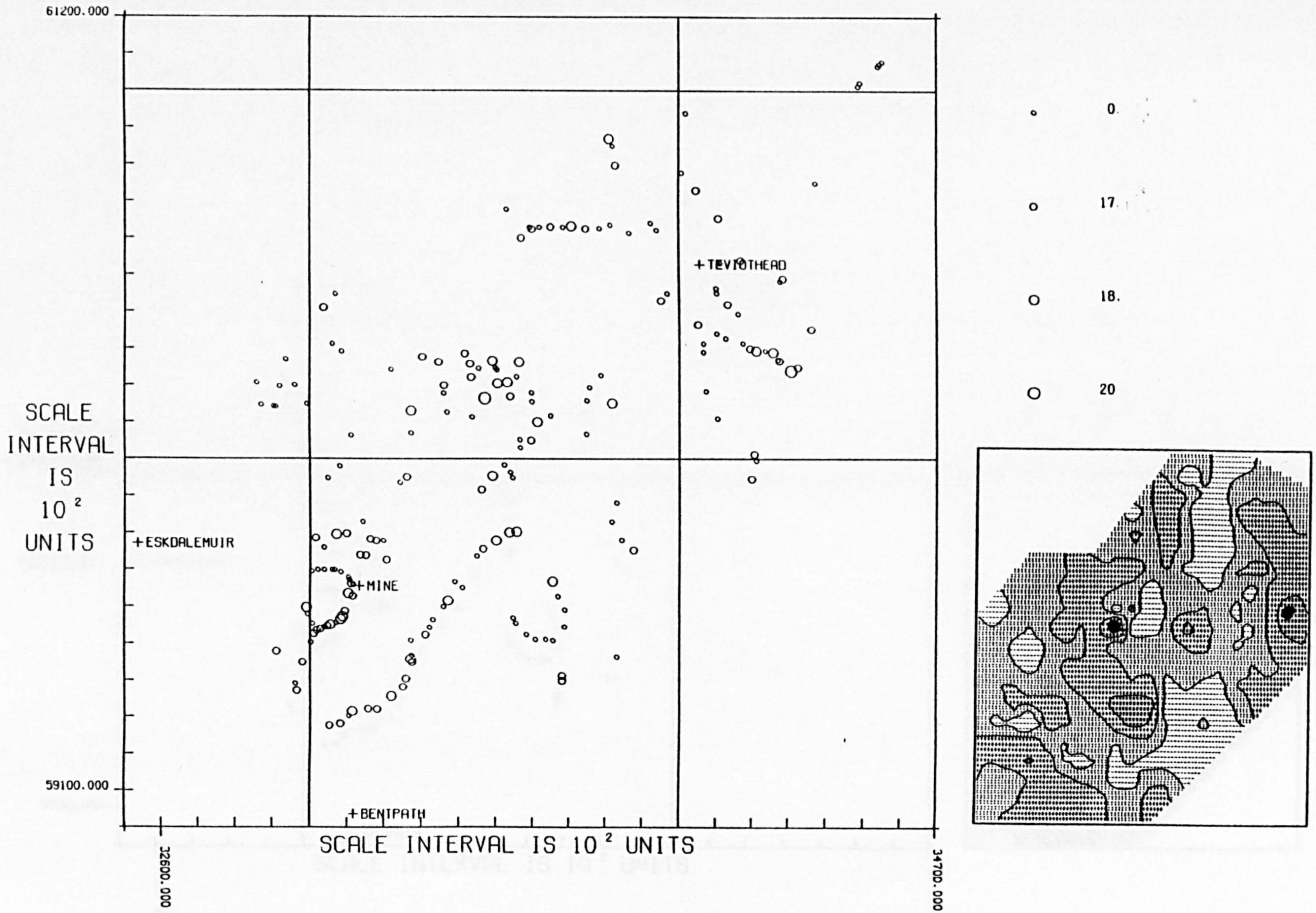

FIGURE 209

FIGURE 210

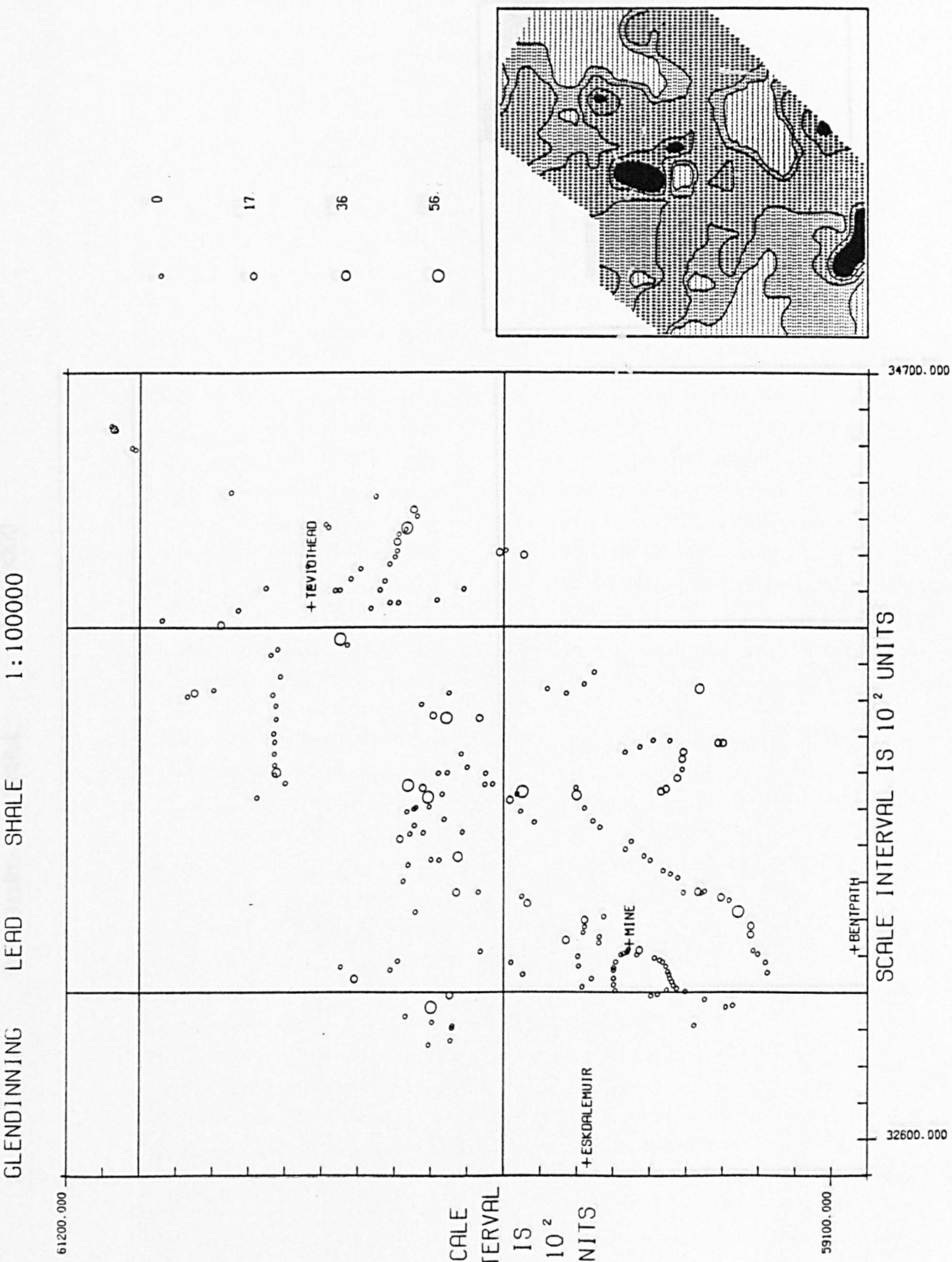
GLENDINNING LEAD SHALE 1:100000
0
17
36
56
+TEVIOTHEAD
+MINE
+BENTPATH
+ESKDALEMUIR
34700.000
32600.000
61200.000
59100.000
SCALE INTERVAL IS 10² UNITS
SCALE INTERVAL IS 10² UNITS

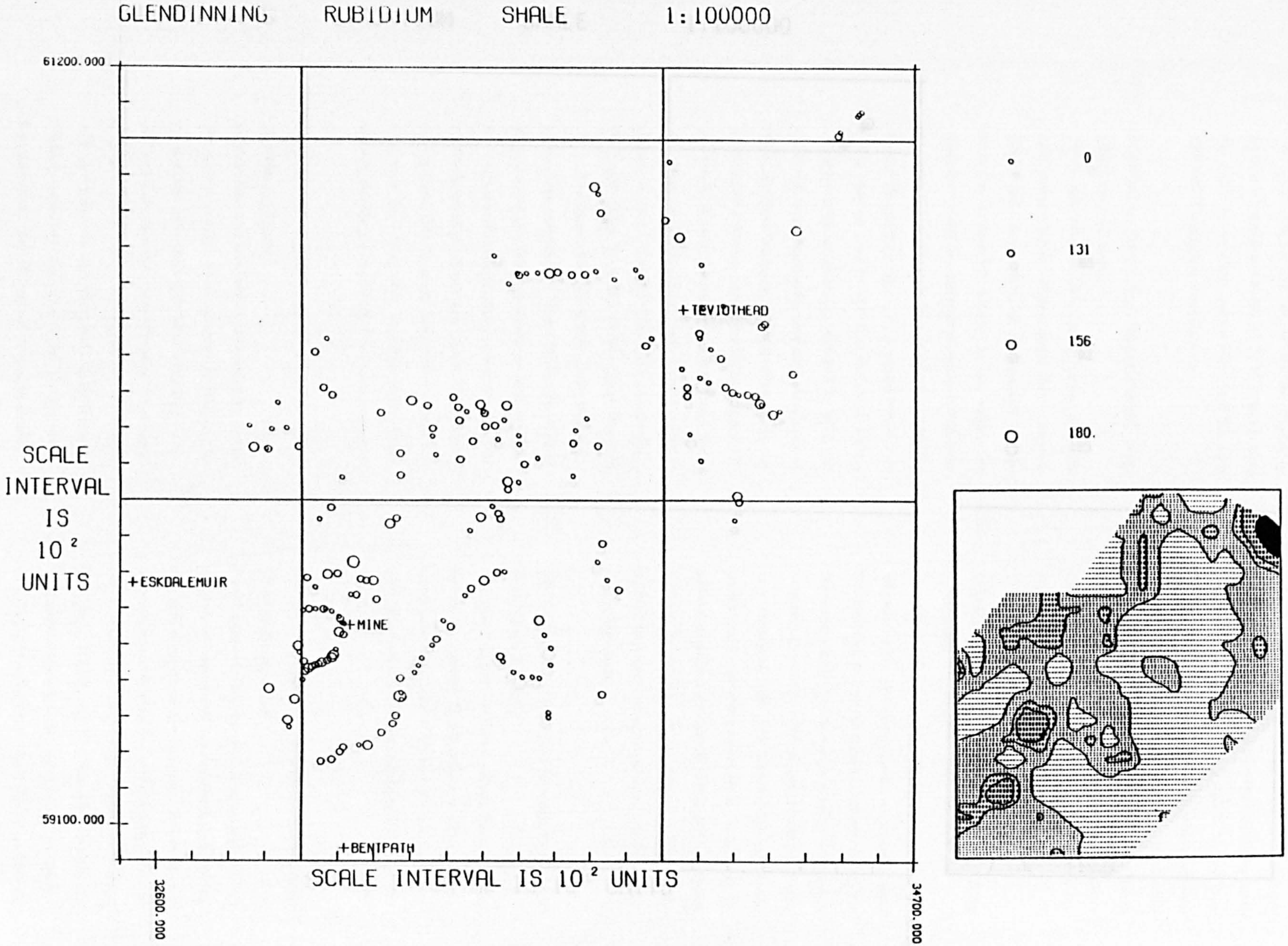
GLENDINNING RUBIDIUM SHALE 1:100000
61200.000
59100.000
SCALE INTERVAL IS 10 2 UNITS
+ESKDALEMUIR
+TEVIOTHEAD
+MINE
+BENTPATH
SCALE INTERVAL IS 10 2 UNITS
3260.000
3470.000
0
131
156
180.

FIGURE 211

FIGURE 212

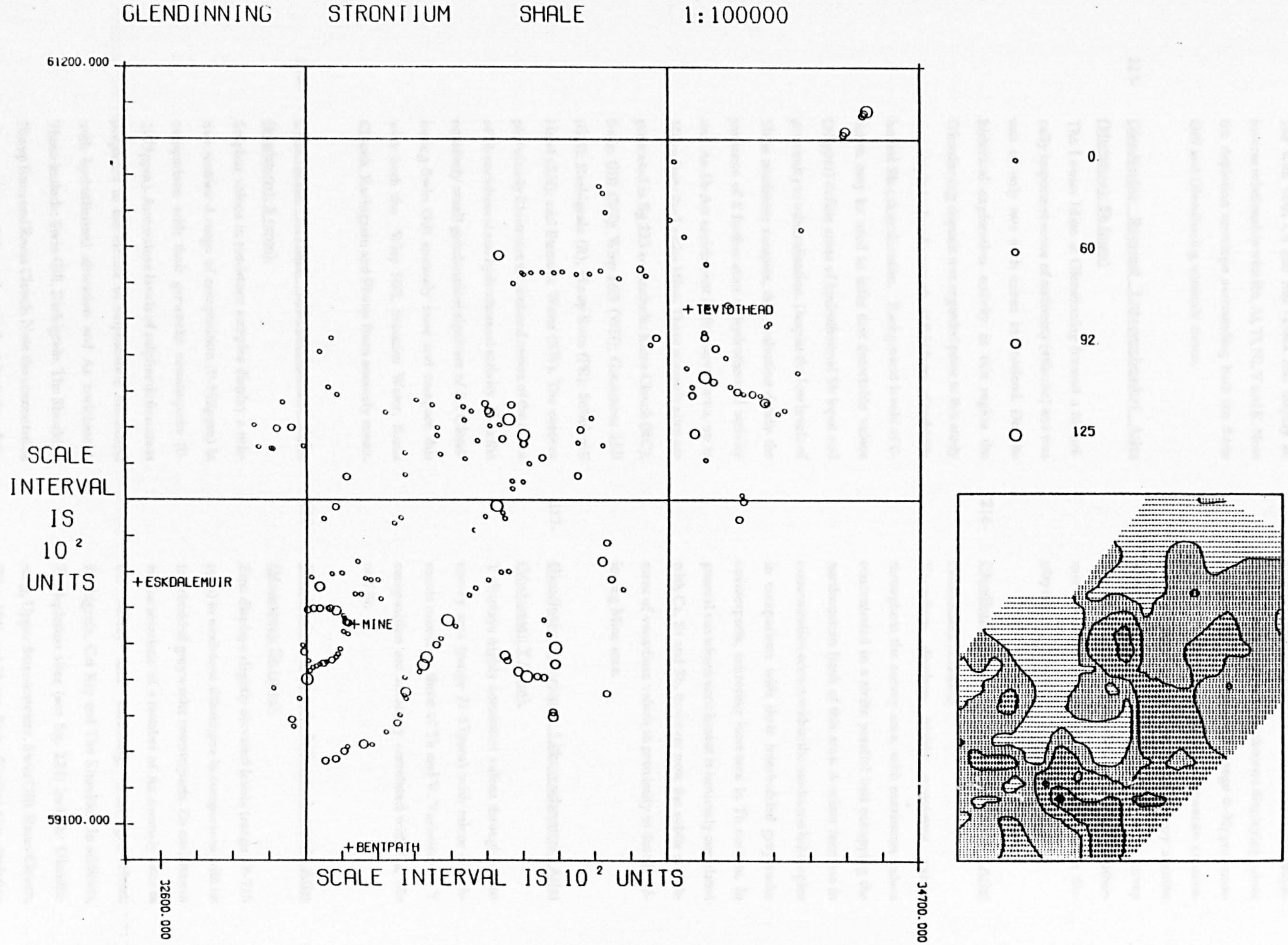

GLENDINNING STRONTIUM SHALE 1:100000
61200.000
59100.000
32600.000
34700.000
SCALE INTERVAL IS 10 ² UNITS
SCALE INTERVAL IS 10 ² UNITS
+ESKDALEMUIR
+MINE
+BENTPATH
+TEVIOTHEAD
0.
60
92
125

systematically lower values (20-278ppm) than their greywacke counterparts. Spatially, Sr values correlate with both Ca and Mn values and display an inverse relationship with Rb, Al, Ti, Ni, V and K. Note the depletion envelope surrounding both the Swin Gill and Glendinning anomaly zones.

213- Glendinning Regional Lithogeochemical Atlas (Mudstone): Sb (ppm)
The Louisa Mine at Glendinning formed a historically important souce of antinomy (stibnite) and was one of only two such mines in Scotland. Despite historical exploration activity in this region the Glendinning deposit was regarded prior to this study as a single isolated example of this form of turbidite hosted Sb-mineralisation. Background levels of 0-2ppm may be used to infer that detectable values (>5ppm) define areas of hydrothermal Sb input and proximity to mineralisation. Despite the low levels of Sb in mudstone samples, this evaluation details the presence of 8 further sites of hydrothermal activity and As-Sb-Au enrichment in the survey area, up to 10km from the Louisa Mine. These anomaly sites are presented in fig 223 and include: Rams Cleuch (RC); Swin Gill (SG); Wisp Hill (WH); Greatmoor Hill (GH); Rashigrain (R); Phaup Burn (PB); Stibbiegill Head (SH); and Stennies Water (SW). The contour plot clearly illustrates the isolated nature of the zones of Sb enrichment and hydrothermal activity. Note the relatively small geochemical signiture of the Glendinning-Swin Gill anomaly zone and compare this with both the Wisp Hill, Stennies Water, Rams Cleuch, Rashigrain and Phaup Burn anomaly zones.

214- Glendinning Regional Lithogeochemical Atlas (Mudstone): S (ppm).
Sulphur values in mudstone samples display a relative restricted range of composition (0-592ppm) in comparison with their grewacke counterparts (0-2975ppm). Anomalous levels of sulphur define areas subjected to the effects of sulphidation associated with hydrothermal alteration and As enrichment. These include: Swin Gill, Rashigrain, The Shoulder-Phaup Burn and Rams Cleuch. Note the concentation of anomalous sulphur values in the tributaries of the Swin Gill zone, at the southern margin of the study area.

215- Glendinning Regional Lithogeochemical Atlas (Mudstone): Th (ppm).
Highly consistent pattern of Th values occur throughout the study area with mudstones displaying minor enrichments in composition (range 0-30ppm) compared with their inter-bedded greywacke counterparts. Slightly elevated Th levels occupy a strike parralel belt on the northwestern flank of the survey area. However, no direct relationship with hydrothermal alteration or As-Sb-Au mineralisation is displayed.

216- Glendinning Regional Lithogeochemical Atlas (Mudstone): V (ppm).
Vanadium displays highly consistent values throughout the survey area, with maximum values concentrated in a strike parallel belt occupying the northwestern flank of this area. A minor increase in concentration occurs within the mudstone lithologies in comparison with their interbedded greywacke counterparts, mirroring increases in Th content. In general vanadium enrichment is inversely correlated with Ca, Sr and Sb, however note the subtle enrichment of vanadium values in proximity to the Glendinning Mine area.

217- Glendinning Regional Lithogeochemical Atlas (Mudstone): Y (ppm).
Y displays highly consistent values throughout the survey area (range 21-57ppm) with minor enrichments mirroring those of Th and V. Variations in Y composition are inversely correlated with Ca, Mn and Sr.

218- Glendinning Regional Lithogeochemical Atlas (Mudstone): Zn (ppm).
Zinc displays slightly elevated levels (range 18-718 ppm) in mudstone lithologies in comparison with its interbedded greywacke counterparts. Zn enrichment is characteristic of a number of As anomaly sites in the survey area including: Stibbiegill Head, Rashigrain, Cat Rig and The Shoulder. In addition, Zn depletion sites (see fig. 224) include: Glendinning, Upper Stennieswater, Swin Gill, Rams Cleuch, Wisp Hill and Phaup Burn. Similar zinc depletion processes were located by Stone (1985) to the west of

FIGURE 213

GLENDINNING ANTIMONY SHALE 1:100000

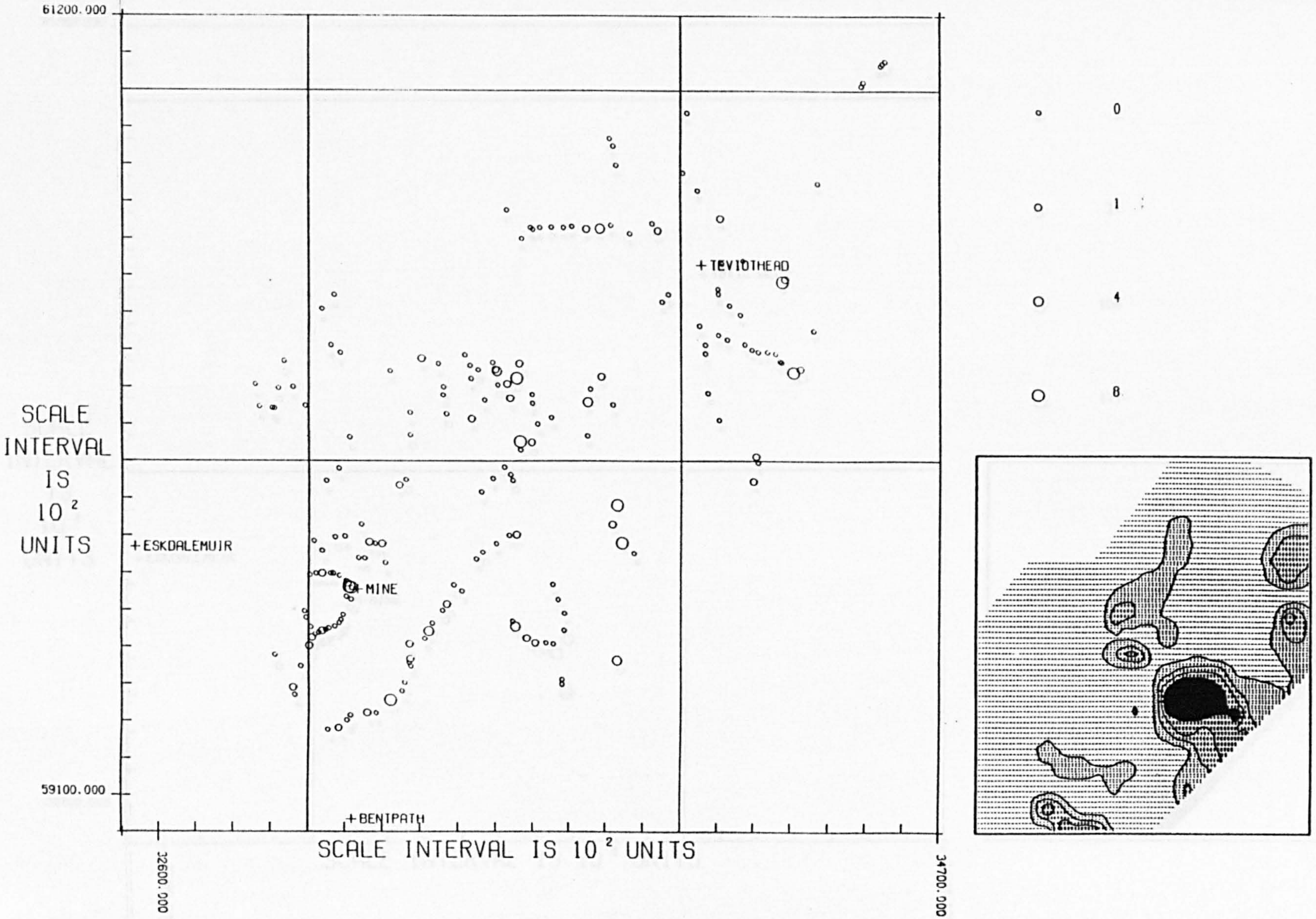

GLENDINNING SULPHUR SHALE 1:100000

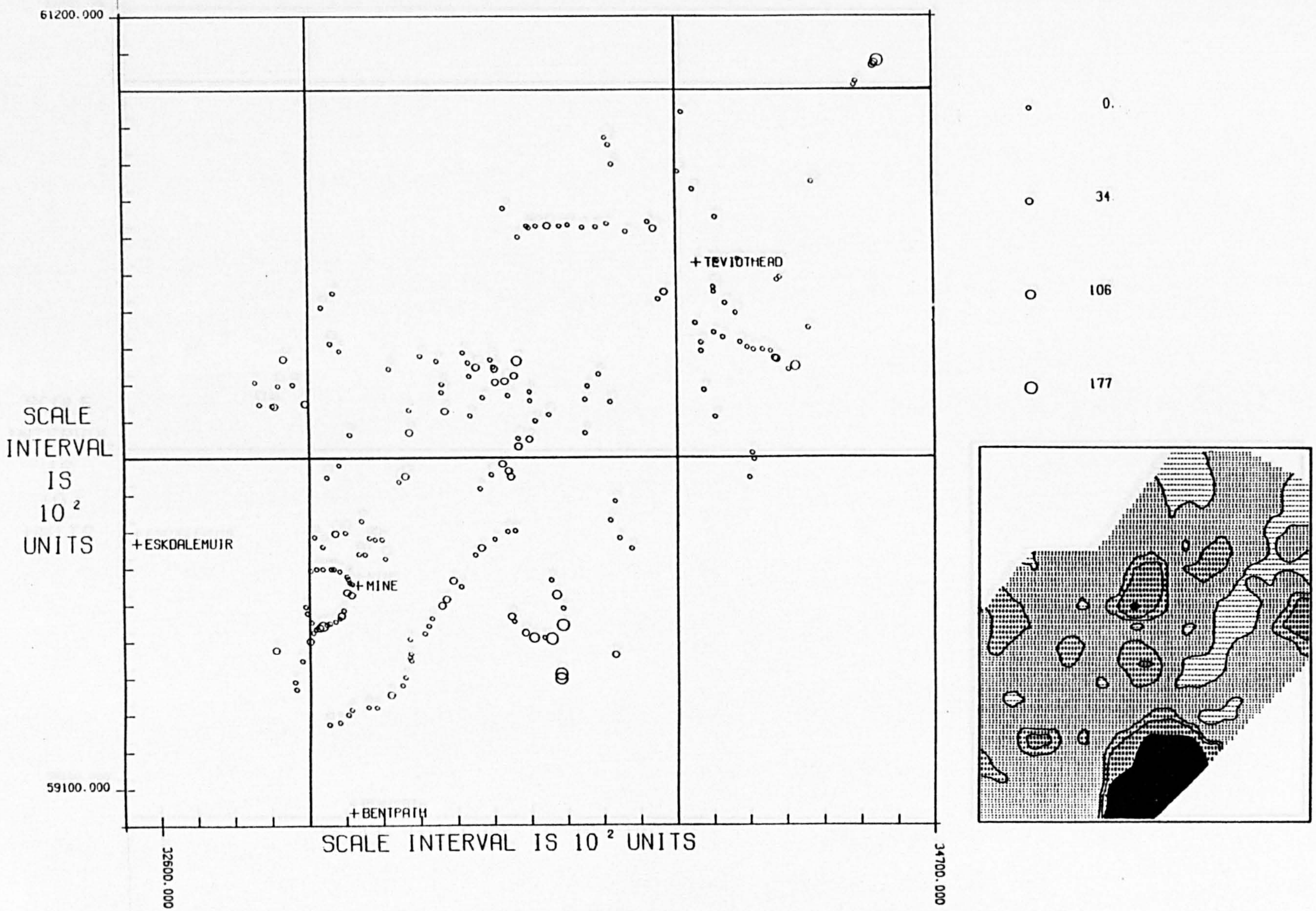

FIGURE 214

GLENDINNING THORIUM SHALE 1:100000

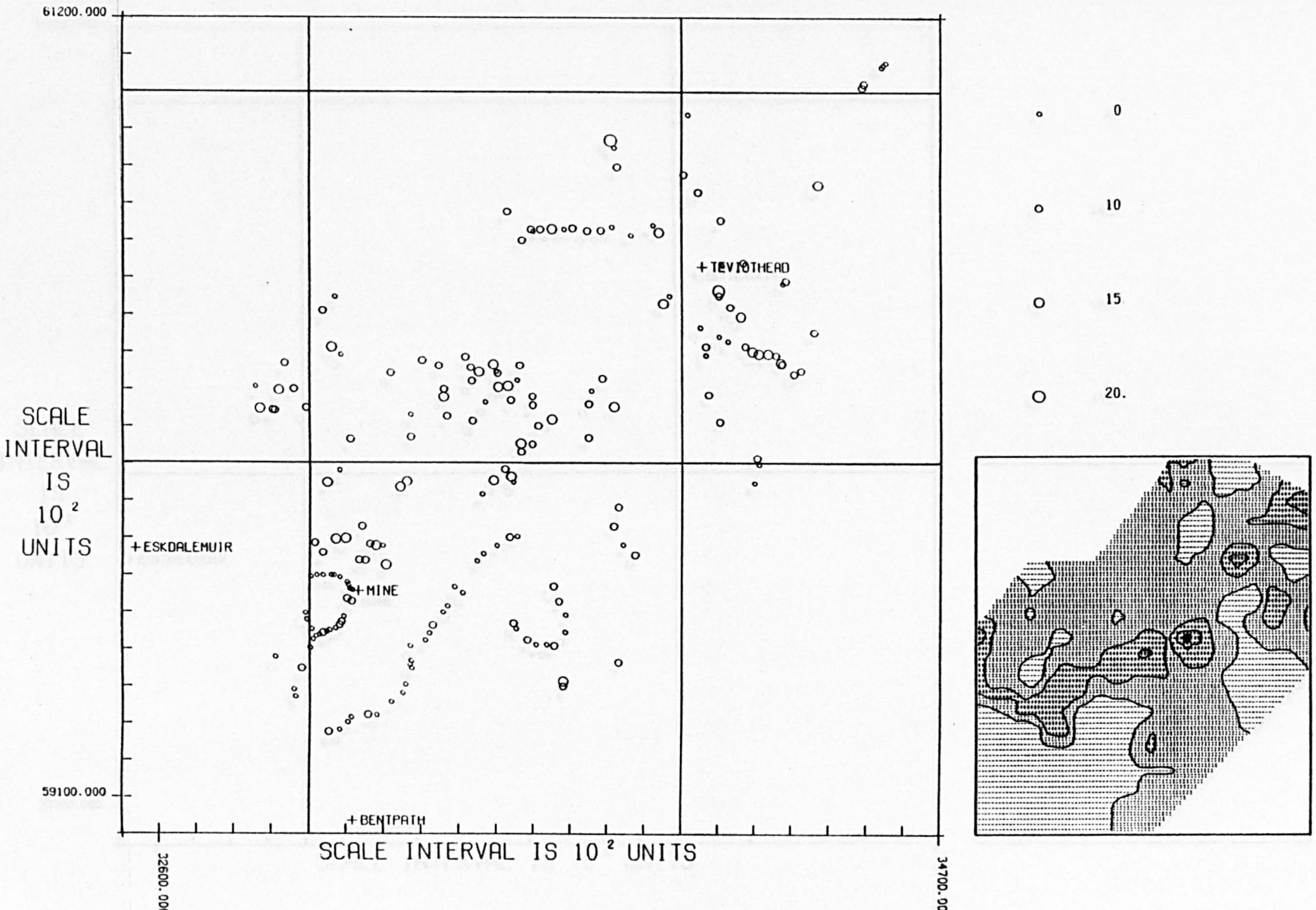

FIGURE 215

GLENDINNING VANADIUM SHALE 1:100000

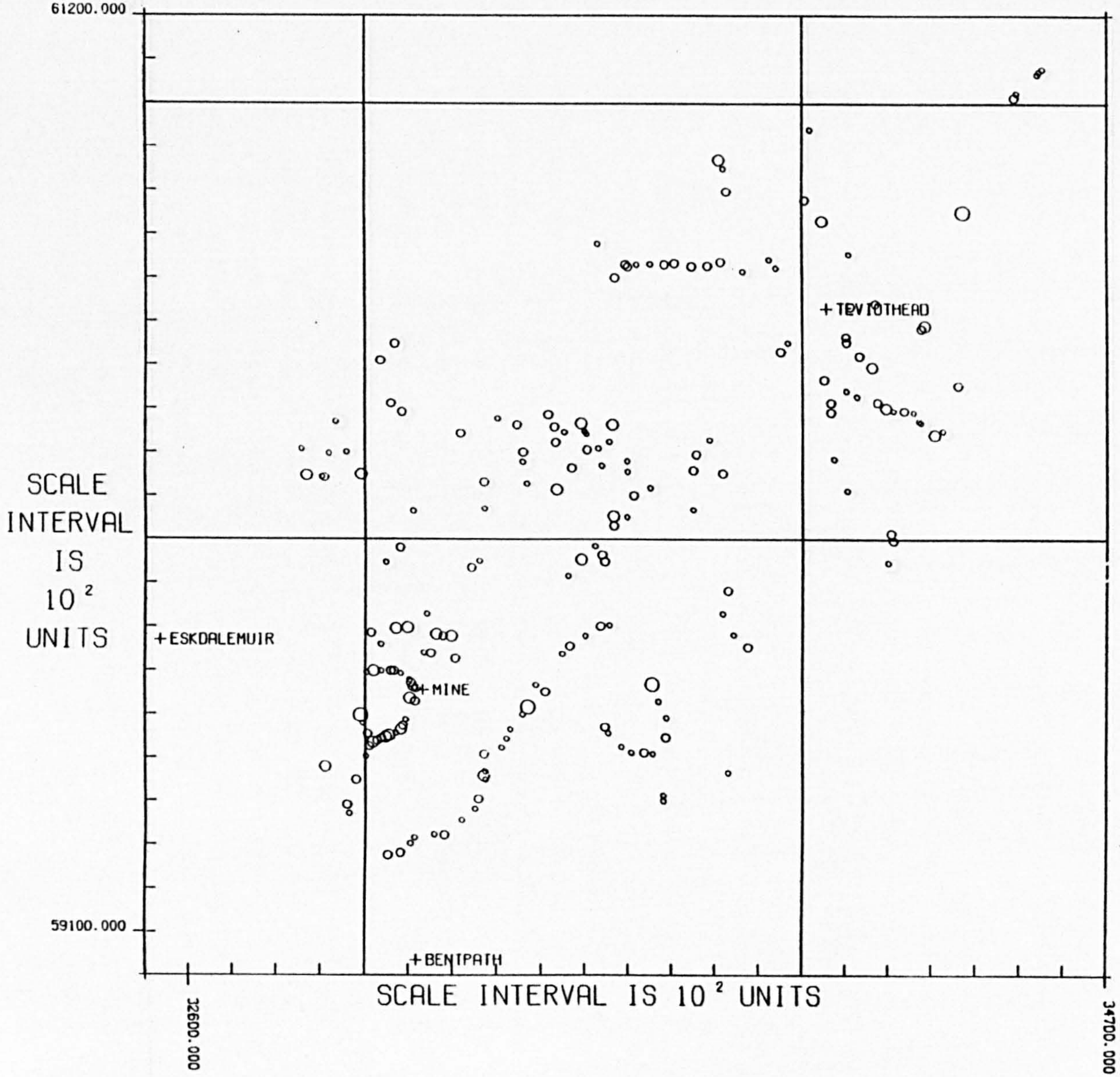

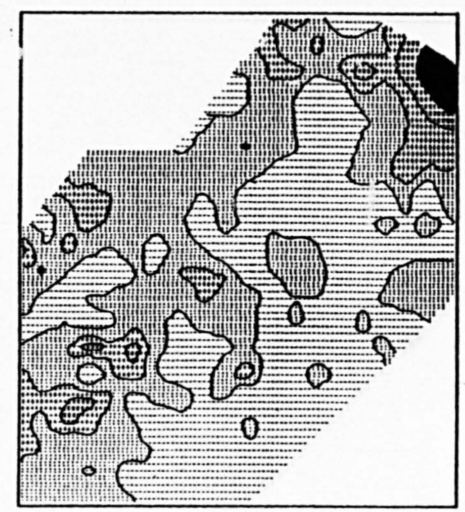

FIGURE 216

FIGURE 217

GLENDINNING YTTRIUM SHALE 1:100000

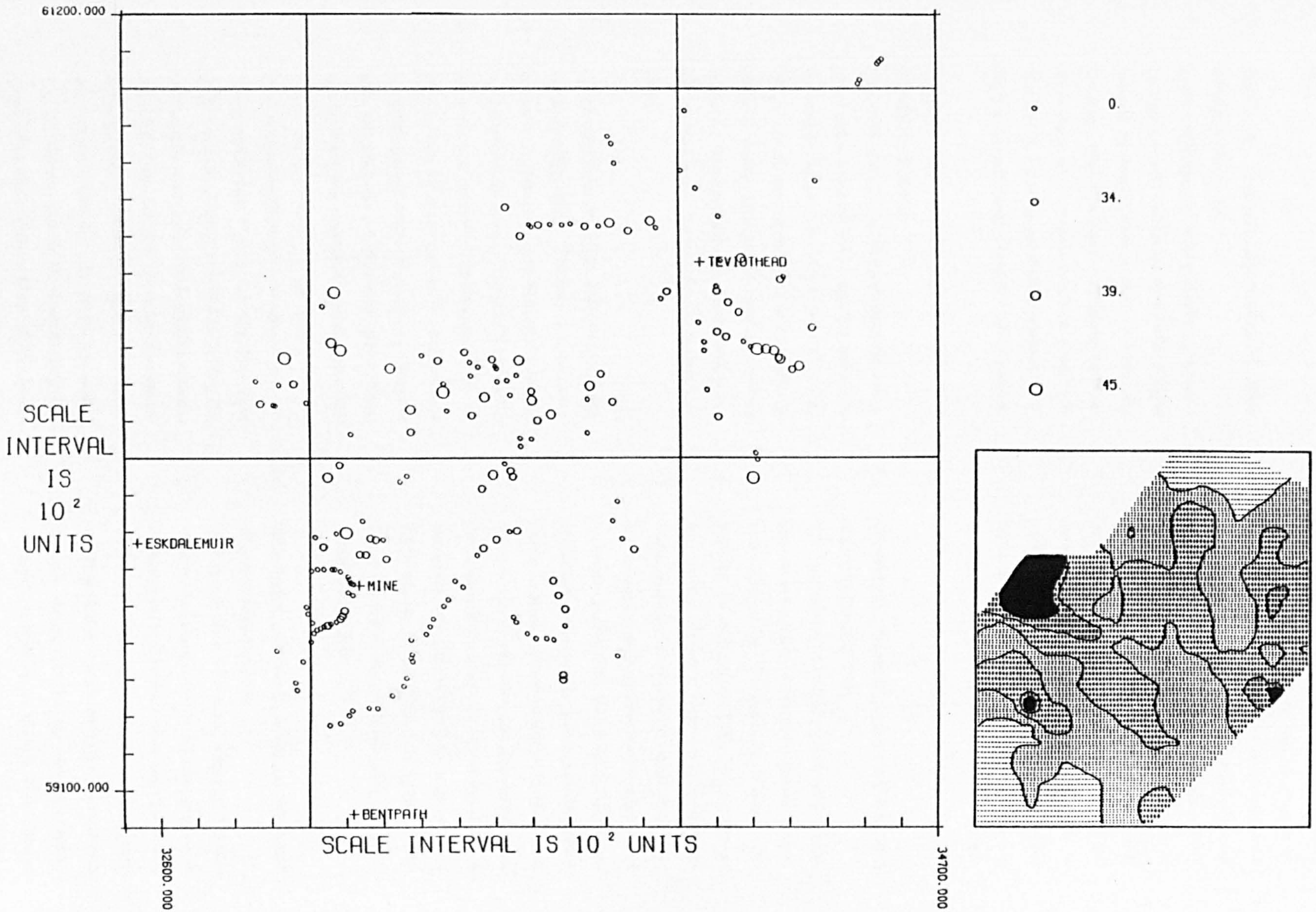

FIGURE 218

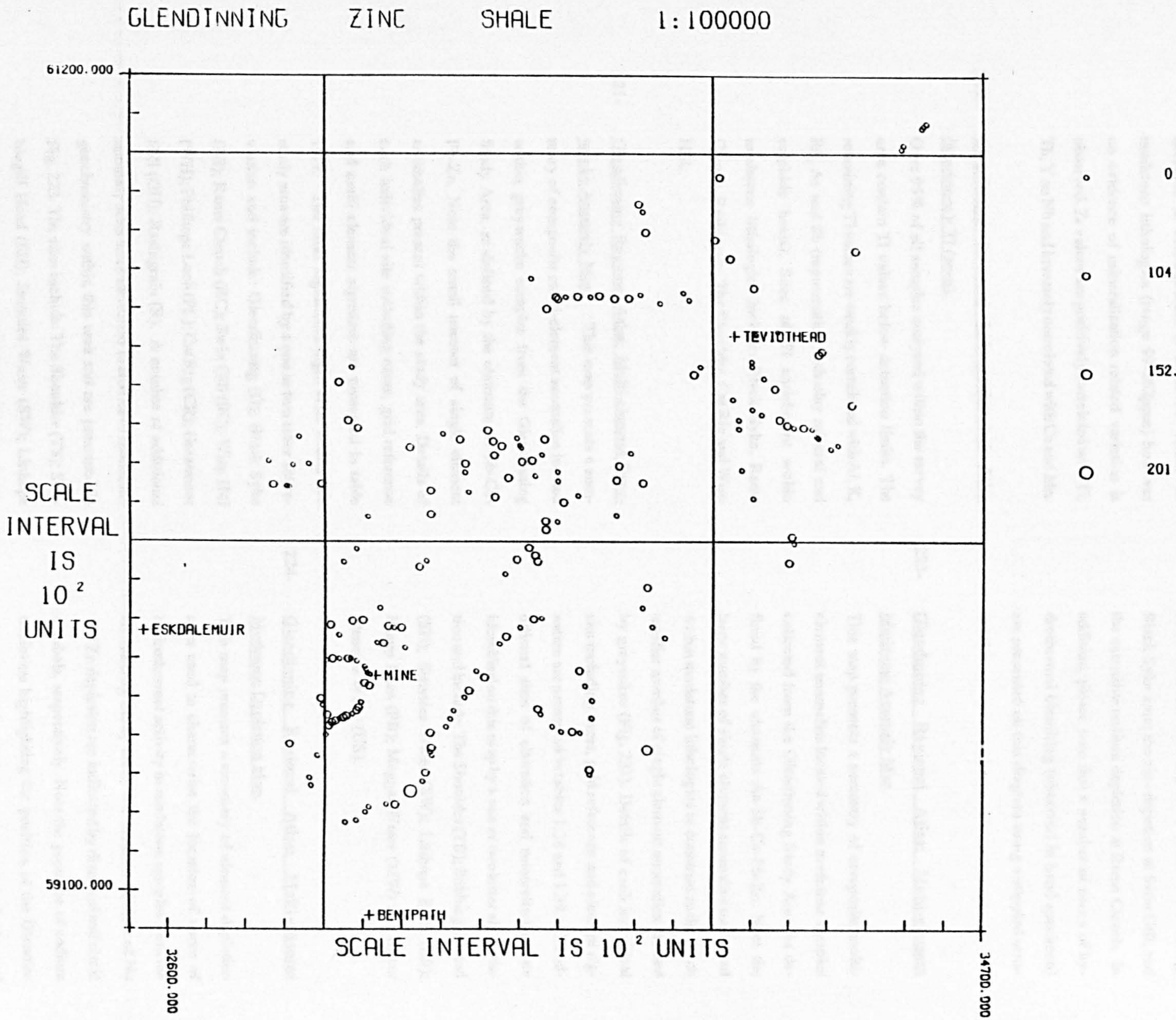
GLENDINNING ZINC SHALE 1:100000
61200.000
59100.000
32600.000
34700.000
SCALE INTERVAL IS 10^2 UNITS
SCALE INTERVAL IS 10^2 UNITS
+ESKDALEMUIR
+MINE
+TEVIOTHEAD
+BENIPATH
0
104
152.
201

Glendinning in the Loch Doon area, where Zn depletion accompanied both As and Pb vein mineralisation.

219- Glendinning Regional Lithogeochemical Atlas (Mudstone): Zr (ppm).
Consistent Zr values are displayed in both greywacke and mudstones throughout the survey area. A slight decrease in concentration is observed within the mudstone lithologies (range 99-262ppm) however no evidence of mineralisation related variation is observed. Zr values are positively correlated with Ti, Th, Y an Nb and inversely correlated with Ca and Mn.

220- Glendinning Regional Lithogeochemical Atlas (Mudstone): Tl (ppm).
Over 95% of all samples analysed within the survey area contain Tl values below detection limits. The remaining Tl values are weakly correlated with Al, K, Rb, As and Sb (representing both clay mineral and sulphide hosts). Sites of Tl enrichment within mudstone lithologies include: Black Syke, Rams Cleuch, Rashigrain, The Shoulder, Cat Rig and Wisp Hill.

221- Glendinning Regional Atlas: Multi-element Greywacke Anomaly Map. This map presents a summary of composite multi-element anomalies located within greywacke samples from the Glendinning Study Area, as defined by the elements As-Sb-Cu-Pb-Zn. Note the small number of single element anomalies present within the study area. Details of each individual site including name, grid reference and multi-element signature are presented in table 1.39. The most significant eight sites within this study area are identified by a one or two letter abbreviation and include: Glendinning (G); Black Syke (BS); Rams Cleuch (RC); Swin Gill (SC); Wisp Hill (WH); Philhope Loch (PL); Cat Rig (CR); Greatmoor Hill (GH); Rashigrain (R). A number of additional anomaly sites were identified in studies of mudstone geochemistry within this area and are presented in Fig. 223. The sites include: The Shoulder (TS); Stibbiegill Head (SH); Stennies Water (SW); Linhope Burn (LB); Phaup Burn (PB); Meggat Water (MW) and Upper Stennies Water (US).

222- Glendinning Regional Atlas: Multi-element Greywacke Depletion Map.
This map presents a summary of element depletion sites used to characterise the location of zones of hydrothermal activity in greywacke samples from the Glendinning Study area. The location of sites of Na and Zn depletion are indicated by diamond and circle symbols, respectively. Note the extensive zone of sodium and zinc depletion in the Glendinning/Black Syke area; the zinc depetion at Swin Gill; and the extensive sodium depletion at Rams Cleuch. In addition, please note that a number of zones of hydrothermal bleaching (observed in hand specimen) are presented on this diagram using a stippled ornament.

223- Glendinning Regional Atlas: Multi-element Mudstone Anomaly Map.
This map presents a summary of composite multi-element anomalies located within mudstone samples collected from the Glendinning Study Area, as defined by the elements As-Sb-Cu-Pb-Zn. Note the large number of single element anomalies contained within mudstone lithologies in constrast to the much smaller number of single element anomalies defined by greyackes (Fig. 221). Details of each individual site including name, grid reference and element signature are presented in tables 1.38 and 1.39. Six additional sites of alteration and mineralisation are identified on this map by a one or two letter abbreviation and include: The Shoulder (TS); Stibbiegill Head (SH); Stennies Water (SW); Linhope Burn (LB); Phaup Burn (PB); Meggat Water (MW) and Upper Stennies Water (US).

224- Glendinning Regional Atlas: Multi-element Mudstone Depletion Map.
This map presents a summary of element depletion sites used to characterise the location of zones of hydrothermal activity in mudstone samples from the Glendinnig Study area. The location of sites of Na and Zn depletion are indicated by diamond and circle symbols, respectively. Note the presence of sodium depletion highlighting the position of the Glendinning area and pointing to zones of hydrothermal activity to the southwest of the main mine area. As

FIGURE 219

GLENDINNING ZIRCONIUM SHALE 1:100000

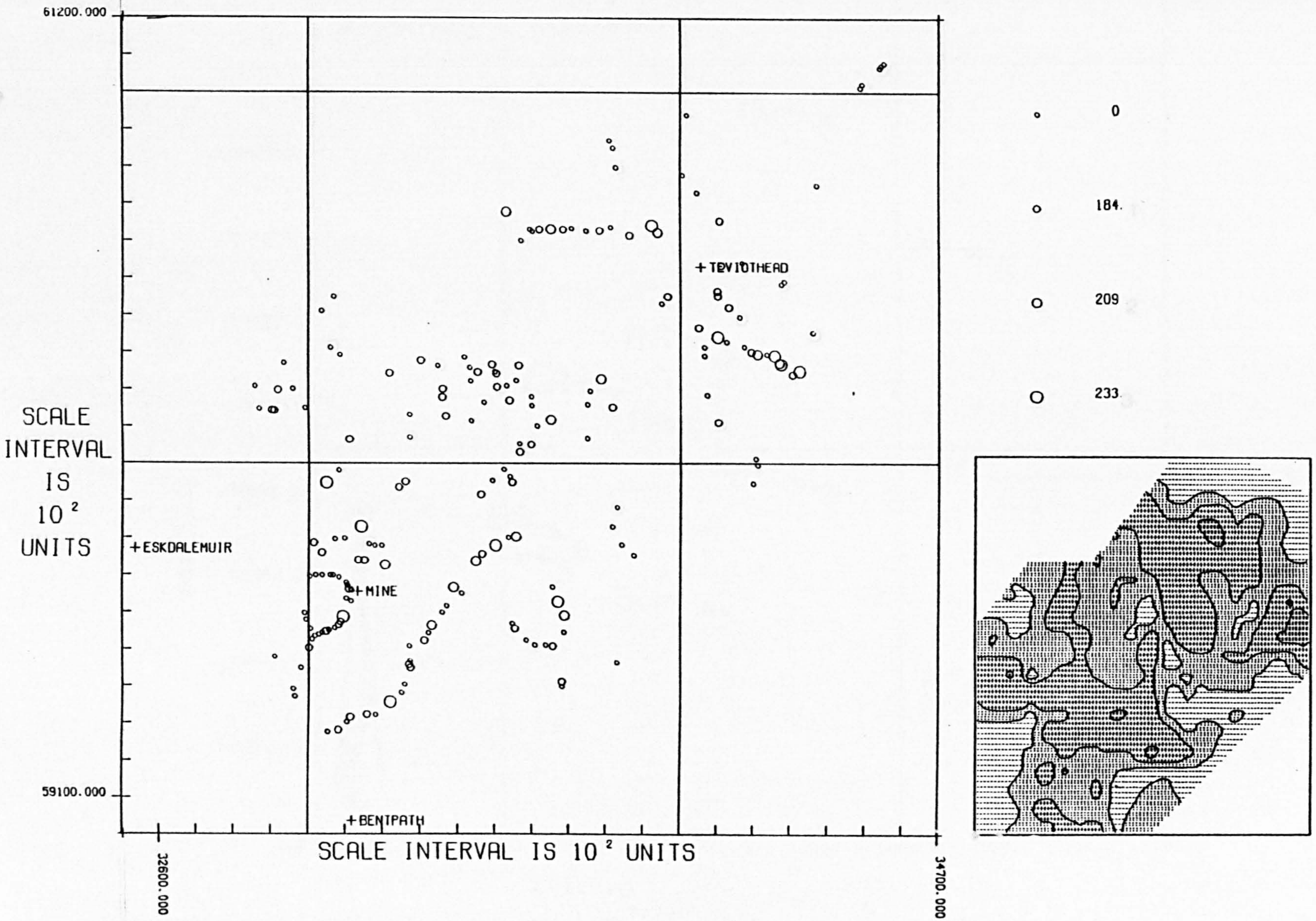

FIGURE 220

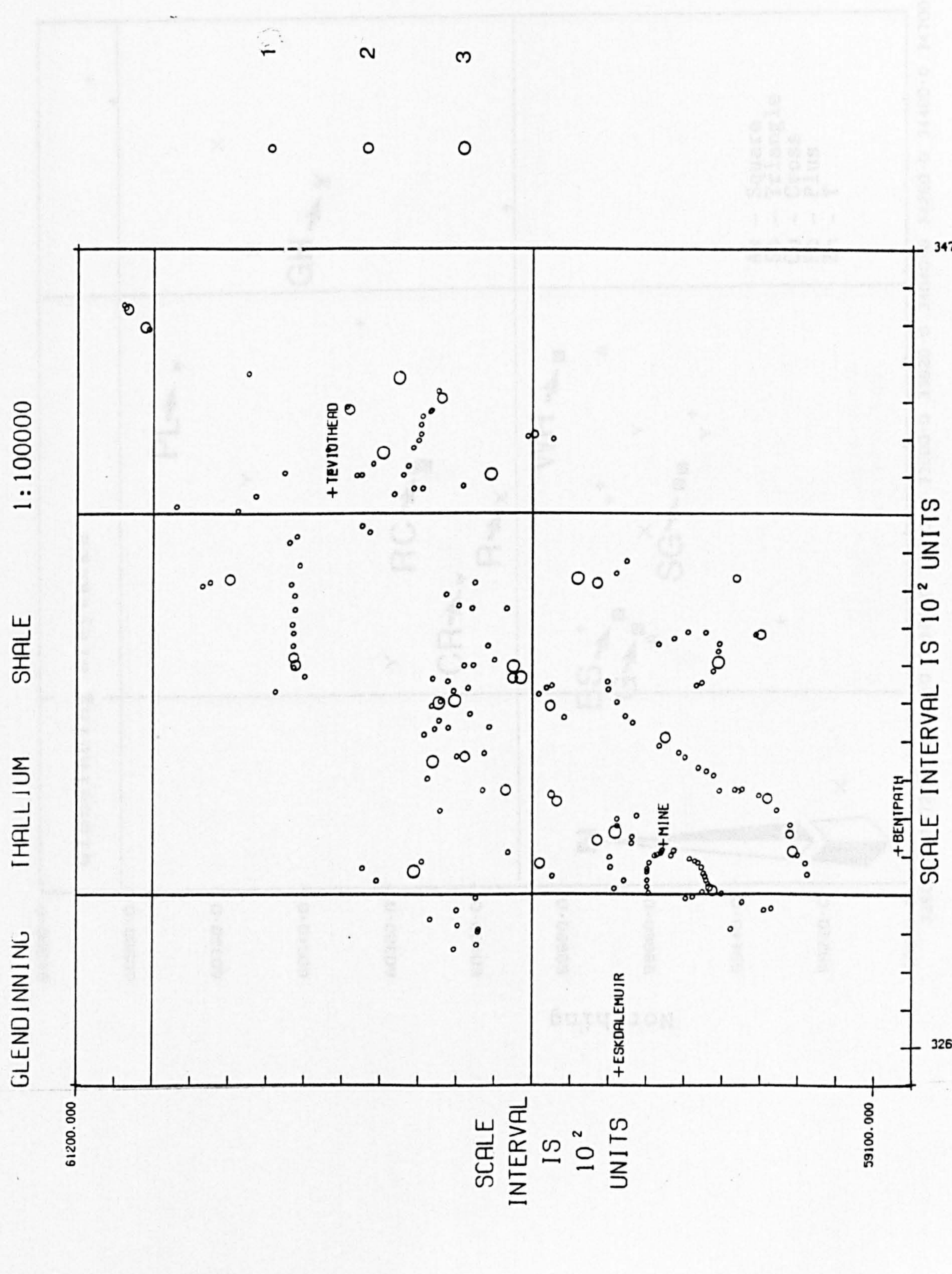
GLENDINNING THALLIUM SHALE 1:100000
1
2
3
34700.000
32600.000
61200.000
59100.000
+TEVIOTHEAD
+MINE
+BENTPATH
+ESKDALEMUIR
SCALE INTERVAL IS 10^2 UNITS
SCALE INTERVAL IS 10^2 UNITS

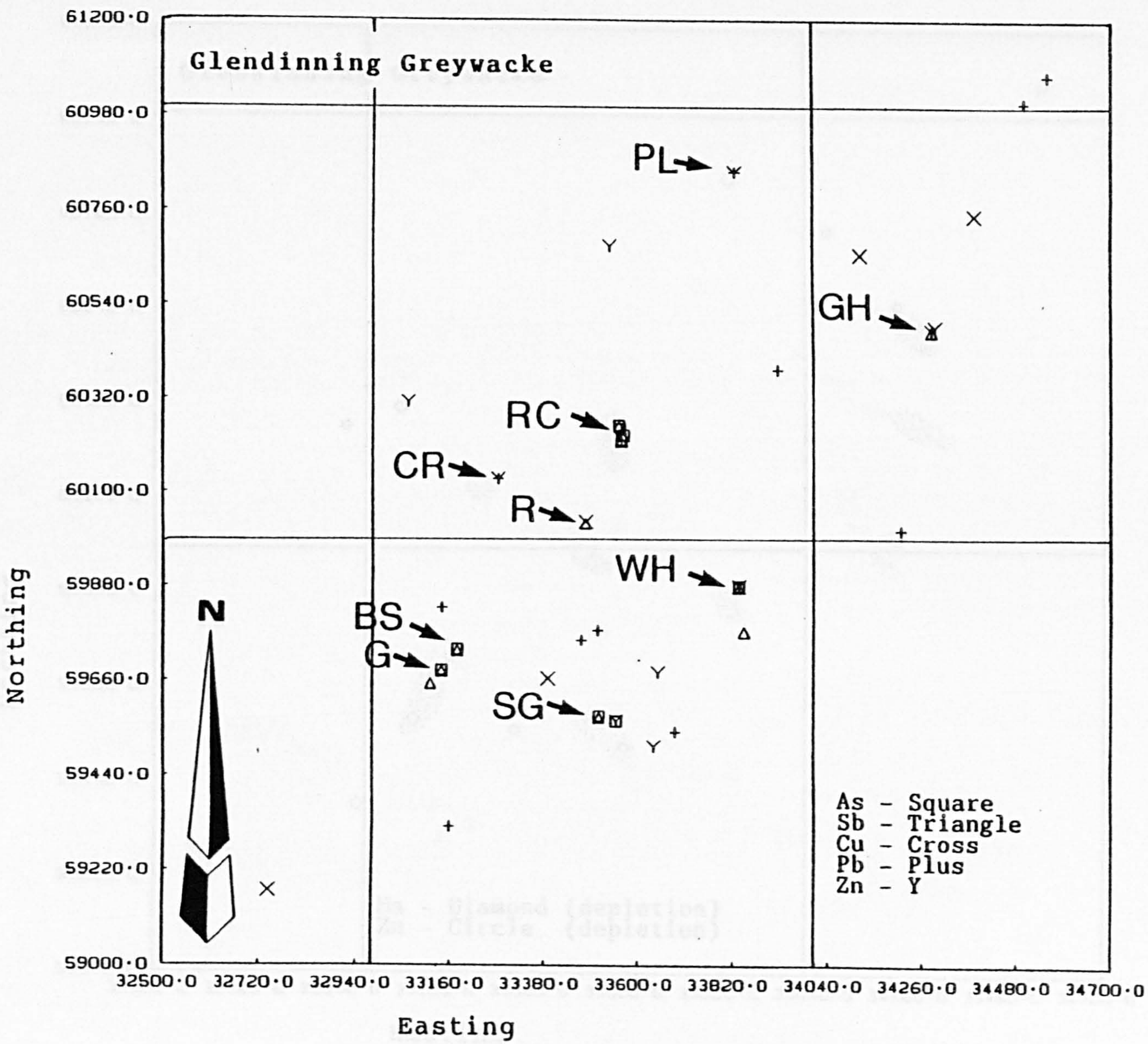
Glendinning Greywacke
PL
GH
RC
CR
R
WH
BS
G
SG
N
As - Square
Sb - Triangle
Cu - Cross
Pb - Plus
Zn - Y
Northing
Easting
61200·0
60980·0
60760·0
60540·0
60320·0
60100·0
59880·0
59660·0
59440·0
59220·0
59000·0
32500·0
32720·0
32940·0
33160·0
33380·0
33600·0
33820·0
34040·0
34260·0
34480·0
34700·0

FIGURE 221

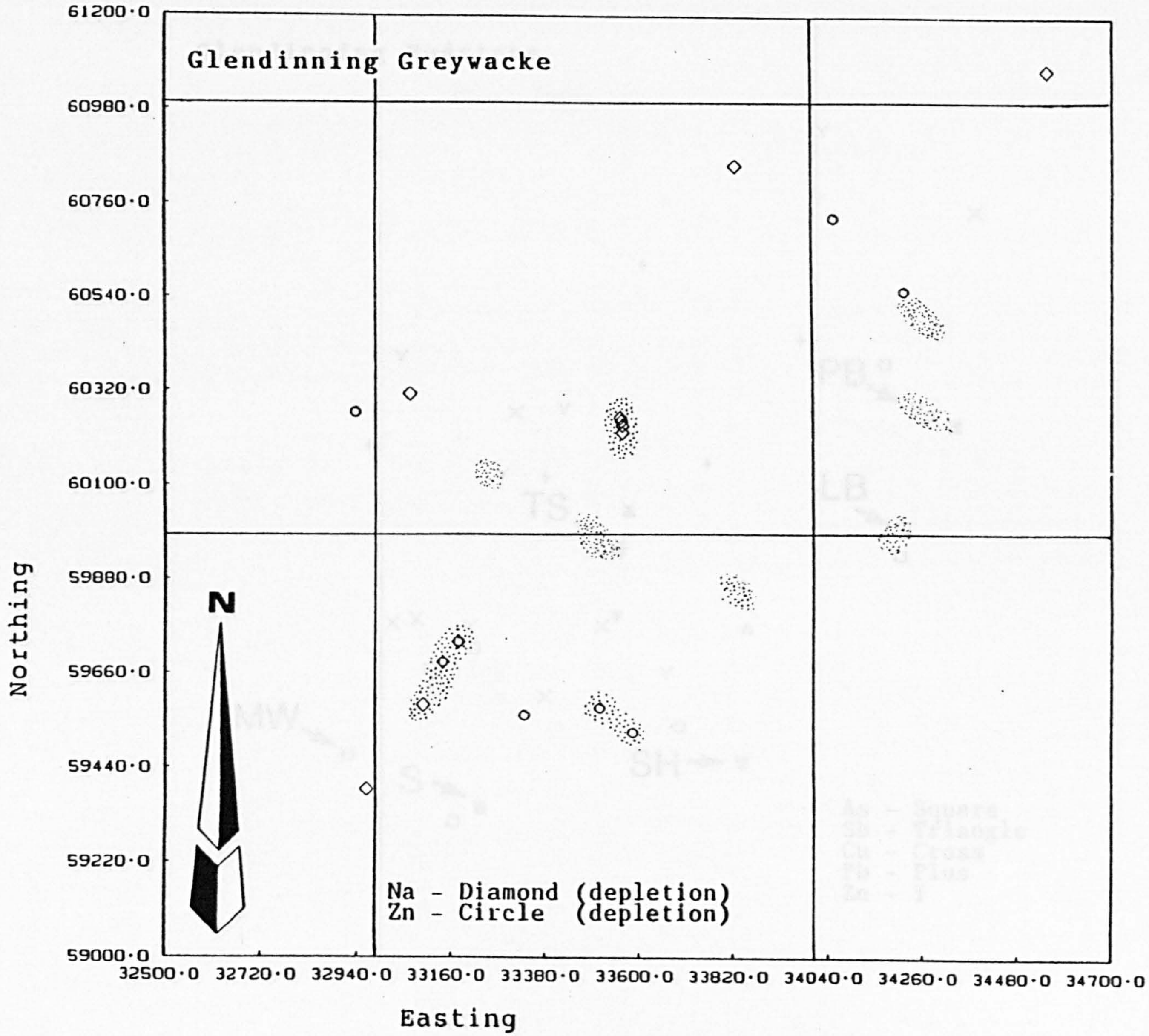
Glendinning Greywacke
Northing
61200·0
60980·0
60760·0
60540·0
60320·0
60100·0
59880·0
59660·0
59440·0
59220·0
59000·0
Easting
32500·0
32720·0
32940·0
33160·0
33380·0
33600·0
33820·0
34040·0
34260·0
34480·0
34700·0
N
Na - Diamond (depletion)
Zn - Circle (depletion)

FIGURE 222

FIGURE 223

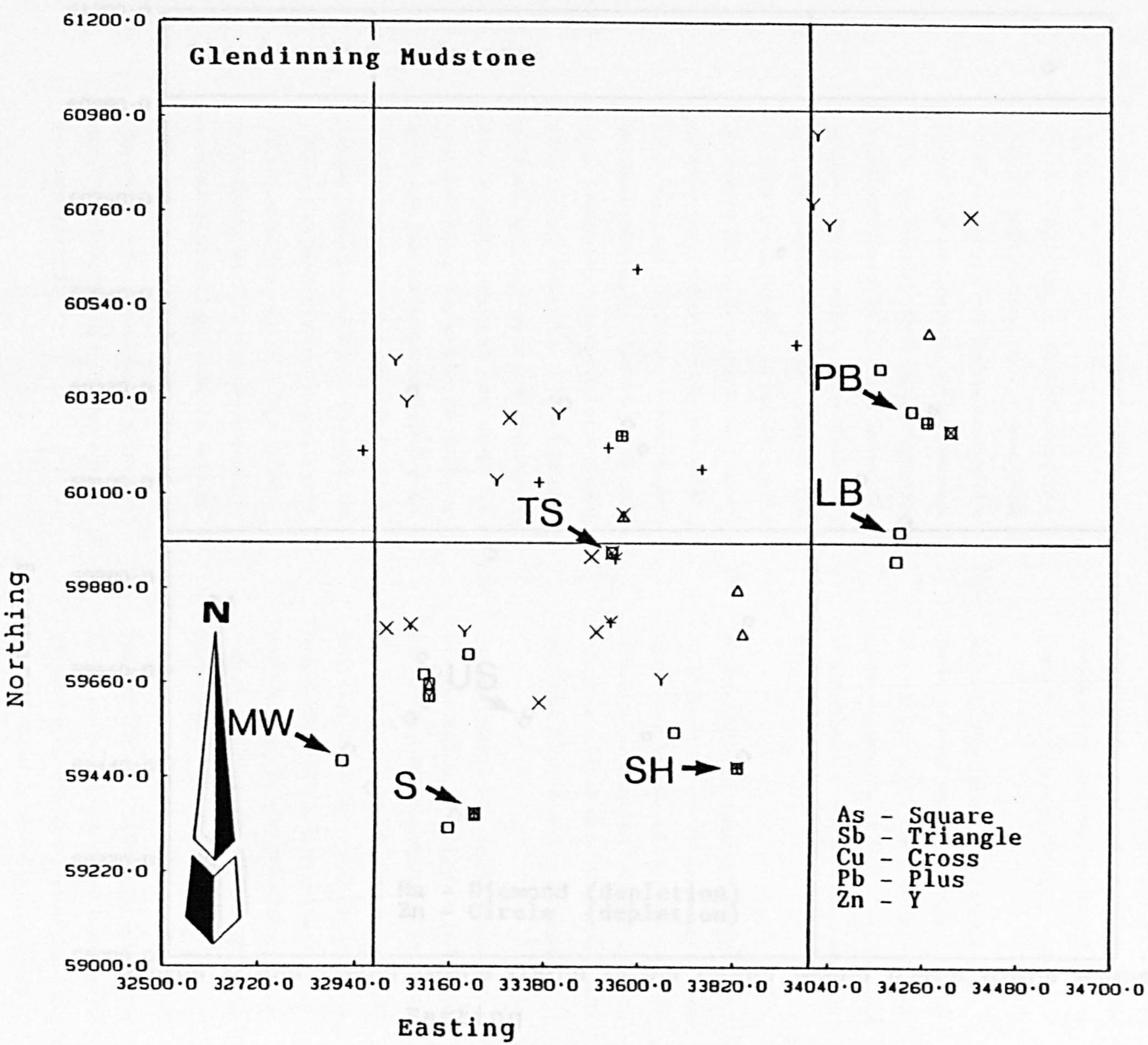

Glendinning Mudstone
Northing
Easting
61200·0
60980·0
60760·0
60540·0
60320·0
60100·0
59880·0
59660·0
59440·0
59220·0
59000·0
32500·0
32720·0
32940·0
33160·0
33380·0
33600·0
33820·0
34040·0
34260·0
34480·0
34700·0
N
PB
LB
TS
MW
S
SH
As - Square
Sb - Triangle
Cu - Cross
Pb - Plus
Zn - Y

FIGURE 224

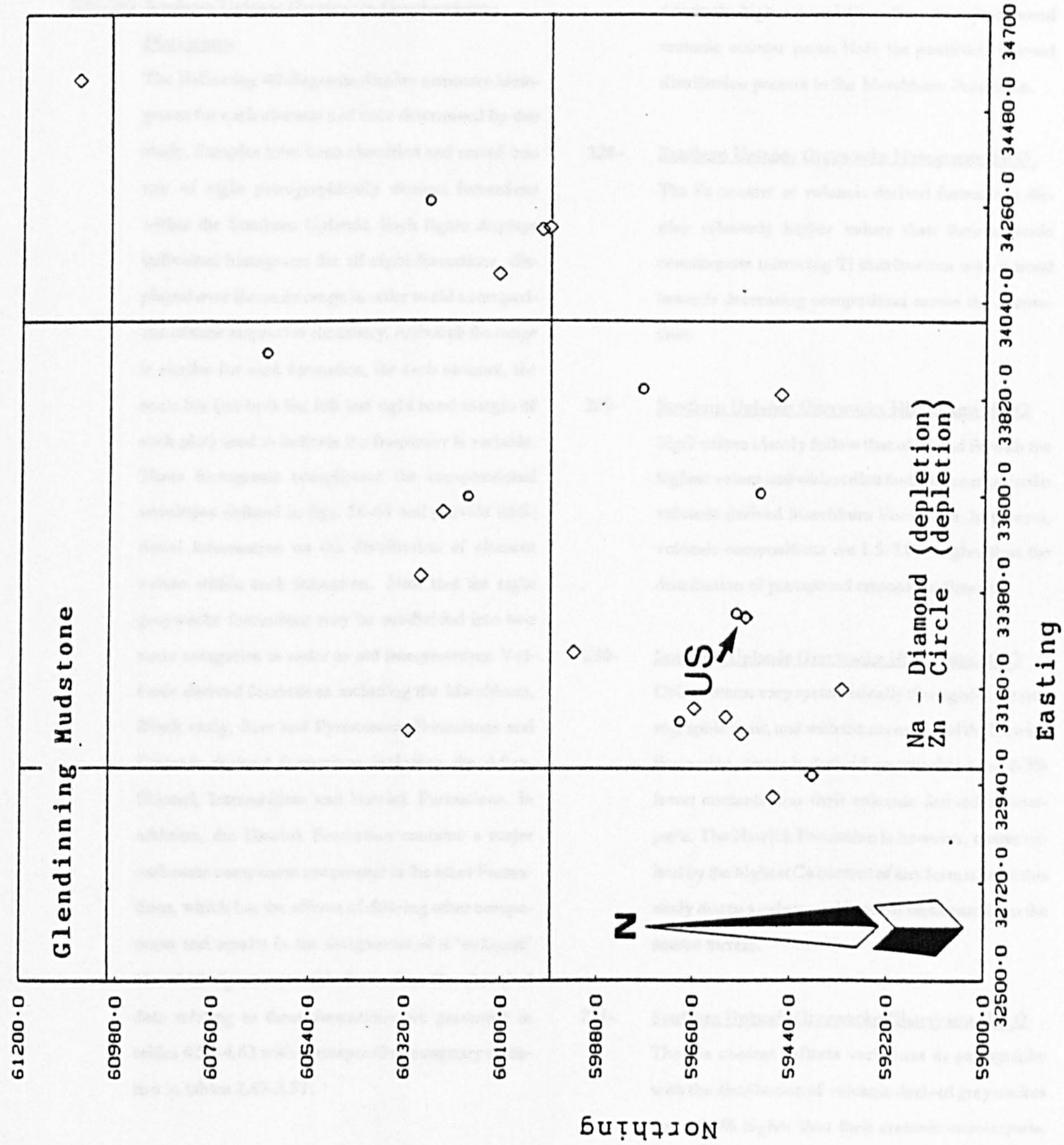
Glendinning Mudstone
US
N
Na - Diamond (depletion)
Zn - Circle (depletion)
Northing
Easting
61200·0
60980·0
60760·0
60540·0
60320·0
60100·0
59880·0
59660·0
59440·0
59220·0
59000·0
32500·0
32720·0
32940·0
33160·0
33380·0
33600·0
33820·0
34040·0
34260·0
34480·0
34700·0

with the greywacke samples, zinc depletion is a characteristic of the Swin Gill, Phaup Burn and Rams Cleuch zones whereas sodium depletion is located in the Wisp Hill, Linhope Burn, Stibbiegill Head, Meggat Water, and Upper Stennies Water and Stennies Water sites.

225-265 Southern Uplands Greywacke Geochemistry : Histograms
The Following 40 diagrams display summary histograms for each element and ratio determined by this study. Samples have been classified and sorted into one of eight petrographically distinct formations within the Southern Uplands. Each figure displays individual histograms for all eight formations, displayed over the same range in order to aid a comparison of their respective chemistry. Although the range is similar for each formation, for each element, the scale bar (on both the left and right hand margin of each plot) used to indicate the frequency is variable. These histograms compliment the compositional envelopes defined in figs. 56-69 and provide additional information on the distribution of element values within each formation. Note that the eight greywacke formations may be subdivided into two main catagories in order to aid interpretation: Volcanic derived formations including the Marchburn, Black craig, Scar and Pyroxenous Formations and Cratonic derived formations including the Afton, Shinnel, Intermediate and Hawick Formations. In addition, the Hawick Formation contains a major carbonate component not present in the other Formations, which has the effecct of diluting other components and results in the assignment of a 'volcanic' chemical signature to this formation. Geochemical data relating to these formations are presented in tables 4.53-4.63 with corresponding summary statistics in tables 2.47-2.57.

225- Southern Uplands Greywacke Histograms: SiO_2
The volcanic Marchburn, Blackcraig, Scar and Pyroxenous Formations display notably lower, negatively skewed SiO_2 population in comparison with their cratonic counterparts. In general, all histograms display highly kurt distribution. Note the low Si distribution of the Hawick Formation.

226- Southern Uplands Greywacke Histograms: Al_2O_3
Little systematic variation in Al_2O_3 composition is observed between volcanic and cratonic formations.

227- Southern Uplands Greywacke Histograms: TiO_2
A general decrease in Ti distribution occurs across the succession with volcanic formations displaying relatively higher populations than their juxtaposed cratonic counter parts. Note the positively skewed distribution present in the Marchburn Formation.

228- Southern Uplands Greywacke Histograms: Fe_2O_3
The Fe content of volcanic derived formations display relatively higher values than their cratonic counterparts mirroring Ti distributions with a trend towards decreasing composition across the succession.

229- Southern Uplands Greywacke Histograms: MgO
MgO values closely follow that of Ti and Fe with the highest values and widest distribution occuring in the volcanic derived Marchburn Formation. In general, volcanic compositions are 1.5-3.0% higher than the distribution of juxtaposed cratonic sediments.

230- Southern Uplands Greywacke Histograms: CaO
CaO contents vary systematically throughout the petrographic units, and with the exception of the Hawick Formation, cratonic derived greywackes have 2-3% lower contents than their volcanic derived counterparts. The Hawick Formation is however, characterised by the highest Ca content of any formation in this study due to a substantial input of carbonate from the source terrain.

231- Southern Uplands Greywacke Histograms: Na_2O
The Na content reflects variations in petrography with the distribution of volcanic derived greywackes up to 0.8% higher than their cratonic counterparts. The effects of Na depletion associated with hydrothermal activity are most clearly observed in the cratonic Afton, Intermediate and Hawick Formations.

232- Southern Uplands Greywacke Histograms: K_2O
Systematic differences in distribution exist between the cratonic and volcanic derived formations. In

FIGURE 225

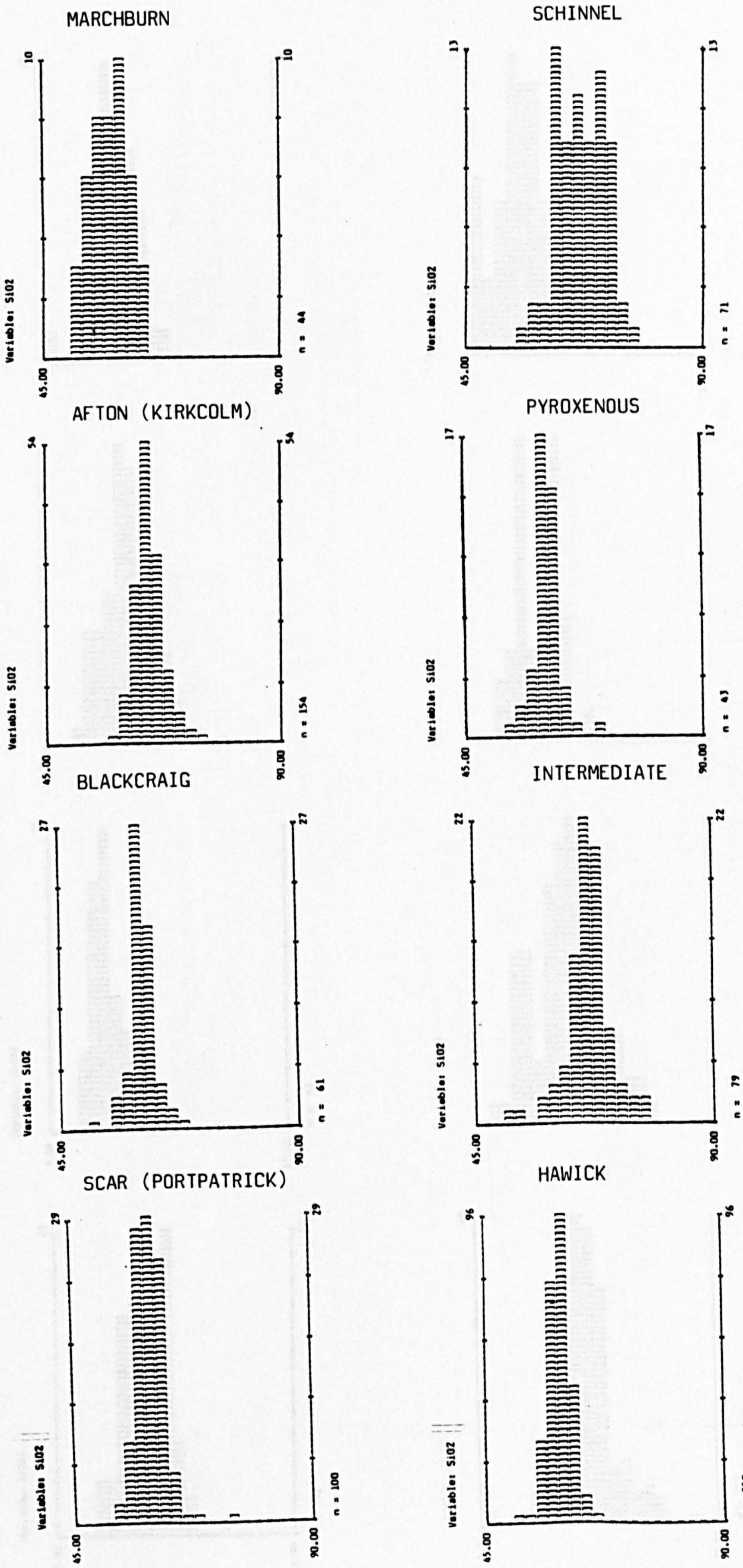
MARCHBURN
Variable: SiO2
45.00
90.00
10
n = 44
SCHINNEL
13
n = 71
AFTON (KIRKCOLM)
54
n = 154
PYROXENOUS
17
n = 43
BLACKCRAIG
27
n = 61
INTERMEDIATE
22
n = 79
SCAR (PORTPATRICK)
29
n = 100
HAWICK
96
n = 258

FIGURE 226

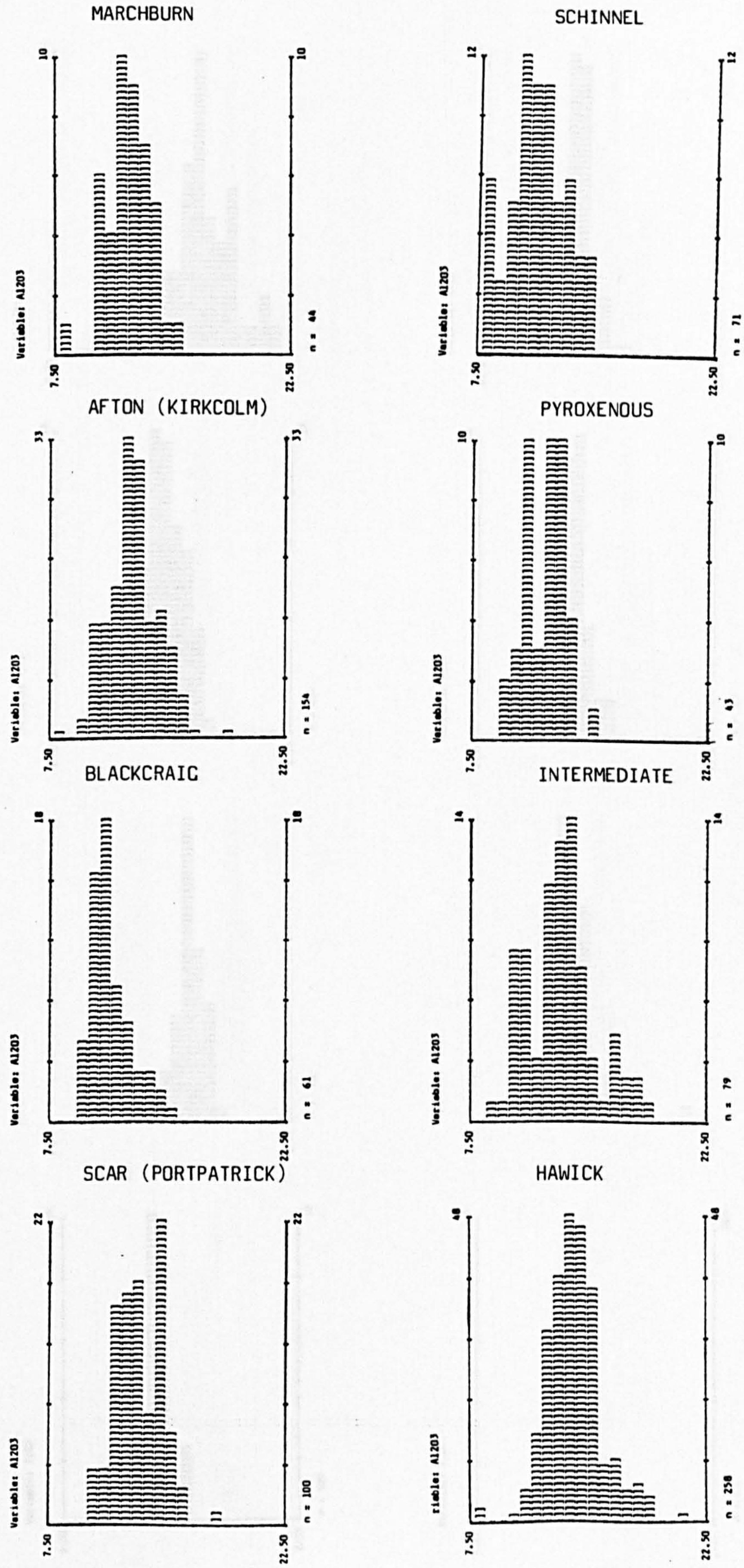
MARCHBURN
Variable: Al203
n = 44
SCHINNEL
Variable: Al203
n = 71
AFTON (KIRKCOLM)
Variable: Al203
n = 154
PYROXENOUS
Variable: Al203
n = 43
BLACKCRAIG
Variable: Al203
n = 61
INTERMEDIATE
Variable: Al203
n = 79
SCAR (PORTPATRICK)
Variable: Al203
n = 100
HAWICK
n = 258
7.50
22.50

FIGURE 227

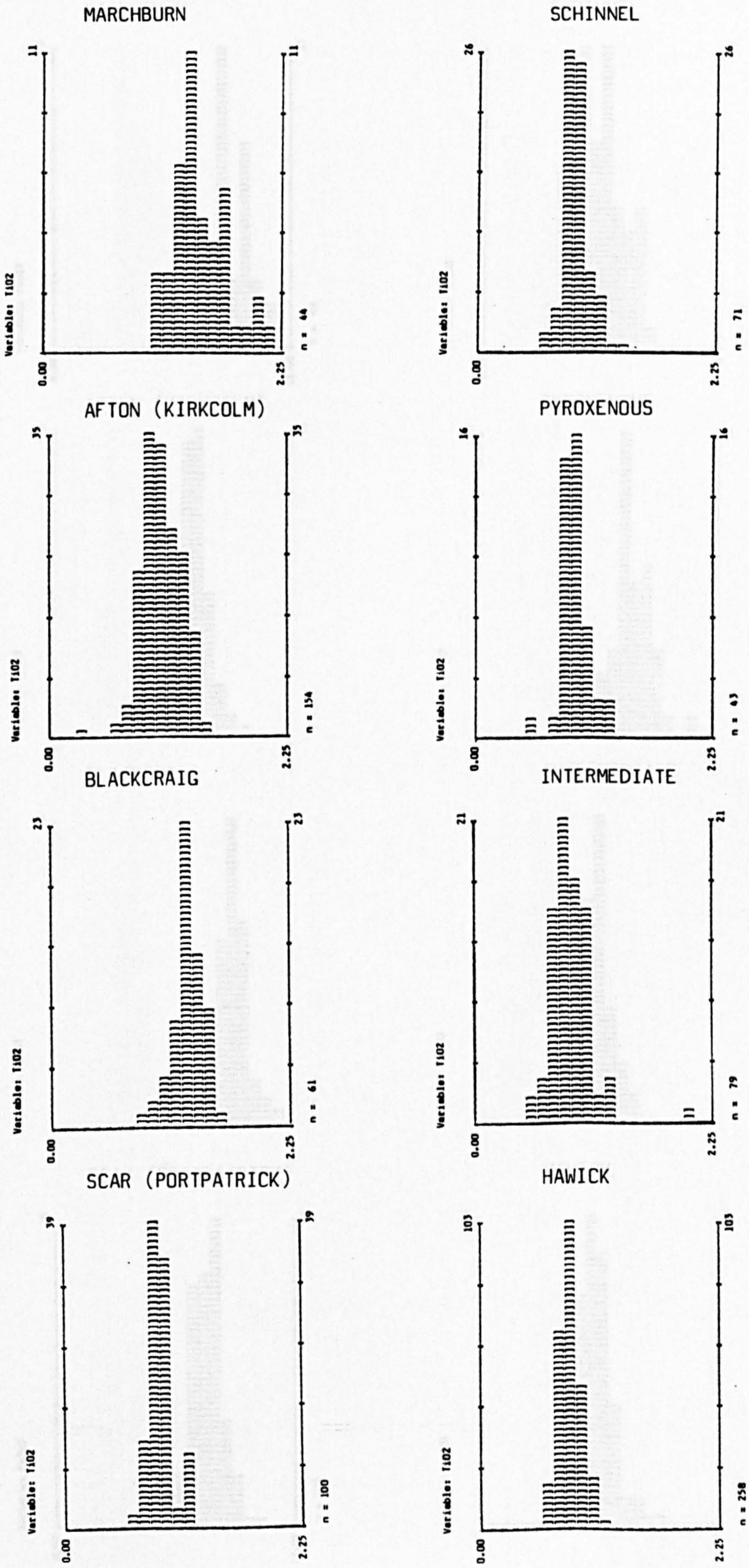
MARCHBURN
Variable: TiO2
0.00
2.25
n = 44
SCHINNEL
Variable: TiO2
0.00
2.25
n = 71
AFTON (KIRKCOLM)
Variable: TiO2
0.00
2.25
n = 134
PYROXENOUS
Variable: TiO2
0.00
2.25
n = 43
BLACKCRAIG
Variable: TiO2
0.00
2.25
n = 61
INTERMEDIATE
Variable: TiO2
0.00
2.25
n = 79
SCAR (PORTPATRICK)
Variable: TiO2
0.00
2.25
n = 100
HAWICK
Variable: TiO2
0.00
2.25
n = 258

FIGURE 228

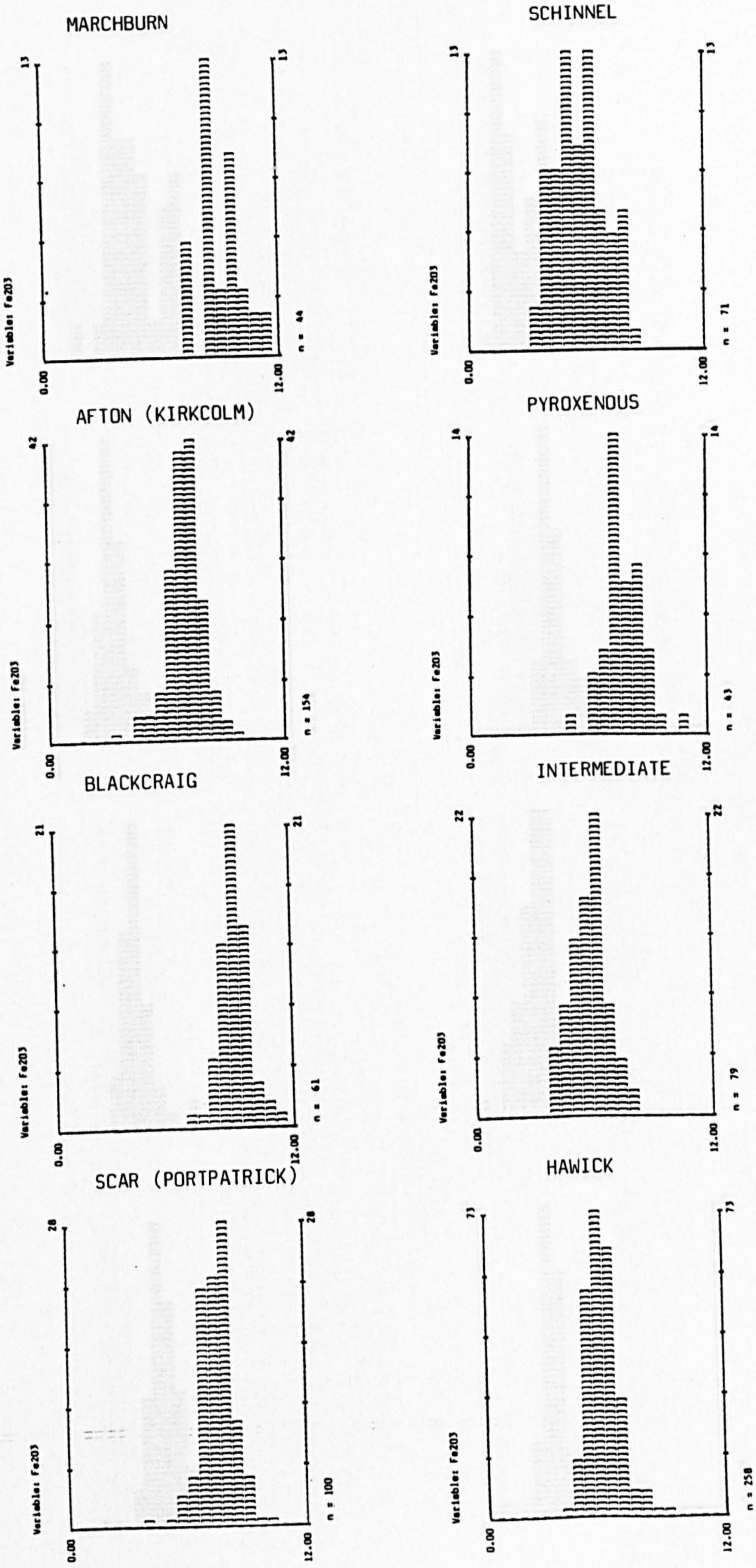
MARCHBURN
13
Variable: Fe2O3
0.00
12.00
n = 44
SCHINNEL
13
Variable: Fe2O3
0.00
12.00
n = 71
AFTON (KIRKCOLM)
42
Variable: Fe2O3
0.00
12.00
n = 154
PYROXENOUS
14
Variable: Fe2O3
0.00
12.00
n = 43
BLACKCRAIG
21
Variable: Fe2O3
0.00
12.00
n = 61
INTERMEDIATE
22
Variable: Fe2O3
0.00
12.00
n = 79
SCAR (PORTPATRICK)
28
Variable: Fe2O3
0.00
12.00
n = 100
HAWICK
73
Variable: Fe2O3
0.00
12.00
n = 258

FIGURE 229

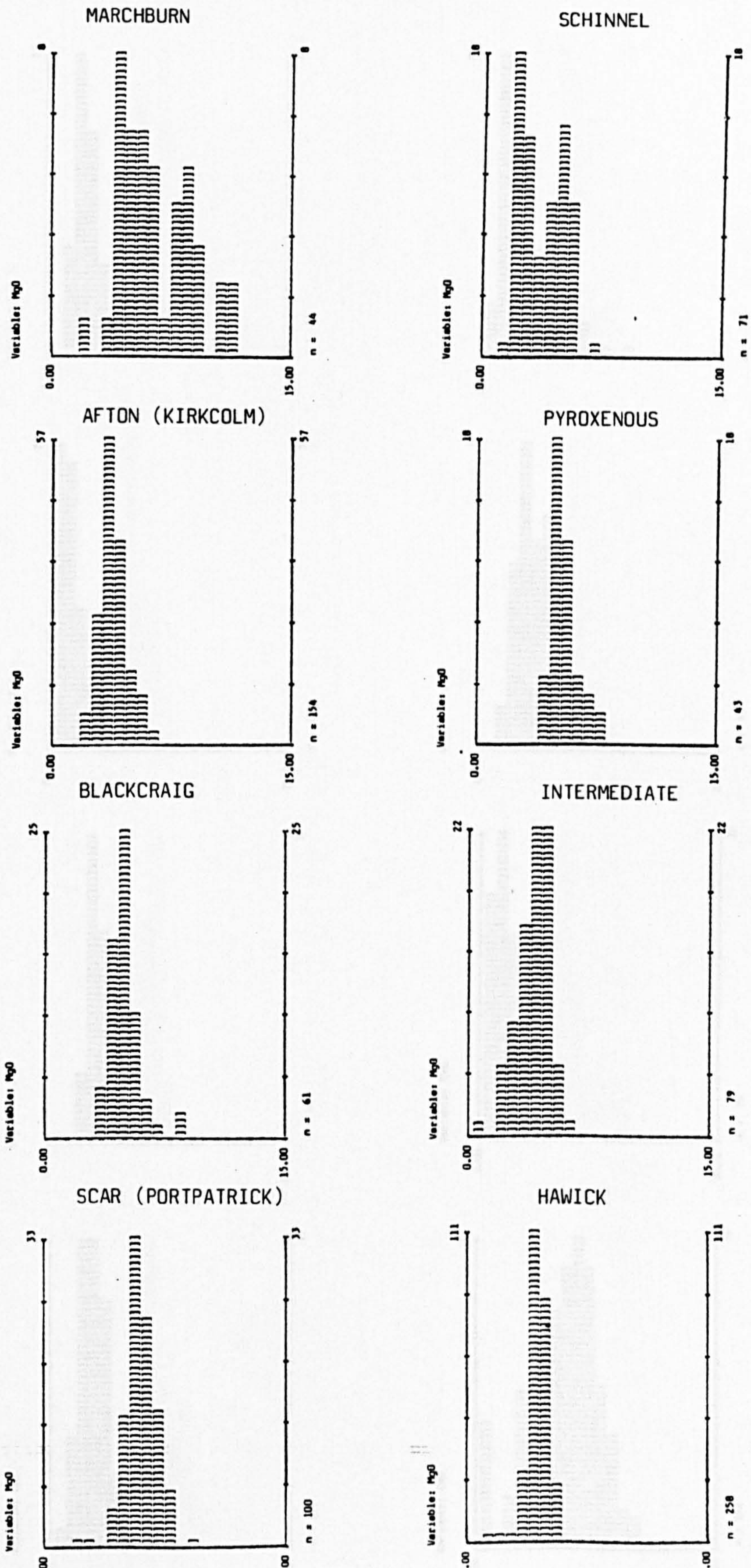
MARCHBURN
Variable: MgO
0.00
15.00
8
n = 44
SCHINNEL
18
n = 71
AFTON (KIRKCOLM)
57
n = 154
PYROXENOUS
18
n = 43
BLACKCRAIG
25
n = 61
INTERMEDIATE
22
n = 79
SCAR (PORTPATRICK)
33
n = 100
HAWICK
111
n = 258

FIGURE 230

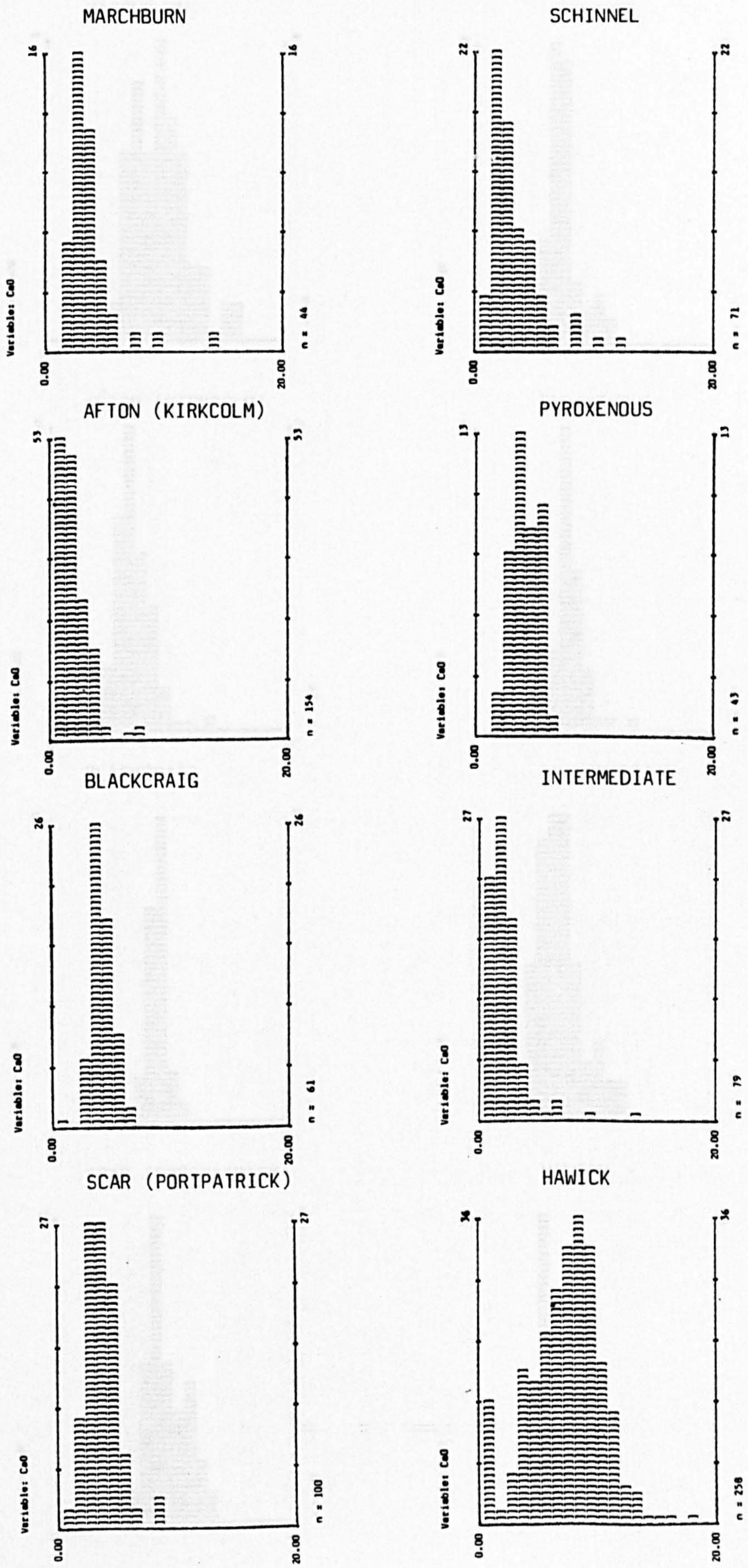
MARCHBURN
SCHINNEL
AFTON (KIRKCOLM)
PYROXENOUS
BLACKCRAIG
INTERMEDIATE
SCAR (PORTPATRICK)
HAWICK
Variable: CaO
0.00
20.00
n = 44
n = 71
n = 154
n = 43
n = 61
n = 79
n = 100
n = 258

FIGURE 231

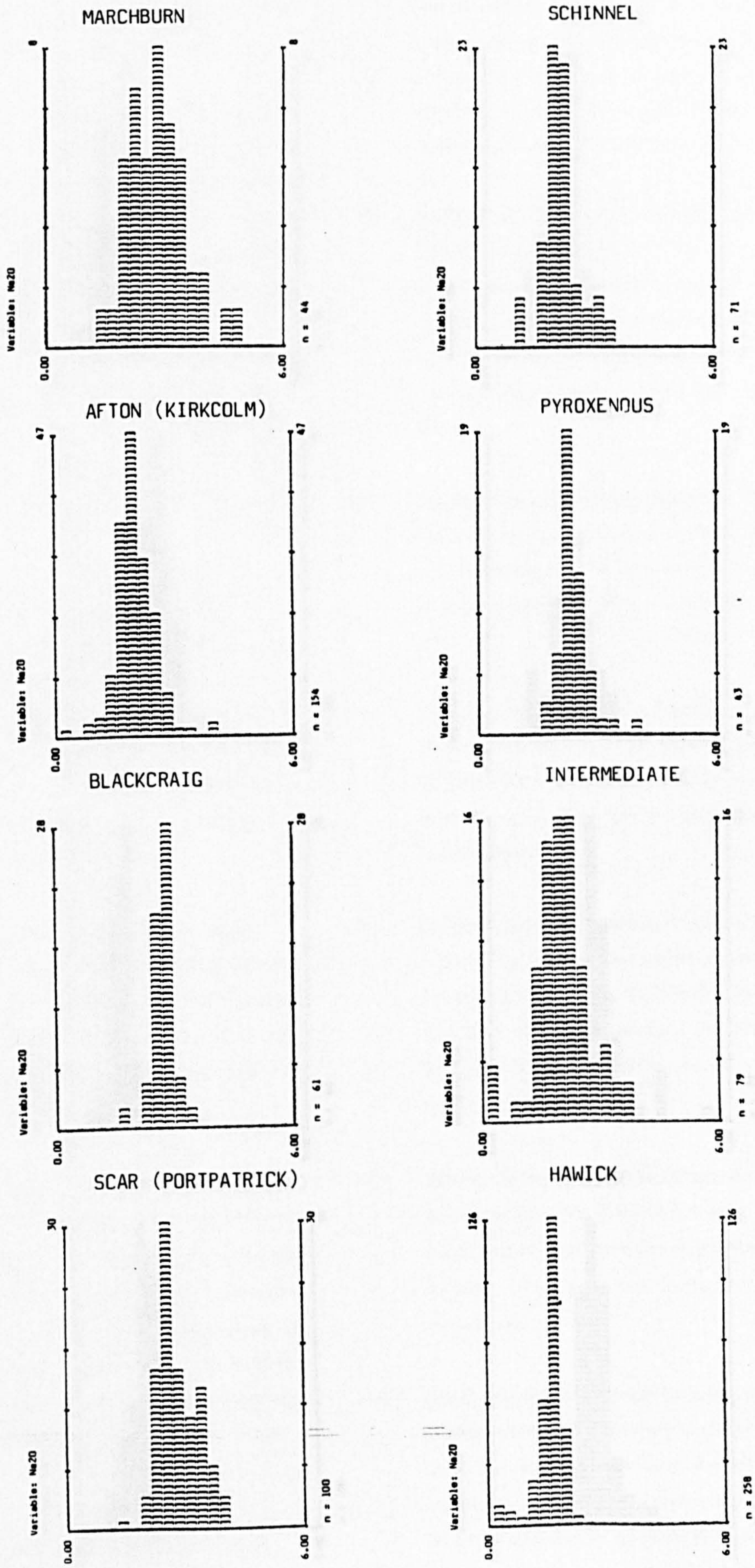
MARCHBURN
SCHINNEL
AFTON (KIRKCOLM)
PYROXENOUS
BLACKCRAIG
INTERMEDIATE
SCAR (PORTPATRICK)
HAWICK

FIGURE 232

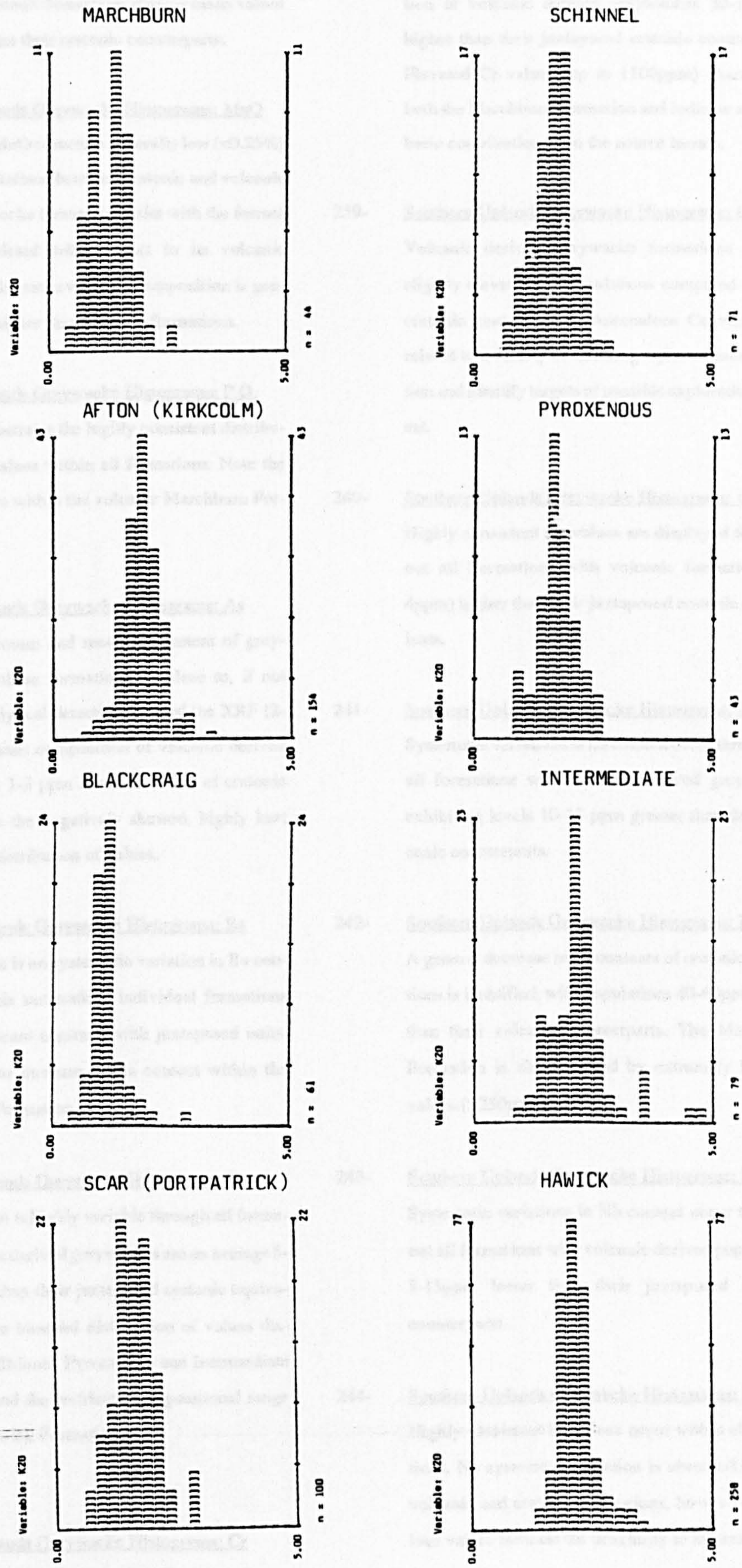
MARCHBURN
Variable: K20
0.00
5.00
n = 44
SCHINNEL
Variable: K20
0.00
5.00
n = 71
AFTON (KIRKCOLM)
Variable: K20
0.00
5.00
n = 156
PYROXENOUS
Variable: K20
0.00
5.00
n = 43
BLACKCRAIG
Variable: K20
0.00
5.00
n = 61
INTERMEDIATE
Variable: K20
0.00
5.00
n = 79
SCAR (PORTPATRICK)
Variable: K20
0.00
5.00
n = 100
HAWICK
Variable: K20
0.00
5.00
n = 258

general the volcanic formations display mean values 0.5% lower than their cratonic counterparts.

233- Southern Uplands Greywacke Histograms: MnO
Although the MnO content is generally low (<0.25%) systematic variations between cratonic and volcanic derived greywacke formations exist with the former relatively depleted with respect to its volcanic counterpart. The mean volcanic composition is generally 0.05% higher than cratonic formations.

234- Southern Uplands Greywacke Histograms: P_2O_5
This figure illustrates the highly consistent distribution of P_2O_5 values within all formations. Note the elevated values within the volcanic Marchburn Formation.

235- Southern Uplands Greywacke Histograms: As
Both the minimum and mean As content of greywackes from these formations lie close to, if not below the analytical detection limit of the XRF (2-3ppm). The mean composition of volcanic derived greywackes is 1-2 ppm lower than that of cratonic samples. Note the negatively skewed, highly kurt (leptokurtic) distribution of values.

236- Southern Uplands Greywacke Histograms: Ba
Although there is no systematic variation in Ba content across this succession, individual formations exhibit significant contrasts with juxtaposed units. Note the major increase in Ba content within the Intermediate Formation.

237- Southern Uplands Greywacke Histograms: Co
The Co content is highly variable through all formations. Volcanic derived greywackes are on average 5-8 ppm lower than their juxtaposed cratonic equivalents. Note the bimodal distribution of values displayed in the Shinnel, Pyroxenous and Intermediate Formations; and the restricted compositional range within the Hawick Formation.

238- Southern Uplands Greywacke Histograms: Cr
A systematic trend of decreasing Cr values occurs throughout the studied Formations with the distribution of volcanic derived greywackes 30-150ppm higher than their juxtaposed cratonic counterparts. Elevated Cr values (up to 1100ppm) characterise both the Marchburn Formation and indicate an ultrabasic contribution from the source terrain.

239- Southern Uplands Greywacke Histograms: Cu
Volcanic derived greywacke formations display slightly elevated Cu populations compared to their cratonic counter parts. Anomalous Cu values are related to a variety of differing styles of mineralisation and identify targets of possible exploration interest.

240- Southern Uplands Greywacke Histograms: Ga
Highly consistent Ga values are displayed throughout all Formations with volcanic formations (3-4ppm) higher than their juxtaposed cratonic equivalents.

241- Southern Uplands Greywacke Histograms: La
Systematic variations in La content occur throughout all formations with cratonic derived greywackes exhibiting levels 10-15 ppm greater than their volcanic counterparts.

242- Southern Uplands Greywacke Histograms: Ni
A general decrease in Ni contents of cratonic formations is identified, with populations 40-60ppm lower than their volcanic counterparts. The Marchburn Formation is characterised by extremely high Ni values (>250ppm).

243- Southern Uplands Greywacke Histograms: Nb
Systematic variations in Nb content occur throughout all formations with volcanic derived populations 5-15ppm lower than their juxtaposed cratonic counterparts.

244- Southern Uplands Greywacke Histograms: Pb
Highly consistent Pb values occur within all formations. No systematic variation is observed between volcanic and cratonic formations, however anomalous values indicate the proximity to mineralisation.

FIGURE 233

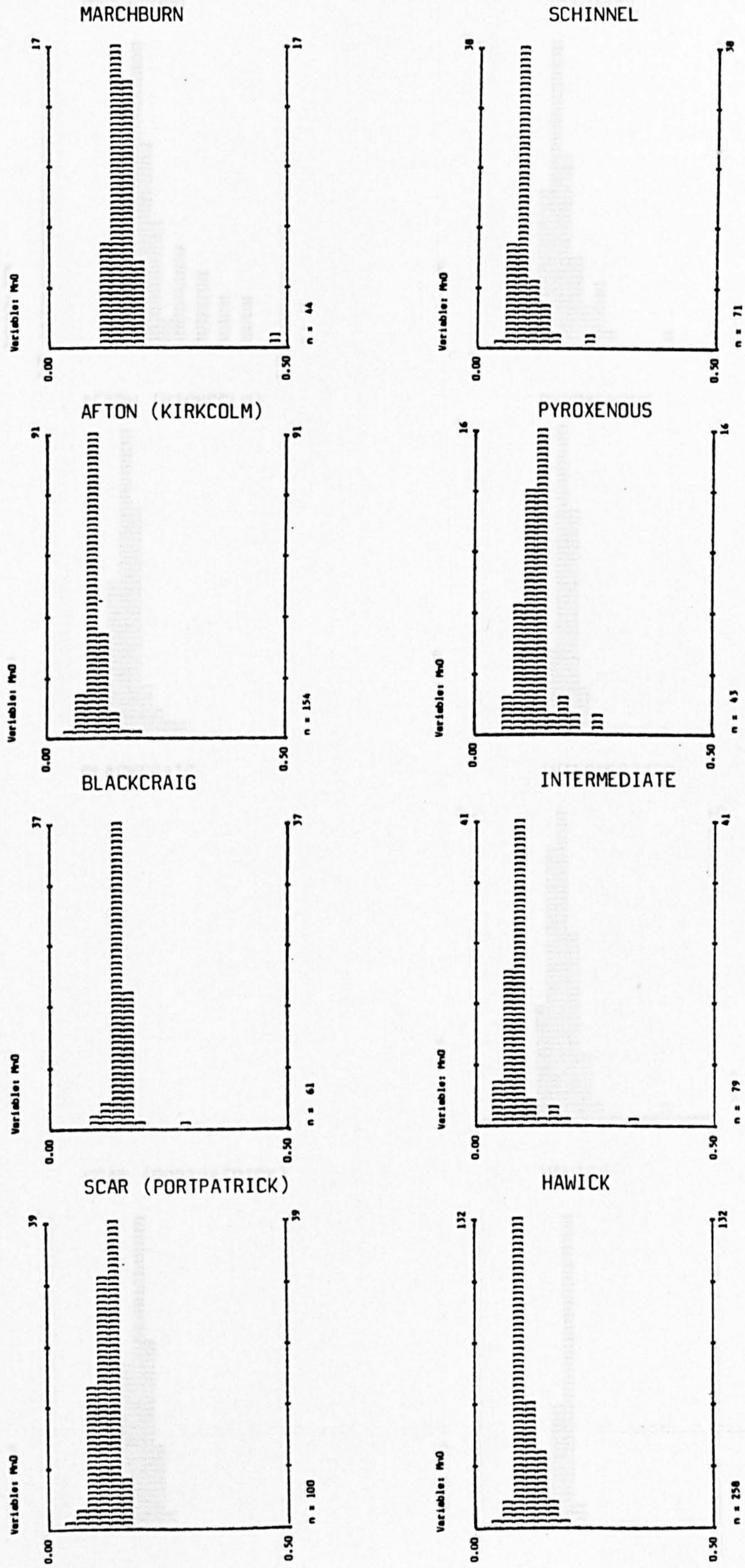
MARCHBURN
SCHINNEL
AFTON (KIRKCOLM)
PYROXENOUS
BLACKCRAIG
INTERMEDIATE
SCAR (PORTPATRICK)
HAWICK
Variable: MnO
0.00
0.50
n = 44
n = 71
n = 154
n = 43
n = 61
n = 79
n = 100
n = 258

FIGURE 234

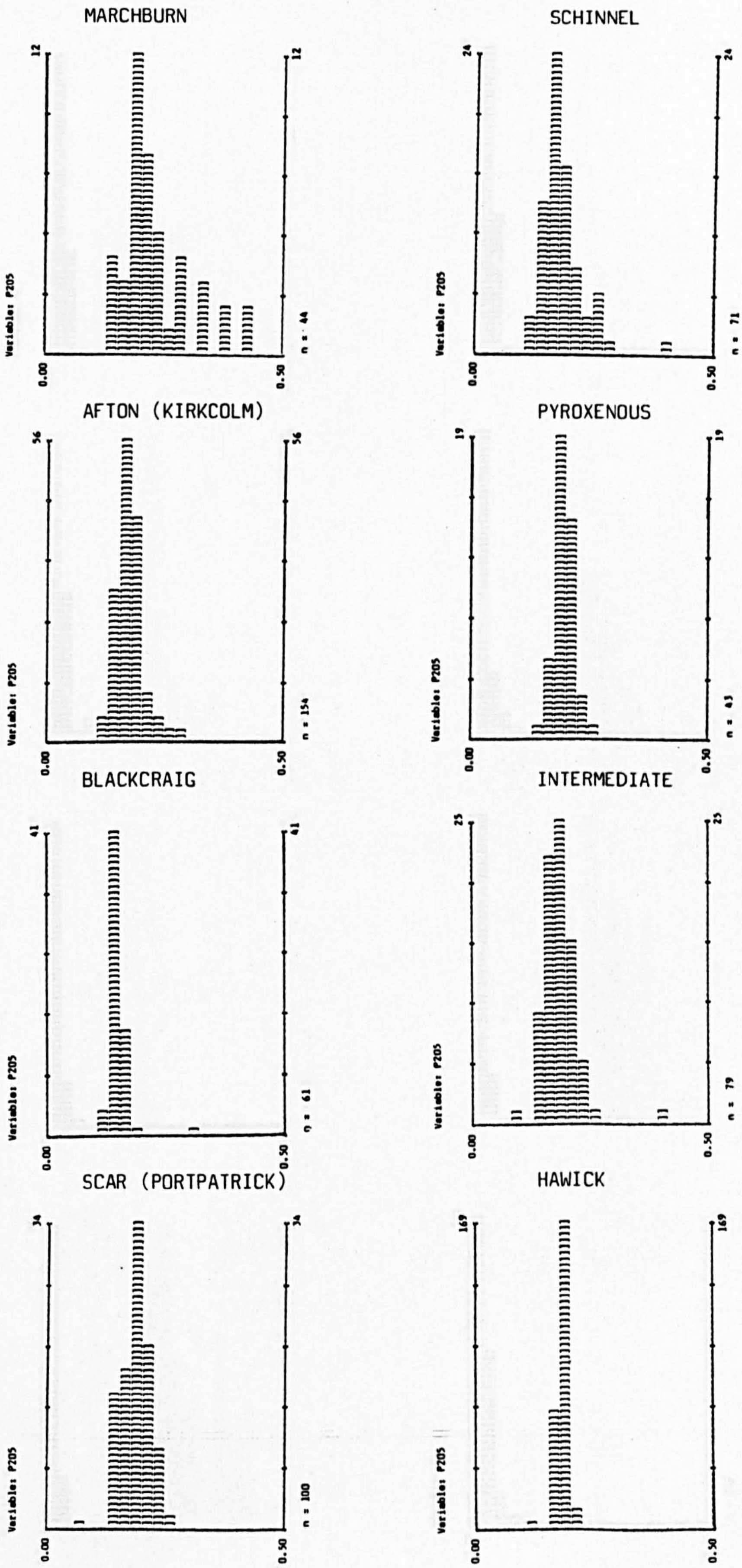
MARCHBURN
Variable: P205
12
0.00
0.50
n = 44
SCHINNEL
Variable: P205
24
0.00
0.50
n = 71
AFTON (KIRKCOLM)
Variable: P205
56
0.00
0.50
n = 154
PYROXENOUS
Variable: P205
19
0.00
0.50
n = 43
BLACKCRAIG
Variable: P205
41
0.00
0.50
n = 61
INTERMEDIATE
Variable: P205
25
0.00
0.50
n = 79
SCAR (PORTPATRICK)
Variable: P205
34
0.00
0.50
n = 100
HAWICK
Variable: P205
169
0.00
0.50

FIGURE 235

MARCHBURN

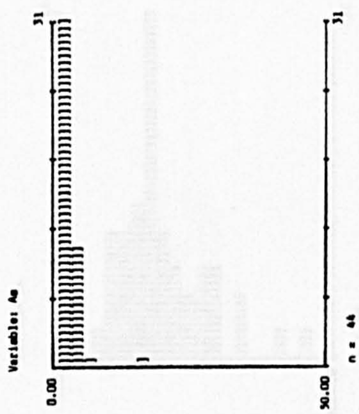

SCHINNEL

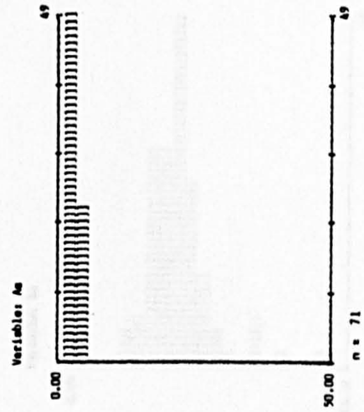

AFTON (KIRKCOLM)

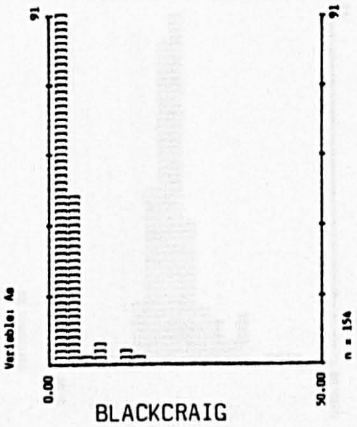

PYROXENOUS

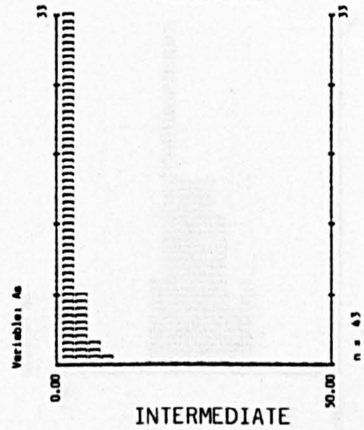

BLACKCRAIG

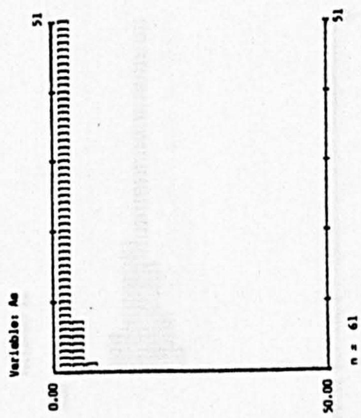

INTERMEDIATE

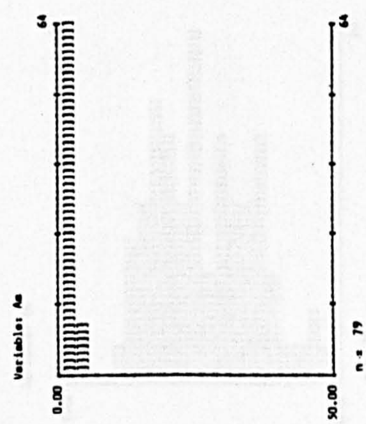

SCAR (PORTPATRICK)

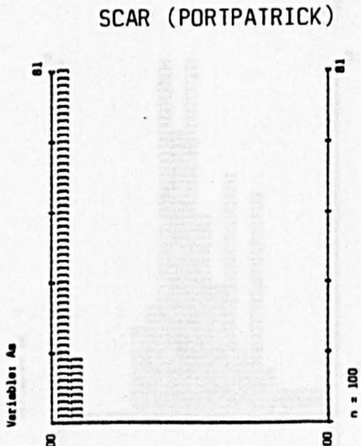

HAWICK

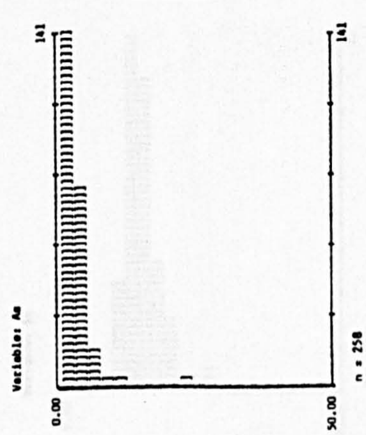

FIGURE 236

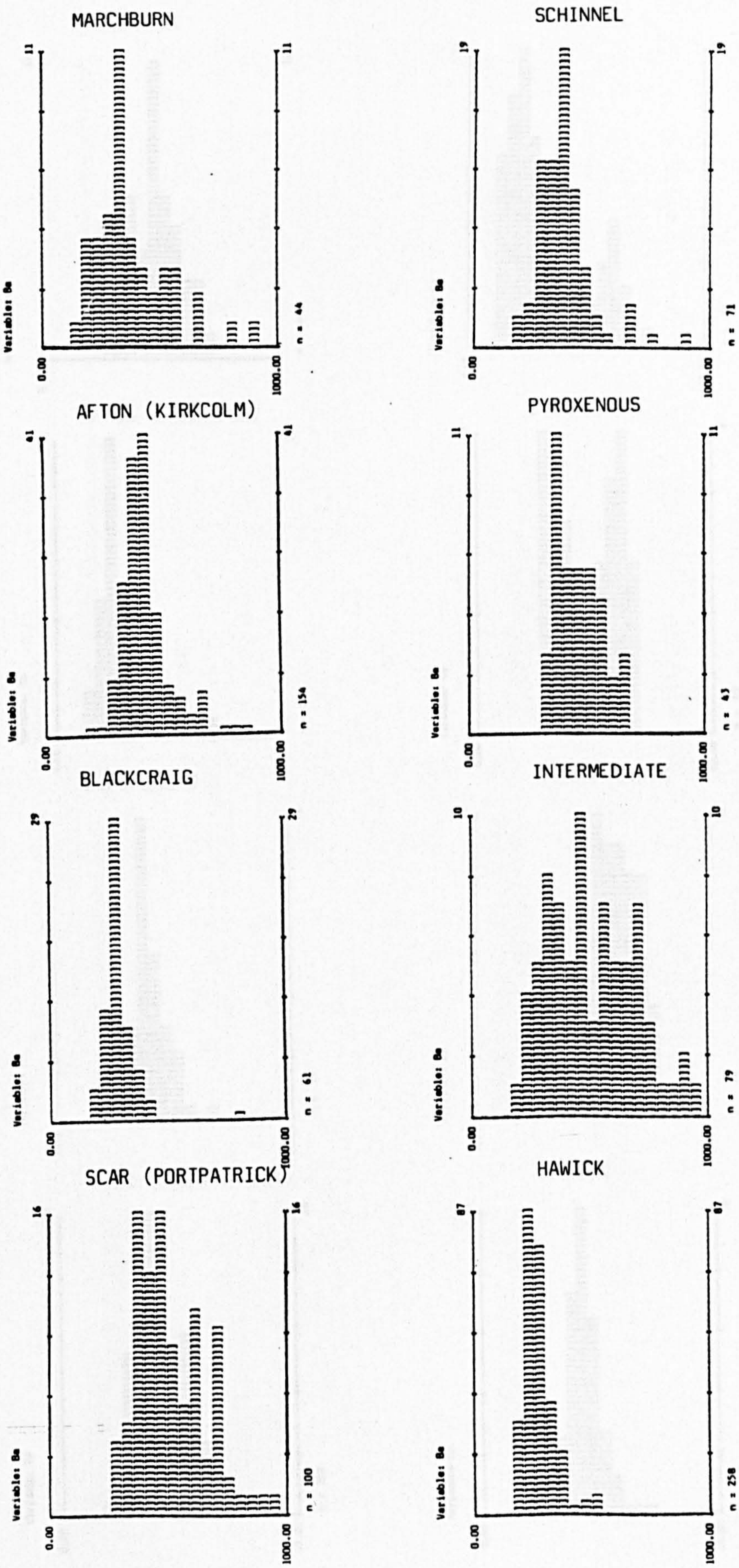
MARCHBURN
Variable: Ba
0.00
1000.00
11
n = 44
SCHINNEL
Variable: Ba
0.00
1000.00
19
n = 71
AFTON (KIRKCOLM)
Variable: Ba
0.00
1000.00
41
n = 154
PYROXENOUS
Variable: Ba
0.00
1000.00
11
n = 43
BLACKCRAIG
Variable: Ba
0.00
1000.00
29
n = 61
INTERMEDIATE
Variable: Ba
0.00
1000.00
10
n = 79
SCAR (PORTPATRICK)
Variable: Ba
0.00
1000.00
16
n = 100
HAWICK
Variable: Ba
0.00
1000.00
87
n = 258

FIGURE 237

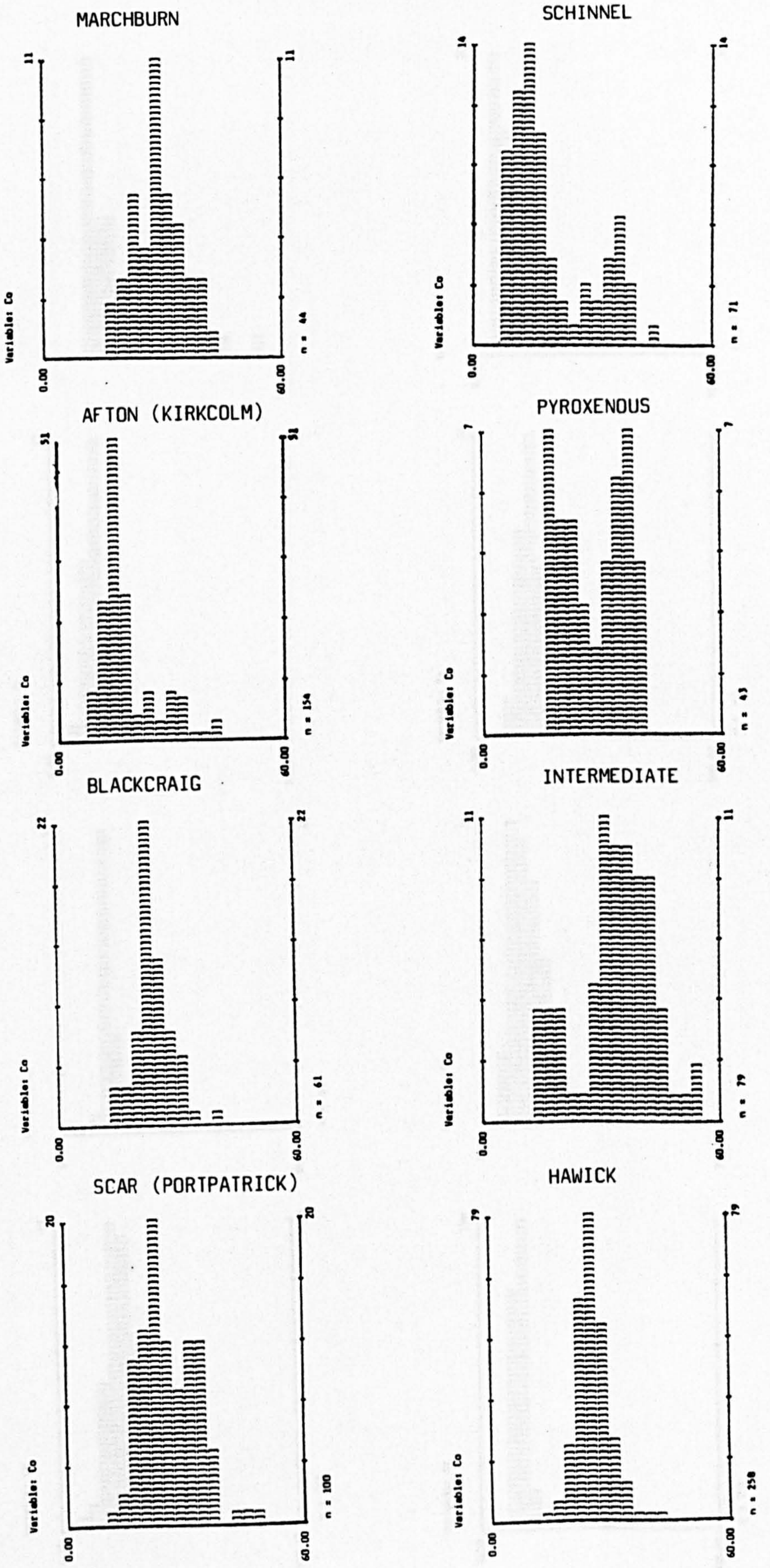
MARCHBURN
Variable: Co
0.00
60.00
n = 44
SCHINNEL
n = 71
AFTON (KIRKCOLM)
n = 154
PYROXENOUS
n = 43
BLACKCRAIG
n = 61
INTERMEDIATE
n = 79
SCAR (PORTPATRICK)
n = 100
HAWICK
n = 250

FIGURE 238

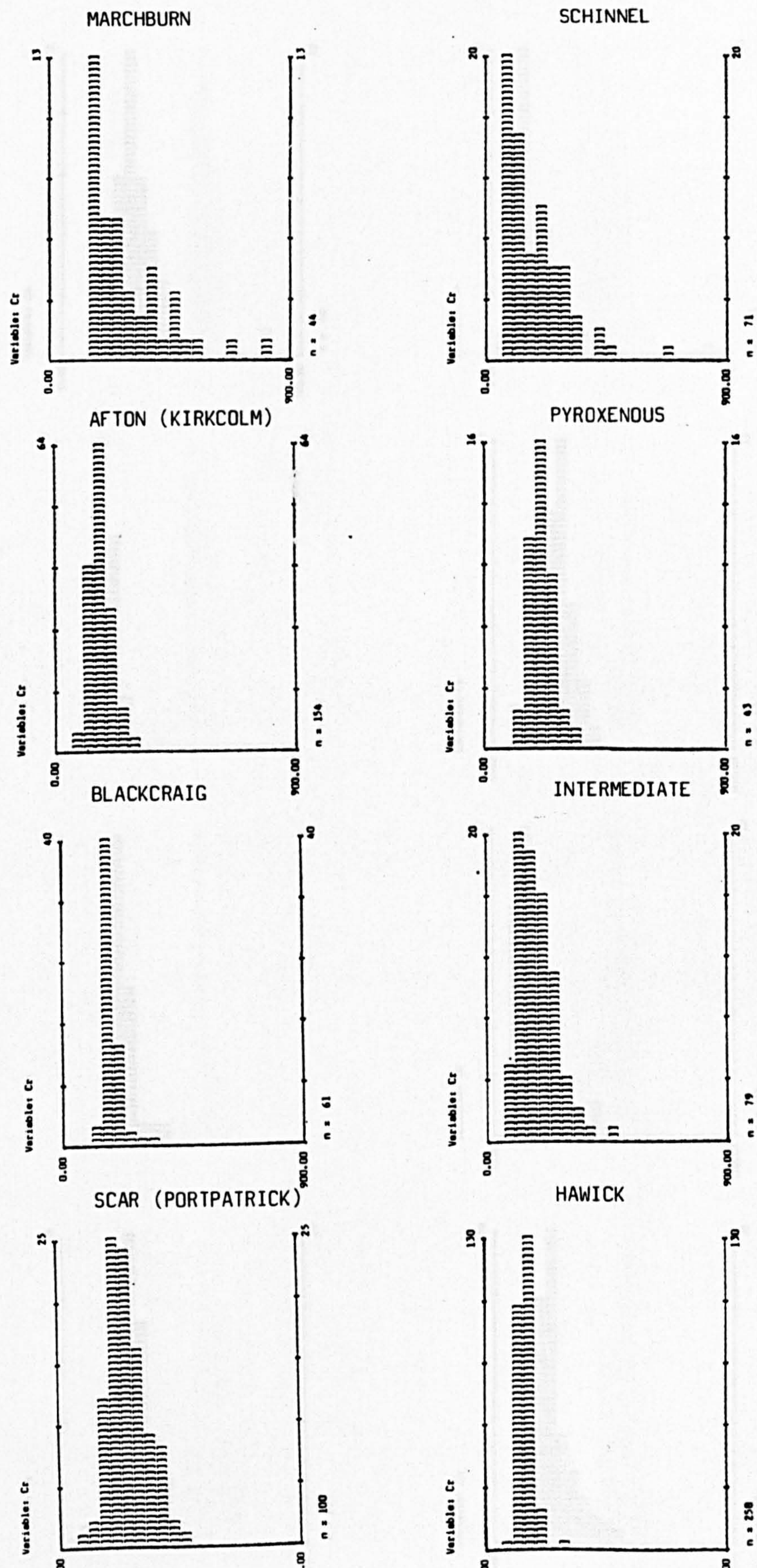
MARCHBURN
SCHINNEL
AFTON (KIRKCOLM)
PYROXENOUS
BLACKCRAIG
INTERMEDIATE
SCAR (PORTPATRICK)
HAWICK
Variable: Cr
0.00
900.00

FIGURE 239

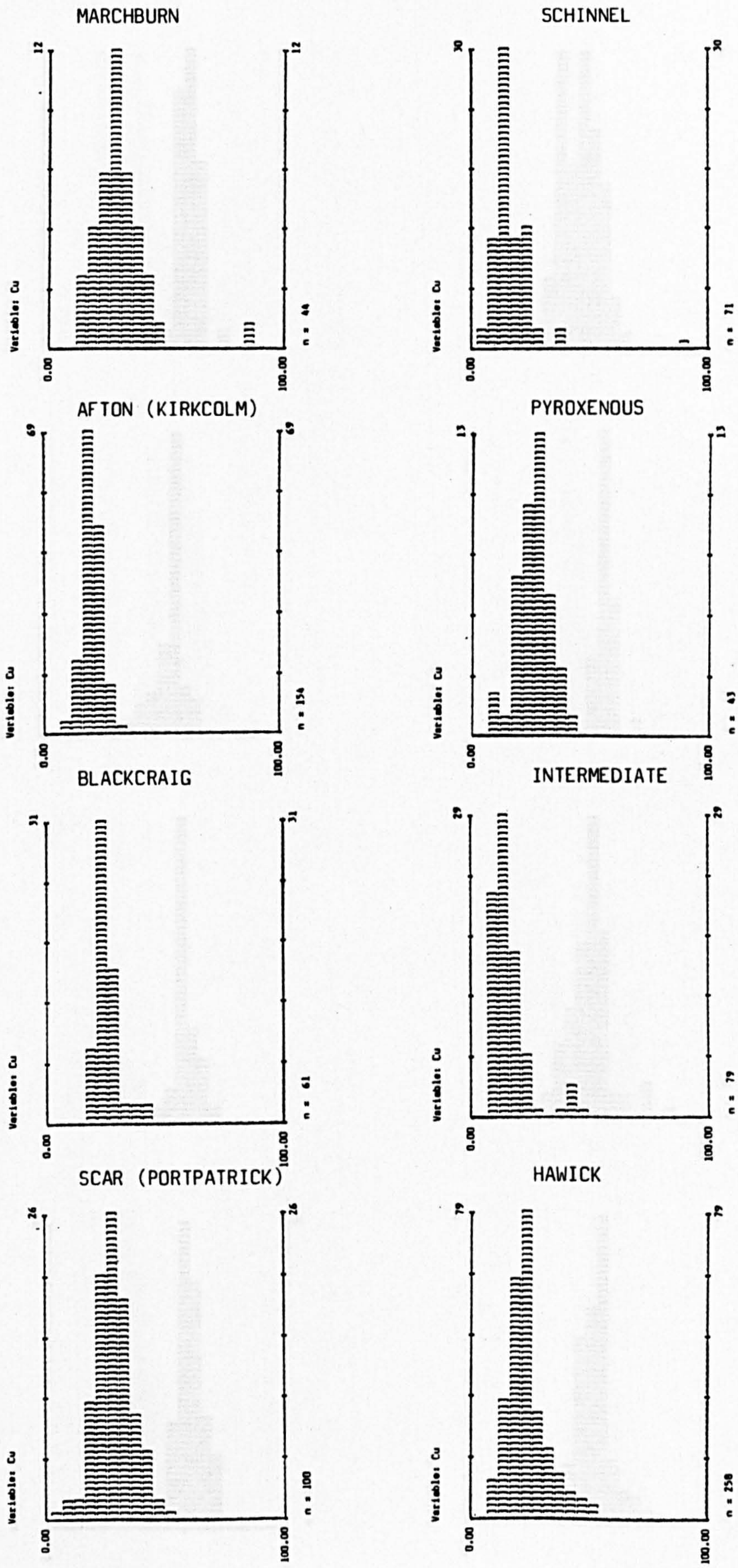
MARCHBURN
SCHINNEL
AFTON (KIRKCOLM)
PYROXENOUS
BLACKCRAIG
INTERMEDIATE
SCAR (PORTPATRICK)
HAWICK
Variable: Cu
0.00
100.00
n = 44
n = 71
n = 154
n = 43
n = 61
n = 79
n = 100
n = 258

FIGURE 240

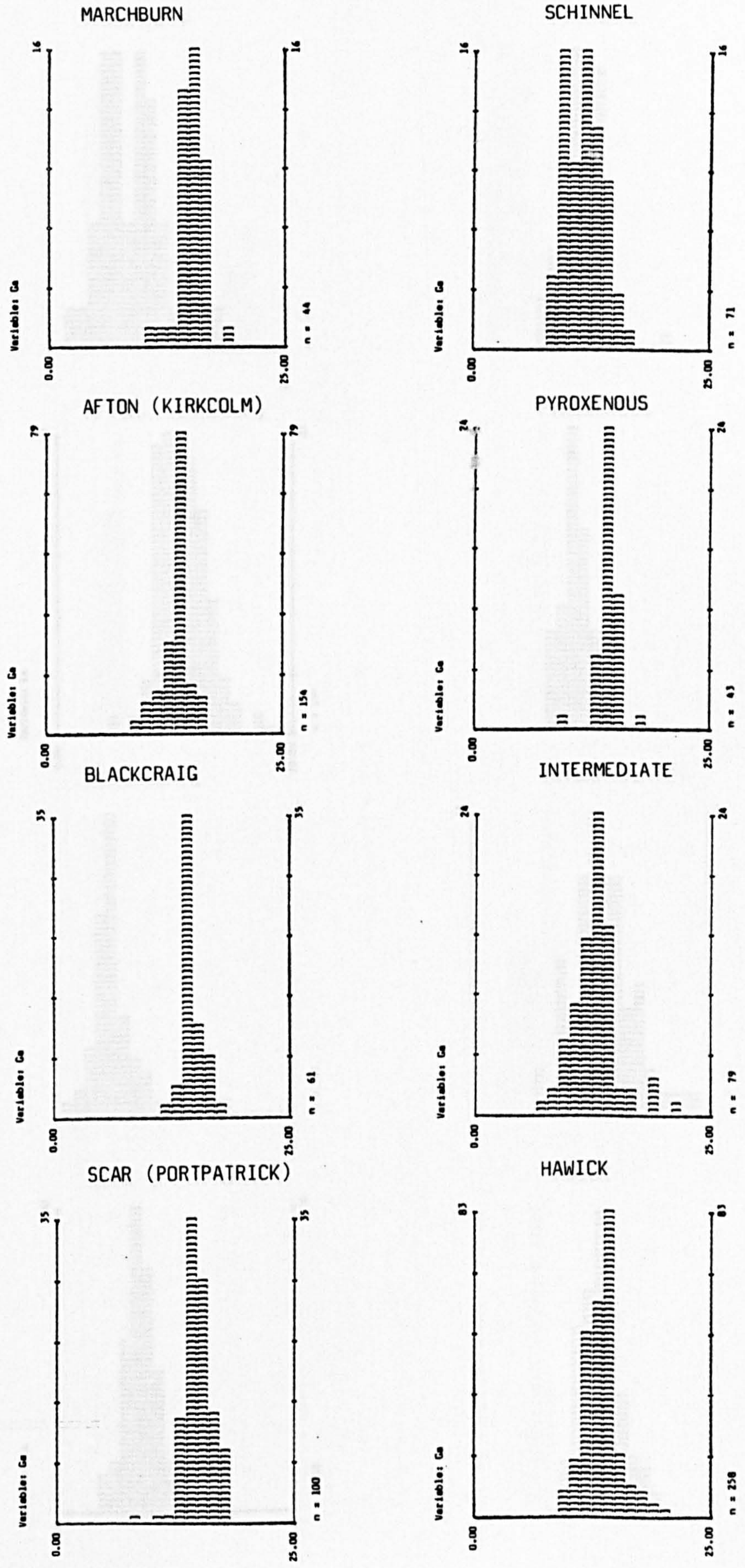
MARCHBURN
SCHINNEL
AFTON (KIRKCOLM)
PYROXENOUS
BLACKCRAIG
INTERMEDIATE
SCAR (PORTPATRICK)
HAWICK
Variable: Ga
0.00
25.00
n = 44
n = 71
n = 154
n = 43
n = 61
n = 79
n = 100
n = 250

FIGURE 241

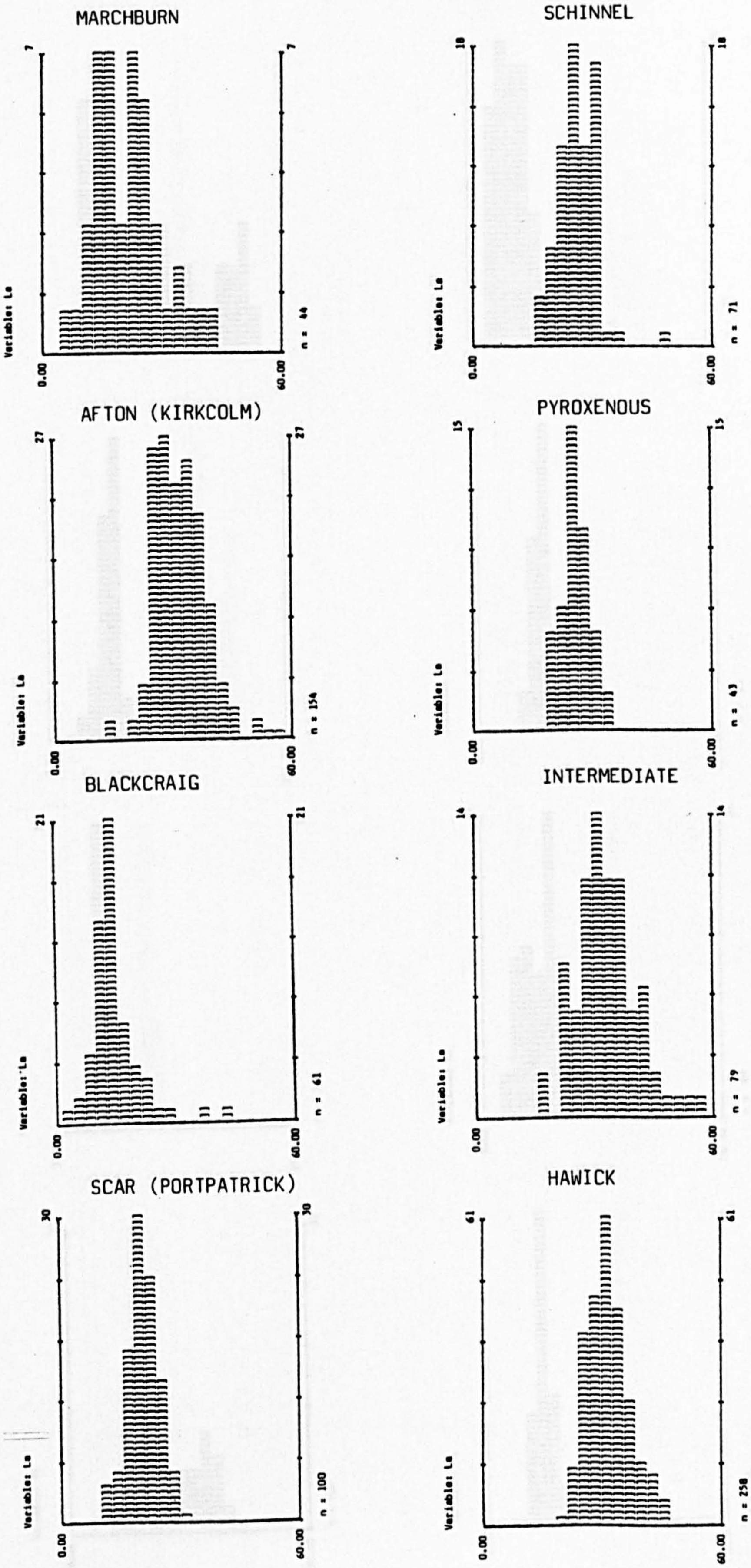
MARCHBURN
7
Variable: La
0.00
60.00
n = 44
SCHINNEL
18
Variable: La
0.00
60.00
n = 71
AFTON (KIRKCOLM)
27
Variable: La
0.00
60.00
n = 154
PYROXENOUS
15
Variable: La
0.00
60.00
n = 43
BLACKCRAIG
21
Variable: La
0.00
60.00
n = 61
INTERMEDIATE
14
Variable: La
0.00
60.00
n = 79
SCAR (PORTPATRICK)
30
Variable: La
0.00
60.00
n = 100
HAWICK
61
Variable: La
0.00
60.00
n = 258

FIGURE 242

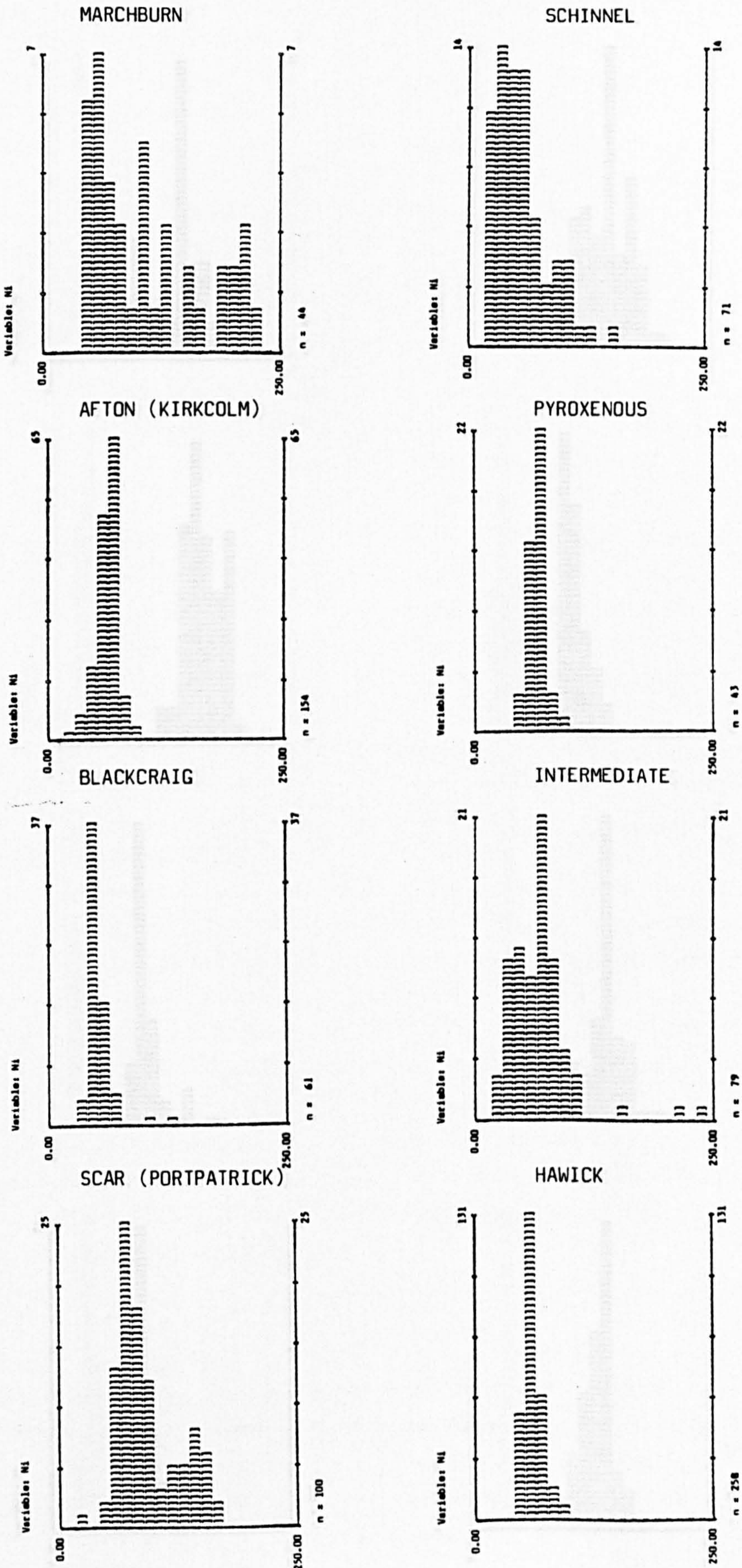
MARCHBURN
7
Variable: Ni
n = 44
0.00
250.00
SCHINNEL
14
Variable: Ni
n = 71
0.00
250.00
AFTON (KIRKCOLM)
65
Variable: Ni
n = 154
0.00
250.00
PYROXENOUS
22
Variable: Ni
n = 43
0.00
250.00
BLACKCRAIG
37
Variable: Ni
n = 61
0.00
250.00
INTERMEDIATE
21
Variable: Ni
n = 79
0.00
250.00
SCAR (PORTPATRICK)
25
Variable: Ni
n = 100
0.00
250.00
HAWICK
131
Variable: Ni
n = 258
0.00
250.00

FIGURE 243

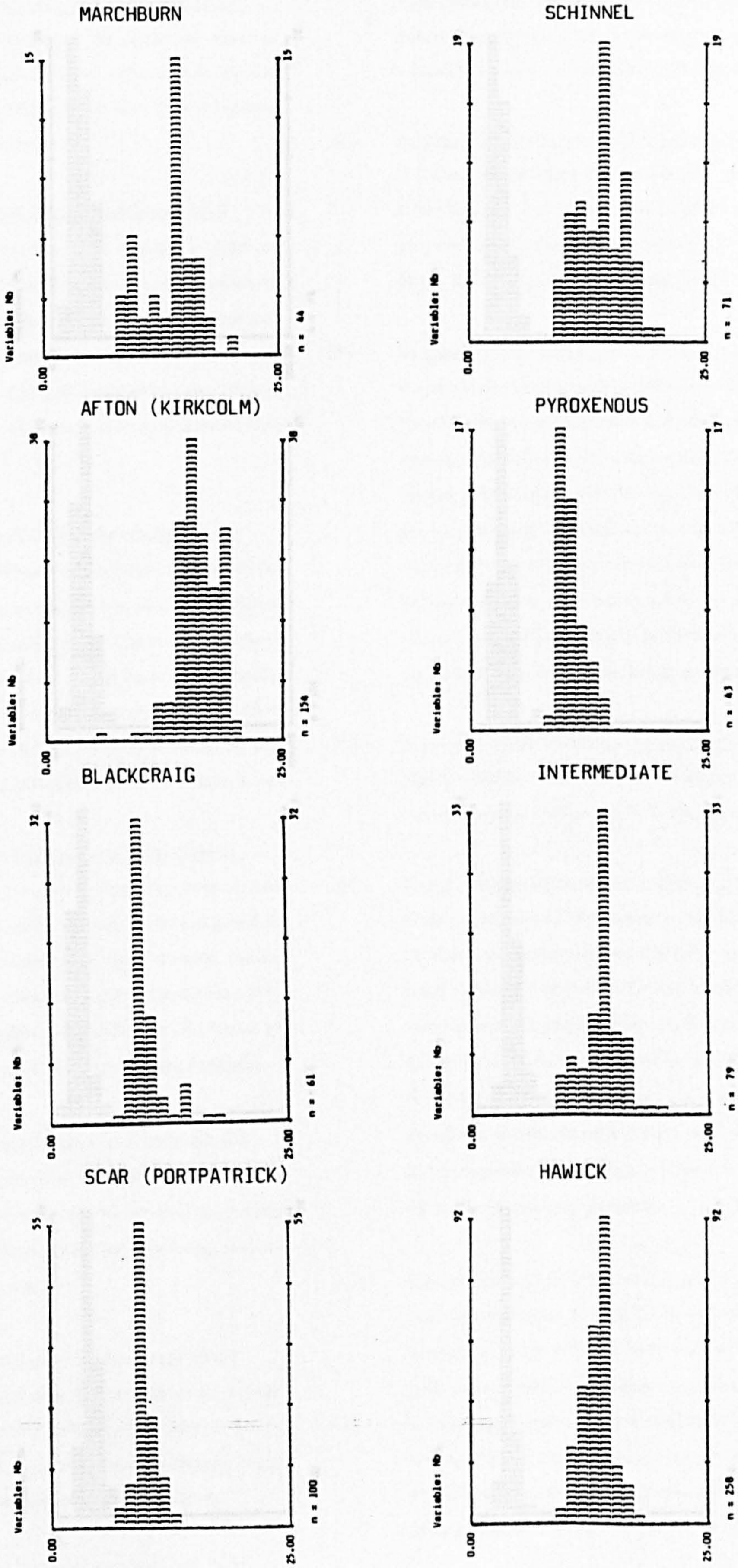
MARCHBURN
SCHINNEL
AFTON (KIRKCOLM)
PYROXENOUS
BLACKCRAIG
INTERMEDIATE
SCAR (PORTPATRICK)
HAWICK
Variable: Nb
0.00
25.00
15
19
38
17
32
33
55
92
n = 44
n = 71
n = 154
n = 43
n = 61
n = 79
n = 100
n = 258

FIGURE 244

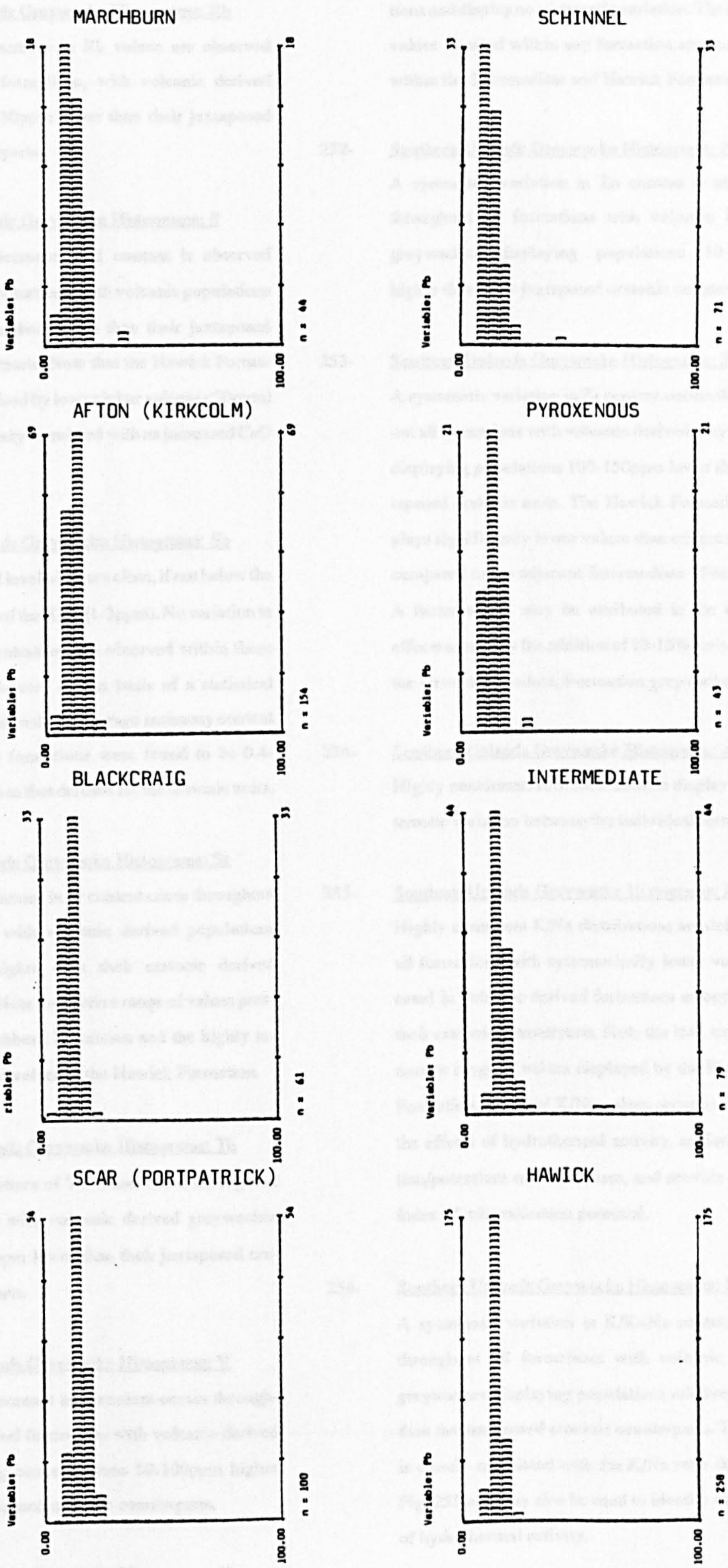
MARCHBURN
n = 46
AFTON (KIRKCOLM)
n = 154
BLACKCRAIG
n = 61
SCAR (PORTPATRICK)
n = 100
SCHINNEL
n = 71
PYROXENOUS
n = 43
INTERMEDIATE
n = 79
HAWICK
n = 238
Variable: Pb
0.00
100.00

245- <u>Southern Uplands Greywacke Histograms: Rb</u>
A systematic increase in Rb values are observed throughout all formations, with volcanic derived populations 20-30ppm lower than their juxtaposed cratonic counterparts.

246- <u>Southern Uplands Greywacke Histograms: S</u>
A systematic decrease in S content is observed throughout all formations, with volcanic populations 200-1000ppm higher values than their juxtaposed cratonic counterparts. Note that the Hawick Formation is characterised by low sulphur values (<50ppm) which are inversely correlated with an increased CaO content.

247- <u>Southern Uplands Greywacke Histograms: Sb</u>
The background level of Sb are close, if not below the detection limits of the XRF (1-3ppm). No variation in antimony concentrations are observed within these formations, however on the basis of a statistical assessment of this data the average antimony content of the volcanic formations were found to be 0.4-1.6ppm lower than that defined for the cratonic units.

248- <u>Southern Uplands Greywacke Histograms: Sr</u>
Systematic variations in Sr content occur throughout all formations with volcanic derived populations 130-200ppm higher than their cratonic derived counterparts. Note the diverse range of values present in the Marchburn Formation and the highly restricted range of values in the Hawick Formation.

249- <u>Southern Uplands Greywacke Histograms: Th</u>
A consistent pattern of Th values occur throughout the succession with volcanic derived greywackes generally 4-6 ppm lower than their juxtaposed cratonic counterparts.

250- <u>Southern Uplands Greywacke Histograms: V</u>
A systematic decrease in V content occurs throughout the individual formations with volcanic derived units exhibiting concentrations 50-100ppm higher than their juxtaposed cratonic counterparts.

251- <u>Southern Uplands Greywacke Histograms: Y</u>
Y values are highly consistent throughout all formations and display no systematic variation. The highest values located within any formation are contained within the Intermediate and Hawick Formation.

252- <u>Southern Uplands Greywacke Histograms: Zn</u>
A systematic variation in Zn content is observed throughout all formations with volcanic derived greywackes displaying populations 10-30ppm higher than their juxtaposed cratonic counterparts.

253- <u>Southern Uplands Greywacke Histograms: Zr</u>
A systematic variation in Zr content occurs throughout all formations with volcanic derived greywackes displaying populations 100-150ppm lower than juxtaposed cratonic units. The Hawick Formation displays significantly lower values than expected when compared to the adjacent Intermediate Formation. A factor which may be attributed to the dilution effects caused by the addition of 10-15% carbonate to the Hawick (Wenlock)Formation greywackes.

254- <u>Southern Uplands Greywacke Histograms: Al/Si</u>
Highly consistent Al/Si distributions display no systematic variation between the individual formations.

255- <u>Southern Uplands Greywacke Histograms: K/Na</u>
Highly consistent K/Na distributions are defined by all formations with systematically lower values located in volcanic derived formations as opposed to their cratonic counterparts. Note the low, extremely narrow range of values displayed by the Blackcraig Formation. Elevated K/Na values serve to illustrate the effects of hydrothermal activity, sodium depletion/potassium metasomatism, and provide a useful index of mineralisation potential.

256- <u>Southern Uplands Greywacke Histograms: K/K+Na</u>
A systematic variation in K/K+Na content occurs throughout all formations with volcanic derived greywackes displaying populations relatively lower than the juxtaposed cratonic counterparts. This ratio is closely associated with the K/Na ratio defined in Fig. 255 and may also be used to identify the effects of hydrothermal activity.

FIGURE 245

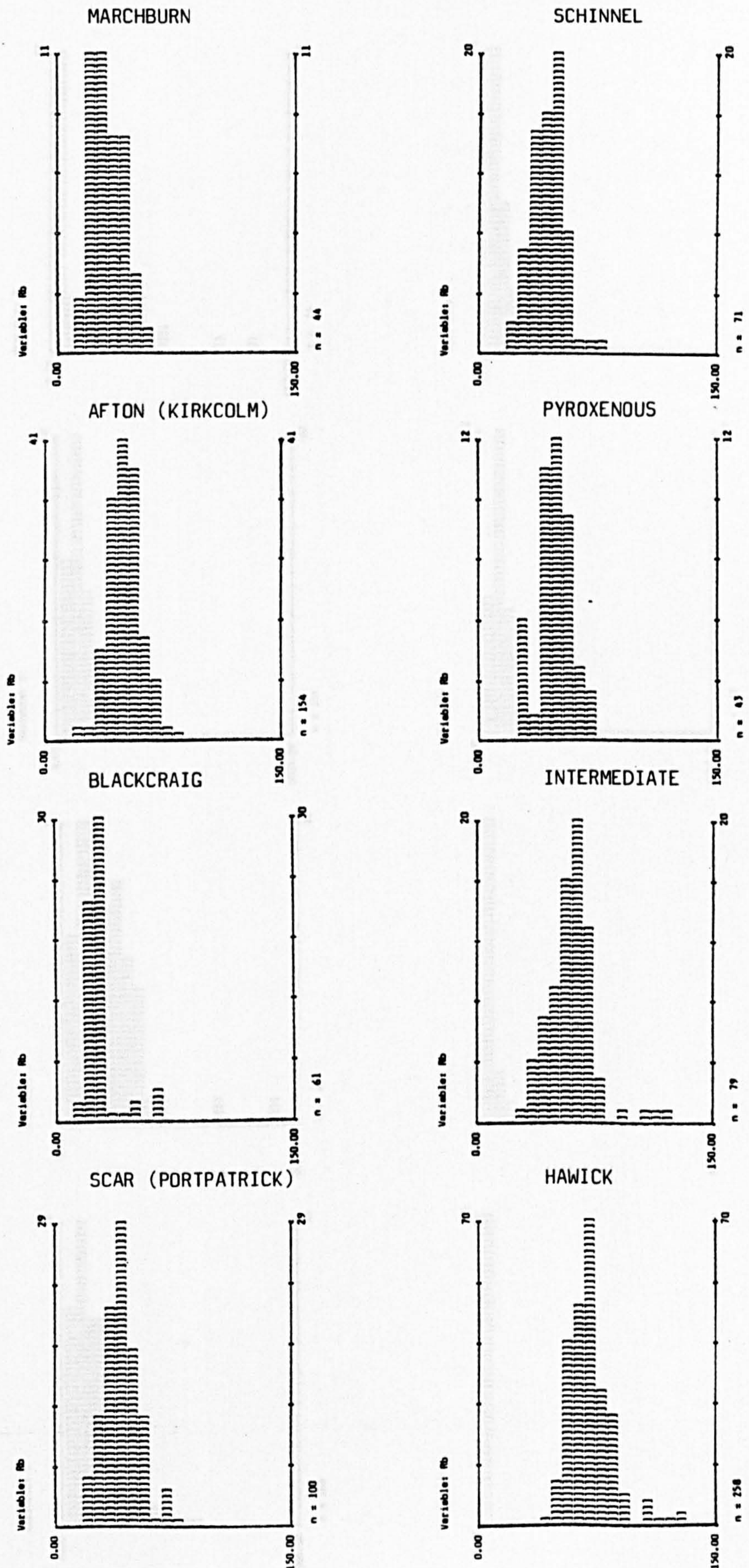
MARCHBURN
11
Variable: Rb
n = 44
0.00
150.00
SCHINNEL
20
Variable: Rb
n = 71
0.00
150.00
AFTON (KIRKCOLM)
41
Variable: Rb
n = 154
0.00
150.00
PYROXENOUS
12
Variable: Rb
n = 43
0.00
150.00
BLACKCRAIG
30
Variable: Rb
n = 61
0.00
150.00
INTERMEDIATE
20
Variable: Rb
n = 79
0.00
150.00
SCAR (PORTPATRICK)
29
Variable: Rb
n = 100
0.00
150.00
HAWICK
70
Variable: Rb
n = 258
0.00
150.00

FIGURE 246

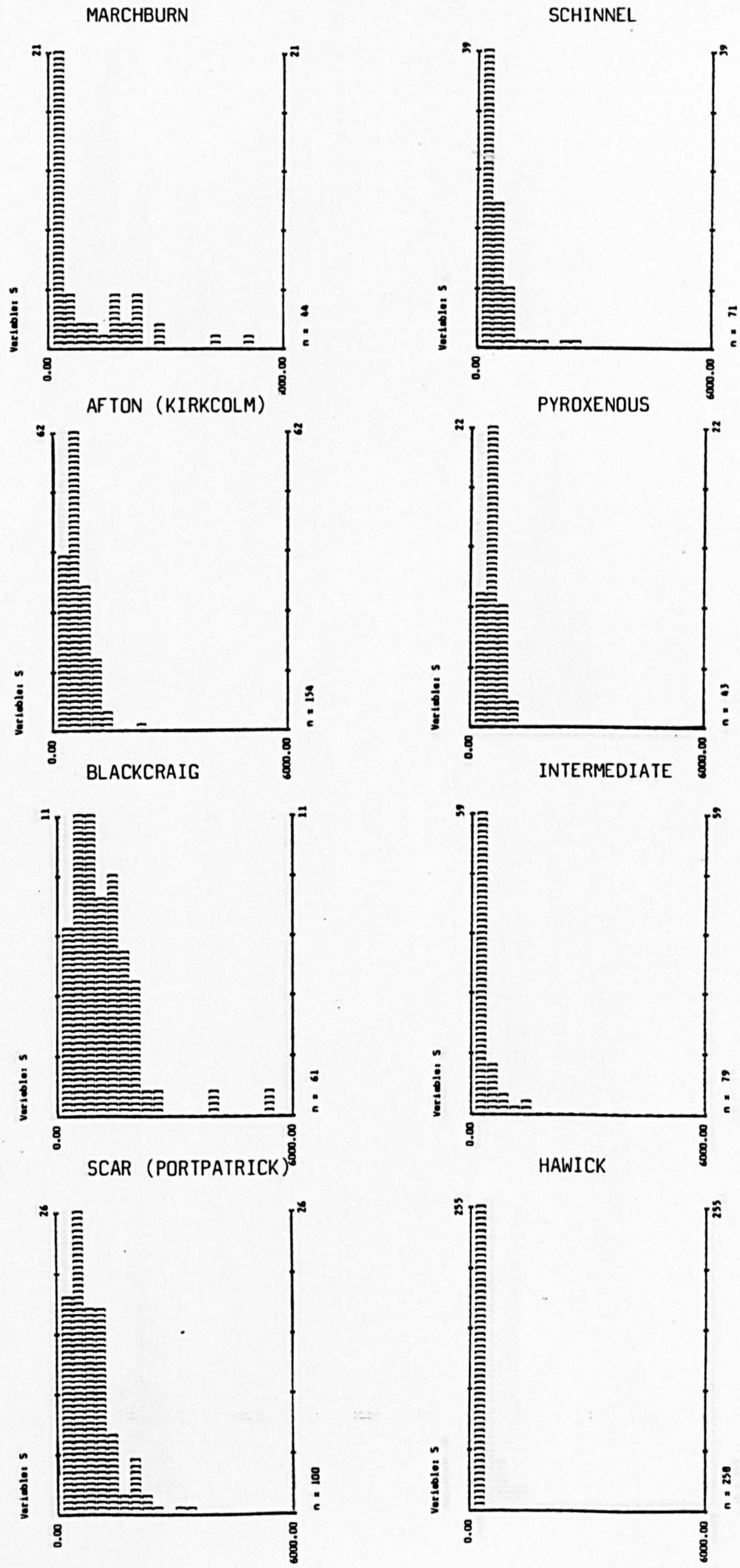
MARCHBURN
SCHINNEL
AFTON (KIRKCOLM)
PYROXENOUS
BLACKCRAIG
INTERMEDIATE
SCAR (PORTPATRICK)
HAWICK

FIGURE 247

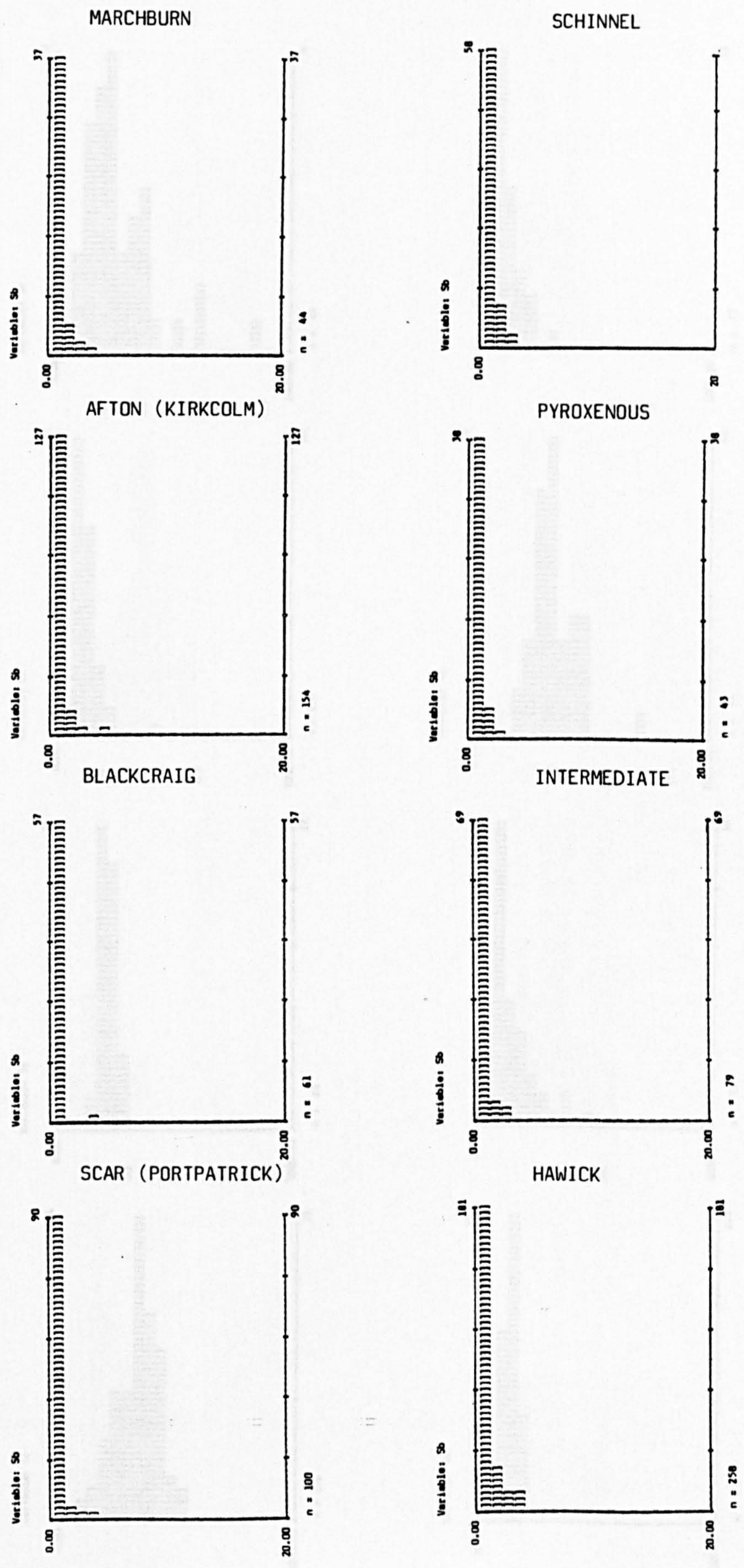
MARCHBURN
Variable: Sb
0.00
20.00
n = 44
SCHINNEL
Variable: Sb
0.00
20
AFTON (KIRKCOLM)
Variable: Sb
0.00
20.00
n = 154
PYROXENOUS
Variable: Sb
0.00
20.00
n = 43
BLACKCRAIG
Variable: Sb
0.00
20.00
n = 61
INTERMEDIATE
Variable: Sb
0.00
20.00
n = 79
SCAR (PORTPATRICK)
Variable: Sb
0.00
20.00
n = 100
HAWICK
Variable: Sb
0.00
20.00
n = 258

FIGURE 248

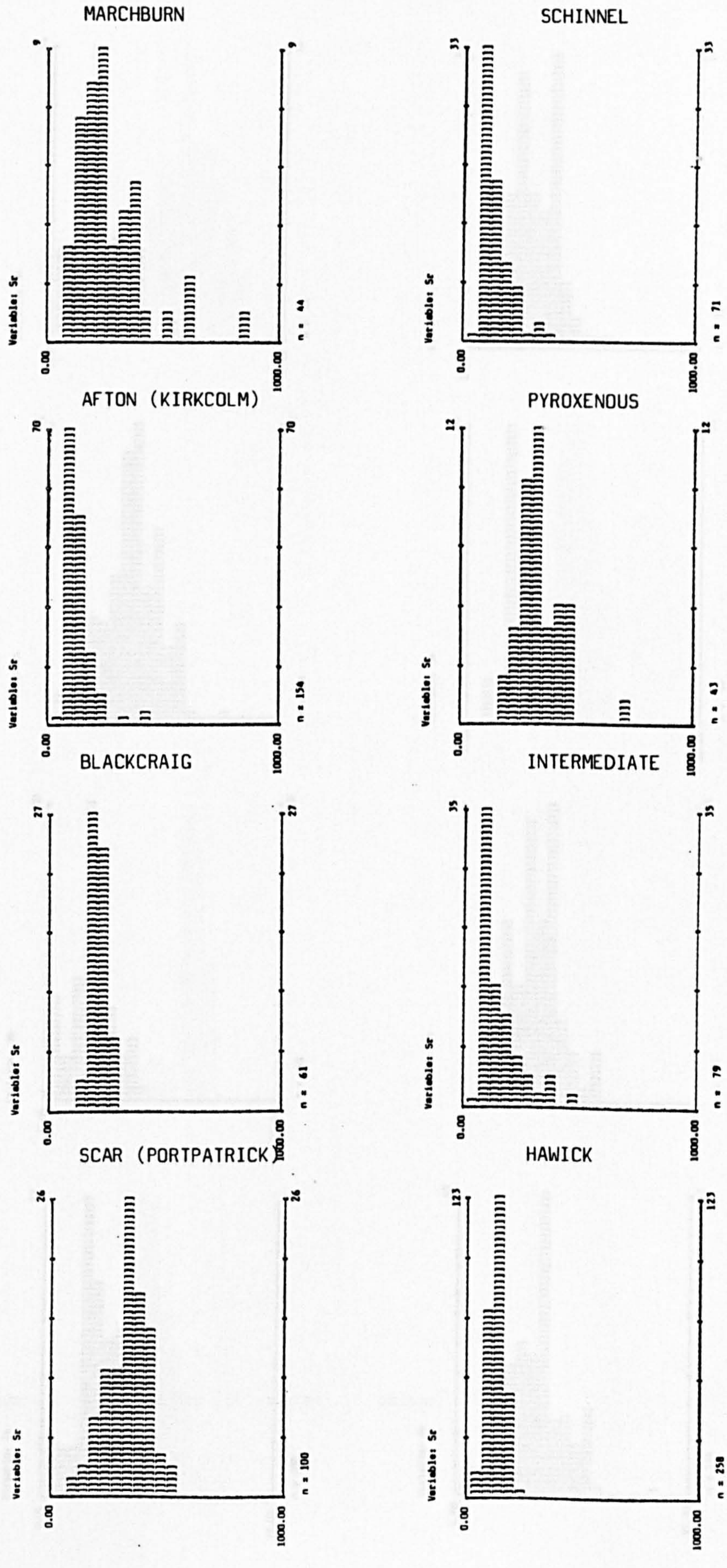
MARCHBURN
SCHINNEL
AFTON (KIRKCOLM)
PYROXENOUS
BLACKCRAIG
INTERMEDIATE
SCAR (PORTPATRICK)
HAWICK
Variable: Sr
0.00
1000.00
n = 44
n = 71
n = 154
n = 43
n = 61
n = 79
n = 100
n = 258

FIGURE 249

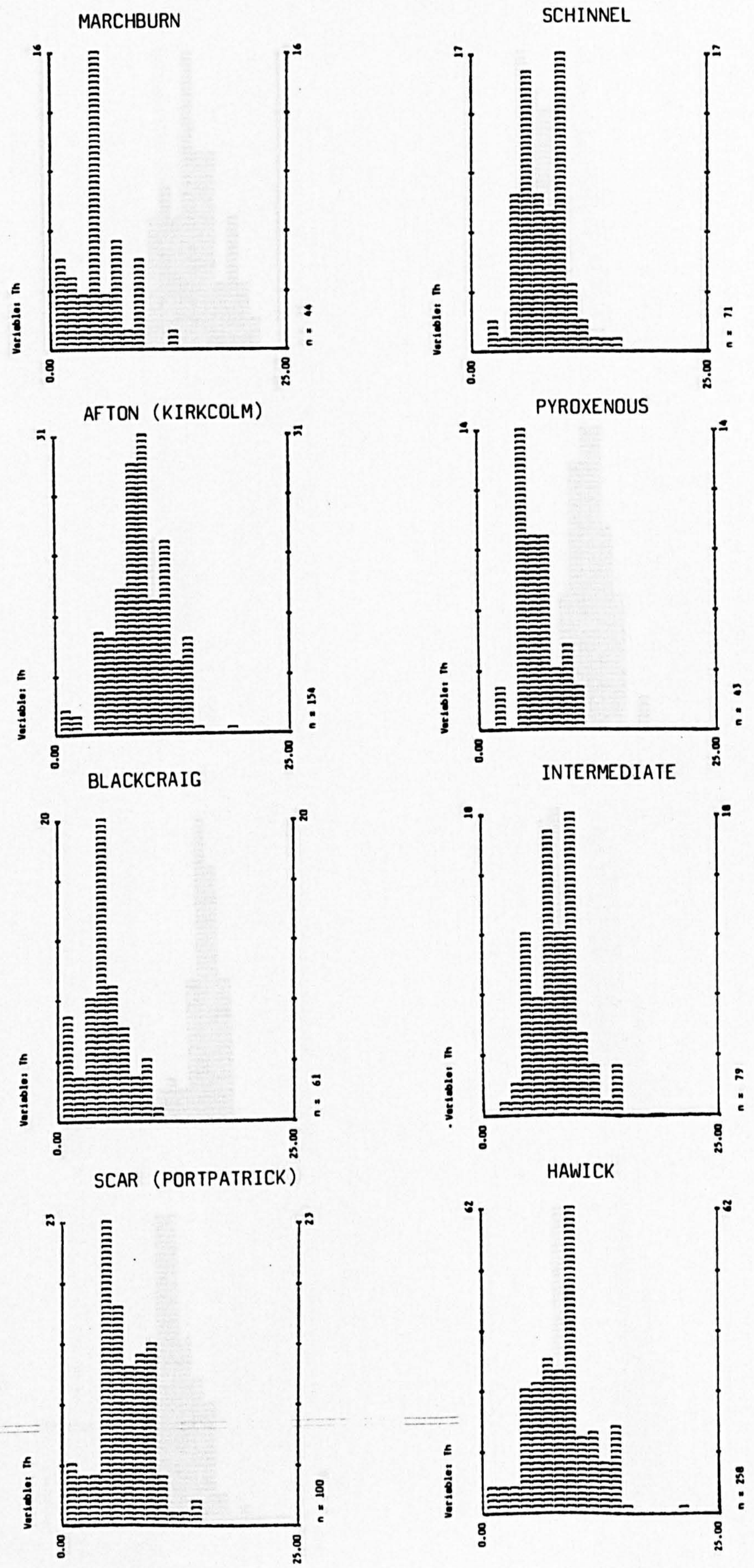
MARCHBURN
16
Variable: Th
n = 44
0.00
25.00
SCHINNEL
17
Variable: Th
n = 71
0.00
25.00
AFTON (KIRKCOLM)
31
Variable: Th
n = 154
0.00
25.00
PYROXENOUS
14
Variable: Th
n = 43
0.00
25.00
BLACKCRAIG
20
Variable: Th
n = 61
0.00
25.00
INTERMEDIATE
18
Variable: Th
n = 79
0.00
25.00
SCAR (PORTPATRICK)
23
Variable: Th
n = 100
0.00
25.00
HAWICK
62
Variable: Th
n = 258
0.00
25.00

FIGURE 250

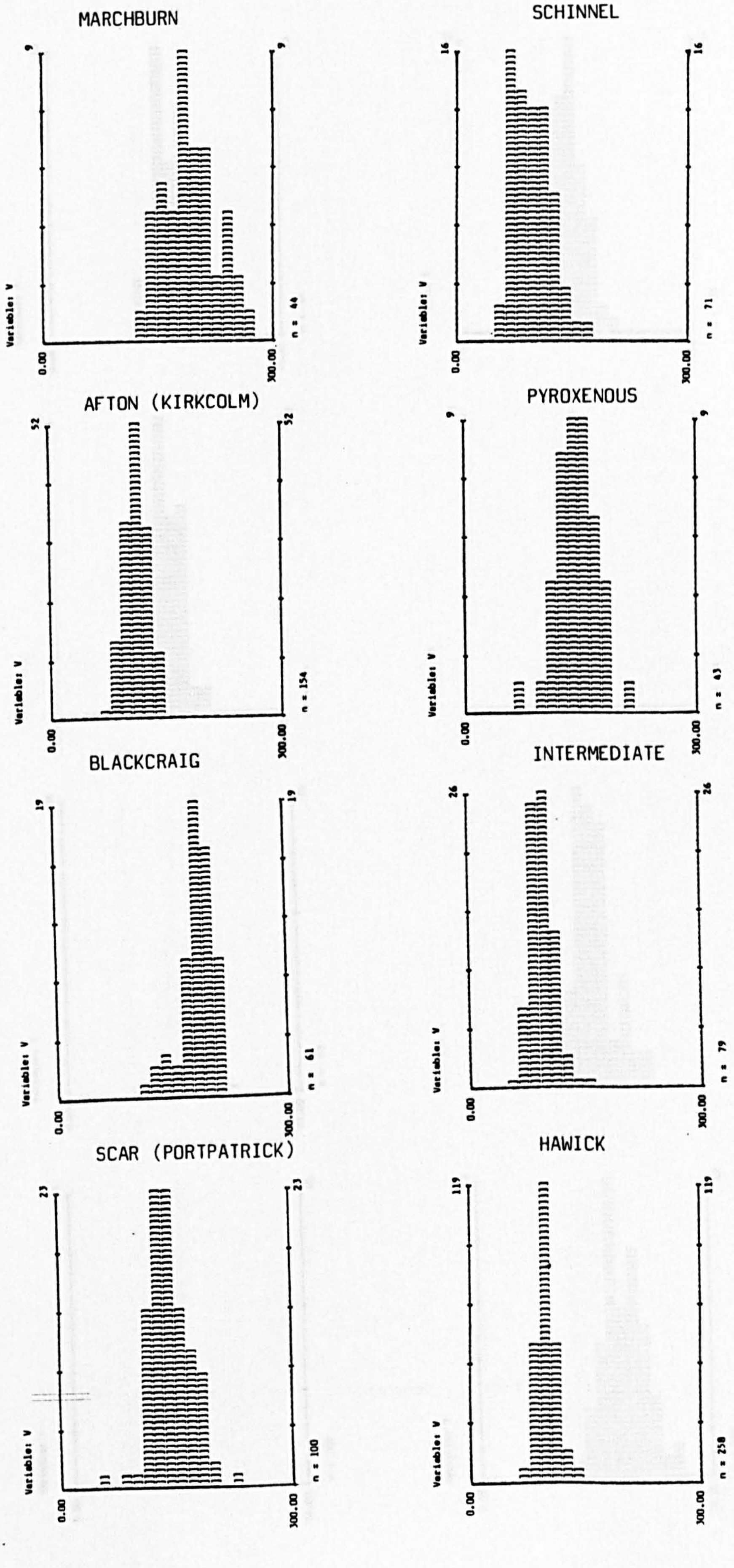
MARCHBURN
SCHINNEL
AFTON (KIRKCOLM)
PYROXENOUS
BLACKCRAIG
INTERMEDIATE
SCAR (PORTPATRICK)
HAWICK
Variable: V
0.00
300.00
n = 44
n = 71
n = 154
n = 43
n = 61
n = 79
n = 100
n = 258

FIGURE 251

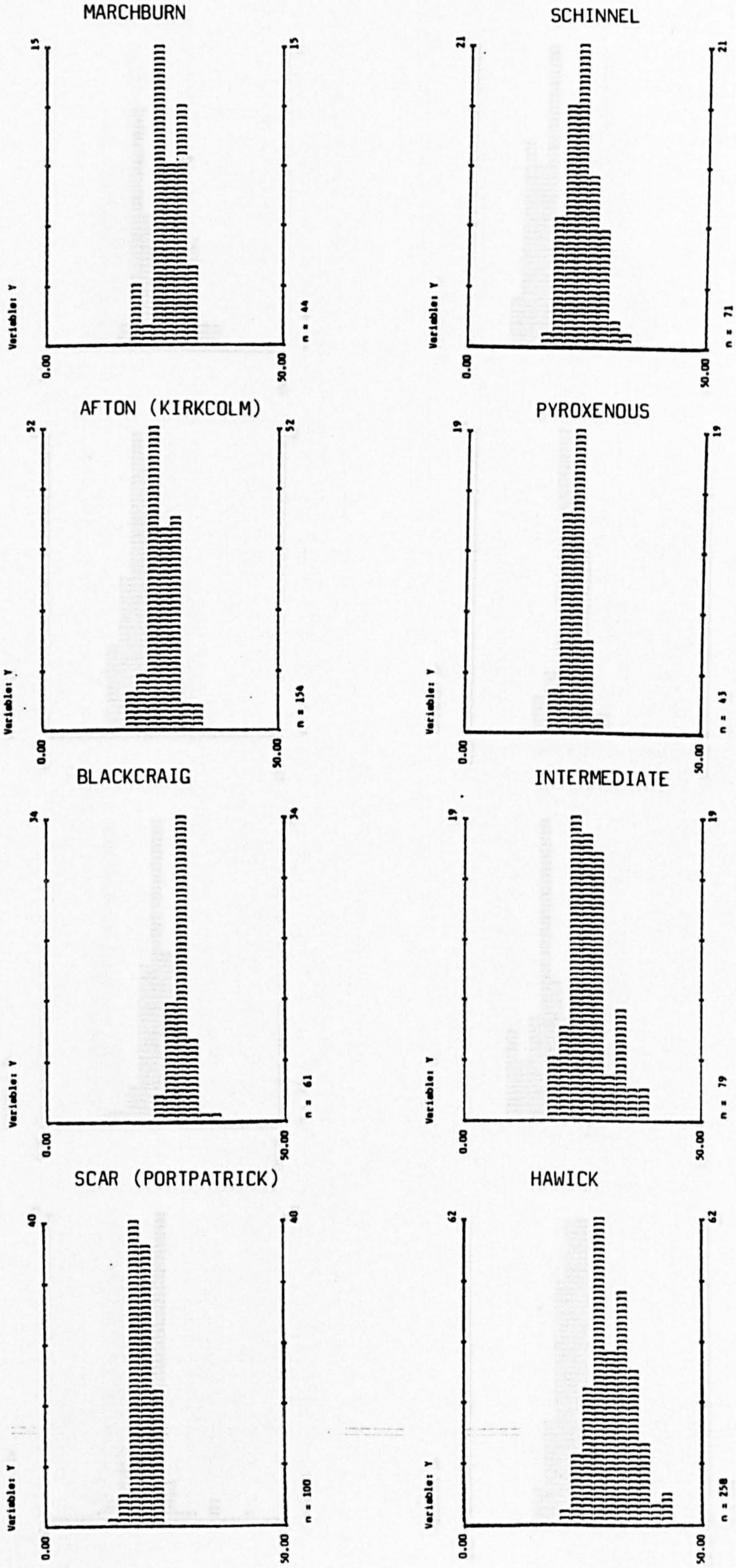
MARCHBURN
15
Variable: Y
n = 44
0.00
50.00
SCHINNEL
21
Variable: Y
n = 71
0.00
50.00
AFTON (KIRKCOLM)
52
Variable: Y
n = 134
0.00
50.00
PYROXENOUS
19
Variable: Y
n = 43
0.00
50.00
BLACKCRAIG
34
Variable: Y
n = 61
0.00
50.00
INTERMEDIATE
19
Variable: Y
n = 79
0.00
50.00
SCAR (PORTPATRICK)
40
Variable: Y
n = 100
0.00
50.00
HAWICK
62
Variable: Y
n = 258
0.00
50.00

FIGURE 252

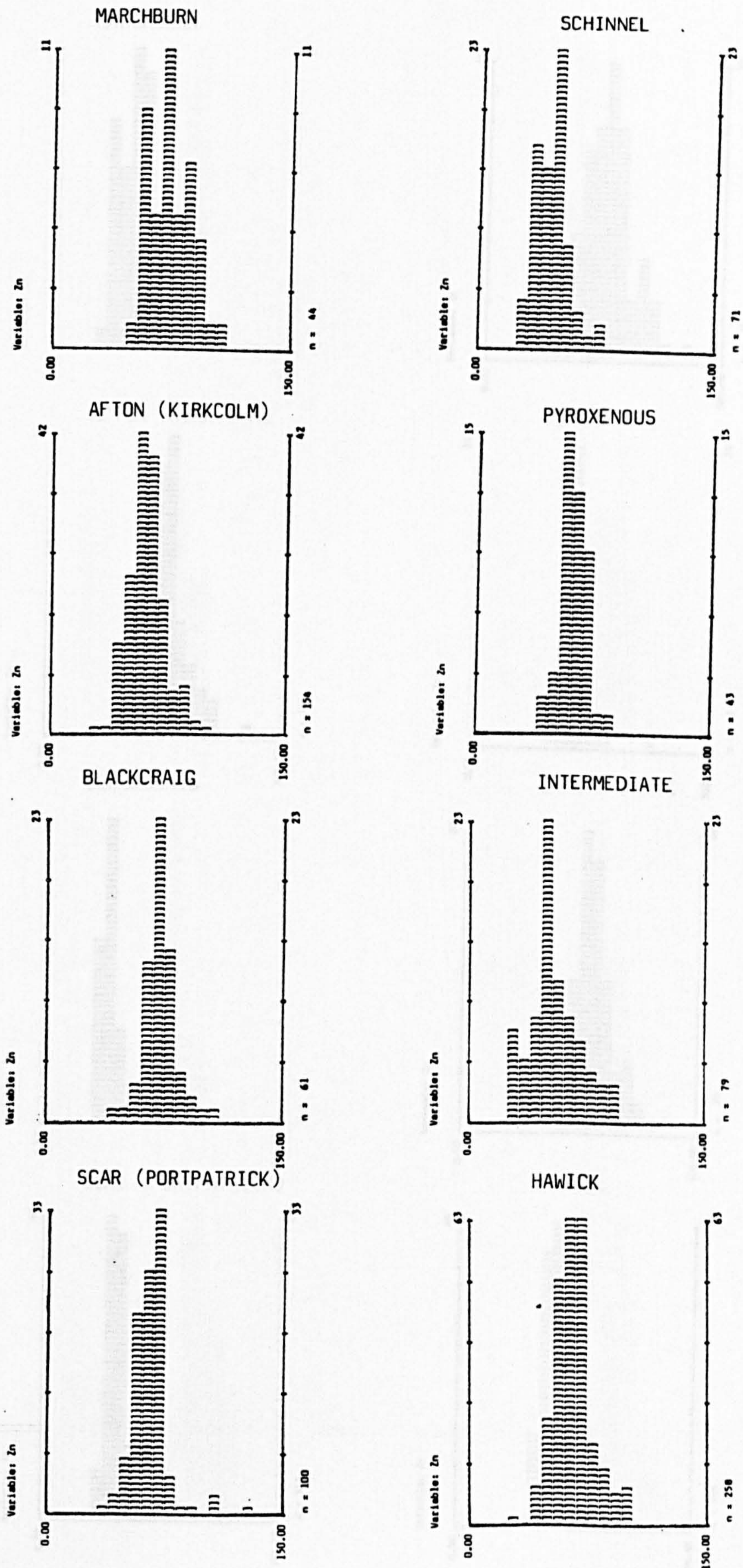
MARCHBURN
SCHINNEL
AFTON (KIRKCOLM)
PYROXENOUS
BLACKCRAIG
INTERMEDIATE
SCAR (PORTPATRICK)
HAWICK
Variable: Zn
0.00
150.00
n = 44
n = 71
n = 154
n = 43
n = 61
n = 79
n = 100
n = 258

FIGURE 253

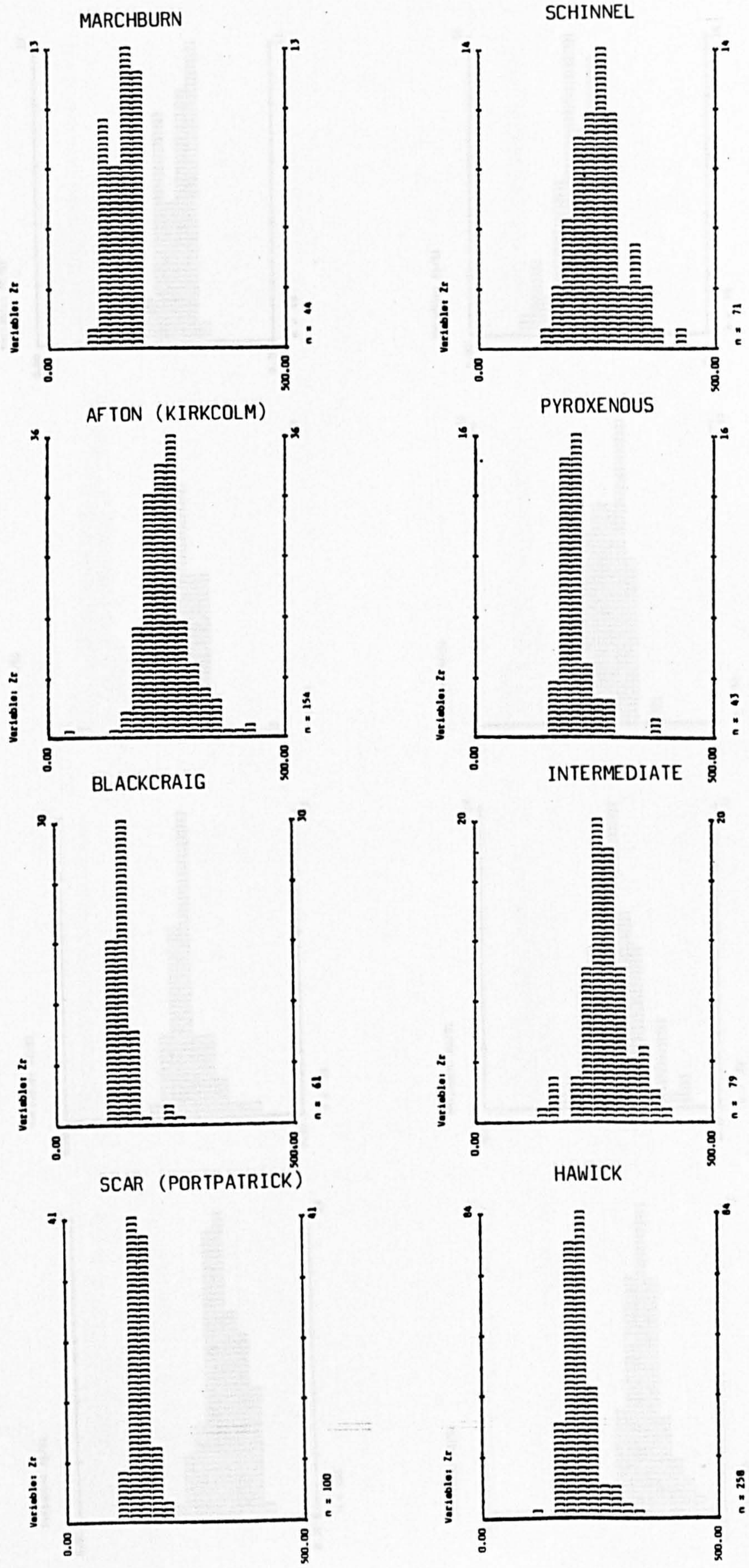
MARCHBURN
13
Variable: Zr
0.00
500.00
n = 44
SCHINNEL
14
Variable: Zr
0.00
500.00
n = 71
AFTON (KIRKCOLM)
36
Variable: Zr
0.00
500.00
n = 154
PYROXENOUS
16
Variable: Zr
0.00
500.00
n = 43
BLACKCRAIG
30
Variable: Zr
0.00
500.00
n = 61
INTERMEDIATE
20
Variable: Zr
0.00
500.00
n = 79
SCAR (PORTPATRICK)
41
Variable: Zr
0.00
500.00
n = 100
HAWICK
84
Variable: Zr
0.00
500.00
n = 258

FIGURE 254

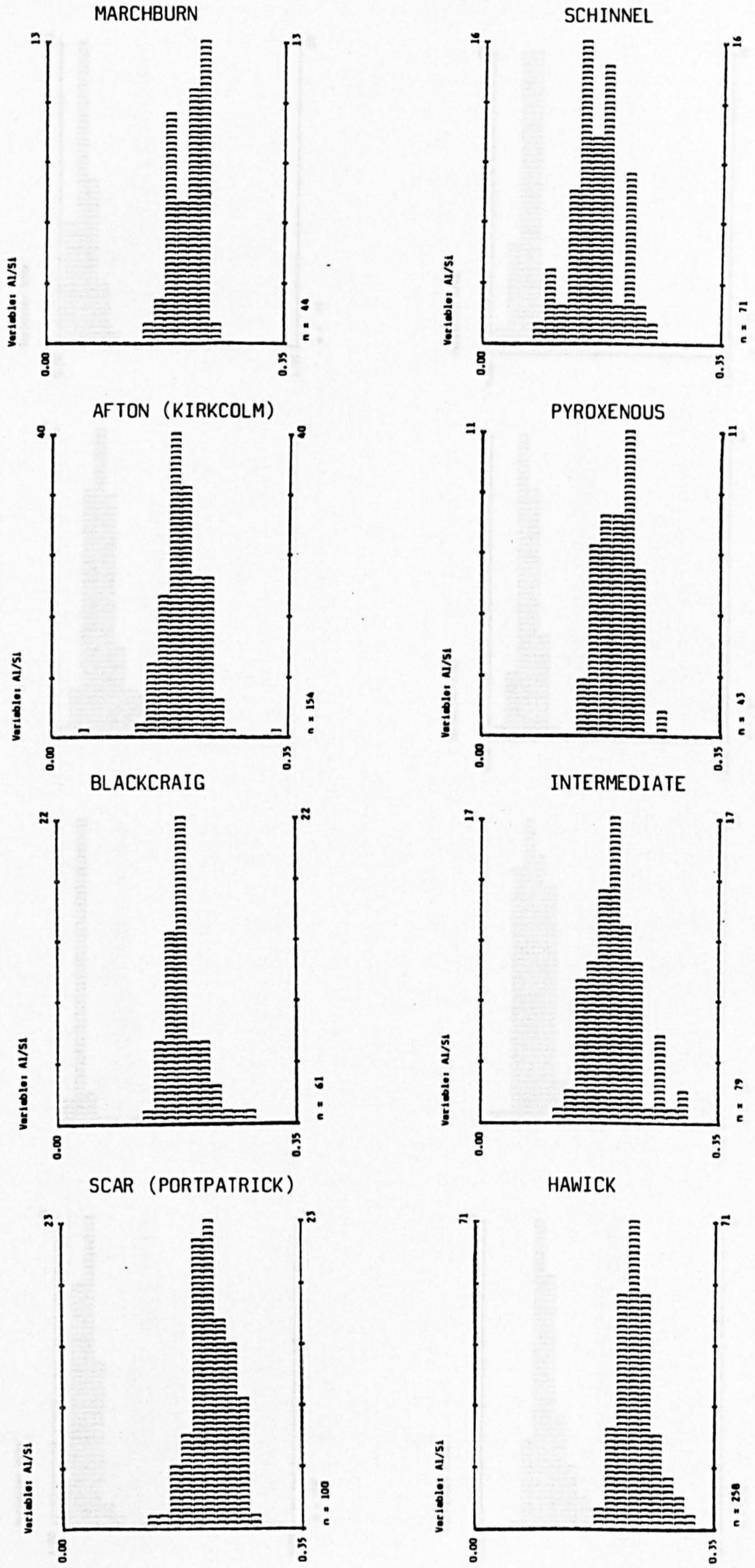
MARCHBURN
SCHINNEL
AFTON (KIRKCOLM)
PYROXENOUS
BLACKCRAIG
INTERMEDIATE
SCAR (PORTPATRICK)
HAWICK

FIGURE 255

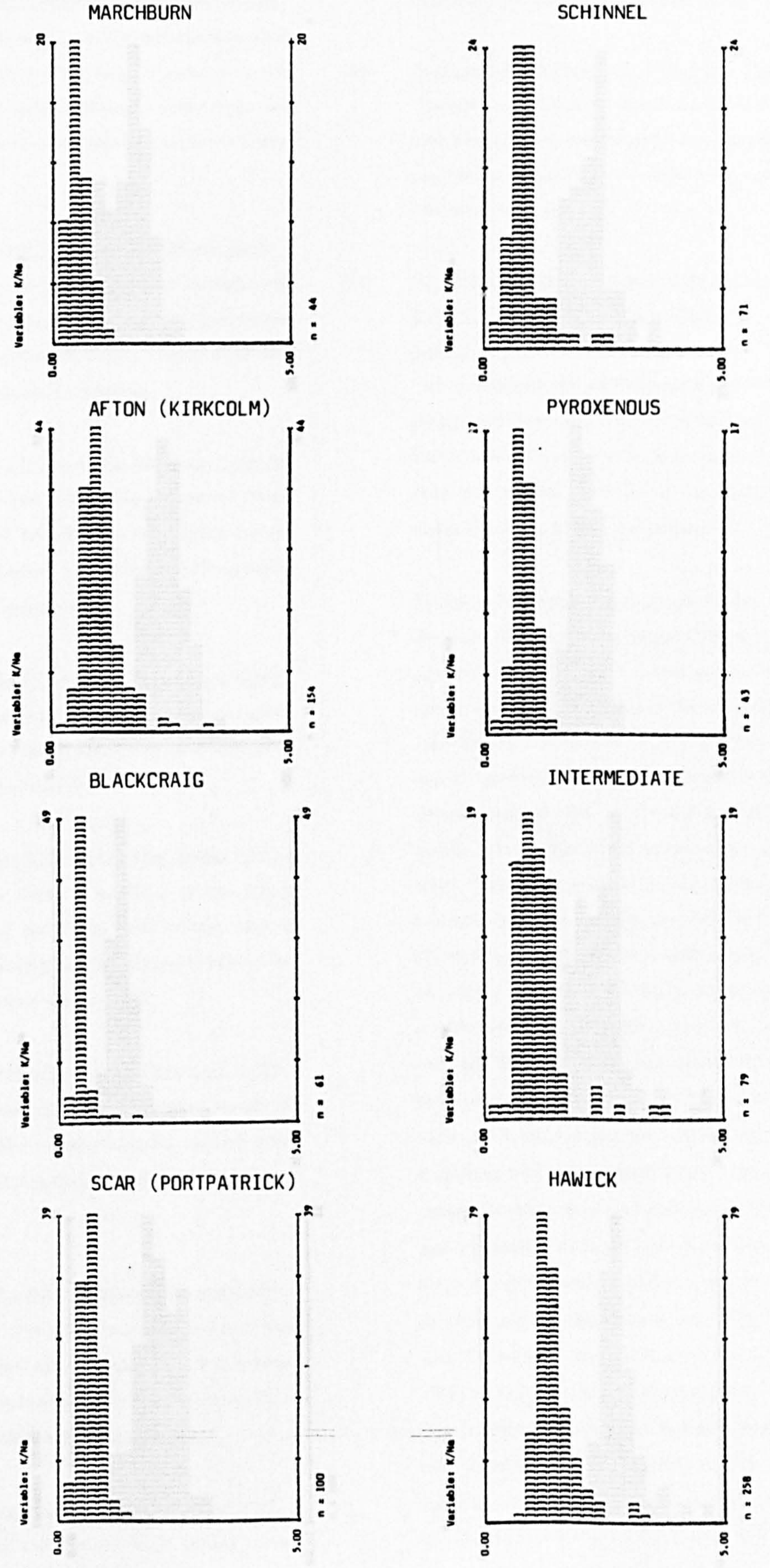
MARCHBURN
Variable: K/Na
0.00
5.00
20
n = 44
SCHINNEL
Variable: K/Na
0.00
5.00
24
n = 71
AFTON (KIRKCOLM)
Variable: K/Na
0.00
5.00
44
n = 154
PYROXENOUS
Variable: K/Na
0.00
5.00
17
n = 43
BLACKCRAIG
Variable: K/Na
0.00
5.00
49
n = 61
INTERMEDIATE
Variable: K/Na
0.00
5.00
19
n = 79
SCAR (PORTPATRICK)
Variable: K/Na
0.00
5.00
39
n = 100
HAWICK
Variable: K/Na
0.00
5.00
79
n = 258

FIGURE 256

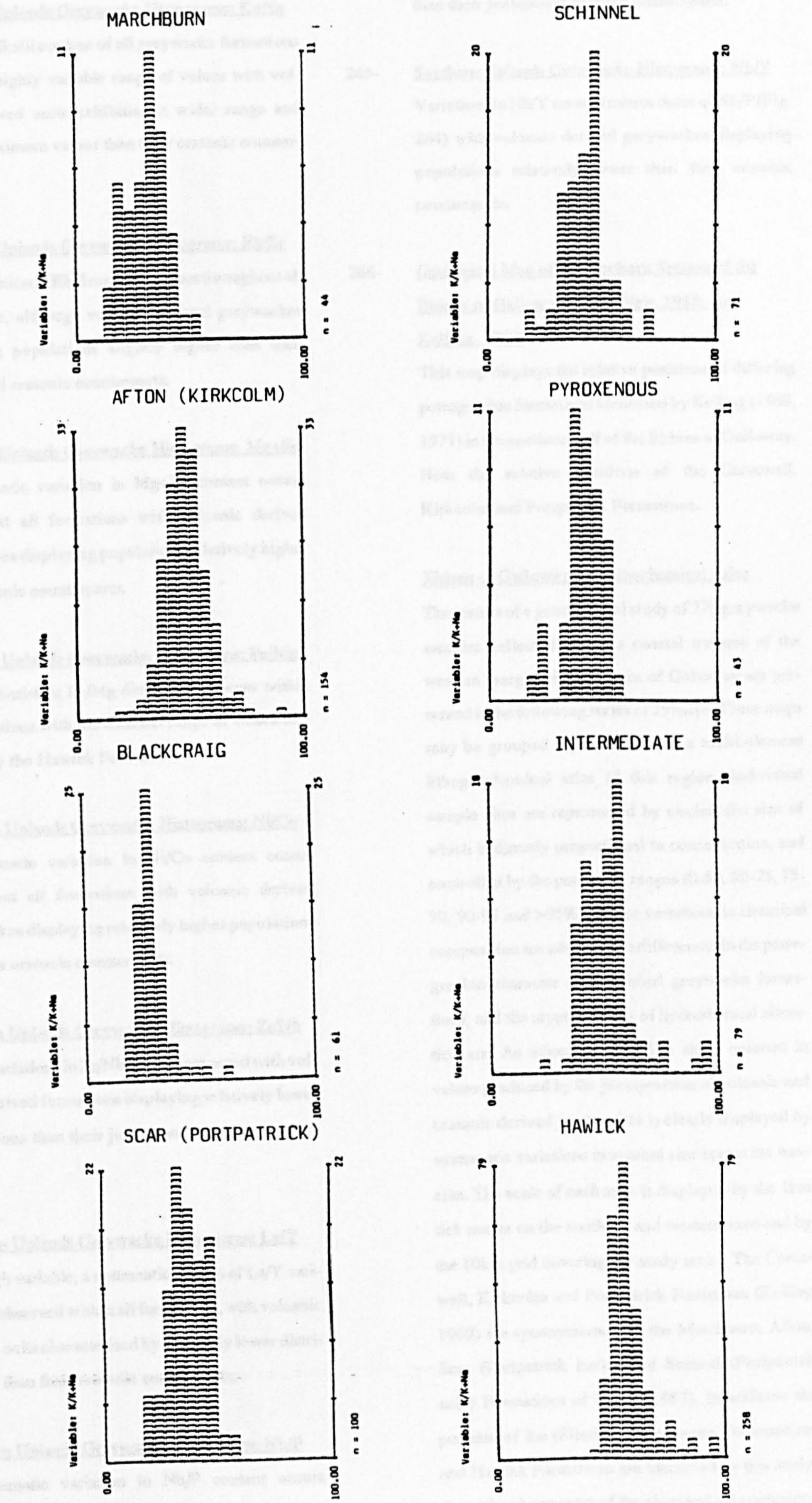
MARCHBURN
SCHINNEL
AFTON (KIRKCOLM)
PYROXENOUS
BLACKCRAIG
INTERMEDIATE
SCAR (PORTPATRICK)
HAWICK
Variable: K/K+Na
0.00
100.00
n = 44
n = 71
n = 154
n = 43
n = 61
n = 79
n = 100
n = 258

257- Southern Uplands Greywacke Histograms: K+Na
The total alkalii content of all greywacke formations display a highly variable range of values with volcanic derived units exhibiting a wider range and higher maximum values than their cratonic counterparts.

258- Southern Uplands Greywacke Histograms: Rb/Sr
Little variation in Rb/Sr content occurs throughout all formations, although volcanic derived greywackes displaying populations slightly higher than their juxtaposed cratonic counterparts.

259- Southern Uplands Greywacke Histograms: Mg+Fe
A systematic variation in Mg+Fe content occurs throughout all formations with volcanic derived greywackes displaying populations relatively higher than cratonic counterparts.

260- Southern Uplands Greywacke Histograms: Fe/Mg
Highly consistent Fe/Mg distributions occur within all formations with the smallest range of values displayed by the Hawick Formation.

261- Southern Uplands Greywacke Histograms: Ni/Co
A systematic variation in Ni/Co content occurs throughout all formations with volcanic derived greywackes displaying relatively higher populations than their cratonic counter parts.

262- Southern Uplands Greywacke Histograms: Zr/Nb
Subtle variations in Zr/Nb content are noted with volcanic derived formations displaying relatively lower populations than their juxtaposed cratonic counterparts.

263- Southern Uplands Greywacke Histograms: La/Y
Although variable, a systematic pattern of La/Y variation is observed within all formations, with volcanic derived units characterised by relatively lower distributions than their cratonic counterparts.

264- Southern Uplands Greywacke Histograms: Nb/P
A systematic variation in Nb/P content occurs throughout all formations with volcanic derived greywackes displaying relatively lower distributions than their juxtaposed cratonic counterparts.

265- Southern Uplands Greywacke Histograms: Nb/Y
Variations in Nb/Y content mirror those of Nb/P (Fig. 264) with volcanic derived greywackes displaying populations relatively lower than their cratonic counterparts.

266- Geological Map of the Northern Section of the Rhinns of Galloway (After Weir, 1985; and Kelling, 1969)
This map displays the relative positions of differing petrographic formations identified by Kelling (1969, 1971) in the northern half of the Rhinns of Galloway. Note the relative positions of the Corsewall, Kirkcolm and Portpatrick Formations.

Rhinns of Galloway Lithogeochemical Atlas
The results of a geochemical study of 279 greywacke samples collected during a coastal traverse of the western margin of the Rhinns of Galloway are presented in the following series of 29 maps. These maps may be grouped together to form a multi-element lithogeochemical atlas of this region. Individual sample sites are represented by circles, the size of which is directly proportional to concentration, and controlled by the percentile ranges (0-50, 50-75, 75-90, 90-95 and >95%). Major variations in chemical composition are attributed to differences in the petrographic character of individual greywacke formations, and the cryptic effects of hydrothermal alteration and As mineralisation. The sharp contrast in values produced by the juxtaposition of volcanic and cratonic derived greywackes is clearly displayed by systematic variations in symbol size across the traverse. The scale of each map is displayed by the 1km tick marks on the southern and western axes and by the 10km grid covering the study area. The Corsewall, Kirkcolm and Portpatrick Formation (Kelling 1969) are synonymous with the Marchburn, Afton, Scar (Portpatrick basic) and Shinnel (Portpatrick acid) Formations of Floyd (1983). In addition the position of the (Silurian) Pyroxenous, Intermediate and Hawick Formations are identified by this study. A graphical summary of the chemical data contained within these maps is presented in fold-out no. 5.

FIGURE 257

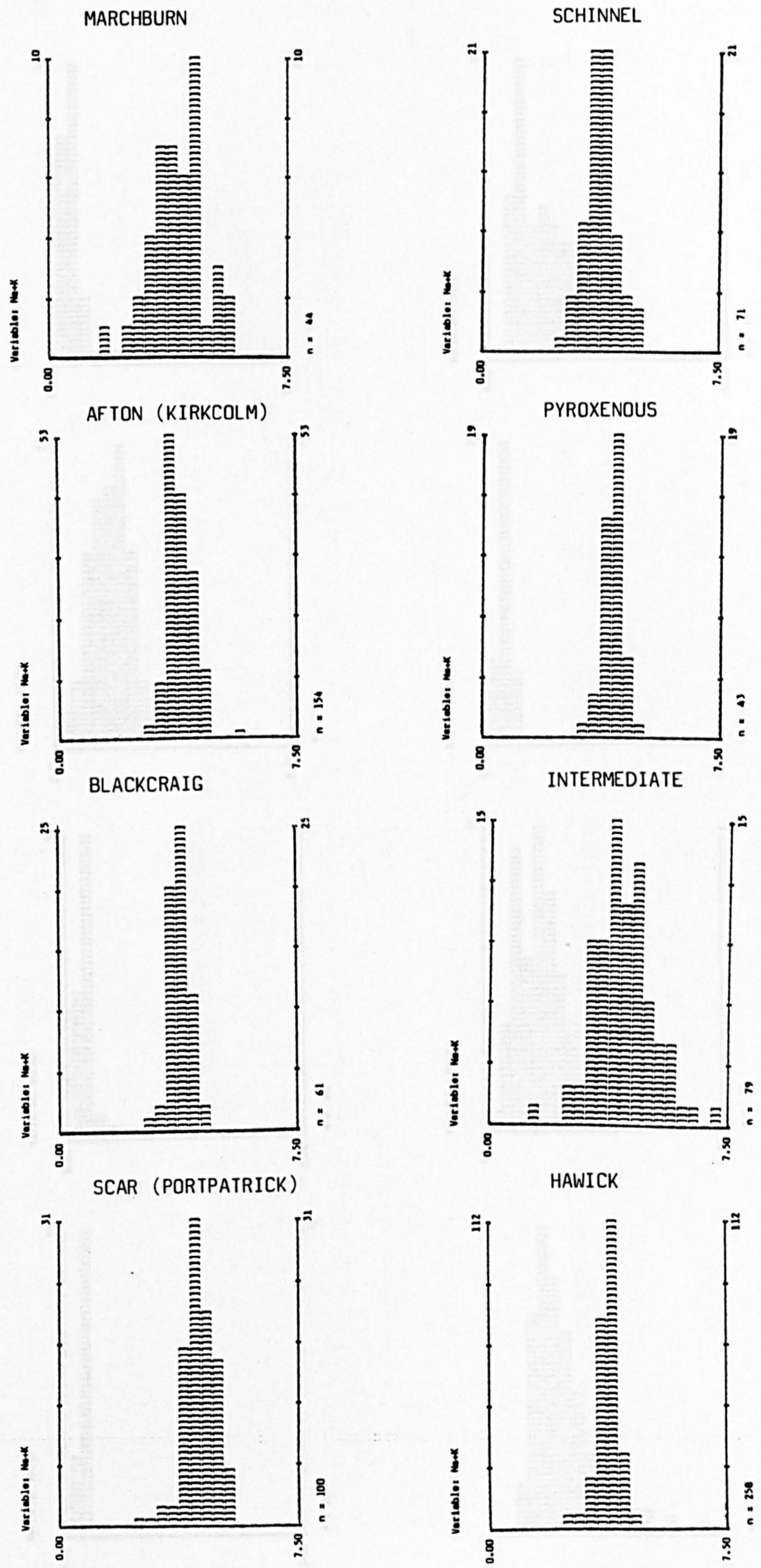
MARCHBURN
Variable: Na+K
10
0.00
7.50
n = 44
SCHINNEL
Variable: Na+K
21
0.00
7.50
n = 71
AFTON (KIRKCOLM)
Variable: Na+K
53
0.00
7.50
n = 154
PYROXENOUS
Variable: Na+K
19
0.00
7.50
n = 43
BLACKCRAIG
Variable: Na+K
25
0.00
7.50
n = 61
INTERMEDIATE
Variable: Na+K
15
0.00
7.50
n = 79
SCAR (PORTPATRICK)
Variable: Na+K
31
0.00
7.50
n = 100
HAWICK
Variable: Na+K
112
0.00
7.50
n = 258

FIGURE 258

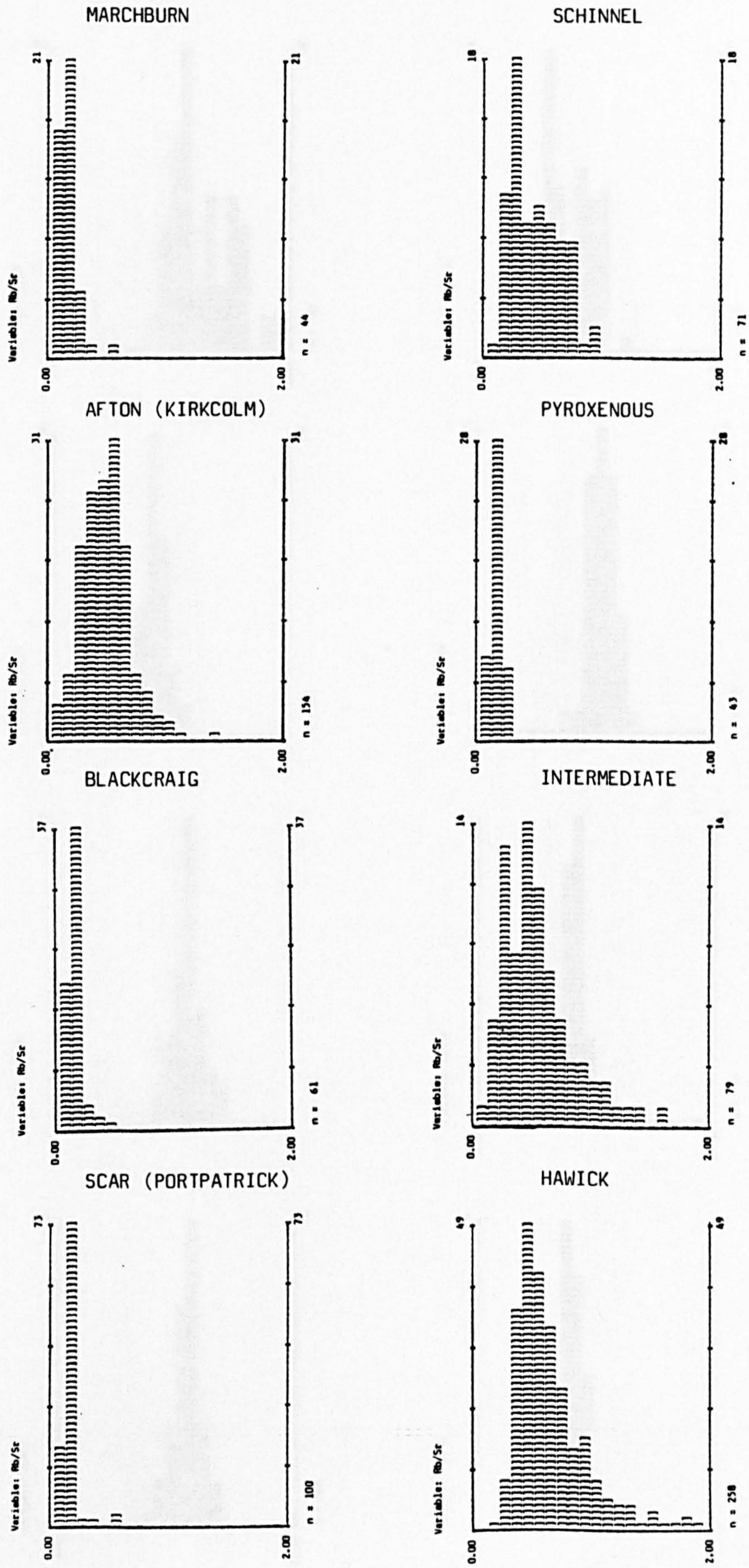
MARCHBURN
SCHINNEL
AFTON (KIRKCOLM)
PYROXENOUS
BLACKCRAIG
INTERMEDIATE
SCAR (PORTPATRICK)
HAWICK
Variable: Rb/Sr
0.00
2.00
n = 44
n = 71
n = 154
n = 43
n = 61
n = 79
n = 100
n = 258

FIGURE 259

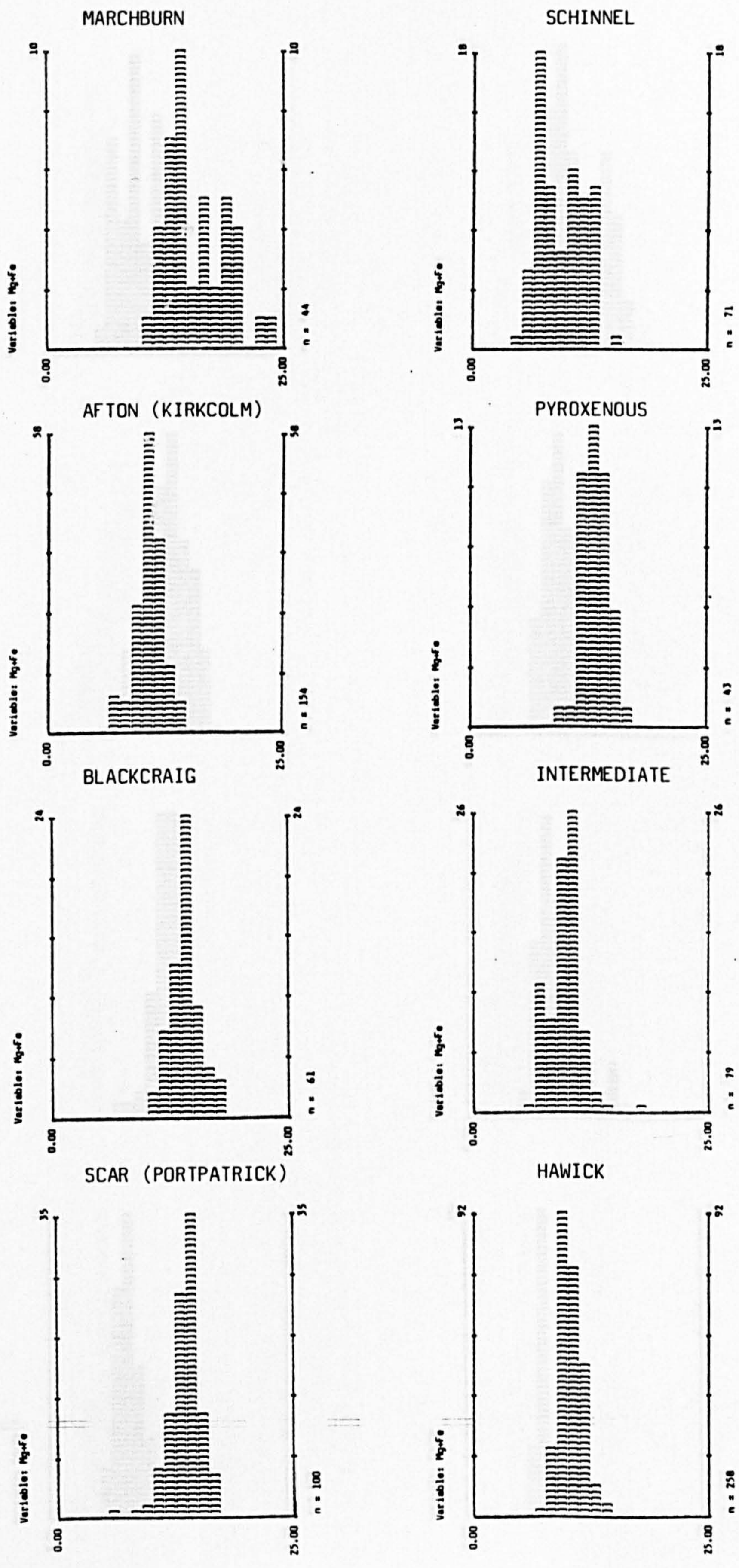
MARCHBURN
SCHINNEL
AFTON (KIRKCOLM)
PYROXENOUS
BLACKCRAIG
INTERMEDIATE
SCAR (PORTPATRICK)
HAWICK
Variable: Mg+Fe
0.00
25.00

FIGURE 260

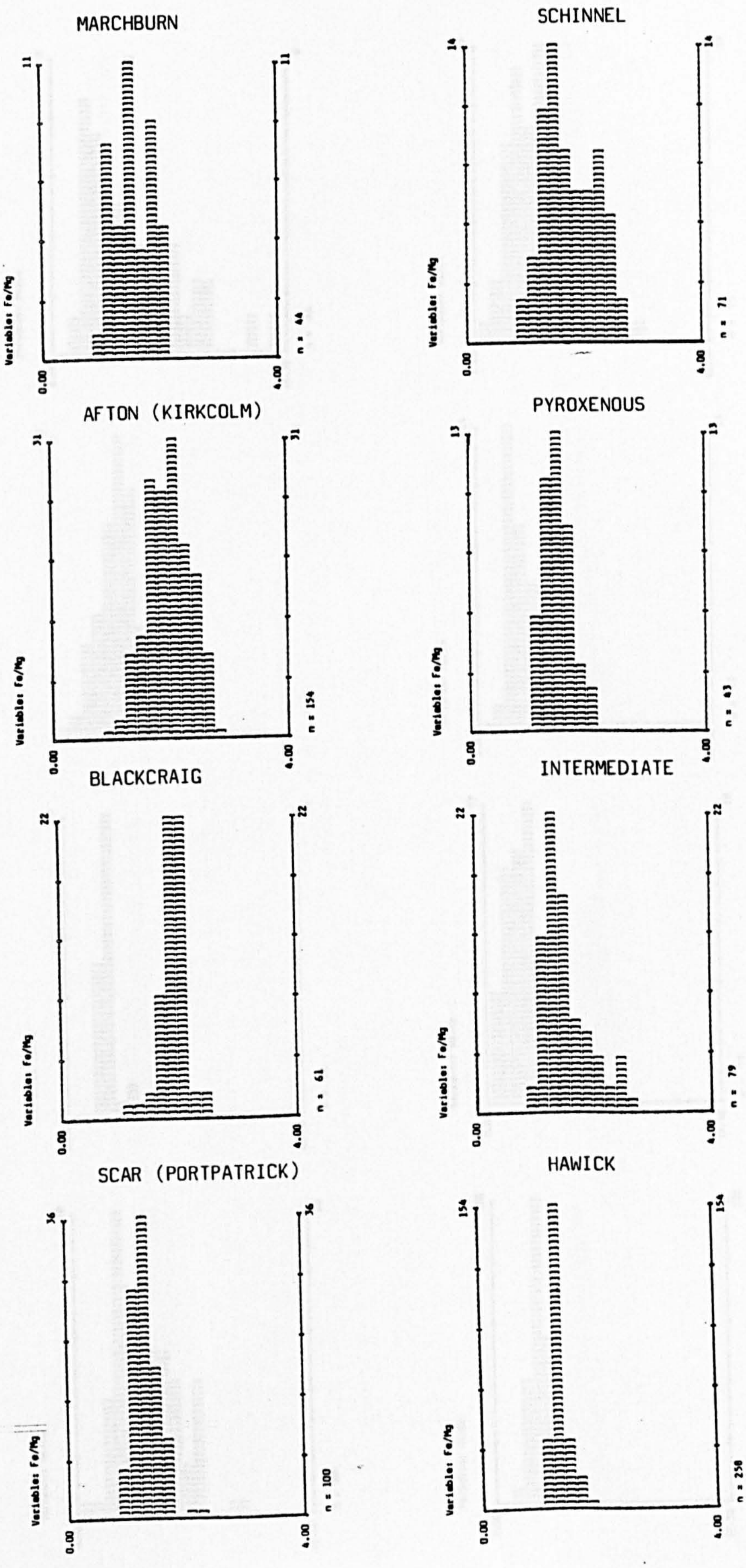
MARCHBURN
11
Variable: Fe/Mg
0.00
4.00
n = 44
SCHINNEL
14
Variable: Fe/Mg
0.00
4.00
n = 71
AFTON (KIRKCOLM)
31
Variable: Fe/Mg
0.00
4.00
n = 154
PYROXENOUS
13
Variable: Fe/Mg
0.00
4.00
n = 43
BLACKCRAIG
22
Variable: Fe/Mg
0.00
4.00
n = 61
INTERMEDIATE
22
Variable: Fe/Mg
0.00
4.00
n = 79
SCAR (PORTPATRICK)
36
Variable: Fe/Mg
0.00
4.00
n = 100
HAWICK
154
Variable: Fe/Mg
0.00
4.00
n = 258

FIGURE 261

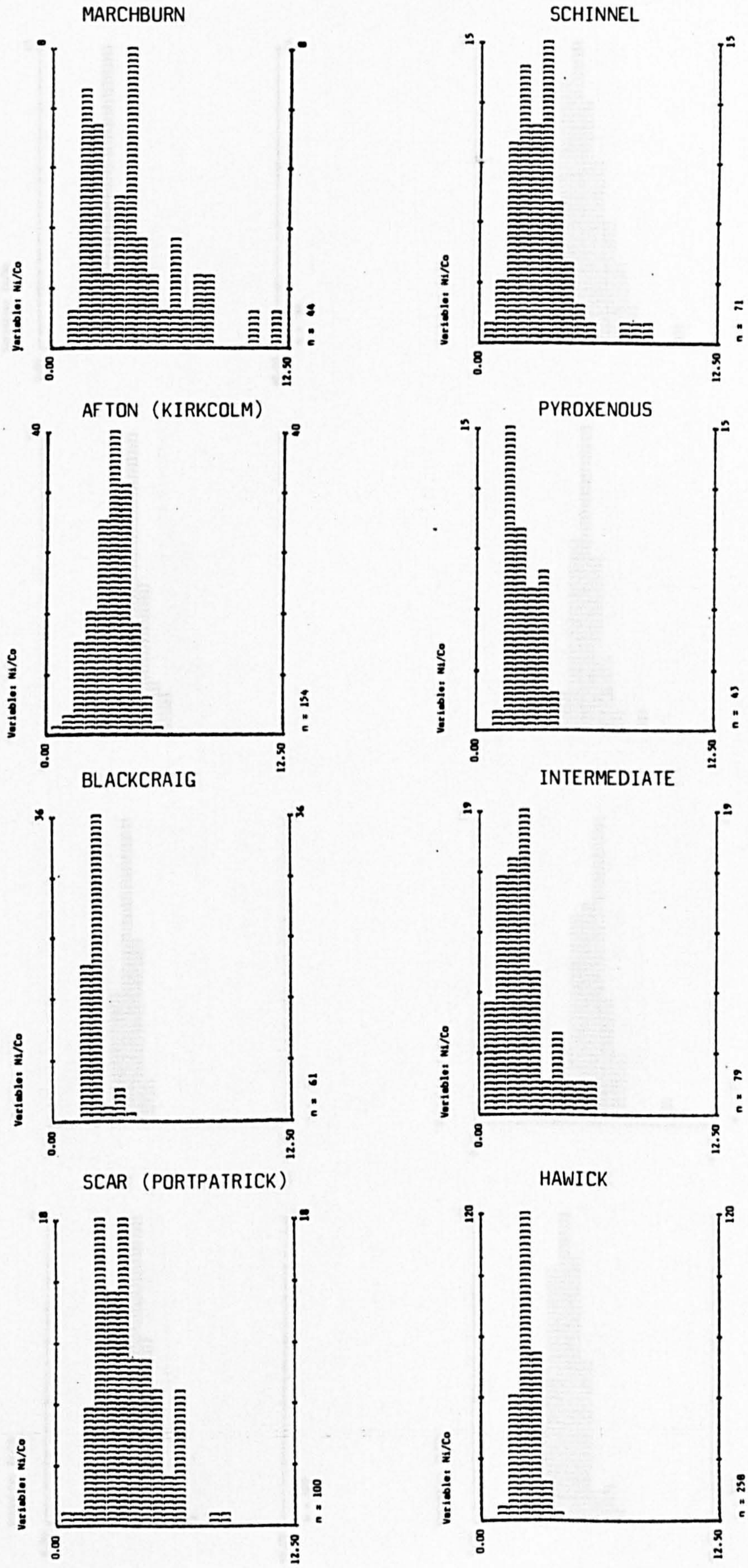
MARCHBURN
Variable: Ni/Co
0.00
12.50
8
n = 44
SCHINNEL
Variable: Ni/Co
0.00
12.50
15
n = 71
AFTON (KIRKCOLM)
Variable: Ni/Co
0.00
12.50
40
n = 154
PYROXENOUS
Variable: Ni/Co
0.00
12.50
15
n = 63
BLACKCRAIG
Variable: Ni/Co
0.00
12.50
36
n = 61
INTERMEDIATE
Variable: Ni/Co
0.00
12.50
19
n = 79
SCAR (PORTPATRICK)
Variable: Ni/Co
0.00
12.50
18
n = 100
HAWICK
Variable: Ni/Co
0.00
12.50
120
n = 258

FIGURE 262

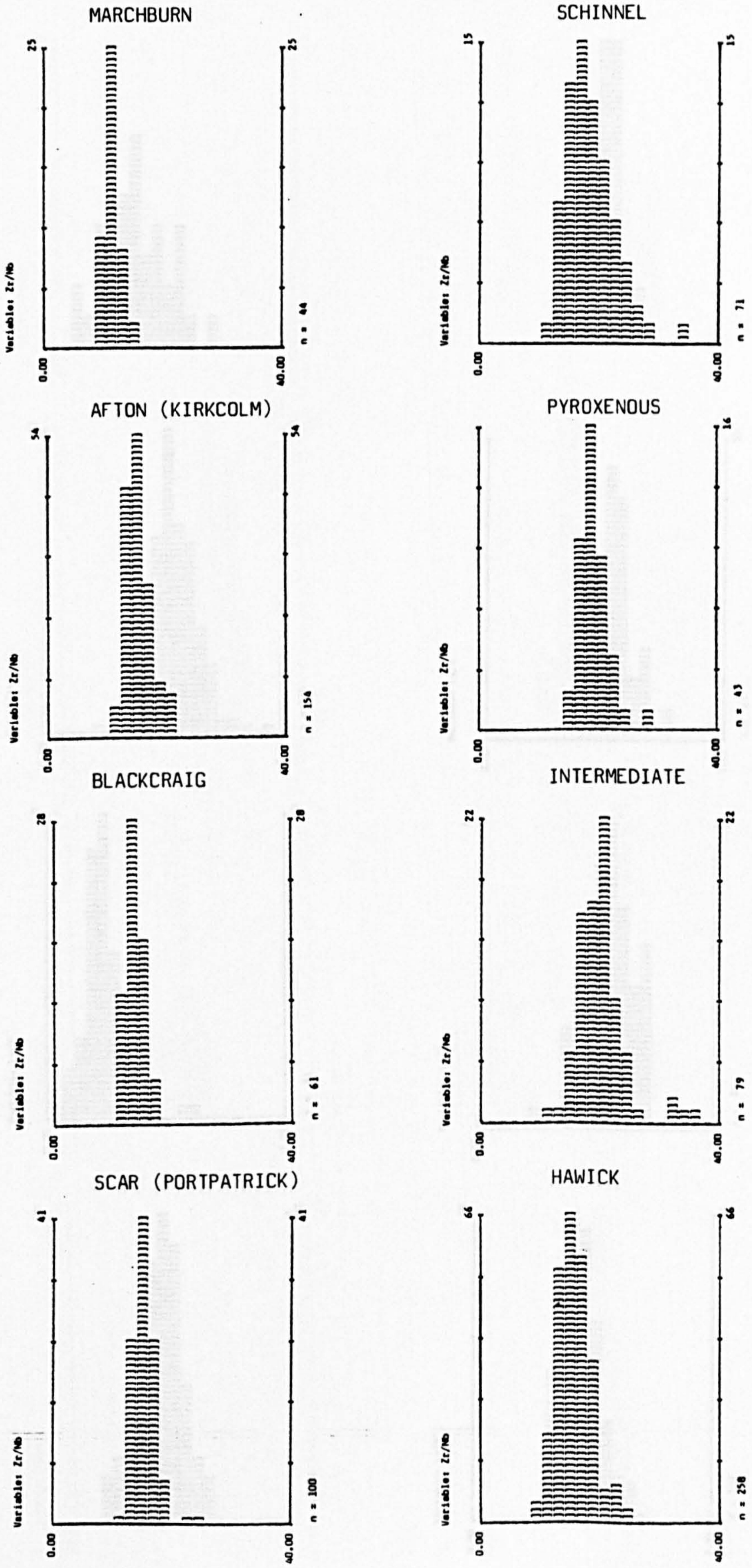
MARCHBURN
SCHINNEL
AFTON (KIRKCOLM)
PYROXENOUS
BLACKCRAIG
INTERMEDIATE
SCAR (PORTPATRICK)
HAWICK
Variable: Zr/Nb
0.00
40.00
n = 44
n = 71
n = 154
n = 43
n = 61
n = 79
n = 100
n = 258

FIGURE 263

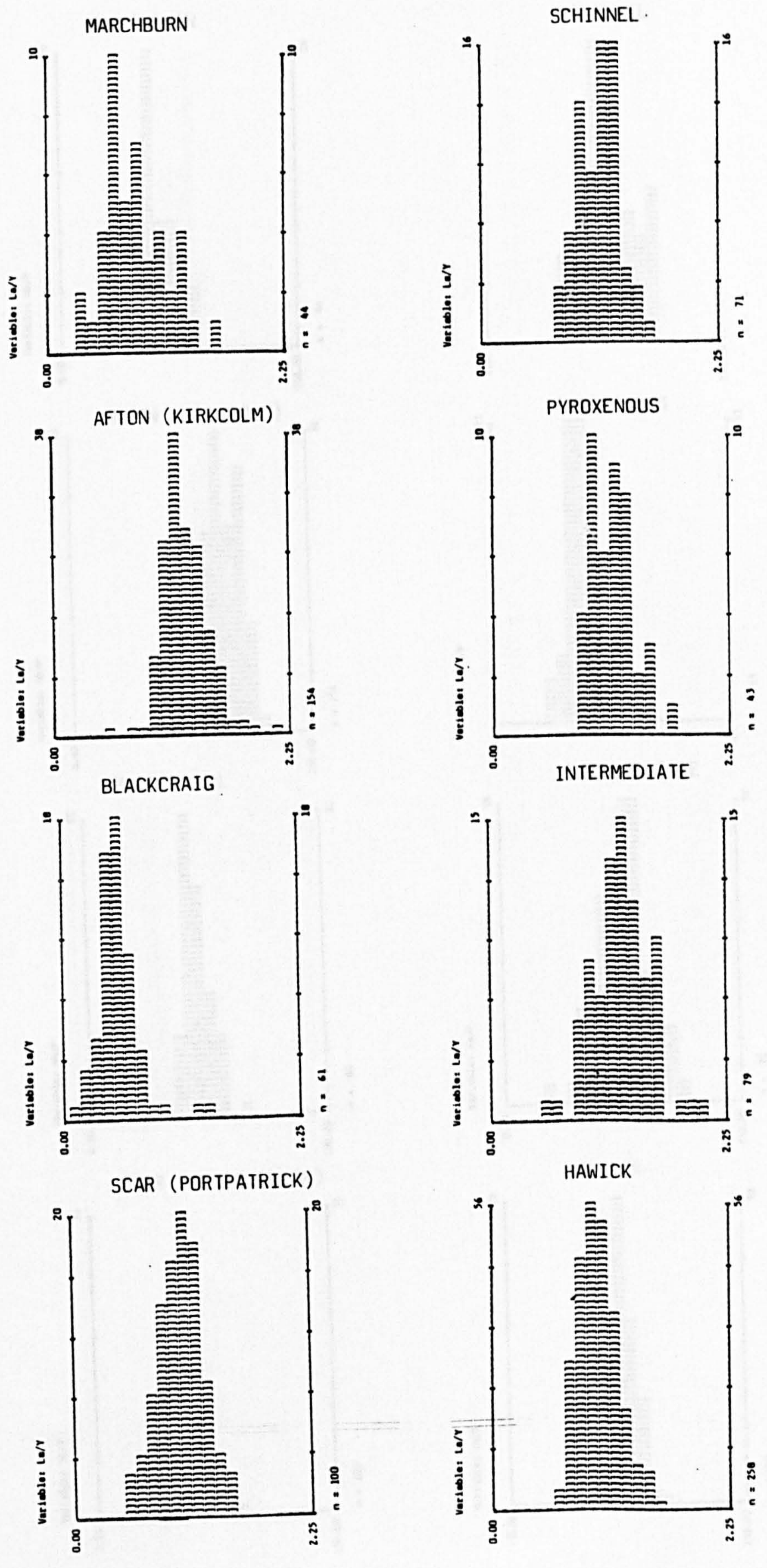
MARCHBURN
SCHINNEL
AFTON (KIRKCOLM)
PYROXENOUS
BLACKCRAIG
INTERMEDIATE
SCAR (PORTPATRICK)
HAWICK
Variable: La/Y
0.00
2.25
n = 44
n = 71
n = 154
n = 43
n = 61
n = 79
n = 100
n = 250

FIGURE 264

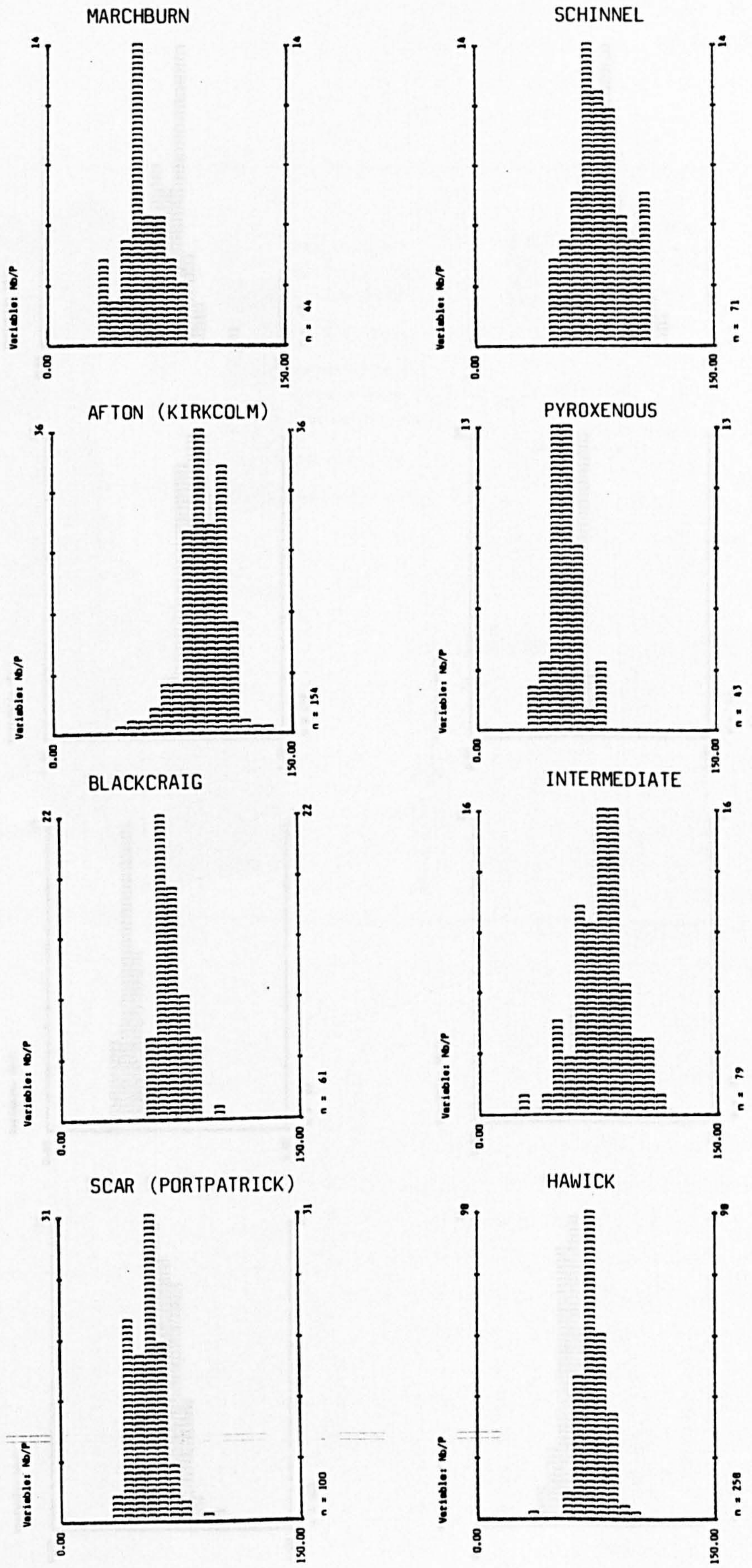
MARCHBURN
14
Variable: Nb/P
0.00
150.00
n = 44
SCHINNEL
14
Variable: Nb/P
0.00
150.00
n = 71
AFTON (KIRKCOLM)
36
Variable: Nb/P
0.00
150.00
n = 154
PYROXENOUS
13
Variable: Nb/P
0.00
150.00
n = 43
BLACKCRAIG
22
Variable: Nb/P
0.00
150.00
n = 61
INTERMEDIATE
16
Variable: Nb/P
0.00
150.00
n = 79
SCAR (PORTPATRICK)
31
Variable: Nb/P
0.00
150.00
n = 100
HAWICK
98
Variable: Nb/P
0.00
150.00
n = 258

FIGURE 265

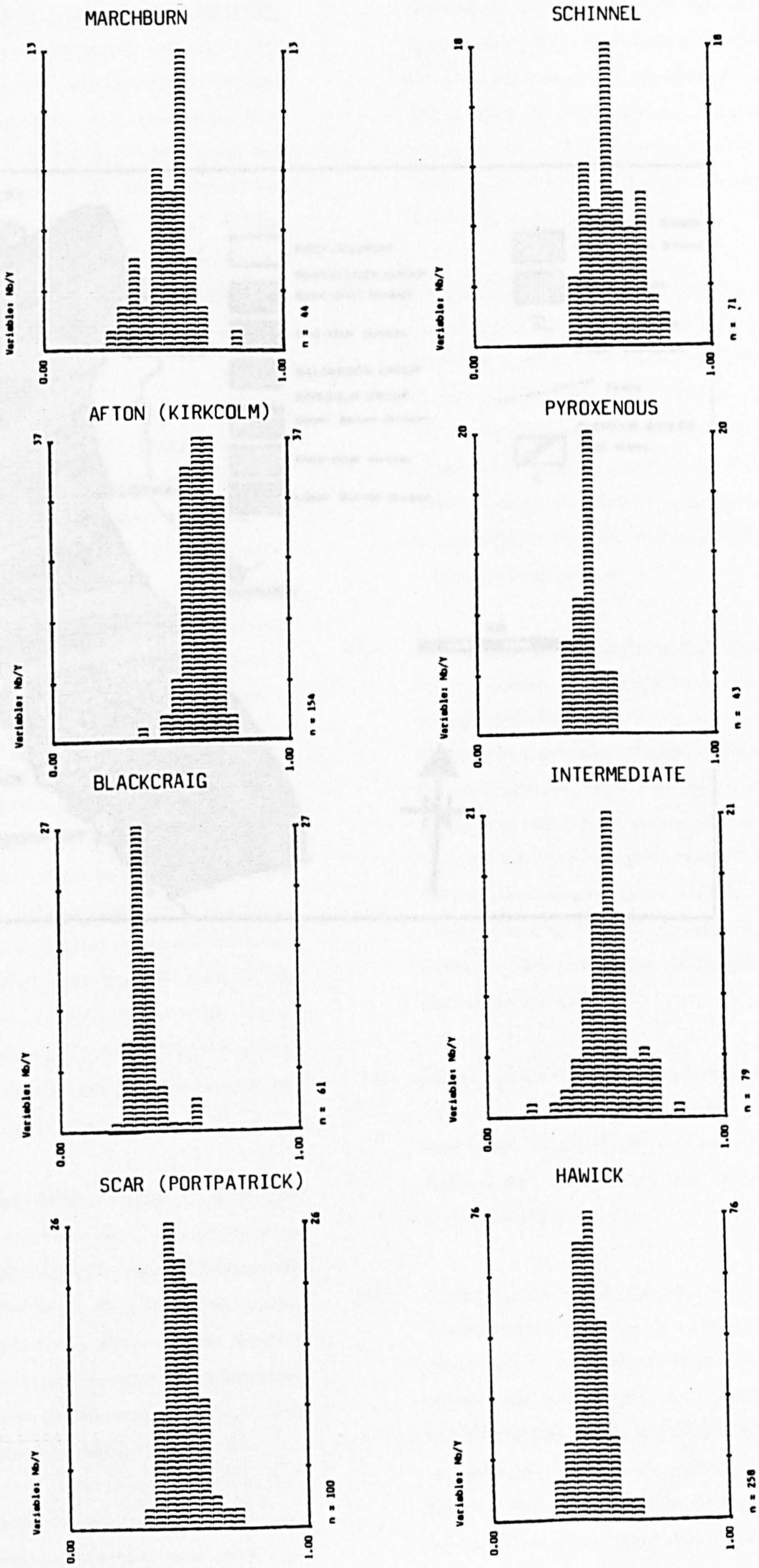
MARCHBURN
13
Variable: Nb/Y
0.00
1.00
n = 44
SCHINNEL
18
Variable: Nb/Y
0.00
1.00
n = 71
AFTON (KIRKCOLM)
37
Variable: Nb/Y
0.00
1.00
n = 154
PYROXENOUS
20
Variable: Nb/Y
0.00
1.00
n = 43
BLACKCRAIG
27
Variable: Nb/Y
0.00
1.00
n = 61
INTERMEDIATE
21
Variable: Nb/Y
0.00
1.00
n = 79
SCAR (PORTPATRICK)
26
Variable: Nb/Y
0.00
1.00
n = 100
HAWICK
76
Variable: Nb/Y
0.00
1.00
n = 258

FIGURE 266

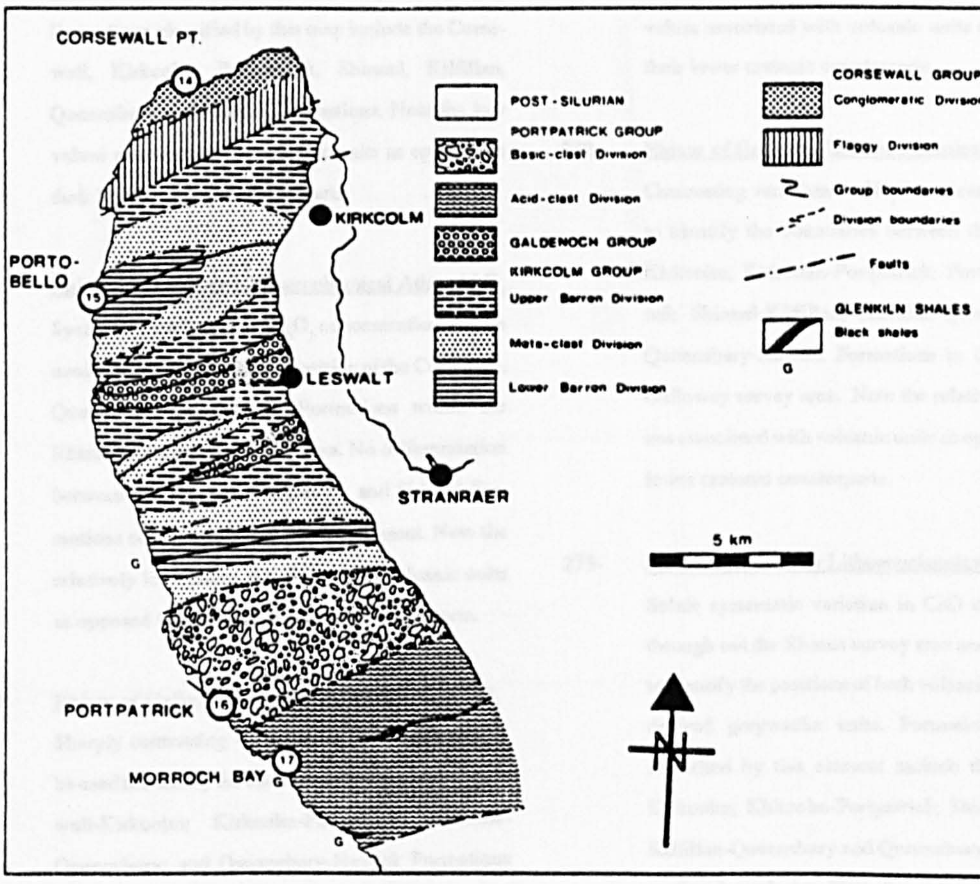

CORSEWALL PT.
14
POST-SILURIAN
PORTPATRICK GROUP
Basic-clast Division
Acid-clast Division
KIRKCOLM
GALDENOCH GROUP
KIRKCOLM GROUP
Upper Barren Division
PORTO-BELLO
15
Meta-clast Division
LESWALT
Lower Barren Division
STRANRAER
G
PORTPATRICK
16
MORROCH BAY
17
CORSEWALL GROUP
Conglomeratic Division
Flaggy Division
Group boundaries
Division boundaries
Faults
GLENKILN SHALES
Black shales
G
5 km
N

267- Rhinns of Galloway Lithogeochemical Atlas: SiO_2
Sharply contrasting, systematic variations in SiO_2 concentration may be used to identify the positions of juxtaposed volcanic and cratonic derived greywacke units within the Rhinns of Galloway survey area. Formations identified by this map include the Corsewall, Kirkcolm, Portpatrick, Shinnel, Kilfillan, Queensbury and Hawick Formations. Note the low values associated with volcanic units as opposed to their higher cratonic counterparts.

268- Rhinns of Galloway Lithogeochemical Atlas: Al_2O_3
Systematic variations in Al_2O_3 concentration may be used to identify the relative position of the Corsewall, Queensbury and Hawick Formations within the Rhinns of Galloway survey area. No differentiation between the Kircolm, Portpatrick and Shinnel Formations could be made using this element. Note the relatively low values associated with volcanic units as opposed to their higher cratonic counterparts.

269- Rhinns of Galloway Lithogeochemical Atlas: TiO_2
Sharply contrasting variations in TiO_2 content may be used to identify the boundaries between the Corsewall-Kirkcolm; Kirkcolm-Portpatrick; Kilfillan-Queensbury; and Queensbury-Hawick Formations in the Rhinns of Galloway survey area. Differentiation between the Portpatrick and Shinnel Formations however, was not possible using the class intervals selected for this diagram. Note the high values associated with volcanic units as opposed to their relatively lower cratonic counterparts.

270- Rhinns of Galloway Lithogeochemical Atlas: Fe_2O_3
Systematic variations in Fe_2O_3 concentration may be used to identify the relative position of the Corsewall, Kirkcolm, Portpatrick, Shinnel, Kilfillan, Queensbury and Hawick Formations within the Rhinns of Galloway survey area. Note the relatively high values associated with volcanic units as opposed to their lower cratonic counterparts.

271- Rhinns of Galloway Lithogeochemical Atlas: MgO
Sharply contrasting, systematic variations in MgO content may be used to identify the positions of both volcanic and cratonic derived greywacke units within the Rhinns of Galloway. Formation boundaries identified by this element include the Corsewall-Kirkcolm; Kirkcolm-Portpatrick; Shinnel-Kilfillan, Kilfillan-Queensbury and Queensbury-Hawick Formation boundaries. Note the extremely high MgO values associated with volcanic units as opposed to their lower cratonic counterparts.

272- Rhinns of Galloway Lithogeochemical Atlas: Na_2O
Contrasting variations in Na_2O content may be used to identify the boundaries between the Corsewall-Kirkcolm; Kirkcolm-Portpatrick; Portpatrick-Shinnel; Shinnel-Kilfillan; Kilfillan-Queensbury; and Queensbury-Hawick Formations in the Rhinns of Galloway survey area. Note the relatively high values associated with volcanic units as opposed to their lower cratonic counterparts.

273- Rhinns of Galloway Lithogeochemical Atlas: CaO
Subtle systematic variation in CaO content occurs through out the Rhinns survey area and may be used to identify the positions of both volcanic and cratonic derived greywacke units. Formation boundaries identified by this element include the Corsewall-Kirkcolm; Kirkcolm-Portpatrick; Shinnel-Kilfillan, Kilfillan-Queensbury and Queensbury-Hawick Formation boundaries. Note the extremely high CaO values associated with the cratonic derived Hawick Formation greywackes.

274- Rhinns of Galloway Lithogeochemical Atlas: K_2O
Contrasting variations in K_2O content may be used to identify the boundaries between the Corsewall-Kirkcolm and Portpatrick-Shinnel Formations in the Rhinns of Galloway.

275- Rhinns of Galloway Lithogeochemical Atlas: MnO
Sharply contrasting, systematic variations in MnO content may be used to identify the positions of both volcanic and cratonic derived greywacke units within the Rhinns of Galloway. Formation boundaries identified by this element include the Corsewall-Kirkcolm; Kirkcolm-Portpatrick; Kilfillan-Queensbury and Queensbury-Hawick Formation boundaries. Note the relatively high MnO values associated with volcanic units in the northern section of the

A LITHOGEOCHEMICAL STUDY OF THE RHYNS OF GALLOWAY, SOUTH WEST SCOTLAND

FIGURE 267

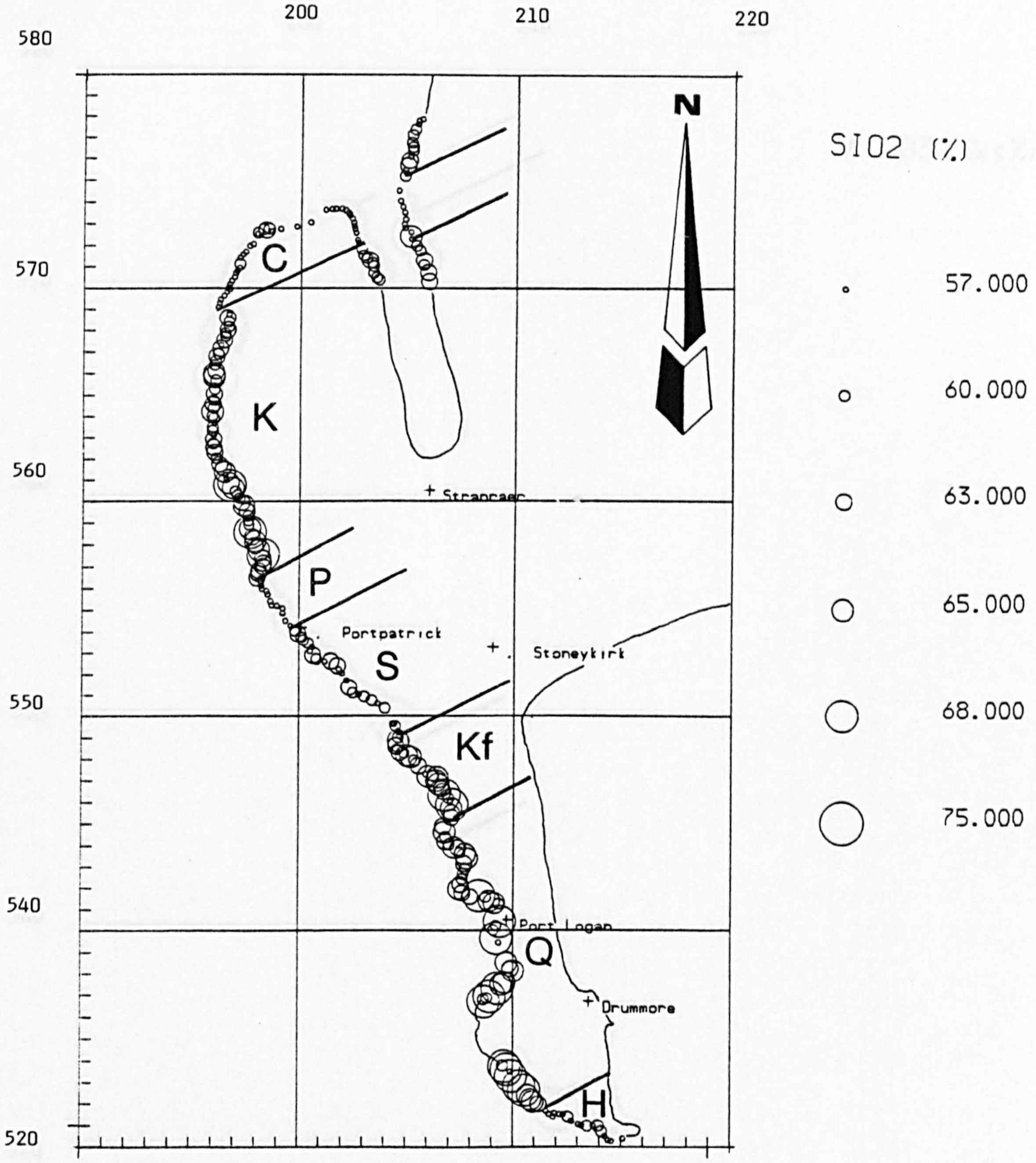

1 : 325,000 (32mm = 10km)

C - CORSEWALL FORMATION (MARCHBURN)
K - KIRKCOLM FORMATION (AFTON)
P - PORTPATRICK FORMATION (SCAR)
S - SCHINNEL FORMATION
Kf- KILFILLAN FORMATION (PYROXENOUS)
Q - QUEENSBURY FORMATION (INTERMEDIATE)
H - HAWICK FORMATION

A LITHOGEOCHEMICAL STUDY OF THE RHYNS OF GALLOWAY, SOUTH WEST SCOTLAND

FIGURE 268

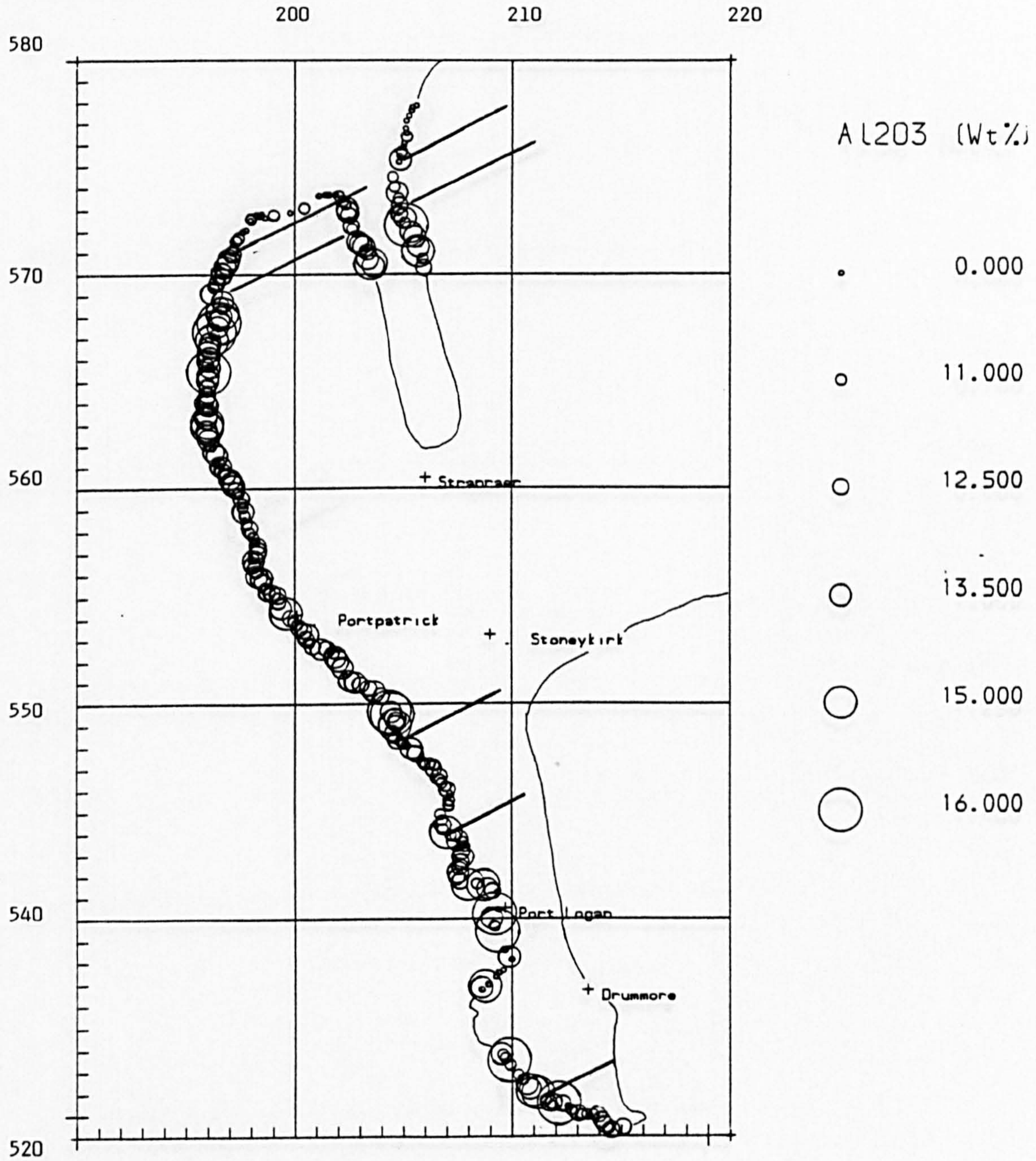

1 : 325,000 (32mm = 10km)

C - CORSEWALL FORMATION (MARCHBURN)
K - KIRKCOLM FORMATION (AFTON)
P - PORTPATRICK FORMATION (SCAR)
S - SCHINNEL FORMATION
Kf- KILFILLAN FORMATION (PYROXENOUS)
Q - QUEENSBURY FORMATION (INTERMEDIATE)
H - HAWICK FORMATION

A LITHOGEOCHEMICAL STUDY OF THE RHYNS OF GALLOWAY, SOUTH WEST SCOTLAND

FIGURE 269

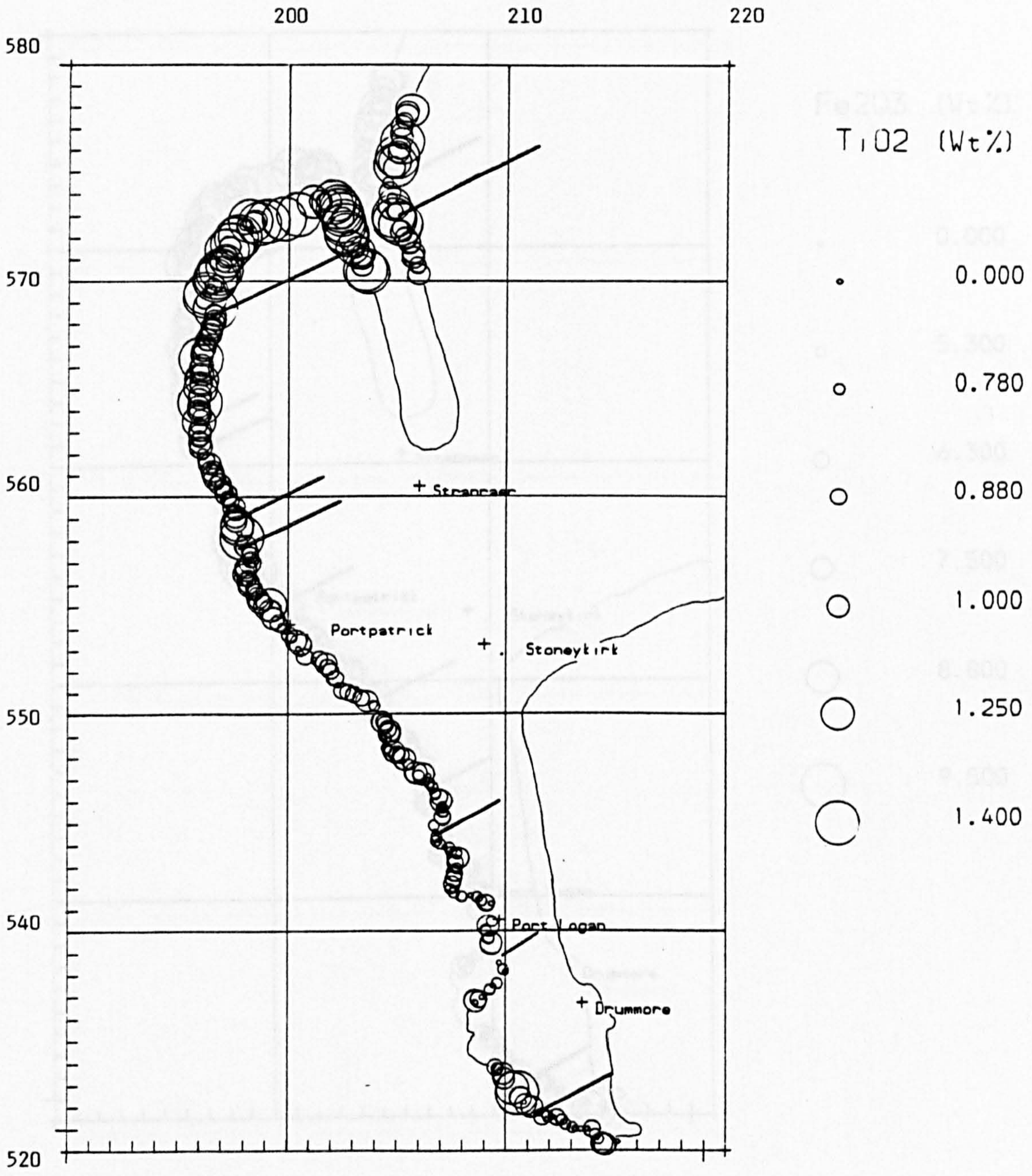

1 : 325,000 (32mm = 10km)

C - CORSEWALL FORMATION (MARCHBURN)
K - KIRKCOLM FORMATION (AFTON)
P - PORTPATRICK FORMATION (SCAR)
S - SCHINNEL FORMATION
Kf- KILFILLAN FORMATION (PYROXENOUS)
Q - QUEENSBURY FORMATION (INTERMEDIATE)
H - HAWICK FORMATION

A LITHOGEOCHEMICAL STUDY OF THE RHYNS OF GALLOWAY, SOUTH WEST SCOTLAND

FIGURE 270

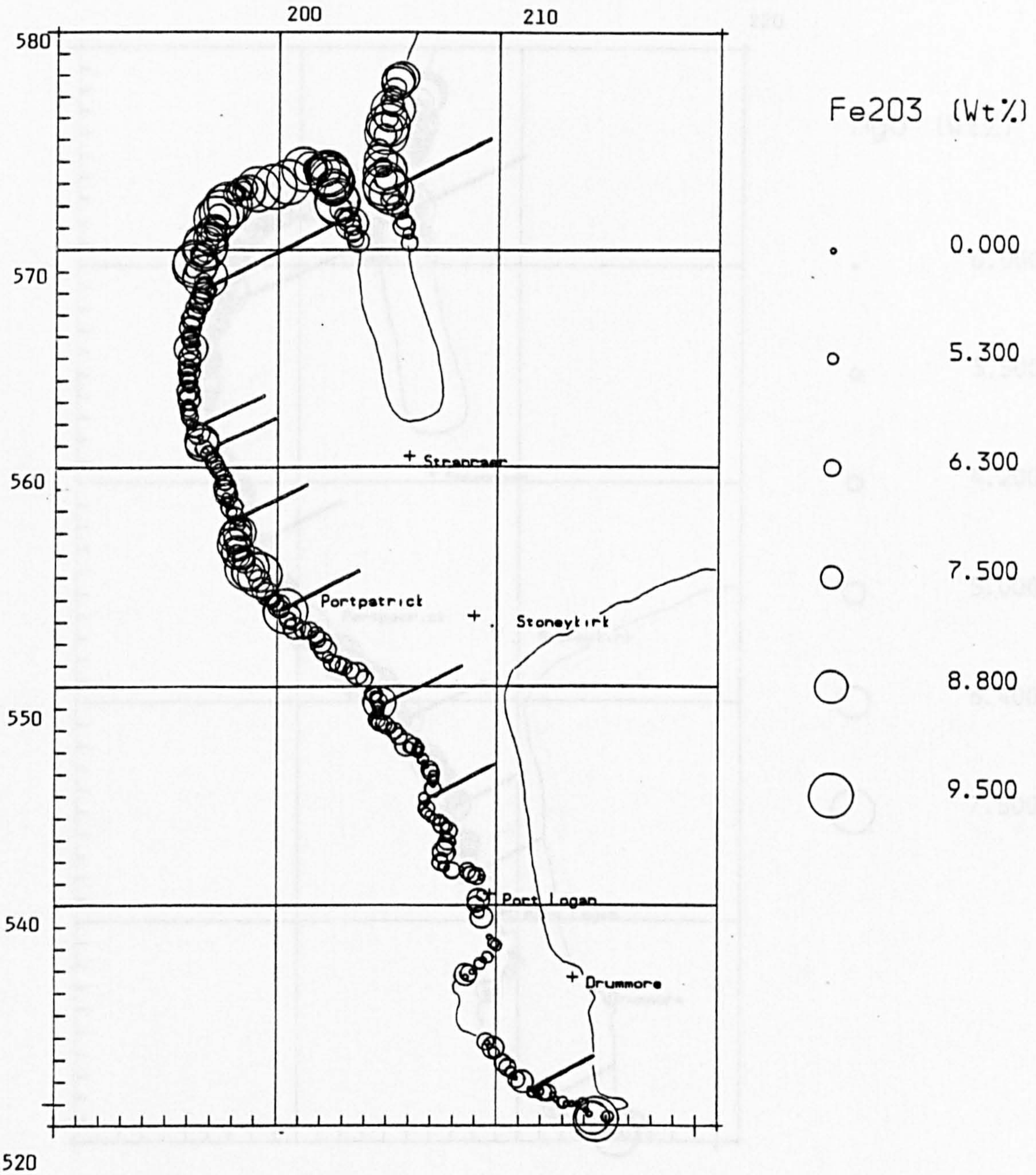

1 : 325,000 (32mm = 10km)

C - CORSEWALL FORMATION (MARCHBURN)
K - KIRKCOLM FORMATION (AFTON)
P - PORTPATRICK FORMATION (SCAR)
S - SCHINNEL FORMATION
Kf- KILFILLAN FORMATION (PYROXENOUS)
Q - QUEENSBURY FORMATION (INTERMEDIATE)
H - HAWICK FORMATION

A LITHOGEOCHEMICAL STUDY OF THE RHYNS OF GALLOWAY, SOUTH WEST SCOTLAND

FIGURE 271

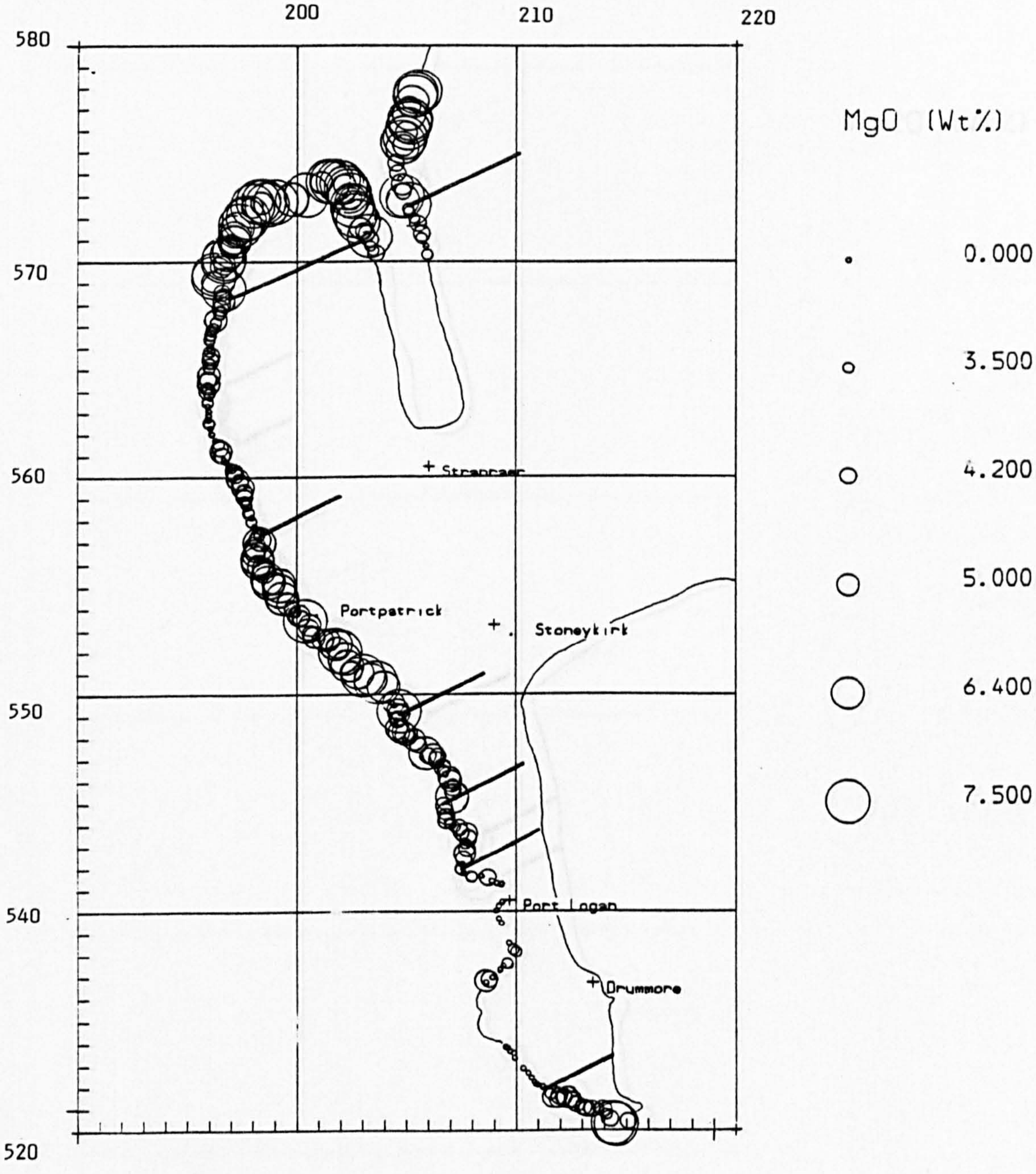

1 : 325,000 (32mm = 10km)

C - CORSEWALL FORMATION (MARCHBURN)
K - KIRKCOLM FORMATION (AFTON)
P - PORTPATRICK FORMATION (SCAR)
S - SCHINNEL FORMATION
Kf- KILFILLAN FORMATION (PYROXENOUS)
Q - QUEENSBURY FORMATION (INTERMEDIATE)
H - HAWICK FORMATION

A LITHOGEOCHEMICAL STUDY OF THE RHYNS OF GALLOWAY, SOUTH WEST SCOTLAND

FIGURE 272

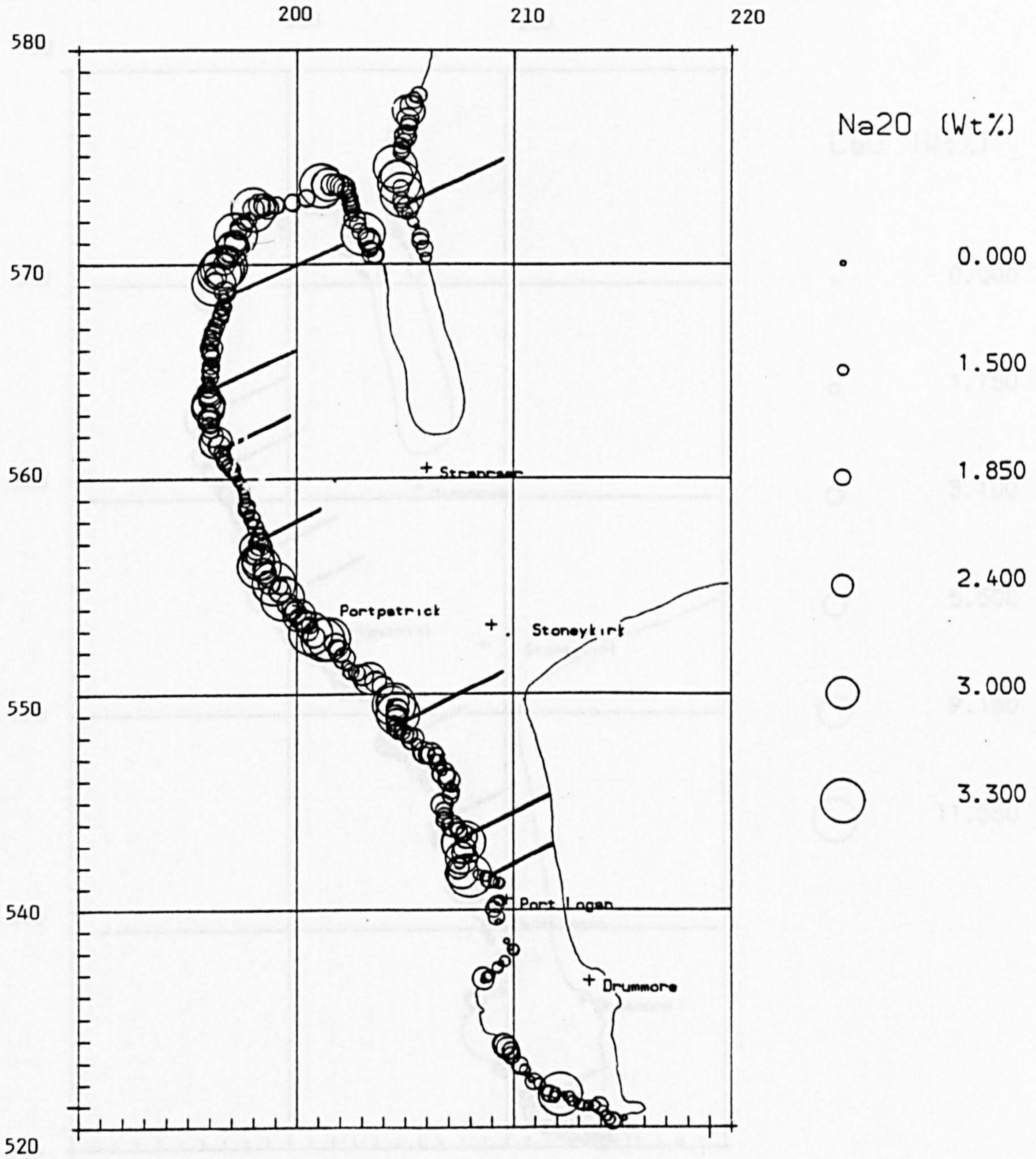

1 : 325,000 (32mm = 10km)

C - CORSEWALL FORMATION (MARCHBURN)
K - KIRKCOLM FORMATION (AFTON)
P - PORTPATRICK FORMATION (SCAR)
S - SCHINNEL FORMATION
Kf- KILFILLAN FORMATION (PYROXENOUS)
Q - QUEENSBURY FORMATION (INTERMEDIATE)
H - HAWICK FORMATION

A LITHOGEOCHEMICAL STUDY OF THE RHYNS OF GALLOWAY, SOUTH WEST SCOTLAND

FIGURE 273

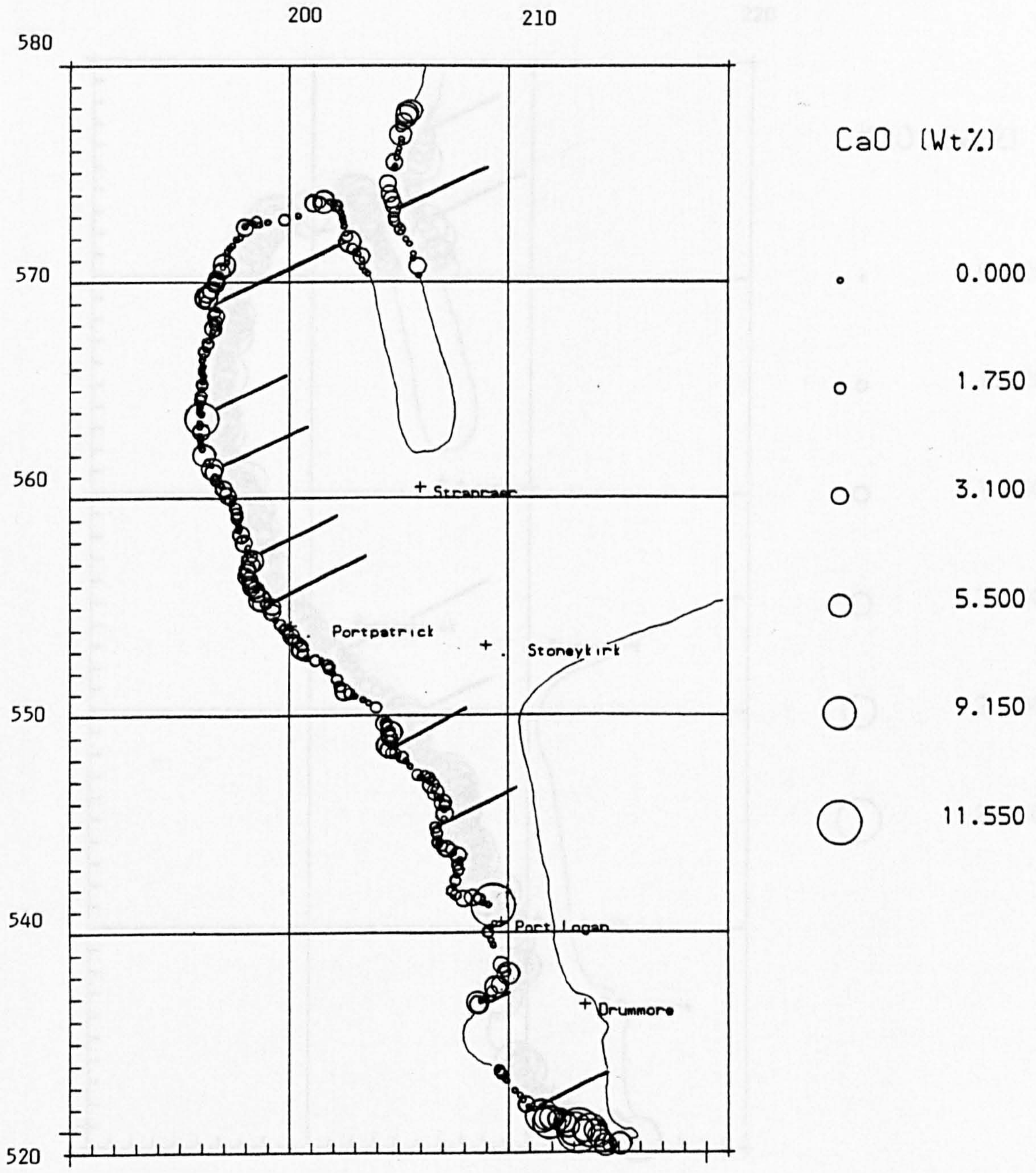

1 : 325,000 (32mm = 10km)

C - CORSEWALL FORMATION (MARCHBURN)
K - KIRKCOLM FORMATION (AFTON)
P - PORTPATRICK FORMATION (SCAR)
S - SCHINNEL FORMATION
Kf- KILFILLAN FORMATION (PYROXENOUS)
Q - QUEENSBURY FORMATION (INTERMEDIATE)
H - HAWICK FORMATION

A LITHOGEOCHEMICAL STUDY OF THE RHYNS OF GALLOWAY, SOUTH WEST SCOTLAND

FIGURE 274

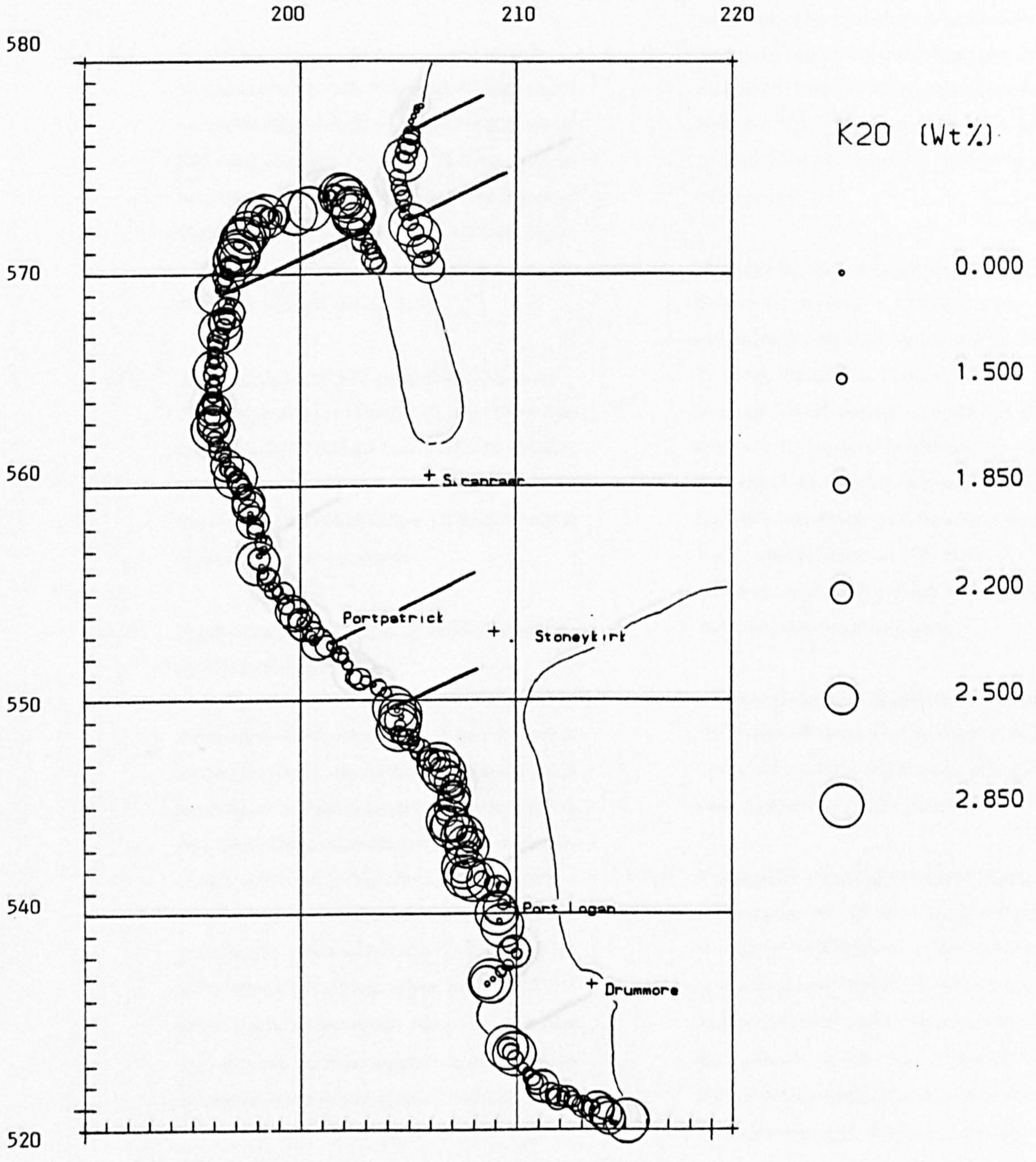

1 : 325,000 (32mm = 10km)

C - CORSEWALL FORMATION (MARCHBURN)
K - KIRKCOLM FORMATION (AFTON)
P - PORTPATRICK FORMATION (SCAR)
S - SCHINNEL FORMATION
Kf- KILFILLAN FORMATION (PYROXENOUS)
Q - QUEENSBURY FORMATION (INTERMEDIATE)
H - HAWICK FORMATION

A LITHOGEOCHEMICAL STUDY OF THE RHYNS OF GALLOWAY, SOUTH WEST SCOTLAND

FIGURE 275

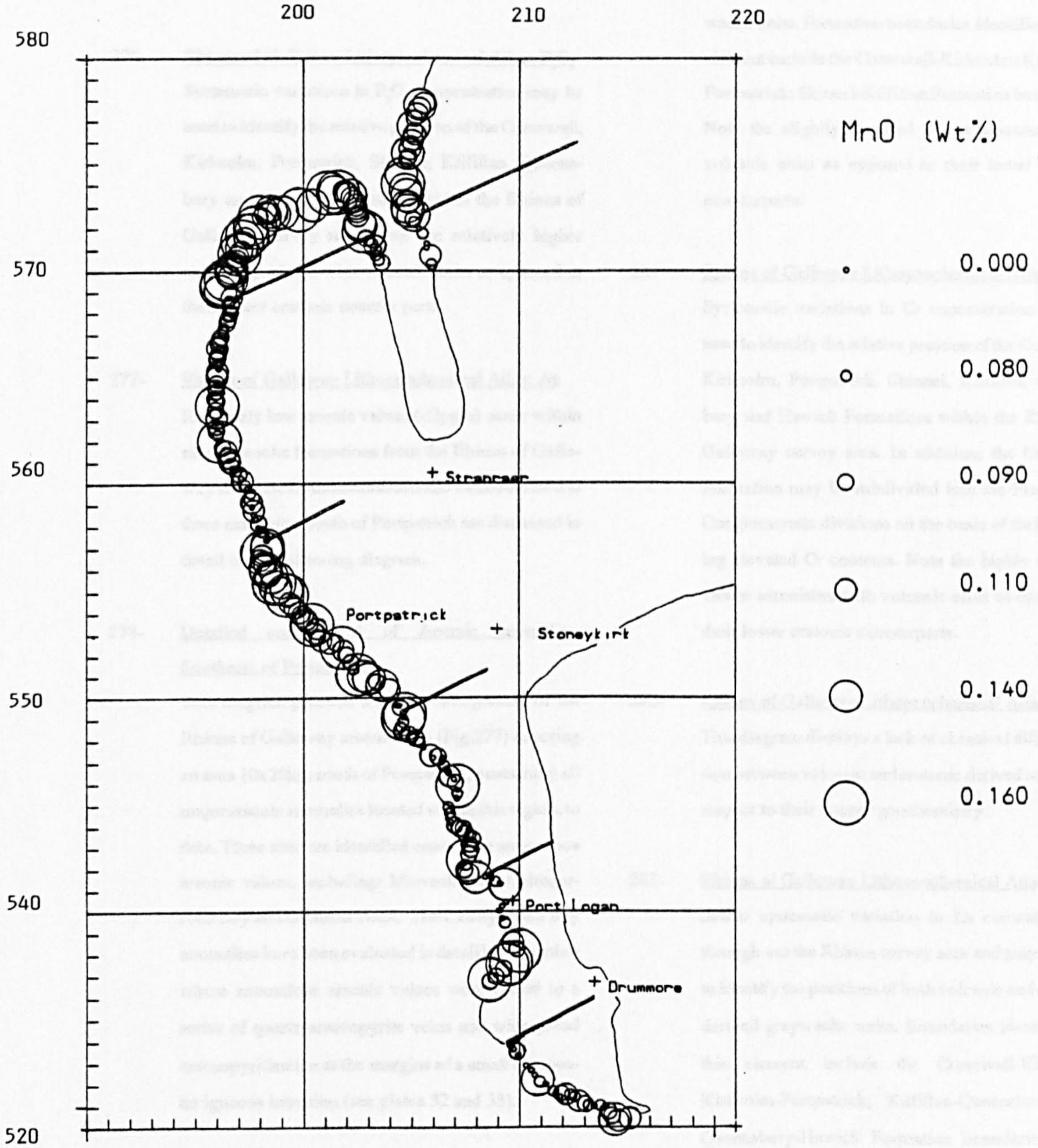

1 : 325,000 (32mm = 10km)

C - CORSEWALL FORMATION (MARCHBURN)
K - KIRKCOLM FORMATION (AFTON)
P - PORTPATRICK FORMATION (SCAR)
S - SCHINNEL FORMATION
Kf - KILFILLAN FORMATION (PYROXENOUS)
Q - QUEENSBURY FORMATION (INTERMEDIATE)
H - HAWICK FORMATION

Rhinns as opposed to their lower cratonic counterparts.

276- Rhinns of Galloway Lithogeochemical Atlas: P_2O_5
Systematic variations in P_2O_5 concentration may be used to identify the relative position of the Corsewall, Kirkcolm, Portpatrick, Shinnel, Kilfillan, Queensbury and Hawick Formations within the Rhinns of Galloway survey area. Note the relatively higher values associated with volcanic units as opposed to their lower cratonic counter parts.

277- Rhinns of Galloway Lithogeochemical Atlas: As
Extremely low arsenic values (<3ppm) occur within all greywacke formations from the Rhinns of Galloway study area. Anomalous arsenic values defined at three main sites south of Portpatrick are discussed in detail in the following diagram.

278- Detailed enlargement of Arsenic anomalies, Southeast of Portpatrick
This diagram presents a partial enlargement of the Rhinns of Galloway arsenic map (Fig.277) covering an area 10x20km south of Portpatrick, containing all major arsenic anomalies located within this region, to date. Three sites are identified containing anomalous arsenic values, including: Morroch Bay, Cairngarroch Bay and Grennan Point. The Cairngarroch Bay anomalies have been evaluated in detail by the author where anomalous arsenic values were traced to a series of quartz-arsenopyrite veins and widespread arsenopyritisation at the margins of a small composite igneous intrusion (see plates 32 and 33).

279- Rhinns of Galloway Lithogeochemical Atlas: Ba
Contrasting variations in Ba content may be used to identify the boundaries between the Corsewall-Kirkcolm; Kirkcolm-Portpatrick; Portpatrick-Shinnel; Shinnel- Kilfillan; Kilfillan-Queensbury; and Queensbury-Hawick Formations in the Rhinns of Galloway survey area. Note the elevated values associated with volcanic units as opposed to their lower cratonic counterparts.

280- Rhinns of Galloway Lithogeochemical Atlas: Co
Subtle variations in Co content occur throughout the Rhinns survey area and may be used to identify the positions of both volcanic and cratonic derived greywacke units. Formation boundaries identified by this element include the Corsewall-Kirkcolm; Kirkcolm-Portpatrick; Shinnel-Kilfillan Formation boundaries. Note the slightly elevated values associated with volcanic units as opposed to their lower cratonic counterparts.

281- Rhinns of Galloway Lithogeochemical Atlas: Cr
Systematic variations in Cr concentration may be used to identify the relative position of the Corsewall, Kirkcolm, Portpatrick, Shinnel, Kilfillan, Queensbury and Hawick Formations within the Rhinns of Galloway survey area. In addition, the Coreswall Formation may be subdivided into the Flaggy and Conglomeratic divisions on the basis of their differing elevated Cr contents. Note the highly elevated values associated with volcanic units as opposed to their lower cratonic counterparts.

282- Rhinns of Galloway Lithogeochemical Atlas: Cu
This diagram displays a lack of chemical differentiation between volcanic and cratonic derived units with respect to their copper geochemistry.

283- Rhinns of Galloway Lithogeochemical Atlas: La
Subtle systematic variation in La content occurs through out the Rhinns survey area and may be used to identify the positions of both volcanic and cratonic derived greywacke units. Boundaries identified by this element include the Corsewall-Kirkcolm; Kirkcolm-Portpatrick; Kilfillan-Queensbury and-Queensbury-Hawick Formation boundaries. Note the relatively low values associated with volcanic units as opposed to their elevated cratonic counterparts.

284- Rhinns of Galloway Lithogeochemical Atlas: Nb
Contrasting variations in Nb content may be used to identify the boundaries between the Corsewall-Kirkcolm; Kirkcolm-Portpatrick; Portpatrick-Shinnel; Shinnel- Kilfillan; Kilfillan-Queensbury; and Queensbury-Hawick Formations in the Rhinns of Galloway survey area. Note the extremely low values associated with volcanic units in comparison with

A LITHOGEOCHEMICAL STUDY OF THE RHYNS OF GALLOWAY, SOUTH WEST SCOTLAND

FIGURE 276

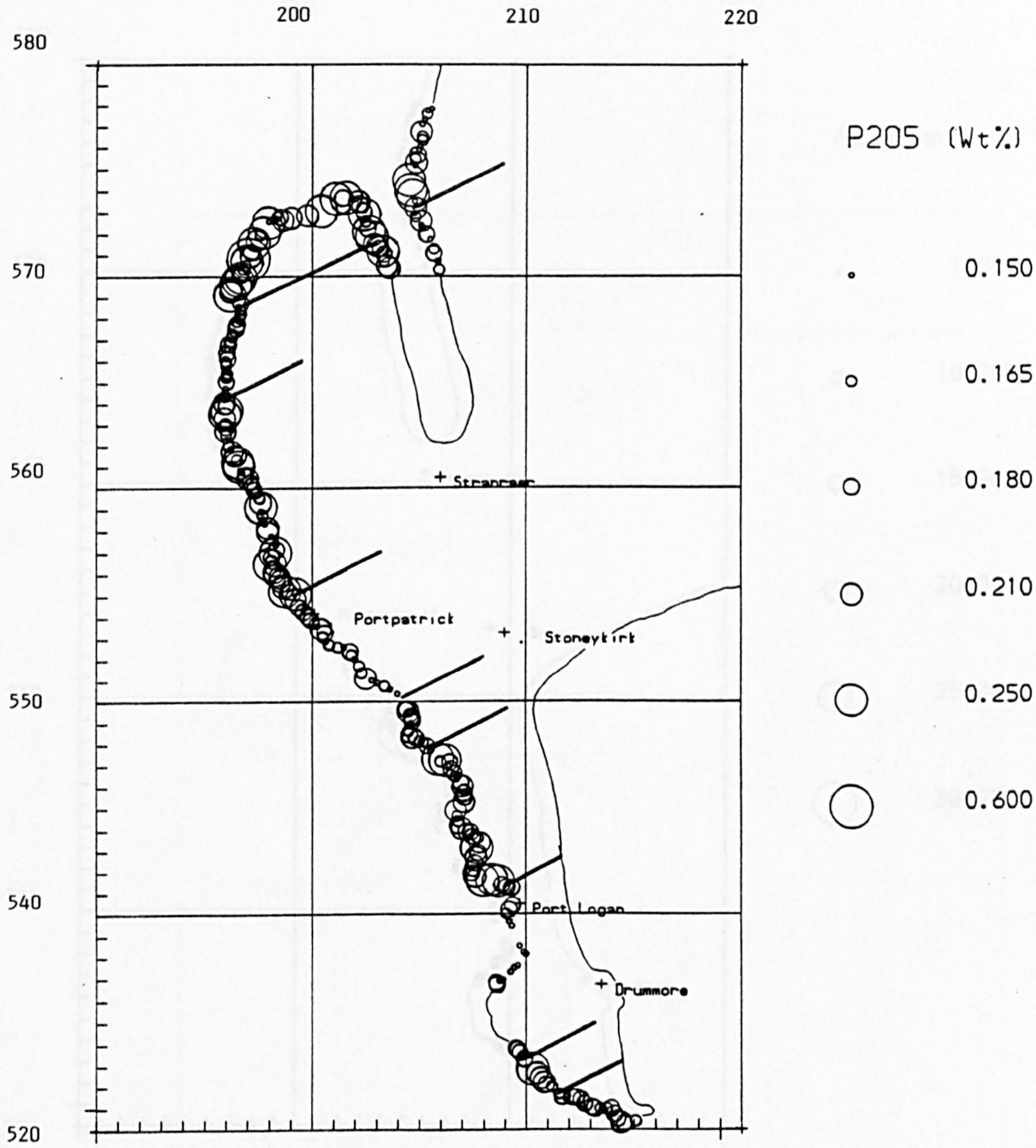

1 : 325,000 (32mm = 10km)

C - CORSEWALL FORMATION (MARCHBURN)
K - KIRKCOLM FORMATION (AFTON)
P - PORTPATRICK FORMATION (SCAR)
S - SCHINNEL FORMATION
Kf- KILFILLAN FORMATION (PYROXENOUS)
Q - QUEENSBURY FORMATION (INTERMEDIATE)
H - HAWICK FORMATION

A LITHOGEOCHEMICAL STUDY OF THE RHYNS OF GALLOWAY, SOUTH WEST SCOTLAND

FIGURE 277

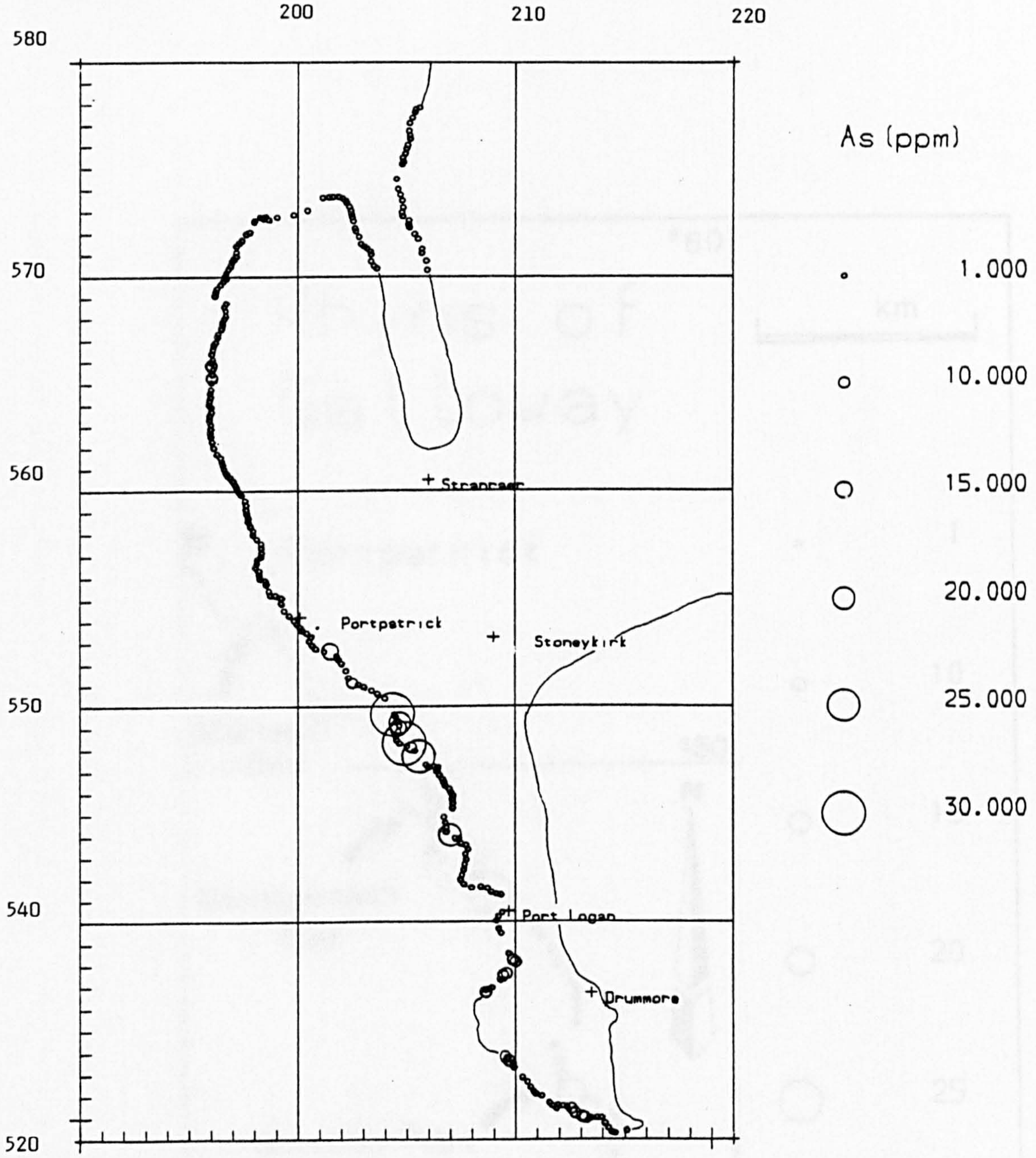

1 : 325,000 (32mm = 10km)

C - CORSEWALL FORMATION (MARCHBURN)
K - KIRKCOLM FORMATION (AFTON)
P - PORTPATRICK FORMATION (SCAR)
S - SCHINNEL FORMATION
Kf- KILFILLAN FORMATION (PYROXENOUS)
Q - QUEENSBURY FORMATION (INTERMEDIATE)
H - HAWICK FORMATION

FIGURE 278

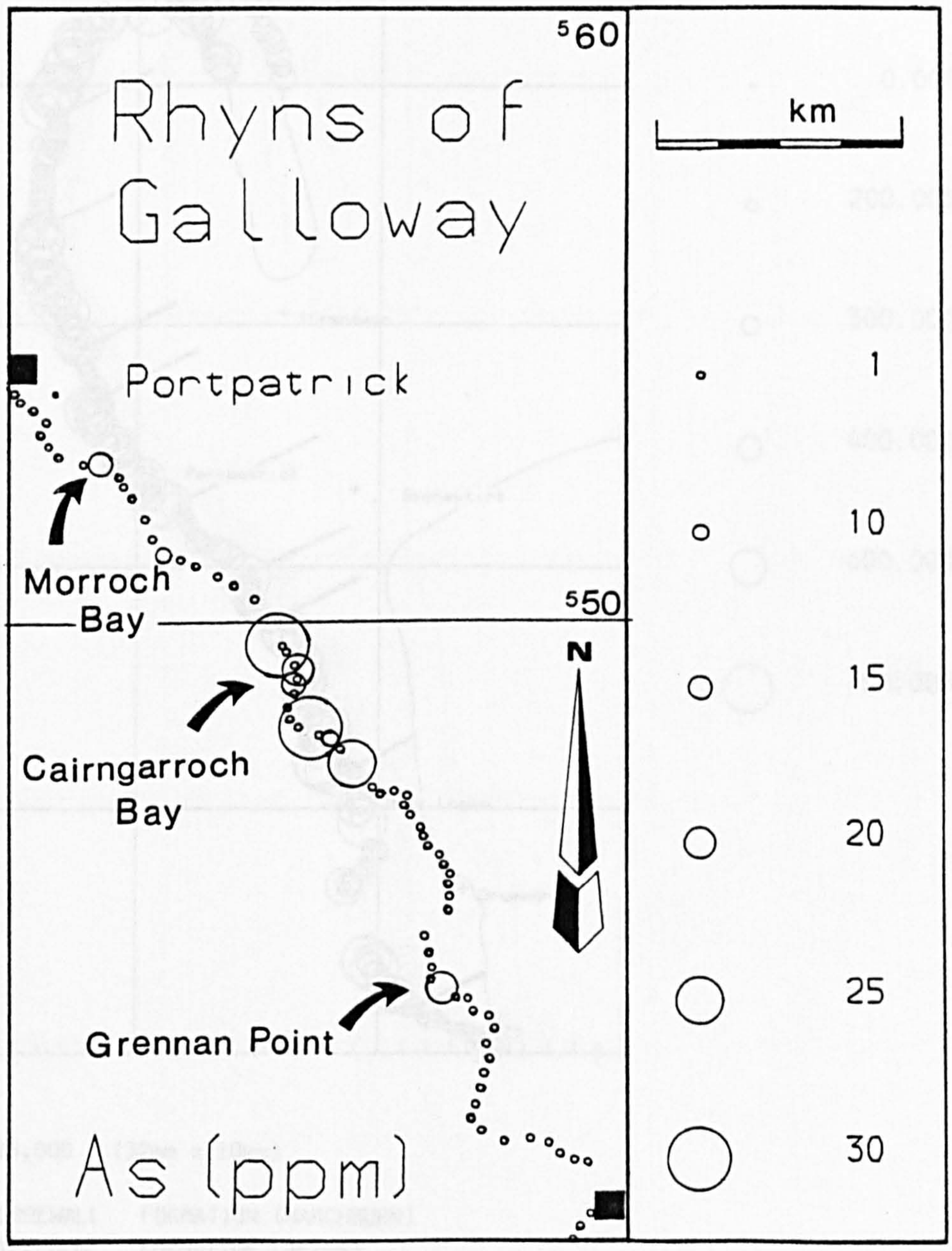
Rhyns of Galloway
560
550
km
Portpatrick
Morroch Bay
Cairngarroch Bay
Grennan Point
N
As (ppm)
1
10
15
20
25
30

A LITHOGEOCHEMICAL STUDY OF THE RHYNS OF GALLOWAY, SOUTH WEST SCOTLAND

FIGURE 279

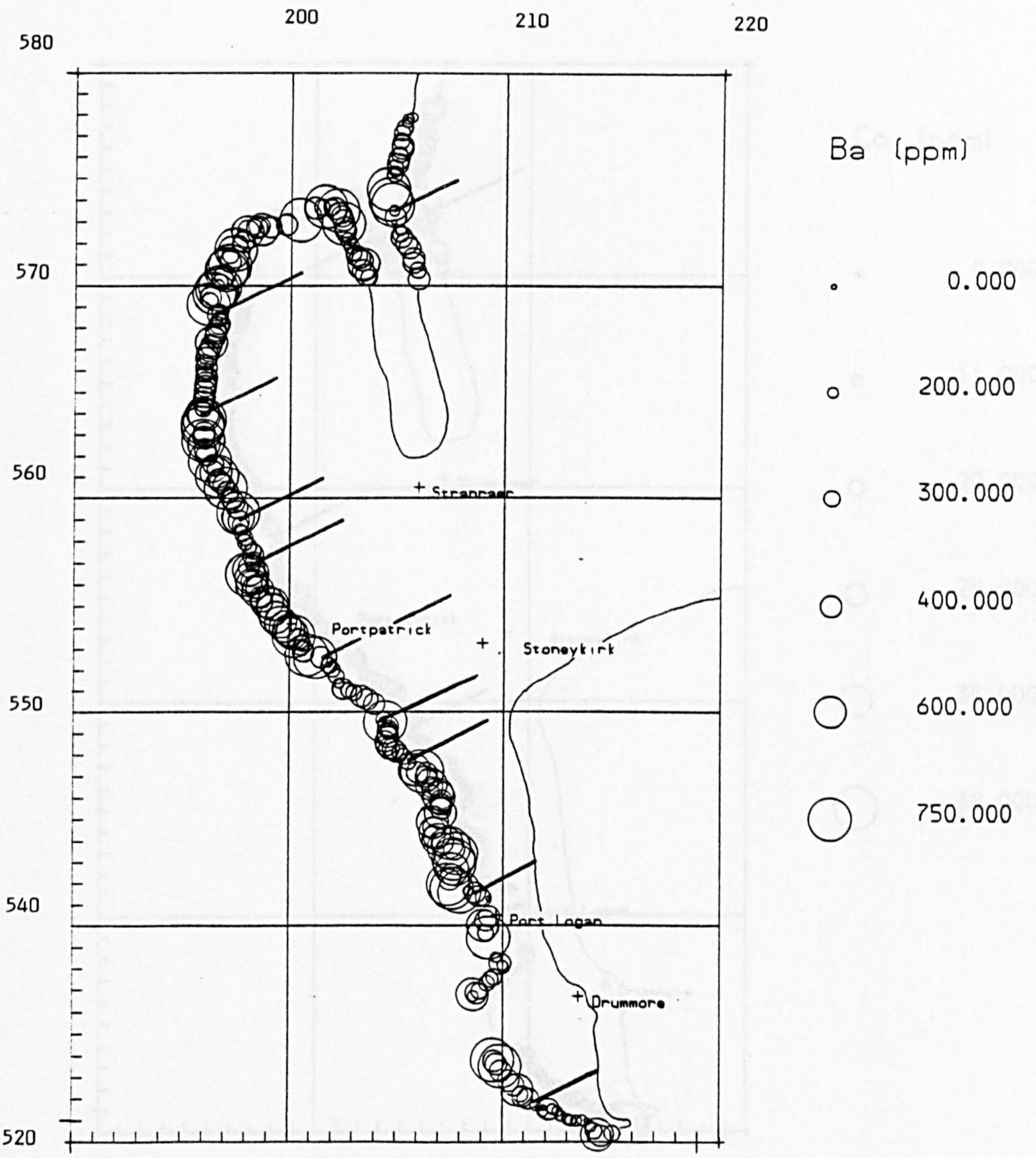

1 : 325,000 (32mm = 10km)

C - CORSEWALL FORMATION (MARCHBURN)
K - KIRKCOLM FORMATION (AFTON)
P - PORTPATRICK FORMATION (SCAR)
S - SCHINNEL FORMATION
Kf- KILFILLAN FORMATION (PYROXENOUS)
Q - QUEENSBURY FORMATION (INTERMEDIATE)
H - HAWICK FORMATION

A LITHOGEOCHEMICAL STUDY OF THE RHYNS OF GALLOWAY, SOUTH WEST SCOTLAND

FIGURE 280

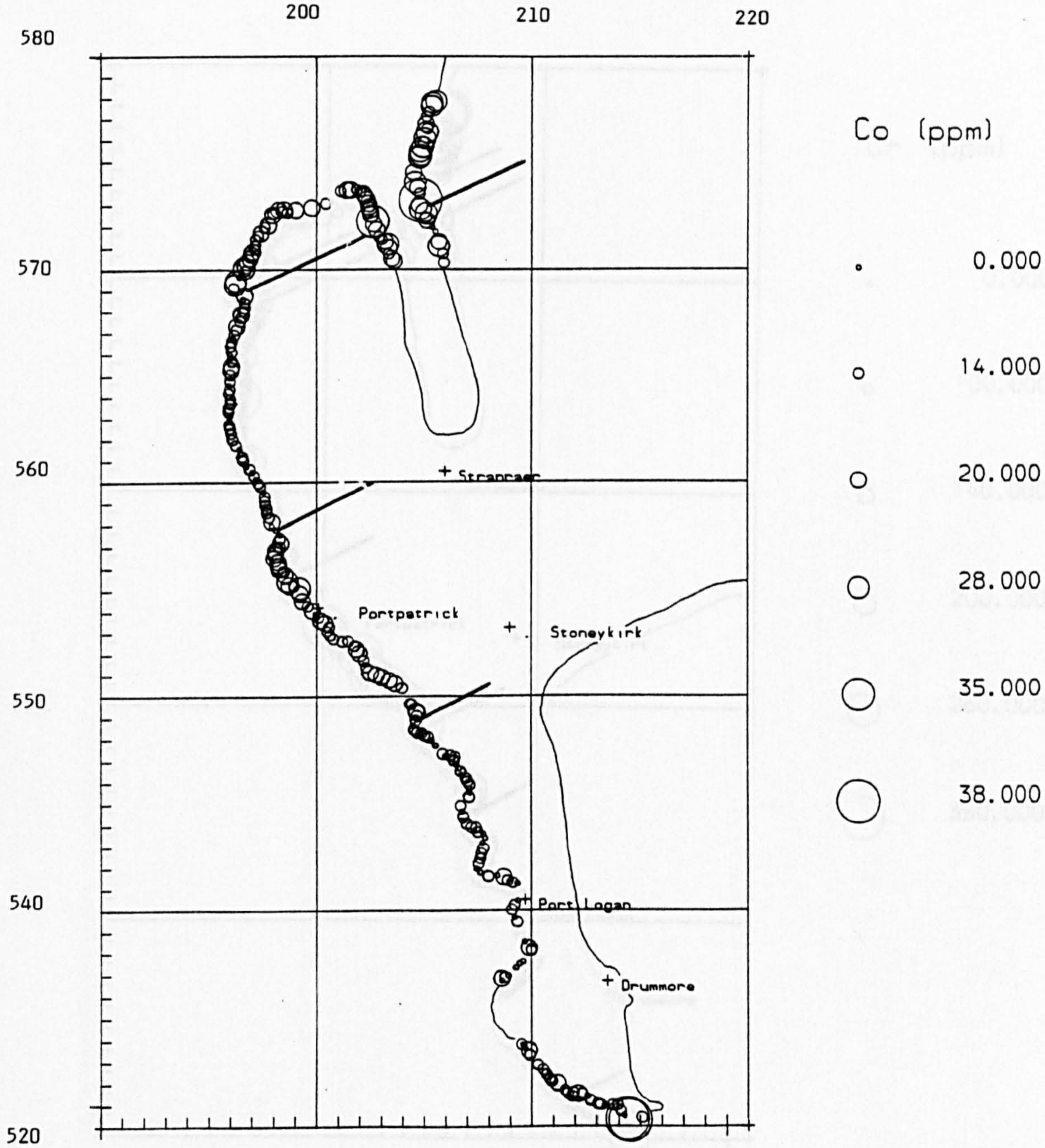

1 : 325,000 (32mm = 10km)

C - CORSEWALL FORMATION (MARCHBURN)
K - KIRKCOLM FORMATION (AFTON)
P - PORTPATRICK FORMATION (SCAR)
S - SCHINNEL FORMATION
Kf- KILFILLAN FORMATION (PYROXENOUS)
Q - QUEENSBURY FORMATION (INTERMEDIATE)
H - HAWICK FORMATION

A LITHOGEOCHEMICAL STUDY OF THE RHYNS OF GALLOWAY, SOUTH WEST SCOTLAND

FIGURE 281

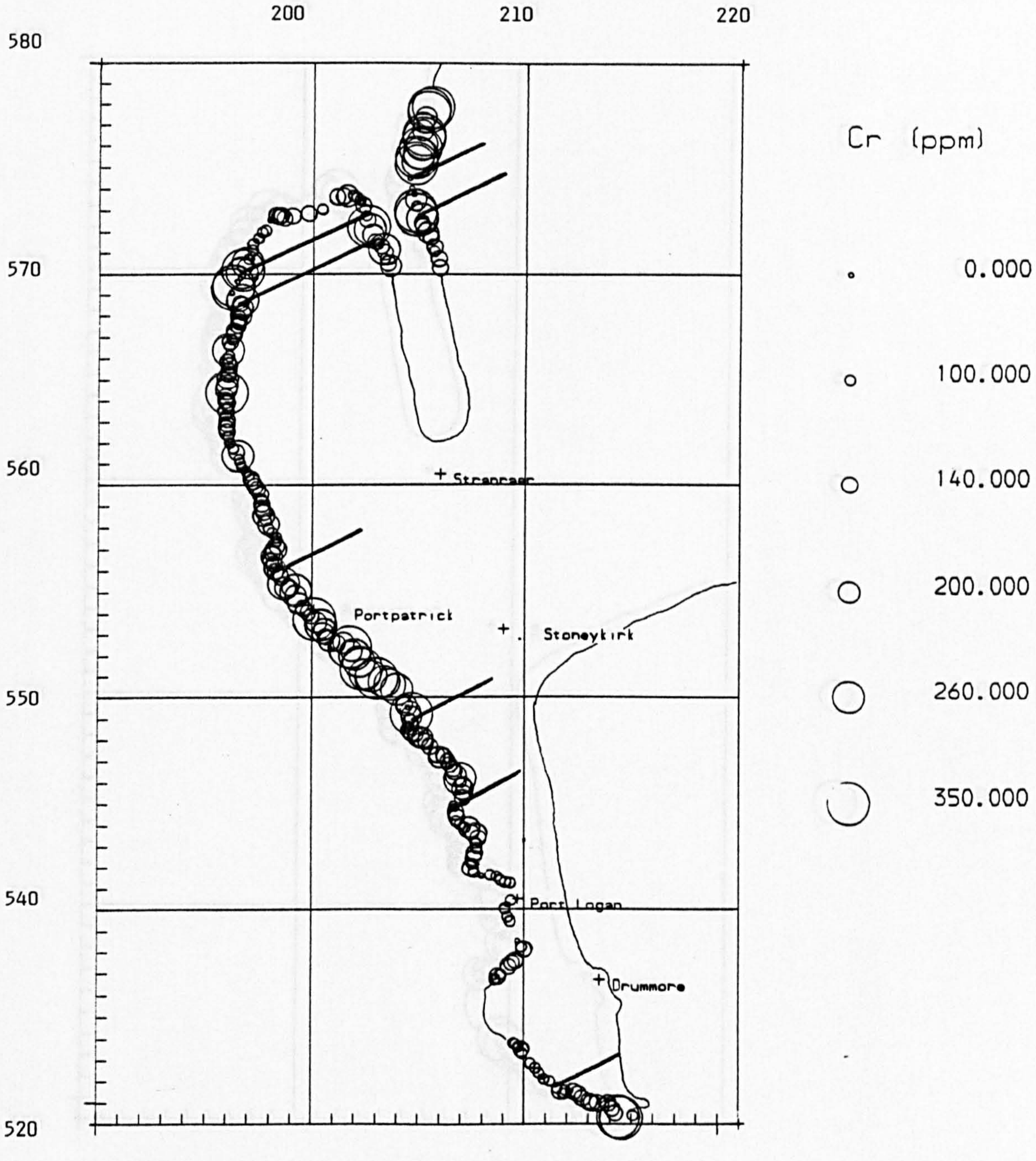

1 : 325,000 (32mm = 10km)

C - CORSEWALL FORMATION (MARCHBURN)
K - KIRKCOLM FORMATION (AFTON)
P - PORTPATRICK FORMATION (SCAR)
S - SCHINNEL FORMATION
Kf- KILFILLAN FORMATION (PYROXENOUS)
Q - QUEENSBURY FORMATION (INTERMEDIATE)
H - HAWICK FORMATION

A LITHOGEOCHEMICAL STUDY OF THE RHYNS OF GALLOWAY, SOUTH WEST SCOTLAND

FIGURE 282

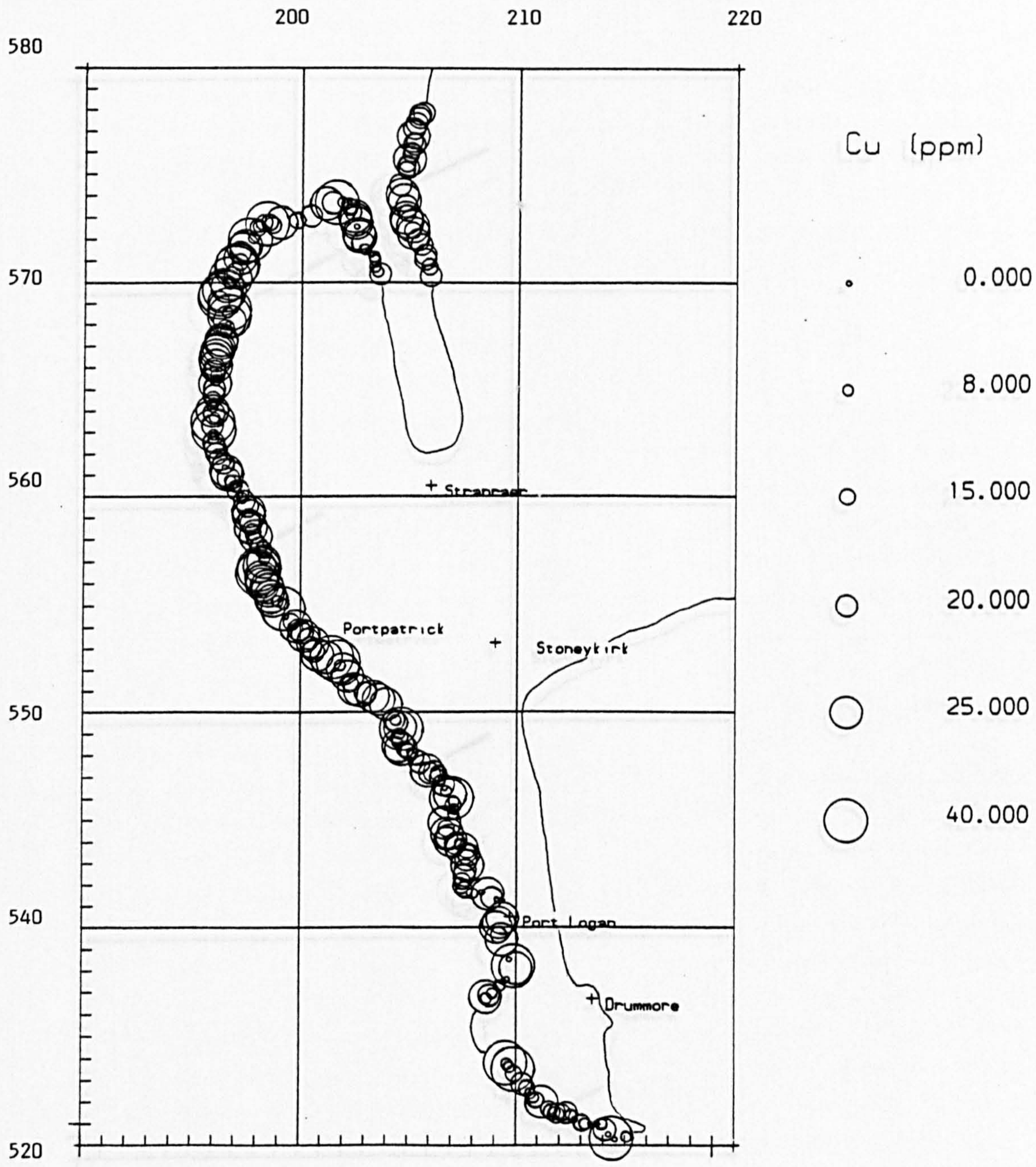

1 : 325,000 (32mm = 10km)

C - CORSEWALL FORMATION (MARCHBURN)
K - KIRKCOLM FORMATION (AFTON)
P - PORTPATRICK FORMATION (SCAR)
S - SCHINNEL FORMATION
Kf- KILFILLAN FORMATION (PYROXENOUS)
Q - QUEENSBURY FORMATION (INTERMEDIATE)
H - HAWICK FORMATION

A LITHOGEOCHEMICAL STUDY OF THE RHYNS OF GALLOWAY, SOUTH WEST SCOTLAND

FIGURE 283

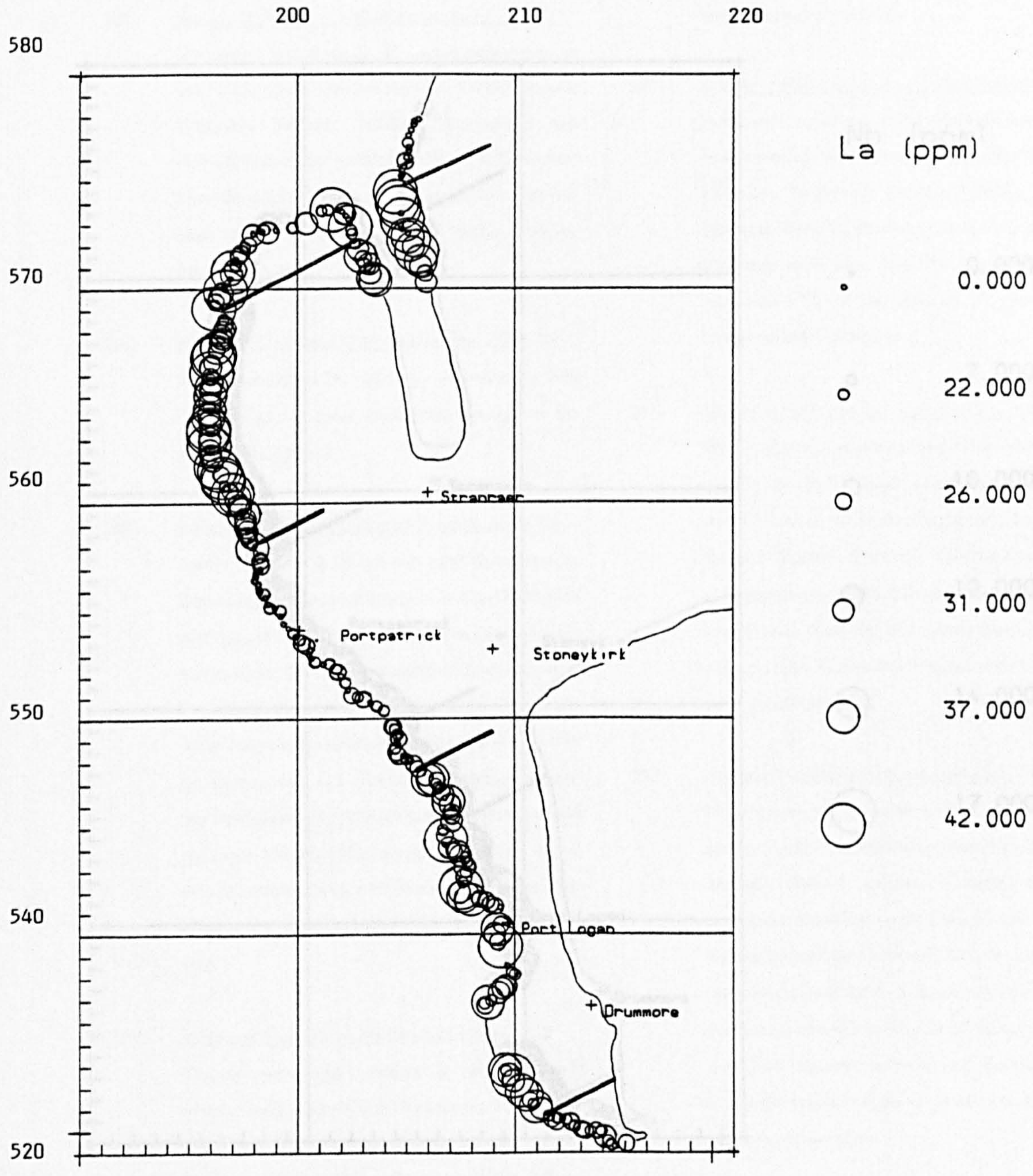

1 : 325,000 (32mm = 10km)

C - CORSEWALL FORMATION (MARCHBURN)
K - KIRKCOLM FORMATION (AFTON)
P - PORTPATRICK FORMATION (SCAR)
S - SCHINNEL FORMATION
Kf- KILFILLAN FORMATION (PYROXENOUS)
Q - QUEENSBURY FORMATION (INTERMEDIATE)
H - HAWICK FORMATION

A LITHOGEOCHEMICAL STUDY OF THE RHYNS OF GALLOWAY, SOUTH WEST SCOTLAND

FIGURE 284

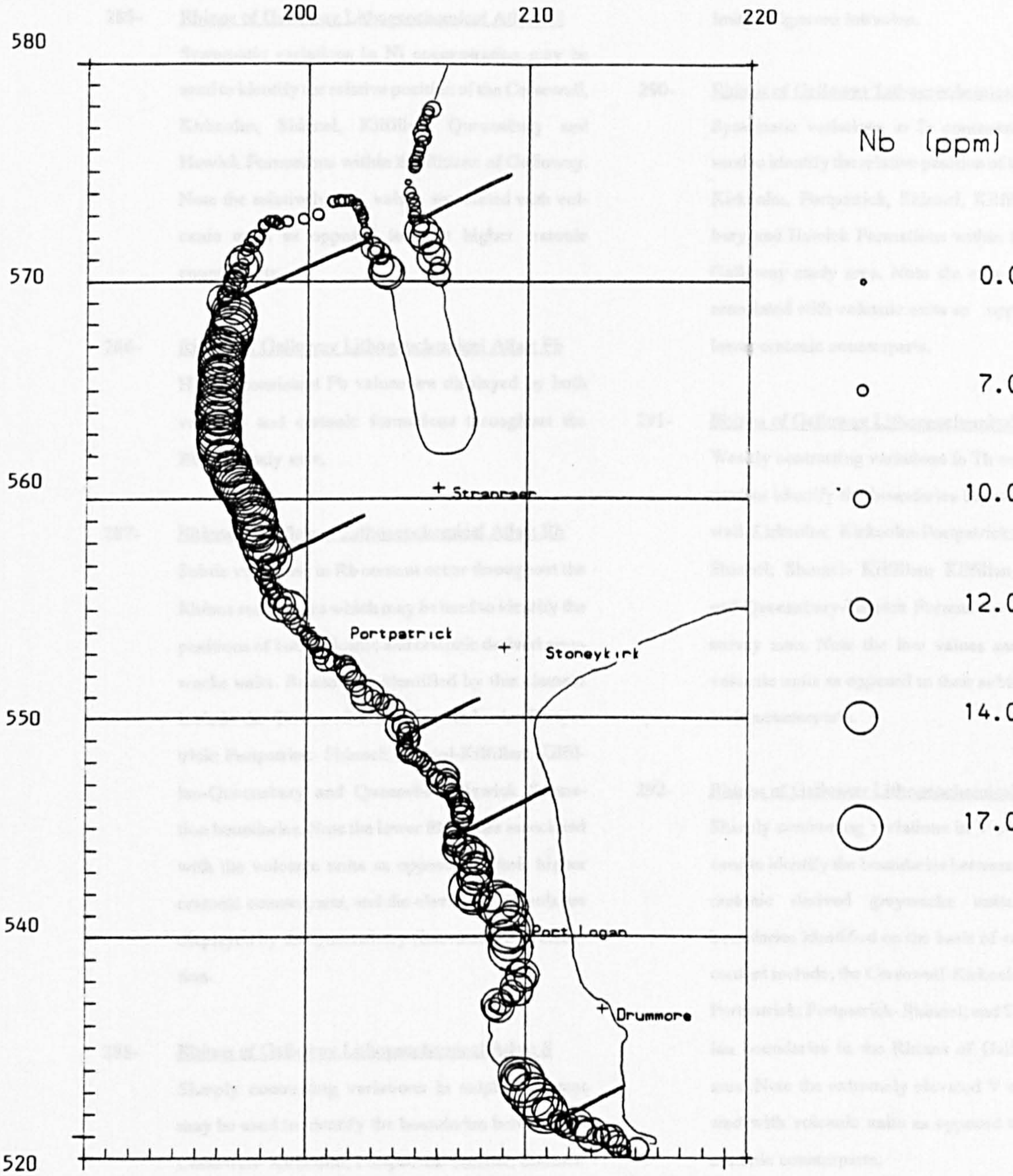

1 : 325,000 (32mm = 10km)

C - CORSEWALL FORMATION (MARCHBURN)
K - KIRKCOLM FORMATION (AFTON)
P - PORTPATRICK FORMATION (SCAR)
S - SCHINNEL FORMATION
Kf- KILFILLAN FORMATION (PYROXENOUS)
Q - QUEENSBURY FORMATION (INTERMEDIATE)
H - HAWICK FORMATION

their higher cratonic counterparts.

285- Rhinns of Galloway Lithogeochemical Atlas: Ni
Systematic variations in Ni concentration may be used to identify the relative position of the Corsewall, Kirkcolm, Shinnel, Kilfillan, Queensbury and Hawick Formations within the Rhinns of Galloway. Note the relatively low values associated with volcanic units as opposed to their higher cratonic counterparts.

286- Rhinns of Galloway Lithogeochemical Atlas: Pb
Highly consistent Pb values are displayed by both volcanic and cratonic formations throughout the Rhinns study area.

287- Rhinns of Galloway Lithogeochemical Atlas: Rb
Subtle variations in Rb content occur throughout the Rhinns survey area which may be used to identify the positions of both volcanic and cratonic derived greywacke units. Boundaries identified by this element include the Corsewall-Kirkcolm; Kirkcolm-Portpatrick; Portpatrick- Shinnel; Shinnel-Kilfillan; Kilfillan-Queensbury and Queensbury-Hawick Formation boundaries. Note the lower Rb values associated with the volcanic units as opposed to their higher cratonic counterparts, and the elevated Rb levels are displayed by the Queensbury (Intermediate) Formation.

288- Rhinns of Galloway Lithogeochemical Atlas: S
Sharply contrasting variations in sulphur content may be used to identify the boundaries between the Corsewall- Kirkcolm; Portpatrick-Shinnel; Shinnel-Kilfillan; Kilfillan-Queensbury; and Queensbury-Hawick Formations in the Rhinns survey area. Note the extremely low values sulphur values identified in both the Corsewall (Lower Ordovician) and Hawick (Silurian) Formations.

289- Rhinns of Galloway Lithogeochemical Atlas: Sb
Note the consistently low Sb values (<4ppm) displayed throughout the succession. A small number of anomalies are identified, located in both Morroch and Cairngarroch Bay's (areas also pinpointed by arsenic geochemistry, see figs. 277 and 278) Logan Bay and the Mull of Galloway. Note the general increase in the background Sb content of greywackes in close proximity to igneous intrusion.

290- Rhinns of Galloway Lithogeochemical Atlas: Sr
Systematic variations in Sr concentration may be used to identify the relative position of the Corsewall, Kirkcolm, Portpatrick, Shinnel, Kilfillan, Queensbury and Hawick Formations within the Rhinns of Galloway study area. Note the elevated Sr values associated with volcanic units as opposed to their lower cratonic counterparts.

291- Rhinns of Galloway Lithogeochemical Atlas: Th
Weakly contrasting variations in Th content may be used to identify the boundaries between the Corsewall-Kirkcolm; Kirkcolm-Portpatrick; Portpatrick-Shinnel; Shinnel- Kilfillan; Kilfillan-Queensbury; and Queensbury-Hawick Formations in the Rhinns survey area. Note the low values associated with volcanic units as opposed to their subtly higher cratonic counterparts.

292- Rhinns of Galloway Lithogeochemical Atlas: V
Sharply contrasting variations in V content may be used to identify the boundaries between volcanic and cratonic derived greywacke units. Formation boundaries identified on the basis of variations in V content include; the Corsewall-Kirkcolm; Kirkcolm-Portpatrick; Portpatrick- Shinnel; and Shinnel-Kilfillan boundaries in the Rhinns of Galloway survey area. Note the extremely elevated V values associated with volcanic units as opposed to their lower cratonic counterparts.

293- Rhinns of Galloway Lithogeochemical Atlas: Y
Subtle variations in Y content occur within greywackes throughout the Rhinns survey area. These variations may be used to identify the positions of both volcanic and cratonic derived greywacke units and their associated boundaries. Formation boundaries identified by Y chemistry include the Corsewall-Kirkcolm; Kirkcolm-Portpatrick; Kilfillan-Queensbury and Queensbury-Hawick boundaries. Note the low values associated with volcanic units as opposed to their relatively higher cratonic counterparts.

A LITHOGEOCHEMICAL STUDY OF THE RHYNS OF GALLOWAY, SOUTH WEST SCOTLAND

FIGURE 285

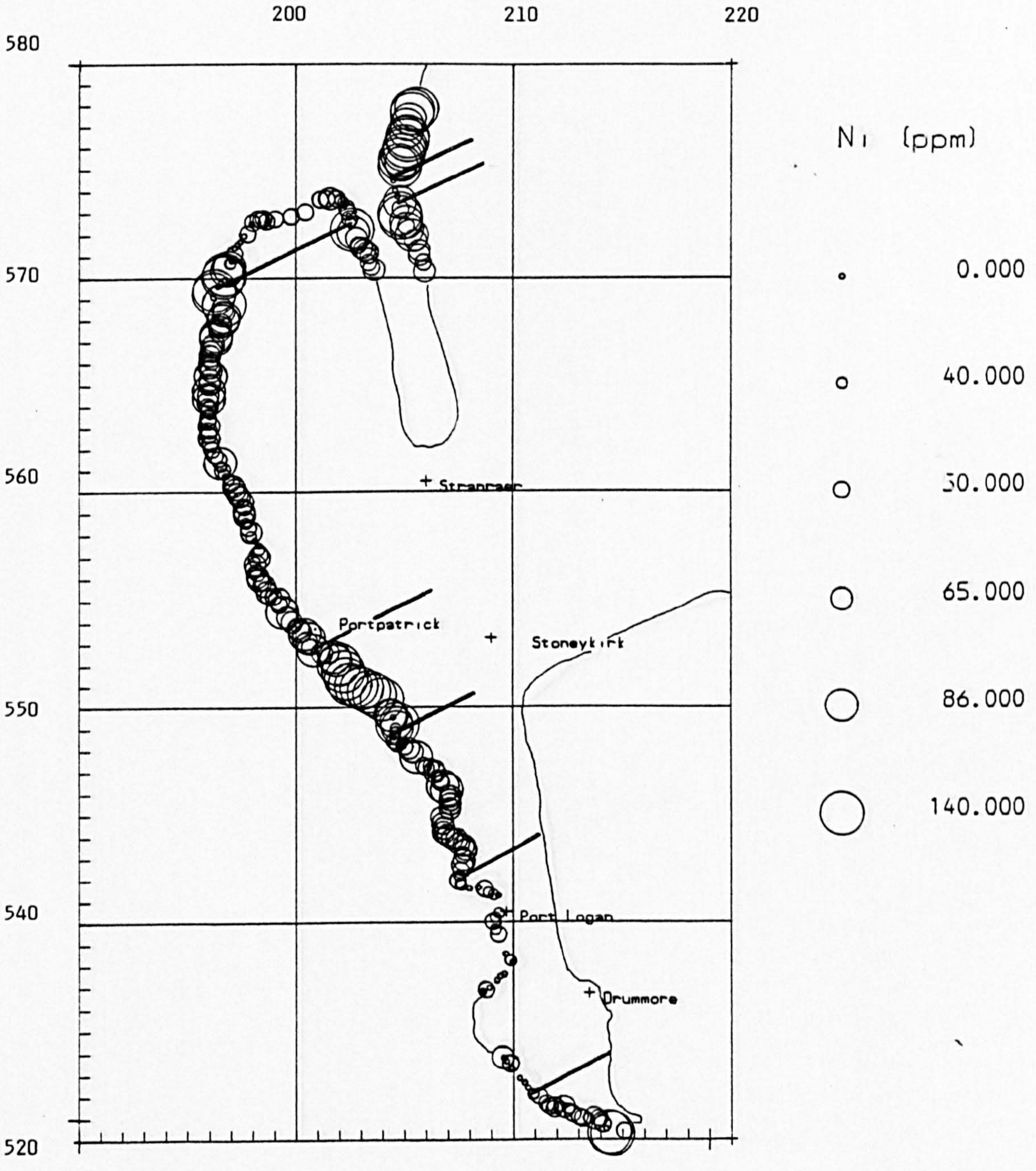

1 : 325,000 (32mm = 10km)

C - CORSEWALL FORMATION (MARCHBURN)
K - KIRKCOLM FORMATION (AFTON)
P - PORTPATRICK FORMATION (SCAR)
S - SCHINNEL FORMATION
Kf- KILFILLAN FORMATION (PYROXENOUS)
Q - QUEENSBURY FORMATION (INTERMEDIATE)
H - HAWICK FORMATION

A LITHOGEOCHEMICAL STUDY OF THE RHYNS OF GALLOWAY, SOUTH WEST SCOTLAND

FIGURE 286

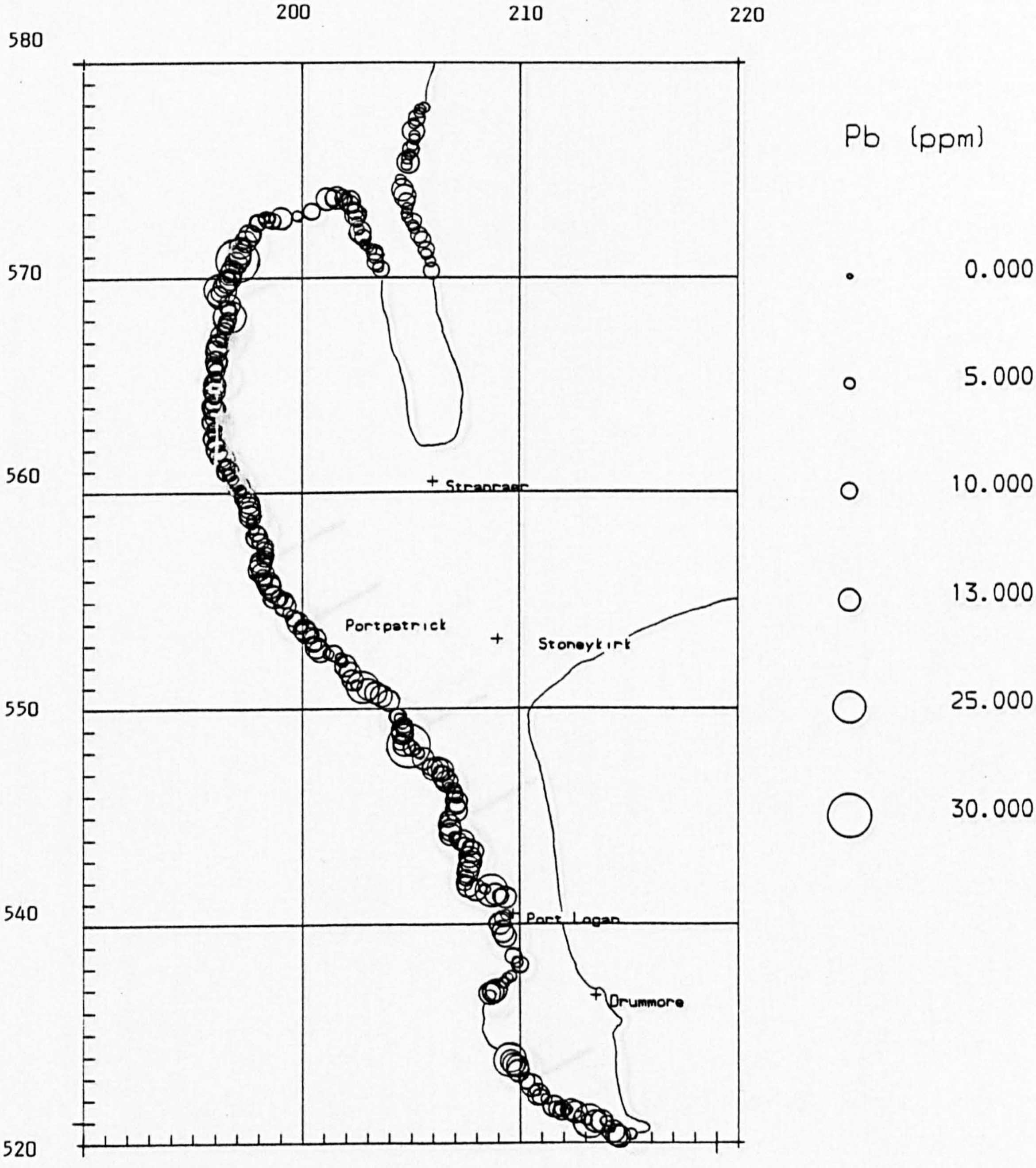

1 : 325,000 (32mm = 10km)

C - CORSEWALL FORMATION (MARCHBURN)
K - KIRKCOLM FORMATION (AFTON)
P - PORTPATRICK FORMATION (SCAR)
S - SCHINNEL FORMATION
Kf- KILFILLAN FORMATION (PYROXENOUS)
Q - QUEENSBURY FORMATION (INTERMEDIATE)
H - HAWICK FORMATION

A LITHOGEOCHEMICAL STUDY OF THE RHYNS OF GALLOWAY, SOUTH WEST SCOTLAND

FIGURE 287

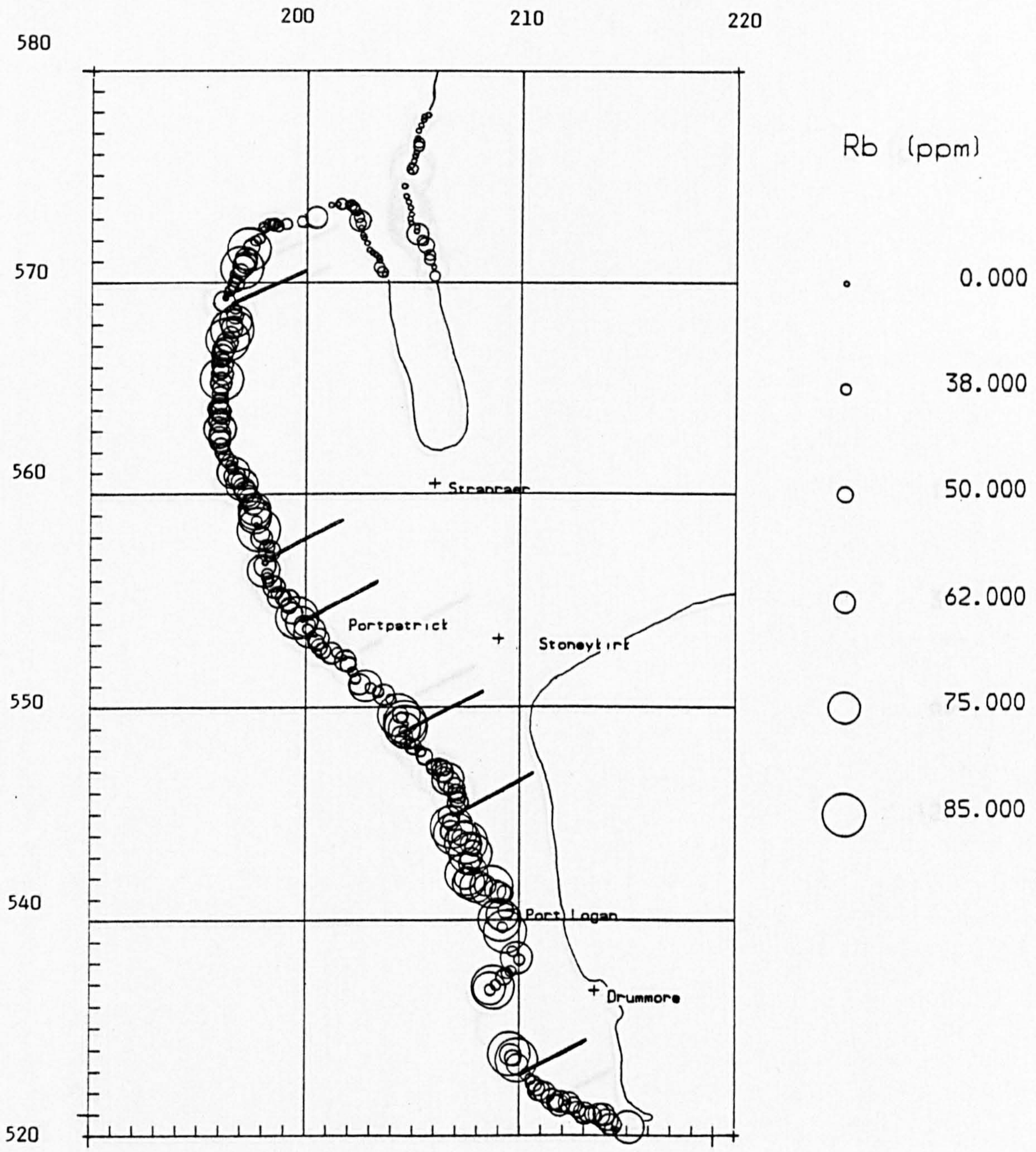

1 : 325,000 (32mm = 10km)

C - CORSEWALL FORMATION (MARCHBURN)
K - KIRKCOLM FORMATION (AFTON)
P - PORTPATRICK FORMATION (SCAR)
S - SCHINNEL FORMATION
Kf- KILFILLAN FORMATION (PYROXENOUS)
Q - QUEENSBURY FORMATION (INTERMEDIATE)
H - HAWICK FORMATION

A LITHOGEOCHEMICAL STUDY OF THE RHYNS OF GALLOWAY, SOUTH WEST SCOTLAND

FIGURE 288

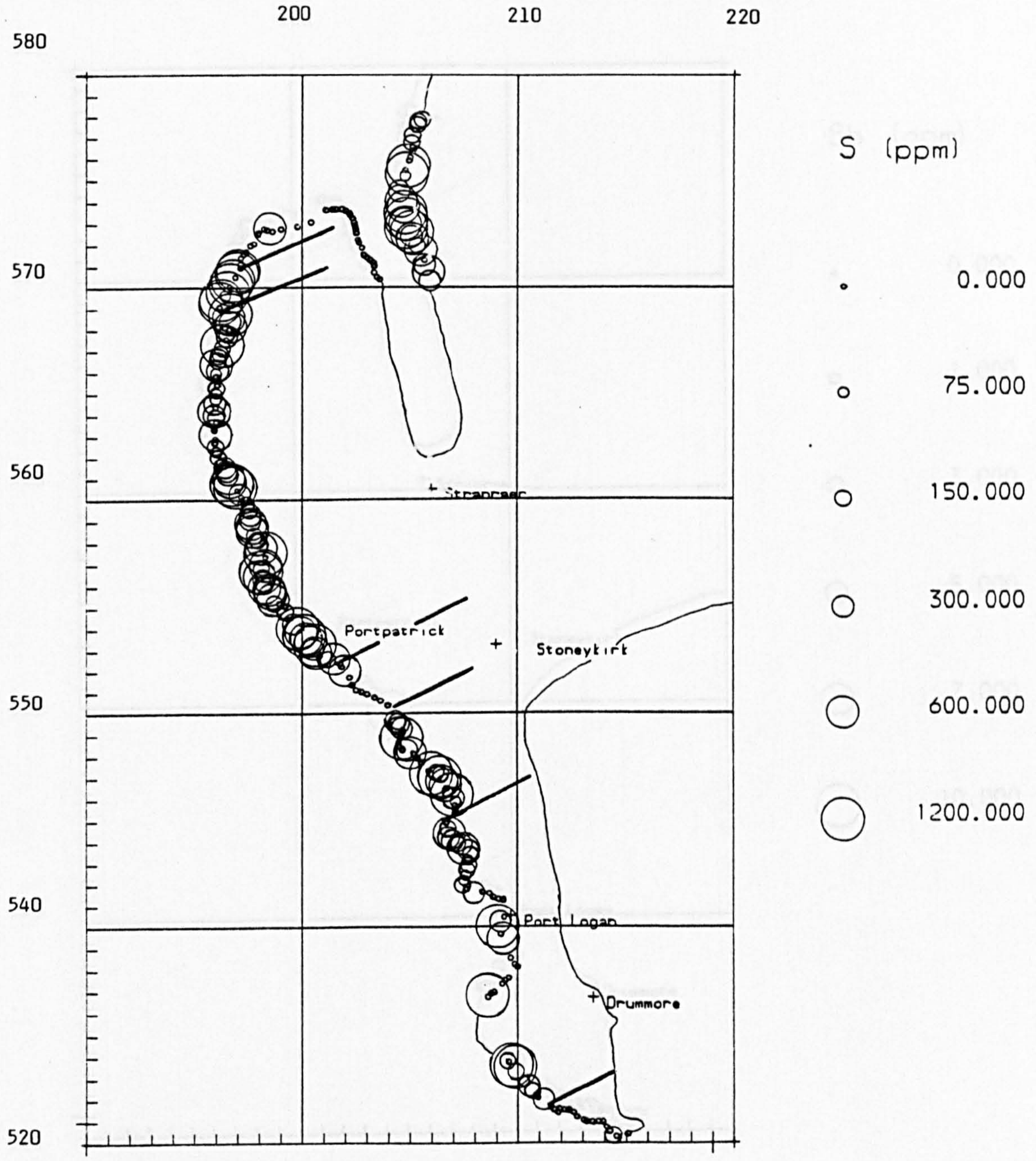

1 : 325,000 (32mm = 10km)

C - CORSEWALL FORMATION (MARCHBURN)
K - KIRKCOLM FORMATION (AFTON)
P - PORTPATRICK FORMATION (SCAR)
S - SCHINNEL FORMATION
Kf- KILFILLAN FORMATION (PYROXENOUS)
Q - QUEENSBURY FORMATION (INTERMEDIATE)
H - HAWICK FORMATION

A LITHOGEOCHEMICAL STUDY OF THE RHYNS OF GALLOWAY, SOUTH WEST SCOTLAND

FIGURE 289

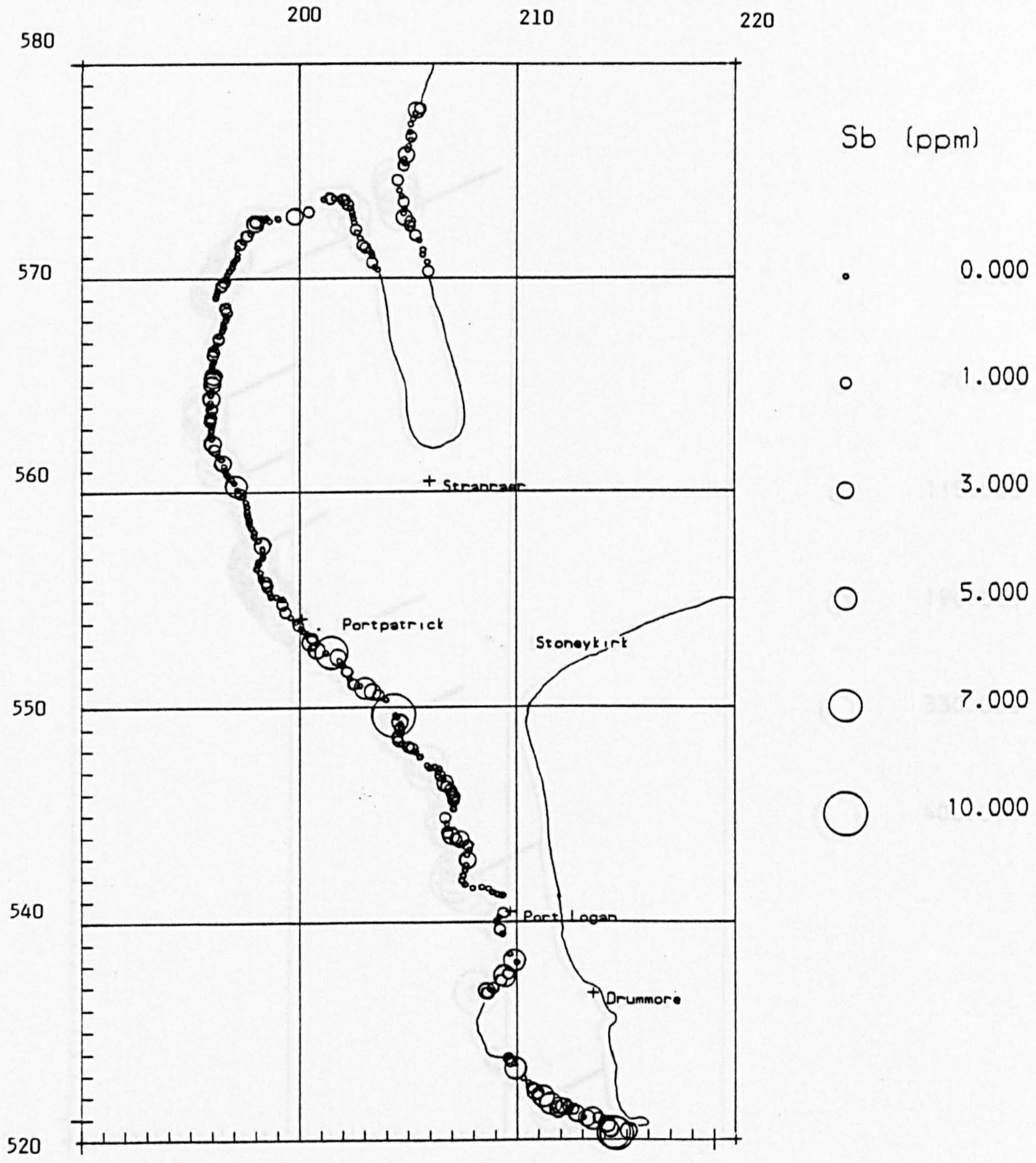

1 : 325,000 (32mm = 10km)

C - CORSEWALL FORMATION (MARCHBURN)
K - KIRKCOLM FORMATION (AFTON)
P - PORTPATRICK FORMATION (SCAR)
S - SCHINNEL FORMATION
Kf- KILFILLAN FORMATION (PYROXENOUS)
Q - QUEENSBURY FORMATION (INTERMEDIATE)
H - HAWICK FORMATION

FIGURE 290

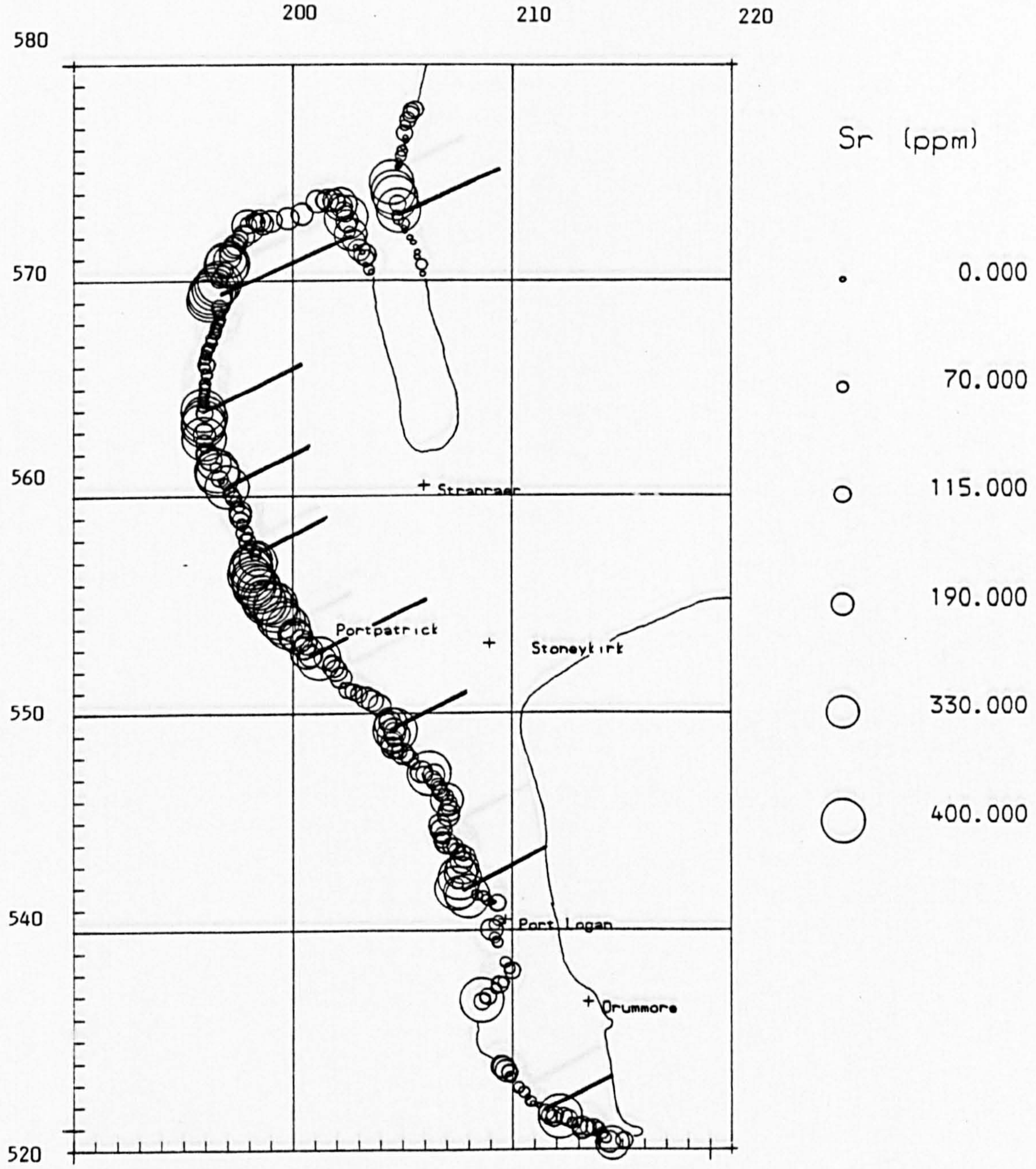

1 : 325,000 (32mm = 10km)

C - CORSEWALL FORMATION (MARCHBURN)
K - KIRKCOLM FORMATION (AFTON)
P - PORTPATRICK FORMATION (SCAR)
S - SCHINNEL FORMATION
Kf- KILFILLAN FORMATION (PYROXENOUS)
Q - QUEENSBURY FORMATION (INTERMEDIATE)
H - HAWICK FORMATION

A LITHOGEOCHEMICAL STUDY OF THE RHYNS OF GALLOWAY, SOUTH WEST SCOTLAND

FIGURE 291

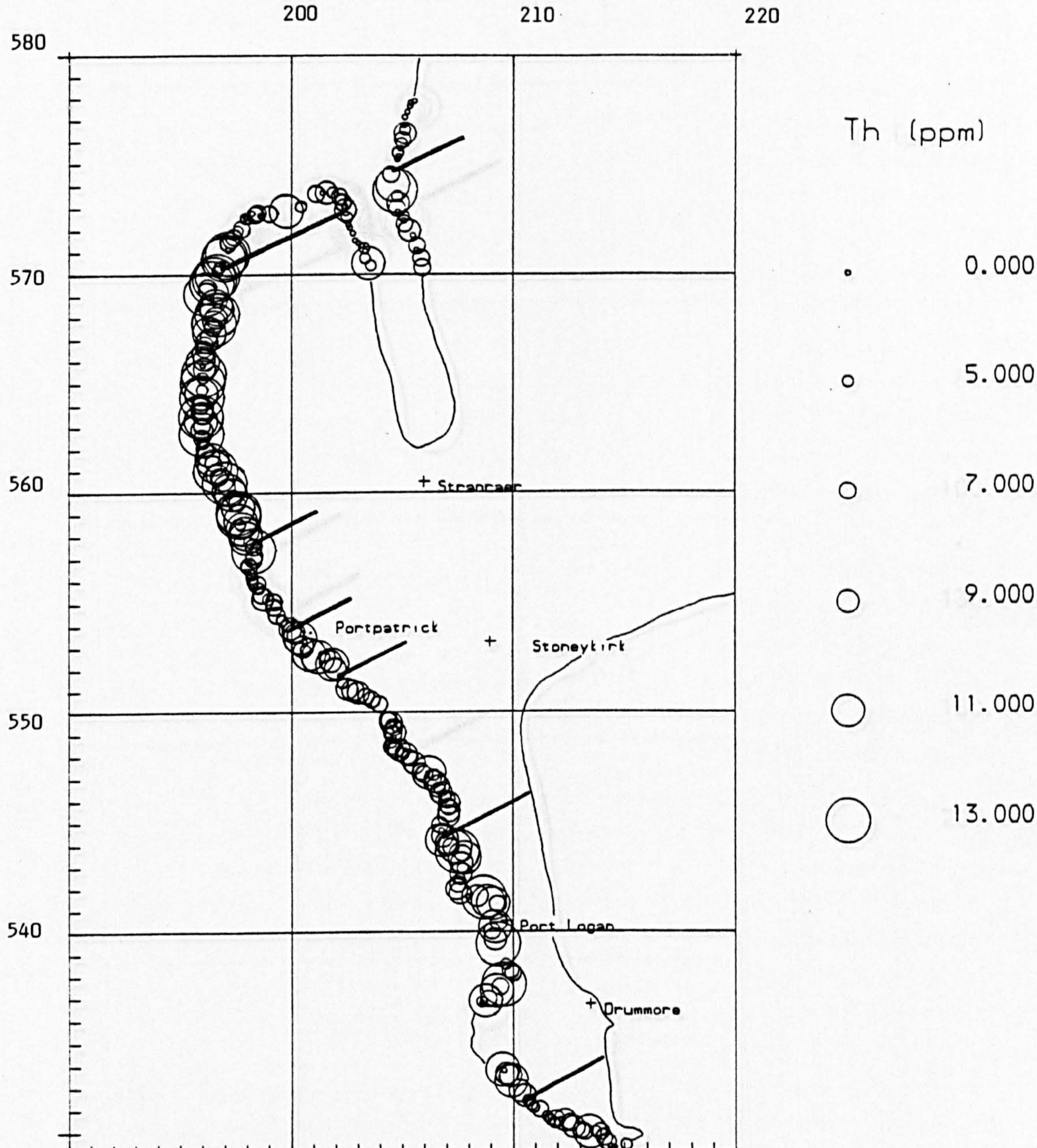

1 : 325,000 (32mm = 10km)

C - CORSEWALL FORMATION (MARCHBURN)
K - KIRKCOLM FORMATION (AFTON)
P - PORTPATRICK FORMATION (SCAR)
S - SCHINNEL FORMATION
Kf- KILFILLAN FORMATION (PYROXENOUS)
Q - QUEENSBURY FORMATION (INTERMEDIATE)
H - HAWICK FORMATION

A LITHOGEOCHEMICAL STUDY OF THE RHYNS OF GALLOWAY, SOUTH WEST SCOTLAND

FIGURE 292

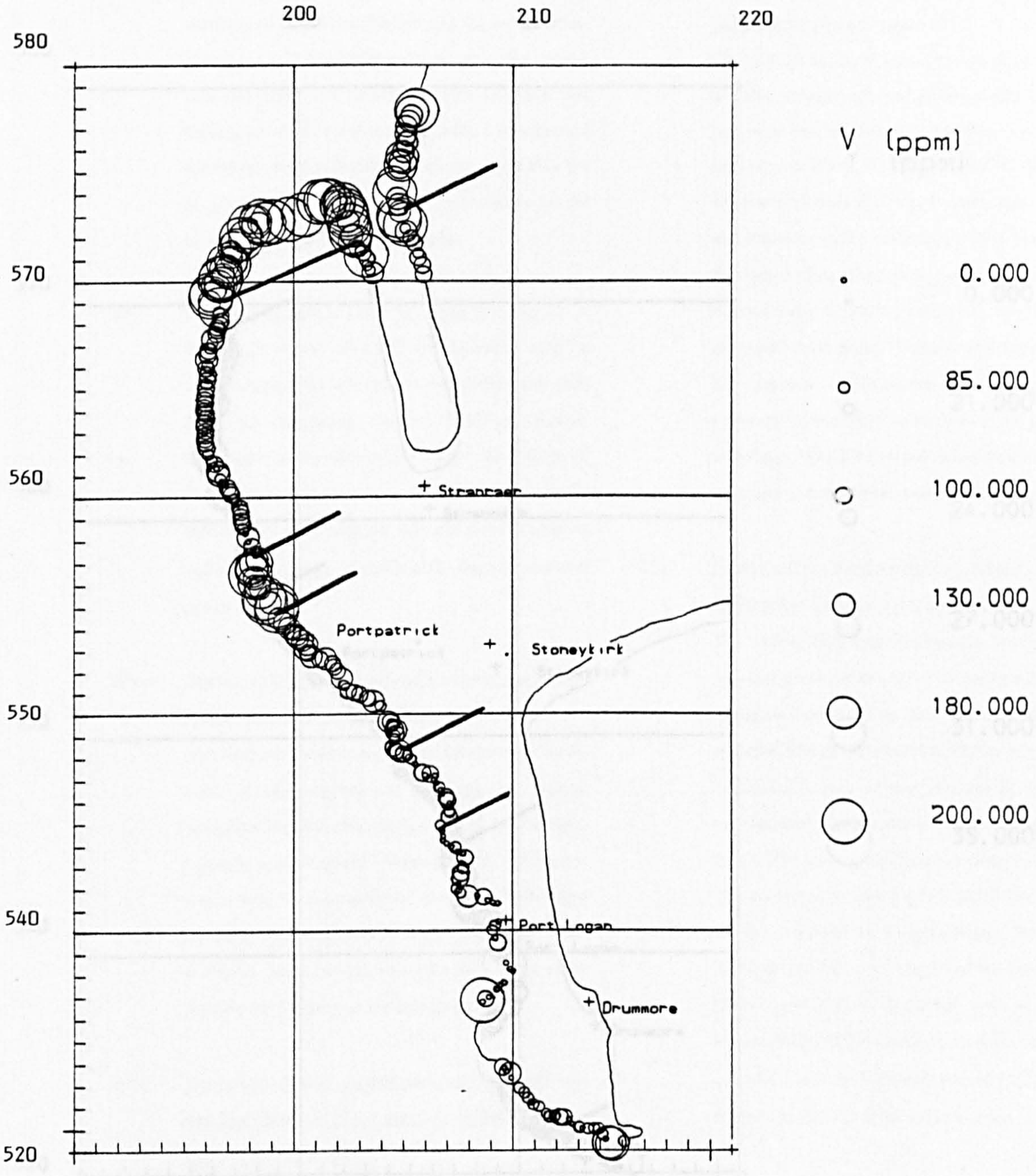

1 : 325,000 (32mm = 10km)

C - CORSEWALL FORMATION (MARCHBURN)
K - KIRKCOLM FORMATION (AFTON)
P - PORTPATRICK FORMATION (SCAR)
S - SCHINNEL FORMATION
Kf- KILFILLAN FORMATION (PYROXENOUS)
Q - QUEENSBURY FORMATION (INTERMEDIATE)
H - HAWICK FORMATION

A LITHOGEOCHEMICAL STUDY OF THE RHYNS OF GALLOWAY, SOUTH WEST SCOTLAND

FIGURE 293

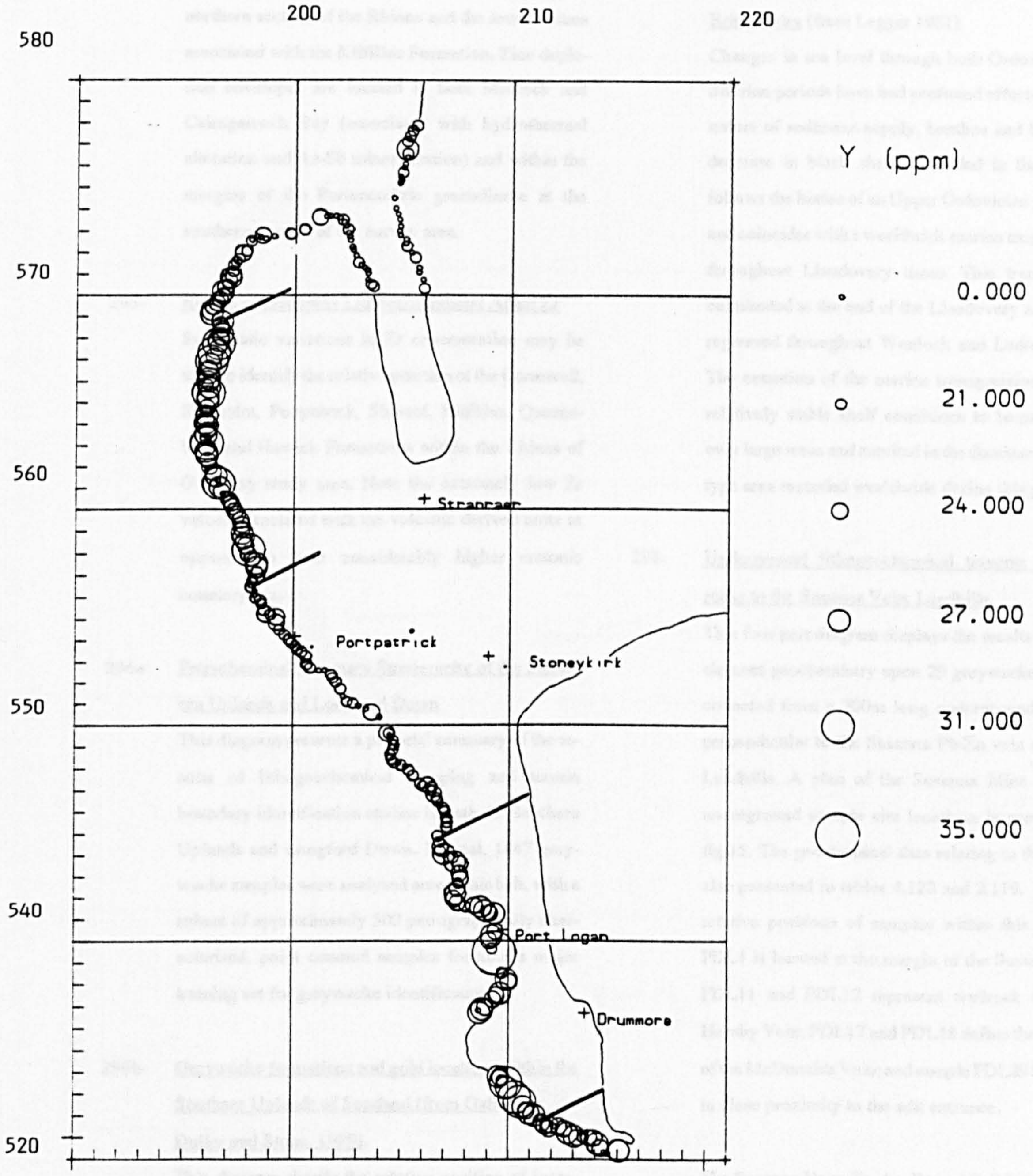

1 : 325,000 (32mm = 10km)

C - CORSEWALL FORMATION (MARCHBURN)
K - KIRKCOLM FORMATION (AFTON)
P - PORTPATRICK FORMATION (SCAR)
S - SCHINNEL FORMATION
Kf- KILFILLAN FORMATION (PYROXENOUS)
Q - QUEENSBURY FORMATION (INTERMEDIATE)
H - HAWICK FORMATION

294- Rhinns of Galloway Lithogeochemical Atlas: Zn
Relatively consistent Zn values displayed in the northern section of the Rhinns and the lower values associated with the Kilfillan Formation. Zinc depletion envelopes are located in both Morroch and Cairngarroch Bay (associated with hydrothermal alteration and As-Sb mineralisation) and within the margins of the Portencorkrie granodiorite at the southern margin of the survey area.

295- Rhinns of Galloway Lithogeochemical Atlas: Zr
Systematic variations in Zr concentration may be used to identify the relative position of the Corsewall, Kirkcolm, Portpatrick, Shinnel, Kilfillan, Queensbury and Hawick Formations within the Rhinns of Galloway study area. Note the extremely low Zr values associated with the volcanic derived units as opposed to their considerably higher cratonic counterparts.

296a- Petrochemical Summary Stratigraphy of the Southern Uplands and Longford Down
This diagram presents a pictorial summary of the results of lithogeochemical mapping and terrain boundary identification studies in both the Southern Uplands and Longford Down. In total, 1847 greywacke samples were analysed across this belt, with a subset of approximately 500 petrographically characterised, point counted samples forming a major training set for greywacke identification.

296b- Greywacke formations and gold locations within the Southern Uplands of Scotland (from Gallagher, Duller and Stone, 1989).
This diagram details the relative position of juxtaposed petrographically and geochemically distinct turbidite formations within the Southern Uplands Study area. Superimposed upon this diagram are the locations of individual in-situ gold occurrences in this region. Note that the identification of in-situ arsenopyrite-hosted gold in the Glendinning, Knipe, Cairngarroch and Talnotry deposits was first recorded by this study.

297- Changes in sea level and associated features through the Lower Palaeozoic stratigraphic Record in the British Isles (from Legget 1981)
Changes in sea level through both Ordovician and Silurian periods have had profound effects upon the nature of sediment supply, benthos and biota. The decrease in black shales recorded in the Silurian follows the hiatus of an Upper Ordovician glaciation and coincides with a worldwide marine transgression throughout Llandovery times. This transgression culminated at the end of the Llandovery and slowly regressed throughout Wenlock and Ludlow times. The cessation of the marine transgression allowed relatively stable shelf conditions to be established over large areas and resulted in the dominantly shelly type area recorded worldwide during this period.

298- Underground lithogeochemical traverse of wall-rocks to the Susanna Vein, Leadhills.
This four part diagram displays the results of multi-element geochemistry upon 29 greywacke samples collected from a 200m long underground traverse perpendicular to the Susanna Pb-Zn vein system at Leadhills. A plan of the Susanna Mine detailing underground sample site locations is presented in fig.15. The geochemical data relating to this plot is also presented in tables 4.122 and 2.119. Note the relative positions of samples within this traverse: PDL1 is located at the margin of the Susanna vein; PDL11 and PDL12 represent wallrock from the Humby Vein; PDL17 and PDL18 define the location of the McDonalds Vein; and sample PDL29 is located in close proximity to the adit entrance.

The Susanna Vein: Fe, As, Ba and Fe/Mg values are elevated in proximity to the Susanna vein whereas La, Pb, Sb, S, Th, K/Na, Al/Ca+Na, Nb/P, Rb/Sr, Ni/Co and Cu/Co exhibit varying degrees of depletion with respect to the average greywacke composition.

The Humby Vein: Al, K, As, Ba, Cu, La, Pb, Rb, Sb, Zn and K/Na, Fe/Mg, Al/Ca+Na, Rb/Sr and Cu/Co values are elevated in proximity to the vein whereas Na, Fe, Mg and Ca exhibit variable levels of depletion with respect to the average greywacke composition.

A LITHOGEOCHEMICAL STUDY OF THE RHYNS OF GALLOWAY, SOUTH WEST SCOTLAND

FIGURE 294

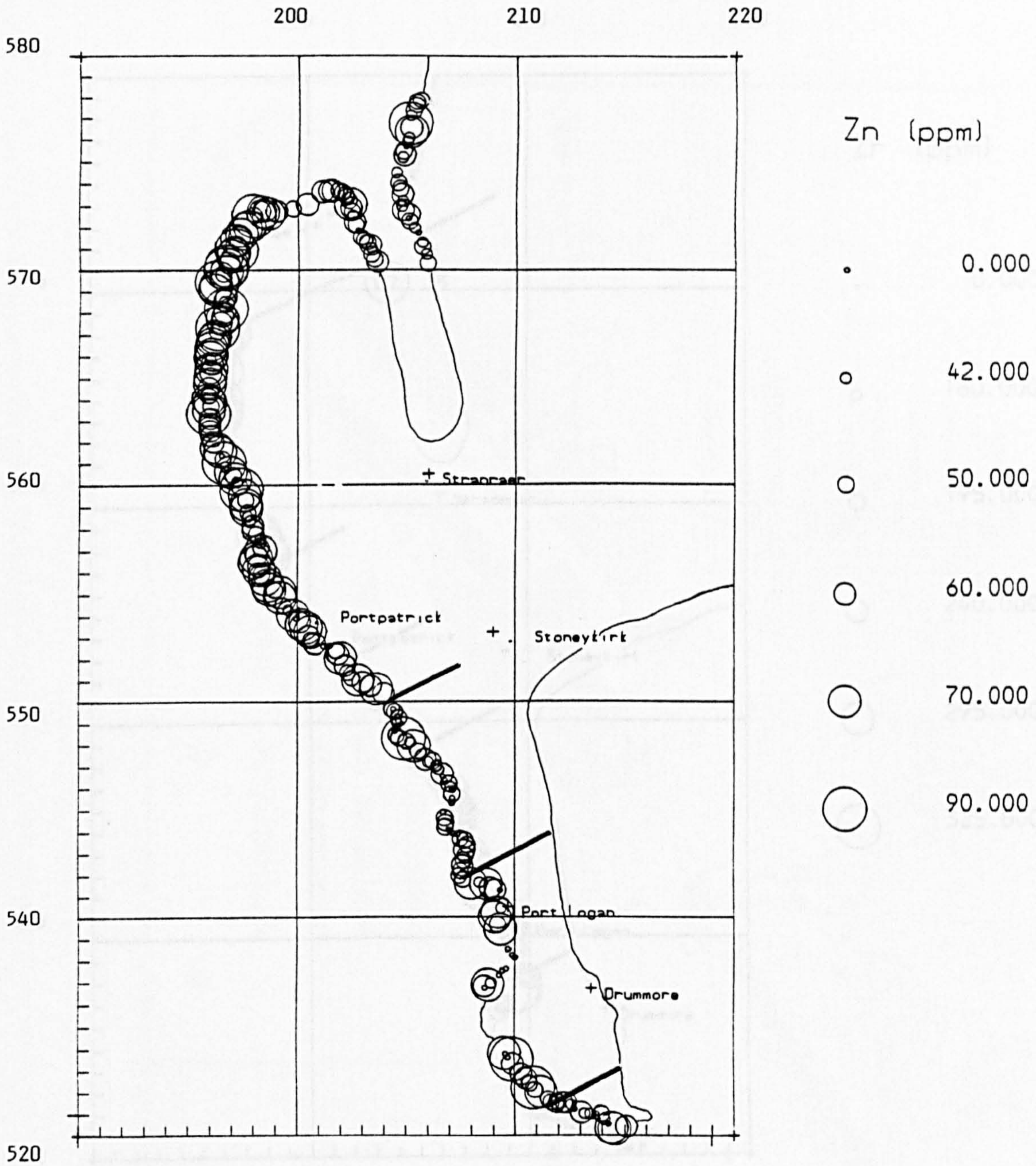

1 : 325,000 (32mm = 10km)

C - CORSEWALL FORMATION (MARCHBURN)
K - KIRKCOLM FORMATION (AFTON)
P - PORTPATRICK FORMATION (SCAR)
S - SCHINNEL FORMATION
Kf- KILFILLAN FORMATION (PYROXENOUS)
Q - QUEENSBURY FORMATION (INTERMEDIATE)
H - HAWICK FORMATION

A LITHOGEOCHEMICAL STUDY OF THE RHYNS OF GALLOWAY, SOUTH WEST SCOTLAND

FIGURE 295

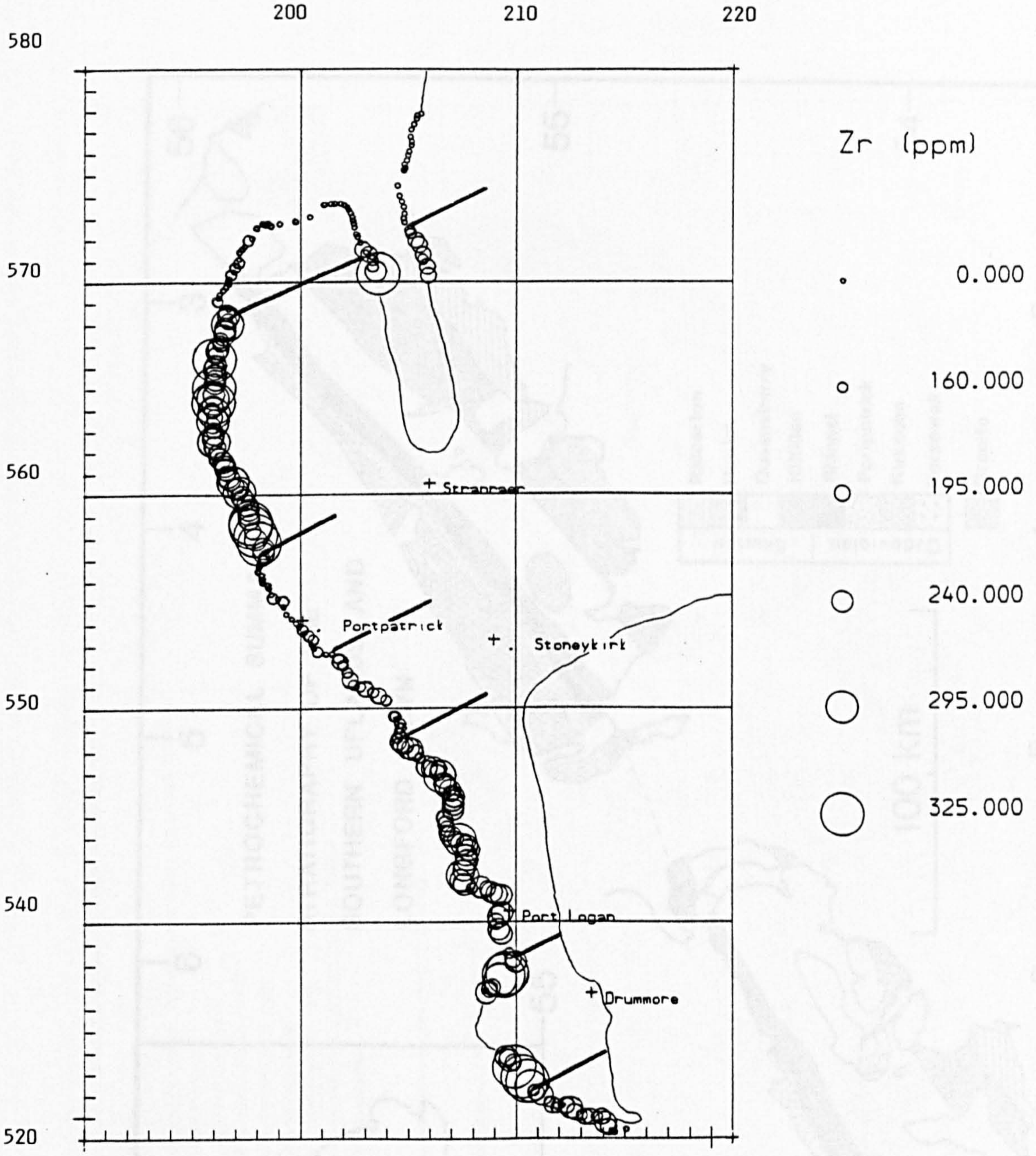

1 : 325,000 (32mm = 10km)

C - CORSEWALL FORMATION (MARCHBURN)
K - KIRKCOLM FORMATION (AFTON)
P - PORTPATRICK FORMATION (SCAR)
S - SCHINNEL FORMATION
Kf- KILFILLAN FORMATION (PYROXENOUS)
Q - QUEENSBURY FORMATION (INTERMEDIATE)
H - HAWICK FORMATION

FIGURE 296

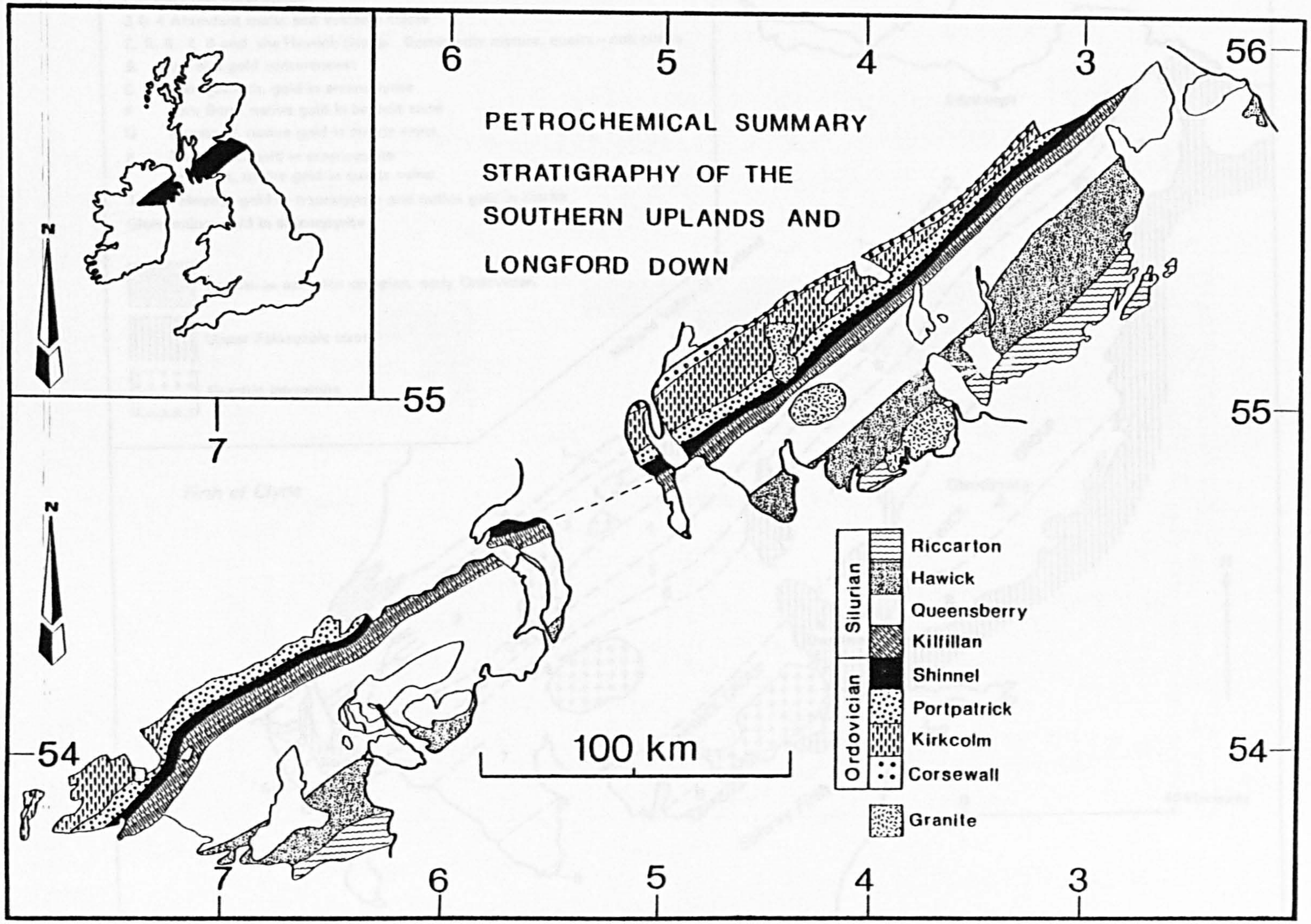
PETROCHEMICAL SUMMARY
STRATIGRAPHY OF THE
SOUTHERN UPLANDS AND
LONGFORD DOWN
N
N
6
5
4
3
56
55
7
55
54
54
100 km
7
6
5
4
3
Silurian
Ordovician
Riccarton
Hawick
Queensberry
Kilfillan
Shinnel
Portpatrick
Kirkcolm
Corsewall
Granite

FIGURE 296

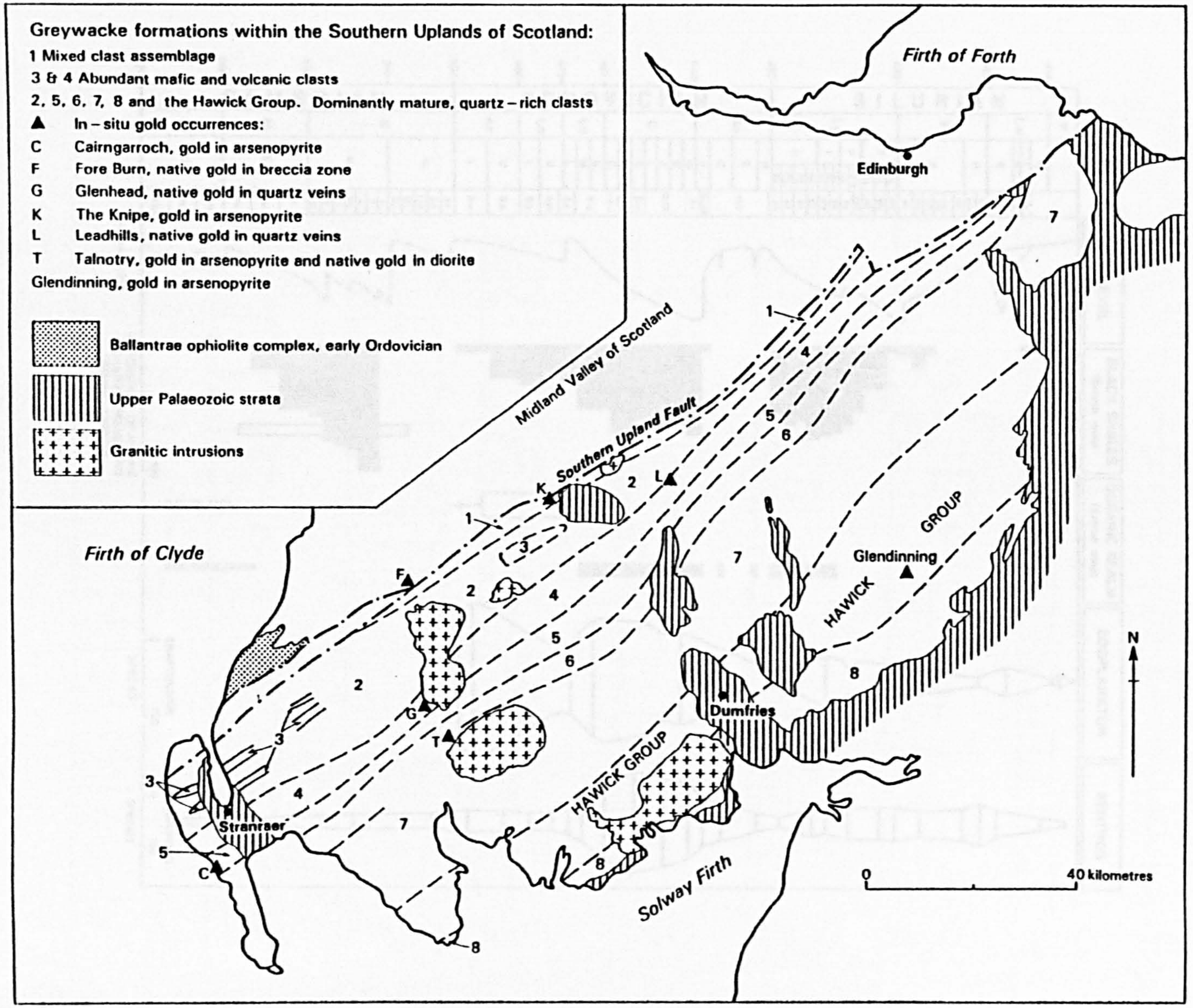

Greywacke formations within the Southern Uplands of Scotland:
1 Mixed clast assemblage
3 & 4 Abundant mafic and volcanic clasts
2, 5, 6, 7, 8 and the Hawick Group. Dominantly mature, quartz – rich clasts
▲ In – situ gold occurrences:
C Cairngarroch, gold in arsenopyrite
F Fore Burn, native gold in breccia zone
G Glenhead, native gold in quartz veins
K The Knipe, gold in arsenopyrite
L Leadhills, native gold in quartz veins
T Talnotry, gold in arsenopyrite and native gold in diorite
Glendinning, gold in arsenopyrite
Ballantrae ophiolite complex, early Ordovician
Upper Palaeozoic strata
Granitic intrusions
Firth of Forth
Edinburgh
Midland Valley of Scotland
Southern Upland Fault
Firth of Clyde
HAWICK GROUP
Glendinning
Dumfries
Stranraer
Solway Firth
N
0
40 kilometres

FIGURE 297

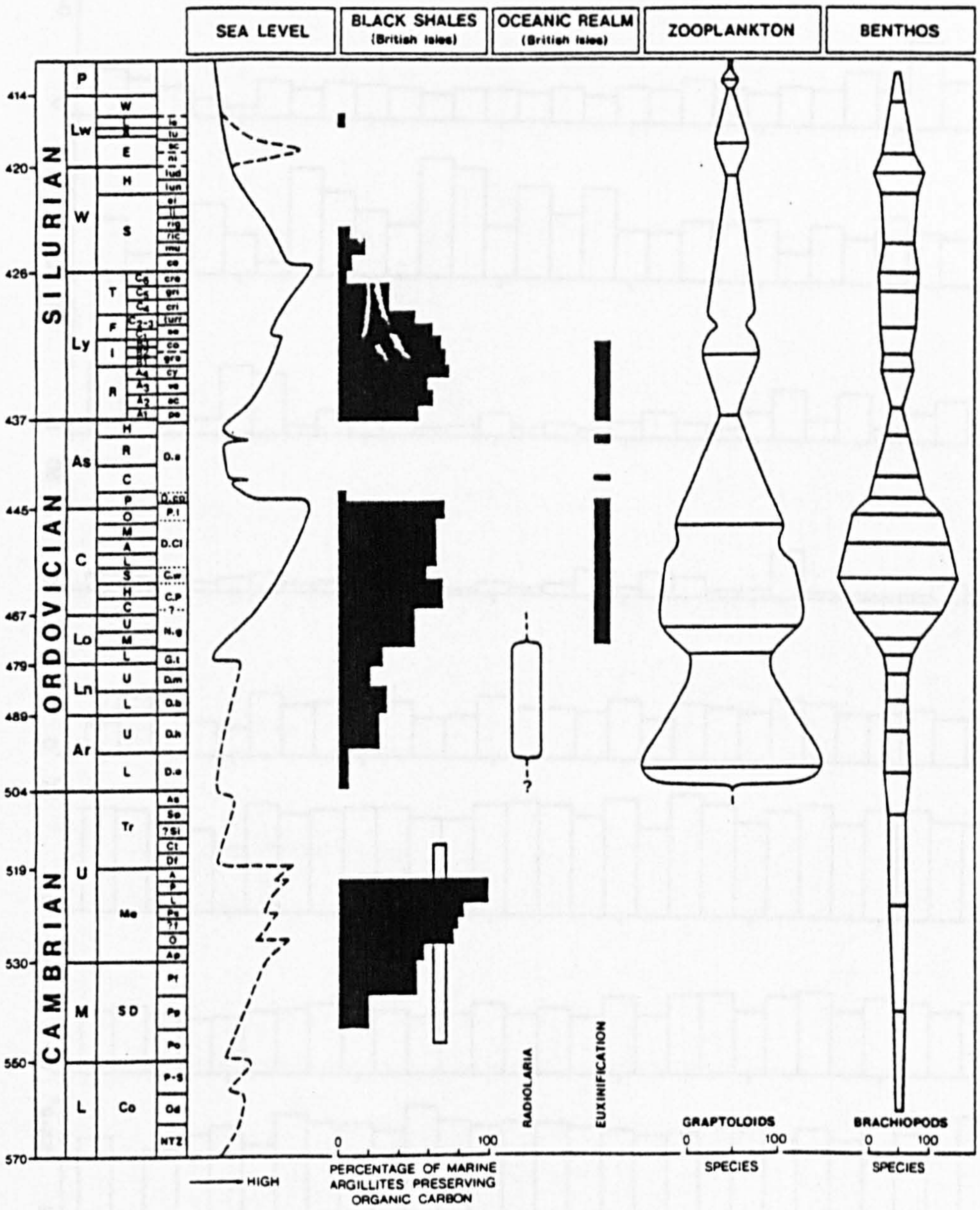
SEA LEVEL
BLACK SHALES (British Isles)
OCEANIC REALM (British Isles)
ZOOPLANKTON
BENTHOS
SILURIAN
ORDOVICIAN
CAMBRIAN
414
420
426
437
445
467
479
489
504
519
530
550
570
HIGH
PERCENTAGE OF MARINE ARGILLITES PRESERVING ORGANIC CARBON
RADIOLARIA
EUXINIFICATION
GRAPTOLOIDS
SPECIES
BRACHIOPODS
SPECIES

FIGURE 298 cont.

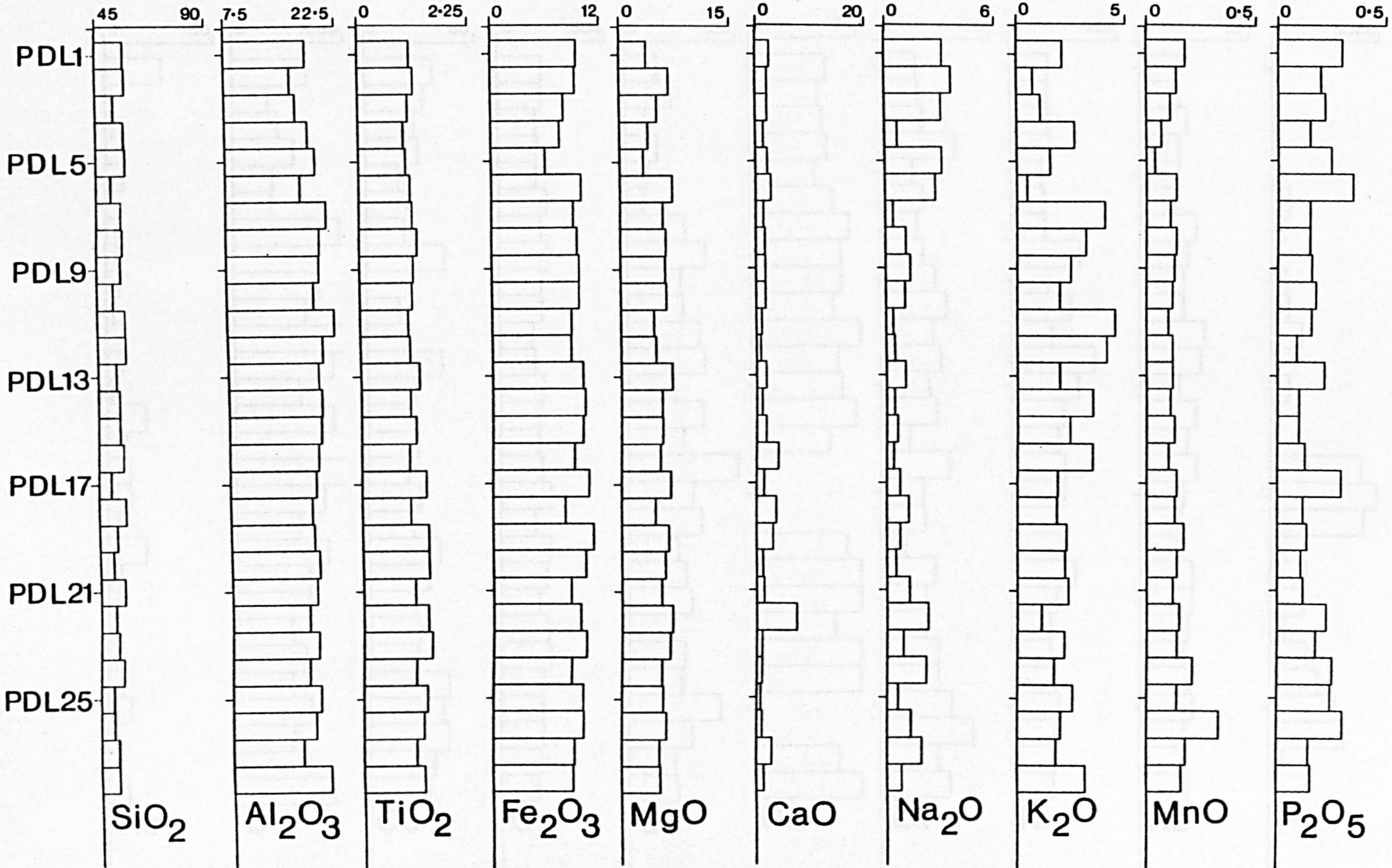

Leadhills : Underground Traverse

FIGURE 298 cont:

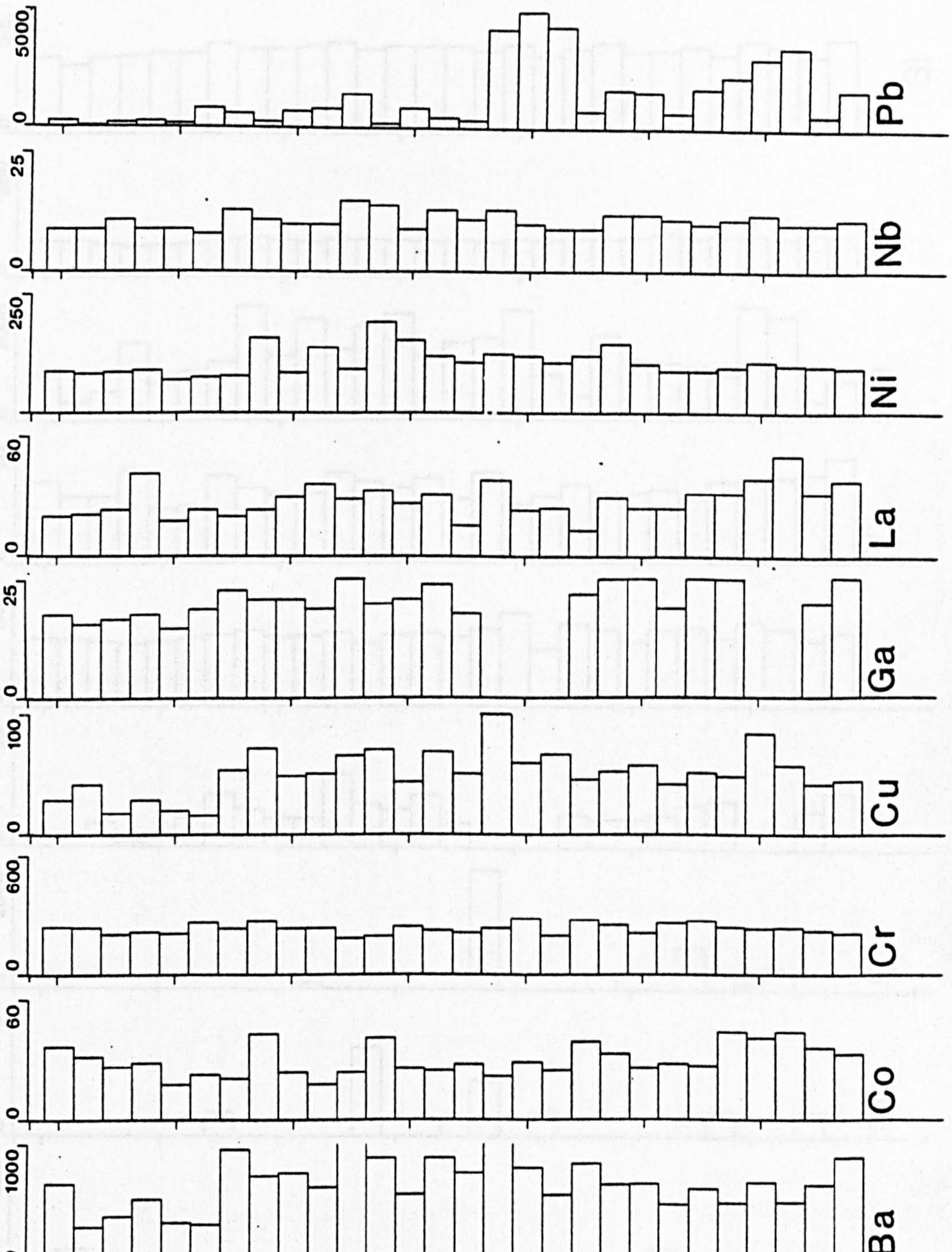

FIGURE 298 cont:

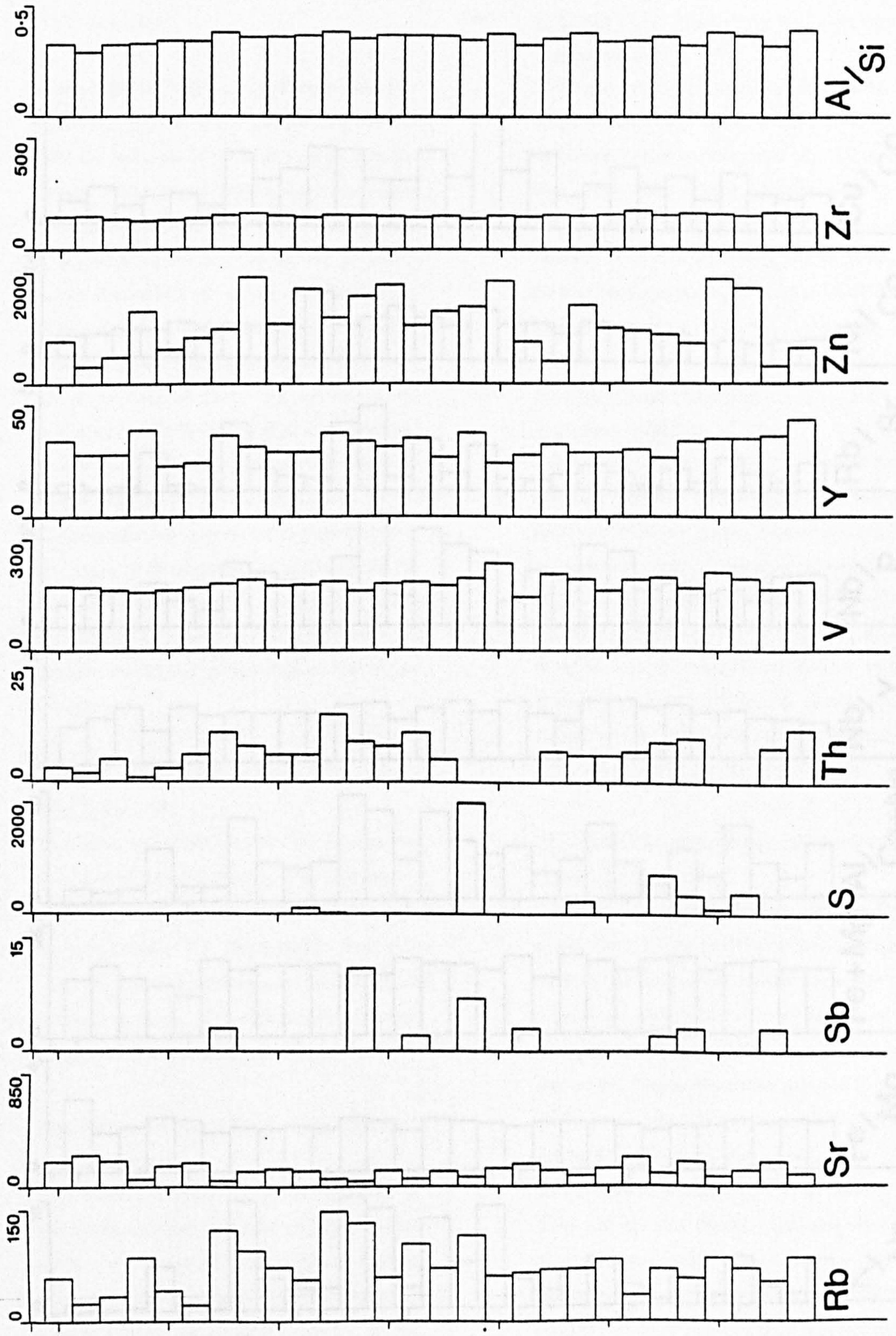

FIGURE 298 cont:

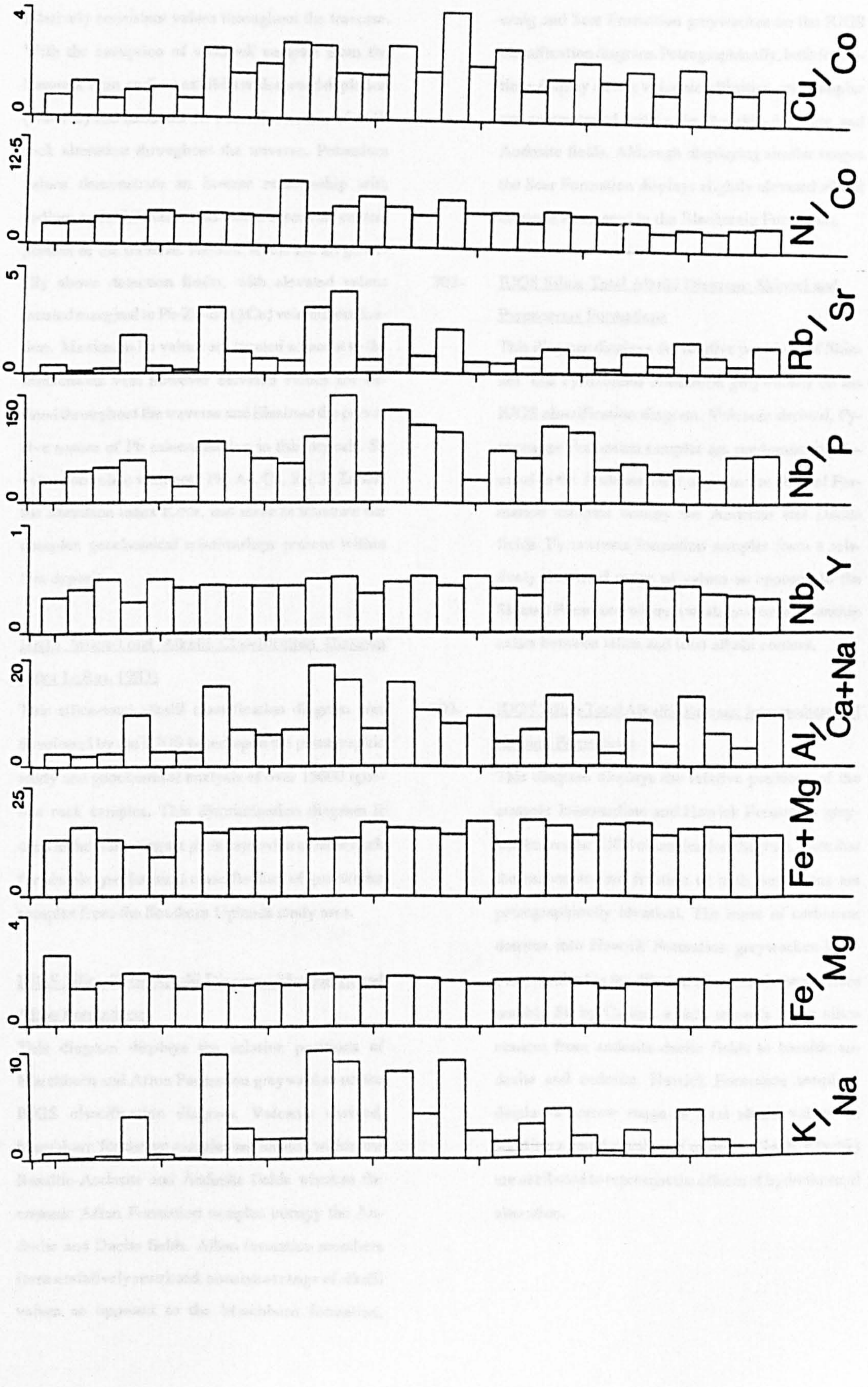

The McDonalds Vein: Fe, Mg, Ca, Pb, Zn, Cu and Sr values are elevated in proximity to the McDonalds vein whereas Na, K, Mg, Fe, Rb, K/Na, Al/Ca+Na, Rb/Sr are depleted.

In general Si, Mn, P, Cr, Nb, V, Y, Zr and Al/Si display relatively consistent values throughout the traverse. With the exception of wallrock samples from the Susanna Vein, sodium exhibits widespread depletion (Na<1%) and indicates the extensive nature of wallrock alteration throughout the traverse. Potassium values demonstrate an inverse relationship with sodium and exhibit elevated values across the central portion of the traverse. Arsenic levels are all generally above detection limits, with elevated values located marginal to Pb-Zn-Ba (±Cu) vein mineralisation. Maximum Pb values are located adjacent to the McDonalds vein however elevated values are defined throughout the traverse and illustrate the pervasive nature of Pb mineralisation in this deposit. Sb values correlate with both Pb, As, Cu, Rb, S, Zn and the alteration index K/Na, and serve to illustrate the complex geochemical relationships present within this deposit.

299- IUGS Silica-Total Alkalii Classification Diagram (after LeBas, 1983)

This silica-total alkalii classification diagram was developed by the IUGS based upon the petrographic study and geochemical analysis of over 15000 igneous rock samples. This discrimination diagram is used in the following six plots to provide a framework for simple geochemical classification of greywacke samples from the Southern Uplands study area.

300- IUGS Silica-Total Alkalii Diagram: Marchburn and Afton Formations.

This diagram displays the relative positions of Marchburn and Afton Formation greywackes on the IUGS classification diagram. Volcanic derived, Marchburn formation samples are located within the Basaltic-Andesite and Andesite fields whereas the cratonic Afton Formation samples occupy the Andesite and Dacite fields. Afton formation members form a relatively restricted, consistent range of alkalii values as opposed to the Marchburn formation, where a strong positive relationship exists between silica and alkalii.

301- IUGS Silica-Total Alkalii Diagram: Blackcraig and Scar Formations.

This diagram displays the relative positions of Blackcraig and Scar Formation greywackes on the IUGS classification diagram. Petrographically, both formations display strong volcanic affinities, and samples are concentrated within the Basaltic-Andesite and Andesite fields. Although displaying similar ranges the Scar Formation displays slightly elevated alkalii contents compared to the Blackcraig Formation.

302- IUGS Silica-Total Alkalii Diagram: Shinnel and Pyroxenous Formations

This diagram displays the relative positions of Shinnel and Pyroxenous Formation greywackes on the IUGS classification diagram. Volcanic derived, Pyroxenous Formation samples are predominantly located in the Andesite field whereas the Shinnel Formation samples occupy the Andesite and Dacite fields. Pyroxenous formation samples form a relatively restricted range of values as opposed to the Shinnel Formation where a weak inverse relationship exists between silica and total alkalii content.

303- IUGS Silica-Total Alkalii Diagram: Intermediate and Hawick Formations

This diagram displays the relative positions of the cratonic Intermediate and Hawick Formation greywackes on the IUGS classification diagram. Note that the carbonate-free fraction of both formations are petrographically identical. The input of carbonate detritus into Hawick Formation greywackes however, resulted in the dilution of major element values notably Si, by Ca and a shift towards lower silica content from andesite-dacite fields to basaltic-andesite and andesite. Hawick Formation members display a narrow range of total alkalii values. In addition a small number of samples (Na+K <3wt%) are attributed to represent the effects of hydrothermal alteration.

FIGURE 299

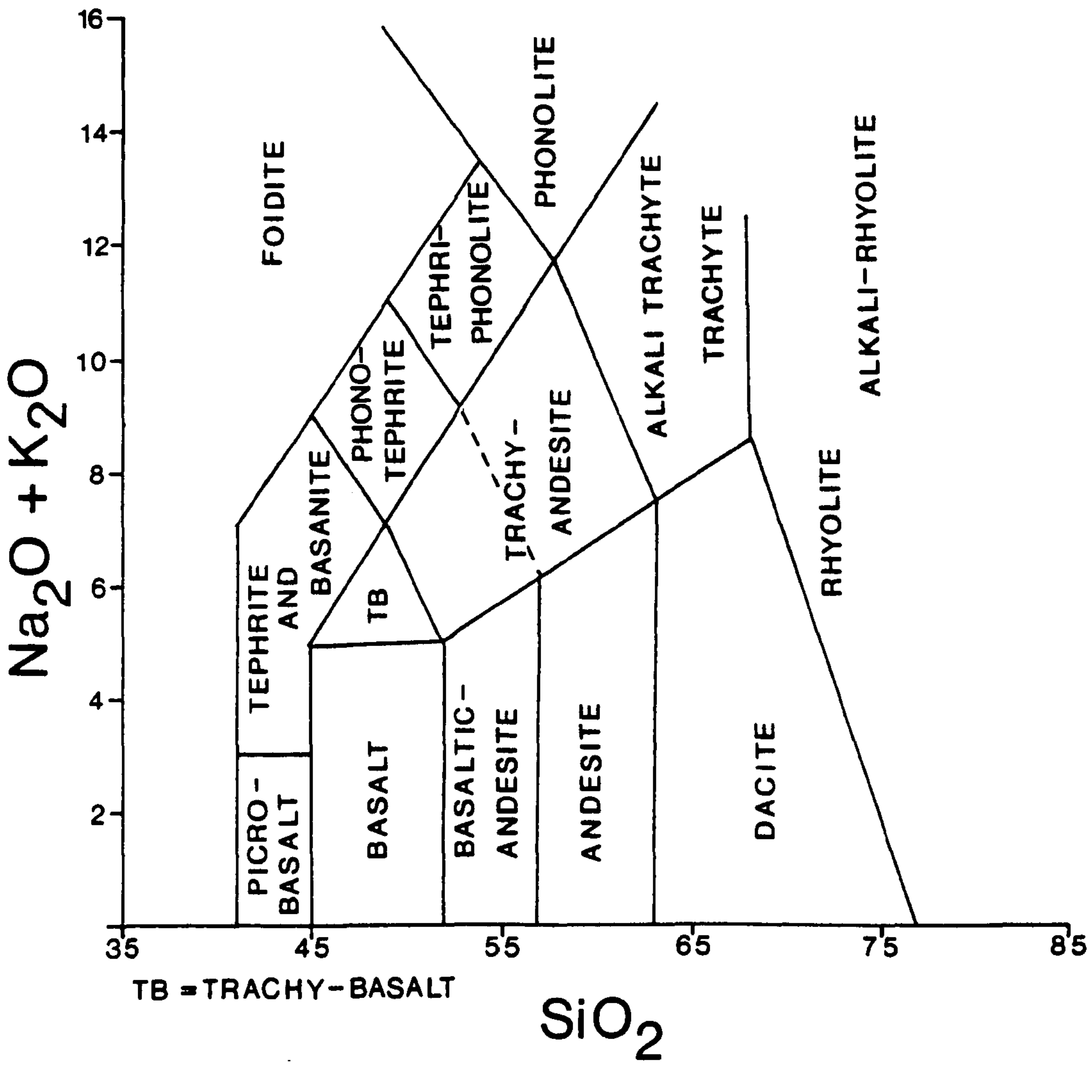
16
14
12
10
8
6
4
2
35
45
55
65
75
85
FOIDITE
PHONOLITE
TEPHRI-
PHONOLITE
PHONO-
TEPHRITE
BASANITE
TEPHRITE
AND
TB
TRACHY-
ANDESITE
ALKALI TRACHYTE
TRACHYTE
ALKALI-RHYOLITE
RHYOLITE
PICRO-
BASALT
BASALT
BASALTIC-
ANDESITE
ANDESITE
DACITE
$Na_2O + K_2O$
SiO_2
TB = TRACHY-BASALT

FIGURE 300

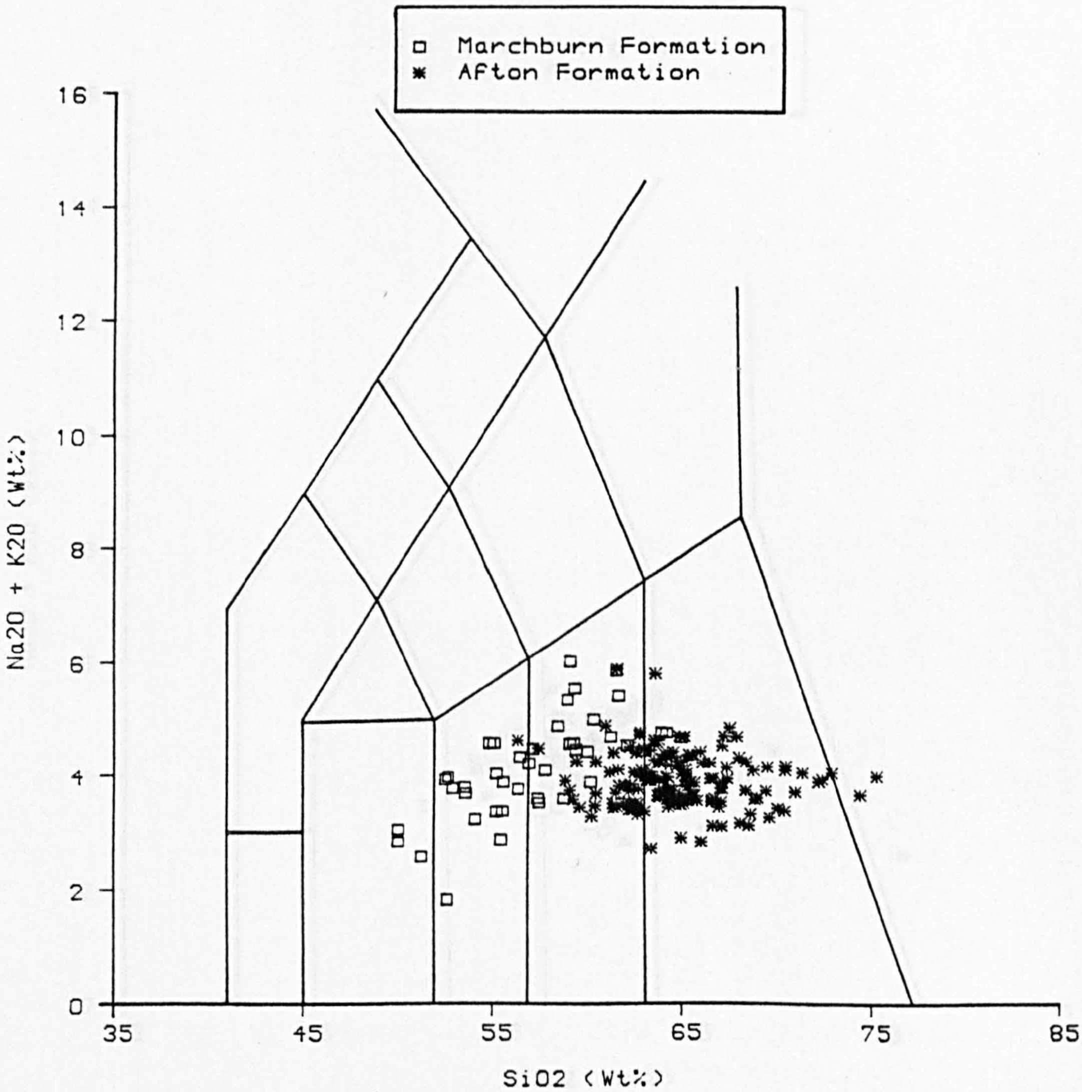

The IUGS Classification Diagram.

FIGURE 301

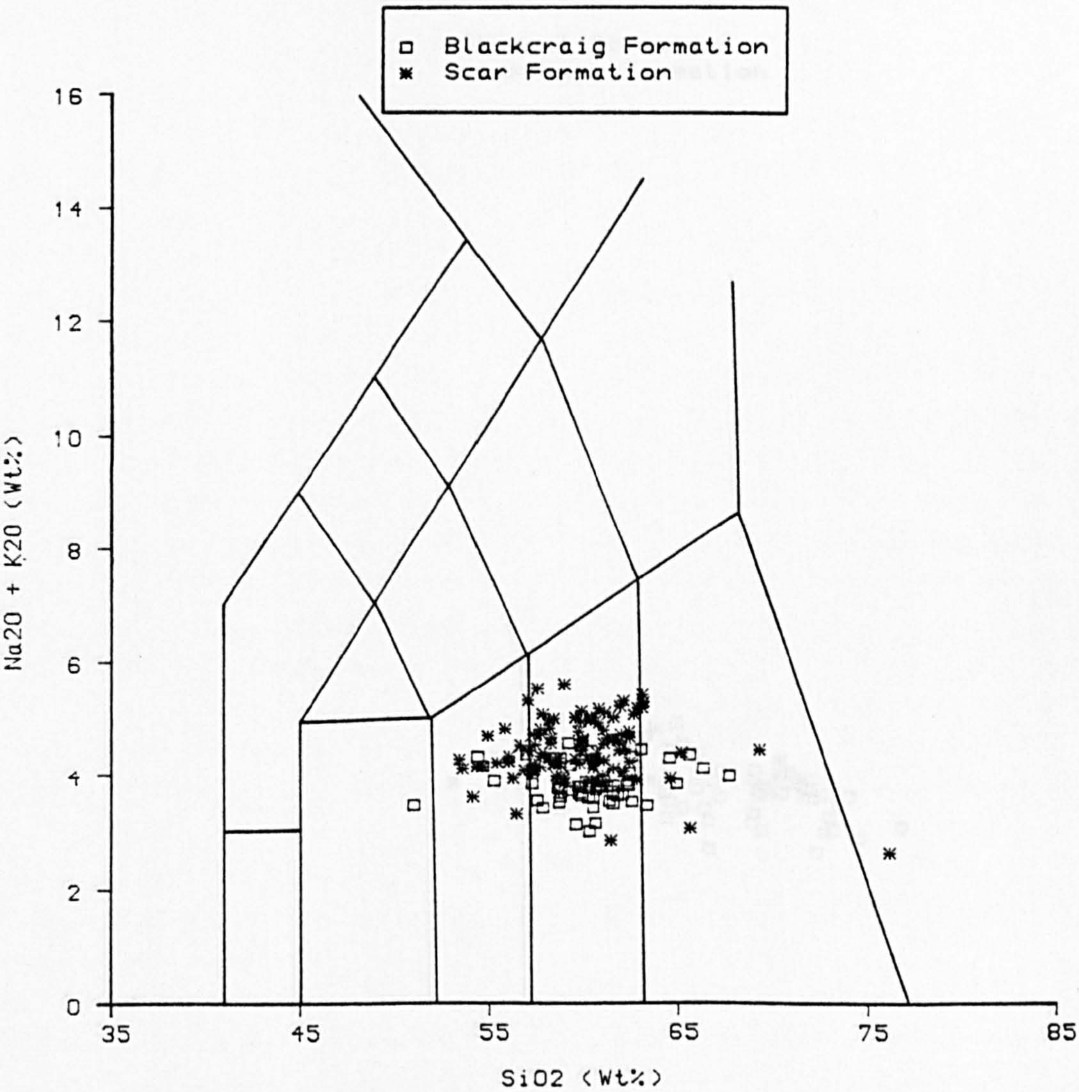

The IUGS Classification Diagram.

FIGURE 302

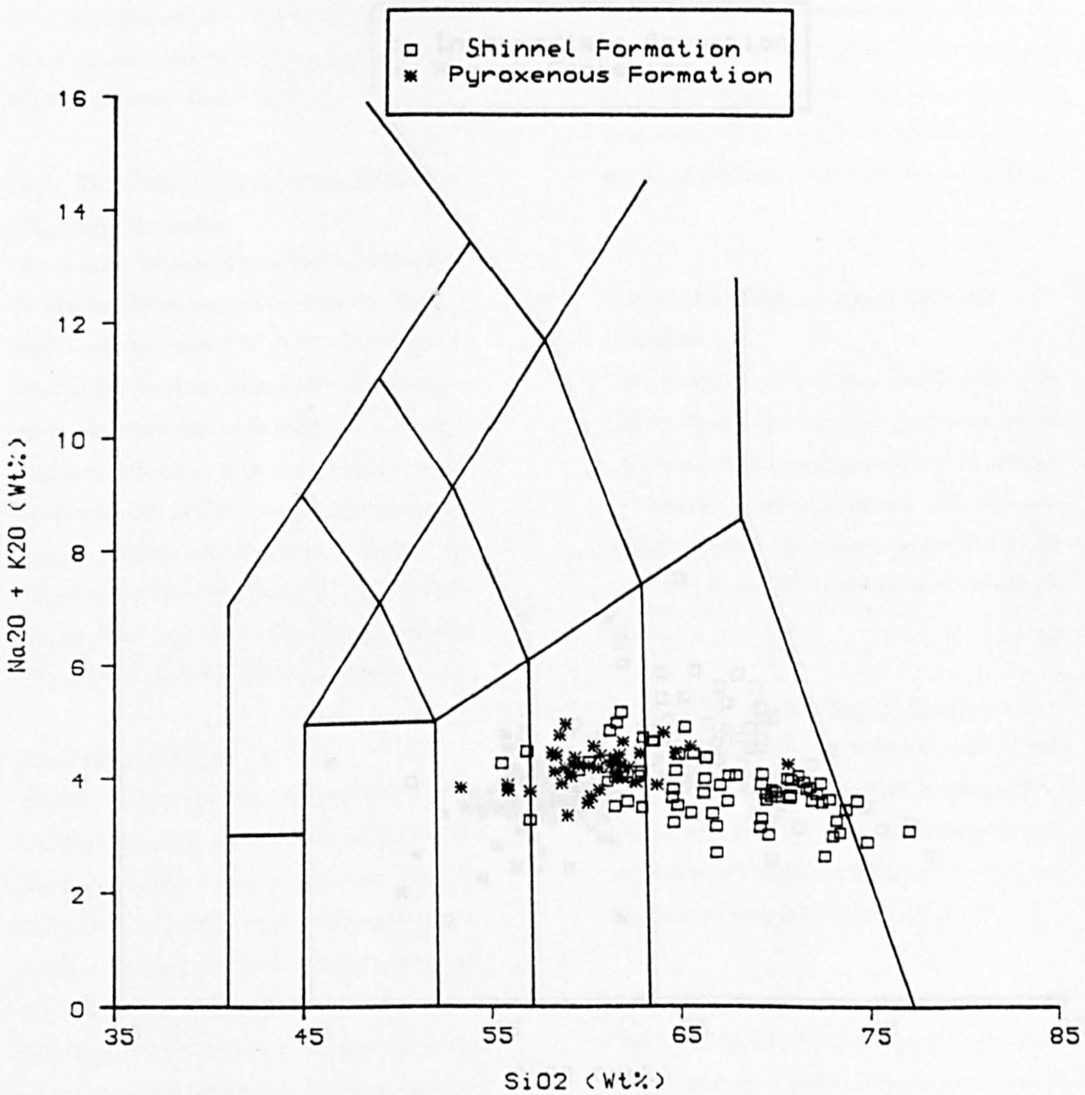

The IUGS Classification Diagram.

FIGURE 303

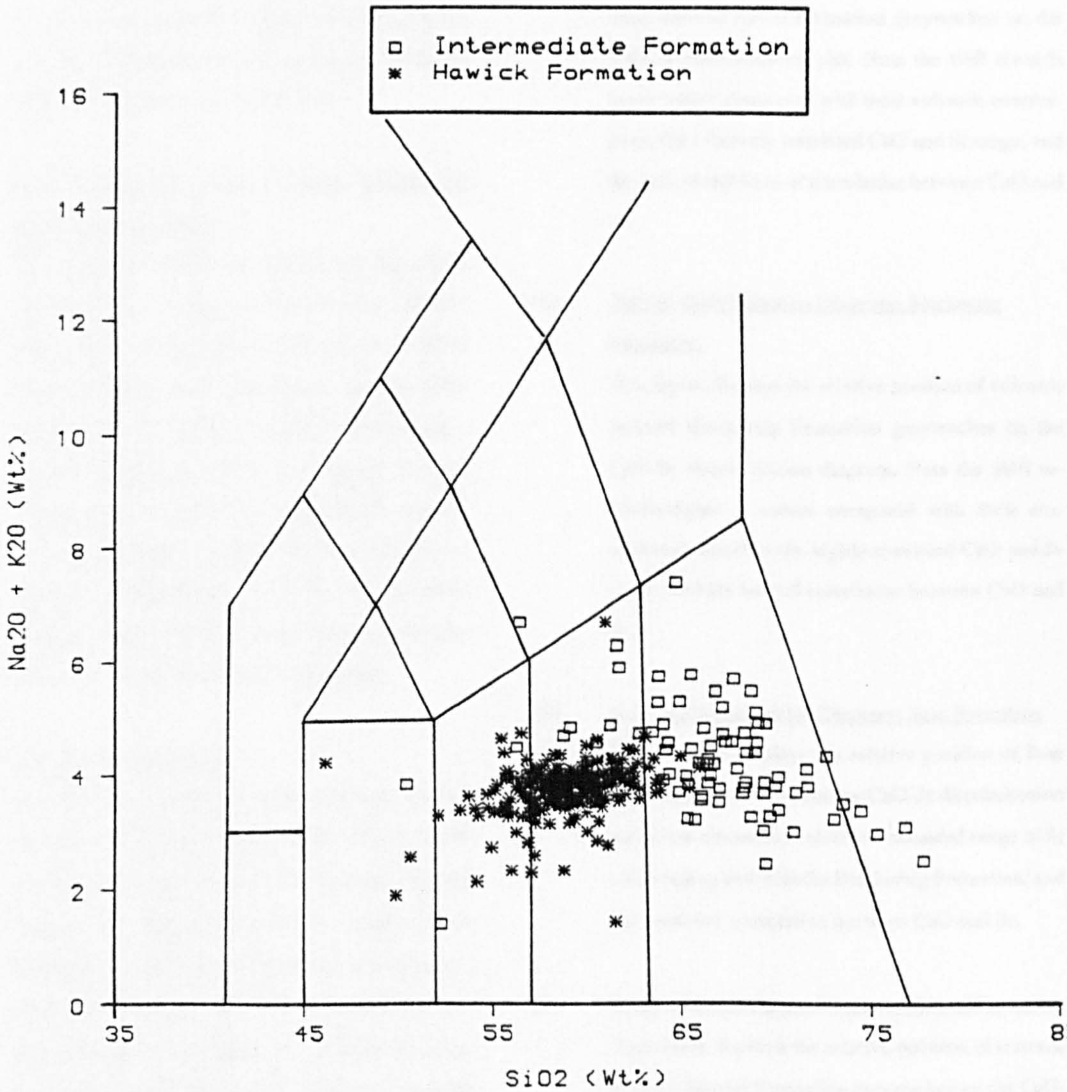

The IUGS Classification Diagram.

304- IUGS Silica-Total Alkalii Diagram: Glendinning Greywacke.
This diagram displays the position of cratonic derived Hawick Formation greywackes from the Glendinning regional study area. Note the relatively narrow, restricted range of total alkalii content which displays a weak positive correlation with silica values. As previously identified in Fig.303, silica values have been systematically depleted by the introduction of carbonate detritus and are located within the basaltic-andesite and andesite fields.

305- IUGS Silica-Total Alkalii Diagram: Glendinning Mineralised Greywacke.
This diagram displays the position of mineralised Hawick Formation greywackes from the Glendinning deposit and should be viewed in comparison with Fig. 304. Note the concentration of values in the basaltic-andesite and andesite fields, which display a decrease in minimum and increase in range of alkalii values compared with their unmineralised counterparts. In addition, a small subset of samples are located within the dacite field (Si > 61%) which indicate silica enrichment (silicification) together with major alkalii depletion (dickitisation).

306-410 Discrimination Diagrams
The following 96 discrimination diagrams display the major chemical characteristics of greywacke formations located within the Southern Uplands Study Area. All samples (with the exception of the Hawick Formation) have been subjected to petrographic examination (Floyd, 1981) and classified into their respective Formations on the basis of point-count and spatial information. Summary statistics relating to each formation are presented in tables 2.50-2.58. A table listing the most widely used greywacke discrimination diagrams and their respective authors is presented in table 1.68.

306- CaO-Sr Discrimination Diagram: Marchburn Formation. The CaO-Sr discrimination diagram defined by Caby (1977) is used in Figs. 306-312 to display the chemical variation present in the major petrographically distinct Formations located in the Southern Uplands Study Area. This figure displays the relative position of Marchburn Formation greywackes on the CaO-Sr discrimination diagram. Note the relatively restricted CaO range (2-5%); the wide range of Sr values (88-857ppm); and the lack of any form of correlation between CaO and Sr.

307- CaO-Sr Discrimination Diagram: Afton Formation
This diagram displays the relative position of cratonic derived Afton Formation greywackes on the CaO-Sr discrimination plot. Note the shift towards lower values compared with their volcanic counterparts; the relatively restricted CaO and Sr range; and the lack of any form of correlation between CaO and Sr.

308- CaO-Sr Discrimination Diagram: Blackcraig Formation.
This figure displays the relative position of volcanic derived Blackcraig Formation greywackes on the CaO-Sr discrimination diagram. Note the shift towards higher values compared with their cratonic counterparts; the highly restricted CaO and Sr range; and the lack of correlation between CaO and Sr.

309- CaO-Sr Discrimination Diagram: Scar Formation
This diagram displays the relative position of Scar Formation greywackes on the CaO-Sr discrimination plot. Note the positive shift and extended range of Sr values compared with the Blackcraig Formation; and the weak (+) correlation between CaO and Sr.

310- CaO-Sr Discrimination Diagram: Shinnel Formation
This figure displays the relative position of cratonic derived Shinnel Formation greywackes on the CaO-Sr discrimination diagram. Note the shift towards lower values compared with their juxtaposed volcanic counterparts; the extended CaO range; and the strong positive correlation between both elements.

311- CaO-Sr Discrimination Diagram: Pyroxenous Formation This diagram displays the relative position of volcanic derived Pyroxenous Formation greywackes on the CaO-Sr discrimination plot. Note the positive shift and extended range of Sr values compared with their cratonic counterparts; the re-

FIGURE 304

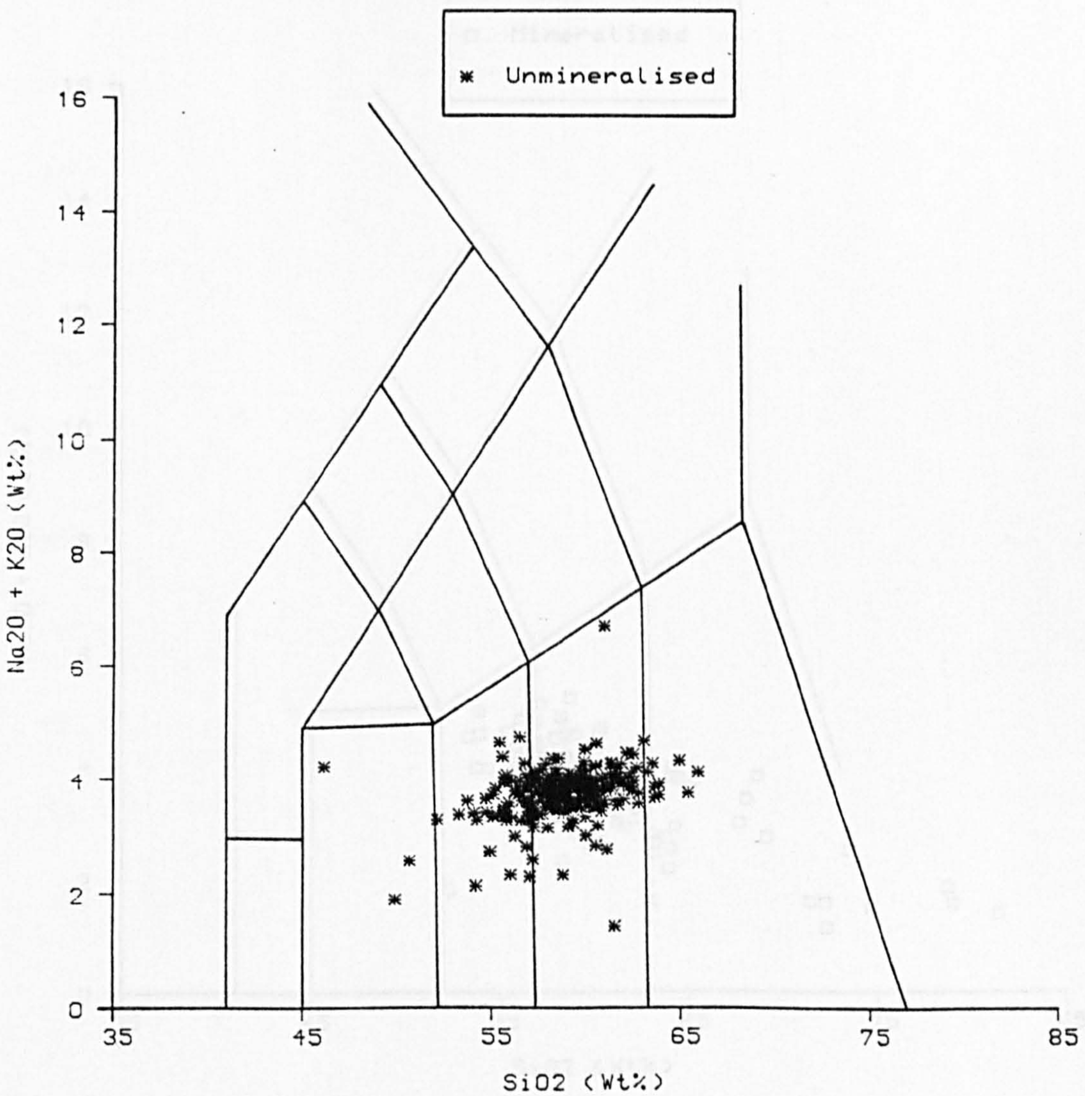

The IUGS Classification Diagram.

FIGURE 305

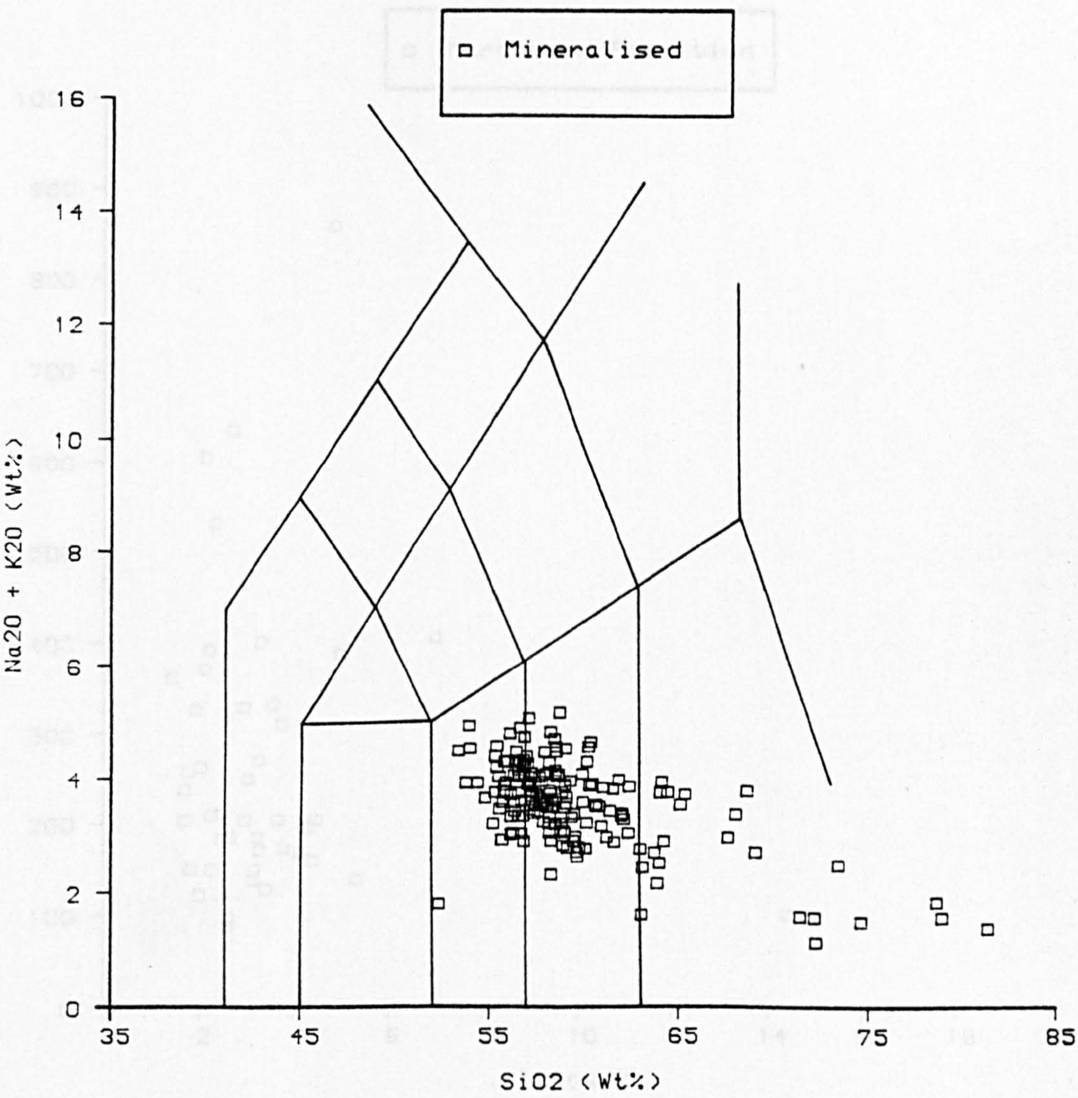

The IUGS Classification Diagram.

FIGURE 306

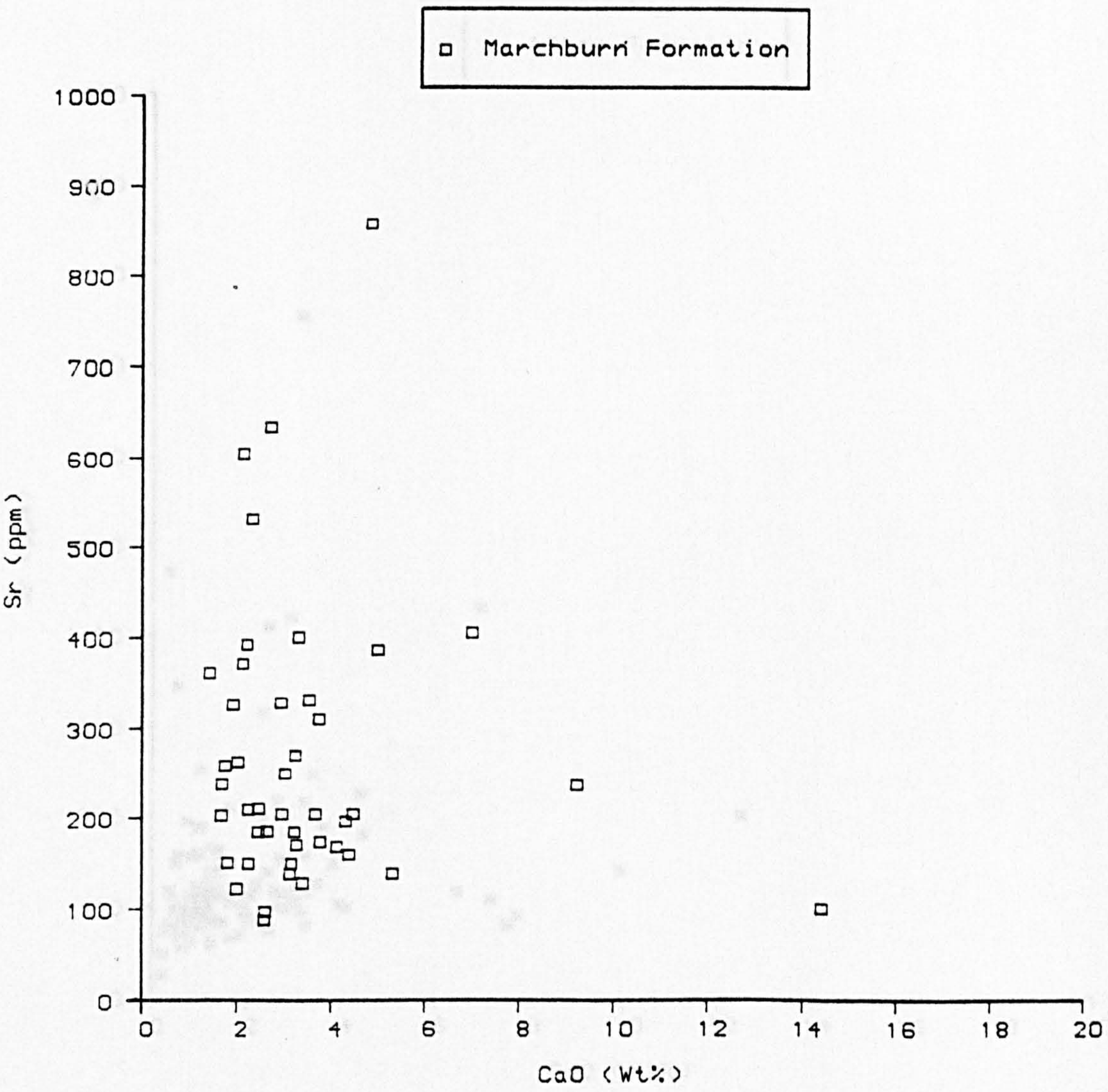

CaO-Sr Discrimination Diagram.

FIGURE 307

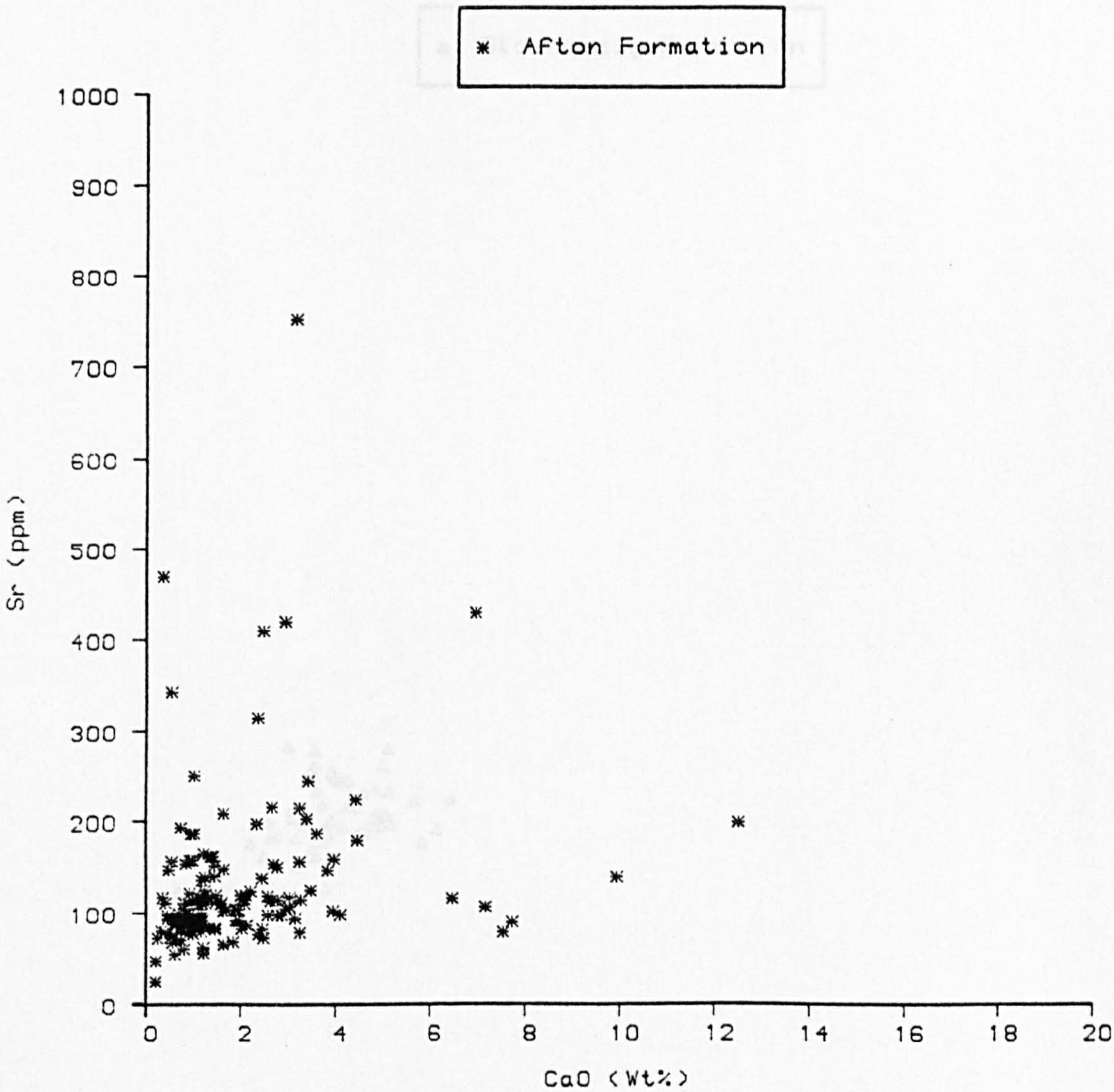

CaO-Sr Discrimination Diagram.

FIGURE 308

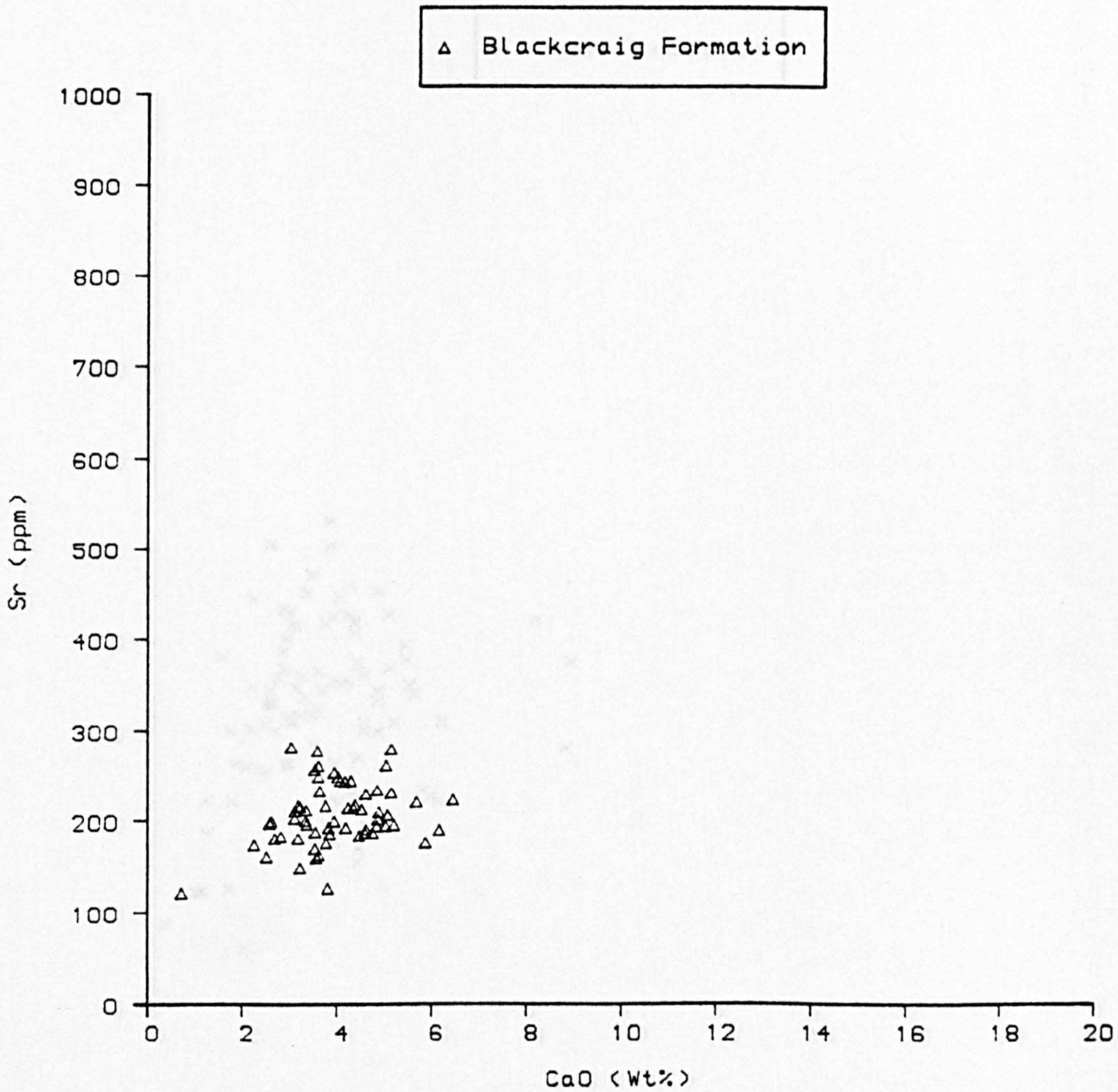

CaO-Sr Discrimination Diagram.

FIGURE 309

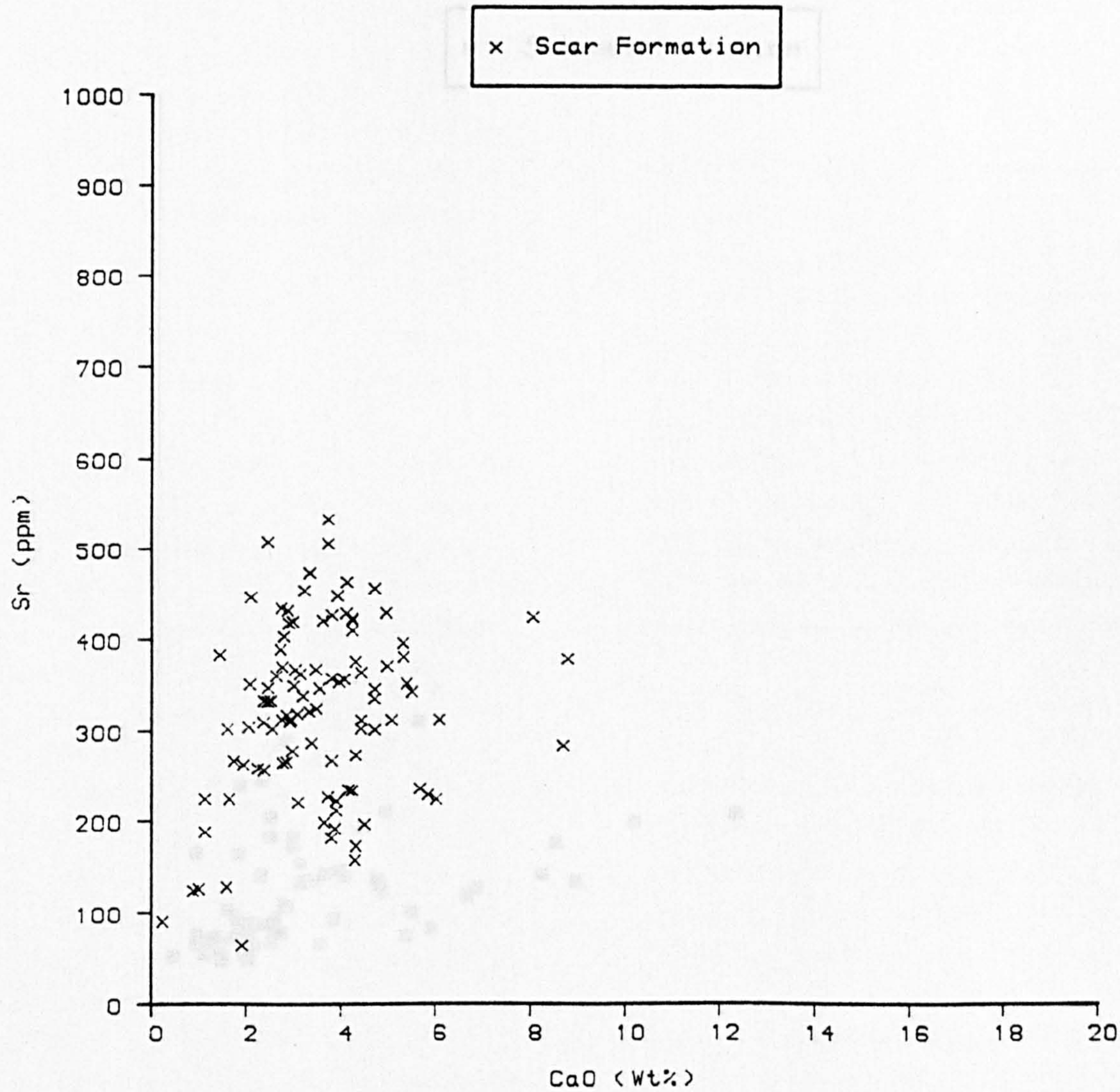

CaO-Sr Discrimination Diagram.

FIGURE 310

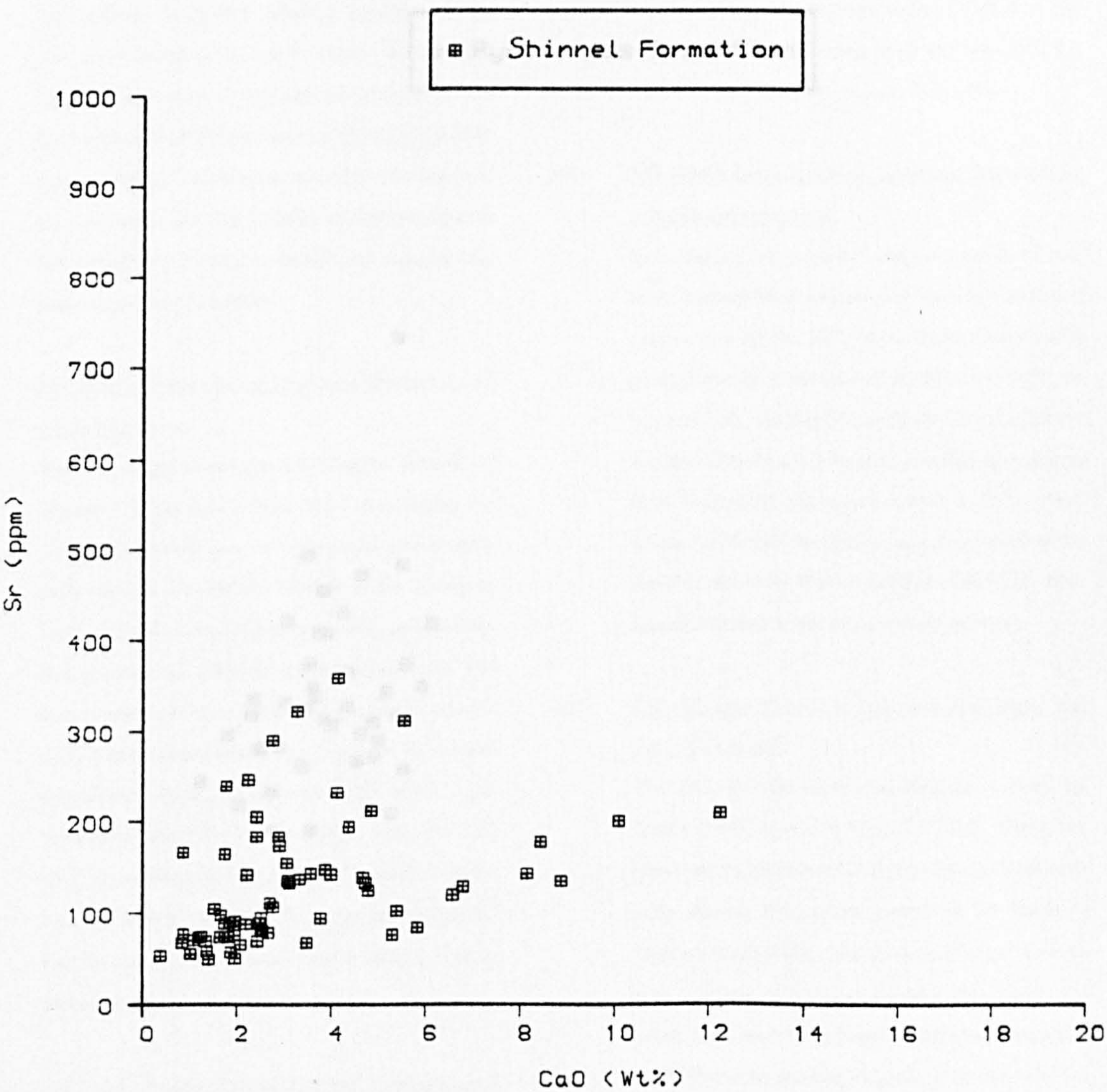

CaO-Sr Discrimination Diagram.

FIGURE 311

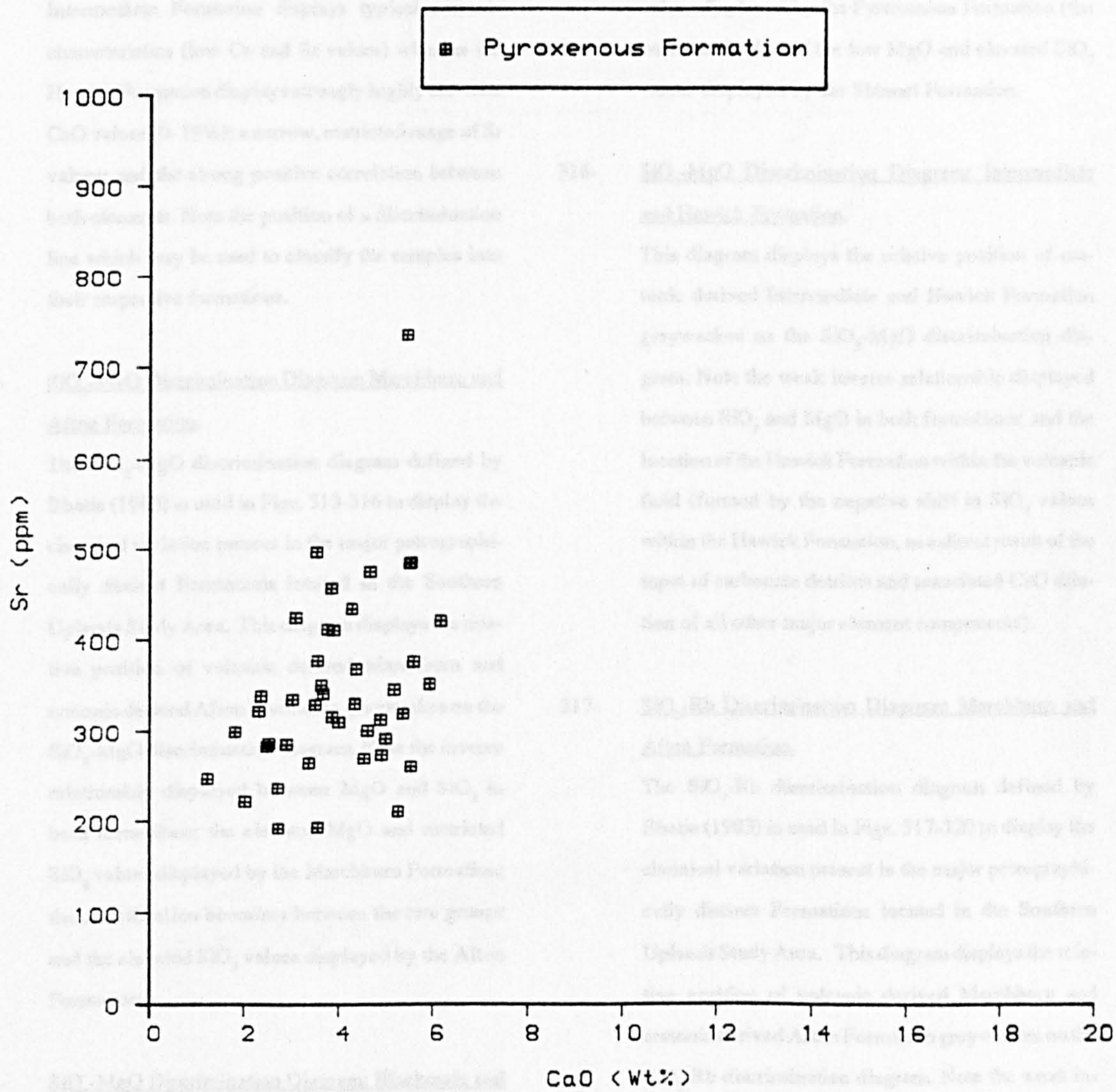

CaO-Sr Discrimination Diagram.

duced range of CaO values; and the weak (+) correlation between both elements.

312- <u>CaO-Sr Discrimination Diagram: Intermediate and Hawick Formation</u>.
This figure displays the relative position of cratonic derived Intermediate and Hawick Formation greywackes on the CaO-Sr discrimination diagram. The Intermediate Formation displays typical cratonic characteristics (low Ca and Sr values) whereas the Hawick Formation displays strongly highly elevated CaO values (0-19%); a narrow, restricted range of Sr values; and the strong positive correlation between both elements. Note the position of a discrimination line which may be used to classify the samples into their respective formations.

313- <u>SiO_2-MgO Discrimination Diagram: Marchburn and Afton Formation</u>.
The SiO_2-MgO discrimination diagram defined by Bhatia (1983) is used in Figs. 313-316 to display the chemical variation present in the major petrographically distinct Formations located in the Southern Uplands Study Area. This diagram displays the relative position of volcanic derived Marchburn and cratonic derived Afton Formation greywackes on the SiO_2-MgO discrimination diagram. Note the inverse relationship displayed between MgO and SiO_2 in both formations; the elevated MgO and restricted SiO_2 values displayed by the Marchburn Formation; the classification boundary between the two groups and the elevated SiO_2 values displayed by the Afton Formation.

314- <u>SiO_2-MgO Discrimination Diagram: Blackcraig and Scar Formation</u>.
This diagram displays the relative position of volcanic derived Blackcraig and Scar Formation greywackes on the SiO_2-MgO discrimination diagram. Note the strong inverse relationship displayed between SiO_2 and MgO in both formations; the elevated MgO values present in the Scar Formation; and the overlapping position of both groups within the volcanic field (defined in fig.316).

315- <u>SiO_2-MgO Discrimination Diagram: Pyroxenous and Shinnel Formation</u>.
This diagram displays the relative position of volcanic derived Pyroxenous and cratonic derived Shinnel Formation greywackes on the SiO_2-MgO discrimination diagram. Note the strong inverse relationship displayed between MgO and SiO_2 in both formations; the elevated MgO and restricted SiO_2 values displayed by the Pyroxenous Formation (the volcanic field); and the low MgO and elevated SiO_2 values displayed by the Shinnel Formation.

316- <u>SiO_2-MgO Discrimination Diagram: Intermediate and Hawick Formation</u>.
This diagram displays the relative position of cratonic derived Intermediate and Hawick Formation greywackes on the SiO_2-MgO discrimination diagram. Note the weak inverse relationship displayed between SiO_2 and MgO in both formations; and the location of the Hawick Formation within the volcanic field (formed by the negative shift in SiO_2 values within the Hawick Formation, as a direct result of the input of carbonate detritus and associated CaO dilution of all other major element components).

317- <u>SiO_2-Rb Discrimination Diagram: Marchburn and Afton Formation.</u>
The SiO_2-Rb discrimination diagram defined by Bhatia (1983) is used in Figs. 317-320 to display the chemical variation present in the major petrographically distinct Formations located in the Southern Uplands Study Area. This diagram displays the relative position of volcanic derived Marchburn and cratonic derived Afton Formation greywackes on the SiO_2-Rb discrimination diagram. Note the weak inverse relationship displayed between Rb and SiO_2 in the Afton formation; the elevated Rb and SiO_2 values displayed by Afton Formation; the classification boundary between the two groups and the restricted SiO_2 and relatively low Rb values displayed by the Marchburn Formation.

318- <u>SiO_2-Rb Discrimination Diagram: Blackcraig and Scar Formation.</u>
This diagram displays the relative position of volcanic derived Blackcraig and Scar Formation grey-

FIGURE 312

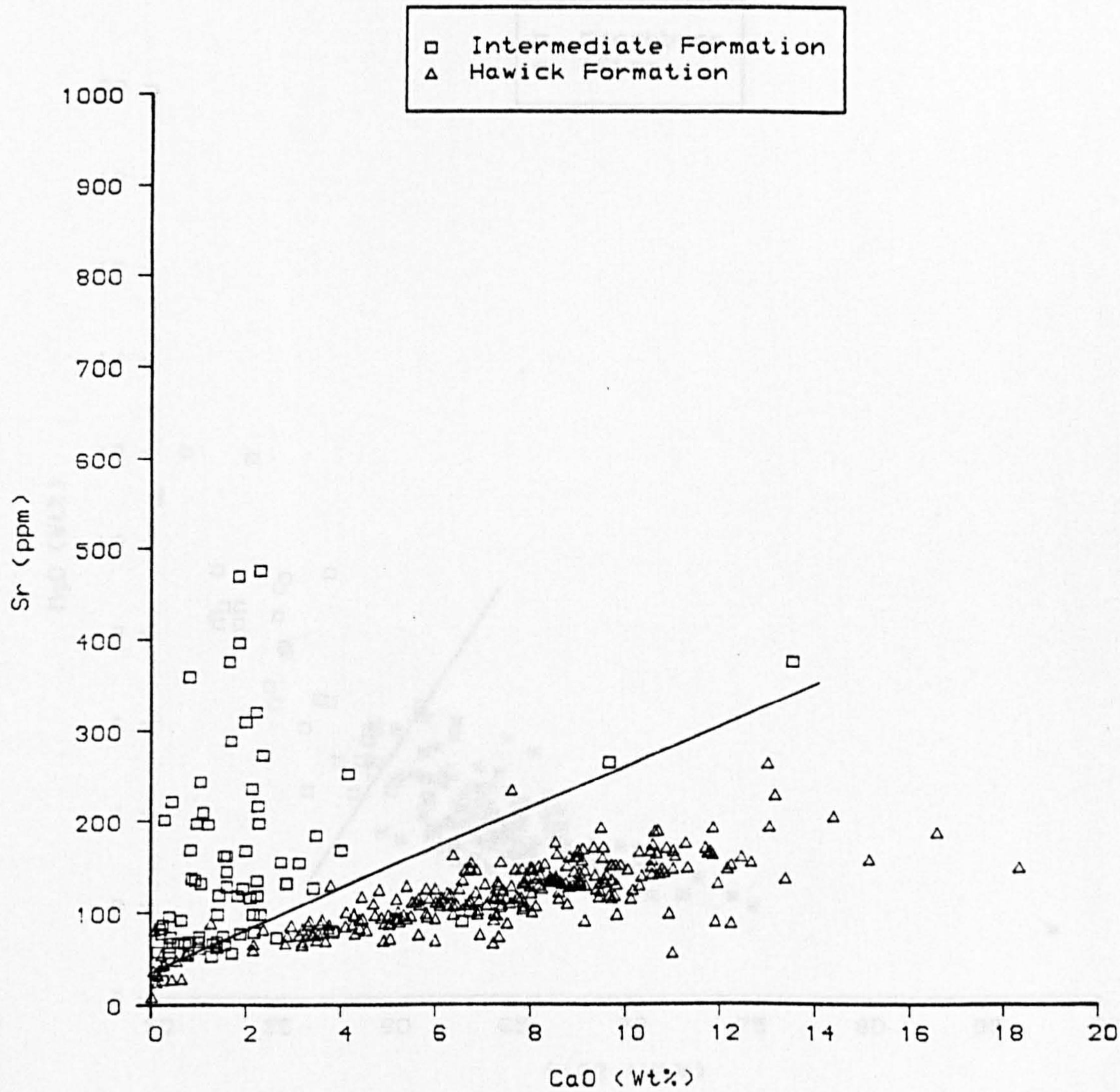

CaO-Sr Discrimination Diagram.

FIGURE 313

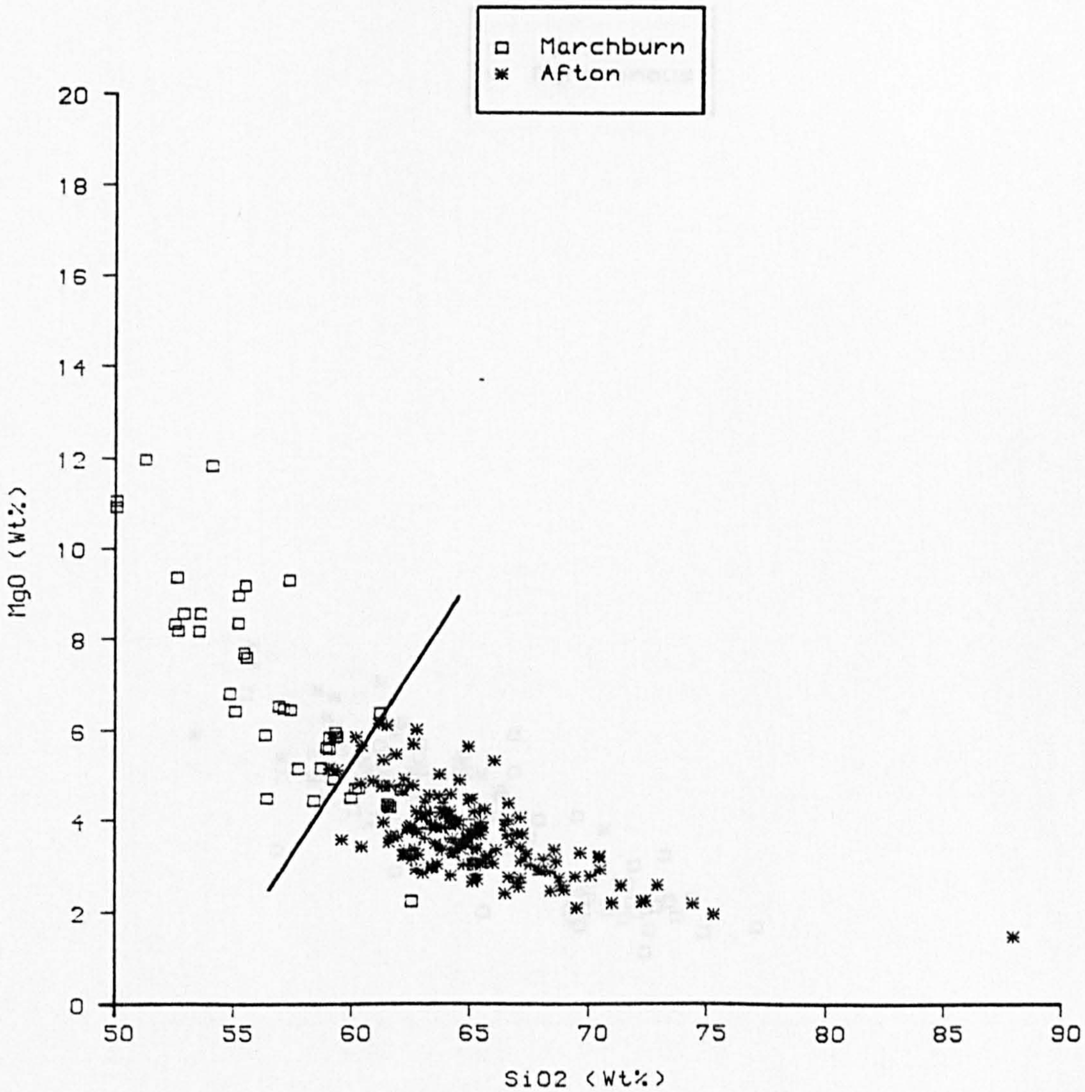

SiO2-MgO Discrimination Diagram (Bhatia, 1983).

FIGURE 314

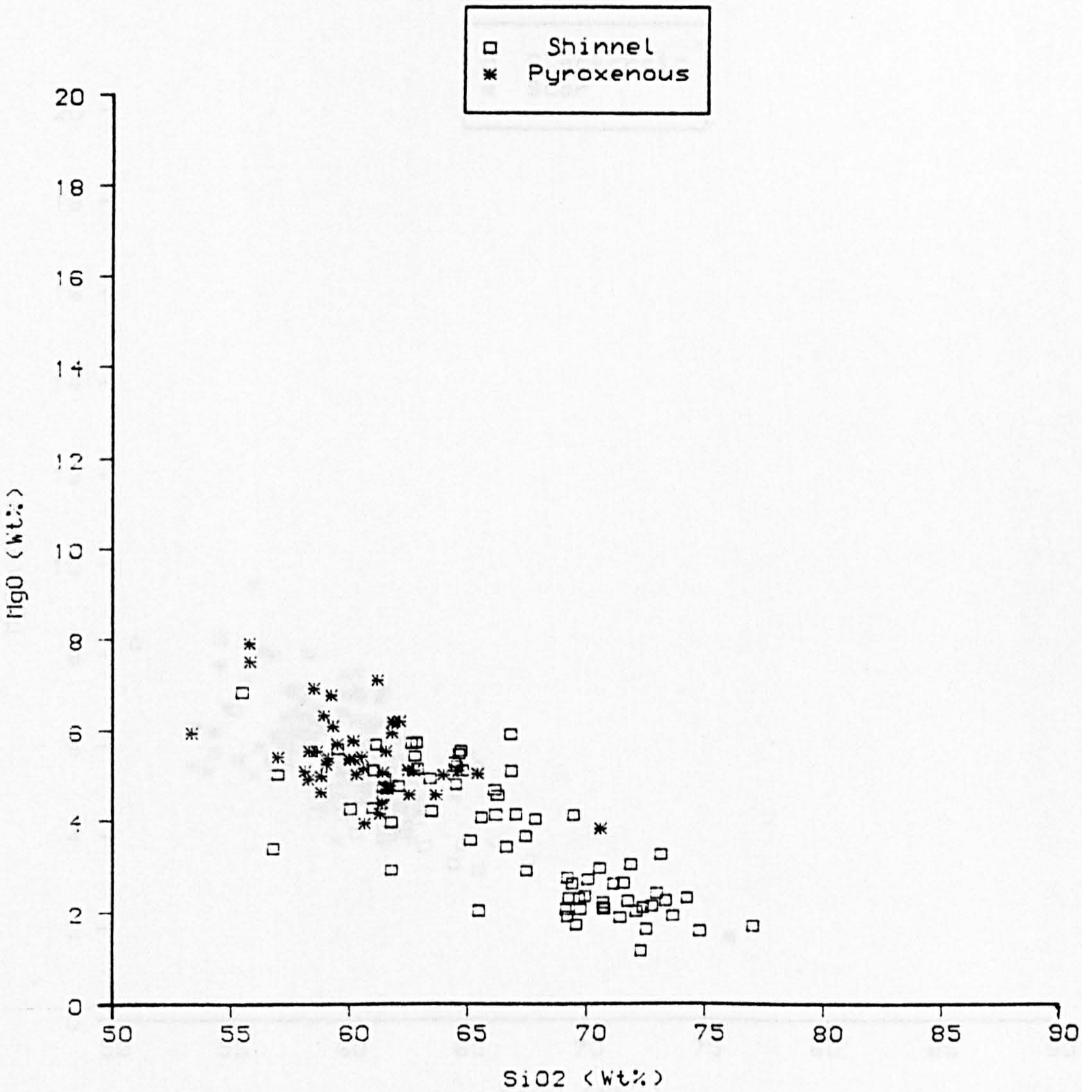

SiO2-MgO Discrimination Diagram (Bhatia, 1983).

FIGURE 315

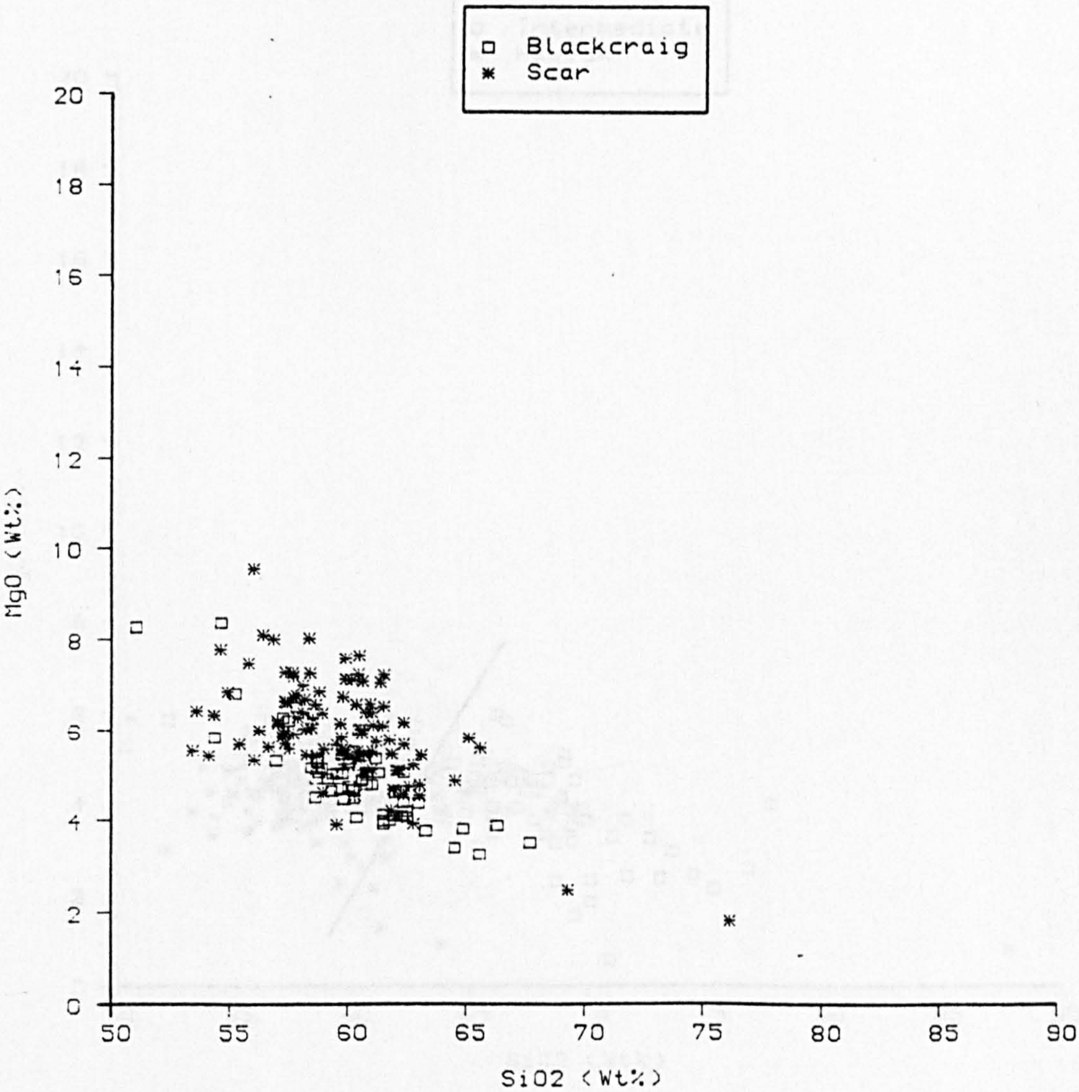

SiO2-MgO Discrimination Diagram (Bhatia, 1983).

FIGURE 316

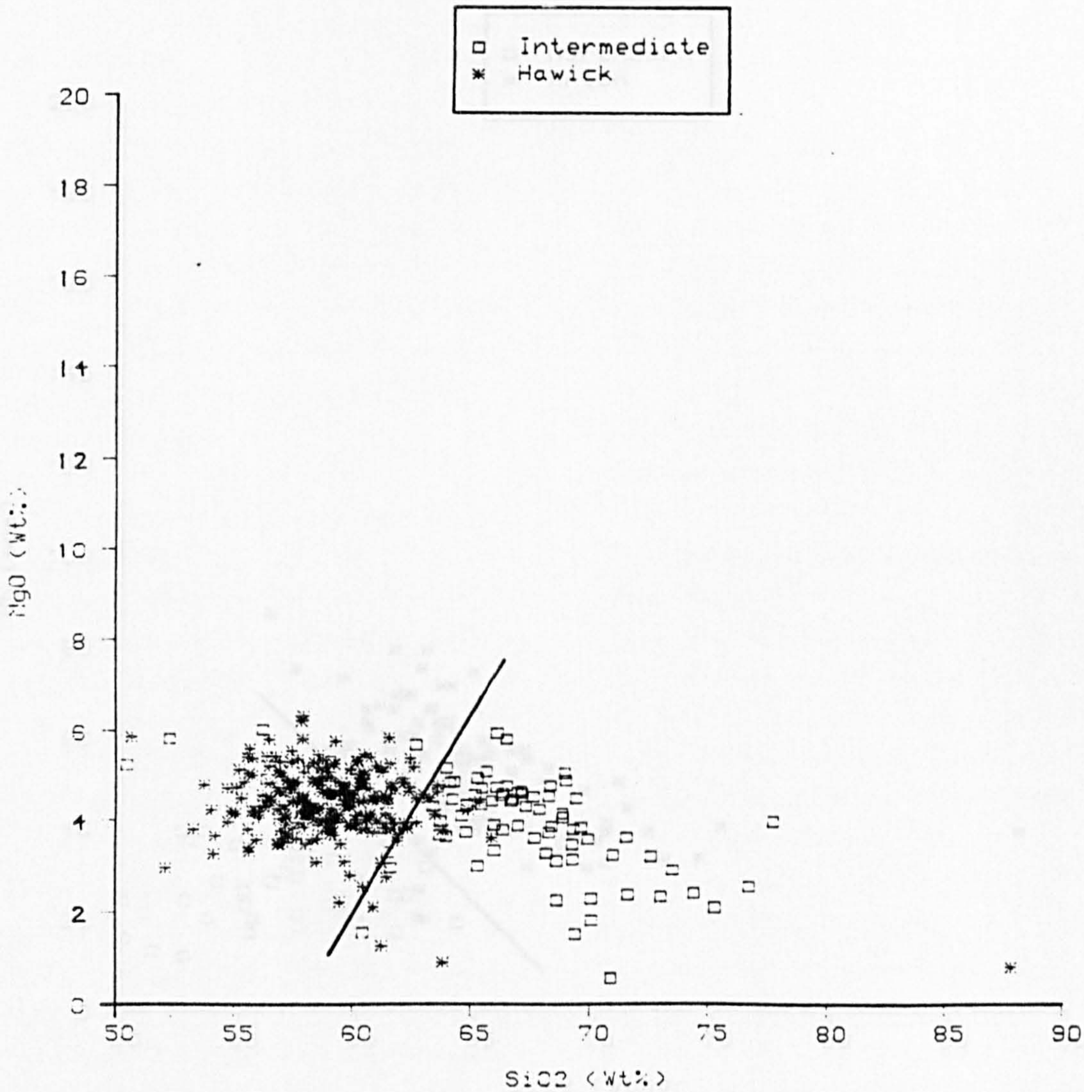

SiO2-MgO Discrimination Diagram (Bhatia, 1983).

FIGURE 317

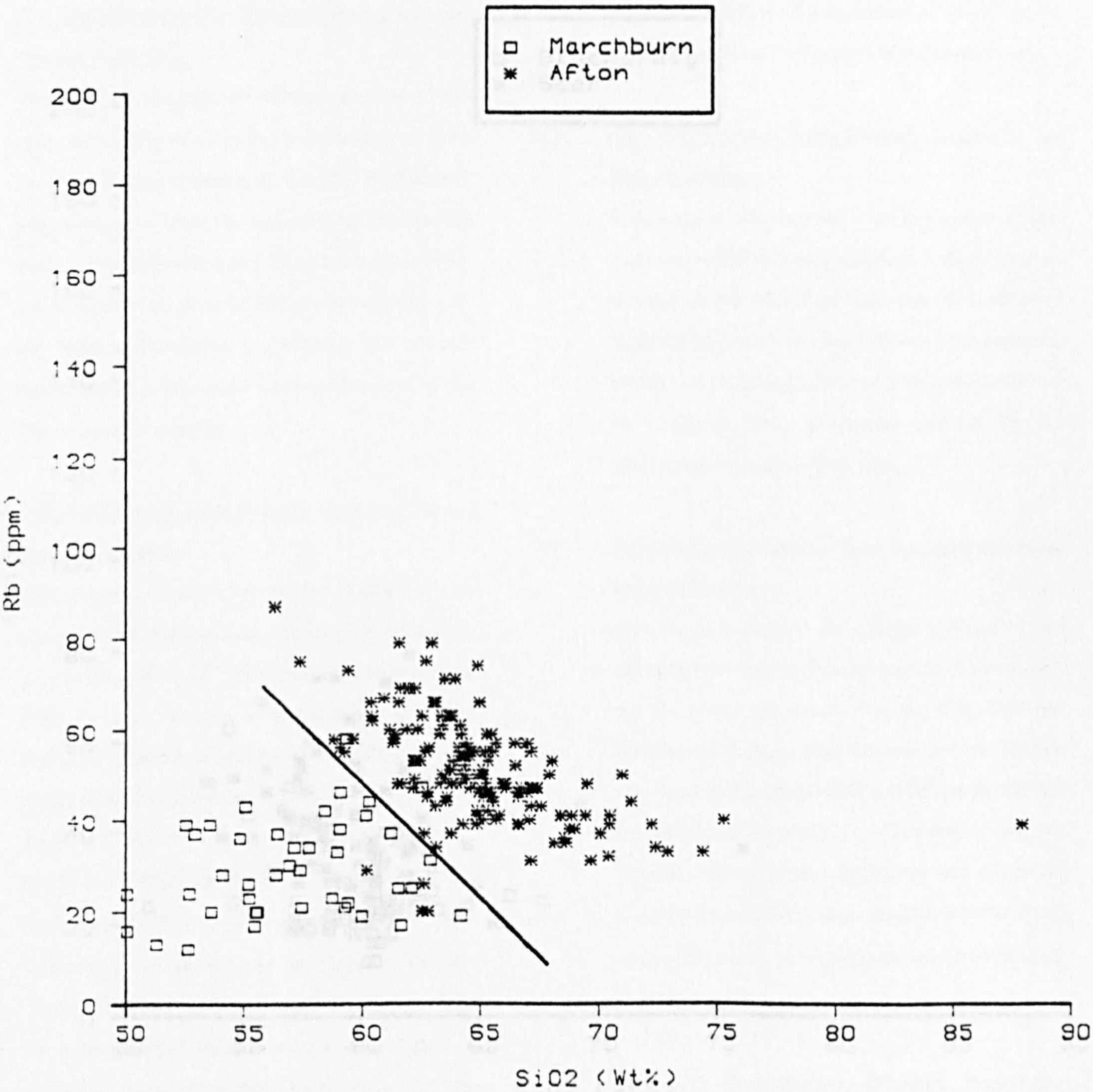

SiO2-Rb Discrimination Diagram (Bhatia, 1983).

FIGURE 318

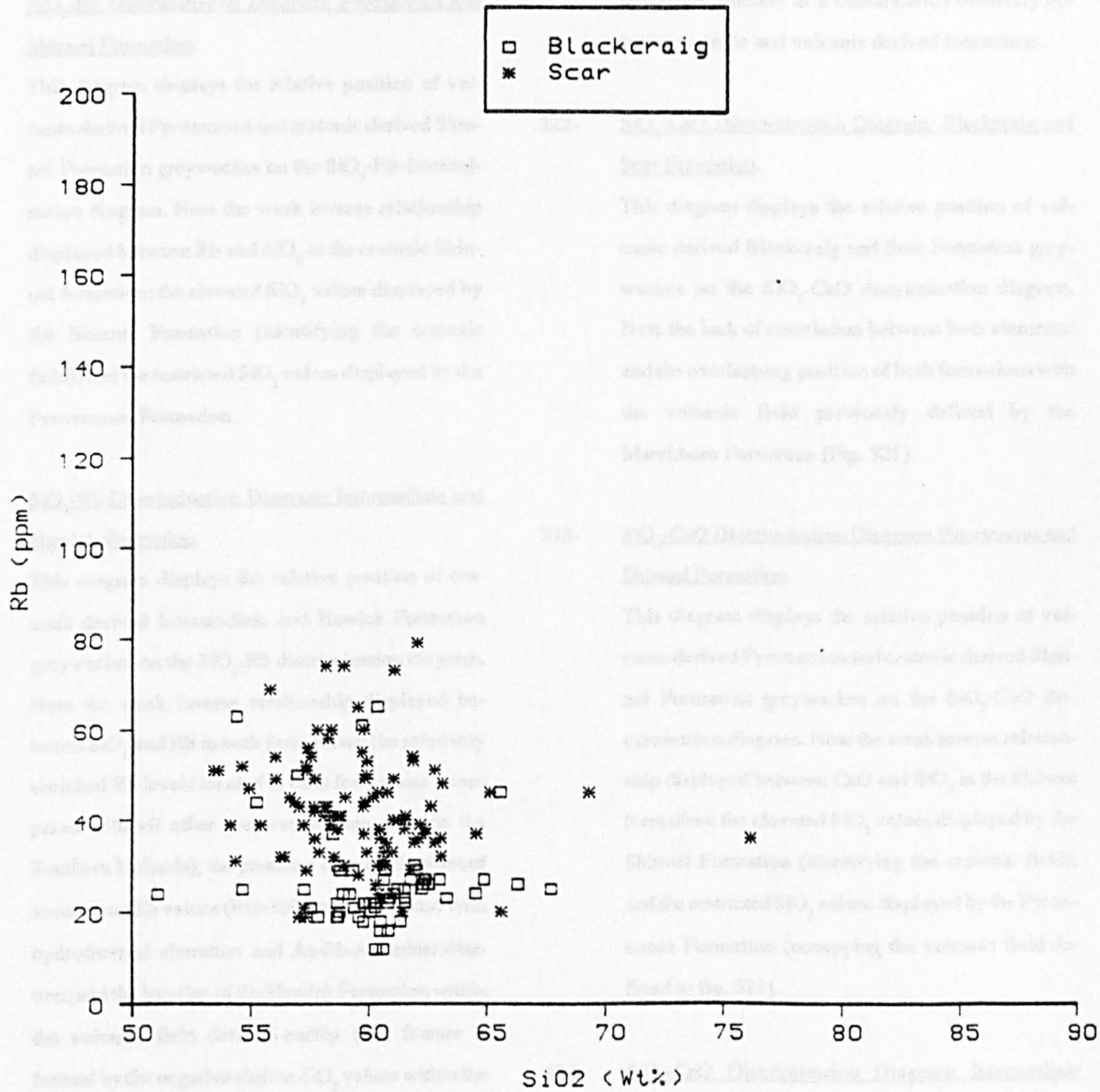

SiO2-Rb Discrimination Diagram (Bhatia, 1983).

wackes on the SiO_2-Rb discrimination diagram. Note the lack of correlation between both elements; the grouping of Blackcraig Formation samples below the Rb=30ppm threshold; the relatively elevated Rb values present in the Scar Formation; and the overlapping position of 75% of both groups within the volcanic field (defined in fig.317).

319- SiO_2-Rb Discrimination Diagram: Pyroxenous and Shinnel Formation.
This diagram displays the relative position of volcanic derived Pyroxenous and cratonic derived Shinnel Formation greywackes on the SiO_2-Rb discrimination diagram. Note the weak inverse relationship displayed between Rb and SiO_2 in the cratonic Shinnel formation; the elevated SiO_2 values displayed by the Shinnel Formation (identifying the cratonic field); and the restricted SiO_2 values displayed by the Pyroxenous Formation.

320- SiO_2-Rb Discrimination Diagram: Intermediate and Hawick Formation
This diagram displays the relative position of cratonic derived Intermediate and Hawick Formation greywackes on the SiO_2-Rb discrimination diagram. Note the weak inverse relationship displayed between SiO_2 and Rb in both formations; the relatively enriched Rb levels located in both formations (compared with all other greywacke formations in the Southern Uplands); the presence of a small subset of anomalous Rb values (Rb>100ppm) associated with hydrothermal alteration and As-Sb-Au mineralisation; and the location of the Hawick Formation within the volcanic field defined earlier (this feature is formed by the negative shift in SiO_2 values within the Hawick Formation, as a direct result of the input of carbonate detritus and associated CaO dilution of all other major element components).

321- SiO_2-CaO Discrimination Diagram: Marchburn and Afton Formation.
The SiO_2-CaO discrimination diagram defined by Bhatia (1983) is used in Figs. 321-324 to display the chemical variation present in the major petrographically distinct Formations located in the Southern Uplands Study Area. This diagram displays the relative position of volcanic derived Marchburn and cratonic derived Afton Formation greywackes on the SiO_2-CaO discrimination diagram. Note the weak inverse relationship displayed between CaO and SiO_2 in both formations; the relatively elevated CaO and restricted SiO_2 values displayed by the Marchburn Formation; the generally lower CaO values displayed by the Afton Formation; and the approximate position of a classification boundary between cratonic and volcanic derived formations.

322- SiO_2-CaO Discrimination Diagram: Blackcraig and Scar Formation.
This diagram displays the relative position of volcanic derived Blackcraig and Scar Formation greywackes on the SiO_2-CaO discrimination diagram. Note the lack of correlation between both elements; and the overlapping position of both formations with the volcanic field previously defined by the Marchburn Formation (Fig. 321).

323- SiO_2-CaO Discrimination Diagram: Pyroxenous and Shinnel Formation.
This diagram displays the relative position of volcanic derived Pyroxenous and cratonic derived Shinnel Formation greywackes on the SiO_2-CaO discrimination diagram. Note the weak inverse relationship displayed between CaO and SiO_2 in the Shinnel formation; the elevated SiO_2 values displayed by the Shinnel Formation (identifying the cratonic field); and the restricted SiO_2 values displayed by the Pyroxenous Formation (occupying the volcanic field defined in fig. 321).

324- SiO_2-CaO Discrimination Diagram: Intermediate and Hawick Formation.
This diagram displays the relative position of cratonic derived Intermediate and Hawick Formation greywackes on the SiO_2-CaO discrimination diagram. Note the major inverse relationship displayed between SiO_2 and CaO and the considerably elevated CaO levels present in the Hawick Formation (max 24.36%) together with correspondingly low SiO_2 levels; the lack of any form of inter-element correlation in the Intermediate Formation; the relatively enriched SiO_2 levels located in the Intermediate For-

FIGURE 319

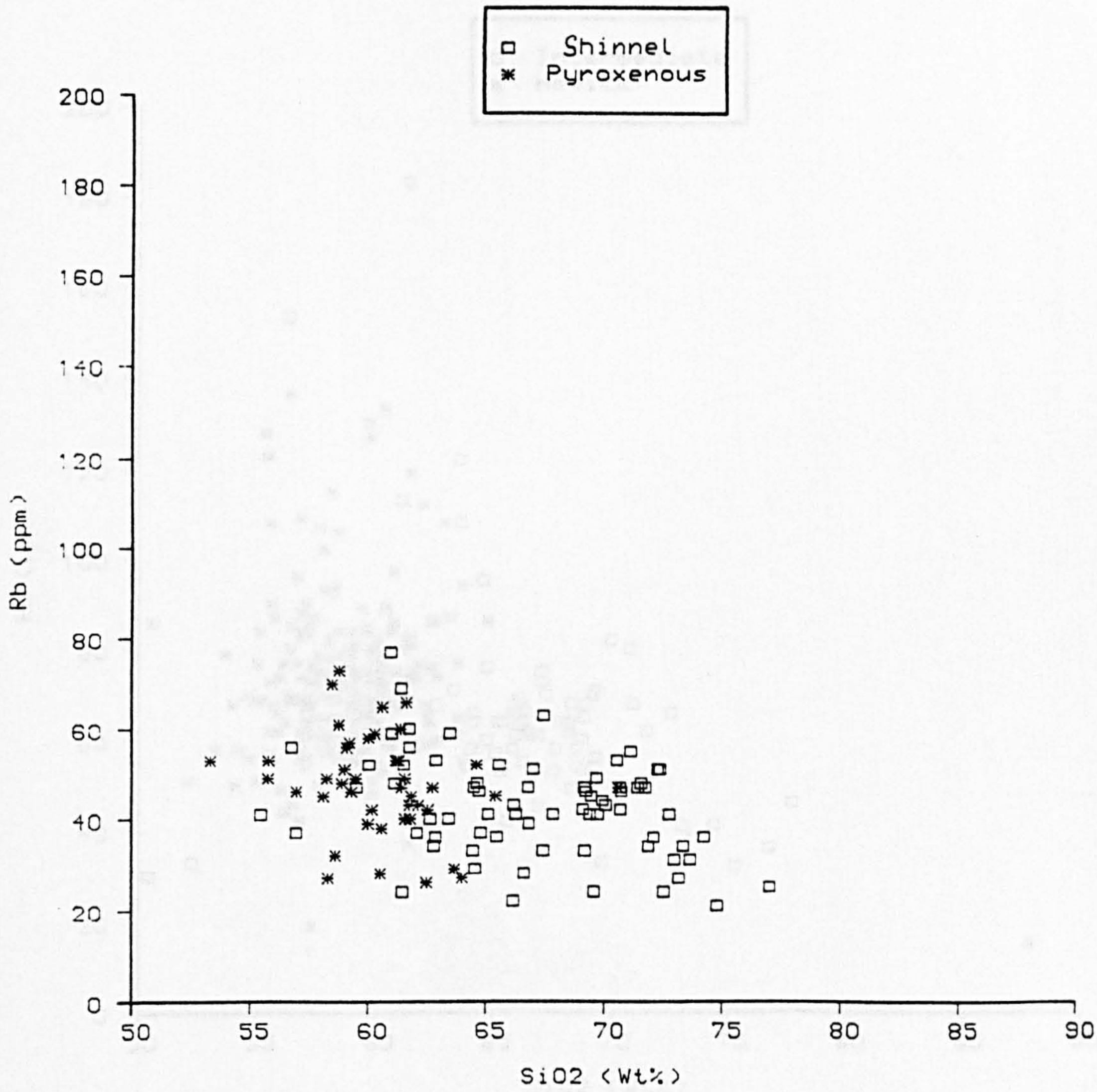

SiO2-Rb Discrimination Diagram (Bhatia, 1983).

FIGURE 320

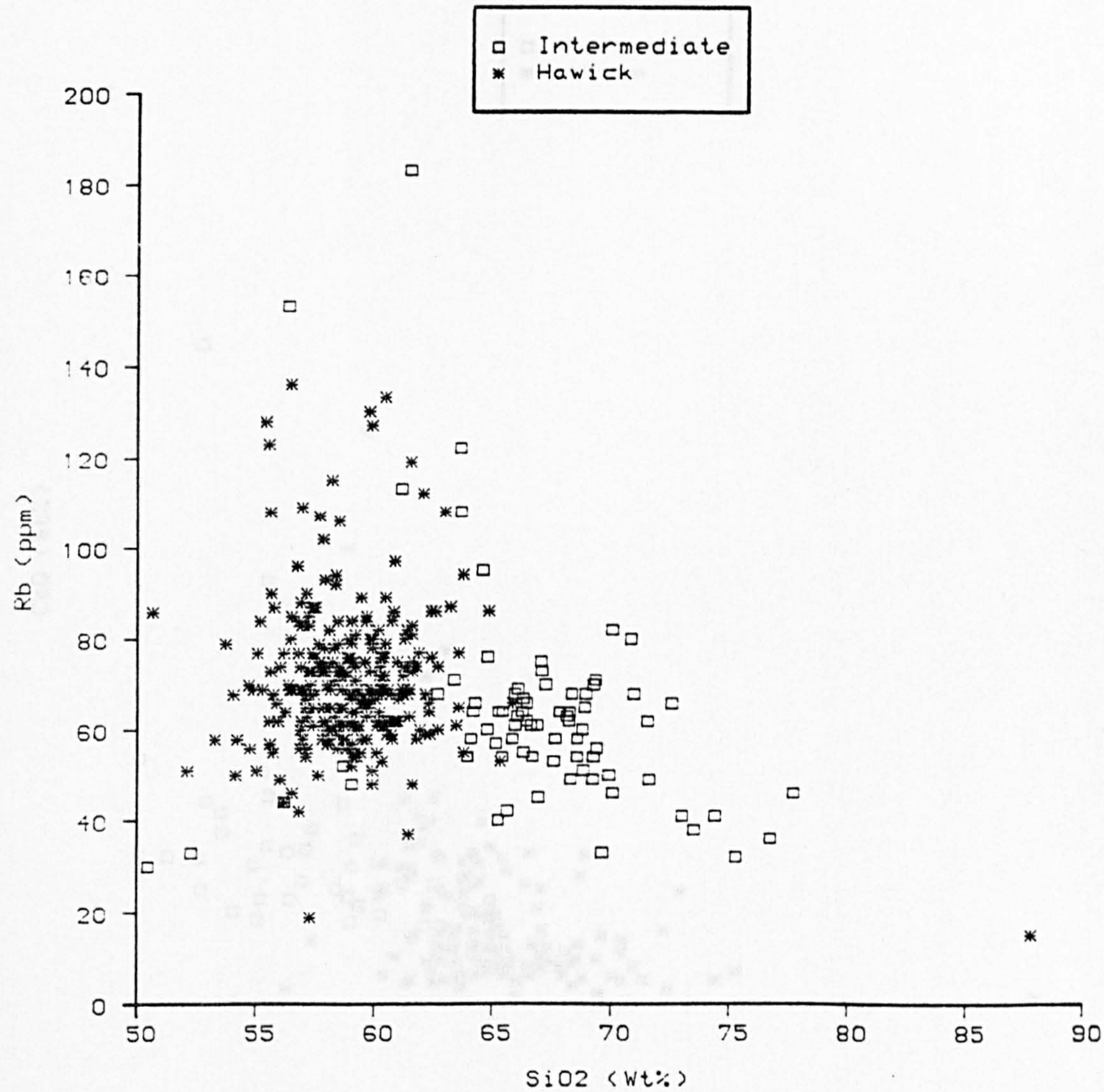

SiO2-Rb Discrimination Diagram (Bhatia, 1983).

FIGURE 321

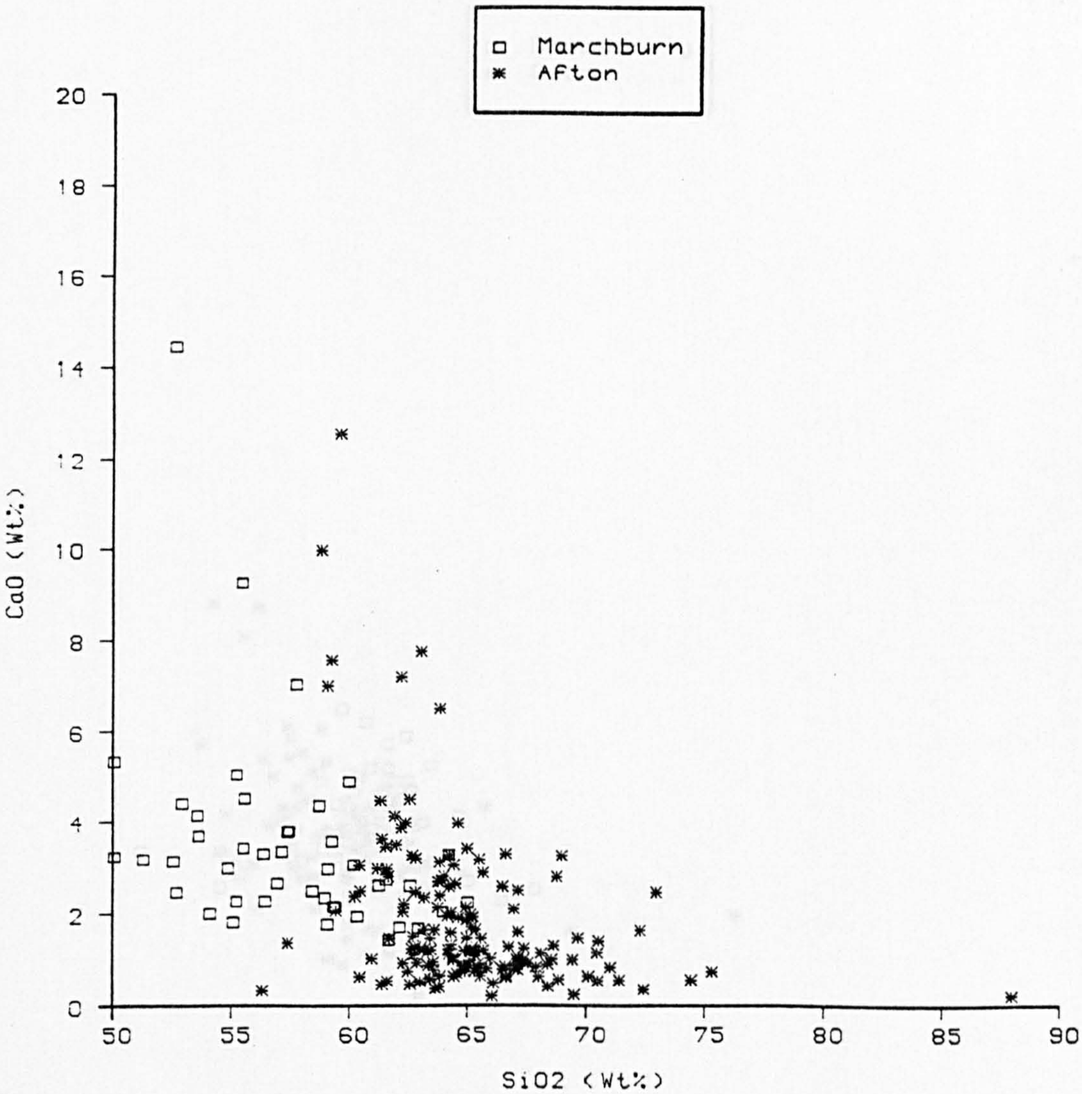

SiO2-CaO Discrimination Diagram (Bhatia, 1983).

FIGURE 322

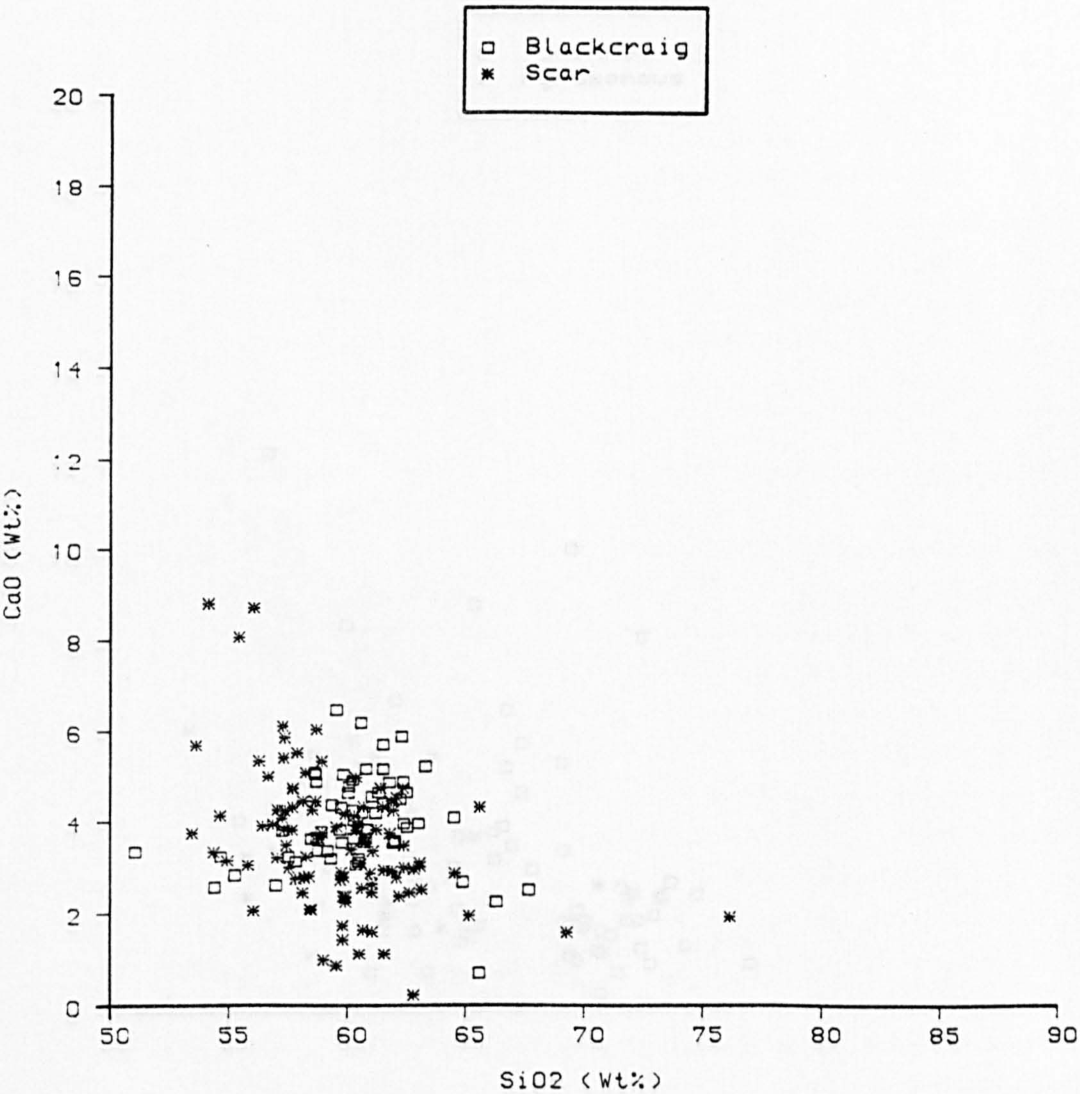

SiO2-CaO Discrimination Diagram (Bhatia, 1983).

FIGURE 323

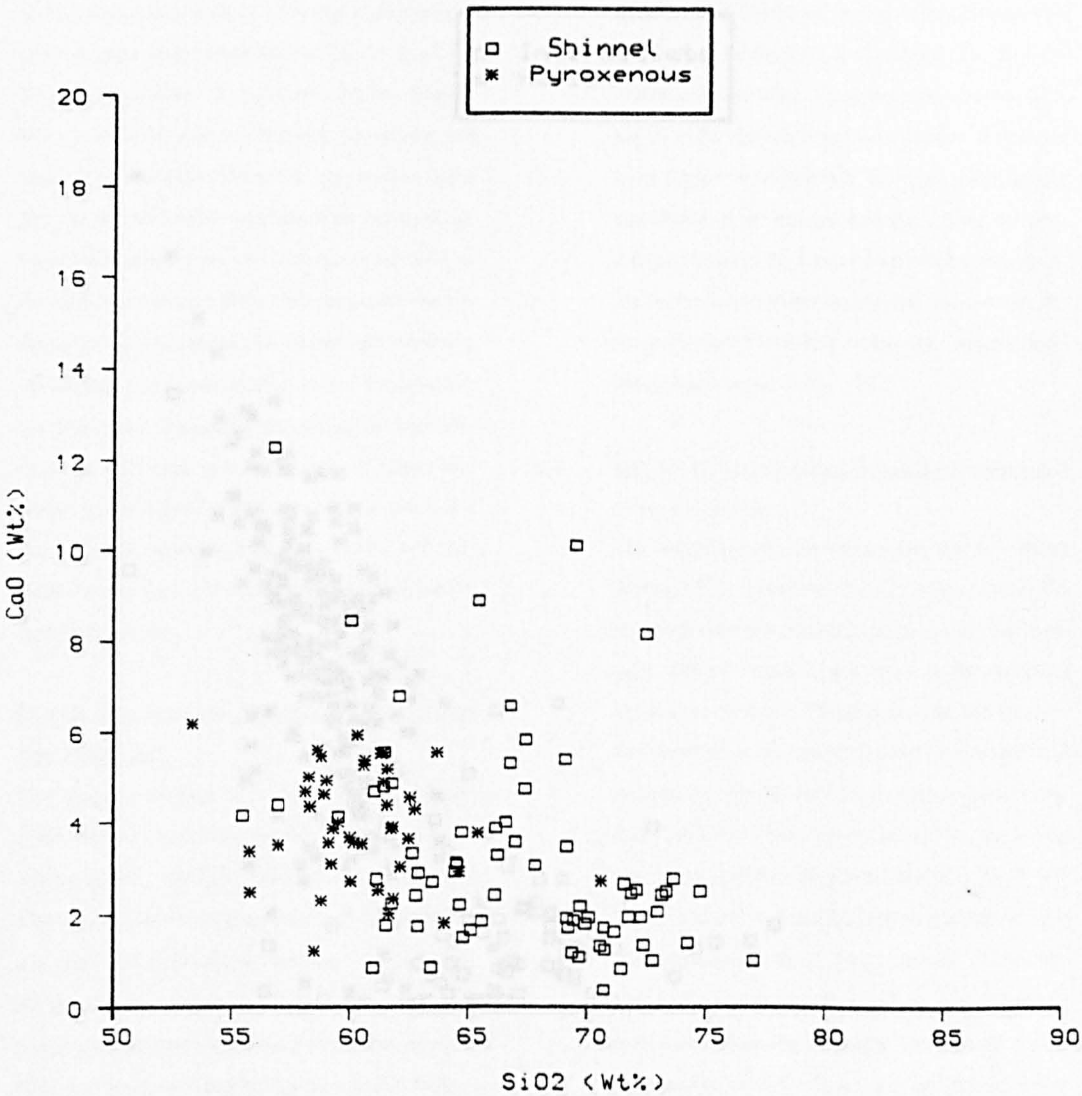

SiO2-CaO Discrimination Diagram (Bhatia, 1983).

FIGURE 324

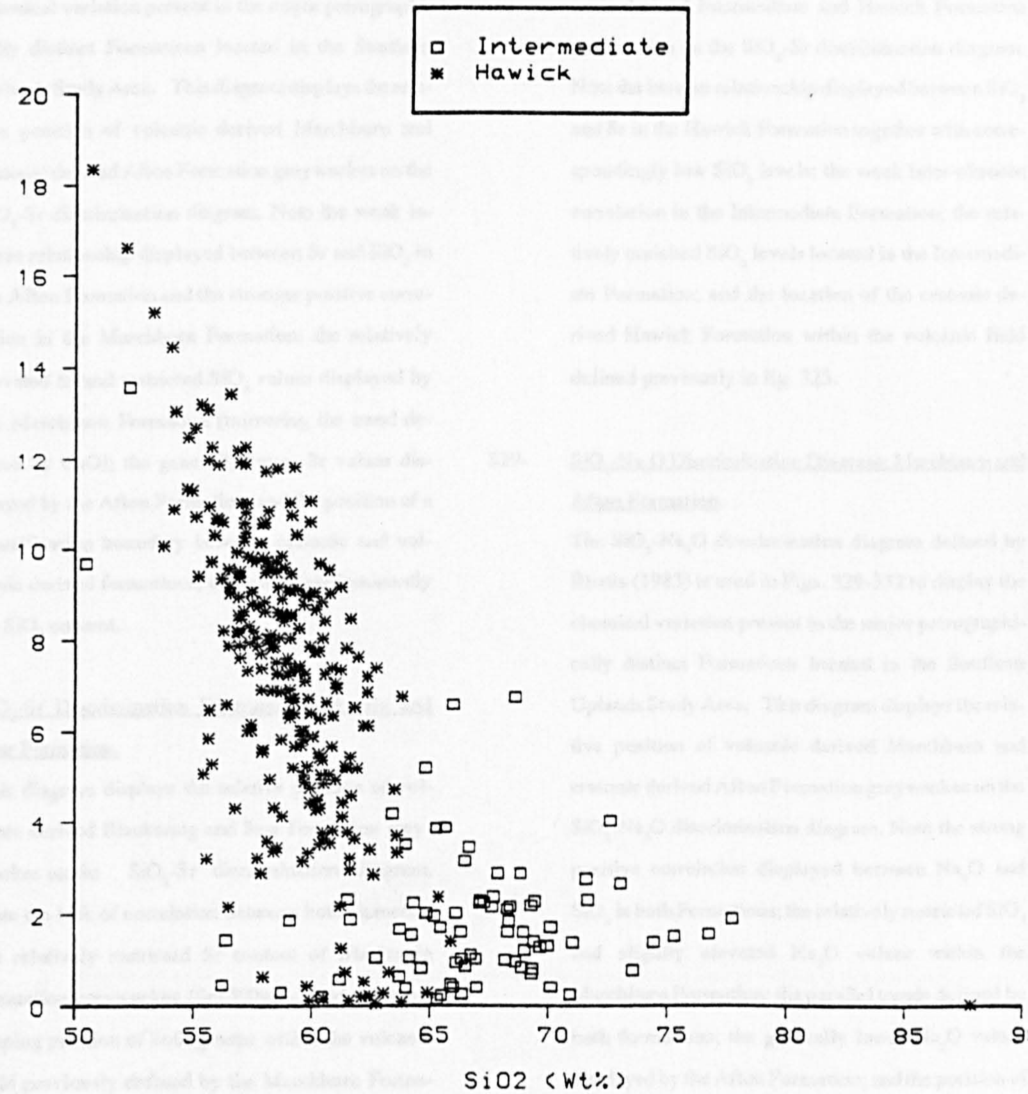

SiO2-CaO Discrimination Diagram (Bhatia, 1983).

mation; and the location of the Hawick Formation within the volcanic field defined previously in fig. 321.

325- <u>SiO_2-Sr Discrimination Diagram: Marchburn and Afton Formation.</u>
The SiO_2-Sr discrimination diagram defined by Bhatia (1983) is used in Figs. 325-328 to display the chemical variation present in the major petrographically distinct Formations located in the Southern Uplands Study Area. This diagram displays the relative position of volcanic derived Marchburn and cratonic derived Afton Formation greywackes on the SiO_2-Sr discrimination diagram. Note the weak inverse relationship displayed between Sr and SiO_2 in the Afton Formation and the stronger positive correlation in the Marchburn Formation; the relatively elevated Sr and restricted SiO_2 values displayed by the Marchburn Formation (mirroring the trend defined by CaO); the generally lower Sr values displayed by the Afton Formation; and the position of a classification boundary between cratonic and volcanic derived formations, controlled predominantly by SiO_2 content.

326- <u>SiO_2-Sr Discrimination Diagram: Blackcraig and Scar Formation.</u>
This diagram displays the relative position of volcanic derived Blackcraig and Scar Formation greywackes on the SiO_2-Sr discrimination diagram. Note the lack of correlation between both elements; the relatively restricted Sr content of Blackcraig Formation greywackes (Sr<300ppm) and the overlapping position of both groups within the volcanic field previously defined by the Marchburn Formation in Fig. 325.

327- <u>SiO_2-Sr Discrimination Diagram: Pyroxenous and Shinnel Formation</u>.
This diagram displays the relative position of volcanic derived Pyroxenous and cratonic derived Shinnel Formation greywackes on the SiO_2-Sr discrimination diagram. Note the weak inverse relationship displayed between Sr and SiO_2 in the Shinnel formation (mirroring the trend defined by CaO); the elevated SiO_2 values displayed by the Shinnel Formation (identifying the cratonic field); and the elevated Sr and restricted SiO_2 values displayed by the Pyroxenous Formation (occupying the volcanic field defined in fig. 325).

328- <u>SiO_2-Sr Discrimination Diagram: Intermediate and Hawick Formation</u>.
This diagram displays the relative position of cratonic derived Intermediate and Hawick Formation greywackes on the SiO_2-Sr discrimination diagram. Note the inverse relationship displayed between SiO_2 and Sr in the Hawick Formation together with correspondingly low SiO_2 levels; the weak inter-element correlation in the Intermediate Formation; the relatively enriched SiO_2 levels located in the Intermediate Formation; and the location of the cratonic derived Hawick Formation within the volcanic field defined previously in fig. 325.

329- <u>SiO_2-Na_2O Discrimination Diagram: Marchburn and Afton Formation</u>.
The SiO_2-Na_2O discrimination diagram defined by Bhatia (1983) is used in Figs. 329-332 to display the chemical variation present in the major petrographically distinct Formations located in the Southern Uplands Study Area. This diagram displays the relative position of volcanic derived Marchburn and cratonic derived Afton Formation greywackes on the SiO_2-Na_2O discrimination diagram. Note the strong positive correlation displayed between Na_2O and SiO_2 in both Formations; the relatively restricted SiO_2 and slightly elevated Na_2O values within the Marchburn Formation; the parallel trends defined by both formations; the generally lower Na_2O values displayed by the Afton Formation; and the position of a classification boundary between cratonic and volcanic derived formations, controlled predominantly by SiO_2 content.

330- <u>SiO_2-Na_2O Discrimination Diagram: Blackcraig and Scar Formation</u>.
This diagram displays the relative position of volcanic derived Blackcraig and Scar Formation greywackes on the SiO_2-Na_2O discrimination diagram. Note the weak positive correlation defined between both elements; the restricted SiO_2 content and gener-

FIGURE 325

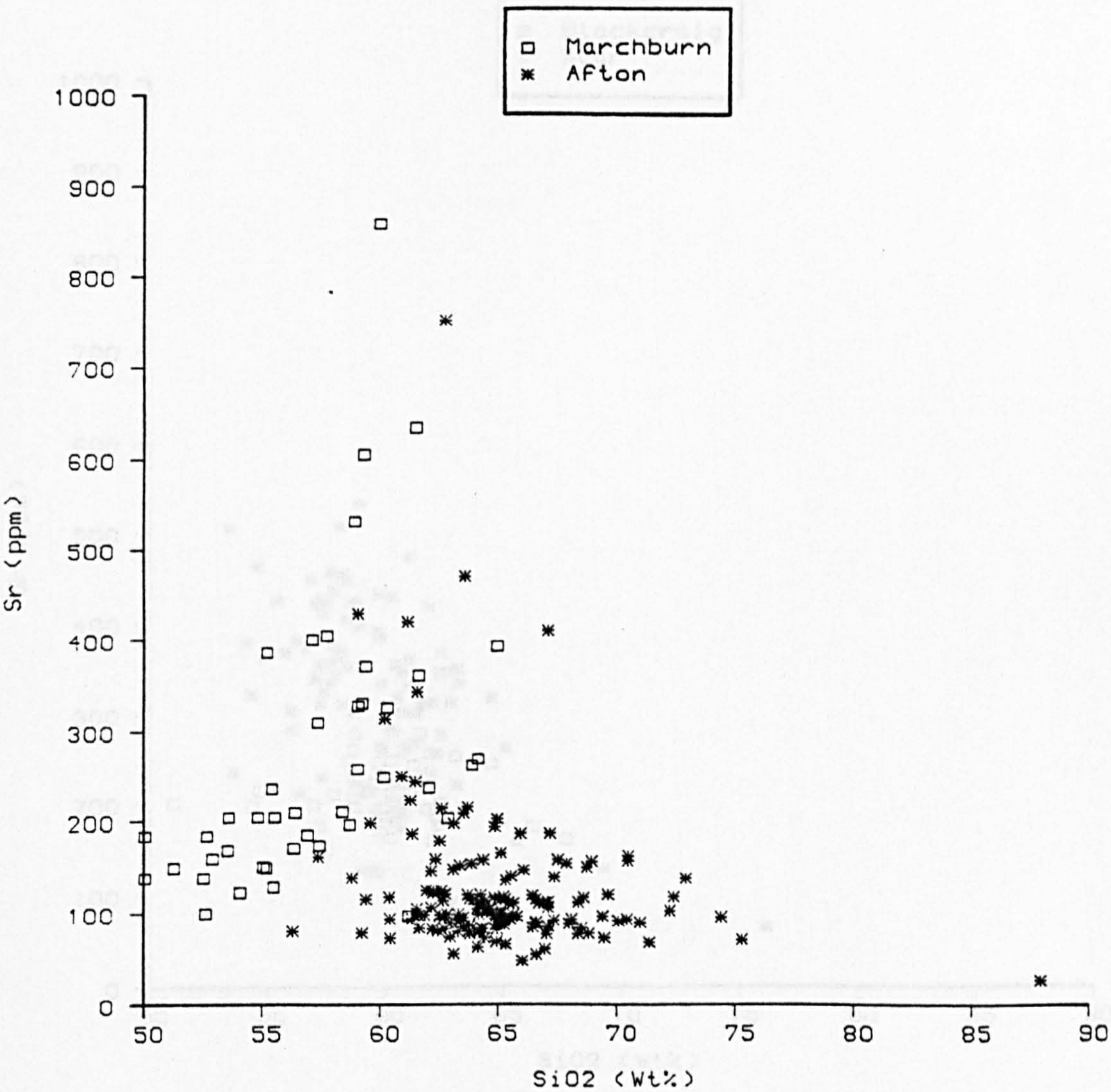

SiO2-Sr Discrimination Diagram (Bhatia, 1983).

FIGURE 326

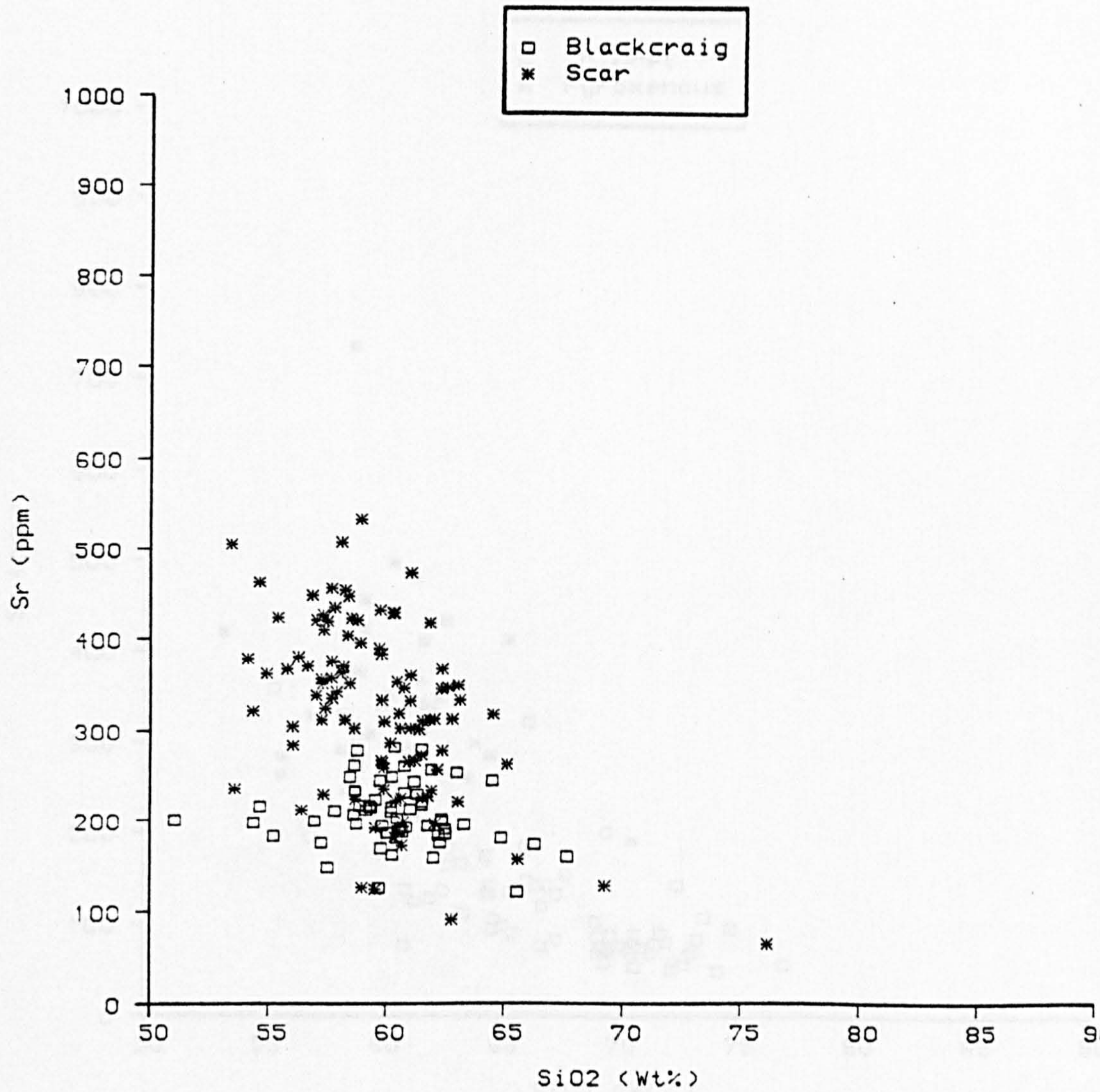

SiO2-Sr Discrimination Diagram (Bhatia, 1983).

FIGURE 327

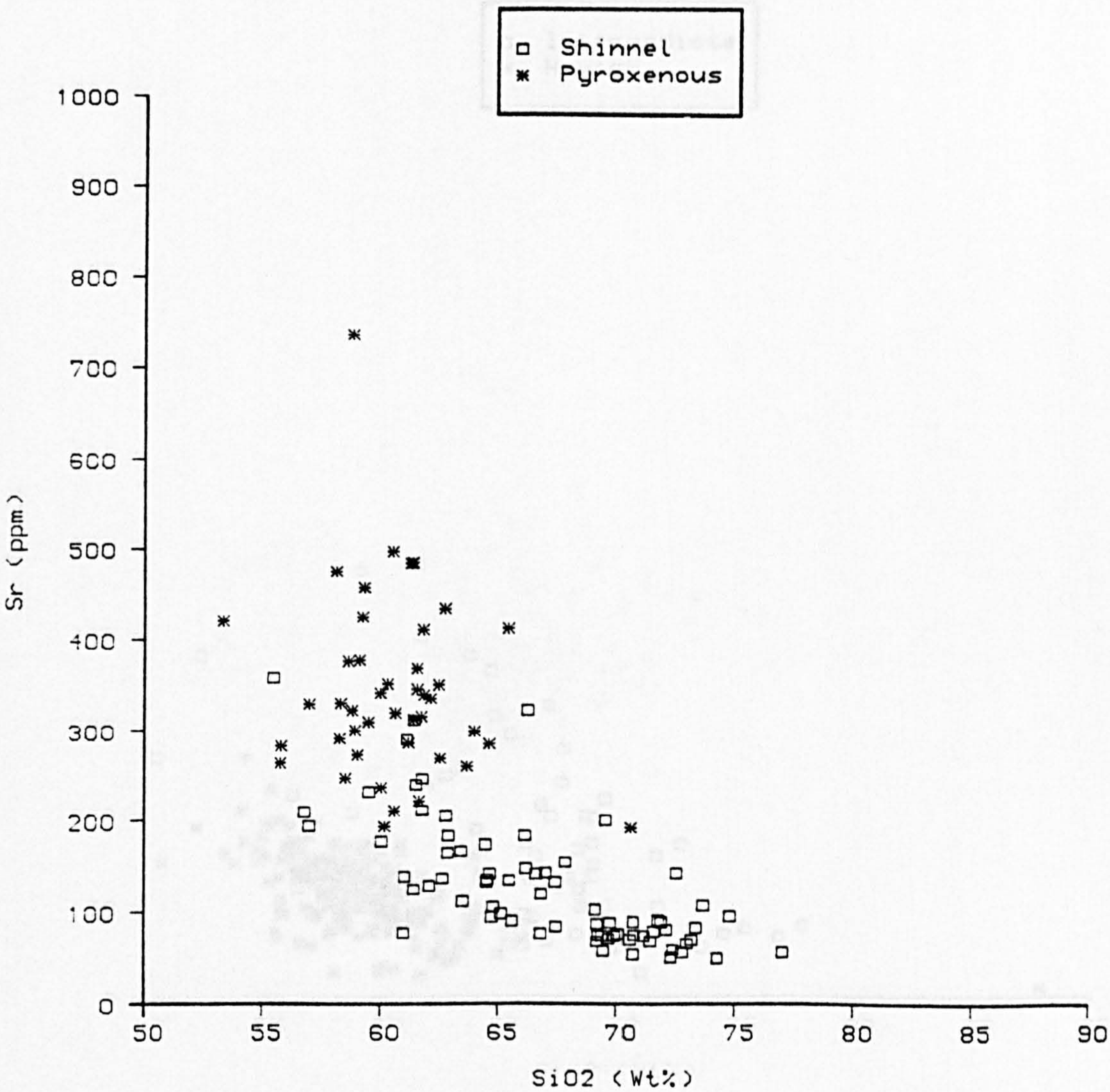

SiO2-Sr Discrimination Diagram (Bhatia, 1983).

FIGURE 328

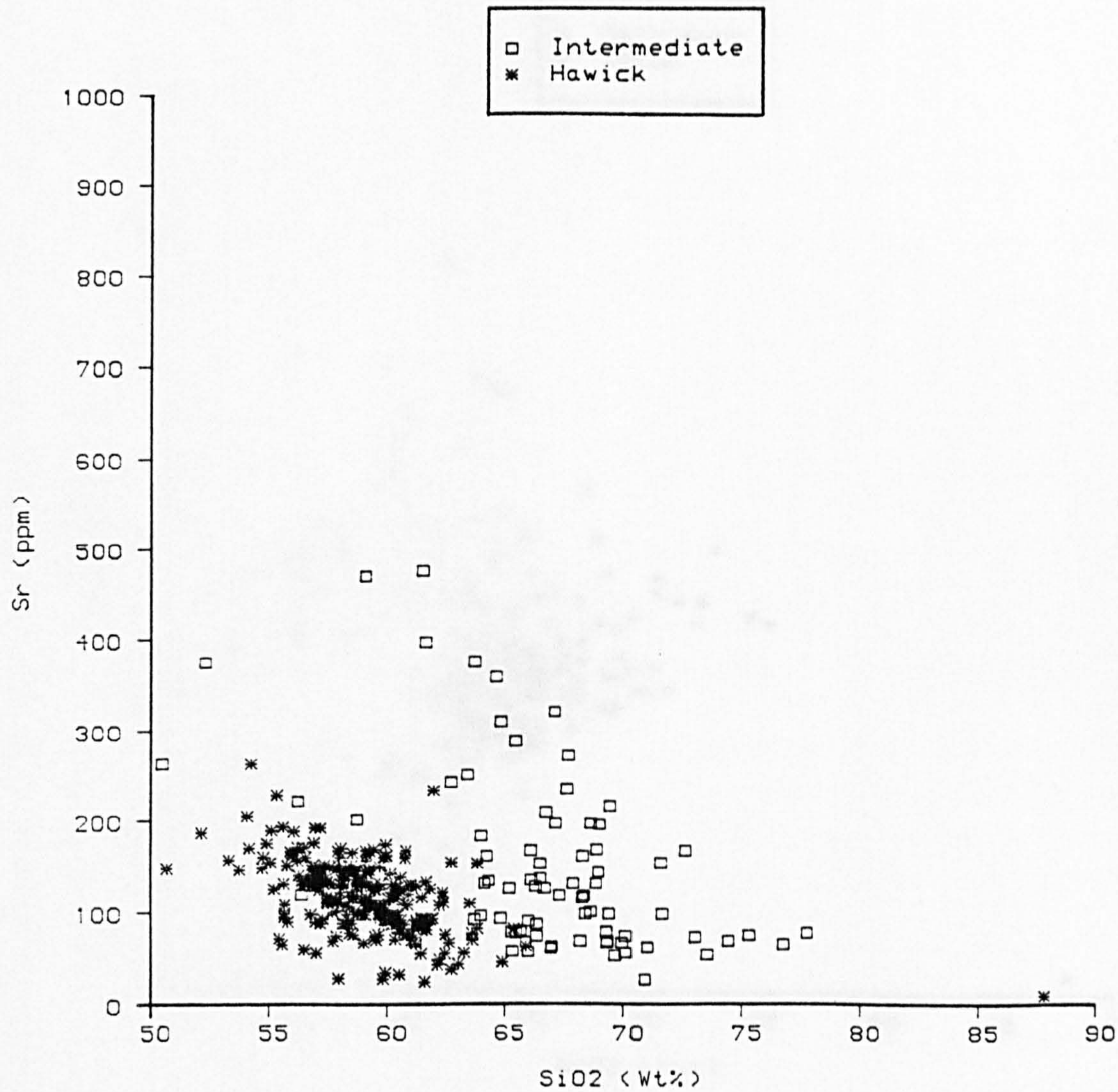

SiO2-Sr Discrimination Diagram (Bhatia, 1983).

FIGURE 329

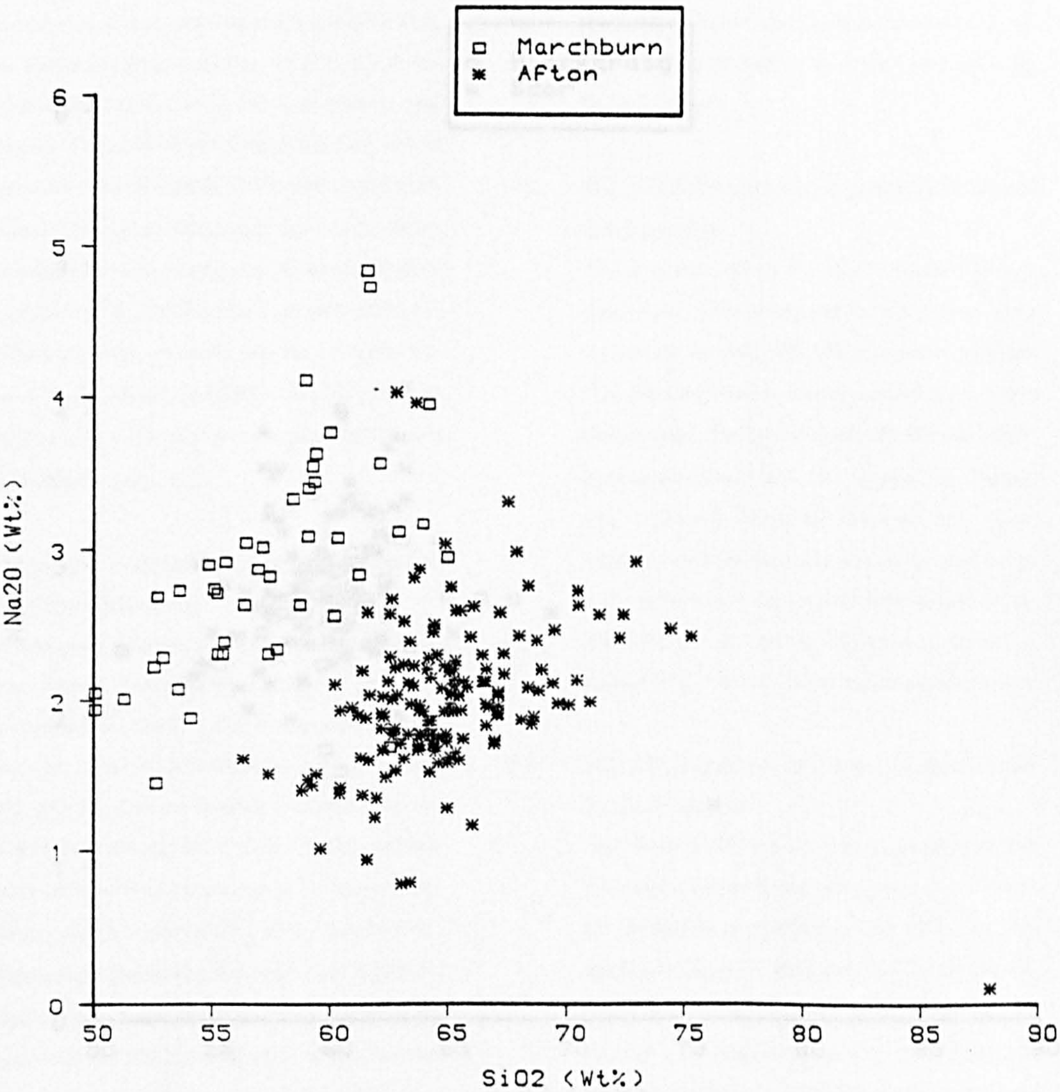

SiO2-Na20 Discrimination Diagram (Bhatia, 1983).

FIGURE 330

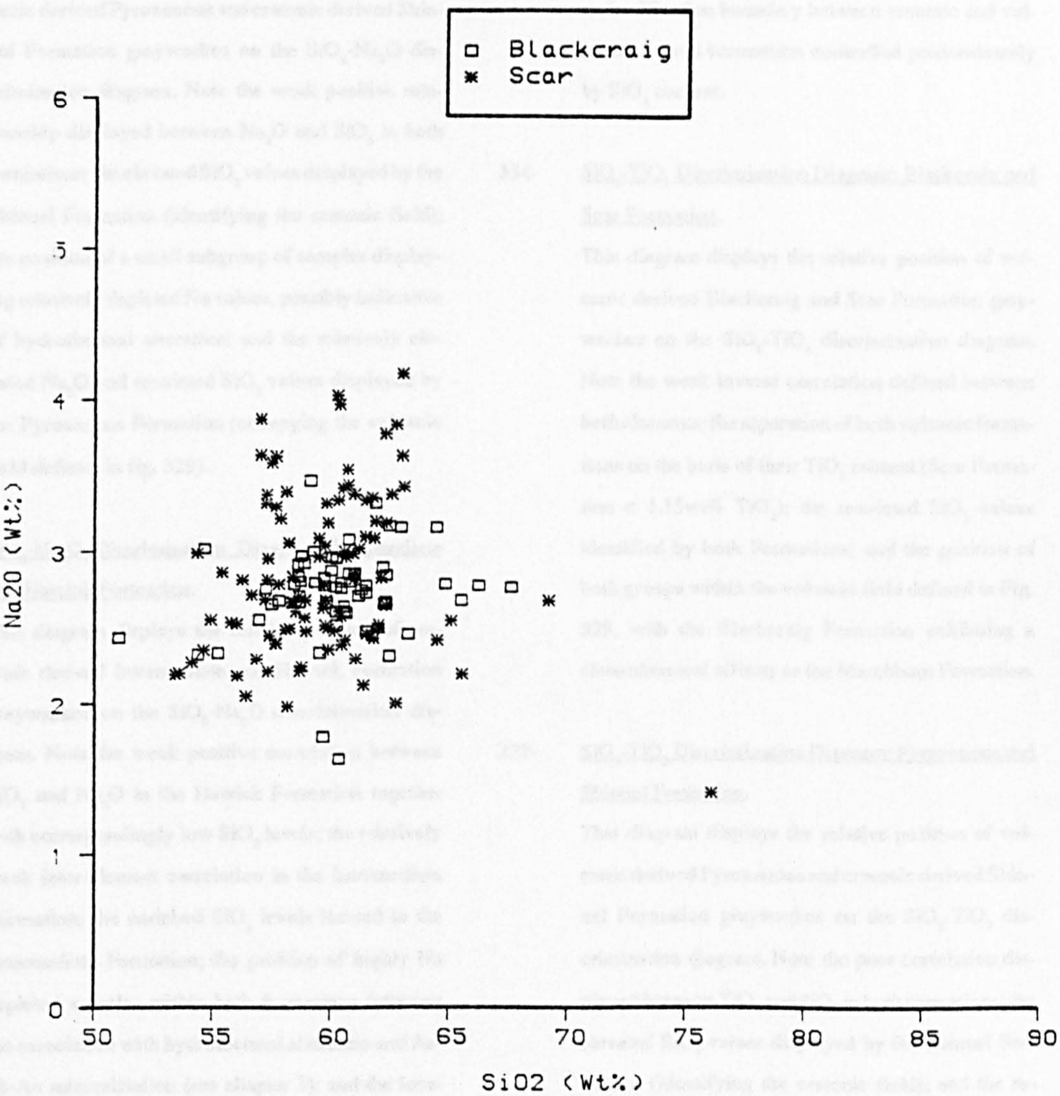

SiO2-Na2O Discrimination Diagram (Bhatia, 1983).

ally elevated Na_2O values identified by both Formations; and the overlapping position of both groups within the volcanic field defined by the Marchburn Formation in Fig. 329.

331- <u>SiO_2-Na_2O Discrimination Diagram: Pyroxenous and Shinnel Formation</u>.

This diagram displays the relative position of volcanic derived Pyroxenous and cratonic derived Shinnel Formation greywackes on the SiO_2-Na_2O discrimination diagram. Note the weak positive relationship displayed between Na_2O and SiO_2 in both formations; the elevated SiO_2 values displayed by the Shinnel Formation (identifying the cratonic field); the position of a small subgroup of samples displaying relatively depleted Na values, possibly indicative of hydrothermal alteration; and the relatively elevated Na_2O and restricted SiO_2 values displayed by the Pyroxenous Formation (occupying the volcanic field defined in fig. 329).

332- <u>SiO_2-Na_2O Discrimination Diagram: Intermediate and Hawick Formation</u>.

This diagram displays the relative position of cratonic derived Intermediate and Hawick Formation greywackes on the SiO_2-Na_2O discrimination diagram. Note the weak positive correlation between SiO_2 and Na_2O in the Hawick Formation together with correspondingly low SiO_2 levels; the relatively weak inter-element correlation in the Intermediate Formation; the enriched SiO_2 levels located in the Intermediate Formation; the position of highly Na depleted samples within both formations inferring the association with hydrothermal alteration and As-Sb-Au mineralisation (see chapter 3); and the location of the cratonic derived Hawick Formation within the volcanic field defined previously in fig. 329.

333- <u>SiO_2-TiO_2 Discrimination Diagram: Marchburn and Afton Formation</u>.

The SiO_2-TiO_2 discrimination diagram defined by Bhatia (1983) is used in Figs. 333-336 to display the chemical variation present in the major petrographically distinct Formations located in the Southern Uplands Study Area. This diagram displays the relative position of volcanic derived Marchburn and cratonic derived Afton Formation greywackes on the SiO_2-TiO_2 discrimination diagram. Note the strong inverse correlation displayed between TiO_2 and SiO_2 in both Formations; the relatively restricted SiO_2 and elevated TiO_2 values displayed by the Marchburn Formation; the single SiO_2-TiO_2 trend defined by both formations; the generally lower TiO_2 values displayed by the Afton Formation; and the position of a classification boundary between cratonic and volcanic derived formations controlled predominantly by SiO_2 content.

334- <u>SiO_2-TiO_2 Discrimination Diagram: Blackcraig and Scar Formation</u>.

This diagram displays the relative position of volcanic derived Blackcraig and Scar Formation greywackes on the SiO_2-TiO_2 discrimination diagram. Note the weak inverse correlation defined between both elements; the separation of both volcanic formations on the basis of their TiO_2 content (Scar Formation < 1.15wt% TiO_2); the restricted SiO_2 values identified by both Formations; and the position of both groups within the volcanic field defined in Fig. 329, with the Blackcraig Formation exhibiting a close chemical affinity to the Marchburn Formation.

335- <u>SiO_2-TiO_2 Discrimination Diagram: Pyroxenous and Shinnel Formation</u>.

This diagram displays the relative position of volcanic derived Pyroxenous and cratonic derived Shinnel Formation greywackes on the SiO_2-TiO_2 discrimination diagram. Note the poor correlation displayed between TiO_2 and SiO_2 in both formations; the elevated SiO_2 values displayed by the Shinnel Formation (identifying the cratonic field); and the restricted TiO_2 content of the volcanic Pyroxenous Formation (<1.15wt%) displaying similar characteristics to the Scar Formation (Fig. 334).

336- <u>SiO_2-TiO_2 Discrimination Diagram: Intermediate and Hawick Formation</u>.

This diagram displays the relative position of cratonic derived Intermediate and Hawick Formation greywackes on the SiO_2-TiO_2 discrimination diagram. Note the poor correlation and wide scatter of SiO_2 and TiO_2 values in both Formations; the rela-

FIGURE 331

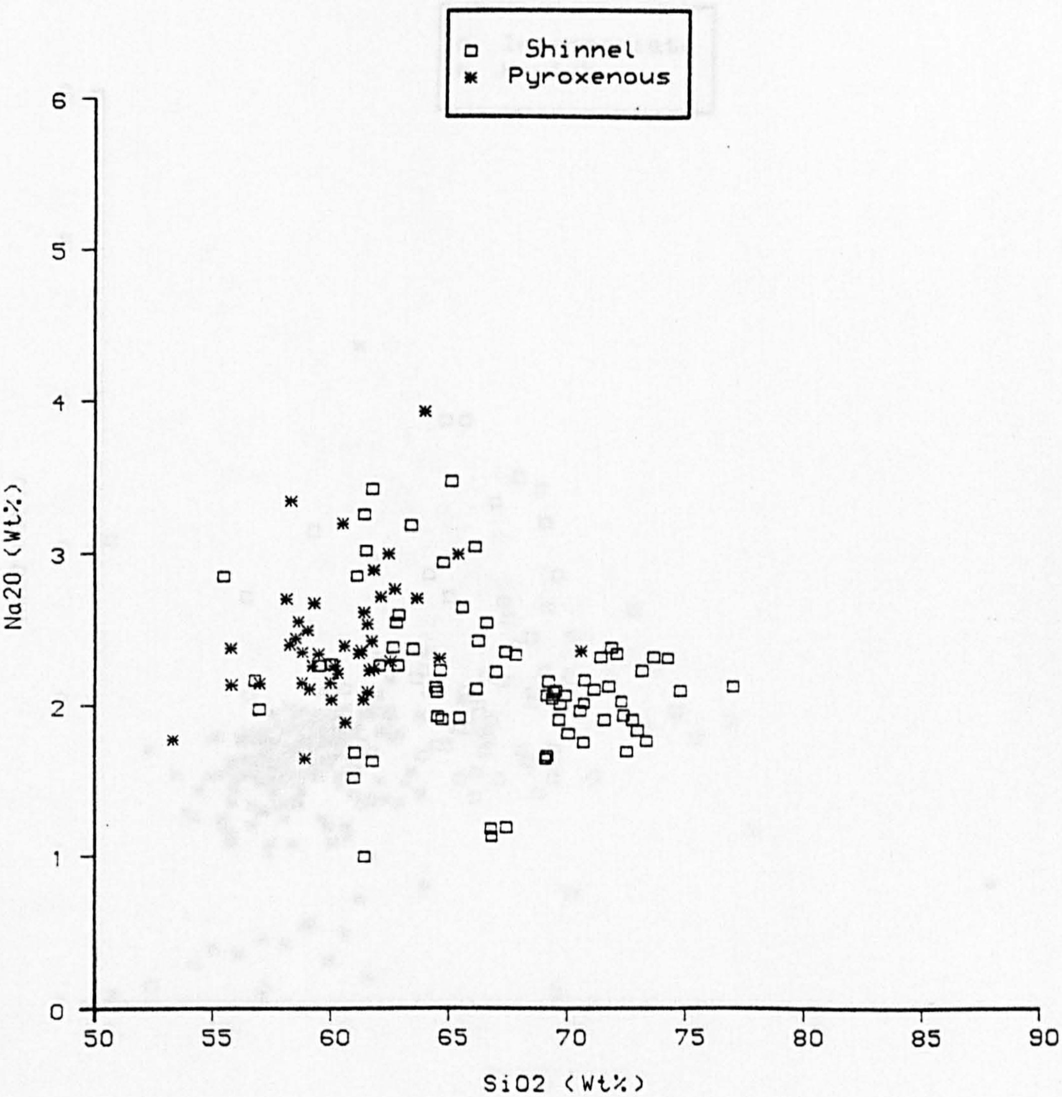

SiO2-Na2O Discrimination Diagram (Bhatia, 1983).

FIGURE 332

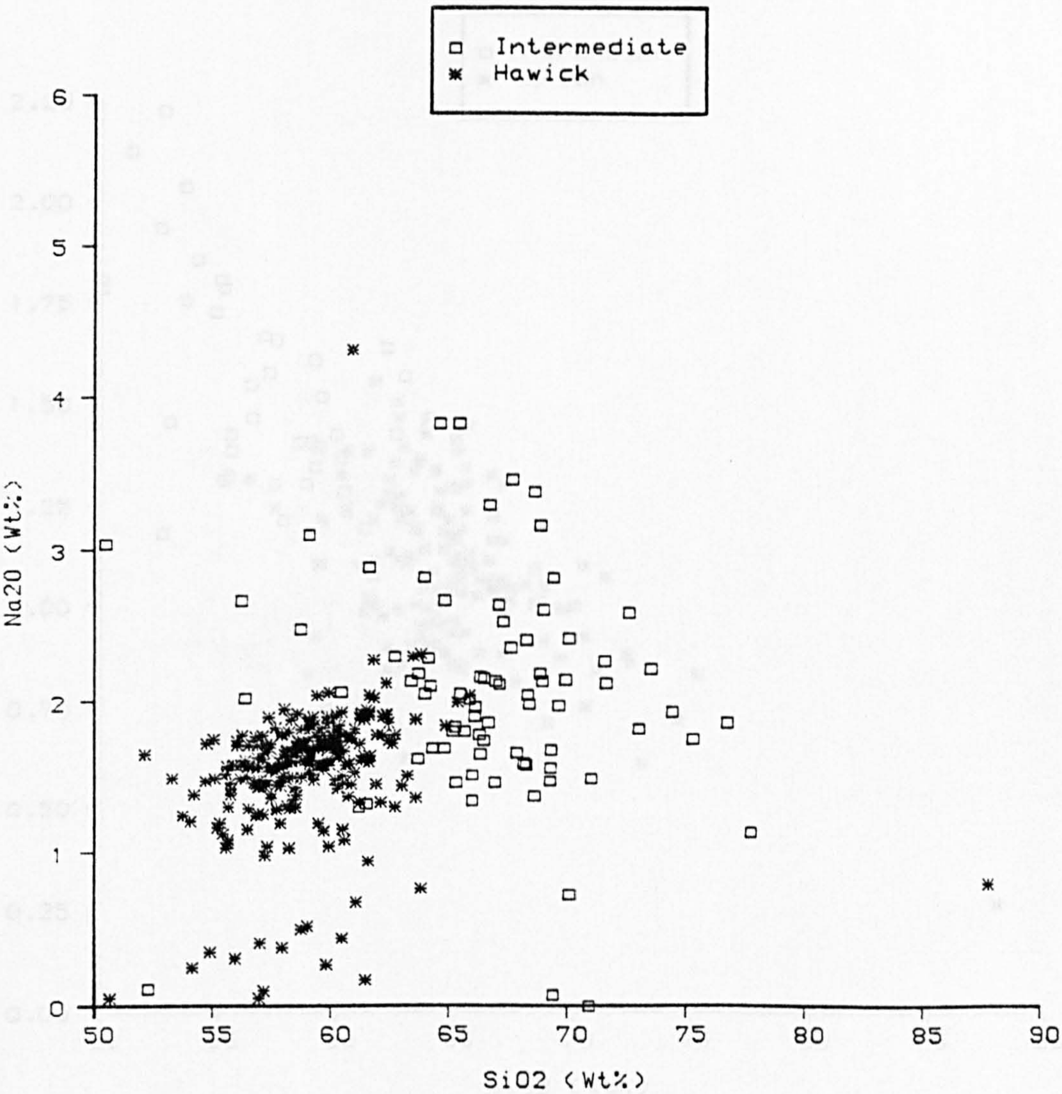

SiO2-Na2O Discrimination Diagram (Bhatia, 1983).

FIGURE 333

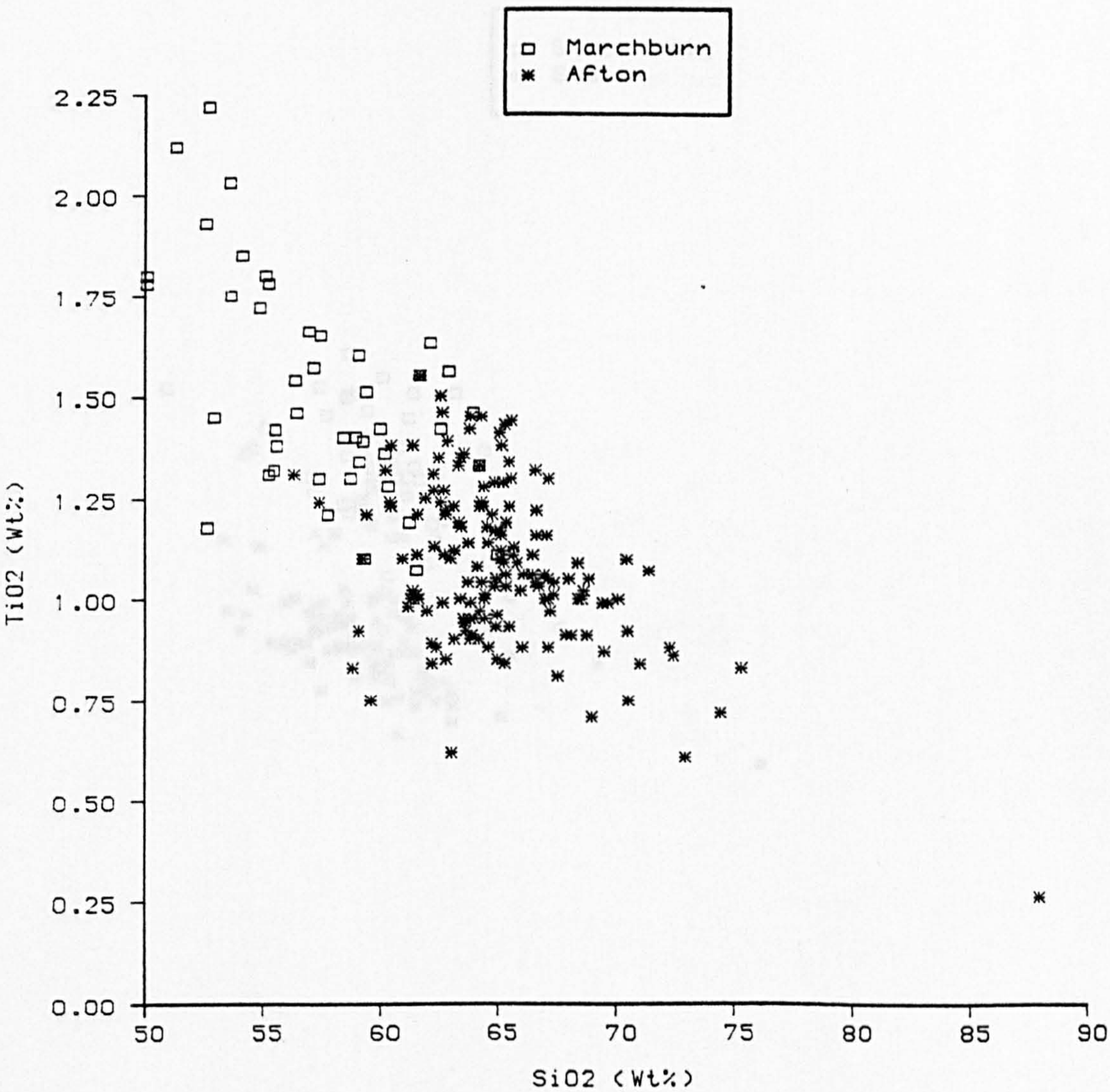

SiO2-TiO2 Discrimination Diagram (Bhatia, 1983).

FIGURE 334

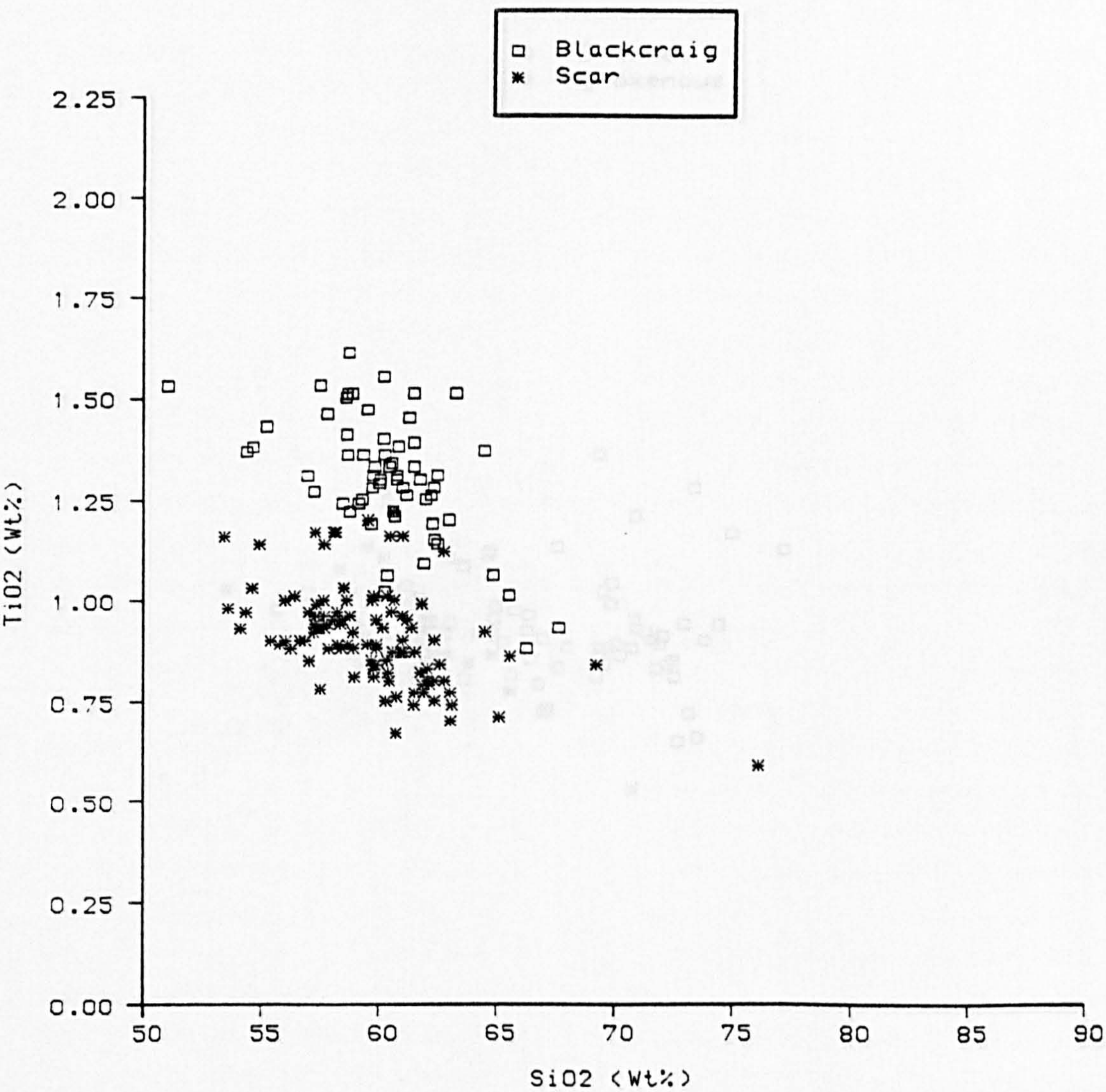

SiO2-TiO2 Discrimination Diagram (Bhatia, 1983).

FIGURE 335

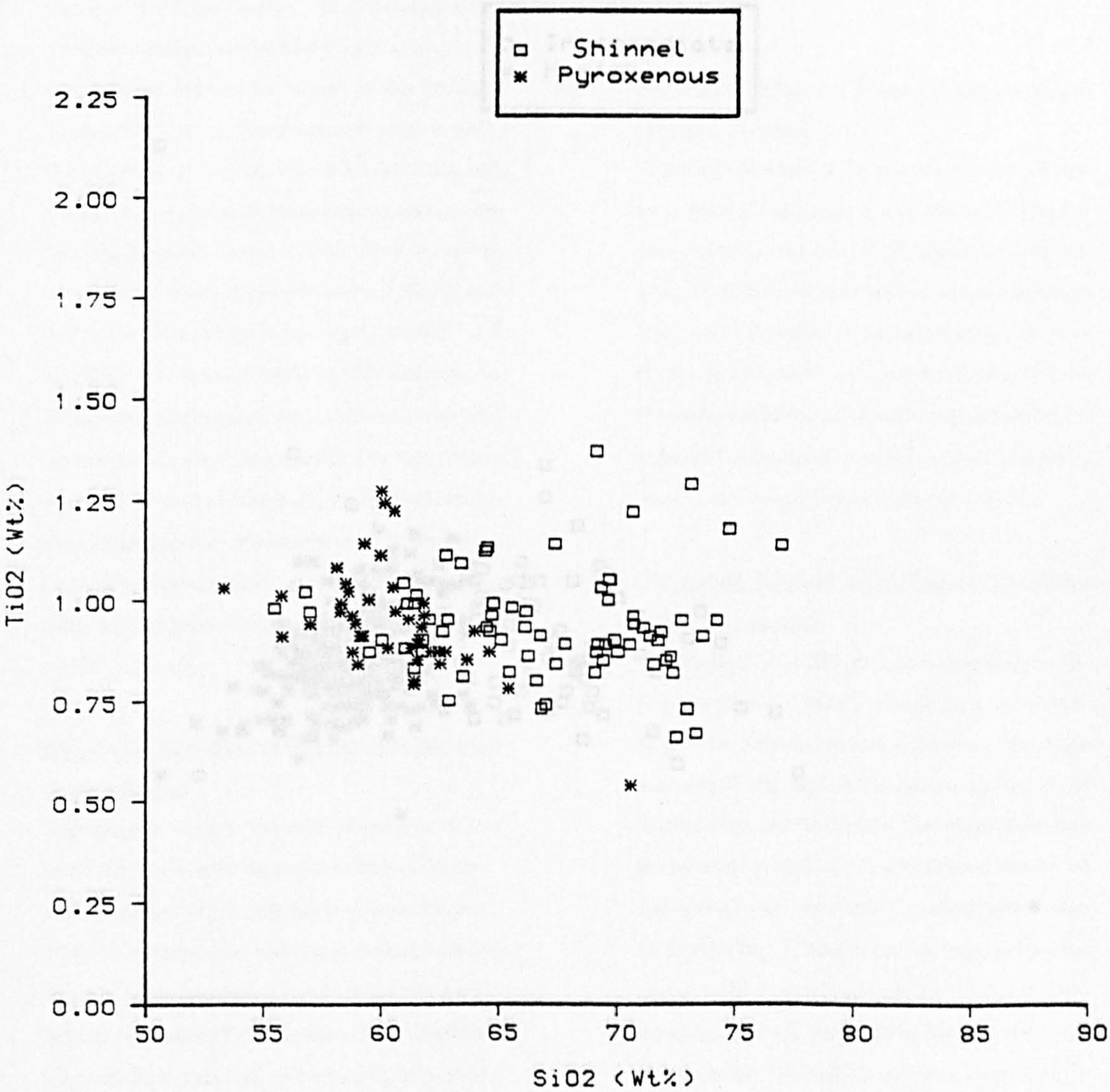

SiO2-TiO2 Discrimination Diagram (Bhatia, 1983).

FIGURE 336

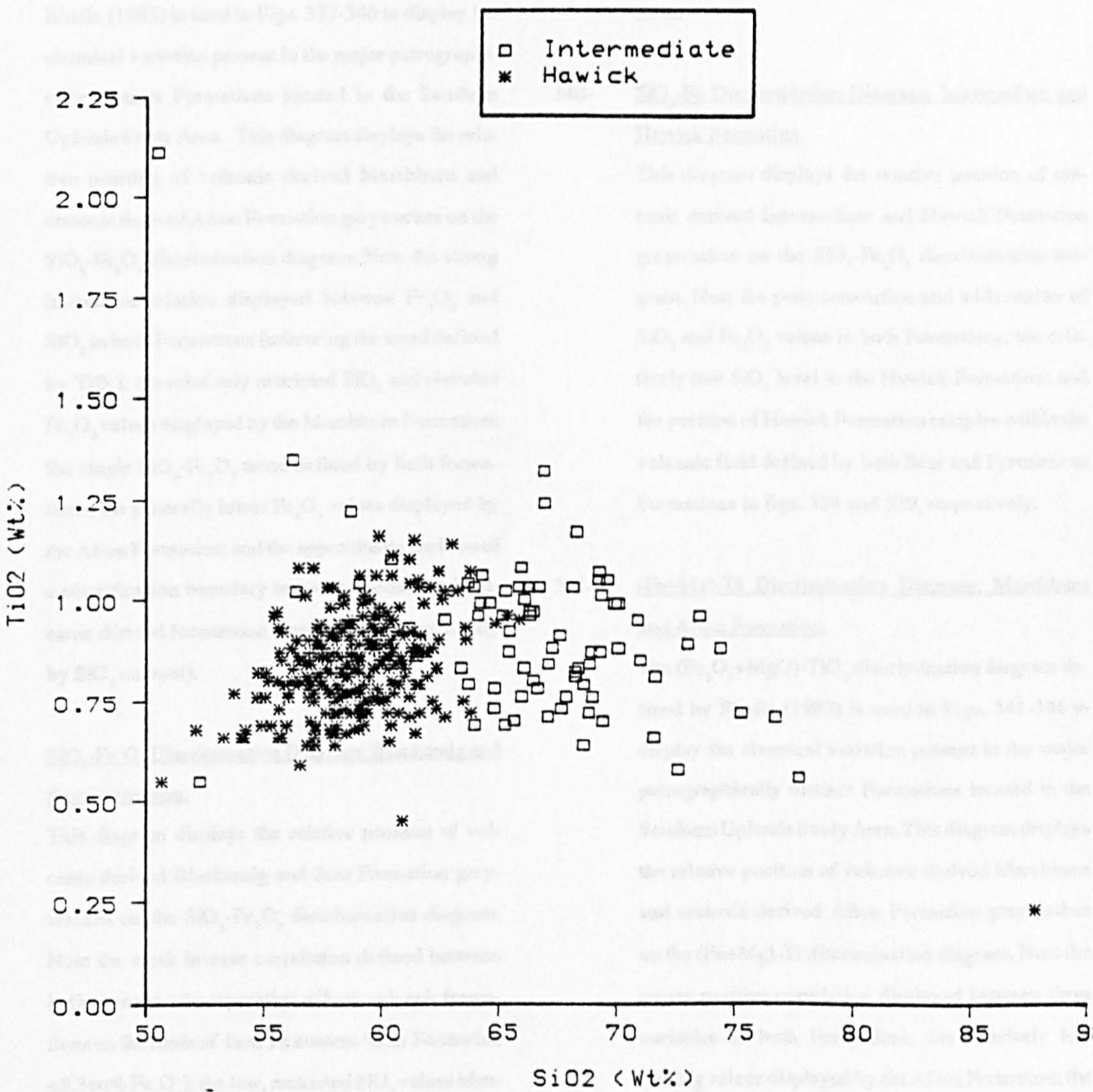

SiO2-TiO2 Discrimination Diagram (Bhatia, 1983).

tively low SiO_2 levels in the Hawick Formation; and the position of Hawick Formation samples within the volcanic field defined by both Scar and Pyroxenous Formations in figs. 334 and 335, respectively.

337- <u>SiO_2-Fe_2O_3 Discrimination Diagram: Marchburn and Afton Formation.</u>

The SiO_2-Fe_2O_3 discrimination diagram defined by Bhatia (1983) is used in Figs. 337-340 to display the chemical variation present in the major petrographically distinct Formations located in the Southern Uplands Study Area. This diagram displays the relative position of volcanic derived Marchburn and cratonic derived Afton Formation greywackes on the SiO_2-Fe_2O_3 discrimination diagram. Note the strong inverse correlation displayed between Fe_2O_3 and SiO_2 in both Formations (mirroring the trend defined by TiO_2); the relatively restricted SiO_2 and elevated Fe_2O_3 values displayed by the Marchburn Formation; the single SiO_2-Fe_2O_3 trend defined by both formations; the generally lower Fe_2O_3 values displayed by the Afton Formation; and the approximate position of a classification boundary between cratonic and volcanic derived formations (controlled predominantly by SiO_2 content).

338- <u>SiO_2-Fe_2O_3 Discrimination Diagram: Blackcraig and Scar Formation.</u>

This diagram displays the relative position of volcanic derived Blackcraig and Scar Formation greywackes on the SiO_2-Fe_2O_3 discrimination diagram. Note the weak inverse correlation defined between both elements; the separation of both volcanic formations on the basis of their Fe content (Scar Formation <8.3wt% Fe_2O_3); the low, restricted SiO_2 values identified by both Formations; the position of both groups within the volcanic field defined by the Marchburn Formation in Fig. 337 with the Blackcraig Formation exhibiting a close chemical affinity to the Marchburn Formation.

339- <u>SiO_2-Fe_2O_3 Discrimination Diagram: Pyroxenous and Shinnel Formation.</u>

This diagram displays the relative position of volcanic derived Pyroxenous and cratonic derived Shinnel Formation greywackes on the SiO_2-Fe_2O_2 discrimination diagram. Note the inverse correlation displayed between Fe_2O_3 and SiO_2 in both formations; the elevated SiO_2 values displayed by the Shinnel Formation (identifying the cratonic field); the single SiO_2-Fe_2O_3 trend defined by both formations; and the elevated Fe_2O_3 content of the volcanic Pyroxenous Formation (<6 wt%) displaying similar characteristics to the Scar and Blackcraig Formations.

340- <u>SiO_2-Fe Discrimination Diagram: Intermediate and Hawick Formation.</u>

This diagram displays the relative position of cratonic derived Intermediate and Hawick Formation greywackes on the SiO_2-Fe_2O_3 discrimination diagram. Note the poor correlation and wide scatter of SiO_2 and Fe_2O_3 values in both Formations; the relatively low SiO_2 level in the Hawick Formation; and the position of Hawick Formation samples within the volcanic field defined by both Scar and Pyroxenous Formations in figs. 338 and 339, respectively.

341- <u>(Fe+Mg)-Ti Discrimination Diagram: Marchburn and Afton Formation.</u>

The (Fe_2O_3+MgO)-TiO_2 discrimination diagram defined by Bhatia (1983) is used in Figs. 341-344 to display the chemical variation present in the major petrographically distinct Formations located in the Southern Uplands Study Area. This diagram displays the relative position of volcanic derived Marchburn and cratonic derived Afton Formation greywackes on the (Fe+Mg)-Ti discrimination diagram. Note the strong positive correlation displayed between these variables in both Formations; the relatively low Fe+Mg values displayed by the Afton Formation; the single trend defined by both formations; the generally lower TiO_2 values displayed by the Afton Formation; and the approximate position of a classification boundary between cratonic and volcanic derived formations.

342- <u>(Fe+Mg)-Ti Discrimination Diagram: Blackcraig and Scar Formation.</u>

This diagram displays the relative position of volcanic derived Blackcraig and Scar Formation greywackes on the (Fe+Mg)-Ti discrimination diagram.

FIGURE 337

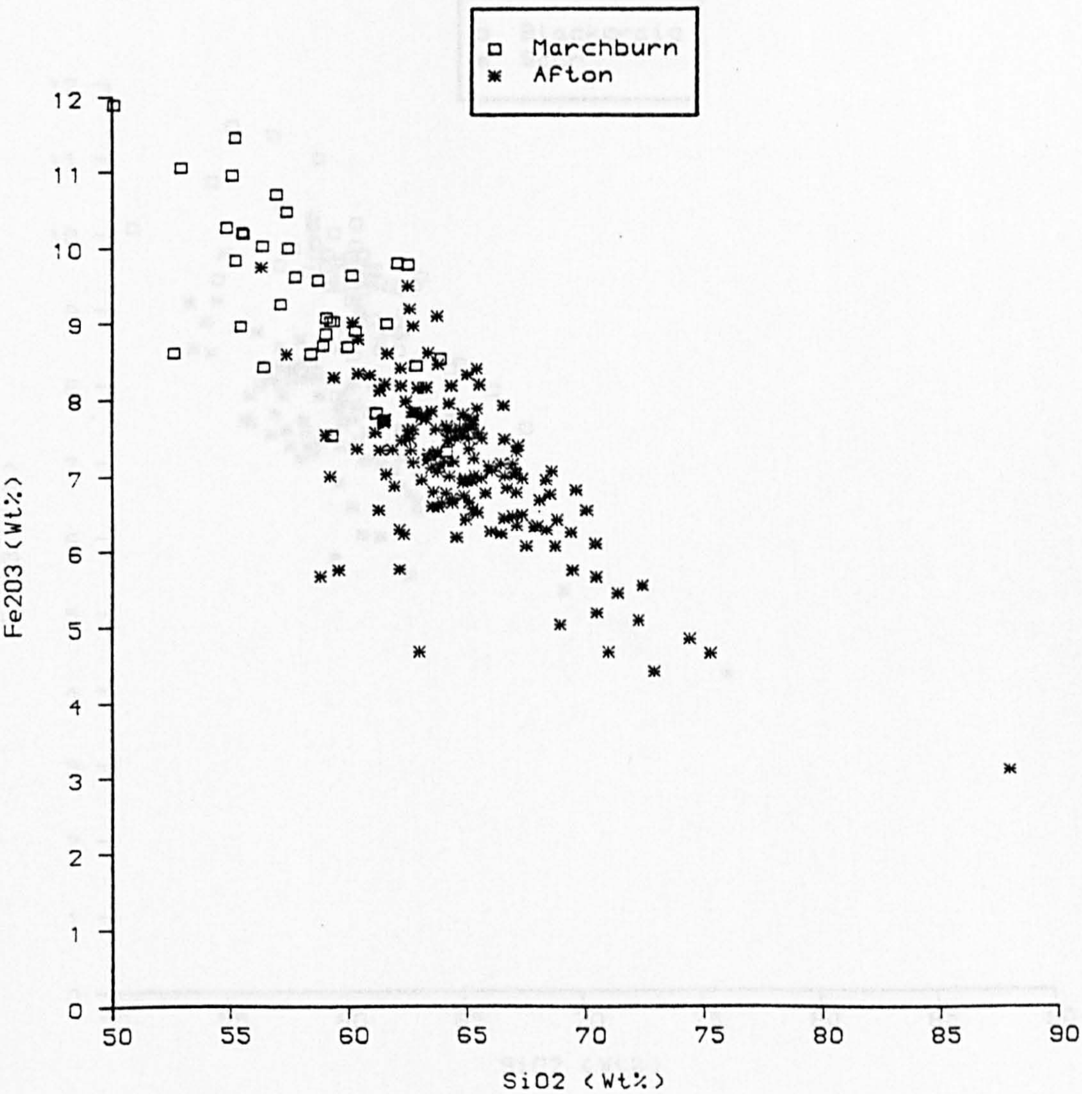

SiO2-Fe2O3 Discrimination Diagram (Bhatia, 1983).

FIGURE 338

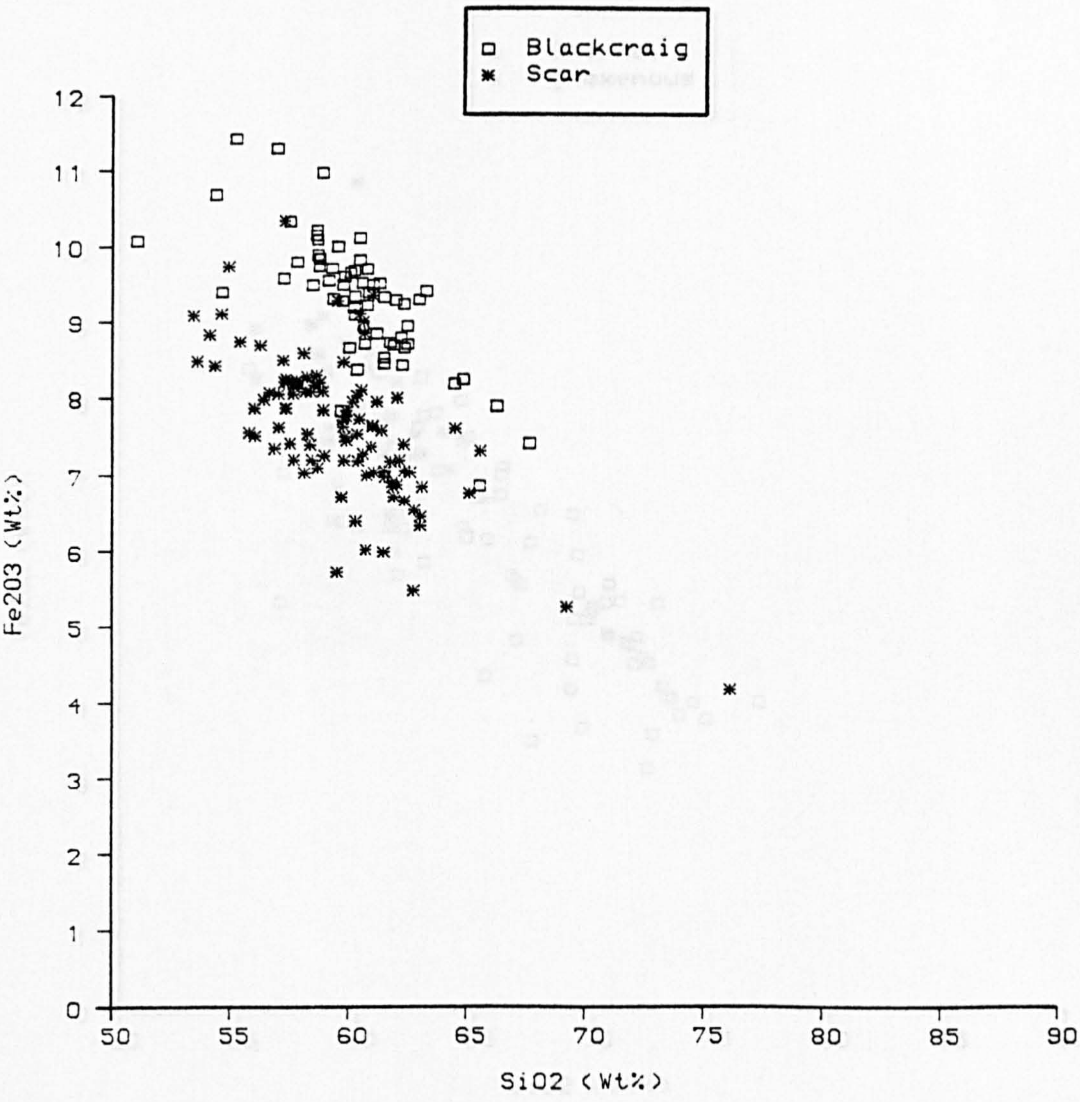

SiO2-Fe2O3 Discrimination Diagram (Bhatia, 1983).

FIGURE 339

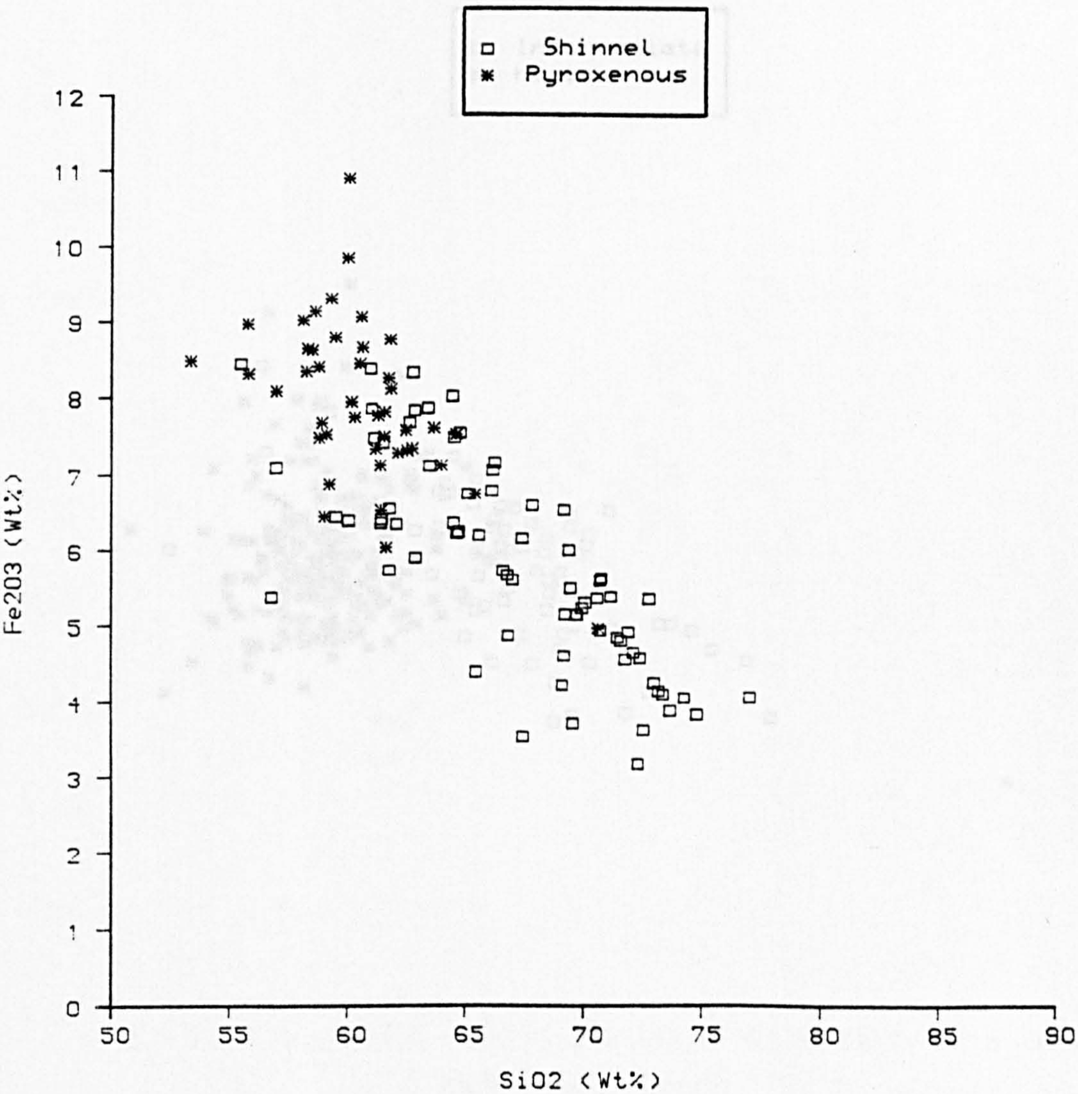

SiO2-Fe2O3 Discrimination Diagram (Bhatia, 1983).

FIGURE 340

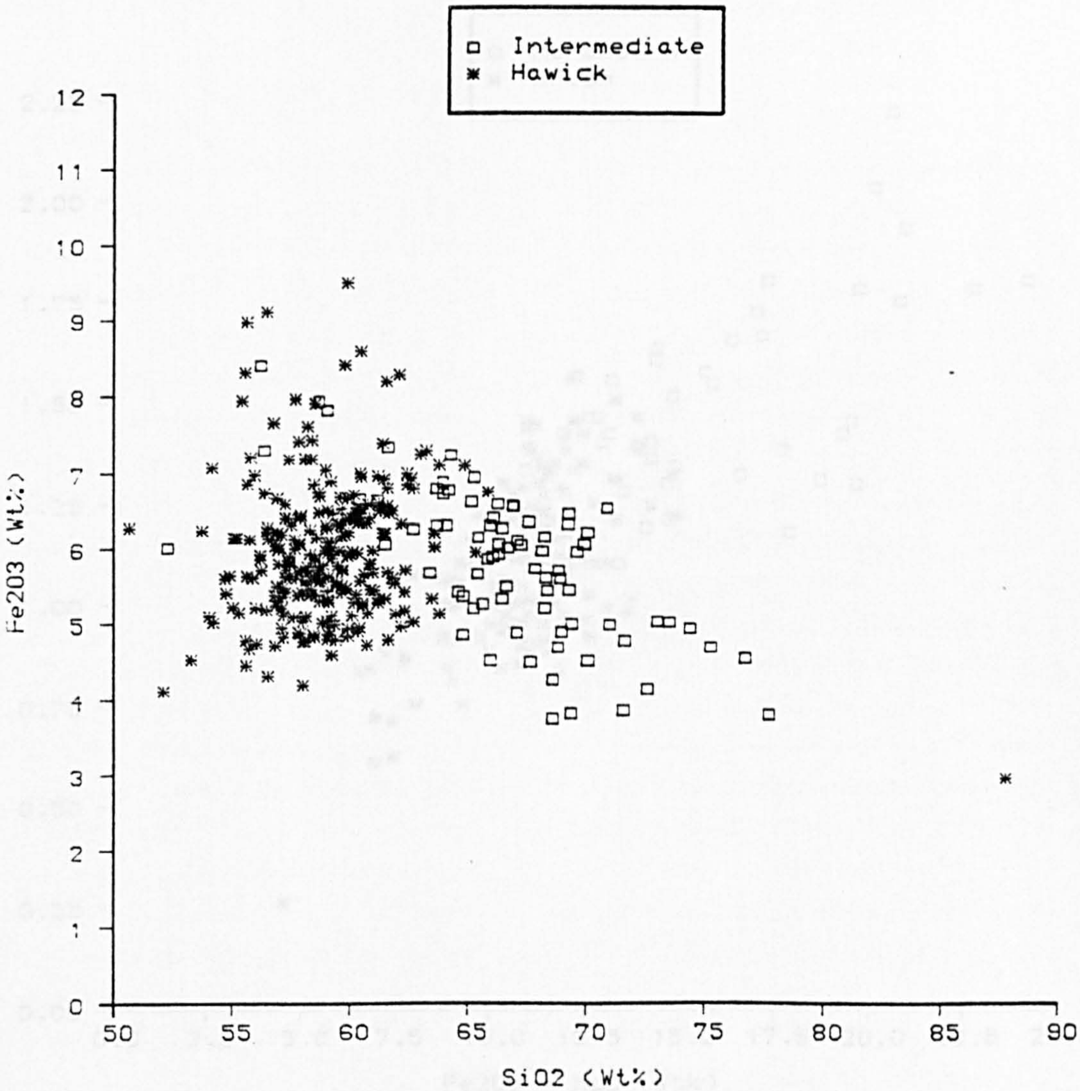

SiO2-Fe2O3 Discrimination Diagram (Bhatia, 1983).

FIGURE 341

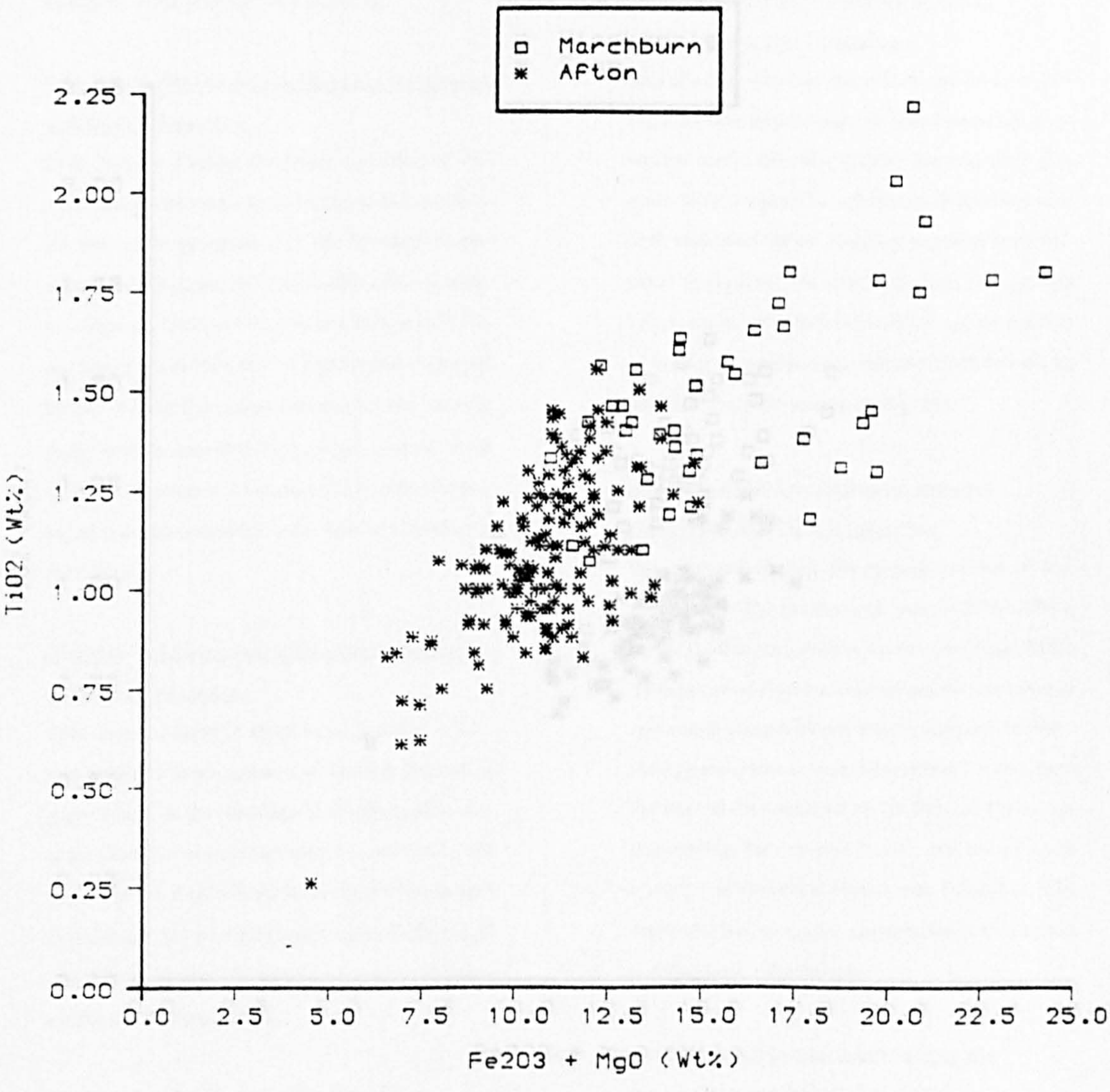

Discrimination Diagram (Bhatia, 1983).

FIGURE 342

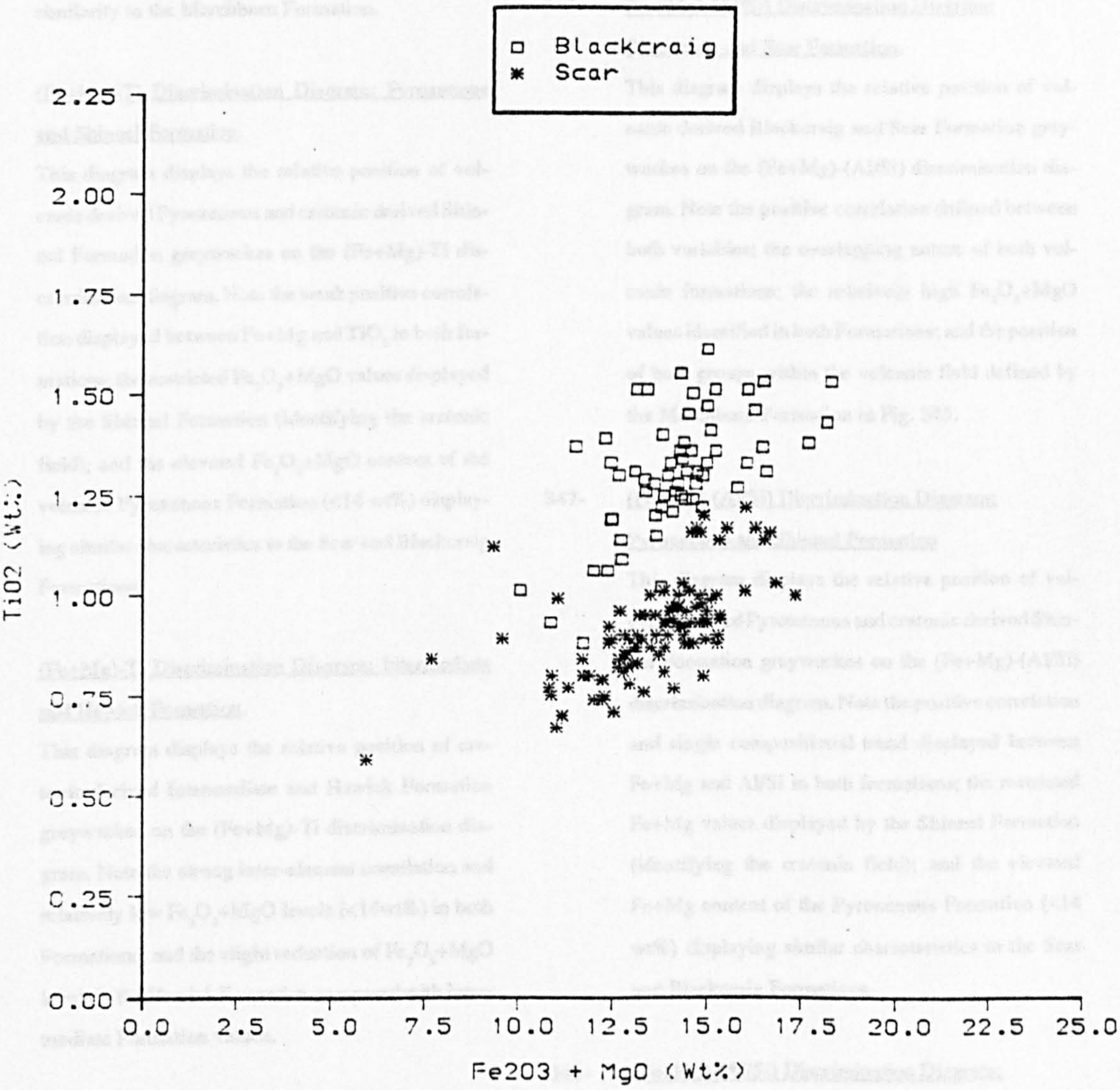

Discrimination Diagram (Bhatia, 1983).

Note the strong positive correlation defined between both elements; the separation of both volcanic formations on the basis of their TiO_2 content (Scar Formation<1.1wt% TiO_2); the relatively high Fe_2O_3+MgO values identified in both Formations; the position of both groups within the volcanic field defined by the Marchburn Formation in Fig. 341 with the Blackcraig Formation exhibiting a close chemical similarity to the Marchburn Formation.

343- <u>(Fe+Mg)-Ti Discrimination Diagram: Pyroxenous and Shinnel Formation</u>.

This diagram displays the relative position of volcanic derived Pyroxenous and cratonic derived Shinnel Formation greywackes on the (Fe+Mg)-Ti discrimination diagram. Note the weak positive correlation displayed between Fe+Mg and TiO_2 in both formations; the restricted Fe_2O_3+MgO values displayed by the Shinnel Formation (identifying the cratonic field); and the elevated Fe_2O_3+MgO content of the volcanic Pyroxenous Formation (<14 wt%) displaying similar characteristics to the Scar and Blackcraig Formations.

344- <u>(Fe+Mg)-Ti Discrimination Diagram: Intermediate and Hawick Formation</u>.

This diagram displays the relative position of cratonic derived Intermediate and Hawick Formation greywackes on the (Fe+Mg)-Ti discrimination diagram. Note the strong inter-element correlation and relatively low Fe_2O_3+MgO levels (<14wt%) in both Formations; and the slight reduction of Fe_2O_3+MgO levels in the Hawick Formation compared with Intermediate Formation values.

345- <u>(Fe+Mg)-(Al/Si) Discrimination Diagram: Marchburn and Afton Formation</u>.

The (Fe+Mg)-(Al/Si) discrimination diagram defined by Bhatia (1983) is used in Figs. 345-348 to display the chemical variation present in the major petrographically distinct Formations located in the Southern Uplands Study Area. This diagram displays the relative position of volcanic derived Marchburn and cratonic derived Afton Formation greywackes on the (Fe+Mg)-(Al/Si) discrimination diagram. Note the weak positive correlation displayed between these variables in both Formations; the relatively low Fe_2O_3 +MgO values displayed by the Afton Formation; the single trend defined by both formations; the generally higher Al/Si values displayed by the Marchburn Formation; and the approximate position of a classification boundary between cratonic and volcanic derived formations.

346- <u>(Fe+Mg)-(Al/Si) Discrimination Diagram: Blackcraig and Scar Formation</u>.

This diagram displays the relative position of volcanic derived Blackcraig and Scar Formation greywackes on the (Fe+Mg)-(Al/Si) discrimination diagram. Note the positive correlation defined between both variables; the overlapping nature of both volcanic formations; the relatively high Fe_2O_3+MgO values identified in both Formations; and the position of both groups within the volcanic field defined by the Marchburn Formation in Fig. 345.

347- <u>(Fe+Mg)-(Al/Si) Discrimination Diagram: Pyroxenous and Shinnel Formation</u>

This diagram displays the relative position of volcanic derived Pyroxenous and cratonic derived Shinnel Formation greywackes on the (Fe+Mg)-(Al/Si) discrimination diagram. Note the positive correlation and single compositional trend displayed between Fe+Mg and Al/Si in both formations; the restricted Fe+Mg values displayed by the Shinnel Formation (identifying the cratonic field); and the elevated Fe+Mg content of the Pyroxenous Formation (<14 wt%) displaying similar characteristics to the Scar and Blackcraig Formations.

348- <u>(Fe+Mg)-(Al/Si) Discrimination Diagram: Intermediate and Hawick Formation</u>

This diagram displays the relative position of cratonic derived Intermediate and Hawick Formation greywackes on the (Fe+Mg)-(Al/Si) discrimination diagram. Note the strong inter-element correlation; the relatively low Fe+Mg levels (<14wt%) in both Formations (defining the cratonic field); and the slight reduction in Fe+Mg and Al/Si levels in the Hawick Formation compared with the juxtaposed Intermediate Formation.

FIGURE 343

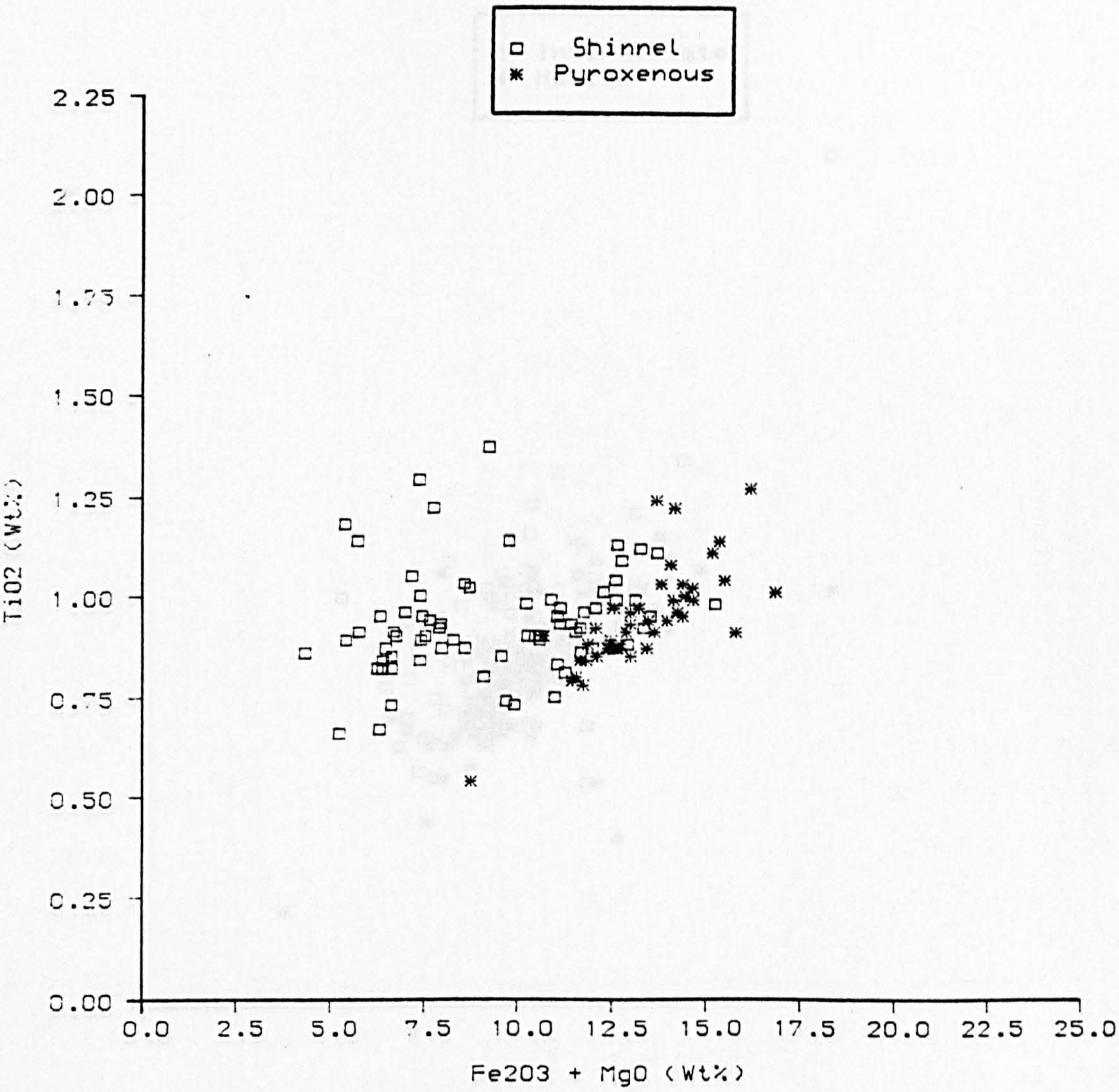

Discrimination Diagram (Bhatia, 1983).

FIGURE 344

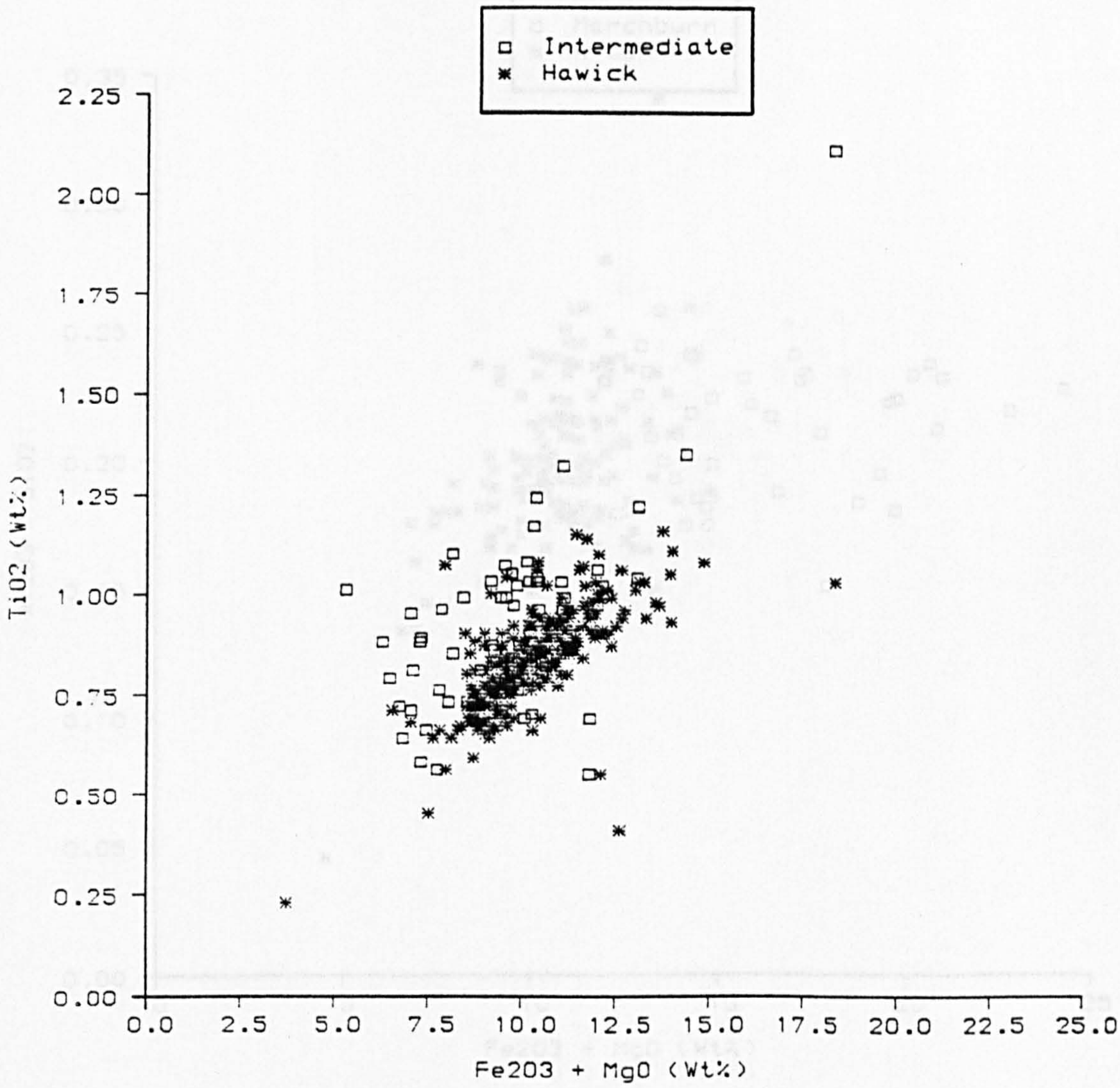

Discrimination Diagram (Bhatia, 1983).

FIGURE 345

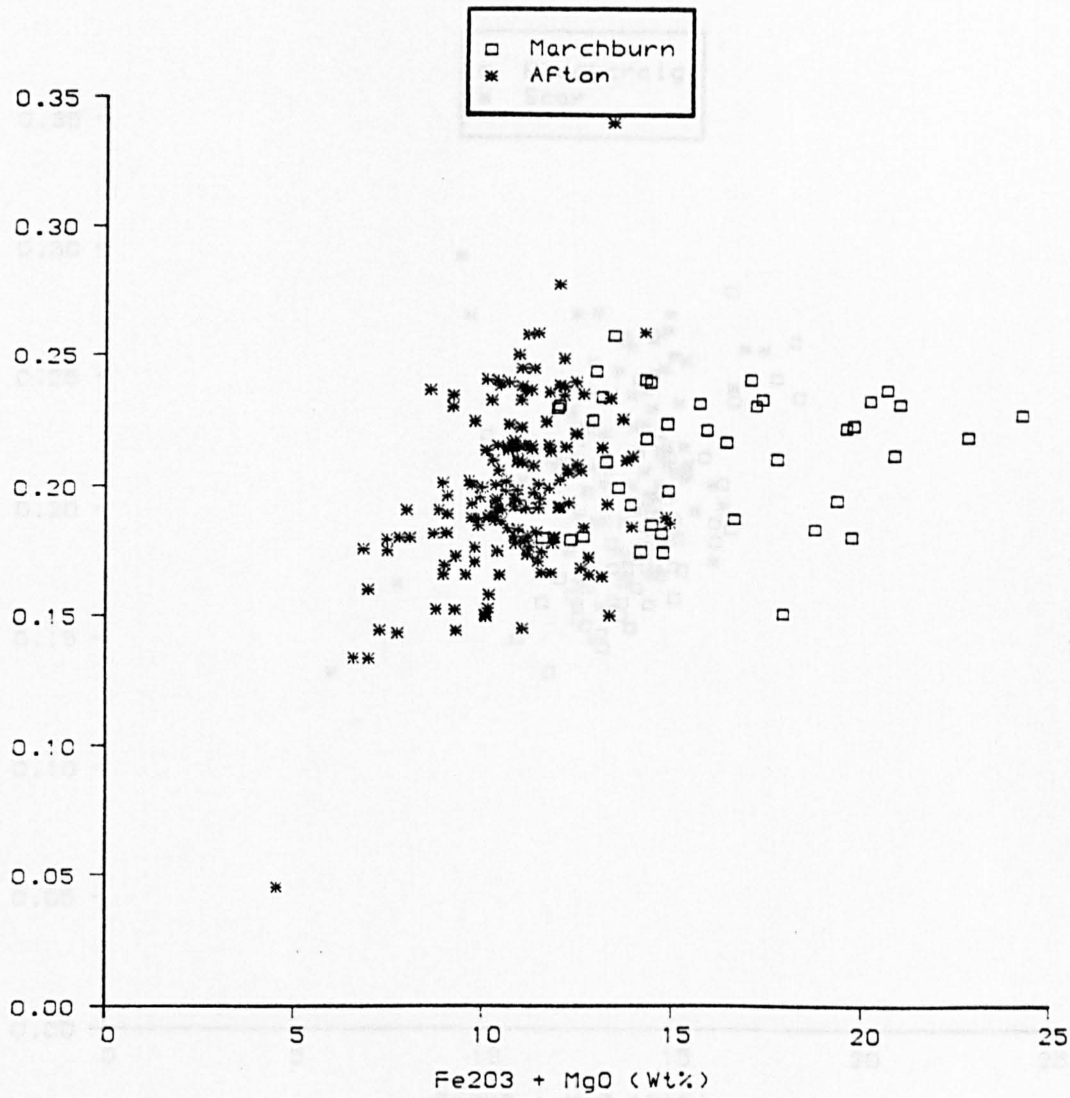

Discrimination Diagram (Bhatia, 1983).

FIGURE 346

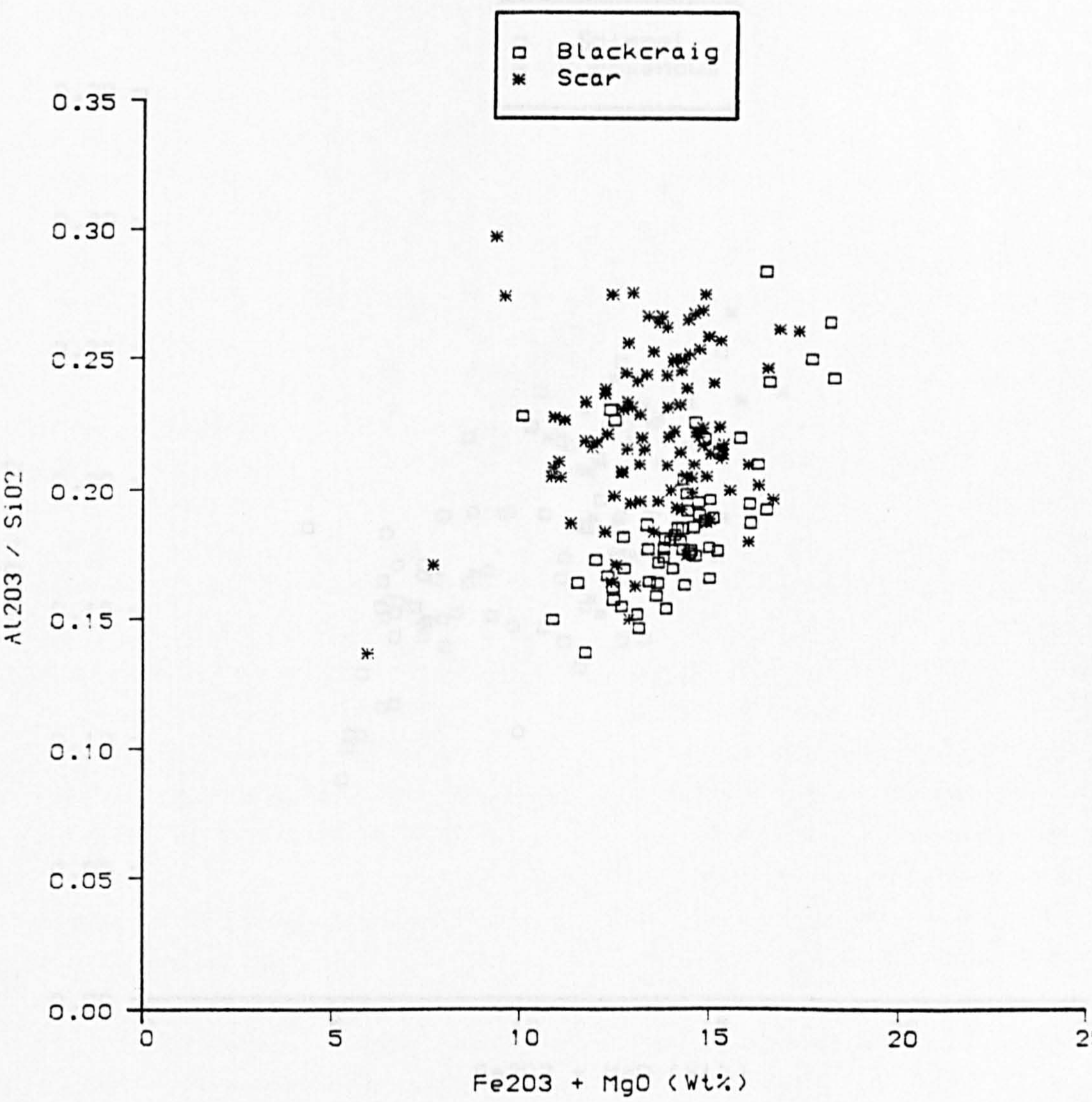

Discrimination Diagram (Bhatia, 1983).

FIGURE 347

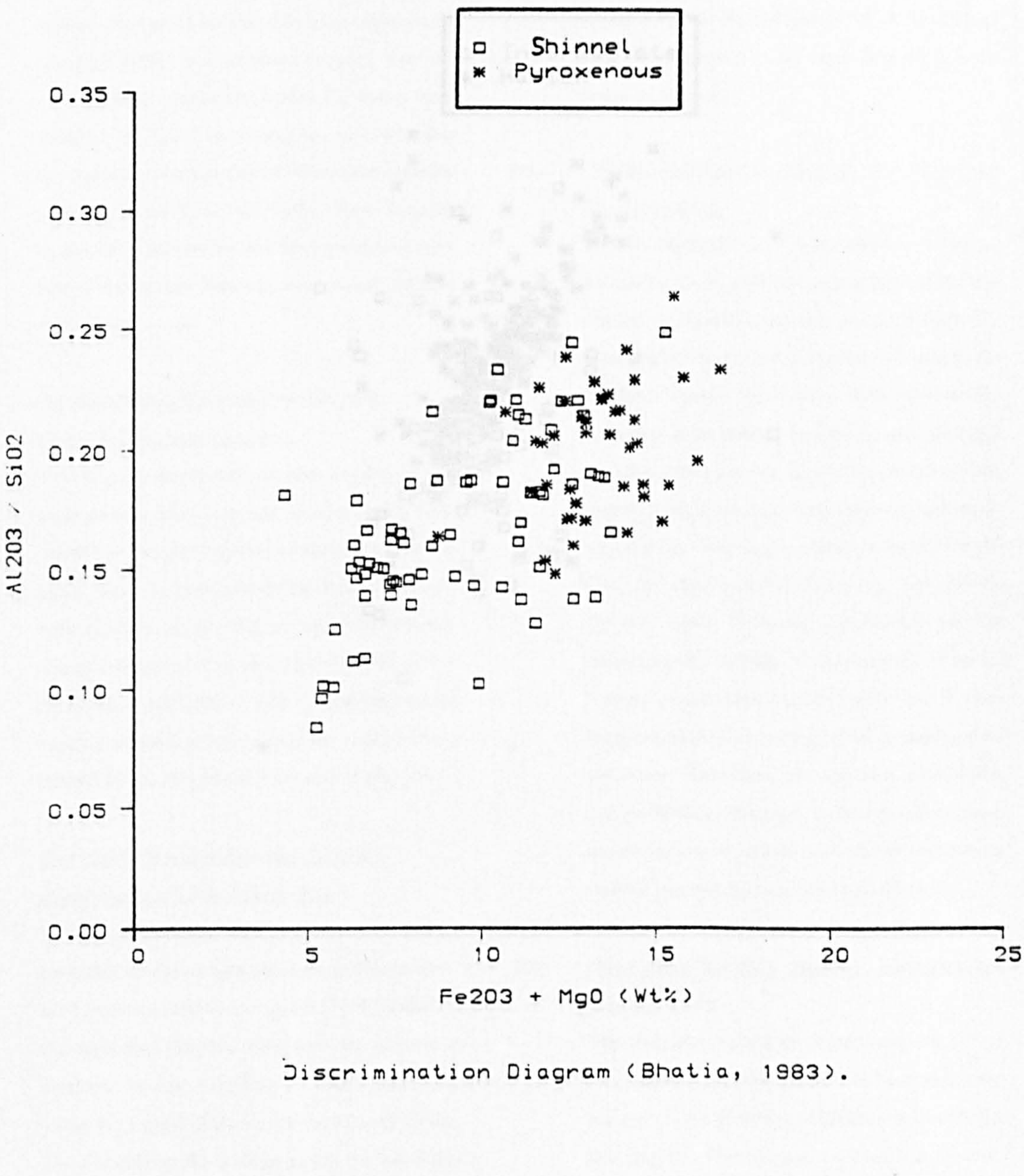

Discrimination Diagram (Bhatia, 1983).

FIGURE 348

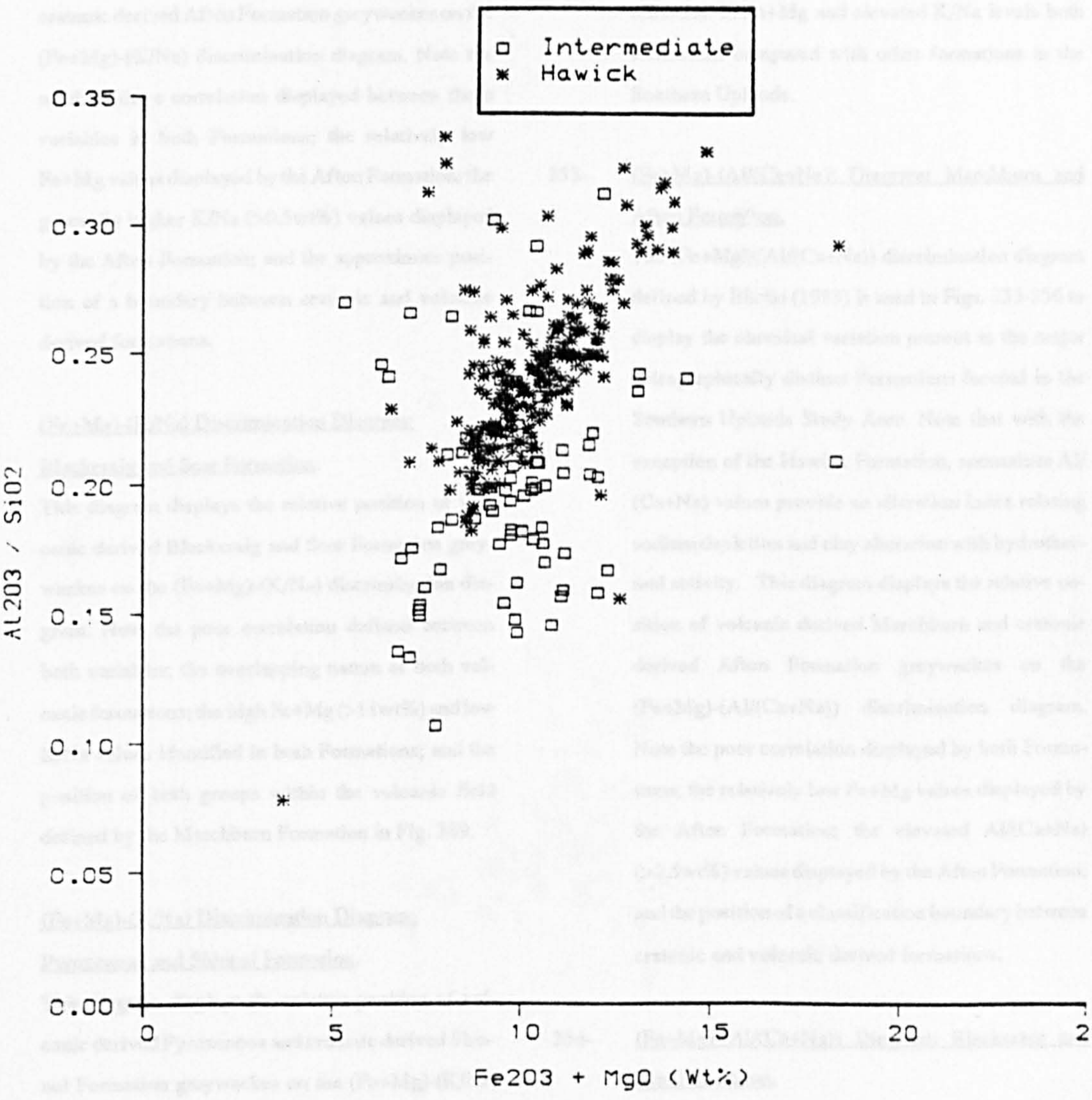

Discrimination Diagram (Bhatia, 1983).

349- (Fe+Mg)-(K/Na) Discrimination Diagram: Marchburn and Afton Formation.

The (Fe+Mg)-(K/Na) discrimination diagram defined by Bhatia (1983) is used in Figs. 349-352 to display the variation present in the major petrographically distinct Formations located in the Southern Uplands Study Area. This diagram displays the relative position of volcanic derived Marchburn and cratonic derived Afton Formation greywackes on the (Fe+Mg)-(K/Na) discrimination diagram. Note the weak positive correlation displayed between these variables in both Formations; the relatively low Fe+Mg values displayed by the Afton Formation; the generally higher K/Na (>0.5wt%) values displayed by the Afton Formation; and the approximate position of a boundary between cratonic and volcanic derived formations.

350- (Fe+Mg)-(K/Na) Discrimination Diagram: Blackcraig and Scar Formation.

This diagram displays the relative position of volcanic derived Blackcraig and Scar Formation greywackes on the (Fe+Mg)-(K/Na) discrimination diagram. Note the poor correlation defined between both variables; the overlapping nature of both volcanic formations; the high Fe+Mg (>11wt%) and low K/Na values identified in both Formations; and the position of both groups within the volcanic field defined by the Marchburn Formation in Fig. 349.

351- (Fe+Mg)-(K/Na) Discrimination Diagram: Pyroxenous and Shinnel Formation.

This diagram displays the relative position of volcanic derived Pyroxenous and cratonic derived Shinnel Formation greywackes on the (Fe+Mg)-(K/Na) discrimination diagram. Note the poor correlation displayed by both variables; the restricted Fe+Mg values (<11 ppm) displayed by the Shinnel Formation (identifying the cratonic field); the low K/Na values and elevated Fe+Mg (>11wt%) content of the volcanic Pyroxenous Formation displaying similar characteristics to the Scar and Blackcraig Formations.

352- (Fe+Mg)-(K/Na) Discrimination Diagram: Intermediate and Hawick Formation.

This diagram displays the relative position of cratonic derived Intermediate and Hawick Formation greywackes on the (Fe+Mg)-(K/Na) discrimination diagram. Note the strong inter-element correlation; the relatively low Fe+Mg levels (<13wt%) in both Formations (the cratonic field); and the slight reduction in Fe+Mg and elevated K/Na levels both formations compared with other formations in the Southern Uplands.

353- (Fe+Mg)-(Al/(Ca+Na)) Diagram: Marchburn and Afton Formation.

The (Fe+Mg)-(Al/(Ca+Na)) discrimination diagram defined by Bhatia (1983) is used in Figs. 353-356 to display the chemical variation present in the major petrographically distinct Formations located in the Southern Uplands Study Area. Note that with the exception of the Hawick Formation, anomalous Al/(Ca+Na) values provide an alteration index relating sodium depletion and clay alteration with hydrothermal activity. This diagram displays the relative position of volcanic derived Marchburn and cratonic derived Afton Formation greywackes on the (Fe+Mg)-(Al/(Ca+Na)) discrimination diagram. Note the poor correlation displayed by both Formations; the relatively low Fe+Mg values displayed by the Afton Formation; the elevated Al/(Ca+Na) (>2.5wt%) values displayed by the Afton Formation; and the position of a classification boundary between cratonic and volcanic derived formations.

354- (Fe+Mg)-(Al/(Ca+Na)) Diagram: Blackcraig and Scar Formation.

This diagram displays the relative position of volcanic derived Blackcraig and Scar Formation greywackes on the (Fe+Mg)-(Al/(Ca+Na)) discrimination diagram. Note the poor correlation defined between both variables; the overlapping nature of both volcanic formations; the high Fe+Mg (>11wt%) and low Al/(Ca+Na) values identified in both Formations; and the position of both groups within the volcanic field defined by the Marchburn Formation in Fig. 353.

FIGURE 349

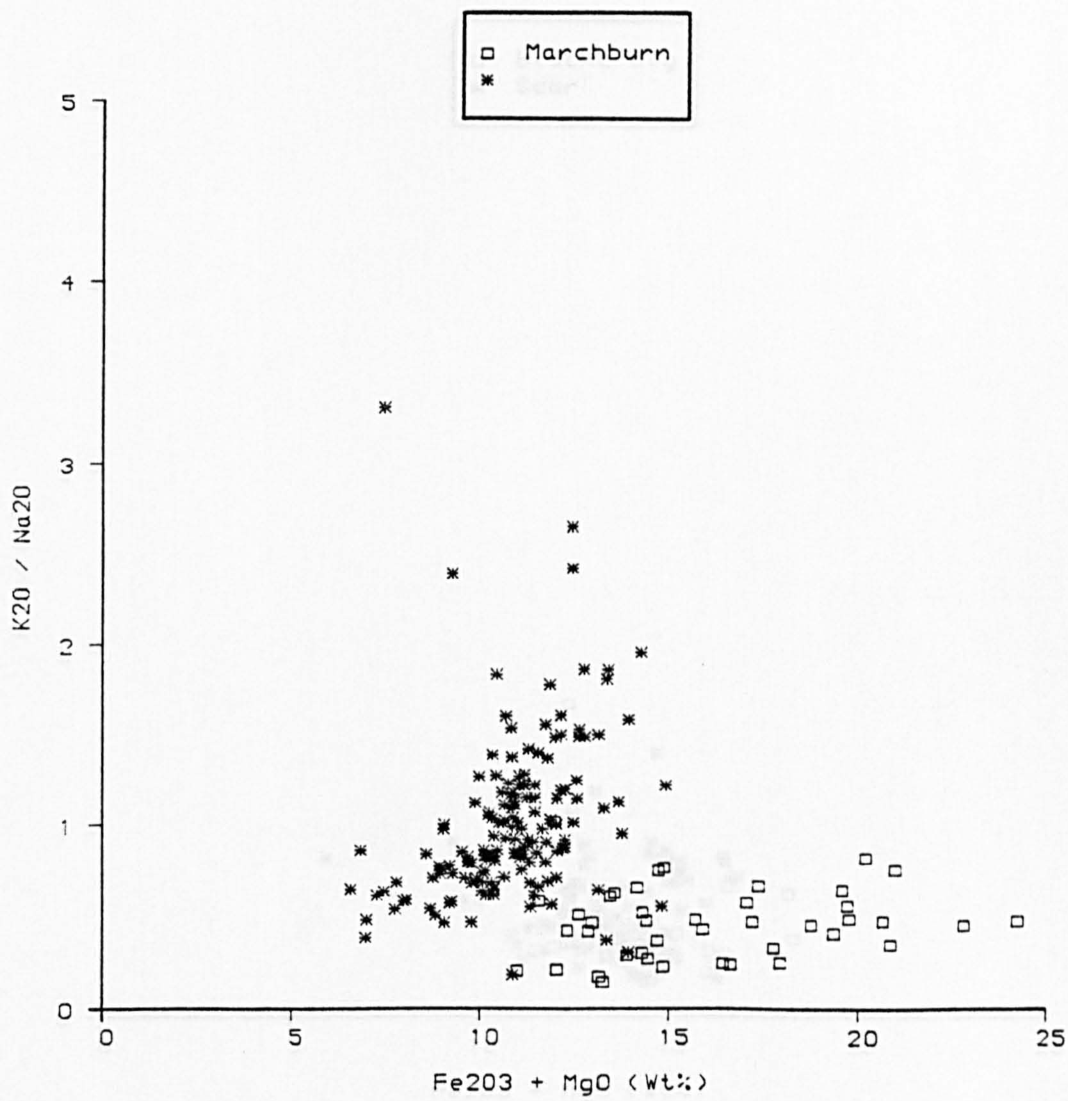

Discrimination Diagram (Bhatia, 1983).

FIGURE 350

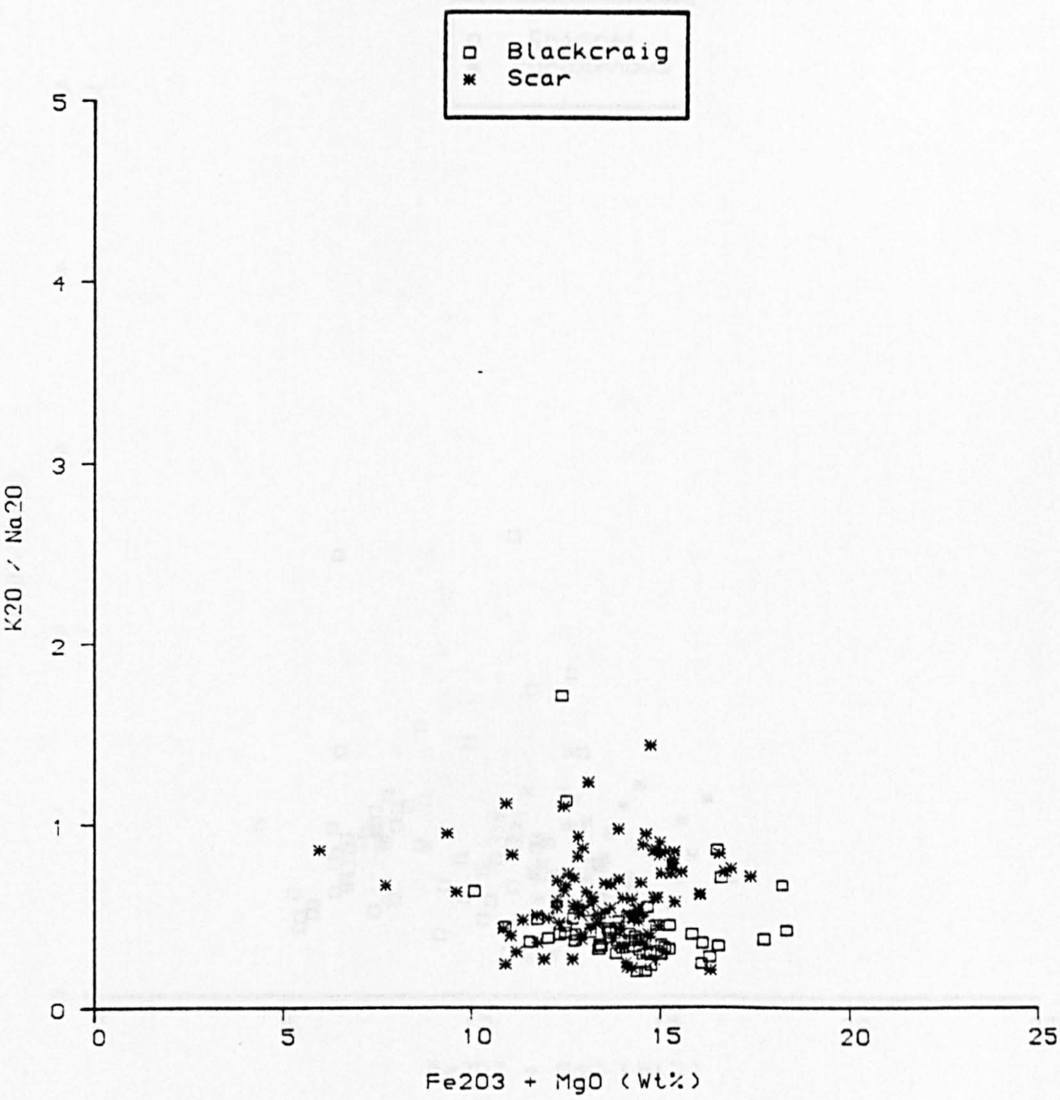

Discrimination Diagram (Bhatia, 1983).

FIGURE 351

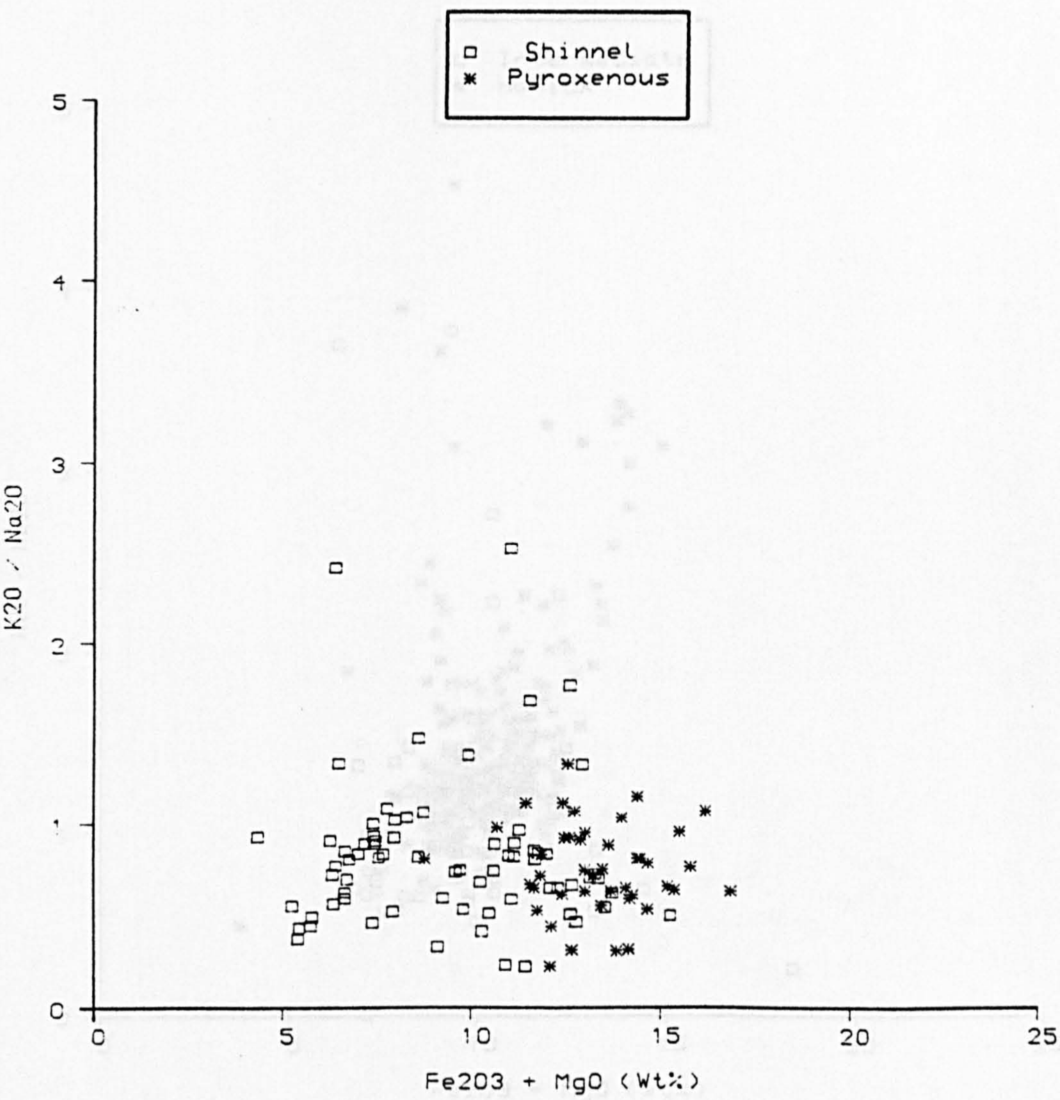

Discrimination Diagram (Bhatia, 1983).

FIGURE 352

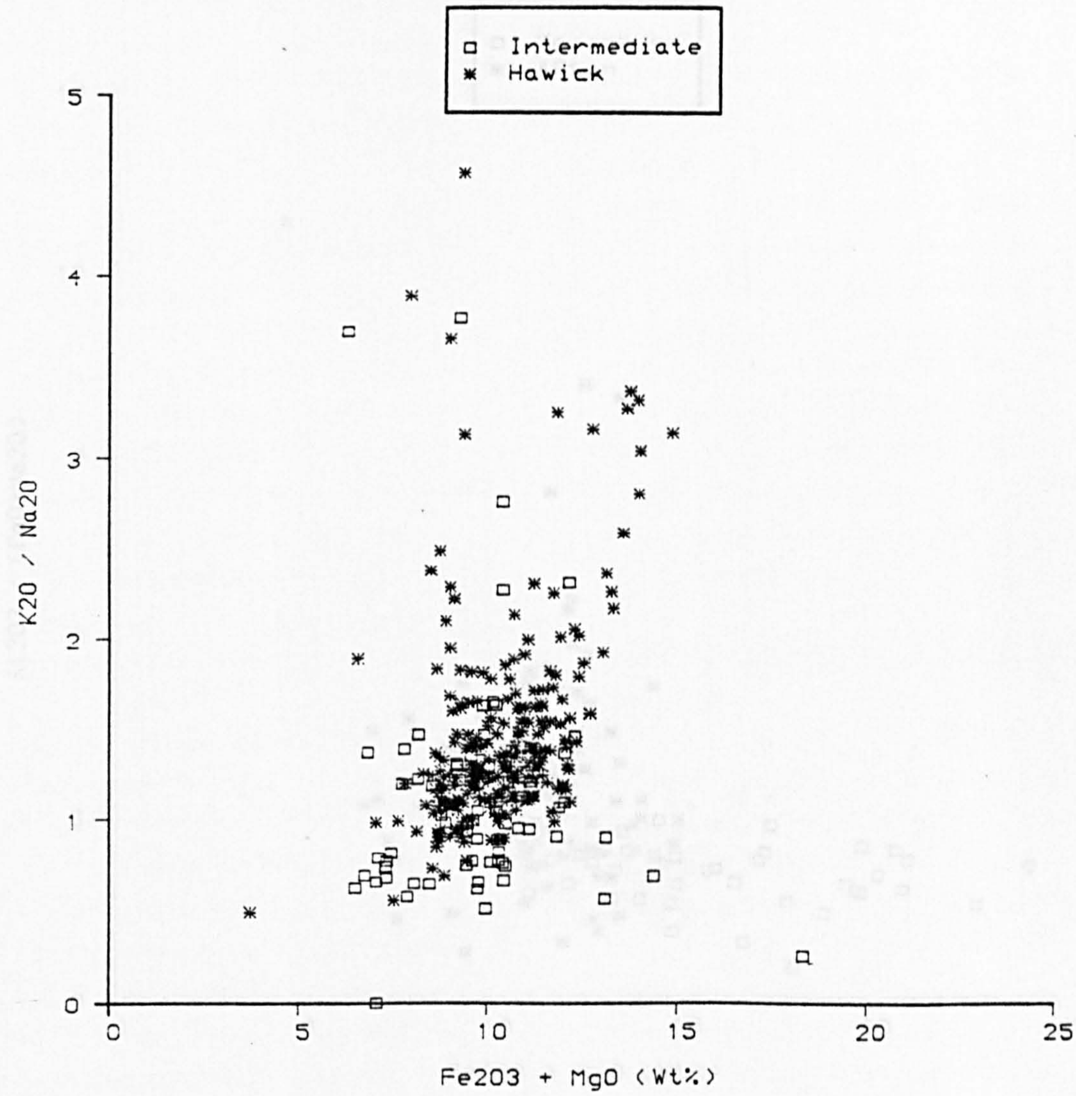

Discrimination Diagram (Bhatia, 1983).

FIGURE 353

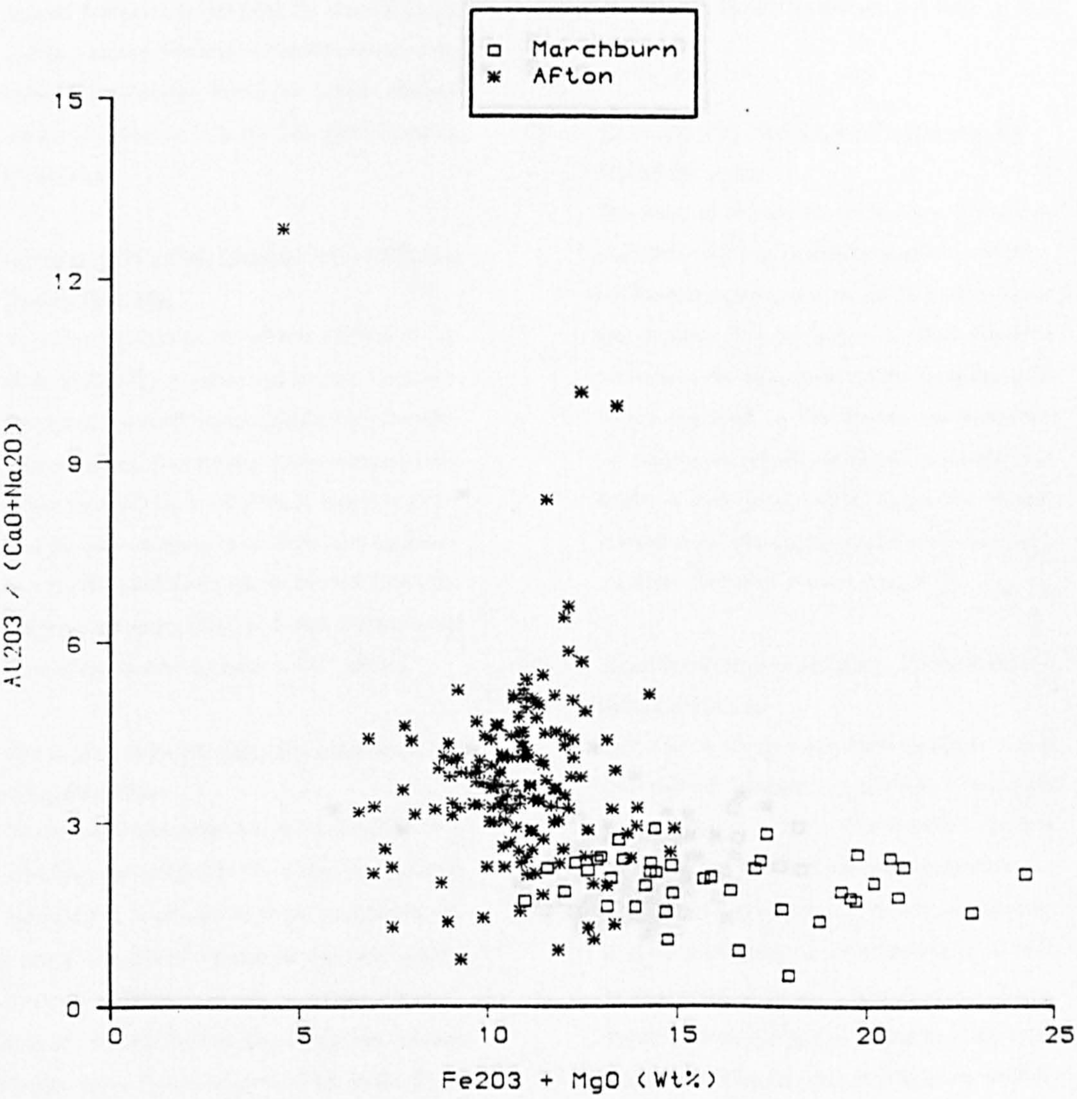

Discrimination Diagram (Bhatia, 1983).

FIGURE 354

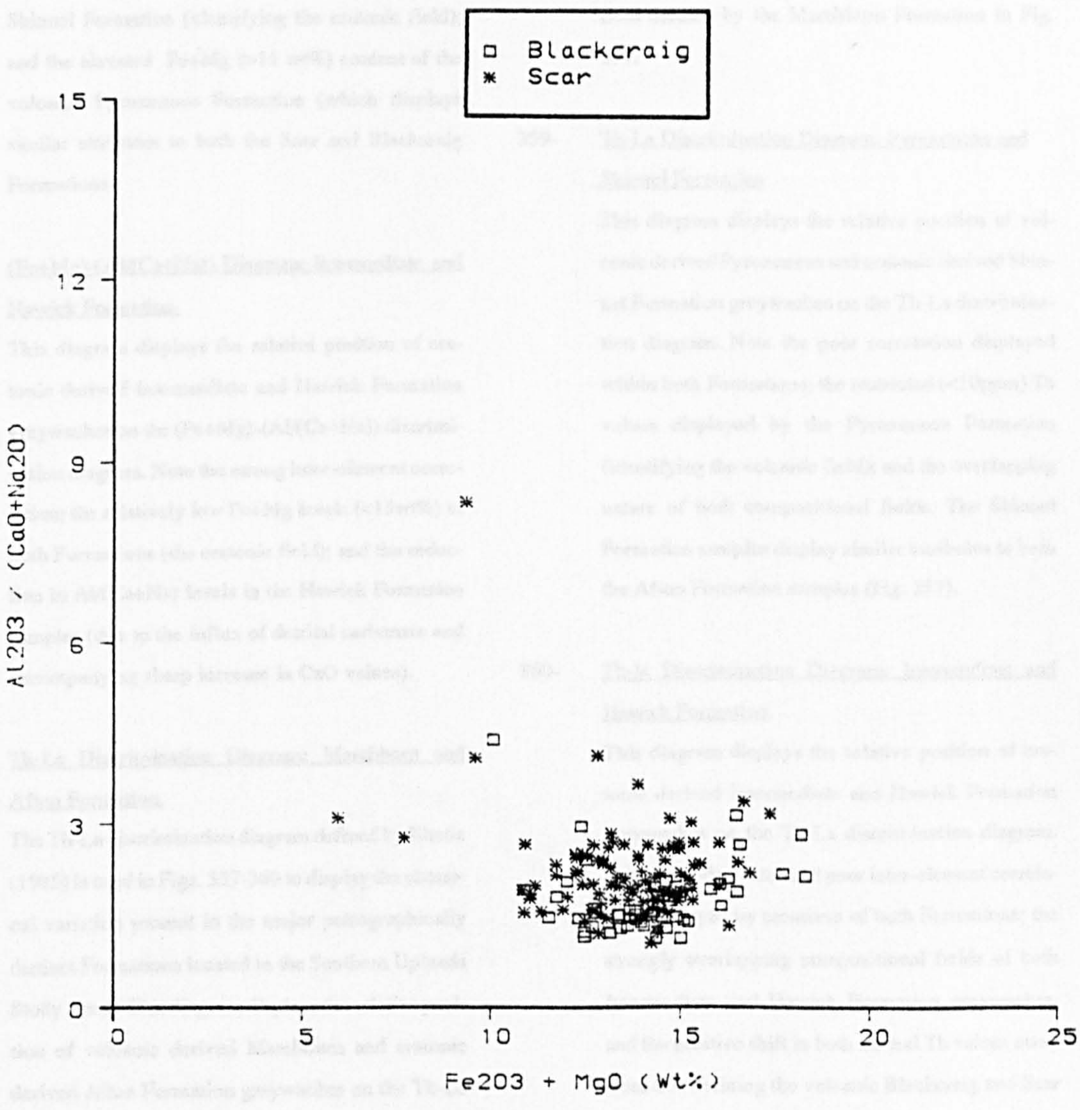

Discrimination Diagram (Bhatia, 1983).

355- (Fe+Mg)-(Al/(Ca+Na)) Diagram: Pyroxenous and Shinnel Formation.
This diagram displays the relative position of volcanic derived Pyroxenous and cratonic derived Shinnel Formation greywackes on the (Fe+Mg)-(Al/(Ca+Na)) discrimination diagram. Note the poor correlation displayed within both Formations; the restricted (<11wt%) Fe+Mg values displayed by the Shinnel Formation (identifying the cratonic field); and the elevated Fe+Mg (>11 wt%) content of the volcanic Pyroxenous Formation (which displays similar attributes to both the Scar and Blackcraig Formations).

356- (Fe+Mg)-(Al/(Ca+Na)) Diagram: Intermediate and Hawick Formation.
This diagram displays the relative position of cratonic derived Intermediate and Hawick Formation greywackes on the (Fe+Mg)-(Al/(Ca+Na)) discrimination diagram. Note the strong inter-element correlation; the relatively low Fe+Mg levels (<13wt%) in both Formations (the cratonic field); and the reduction in Al/(Ca+Na) levels in the Hawick Formation samples (due to the influx of detrital carbonate and accompanying sharp increase in CaO values).

357- Th-La Discrimination Diagram: Marchburn and Afton Formation.
The Th-La discrimination diagram defined by Bhatia (1985) is used in Figs. 357-360 to display the chemical variation present in the major petrographically distinct Formations located in the Southern Uplands Study Area. This diagram displays the relative position of volcanic derived Marchburn and cratonic derived Afton Formation greywackes on the Th-La discrimination diagram. Note the positive correlation displayed by both Formations; the relatively low La and Th values displayed by the Marchburn Formation; the elevated La (>20ppm) and Th (>5ppm) values displayed by the cratonic Afton Formation; and the position of a approximate discrimination boundary between cratonic and volcanic derived formations.

358- Th-La Discrimination Diagram: Blackcraig and Scar Formation. This diagram displays the relative position of volcanic derived Blackcraig and Scar Formation greywackes on the La-Th discrimination diagram. Note the weak positive correlation defined between La and Th; the overlapping compositional fields and generally low (<10ppm) Th levels in both Formations; the relatively low La values (<17ppm) identifying Blackcraig Formation samples; and the concentration of both groups within the volcanic field defined by the Marchburn Formation in Fig. 357.

359- Th-La Discrimination Diagram: Pyroxenous and Shinnel Formation
This diagram displays the relative position of volcanic derived Pyroxenous and cratonic derived Shinnel Formation greywackes on the Th-La discrimination diagram. Note the poor correlation displayed within both Formations; the restricted (<10ppm) Th values displayed by the Pyroxenous Formation (identifying the volcanic field); and the overlapping nature of both compositional fields. The Shinnel Formation samples display similar attributes to both the Afton Formation samples (Fig. 357).

360- Th-la Discrimination Diagram: Intermediate and Hawick Formation.
This diagram displays the relative position of cratonic derived Intermediate and Hawick Formation greywackes on the Th-La discrimination diagram. Note the wide scatter and poor inter-element correlation displayed by members of both Formations; the strongly overlapping compositional fields of both Intermediate and Hawick Formation greywackes; and the positive shift in both La and Th values away from that defining the volcanic Blackcraig and Scar Formations.

361- (K/K+Na)-(K+Na) Discrimination Diagram: Marchburn and Afton Formation.
The (K/K+Na)-(K+Na) diagram defined by Cathelineau (1983) is used in Figs. 361-365 to display the chemical variation present in the major petrographically distinct Formations located in the Southern Uplands Study Area. The K/K+Na variable is used by Cathelineau (op. cit) to assess the level of potassic metasomatism present within individual samples,

FIGURE 355

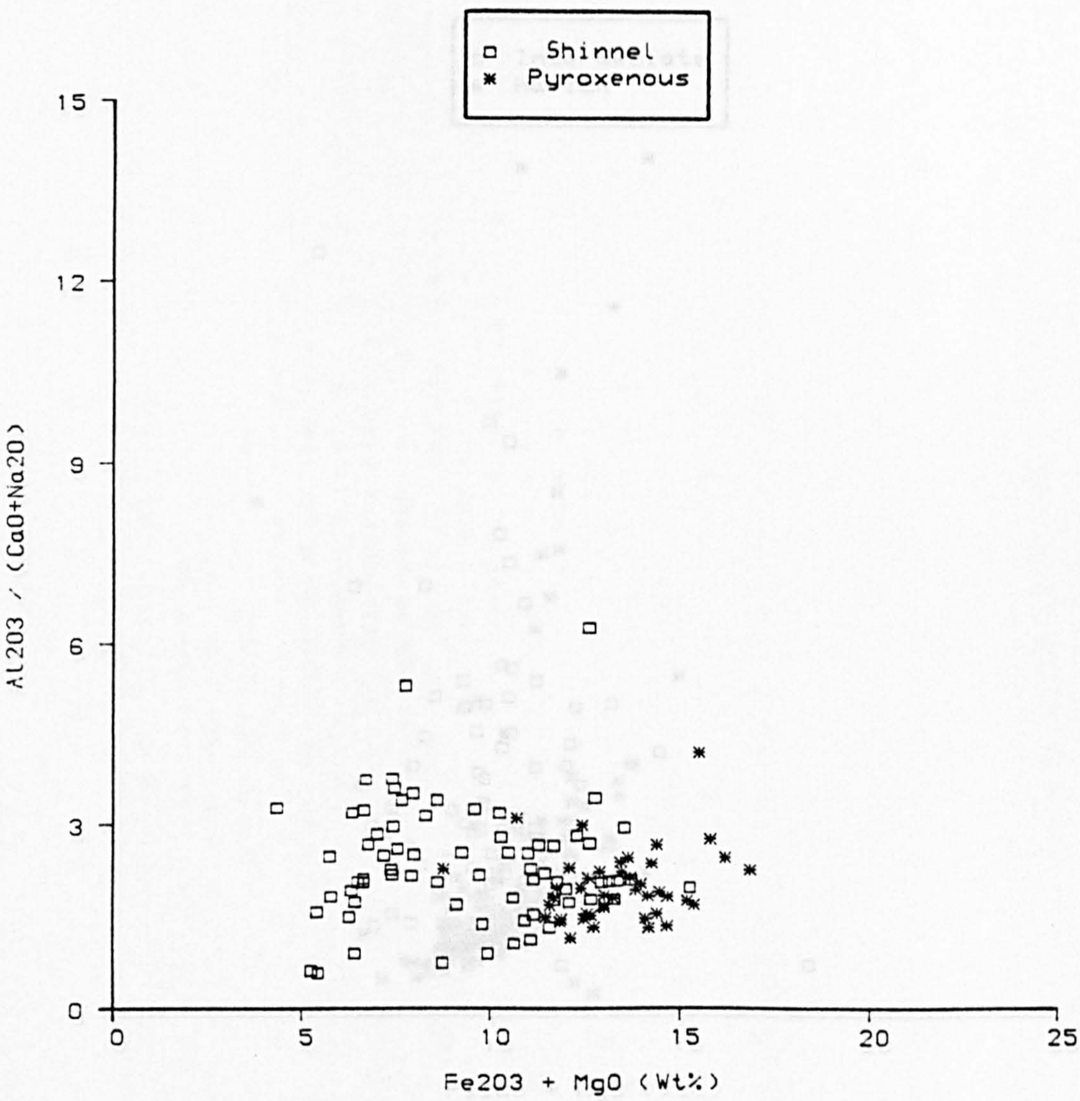

Discrimination Diagram (Bhatia, 1983).

FIGURE 356

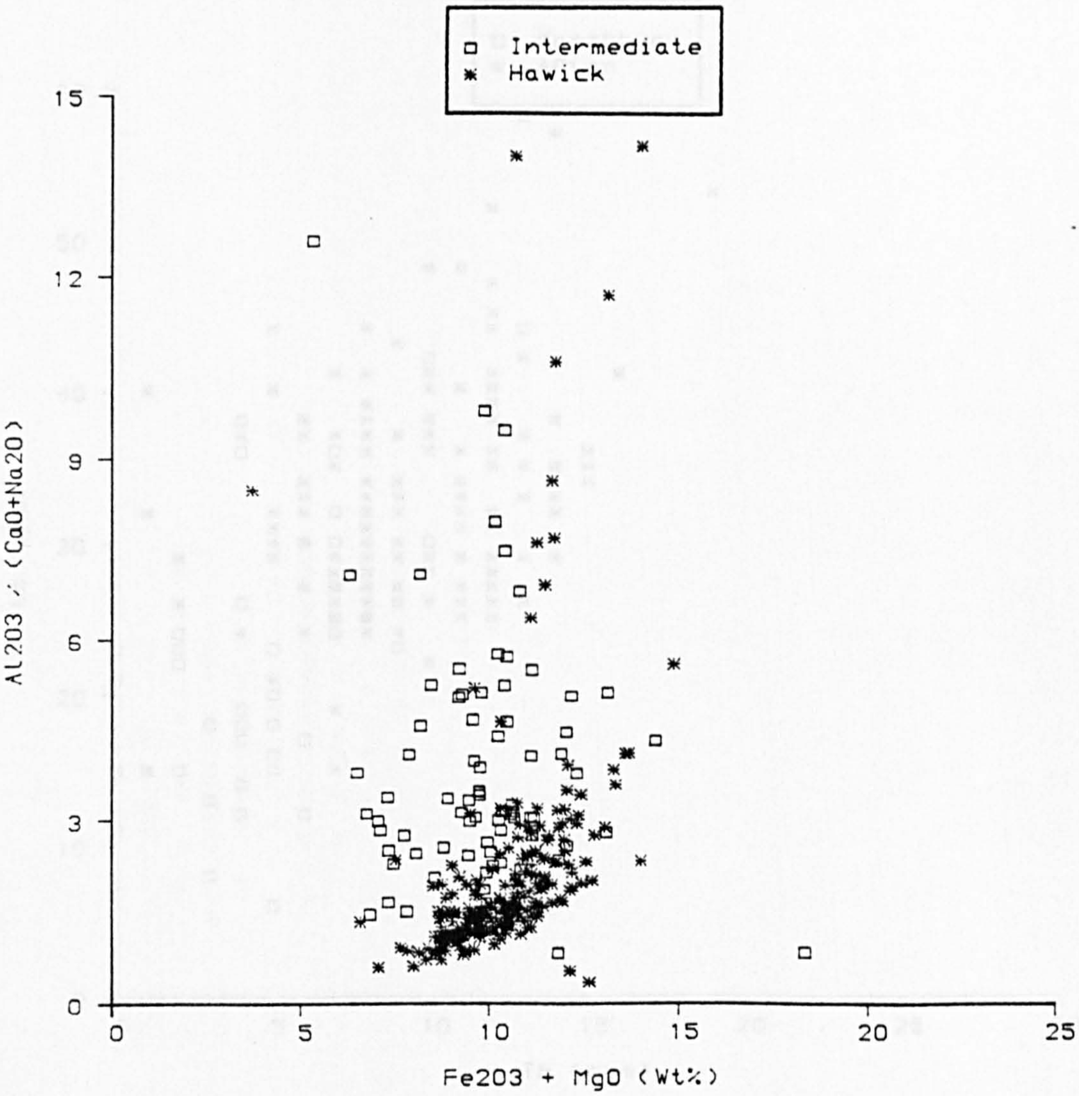

Discrimination Diagram (Bhatia, 1983).

FIGURE 357

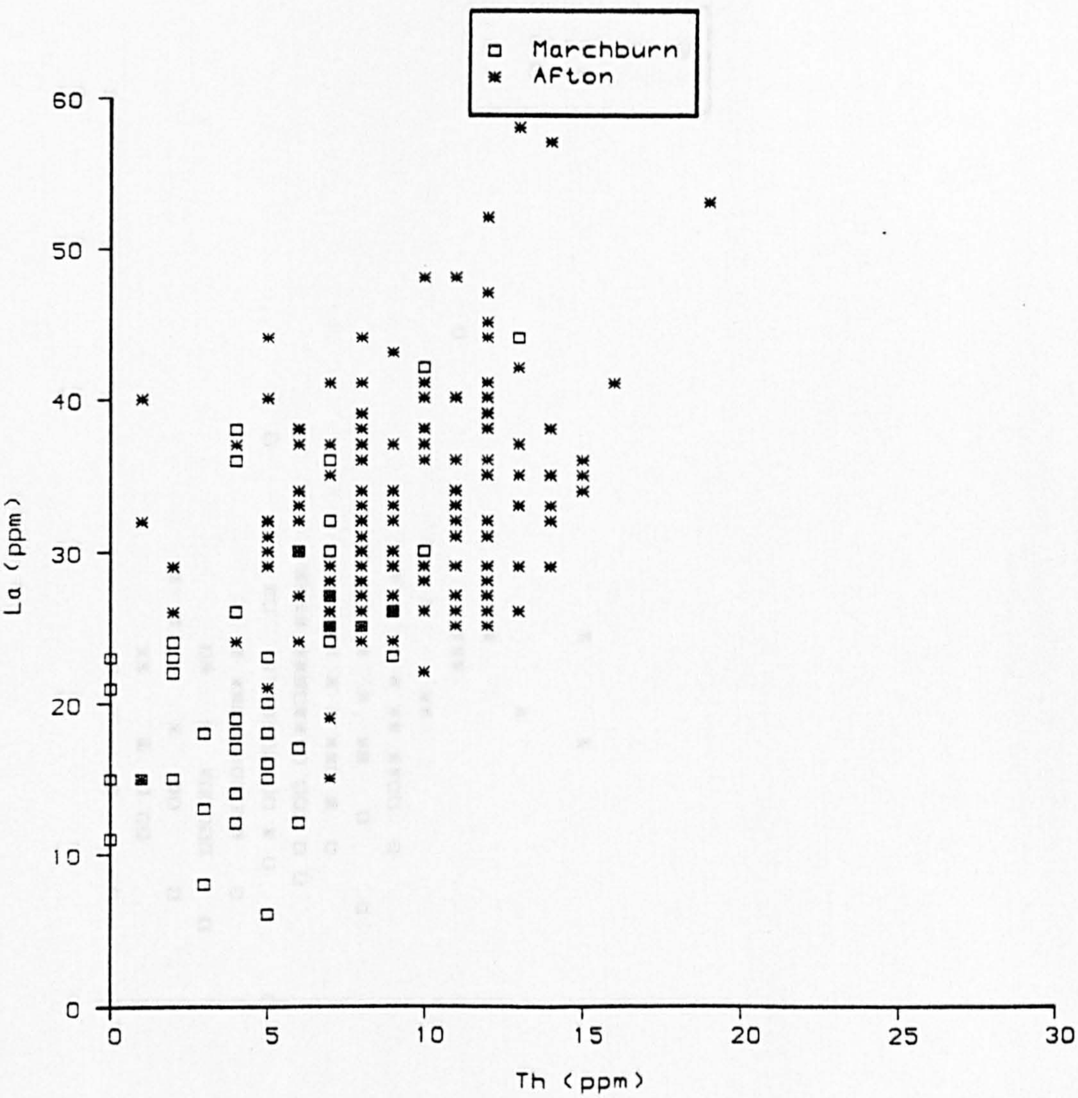

Discrimination Diagram (Bhatia, 1985).

FIGURE 358

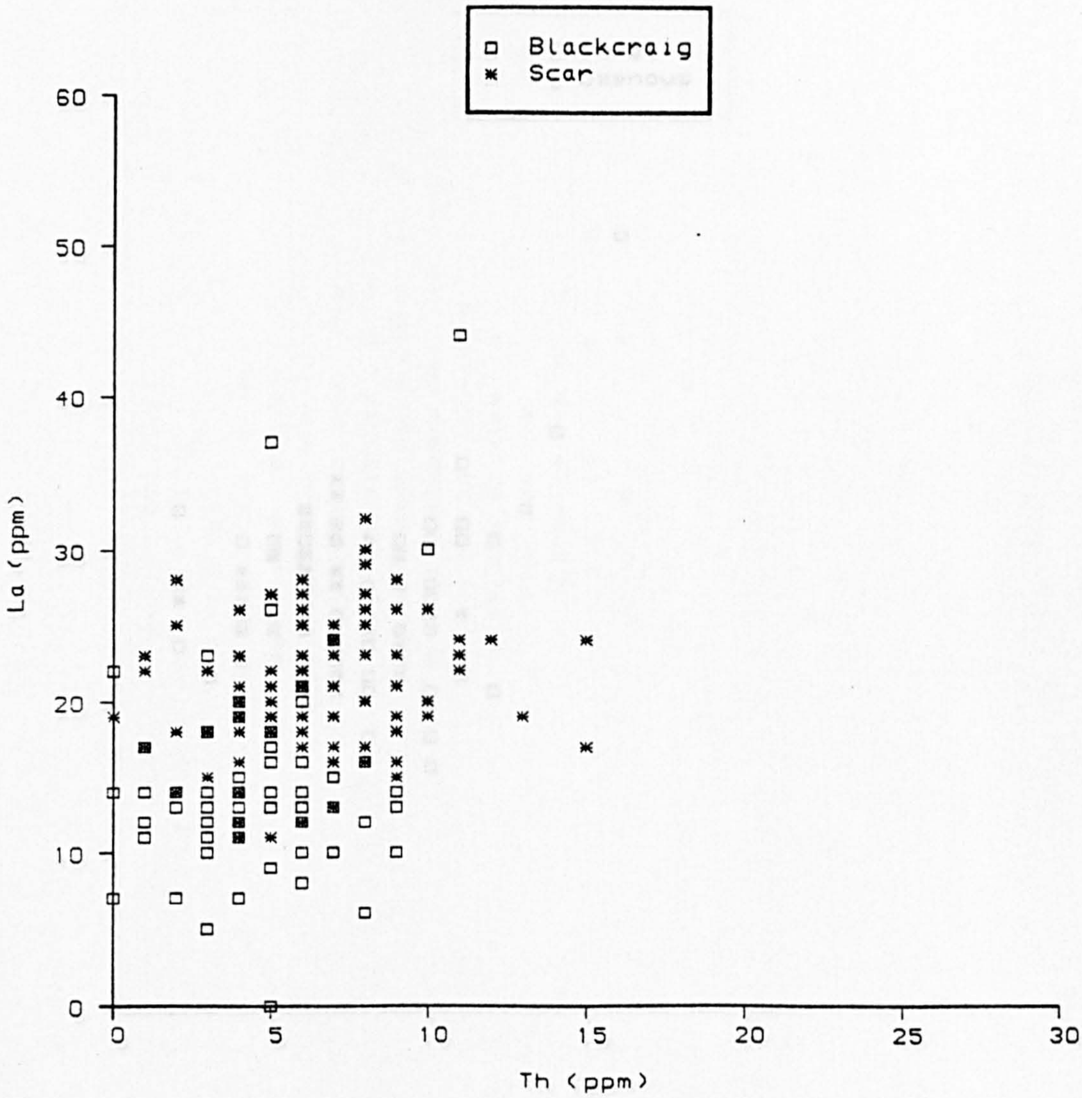

Discrimination Diagram (Bhatia, 1985).

FIGURE 359

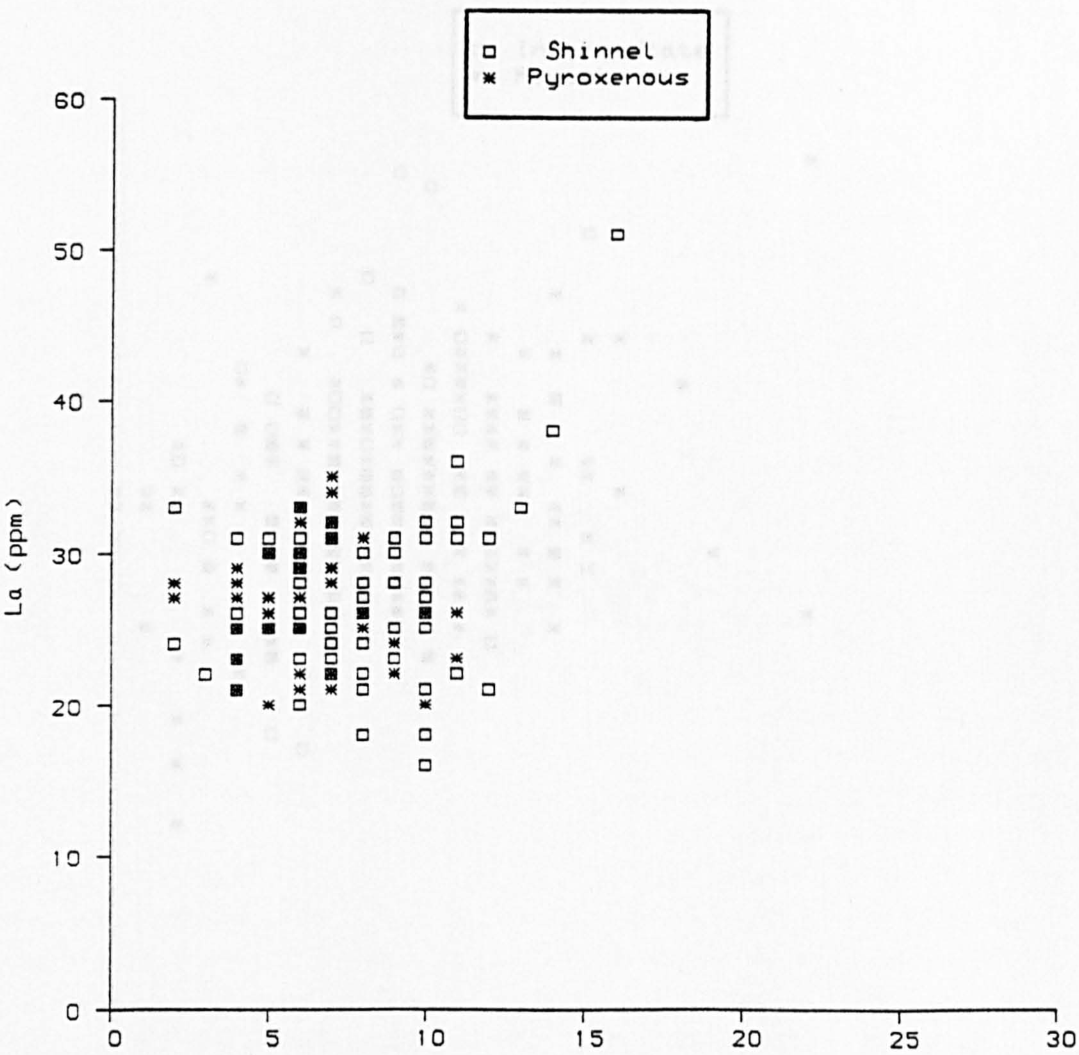

Discrimination Diagram (Bhatia, 1985).

FIGURE 360

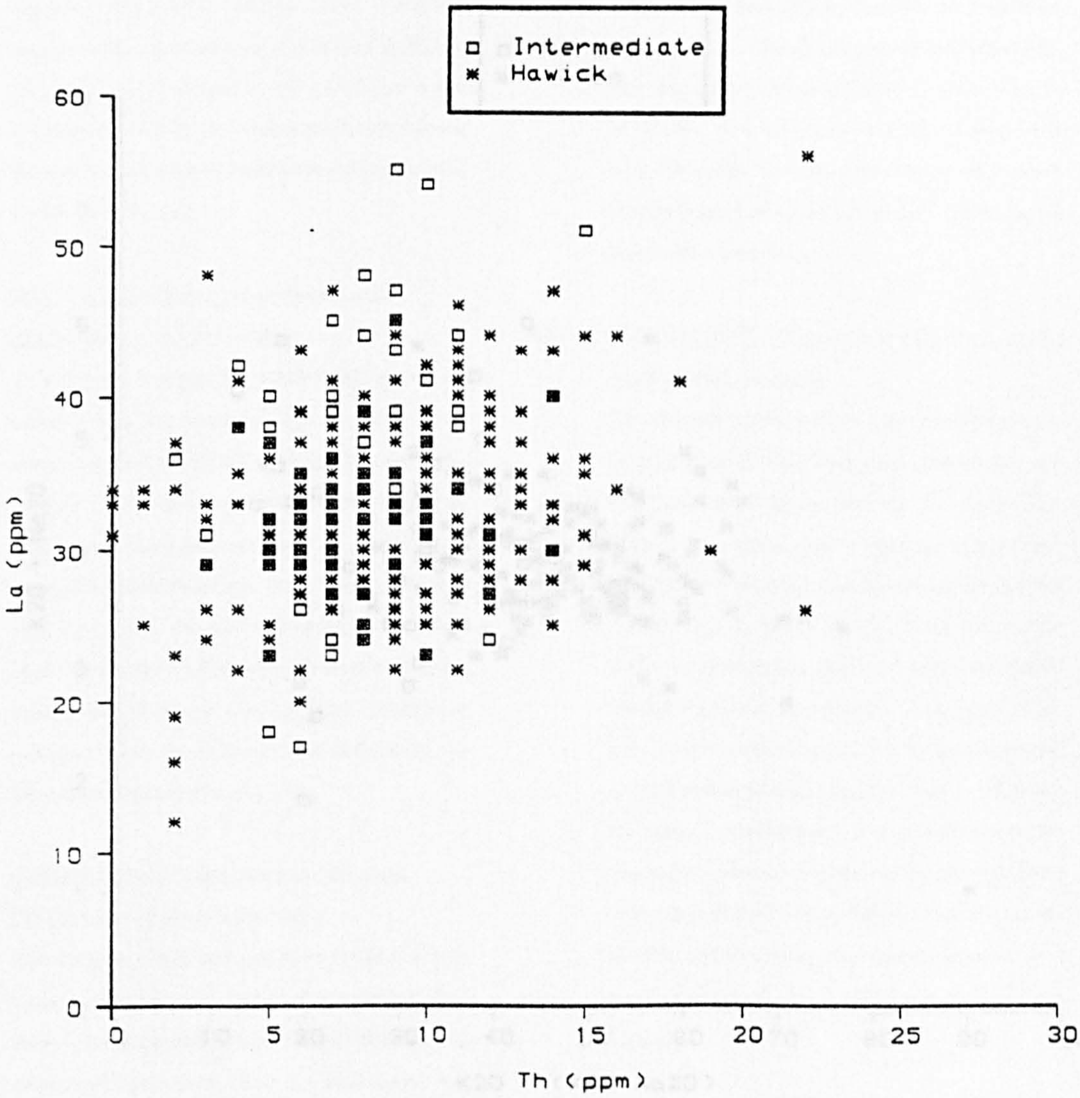

Discrimination Diagram (Bhatia, 1985).

FIGURE 361

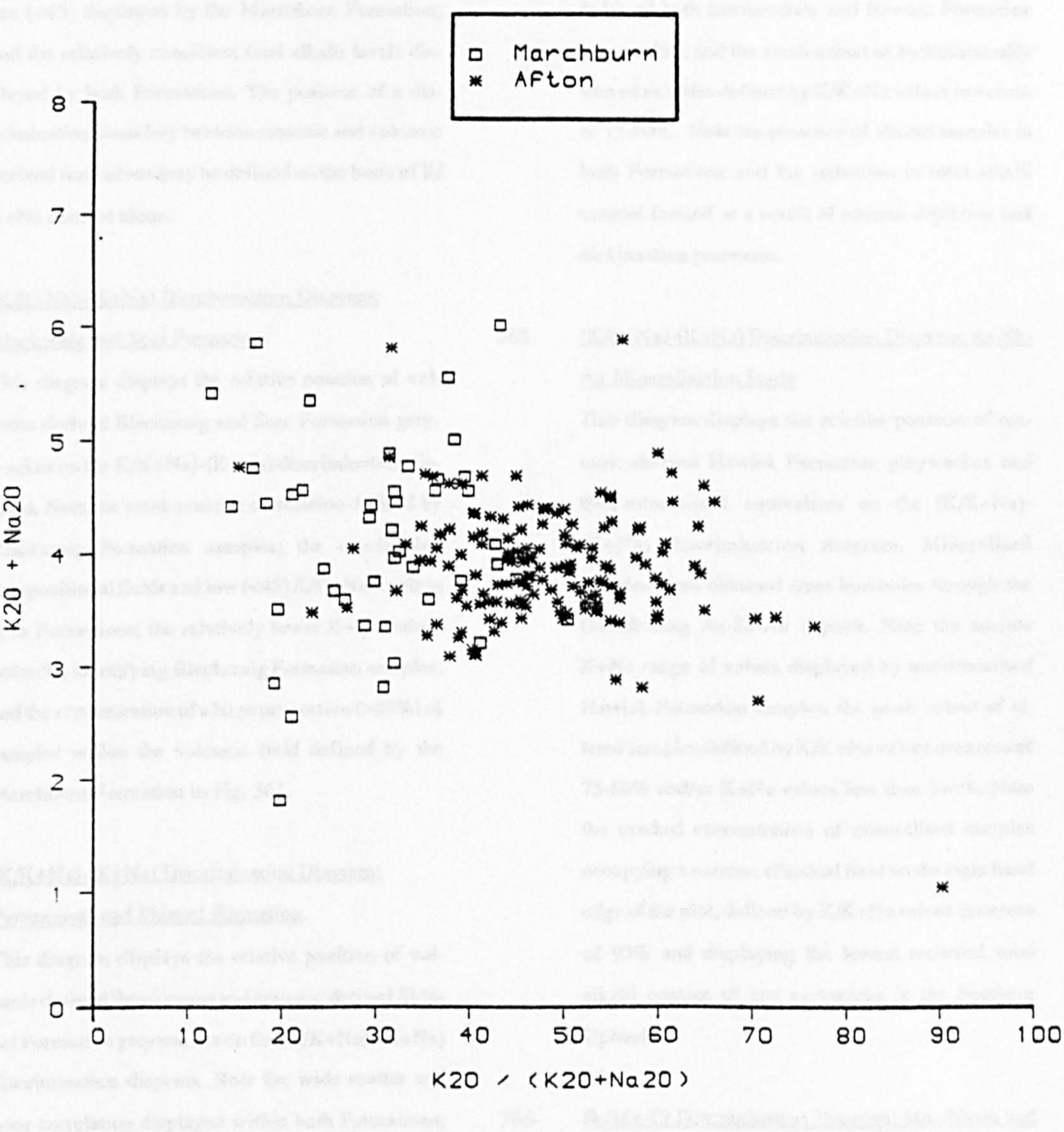

Total Alkalii Discrimination Diagram (Cathelineau, 1983).

and this is compared with the total alkalii content of the samples in order to assess the possible effects of sodium addition or depletion. This diagram displays the relative position of volcanic derived Marchburn and cratonic derived Afton Formation greywackes on the (K/K+Na)-(K+Na) discrimination diagram. Note the wide scatter and poor correlation displayed by both Formations; the relatively low K/K+Na values (<45) displayed by the Marchburn Formation; and the relatively consistent total alkalii levels displayed by both Formations. The position of a discrimination boundary between cratonic and volcanic derived formations may be defined on the basis of K/K+Na content alone.

362- <u>(K/K+Na)-(K+Na) Discrimination Diagram: Blackcraig and Scar Formation</u>.

This diagram displays the relative position of volcanic derived Blackcraig and Scar Formation greywackes on the K/K+Na)-(K+Na) discrimination diagram. Note the weak positive correlation defined by Blackcraig Formation samples; the overlapping compositional fields and low (<45) K/K+Na levels in both Formations; the relatively lower K+Na values (<4wt%) identifying Blackcraig Formation samples; and the concentration of a large proportion (>80%) of samples within the volcanic field defined by the Marchburn Formation in Fig. 361.

363- <u>(K/K+Na)-(K+Na) Discrimination Diagram: Pyroxenous and Shinnel Formation</u>.

This diagram displays the relative position of volcanic derived Pyroxenous and cratonic derived Shinnel Formation greywackes on the (K/K+Na)-(K+Na) discrimination diagram. Note the wide scatter and poor correlation displayed within both Formations; the large range of K/K+Na values displayed by the Shinnel Formation; the narrow, restricted range of K+Na values displayed by the Pyroxenous Formation and the overlapping nature of both compositional fields.

364- <u>(K/K+Na)-(K+Na) Discrimination Diagram: Intermediate and Hawick Formation</u>.

This diagram displays the relative position of cratonic derived Intermediate and Hawick Formation greywackes on the (K/K+Na)-(K+Na) discrimination diagram. Note the wide scatter and poor interelement correlation displayed by the Intermediate Formation; the relatively restricted compositional field and the narrow K+Na range of values displayed by the Hawick Formation; the positive shift in values of both formations to within the cratonic field (K/K+Na >45); the strongly overlapping compositional fields of both Intermediate and Hawick Formation greywackes; and the small subset of hydrothermally altered samples defined by K/K+Na values in excess of 75-80%. Note the presence of altered samples in both Formations and the reduction in total alkalii content formed as a result of sodium depletion and dickitisation processes.

365- <u>(K/K+Na)-(K+Na) Discrimination Diagram: As-Sb-Au Mineralisation Study</u>

This diagram displays the relative position of cratonic derived Hawick Formation greywackes and their mineralised equivalents on the (K/K+Na)-(K+Na) discrimination diagram. Mineralised samples were obtained from boreholes through the Glendinning As-Sb-Au deposit. Note the narrow K+Na range of values displayed by unmineralised Hawick Formation samples; the small subset of altered samples defined by K/K+Na values in excess of 75-80% and/or K+Na values less than 3wt%. Note the marked concentration of mineralised samples occupying a narrow, elliptical field on the right hand edge of the plot, defined by K/K+Na values in excess of 90% and displaying the lowest recorded total alkalii content of any greywacke in the Southern Uplands.

366- <u>Fe/Mg-Cr Discrimination Diagram: Marchburn and Afton Formation</u>.

The (Fe/Mg)-Cr discrimination diagram defined by Ricci and Sabatini (1976) is used in Figs. 366-369 to display the chemical variation present in the major petrographically distinct Formations located in the Southern Uplands Study Area. Ricci and Sabatini (op. cit) used this diagram to demonstrate the relationship between the presence of mafic clast components and elevated Cr values (up to 450ppm). In addition, the negative correlation between Cr and Fe/

FIGURE 362

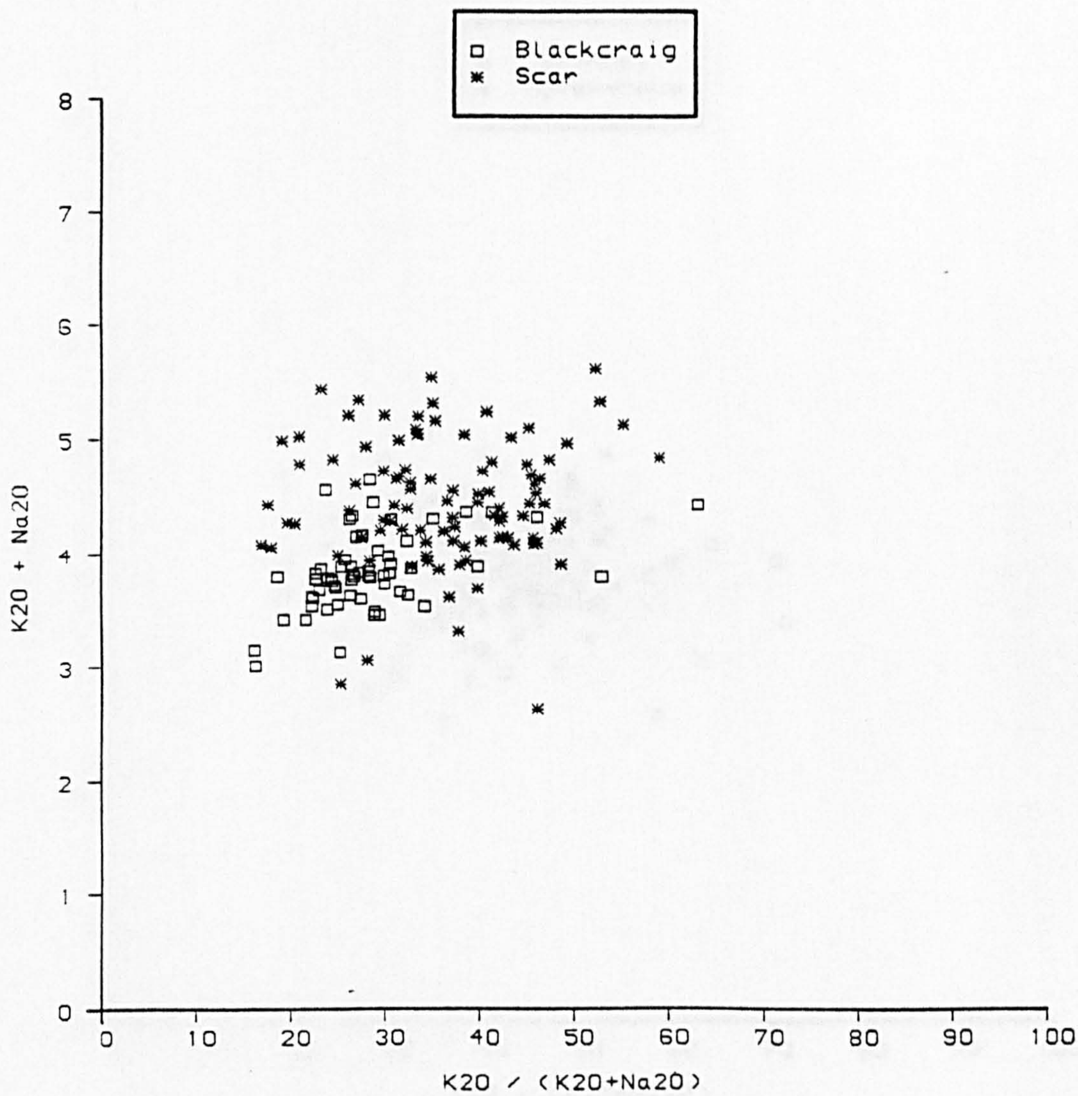

Total Alkalii Discrimination Diagram (Cathelineau, 1983).

FIGURE 363

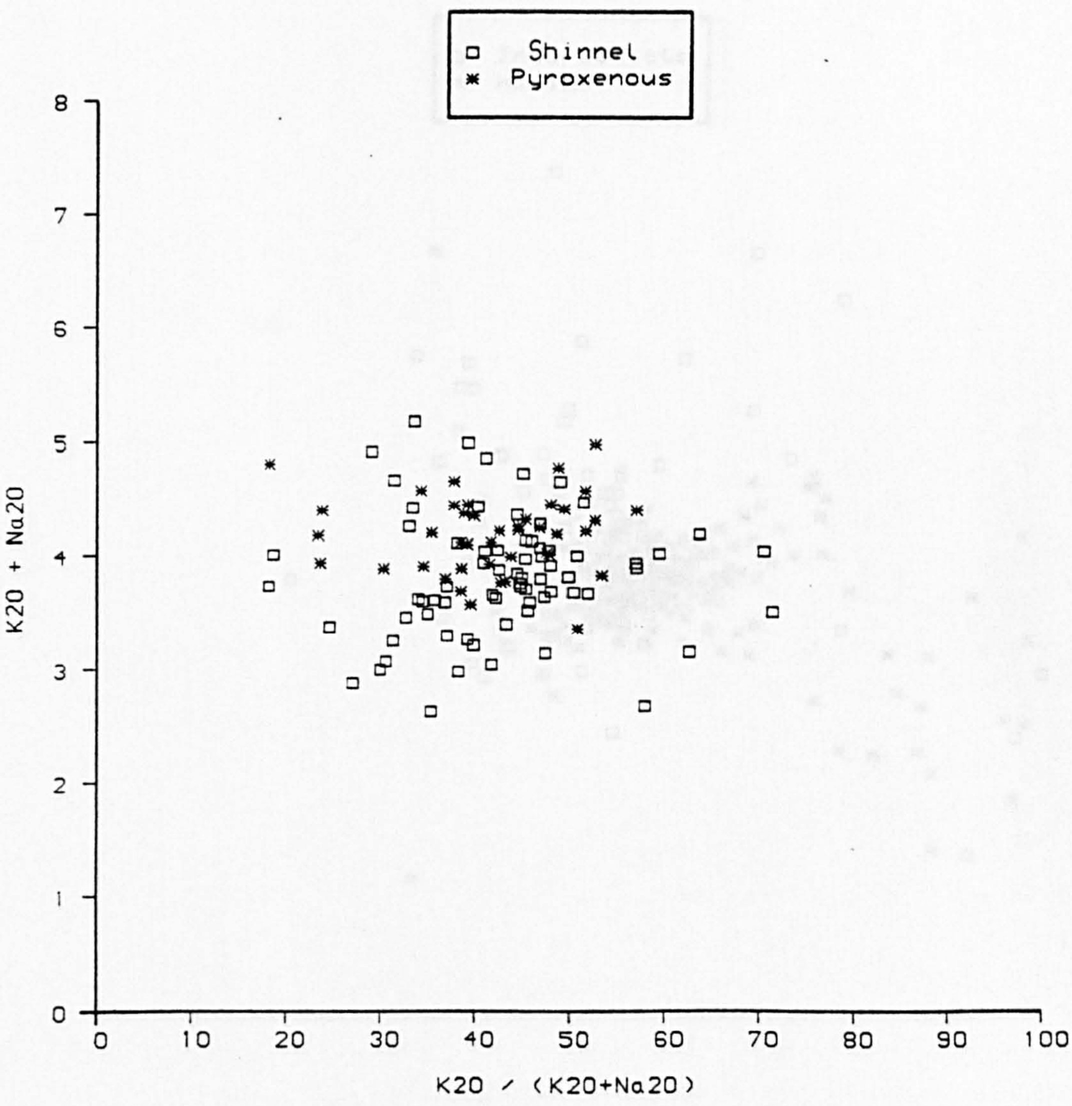

Total Alkalii Discrimination Diagram (Cathelineau, 1983).

FIGURE 364

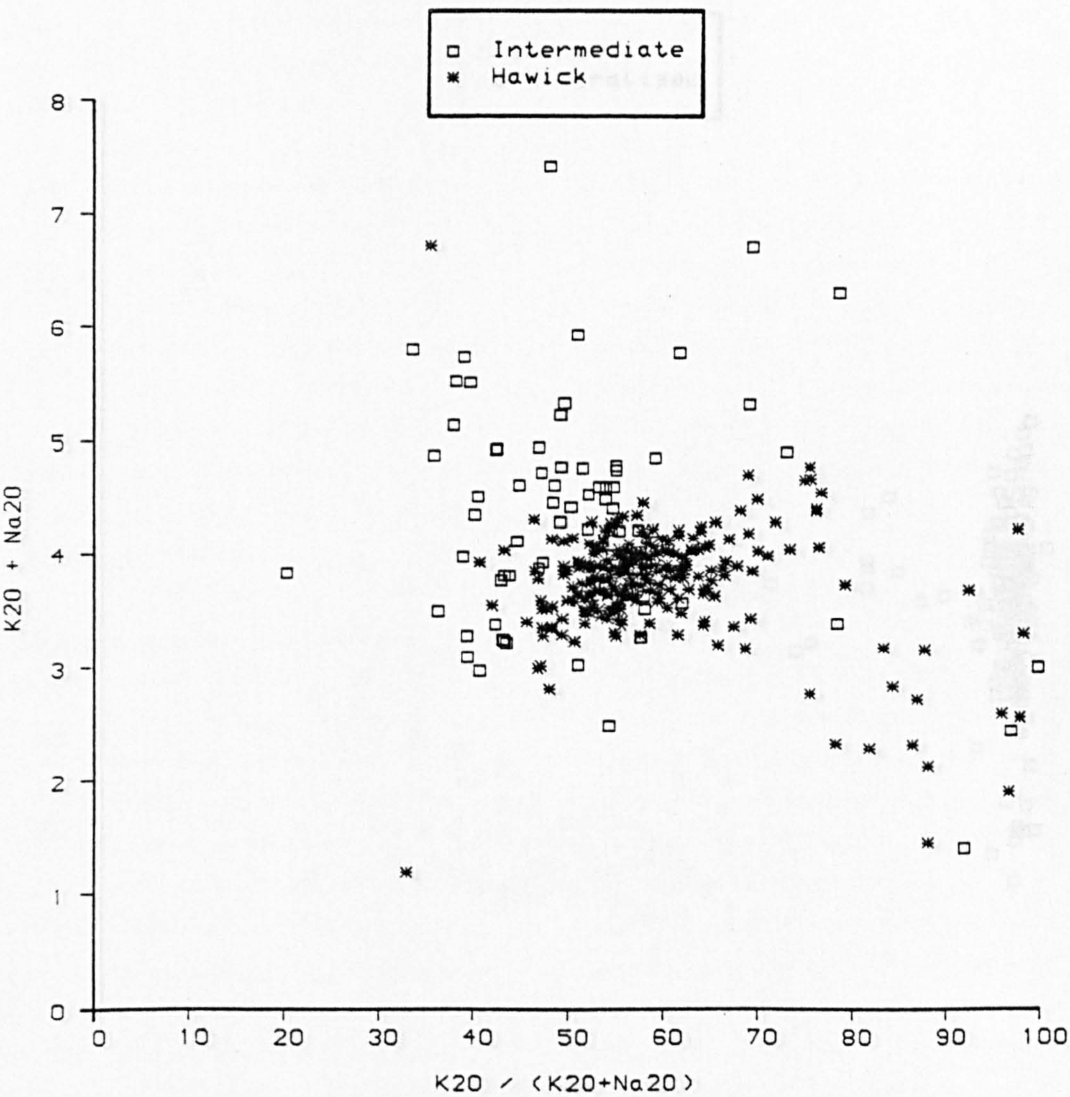

Total Alkalii Discrimination Diagram (Cathelineau, 1983).

FIGURE 365

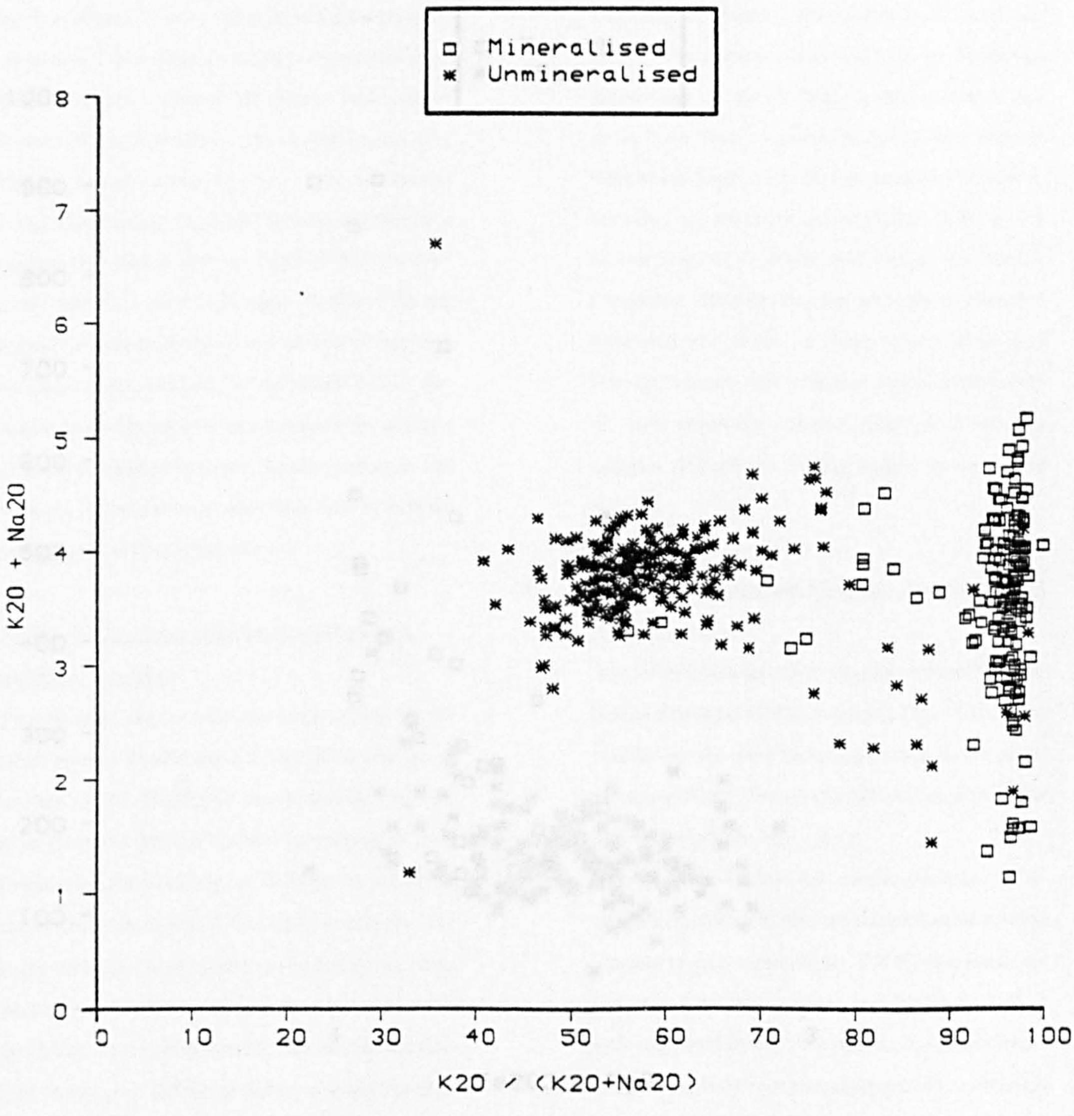

Total Alkalii Discrimination Diagram (Cathelineau, 1983).

FIGURE 366

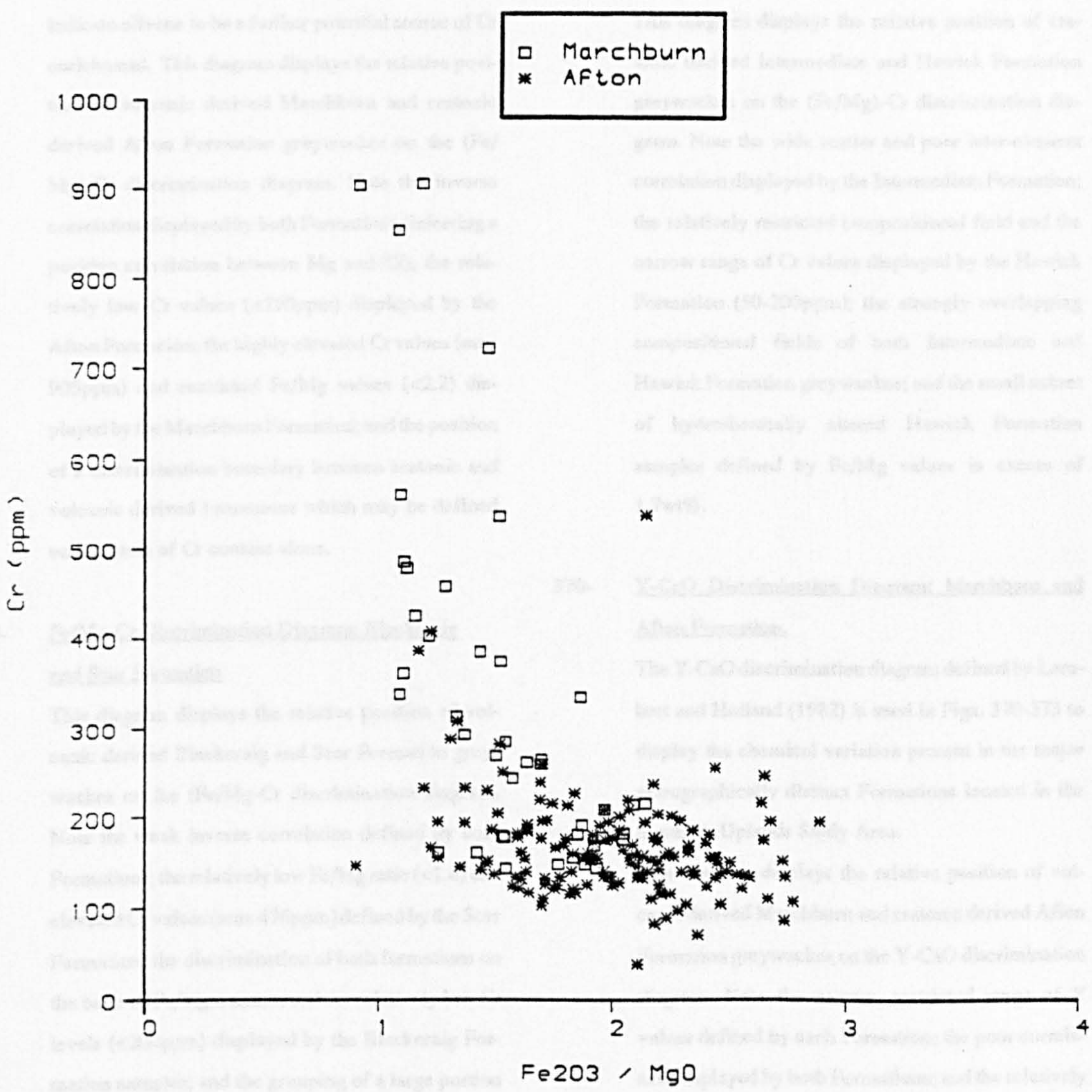

Discrimination Diagram (Ricci, 1978).

Mg was used to suggest a close magmatic relationship within the source material and to rule out any geochemical differentiation of Cr relative to Mg in the sedimentary, diagenetic or metamorphic environments. Both Cr-rich pyroxenes and/or Cr-rich spinels provide the likely sources of Cr enrichment in the Southern Uplands Study area. In addition, elevated Ni values (particularly the Marchburn Formation) indicate olivene to be a further potential source of Cr enrichment. This diagram displays the relative position of volcanic derived Marchburn and cratonic derived Afton Formation greywackes on the (Fe/Mg)-Cr discrimination diagram. Note the inverse correlation displayed by both Formations (inferring a positive correlation between Mg and Cr); the relatively low Cr values (<250ppm) displayed by the Afton Formation; the highly elevated Cr values (max 905ppm) and restricted Fe/Mg values (<2.2) displayed by the Marchburn Formation; and the position of a discrimination boundary between cratonic and volcanic derived formations which may be defined on the basis of Cr content alone.

367- <u>Fe/Mg-Cr Discrimination Diagram: Blackcraig and Scar Formation</u>

This diagram displays the relative position of volcanic derived Blackcraig and Scar Formation greywackes on the (Fe/Mg-Cr discrimination diagram. Note the weak inverse correlation defined by both Formations; the relatively low Fe/Mg ratio (<1.6) and elevated Cr values (max 476ppm) defined by the Scar Formation; the discrimination of both formations on the basis of Fe/Mg content; and the relatively low Cr levels (<200ppm) displayed by the Blackcraig Formation samples; and the grouping of a large portion (>95%) of samples within the volcanic field defined by the Marchburn Formation in Fig. 366.

368- <u>Fe/Mg-Cr Discrimination Diagram: Pyroxenous and Shinnel Formation</u>.

This diagram displays the relative position of volcanic derived Pyroxenous and cratonic derived Shinnel Formation greywackes on the (Fe/Mg)-Cr discrimination diagram. Note the narrow range of Fe/Mg and Cr values displayed by the Pyroxenous Formation (located within the volcanic field); the apparently bimodal grouping of values within the Shinnel Formation (a high Cr group displaying an inverse relationship with Fe/Mg and a low Cr group displaying a poor correlation with Fe/Mg); and the overlapping nature of both compositional fields.

369- <u>Fe/Mg-Cr Discrimination Diagram: Intermediate and Hawick Formation</u>

This diagram displays the relative position of cratonic derived Intermediate and Hawick Formation greywackes on the (Fe/Mg)-Cr discrimination diagram. Note the wide scatter and poor inter-element correlation displayed by the Intermediate Formation; the relatively restricted compositional field and the narrow range of Cr values displayed by the Hawick Formation (50-200ppm); the strongly overlapping compositional fields of both Intermediate and Hawick Formation greywackes; and the small subset of hydrothermally altered Hawick Formation samples defined by Fe/Mg values in excess of 1.7wt%.

370- <u>Y-CaO Discrimination Diagram: Marchburn and Afton Formation.</u>

The Y-CaO discrimination diagram defined by Lambert and Holland (1982) is used in Figs. 370-373 to display the chemical variation present in the major petrographically distinct Formations located in the Southern Uplands Study Area.

This diagram displays the relative position of volcanic derived Marchburn and cratonic derived Afton Formation greywackes on the Y-CaO discrimination diagram. Note the narrow, restricted range of Y values defined by each Formation; the poor correlation displayed by both Formations; and the relatively elevated Sr levels (>150 ppm) displayed by the Marchburn Formation, controlling the position of a discrimination boundary between cratonic and volcanic derived formations.

371- <u>Y-CaO Discrimination Diagram: Blackcraig and Scar Formation.</u>

This diagram displays the relative position of volcanic derived Blackcraig and Scar Formation greywackes on the Y-CaO discrimination diagram. Note the poor correlation defined by both Formations; the

FIGURE 367

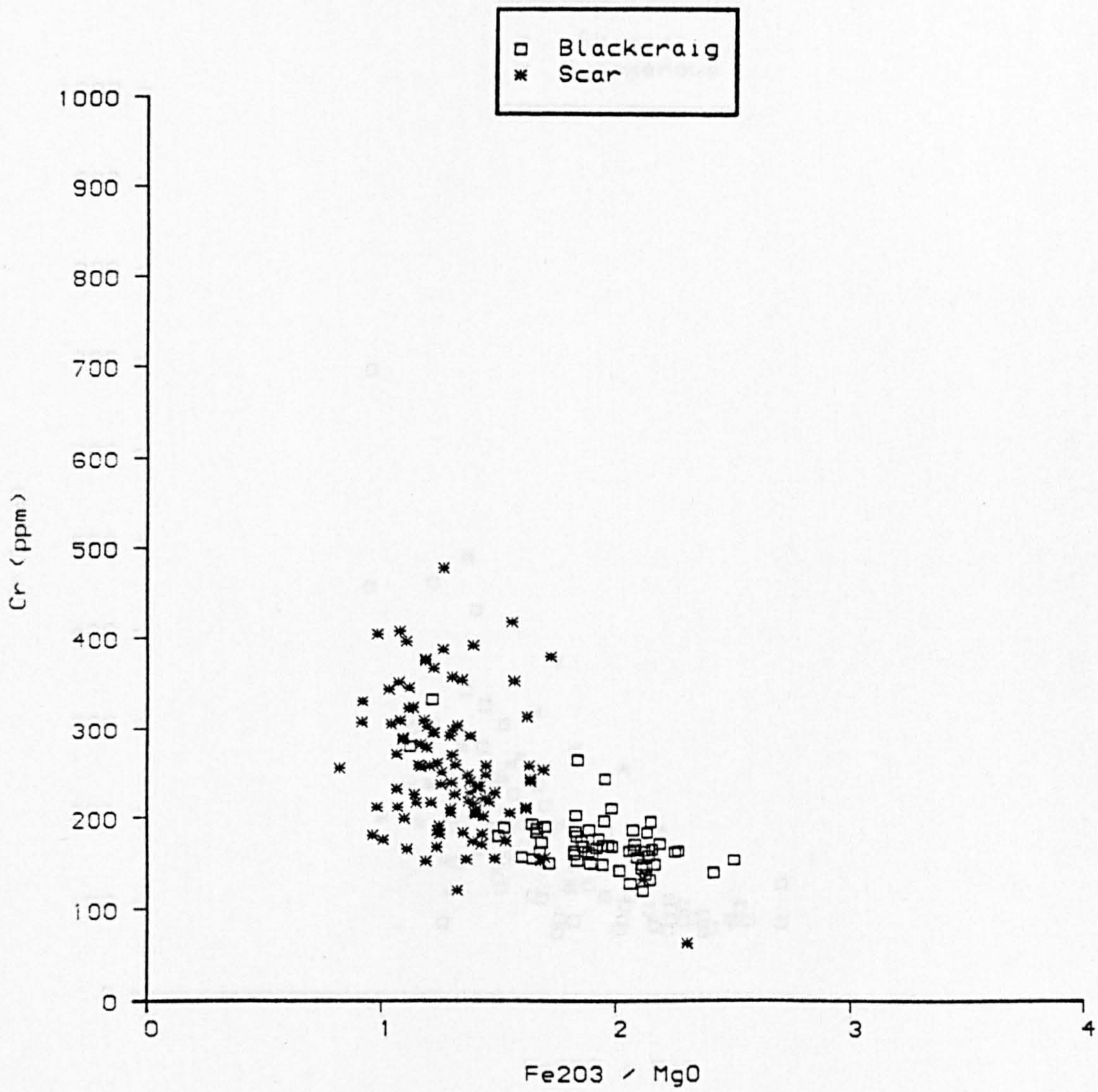

Discrimination Diagram (Ricci, 1978).

FIGURE 368

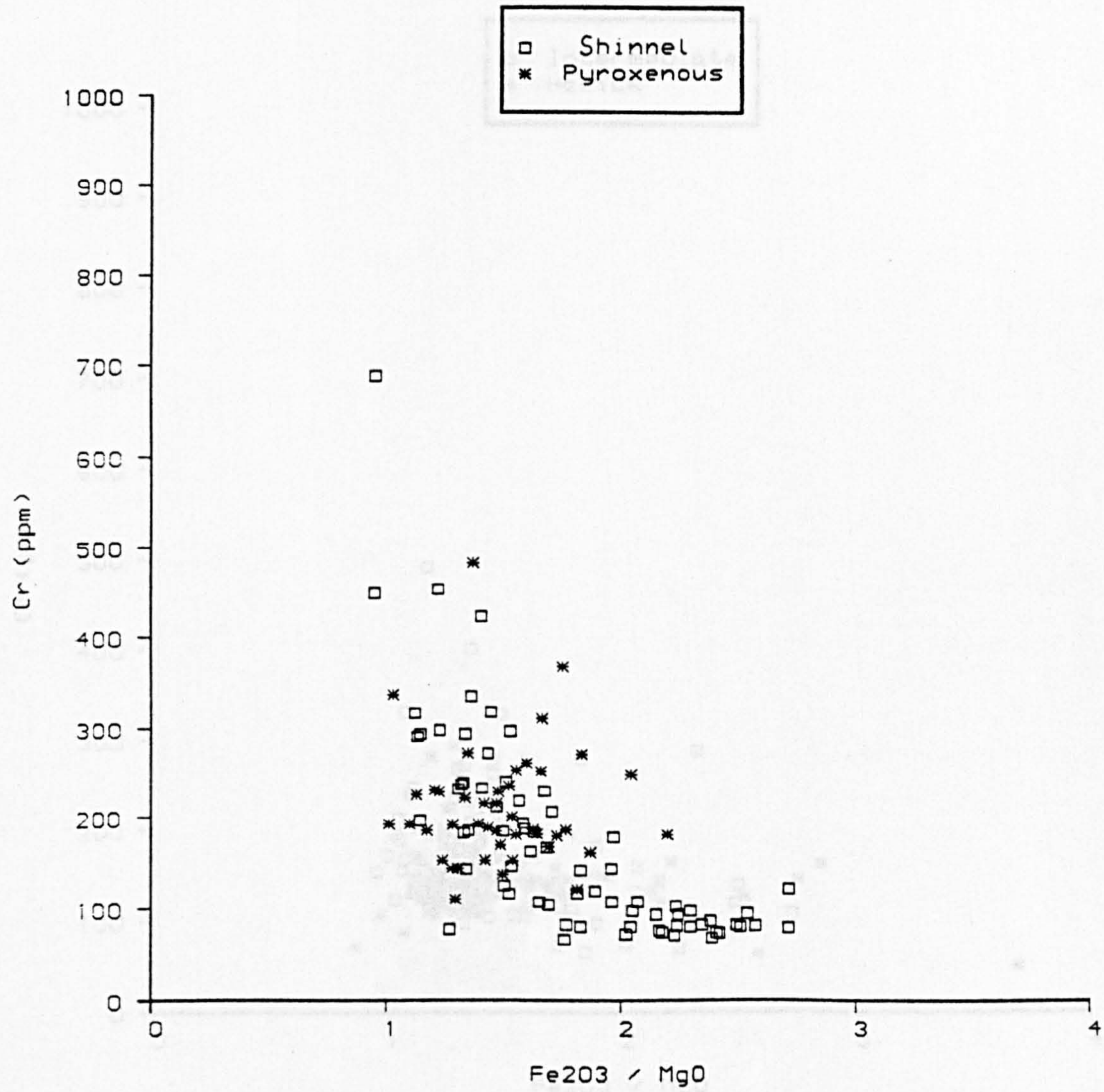

Discrimination Diagram (Ricci, 1978).

FIGURE 369

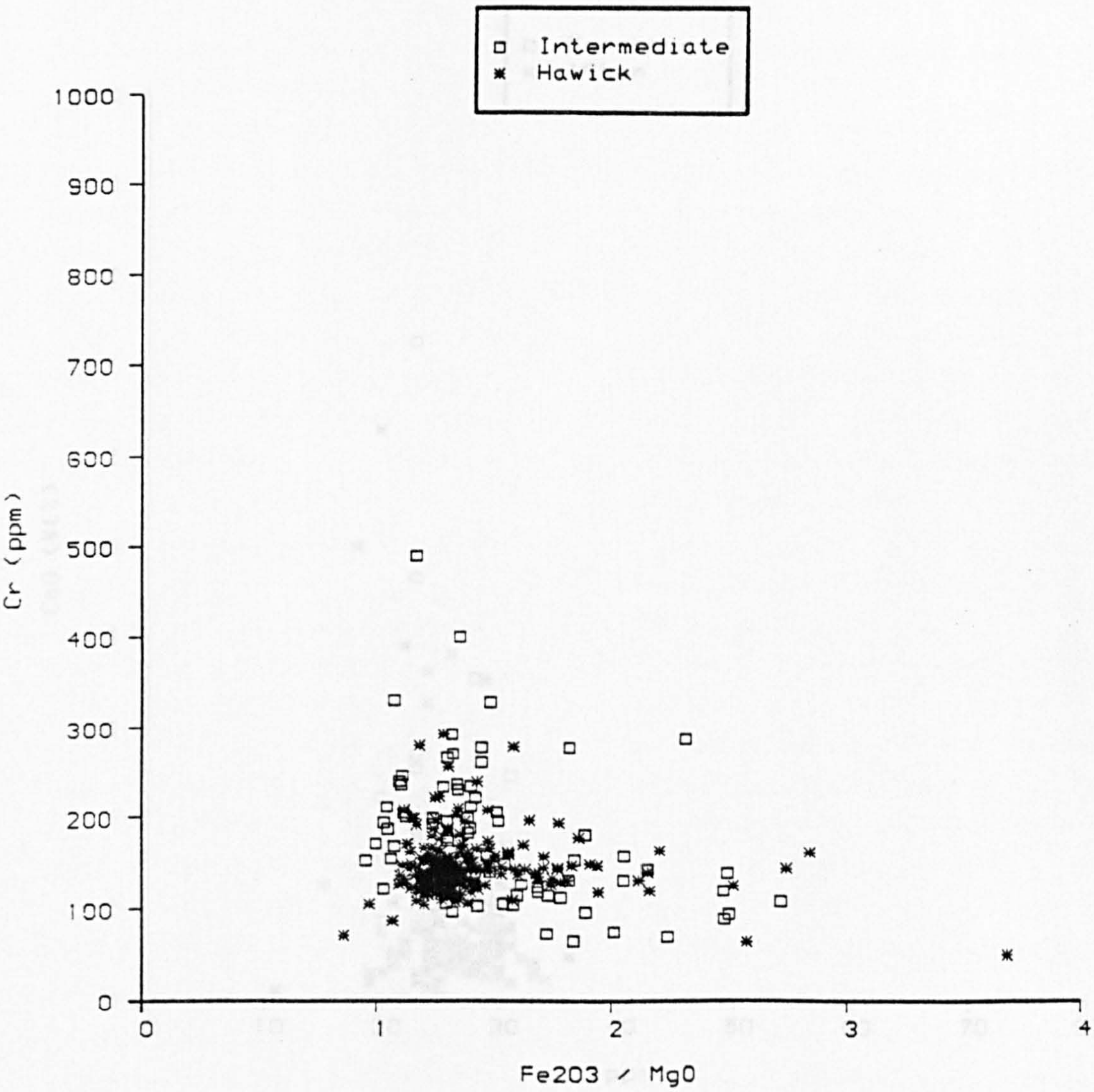

Discrimination Diagram (Ricci, 1978).

FIGURE 370

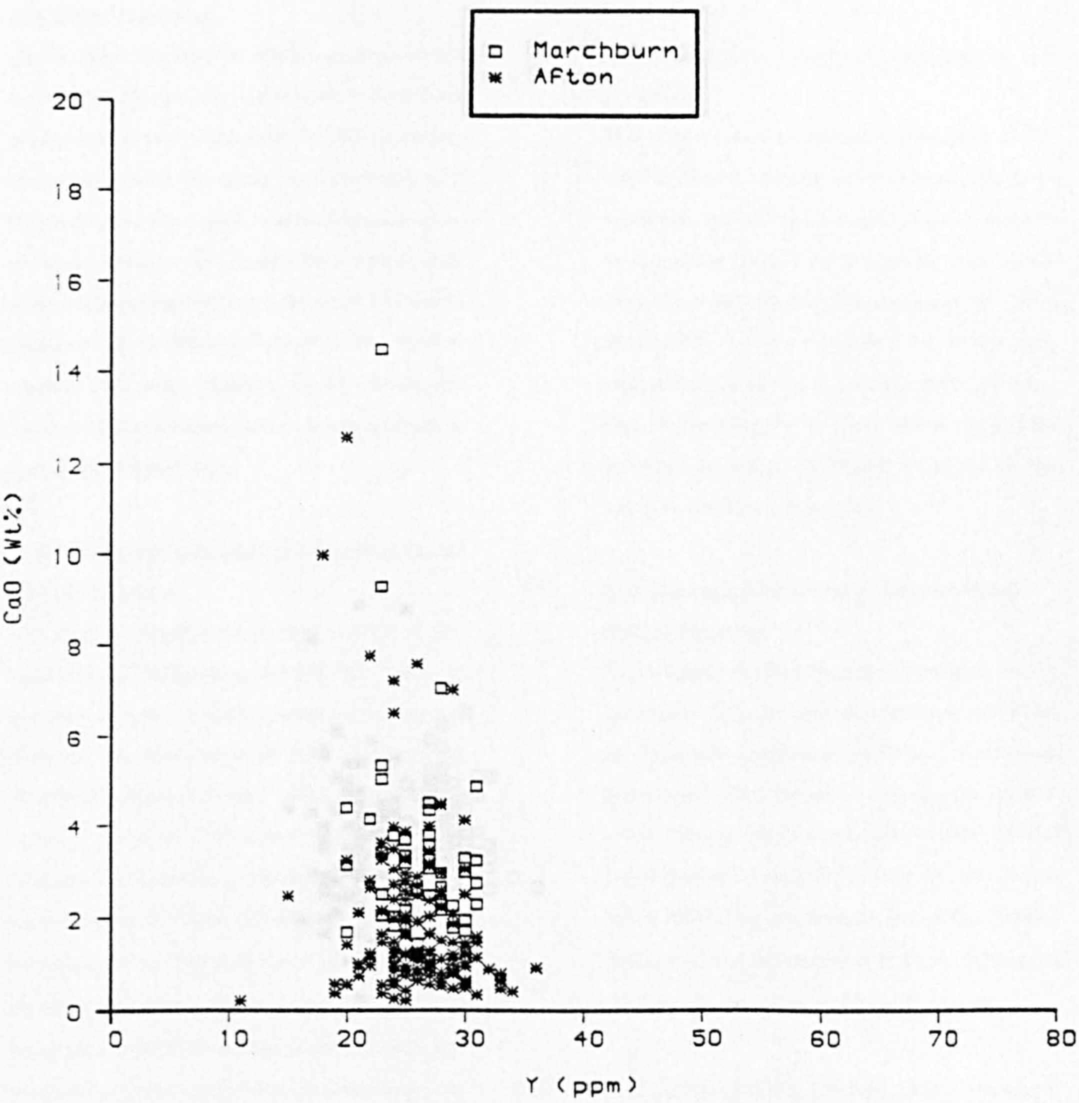

Discrimination Diagram (Lambert, Holland and Winchester)

FIGURE 371

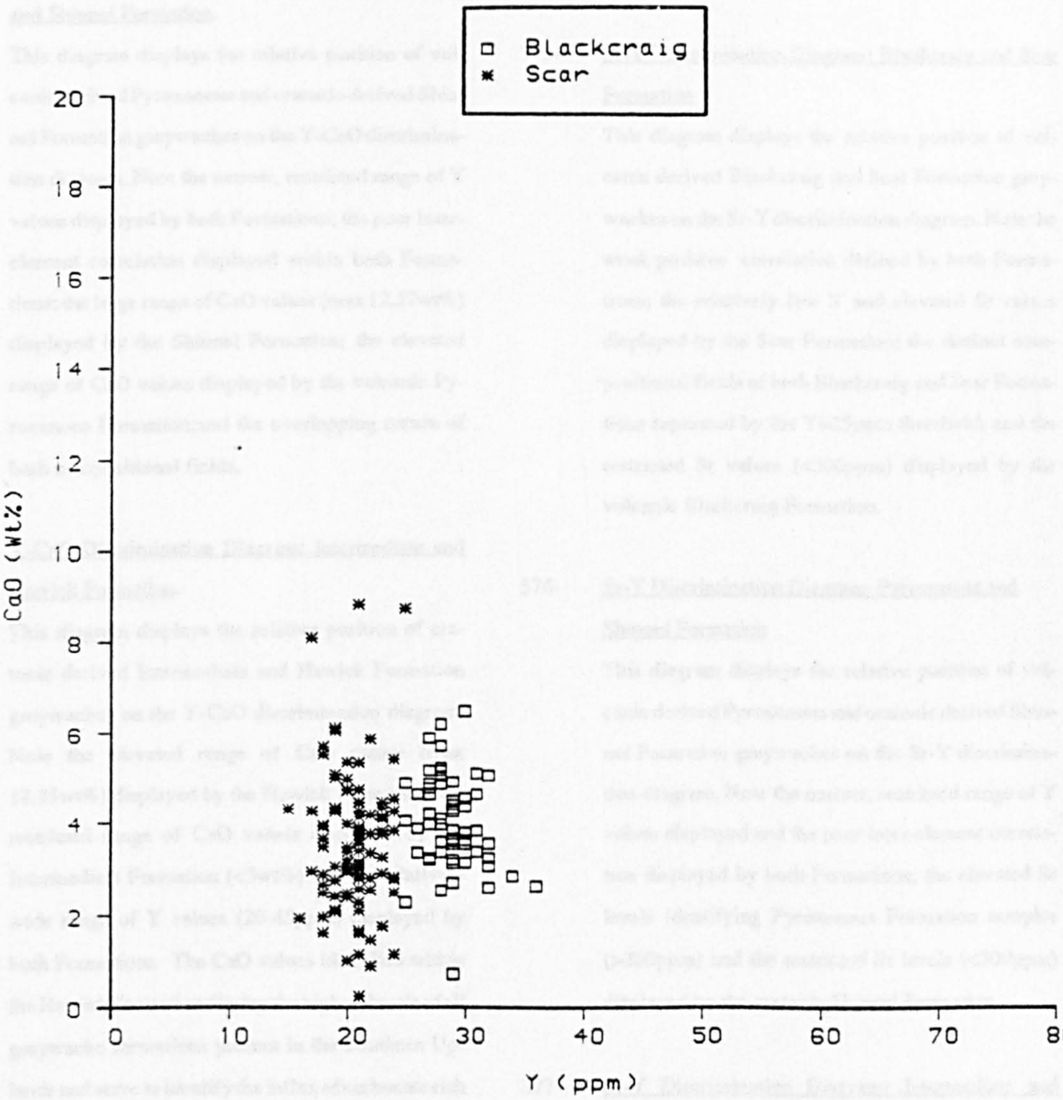

Discrimination Diagram (Lambert, Holland and Winchester)

relatively low Y values displayed by the Scar Formation; the distinct compositional fields of both Blackcraig and Scar Formations separated by the Y=25ppm threshold; and the slight positive shift in CaO values displayed by the volcanic Blackcraig Formation.

372- <u>Y-CaO Discrimination Diagram: Pyroxenous and Shinnel Formation</u>.

This diagram displays the relative position of volcanic derived Pyroxenous and cratonic derived Shinnel Formation greywackes on the Y-CaO discrimination diagram. Note the narrow, restricted range of Y values displayed by both Formations; the poor inter-element correlation displayed within both Formations; the large range of CaO values (max 12.27wt%) displayed by the Shinnel Formation; the elevated range of CaO values displayed by the volcanic Pyroxenous Formation;and the overlapping nature of both compositional fields.

373- <u>Y-CaO Discrimination Diagram: Intermediate and Hawick Formation</u>.

This diagram displays the relative position of cratonic derived Intermediate and Hawick Formation greywackes on the Y-CaO discrimination diagram. Note the elevated range of CaO values (max 18.35wt%) displayed by the Hawick Formation, the restricted range of CaO values displayed by the Intermediate Formation (<3wt%) and the relatively wide range of Y values (20-45ppm) displayed by both Formations. The CaO values identified within the Hawick Formation display the highest levels of all greywacke formations present in the Southern Uplands and serve to identify the influx of carbonate rich detritus from the source terrain.

374- <u>Sr-Y Discrimination Diagram: Marchburn and Afton Formation</u>.

The Sr-Y discrimination diagram defined by Lambert and Holland (1982) is used in Figs. 374-377 to display the chemical variation present in the major petrographically distinct Formations located in the Southern Uplands Study Area. This diagram displays the relative position of volcanic derived Marchburn and cratonic derived Afton Formation greywackes on the Sr-Y discrimination diagram. Note the narrow, restricted range of Y values defined by both Formations; the poor correlation displayed by both Formations; and the relatively elevated CaO levels (>1.5 wt%) displayed by the Marchburn Formation. The position of a discrimination boundary between cratonic and volcanic derived formations are poorly constrained on this diagram.

375- <u>Sr-Y Discrimination Diagram: Blackcraig and Scar Formation</u>

This diagram displays the relative position of volcanic derived Blackcraig and Scar Formation greywackes on the Sr-Y discrimination diagram. Note the weak positive correlation defined by both Formations; the relatively low Y and elevated Sr values displayed by the Scar Formation; the distinct compositional fields of both Blackcraig and Scar Formations separated by the Y=25ppm threshold; and the restricted Sr values (<300ppm) displayed by the volcanic Blackcraig Formation.

376- <u>Sr-Y Discrimination Diagram: Pyroxenous and Shinnel Formation</u>

This diagram displays the relative position of volcanic derived Pyroxenous and cratonic derived Shinnel Formation greywackes on the Sr-Y discrimination diagram. Note the narrow, restricted range of Y values displayed and the poor inter-element correlation displayed by both Formations; the elevated Sr levels identifying Pyroxenous Formation samples (>300ppm) and the restricted Sr levels (<300ppm) displayed by the cratonic Shinnel Formation.

377- <u>Sr-Y Discrimination Diagram: Intermediate and Hawick Formation</u>

This diagram displays the relative position of cratonic derived Intermediate and Hawick Formation greywackes on the Sr-Y discrimination diagram. Note the relatively restricted range of Sr values (max 263ppm) displayed by the Hawick Formation, the elevated range of Sr values displayed by the Intermediate Formation (max 510ppm) and the comparatively wide range of Y values (20-45ppm) displayed by both Formations.

FIGURE 372

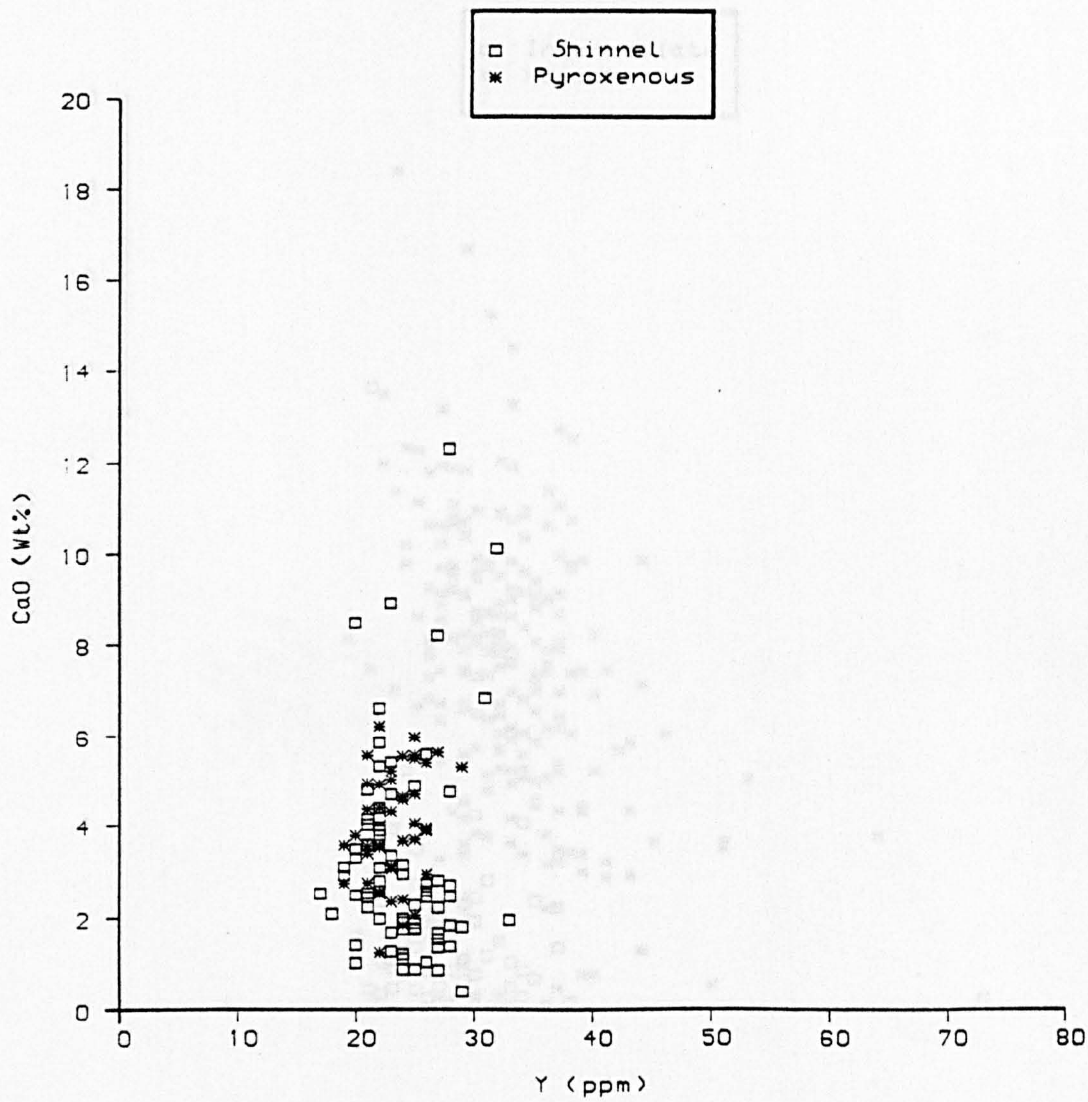

Discrimination Diagram (Lambert, Holland and Winchester)

FIGURE 373

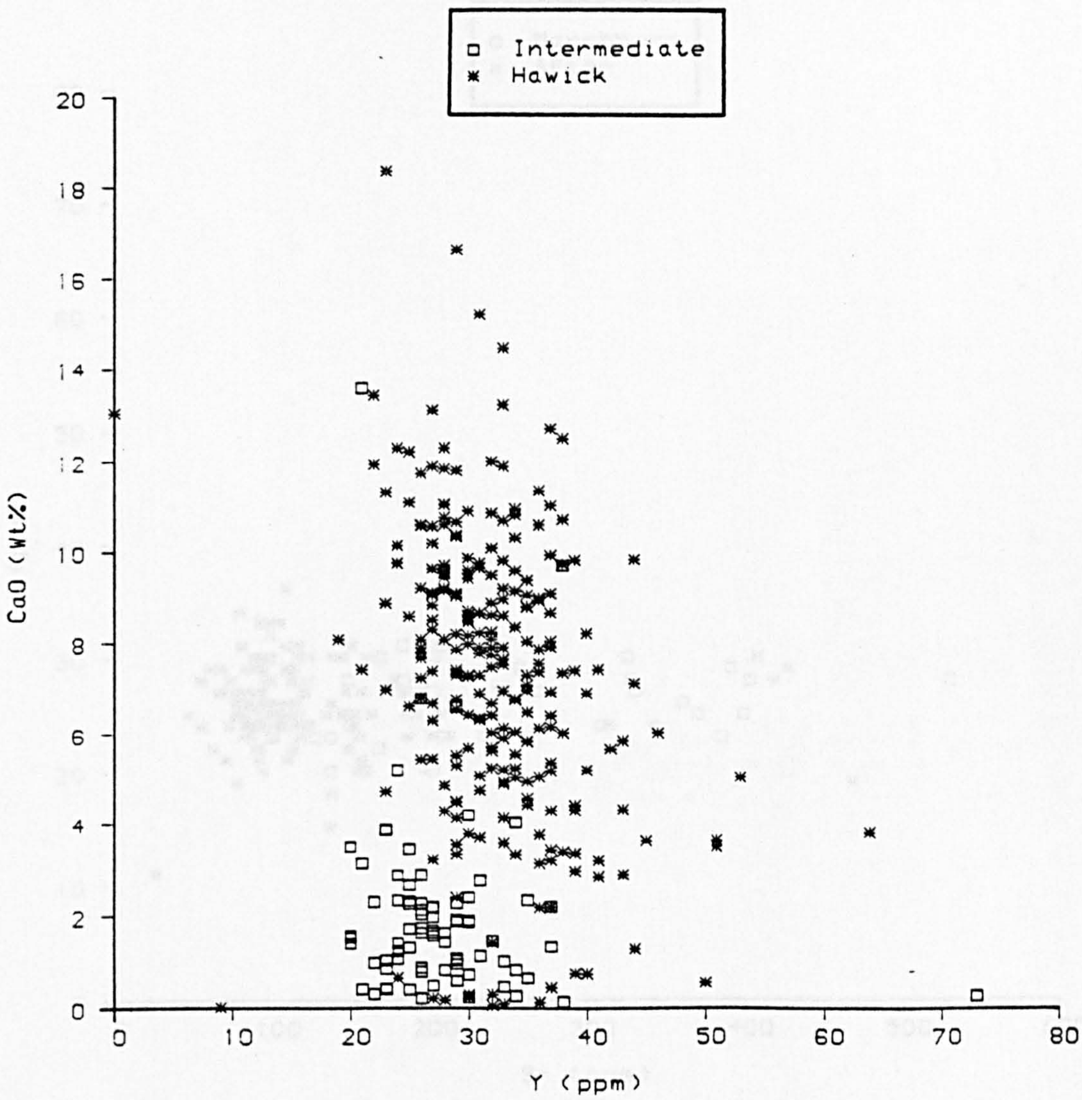

Discrimination Diagram (Lambert, Holland and Winchester)

FIGURE 374

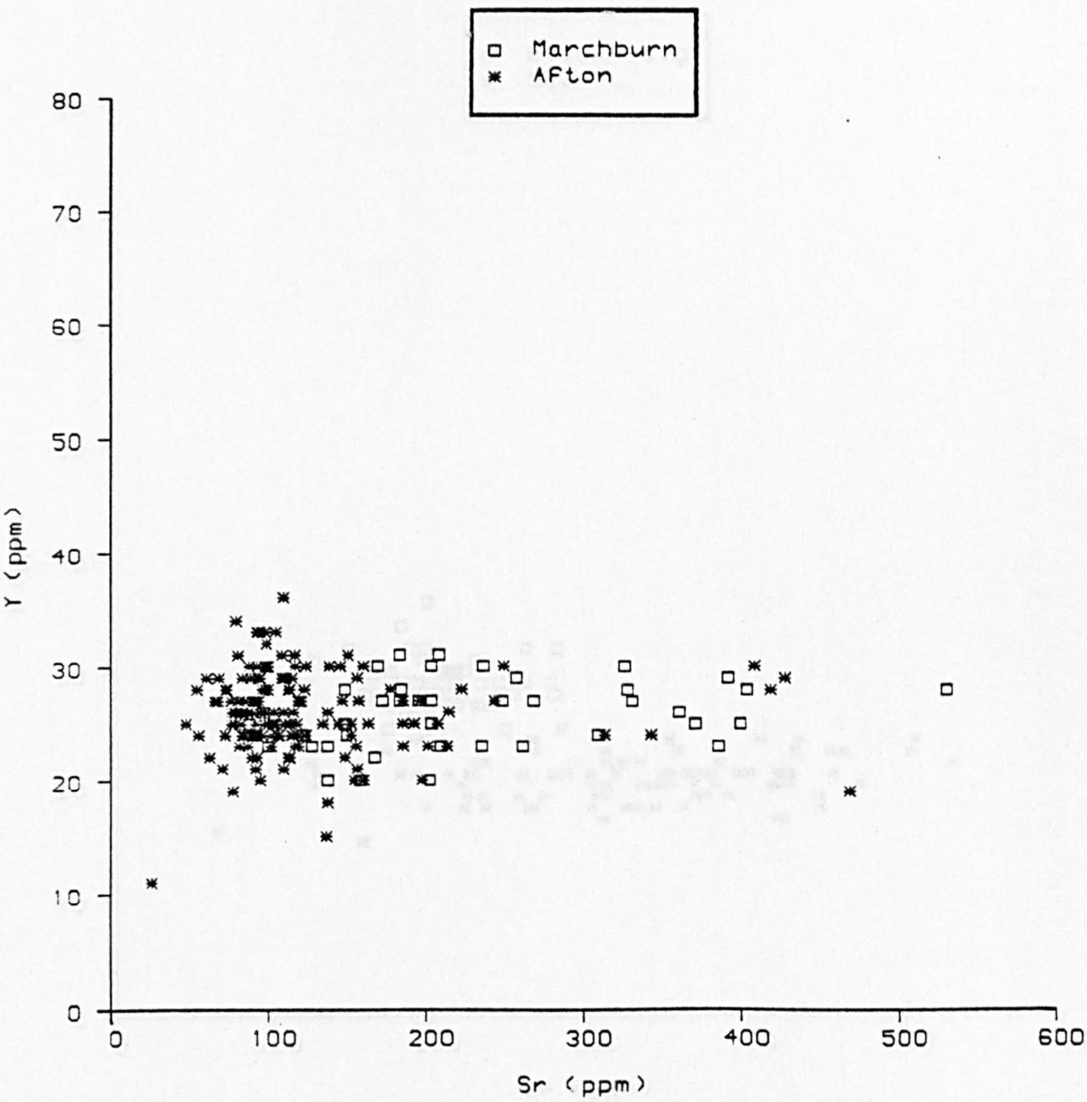

Discrimination Diagram (Lambert, Holland and Winchester)

FIGURE 375

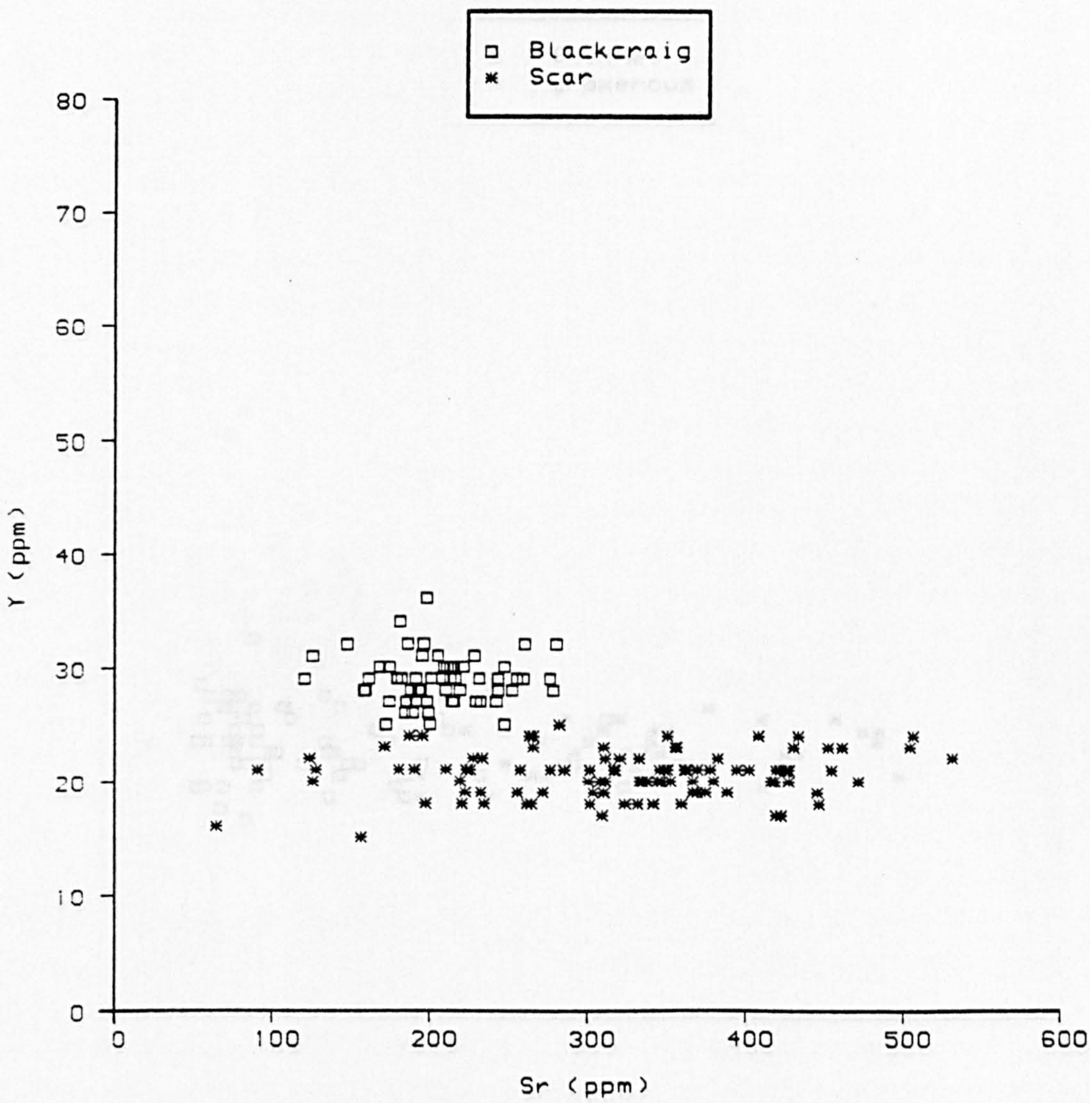

Discrimination Diagram (Lambert, Holland and Winchester)

FIGURE 376

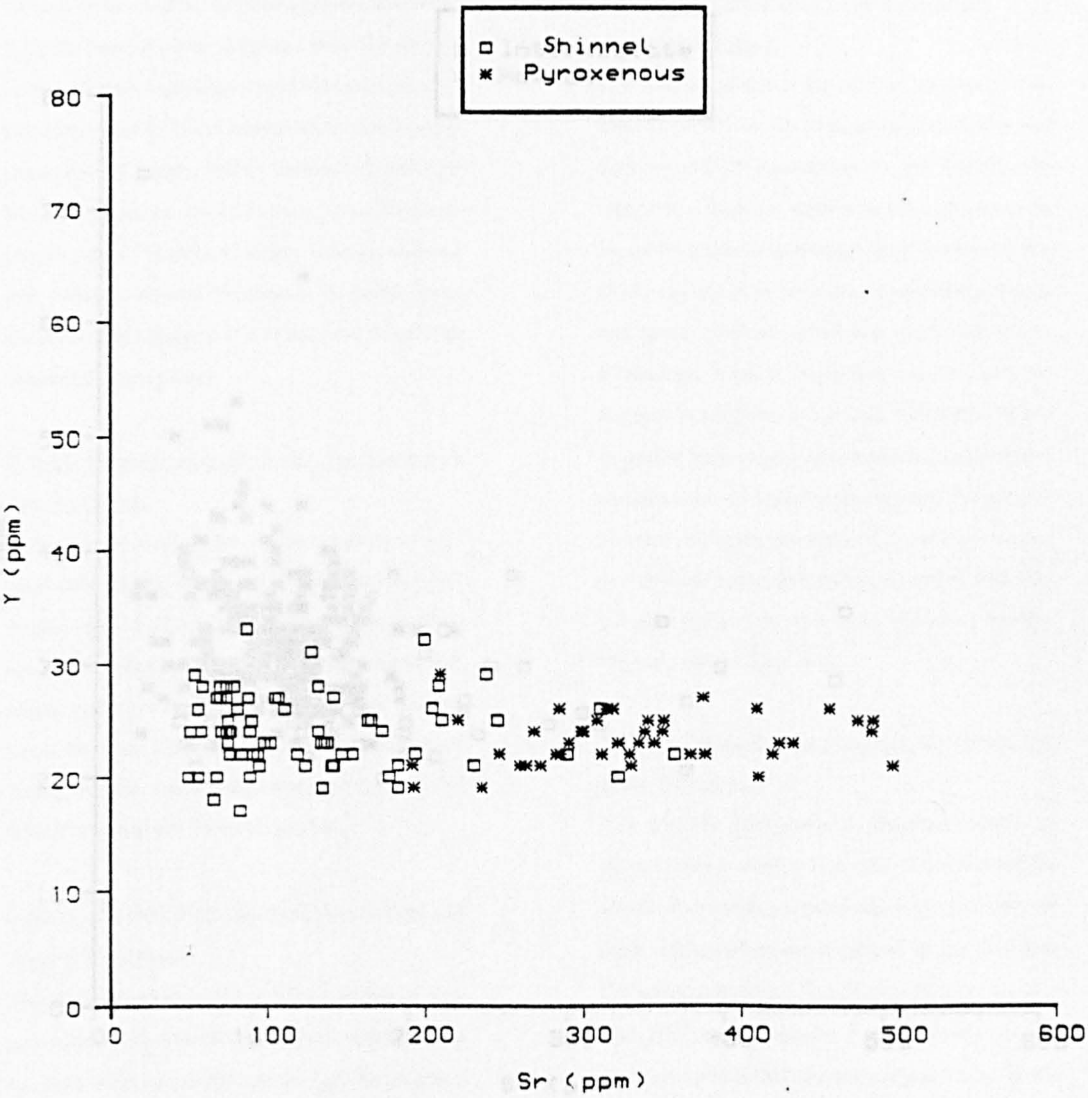

Discrimination Diagram (Lambert, Holland and Winchester)

FIGURE 377

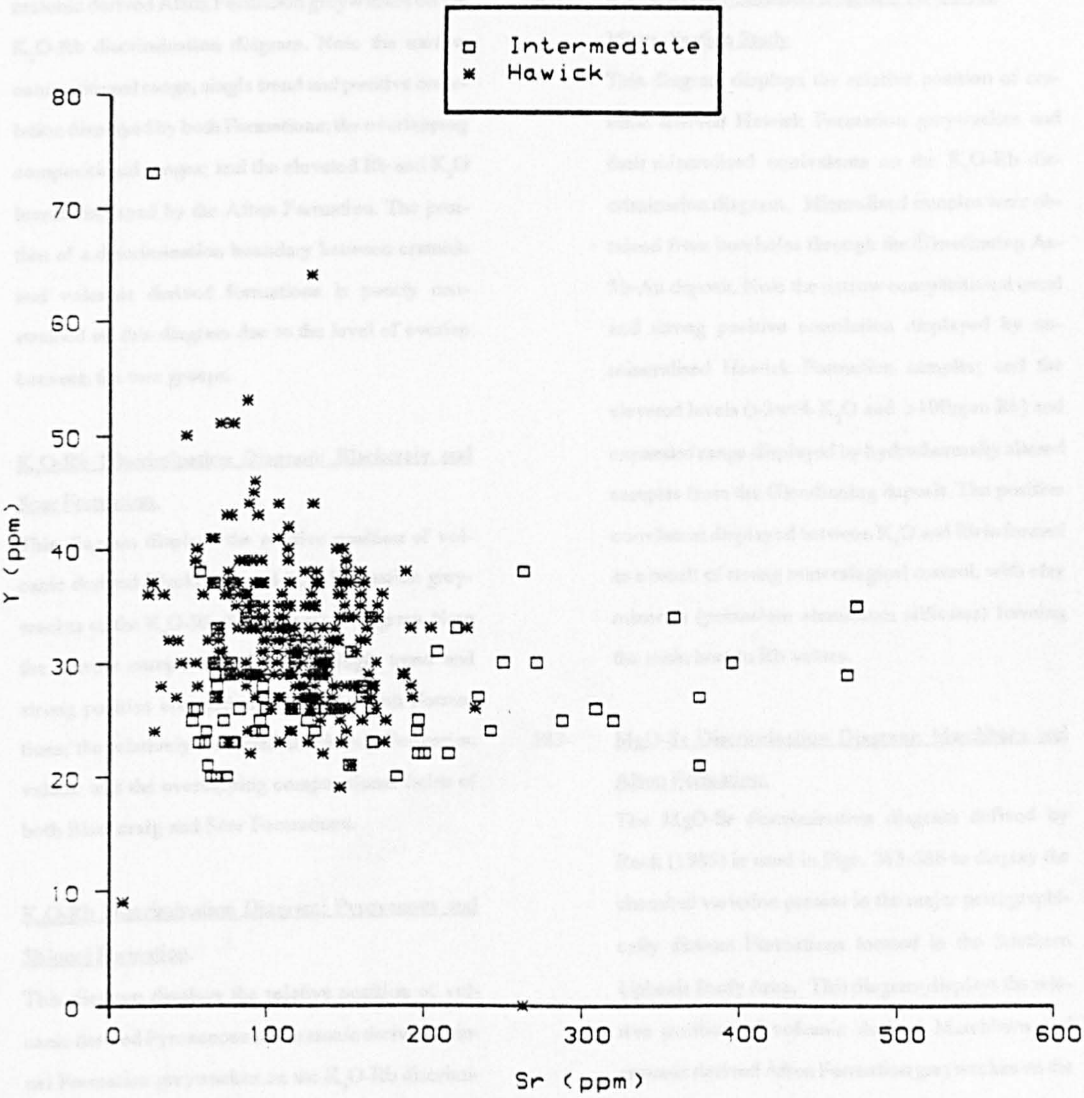

Discrimination Diagram (Lambert, Holland and Winchester)

378- K_2O-Rb Discrimination Diagram: Marchburn and Afton Formation

The K_2O-Rb discrimination diagram defined by Rock (1985) is used in Figs. 378-382 to display the chemical variation present in the major petrographically distinct Formations located in the Southern Uplands Study Area. This diagram displays the relative position of volcanic derived Marchburn and cratonic derived Afton Formation greywackes on the K_2O-Rb discrimination diagram. Note the narrow compositional range, single trend and positive correlation displayed by both Formations; the overlapping compositional ranges; and the elevated Rb and K_2O levels displayed by the Afton Formation. The position of a discrimination boundary between cratonic and volcanic derived formations is poorly constrained on this diagram due to the level of overlap between the two groups.

379- K_2O-Rb Discrimination Diagram: Blackcraig and Scar Formation.

This diagram displays the relative position of volcanic derived Blackcraig and Scar Formation greywackes on the K_2O-Rb discrimination diagram. Note the narrow compositional range, single trend and strong positive correlation defined by both Formations; the relatively restricted Blackcraig Formation values; and the overlapping compositional fields of both Blackcraig and Scar Formations.

380- K_2O-Rb Discrimination Diagram: Pyroxenous and Shinnel Formation.

This diagram displays the relative position of volcanic derived Pyroxenous and cratonic derived Shinnel Formation greywackes on the K_2O-Rb discrimination diagram. Note as in previous K_2O-Rb plots, the narrow compositional range single trend and strong positive correlation displayed by both Formations; and the closely overlapping compositional fields of both groups.

381- K_2O-Rb Discrimination Diagram: Intermediate and Hawick Formation.

This diagram displays the relative position of cratonic derived Intermediate and Hawick Formation greywackes on the K_2O-Rb discrimination diagram. Note the narrow compositional range, single trend and strong positive correlation displayed by both Formations; the overlapping compositional fields of both groups; and the elevated values (>3wt% K_2O and >100ppm Rb) displayed by both Formations indicative of hydrothermally altered samples (see Fig. 382).

382- K_2O-Rb Discrimination Diagram: As-Sb-Au Mineralisation Study

This diagram displays the relative position of cratonic derived Hawick Formation greywackes and their mineralised equivalents on the K_2O-Rb discrimination diagram. Mineralised samples were obtained from boreholes through the Glendinning As-Sb-Au deposit. Note the narrow compositional trend and strong positive correlation displayed by unmineralised Hawick Formation samples; and the elevated levels (>3wt% K_2O and >100ppm Rb) and expanded range displayed by hydrothermally altered samples from the Glendinning deposit. The positive correlation displayed between K_2O and Rb is formed as a result of strong mineralogical control, with clay minerals (potassium aluminium sillicates) forming the main host to Rb values.

383- MgO-Sr Discrimination Diagram: Marchburn and Afton Formation.

The MgO-Sr discrimination diagram defined by Rock (1985) is used in Figs. 383-386 to display the chemical variation present in the major petrographically distinct Formations located in the Southern Uplands Study Area. This diagram displays the relative position of volcanic derived Marchburn and cratonic derived Afton Formation greywackes on the MgO-Sr discrimination diagram. Note the wide scatter and inverse relationship displayed between MgO and Sr in the Marchburn Formation; the narrow restricted range of MgO and Sr values (MgO <6wt% and Sr <200wt%) displayed by the Afton Formation; and the classification boundary between the two groups.

384- MgO-Sr Discrimination Diagram: Blackcraig and Scar Formation. This diagram displays the relative position of volcanic derived Blackcraig and Scar

FIGURE 378

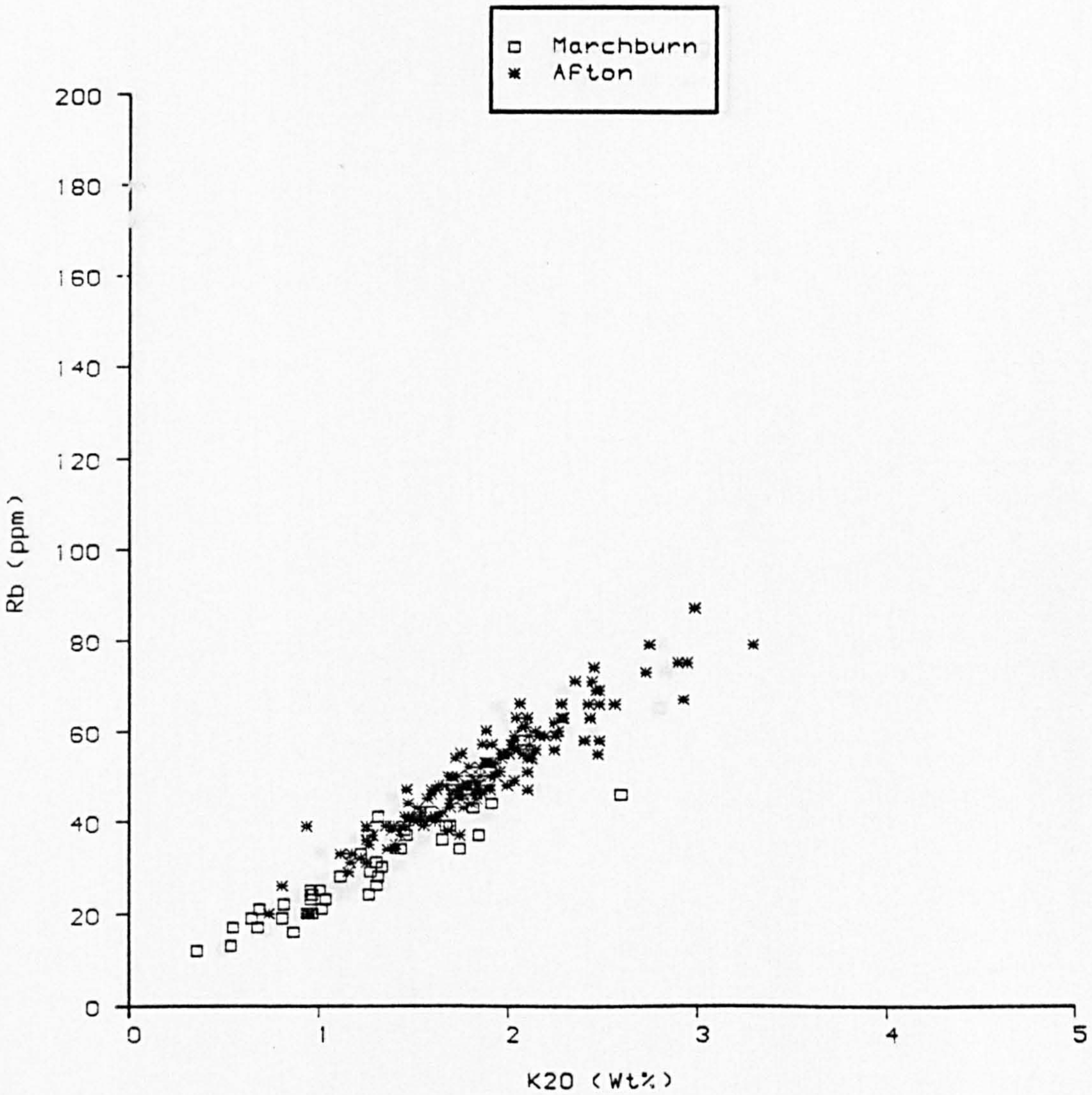

Discrimination Diagram (Rock, 1985)

FIGURE 379

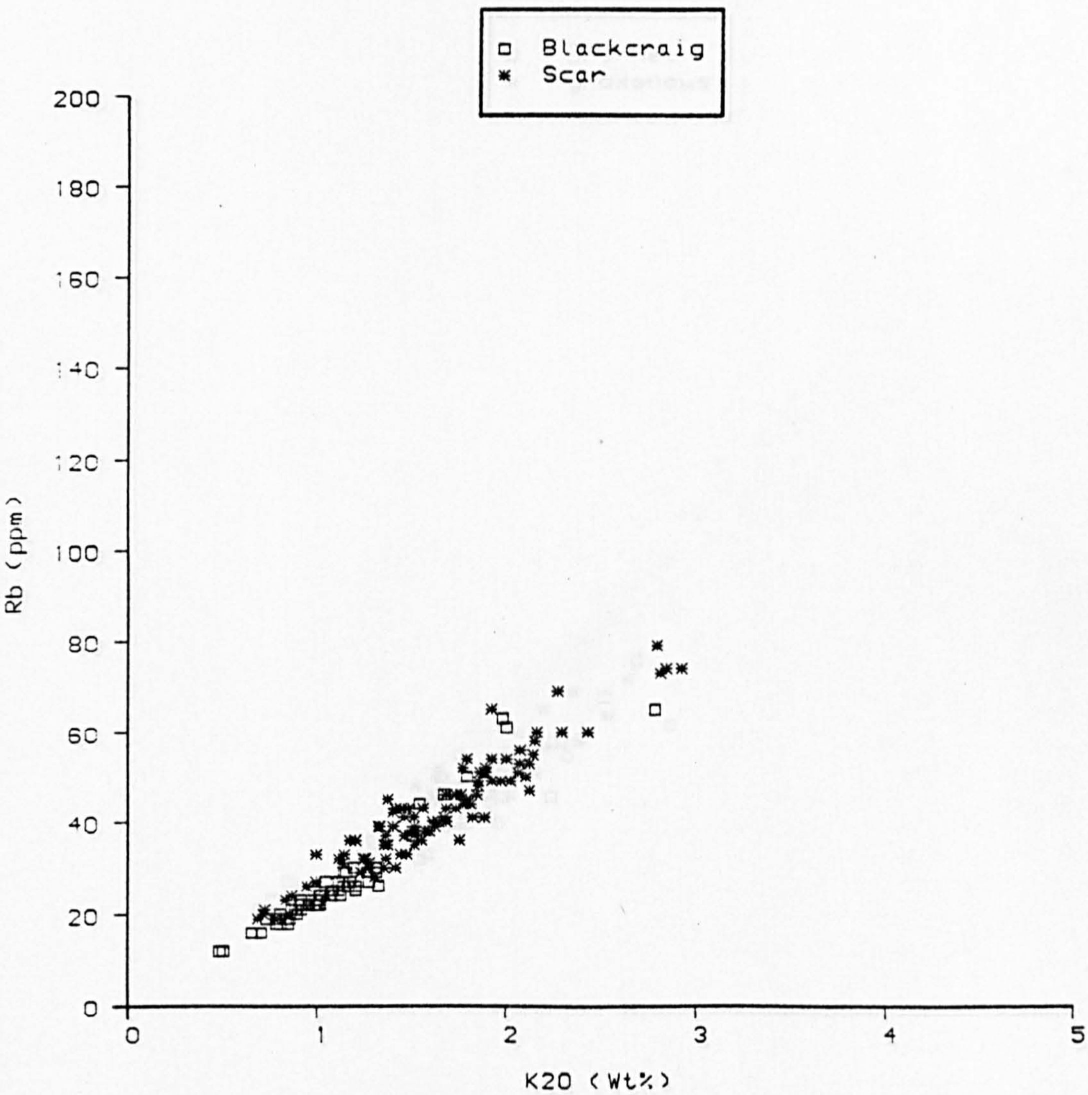

Discrimination Diagram (Rock, 1985)

FIGURE 380

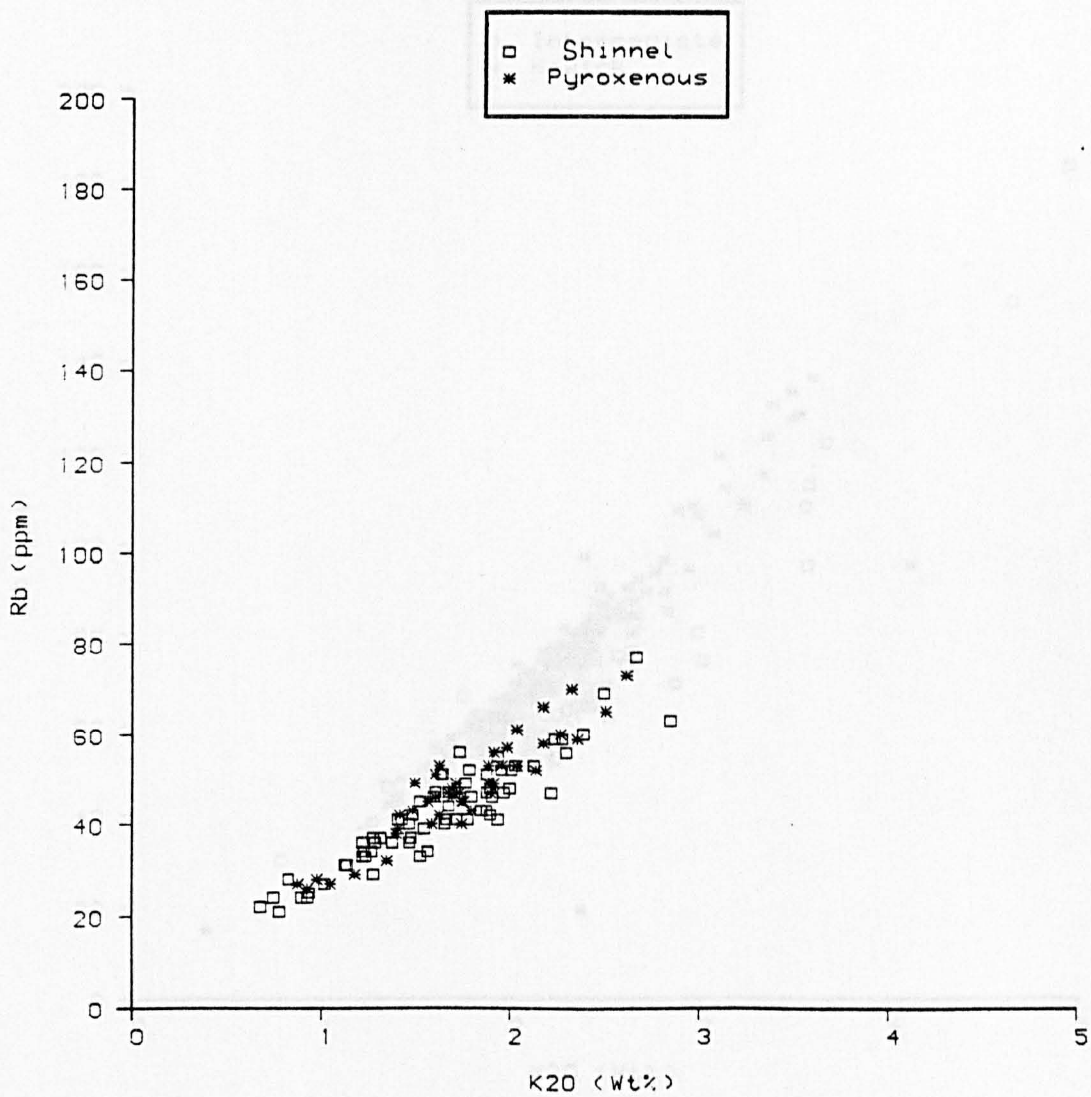

Discrimination Diagram (Rock, 1985)

FIGURE 381

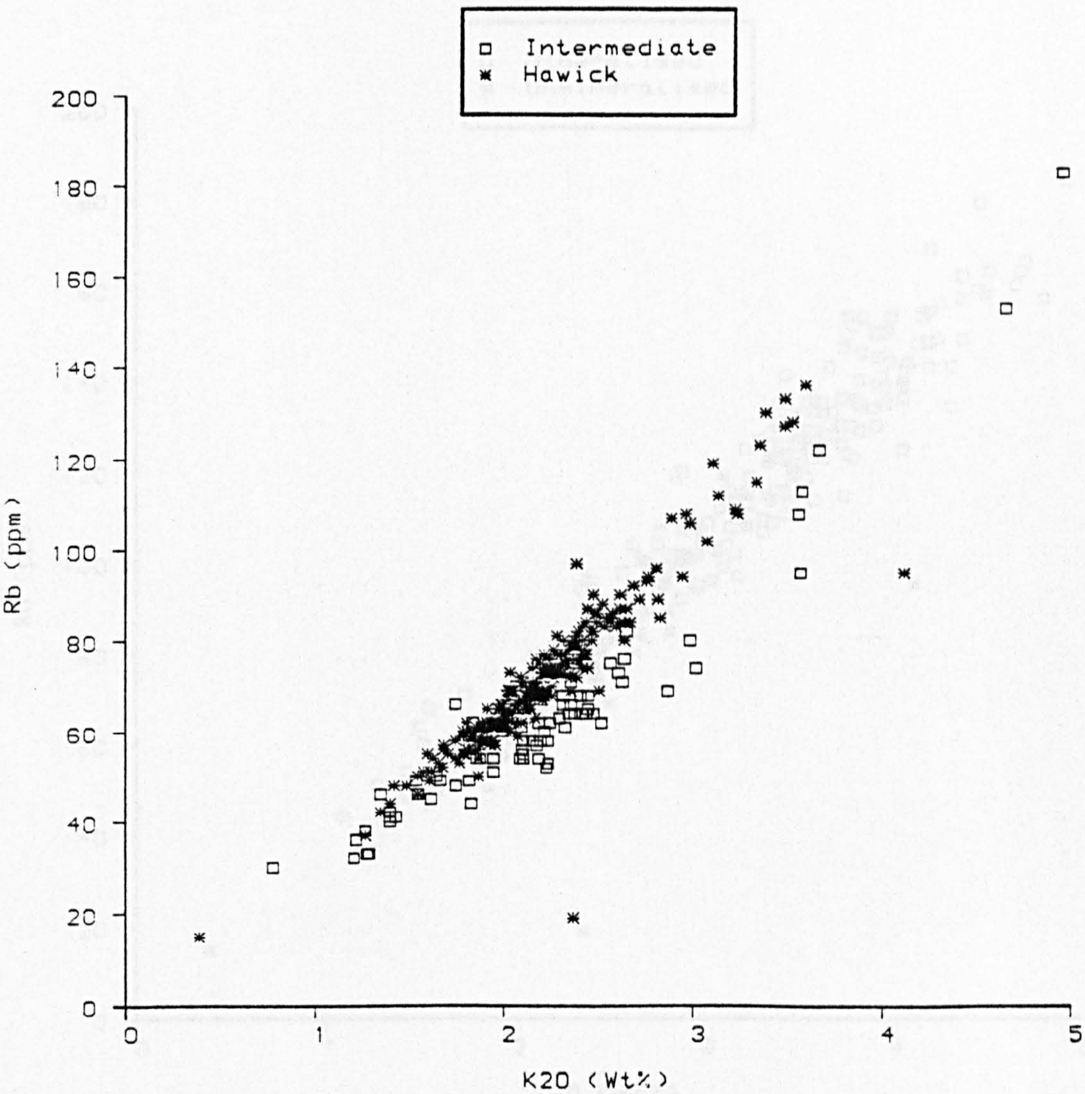

Discrimination Diagram (Rock, 1985)

FIGURE 382

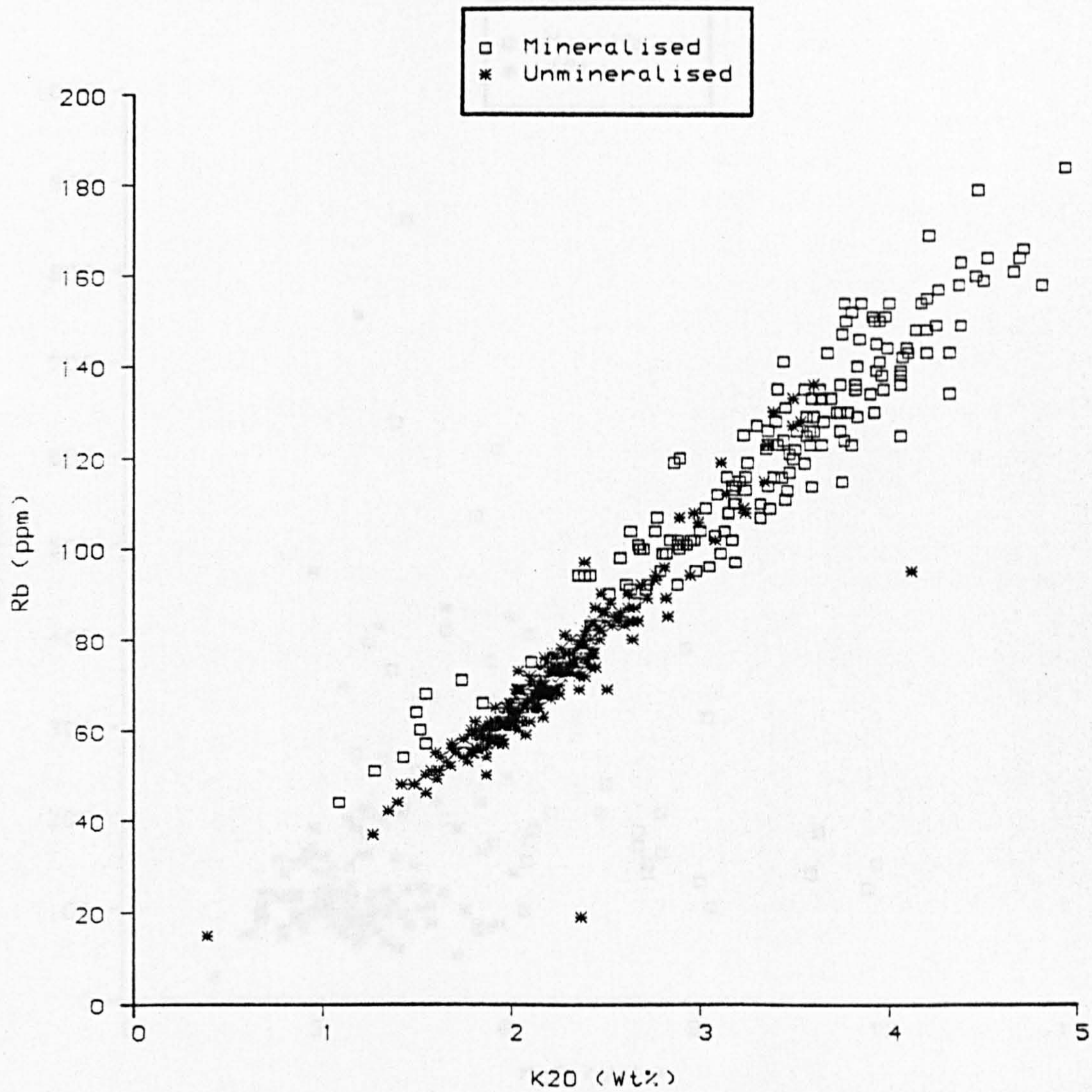

Discrimination Diagram (Rock, 1985)

FIGURE 383

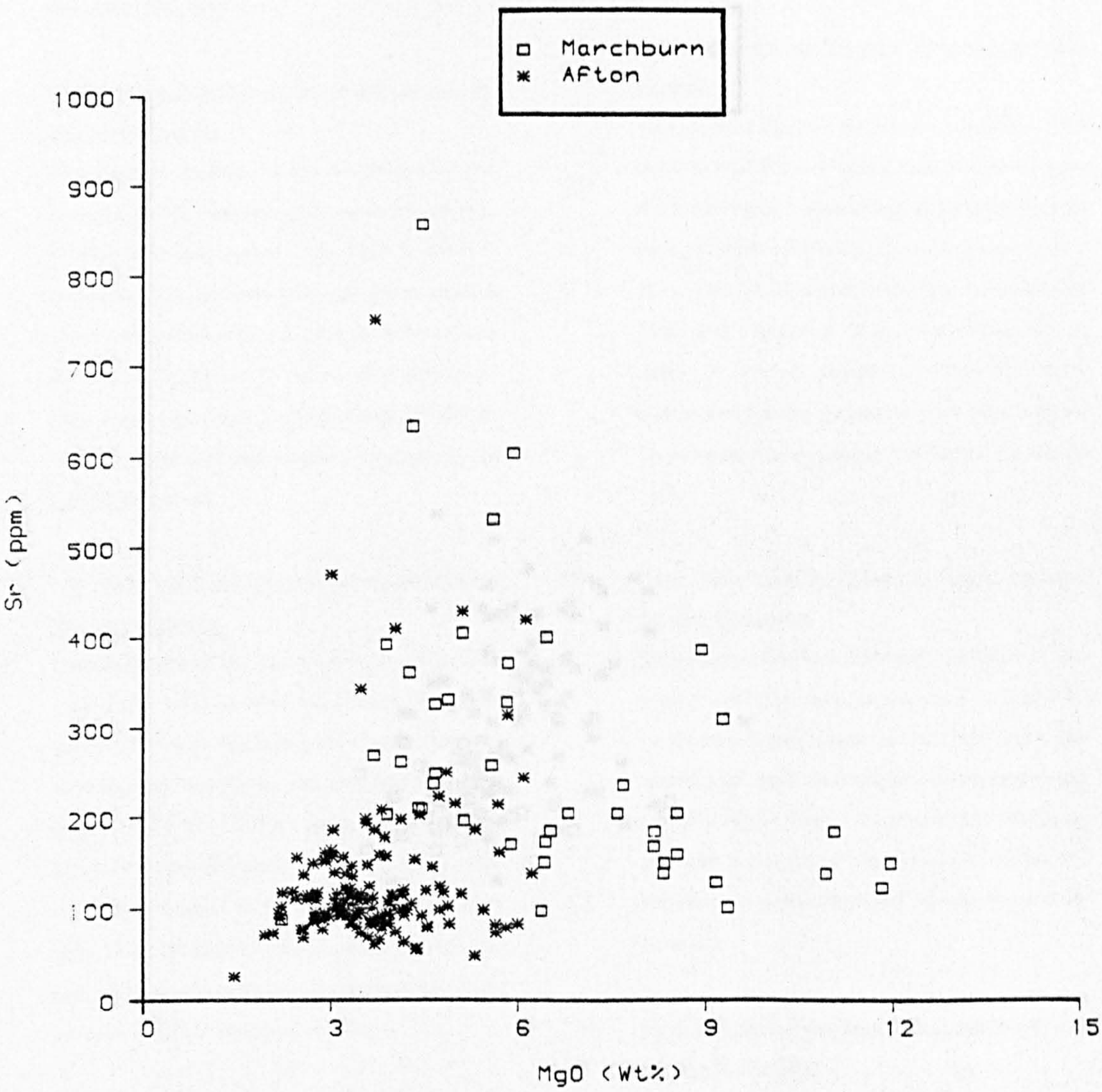

Discrimination Diagram (Rock, 1985)

FIGURE 384

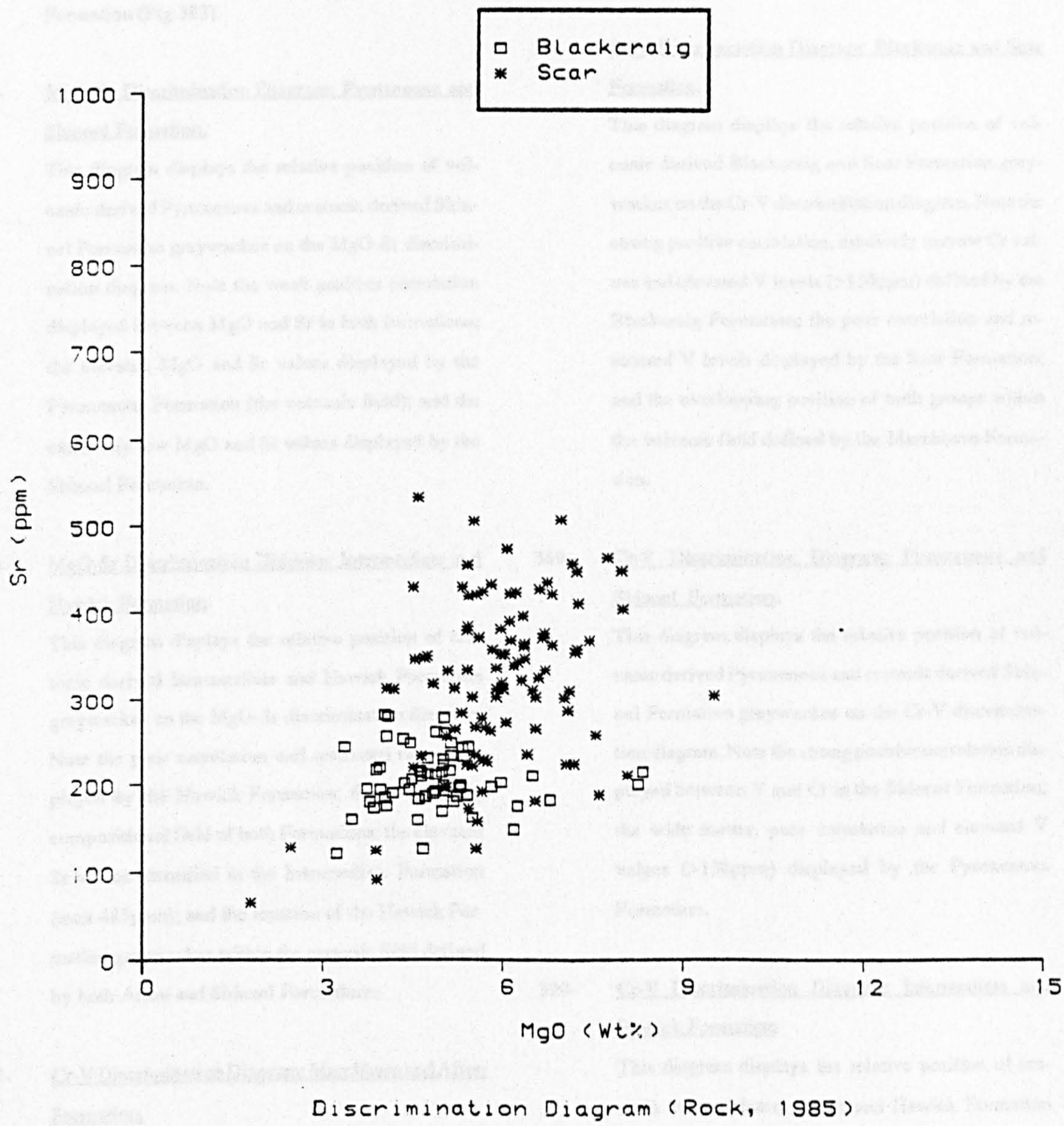
Blackcraig
Scar
Sr (ppm)
1000
900
800
700
600
500
400
300
200
100
0
0
3
6
9
12
15
MgO (Wt%)
Discrimination Diagram (Rock, 1985)

Formation greywackes on the MgO-Sr discrimination diagram. Note the wide scatter, and poor correlation displayed between Sr and MgO in the Scar Formation; the weak positive correlation and relatively restricted MgO and Sr values (MgO <6wt% and Sr <200wt%) present in the Blackcraig Formation; and the overlapping position of both groups within the volcanic field defined by the Marchburn Formation (Fig.383).

385- MgO-Sr Discrimination Diagram: Pyroxenous and Shinnel Formation.
This diagram displays the relative position of volcanic derived Pyroxenous and cratonic derived Shinnel Formation greywackes on the MgO-Sr discrimination diagram. Note the weak positive correlation displayed between MgO and Sr in both formations; the elevated MgO and Sr values displayed by the Pyroxenous Formation (the volcanic field); and the extremely low MgO and Sr values displayed by the Shinnel Formation.

386- MgO-Sr Discrimination Diagram: Intermediate and Hawick Formation.
This diagram displays the relative position of cratonic derived Intermediate and Hawick Formation greywackes on the MgO-Sr discrimination diagram. Note the poor correlation and restricted range displayed by the Hawick Formation; the overlapping compositional field of both Formations; the elevated Sr values identified in the Intermediate Formation (max 485ppm); and the location of the Hawick Formation greywackes within the cratonic field defined by both Afton and Shinnel Formations;

387- Cr-V Discrimination Diagram: Marchburn and Afton Formation.
The Cr-V discrimination diagram defined by Rock (1985) is used in Figs. 387-390 to display the chemical variation present in the major petrographically distinct Formations located in the Southern Uplands Study Area. This diagram displays the relative position of volcanic derived Marchburn and cratonic derived Afton Formation greywackes on the Cr-V discrimination diagram. Note the narrow, relatively restricted range of V values (<150ppm) defined by the Afton Formation; the strong positive correlation displayed by both groups; and the elevated V and Cr levels (>130ppm and 200-905ppm respectively) displayed by the Marchburn Formation. The position of a discrimination boundary between cratonic and volcanic derived formations may be identified solely on the basis of V content (Cratonic Formations <130ppm).

388- Cr-V Discrimination Diagram: Blackcraig and Scar Formation.
This diagram displays the relative position of volcanic derived Blackcraig and Scar Formation greywackes on the Cr-V discrimination diagram. Note the strong positive correlation, relatively narrow Cr values and elevated V levels (>130ppm) defined by the Blackcraig Formation; the poor correlation and restricted V levels displayed by the Scar Formation; and the overlapping position of both groups within the volcanic field defined by the Marchburn Formation.

389- Cr-V Discrimination Diagram: Pyroxenous and Shinnel Formation.
This diagram displays the relative position of volcanic derived Pyroxenous and cratonic derived Shinnel Formation greywackes on the Cr-V discrimination diagram. Note the strong positive correlation displayed between V and Cr in the Shinnel Formation; the wide scatter, poor correlation and elevated V values (>130ppm) displayed by the Pyroxenous Formation.

390- Cr-V Discrimination Diagram: Intermediate and Hawick Formation.
This diagram displays the relative position of cratonic derived Intermediate and Hawick Formation greywackes on the Cr-V discrimination diagram. Note the strong positive correlation, overlapping compositional field and restricted Cr and V values displayed by both Formations; and the location of both Hawick and Intermediate Formation greywackes within the cratonic field defined by both Afton and Shinnel Formations;

FIGURE 385

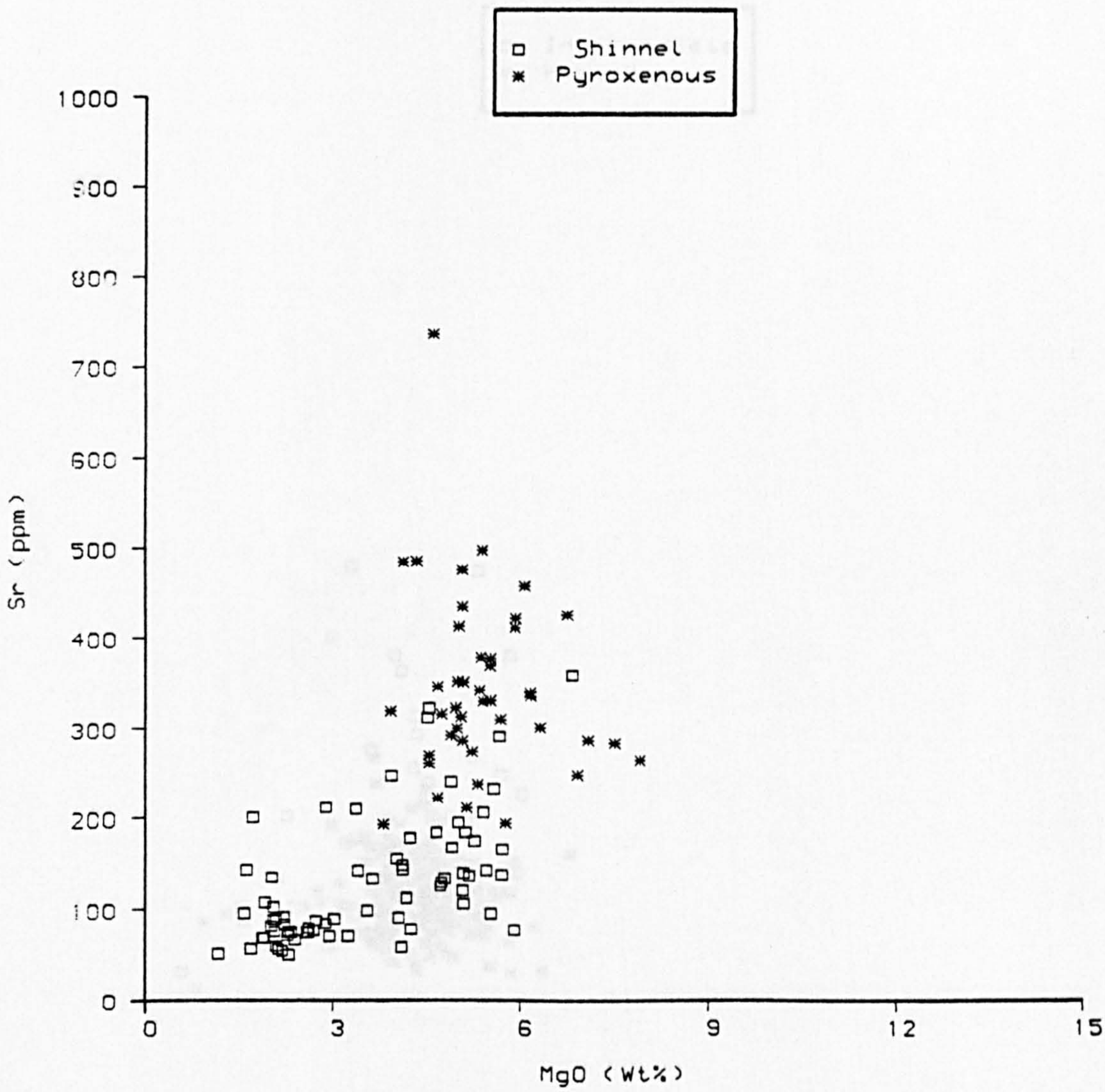

Discrimination Diagram (Rock, 1985)

FIGURE 386

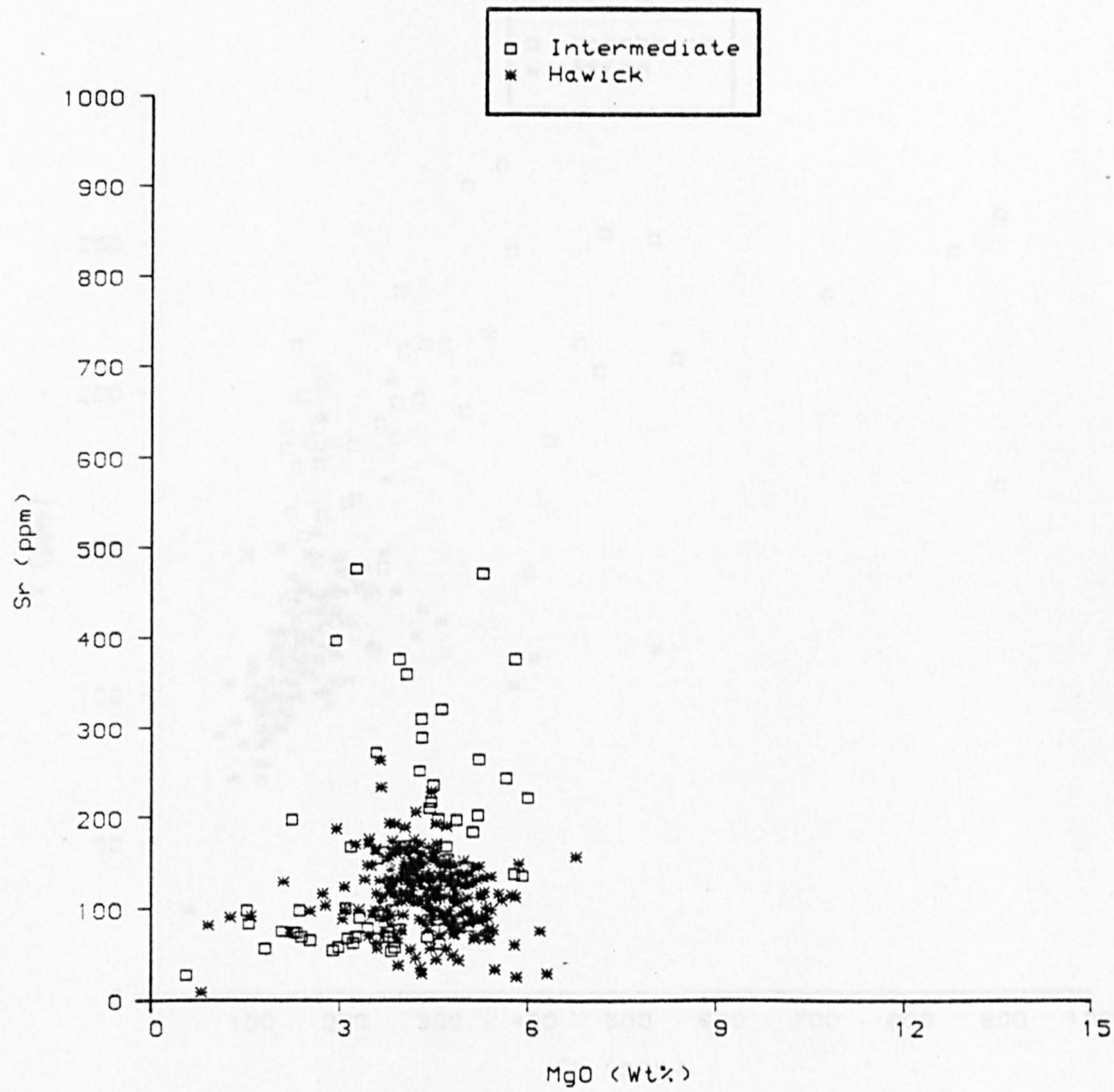

Discrimination Diagram (Rock, 1985)

FIGURE 387

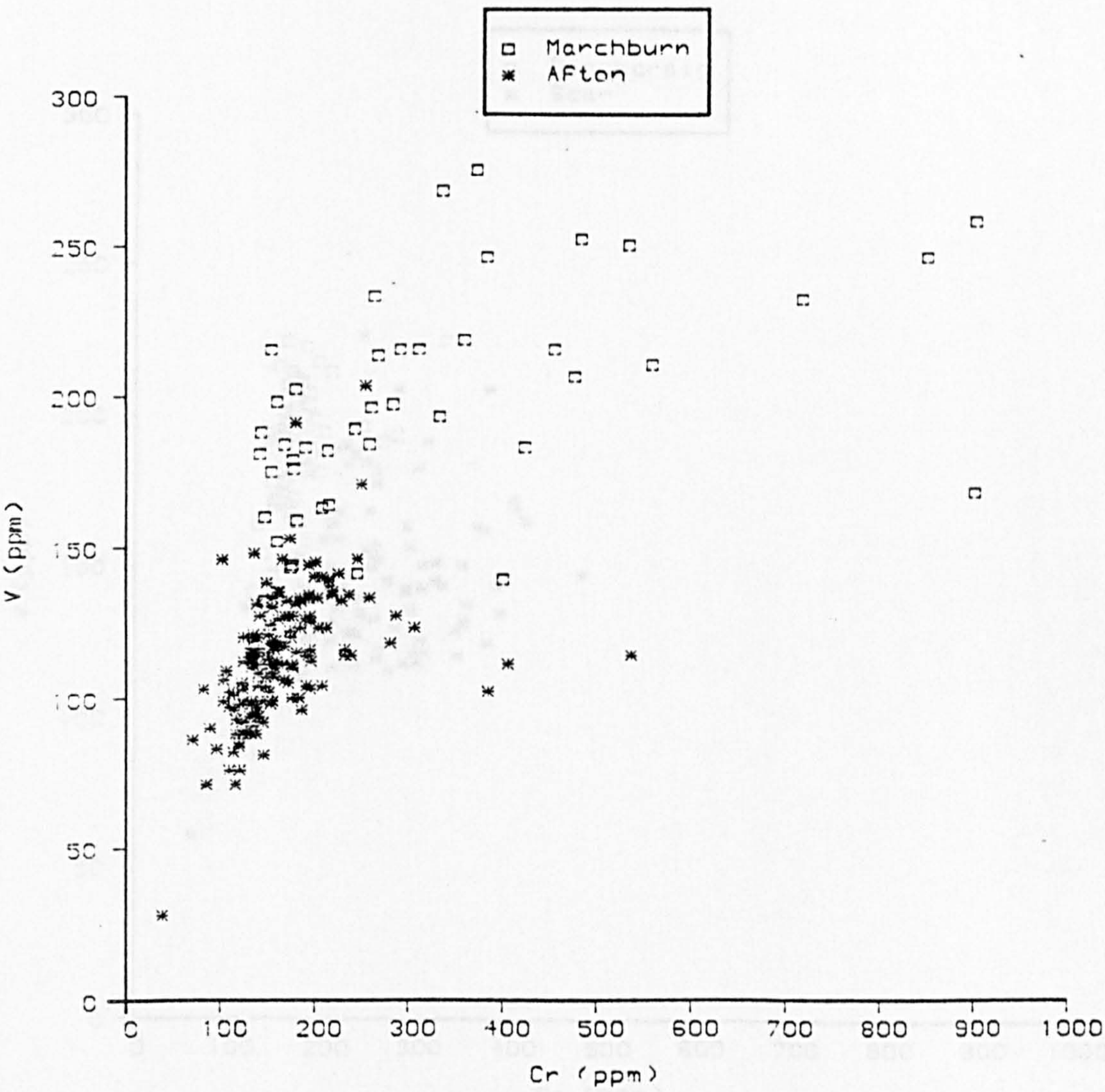

Discrimination Diagram (Rock, 1985)

FIGURE 388

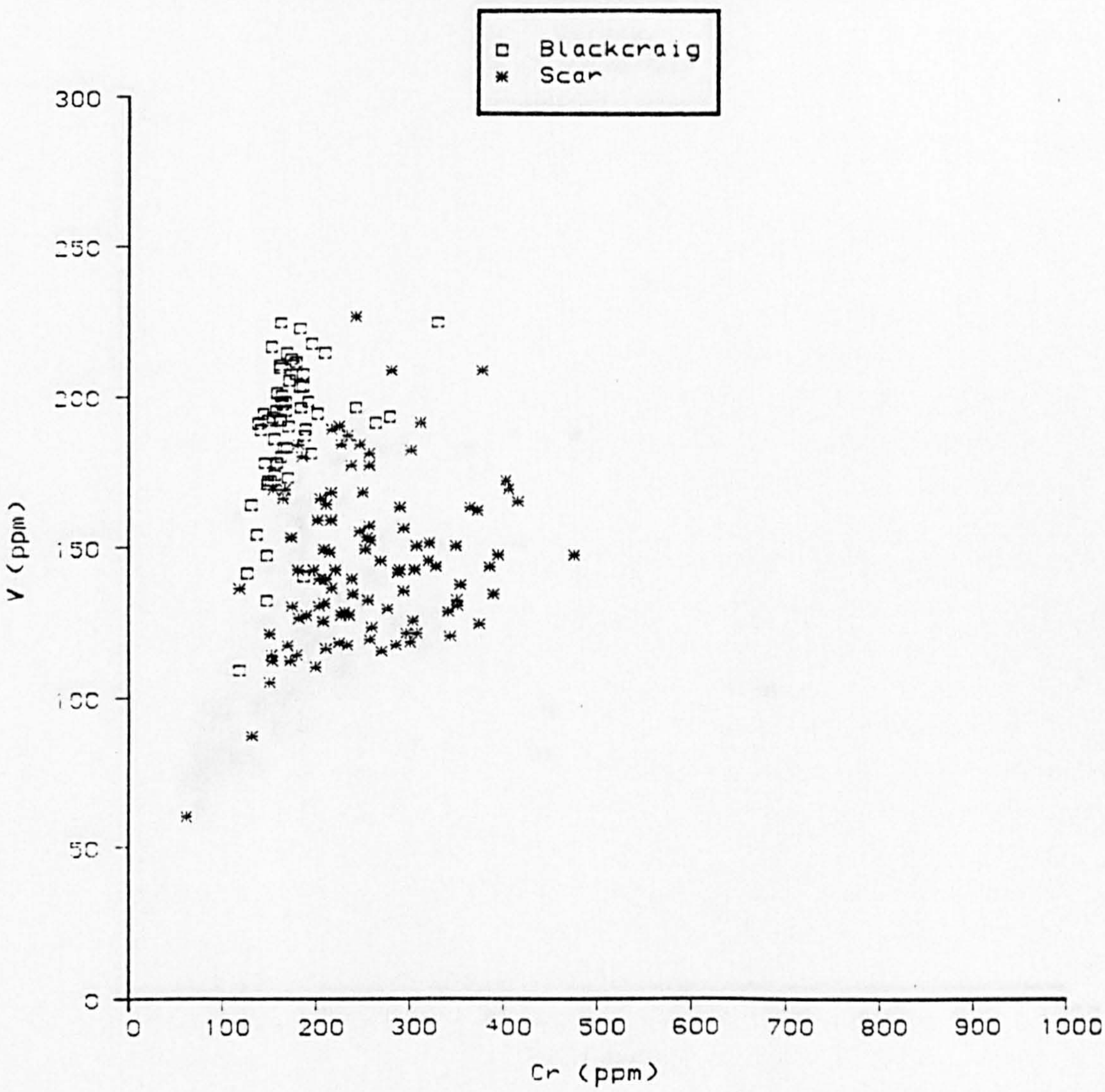

Discrimination Diagram (Rock, 1985)

FIGURE 389

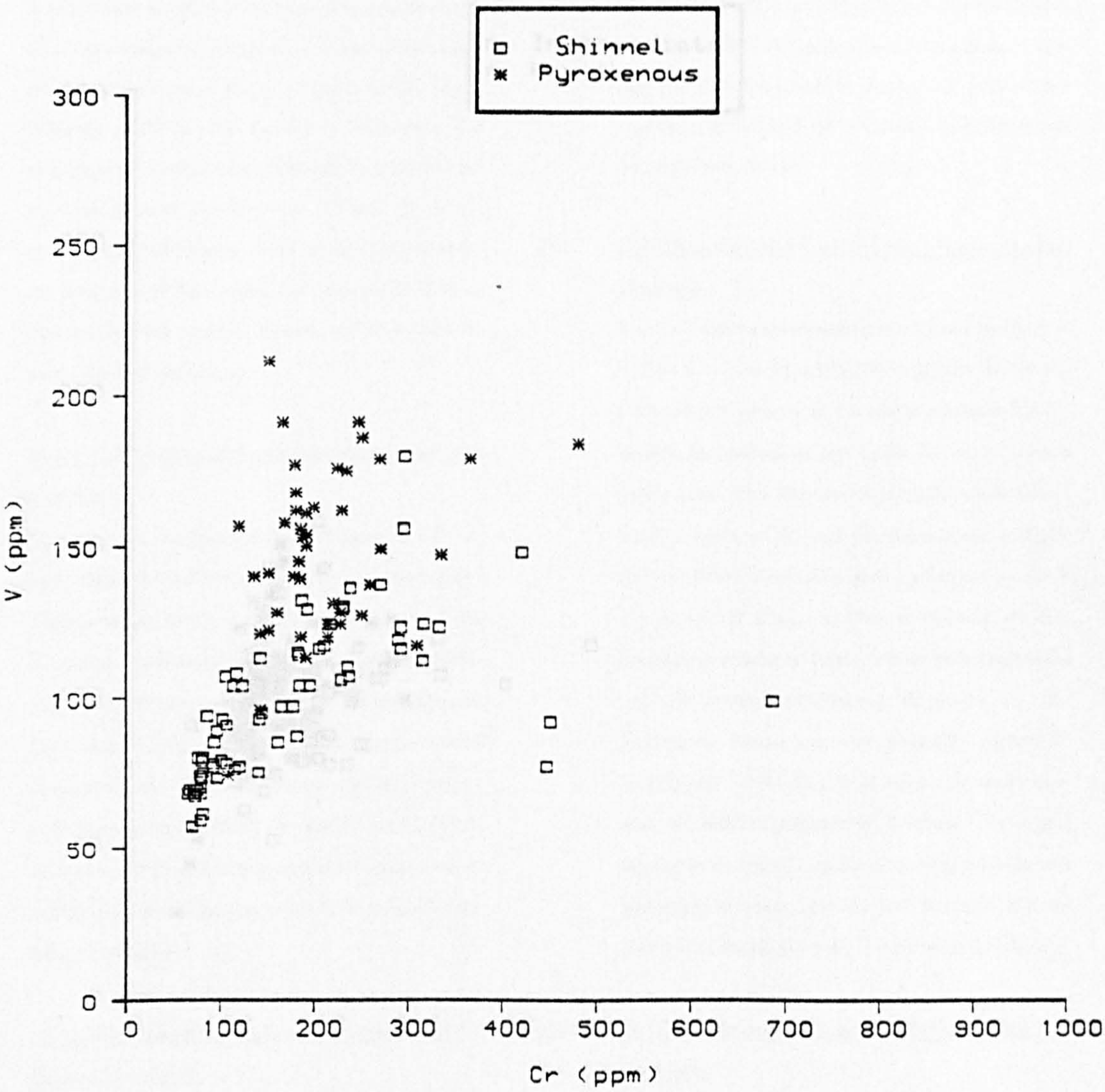

Discrimination Diagram (Rock, 1985)

FIGURE 390

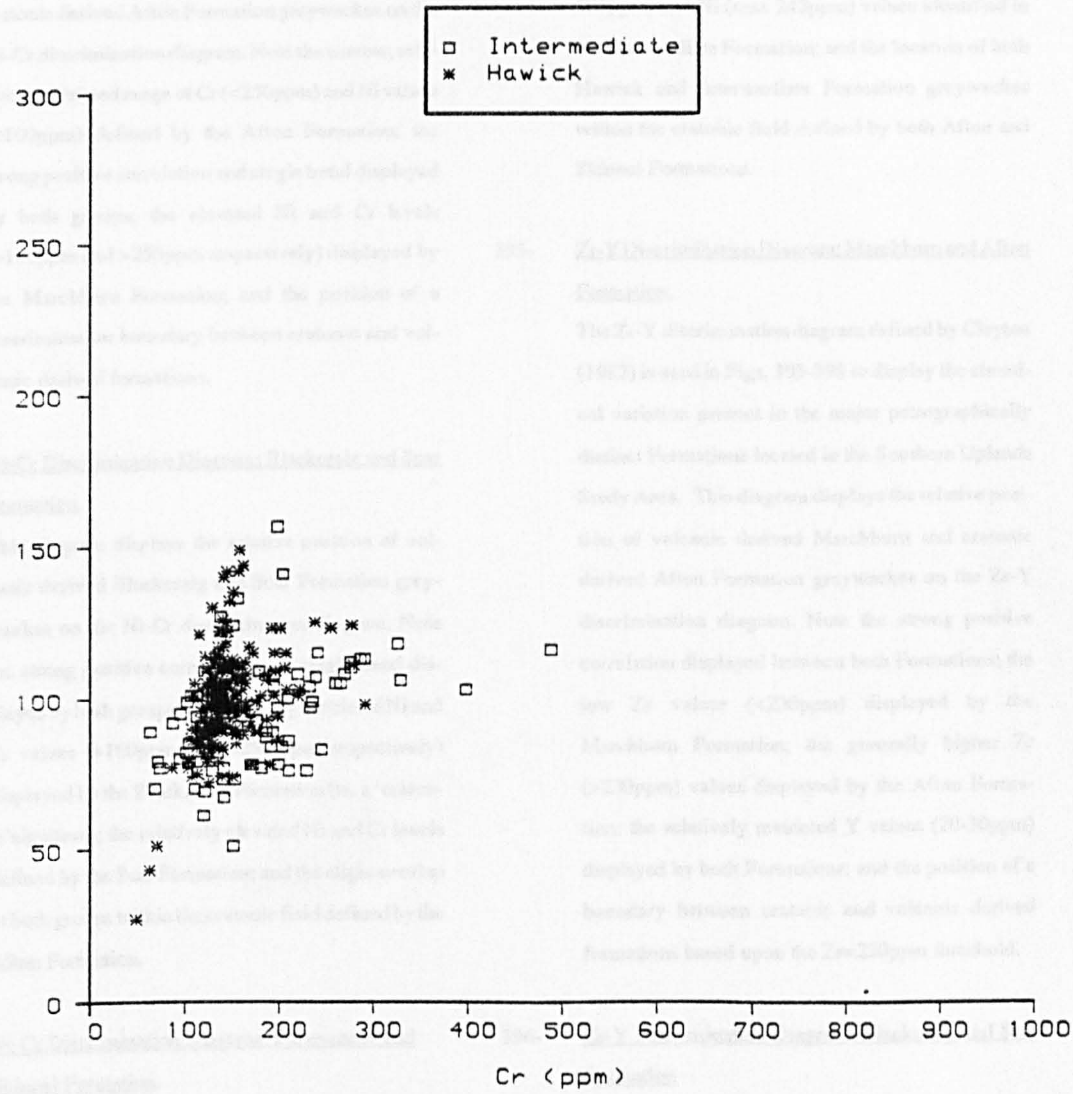

Discrimination Diagram (Rock, 1985)

391- Ni-Cr Discrimination Diagram: Marchburn and Afton Formation.

The Ni-Cr discrimination diagram defined by Clayton (1982) is used in Figs. 391-394 to display the chemical variation present in the major petrographically distinct Formations located in the Southern Uplands Study Area. This diagram displays the relative position of volcanic derived Marchburn and cratonic derived Afton Formation greywackes on the Ni-Cr discrimination diagram. Note the narrow, relatively restricted range of Cr (<250ppm) and Ni values (<100ppm) defined by the Afton Formation; the strong positive correlation and single trend displayed by both groups; the elevated Ni and Cr levels (>100ppm and >250ppm respectively) displayed by the Marchburn Formation; and the position of a discrimination boundary between cratonic and volcanic derived formations.

392- Ni-Cr Discrimination Diagram: Blackcraig and Scar Formation.

This diagram displays the relative position of volcanic derived Blackcraig and Scar Formation greywackes on the Ni-Cr discrimination diagram. Note the strong positive correlation and single trend displayed by both groups; the relatively restricted Ni and Cr values (>100ppm and >250 ppm respectively) displayed by the Blackcraig Formation (ie. a 'cratonic' signiture); the relatively elevated Ni and Cr levels defined by the Scar Formation; and the slight overlap of both groups within the cratonic field defined by the Afton Formation.

393- Ni-Cr Discrimination Diagram: Pyroxenous and Shinnel Formation.

This diagram displays the relative position of volcanic derived Pyroxenous and cratonic derived Shinnel Formation greywackes on the Ni-Cr discrimination diagram. Note the overlapping position of both Formations; the strong positive correlation displayed between Cr and Ni in the Pyroxenous Formation; and the apparent bimodal nature of Shinnel Formation, with the first group distinguished by low Ni and Cr values and a strong positive correlation, and the second group identified by relatively higher Cr and Ni values, a wide scatter and poor correlation.

394- Ni-Cr Discrimination Diagram: Intermediate and Hawick Formation.

This diagram displays the relative position of cratonic derived Intermediate and Hawick Formation greywackes on the Ni-Cr discrimination diagram. Note the strong positive correlation, overlapping compositional field and restricted Cr and Ni values displayed by both Formations; the elevated Cr (max 505ppm) and Ni (max 243ppm) values identified in the Intermediate Formation; and the location of both Hawick and Intermediate Formation greywackes within the cratonic field defined by both Afton and Shinnel Formations.

395- Zr-Y Discrimination Diagram: Marchburn and Afton Formation.

The Zr-Y discrimination diagram defined by Clayton (1982) is used in Figs. 395-398 to display the chemical variation present in the major petrographically distinct Formations located in the Southern Uplands Study Area. This diagram displays the relative position of volcanic derived Marchburn and cratonic derived Afton Formation greywackes on the Zr-Y discrimination diagram. Note the strong positive correlation displayed between both Formations; the low Zr values (<230ppm) displayed by the Marchburn Formation; the generally higher Zr (>230ppm) values displayed by the Afton Formation; the relatively restricted Y values (20-30ppm) displayed by both Formations; and the position of a boundary between cratonic and volcanic derived formations based upon the Zr=230ppm threshold.

396- Zr-Y Discrimination Diagram: Blackcraig and Scar Formation

This diagram displays the relative position of volcanic derived Blackcraig and Scar Formation greywackes on the Y-Zr discrimination diagram. Note the strong positive correlation displayed by both Formations; the parallel trend displayed by both groups; and the relatively restricted Y values (<24ppm) displayed by the Scar Formation; and the location of both Formations within the volcanic field defined by the Marchburn Formation.

FIGURE 391

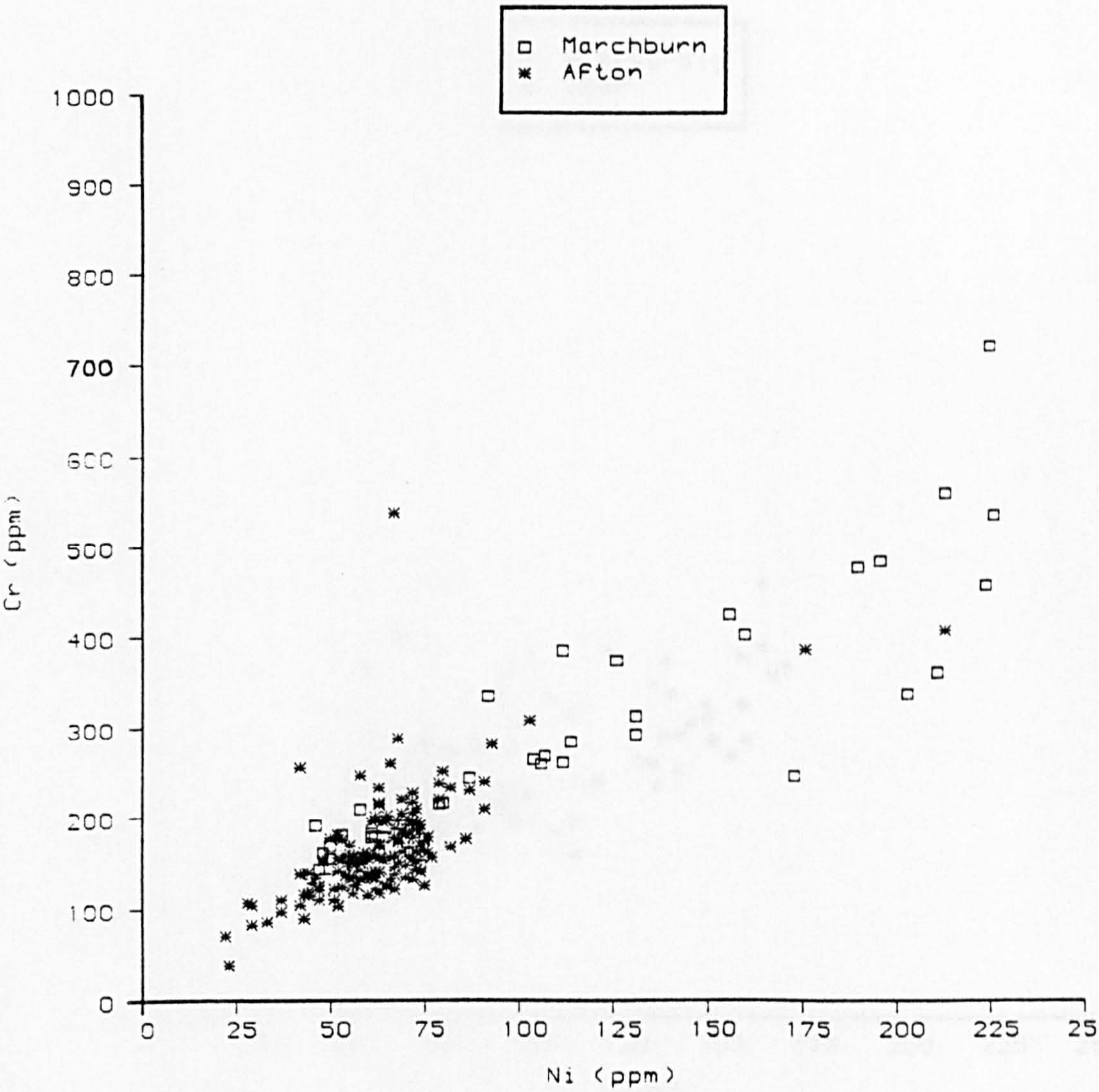

Discrimination Diagram (Clayton)

FIGURE 392

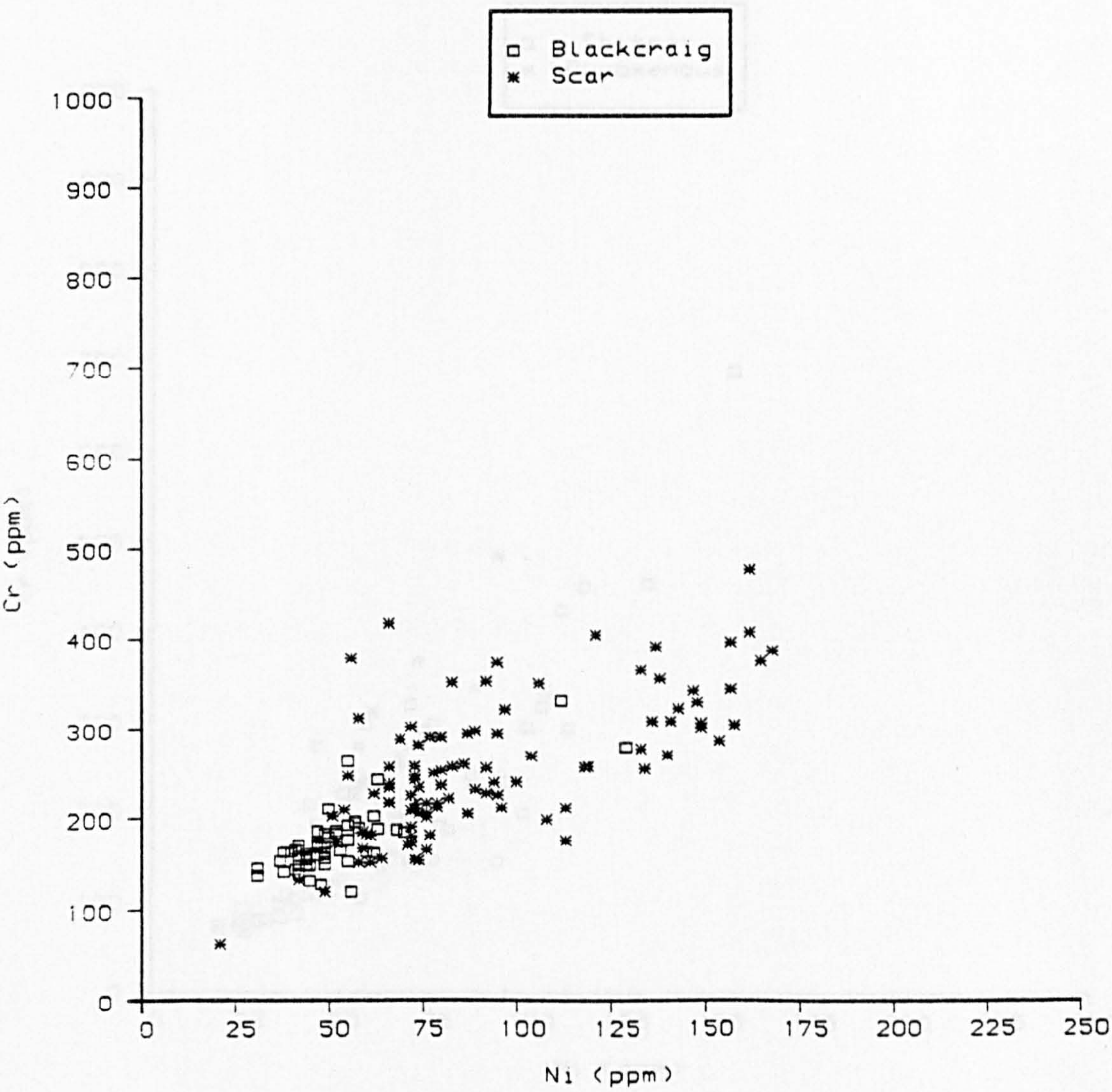

Discrimination Diagram (Clayton)

FIGURE 393

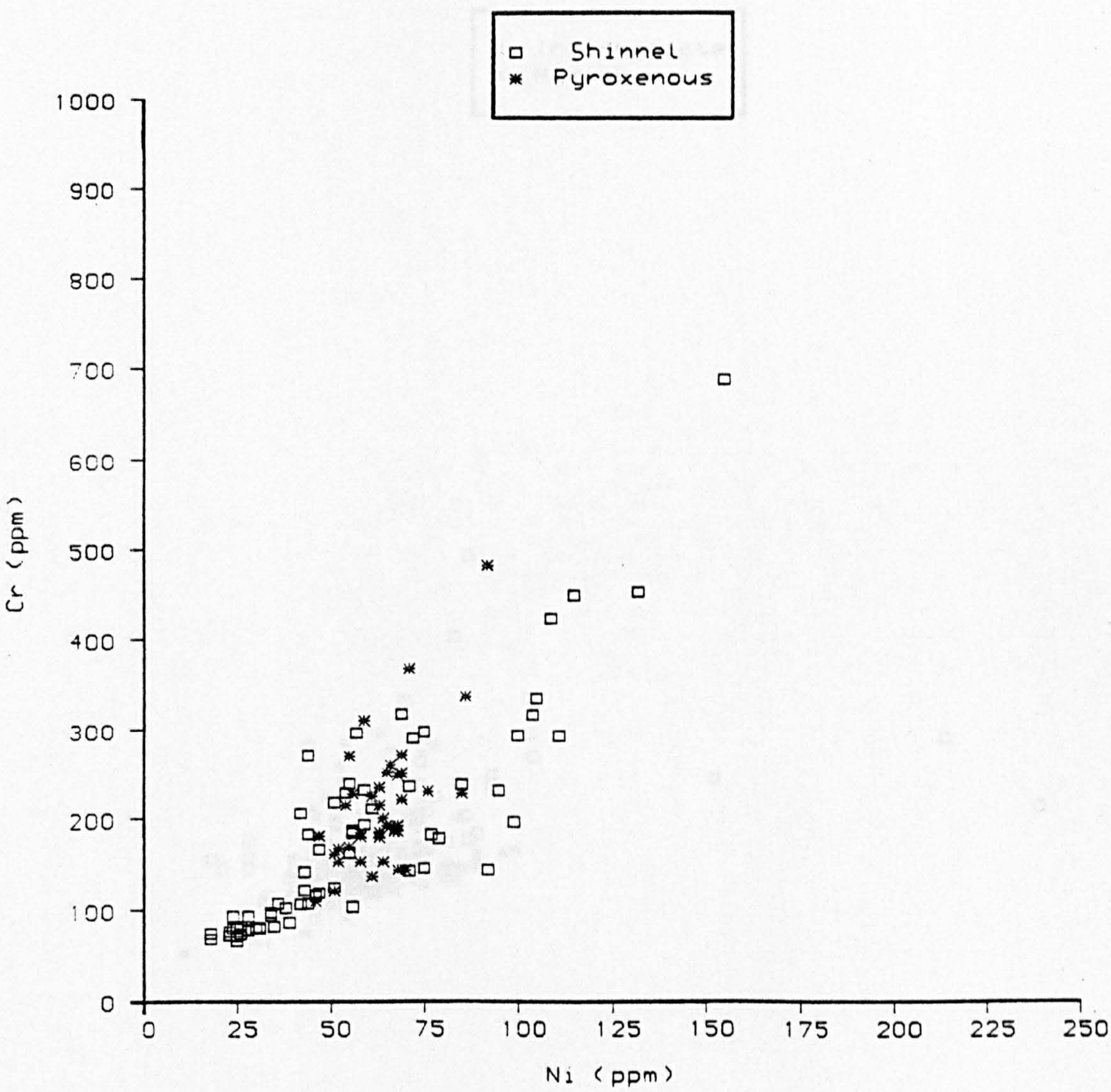

Discrimination Diagram (Clayton)

FIGURE 394

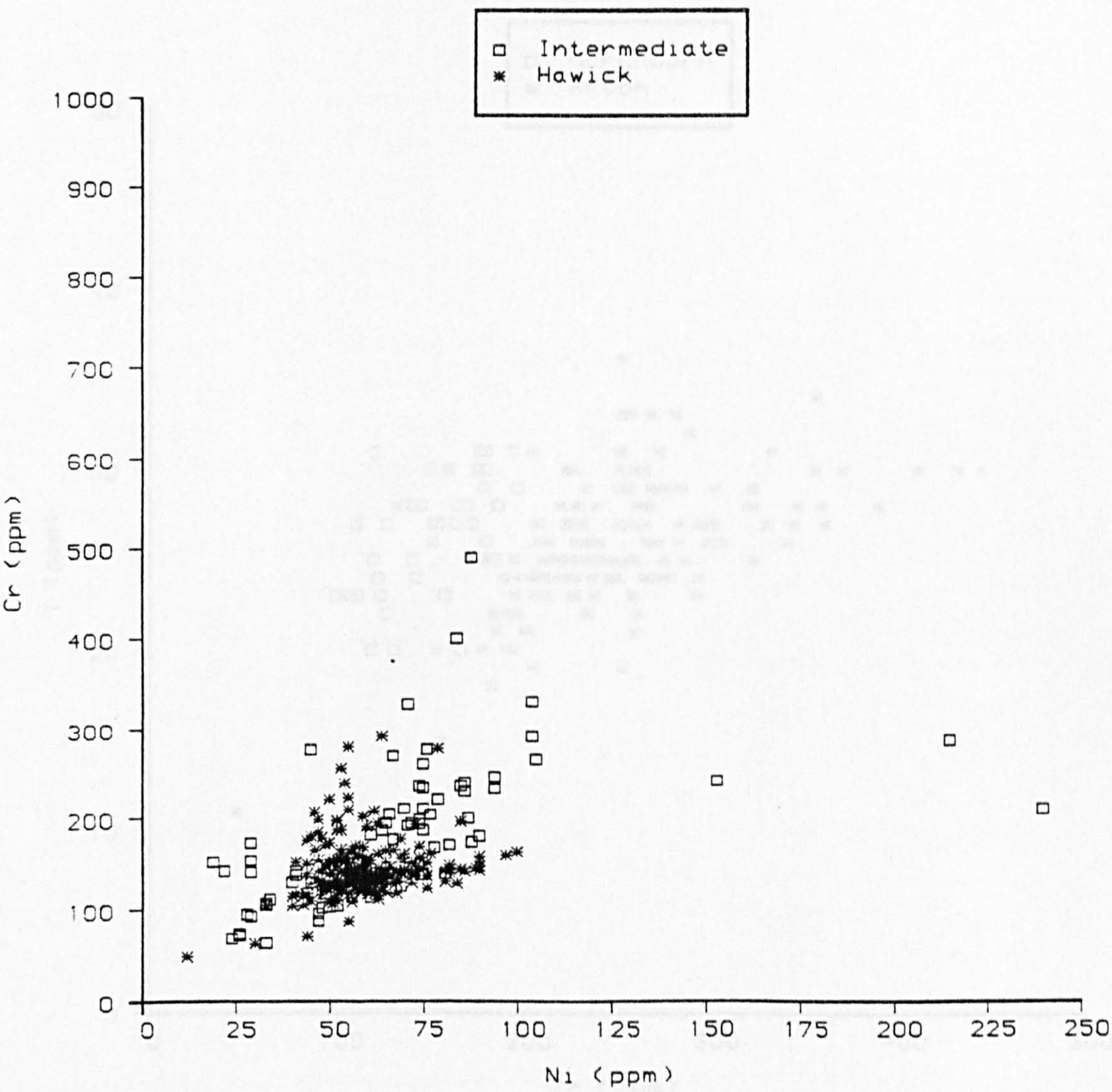

Discrimination Diagram (Clayton)

FIGURE 395

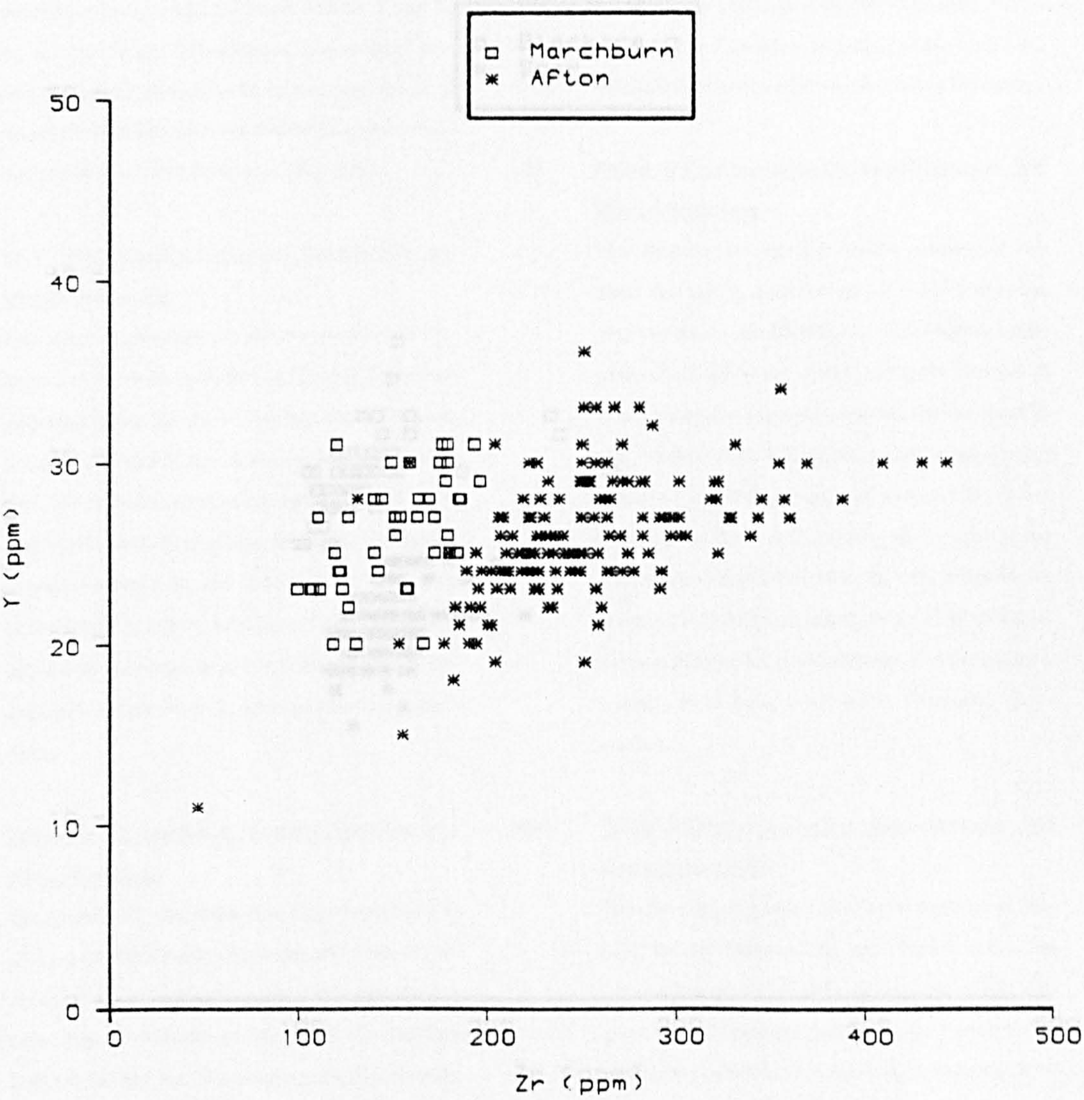

Discrimination Diagram (Clayton)

FIGURE 396

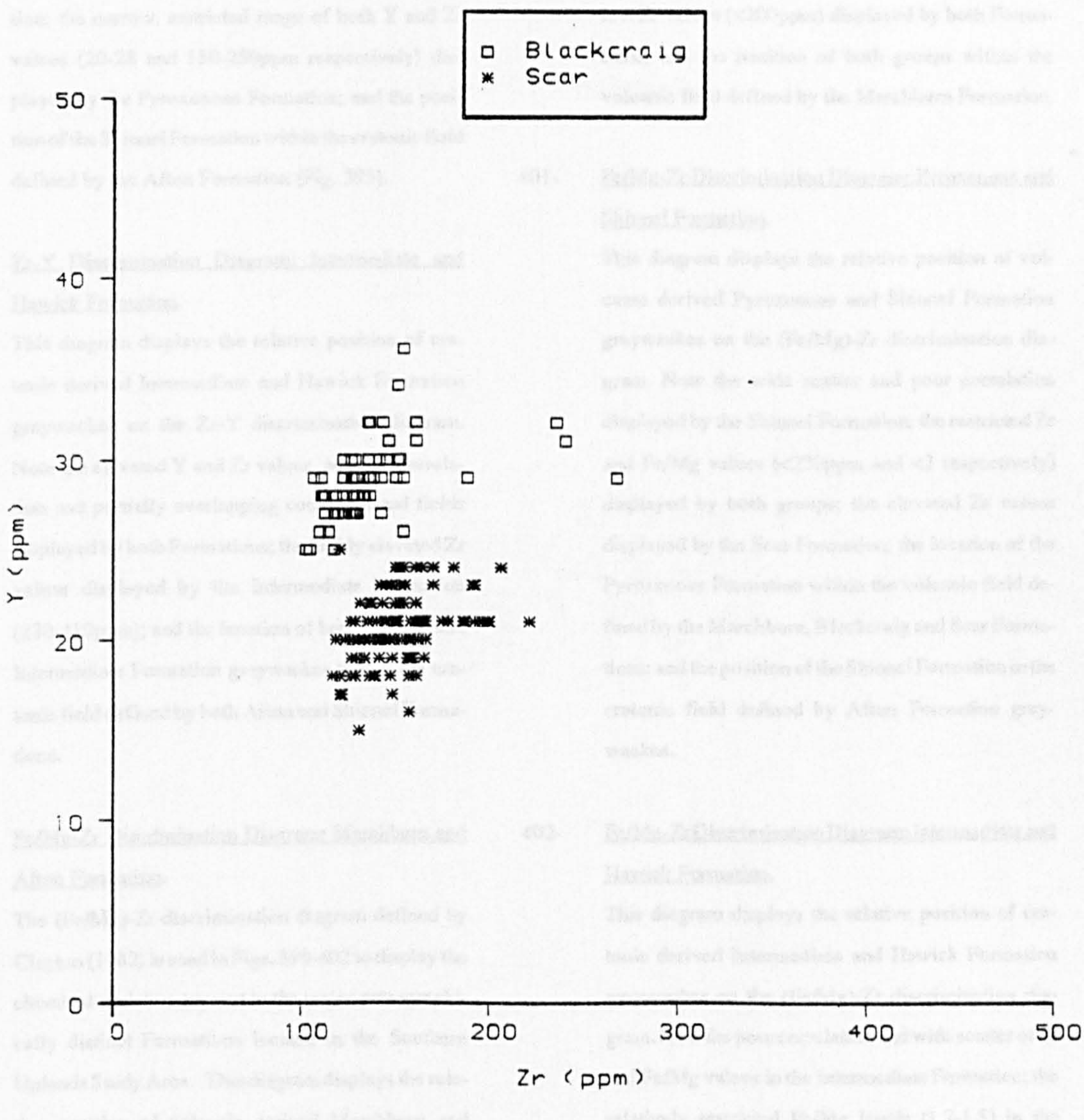

Discrimination Diagram (Clayton)

397- Zr-Y Discrimination Diagram: Pyroxenous and Shinnel Formation

This diagram displays the relative position of volcanic derived Pyroxenous and cratonic derived Shinnel Formation greywackes on the Zr-Y discrimination diagram. Note the slightly overlapping compositional fields; the positive correlation and elevated Zr values (>200ppm) displayed by the Shinnel Formation; the narrow, restricted range of both Y and Zr values (20-28 and 150-250ppm respectively) displayed by the Pyroxenous Formation; and the position of the Shinnel Formation within the cratonic field defined by the Afton Formation (Fig. 395).

398- Zr-Y Discrimination Diagram: Intermediate and Hawick Formation.

This diagram displays the relative position of cratonic derived Intermediate and Hawick Formation greywackes on the Zr-Y discrimination diagram. Note the elevated Y and Zr values, positive correlation and partially overlapping compositional fields displayed by both Formations; the highly elevated Zr values displayed by the Intermediate Formation (230-410ppm); and the location of both Hawick and Intermediate Formation greywackes within the cratonic field defined by both Afton and Shinnel Formations.

399- Fe/Mg-Zr Discrimination Diagram: Marchburn and Afton Formation.

The (Fe/Mg)-Zr discrimination diagram defined by Clayton (1982) is used in Figs. 399-402 to display the chemical variation present in the major petrographically distinct Formations located in the Southern Uplands Study Area. This diagram displays the relative position of volcanic derived Marchburn and cratonic derived Afton Formation greywackes on the (Fe/Mg)-Zr discrimination diagram. Note the strong positive correlation displayed by Marchburn Formation samples; the wide scatter and elevated Zr values (>230ppm) displayed by the Afton Formation; the generally lower Zr (<230ppm) values displayed by the Marchburn Formation; and the position of a boundary between cratonic and volcanic derived formations based upon the Zr=230ppm threshold.

400- Fe/Mg-Zr Discrimination Diagram: Blackcraig and Scar Formation.

This diagram displays the relative position of volcanic derived Blackcraig and Scar Formation greywackes on the (Fe/Mg)-Zr discrimination diagram. Note the weak inverse correlation and single trend displayed by both Formations; the restricted (Fe/Mg) values (<1.7) displayed by the Scar Formation; the low Zr values (<200ppm) displayed by both Formations; and the position of both groups within the volcanic field defined by the Marchburn Formation.

401- Fe/Mg-Zr Discrimination Diagram: Pyroxenous and Shinnel Formation.

This diagram displays the relative position of volcanic derived Pyroxenous and Shinnel Formation greywackes on the (Fe/Mg)-Zr discrimination diagram. Note the wide scatter and poor correlation displayed by the Shinnel Formation; the restricted Zr and Fe/Mg values (<230ppm and <2 respectively) displayed by both groups; the elevated Zr values displayed by the Scar Formation; the location of the Pyroxenous Formation within the volcanic field defined by the Marchburn, Blackcraig and Scar Formations; and the position of the Shinnel Formation in the cratonic field defined by Afton Formation greywackes.

402- Fe/Mg-Zr Discrimination Diagram: Intermediate and Hawick Formation.

This diagram displays the relative position of cratonic derived Intermediate and Hawick Formation greywackes on the (Fe/Mg)-Zr discrimination diagram. Note the poor correlation and wide scatter of Zr and Fe/Mg values in the Intermediate Formation; the relatively restricted Fe/Mg levels (1.2-1.5) in the Hawick Formation (with the exception of hydrothermally altered Fe-rich samples); the position of Hawick Formation samples within the volcanic field defined by the Scar and Pyroxenous Formations; and the location of Intermediate Formation samples within the cratonic field defined by the Afton and Shinnel Formations.

403- Zr-TiO_2 Discrimination Diagram: Marchburn and Afton Formation. The Zr-TiO_2 discrimination dia-

FIGURE 397

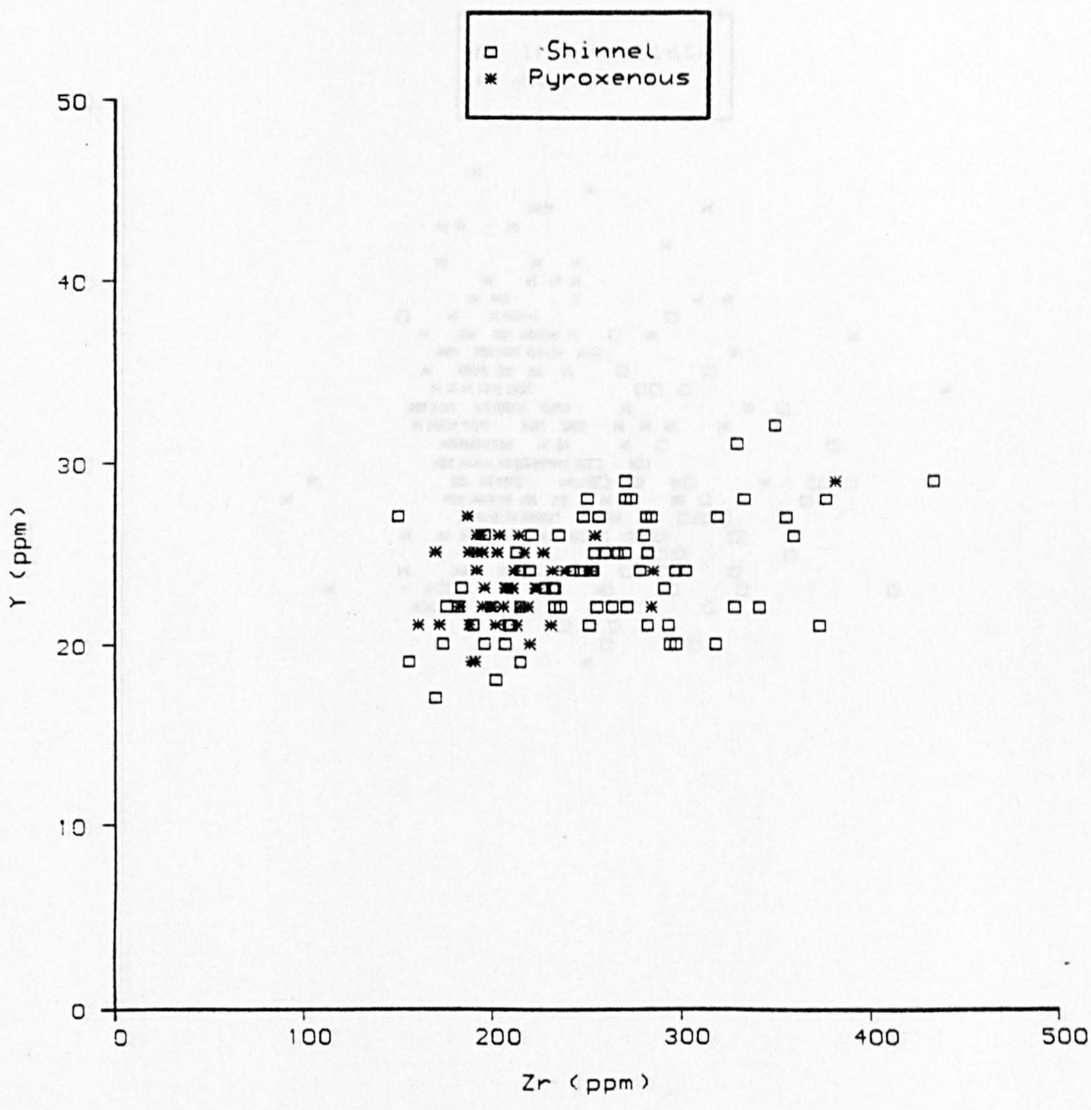

Discrimination Diagram (Clayton)

FIGURE 398

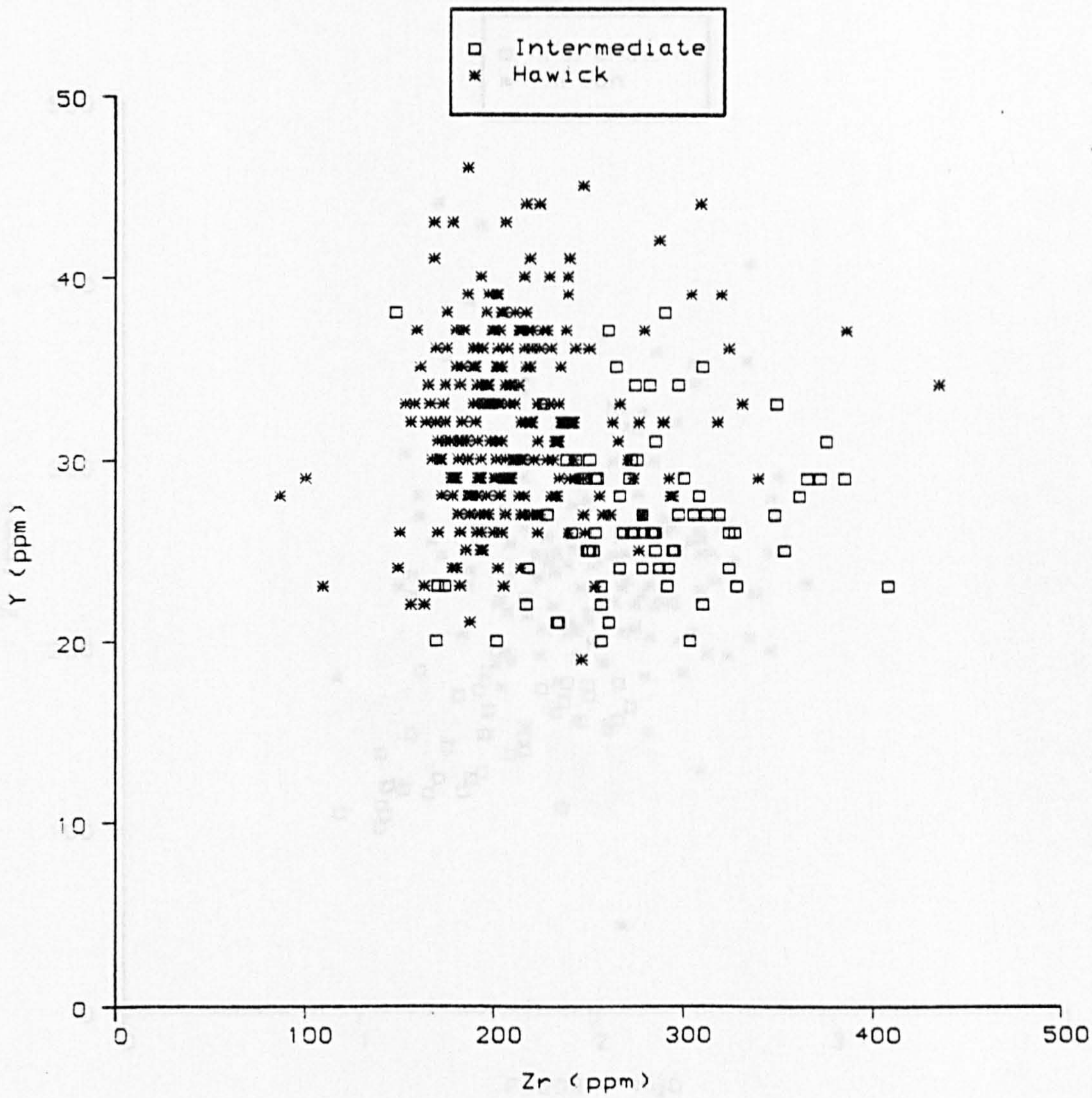

Discrimination Diagram (Clayton)

FIGURE 399

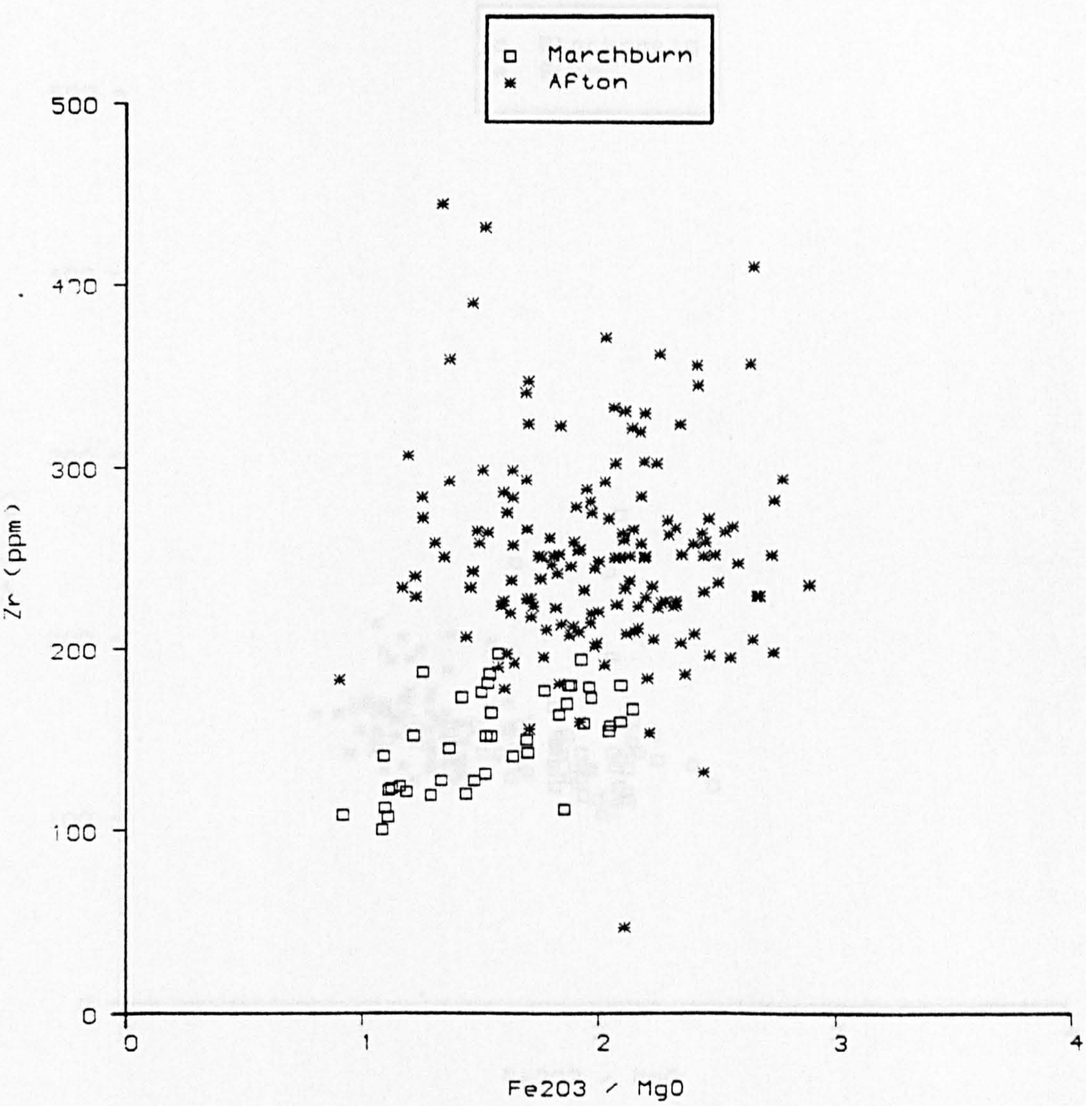

Discrimination Diagram (Clayton)

FIGURE 400

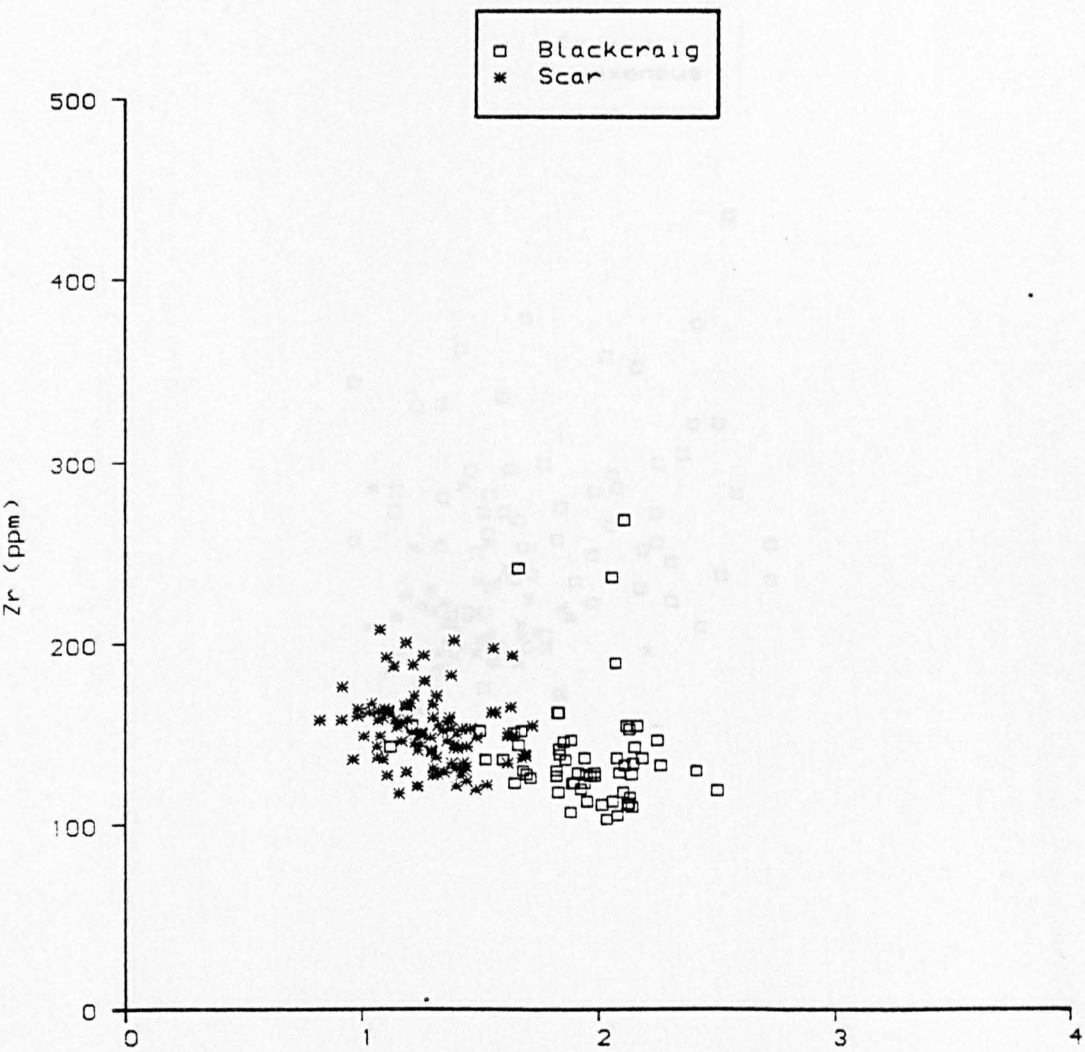

Discrimination Diagram (Clayton)

FIGURE 401

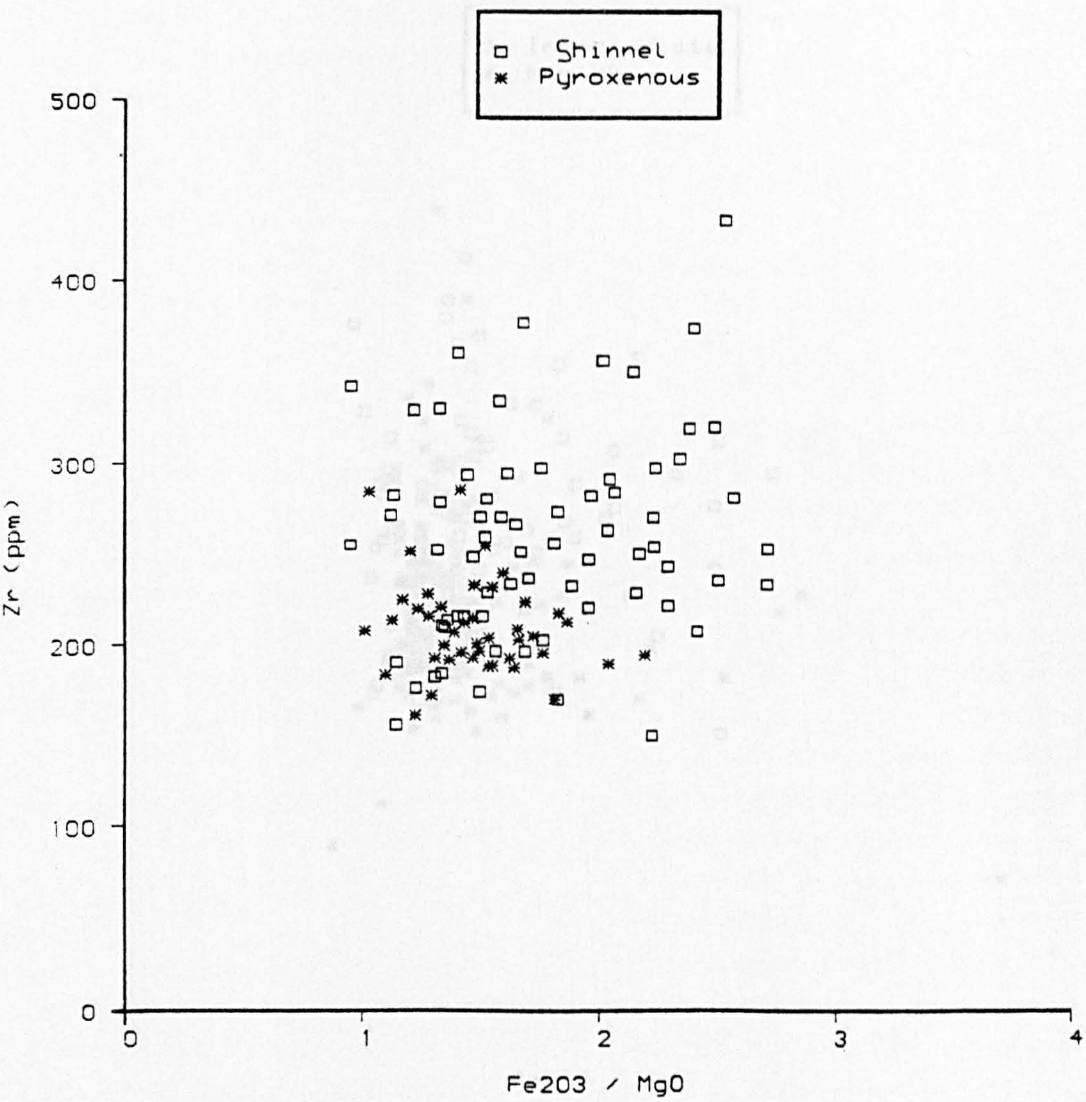

Discrimination Diagram (Clayton)

FIGURE 402

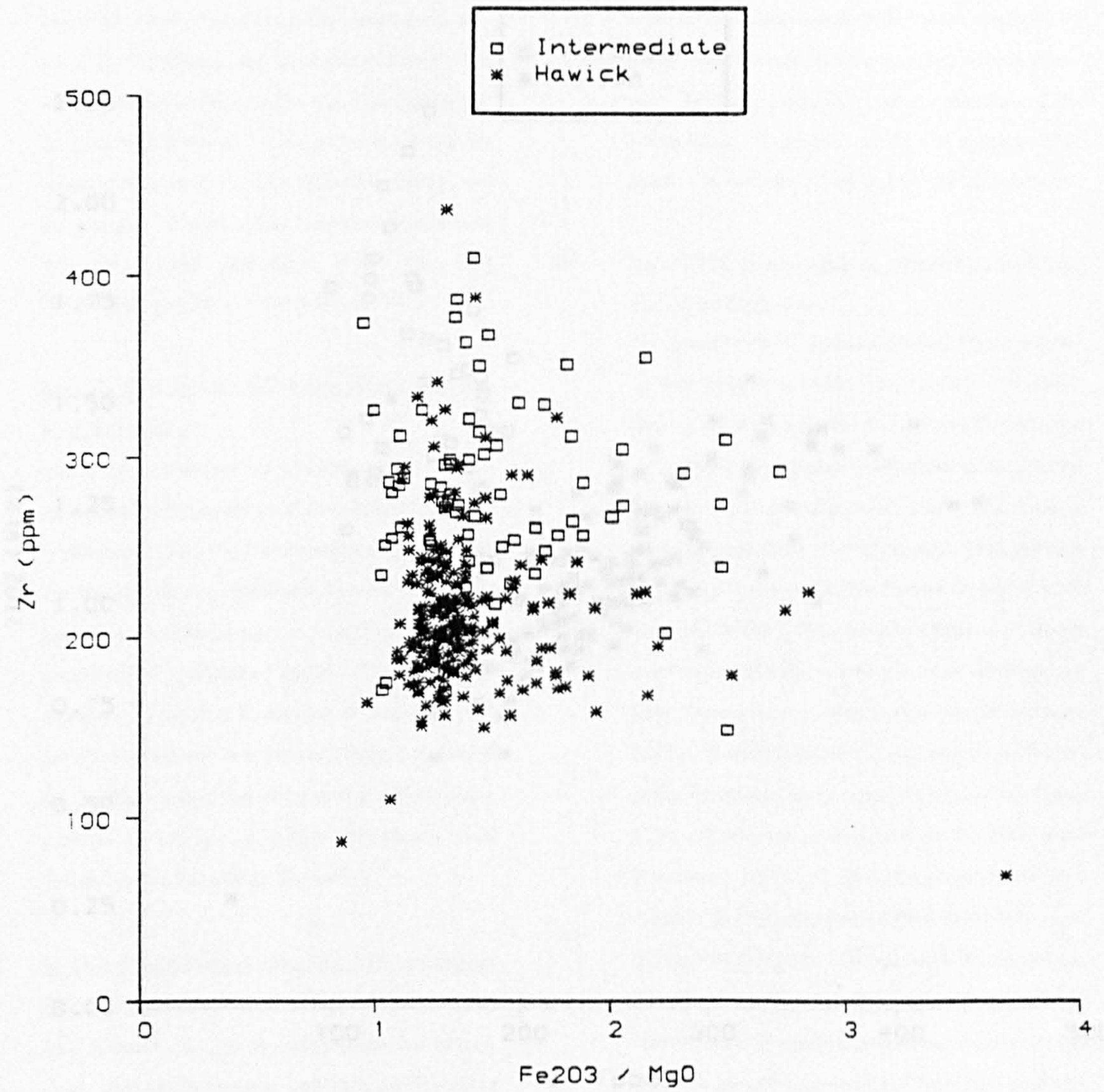

Discrimination Diagram (Clayton)

FIGURE 403

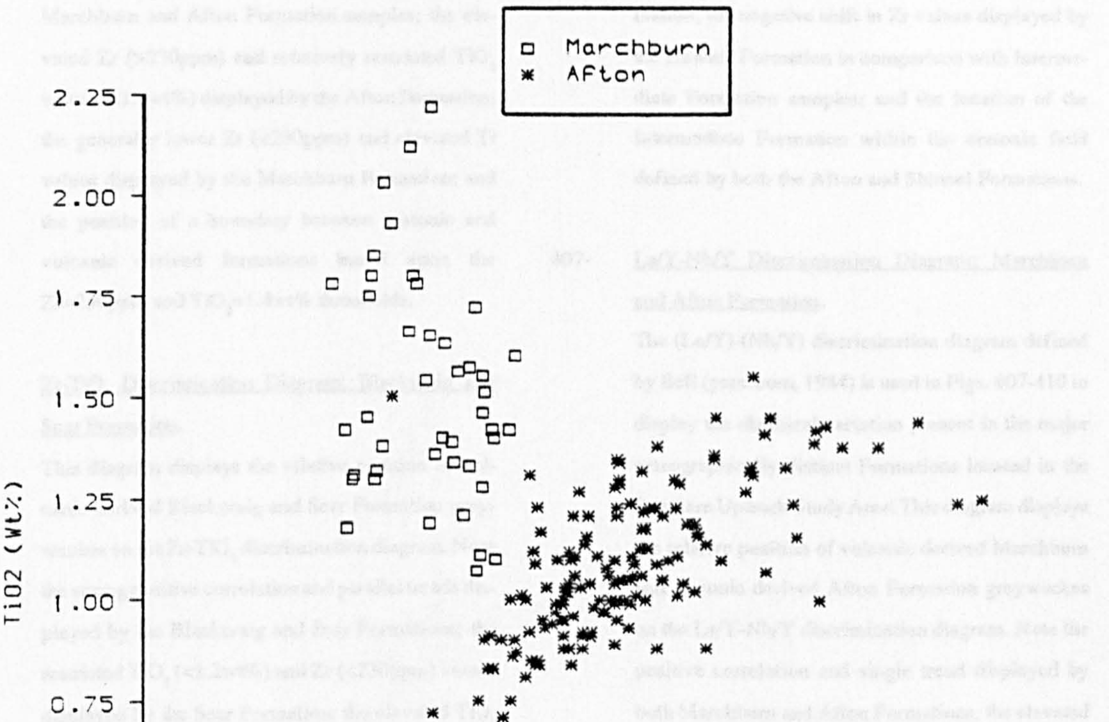

Discrimination Diagram (Pierce and Cann)

gram defined by Pierce (1982) is used in Figs. 403-406 to display the chemical variation present in the major petrographically distinct Formations located in the Southern Uplands Study Area. This diagram displays the relative position of volcanic derived Marchburn and cratonic derived Afton Formation greywackes on the Zr-TiO_2 discrimination diagram. Note the strong positive correlation displayed both Marchburn and Afton Formation samples; the elevated Zr (>230ppm) and relatively restricted TiO_2 values (<1.4wt%) displayed by the Afton Formation; the generally lower Zr (<230ppm) and elevated Ti values displayed by the Marchburn Formation; and the position of a boundary between cratonic and volcanic derived formations based upon the Zr=230ppm and TiO_2=1.4wt% thresholds.

404- <u>Zr-TiO_2 Discrimination Diagram: Blackcraig and Scar Formation</u>.

This diagram displays the relative position of volcanic derived Blackcraig and Scar Formation greywackes on the Zr-TiO_2 discrimination diagram. Note the strong positive correlation and parallel trends displayed by the Blackcraig and Scar Formations; the restricted TiO_2 (<1.2wt%) and Zr (<230ppm) values displayed by the Scar Formation; the elevated TiO_2 (>1.2wt%) and low Zr values (<200ppm) displayed by the Blackcraig Formation; and the overlapping position of both groups within the volcanic field defined by the Marchburn Formation.

405- <u>Zr-TiO_2 Discrimination Diagram: Pyroxenous and Shinnel Formation</u>

This diagram displays the relative position of volcanic derived Pyroxenous and Shinnel Formation greywackes on the Zr-TiO_2 discrimination diagram. Note the wide scatter, elevated Zr levels (>200ppm) and weak positive correlation displayed by Shinnel Formation samples; the restricted Zr and TiO_2 values (<230ppm and 0.75-1.1wt% respectively) displayed by the Pyroxenous Formation; the location of the Pyroxenous Formation within the volcanic field defined by the Marchburn, Blackcraig and Scar Formations; and the location of both Formations within the cratonic field defined by Afton Formation greywackes.

406- <u>Zr-TiO_2 Discrimination Diagram: Intermediate and Hawick Formation</u>.

This diagram displays the relative position of cratonic derived Intermediate and Hawick Formation greywackes on the Zr-TiO_2 discrimination diagram. Note the poor correlation and wide scatter of Zr and TiO_2 values in both Formations; the relatively elevated Zr levels (>230 ppm) in the Intermediate Formation; the negative shift in Zr values displayed by the Hawick Formation in comparison with Intermediate Formation samples; and the location of the Intermediate Formation within the cratonic field defined by both the Afton and Shinnel Formations.

407- <u>La/Y-Nb/Y Discrimination Diagram: Marchburn and Afton Formation</u>.

The (La/Y)-(Nb/Y) discrimination diagram defined by Bell (pers. com, 1984) is used in Figs. 407-410 to display the chemical variation present in the major petrographically distinct Formations located in the Southern Uplands Study Area. This diagram displays the relative position of volcanic derived Marchburn and cratonic derived Afton Formation greywackes on the La/Y-Nb/Y discrimination diagram. Note the positive correlation and single trend displayed by both Marchburn and Afton Formations; the elevated La/Y (>1) and Nb/Y (>0.55) values displayed by the Afton Formation; the generally lower La/Y (<1) and Nb/Y (<0.55) values displayed by the Marchburn Formation; and the position of a boundary between cratonic and volcanic derived formations defined on the basis of the La/Y=1.00 threshold. The higher La/Y values displayed by relatively acid, cratonically derived Afton Formation greywackes may be used to infer the relative enrichment of light rare earth elements.

408- <u>La/Y-Nb/Y Discrimination Diagram: Blackcraig and Scar Formation</u>.

This diagram displays the relative position of volcanic derived Blackcraig and Scar Formation greywackes on the La/Y-Nb/Y discrimination diagram. Note the correlation and single trend displayed by both Formations; the elevated La/Y (>1) values displayed by the Scar Formation; the relatively low La/Y and Nb/Y values identifying the Blackcraig For-

FIGURE 404

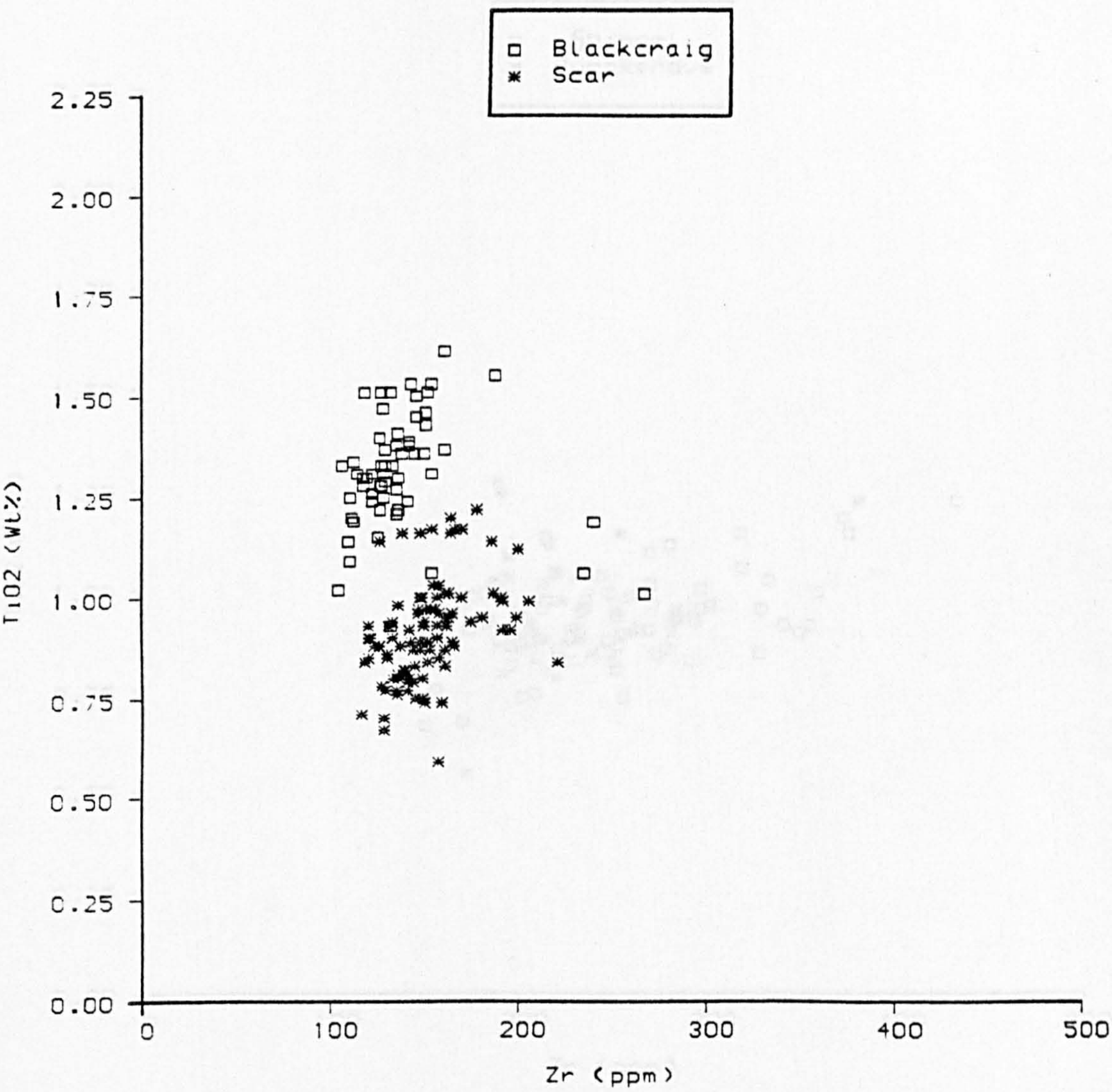

Discrimination Diagram (Pierce and Cann)

FIGURE 405

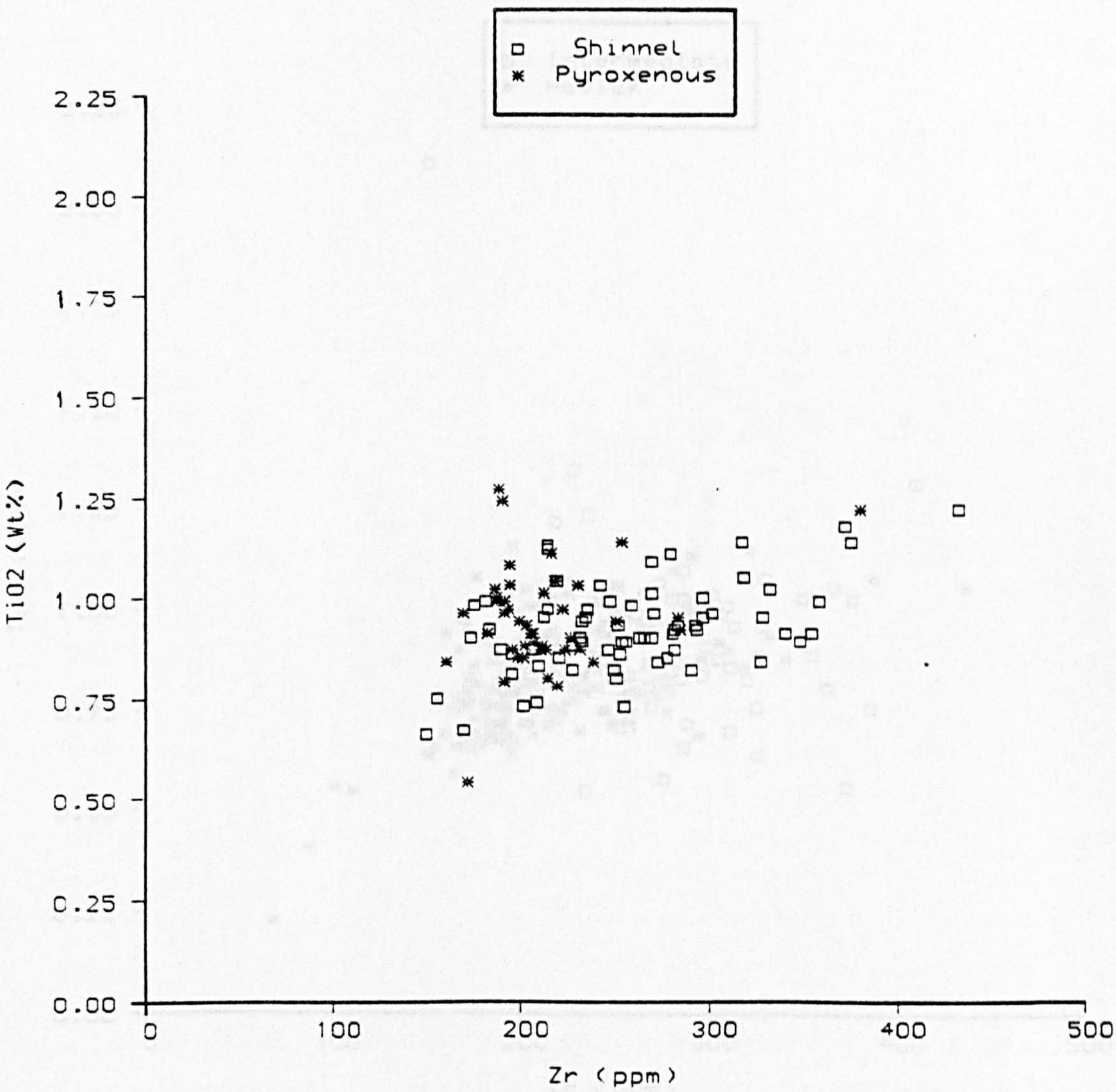

Discrimination Diagram (Pierce and Cann)

FIGURE 406

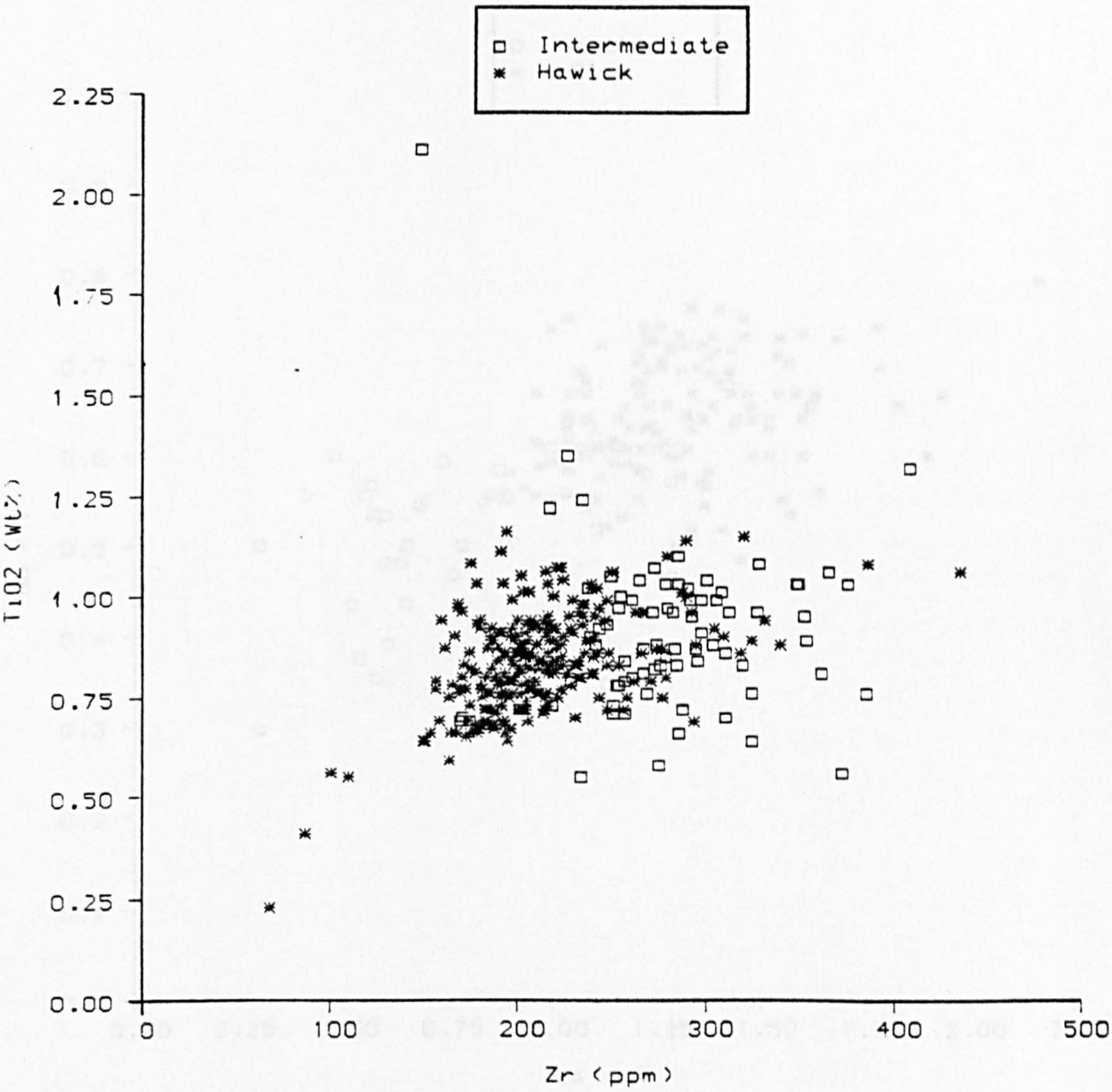

Discrimination Diagram (Pierce and Cann)

FIGURE 407

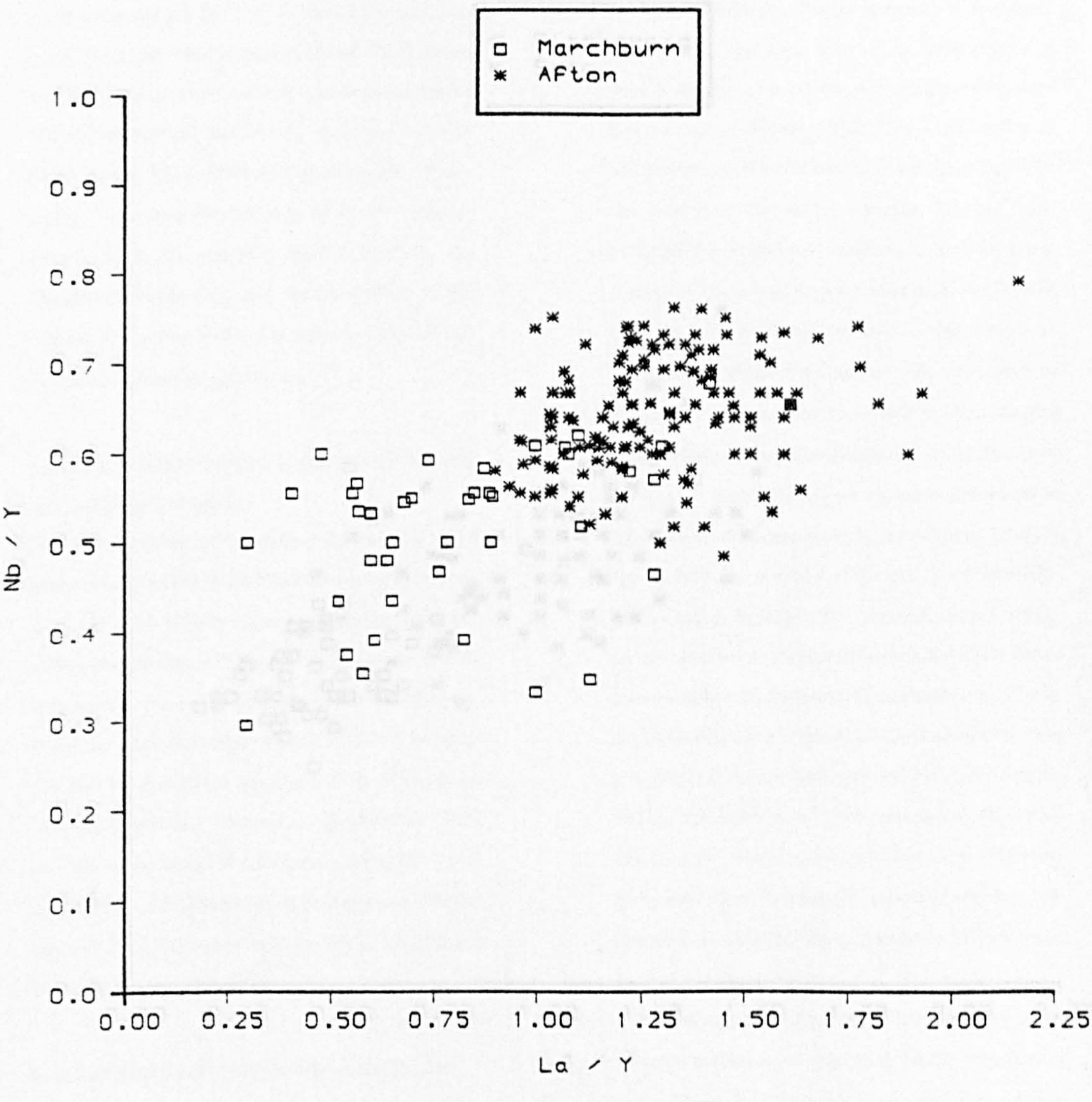

Discrimination Diagram.

FIGURE 408

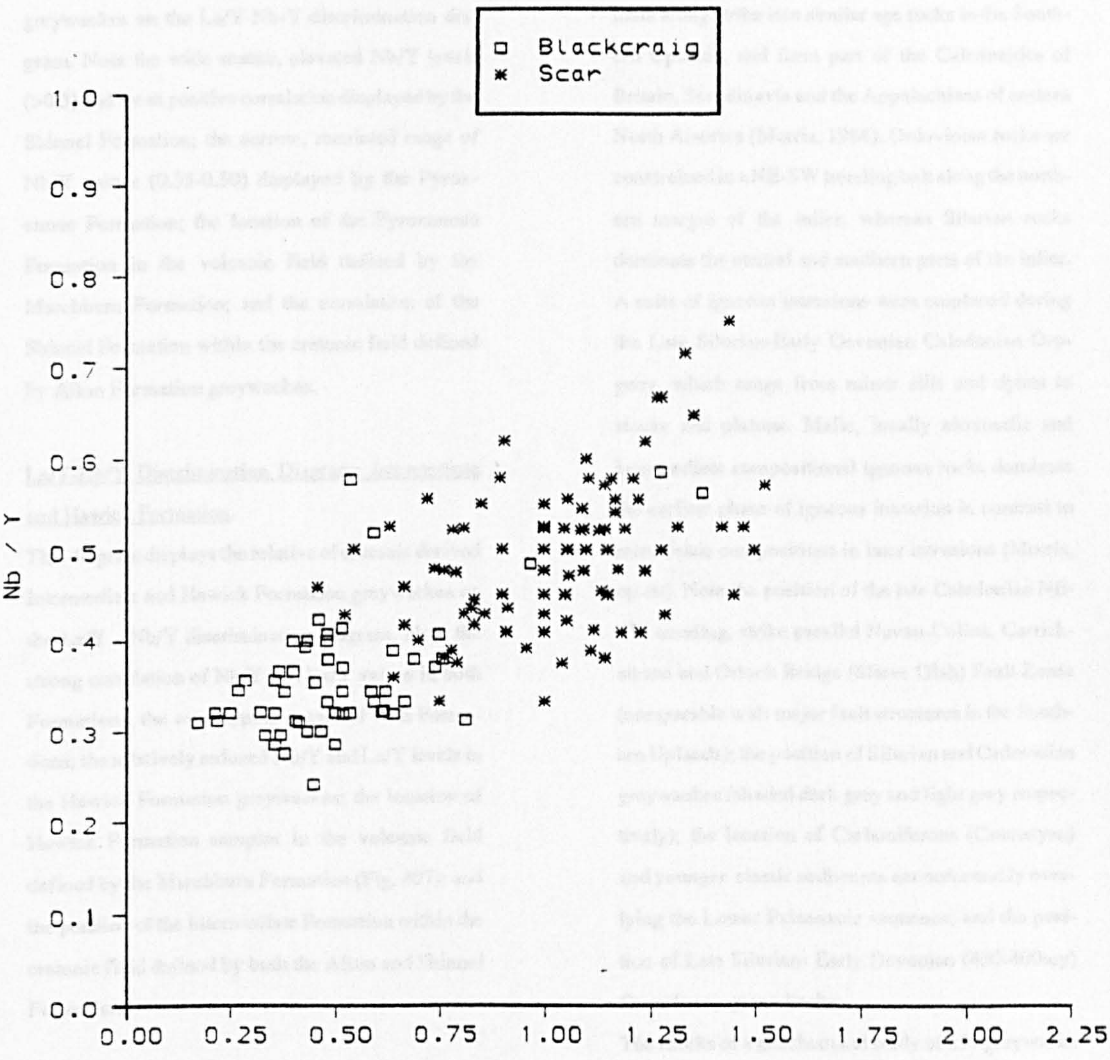

Discrimination Diagram.

mation; and the overlapping position of both groups within the volcanic field defined by the Marchburn Formation.

409- La/Y-Nb/Y Discrimination Diagram: Pyroxenous and Shinnel Formation.

This diagram displays the relative position of volcanic derived Pyroxenous and Shinnel Formation greywackes on the La/Y-Nb-Y discrimination diagram. Note the wide scatter, elevated Nb/Y levels (>0.5) and weak positive correlation displayed by the Shinnel Formation; the narrow, restricted range of Nb/Y values (0.35-0.50) displayed by the Pyroxenous Formation; the location of the Pyroxenous Formation in the volcanic field defined by the Marchburn Formation; and the correlation of the Shinnel Formation within the cratonic field defined by Afton Formation greywackes.

410- La/Y-Nb/Y Discrimination Diagram: Intermediate and Hawick Formation.

This diagram displays the relative of cratonic derived Intermediate and Hawick Formation greywackes on the La/Y - Nb/Y discrimination diagram. Note the strong correlation of Nb/Y and La/Y values in both Formations; the overlapping nature of both Formations; the relatively reduced Nb/Y and La/Y levels in the Hawick Formation greywackes; the location of Hawick Formation samples in the volcanic field defined by the Marchburn Formation (Fig. 407); and the position of the Intermediate Formation within the cratonic field defined by both the Afton and Shinnel Formations.

411- Longford Down Lithogeochemical Survey Area: Geological Map

This diagram displays a summary geological map of the Longford Down Study Area in the Republic of Ireland (after Morris, 1978, 1979 and 1985). This area includes counties Louth and Monaghan, a substantial part of County Cavan and parts of Counties Leitrim, Longford, Meath and Roscommon. This area of undulating lowland was geologically mapped by the Geological Survey of Ireland during the 19th century and resulted in the publication of summary 1 inch:1 mile scale geological maps and memoirs. Subsequent to this study various parts of the inlier have been remapped by both the Geological Survey and individual researchers. The metallic mineral deposits which occur in the inlier have in general been subjected to little investigation, however Morris (1984) presented a summary of all metallic mineral deposits of the Longford-Down. The Longford-Down Inlier is composed of Ordovician and Silurian rocks which continue along strike into similar age rocks in the Southern Uplands, and form part of the Caledonides of Britain, Scandinavia and the Appalachians of eastern North America (Morris, 1984). Ordovician rocks are constrained in a NE-SW trending belt along the northern margin of the inlier, whereas Silurian rocks dominate the central and southern parts of the inlier. A suite of igneous intrusions were emplaced during the Late Silurian-Early Devonian Caledonian Orogeny, which range from minor sills and dykes to stocks and plutons. Mafic, locally ultramafic and intermediate compositional igneous rocks dominate the earliest phase of igneous intrusion in contrast to more felsic compositions in later intrusions (Morris, op.cit). Note the position of the late Caledonian NE-SW trending, strike parallel Navan-Collon, Carrickateane and Orloch Bridge (Slieve Glah) Fault Zones (comparable with major fault structures in the Southern Uplands); the position of Silurian and Ordovician greywackes (shaded dark grey and light grey respectively); the location of Carboniferous (Courceyan) and younger clastic sediments unconformably overlying the Lower Palaeozoic sequence; and the position of Late Silurian- Early Devonian (430-400my) Crossdoney granodiorite.

The results of a geochemical study of 297 greywacke samples collected for this study by Dr John Morris (Irish Geological Survey) on a 'dog leg' traverse across the Longford Down Study Area are presented in a series of 1:400,000 scale maps which form a multi-element lithogeochemical atlas of this region (Figs 411-441). The sampling pattern selected in this study was chosen to maximise coverage, include areas with strong stratigraphic and petrographic controls and avoid the Clontibret region and other mineralised areas. Individual sample sites are represented by circles, the size of which is proportional to concentration, and controlled by specific percentile ranges

FIGURE 409

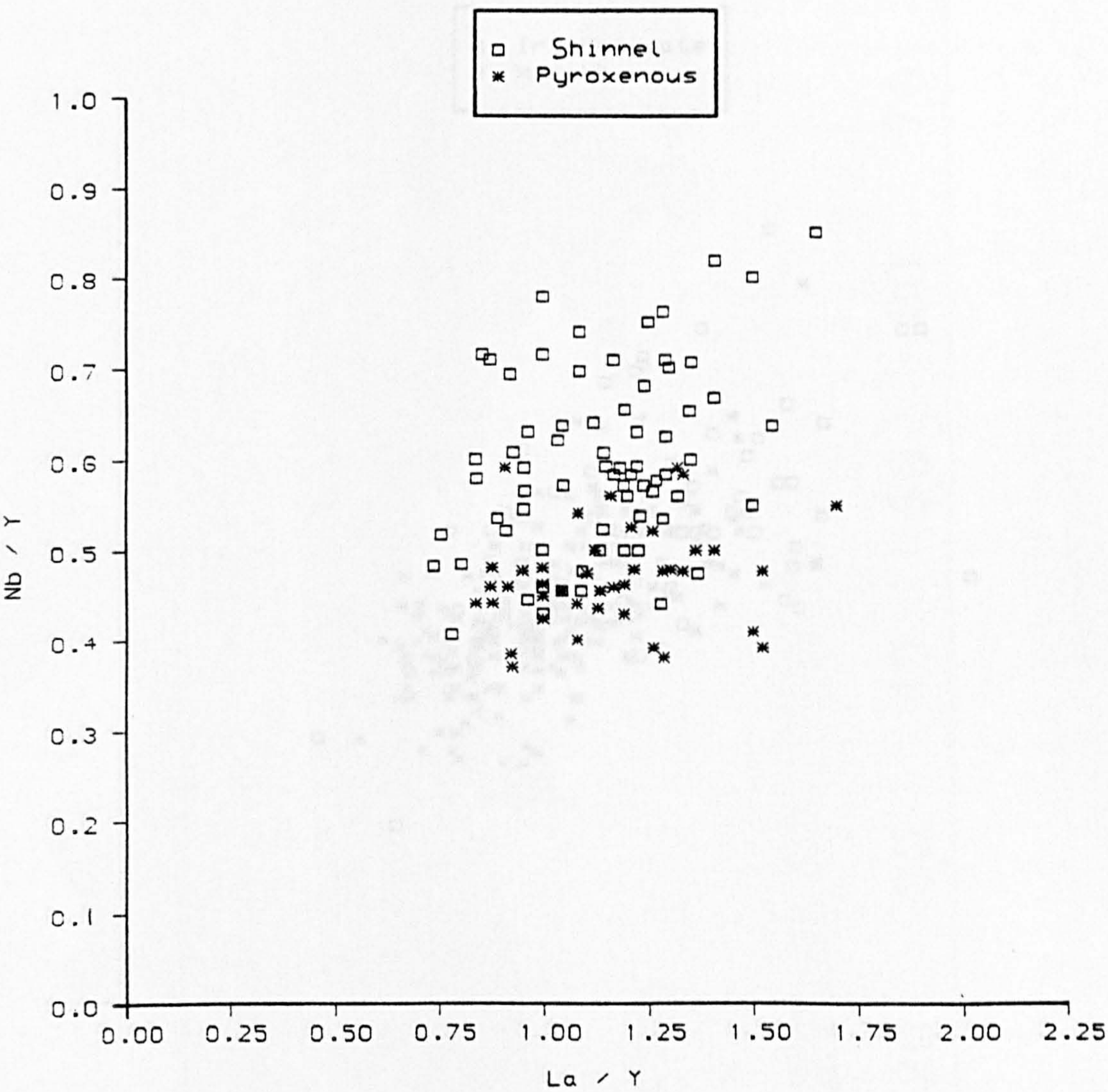

Discrimination Diagram.

FIGURE 410

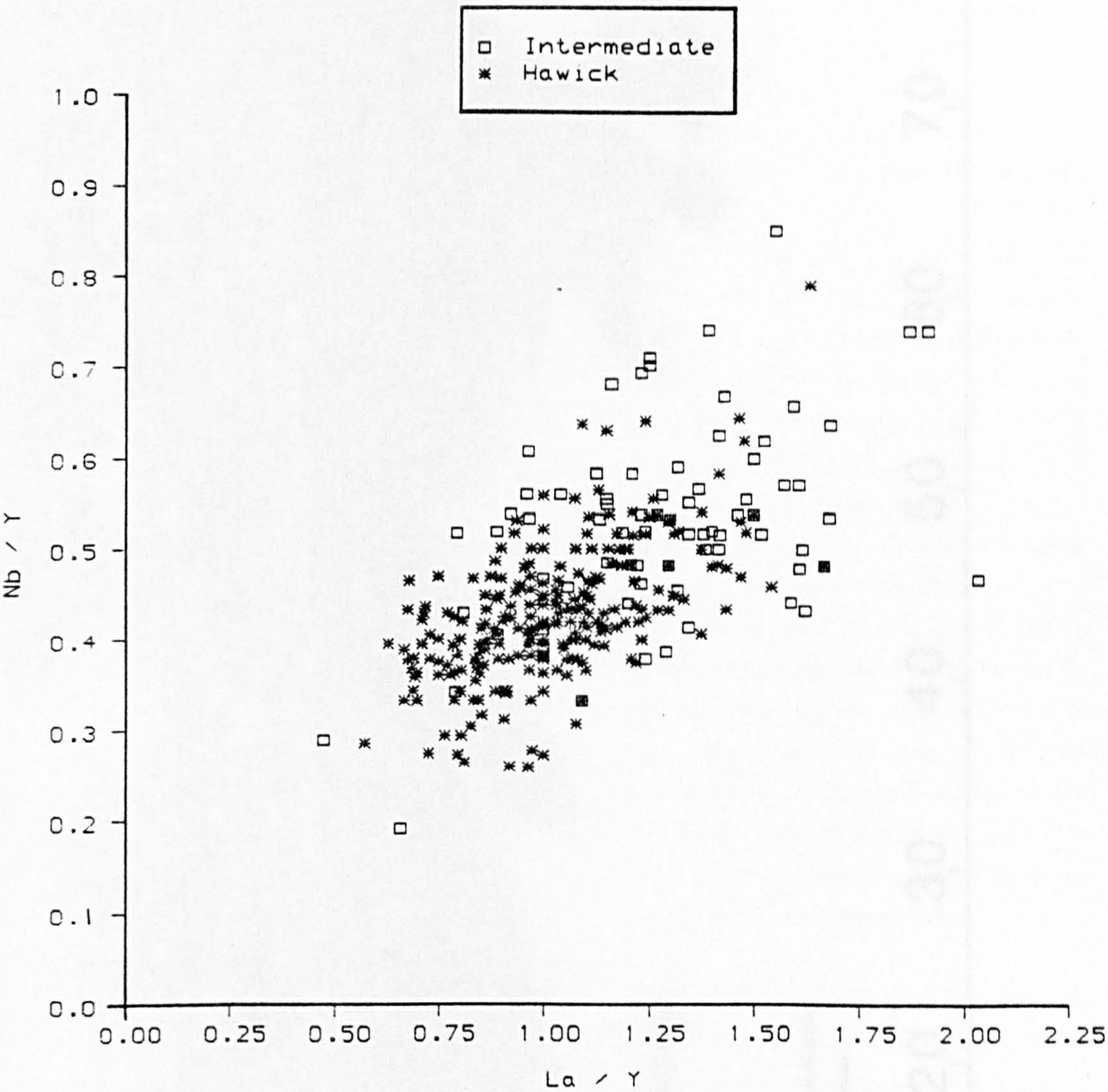

Discrimination Diagram.

FIGURE 411

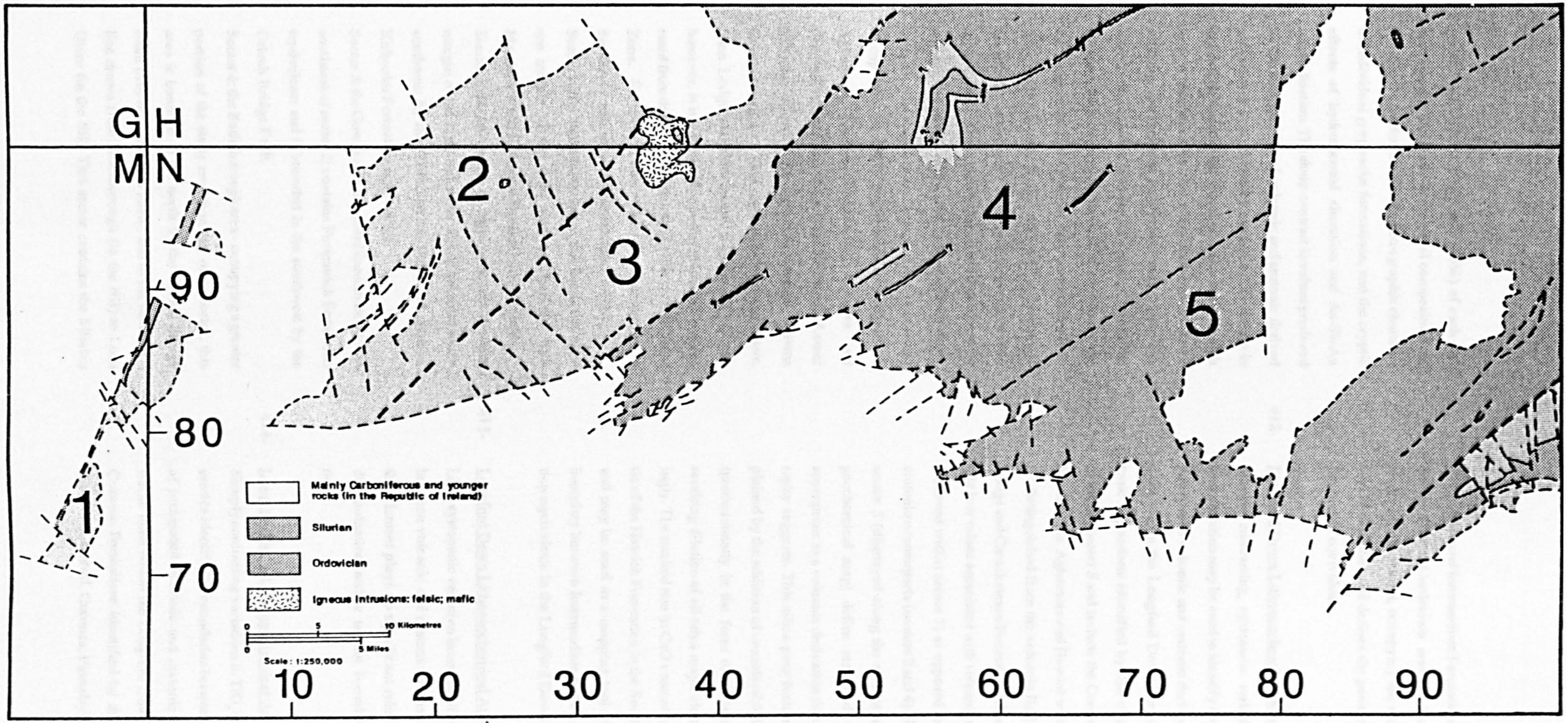

G
H
M
N
1
2
3
4
5
90
80
70
10
20
30
40
50
60
70
80
90
Mainly Carboniferous and younger rocks (in the Republic of Ireland)
Silurian
Ordovician
Igneous intrusions: felsic; mafic
0
5
10 Kilometres
0
5 Miles
Scale: 1:250,000

(0-50, 50-75, 75-90, 90-95 and >95%) of each element. Major variations in chemical composition are attributed to differences in the petrographic character of individual greywacke formations, and the cryptic effects of hydrothermal alteration and As-Sb-Au mineralisation. The sharp contrast in values produced by the juxtaposition of volcanic and cratonic derived greywackes is displayed by systematic variations in symbol size across the traverse. The scale of each map is displayed by the 10km tick marks on the southern and western axes which may be used to identify the relative position of samples within the 100km Irish Survey grid cells G, H, M and N covering the study area. The chemical data contained within these maps is located in table 4.81-4.92 and presented graphically as a number of composite profiles within foldout no. 4. Three regional scale stratigraphic units are defined in this study area, namely the Strokestown, Gowna and Hawick Groups. The Strokestown Group (Morris, 1987) comprises five Formations: Aghamore, Lackan, Finnalayhta, Coronea and Cornhill, which range in age from Llanvirn to Lower Silurian; whereas the Llandeilo-Caradoc Gowna Group consists of three formations: Carackateane, Glen Lodge and Red Island. The Hawick Group however, is not subdivided in this study, but is separated from the Gowna Group by the Slieve Glah Shear Zone. For the purposes of the following discussion the survey area may be divided into 5 sectors:

Sector 1: the Strokestown Inlier, this forms the western margin of the field area and contains both Marchburn and Kirkcolm Formation equivalents.

Sector 2: the Arva area - occupying the northwestern margin of the main inlier this area is bounded to the southwest by the Carrickateane Fault and contains Kirkcolm Formation equivalents.

Sector 3: the Gowna area is located immediately to the southeast of sector 2; contains Portpatrick Formation equivalents and is bounded in the southwest by the Orloch Bridge Fault.

Sector 4: the Bailieborough area - occupying a greater portion of the study area than any other sector, this area is bounded to the north by the Orloch Bridge Fault (Slieve Glah Shear Zone) and to the south by a line drawn from Jonesborough (in the NE) to Loch Glore (in the SE). This sector contains the Silurian Pyroxenous and Intermediate Formation equivalents.

Sector 5: the Castletown area, is located to the southeast of sector 4, occupying the remaining portion of the Inlier and defines the position of Hawick Formation equivalents.

412- <u>Longford Down Lithogeochemical Atlas : SiO_2 (%)</u>

Sharply contrasting, systematic variations in SiO_2 concentration may be used to identify the positions of juxtaposed volcanic and cratonic derived greywacke units within the Longford Down survey area. Cratonic Formations identified by this element are detailed in chapter 5 and include the Cornhill, Coronea, Finnalayhta, Aghamore and Hawick units which may be distinguished from the volcanic Red Island, Glen Lodge and Carackateane Formations. Note the generally low values associated with volcanic units (clearly observed within sector 3) as opposed to their higher cratonic counterparts (sectors 2 and 4). Samples from sector 5 (displayed along the eastern margin of the geochemical map) define restricted values more appropriate to a volcanic derivation that their petrography suggests. This silica-poor feature may be explained by the addition of considerable CaO addition (predominantly in the form of carbonate) and the resulting dilution of all other major elements accordingly. The marked rise in CaO content is characteristic of the Hawick Formation in the Southern Uplands and may be used as a mapping tool to identify the boundary between Intermediate and Hawick Formation equivalents in the Longford Down.

413- <u>Longford Down Lithogeochemical Atlas : Al_2O_3 (%)</u>

Little systematic variation in composition is observed between volcanic and cratonic formations. As such this element plays no significant role in greywacke discrimination and/or terrain boundary identification.

414- <u>Longford Down Lithogeochemical Atlas : TiO_2 (%)</u>

Sharply contrasting variations in TiO_2 content may be used to identify the boundaries between the positions of juxtaposed volcanic and cratonic derived greywacke units within the Longford Down survey area. Cratonic Formations identified by this element include the Cornhill, Coronea, Finnalayhta, Aghamore

FIGURE 412

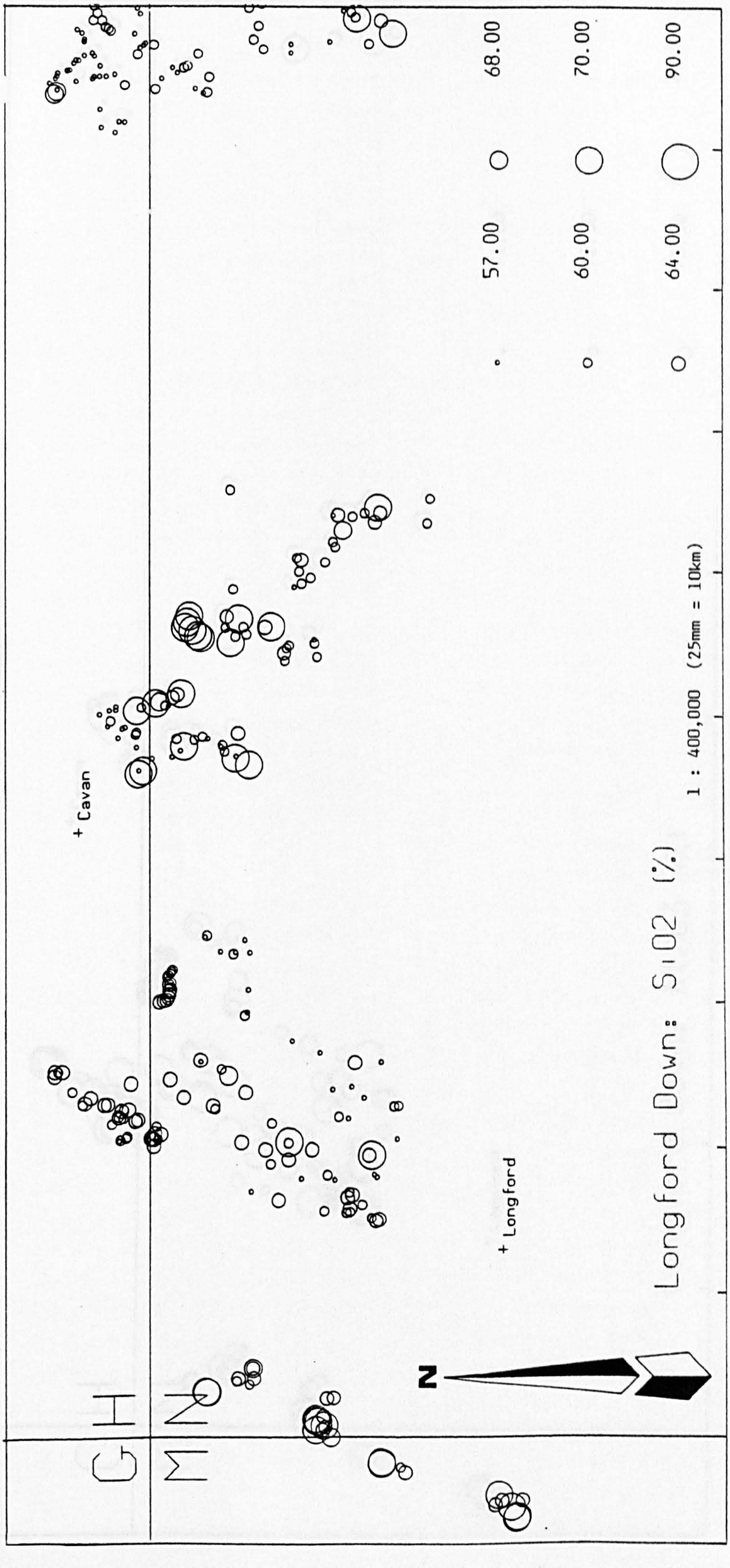
GHM
+ Cavan
+ Longford
N
57.00
68.00
60.00
70.00
64.00
90.00
Longford Down: SiO2 (%)
1 : 400,000 (25mm = 10km)

FIGURE 413

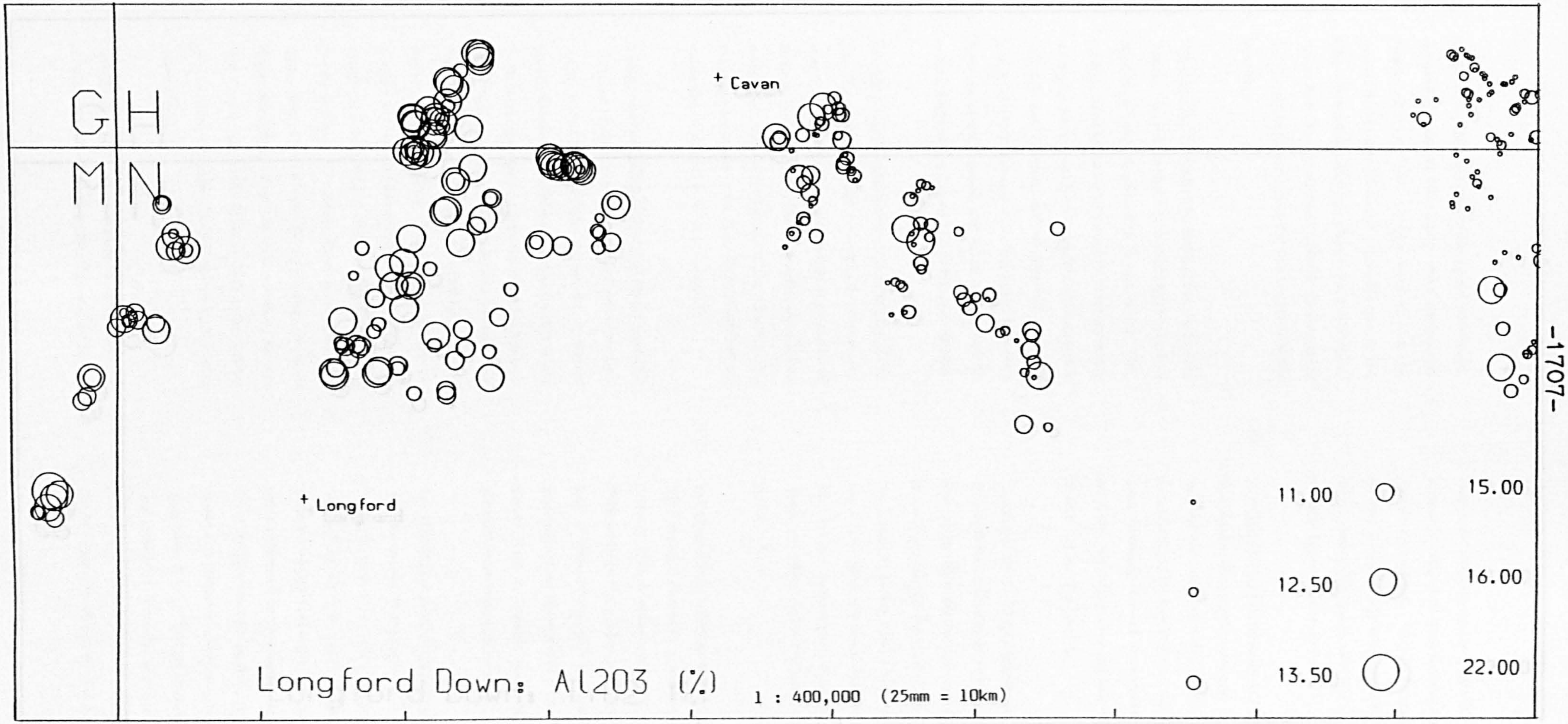

G H
M N
Cavan
Longford
Longford Down: Al203 (%)
1 : 400,000 (25mm = 10km)
11.00
12.50
13.50
15.00
16.00
22.00
-1707-

FIGURE 414

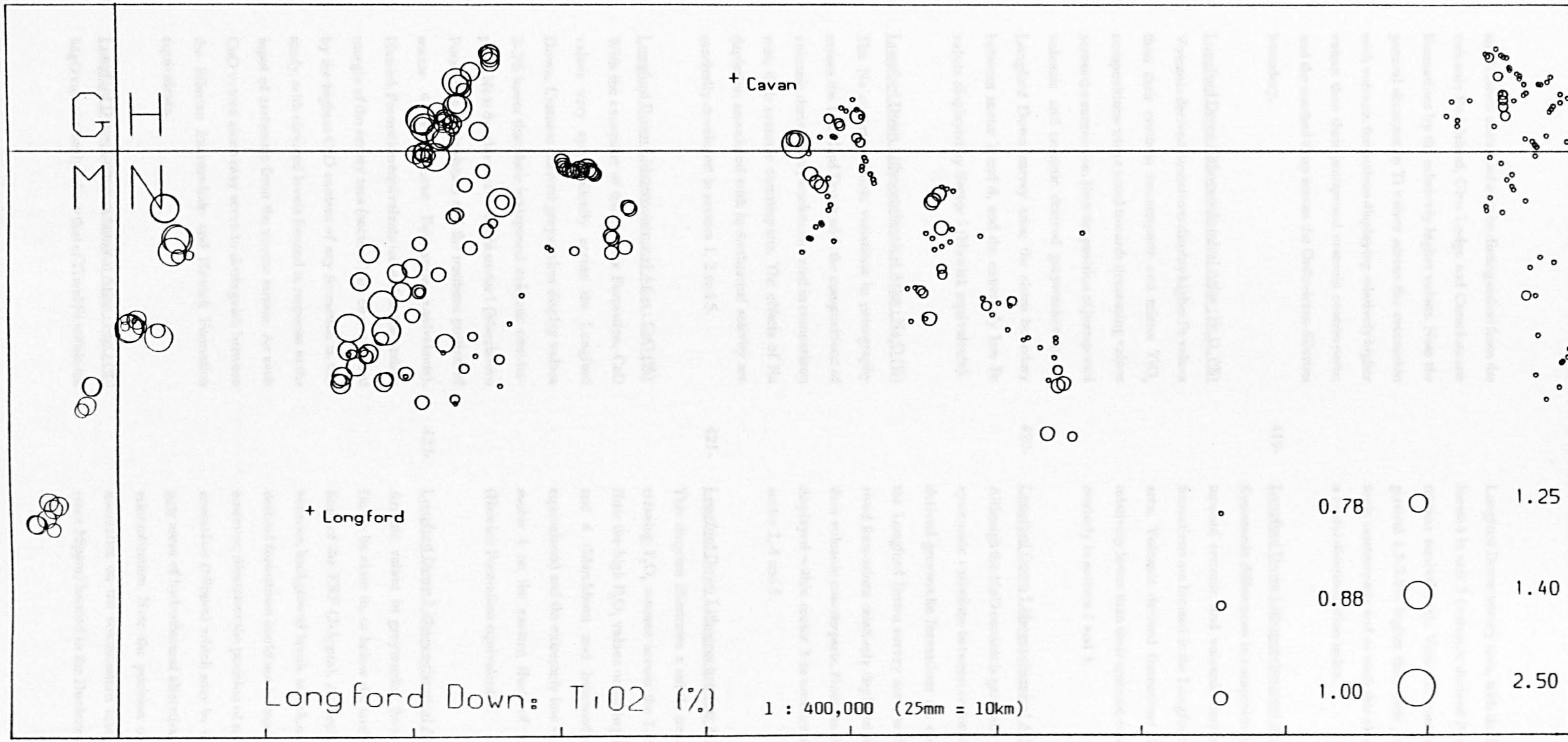
G
H
M
N
+ Cavan
+ Longford
0.78
0.88
1.00
1.25
1.40
2.50
Longford Down: TiO2 (%)
1 : 400,000 (25mm = 10km)

and Hawick units; and may be distinguished from the volcanic Red Island, Glen Lodge and Carackateane Formations by the relatively higher values. Note the general decrease in Ti values across the succession with volcanic formations displaying relatively higher values than their juxtaposed cratonic counterparts; and the marked drop across the Ordovician-Silurian boundary.

415- Longford Down Lithogeochemical Atlas : Fe_2O_3 (%)
Volcanic derived formations display higher Fe values than their cratonic counterparts and mirror TiO_2 compositions with a trend towards decreasing values across the succession. Note the position of juxtaposed volcanic and cratonic derived greywackes in the Longford Down survey area; the sharp boundary between sector 3 and 4, and the extremely low Fe values displayed by Sector 5 (Hawick equivalents).

416- Longford Down Lithogeochemical Atlas : Na_2O (%)
The Na content reflects variations in petrography across the Longford Down with the compositions of volcanic derived greywackes elevated in comparison with their cratonic counterparts. The effects of Na depletion associated with hydrothermal activity are markedly developed in sectors 1, 2 and 5.

417- Longford Down Lithogeochemical Atlas : CaO (%)
With the exception of the Hawick Formation, CaO values vary systematically across the Longford Down. Cratonic derived greywackes display values 2-3% lower than their juxtaposed volcanic counterparts. Note the elevated values in sector 1 (Marchburn Formation equivalents) and the northern portion of sector 4 (Pyroxenous Formation equivalents). Hawick Formation equivalents located on the eastern margin of the survey area (sector 5) are characterised by the highest CaO content of any formation in this study, with elevated levels formed in response to the input of carbonate from the source terrain. As such CaO values alone may serve to distinguish between the Silurian Intermediate and Hawick Formation equivalents.

418- Longford Down Lithogeochemical Atlas : MgO (%)
MgO values closely follow that of Ti and Fe within the Longford Down survey area, with the highest values located in unit 3 (volcanic derived Pyroxenous Formation equivalents). Volcanic composition are in general 1.5-3.0% higher than their juxtaposed cratonic counterparts and as such this element provides a useful discrimination index.

419- Longford Down Lithogeochemical Atlas : K_2O (%)
Systematic differences in composition between juxtaposed cratonic and volcanic derived greywacke formations are located in the Longford Down survey area. Volcanic derived formations display values relatively lower than their cratonic counterparts particularly in sectors 1 and 3.

420- Longford Down Lithogeochemical Atlas : MnO (%)
Although the MnO content is generally low (<0.25%) systematic variations between cratonic and volcanic derived greywacke formations are observed within the Longford Down survey area, with cratonic derived formations relatively depleted with respect to their volcanic counterparts. Note the elevated values displayed within sector 3 in contrast to the cratonic sector 2, 4 and 5.

421- Longford Down Lithogeochemical Atlas : P_2O_5 (%)
This diagram illustrates a subtle trend towards decreasing P_2O_5 content across the Longford Down. Note the high P_2O_5 values occurring in the sector 1 and 4 (Marchburn and Intermediate Formation equivalents) and the extremely low values located in sector 4 on the eastern flank of this study area (Hawick Formation equivalents).

422- Longford Down Lithogeochemical Atlas : As (ppm)
Arsenic values in greywackes from the Longford Down lie close to, or below the analytical detection limit of the XRF (2-3ppm). As such, a comparison between background levels in volcanic and cratonic derived formations could not be made. This diagram however, illustrates the position of numerous arsenic anomalies (>8ppm) which may be used to pinpoint new areas of hydrothermal alteration and As-Sb-Au mineralisation. Note the position of major arsenic anomalies on the southeastern margin of sector 5 (max 55ppm) located in the Dunleer township, adja-

FIGURE 415

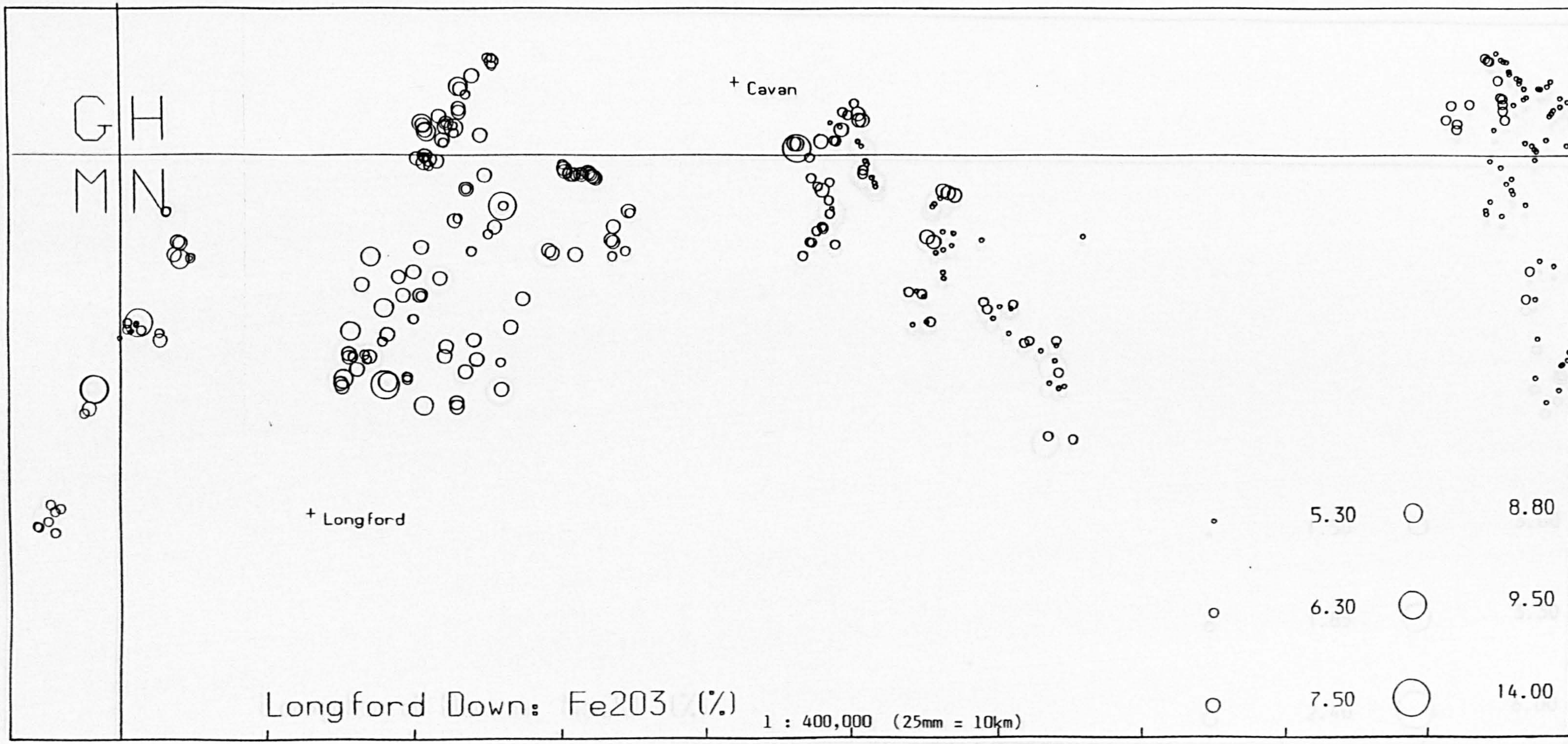
G H
M N
+ Cavan
+ Longford
5.30
8.80
6.30
9.50
7.50
14.00
Longford Down: Fe2O3 (%)
1 : 400,000 (25mm = 10km)

FIGURE 416

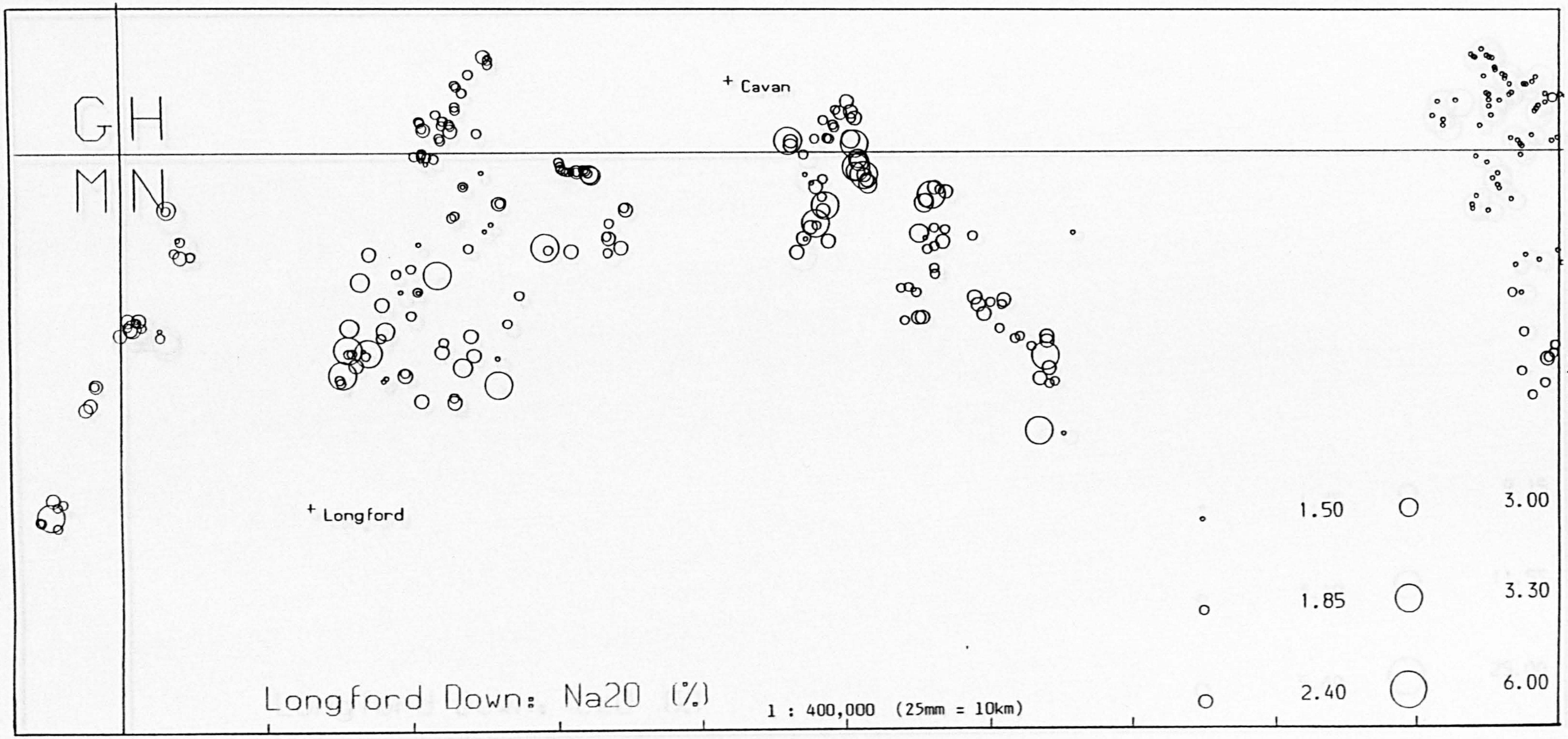
G H
M N
+ Cavan
+ Longford
1.50
1.85
2.40
3.00
3.30
6.00
Longford Down: Na2O (%)
1 : 400,000 (25mm = 10km)

FIGURE 417

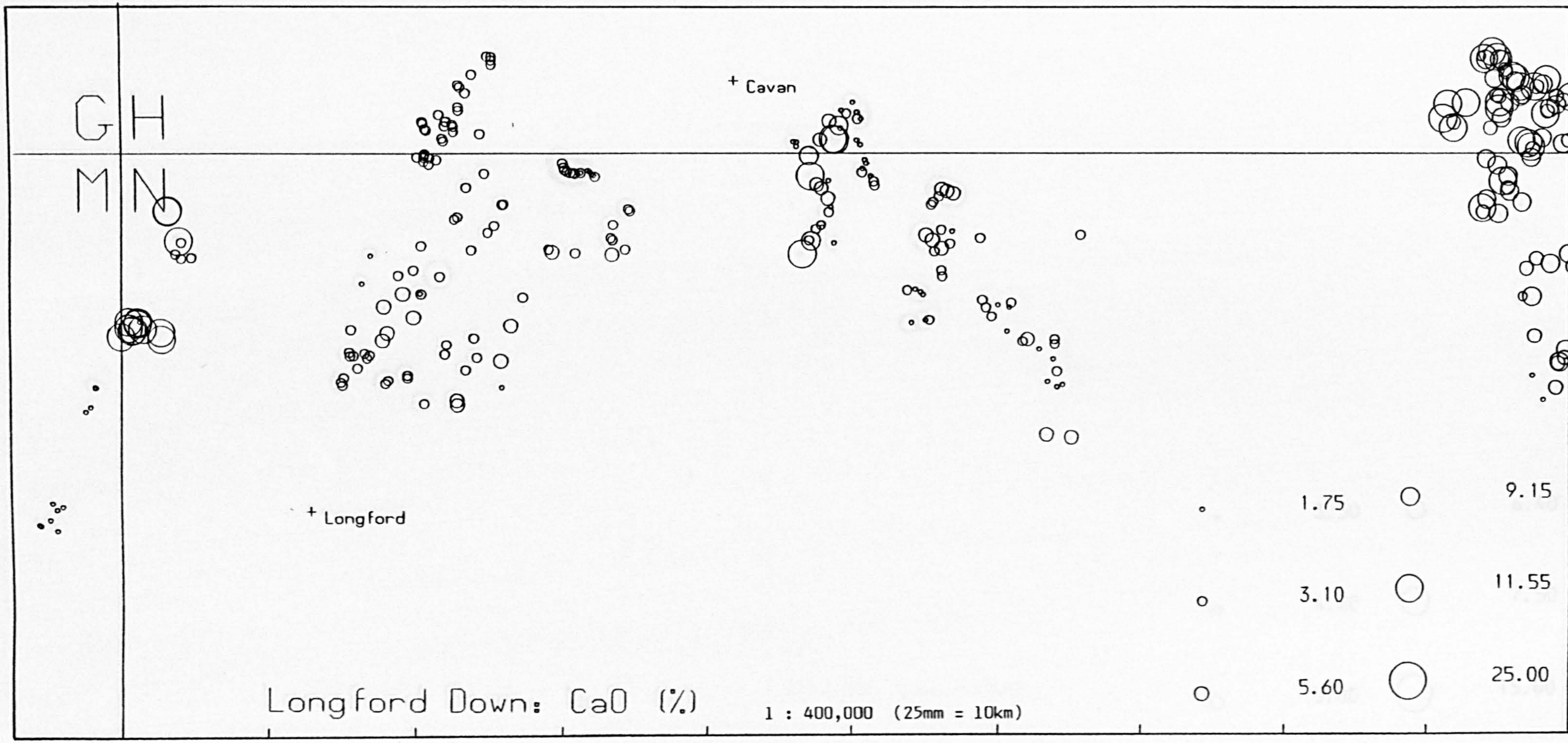
G H
M N
+ Cavan
+ Longford
1.75
3.10
5.60
9.15
11.55
25.00
Longford Down: CaO (%)
1 : 400,000 (25mm = 10km)

FIGURE 418

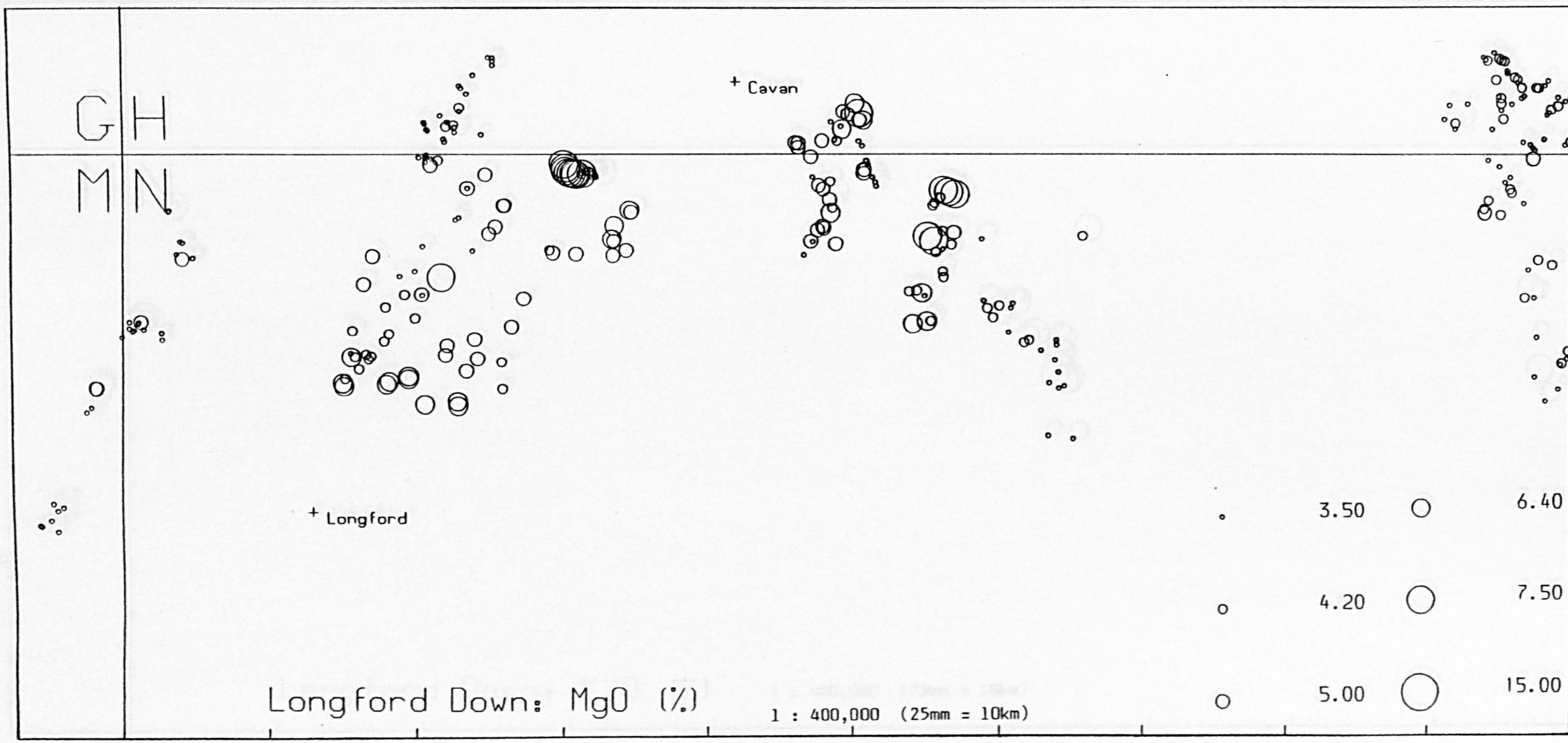
G H
M N
+ Cavan
+ Longford
3.50
4.20
5.00
6.40
7.50
15.00
Longford Down: MgO (%)
1 : 400,000 (25mm = 10km)

FIGURE 419

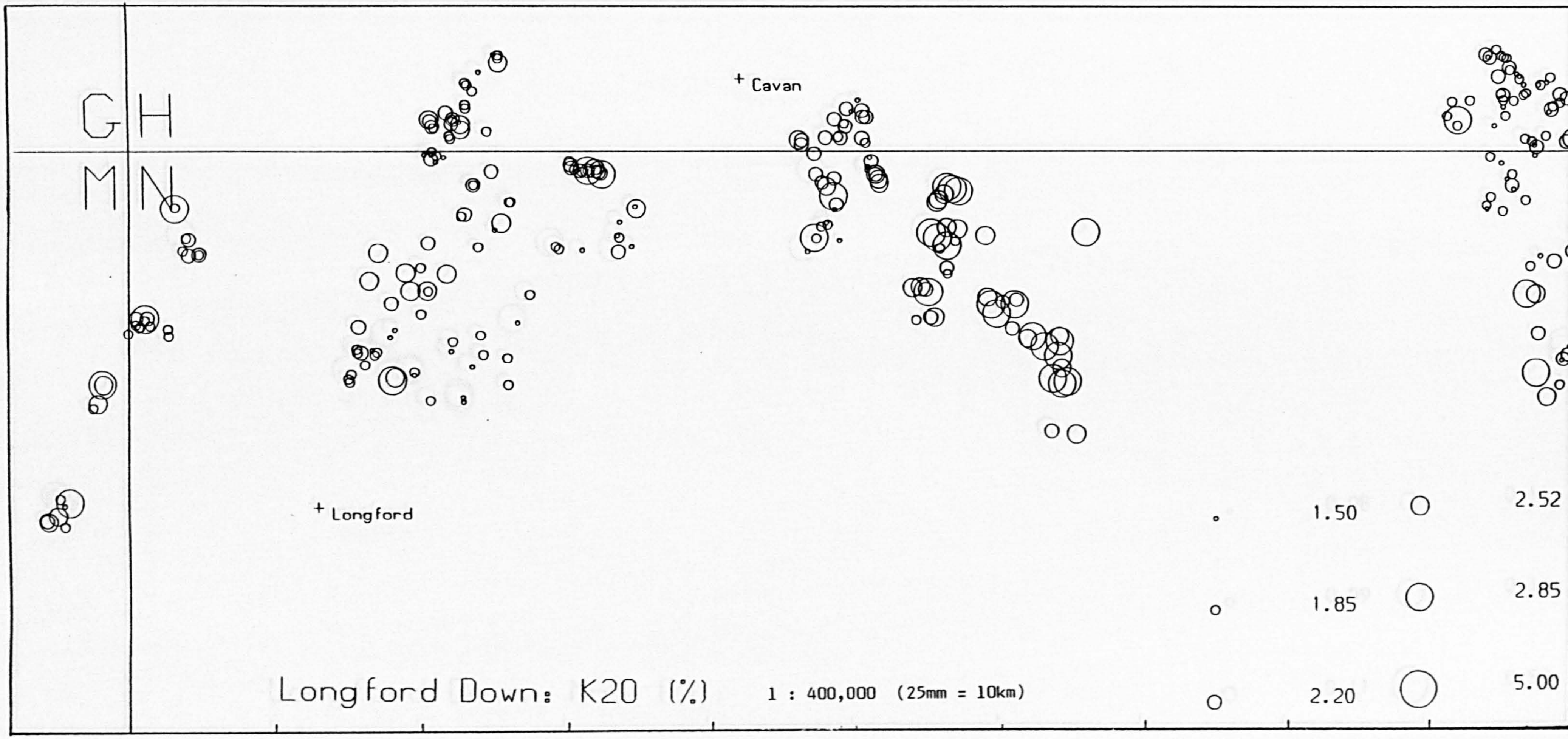
G
H
M
N
+ Cavan
+ Longford
1.50
1.85
2.20
2.52
2.85
5.00
Longford Down: K20 (%)
1 : 400,000 (25mm = 10km)

FIGURE 420

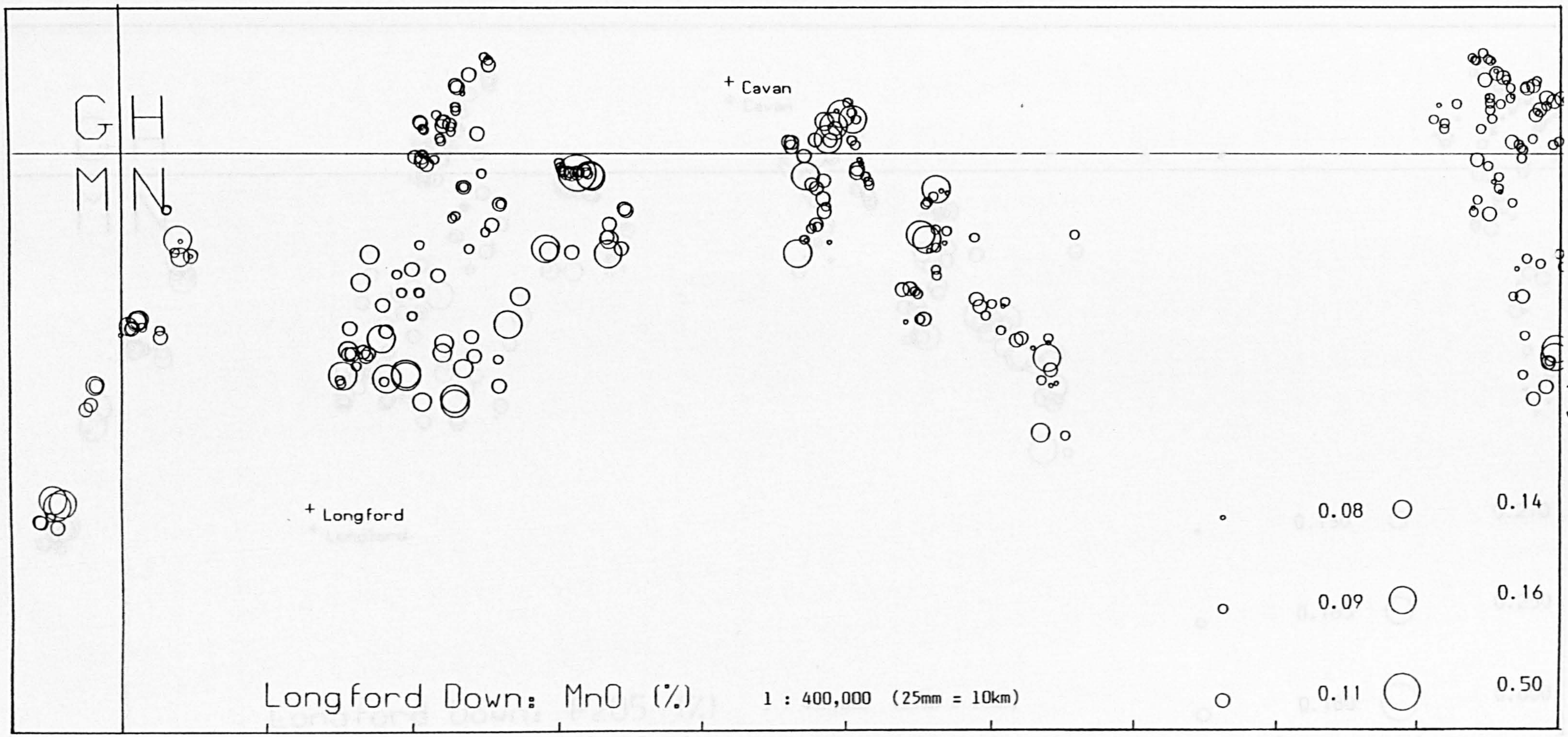
G
H
M
N
Cavan
Longford
0.08
0.09
0.11
0.14
0.16
0.50
Longford Down: MnO (%)
1 : 400,000 (25mm = 10km)

FIGURE 421

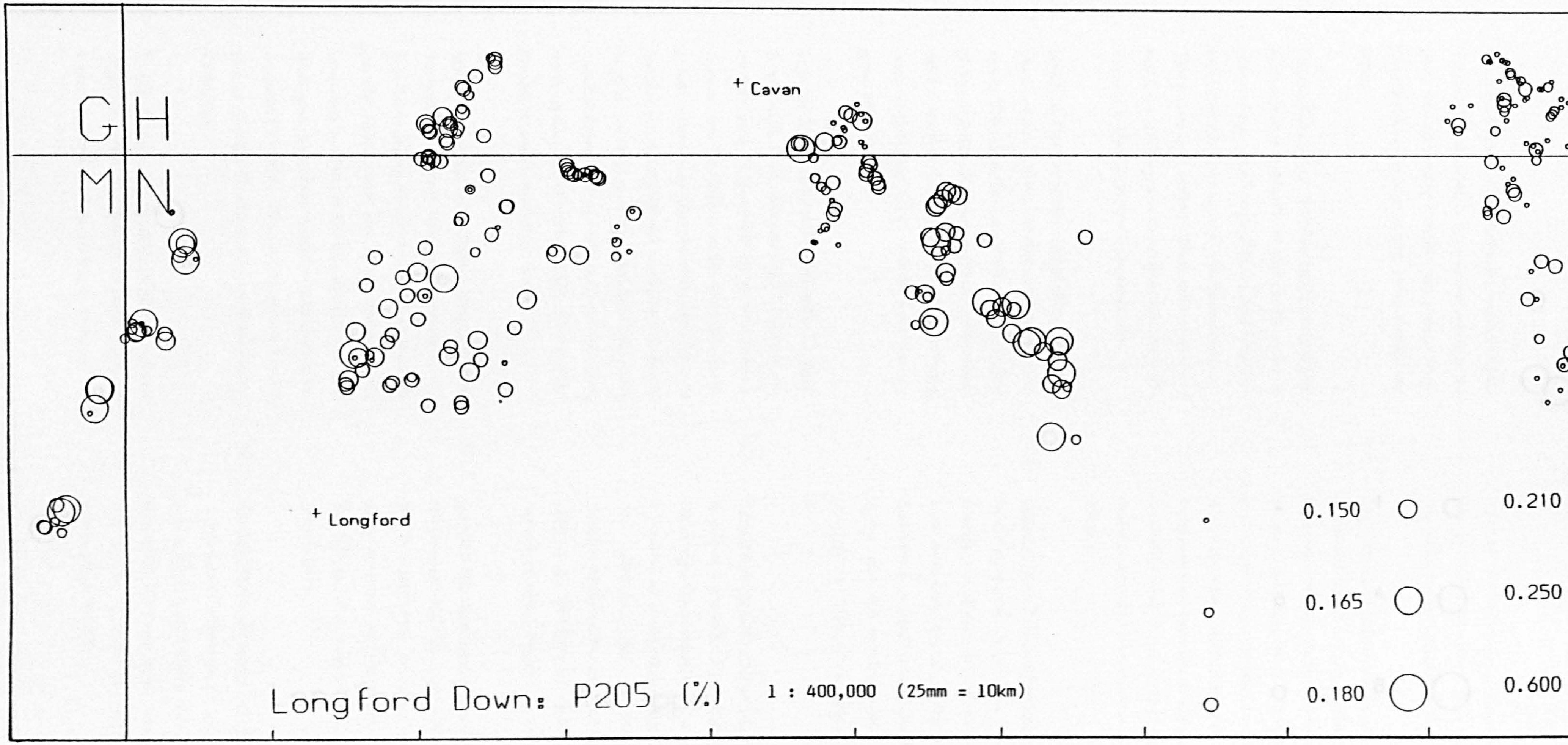

G
H
M
N
+ Cavan
+ Longford
Longford Down: P205 (%)
1 : 400,000 (25mm = 10km)
0.150
0.165
0.180
0.210
0.250
0.600

FIGURE 422

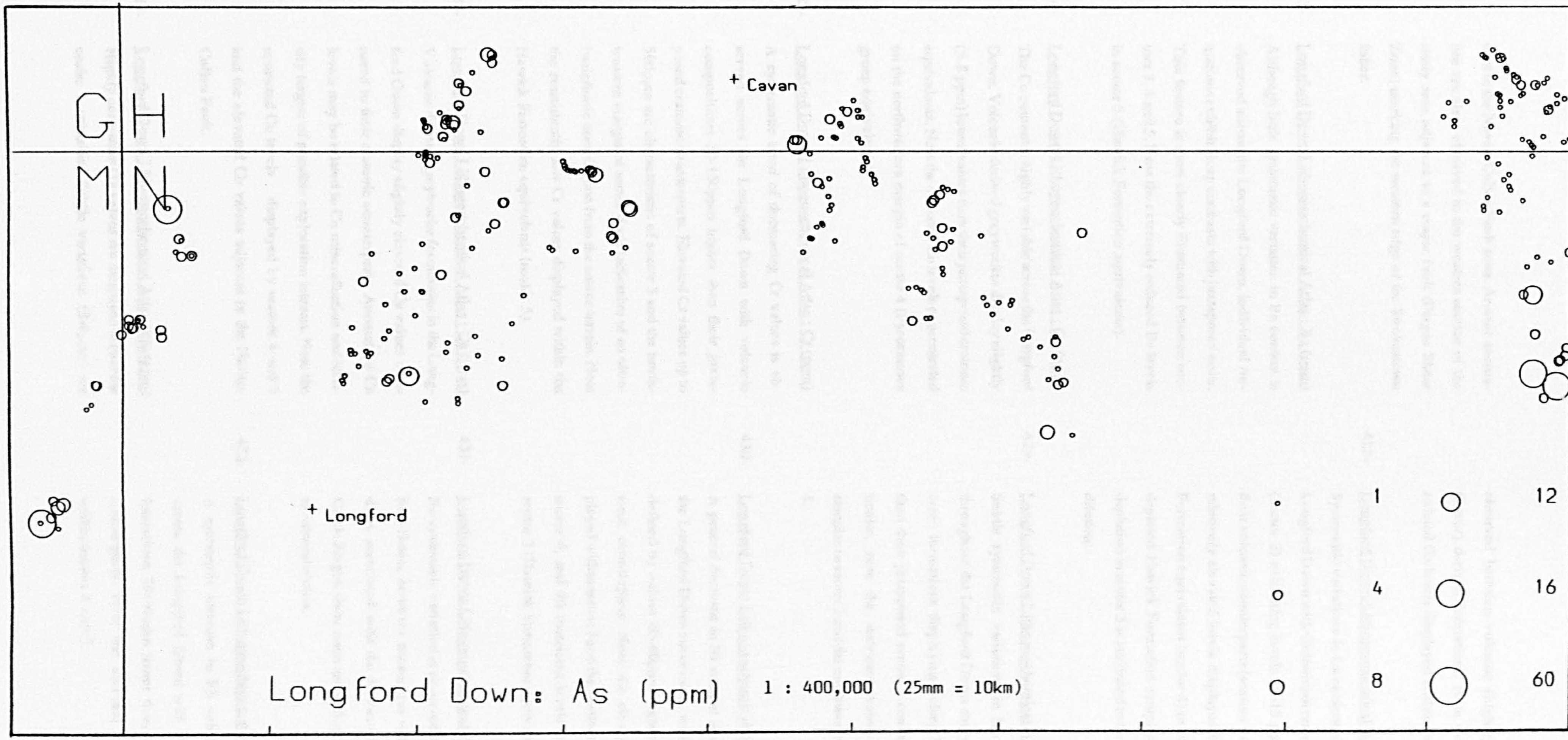
G
H
M
N
+ Cavan
+ Longford
1
4
8
12
16
60
Longford Down: As (ppm)
1 : 400,000 (25mm = 10km)

cent to the Navan-Collon Fault zone. Arsenic anomalies are also observed in the western section of the study area adjacent to a major fault (Fergus Shear Zone) marking the western edge of the Strokestown Inlier.

423- Longford Down Lithogeochemical Atlas : Ba (ppm)
Although little systematic variation in Ba content is observed across the Longford Down, individual formations exhibit sharp contrasts with juxtaposed units. This feature is most clearly illustrated between sectors 3, 4 and 5. Note the extremely reduced Ba levels in sector 5 (Hawick Formation equivalents).

424- Longford Down Lithogeochemical Atlas : Co (ppm)
The Co content is highly variable across the Longford Down. Volcanic derived greywackes display slightly (5-8 ppm) lower values than their juxtaposed cratonic equivalents. Note the elevated Co levels concentrated on the northwestern margin of sector 4 (Pyroxenous group equivalents).

425- Longford Down Lithogeochemical Atlas : Cr (ppm)
A systematic trend of decreasing Cr values is observed across the Longford Down with volcanic compositions 30-150ppm higher than their juxtaposed cratonic counterparts. Elevated Cr values up to 590ppm are characteristic of sector 3 and the northwestern margin of sector 4 are indicative of an ultrabasic/basic contribution from the source terrain. Note the consistently low Cr values displayed within the Hawick Formation equivalents (sector 5).

426- Longford Down Lithogeochemical Atlas : Cu (ppm)
Volcanic derived greywacke formations in the Longford Down display slightly elevated Cu values compared to their cratonic counterparts. Anomalous Cu levels may be related to Cu mineralisation and identify targets of possible exploration interest. Note the restricted Cu levels displayed by sectors 4 and 5 and the elevated Cu values adjacent to the Navan-Collon Fault.

427- Longford Down Lithogeochemical Atlas : Ga (ppm)
Highly consistent Ga values are displayed across the entire succession. Subtle variations (3-4ppm) are observed between volcanic (higher) and cratonic (lower) derived formations. Note the relatively restricted Ga levels displayed within sectors 4 and 5.

428- Longford Down Lithogeochemical Atlas : La (ppm)
Systematic variations in La content occur across the Longford Down with Ordovician cratonic formations (sector 2) exhibiting levels 10-15 ppm greater than their volcanic counterparts (sectors 1 and 3). Note the relatively elevated levels displayed by Intermediate Formation equivalents (sector 4) in comparison with depleted Hawick Formation samples (sector 5). La depletion in sector 5 is attributed to the effects of CaO dilution.

429- Longford Down Lithogeochemical Atlas : Nb (ppm)
Subtle systematic variations in Nb content occur throughout the Longford Down study area with volcanic formations displaying values 5-15ppm lower than their juxtaposed cratonic counterparts. In particular, note the restricted values displayed by samples in sector 3 and the northwest margin of sector 4.

430- Longford Down Lithogeochemical Atlas : Ni (ppm)
A general decrease in Ni content is observed across the Longford Down succession, with volcanic units defined by values 40-60ppm higher than their cratonic counterparts. Note the elevated values displayed within sector 3 and the northwestern margin of sector 4; and the restricted levels contained within sector 5 (Hawick Formation equivalents).

431- Longford Down Lithogeochemical Atlas : Pb (ppm)
No systematic variation is observed within the Longford Down, however anomalous values particularly those associated with the Navan-Collon Fault and Castle Fergus shear zone are indicative of proximity to mineralisation.

432- Longford Down Lithogeochemical Atlas : Rb (ppm)
A systematic increase in Rb values are observed across the Longford Down with volcanic derived formations 20-30ppm lower than their juxtaposed counterparts. Note the elevated levels displayed within sectors 4 and 5.

FIGURE 423

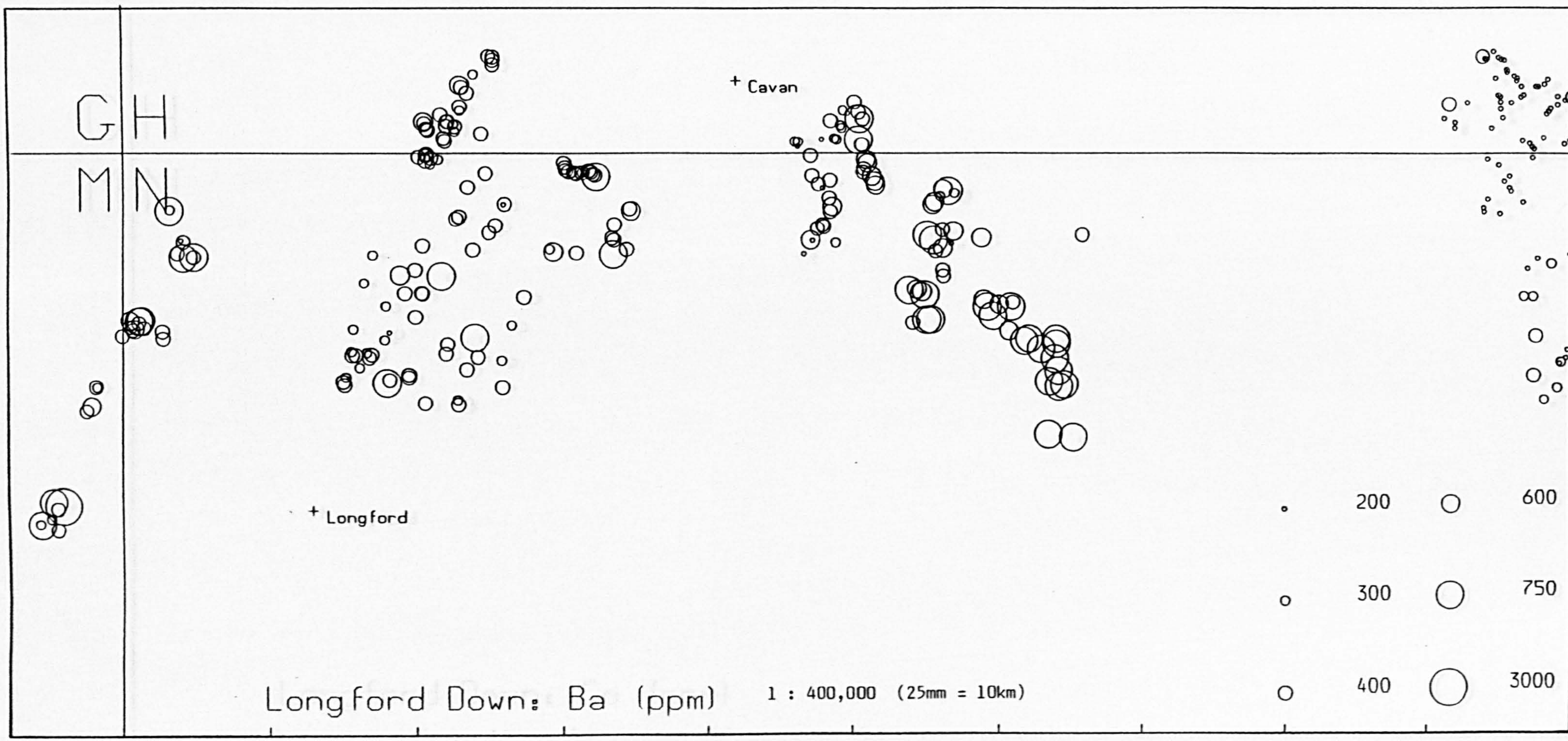
G
H
M
N
+ Cavan
+ Longford
200
300
400
600
750
3000
Longford Down: Ba (ppm)
1 : 400,000 (25mm = 10km)

FIGURE 424

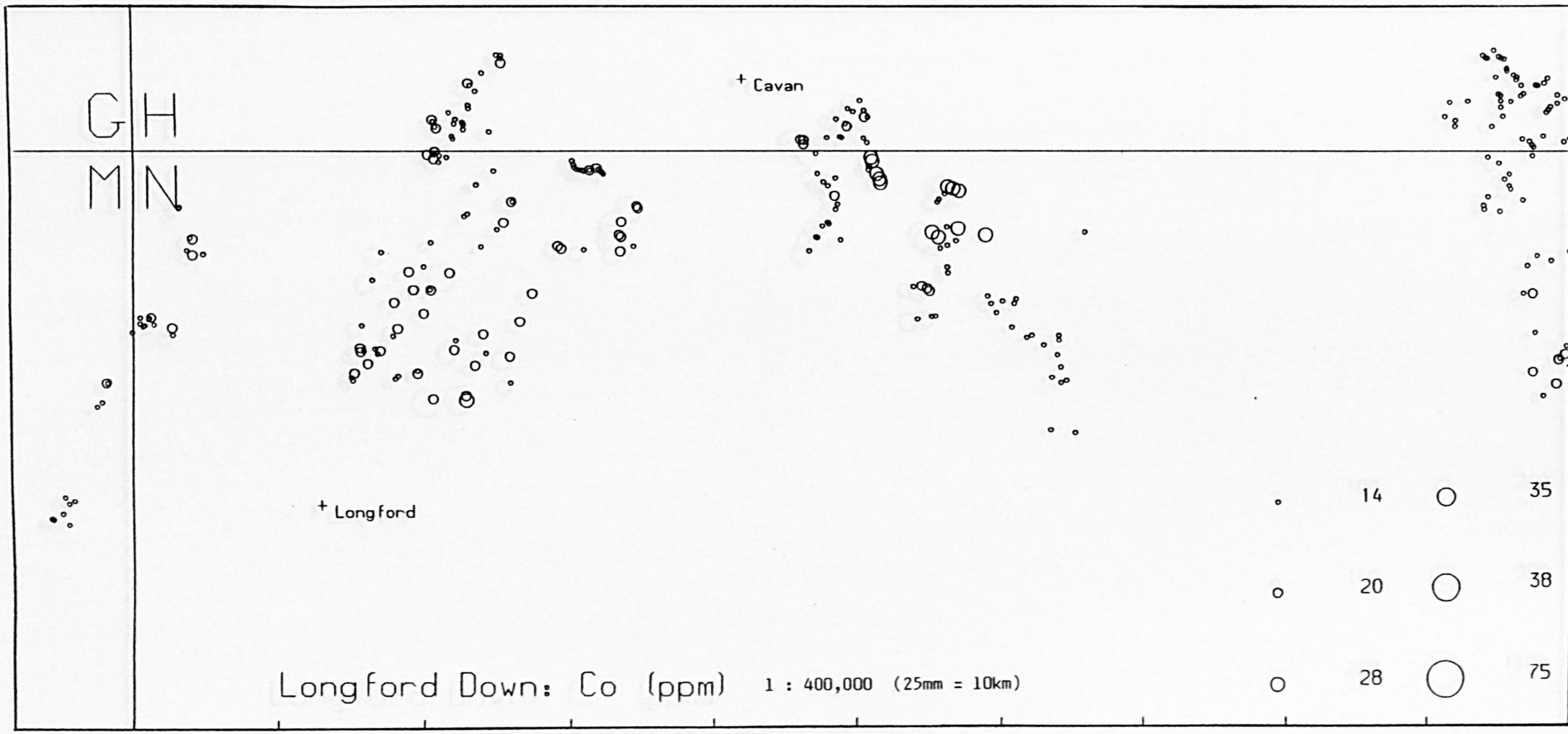

G
H
M
N
Cavan
Longford
-1720-
14
20
28
35
38
75
Longford Down: Co (ppm)
1 : 400,000 (25mm = 10km)

FIGURE 425

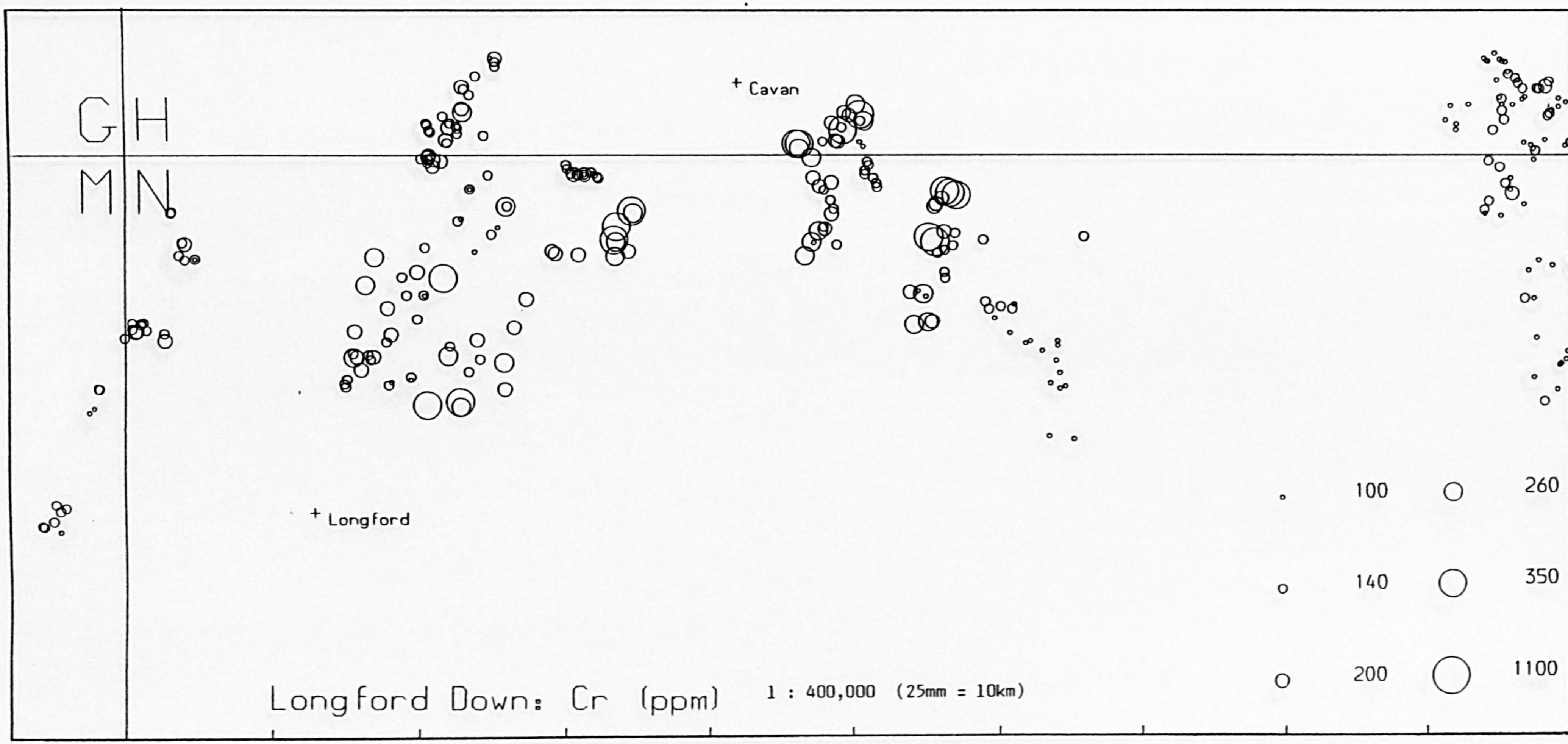
G H
M N
+ Cavan
+ Longford
100
260
140
350
200
1100
Longford Down: Cr (ppm)
1 : 400,000 (25mm = 10km)

FIGURE 426

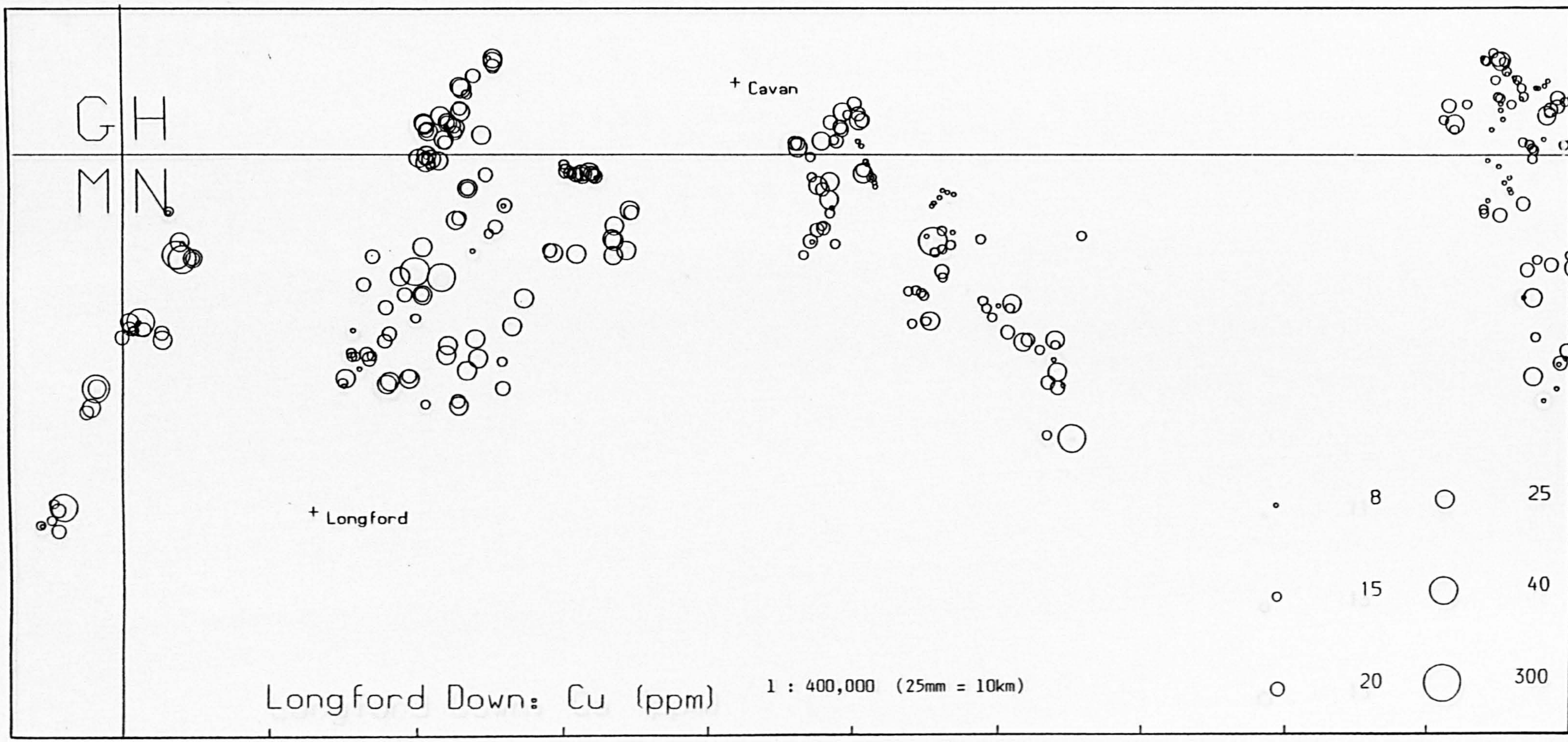

G H
M N
+ Cavan
+ Longford
8
25
15
40
20
300
Longford Down: Cu (ppm)
1 : 400,000 (25mm = 10km)

FIGURE 427

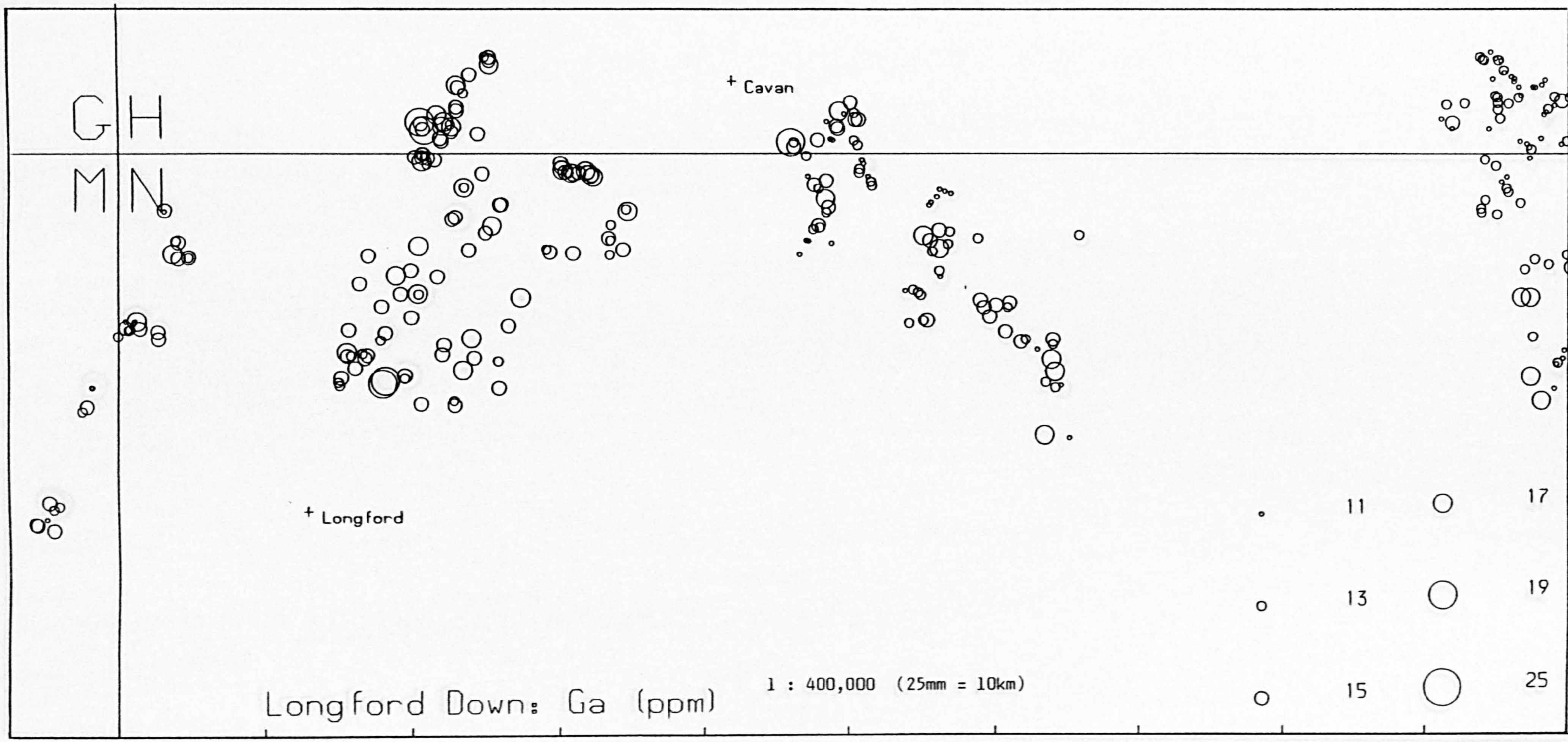

G H
M N
+ Cavan
+ Longford
Longford Down: Ga (ppm)
1 : 400,000 (25mm = 10km)
11
13
15
17
19
25

FIGURE 428

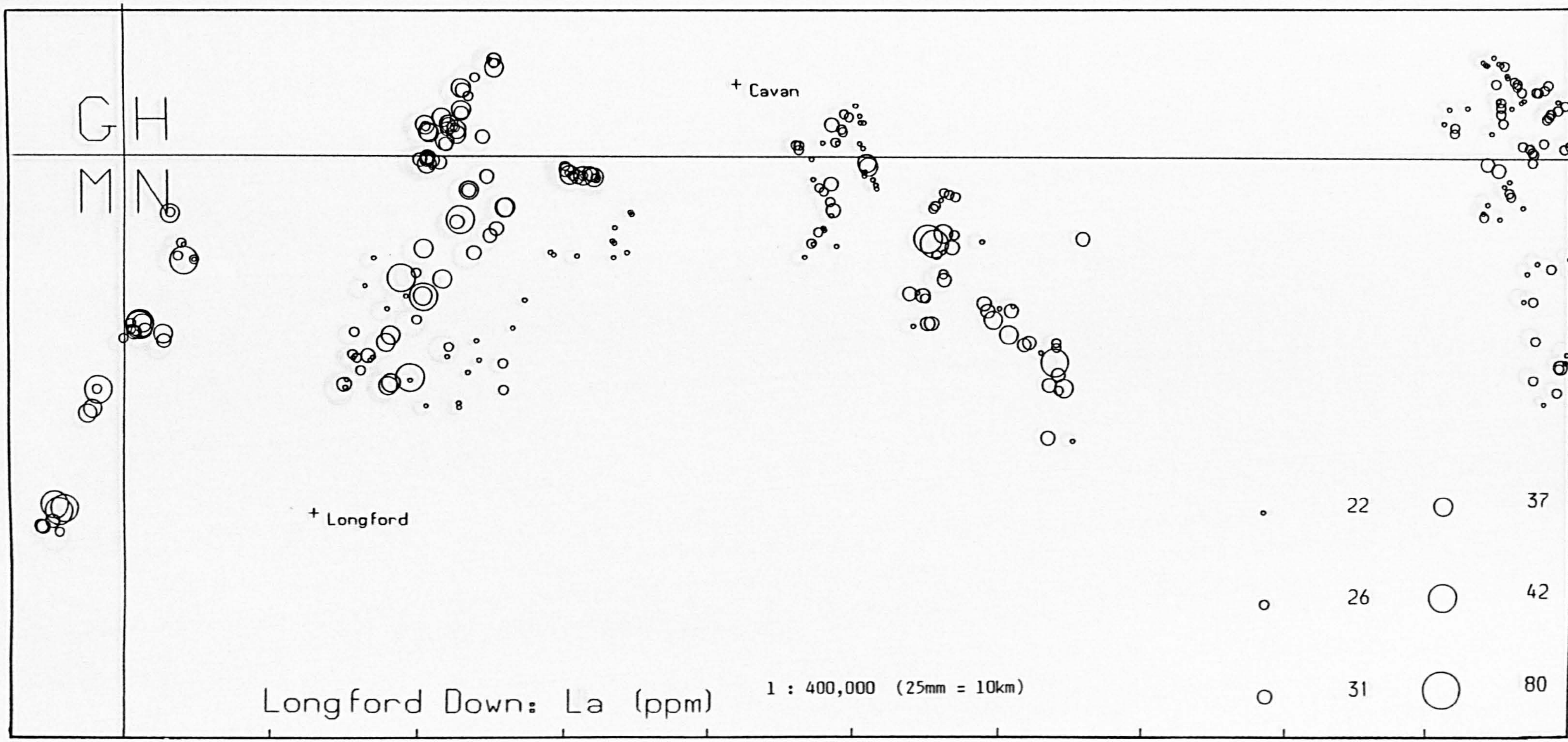
G H
M N
+ Cavan
+ Longford
22
26
31
37
42
80
Longford Down: La (ppm)
1 : 400,000 (25mm = 10km)

FIGURE 429

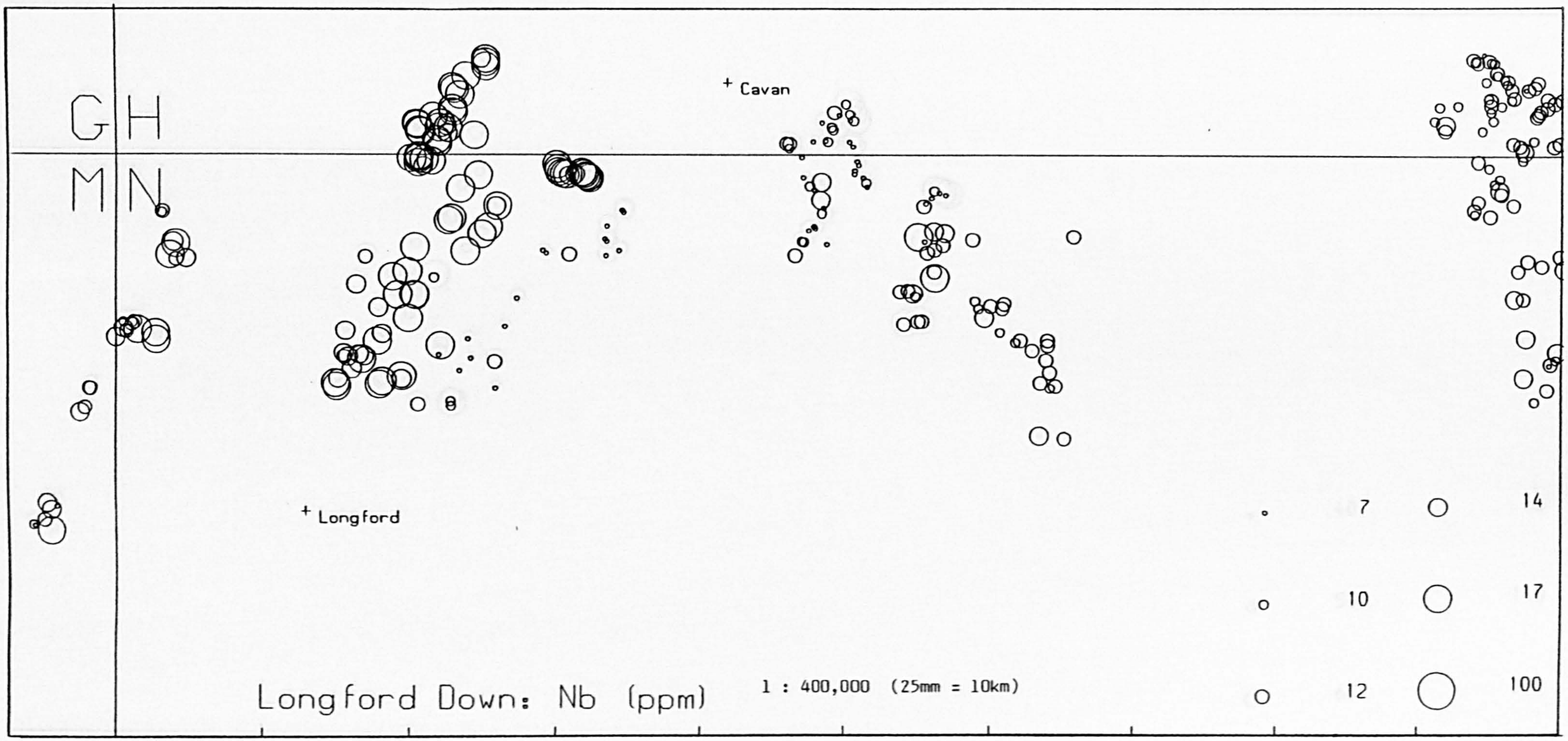
G H
M N
+ Cavan
+ Longford
7
14
10
17
12
100
Longford Down: Nb (ppm)
1 : 400,000 (25mm = 10km)

FIGURE 430

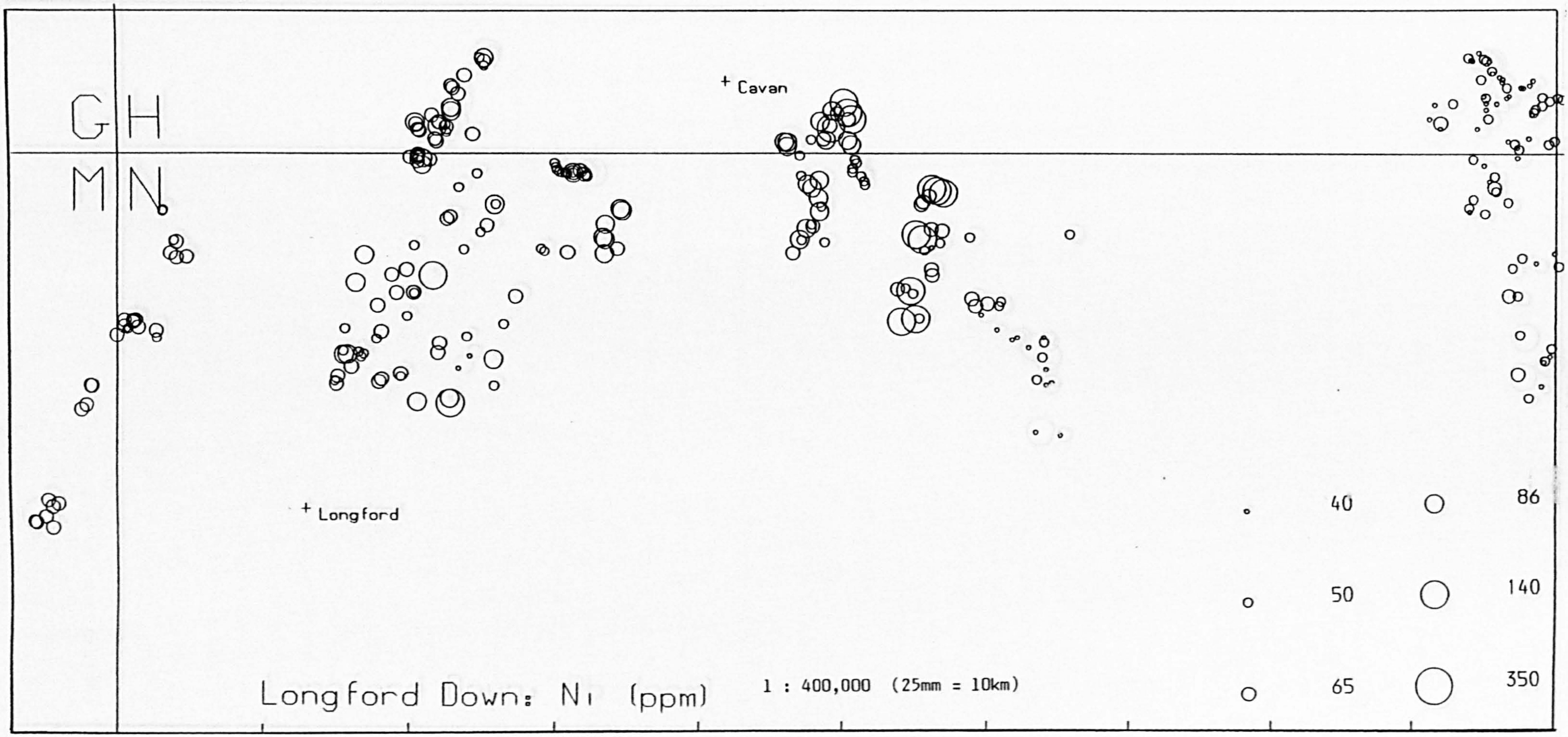
G H
M N
+ Cavan
+ Longford
40
50
65
86
140
350
Longford Down: Ni (ppm)
1 : 400,000 (25mm = 10km)

FIGURE 431

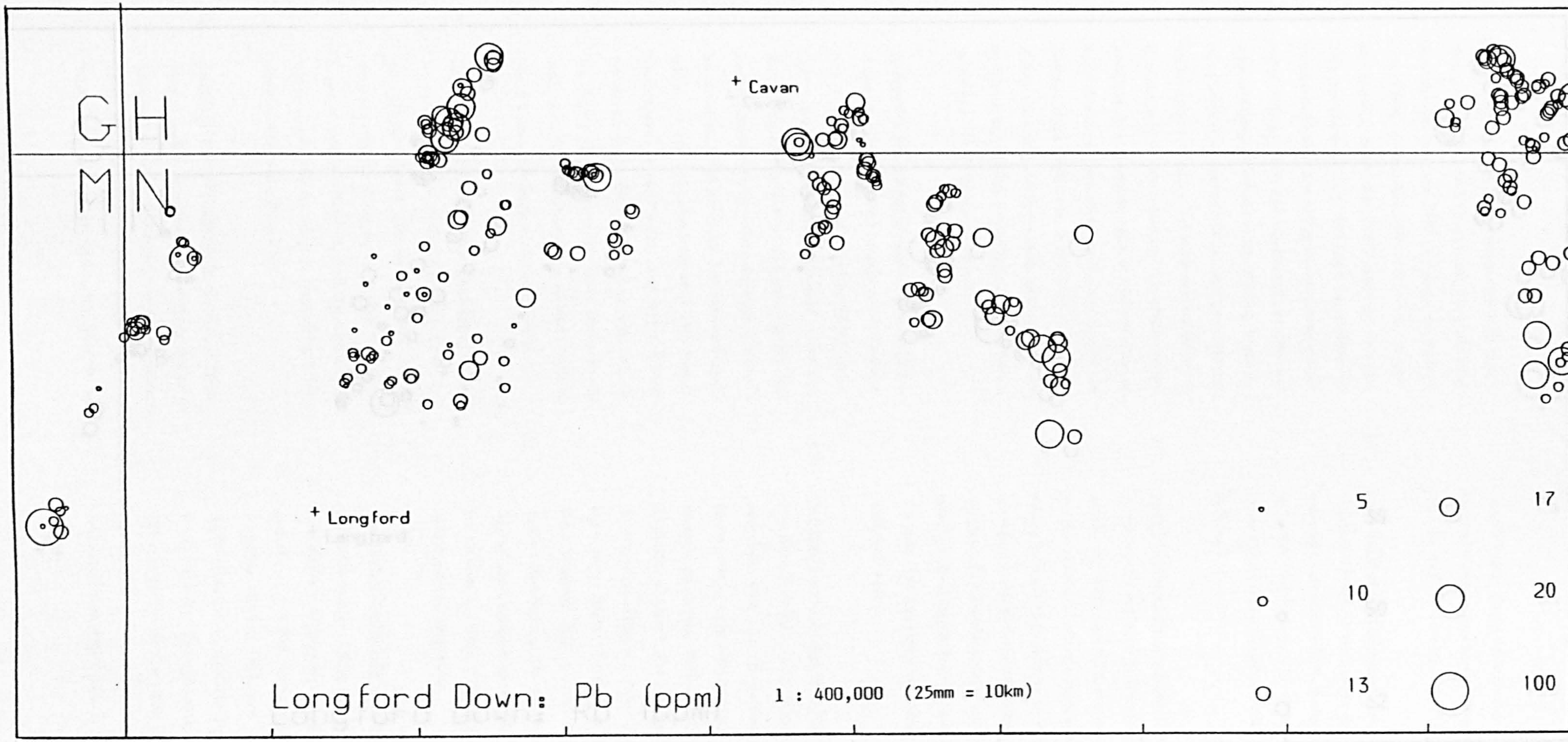
G H
M N
+ Cavan
+ Longford
5
10
13
17
20
100
Longford Down: Pb (ppm)
1 : 400,000 (25mm = 10km)

FIGURE 432

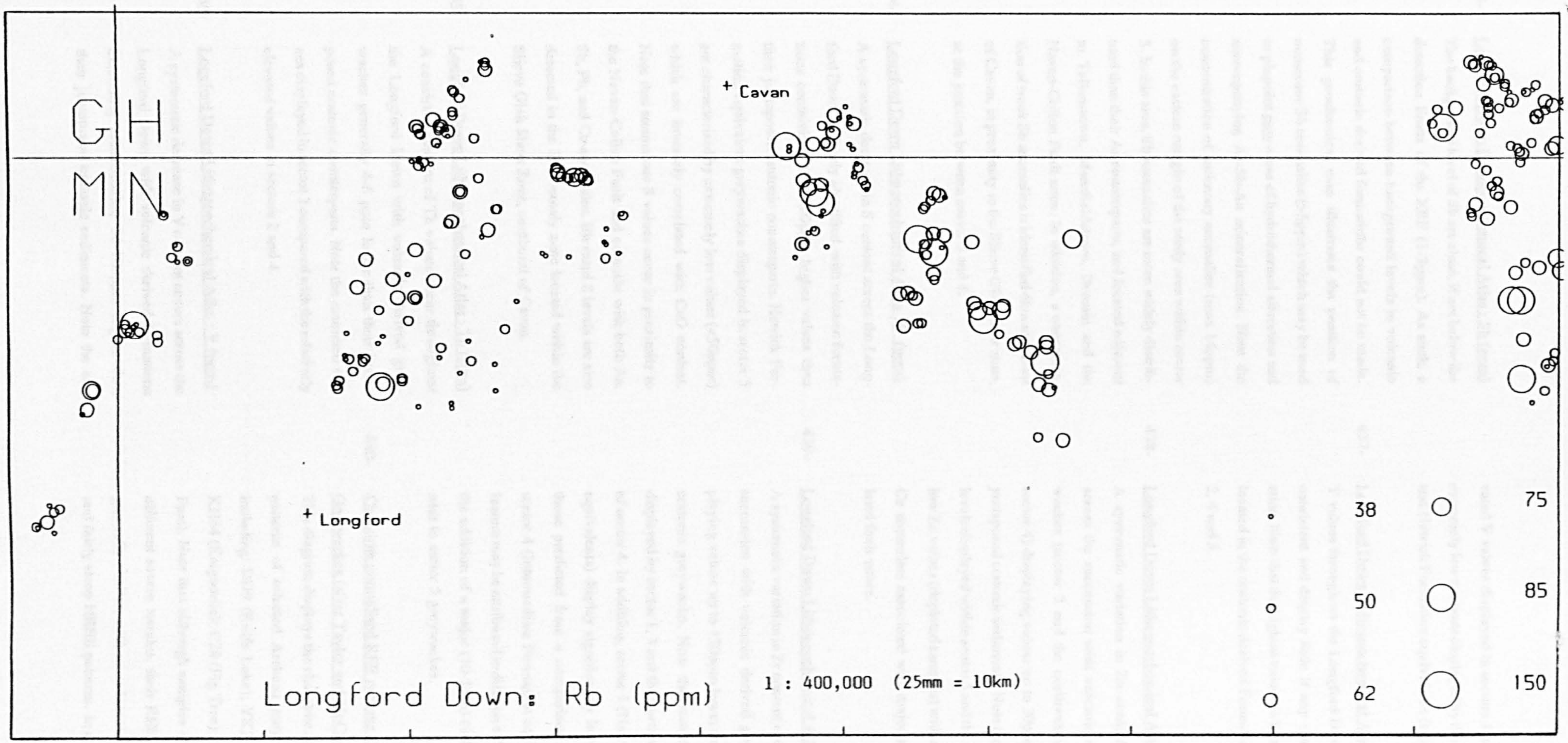
G
H
M
N
+ Cavan
+ Longford
Longford Down: Rb (ppm)
1 : 400,000 (25mm = 10km)
38
50
62
75
85
150

433- <u>Longford Down Lithogeochemical Atlas : Sb (ppm)</u>
The background level of Sb are close, if not below the detection limits of the XRF (1-3ppm). As such, a comparison between background levels in volcanic and cratonic derived formations could not be made. This geochemical map illustrates the position of numerous Sb anomalies (>5ppm) which may be used to pinpoint <u>new</u> areas of hydrothermal alteration and accompanying As-Sb-Au mineralisation. Note the concentration of antimony anomalies (max 14ppm) on the eastern margin of the study area within sector 5. In this area, Sb anomalies are more widely distributed than their As counterparts, and located adjacent to Tallanstown, Mansfieldstown, Dromin and the Navan-Collon Fault zone. In addition, a concentration of weak Sb anomalies is identified 4km southeast of Cavan, in proximity to the Slieve Glah shear zone, at the junction between sector 3 and 4.

434- <u>Longford Down Lithogeochemical Atlas : S (ppm)</u>
A systematic decrease in S content across the Longford Down is clearly identified, with volcanic formations containing 200-1000ppm higher values than their juxtaposed cratonic counterparts. Hawick Formation equivalent greywackes displayed in sector 5 are characterised by extremely low values (<50ppm) which are inversely correlated with CaO content. Note that anomalous S values occur in proximity to the Navan-Collon Fault and coincide with both As, Sb, Pb, and Cu anomalies. Elevated S levels are also detected in the Sb anomaly zone located within the Slieve Glah Shear Zone, southeast of Cavan.

435- <u>Longford Down Lithogeochemical Atlas : Th (ppm)</u>
A consistent pattern of Th values occur throughout the Longford Down with volcanic derived greywackes generally 4-6 ppm lower than their juxtaposed cratonic counterparts. Note the restricted values displayed in sector 3 compared with the relatively elevated values in sectors 2 and 4.

436- <u>Longford Down Lithogeochemical Atlas : V (ppm)</u>
A systematic decrease in V content occurs across the Longford Down with volcanic derived formations exhibiting concentration 50-100ppm higher than their juxtaposed cratonic sediments. Note the elevated V values displayed in sectors 1 and 3; and the extremely low contents displayed by the Intermediate and Hawick Formation equivalents (sectors 4 and 5).

437- <u>Longford Down Lithogeochemical Atlas : Y (ppm)</u>
Y values throughout the Longford Down are highly consistent and display little if any systematic variation. Note that the highest values in this sequence are located in the cratonic derived Formations of sectors 2, 4 and 5.

438- <u>Longford Down Lithogeochemical Atlas : Zn (ppm)</u>
A systematic variation in Zn content is observed across the succession with volcanic derived greywackes (sector 3 and the northwestern margin of sector 4) displaying values up to 30ppm higher than juxtaposed cratonic sediments. Note the restricted Zn levels displayed within sector 5 and the association of low Zn values (depleted samples) with As, Sb, Pb and Cu anomalies associated with major shear zone related fault zones.

439- <u>Longford Down Lithogeochemical Atlas : Zr (ppm)</u>
A systematic variation in Zr content occurs across the succession with volcanic derived greywackes displaying values up to 150ppm lower than juxtaposed cratonic greywacke. Note the restricted Zr levels displayed by sector 1, 3 and the northwestern margin of sector 4. In addition, sector 5 (Hawick Formation equivalents) display significantly lower values than those predicted from a comparison with adjacent sector 4 (Intermediate Formation equivalents). This feature may be attributed to dilution effects formed by the addition of a major (10-15%) carbonate component to sector 5 greywackes.

440- <u>Chondrite normalised REE patterns for Archean Greywackes (after Taylor and McClennan, 1985)</u>
This diagram displays the chondrite normalised REE patterns of selected Archean greywacke samples including: DD9 (Knife Lake); YK2 (Yellowknife); KH44 (Kalgoorlie); C28 (Fig Tree); and G21 (South Pass). Note that although samples are derived from different source terrains, their REE patterns are all generally similar, with no substantial Eu-anomalies and fairly steep HREE patterns. In comparison with

FIGURE 433

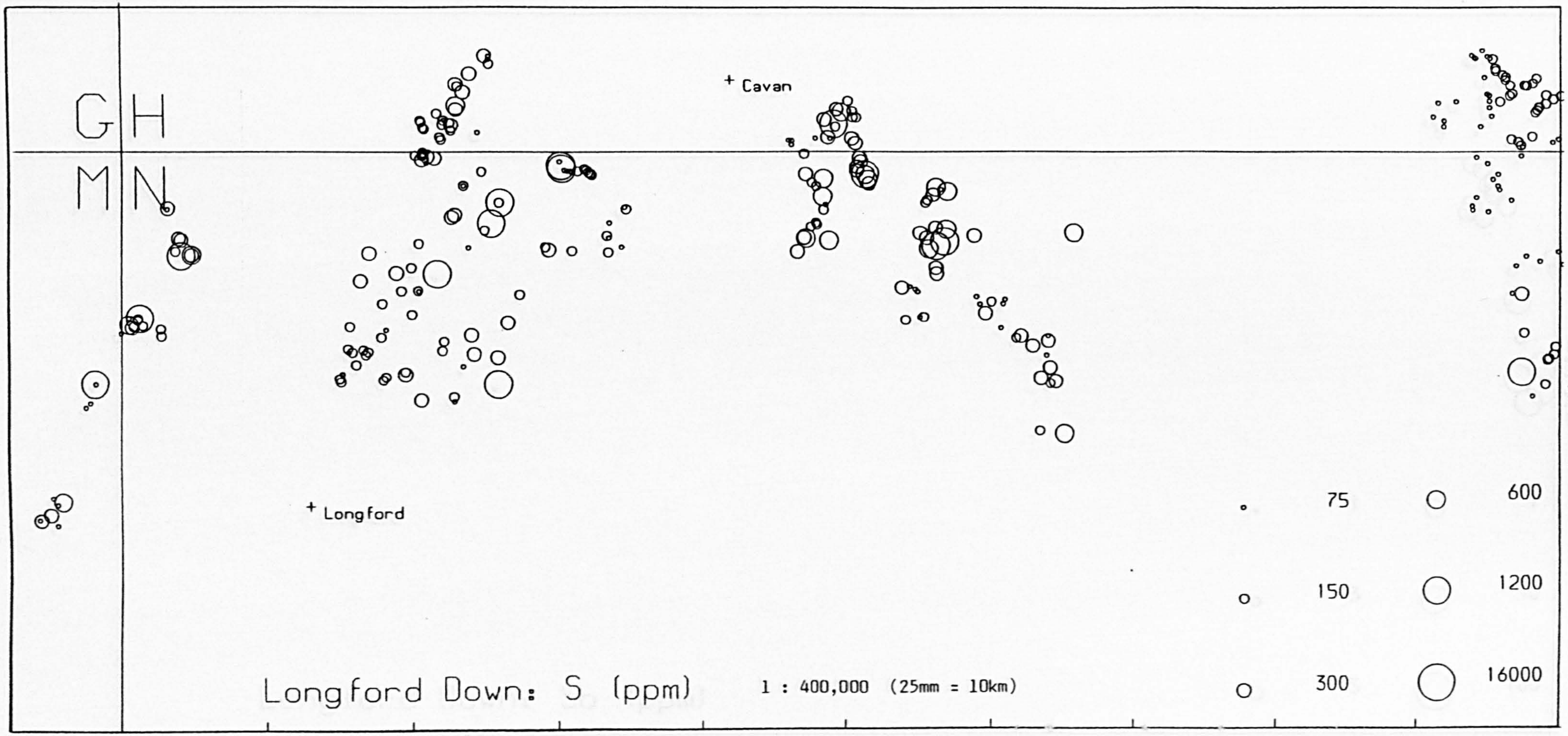
GH
MN
+ Cavan
+ Longford
75
150
300
600
1200
16000
Longford Down: S (ppm)
1 : 400,000 (25mm = 10km)

FIGURE 434

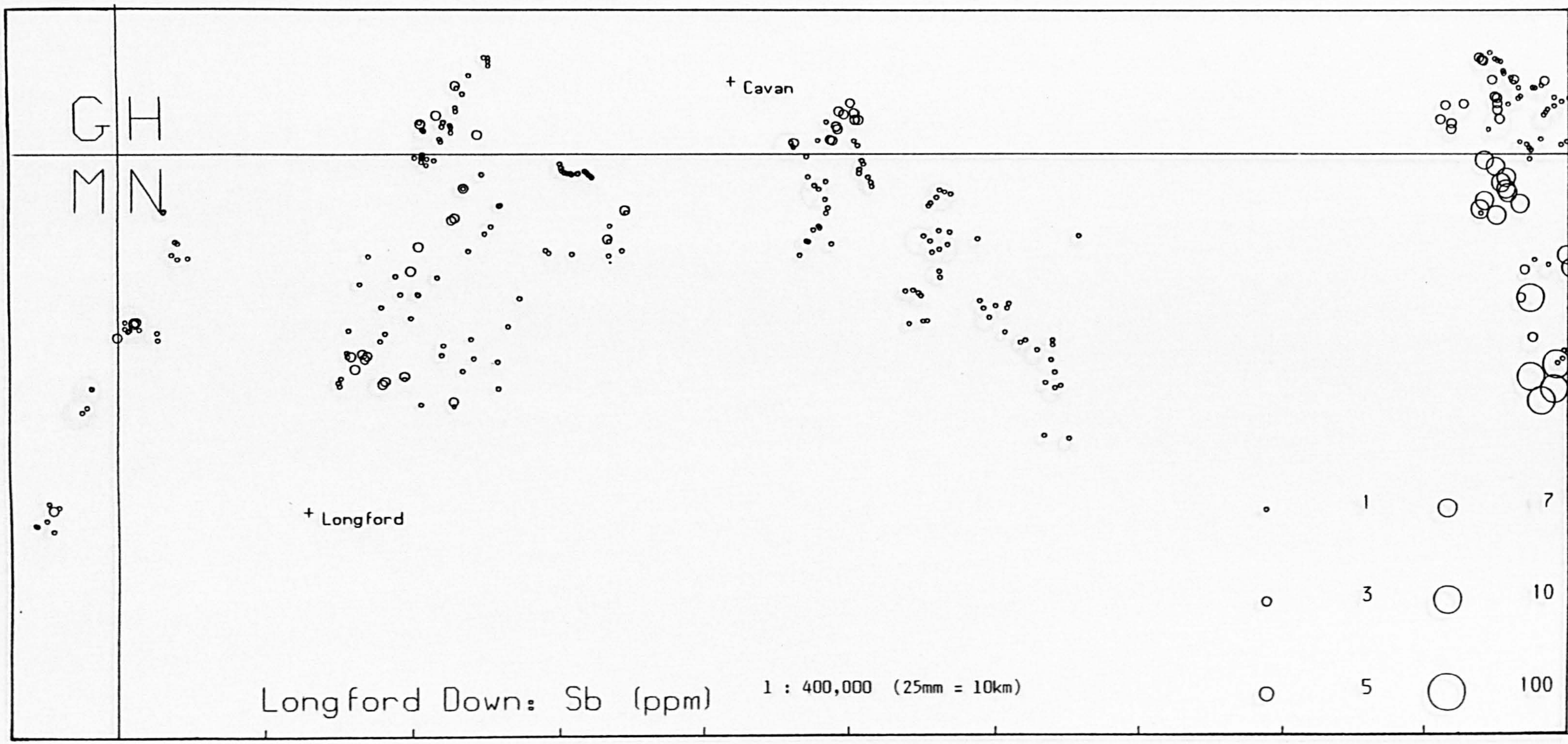
G H
M N
+ Cavan
+ Longford
Longford Down: Sb (ppm)
1 : 400,000 (25mm = 10km)
1
3
5
7
10
100

FIGURE 435

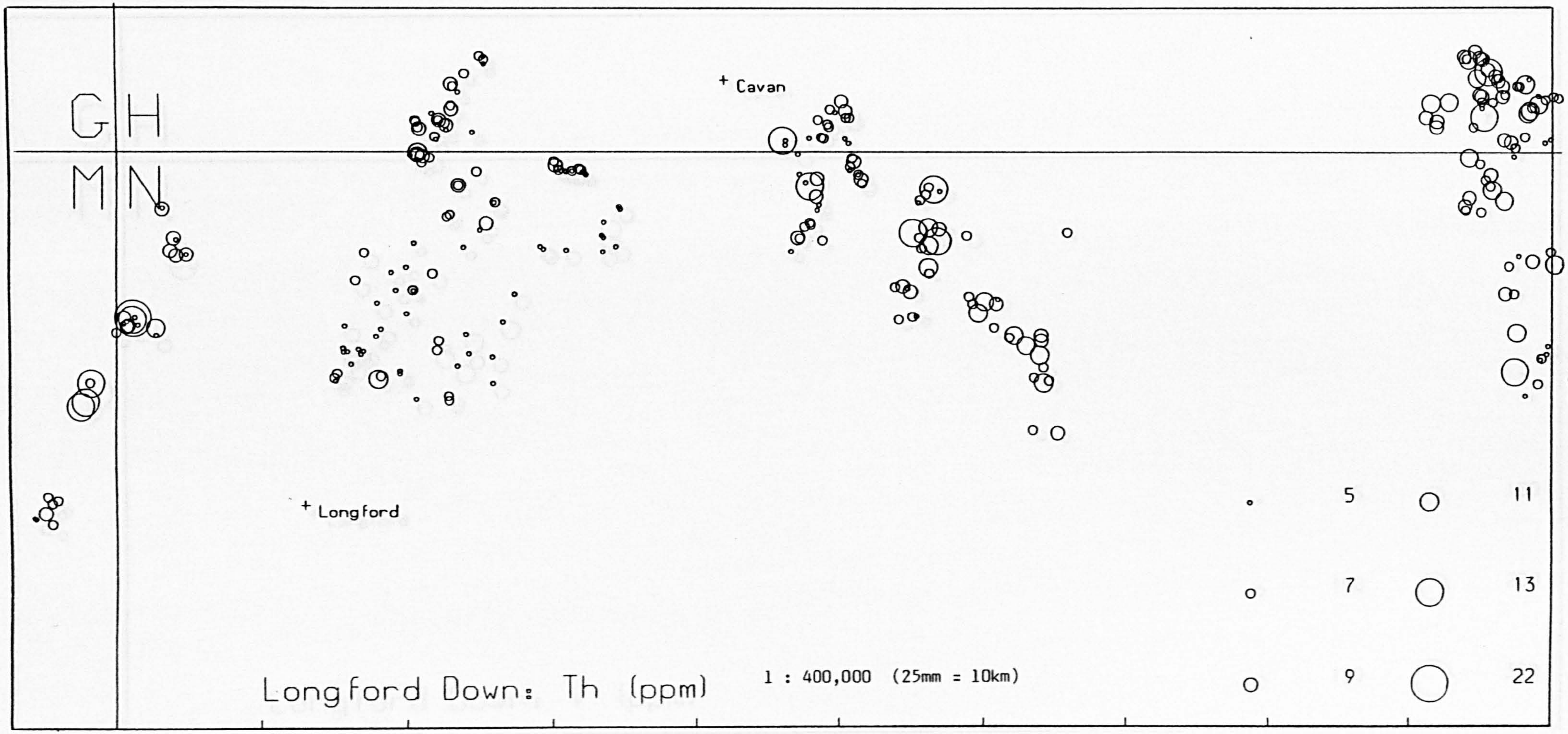

G
H
M
N
+ Cavan
+ Longford
5
11
7
13
9
22
Longford Down: Th (ppm)
1 : 400,000 (25mm = 10km)

FIGURE 436

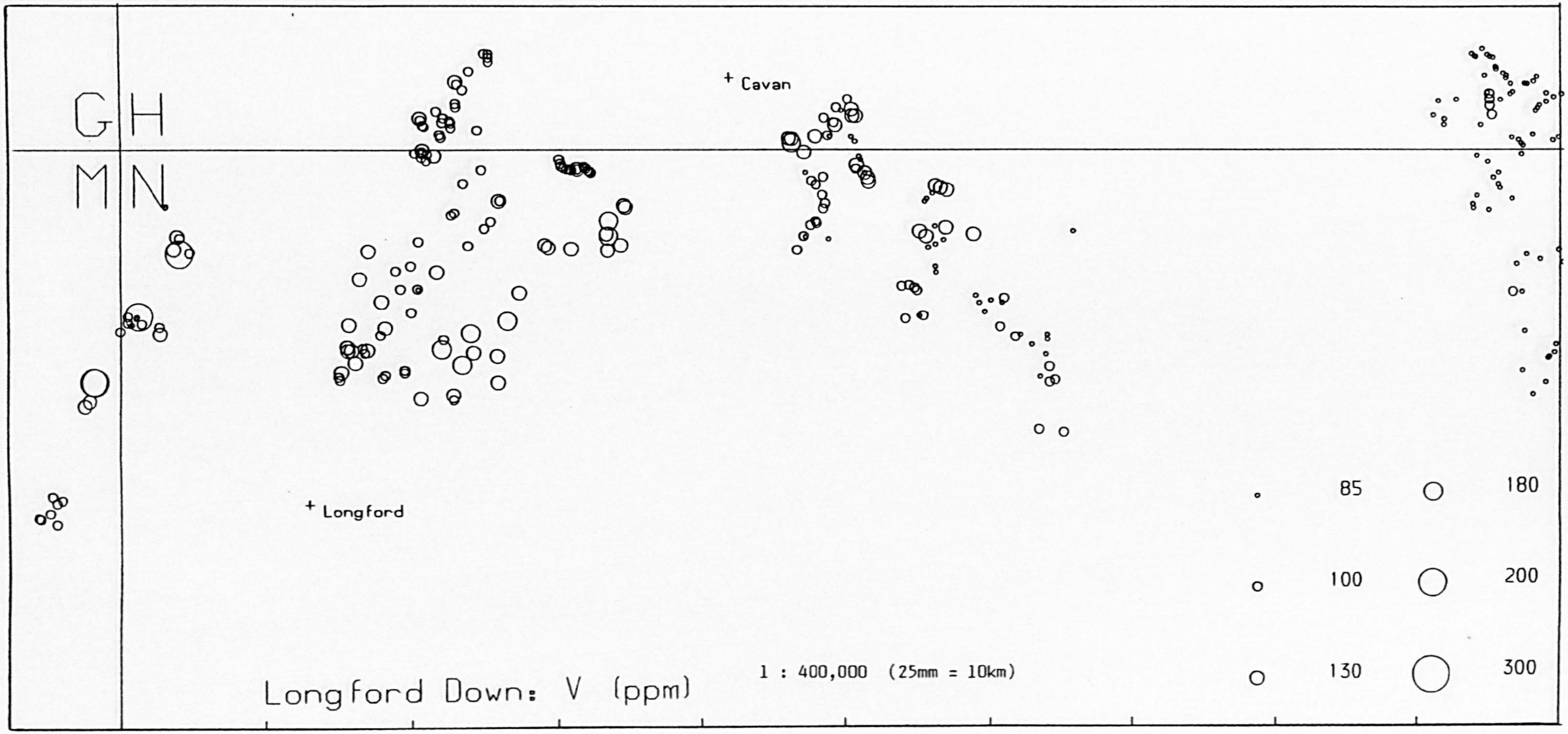

-1733-

FIGURE 437

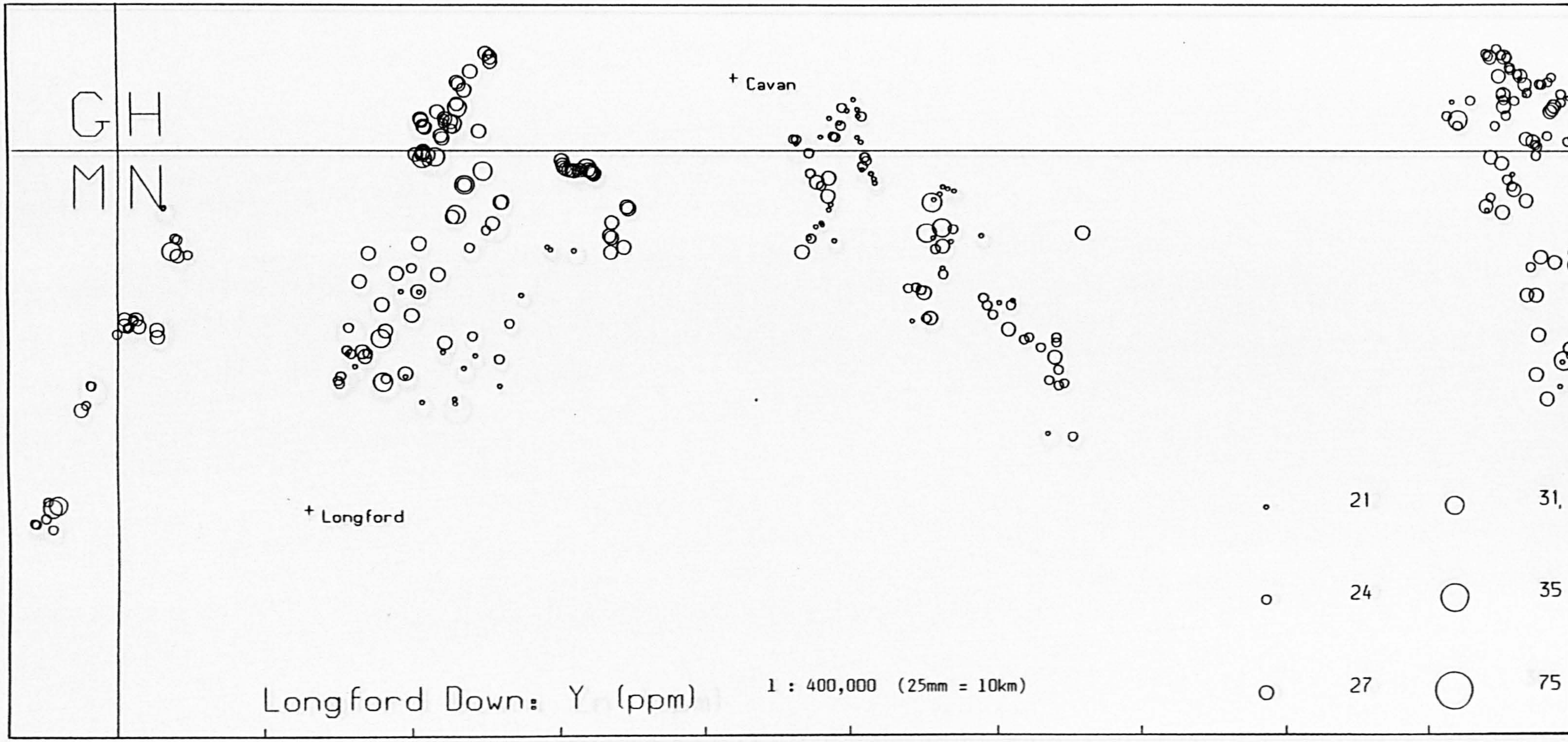
G
H
M
N
+ Cavan
+ Longford
21
31
24
35
27
75
Longford Down: Y (ppm)
1 : 400,000 (25mm = 10km)

FIGURE 438

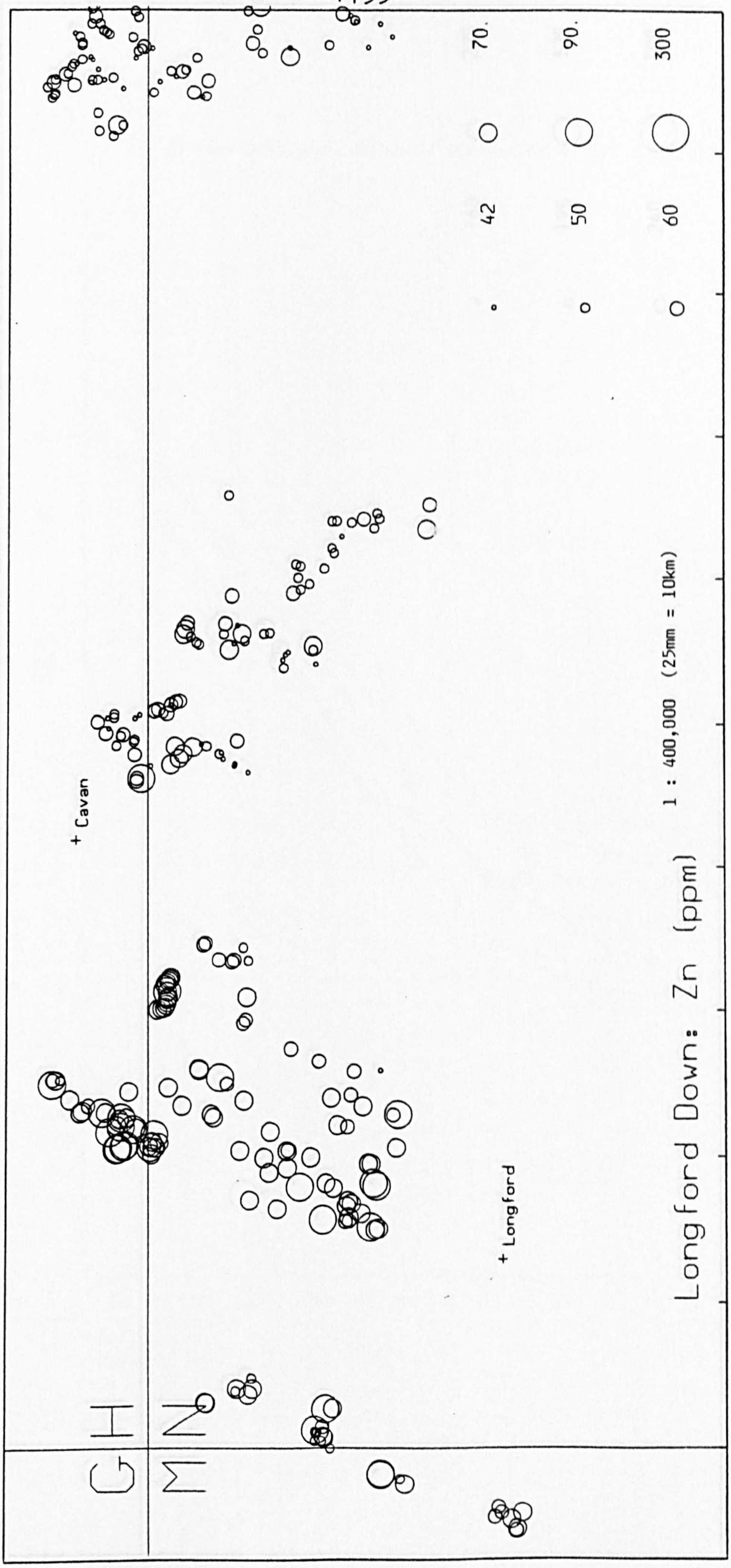
G H
M N
+ Cavan
+ Longford
42
70
50
90
60
300
1 : 400,000 (25mm = 10km)
Longford Down: Zn (ppm)

FIGURE 439

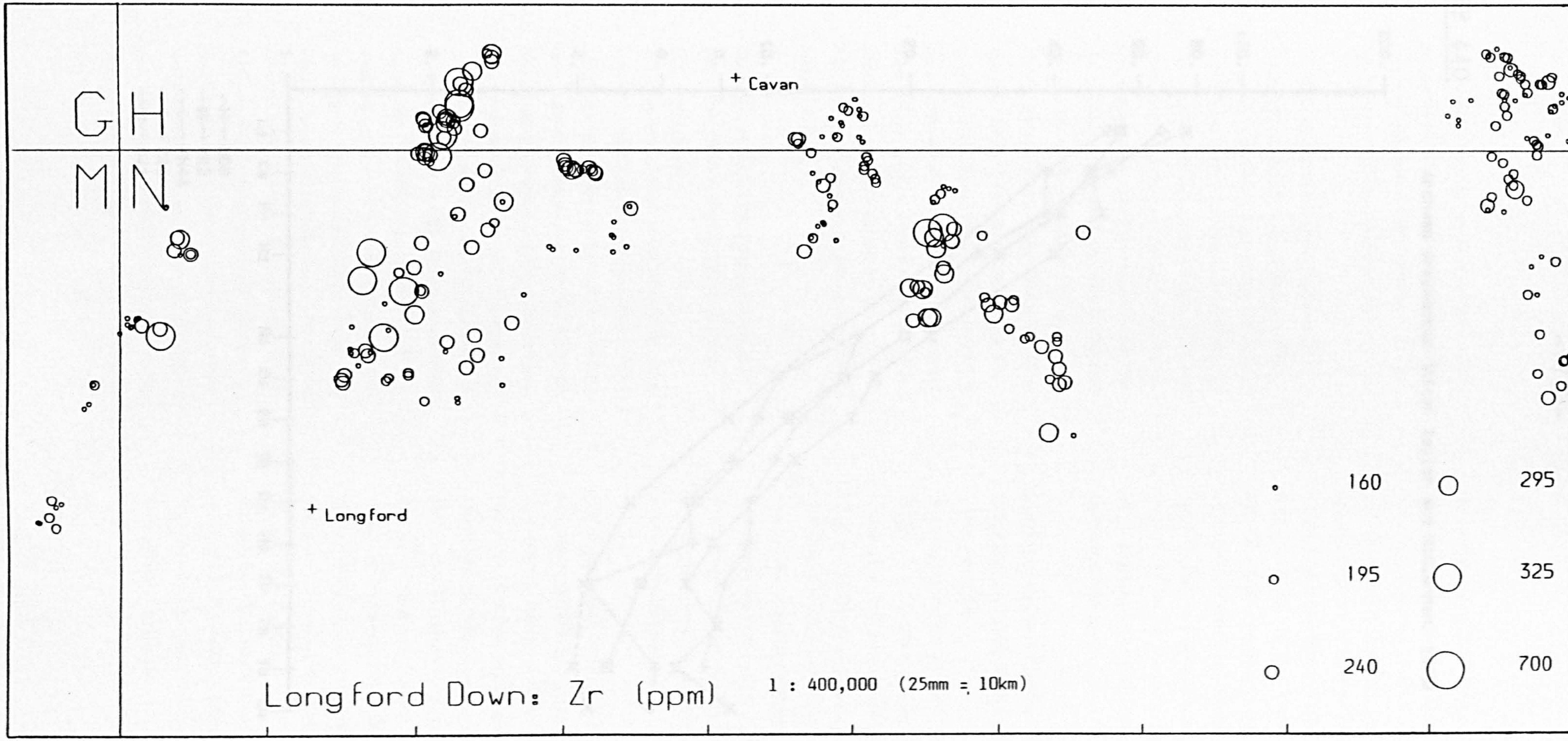
G
H
M
N
+ Cavan
+ Longford
Longford Down: Zr (ppm)
1 : 400,000 (25mm = 10km)
160
295
195
325
240
700

FIGURE 440

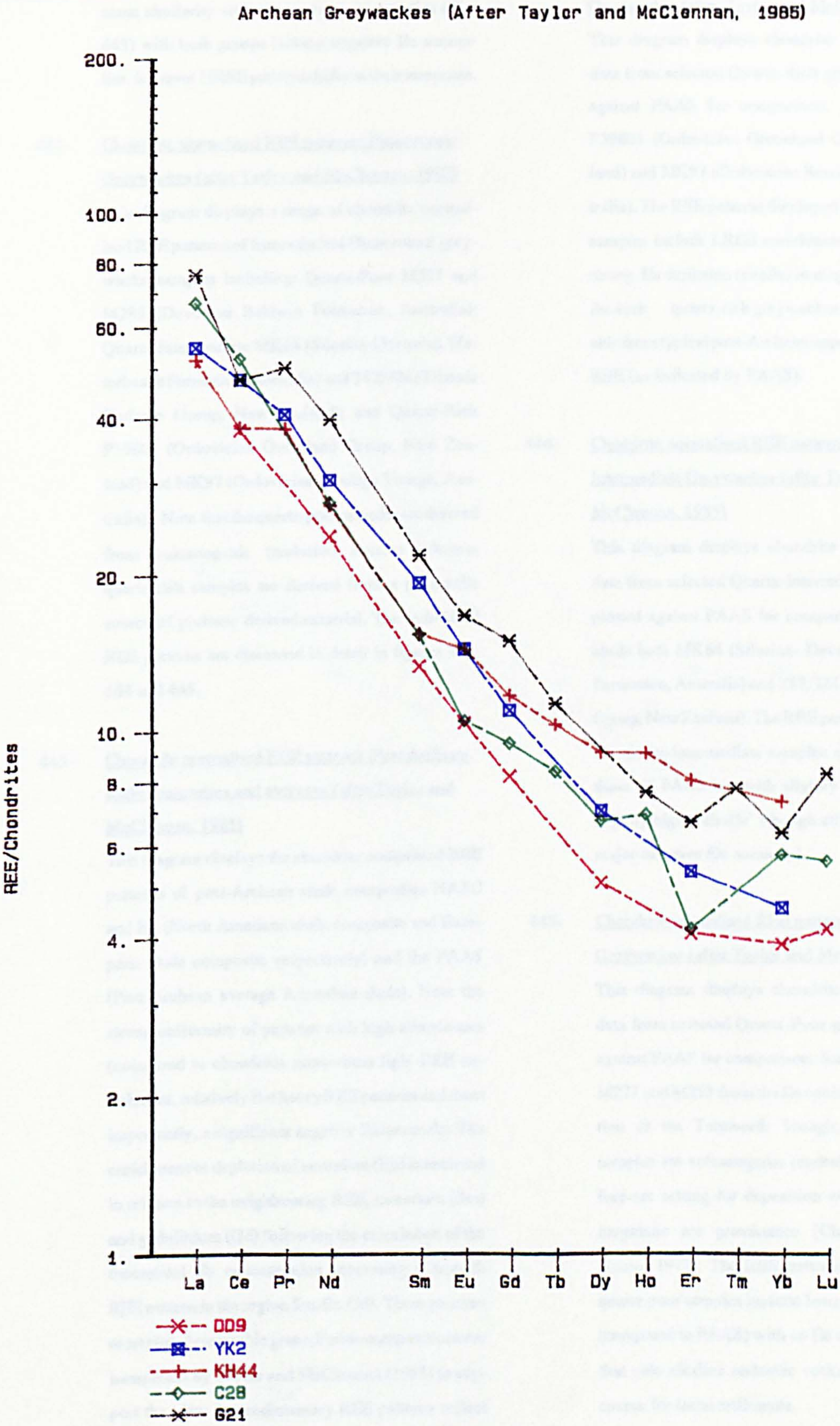
Archean Greywackes (After Taylor and McClennan, 1985)
REE/Chondrites
200.
100.
80.
60.
40.
20.
10.
8.
6.
4.
2.
1.
La
Ce
Pr
Nd
Sm
Eu
Gd
Tb
Dy
Ho
Er
Tm
Yb
Lu
DD9
YK2
KH44
C28
G21

post-Archean greywackes, these samples exhibit some similarity with the quartz-poor varieties (Fig. 445) with both groups lacking negative Eu-anomalies, however HREE patterns differ in their steepness.

441- Chondrite normalised REE patterns: Phanerozoic Greywackes (after Taylor and McClennan, 1985)
This diagram displays a range of chondrite normalised REE patterns of from selected Phanerozoic greywacke samples including: Quartz-Poor M277 and M285 (Devonian Baldwin Formation, Australia); Quartz-Intermediate MK64 (Silurian-Devonian Waterbeach Formation, Australia) and T82/324 (Triassic Torlesse Group, New Zealand); and Quartz-Rich P39803 (Ordovician Greenland Group, New Zealand) and MK97 (Ordovician Bendigo Trough, Australia). Note that the quartz-poor samples are derived from volcanogenic (andesite) sources whereas quartz-rich samples are derived from a polycyclic source of plutonic derived material. The individual REE patterns are discussed in detail in figures 443, 444 and 445.

442- Chondrite normalised REE patterns: Post Archean shale composites and averages (after Taylor and McClennan, 1985)
This diagram displays the chondrite normalised REE patterns of post-Archean shale composites NASC and ES (North American shale composite and European shale composite respectively) and the PAAS (Post-Archean average Australian shale). Note the strong uniformity of patterns with high abundances (compared to chondritic meteorites) light REE enrichment, relatively flat heavy REE patterns and most importantly, a significant negative Eu-anomaly. The enrichment or depletion of europium (Eu) is assessed in relation to the neighbouring REE, samarium (Sm) and gadolinium (Gd) following the calculation of the theoretical Eu concentration (assuming a smooth REE pattern in the region Sm-Eu-Gd). These patterns most closely resemble granodioritic compositions are interpreted by Taylor and McClennan (1985) to support the view that sedimentary REE patterns reflect the upper continental crust exposed to weathering and erosion.

443- Chondrite normalised REE patterns: Quartz Rich Greywackes (after Taylor and McClennan, 1985)
This diagram displays chondrite normalised REE data from selected Quartz-Rich greywackes plotted against PAAS for comparison. Samples include P39803 (Ordovician Greenland Group, New Zealand) and MK97 (Ordovician Bendigo Trough, Australia). The REE patterns displayed by the quartz-rich samples include LREE enrichment ($La_N/Y_N>8$) and strong Eu depletion (similar in magnitude to PAAS). As such quartz-rich greywackes are indistinguishable from typical post-Archean upper crust in terms of REE (as indicated by PAAS).

444- Chondrite normalised REE patterns: Quartz Intermediate Greywackes (after Taylor and McClennan, 1985)
This diagram displays chondrite normalised REE data from selected Quartz-Intermediate greywackes plotted against PAAS for comparison. Samples include both MK64 (Silurian- Devonian Waterbeach Formation, Australia) and T82/324 (Triassic Torlesse Group, New Zealand). The REE patterns displayed by the quartz-intermediate samples essentially parallel those of PAAS but with slightly lower LREE and slightly higher Eu/Eu* (though still demonstrating a major negative Eu-anomaly).

445- Chondrite normalised REE patterns: Quartz Poor Greywackes (after Taylor and McClennan, 1985)
This diagram displays chondrite normalised REE data from selected Quartz-Poor greywackes plotted against PAAS for comparison. Samples include both M277 and M285 from the Devonian Baldwin Formation of the Tamworth Trough, Australia. These samples are volcanogenic (andesite) in origin and a fore-arc setting for deposition with an undissected magmatic arc provenance (Chappell, 1968 and Nance, 1977). The REE patterns displayed by the quartz poor samples include lower LREE and La/Yb (compared to PAAS) with no Eu depletion. It is clear that calc-alkaline andesitic rocks were the primary source for these sediments.

FIGURE 441

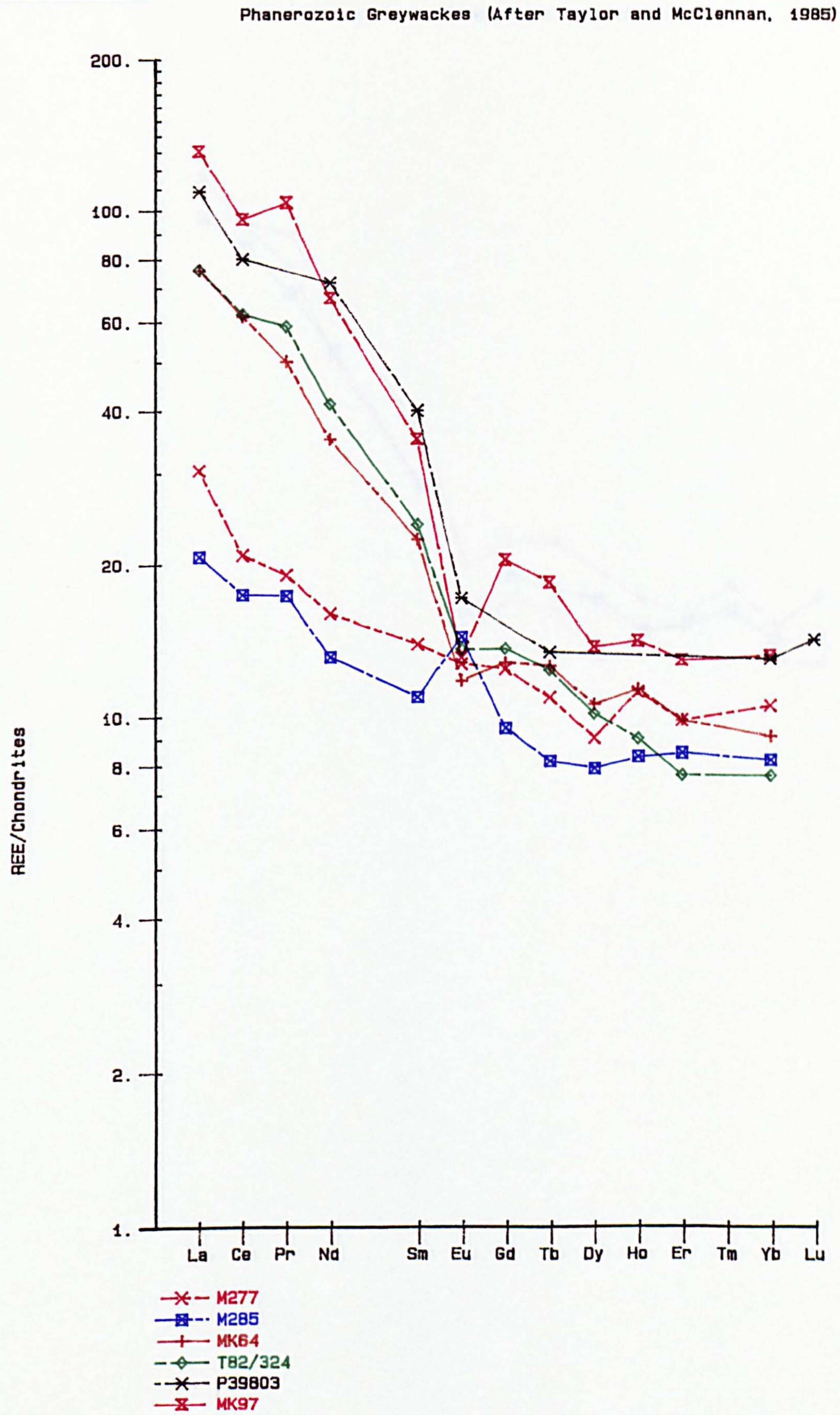
Phanerozoic Greywackes (After Taylor and McClennan, 1985)
REE/Chondrites
200.
100.
80.
60.
40.
20.
10.
8.
6.
4.
2.
1.
La
Ce
Pr
Nd
Sm
Eu
Gd
Tb
Dy
Ho
Er
Tm
Yb
Lu
M277
M285
MK64
T82/324
P39803
MK97

FIGURE 442

Post Archean Shale Composites and Averages :

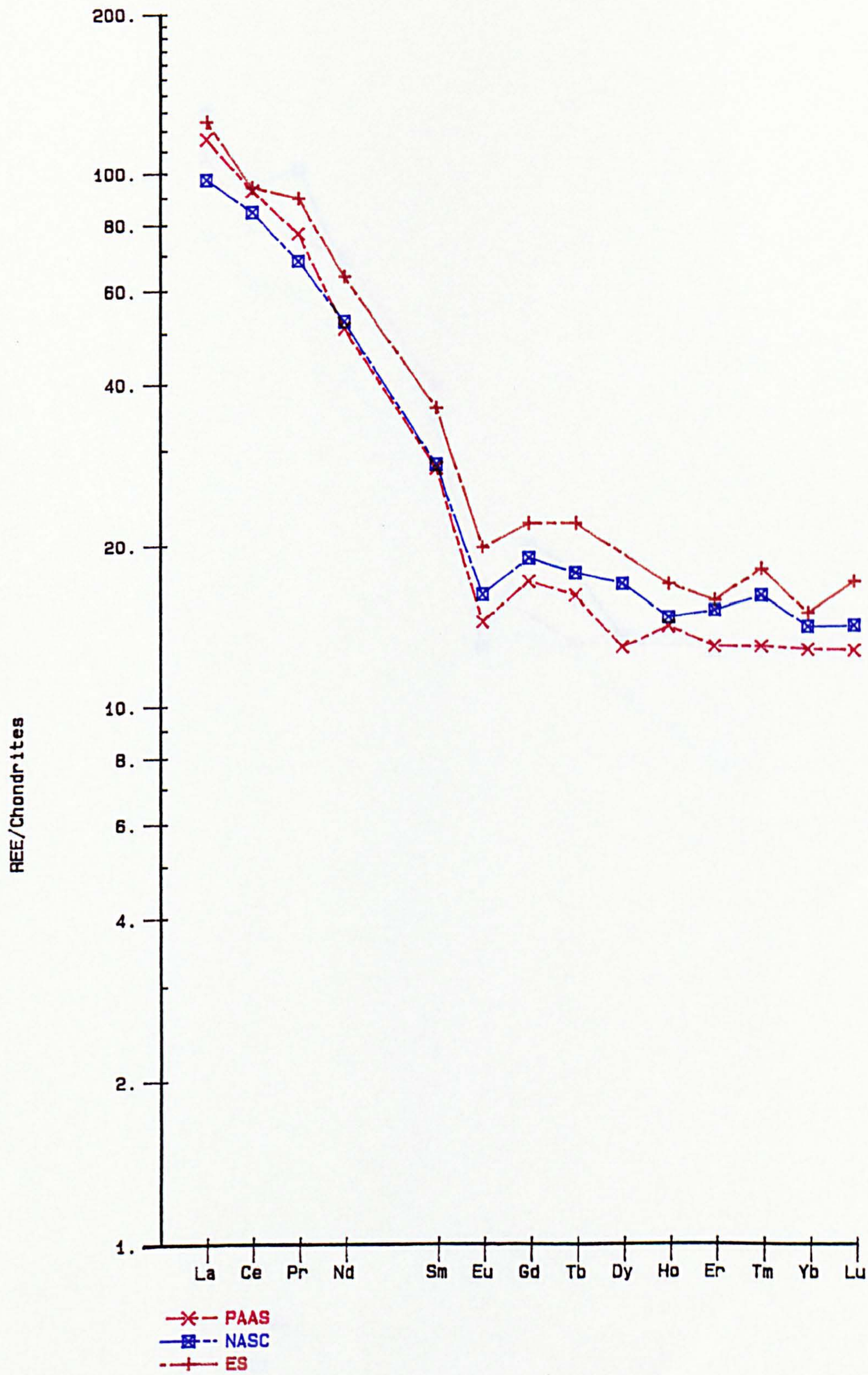

FIGURE 443

Quartz-rich Greywacke :

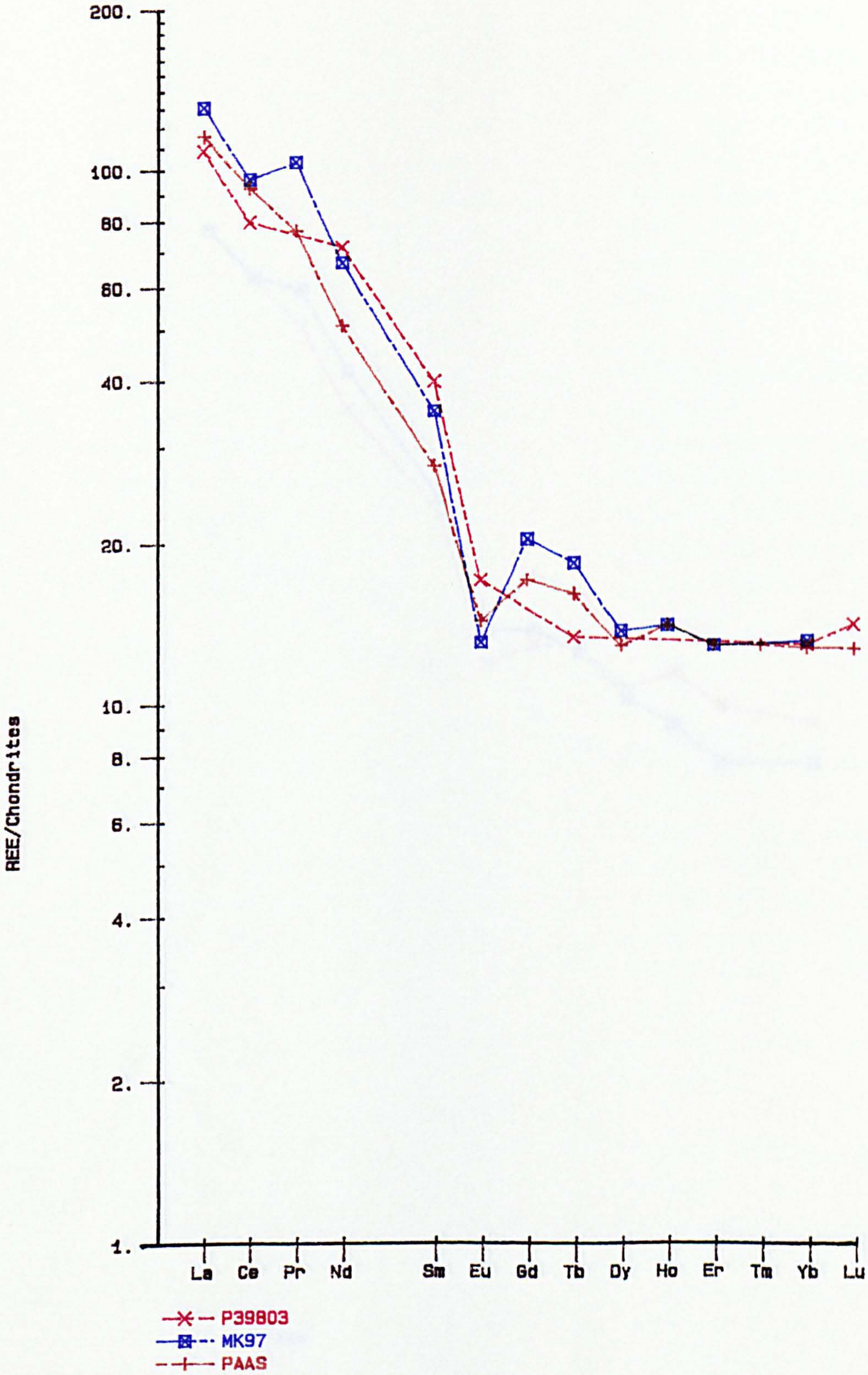

FIGURE 444

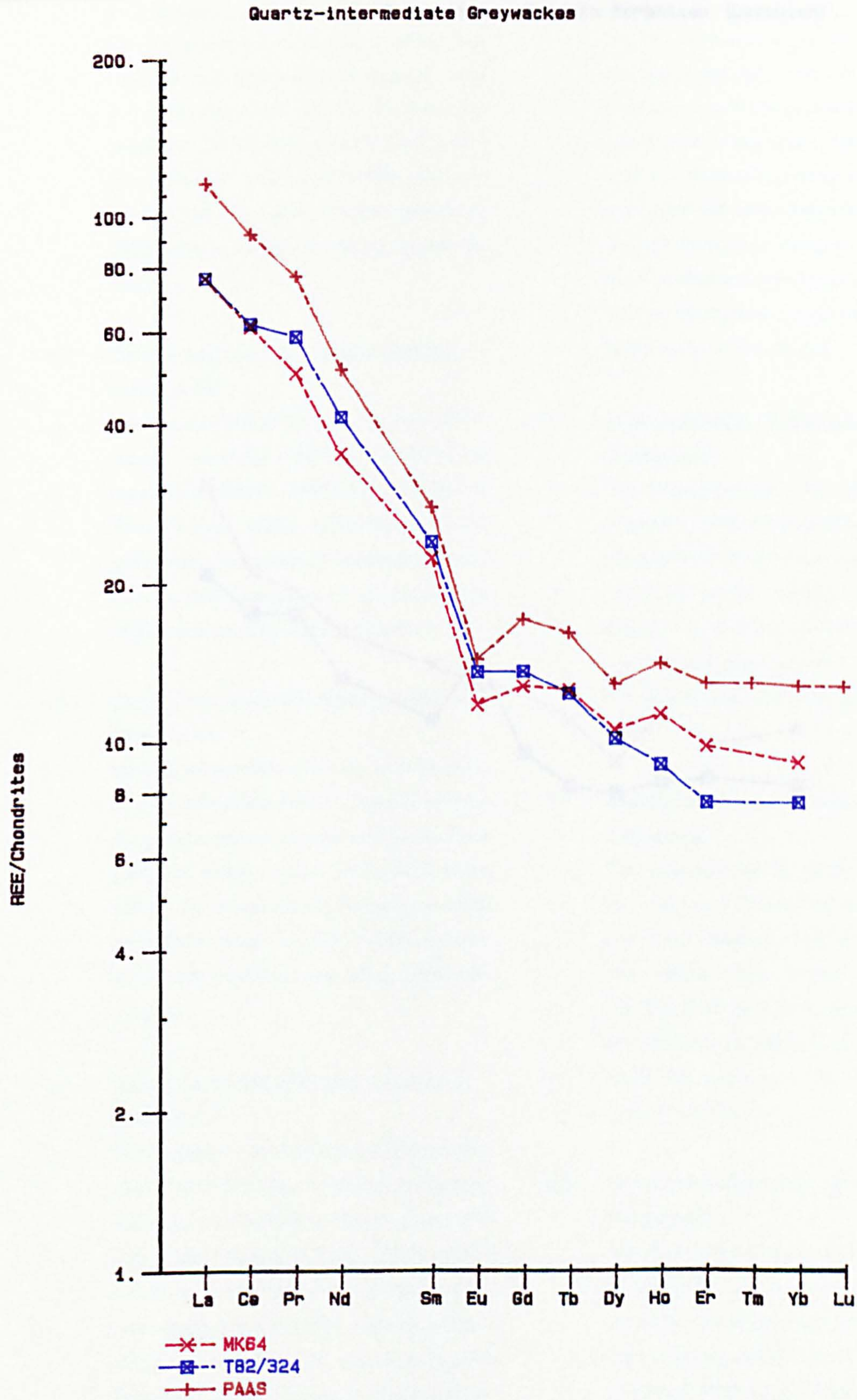
Quartz-intermediate Greywackes
200.
100.
80.
60.
40.
20.
10.
8.
6.
4.
2.
1.
REE/Chondrites
La
Ce
Pr
Nd
Sm
Eu
Gd
Tb
Dy
Ho
Er
Tm
Yb
Lu
MK64
T82/324
PAAS

FIGURE 445

Quartz-poor Greywackes : Baldwin Formation (Devonian).

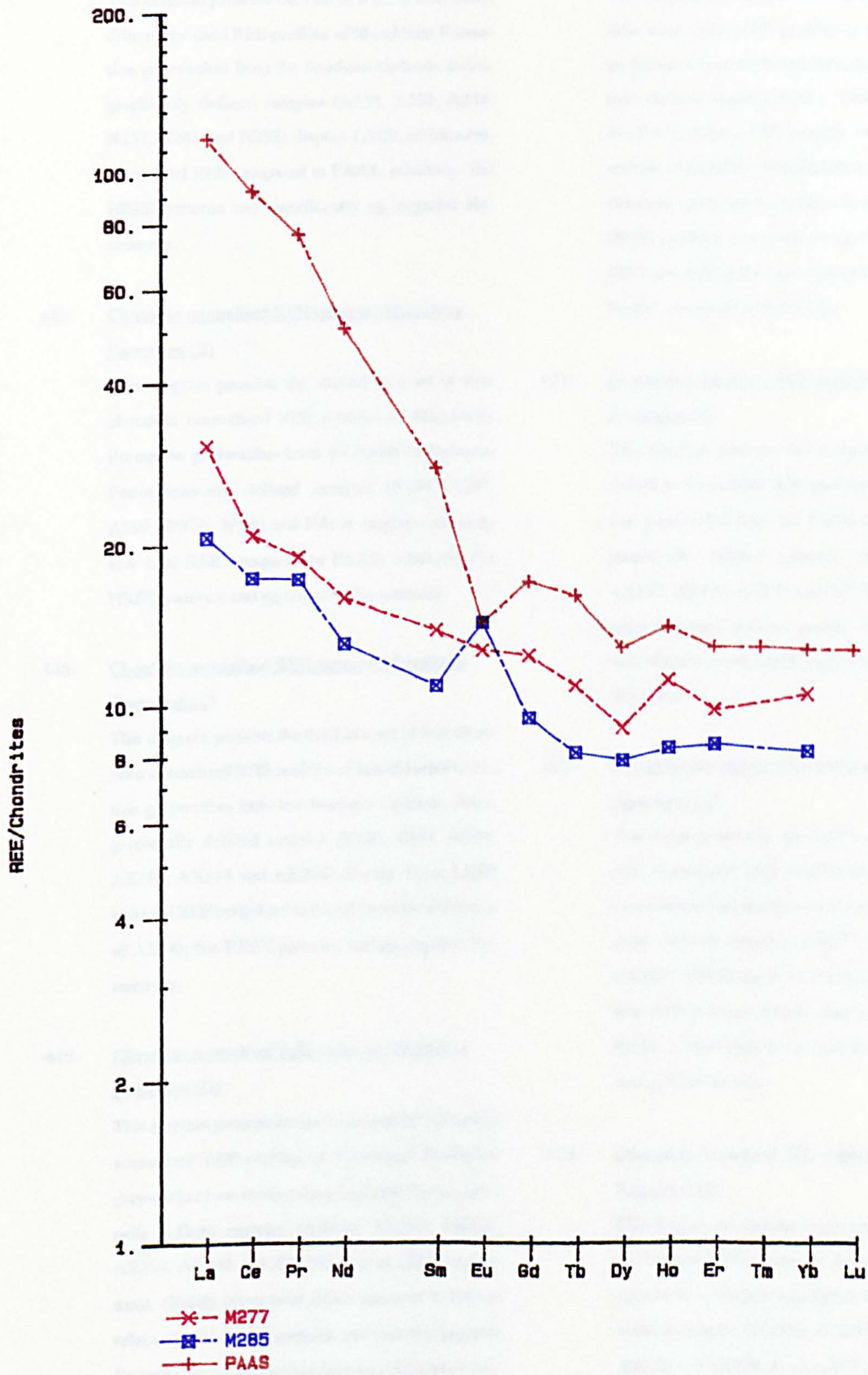

446- Chondrite normalised REE patterns: Marchburn Formation (A)

This diagram presents the first in a set of four chondrite normalised REE profiles of Marchburn Formation greywackes from the Southern Uplands. Petrographically defined samples (A232, A233, A234, N237, N241 and N292) display LREE enrichment; lower total REE compared to PAAS; relatively flat HREE patterns and significantly no negative Eu-anomaly.

447- Chondrite normalised REE patterns: Marchburn Formation (B)

This diagram presents the second in a set of four chondrite normalised REE profiles of Marchburn Formation greywackes from the Southern Uplands. Petrographically defined samples (N294, A297, A299, W379, W380 and N413) display extremely low total REE compared to PAAS; relatively flat HREE patterns; and no negative Eu-anomaly.

448- Chondrite normalised REE patterns: Marchburn Formation (C)

This diagram presents the third in a set of four chondrite normalised REE profiles of Marchburn Formation greywackes from the Southern Uplands. Petrographically defined samples (N426, C472, AX54, AX156, AX214 and AX215) display lower LREE and total REE compared to PAAS (with the exception of AX54); flat HREE patterns; and no negative Eu-anomaly.

449- Chondrite normalised REE patterns: Marchburn Formation (D)

This diagram presents the last in a set of four chondrite normalised REE profiles of Marchburn Formation greywackes from the Southern Uplands. Petrographically defined samples (AX216, AX217, AX224, AX292, AX293 and AX294) display LREE enrichment, slightly lower total REE compared to PAAS; relatively flat HREE patterns and lack the negative Eu-anomaly associated with quartz-rich, cratonic derived sediments. On the basis of the REE evidence presented in Figs. 446-449 it is clear that calc-alkaline andesitic rocks were the primary source for Marchburn Formation greywackes.

450- Chondrite normalised REE patterns: Afton Formation (A)

This diagram presents the first in a set of four chondrite normalised REE profiles of Afton Formation greywackes from the Southern Uplands. Petrographically defined samples (A222, E452, K462, A463 and C471) display REE patterns essentially parallel to those of PAAS but with slightly lower total REE enrichment (particularly notable in the relatively flat HREE profile); and (with the exception of samples E452 and K462) Eu depletion (with slightly higher Eu/Eu* compared with PAAS).

451- Chondrite normalised REE patterns: Afton Formation (B)

This diagram presents the second in a set of four chondrite normalised REE profiles of Afton Formation greywackes from the Southern Uplands. Petrographically defined samples (AX131, AX132, AX133, AX134, AX135 and AX136) display highly consistent REE patterns parallel to those of PAAS with slightly lower LREE enrichment and strong Eu depletion.

452- Chondrite normalised REE patterns: Afton Formation (C)

This diagram presents the third in a set of four chondrite normalised REE profiles of Afton Formation greywackes from the Southern Uplands. Petrographically defined samples (AX137, AX140, AX141, AX149, AX170 and AX171) display highly consistent REE patterns which closely parallel those of PAAS, with slightly lower total REE enrichment and strong Eu depletion.

453- Chondrite normalised REE patterns: Afton Formation (D)

This diagram presents the last in a set of four chondrite normalised REE profiles of Afton Formation greywackes from the Southern Uplands. Petrographically defined samples (AX172, AX202, AX204, AX222, AX223 and AX296) display REE patterns essentially parallel to those of PAAS but with slightly lower total REE enrichment; and Eu depletion. Sample AX298 however, displays lower total REE levels and no negative Eu anomaly. On the basis of REE evidence

FIGURE 446

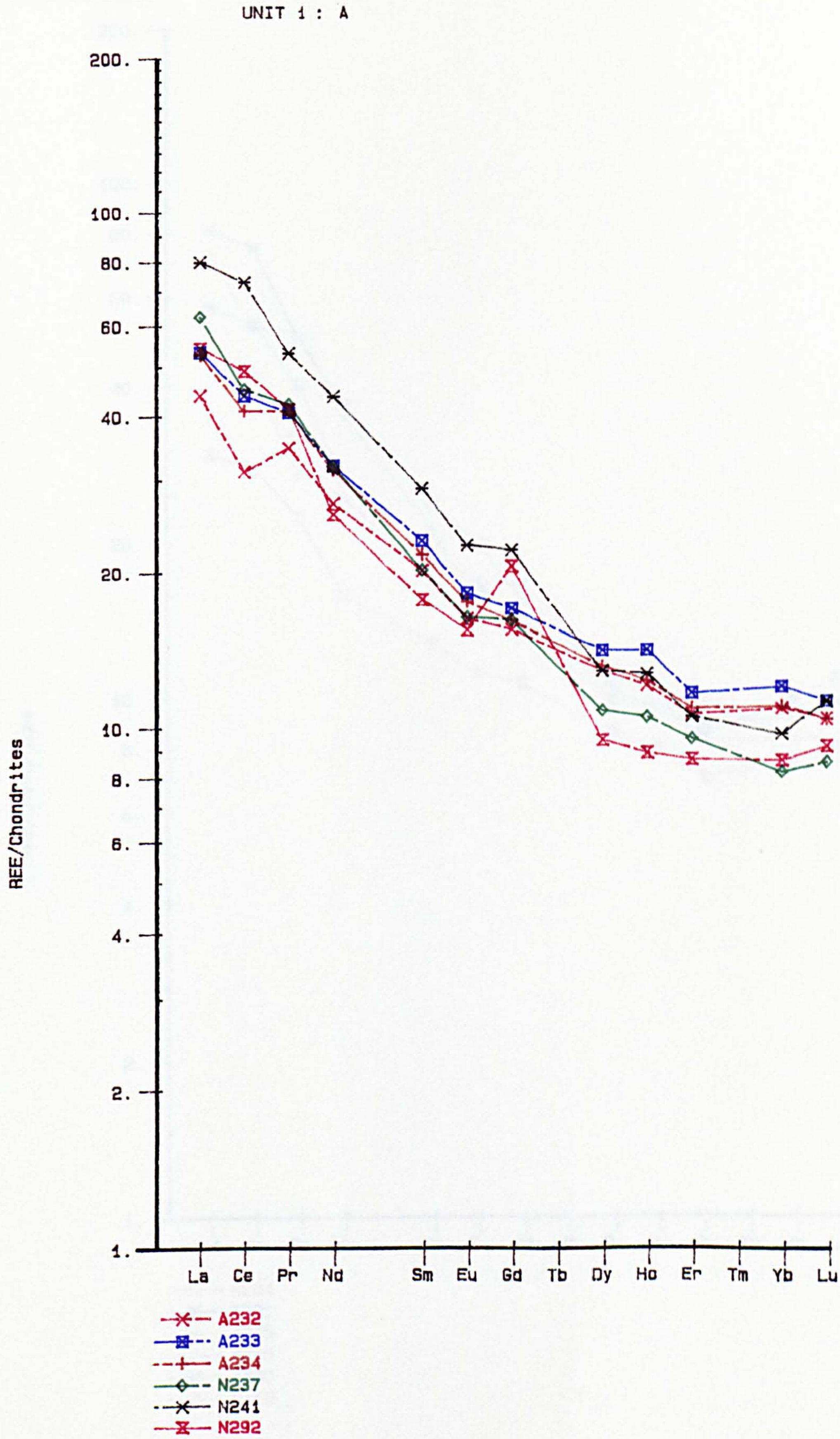
UNIT 1 : A
200.
100.
80.
60.
40.
20.
10.
8.
6.
4.
2.
1.
REE/Chondrites
La
Ce
Pr
Nd
Sm
Eu
Gd
Tb
Dy
Ho
Er
Tm
Yb
Lu
A232
A233
A234
N237
N241
N292

FIGURE 447

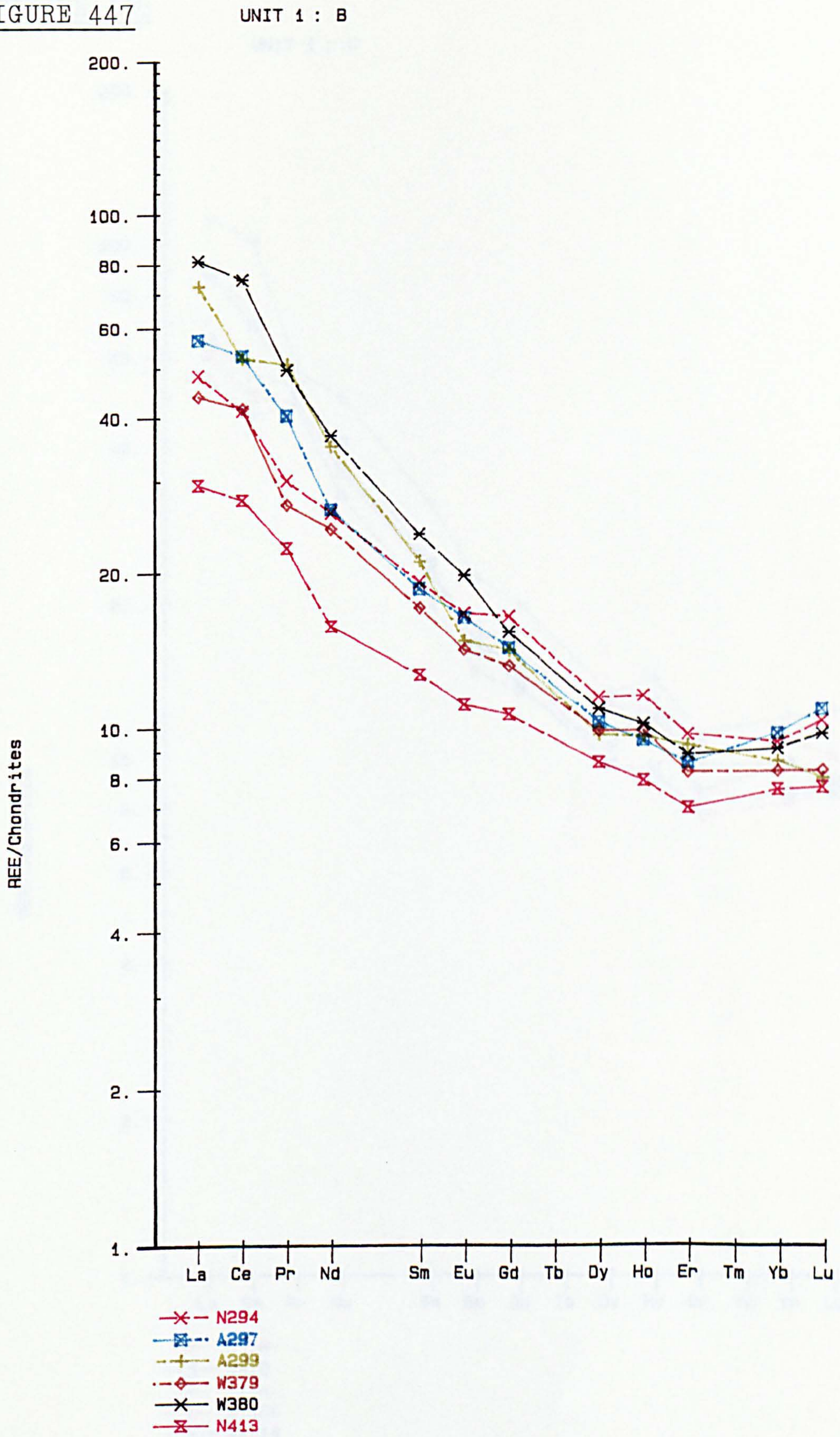
UNIT 1 : B
200.
100.
80.
60.
40.
20.
10.
8.
6.
4.
2.
1.
REE/Chondrites
La
Ce
Pr
Nd
Sm
Eu
Gd
Tb
Dy
Ho
Er
Tm
Yb
Lu
N294
A297
A299
W379
W380
N413

FIGURE 448

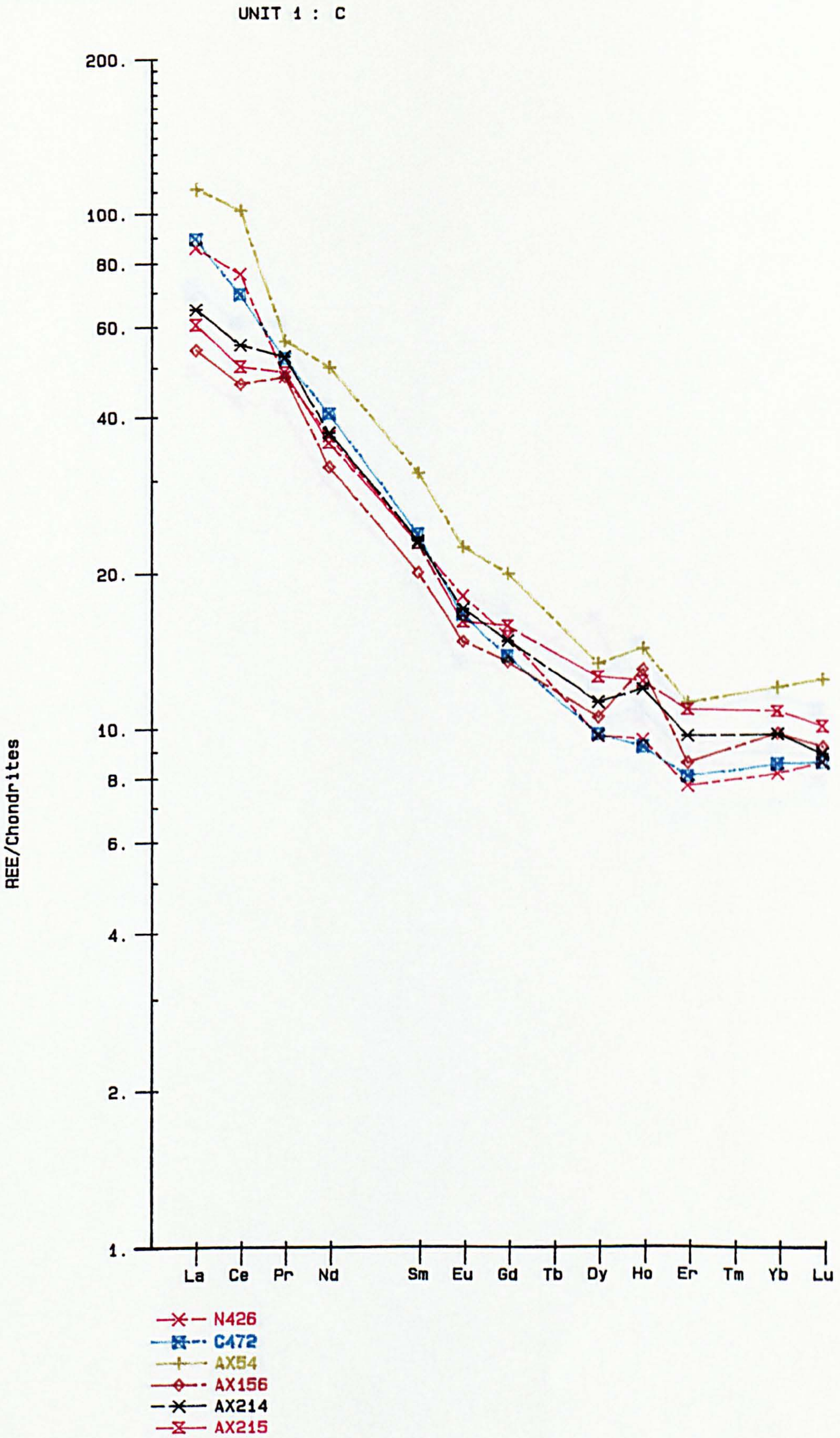
UNIT 1 : C
200.
100.
80.
60.
40.
20.
10.
8.
6.
4.
2.
1.
REE/Chondrites
La
Ce
Pr
Nd
Sm
Eu
Gd
Tb
Dy
Ho
Er
Tm
Yb
Lu
N426
C472
AX54
AX156
AX214
AX215

FIGURE 449

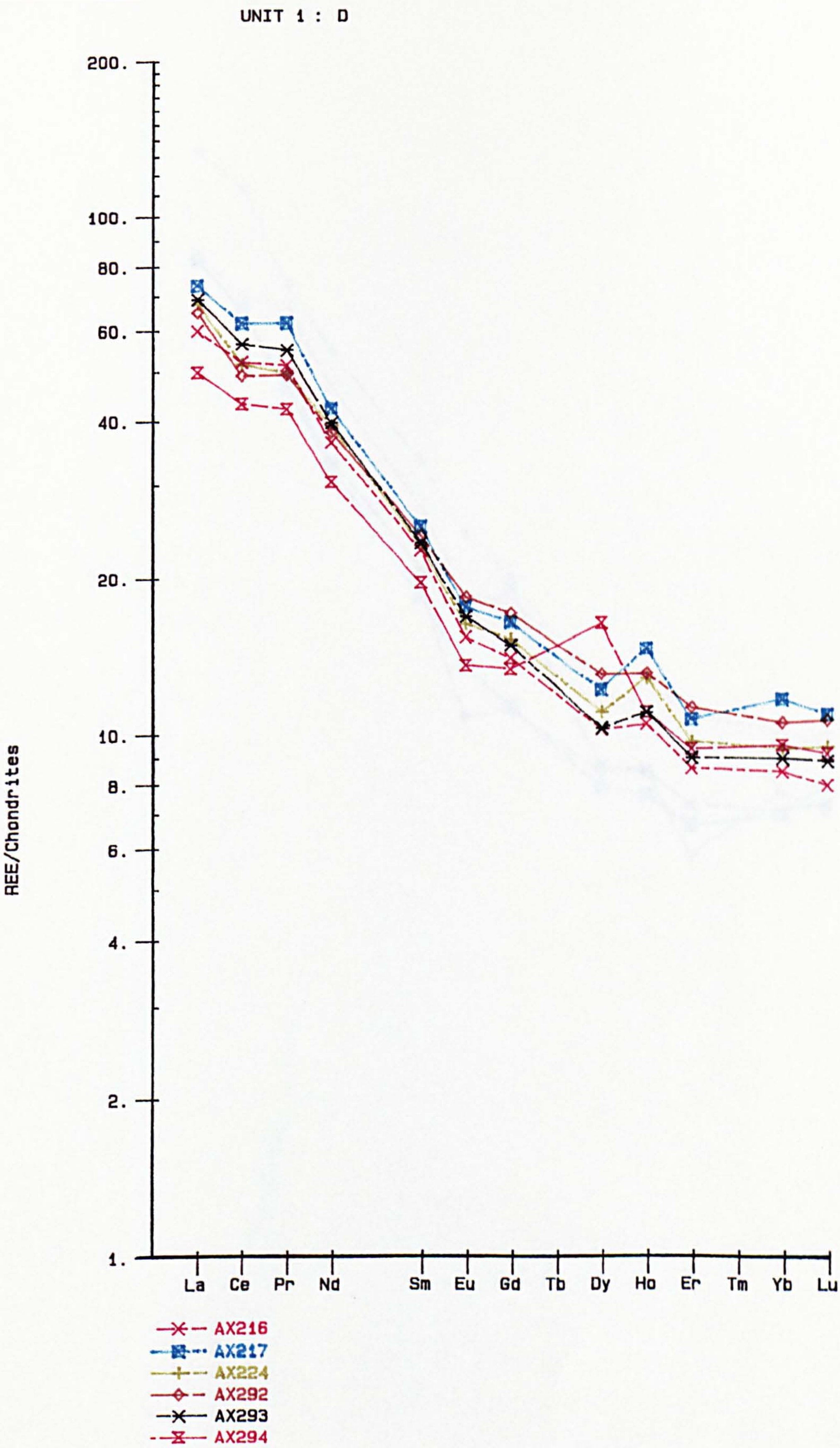
UNIT 1 : D
200.
100.
80.
60.
40.
20.
10.
8.
6.
4.
2.
1.
REE/Chondrites
La
Ce
Pr
Nd
Sm
Eu
Gd
Tb
Dy
Ho
Er
Tm
Yb
Lu
AX216
AX217
AX224
AX292
AX293
AX294

FIGURE 450

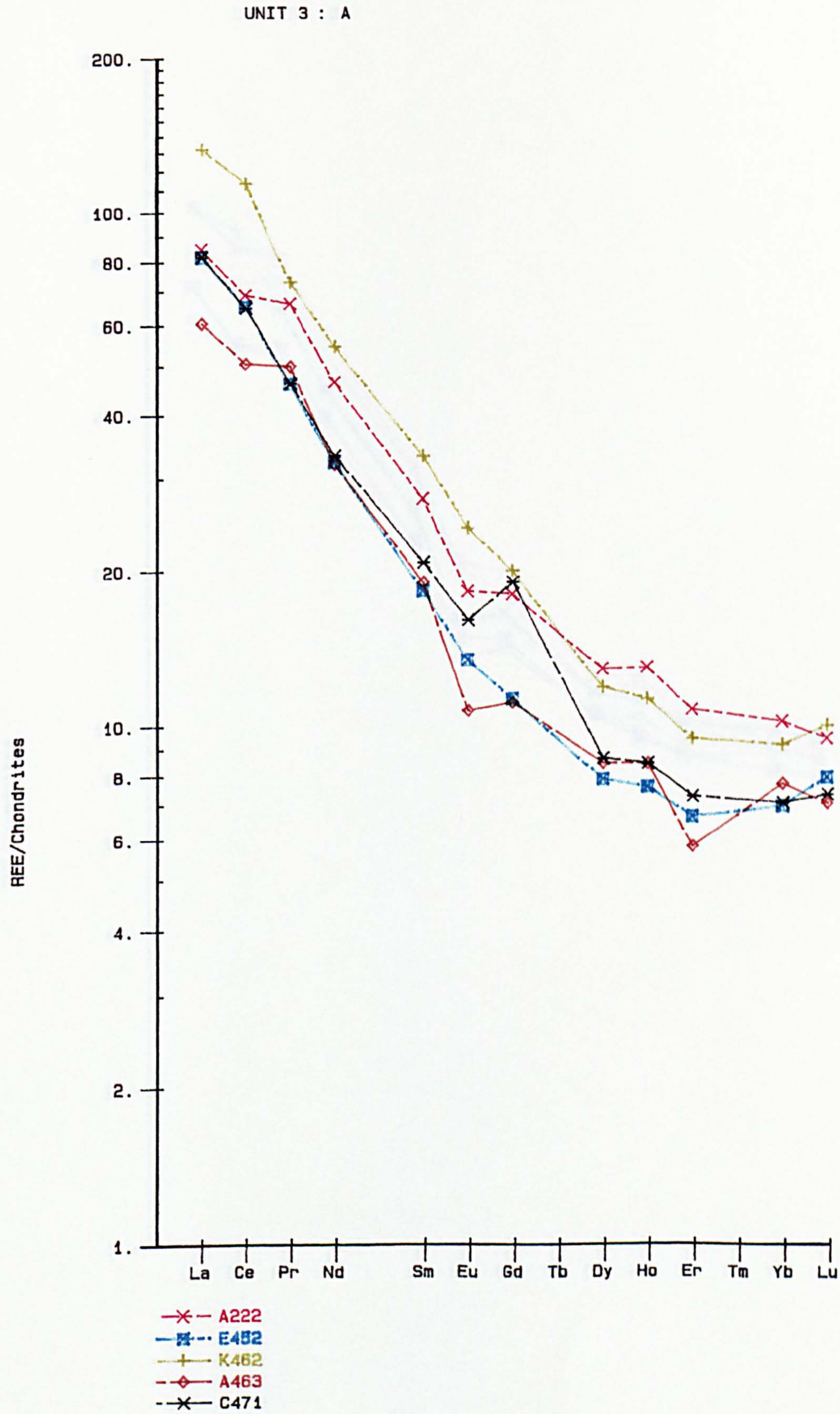
UNIT 3 : A
200.
100.
80.
60.
40.
20.
10.
8.
6.
4.
2.
1.
REE/Chondrites
La
Ce
Pr
Nd
Sm
Eu
Gd
Tb
Dy
Ho
Er
Tm
Yb
Lu
A222
E452
K462
A463
C471

FIGURE 451

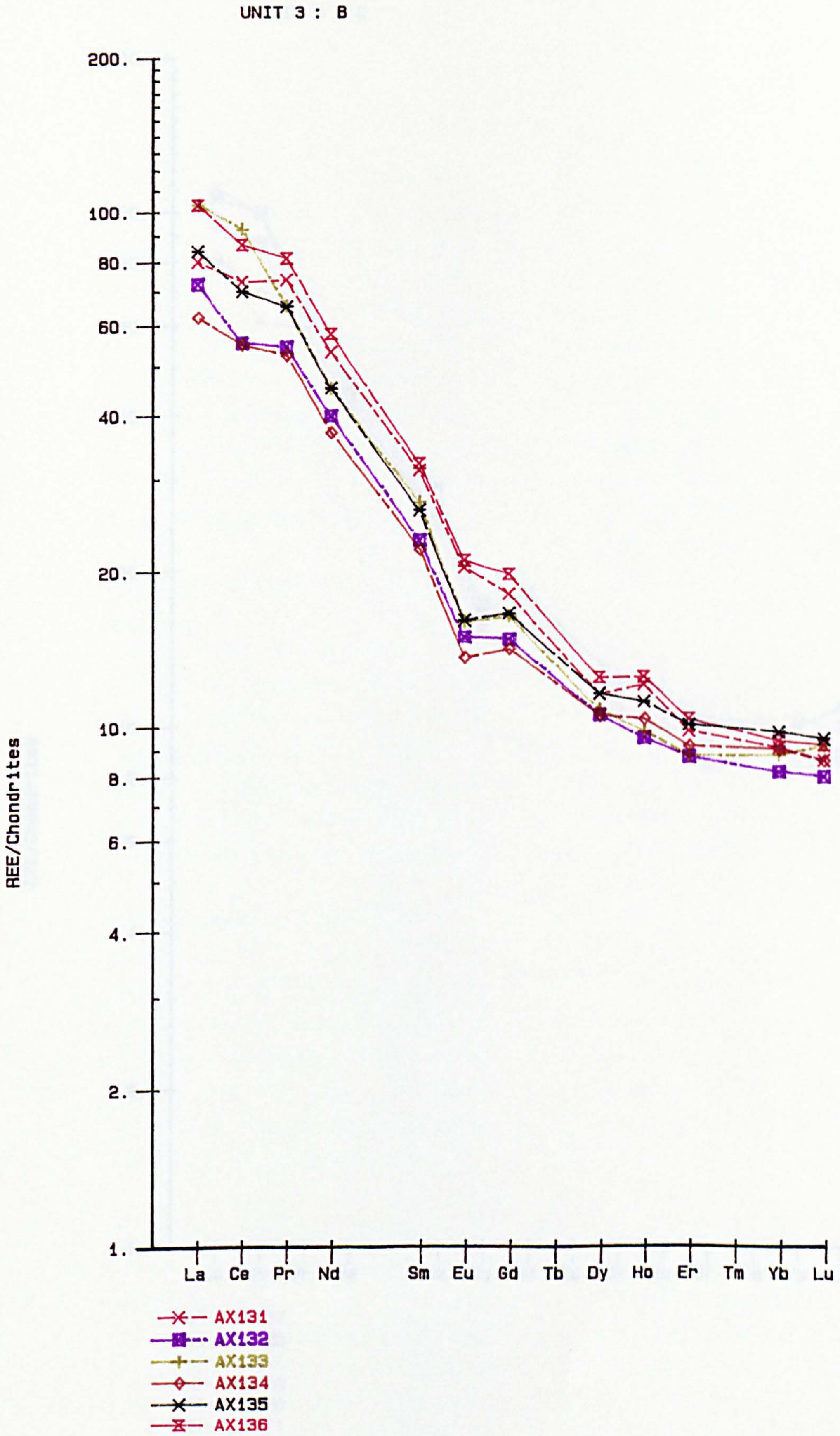
UNIT 3 : B
200.
100.
80.
60.
40.
20.
10.
8.
6.
4.
2.
1.
REE/Chondrites
La
Ce
Pr
Nd
Sm
Eu
Gd
Tb
Dy
Ho
Er
Tm
Yb
Lu
AX131
AX132
AX133
AX134
AX135
AX136

FIGURE 452

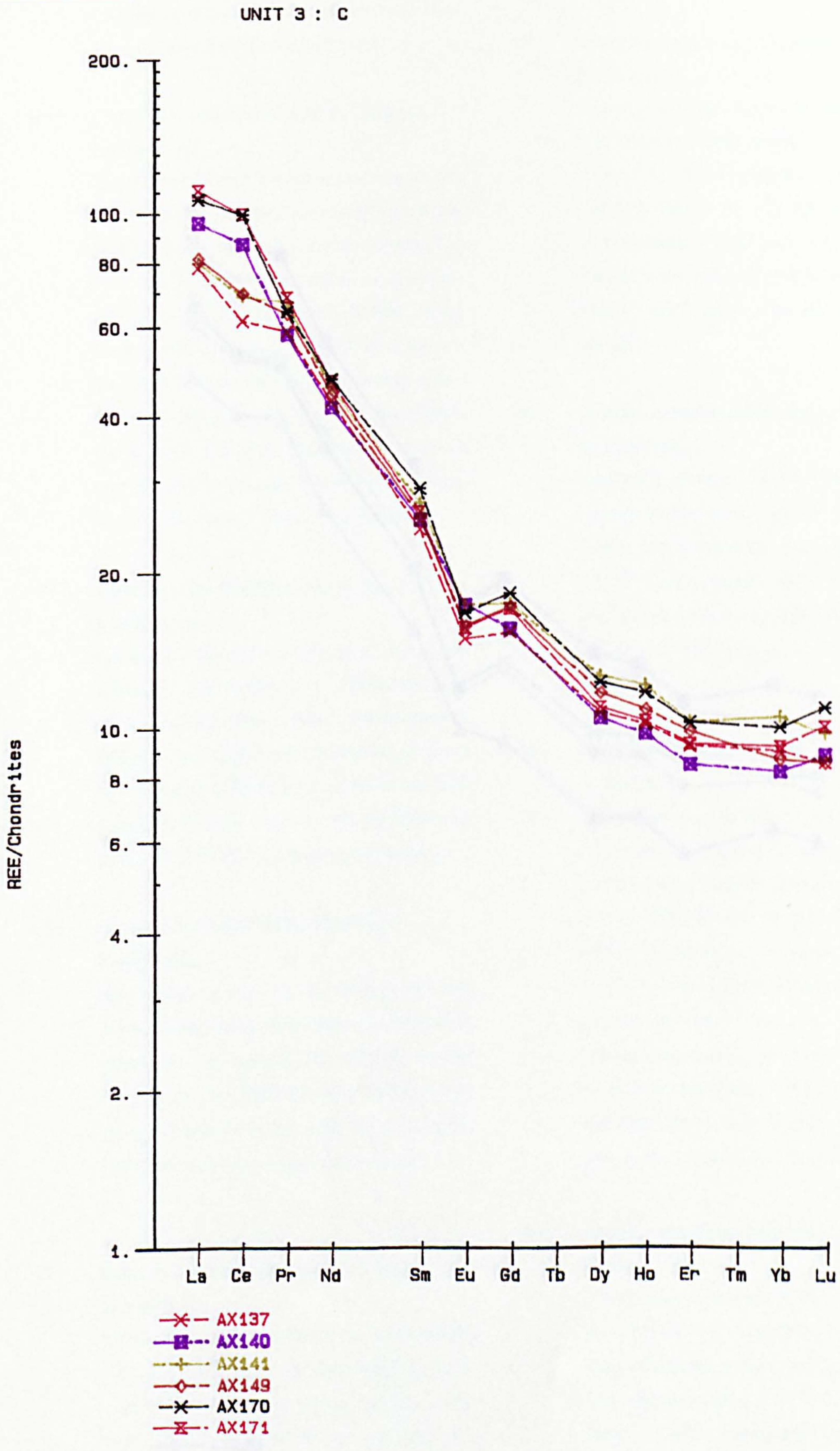
UNIT 3 : C
200.
100.
80.
60.
40.
20.
10.
8.
6.
4.
2.
1.
REE/Chondrites
La
Ce
Pr
Nd
Sm
Eu
Gd
Tb
Dy
Ho
Er
Tm
Yb
Lu
AX137
AX140
AX141
AX149
AX170
AX171

FIGURE 453

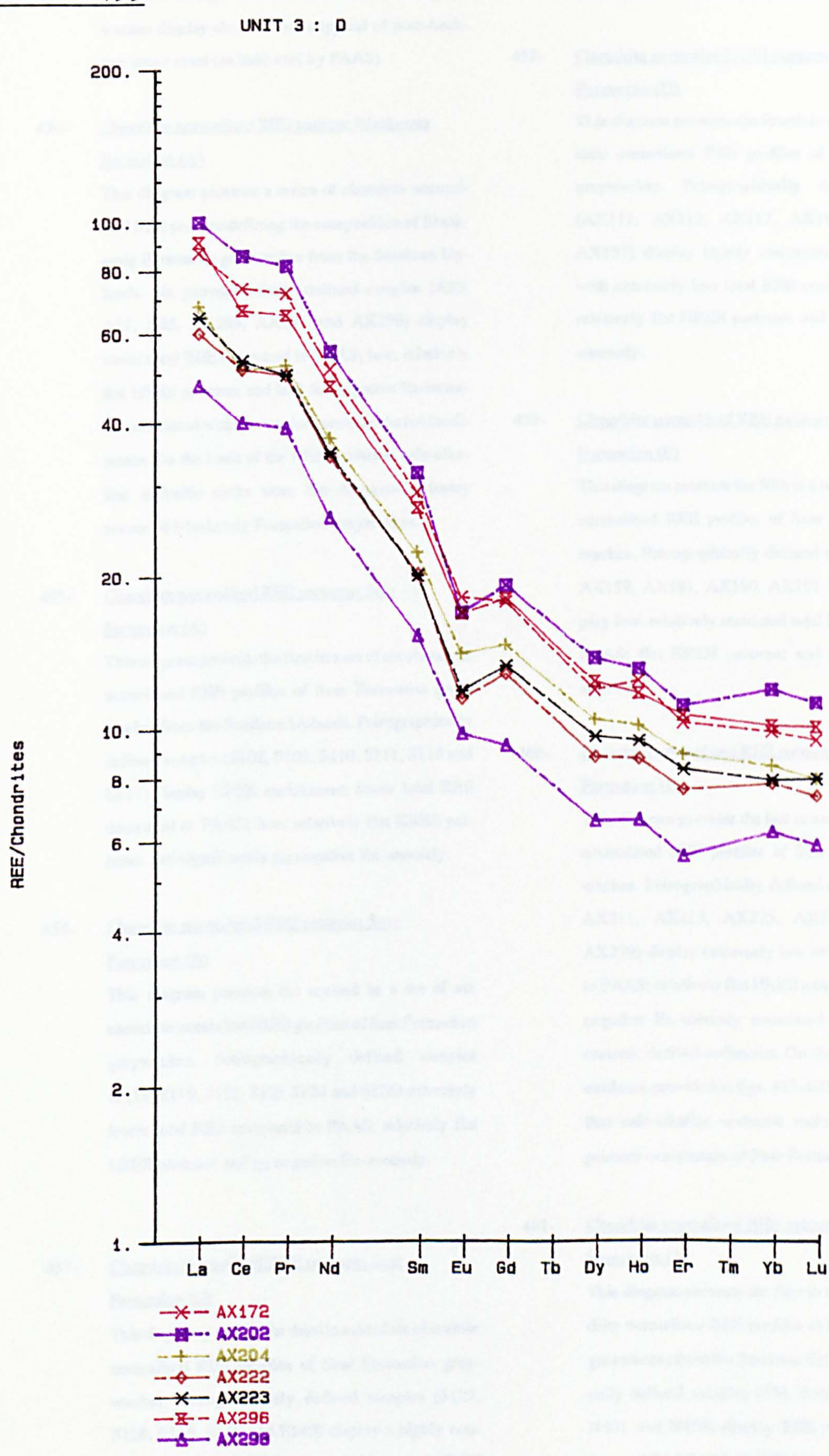
UNIT 3 : D
REE/Chondrites
200.
100.
80.
60.
40.
20.
10.
8.
6.
4.
2.
1.
La
Ce
Pr
Nd
Sm
Eu
Gd
Tb
Dy
Ho
Er
Tm
Yb
Lu
AX172
AX202
AX204
AX222
AX223
AX296
AX298

presented in Figs. 450-453 Afton Formation greywackes display characteristics typical of post-Archean upper crust (as indicated by PAAS).

454- Chondrite normalised REE pattern: Blackcraig Formation (A)

This diagram presents a series of chondrite normalised REE profiles defining the composition of Blackcraig Formation greywackes from the Southern Uplands. Six petrographically defined samples (A20, A21, A45, AX288, AX289 and AX290) display lower total REE compared to PAAS; low, relatively flat HREE patterns; and lack the negative Eu-anomaly associated with quartz-rich, cratonic derived sediments. On the basis of the REE evidence, calc-alkaline andesitic rocks were the dominant primary source of Blackcraig Formation greywackes.

455- Chondrite normalised REE patterns: Scar Formation (A)

This diagram presents the first in a set of six chondrite normalised REE profiles of Scar Formation greywackes from the Southern Uplands. Petrographically defined samples (S102, S105, S110, S111, S116 and E117) display LREE enrichment; lower total REE compared to PAAS; low, relatively flat HREE patterns; and significantly no negative Eu-anomaly.

456- Chondrite normalised REE patterns: Scar Formation (B)

This diagram presents the second in a set of six chondrite normalised REE profiles of Scar Formation greywackes. Petrographically defined samples (S118, S119, S121, S122 S124 and S126) extremely lower total REE compared to PAAS; relatively flat LREE patterns; and no negative Eu-anomaly.

457- Chondrite normalised REE patterns: Scar Formation (C)

This diagram presents the third in a set of six chondrite normalised REE profiles of Scar Formation greywackes. Petrographically defined samples (S127, S128, E136, E139 and E140) display a highly constrained pattern of REE values with low total REE compared to PAAS; low, relatively flat HREE patterns; and the absence of a negative Eu-anomaly.

458- Chondrite normalised REE patterns: Scar Formation (D)

This diagram presents the fourth in a set of six chondrite normalised REE profiles of Scar Formation greywackes. Petrographically defined samples (AX111, AX112, AX117, AX119, AX124 and AX157) display tightly constrained REE patterns with extremely low total REE compared to PAAS; relatively flat HREE patterns; and no negative Eu-anomaly.

459- Chondrite normalised REE patterns: Scar Formation (E)

This diagram presents the fifth in a set of six chondrite normalised REE profiles of Scar Formation greywackes. Petrographically defined samples (AX158, AX159, AX181, AX190, AX191 and AX200) display low, relatively restricted total REE compared to PAAS; flat HREE patterns; and no negative Eu-anomaly.

460- Chondrite normalised REE patterns: Scar Formation (F)

This diagram presents the last in a set of six chondrite normalised REE profiles of Scar Formation greywackes. Petrographically defined samples (AX210, AX211, AX213, AX275, AX277, AX278 and AX279) display extremely low total REE compared to PAAS; relatively flat HREE patterns; and lacks the negative Eu-anomaly associated with quartz-rich, cratonic derived sediments. On the basis of the REE evidence provided in figs. 455-460 it may be inferred that calc-alkaline andesitic rocks formed a major primary component of Scar Formation greywackes.

461- Chondrite normalised REE patterns: Shinnel Formation (A)

This diagram presents the first in a set of three chondrite normalised REE profiles of Shinnel Formation greywackes from the Southern Uplands. Petrographically defined samples (S54, S56, S58, S64, N400, N401 and N456) display REE patterns parallel to those of PAAS with slightly lower total REE levels; and Eu depletion anomalies.

FIGURE 454

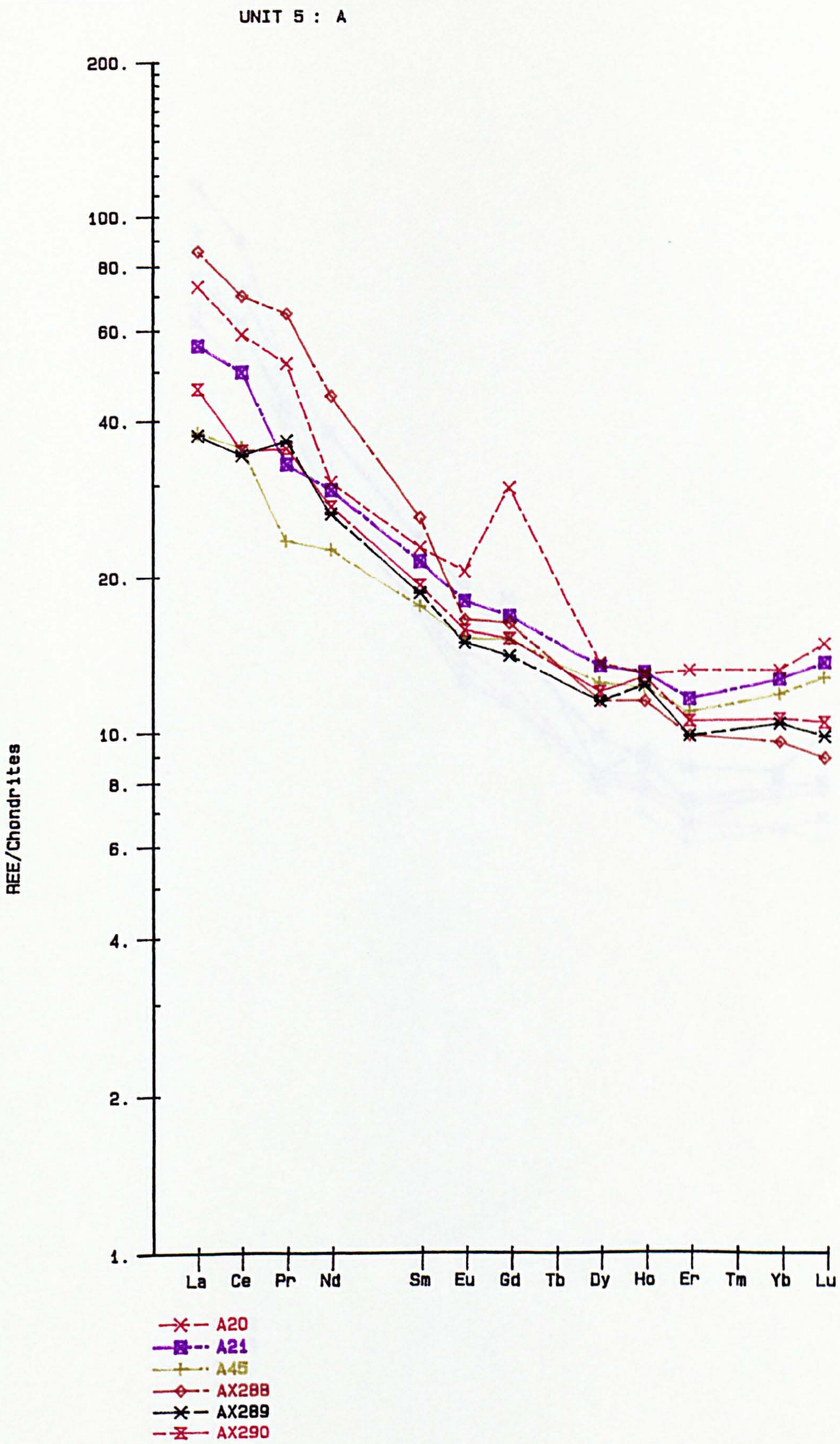
UNIT 5 : A
200.
100.
80.
60.
40.
20.
10.
8.
6.
4.
2.
1.
REE/Chondrites
La
Ce
Pr
Nd
Sm
Eu
Gd
Tb
Dy
Ho
Er
Tm
Yb
Lu
A20
A21
A45
AX288
AX289
AX290

FIGURE 455

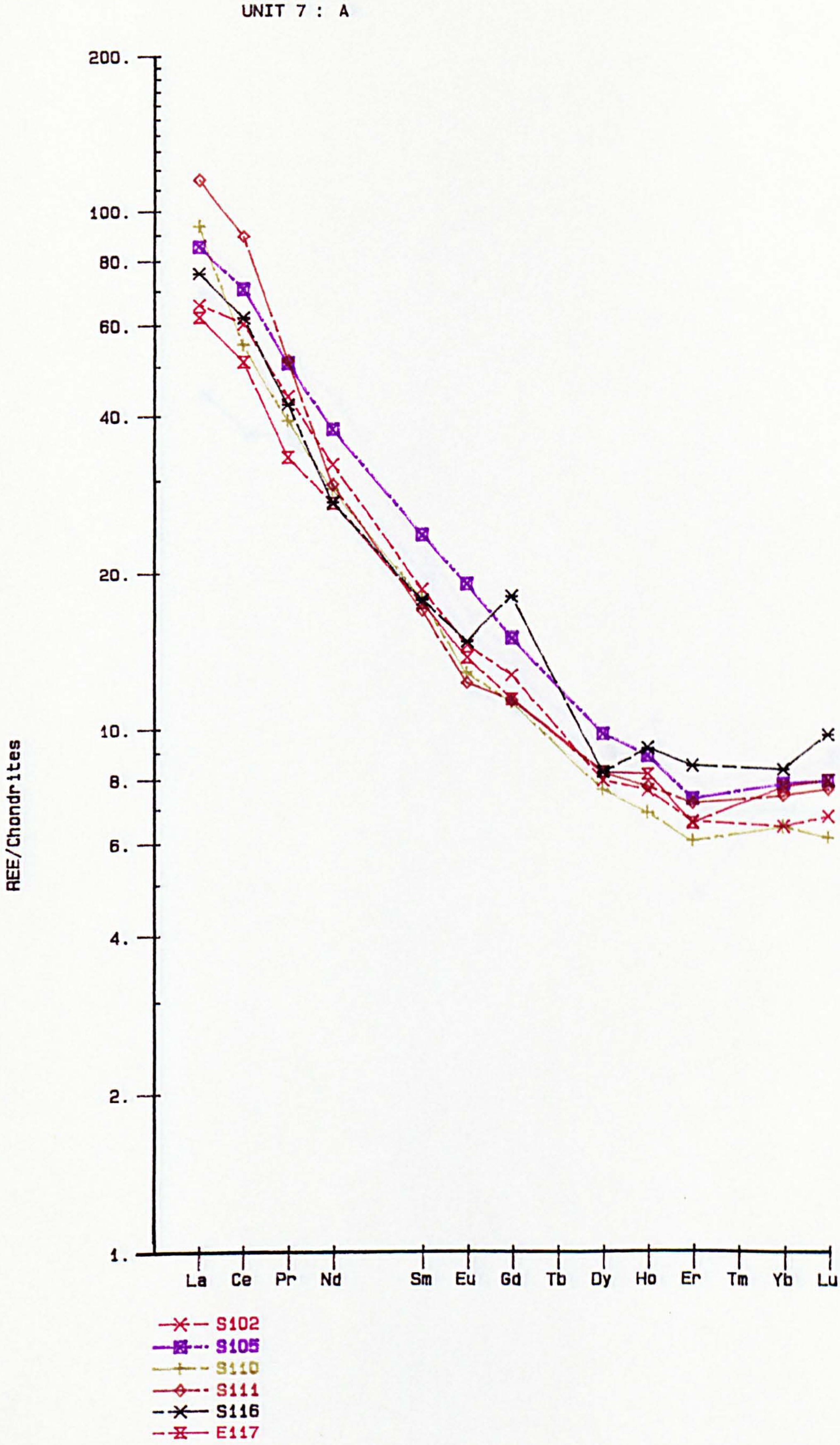
UNIT 7 : A
REE/Chondrites
200.
100.
80.
60.
40.
20.
10.
8.
6.
4.
2.
1.
La
Ce
Pr
Nd
Sm
Eu
Gd
Tb
Dy
Ho
Er
Tm
Yb
Lu
S102
S105
S110
S111
S116
E117

FIGURE 456

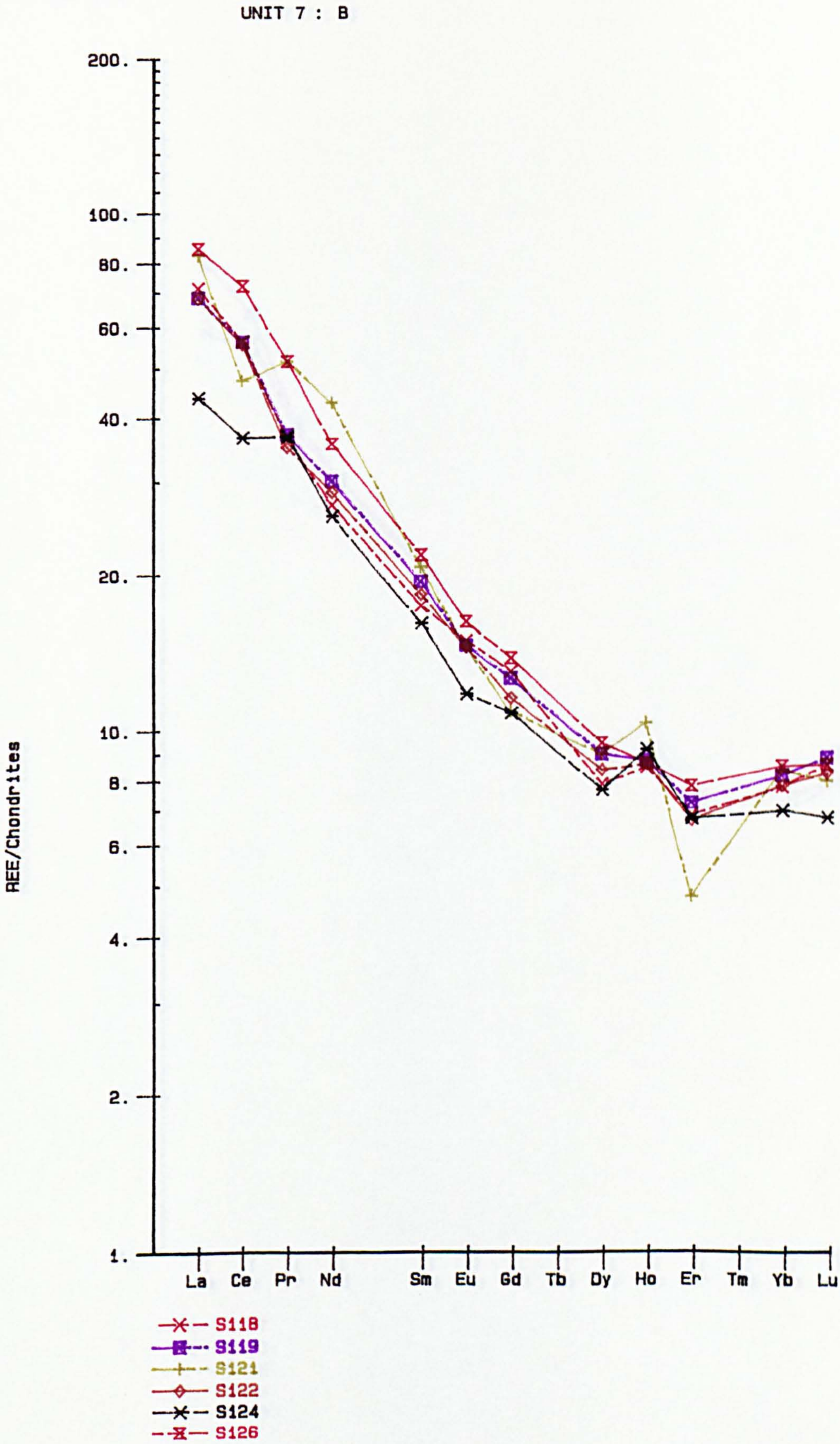
UNIT 7 : B
200.
100.
80.
60.
40.
20.
10.
8.
6.
4.
2.
1.
REE/Chondrites
La
Ce
Pr
Nd
Sm
Eu
Gd
Tb
Dy
Ho
Er
Tm
Yb
Lu
S118
S119
S121
S122
S124
S126

FIGURE 457

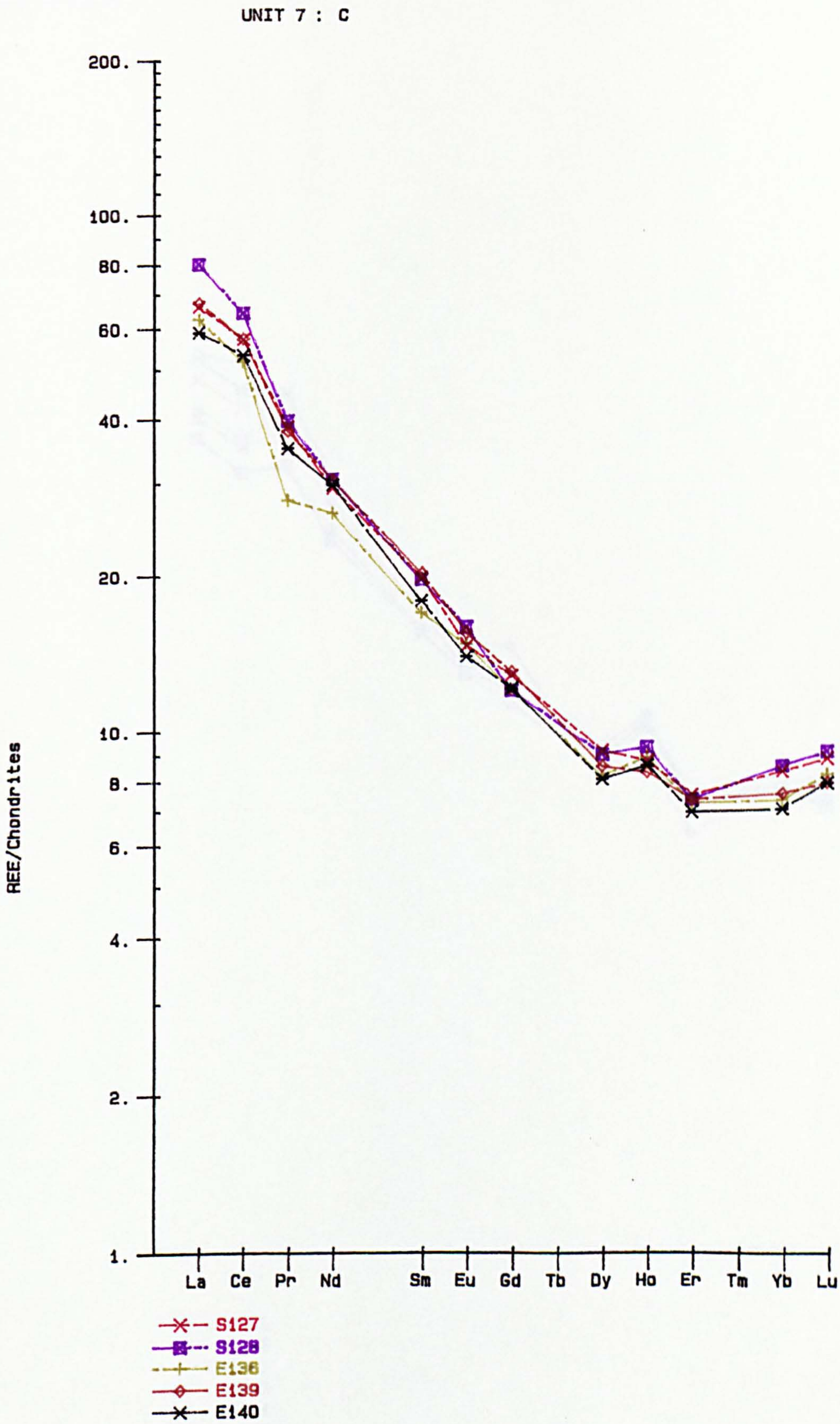
UNIT 7 : C
200.
100.
80.
60.
40.
20.
10.
8.
6.
4.
2.
1.
REE/Chondrites
La
Ce
Pr
Nd
Sm
Eu
Gd
Tb
Dy
Ho
Er
Tm
Yb
Lu
S127
S128
E136
E139
E140

FIGURE 458

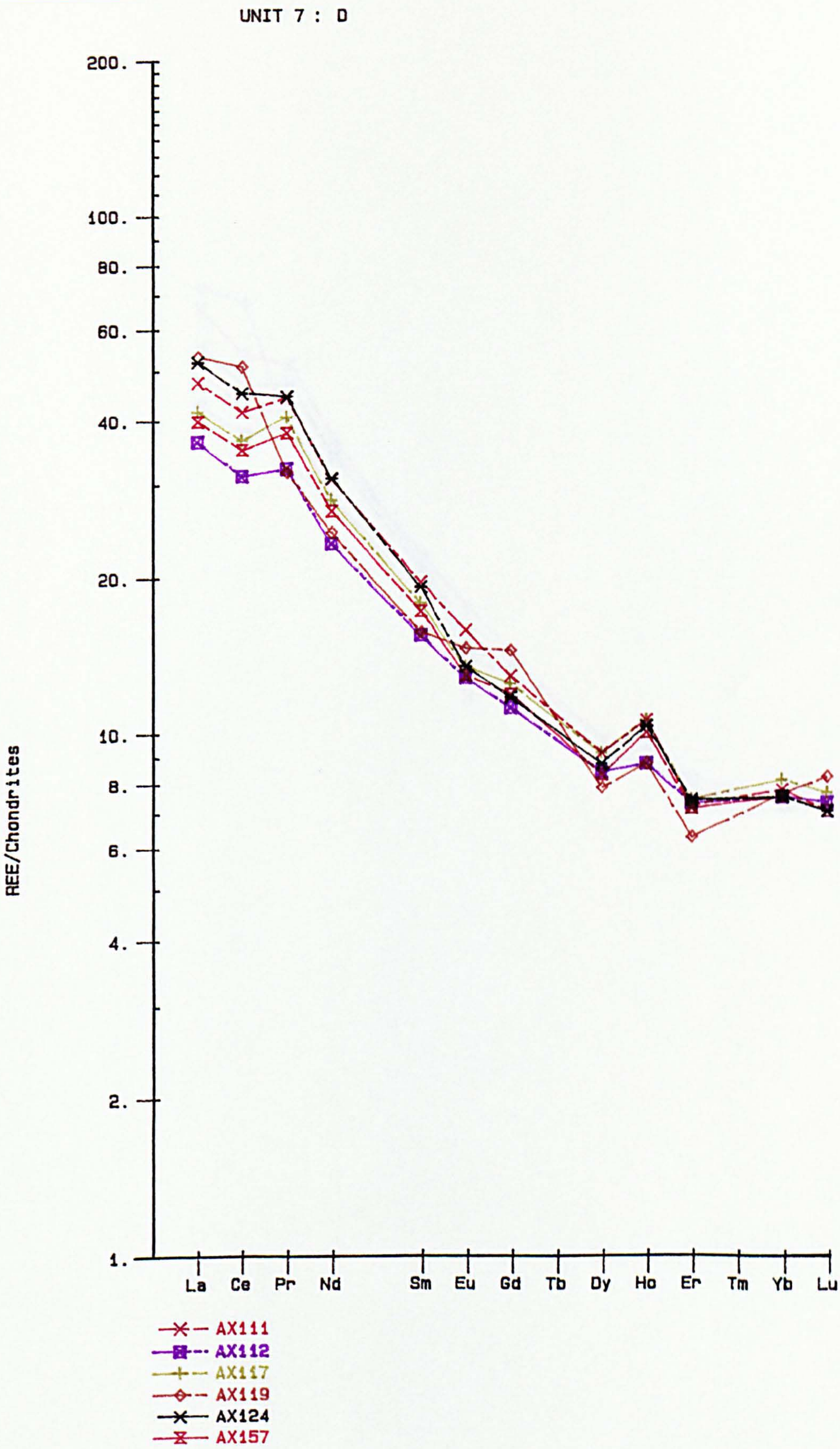
UNIT 7 : D
200.
100.
80.
60.
40.
20.
10.
8.
6.
4.
2.
1.
REE/Chondrites
La
Ce
Pr
Nd
Sm
Eu
Gd
Tb
Dy
Ho
Er
Tm
Yb
Lu
AX111
AX112
AX117
AX119
AX124
AX157

FIGURE 459

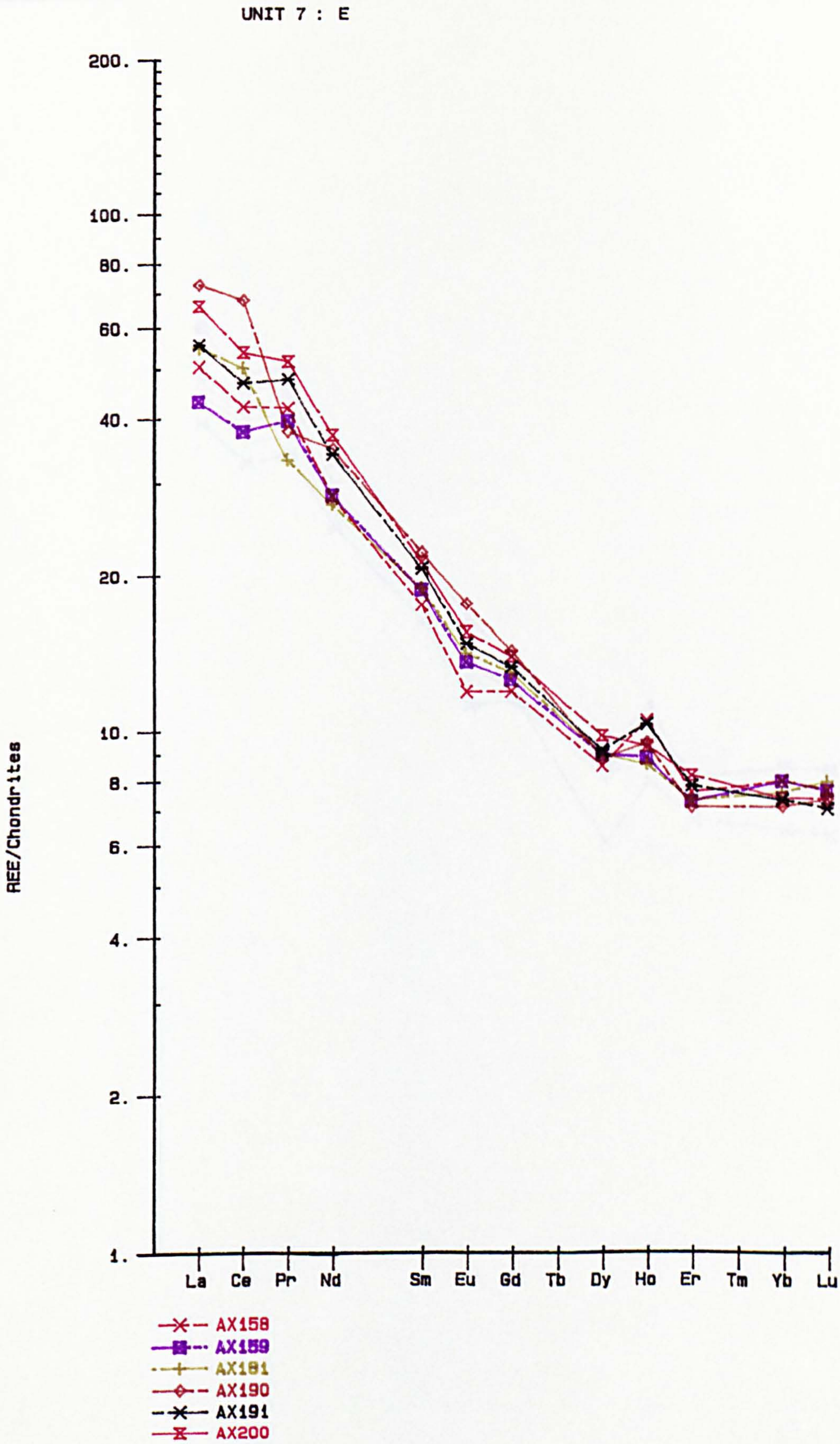
UNIT 7 : E
200.
100.
80.
60.
40.
20.
10.
8.
6.
4.
2.
1.
REE/Chondrites
La
Ce
Pr
Nd
Sm
Eu
Gd
Tb
Dy
Ho
Er
Tm
Yb
Lu
AX158
AX159
AX181
AX190
AX191
AX200

FIGURE 460

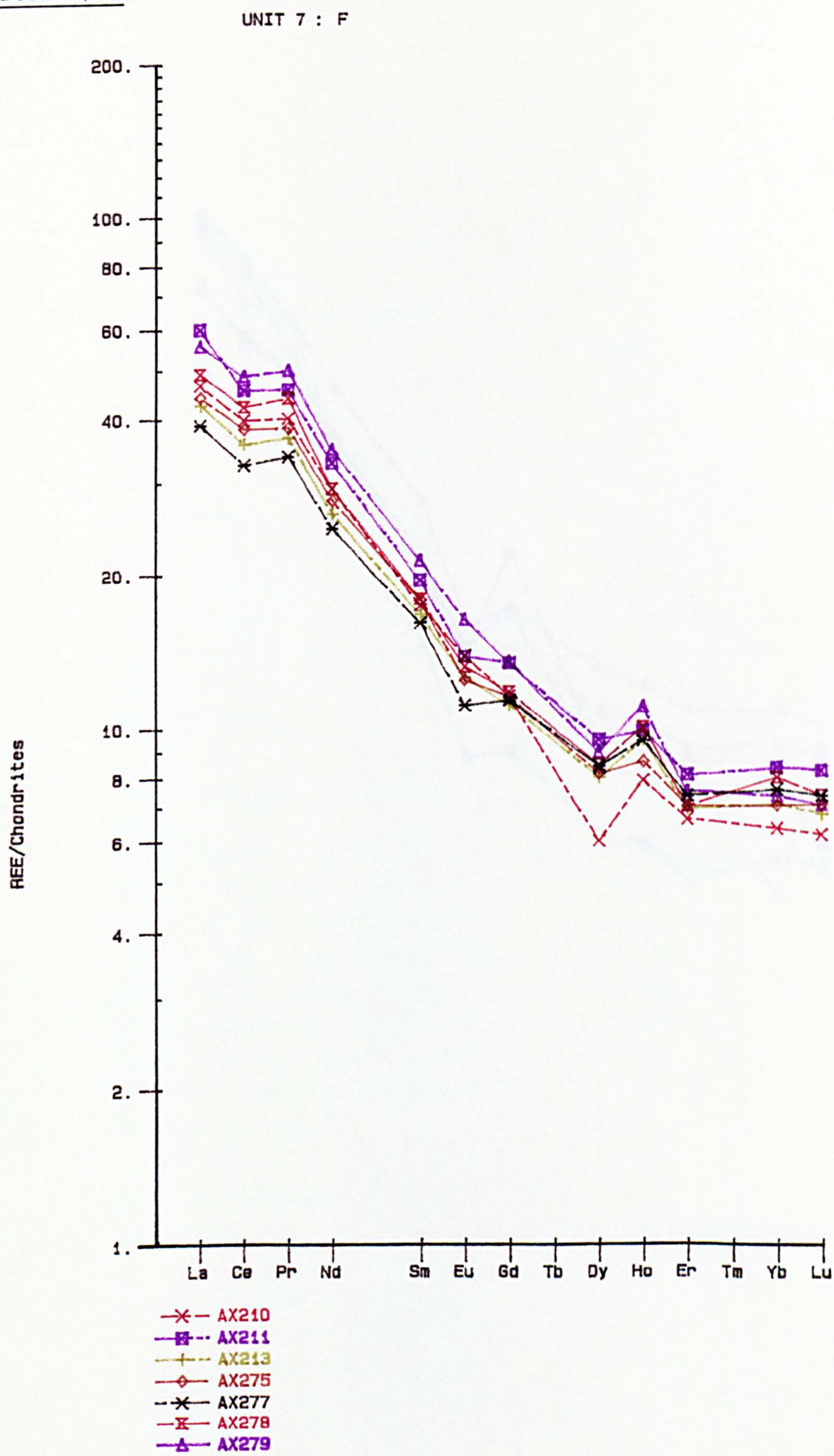
UNIT 7 : F
200.
100.
80.
60.
40.
20.
10.
8.
6.
4.
2.
1.
REE/Chondrites
La
Ce
Pr
Nd
Sm
Eu
Gd
Tb
Dy
Ho
Er
Tm
Yb
Lu
AX210
AX211
AX213
AX275
AX277
AX278
AX279

FIGURE 461

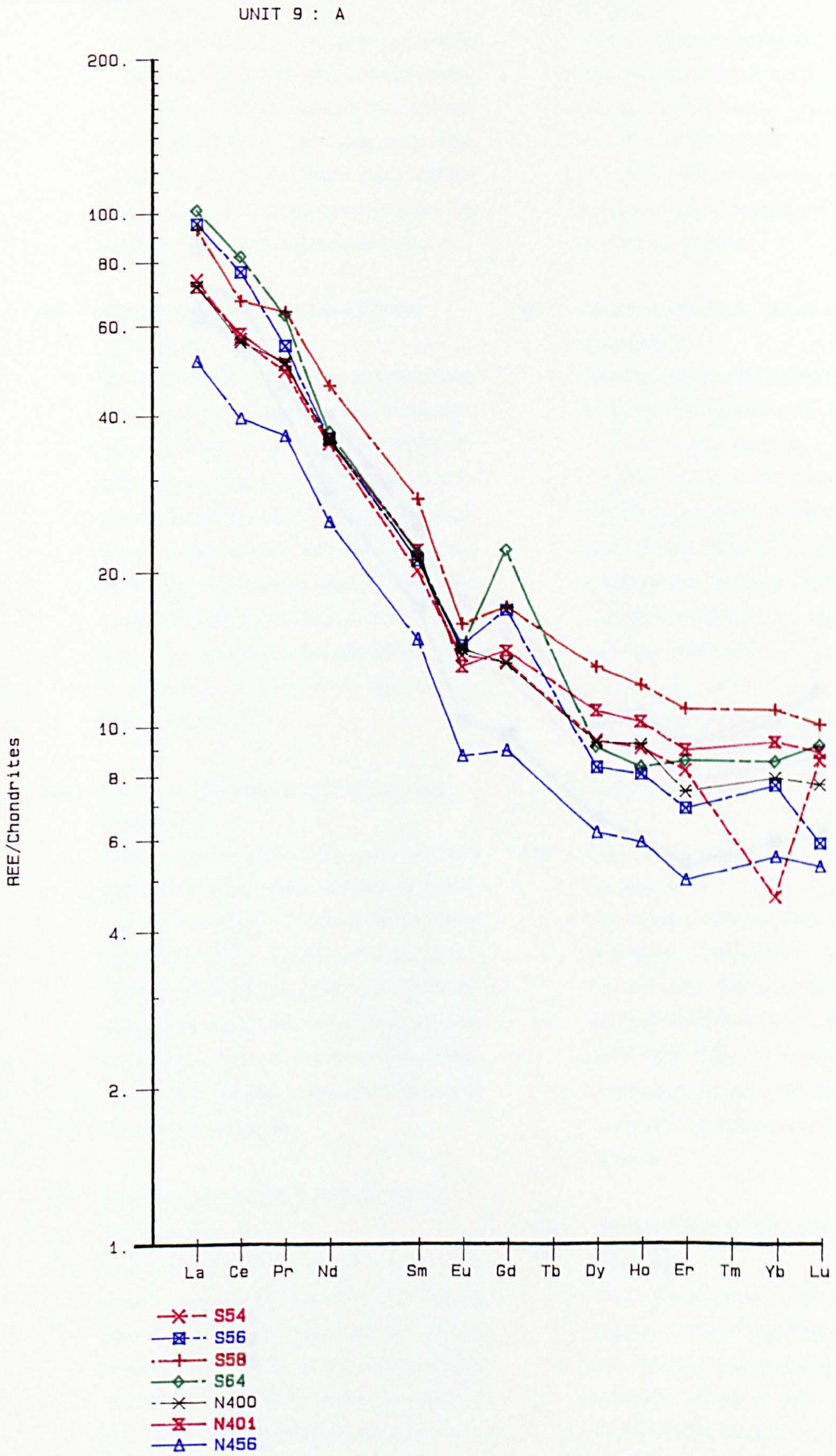
UNIT 9 : A
REE/Chondrites
200.
100.
80.
60.
40.
20.
10.
8.
6.
4.
2.
1.
La
Ce
Pr
Nd
Sm
Eu
Gd
Tb
Dy
Ho
Er
Tm
Yb
Lu
S54
S56
S58
S64
N400
N401
N456

FIGURE 462

UNIT 9 : B

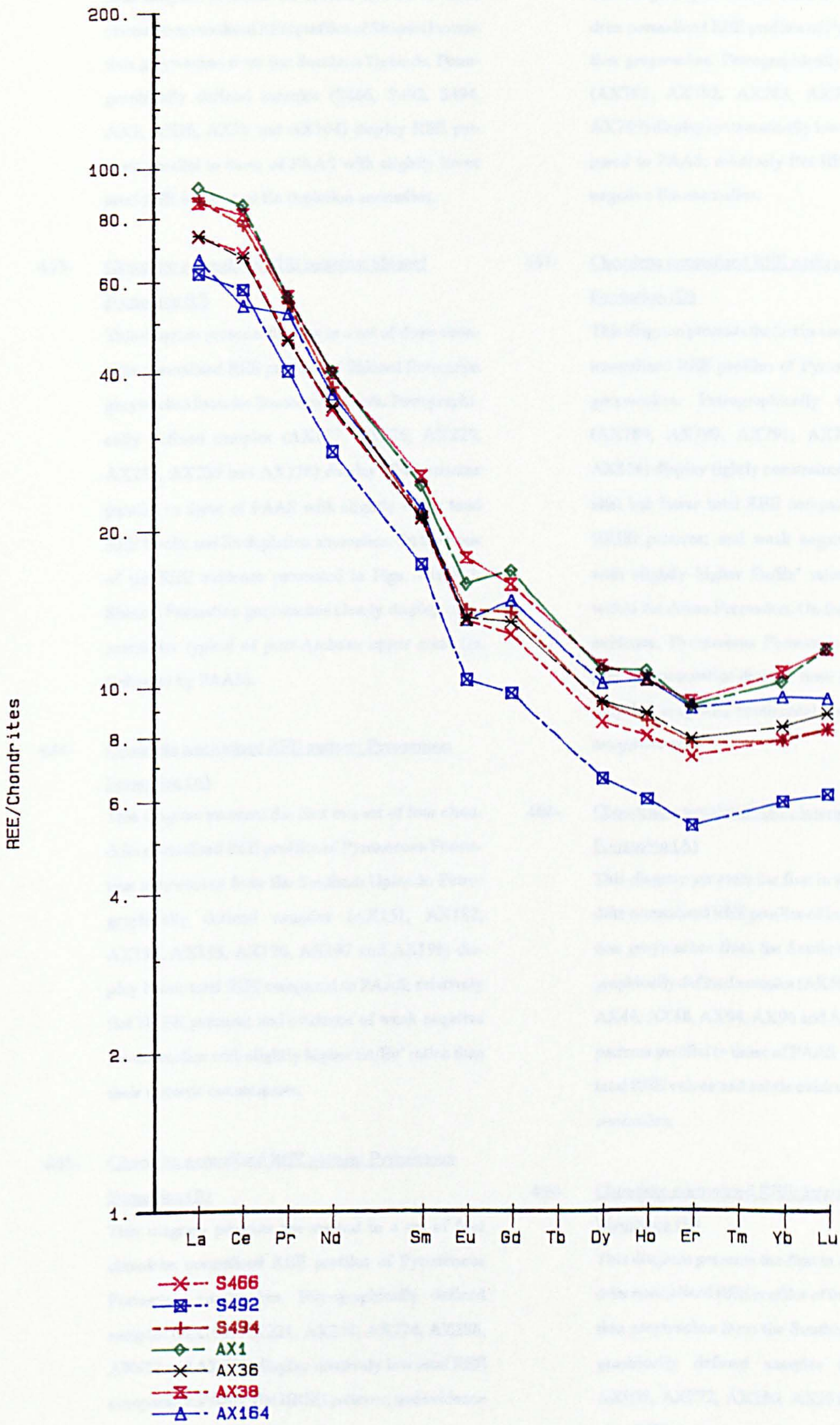

462- Chondrite normalised REE patterns: Shinnel Formation (B)

This diagram presents the second in a set of three chondrite normalised REE profiles of Shinnel Formation greywackes from the Southern Uplands. Petrographically defined samples (S466, S492, S494, AX1, AX36, AX38 and AX164) display REE patterns parallel to those of PAAS with slightly lower total REE levels; and Eu depletion anomalies.

463- Chondrite normalised REE patterns: Shinnel Formation (C)

This diagram presents the last in a set of three chondrite normalised REE profiles of Shinnel Formation greywackes from the Southern Uplands. Petrographically defined samples (AX177, AX226, AX229, AX235, AX236 and AX276) display REE patterns parallel to those of PAAS with slightly lower total REE levels; and Eu depletion anomalies. On the basis of the REE evidence presented in Figs. 461-463, Shinnel Formation greywackes clearly display characteristics typical of post-Archean upper crust (as indicated by PAAS).

464- Chondrite normalised REE pattern: Pyroxenous Formation (A)

This diagram presents the first in a set of four chondrite normalised REE profiles of Pyroxenous Formation greywackes from the Southern Uplands. Petrographically defined samples (AX151, AX182, AX194, AX195, AX196, AX197 and AX198) display lower total REE compared to PAAS; relatively flat HREE patterns; and evidence of weak negative Eu-anomalies with slightly higher Eu/Eu* ratios than their cratonic counterparts.

465- Chondrite normalised REE pattern: Pyroxenous Formation (B)

This diagram presents the second in a set of four chondrite normalised REE profiles of Pyroxenous Formation greywackes. Petrographically defined samples (AX199, AX221, AX238, AX274, AX286, AX657 and AX659) display relatively low total REE compared to PAAS; flat HREE patterns; and evidence of weak negative Eu-anomalies.

466- Chondrite normalised REE pattern: Pyroxenous Formation (C)

This diagram presents the third in a set of four chondrite normalised REE profiles of Pyroxenous Formation greywackes. Petrographically defined samples (AX781, AX782, AX783, AX784, AX785 and AX789) display systematically lower total REE compared to PAAS; relatively flat HREE patterns; and negative Eu-anomalies.

467- Chondrite normalised REE pattern: Pyroxenous Formation (D)

This diagram presents the last in a set of four chondrite normalised REE profiles of Pyroxenous Formation greywackes. Petrographically defined samples (AX789, AX790, AX791, AX796, AX797 and AX834) display tightly constrained values with parallel but lower total REE compared to PAAS; flat HREE patterns; and weak negative Eu-anomalies with slightly higher Eu/Eu* ratios than identified within the Afton Formation. On the basis of the REE evidence, Pyroxenous Formation greywackes display characteristics derived from sources including recycled orogenic, continental block and dissected magmatic arc.

468- Chondrite normalised REE: Intermediate Formation (A)

This diagram presents the first in a set of three chondrite normalised REE profiles of Intermediate Formation greywackes from the Southern Uplands. Petrographically defined samples (AK502, AK674, AX44, AX46, AX48, AX94, AX96 and AX97) display REE patterns parallel to those of PAAS with slightly lower total REE values and subtle evidence of negative Eu-anomalies.

469- Chondrite normalised REE: Intermediate Formation (B)

This diagram presents the first in a set of three chondrite normalised REE profiles of Intermediate Formation greywackes from the Southern Uplands. Petrographically defined samples (AX107, AX108, AX109, AX272, AX280, AX281 and AX283) display REE patterns parallel to those of PAAS with lower total REE values; and strong negative Eu-anomalies.

FIGURE 463

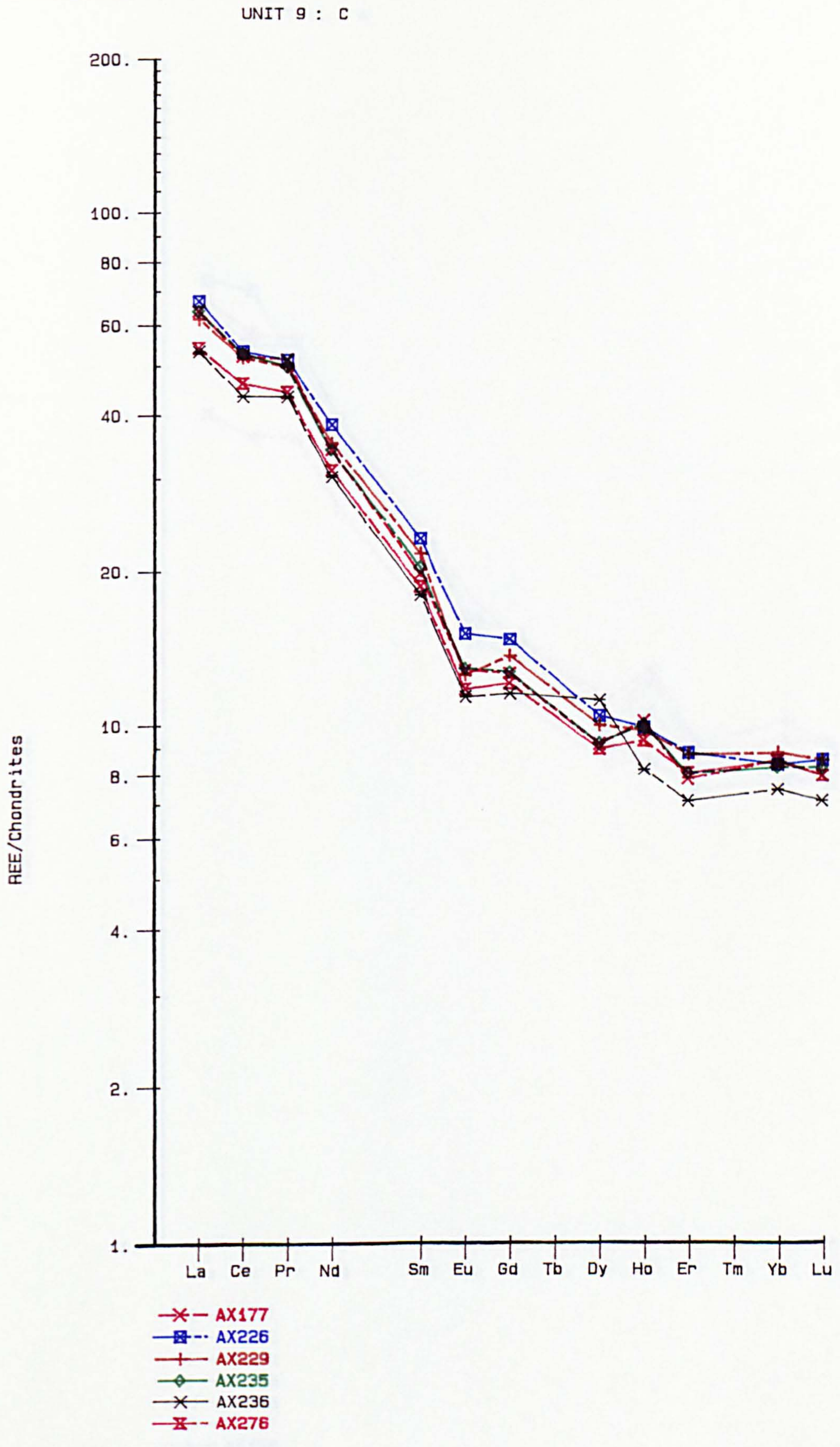
UNIT 9 : C
REE/Chondrites
200.
100.
80.
60.
40.
20.
10.
8.
6.
4.
2.
1.
La
Ce
Pr
Nd
Sm
Eu
Gd
Tb
Dy
Ho
Er
Tm
Yb
Lu
AX177
AX226
AX229
AX235
AX236
AX276

FIGURE 464

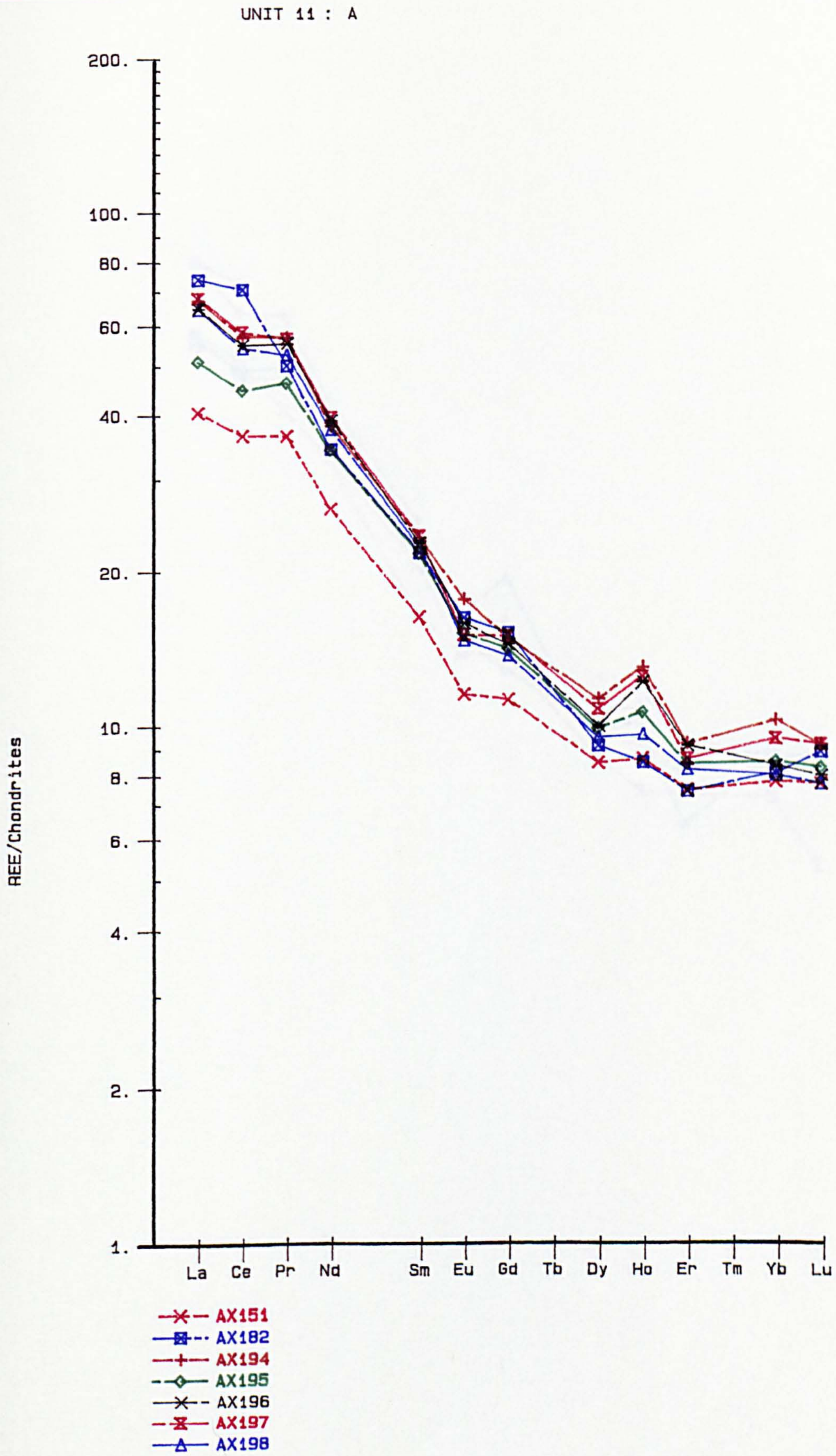
UNIT 11 : A
200.
100.
80.
60.
40.
20.
10.
8.
6.
4.
2.
1.
REE/Chondrites
La
Ce
Pr
Nd
Sm
Eu
Gd
Tb
Dy
Ho
Er
Tm
Yb
Lu
AX151
AX182
AX194
AX195
AX196
AX197
AX198

FIGURE 465

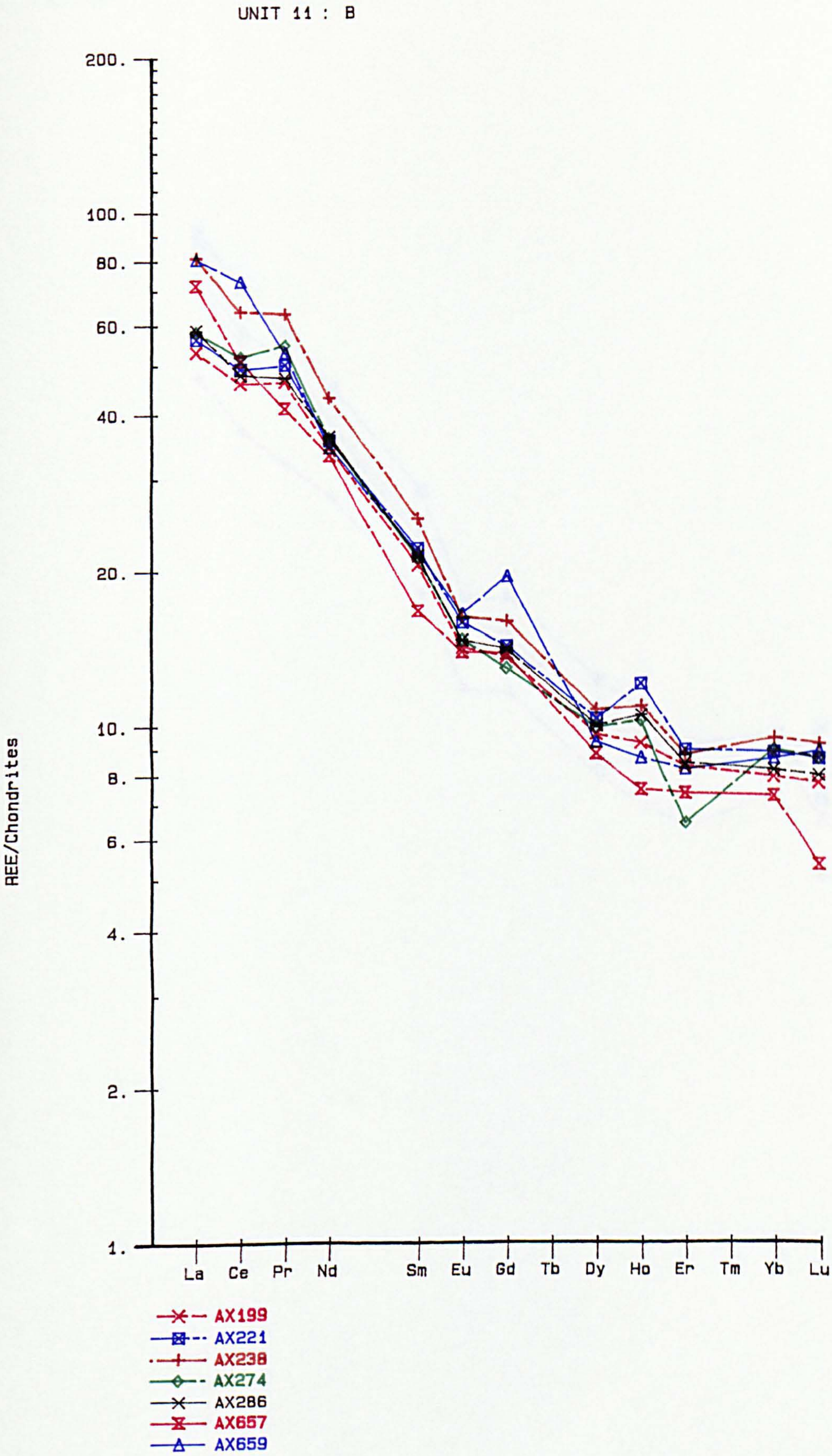
UNIT 11 : B
200.
100.
80.
60.
40.
20.
10.
8.
6.
4.
2.
1.
REE/Chondrites
La
Ce
Pr
Nd
Sm
Eu
Gd
Tb
Dy
Ho
Er
Tm
Yb
Lu
AX199
AX221
AX238
AX274
AX286
AX657
AX659

FIGURE 466

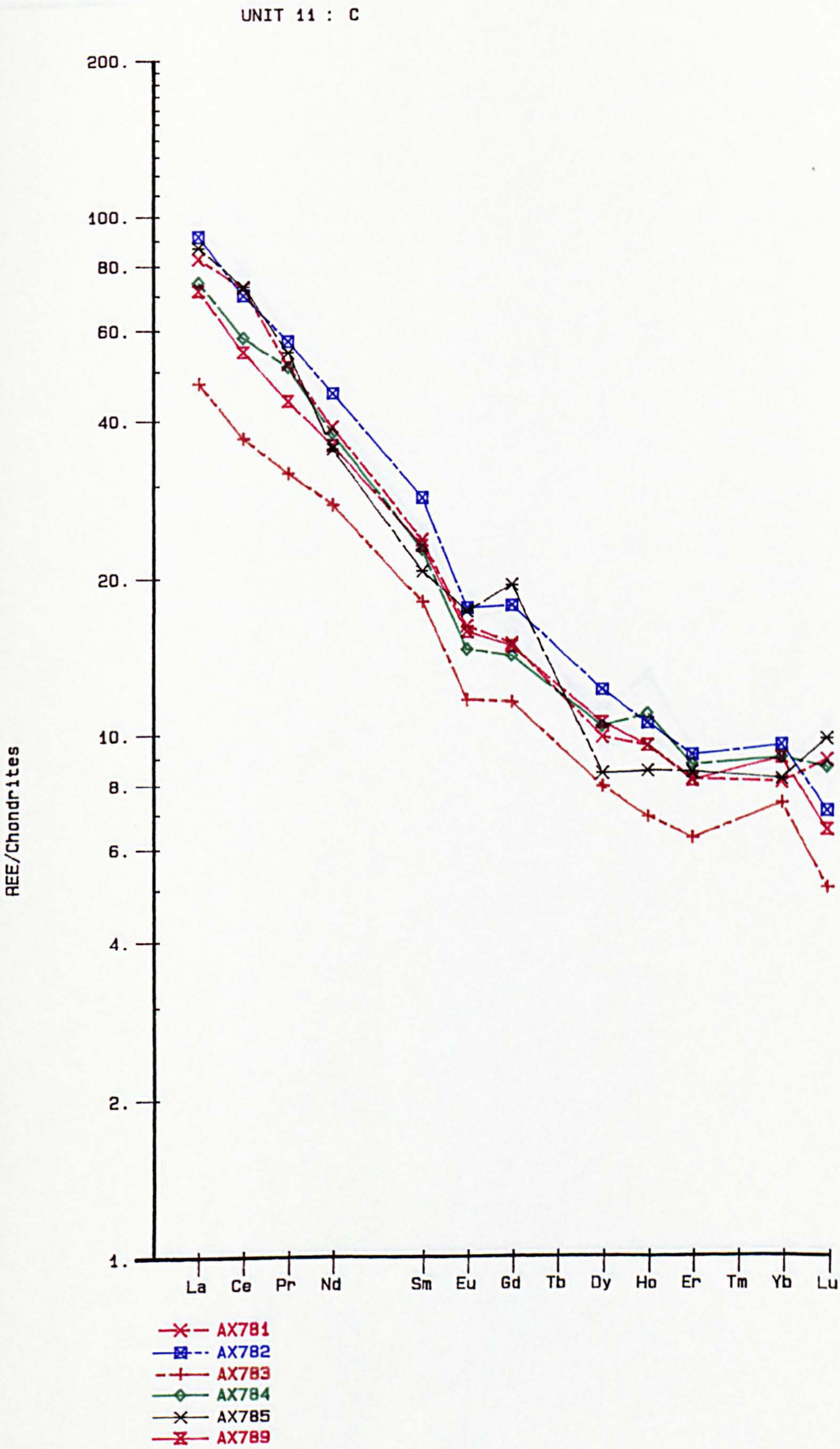
UNIT 11 : C
200.
100.
80.
60.
40.
20.
10.
8.
6.
4.
2.
1.
REE/Chondrites
La
Ce
Pr
Nd
Sm
Eu
Gd
Tb
Dy
Ho
Er
Tm
Yb
Lu
AX781
AX782
AX783
AX784
AX785
AX789

FIGURE 467

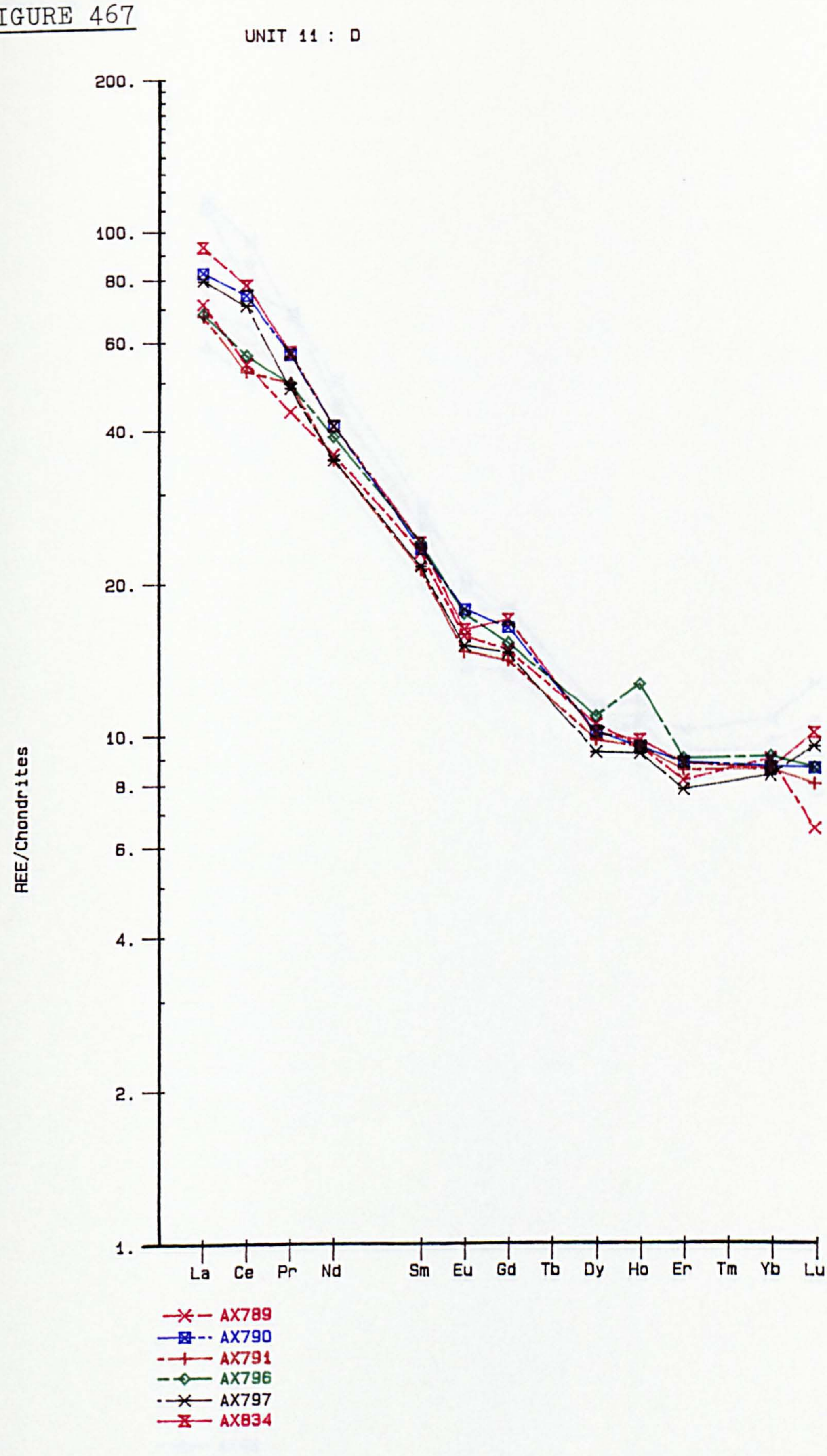
UNIT 11 : D
200.
100.
80.
60.
40.
20.
10.
8.
6.
4.
2.
1.
REE/Chondrites
La
Ce
Pr
Nd
Sm
Eu
Gd
Tb
Dy
Ho
Er
Tm
Yb
Lu
AX789
AX790
AX791
AX796
AX797
AX834

FIGURE 468

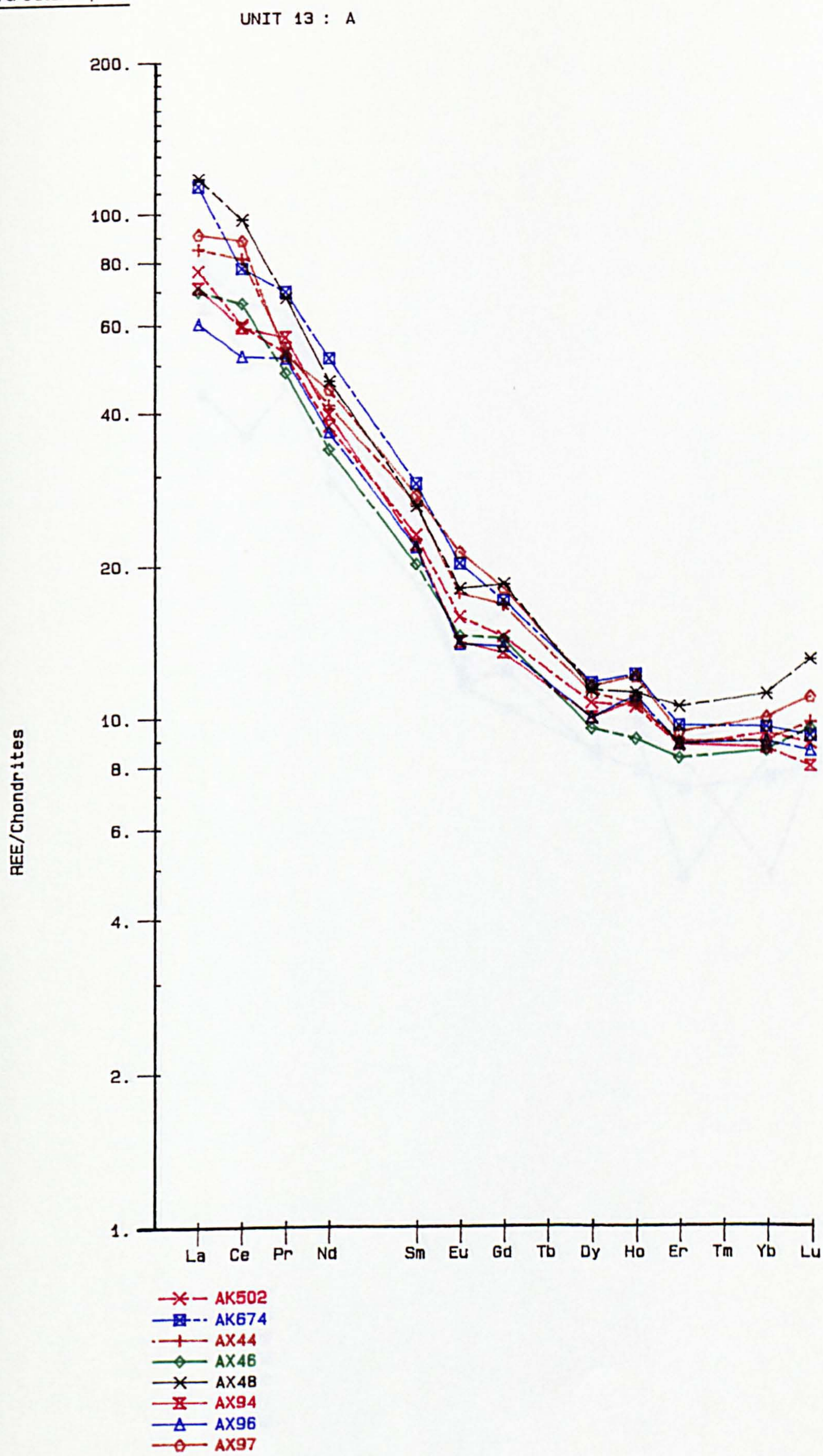
UNIT 13 : A
200.
100.
80.
60.
40.
20.
10.
8.
6.
4.
2.
1.
REE/Chondrites
La
Ce
Pr
Nd
Sm
Eu
Gd
Tb
Dy
Ho
Er
Tm
Yb
Lu
AK502
AK674
AX44
AX46
AX48
AX94
AX96
AX97

FIGURE 469

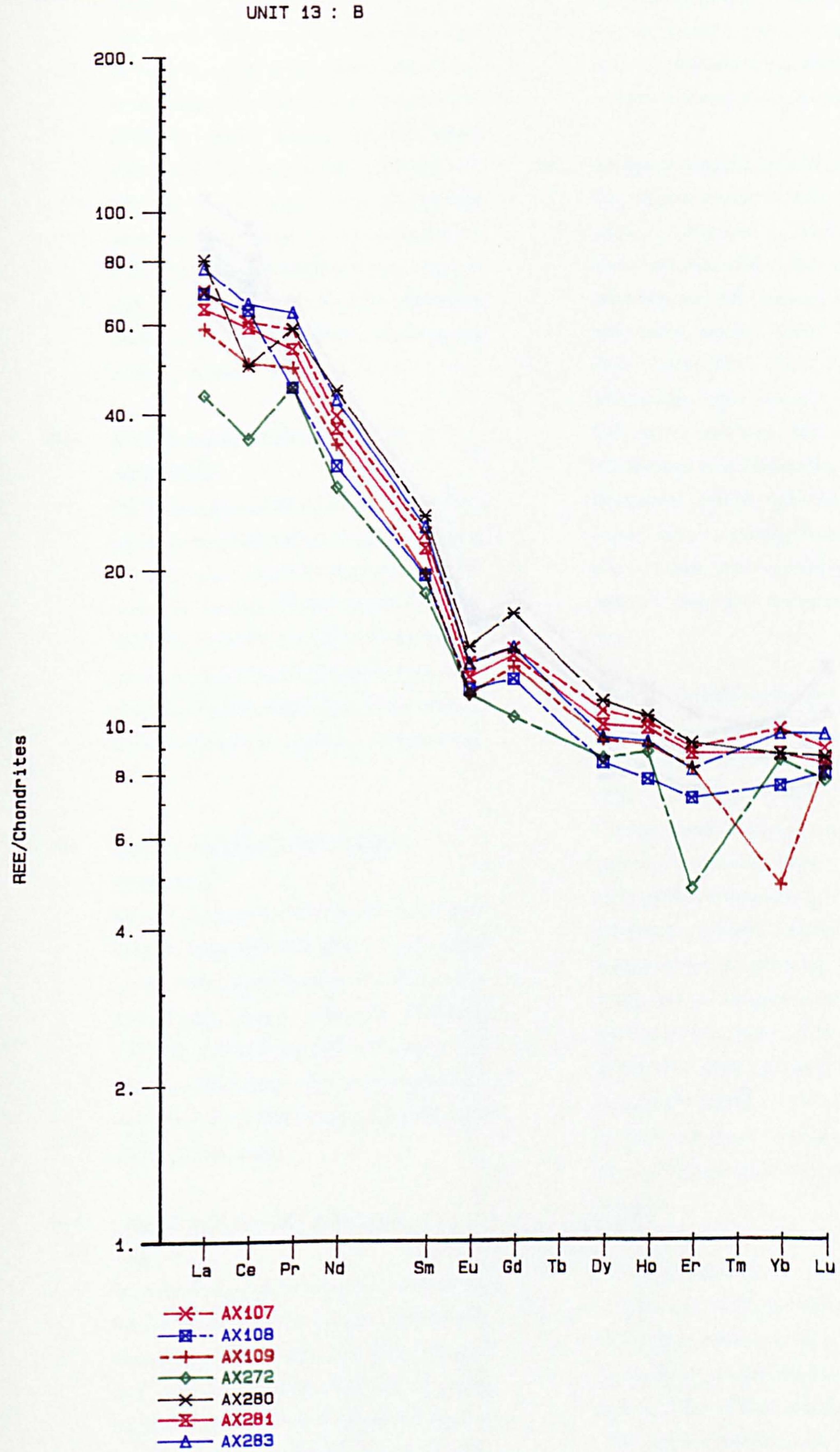

UNIT 13 : B
200.
100.
80.
60.
40.
20.
10.
8.
6.
4.
2.
1.
REE/Chondrites
La
Ce
Pr
Nd
Sm
Eu
Gd
Tb
Dy
Ho
Er
Tm
Yb
Lu
AX107
AX108
AX109
AX272
AX280
AX281
AX283

FIGURE 470

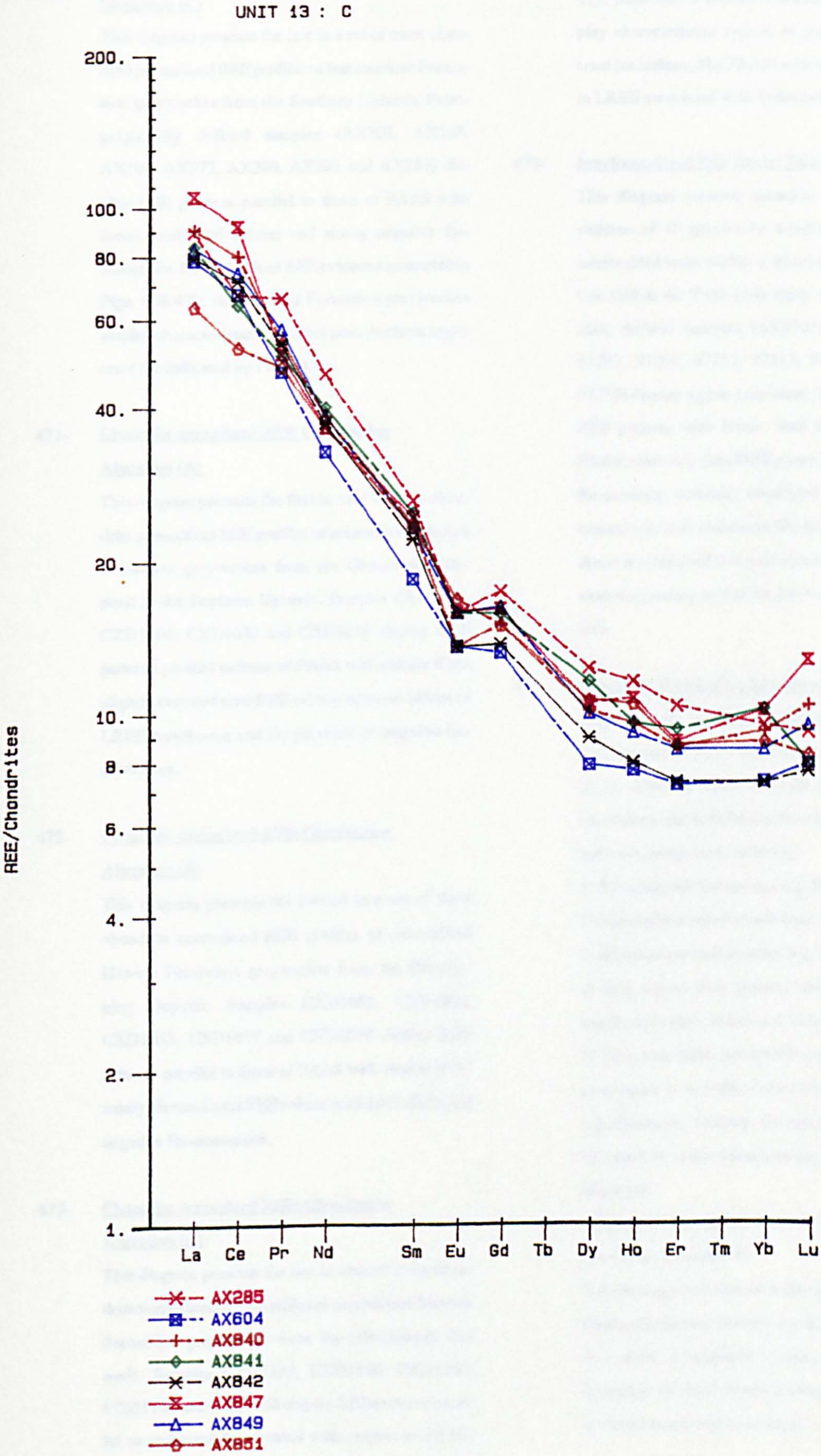
UNIT 13 : C
REE/Chondrites
200.
100.
80.
60.
40.
20.
10.
8.
6.
4.
2.
1.
La
Ce
Pr
Nd
Sm
Eu
Gd
Tb
Dy
Ho
Er
Tm
Yb
Lu
AX285
AX604
AX840
AX841
AX842
AX847
AX849
AX851

470- Chondrite normalised REE: Intermediate Formation (C)

This diagram presents the last in a set of three chondrite normalised REE profiles of Intermediate Formation greywackes from the Southern Uplands. Petrographically defined samples (AX107, AX108, AX109, AX272, AX280, AX281 and AX283) display REE patterns parallel to those of PAAS with lower total REE values; and strong negative Eu-anomalies. On the basis of REE evidence presented in Figs. 468-470, Intermediate Formation greywackes display characteristics typical of post-Archean upper crust (as indicated by PAAS).

471- Chondrite normalised REE: Glendinning Alteration (A)

This diagram presents the first in a set of three chondrite normalised REE profiles of mineralised Hawick Formation greywackes from the Glendinning Deposit in the Southern Uplands. Samples CXD1005, CXD1006, CXD1030 and CXD1050 display REE patterns parallel to those of PAAS with similar if not slightly elevated total REE values; subtle evidence of LREE enrichment and the presence of negative Eu-anomalies.

472- Chondrite normalised REE: Glendinning Alteration (B)

This diagram presents the second in a set of three chondrite normalised REE profiles of mineralised Hawick Formation greywackes from the Glendinning Deposit. Samples CXD1051, CXD1052, CXD1053, CXD1077 and CXD1078 display REE patterns parallel to those of PAAS with similar if not subtly elevated total REE values; enriched LREE; and negative Eu-anomalies.

473- Chondrite normalised REE: Glendinning Alteration (C)

This diagram presents the last in a set of three chondrite normalised REE profiles of mineralised Hawick Formation greywackes from the Glendinning Deposit. Samples CXD1159, CXD1160, CXD1165, CXD1166 and CXD1168 display REE patterns parallel to and partially elevated with respect to PAAS; together with corresponding negative Eu-anomalies. On the basis of REE evidence presented in Figs. 471-473, mineralised Hawick Formations samples display characteristics typical of post-Archean upper crust (as indicated by PAAS) with subtle enrichments in LREE associated with hydrothermal alteration.

474- Interformational REE Study: Tala Linn Study Area

This diagram presents chondrite normalised REE patterns of 10 greywacke samples collected from interbedded units within a 40m long measured section within the Talla Linn study area. Petrographically defined samples (AX97201, 97203, 97205, 97207, 97209, 97211, 97213, 97215, 97217 and 97219) display highly consistent, tightly constrained REE patterns with lower total REE compared to PAAS; relatively flat HREE patterns; and no negative Eu-anomaly, normally associated with quartz-rich, cratonic derived sediments. On the basis of this evidence it is inferred that calc-alkaline andesitic rocks were the primary source for greywackes in this study area.

475 - Simplified Model of the Metallogenesis of As-Sb-Au Deposits in the British Caledonides

This diagram present a simplified graphical summary of the differing styles of As-Sb-Au mineralisation identified in the British Isles. Seven major types of deposit are recognised, including:

1) Metalliferous hot springs (eg. Rhynie)
2) Mineralized breccias and faults (eg. Glendinning)
3) Mineralized fault systems (eg. Clontibret)
4) Mineralized fault systems and minor intrusions (eg. Penkiln Burn, Glenhead, Talnotry Copper mine)
5) Vein mineralization related to major intrusions:-
a) marginal to or at the contact with major intrusions (eg. Glenhead, Talnotry, Cairngarroch, The Knipe);
b) hosted by major intrusions (eg. Black Stockarton Moor); or
c) hosted by igneous breccias and agglomerates (eg. Fore Burn, Kilmelford).

It is not suggested that each different style of mineralisation is present in every deposit, however a tentative model is proposed relating the nature of the deposit to depth of emplacement, and an increasing igneous component with depth.

FIGURE 471

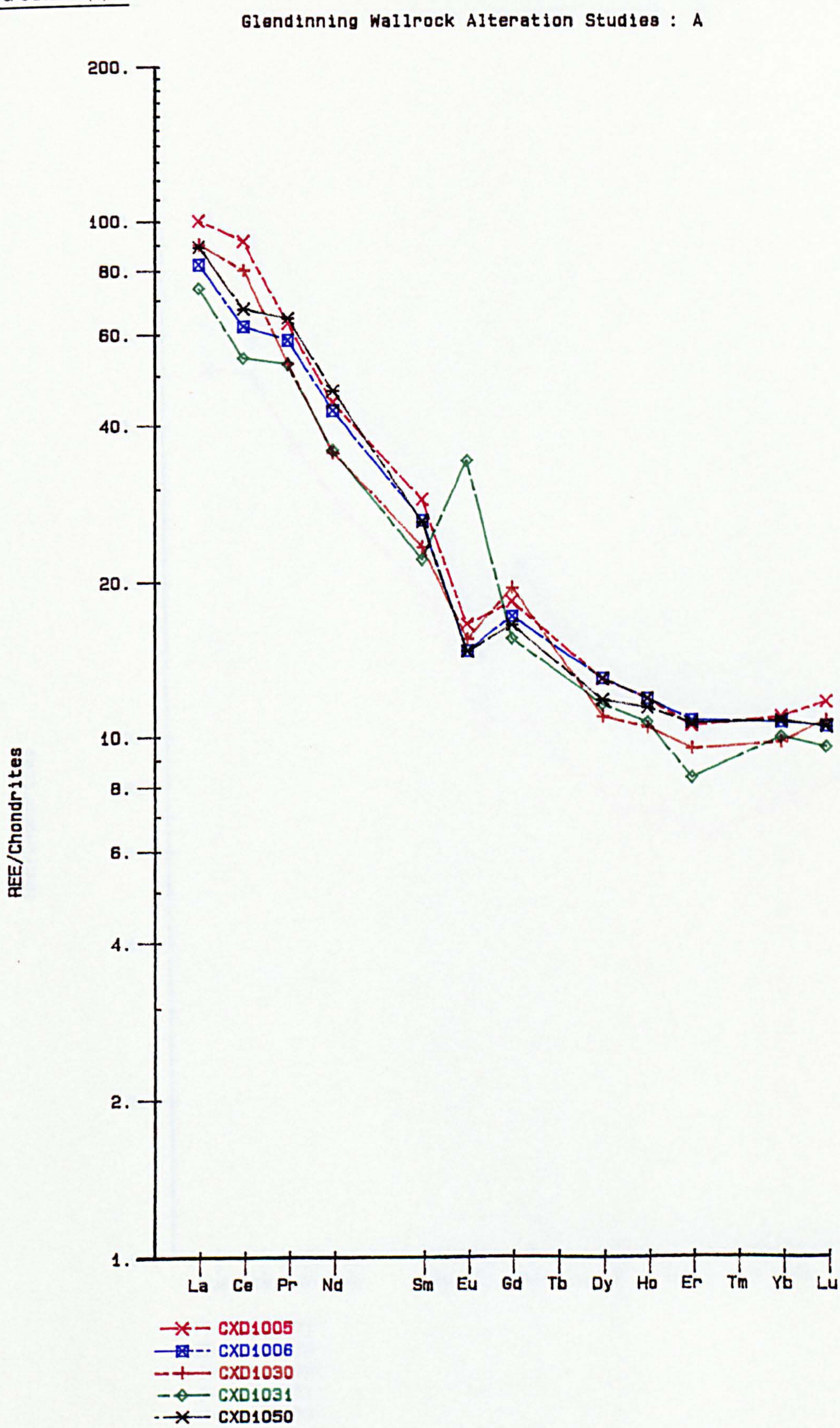
Glendinning Wallrock Alteration Studies : A
REE/Chondrites
200.
100.
80.
60.
40.
20.
10.
8.
6.
4.
2.
1.
La
Ce
Pr
Nd
Sm
Eu
Gd
Tb
Dy
Ho
Er
Tm
Yb
Lu
CXD1005
CXD1006
CXD1030
CXD1031
CXD1050

FIGURE 472

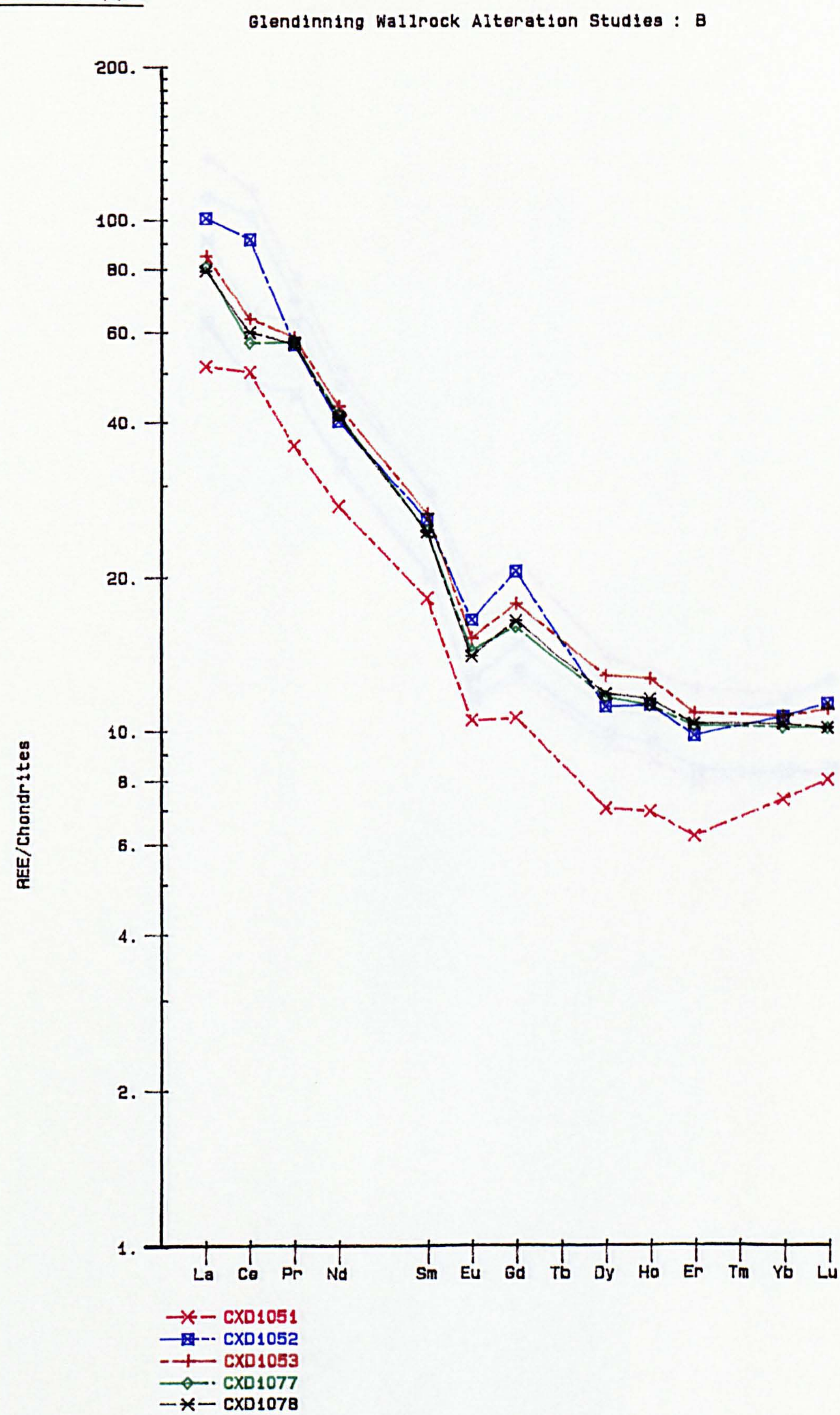
Glendinning Wallrock Alteration Studies : B
REE/Chondrites
200.
100.
80.
60.
40.
20.
10.
8.
6.
4.
2.
1.
La Ce Pr Nd Sm Eu Gd Tb Dy Ho Er Tm Yb Lu
CXD1051
CXD1052
CXD1053
CXD1077
CXD1078

FIGURE 473

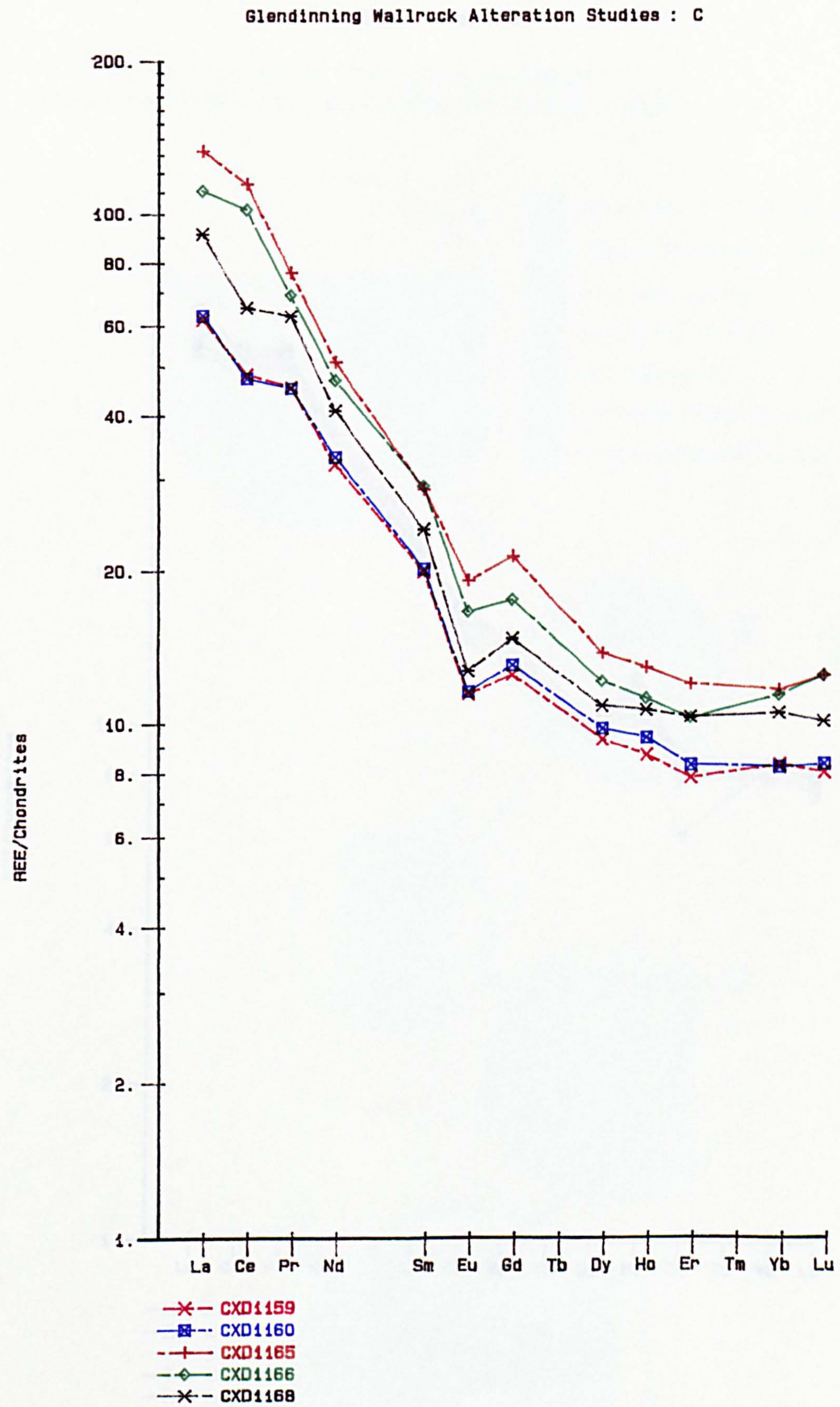
Glendinning Wallrock Alteration Studies : C
200.
100.
80.
60.
40.
20.
10.
8.
6.
4.
2.
1.
REE/Chondrites
La
Ce
Pr
Nd
Sm
Eu
Gd
Tb
Dy
Ho
Er
Tm
Yb
Lu
CXD1159
CXD1160
CXD1165
CXD1166
CXD1168

FIGURE 474

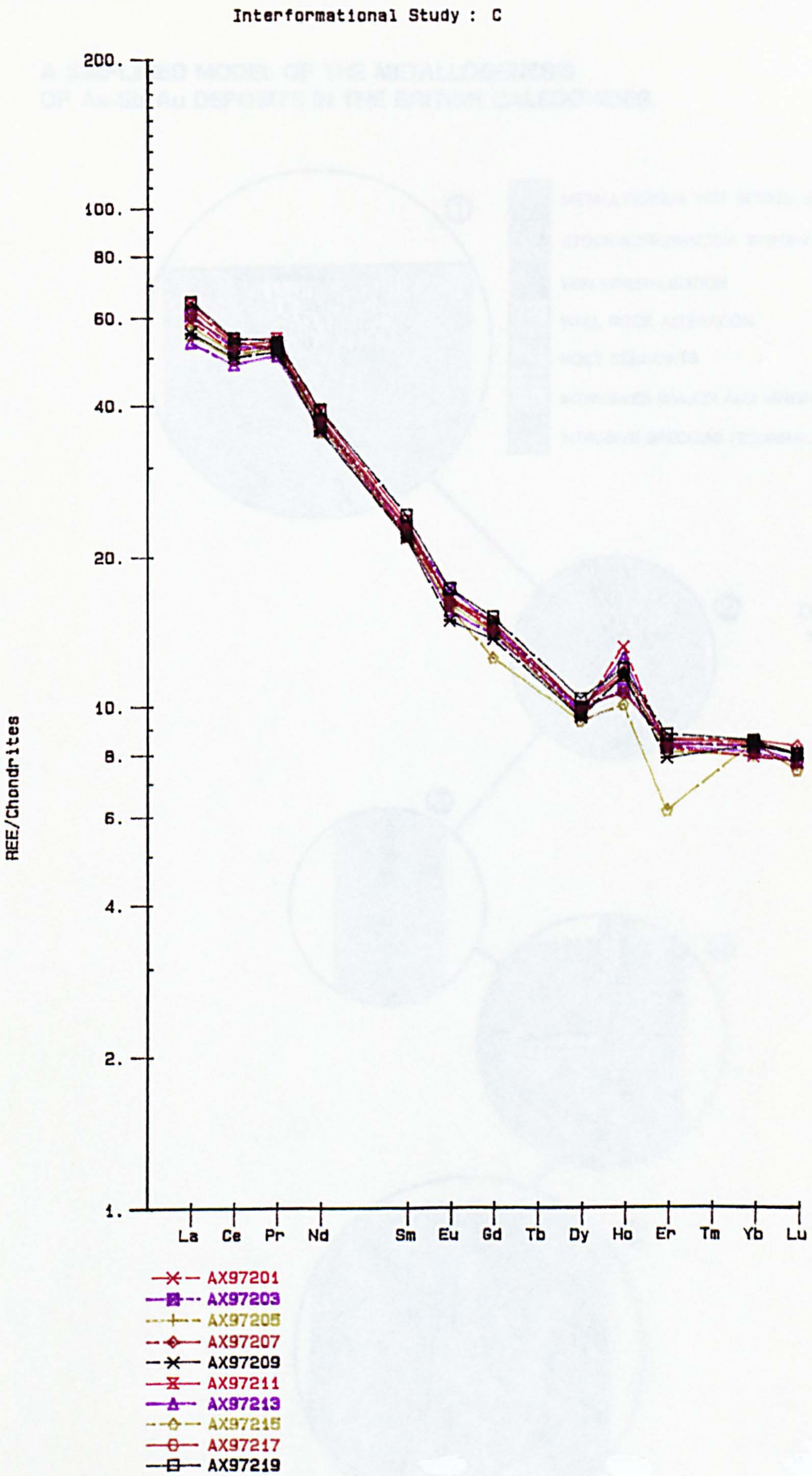
Interformational Study : C
200.
100.
80.
60.
40.
20.
10.
8.
6.
4.
2.
1.
REE/Chondrites
La
Ce
Pr
Nd
Sm
Eu
Gd
Tb
Dy
Ho
Er
Tm
Yb
Lu
AX97201
AX97203
AX97205
AX97207
AX97209
AX97211
AX97213
AX97215
AX97217
AX97219

FIGURE 475

A SIMPLIFIED MODEL OF THE METALLOGENESIS OF As-Sb-Au DEPOSITS IN THE BRITISH CALEDONIDES.